17.4.91

AJR

CUK-H03574-28-P024458

28

American
Journal of
Roentgenology

May 1990

Better catheter tip control starts with better fingertip control.

An easy-to-handle winged and ribbed hub is only one of the ways our new E-Z-Flow™ angiography catheters can be a big improvement over the catheter you now may be using.

Control is also enhanced by the excellent curve memory of our new, smooth nylon composite material, and the outstanding torque characteristics of our reliable one-piece design. The perfectly round lumen of our precision-formed tip follows guidewires precisely, with no gaps that can snag on tissue. And better radiopacity gives you excellent visualization.

E-Z-Flow catheters are available from authorized E-Z-EM distributors worldwide, and are fully supported by our network of technical representatives. For more information, call us at 1-800-544-4624.

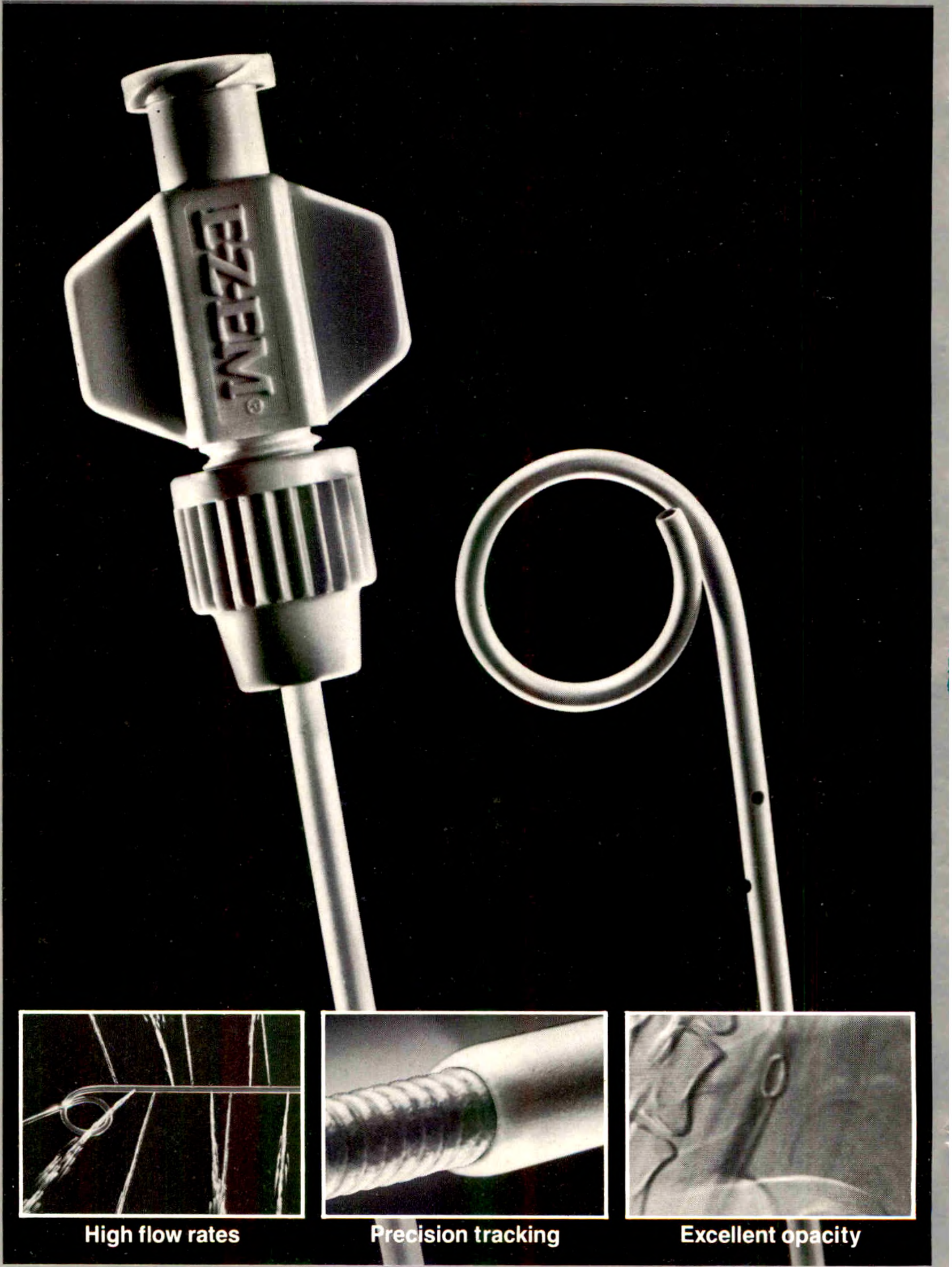

For both the patient and the practitioner, E-Z-EM products set the standards for convenience, safety, and quality in:

- GI Radiology
- Interventional Radiology
- CT Scanning
- Ultrasound
- Magnetic Resonance Imaging
- Angiography
- CEA Immunostaining
- Radiation Oncology
- Patient Prepping
- Protective Products
- Computerized Information Management Systems

E-Z-EM®

E-Z-EM, Inc.
7 Portland Avenue
Westbury, NY 11590

Circle 5 on the Reader Service Card

© 1989, E-Z-EM, Inc.

12. 4. 91

Official Journal of the American Roentgen Ray Society

AJR

American Journal of Roentgenology
Diagnostic Imaging and Related Sciences

Editor-In-Chief Robert N. Berk, *La Jolla, California*
University of California, San Diego
School of Medicine and Medical Center

Editor Emeritus Melvin M. Figley, *Seattle, Washington*

Associate Editor Saskia von Waldenburg Hilton, *San Diego, California*

Consulting Editor Michael S. Huckman, *Chicago, Illinois*

Statistician Charles C. Berry, *San Diego, California*

Editorial Board

John R. Amberg
Itamar Aviad
Mark E. Baker
Lawrence W. Bassett
Michael A. Bettmann
Felix S. Chew
N. Reed Dunnick
David K. Edwards
Ronald G. Evens
David S. Feigin
Sandra K. Fernbach
Richard H. Gold
William R. Hendee
John R. Hesselink
Charles B. Higgins
Melvyn T. Korobkin
Faye C. Laing
Thomas L. Lawson
Robert G. Levitt
Bruce L. McClennan
Richard P. Moser
Albert A. Moss
Jeffrey H. Newhouse
Donald L. Resnick
Stewart R. Reuter
Charles A. Rohrmann, Jr.
Peter M. Ronai
Sjef H. J. Ruijs
Stuart S. Sagel
David J. Sartoris
Stefan C. Schatzki
William P. Shuman
Edward A. Sickles
Barry A. Siegel
David D. Stark
Edward T. Stewart
Murali Sundaram
Eric vanSonnenberg
Robert K. Zeman

Editorial Staff: Margaret Levene, *managing editor*; Katie L. Spiller, Barbara Rose, Barbara L. Halliburton, and Janine Anderson, *manuscript editors*; Nancy Rydbeck, *office manager*; Sheri Smith, *administrative assistant*; Sandra L. Griffin, *administrative secretary*.

P24458

AJR, AMERICAN JOURNAL OF ROENTGENOLOGY (ISSN 0361 803X) is the official journal of the American Roentgen Ray Society and is published monthly by Williams & Wilkins, 428 E. Preston St., Baltimore, MD 21202. Annual dues include $50 for journal subscription. Second-class postage paid at Baltimore, MD, and at additional mailing offices. Postmaster, send address changes (Form 3579) to AJR, 428 E. Preston St., Baltimore, MD 21202. Subscription rates $110 ($155 foreign, $244 Japan); institutions $120 ($165 foreign, $254 Japan); in training $25 ($70 foreign, $159 Japan); single copy $16 ($19 foreign). Japanese rates include airfreight. Japanese yen price is available from our sole agent USACO Corporation, 13-12, Shimbashi 1-Chome, Minato-Ku, Tokyo 105, Japan, telephone 03-502-6471. Airmail rates furnished on request. Indexed by *Current Contents* and *Index Medicus*. Copyright © 1990 by American Roentgen Ray Society. 0361-803X/90$2.00

GET THE MOST OUT OF IMAGING PROCEDURES

NEW!

Fetal Sectional Anatomy and Ultrasonography

Lewis H. Nelson III, MD and Walter J. Bo., PhD

Enhance your interpretive skills with the one text that helps you translate the two-dimensional images on paper to the three-dimensional image you actually see.

Combining images and drawings, this text-free atlas provides the facts you need to get the most out of ultrasonographic procedures. Anatomical sections that feature both sagittal and transverse orientation make this book easy to use during scanning, while the clearly-labeled illustrations eliminate the need for cross-referencing to tables.

Drs. Nelson and Bo have created an atlas which employs not only ultrasonography, but also magnetic resonance imaging and computer tomography as imaging modalities to present a complete reference of fetal anatomy. Serial transverse sections of a mid-pregnancy male fetus and sagittal sections of a term, anencephalic female fetus are labeled on the actual image for easy identification at a glance.

1988/224 pages/365 illustrations/6400-2/$65.00/$78.00 outside the US and Canada

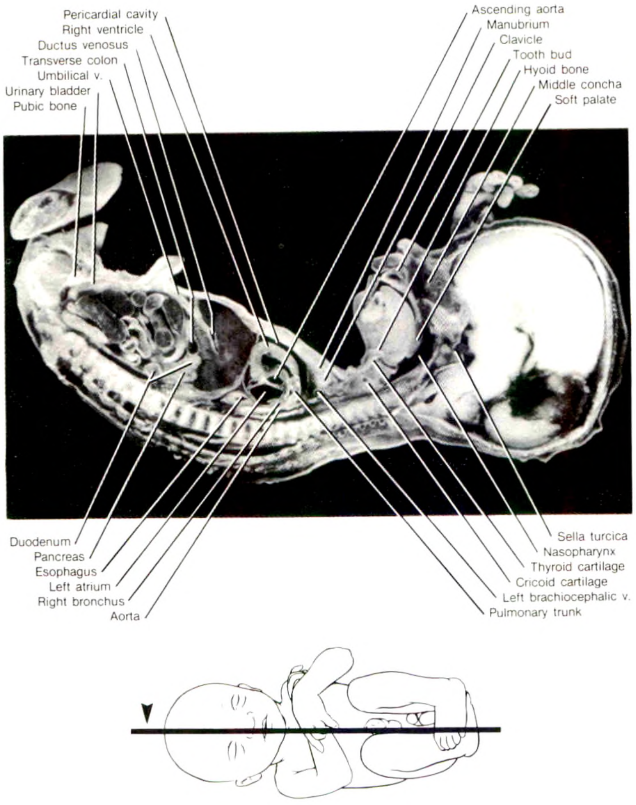

Ordering is as easy as picking up your phone:

In the US just dial, toll-free
1-800-638-0672.

30 day FREE trial for all books! (US only)

NEW!

Computed Cranial and Spinal Imaging

A Practical Introduction

John M. Stevens

Superb illustrations and eminent authors distinguish this new work on optimal imaging of neurological disorders.

From initial choice of imaging modality through interpretation of results, this text spells out exactly how to approach investigation and management decisions, with the strengths, limitations, and uses of CT and MRI examined clearly and in detail. Both normal and pathological appearances of the brain, spine, paranasal sinuses, and orbits are examined with extensive accompanying illustrations. You'll also find essential information on when to administer intravenous or intrathecal contrast enhancement.

1988/224 pages/illustrated/7931-X/$44.95 (available only in North America)

SANS TACHE

Williams & Wilkins

428 East Preston Street
Baltimore, Maryland 21202

Broadway House
2-6 Fulham Broadway
London SW6 1AA England

NELSAD 96707-0 88

AJR Guidelines for Authors

Address new and revised manuscripts, correspondence, and classified ads to the Editor:

AJR Editorial Office
2223 Avenida de la Playa, Suite 200
La Jolla, CA 92037-3218
Telephone: (619) 459-2229; FAX: (619) 459-8814

Inquiries regarding subscriptions, display advertising, reprints, or permission to republish *AJR* material should be addressed to the publisher:

The Williams & Wilkins Co.
428 E. Preston St.
Baltimore, MD 21202 Telephone: 1-800-638-6423

The *AJR* publishes original contributions to the advancement of medical diagnosis and treatment. Submitted manuscripts should not contain previously published material and should not be under consideration for publication elsewhere. Papers dealing with neuroradiology should be addressed to: American Journal of Neuroradiology, Dept. of Radiology, Massachusetts General Hospital, Boston, MA 02114. At the discretion of the *AJR* Editor, *AJNR* articles that are of interest to the general reader may be republished in the *AJR*. Neuroradiologic papers sent to the *AJR* will be forwarded to the Editorial Office of the *AJNR*.

Manuscript decisions are based on peer review. Reviewers receive manuscripts without title pages to ensure an unbiased review. Statements made in the article, including changes made by the Editor or manuscript editor, are the responsibility of the author and not of the *AJR* or its publisher. Authors will be sent the edited manuscript, galley proof, and proofs of illustrations. If the corresponding author will be unavailable to review galleys, arrangements should be made for a coauthor or colleague to read and return the proof.

The following guidelines are based on instructions set forth in the **Uniform Requirements for Manuscripts Submitted to Biomedical Journals** (*Ann Intern Med* **1988;**108:258–265). Articles will be edited, however, to conform to the individual style of AJR.

General Guidelines for Major Papers

Abstract. Clearly state (in 200 words or less) the purpose, methods, results, and conclusions of the study. Include actual data.

Introduction. Briefly describe the purpose of the investigation and explain why it is important.

Methods. Describe the research plan, the materials (or subjects), and the methods used, in that order. Explain in detail how disease was confirmed and how subjectivity in observations was controlled.

Results. Present results in a clear, logical sequence. If tables are used, do not duplicate tabular data in text, but do describe important trends and points.

Discussion. Describe the limitations of the research plan, materials (or subjects), and methods, considering both the purpose and the outcome of the study. When results differ from those of previous investigators, explain the discrepancy.

AUTHOR'S CHECKLIST

For priority handling, complete the following checklist, sign the copyright form on the reverse side of this page, and include both with the manuscript.

________ Two copies of the manuscript (the original and a photocopy) and two complete sets of figures are submitted. One copy has been retained by the author.

________ If appropriate, *AJR* Guidelines for case reports, technical notes, pictorial essays, or letters to the Editor have been followed. (See page A5.)

________ The manuscript, including references, figure legends, and tables, is typed double-spaced on 8½ × 11 in. (21.6 × 27.9 cm) *nonerasable* paper. Right-hand margins are not justified.

________ All manuscript pages are numbered consecutively beginning with the abstract. Authors' names do not appear on the manuscript pages.

________ The manuscript is organized as follows: title page, blind title page (title only), abstract, introduction, methods, results, discussion, acknowledgments, references, tables, figure legends, and figures.

________ Informed consent has been obtained from patients who participated in clinical investigations. If experiments were performed on animals, authors complied with NIH guidelines for use of laboratory animals.

________ Use of unfamiliar acronyms and abbrevations is kept to a minimum. When abbreviations are used they are defined at first mention, followed by the abbreviation in parentheses.

________ Metric measurements are used throughout, or the metric equivalent is given in parentheses.

________ Names and locations (city and state only) of manufacturers are given for equipment and nongeneric drugs.

Title Page

________ The following information is given: title of article; names and complete addresses (including zip code) of all authors; current addresses of authors who have moved since study; acknowledgment of grant or other assistance. The corresponding author is clearly identified, and a current address, phone number, and FAX number are given.

________ Two copies of a blind title page are included giving only the title (without the authors' names) for use in the review process.

Abstract

________ An abstract of approximately 200 words concisely states the purpose, methods, and results of the study in one paragraph. Actual data are included. Conclusions are stated in a second, summary paragraph.

________ No abbreviations or reference citations are used.

References

________ References (not to exceed 35) are typed double-spaced starting on a separate page and are **numbered consecutively in the order in which they appear in the text**.

________ All references are cited in the text and are enclosed in brackets and typed on line with the text (not superscript).

________ Unpublished data are not cited in the reference list, but are cited parenthetically in the text, for example, (Smith DJ, personal communication), (Smith DJ, unpublished data). This includes papers submitted, but not yet accepted, for publication.

________ Inclusive page numbers (e.g., 333–335) are given for all references.

________ Journal names are abbreviated according to *Index Medicus*.

________ Style and punctuation of references follow the format illustrated in the following examples (all authors are listed when six or fewer; when seven or more authors, the first three are listed, followed by "et al."):

Journal article

1. Long RS, Roe EW, Wu EU, et al. Membrane oxygenation: radiographic appearance. *AJR* **1986**;146:1257–1260

Book

2. Smith LW, Cohen AR. *Pathology of tumors*, 6th ed. Baltimore: Williams & Wilkins, **1977**:100–109

Chapter in a book

3. Breon AJ. Serum monitors of bone metastasis. In: Clark SA, ed. *Bone metastases*. Baltimore: Williams & Wilkins, **1983**:165–180

Paper presented at a meeting

4. Lau FS, Kirk AN. MR imaging of the spine. Presented at the annual meeting of the American Roentgen Ray Society, Washington, DC, April **1986**

Tables

________ Each table is typed double-spaced on a separate page without vertical or horizontal rules; each has a short, descriptive title. Tables do not exceed two pages in length and contain at least four lines of data.

________ Tables are numbered in the order in which they are cited in the text.

________ Abbreviations are defined in an explanatory note below each table.

________ Tables are self-explanatory and do not duplicate data given in the text or figures.

________ All arithmetic (percentages, totals, differences) has been double checked for accuracy, and tabular data agree with data given in the text.

Figures and Legends

________ Two complete sets of original figures are submitted unmounted in labeled envelopes.

________ Figures are clean, unscratched, 5 × 7 in. (13 × 18 cm) glossy prints with **white borders.** A separate print is submitted for each figure *part*.

________ All figure parts relating to one patient have the same figure number.

________ Each figure is labeled on the back with the figure number and an arrow indicating "top." For black-and-white figures, labeling is done on a gummed label, which is then affixed to the back of the print. *Never* use labels on color figures, but write figure number on the back lightly in pencil. *Never* use ink on front or back of any figures.

________ Author's names are *not* written on the backs of figures.

________ Only removable (rub-on) arrows and letters are used on the figures. Symbols are uniform in size and style and are not broken or cracked.

________ Images are uniform in size and magnification.

________ Line drawings are done in black ink on a white background. They are professional in quality, and all use the same size type. (Only glossy prints are acceptable.)

________ Written permission has been obtained for use of all previously published illustrations (and copies of permission letters are included), and an appropriate credit line is given in the legends.

________ Legends are typed double-spaced, and figure numbers correspond with the order in which the figures are cited in the text.

Transfer of Copyright Agreement, Conflict of Interest Acknowledgment, Certification of Coauthors, and Exclusive Publication Statement

Complete copyright to the article entitled: ____

____

is hereby transferred to the American Roentgen Ray Society (for United States government employees to the extent transferable), effective if and when the article is accepted for publication in the *American Journal of Roentgenology*. In the case of the authors who are officers or employees of the United States government, the American Roentgen Ray Society recognizes that works prepared by officers or employees of the United States government as part of their official government duties are in the public domain.

Authors reserve all proprietary rights other than copyright, such as patent rights and the right to use all or part of this article in future works of their own. The authors retain the right of replication, subject only to crediting the original source of publication and receiving written permission from the publisher.

Authors guarantee that this manuscript contains no matter that is libelous or otherwise unlawful, invades individual privacy, or infringes any proprietary rights.

Authors understand that they will receive no royalty or other compensation from the American Roentgen Ray Society or the publisher.

Authors guarantee that the editor has been or will be informed of any proprietary or commercial interest or conflicts of interest the authors may have that relate directly or indirectly to the subject of this article.

All authors certify that they have made substantive and specific intellectual contributions to the article and assume public responsibility for its content.

Finally, the authors certify that none of the material in this manuscript has been published previously or is currently under consideration for publication elsewhere.

------------------------	------------------------	------------------------
First author/date	Second author	Third author
------------------------	------------------------	------------------------
Fourth author	Fifth author	Sixth author

This agreement must be signed by all authors in order for the manuscript to be published.

Case Reports

A case report is a brief description of a special case that provides a message that transcends the individual patient.

Format. There is no abstract. The introduction should be a short paragraph giving the general background and the specific interest of the case. No more than one case should be described in detail (similar ones can be mentioned briefly in the discussion). Emphasis should be on the radiologic aspects; clinical information must be limited to that necessary to provide a background for the radiology. The discussion should be succinct and should focus on the specific message and relevance of radiologic methods. A review of the literature is not appropriate.

Length. Maximum of five double-spaced, typewritten pages, including the references but not the title page or figure legends.

References. Maximum of eight.

Figures. Maximum of three or four, unless the text is shortened accordingly. Legends must not repeat the text.

Tables and Acknowledgments. Not appropriate in case reports.

Pictorial Essays

A pictorial essay is an article that conveys its message through illustrations and their legends. Unlike other *AJR* articles, which are based on original research, pictorial essays serve primarily as teaching tools, like exhibits at a scientific meeting. They are not encyclopedic book chapters. The abstract should be a short, introductory paragraph.

Length. Maximum of four double-spaced, typewritten pages, including the references but not the title page or figure legends.

References. Maximum of four.

Figures. Maximum of 30 figure *parts*. Number should be as few as necessary to convey the message of the paper.

Tables and Acknowledgments. Not appropriate in pictorial essays.

Opinions, Commentaries, and Perspectives

Opinions, commentaries, and perspectives are special articles dealing with controversial topics or issues of special concern to radiologists.

Format. Include a title page but no abstract. Headings may be used to break up the text.

Length. Maximum of five double-spaced, typewritten pages.

References. Maximum of five.

Tables and Figures. Maximum of four.

Technical Notes

A technical note is a brief description of a specific technique or procedure, modification of a technique, or equipment of interest to radiologists.

Format. No abstract, headings, or subheadings are required. If headings are used, they should be a combination of "Case Report," "Materials and Methods," "Results," and "Discussion." A brief one-paragraph introduction should be included to give the general background. Discussion should be limited to the specific message, including the uses of the technique or equipment. Literature reviews and lengthy case reports are not appropriate.

Length. Maximum of five double-spaced, typewritten pages, including the references but not the title page or figure legends.

References. Maximum of eight.

Figures. Maximum of two, unless the text is shortened accordingly.

Tables and Acknowledgments. Not appropriate in technical notes.

Letters to the Editor and Replies

Letters to the Editor and Replies should offer objective and constructive criticism of published articles. Letters may also discuss matters of general interest to radiologists. Do not end a letter with a hand-written signature.

Format. All letters should be typed double-spaced on nonletterhead paper, with no greeting or salutation. Name and affiliation should appear at the end of the letter. Titles for letters should be short and pertinent. The title for a reply is simply "Reply."

Length. Maximum of two double-spaced, typewritten pages, including references.

References. Maximum of four.

Figures. Maximum of two.

Tables and Acknowledgments. Not appropriate in Letters to the Editor and Replies.

Computer Page Articles

Articles published on the computer page deal with practical computer applications to radiology.

Format. Include a title page but no abstract.

Length. Maximum of eight double-spaced, typewritten pages.

References. Maximum of five.

Figures and Tables. Maximum of five. Computer printouts are not acceptable. Figures must be submitted as 5 × 7 in. glossy prints.

All submissions to the *AJR* must be accompanied by a completed copy of the Author's Checklist and the signed Copyright Agreement.

CHAIRMAN OF RADIOLOGY

300-bed university affiliated Philadelphia teaching hospital with renowned Radiology Department has begun search for an especially qualified person. Board certification is minimal requirement. Depth of experience and strong adminstrative skills essential. This is a unique and challenging opportunity. Highly qualified radiology staff exists, as well as general medical staff in full range of specialities. Department is well-equipped with CT scan and MRI. School of X-Ray Technology as well as radiology residency. Contractual arrangements open. Your curriculum vitae will receive prompt and confidential treatment. Replies should be forwarded to:

C-50, P.O. Box 2045
Philadelphia, PA 19103

Equal Opportunity Employer, M/F

VASCULAR/INTERVENTIONAL AND NUCLEAR MEDICINE/IMAGING
TWO POSITIONS

The ten member imaging section of the Guthrie Clinic - Robert Packer Hospital desires associates with Fellowship training in the above modalities.

The Guthrie Clinic is a 220 physician multi-specialty clinic serving the Southern Tier of New York and the Northern Tier of Pennsylvania in the beautiful endless mountains.

Outstanding practice opportunities in an environment free of urban hassle.

Please send letter of inquiry with curriculum vitae:

Guthrie Clinic
Sayre, PA 18840
717-888-5858
Attn: G.V. Ippolito
Vice President

CHIEF OF DIAGNOSTIC IMAGING

Hawaii Permanente Medical Group, Inc., a large multi-specialty group practice, is seeking a radiologist with management experience to direct the professional activities of diagnostic imaging for Kaiser Permanente on the island of Oahu.

Approximately 120,000 procedures are performed annually at the 200-bed medical center and detached clinics. CT, ultrasound, nuclear medicine, angiography, and other standard modalities are provided. MRI is planned for 1991.

Contact:

Michael Chaffin, M.D.
at 808-834-9112 or send
curriculum vitae to
3288 Moanalua Road
Honolulu, HI 96819.

An equal opportunity employer

UNIVERSITY OF Miami
SCHOOL OF MEDICINE

Department of Radiology is recruiting faculty for the UM/Jackson Memorial Medical Center, a 1300 bed tertiary care referral center. Positions available to meet expanding clinical and academic programs in:

ABDOMINAL IMAGING
MUSCULOSKELETAL IMAGING
NUCLEAR MEDICINE
PEDIATRIC RADIOLOGY
THORACIC IMAGING

Candidates must be Board certified or eligible, with fellowship training or equivalent experience. Rank and salary commensurate with qualifications. Send C.V. to:

C.A. Poole, M.D.
Professor and Chairman
Department of Radiology (R-130)
University of Miami
School of Medicine
P.O. Box 016960
Miami, Florida 33101

An Affirmative Action/Equal Opportunity Employer

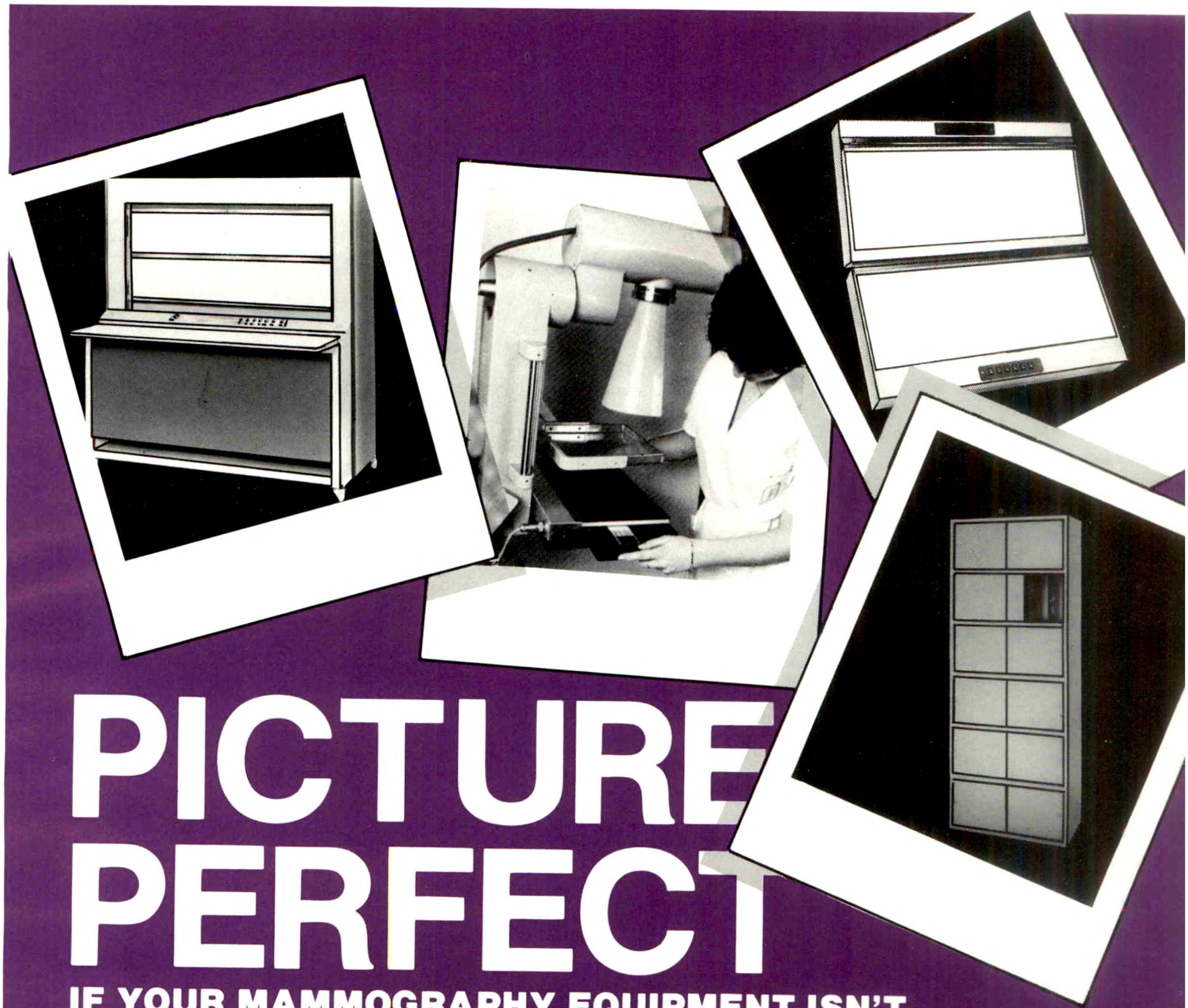

PICTURE PERFECT

IF YOUR MAMMOGRAPHY EQUIPMENT ISN'T THE "PICTURE" OF EFFICIENCY,

YOUR PRODUCTIVITY AND PERFORMANCE WILL BE OUT OF FOCUS!

For over 40 years, specially-dedicated S & S x-ray equipment and accessories have been improving Radiologists' efficiency and productivity. Specially-dedicated mammography equipment includes:

MOBILE *MOTORIZED VIEWERS*

Hold *Mammography* radiographs for random access recall and viewing within 7 seconds! Individual on-off light switches control divided viewing areas.

MODELS:

MV810-170: 10 viewing areas for 170 8x10" films
MV 1824-272: 16 viewing areas for 272 18x24cm films
MV2430-204: 12 viewing areas for 204 24x30cm films

S & S *MAMMOGRAPHY ILLUMINATORS:*

The standard for illumination excellence. Surface or recessed mounting is available for 1 to 6 banks—1 over 1 up to 6 over 6. Individual on-off light controls for ***each*** viewing section reduce glare and prevent spill-over. Single or two tier models for straight or angulated viewing include:

MODELS:

147000: Series for 8x10/18x24cm films
146000: Series for 24x30cm films

MAMMOGRAPH-SIZED VERTIFILE:

Doubles capacity over conventional drawer files. Adjustable partitions. Available with or without sliding door closures.

MODELS:

871: 1 shelf (2 doors) 14x30x13½"
873: 3 shelves (6 doors) 14x30x37¾"
876: 6 shelves (12 doors) 14x30x74½"

ADD-ON *MOVING GRID BUCKY SYSTEM:*

Converts existing non-Bucky mammography equipment. Improves contrast and micro-calcification visibility. Eliminates grid lines. Reduces scattered radiation.

MODELS:

MB-12: for 18x24cm film
MB-24: for 24x30cm film

See your local x-ray dealer or call S & S directly for *Picture Perfect* mammography equipment and our expanded line of radiological equipment and accessories.

S & S X-RAY PRODUCTS, INC.
1101 Linwood Street, Brooklyn, NY 11208
TOLL FREE: 800/347-XRAY ■ **NY STATE:** 718/649-8500 ■ **FAX:** 718/257-0219

CIRCLE 9 ON READER SERVICE CARD

AJR Business and Subscriber Information

The American Roentgen Ray Society

AJR, American Journal of Roentgenology, is published monthly to disseminate research on current developments in the radiologic sciences and commentary on topics related to radiology. It is published by the American Roentgen Ray Society, 1891 Preston White Dr., Reston, VA 22091; (703) 648-8992. Inquiries regarding society business, the annual ARRS meeting, and membership should be addressed to the Society at the above address.

Correspondence Concerning the *AJR*

Correspondence regarding display (not classified) advertising, subscriptions, address changes, reprints, and permission requests should be addressed to Williams & Wilkins, 428 E. Preston St., Baltimore, MD 21202; (301) 528–4000.

Correspondence regarding editorial matters and classified advertising should be addressed to Editorial Office, AJR, 2223 Avenida de la Playa, Ste. 200, La Jolla, CA 92037-3218; telephone (619) 459-2229; FAX (619) 459-8814. For information on manuscript submission, see Guidelines for Authors, pages A3–A5.

Subscriber Information

Subscription requests and inquiries should be sent to Williams & Wilkins, 428 E. Preston St., Baltimore, MD 21202. ARRS annual dues include $50 for journal subscription. Subscription rates are as follows: nonmembers, $110/year ($155 foreign, $244.00 Japan); institutions, $120 ($165 foreign, $254.00 Japan); nonmember in-training, $25 ($70 foreign, $159.00 Japan). Single copies of the Journal may be purchased for $16 ($19 foreign). Airmail rates will be furnished on request.

Japanese rates include airfreight. Japanese yen price is available from our sole agent, USACO Corporation, 13-12, Shimbashi 1-Chome, Minato-Ku, Tokyo 105, Japan; telephone 03-502-6471.

Call toll-free, 1-800-638-6423 (in Maryland call 1-800-638-4007), with subscription questions or problems. Please have the mailing label from your latest issue available when you call.

If a subscriber receives a damaged copy of the *AJR* or fails to receive an issue, the subscriber should notify Williams & Wilkins (428 E. Preston St., Baltimore, MD 21202) within 60 days of publication (90 days for foreign subscribers) and that issue will be replaced.

Change of address information should be sent to Williams & Wilkins, 428 E. Preston St., Baltimore, MD 21202. Allow 90 days for address changes.

Copyrights, Permissions, and Reprints

The American Roentgen Ray Society holds the copyright for all material published in the *AJR*. No part of this publication may be reproduced without permission from the ARRS. Requests for such permission should be addressed to Williams & Wilkins, 428 E. Preston St., Baltimore, MD 21202.

For reprints of a particular article, please contact the author designated in the footnotes for that article.

Indexes

The *AJR* provides volume and yearly indexes (subject and author) in the June and December issues each year. *AJR* articles are also indexed in *Current Contents*, *Index Medicus*, and the cumulative index published by *Radiology*.

Adrenal Imaging: Current Status

N. Reed Dunnick[1]

The development of cross-sectional imaging techniques has dramatically improved our ability to examine the adrenal glands. No longer requiring time-consuming or invasive procedures such as arteriography, venography, or venous sampling, the adrenal glands are readily imaged with CT, sonography, and MR imaging.

The most common indication for adrenal imaging is the detection of metastatic disease. Although tumor metastases as small as 1 cm are easily detected by CT, they must be distinguished from benign adenomas. Furthermore, diseases of the adrenal glands may become manifest as a result of hormone excess or deficiency. Thus, adrenal diseases may be considered as hyperfunctional disorders, adrenal insufficiency, or diseases in which adrenal function is normal. As these hormones can readily be measured, there is seldom doubt in which category a patient belongs.

Diseases Associated with Increased Function

Cortex

Cushing syndrome results from excess glucocorticoids, from either exogenous or endogenous sources. Exogenous Cushing syndrome is seen in patients being treated with large doses of steroids. Endogenous Cushing syndrome is due to overproduction of cortisol by the adrenal cortex. This can be due to an autonomous adrenal tumor, benign or malignant, or due to adrenal hyperplasia from unregulated production of adrenocorticotropic hormone (ACTH).

Cushing disease refers to bilateral adrenal hyperplasia due to overproduction of ACTH by a pituitary adenoma. However, a pituitary adenoma is not always the source of ACTH in patients with adrenal hyperplasia; a variety of other tumors, such as oat-cell carcinoma; bronchial carcinoid adenomas; and tumors of the ovary, pancreas, thymus, and thyroid, as well as pheochromocytomas, also may secrete ACTH [1].

Approximately 70% of cases of endogenous Cushing syndrome are caused by bilateral adrenal hyperplasia. The vast majority of these patients have a pituitary adenoma secreting increased amounts of ACTH. Ectopic sources of ACTH cause approximately 10% of cases [2].

A few patients with adrenal hyperplasia have macronodules that can be seen in the adrenal glands on CT scans. These macronodules usually measure less than 3 cm and may be less than 1 cm in diameter [3]. Macronodular hyperplasia is due to an ACTH-secreting pituitary microadenoma in the majority of cases.

Primary pigmented nodular adrenocortical disease is a rare cause of Cushing syndrome most often found in children or young adults. Cortisol is produced by pigmented nodules of hyperplastic cells [4]. The treatment of primary pigmented nodular adrenocortical disease is bilateral adrenalectomy with steroid replacement.

A benign but autonomous adrenal cortical adenoma is the cause of approximately 20% of cases of endogenous Cushing syndrome and a primary adrenal cortical carcinoma is responsible for about 10% of cases [5]. The prevalence of carcinoma is even higher among children.

Primary aldosteronism, or Conn syndrome, is the result of excess aldosterone produced by the adrenal glands. As with

---

Received November 13, 1989; accepted after revision December 20, 1989.
Delivered as the Malcolm B. Hanson Lecture at the University of Minnesota, Minneapolis, September 1988.

[1] Department of Radiology, Box 3808, Duke University Medical Center, Durham, NC 27710.

AJR **154:927-936, May 1990** 0361-803X/90/1545-0927 © American Roentgen Ray Society

Cushing syndrome, it may be caused by either adrenal hyperplasia or a primary adrenal tumor. A benign but unregulated aldosterone-secreting adenoma is the most common cause of primary aldosteronism, being responsible for almost 80% of cases. Bilateral adrenal hyperplasia accounts for 20% of cases. Rarely does a primary adrenocortical carcinoma secrete enough aldosterone to cause a recognizable clinical syndrome [6].

The rare adrenogenital syndromes result from an inborn error in the adrenal enzyme system that blocks or impairs the synthesis of cortisol or aldosterone. Each different enzyme deficiency results in a different form of congenital adrenal hyperplasia [7]. The clinical manifestations are determined by the degree of deficiency of cortisol or aldosterone and by the biological properties of the biochemical intermediates that are formed and secreted in excess.

Androgen-producing tumors are rare, may be benign or malignant, and may occur in either males or females at any age. Patients whose virilization is due to a tumor usually present at a later age than do those with congenital adrenal hyperplasia. The typical clinical manifestations include amenorrhea, hirsutism, enlargement of the clitoris, and deepening of the voice [6].

Feminizing tumors are quite rare. They are usually seen in men but have been reported in prepubertal girls and postmenopausal women. Gynecomastia is the predominant clinical manifestation [6].

The most valuable technique for examining the adrenal glands is CT. The perinephric fat present in most patients allows the adrenal gland to be displayed clearly, and tumors as small as 10 mm in diameter are routinely identified. The adrenal glands must be examined carefully by using contiguous 5-mm collimated slices. Even narrower collimation may be used to clarify equivocal findings. IV contrast material is not usually needed, but may be used to distinguish an adrenal mass from the upper pole of the kidney.

The adenomas in Conn syndrome are usually the most difficult to detect because they tend to be the smallest, averaging less than 2 cm in diameter (Fig. 1) [8–11]. Careful study of the adrenal gland is required; narrowly collimated sections may be needed. The left adrenal gland may be particularly troublesome.

Cushing syndrome, on the other hand, is relatively easy to examine with CT. The tumors in these patients are larger than those causing Conn syndrome and the adrenal glands are clearly defined by the abundant retroperitoneal fat [8]. Any tumor that is greater than 4 cm in diameter or shows central necrosis is suspicious for malignancy and may be a primary adrenocortical carcinoma rather than an adenoma [12, 13].

Bilateral adrenal hyperplasia is seen as enlargement of the entire adrenal gland, but without a focal mass (Fig. 2). The limbs of the adrenal are both thicker and longer, and they are seen over a larger series of CT sections.

Enlargement of the adrenal gland is usually more obvious in patients with Cushing syndrome than in those with Conn syndrome. However, there is significant overlap with the appearance of normal adrenal glands, and hyperplasia should not be diagnosed solely on the basis of morphology.

Patients with primary pigmented nodular adrenocortical disease may demonstrate adrenal nodularity. If the nodules are small, the adrenal glands may appear normal on CT. However, Doppman et al. [4] recently reported detecting unilateral or bilateral nodularity in six of eight patients studied.

Venography can be used to provide samples of blood from the adrenal veins for hormone analysis. Venous sampling can be quite valuable in patients with Conn syndrome as the aldosterone-secreting adenoma is often less than 1 cm and may be too small to be detected by CT [8, 9, 14]. It is rarely needed in Cushing syndrome but may be used in patients with masculinizing or feminizing tumors.

An additional venous sampling technique is occasionally used in patients with Cushing syndrome due to bilateral adrenal hyperplasia. In these patients, the source of the ACTH is usually a pituitary adenoma but may be an ectopic source, such as a lung tumor. In this situation, blood samples are obtained from the right and left petrosal sinuses, and ACTH is measured [15].

The perinephric fat provides excellent contrast for MR as well as CT [16]. Although the spatial resolution of MR is still inferior to that of CT, the additional parameters that are

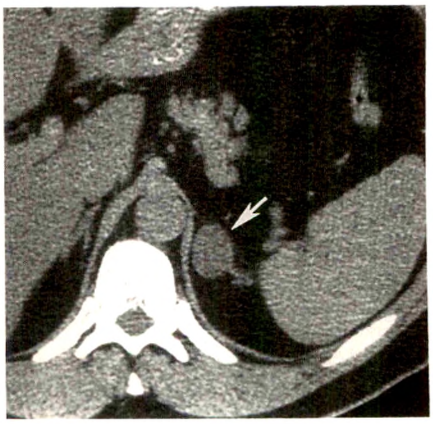
1

Fig. 1.—Aldosteronoma. Aldosterone-secreting adenoma is identified on CT scan in left adrenal gland (*arrow*) in patient with primary aldosteronism.

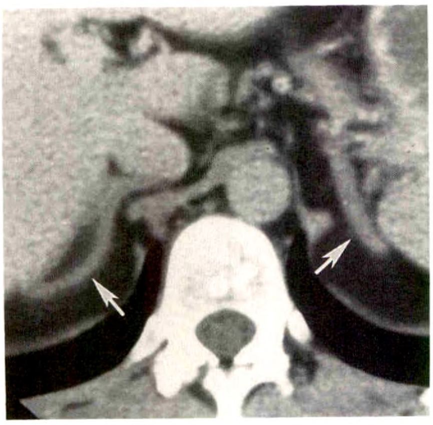
2

Fig. 2.—Adrenal hyperplasia. Bilateral adrenal hyperplasia is seen on CT scan in patient with Cushing syndrome. Adrenal glands are enlarged (*arrows*) but do not demonstrate focal mass.

available, especially to distinguish benign from malignant lesions, may prove quite useful. For most patients with hyperfunction of the adrenal cortex, however, MR does not provide additional information after a CT examination [17].

Cortical imaging agents have been developed that can localize hyperfunctioning adrenal cortical tumors, particularly in patients with Cushing syndrome. The labeling agent ^{131}I-6,beta-iodomethyl-19-norcholesterol (NP-59) is administered IV and scans are obtained after a delay of 2–5 days [18]. However, NP-59 is an investigational drug and is not commercially available. Furthermore, the success of CT in localizing these adrenal tumors has made this examination unnecessary in most centers.

Medulla

Pheochromocytomas are tumors composed of chromaffin cells and are usually located in the adrenal medulla. Extraadrenal pheochromocytoma (paragangliomas) are found most commonly along the sympathetic chain in the retroperitoneum.

Pheochromocytomas are associated with other endocrine tumors. The multiple endocrine neoplasia (MEN) syndrome, type IIa, includes medullary carcinoma of the thyroid and parathyroid hyperplasia as well as pheochromocytoma. Type IIb MEN syndrome comprises pheochromocytoma; medullary carcinoma of the thyroid; and mucocutaneous manifestations including mucosal neuromas, intestinal ganglioneuromatosis, and a marfanoid habitus. All manifestations of the syndrome may not occur at the same time. Thus, a careful history of a previous endocrine abnormality should be obtained when examining patients who may fall into these categories. These abnormalities are inherited in an autosomal-dominant fashion.

Pheochromocytoma is associated with neurofibromatosis and the von Hippel–Lindau syndrome. There is also a syndrome of familial pheochromocytomas not associated with other endocrine tumors.

Although 90% of all pheochromocytomas are located in the adrenal medulla, there is a striking difference between sporadic tumors and those associated with the MEN syndromes. The sporadic pheochromocytomas are located outside the adrenal gland in as many as 25% of cases, whereas those associated with the MEN II syndromes are virtually always intraadrenal [19]. Pheochromocytomas found in MEN II patients are usually multicentric and involve both adrenal glands in more than 80% of cases. Pheochromocytomas are usually benign, but approximately 13% demonstrate malignant behavior.

If a pheochromocytoma is suspected, the diagnosis can be made by measuring elevated levels of serum or urine catecholamines. Urinary metanephrines or vanillylmandelic acid are elevated in over 90% of patients when 24-hr urine collections are measured. Epinephrine, norepinephrine, and dopamine can be measured by liquid chromatography, which further aids in the diagnosis. Several separate determinations should be made because of the episodic hormone secretion found in these patients. Furthermore, patients taking medications such as methyldopa or Mandelamine may have falsely high catecholamine levels.

As with tumors of the adrenal cortex, CT is the primary localizing examination [20]. IV contrast injection is seldom needed because the tumors are usually easily seen (Fig. 3). As glucagon may induce a hypertensive crisis, it should not be used in patients undergoing abdominal CT to identify a suspected pheochromocytoma. Most intraadrenal pheochromocytomas are detected and a sensitivity of 95% can be expected [6]. Care must be taken when examining patients with the MEN syndrome, however, as the tumors in these patients are often smaller. Sonography may be helpful in children, where the relative lack of retroperitoneal fat makes CT evaluation difficult.

Pheochromocytomas are both identified and characterized by MR. T1-weighted sequences are used to identify the mass and the high signal intensity seen on T2-weighted images helps to characterize it as a pheochromocytoma. This intense T2-weighted signal helps to distinguish a pheochromocytoma from an adrenal adenoma [21].

The spatial resolution of MR is inferior to that of CT, so routine scanning of the adrenal glands and retroperitoneum is still best done with CT. However, MR can be quite valuable in the identification of lesions in areas that may be a problem for CT. Tumors in the wall of the urinary bladder or the paracardiac region are often problematic on CT but clearly recognized with MR. Also, postoperative patients in whom retroperitoneal tissue planes are disrupted may be difficult to examine with CT [22].

Metaiodobenzylguanidine (MIBG) is an analog of guanethidine that is taken up by adrenergic tissue. When MIBG is labeled with a radionuclide, pheochromocytomas can be localized (Fig. 3) [23]. Iodine-131 is the most commonly used isotope, but iodine-123 has been advocated as having better detection efficiency and superior dosimetry.

The overall accuracy of MIBG is similar to that of CT and MR imaging; however, scintigraphy has several advantages. With a single injection of radionuclide the entire body can be scanned. This is particularly helpful for ectopic tumors or in the detection of metastatic deposits. MIBG also can detect medullary hyperplasia, which is seen in patients with MEN syndromes and may be an early manifestation of a developing pheochromocytoma.

However, MIBG is not widely used to detect or localize pheochromocytomas. Although ^{131}I-MIBG has gained Food and Drug Administration approval, it is not universally available. Furthermore, the spatial resolution is poor and studies require 1–3 days to complete.

Diseases Associated with Decreased Function

Primary adrenal insufficiency, or Addison disease, occurs only after at least 90% of the adrenal cortex has been destroyed. Idiopathic adrenal atrophy is the most common cause in the United States and it is most likely an autoimmune disorder. The other common cause of Addison disease is destruction of the adrenal glands by a granulomatous disease, usually tuberculosis. However, other causes such as infarction, amyloidosis, hemorrhage, or destruction by histoplasmosis, blastomycosis, disseminated fungal infection, lymphoma, and metastatic tumor (Fig. 4) have been reported.

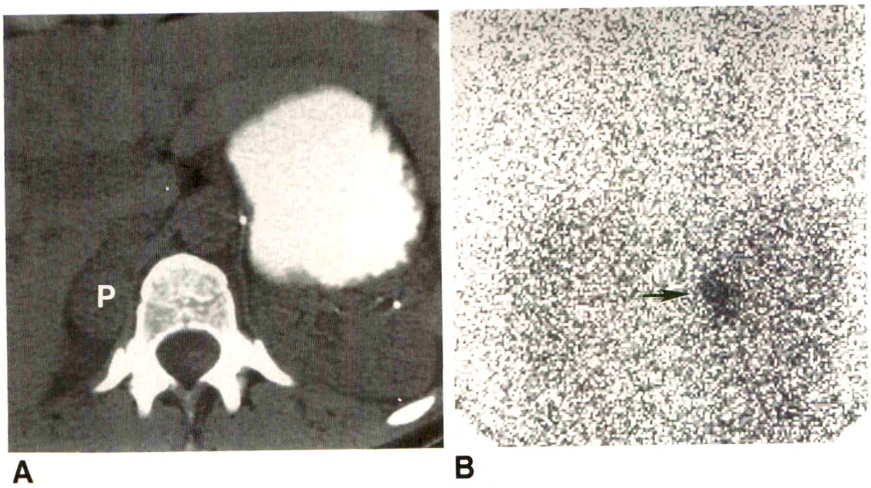

Fig. 3.—Pheochromocytoma.

A, Unenhanced CT scan shows right adrenal pheochromocytoma (P).

B, On scintigram, area of increased activity (*arrow*) after injection of metaiodobenzylguanidine (MIBG) correlates with right adrenal pheochromocytoma.

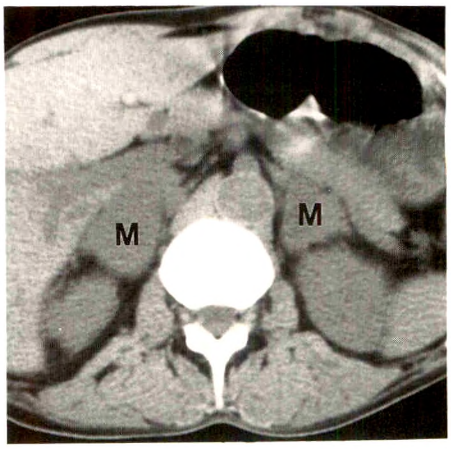

Fig. 4.—Adrenal insufficiency. CT scan shows bilateral adrenal metastases (M) from primary lung carcinoma that have destroyed enough adrenal tissue to cause adrenal insufficiency.

The radiologic manifestations of adrenal insufficiency depend on the cause of adrenal dysfunction. The plain abdominal radiograph may reveal adrenal calcification commonly seen in tuberculosis or histoplasmosis.

The most useful examination is CT, which defines the size and shape of the adrenal glands. In idiopathic Addison disease, cortical atrophy is so severe that the adrenal glands may be difficult to detect [24].

Granulomatous involvement by either tuberculosis or histoplasmosis is usually bilateral. The glands are enlarged but often maintain a normal configuration. Calcification is common [25].

If adrenal hemorrhage is acute, it may be recognized by the increased density of the recent hemorrhage [26, 27]. As the density of the hematoma decreases, it becomes indistinguishable from other adrenal masses. Although adrenal metastases are common, adrenal insufficiency rarely occurs. This is because so much of the adrenal cortex must be destroyed before insufficiency ensues [28].

Diseases Associated with Normal Function

Adenoma

Benign, nonhyperfunctioning adrenal adenomas are commonly encountered on abdominal CT examinations. Commons and Callaway [29] found adenomas greater than 3 mm in 2.86% of 7437 autopsies. The prevalence of adenomas was higher among older patients and those with diabetes or hypertension.

Adenomas consist of cords of clear cells separated by fibrovascular trabeculae. It is often difficult to distinguish a benign adenoma from an adrenal cortical carcinoma. Although carcinomas are more likely to have hemorrhage, necrosis, pleomorphism, and giant cells, these features also may be seen in benign adenomas.

Nonhyperfunctioning adenomas are almost always detected as an incidental finding. Occasionally, they are large enough to cause pain or compress adjacent structures.

Most adenomas are detected during CT examination of the upper abdomen. Typically, the nonhyperfunctioning adenoma is a well-defined, rounded, homogeneous mass (Fig. 5) [31]. Calcification may occur, but is uncommon. Central necrosis or hemorrhage is rare. The density ranges from approximately 0 to 30 H; a higher lipid content is presumably responsible for the lower-density lesions [32].

MR can detect adrenal masses larger than 1.5 cm almost as well as CT can [33]. Furthermore, MR may be used to characterize adrenal masses, but these data are still incomplete. Nonhyperfunctioning adenomas may be less intense than adenomas secreting aldosterone or cortisol, but this has been difficult to demonstrate [34]. However, this is seldom a clinical problem because adrenal hyperfunction can be assessed by measuring serum hormone levels. More importantly, because benign adenomas have the signal intensity of normal adrenal tissue, MR may be useful in distinguishing an adenoma from metastatic tumor (Fig. 5).

Carcinoma

Primary adrenal cortical carcinoma is an uncommon malignancy that occurs with a frequency of approximately one case per million people. Men and women are affected equally, but functional tumors are more common among females. Although the median age at presentation is the fifth decade, patients from 1 to 80 years old have been reported.

Adrenal carcinomas occur more commonly in the left gland than the right, and up to 10% may be bilateral. They are usually quite large at presentation, although a tumor as small as 1 cm has been reported. The most common presentation of patients with an adrenal carcinoma is abdominal pain or a palpable mass. Approximately half of these tumors are functional and may be detected by the manifestations of excess hormone production [35, 36]; Cushing syndrome is most frequent, followed by virilization and feminization. Hyperaldosteronism is rarely due to carcinoma.

The typical CT appearance of adrenal carcinoma is a large mass with central areas of low attenuation representing tumor necrosis (Fig. 6) [12, 13]. Calcification is seen in approximately 30% of cases. Evidence of hepatic or regional lymph-node metastases also may be seen on CT. Extension of tumor into the left renal vein or inferior vena cava may also be detected with CT. If a bolus technique is used for contrast injection, CT may define the extent of tumor thrombus. If this delineation is not clear, additional studies such as venacavography [37] or MR may be needed.

The most difficult area for CT staging of adrenal carcinoma has been the detection of direct hepatic extension. If a fat plane exists between the tumor and the liver, there is no hepatic involvement. However, if there is no fat plane, it is impossible to predict the presence or absence of liver invasion.

MR imaging is often used to evaluate a suspected adrena carcinoma. The high signal intensity on T2-weighted images further supports the malignant diagnosis [38]. Venous extension also can be detected by using limited-flip-angle techniques (Fig. 7).

Myelolipoma

A myelolipoma is a benign tumor composed of mature adipose cells and hematopoietic tissue. The gross appearance resembles fatty tissue but may contain patchy red areas of blood-forming cells. It is an uncommon lesion with only approximately 250 cases reported in the literature [39].

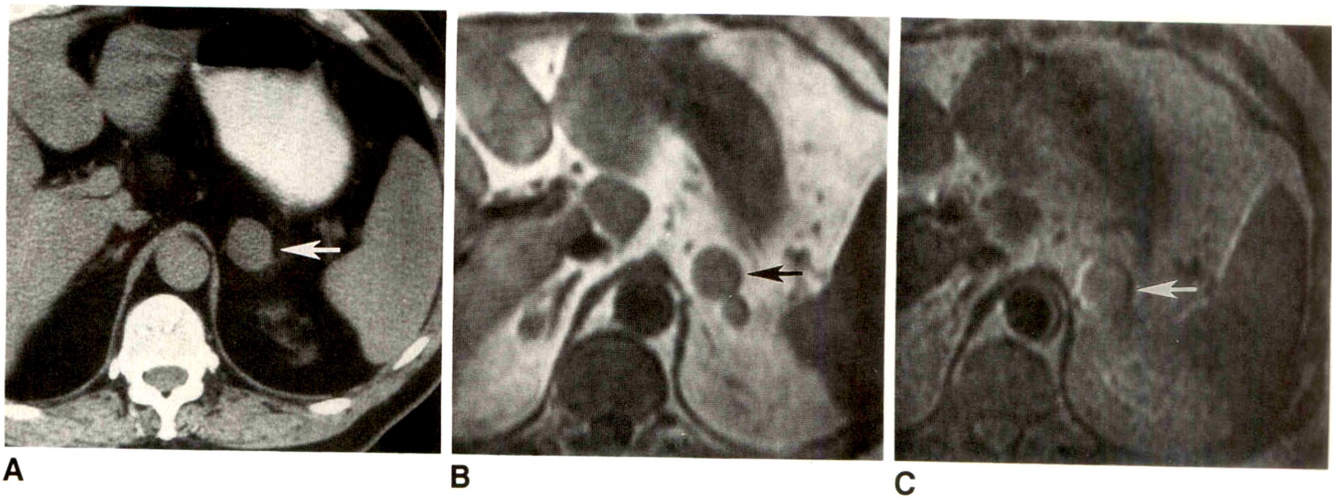

Fig. 5.—Nonhyperfunctioning adenoma.
A, Unenhanced abdominal CT scan reveals well-defined ovoid left adrenal mass (*arrow*).
B, MR image, SE 500/20 (TR/TE), shows features of benign adrenal adenoma (*arrow*) (T2 relaxation time = 54 msec).
C, MR image, 2500/80. Benign adenoma (*arrow*) has more signal than liver.
(*B* and *C* reprinted with permission from Baker et al. [30].)

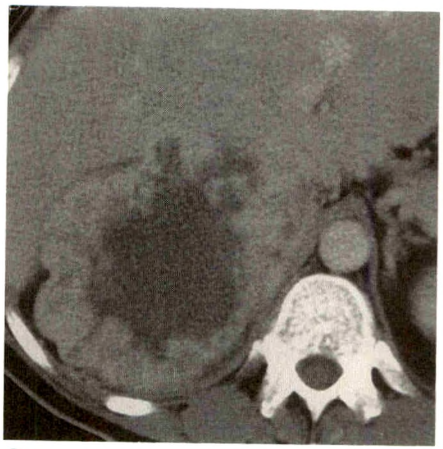

6

Fig. 6.—Adrenocortical carcinoma. Large, irregular mass shown on CT scan demonstrates central necrosis.

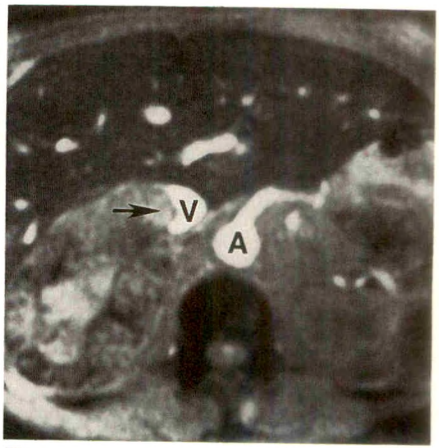

7

Fig. 7.—Adrenocortical carcinoma. Limited-flip-angle technique (gradient-recalled acquisition in the steady state) clearly defines flowing blood in aorta (A) and inferior vena cava (V) on this MR image. Venous extension of adrenocortical carcinoma into inferior cava is seen (*arrow*).

The tumors are functionally inactive and are usually detected as an incidental finding. Occasionally, large tumors may cause pain or present with displacement of adjacent organs. Retroperitoneal hemorrhage has been reported.

Sonography reveals a highly echogenic mass. If the tumor is 4 cm or larger, a propagation speed artifact may be present [40]. This apparent posterior displacement of an acoustic interface such as the diaphragm is due to the relatively slow speed of sound through fat, as compared with the speed assumed in signal processing [41]. This appearance is suggestive of a myelolipoma; however, it cannot be clearly distinguished from a retroperitoneal lipoma or liposarcoma. If the tumor is small or the patient has abundant retroperitoneal fat, the myelolipoma may be difficult to distinguish from perirenal fat.

The most definitive radiologic examination is CT [40, 41]. A fatty adrenal mass is virtually diagnostic of a myelolipoma. Unenhanced scans are usually adequate to make the diagnosis (Fig. 8). Contrast administration may mask the fat density of a myelolipoma. Although not yet reported, an adrenal lipoma or liposarcoma could mimic this appearance. A case of adenocarcinoma metastatic to the adrenal gland simulating myelolipoma has been reported [42]. MR imaging also can image myelolipomas but does not add information to what is gained with CT.

The demonstration of macroscopic fat in an adrenal mass on CT is usually sufficient to diagnose a myelolipoma. Occasionally, cases may not have sufficient fatty components to demonstrate fat density. Narrow collimated scans may help by reducing partial-volume artifacts. The diagnosis also can be made by percutaneous biopsy [43].

Hemorrhage

Adrenal hemorrhage may be spontaneous, traumatic, or related to anticoagulation. Spontaneous adrenal hemorrhage often occurs in patients with septicemia, hypertension, renal vein thrombosis, or adrenal disease such as a tumor. It more commonly involves the right rather than the left adrenal gland.

Adrenal hemorrhage is more common in neonates than in older children or adults. It may be due to the trauma of delivery, asphyxia, septicemia, or abnormal clotting factors [44]. It is bilateral in only about 10% of cases. If the hemorrhage is large, a palpable mass, anemia, or prolonged jaundice may occur. Adrenal insufficiency is rare in the neonate. Hemorrhage can usually be distinguished from a tumor such as neuroblastoma and surgery avoided. Most adrenal hematomas will be resorbed, but some may liquify and persist as an adrenal pseudocyst.

When adrenal hemorrhage occurs in the older child or adult, it is often due to trauma or associated with systemic illness or anticoagulation. When related to anticoagulation therapy, it usually occurs during the first 3 weeks of therapy [45]. However, it is not due to excessive anticoagulation, as associated hemorrhage does not occur in other areas.

Adrenal hemorrhage may occur in up to 25% of severely traumatized patients; approximately 20% of cases are bilateral. The right adrenal gland is involved much more commonly than the left [46]. This may be due to an acute rise in venous pressure, which is more directly transmitted to the right adrenal gland because the right adrenal vein enters the inferior vena cava directly. The hematoma is usually found in the adrenal medulla with stretching of the surrounding cortex.

The most reliable method of identifying adrenal hemorrhage is CT. Initially the hematoma has a high density, 50–90 H (Fig. 9) [47]. Follow-up studies usually show resorption of the hematoma and a gradual decrease in density to near that of water [48].

Sonography is often used to detect adrenal hemorrhage in children. With sonography, adrenal hemorrhage is seen as an anechoic mass that may displace or compress the upper pole of the kidney. Occasionally sufficient echogenicity may be

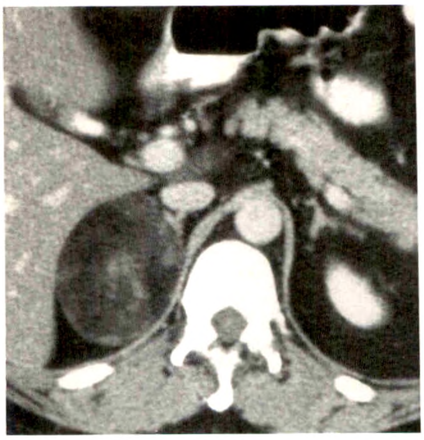

Fig. 8.—Myelolipoma. Macroscopic fat is clearly detected on CT scan in this adrenal myelolipoma.

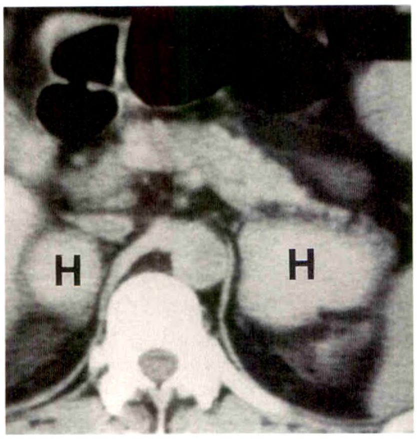

Fig. 9.—Adrenal hemorrhage. CT scan shows bilateral high-density adrenal masses (H) in patient with acute adrenal hemorrhage. (Reprinted with permission from Dunnick [71].)

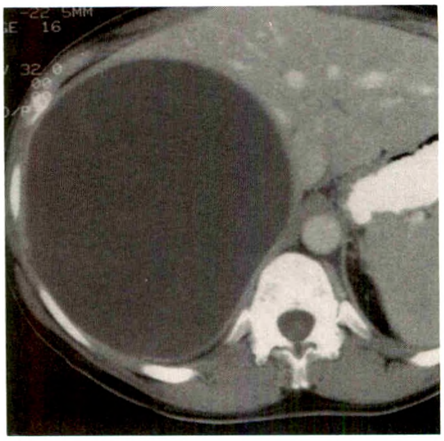

Fig. 10.—Adrenal cyst. CT scan shows a huge cystic mass in right adrenal gland. Thickened wall suggests pseudocyst.

seen to suggest a solid mass. Sequential examinations usually show a progressive decrease in size. MR imaging of adrenal hemorrhage has also been reported [49]. The MR appearance reflects the evolution from acute to chronic stages with hemoglobin breakdown.

Cysts

Adrenal cysts are uncommon lesions that may occur at any age. They involve the right and left glands equally, but have a 3:1 female predilection [50].

There are several recognized causes of adrenal cysts. Endothelial cysts are the most common, accounting for approximately 45% of all adrenal cysts [51]. They have an endothelial lining and may be lymphatic or angiomatous in origin. Lymphangiomatous cysts are more common and probably arise from blockage of a lymph duct.

Epithelial cysts are quite uncommon, as they make up only 9% of adrenal cysts. They have a cylindric epithelium and include cystic adenomas.

Parasitic cysts are the least common variety, making up only 7% of the total. They are usually echinococcal in origin and are associated with widespread disease.

Pseudocysts are the second most common variety; they make up 39% of adrenal cysts. They are probably caused by adrenal hemorrhage into either a normal or abnormal gland. The lining is not covered by epithelium. Pseudocysts are most commonly detected radiologically, because they tend to be larger than endothelial cysts [52].

Sonography shows a cystic suprarenal mass. Unlike renal cysts, adrenal cysts often exhibit a thick wall (Fig. 10). Pseudocysts also may have internal septa. If a soft-tissue masslike component is present, surgery may be required to exclude a neoplasm.

Similar findings are detected with CT. The density of the fluid can be measured, and calcification is easier to detect with CT than with sonography. However, it may still be difficult to exclude malignancy. Cyst aspiration can be helpful if the fluid is clear and the cytology benign.

Metastases

The adrenal glands are a common site of metastatic disease. In a series of 1000 consecutive autopsies of cadavers with an epithelial malignancy, Abrams et al. [53] found 27% to have adrenal metastases.

The radiologic appearance of adrenal metastases is not specific. They may be large or small, unilateral or bilateral. A metastasis is a solid mass, and when less than 3 cm in diameter, is usually homogeneous. Larger lesions may show central necrosis or areas of hemorrhage. Thus, an adrenal metastasis cannot be distinguished clearly from benign lesions such as an adenoma, hematoma, pseudocyst, or inflammatory mass on the basis of its morphology.

Nevertheless, several investigators have tried to identify criteria that would allow the diagnosis of a benign or malignant cause on the basis of CT criteria. Features that suggest a malignant lesion include a large size (>3 cm), poorly defined margins, invasion of adjacent structures, inhomogeneous attenuation, and a thick irregular enhancing rim (Fig. 11) [54]. Small ovoid lesions with a thin rim and homogeneous density are more likely to be benign.

In many patients, there is evidence of widespread metastatic disease involving the lungs, liver, and retroperitoneal lymph nodes as well as the adrenal glands. In these patients it is relatively unimportant whether the adrenal mass represents metastatic tumor. However, in some patients an adrenal mass may be the only evidence of metastatic disease. This can be a critical distinction because it may change the therapy from an attempt at cure to palliation.

Several radiologic procedures can be used to distinguish an adrenal metastasis from a benign lesion such as an adenoma. The nature of an adrenal mass can be predicted with MR. Metastases typically have a higher signal intensity on T2-weighted sequences (Fig. 12). Several methods have been used to show this difference. As the normal adrenal gland is small, it is difficult to measure the signal from normal adrenal cortex. Thus, a ratio of the intensity of the adrenal tumor and adjacent liver [55, 56], muscle, or fat [57] has been used. Data from several studies suggest there are cutoff points below which all lesions are adenomas and above which all lesions are metastases. However, this leaves an overlap group that contains 21–31% of cases. Others have used calculated T1 values to distinguish benign from malignant masses, but similar overlap has been observed [58].

Most of the early studies that used MR to distinguish a benign adenoma from an adrenal metastasis used low-field-strength (0.35–0.5 T) units. More recently, MR imaging at 1.5 T has been applied to this problem. We [30] and others [59] have found that the T2 relaxation time of the adrenal mass is the most useful parameter; however, atypical cases still occur (Fig. 13).

MR spectroscopy can provide additional information that may help to distinguish an adrenal adenoma from carcinoma. Leroy-Willig et al. [60] found that the lipid content as measured by proton spectroscopy was significantly lower in carcinomas than adenomas.

Adrenal cortical scintigraphy also has been applied to this problem. Because benign adenomas take up a cortical labeling agent such as NP-59, they can be distinguished from nonadenomatous masses. Absence of uptake is not specific, however, as neither a cyst, a hematoma, nor an inflammatory mass will take up the radionuclide. Thus, a benign mass cannot be distinguished from a metastasis with this examination.

Francis et al. [61] applied NP-59 scintigraphy to 28 oncologic patients and a unilateral adrenal mass. Each of 14 patients with increased radionuclide uptake had an adenoma. None of the 11 patients with decreased uptake on the side of the mass had an adenoma; nine had metastases and two had cysts. Uptake was indeterminant in three patients. Despite these encouraging results, however, adrenal scintigraphy is not widely used to distinguish benign from malignant adrenal masses.

Percutaneous aspiration biopsy is the most definitive method of confirming metastatic disease [62–65]. With experienced cytopathologists, the positive predictive value approaches 100%. A negative aspiration is not as diagnostic because sampling error or an inadequate specimen may preclude a confident diagnosis. The overall accuracy reported for percutaneous adrenal biopsy ranges from 80% to 100%. The results will vary with the patient population and types of lesions aspirated. Positive results indicate malignancy. Negative aspirations can be repeated to increase the confidence that the lesion is benign.

Adrenal biopsy is an invasive procedure and complications may occur. The most common complication is pneumothorax [62]. Pneumothoraces are usually small and resolve spontaneously. Large or symptomatic pneumothoraces should be treated with a small chest tube that can be placed under fluoroscopic guidance by the radiologist [66, 67]. Tumor seeding of the needle tract and bacteremia are rare. Pancreatitis may occur and can be a serious complication. Thus, the pancreas should be avoided if possible. Many patients will have a small amount of bleeding but this is seldom symptomatic.

The most worrisome complication of percutaneous needle biopsy of an adrenal mass is precipitation of a hypertensive crisis by a pheochromocytoma [68]. This may be fatal despite regaining control of the blood pressure. Screening catecholamines may be useful in hypertensive patients, but may not be elevated in an intermittently functioning pheochromocytoma.

Lymphoma

Involvement of the adrenal gland by malignant lymphoma is more common with non-Hodgkin lymphoma than with Hodgkin disease. Most patients have a diffuse rather than nodular form of lymphoma. In a review of 173 patients with non-Hodgkin lymphoma, Paling and Williamson [69] found evidence on CT of adrenal involvement in seven patients (4%) during some portion of the course of their disease.

The adrenal glands are seldom an isolated site of disease, although other involvement may be distant. In most patients, however, retroperitoneal lymphoma also is present. Bilateral adrenal involvement is seen in about half the cases. Even with extensive disease, adrenal insufficiency is rare. The techniques with which adrenal lymphoma can be identified are sonography, CT, and MR imaging. On sonography, lymphoma appears as a well-defined, relatively echopenic homogeneous tissue mass. If extensive retroperitoneal disease is present, it may be difficult to identify the adrenal glands.

CT provides the best morphologic delineation. The adrenal glands are enlarged with either a rounded mass or more symmetric enlargement, preserving the basic glandular configuration (Fig. 14). The tissue is usually homogeneous and shows contrast enhancement. There is, however, no pathognomonic pattern to indicate lymphomatous involvement.

Pseudotumors

Retroperitoneal fat provides the contrast needed to demonstrate the adrenal glands. When there is a paucity of fat in the perirenal space the adrenal glands are difficult to evaluate. Furthermore, large masses may compress the normal adrenal gland so that it is impossible to determine the organ of origin.

Abnormalities in the upper abdomen may simulate an adrenal mass. In addition to creating diagnostic confusion, percutaneous biopsy may be attempted. An appreciation of some of the causes of an adrenal pseudotumor may help avoid these pitfalls.

Lesions that may simulate an adrenal mass on either side include an exophytic renal mass. An adrenal mass on the right side may be mimicked by a hepatic mass, interposition of the colon into the hepatorenal recess, or a dilated inferior vena cava.

Adrenal pseudotumors on the left side are more common [70]. They include splenic lobulations, an accessory spleen, tortuous splenic vessels, and a splenic artery aneurysm. The tail of the pancreas may extend to the adrenal area and mimic a left adrenal lesion. Although the stomach should be clearly distinguished by oral contrast material, a gastric diverticulum may present a diagnostic problem.

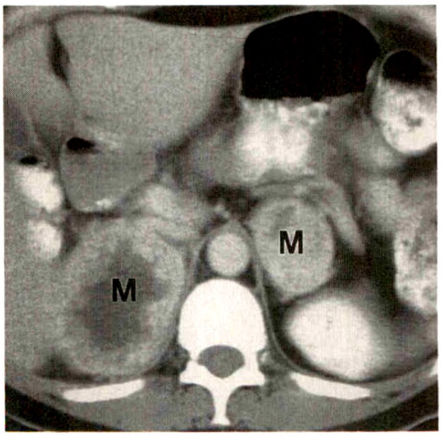

11

Fig. 11.—Adrenal metastases. CT scan shows bilateral adrenal masses (M) with inhomogeneous enhancement and thick irregular walls in patient with renal adenocarcinoma.

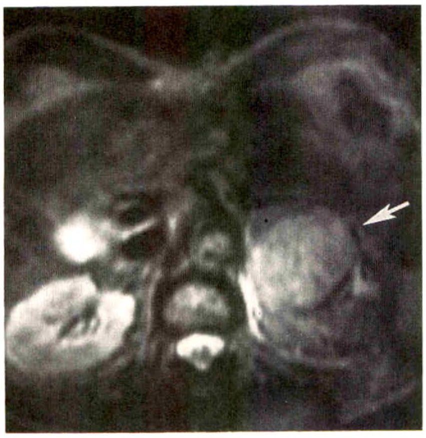

12

Fig. 12.—Typical adrenal metastasis from oat cell carcinoma of the lung. On this 2500/80 (TR/TE) MR image, mass (*arrow*) is hyperintense with a T2 relaxation time of 75 msec. (Reprinted with permission from Baker et al. [30].)

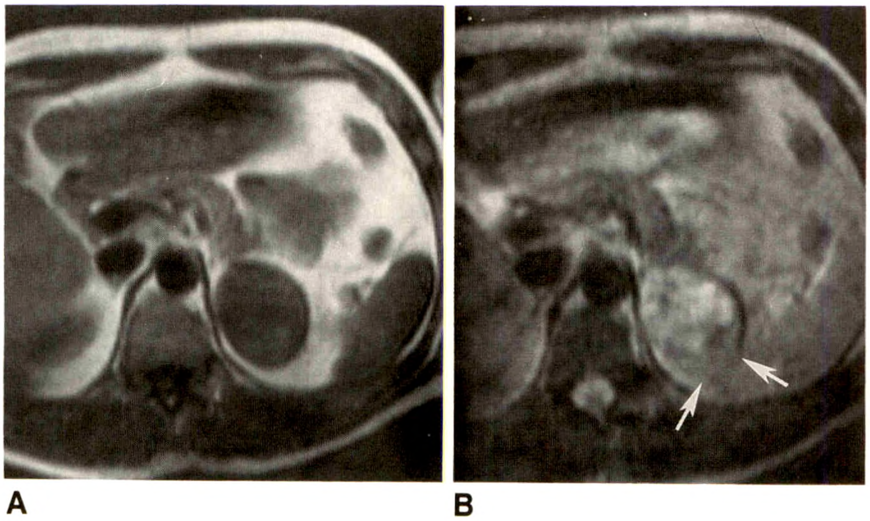

Fig. 13.—Atypical nonhyperfunctioning adenoma.
***A* and *B*, 500/20 (TR/TE) (*A*) and 2500/80 (*B*) spin-echo MR images. Atypical features are seen on long TR/TE sequence: hyperintensity in major portions of mass (T2 relaxation time = 94 msec). There is a rim of more "normal" adrenal signal peripherally in *B* (*arrows*). Hyperintense area was hemorrhagic on pathologic examination. (Reprinted with permission from Baker et al. [30].)**

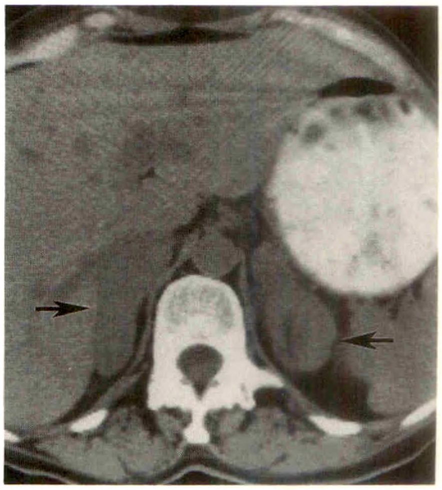

Fig. 14.—Lymphoma. CT shows bilateral adrenal masses with preservation of glandular configuration (*arrows*).

Careful attention to the adrenal glands and use of oral contrast material should distinguish most confusing structures. A bolus IV injection of contrast material should further delineate vascular structures. Repeated sections with narrow collimation also may help to elucidate the true nature of these lesions. If the diagnosis is still in doubt, however, an additional study such as sonography or MR imaging may be needed for a confident diagnosis.

REFERENCES

1. Doppman JL, Nieman L, Miller DL, et al. Ectopic adrenocorticotropic hormone syndrome: localization studies in 28 patients. *Radiology* **1989**; 172:115–124
2. Falke THM. Clinical and histopathological basis of adrenal imaging. In: Drukkerij HJ, Pasmans BV, eds. *Localization and identification of adrenocortical and sympathomedullary disorders with CT and MRI*. S-Gravenhage Den Haag, **1989**:15–66
3. Doppman JL, Miller DL, Dwyer AJ, et al. Macronodular adrenal hyperplasia in Cushing disease. *Radiology* **1988**;166:347–352
4. Doppman JL, Travis WD, Nieman L, et al. Cushing syndrome due to primary pigmented nodular adrenocortical disease: findings at CT and MR imaging. *Radiology* **1989**;172:415–420
5. Leder LD, Richter HS. Pathology of renal and adrenal neoplasms. In: Lohr E, Leder LD, eds. *Renal and adrenal tumors*, 2nd ed. New York: Springer-Verlag, **1987**:1–68
6. Dunnick NR. The adrenal gland. In: Taveras JM, Ferrucci JT, eds. *Radiology: diagnosis, imaging, intervention.* Philadelphia: Lippincott, **1988**
7. Drucker S, New MI. Disorders of adrenal steroidogenesis. *Pediatr Adolesc Endocrinol* **1987**;34:1055–1065
8. Dunnick NR, Doppman JL, Gill JR, et al. Localization of functional adrenal tumors by computed tomography and venous sampling. *Radiology* **1982**;142:429–433
9. Geisinger MA, Zelch MG, Bravo EL, et al. Primary hyperaldosteronism: comparison of CT, adrenal venography and venous sampling. *AJR* **1983**; 141:299–302
10. Kenney PJ, Streeten DP, Anderson GH. Difficulties in the prospective diagnosis of functional adrenal diseases by CT. *Urol Radiol* **1986**;8: 184–189
11. Moulton JS, Moulton JS. CT of the adrenal glands. *Semin Roentgenol* **1988**;23:288–303
12. Dunnick NR, Heaston D, Halvorsen R, et al. CT appearance of adrenal cortical carcinoma. *J Comput Assist Tomogr* **1982**;6:978–982
13. Fishman EK, Deutch BM, Hartman DS, Goldman SM, Zerhouni EA, Siegelman SS. Primary adrenocortical carcinoma: CT evaluation with clinical correlation. *AJR* **1987**;148:531–535
14. Dunnick NR, Doppman JL, Mills SR, Gill JR Jr. Preoperative diagnosis and localization of aldolsteronomas by measurement of corticosteroids in adrenal venous blood. *Radiology* **1979**;133:331–333
15. Doppman JL, Oldfield E, Krudy AG, et al. Petrosal sinus sampling for Cushing syndrome: anatomical and technical considerations. *Radiology* **1984**;150:99–103
16. Dunnick NR. CT and MRI of adrenal lesions. *Urol Radiol* **1988**;10:12–16
17. Ikeda DM, Francis IR, Glazer GM, et al. The detection of adrenal tumors and hyperplasia in patients with primary aldosteronism: comparison of scintigraphy, CT, and MR imaging. *AJR* **1989**;153:301–306
18. Gross MD, Thompson NW, Beierwaltes WH. Scintigraphic approach to the localization of adrenal lesions causing hypertension. *Urol Radiol* **1982**;3: 241–244
19. Cho KJ, Freier DT, McCormick TL, et al. Adrenal medullary disease in multiple endocrine neoplasia type II. *AJR* **1980**;134:23–29
20. Welch TJ, Sheedy PF II, van Heerden JA, et al. Pheochromocytoma: value of computed tomography. *Radiology* **1983**;148:501–503
21. Reinig JW, Doppman JL, Dwyer AJ, et al. Adrenal masses differentiated by MR. *Radiology* **1986**;158:81–84
22. Fink IJ, Reinig JW, Dwyer AJ, et al. MR imaging of pheochromocytomas. *J Comput Assist Tomogr* **1985**;9:454–458
23. Swensen SJ, Brown ML, Sheps SG, et al. Use of ^{131}I-MIBG scintigraphy in the evaluation of suspected pheochromocytoma. *Mayo Clin Proc* **1985**; 60:299–304
24. Eason RJ, Croxson MS, Perry MC, Somerfield SD. Addison disease, adrenal autoantibodies and computerized adrenal tomography. *NZ Med J* **1982**;95:569–573
25. Wilson DA, Muchmore HG, Tisdal RG, et al. Histoplasmosis of the adrenal glands studies by CT. *Radiology* **1984**;150:779–783
26. Ling D, Korobkin M, Silverman PM, Dunnick NR. CT demonstration of bilateral adrenal hemorrhage. *AJR* **1983**;141:307–308
27. Doppman JL, Gill JR, Nienhius AW, et al. CT findings in Addison disease. *J Comput Assist Tomogr* **1982**;6:757–761
28. Seidenwurm DJ, Elmer EB, Kaplan LM, et al. Metastases to the adrenal

glands and the development of Addison disease. *Cancer* **1984**;54: 552–557

29. Commons RR, Callaway CP. Adenomas of the adrenal cortex. *Arch Intern Med* **1948**;81:37–41
30. Baker ME, Blinder R, Spritzer C, Leight GS, Herfkens RJ, Dunnick NR. MR evaluation of adrenal masses at 1.5 T. *AJR* **1989**;153:307–312
31. Mitnick JS, Bosniak MA, Megibow AJ, Naidich DP. Nonfunctioning adrenal adenomas discovered incidentally on computed tomography. *Radiology* **1983**;148:495–499
32. Schaner EG, Dunnick NR, Doppman JL, et al. Adrenal cortical tumors with low attenuation coefficients: a pitfall in computed tomography diagnosis. *J Comput Assist Tomogr* **1978**;2:11–15
33. Schultz CL, Haaga JR, Fletcher BD, et al. Magnetic resonance imaging of the adrenal glands: a comparison with computed tomography. *AJR* **1984**;143:1235–1240
34. Remer EM, Weinfield RM, Glazer GM, et al. Hyperfunctioning and nonhyperfunctioning benign adrenal cortical lesions: characterization and comparison with MR imaging. *Radiology* **1989**;171:681–685
35. Bodie B, Novick AC, Pontes JE, et al. The Cleveland Clinic experience with adrenal cortical carcinoma. *J Urol* **1989**;141:257–260
36. Hutter AM, Kayhoe DE. Adrenal cortical carcinoma. *Am J Med* **1966**; 41:572–580
37. Dunnick NR, Doppman JL, Geelhoed GW. Intravenous extension of endocrine tumors. *AJR* **1980**;135:471–476
38. Smith SM, Patel SK, Turner DA, Matalon TAS. Magnetic resonance imaging of adrenal cortical carcinoma. *Urol Radiol* **1989**;11:1–6
39. Dieckmann KP, Hamm B, Pickartz H, et al. Adrenal myelolipoma: clinical, radiologic and histologic features. *Urology* **1987**;29:1–8
40. Musante F, Derchi LE, Zappasodi F, et al. Myelolipoma of the adrenal gland: sonographic and CT features. *AJR* **1988**;151:961–964
41. Vick CW, Zeman RK, Mannes E, et al. Adrenal myelolipoma: CT and ultrasound findings. *Urol Radiol* **1984**;6:7–13
42. Greene KM, Brantly PN, Thompson WR. Adenocarcinoma metastatic to the adrenal gland simulating myelolipoma: CT evaluation. *J Comput Assist Tomogr* **1985**;9:820–821
43. Gould JD, Mitty HA, Pertsemlidis D, Szporn AH. Adrenal myelolipoma: diagnosis by fine-needle aspiration. *AJR* **1987**;148:921–922
44. Khuri FJ, Alton DJ, Hardy BE, et al. Adrenal hemorrhage in neonates: report of 5 cases and review of the literature. *J Urol* **1980**;124:684–687
45. Itoh K, Yamashita K, Satoh Y, Sawada H. MR imaging of bilateral adrenal hemorrhage. *J Comput Assist Tomogr* **1988**;12:1054–1056
46. Murphy BJ, Casillas J, Yrizarry JM. Traumatic adrenal hemorrhage radiologic findings. *Radiology* **1988**;169:701–703
47. Dunnick NR. Metabolic abnormalities of the adrenal cortex. In: Pollack H, ed. *Clinical urography*. Philadelphia: Saunders, **1990**:2313–2337
48. Ling D, Korobkin M, Silverman PM, Dunnick NR. CT demonstration of bilateral adrenal hemorrhage. *AJR* **1983**;141:307–308
49. Falke THM, te Strake L, Sandler MP, et al. Magnetic resonance imaging of the adrenal glands. *RadioGraphics* **1987**;7:343–370
50. Cheema P, Cartegena R, Staubitz W. Adrenal cysts: diagnosis and treatment. *J Urol* **1981**;126:396–399
51. Ghandur-Mnaymneh L, Slim M, Muakassa K. Adrenal cysts: pathogenesis and histological identification with a report of 6 cases. *J Urol* **1979**;122: 87–91
52. Johnson CD, Baker ME, Dunnick NR. CT demonstration of an adrenal pseudocyst. *J Comput Assist Tomogr* **1985**;9:817–819
53. Abrams HL, Spiro R, Goldstein N. Metastases in carcinoma: analysis of 1000 autopsied cases. *Cancer* **1950**;3:74–85
54. Berland LL, Koslin DB, Kenney PJ, et al. Differentiation between small benign and malignant adrenal masses with dynamic incremented CT. *AJR* **1988**;151:95–101
55. Reinig JW, Doppman JL, Dwyer AJ, Frank J. MRI of indeterminate adrenal masses. *AJR* **1986**;147:493–496
56. Glazer GM, Woolsey EJ, Borrello J, et al. Adrenal tissue characterization using MR imaging. *Radiology* **1986**;158:73–79
57. Chang A, Glazer HS, Lee JKT, et al. Adrenal gland: MR imaging. *Radiology* **1987**;163:123–128
58. Chezmar JL, Robbins SM, Nelson RC, et al. Adrenal masses: characterization with T1-weighted MR imaging. *Radiology* **1988**;166:357–359
59. Kier R, McCarthy S. MR characterization of adrenal masses: field strength and pulse sequence considerations. *Radiology* **1989**;171:671–674
60. Leroy-Willig A, Bittoun J, Luton JP, et al. In vivo MR spectroscopic imaging of the adrenal glands: distinction between adenomas and carcinomas larger than 15 mm based on lipid content. *AJR* **1989**;153:771–773
61. Francis IR, Smid A, Gross MD, et al. Adrenal masses in oncologic patients: functional and morphologic evaluation. *Radiology* **1988**;166:353–356
62. Bernardino ME, Walther MM, Phillips VM, et al. CT-guided adrenal biopsy: accuracy, safety, and indications. *AJR* **1985**;144:67–69
63. Koenker RM, Mueller PR, vanSonnenberg E. Interventional radiology of the adrenal glands. *Semin Roentgenol* **1988**;22:314–322
64. Oliver TW Jr, Bernardino ME, Miller JI, et al. Isolated adrenal masses in nonsmall-cell bronchogenic carcinoma. *Radiology* **1984**;153:217–218
65. Pagani JJ. Nonsmall cell lung carcinoma adrenal metastases: computed tomography and percutaneous needle biopsy in their diagnosis. *Cancer* **1984**;53:1058–1060
66. Casola G, vanSonnenberg E, Keightley A, et al. Pneumothorax: radiologic treatment with small catheters. *Radiology* **1988**;166:89–91
67. Perlmutt LM, Johnston WW, Dunnick NR. Percutaneous transthoracic needle aspiration: a review. *AJR* **1989**;152:451–455
68. Casola G, Nicolet V, vanSonnenberg E, et al. Unsuspected pheochromocytoma: risk of blood-pressure alterations during percutaneous adrenal biopsy. *Radiology* **1986**;156:733–735
69. Paling MR, Williamson BRJ. Adrenal involvement in non-Hodgkin lymphoma. *AJR* **1983**;141:303–305
70. Berliner L, Bosniak MA, Megibow A. Adrenal pseudotumors on computed tomography. *J Comput Assist Tomogr* **1982**;6:281–285
71. Dunnick NR. Metabolic abnormalities of the adrenal cortex. In: Putnam CA, Ravin CE, eds. *Textbook of diagnostic imaging*. Philadelphia: Saunders, **1988**

Review Article

MR Angiography

Robert R. Edelman,[1] Heinrich P. Mattle,[1,2] Dennis J. Atkinson,[1,3] and Henri M. Hoogewoud[1,4]

The capability for studying blood flow noninvasively with MR was recognized long before the implementation of the first MR imaging systems [1–3]. MR imaging quickly proved superior to CT for assessing blood vessels. However, early studies, which relied on the conventional spin-echo (SE) pulse sequence, had significant limitations. Flowing blood may produce complex signal patterns, depending on the flow velocity, direction, and profile, and these appearances may not be evaluated unambiguously on SE images [4]. The introduction of newer techniques such as two-dimensional (2-D) and three-dimensional (3-D) gradient-echo (GRE) pulse sequences, flow compensation, and RF presaturation has vastly expanded MR's capabilities for showing vessel patency and direction of flow, and for quantifying flow velocities and flow volumes [5, 6]. These techniques became the foundation for the field of MR angiography. In this article, technical and clinical developments in the field of MR angiography will be reviewed, with an emphasis on current and future clinical applications as well as practical limitations.

Flow Effects and Techniques for Manipulating Flow Contrast

The process of creating an MR image involves the application of RF and gradient pulses. Fresh spins first entering the imaging volume have not been recently affected by RF pulses and are unsaturated; they therefore produce an intense signal. This effect, which is most pronounced in the entrance slice, is called *flow-related* or *paradoxical* enhancement. A competing effect is that caused by the washout of flowing spins from the slice during the imaging process [7]. When images are obtained with an SE pulse sequence, spins must remain in the slice sufficiently long to be exposed to both the 90° and 180° RF pulses (i.e., for a time interval of at least ½TE). With fast flow, washout effects tend to dominate, so that flowing blood appears dark. Washout effects can be accentuated by the use of thin slices and/or long TE; this is one method for obtaining "black-blood" images. *Presaturation* techniques, which incorporate one or more additional RF pulses prior to the pulse sequence, are also useful to produce black-blood images [8, 9]. The basic principle is that an extra RF pulse (typically near 90°) can be applied outside the imaging volume to saturate inflowing spins without altering the signal intensity of stationary tissues within the imaging volume. The inflowing, presaturated spins then appear dark when imaged with the regular pulse sequence. The technique eliminates ghost artifacts from pulsatile flow and readily distinguishes thrombus from flowing blood.

Flowing blood can be made to appear bright by the combination of the GRE pulse sequence and flow compensation. In the GRE sequence, the echo is refocused without a 180° RF pulse simply by a reversal of the imaging gradients, so that stationary spins have no net phase shift at the echo time (TE) [10]. The absence of the 180° pulse makes washout effects negligible. However, phase shifts produced by flow across the magnetic field gradients [11] interfere with the

---

Received September 14, 1989; accepted after revision November 27, 1989.

[1] Department of Radiology, Beth Israel Hospital, 330 Brookline Ave., Boston, MA 02215. Address reprint requests to R. R. Edelman.

[2] Department of Radiology, New England Deaconess Hospital, 185 Pilgrim Rd., Boston, MA 02215.

[3] Siemens Medical Systems, Iselin, NJ 08830.

[4] Département de Radiologie, Hôpital Cantonal, 1700 Fribourg, Switzerland.

AJR 154:937–946, May 1990 0361–803X/90/1545–0937 © American Roentgen Ray Society

creation of bright blood GRE images. These phase shifts result in flow-related dephasing and signal loss [12]. In order to make the flowing spins appear brighter, *flow compensation* (also called gradient motion rephasing, gradient motion nulling, or motion artifact suppression technique) is applied [13, 14]. The pulse sequence is modified by the addition of one or more gradient pulses, which are precisely calibrated to eliminate phase shifts from both stationary and flowing spins. At least three gradient pulses are needed to correct for first-order (velocity) phase shifts, and more pulses are needed for higher-order effects (e.g., acceleration, jerk). Given that the additional gradient pulses needed for higher-order flow compensation prolong the TE, there is little clinical benefit in applying flow compensation of higher than first order. The efficacy of flow compensation is improved by using a very short TE. This can be achieved by shifting the center of the readout period with respect to the peak of the echo (asymmetric sampling), at the expense of some loss of spatial resolution.

MR Angiography

Abnormalities involving large blood vessels, such as abdominal aortic aneurysms, are usually well evaluated by using standard 2-D SE and GRE images. However, detailed evaluation of vascular anatomy in smaller vessels, such as the renal or carotid arteries, requires the application of a more sophisticated approach. In order to overcome the restrictions inherent to tomographic images for evaluating blood vessels crossing several image slices, a variety of *projection imaging* techniques have been developed. Similar to a conventional angiogram, a projection image displays some, or all, blood vessels coursing through a large thickness of the body.

Two general approaches have been studied for producing such MR angiograms. The first approach involves acquiring a series of contiguous, thin-slice "bright-blood" images with a 3-D or 2-D GRE pulse sequence, and then postprocessing these images. The second method involves the direct acquisition of an image encompassing the blood vessels within a large thickness of the body. MR angiography may be further categorized according to the means for generating flow contrast. Techniques that rely on the inflow of unsaturated spins into the imaging volume, in order to make blood vessels appear brighter than stationary spins, are classified as time-of-flight or magnetization recovery. Techniques that rely on the application of gradient pulses, in order to produce different phase shifts for flowing and stationary spins, are called phase contrast.

3-D Time-of-Flight Acquisition

Three-dimensional GRE imaging allows a series of very thin (1–2 mm), contiguous slices to be obtained, with better signal to noise and shorter TE than is available by 2-D methods. The 3-D sequence differs from a 2-D sequence in one important respect. First, a relatively thick volume or "slab" of tissue (typically 32 mm or thicker), rather than a thin slice, is excited by the RF pulse. Thin, contiguous slices, or *partitions*, are then produced by phase-encoding the excited slab along the slice-selection axis, in addition to the standard in-plane phase-encoding process. The individual slices are postprocessed by using a *maximum-intensity-projection* (MIP) algorithm (Fig. 1). The computer projects a line (or ray) through the slices along a user-defined viewing angle. The brightest pixel along this line is then placed into the projection image; on GRE images, this pixel usually represents flowing blood. The procedure is repeated for each pixel in the projection image. In the final projection angiogram, blood vessels appear bright and stationary tissues appear dark. An advantage of this method is that, once the images have been acquired, they may be postprocessed along any viewing angle to eliminate vascular overlap and permit optimal assessment of stenoses.

Sequential 2-D Acquisition

The 3-D GRE acquisition has significant drawbacks for the evaluation of veins and severely diseased arteries, because blood flowing slowly within the thick imaging volume becomes saturated and flow contrast is lost. Three-dimensional acquisitions are also particularly sensitive to motion such as respiration or swallowing. The sequential 2-D acquisition method helps to overcome these limitations [15]. A series of contiguous or overlapping 2-D flow-compensated GRE images are acquired sequentially, spanning the region of interest. The images are then postprocessed by using the MIP algorithm to produce projection images. Unlike a 3-D acquisition, which requires several minutes, the individual 2-D acquisitions can each be completed in just a few seconds. This is fast enough that breath-holding can be used to eliminate respiratory artifacts (Fig. 2). We have found that the efficiency of the sequential 2-D study is markedly improved by acquiring multiple slices simultaneously during each breath-hold. This can be done without compromising flow contrast if thin slices are used and they are separated by a gap of several times the slice thickness. For instance, typical scan variables for each breath-hold acquisition would be 51/10/30°/1 (TR/TE/flip an-

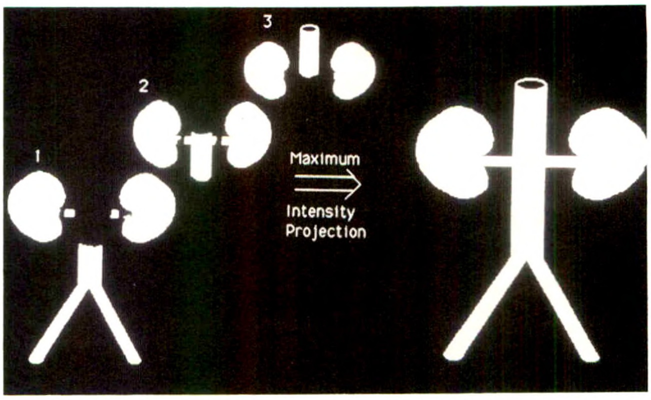

Fig. 1.—Schematic of maximum-intensity-projection algorithm, as applied to sequential 2-D study of renal arteries. Brightest pixels are extracted from slices, along a ray projected through images at user-defined viewing angle. These pixels are then combined into a projection image, which overcomes limitations inherent to tomographic images for displaying tortuous blood vessels.

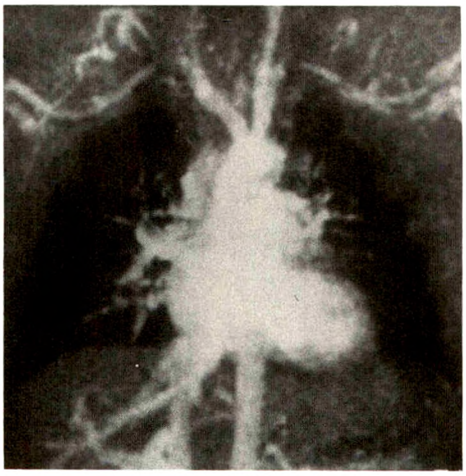

Fig. 2.—Sequential 2-D angiogram of chest in a normal subject. Scan variables: 30/10/30°/1 (TR/TE/flip angle/NEX), one slice per breath-hold, 5-mm slice thickness, and 1-mm overlap between sequential slices.

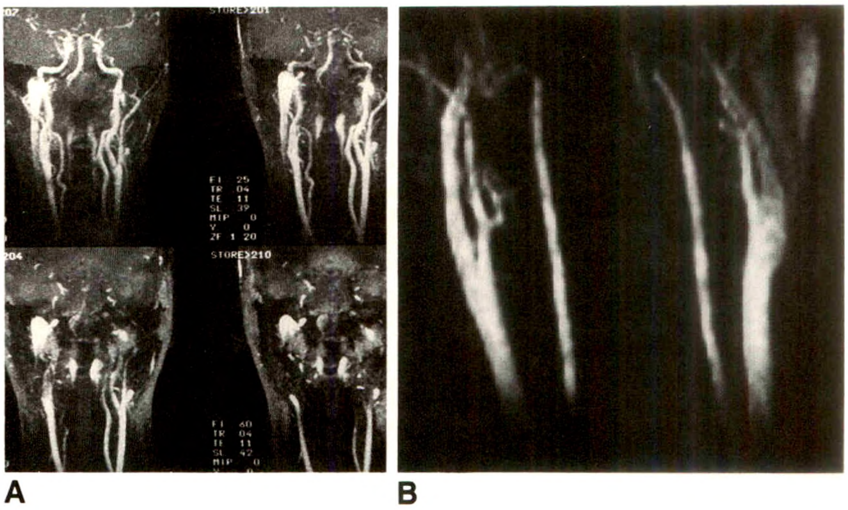

Fig. 3.—*A*, Effect of flip angle on flow contrast for 3-D time-of-flight MR angiogram. Large flip angles (e.g., 60°, lower right) produce best flow contrast for inflowing spins within first few centimeters of carotid arteries. Smaller flip angles (e.g., 15°, upper left) provide better visualization of vessels deep within imaging volume, such as intracranial arteries. (Courtesy of G. Laub.)

B, Saturation effects are largely avoided by using an axial excitation. MR angiogram of normal carotid bifurcations, obtained with a 3-D flow-compensated gradient-echo acquisition, axial excitation, and coronal signal readout. Scan variables: 49/9/20°/1 (TR/TE/flip angle/NEX), 10-cm-thick axial excitation volume, 64 partitions, 1.5-mm partition thickness, 256 × 192 acquisition matrix, 25-cm field of view, and 8-min scan time. Excellent vascular detail was obtained with this method. Presaturation eliminated signal from jugular veins as well as wraparound along slice-selection direction.

gle/number of excitations [NEX]), 256 × 256 acquisition matrix, 38-cm field of view, and three slices acquired simultaneously with a slice thickness of 5 mm and 20-mm interslice gap.

Compared with the 3-D method, angiograms acquired by using the sequential 2-D method consistently show better flow contrast for vessels with low or moderate flow velocities, because the thin slice thickness maximizes flow-related enhancement and minimizes in-plane saturation. Sequential 2-D acquisitions are better than 3-D acquisitions for showing abdominal and intracranial venous structures and small arteries. Conversely, rapid arterial flow in stationary body parts (e.g., in the circle of Willis) is rendered better by 3-D than 2-D methods, because flow-related dephasing is reduced by the thinner slices (i.e., smaller voxel) and shorter TE available with 3-D imaging.

With either 2-D or 3-D methods, the proper selection of flip angle is essential to maximize flow-related enhancement while minimizing saturation (Fig. 3A). With 2-D methods, satisfactory results are usually obtained with a TR of approximately 30 msec and a flip angle of approximately 30°. With 3-D methods, large flip angles (e.g., 60°) produce the best flow contrast for inflowing spins within the first few centimeters of the imaging volume, but smaller flip angles (e.g., 20°) provide better visualization of vessels deep within the imaging volume [16]. Also, thick imaging volumes (e.g., 100 mm) produce more saturation and worse flow contrast than relatively thinner volumes (e.g., 32 mm). A potential compromise is to perform sequential 3-D acquisitions by using thin slabs and a reduced number of partitions to preserve flow contrast while obtaining the benefits of a 3-D sequence.

Gd-DTPA enhancement can also be used to improve flow contrast, but its use entails certain drawbacks. First, tissues other than blood vessels (e.g., nasal mucosa, choroid plexus, pituitary gland) will enhance and be shown inappropriately on MR angiograms that use MIP postprocessing. Second, presaturation is rendered ineffective by the shortened T1 relaxation time of gadolinium-enhanced blood [17].

The choice of transmitter coil is also of significance. For instance, when the head coil is used as the transmitter for imaging of the carotid bifurcation, the RF excitation is limited to the head and upper neck. As a result, there is prominent flow-related enhancement within the carotid arteries. On the other hand, if the body coil is used as the transmitter for a sagittal or coronal acquisition, then the RF excitation will affect the great vessels within the chest, as well as within the neck. This results in saturation of the spins flowing into the carotid bifurcation, and loss of flow contrast. The problem may be overcome by use of an axial RF excitation through the neck, which does not affect the chest, followed by readout in the coronal or sagittal plane (Fig. 3B).

Projection Acquisition Methods

Methods that use direct acquisition of projection images differ substantially from those already discussed in that the acquired images span a large thickness of the body. The acquisition strategy is to uniquely identify moving spins by changing their appearance in the two images, while maintaining an identical appearance of stationary spins. By simply subtracting one image from the other, the signals from the background tissues are eliminated and only the blood vessels are shown. The basic principle of the technique is analogous to digital subtraction angiography; however, modifications to the pulse sequence substitute for the effect of an iodinated contrast agent.

An early implementation of the projection acquisition method used cardiac gating to produce differences in vascular signal. Vascular signal is greater on SE images during slow diastolic flow than during rapid systolic flow. By subtracting a projection image gated to diastole from one gated to systole, Wedeen et al. [18] created MR angiograms of the peripheral arterial circulation. Better results are obtained if flow-sensitizing gradients are also used. One projection image is acquired with flow compensation to enhance vascular signal, and another with dephasing gradients to eliminate it. A limitation of this method is that it may be difficult to completely dephase very slow flow (e.g., in severely stenotic arteries), so that flow contrast may be limited.

Dumoulin et al. [19, 20] proposed an alternative projection acquisition approach. Two projection images are acquired with bipolar flow-sensitizing gradients of opposite polarities, which produce phase shifts (θ) of opposite sign for moving spins. Complex image subtraction then produces flow contrast proportional to 2 sin θ. One drawback of this phase-contrast method is aliasing: if the phase shift is more than 360°, then the phase shift becomes ambiguous. For instance, rapid flow with a phase shift of 400° may be interpreted identically to slower flow with a shift of 40°. As a result of aliasing, there may be low signal and poor flow contrast despite brisk flow. Therefore, the flow-sensitizing gradients should be calibrated for the specific range of velocities that exists within the vessel of interest.

The combination of flow-sensitizing gradients and complex image subtraction has also been incorporated into 3-D acquisitions (*3-D phase-contrast angiography*) [21]. For small arteries and veins in stationary tissues (e.g., brain or hand), the method produces better flow contrast than the time-of-flight 3-D methods described above [22]. However, the phase-contrast method requires 3-D data to be acquired with multiple permutations of the flow-sensitizing gradients, so that acquisition times are much longer than for the time-of-flight approach. Moreover, it requires much more intensive postprocessing of the data, and is sensitive to aliasing. The complex subtraction used for phase-contrast angiography is also extremely sensitive to spurious phase shifts produced by gradient-induced eddy currents, so that use of properly calibrated eddy current compensation is essential. Active gradient shielding has proved helpful to achieve this.

A number of other methods for MR angiography have been proposed, although to date no substantial clinical results have been obtained with them. For instance, flow contrast can be produced in a pair of projection images by acquiring one image with, and one without, presaturation or preinversion [23, 24]. However, the effectiveness of presaturation for eliminating vascular signal decreases with distance from the presaturation slab, so that the method is not useful for large-field-of-view applications (e.g., imaging the aorta). Other proposed methods include line-scan angiography [25] and a modified driven-equilibrium sequence [26].

Flow Measurement

A variety of methods are available for measuring flow velocities. These methods fall into two groups, depending on whether they assess changes in proton phase or magnetization. *Phase techniques* rely on the fact that constant velocity flow along a magnetic field gradient produces shifts in the phase of the MR signal that are proportional to the velocity [27]. The phase information is not apparent on standard images, which are reconstructed from the signal magnitude. However, phase-sensitive images can also be reconstructed. In these images, the pixel intensity is directly proportional to phase and, therefore, velocity. Phase imaging methods have been applied to large vessels such as the aorta [28] and pulmonary arteries, for instance, permitting cardiac shunts to be quantified, to separate the true and false lumens of an aortic dissection [29], or to distinguish thrombus from slow flow [30].

Time-of-flight methods rely on specific temporal and spatial changes in longitudinal magnetization rather than phase [31]. An example is bolus tracking. If a bolus of blood is "tagged" by a thin presaturation slab, then the motion of the bolus can be imaged over the cardiac cycle by obtaining multiple data readouts with a cine GRE pulse sequence [32]. The tagged bolus appears dark, contrasting sharply with the adjoining bright flowing blood. Velocity is quantified simply as distance traveled divided by the time between tagging and data readouts. Replay of the images in a closed movie loop permits a visual appreciation of the flow velocities and profiles. Unlike the case of arterial flow, cardiac gating is not required for flow measurements in most veins, since venous flow is relatively steady. This permits chest and abdominal flow measurements to be completed within a breath-hold.

Clinical Results

Despite the variety of methods now available for MR angiography, there has been a dearth of clinical studies. Pending the performance of well-controlled studies at multiple institutions, applying standardized techniques to large numbers of subjects, any conclusions one may draw about the clinical utility of MR angiography must be considered tentative.

Extracranial Carotid Circulation

Atherosclerosis affecting the extracranial carotid circulation is a significant cause of thromboembolic stroke. The gold standard to assess atherosclerotic changes is contrast angiography. Duplex sonography has proved to be an accurate, inexpensive screening technique for disease affecting the extracranial carotid. However, it provides incomplete plaque characterization, patent vessels may be falsely diagnosed as occluded, and it can evaluate the intracranial cerebral cir-

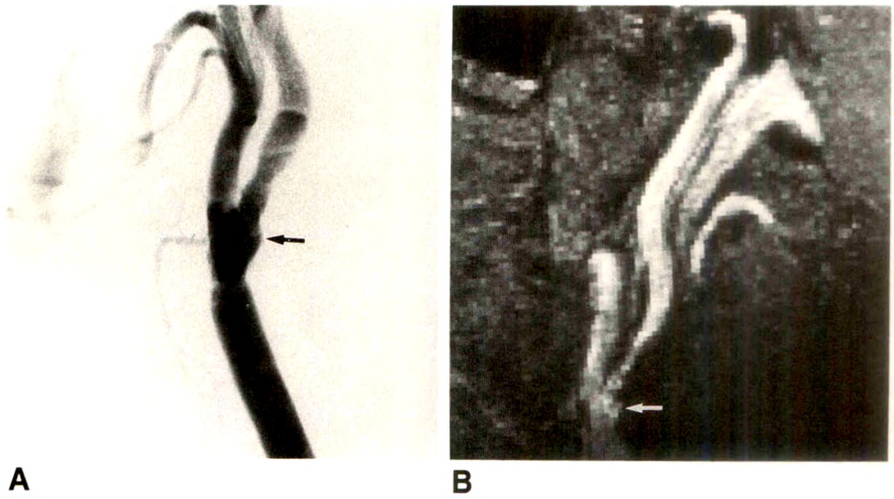

Fig. 4.—*A* and *B*, Carotid arteriogram (*A*) and 3-D MR angiogram (*B*) in a patient with moderate stenosis of proximal internal carotid artery. Scan variables: 40/8/15°/1 (TR/TE/flip angle/NEX), 40-mm 3-D slab thickness, and 32 partitions with 1.25-mm slice thickness. There is good correlation between the two images. However, MR angiogram exaggerates degree of stenosis. Ulceration (*arrows*).

culation only when combined with transcranial Doppler sonography.

Masaryk et al. [33] have used time-of-flight 3-D acquisitions, postprocessed by using the MIP algorithm, for studies of the carotid bifurcation (Fig. 4). MR angiography correctly classified 21 of 22 stenoses and occlusions of the internal carotid artery. One problem was that lesser stenoses were sometimes overgraded as severe stenoses. This error is produced by the presence of turbulent (i.e., chaotic) flow distal to the stenosis, which results in signal loss that is not entirely recovered by the application of flow compensation. The problem is ameliorated, but not eliminated, by the use of a very short TE (e.g., 7 msec). In addition, with the low flow velocities that can exist in severely stenotic arteries, flow contrast will be reduced by saturation effects as the blood flows within the imaging volume. Keller et al. [34] have applied sequential 2-D, rather than 3-D, acquisitions with very thin slices (e.g., nominal slice thickness of 1 mm) to reduce these saturation effects, with promising results. However, the signal-to-noise ratios of these images are poorer than those obtained by 3-D acquisitions. Both methods are also suboptimal for detecting plaque ulcerations, because the relative stasis of blood within these lesions fails to produce adequate flow contrast. Better evaluation of ulcerations might be obtained by using more anatomic black-blood imaging methods. Because of its greater availability and lower cost, duplex sonography remains the screening method of choice for carotid bifurcation disease, although MR angiography may be useful for selected cases with technically inadequate or ambiguous sonography. In particular, we expect that MR will prove more accurate for differentiating a severely stenotic vessel from a thrombosed one. This distinction is important, because a stenotic vessel, unlike a thrombosed one, may be amenable to surgical treatment [35]. However, further study is needed to determine whether MR might obviate conventional angiography in this application.

Intracranial Vessels

Preliminary studies suggest that MR angiography may have a useful role in the evaluation of a variety of cerebrovascular disorders. One study of intracranial aneurysms, that used both SE imaging and MR angiography detected 17 of 19 aneurysms [36]. MR angiography increased the sensitivity for aneurysms, compared with SE images alone. However, there are several pitfalls in the use of MR angiography for this diagnosis. MR angiography fails to detect thrombosed aneurysms, as well as those containing very slow flow, and will underestimate the size of aneurysms containing turbulent flow. Moreover, substances having short T1 relaxation times such as extracellular methemoglobin and proteinaceous solutions, which may be present in subarachnoid or intracerebral hemorrhages and in thrombosed vessels, can appear bright on MR angiograms, which use MIP postprocessing. For optimal evaluation, it is therefore essential that both black-blood SE images and bright-blood angiograms be obtained (Fig. 5). In the setting of relatively modest clinical suspicion (e.g., family history of berry aneurysms involving the circle of Willis), MR may be useful for the initial imaging evaluation. However, one should note that the 89% accuracy reported in the study of Masaryk et al. [36] is inferior to the results with thin-section contrast-enhanced CT [37]. Also, MR should not, at the present stage of development, substitute for contrast angiography in patients with high clinical suspicion (e.g., evidence of subarachnoid hemorrhage).

MR imaging, with conventional SE techniques, has proved to be a good means for detecting and characterizing intracranial arteriovenous malformations. Rapidly flowing blood appears dark, but may be impossible to differentiate from calcification; this differentiation is better made by MR angiography [38, 39]. It has been shown that 3-D MR angiography delineates the nidus and major feeding vessels, whereas sequential 2-D MR angiography better renders the draining veins (Fig. 6) [40]. Moreover, presaturation techniques allow the different vascular territories contributing to the malformation to be precisely mapped. In order to accomplish this, a presaturation slab is applied to a single feeding vessel, such as a middle cerebral artery, without affecting other major intracranial arteries. The presaturation eliminates signal only within that portion of the malformation supplied by the presaturated vessel. Thus, by using this technique of *selective MR arteri-*

P 24458

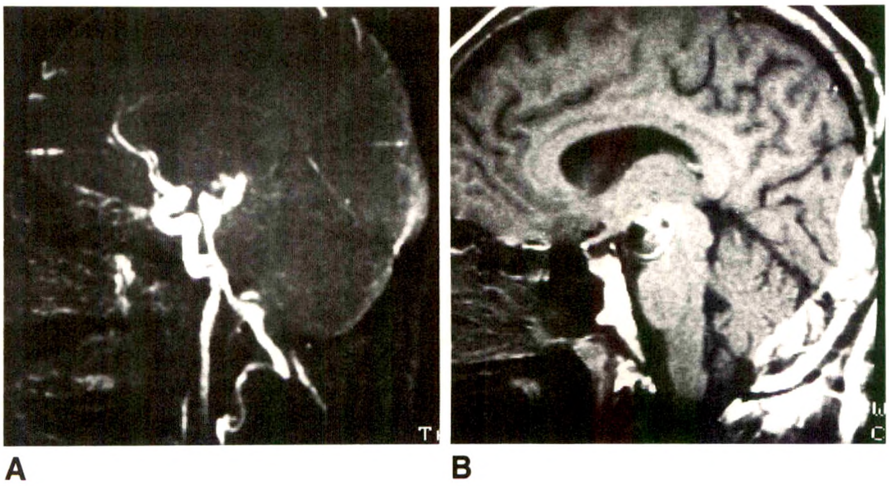

Fig. 5.—*A*, Giant aneurysm at top of basilar artery seen on sagittal 3-D angiogram. Methemoglobin or proteinaceous substances, as well as flowing spins, may appear bright on gradient-echo images; therefore, clot can be mistaken for flow.

B, SE MR image obtained with presaturation more accurately delineates extent of clot from open lumen of aneurysm. (Reprinted with permission from Edelman et al. [5].)

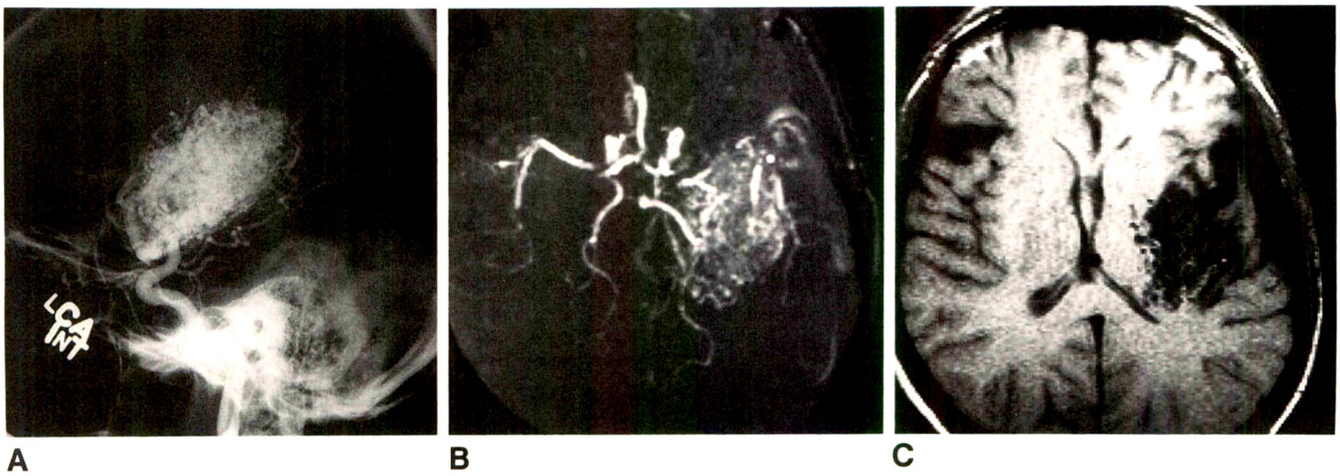

Fig. 6.—Left parietotemporal arteriovenous malformation.

A, Conventional carotid angiogram.

B, Axial 3-D MR angiogram.

C, SE MR image with flow presaturation. Nidus is well seen on both SE image and MR angiogram. (Reprinted with permission from Edelman et al. [40].)

ography, it is not essential that the entire vascular tree be shown for functional information about the malformation to be determined.

MR angiography can also be applied to the study of collateral circulation in the cerebrovascular system (Fig. 7) [41]. Currently, the only noninvasive means for demonstrating cross-flow through the circle of Willis is by using transcranial Doppler imaging. This technique is a useful bedside tool for the evaluation of stroke patients [42]. However, there are many possible pitfalls, especially in the assessment of the posterior circulation. On the other hand, MR angiography with time-of-flight or phase-contrast 3-D techniques shows vascular anatomy but, as it is usually implemented, fails to provide functional information. Selective MR angiography with presaturation is an accurate means for showing origin and directionality of flow. Collateral flow or the presence of a fetal posterior circulation, which may not be apparent on standard MR angiograms, is readily shown by the selective method.

MR venography of the cerebral sinuses and veins is also feasible [15]. For this purpose, sequential 2-D MR angiography is performed with presaturation of the arterial inflow, so that only veins are depicted. The effect of presaturation does not carry through to the veins, because the flowing spins remagnetize during the few seconds of transit through the capillary circulation. This technique may prove useful for the evaluation of suspected sinus thrombosis and venous malformations. MR can also be applied to the measurement of intracranial venous flow, which is not possible by other noninvasive means. For instance, bolus tracking has been used to measure blood flow within the superior sagittal sinus, which might be an indicator of cortical blood flow [43]. Dynamic changes in cerebral blood flow with maneuvers such as hyperventilation are readily shown. In animals and humans, regional perfusion of the brain [44], heart [45], and kidneys [46] has also been assessed qualitatively by dynamic first-pass MR imaging with paramagnetic or superparamagnetic contrast agents, although quantitation is a more difficult task.

Body Angiography

Sequential breath-hold 2-D acquisitions can be applied to the evaluation of the vasculature within the chest and abdo-

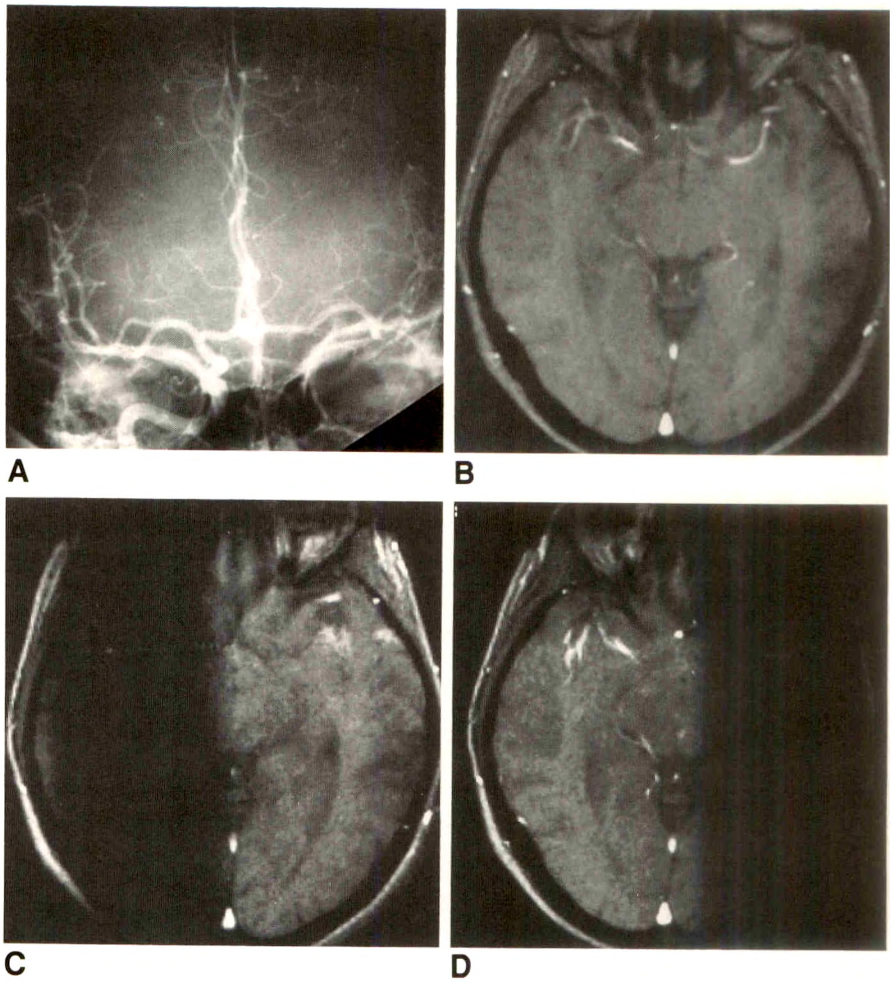

Fig. 7.—*A*, Conventional arteriogram in patient with occlusion of left internal carotid artery shows collateral flow from right to left internal carotid artery territory over anterior communicating artery.

B, Axial 2-D gradient-echo MR image, 30/10/30°/1 (TR/TE/flip angle/NEX), shows flow in both middle cerebral arteries. Information about origin of flow is not available from this image.

C, Presaturation of right carotid artery eliminated signal in left middle cerebral artery, indicating origin of flow from right side.

D, Presaturation of left carotid artery does not affect signal in right middle cerebral artery. (Reprinted with permission from Edelman et al. [41].)

men (Figs. 2 and 8A) [15]. Venograms of the hepatic and portal venous systems are created, without overlap from arteries, by applying presaturation to the distal thoracic aorta. Esophageal, gastric, and splenic varices are demonstrated without regard to body habitus, a significant advantage compared with sonography (Fig. 8B). Patency of the main portal vein and the flow velocity and direction are quickly determined with MR by using bolus tracking (Figs. 8C and 8D) [47]. Projection acquisition techniques such as phase-contrast angiography have also been applied to the study of the abdominal vasculature [48]. Although sonography may remain as the initial technique for evaluation of patients with portal hypertension, the role of MR angiography is increasing.

MR may be superior to CT in depicting abdominal aortic aneurysms because of its capability for showing the entire length of the lesion in a single image. However, the interpretation of complex signal intensities in regions of slow or turbulent flow is difficult. MR may also prove useful for the initial evaluation of patients with suspected renovascular hypertension (Fig. 9). In a prospective study of 25 patients with 55 renal arteries, MR angiography with the sequential 2-D approach had a sensitivity of 100% for detecting renal artery stenoses of moderate (≥50%) or more severe degree [49]. MR incorrectly overgraded the degree of renal artery stenosis in four of 55 renal arteries (specificity = 92%). MR also correctly determined the number of renal arteries in all cases. However, MR was not adequate for evaluation of the distal portions of the renal arteries. Aortic plaque, which appears dark on GRE images, is well shown.

Perhaps of even greater potential clinical value, MR angiography has been used to quantify flow volumes in the renal veins, which allows the hemodynamic significance of renal artery stenoses to be assessed. This is not possible by other noninvasive means or conventional angiography. Renal vein flow is nearly equal to renal blood flow. In 12 healthy subjects, side-to-side differences in renal vein flow were minimal. However, in five patients with unilateral renal artery stenosis, a marked reduction in blood flow was shown on the side of the stenosis (Hoogewoud HM, Edelman RR, Mattle HP, et al., unpublished data). Further study is needed in this area.

Less success has been achieved in studying the peripheral arterial circulation, and reports to date have been anecdotal. Difficulties include the need to obtain high spatial resolution over a large field of view and the presence of slow or turbulent flow in association with stenoses. Single-slice 2-D GRE can be used to assess deep venous thrombosis [50], but MR faces stiff competition from noninvasive studies such as duplex sonography. The capability for differentiating acute from chronic thrombosis and for demonstrating the presence of collateral circulation must also be developed. Application of

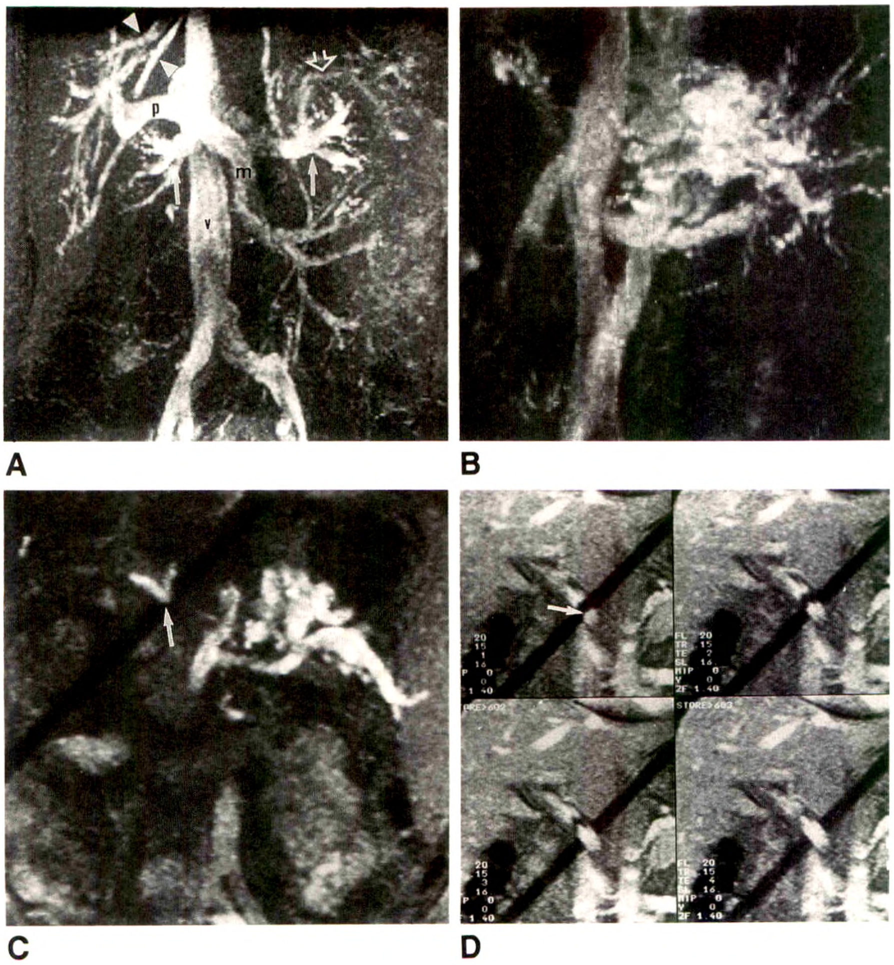

Fig. 8.—*A*, Sequential 2-D venogram of upper abdomen in a normal subject. Scan variables for each breath-hold acquisition: 72/10/35°/1 (TR/TE/flip angle/NEX), three slices per breath-hold, 5-mm slice thickness with 40-mm interslice gap, 256 × 192 acquisition matrix, and 38-cm field of view. The thickness of the projection image, created from multiple overlapping breath-hold acquisitions, is 120 mm. Presaturation slab (black stripe across top of image) above diaphragm eliminates signal from arterial blood flowing into abdomen. Inferior vena cava (v) and iliac veins, superior mesenteric vein (m) and small branches, renal veins (*solid arrows*), main portal vein (p) and its intrahepatic branches, and hepatic veins (*arrowheads*) are visualized. Splenic vein (*open arrow*) is not well shown because it is partially outside imaging volume.

B, Sequential 2-D MR angiogram in patient with liver cirrhosis reveals massive gastric varices. Because arterial presaturation was not applied, there is overlap of aorta and portal venous system.

C, Bolus tracking study of portal vein displays reversed flow. In order to eliminate vascular overlap, range of slices used for postprocessing was restricted to exclude aorta. Tagged bolus (*arrow*), which appears dark, is observed to move away from liver.

D, Bolus tracking study of normal portal vein. Tagged bolus (*arrow*) is seen to move toward liver in sequential images. (Reprinted with permission from Edelman et al. [47].)

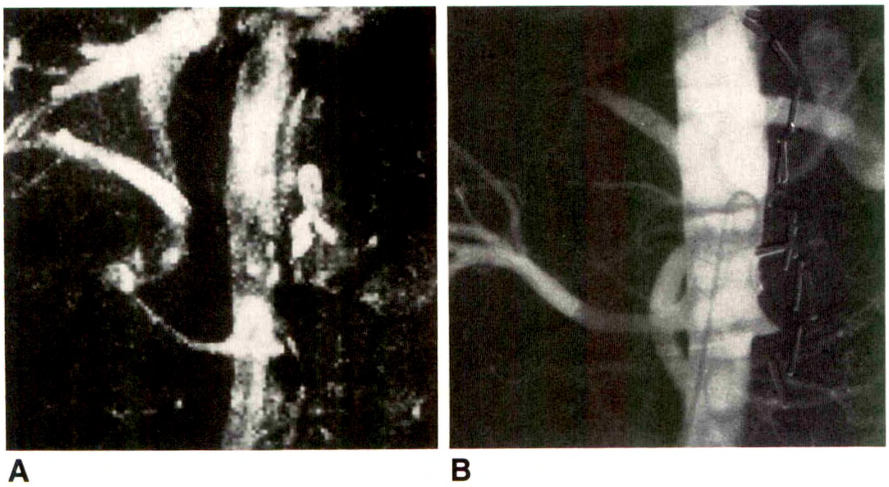

Fig. 9.—*A* and *B*, Sequential 2-D MR angiogram (*A*) (scan variables: 30/10/30°/1[TR/TE/flip angle/NEX], one slice per breath-hold, 5-mm slice thickness, and 1-mm overlap between sequentially acquired coronal slices) shows occlusion of left renal artery and correlates well with conventional angiogram (*B*). Distal portion of right renal artery is not optimally assessed in projection image because of current limitations of the technique. (Reprinted with permission from Kim et al. [49].)

MR angiography to the deep venous system is impeded by the phasic low-flow velocities, or stasis, present in these vessels. MR contrast agents such as Gd-DTPA, in conjunction with 2-D or 3-D acquisition methods and postprocessing by the MIP algorithm, might be useful in overcoming this problem, but would increase the cost and make the examination invasive.

MR angiography of the coronary arteries is, without question, the most challenging task for flow researchers, and may in fact prove to be a technical impossibility. The combination of the small size of the vessels (less than 5 mm diameter) with both cardiac and respiratory motion represents a daunting obstacle. Nonetheless, coronary arteries are occasionally visualized on standard gated SE and cine GRE studies [6, 51]. In order to produce MR angiograms of the native coronary arteries, one group has applied a technique by which two projection images are acquired, in one of which the aortic root has been preinverted [52]. In principle, the preinversion will affect only signal from blood washing into the coronary ostia, so that a subtraction image would show only the coronary arteries without signal from the ventricular cavities. To date, there have been no convincing results. Better success has been achieved in the study of coronary artery bypass grafts [53–55]. Cine GRE imaging has proved to be an accurate method for determining bypass graft patency, although the proper interpretation of these images requires considerable experience because of the complex courses of the grafts, and these tomographic images are not adequate for evaluating graft stenosis. Full acceptance of MR by cardiologists and cardiac surgeons for evaluation of bypass grafts will probably await the successful application of angiographic techniques.

Conclusions

Within just a few years, the field of MR angiography has evolved from a haphazard probing of technical possibilities to a level where applications are undergoing clinical trials. At present, MR angiography should not be considered directly competitive with contrast angiography because of the higher spatial resolution and more reliable depiction of vascular anatomy by the latter method. Nonetheless, MR angiography is often helpful as an adjunct to conventional MR imaging methods for improving the depiction of vascular anatomy and function. Preliminary studies suggest that MR angiography may be useful for the study of the portal venous system and other abdominal vessels, intracranial aneurysms and vascular malformations, cerebral venous and sinus thrombosis, and, in selected cases, for the evaluation of the carotid bifurcation. Further improvements will result from the implementation of shorter TEs, reconstruction schemes that can be applied to asymmetrically sampled data to improve spatial resolution [56], and optimized fast imaging techniques. With continued technical progress and the performance of carefully designed clinical studies, MR angiography will probably become a standard tool for the evaluation of vascular disorders.

REFERENCES

1. Hahn HL. Spin echoes. *Phys Rev* **1950**;80:580–594
2. Suryan G. Nuclear resonance in flowing liquids. *Proc Indian Acad Sci [A]* **1951**;33:107–111
3. Singer JR. NMR diffusion and flow measurements and an introduction to spin-phase graphing. *J Phys [E]* **1978**;11:281–291
4. Axel L. Blood flow effects in magnetic resonance. *AJR* **1984**;143:1157–1166
5. Edelman RR, Rubin JB, Buxton RR. Flow. In: Edelman RR, Hesselink JR, eds. *Clinical magnetic resonance imaging*. Philadelphia: Saunders, **1990** (in press)
6. Alfidi RJ, Masaryk TJ, Haacke EM, et al. MR angiography of peripheral, carotid, and coronary arteries. *AJR* **1987**;149:1097–1109
7. Bradley WG, Waluch V, Lai K-S, et al. The appearance of rapidly flowing blood on MR images. *AJR* **1984**;143:1167–1174
8. Edelman RR, Atkinson DJ, Silver MS. FRODO pulses: a new method for elimination of motion, flow and wraparound artifact. *Radiology* **1988**;166:231–236
9. Felmlee JP, Ehman RL. Spatial presaturation: a method for suppressing

9. Felmlee JP, Ehman RL. Spatial presaturation: a method for suppressing flow artifacts and improving depiction of vascular anatomy in MRI. *Radiology* **1987**;164:559–564

10. Frahm J, Haase A, Mattaei D. Rapid NMR imaging of dynamic processes using the FLASH technique. *Magn Reson Med* **1986**;3:321–327
11. Singer JR. NMR diffusion and flow measurements and an introduction to spin-phase graphing. *J Phys [E]* **1978**;11:281–291
12. von Schulthess GK, Higgins CB. Blood flow imaging with MR: spin-phase phenomenon. *Radiology* **1985**;157:687–695
13. Laub GA, Kaiser WA. MR angiography with gradient motion rephasing. *J Comput Assist Tomogr* **1988**;12:377–382
14. Haacke EM, Lenz G. Improving MR image quality in the presence of motion by using rephasing gradients. *AJR* **1987**;148:1251–1258
15. Edelman RR, Wentz KU, Mattle H, et al. Projection arteriography and venography: initial clinical results with MR. *Radiology* **1989**;172:351–357
16. Ruggieri PM, Laub GA, Masaryk TJ, Modic MT. Intracranial circulation: pulse-sequence considerations in three-dimensional (volume) MR angiography. *Radiology* **1989**;171:785–791
17. Edelman RR, Siegel JB, Singer A, Dupuis K, Longmaid HE. Dynamic MR imaging of the liver with Gd-DTPA: initial clinical results. *AJR* **1989**;153:1213–1219
18. Wedeen VJ, Meuli RA, Edelman RR, et al. Projective imaging of pulsatile flow with magnetic resonance. *Science* **1985**;230:946–948
19. Dumoulin CL, Hart HR. MR angiography. *Radiology* **1986**;61:717–720
20. Dumoulin CL, Souza SP, Walker MF, Yoshitome E. Time-resolved MR angiography. *Magn Reson Med* **1988**;6:275–286
21. Dumoulin CL, Souza SP, Walker MF, Wagle W. Three-dimensional phase contrast angiography. *Magn Reson Med* **1989**;9:139–149
22. Chao PW, Goldberg H, Dumoulin CL, Wehrli FW. Comparison of time of flight versus phase contrast techniques: visualization of the intra- and extracerebral carotid artery. In: *Book of abstracts: Society of Magnetic Resonance in Medicine 1989*, vol. 1. Berkeley, CA: Society of Magnetic Resonance in Medicine, **1989**:165
23. Dixon WT, Du LN, Faul DD, et al. Projection angiograms of blood labeled by adiabatic fast passage. *Magn Reson Med* **1986**;3:454–462
24. Nishimura DG, Macovski A, Pauly JM. Considerations of MR angiography by selective inversion recovery. *Magn Reson Med* **1988**;7:472–484
25. Pauly J, Nishimura D, Macovski A. Line scan MR angiography. In: *Book of abstracts: Society of Magnetic Resonance in Medicine 1987*, vol. 1. Berkeley, CA: Society of Magnetic Resonance in Medicine, **1987**:28
26. Pauly J, Nishimura D, Macovski A. Robust velocity selective excitation. In: *Book of abstracts: Society of Magnetic Resonance in Medicine 1987*, vol 1. Berkeley, CA: Society of Magnetic Resonance in Medicine, **1987**:27
27. Wedeen VJ, Rosen BR, Chesler D, Brady TJ. MR velocity imaging by phase display. *J Comput Assist Tomogr* **1985**;9:530–536
28. Maier SE, Meier D, Boesiger P, Moser UT, Vieli A. Human abdominal aorta: comparative measurements of blood flow with MR imaging and multigated Doppler US. *Radiology* **1989**;171:487–492
29. Dinsmore RE, Wedeen VJ, Miller SW, et al. MRI of dissection of the aorta: recognition of the intimal tear and differential flow velocities. *AJR* **1986**;146:1286–1288
30. White EM, Edelman RR, Wedeen VJ, Brady TJ. Intravascular signal in MR imaging: use of phase display for differentiation of blood flow signal from intraluminal disease. *Radiology* **1986**;161:245–249
31. Wehrli FW, Shimakawa A, Gullberg GT, MacFall JR. Time-of-flight MR flow imaging: selective saturation recovery with gradient refocusing. *Radiology* **1986**;160:781–785
32. Edelman RR, Mattle H, Kleefield J, Silver MS. Quantification of blood flow with dynamic MR imaging and presaturation bolus tracking. *Radiology* **1989**;171:551–556
33. Masaryk TJ, Modic MT, Ruggieri PM, et al. Three-dimensional (volume) gradient-echo imaging of the carotid bifurcation: preliminary clinical experience. *Radiology* **1989**;171:801–806
34. Keller PJ, Drayer BP, Fram EK, Williams KD, Dumoulin CL, Souza SP. MR angiography with two-dimensional acquisition and three-dimensional display: work in progress. *Radiology* **1989**;173:527–532
35. O'Leary DH, Mattle H, Potter JE. Atheromatous pseudo-occlusion of the internal carotid artery: a review of 34 patients. *Stroke* **1989**;20:1168–1173
36. Masaryk TJ, Modic MT, Ross JS, Ruggieri P, VanDyke C, Tkach J. MR angiography of intracranial aneurysms (abstr). *AJNR* **1989**;10:893–894
37. Schmid UD, Steiger HJ, Huber P. Accuracy of high resolution computed tomography in direct diagnosis of cerebral aneurysms. *Neuroradiology* **1987**;29:152–159

38. Smith HJ, Strother CM, Kikuchi Y, et al. MR imaging in the management of supratentorial intracranial AVMs. *AJNR* **1988**;9:225–235
39. Needell WM, Maravilla KR. MR flow imaging in vascular malformations using gradient recalled acquisitions. *AJNR* **1988**;9:637–642
40. Edelman RR, Wentz KU, Mattle H, et al. Intracerebral arteriovenous malformations: evaluation with selective MR angiography and venography. *Radiology* **1989**;173:831–837
41. Edelman RR, Mattle H, O'Reilly GV, Wentz KU, Liu C, Zhao B. Magnetic resonance imaging of flow dynamics in the circle of Willis. *Stroke* **1990**;21:56–65
42. Mattle H, Grolimund P, Huber P, Sturzenegger M, Zurbrügg HR. Transcranial Doppler sonographic findings in middle cerebral artery disease. *Arch Neurol* **1988**;45:289–295
43. Mattle H, Edelman RR, Reis MA, Atkinson DJ. Flow quantification in the superior sagittal sinus using magnetic resonance. *Neurology* (in press)
44. Rosen BR, Belliveau JW, Chien D. Perfusion imaging by nuclear magnetic resonance. *Magn Reson Q* **1989**;5:263–281
45. Atkinson DJ, Burstein D, Edelman RR. Evaluation of first-pass cardiac perfusion by ultrafast magnetic resonance imaging. *Radiology* (in press)
46. Choyke PL, Frank JA, Girton ME, et al. Dynamic Gd-DTPA-enhanced MR imaging of the kidney: experimental results. *Radiology* **1989**;170:713–720
47. Edelman RR, Zhao B, Liu C, et al. Magnetic resonance angiography and flow velocity quantification in the portal venous system. *AJR* **1989**;153:755–760
48. Vock P, Terrier F, Wegmüller H, Strauch E, Souza SP, Dumoulin CL. MR angiography of abdominal vessels. In: *Book of abstracts: Society of Magnetic Resonance in Medicine 1989*. Berkeley, CA: Society of Magnetic Resonance in Medicine, **1989**:1012
49. Kim D, Edelman RR, Kent C, Porter D, Skillman J. MR angiography of the renal arteries and abdominal aorta. *Radiology* (in press)
50. Spritzer CE, Sussman SK, Blinder RA, et al. DVT evaluation with limited flip angle gradient-refocused MRI: preliminary experience. *Radiology* **1988**;166:371–375
51. Paulin S, von Schulthess GK, Fossel E, Krayenbuehl HP. MR imaging of the aortic root and proximal coronary arteries. *AJR* **1987**;148:665–670
52. Nishimura D, Macovski A, Pauly J. Coronary angiography by selective inversion recovery. In: *Book of abstracts: Society of Magnetic Resonance in Medicine 1988*. Berkeley, CA: Society of Magnetic Resonance in Medicine, **1988**:726
53. Rubinstein RI, Askenase AD, Thickman D, et al. Magnetic resonance imaging to evaluate patency of aortocoronary bypass grafts. *Circulation* **1987**;76:786–791
54. Jenkins JP, Love HG, Foster CJ, et al. Detection of coronary artery bypass graft patency as assessed by magnetic resonance imaging. *Br J Radiol* **1988**;61:2–4
55. White RD, Pflugfelder PW, Lipton MJ, Higgins CB. Coronary artery bypass grafts: evaluation of patency with cine MR imaging. *AJR* **1988**;150:1271–1274
56. Haacke EM, Lindskog E, Lin W. Half Fourier imaging: a partially phase constrained iterative reconstruction scheme and an evaluation of several fast reconstruction schemes (abstr). In: *Book of abstracts: Society of Magnetic Resonance in Medicine 1989*. Berkeley, CA: Society of Magnetic Resonance in Medicine, **1989**:363

Progress in Radiology

Percutaneous Ethanol Injection Therapy for the Treatment of Hepatocellular Carcinoma

Shuichiro Shiina,[1] Kazumi Tagawa,[2] Tadao Unuma,[2] and Akira Terano[1]

Hepatocellular carcinoma is one of the most common malignant neoplasms in the world, particularly in Asian and African countries [1]. Recently, various imaging techniques, especially sonography, and measurement of serum alpha-fetoprotein levels have been used successfully in the detection of these tumors. More and more early cases are being detected as a result of screening of high-risk groups, such as hepatitis B surface antigen carriers and patients with chronic liver disease. About two-thirds of hepatocellular carcinomas found by screening of high-risk groups are unifocal and less than 3 cm in diameter [2, 3].

Curative surgical resection of the primary tumor in the liver has been the therapeutic technique most likely to result in complete remission and extended survival. The resectability rate of hepatocellular carcinoma, however, has remained rather low. Most patients with hepatocellular carcinoma have underlying liver cirrhosis and their severe liver dysfunction often makes hepatectomy impossible, even when the cancer is found in an early stage. The Liver Cancer Study Group in Japan reported that only 1382 (19%) of 7320 cases of primary liver cancer were resectable [4].

When hepatocellular carcinoma is unresectable because of advanced cancer or poor surgical risk, transcatheter arterial embolization or chemotherapy has been a treatment of choice. However, the value of transcatheter arterial embolization is limited [5, 6]: even small hepatocellular carcinomas often invade the capsule (intercapsular invasion) and sometimes extend beyond the capsule (extracapsular invasion); transcatheter arterial embolization is ineffective against these forms of extension. Long-term survival rates in patients treated by arterial embolization are low; Yamada et al. [7] reported that in 838 cases of hepatocellular carcinoma treated with transcatheter arterial embolization, the 3- and 5-year survival rates were 12% and 6%, respectively. Results with standard chemotherapy for hepatocellular carcinoma have also been far from satisfactory, with a response rate around 10% [8].

Sonographically guided percutaneous ethanol injection therapy was first reported in 1983 by Sugiura et al. [9] and has recently attracted a great deal of attention in the treatment of liver neoplasms [10–17].

In this procedure, absolute ethanol is injected into the lesion through a fine needle. Absolute ethanol has been widely used in various therapeutic procedures, such as transcatheter arterial embolization therapy of renal tumors [18], thrombotherapy of esophageal varices [19], and percutaneous injection therapy of secondary hyperparathyroidism [20]. Absolute ethanol destroys tumor tissue mainly because of its dehydrative and protein degenerative effects and partly because of its thromboembolic effect [15]. Although some investigators have used other agents for injection therapy of hepatocellular carcinoma, such as immunochemotherapeutic agents [21] and chemotherapeutic agents [22], they were not as efficacious as absolute ethanol.

In this review, we will discuss the indications and contraindications of percutaneous ethanol injection for treatment of hepatocellular carcinoma, preparation of the patient, technical aspects, efficacy, and complications.

Received August 23, 1989; accepted after revision December 8, 1989.

[1] Second Department of Internal Medicine, Faculty of Medicine, University of Tokyo, Hongo 7-3-1, Bunkyo-ku, Tokyo 113, Japan. Address reprint requests to S. Shiina.

[2] Department of Gastroenterology, Mitsui Memorial Hospital, Kandaizumi-cho 1, Chiyoda-ku, Tokyo 101, Japan.

AJR 154:947–951, May 1990 0361–803X/90/1545–0947 © American Roentgen Ray Society

Indications

Percutaneous ethanol injection therapy has been performed mainly in patients with hepatocellular carcinoma [9–17]. There also have been a few reports on the use of the therapy for the treatment of metastatic liver tumors [10, 14], cholangiocarcinoma [14], peritoneal lymph-node metastasis [14], adenomatous hyperplastic nodules in the cirrhotic liver [23], and tumor thrombosis of hepatocellular carcinoma in the portal vein [24].

Most investigators perform the therapy for tumors of up to 5 cm in diameter, although the optimal tumor size for ethanol injection is considered to be less than 3 cm in diameter. Histopathologic examination shows that areas of at least 3 cm in diameter are almost completely necrotic in all cases [11, 12]. The injected ethanol may distribute only in a limited area; it may simply escape into the blood stream beyond this radius. Most investigators perform percutaneous ethanol injection for patients with up to three lesions, although single lesions are considered optimal for the therapy.

In cases of larger tumors or multiple lesions, percutaneous ethanol injection can be performed to reduce the tumor burden. In such cases, the tumor frequently invades vessels involved by intrahepatic metastasis. Therefore, ethanol injection, which has only local effect, should be combined with transcatheter arterial embolization. Specifically, the main tumor or tumors should be treated by the combination of ethanol injection and arterial embolization; lesions that cannot be detected by sonography should be controlled by arterial embolization. Percutaneous ethanol injection can be performed not only in patients with Child class A or B disease, but also in patients with Child class C disease (Table 1) [25], as the change in liver function after ethanol injection is only mild and transient.

Contraindications

Patients with ascites, a marked bleeding tendency, or extrahepatic metastasis are excluded from percutaneous ethanol injection. Absence of ascites must be confirmed by sonography, and the prothrombin time and platelet count must be checked before the therapy. The procedure is performed only in patients whose prothrombin time is more than 35% and whose platelet count is more than 40,000/mm^3.

TABLE 1: Condition of Patients According to Liver Disease Classification of Child [25]

Variable	Category		
	A, Minimal	B, Moderate	C, Advanced
Nutrition	Excellent	Good	Poor, "wasting"
Encephalopathy	None	Minimal	Advanced, "coma"
Ascites	None	Easily controlled	Poorly controlled
Serum bilirubin (mg/dl)	Below 2	2–3	Over 3
Serum albumin (g/dl)	Over 3.5	3–3.5	Below 3

Technique

Preliminary sonograms should be obtained to select the optimal approach. The patient should fast for at least 6 hr before the therapy and should be given premedications for analgesia and sedation.

The tumor puncture is usually performed with a 21- or 22-gauge, 15- or 20-cm puncture needle suitable for sonographic guidance. The shorter needle is easier to control than the longer one.

Sterile physiologic saline is used as the coupling agent for the sonography. The lesion is scanned with a puncture transducer and the site for insertion of the needle is selected. After local anesthesia is administered, the puncture needle is introduced into the lesion under sonographic observation. It is critical to introduce the needle without bending it. Any deviation from the scanning plane makes it difficult to observe the needle tip and to puncture the lesion. During insertion of the needle, the patient is asked to hold his or her breath in the proper phase of respiration.

Absolute ethanol is injected under sonographic observation. Ethanol is injected into the lesion at one or more locations in one treatment session. If influx of the ethanol into vessels or bile ducts is observed, the injection is stopped immediately to avoid injury of the vessels or the bile ducts. In order to reduce reflux of the injected ethanol through the puncture track into the peritoneal cavity, which is probably the main cause of abdominal discomfort, the needle is left in place for a few minutes after the injection.

In most cases, 2–8 ml of ethanol is injected in one treatment session and the injection is repeated two or three times per week until the sum of the injected ethanol reaches the intended volume [9–17]. The total volume of ethanol that should be injected is calculated according to the formula

$$V = \tfrac{4}{3}\pi(r + 0.5)^3 \text{ (ml)},$$

where V is the volume of ethanol and r is the radius (in centimeters) of the lesion. Addition of the 0.5 (cm) provides a safety margin, which is based on the concept that a certain amount of the surrounding tissue at the periphery of the lesion as well as the lesion itself must be destroyed to ensure cure of the lesion. For example, 13.5 ml of ethanol should be injected into a lesion 2.0 cm in diameter and 32 ml should be injected into a lesion 3.0 cm in diameter. However, the volume and number of injections are modified depending on patient compliance, lesion location, and postcontrast CT findings after therapy. It usually takes only 10–20 min to complete the procedure. After therapy, the patient should remain in bed for at least 3 hr.

Complications

Common adverse effects of percutaneous ethanol injection are transient pain at the site of the injection, fever, and alcohol intoxication. None of these requires any special treatment. The pain and fever can be reduced to a great degree by leaving the needle in place for a few minutes after the injection, which prevents reflux of the injected ethanol into the peritoneal cavity.

The alterations in liver function that follow ethanol injection are much milder than changes that occur after surgical resection or transcatheter arterial embolization. Thus, ethanol injection can be considered even in cases of advanced liver cirrhosis.

Serious complications reported are intraperitoneal hemorrhage due to necrosis of the tumor [12], ascites [13], right pleural effusion [13], jaundice due to hepatic decompensation [13], intraperitoneal hemorrhage due to the injury of a vessel in the omentum that covered the atrophic liver [15], jaundice probably due to injury of a bile duct [15], hepatic infarction probably due to influx of the ethanol into vessels [15], and transient hypotension [15]. Fujimoto [15] reported that major complications occurred in eight (2.8%) of 289 procedures.

There have been no reports of metastasis or local dissemination of tumor occurring after percutaneous ethanol injection. An animal experiment [15] showed that injected ethanol damages the cancer cells immediately, which suggests that metastasis or dissemination does not occur easily with this procedure. No deaths directly related to ethanol injection have been reported.

Histopathologic Evaluation of Efficacy

The short-term efficacy of the therapy is best evaluated by histopathologic examination. We have examined 13 cases in this way and found that the lesion was completely necrotic in nine cases, 90% necrotic in three cases, and 70% necrotic in the other case [11, 12]. Other investigators also found that percutaneous ethanol injection destroyed the lesion completely in most cases. Sheu et al. [13] found that in the six patients who subsequently underwent surgical resection, four had complete necrosis of the tumor and the other two had only a small peripheral residual of viable tumor remaining. Suyama et al. [14] found that the tumor showed complete necrosis in two of the six cases that were histopathologically examined. Fujimoto [15] reported that complete necrosis of the tumor was observed in two of the four resected cases after percutaneous ethanol injection. Livraghi et al. [17] reported that no viable tumor cells were detected in four patients who subsequently underwent surgery. The size of the lesion, presence or absence of internal septation, volume of injected ethanol, and accuracy of the injection are the major factors that determine whether the lesion becomes completely necrotic or not.

In our previous study [11, 12], histopathologic examination also showed that the capsule and a certain amount of the surrounding tissue as well as the tumor itself degenerate in response to the alcohol (Fig. 1). This finding proves that, unlike transcatheter arterial embolization [26], ethanol injection can be effective for intercapsular and extracapsular invasion. The fact that ethanol injection is efficacious for these forms of extension, which are frequently found even in small hepatocellular carcinomas, is important if cure is to be expected.

In the four cases in which some portion of the tumor was found intact in our previous study [11, 12], the viable tumor tissue was along the edge of the lesion, in portions isolated by septa or in daughter nodules. Therefore, ethanol should be injected not only into the center of the tumor but also into sites close to the edge.

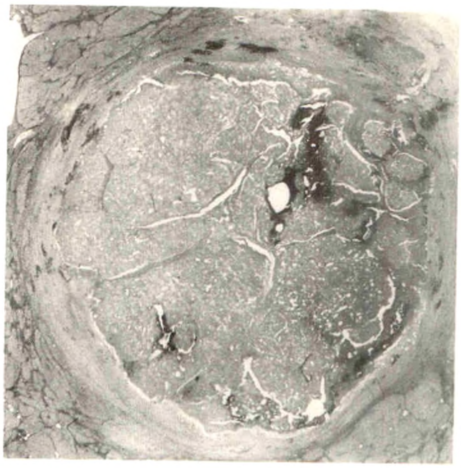

Fig. 1.—Macroscopic appearance of fixed resected liver specimen after ethanol injection of hepatocellular carcinoma. Capsule and a certain amount of surrounding liver parenchyma as well as tumor are necrotic.

The value of fine-needle biopsy in following the results of ethanol injection, although it is definitively capable of indicating necrosis of the tumor, is limited because the tissue obtained by the biopsy does not always represent that of the entire tumor.

Imaging Techniques to Evaluate the Results of Ethanol Injection

Evaluation with radiologic imaging is important to determine if the treated tumor is completely necrotic and to detect any recurrence early. CT with contrast enhancement and angiography are the most useful for this purpose [5].

In our previous study [12], treated lesions did not enhance after IV contrast administration in CT examinations performed 1–6 months after the therapy, a period corresponding to devascularization of the lesions (Fig. 2). Angiography performed 3–6 months after therapy did not show tumor stain in any case (Fig. 3). Neither of these procedures showed evidence of viable cancer tissue in any case during that period. Complete necrosis is likely if the normal liver tissue at the periphery of the tumor does not enhance on CT scans.

Although the sonographic features of the tumor change after ethanol injection, sonography cannot be used to confirm complete necrosis of the tumor. In general, hypoechoic tumors become hyperechoic and hyperechoic tumors become heterogeneous after ethanol injections (Fig. 4) [12].

To detect any growth of a small amount of viable tumor, periodic imaging studies are essential. If recurrence of the tumor is detected, the lesion can be retreated by percutaneous injection of ethanol.

Evaluation of Efficacy by Serum Tumor Markers

Serum tumor markers such as alpha-fetoprotein and plasma-abnormal prothrombin [27] are useful to evaluate the efficacy of percutaneous ethanol injection providing the markers are elevated before treatment. In our study [12], serum

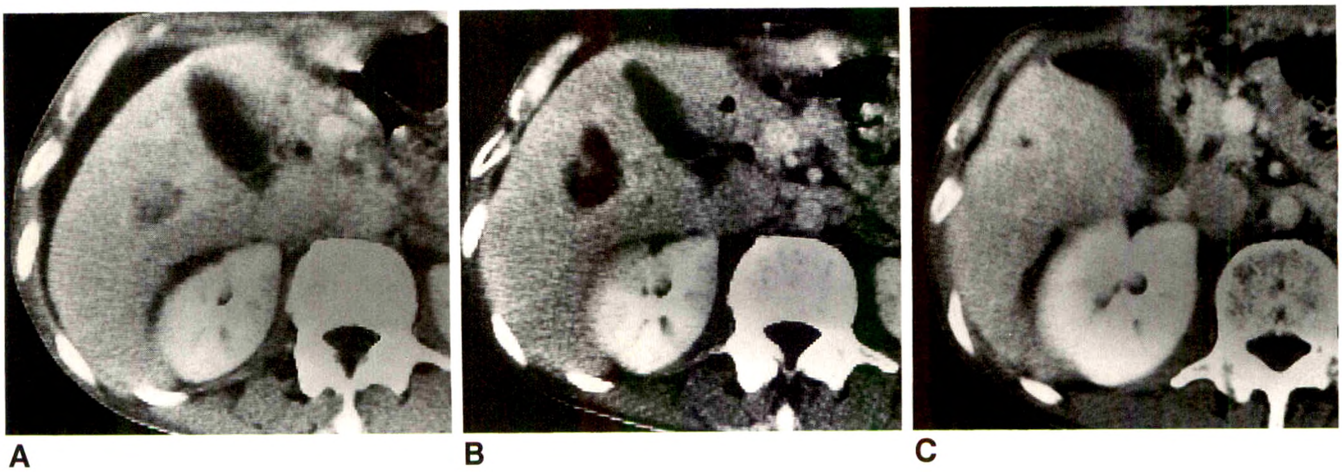

Fig. 2.—Hepatocellular carcinoma.
A, Before ethanol injection. CT scan with contrast enhancement shows hypodense solitary mass in right lobe.
B, 2 weeks after six injections. CT scan shows completely nonenhanced area in right lobe.
C, 1 year after treatment. CT scan shows decrease in size of nonenhanced area.

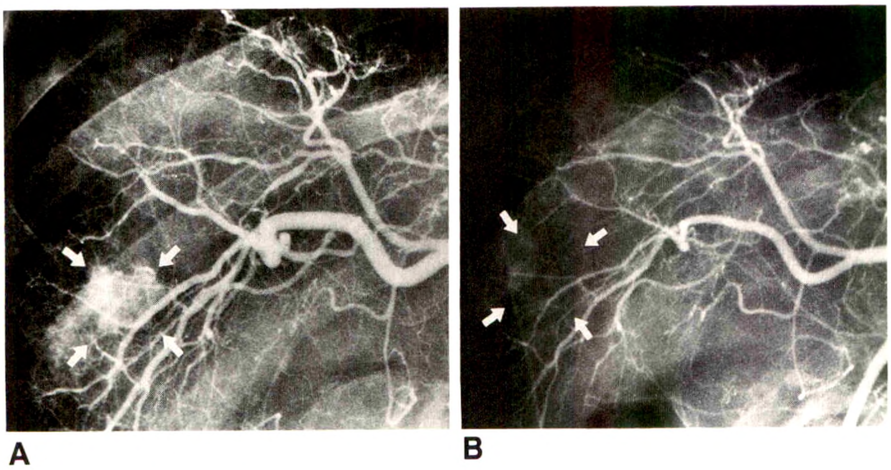

Fig. 3.—Hepatocellular carcinoma.
A, Before ethanol injection. Angiogram shows tumor stain 2 cm in diameter in right lobe (*arrows*).
B, 6 months after treatment. Tumor stain no longer exists (*arrows*).

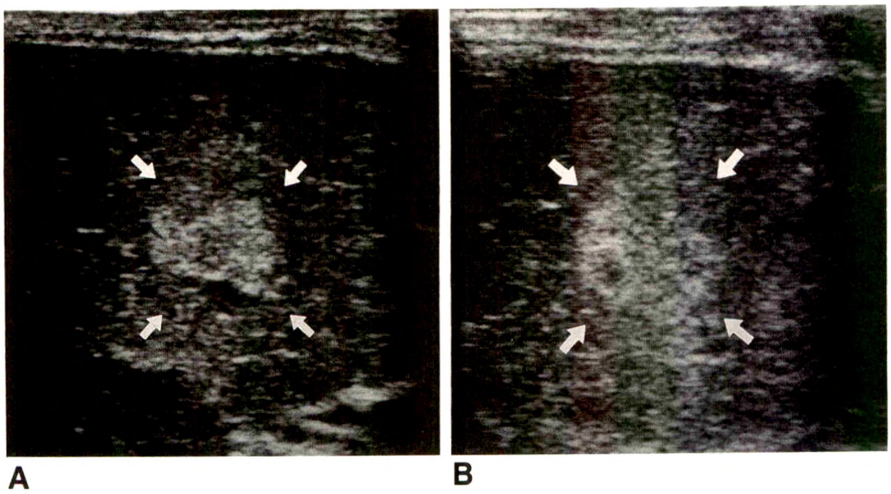

Fig. 4.—Hepatocellular carcinoma.
A, Before ethanol injection. Sonogram shows hyperechoic lesion in right lobe (*arrows*).
B, 1 week after six injections. Lesion is heterogeneous and its margin is indistinct (*arrows*).

alpha-fetoprotein levels decreased after therapy in all cases with a single lesion, if the serum alpha-fetoprotein level was more than 100 ng/ml before therapy.

Long-term Survival Rates

The follow-up periods have not been long enough to compare the long-term survival rates of patients treated by ethanol injection with those of patients treated by other techniques.

To date, the best study on long-term survival rates of patients treated by percutaneous ethanol injection is that of Ebara et al. [16]. They treated 59 cases of hepatocellular carcinoma in which the diameter of the tumor was 3 cm or less and the number of the lesions was not more than three by ethanol injection. They reported that the 1-, 2-, 3-, and 4-year survival rates were 96%, 86%, 79%, and 79%, respectively. They compared these long-term survival rates with those of 41 patients with tumors 3 cm or less in diameter who underwent surgical resection and concluded that the patients treated by ethanol injection had significantly higher survival rates than those who underwent hepatectomy. Although they used historical controls and the follow-up period was only 4 years, the results suggest that percutaneous ethanol injection can be an alternative to surgery for the curative treatment of small hepatocellular carcinoma. Livraghi et al. [17] reported that the 1-year survival rate of 12 patients was 92%. Randomized trials to compare long-term survival rates of patients treated by percutaneous ethanol injection with those of patients treated by other therapies have not been conducted.

New Devices and Methods for Percutaneous Ethanol Injection Therapy

For the treatment to be effective, the tip of the puncture needle must be accurately placed in the lesion. However, after repeated injections, the tumor often becomes difficult to identify. To solve this problem, Sheu et al. [28] implanted one or more small steel coils into the tumor before treatment. Even after the sonographic image of the tumor was obscured, they could still inject ethanol on the basis of the location of the coil. Their procedure, however, seems to be rather complicated. They have to puncture the lesion twice, first to place the coil and second to inject ethanol. Furthermore, they have to use relatively thick needles (18-gauge) so that the coil can be delivered through the needles.

We have found that a small amount of Gelfoam powder (Upjohn Co., Kalamazoo, MI) injected in the lesion can serve as a marker for ethanol injection [29]. As yet, percutaneous ethanol injection therapy has been limited to small lesions, because it is virtually impossible to inject ethanol throughout large lesions. However, if ethanol and Gelfoam are injected through the same needle, the exact place where the ethanol is injected can be identified afterward. Thus, by using the Gelfoam injection as a marker, it might be possible to inject ethanol into every part of large tumors.

Sheu et al. [28] designed a new puncture needle with multiple side holes to achieve more homogeneous and even distribution of the ethanol. Ido et al. [30] injected ethanol into the tumor under peritoneoscopic sonographic guidance. With this procedure, the patient did not need to hold his or her breath and the needle could be placed in the lesion for a long period. Thus, a large amount of ethanol could be injected at once, which enabled them to complete the therapy in one treatment session. Hirano et al. [31] reported that injection of a mixture of Lipiodol and ethanol showed the area of necrosis more accurately with CT.

REFERENCES

1. Prevention of liver cancer: report of WHO meeting. In: *World Health Organization technical report series*. Geneva: World Health Organization, **1983**:7–8
2. Kubo Y, Okuda K, Musha H, et al. Detection of hepatocellular carcinoma during a clinical follow-up of chronic liver disease. *Gastroenterology* **1978**;74:578–580
3. Liaw YF, Tai DI, Chu CM, et al. Early detection of hepatocellular carcinoma in patients with chronic type B hepatitis. *Gastroenterology* **1986**;90: 263–267
4. Liver Cancer Study Group of Japan. *Survey and follow-up study of primary liver cancer in Japan*, report 8. Kyoto: Shinko-insatsu, **1988**:63–85
5. Nakamura H, Tanaka T, Hori S, et al. Transcatheter embolization of hepatocellular carcinoma: assessment of efficacy in cases of resection following embolization. *Radiology* **1983**;147:401–405
6. Hsu HC, Wei TC, Tsang YM, et al. Histological assessment of resected hepatocellular carcinoma after transcatheter hepatic arterial embolization. *Cancer* **1986**;57:1184–1191
7. Yamada R, Kitayama K, Sato M, et al. Transcatheter arterial embolization in the treatment of primary liver cancer. In: *Diseases of the liver and biliary system*, vol. 2. Tokyo: Nihon Rinsho, **1988**:161–166
8. Bhardwaj S, Bruckner HW, Holland JF. Therapy of malignant tumors of the liver. In: Berk JE, Haubrich WS, Kalser MH, Roth JLA, Schaffner F, eds. *Bockus gastroenterology*, 4th ed. Philadelphia: Saunders, **1985**: 3388–3397
9. Sugiura N, Takara K, Ohto M, et al. Percutaneous intratumoral injection of ethanol under ultrasound imaging for treatment of small hepatocellular carcinoma. *Acta Hepatol Jpn* **1983**;24:920
10. Livraghi T, Festi D, Monti F, Salmi A, Vettori C. US-guided percutaneous alcohol injection of small hepatic and abdominal tumors. *Radiology* **1986**;161:309–312
11. Tagawa K, Muto H, Yasuda H, Unuma T, Shiina S. Therapeutic effects of ultrasonically guided ethanol injection for treatment of hepatocellular carcinoma. *Jpn J Med Ultrasonics* **1987**;14:743–744
12. Shiina S, Yasuda H, Muto H, et al. Percutaneous ethanol injection in the treatment of liver neoplasms. *AJR* **1987**;149:949–952
13. Sheu JC, Sung JL, Huang GT, et al. Intratumor injection of absolute ethanol under ultrasound guidance for the treatment of small hepatocellular carcinoma. *Hepatogastroenterology* **1987**;34:255–261
14. Suyama Y, Horishi M, Ebisui S, et al. US guided intratumoral ethanol injection therapy to small liver cancer: clinical evaluation for twenty cases. *Nippon Gan Chiryo Gakkai Shi* **1987**;22:818–826
15. Fujimoto T. The experimental and clinical studies of percutaneous ethanol injection therapy (PEIT) under ultrasonography for small hepatocellular carcinoma. *Acta Hepatol Jpn* **1988**;29:52–59
16. Ebara M, Nihei T, Ohto M. Intratumoral injection of absolute ethanol for treatment of small hepatocellular carcinoma. *Naika* **1988**;61:665–669
17. Livraghi T, Salmi A, Bolondi L, et al. Small hepatocellular carcinoma: percutaneous alcohol injection—results in 23 patients. *Radiology* **1988**;168:313–317
18. Ellman BA, Parkhill BJ, Curry TS, et al. Ablation of renal tumors with absolute ethanol: a new technique. *Radiology* **1981**;141:619–626
19. Yune HY, Klatte EC, Richmond BD, Rabe FE. Absolute ethanol in thrombotherapy of bleeding esophageal varices. *AJR* **1982**;138:1137–1141
20. Solbiati L, Giangrande A, Pra LD, Bellotti E, Cantú P, Ravetto C. Percutaneous ethanol injection of parathyroid tumors under US guidance: treatment for secondary hyperparathyroidism. *Radiology* **1985**;155:607–610
21. Imaoka S, Sasaki Y, Matsui Y, et al. Evaluation of intratumoral injection of an immunoprotentiator (OK-432) in patients with hepatocellular carcinoma. *Nippon Gan Chiryo Gakkai Shi* **1982**;17:1957–1962
22. Onodera H, Oikawa M, Abe M, Chida N, Kimura S, Gotoh Y. Ultrasonographically guided percutaneous direct injection therapy for unresectable hepatoma. *Jpn J Clin Radiol* **1986**;31:1461–1464
23. Livraghi T, Sangalli G, Vettori C. Adenomatous hyperplastic nodules in the cirrhotic liver: a therapeutic approach. *Radiology* **1989**;170:155–157
24. Shinagawa T, Iino Y, Ukaji H, et al. Percutaneous ethanol injection in the treatment of portal tumor thrombus in hepatocellular carcinoma. *Acta Hepatol Jpn* **1989**;30:109
25. Child CG III. *Hepatic circulation and portal hypertension*. Philadelphia: Saunders, **1954**
26. Kobayashi T, Ohto M, Sumida M, et al. A clinical and histopathological study on therapeutic effects of transcatheter arterial embolization for small hepatocellular carcinoma. *Nippon Shokakibyo Gakkai Zasshi* **1983**;80: 2574–2583
27. Fujiyama S, Morishita T, Hashiguchi O, Sato T. Plasma abnormal prothrombin (des-gamma-carboxy prothrombin) as a marker of hepatocellular carcinoma. *Cancer* **1988**;61:1621–1628
28. Sheu JC, Huang GT, Chen DS, et al. Small hepatocellular carcinoma: intratumor ethanol treatment using new needle and guidance systems. *Radiology* **1987**;163:43–48
29. Shiina S, Komatsu Y, Shiratori Y, et al. Sonographically guided percutaneous injection of ethanol for treatment of hepatocellular carcinoma: value of Gelfoam to mark the lesion (letter). *AJR* **1989**;153:430
30. Ido K, Hitomi N, Kawamoto T, Tanaka H, Ohtani M, Kimura K. Ethanol injection therapy for the treatment of small hepatocellular carcinoma under peritoneoscopic ultrasound guidance. *Acta Hepatol Jpn* **1988**;29:1121
31. Hirano M, Tohara K, Sakaguchi S, Okumura M. Therapeutic percutaneous injection of lipiodol-ethanol solution for hepatocellular carcinoma. *Acta Hepatol Jpn* **1989**;30:383–384

Memorial

Glen W. Hartman, Secretary of the ARRS, 1936–1990

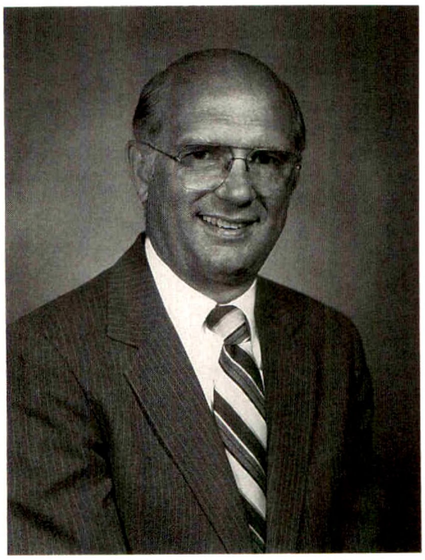

On February 18, 1990, the short life of Glen Hartman came to an abrupt end. His was a life full of achievement with a sure promise of more to come. An 18-month battle with malignant disease—a battle he appeared to be winning—took a quick turn with shocking and perhaps merciful suddenness.

Glen was educated at the University of Wisconsin, receiving his M.D. degree from that school in 1961. After his residency in radiology at the Mayo Graduate School of Medicine and an additional year of graduate study at the University College Hospital in London, he joined the staff of the Mayo Clinic where he remained one its most distinguished members until his death.

At the Mayo Clinic, Glen served as the chairman of the department of diagnostic radiology from 1975 to 1979 and as chairman of the Health-Related Sciences Education Committee. He was also president of the Mayo Clinic staff from 1985 to 1986. Perhaps his most prestigious appointment at that institution was as the first head of the newly formed Mayo Medical Ventures. Among other activities, he served as the publisher of the *Mayo Medical Newsletter*.

Teaching, writing, and publishing all came easily to him. In addition to his work in the education programs of national and international societies, he served as professor of radiology at the Mayo Medical School.

Despite serving in a busy department in which he helped develop uroradiology as a subspecialty, he had time for other activities, serving as president of the Minnesota Radiological Society and president of the Society of Uroradiology as well as a member of the committee on written examinations of the American Board of Radiology.

In the American Roentgen Ray Society, Glen was chairman of instructional courses from 1984 to 1986, when he assumed the post of secretary. At the time of his death, he was busy planning the next meeting. At that meeting the Gold Medal of the ARRS will be awarded to him posthumously.

He was so effective in all of these positions that he was constantly called upon to undertake new challenges. He served as chairman of the Intersociety Commission of the American College of Radiology as well as a member of the Board of Chancellors of that organization.

Because of his work on the Intersociety Commission, he became very interested in the potential for multisocietal activity. He conceived the idea of a centennial celebration of radiology in 1995. Working with every major radiologic society, he formed a separate corporation, Radiology Centennial Incorporated, which has been working under his leadership to make 1995 a banner year in radiologic history.

Glen loved radiology, the Mayo Clinic, his church, but most of all his family. He derived much of his strength, energy, and good humor from his wife, Dorothy, for theirs was a match made in heaven. He never boasted about his three children, Tom, Laura, and Bob, but with the slightest urging, his pride in them would burst forth and run like a Minnesota mountain stream. When he first learned of his illness, Glen never lost faith that as a family they could overcome almost anything.

Their loss is surely the greatest, but Glen was so important to our specialty that many of us feel his loss almost as keenly. When we celebrate the centennial of radiology in 1995 there will be something missing, but I shall try to fill that void by treating the event as a celebration of his life. It has been said that there is no indispensable man. Whoever believes that never knew Glen Hartman.

Raymond A. Gagliardi
Pontiac, MI 72903

Review Article

Physiology and Radiology of the Normal Oral and Pharyngeal Phases of Swallowing

Wylie J. Dodds,[1] Edward T. Stewart,[1] and Jeri A. Logemann[2]

During the past decade, considerable interest has developed in the radiologic examination of the oral and pharyngeal phases of swallowing [1]. This interest has been stimulated by advances in swallowing therapy. In this report, we review (1) the normal physiology of swallowing, (2) methods for radiologic examination of the mouth and pharynx, and (3) the radiologic appearance of normal oral and pharyngeal swallowing. See pages 965–974 for a report on abnormalities of swallowing and therapeutic techniques designed to improve abnormal oral and pharyngeal swallowing functions.

Normal Physiology

Swallowing normally occurs as an orderly physiologic process that transports ingested material and saliva from the mouth to the stomach [2, 3]. This process usually occurs so smoothly and effortlessly that it belies the complexity of the neuromuscular apparatus that executes and orchestrates the swallowing sequence. Generally, swallowing is considered to be voluntary because deglutition can be elicited by cerebral input when one thinks "swallow." Many swallows, however, particularly those between meals, occur without conscious input. Spontaneous swallowing occurs at about 1/min in awake subjects [4]. This high swallowing rate is initiated by salivation, which occurs at about 0.5 ml/min and must either be swallowed or expectorated. The high basal rate of swallowing during wakefulness leads to about 1000 swallows daily or 3 to 4 million per decade. Although the majority of swallows occur subconsciously in response to salivation, some saliva swallows are voluntary, and close clustering of voluntary swallows is evoked consciously during eating. During eating, swallowing is associated with increased salivation, which facilitates the initiation of swallowing and acts as a lubricant. During sleep, salivation and swallows nearly cease [5], but the awake pattern recurs rapidly during arousals from sleep.

Phases of Swallowing

For descriptive purposes, swallowing is divided into four phases: (1) preparatory phase, (2) oral phase, (3) pharyngeal phase, and (4) esophageal phase. The preparatory phase involves mastication of a bolus and mixing it with saliva. The bolus is sized, shaped, and positioned on the tongue ready for swallowing. During the oral phase, the bolus is propelled from the oral cavity into the pharynx. The normal pharyngeal phase involves bolus transport from the oropharynx into the esophagus without aspiration. During the esophageal phase, not discussed further in this report, the bolus is propelled the length of the esophagus into the stomach.

Anatomy

The anatomic components of the head and neck swallowing apparatus include (1) bony and cartilaginous support structures, (2) striated muscles, and (3) neural elements. The bony

---

Received October 10, 1989; accepted after revision November 21, 1989.

[1] Department of Radiology, the Medical College of Wisconsin, Froedtert Memorial Lutheran Hospital, 9200 W. Wisconsin Ave., Milwaukee, WI 53226. Address reprint requests to W. J. Dodds.

[2] Department of Communication Sciences and Disorders, Neurology and Otolaryngology–Head and Neck Surgery, Northwestern University, Evanston, IL 60208.

AJR **154:953–963, May 1990** 0361–803X/90/1545–0953 © American Roentgen Ray Society

maxillary palatal arch apposes the tongue during the oral phase of swallowing. Another solid structure is the hinged mandible that allows chewing during the preparatory phase, but becomes fixed in a closed position during swallowing. The pharyngobasilar fascia originates from the basiocciput of the skull and anchors the pharynx to the skull base. The cervical spine provides a firm but flexible posterior support for the pharynx. Membranous planes that ensheathe the pharynx allow its free axial movement during swallowing. Suspended by the suprahyoid musculature, the hyoid bone serves as an intermediate supporting structure for the larynx and platform for the tongue (Fig. 1). The thyrohyoid membrane and thyrohyoid muscles connect the larynx to the hyoid. The larynx forms the anterior wall of the hypopharynx, and the posterior tongue forms the anterior wall of the oropharynx.

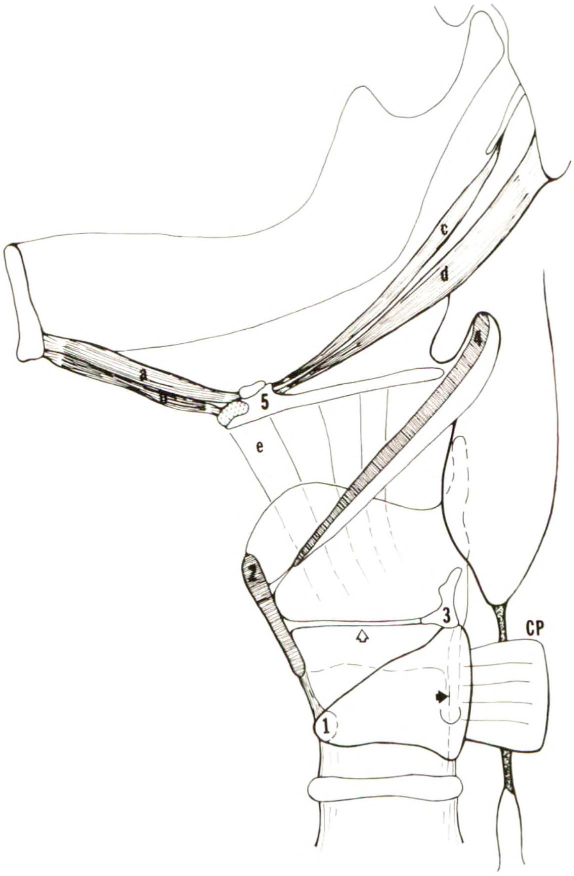

Fig. 1.—Schematic representation of suspension of hyoid and larynx. Hyoid (5) is suspended from mandible and skull by four suprahyoid muscles: anterior pair—geniohyoid (b) and anterior digastric (a); posterior pair—stylohyoid (c) and posterior digastric (d). These muscles generate a superior and anterior movement of hyoid during swallowing. Larynx is attached to hyoid by paired thyroglossus muscles (e) and thyrohyoid membrane (*not shown*). Larynx consists of following cartilages: epiglottic (4), thyroid (2), cricoid (1), and arytenoid (3). Epiglottis is attached anteriorly to thyroid cartilage, just superior to ventral attachment of vocal cords (*open arrow*) on thyroid cartilage. Posteriorly, vocal cords attach to vocal process of arytenoids. Arytenoids sit on superior margin of cricoid plate. Posterior border of trachea is indicated by *solid arrow*. Just below this arrow is a hinge joint between inferior cornu of thyroid cartilage and cricoid cartilage. Shortening of cricothyroid muscle (*not shown*) approximates anterior thyroid cartilage to anterior rim of cricoid cartilage. This movement passively tenses vocal cords and tucks introitus of laryngeal vestibule ventrally under free margin of epiglottis. During swallowing, larynx makes a superoanterior excursion because of its attachments to hyoid. Thyrohyoid muscles (e) contract so that larynx approximates and becomes locked to hyoid. Thus, superior movement of larynx exceeds that of hyoid. Shortening of thyrohyoid muscles also rotates epiglottis into a horizontal position. Because of its attachment to cricoid, cricopharyngeus (CP) moves superiorly about 1.5 cm during swallow-induced orad excursion of larynx.

Muscular Components and Their Innervation

A total of 31 paired striated muscles are involved during the preparatory and oral-pharyngeal phases of swallowing. The muscles of the mandible are supplied exclusively by the mandibular branch (V_3) of the trigeminal nerve. The facial-muscle movement, supplied by the facial nerve (VII), plays an important role during chewing. Tongue movement is the major action during chewing and during the oral phase of swallowing, as well as a major component of the pharyngeal phase of swallowing. Tongue movement is determined by the four intrinsic and four extrinsic muscles of the tongue. The intrinsic tongue musculature is innervated by the hypoglossal nerve (XII), and the four extrinsic muscles with the exception of the palatoglossus (X) are innervated by the ansa cervicalis (C_1–C_2), which courses with the hypoglossal nerve. The musculature of the soft palate is under vagal (X) control, except for the tensor veli palatini, which is innervated by V_3. With the exception of the stylopharyngeus, innervated by the glossopharyngeal nerve (IX), all of the pharyngeal muscles (constrictors and levators) including the cricopharyngeus, are innervated by the vagus. Further, the vagus innervates all the intrinsic muscles of the larynx. Seven paired laryngeal muscles are innervated by the vagal recurrent laryngeal nerves, and one pair (the cricothyroids) is innervated by the vagal superior laryngeal nerves. Hyoid and laryngeal movement are produced by suprahyoid and infrahyoid muscle groups innervated by V_3, VII, and the ansa cervicalis (C_1–C_2).

In summary, the muscles of mastication are all innervated by V_3, whereas cranial nerves XII and the ansa cervicalis (C_1–C_2) control the tongue. With few exceptions, the vagus (X) controls the muscles of the palate, pharynx, and larynx. Multiple cranial nerves regulate deglutitive movement of the hyoid and larynx.

Neural Control

The neural control of swallowing involves four major components: (1) efferent motor fibers contained in cranial nerves and the ansa cervicalis; (2) afferent sensory fibers contained in cranial nerves; (3) cerebral, midbrain, and cerebellar fibers that synapse within the midbrain swallowing centers; and (4) paired swallowing centers located in the brainstem. Fibers from the higher CNS centers and oral-pharyngeal sensory fibers send input signals to the brainstem swallowing centers that process the information. Output signals pass via the cranial nerves that operate the muscle machinery of swallowing.

Input Afferent Signals

Sensory cranial nerve input that initiates swallowing goes directly to the swallowing centers, and is provided mainly by cranial nerves IX and X, with some participation by the maxillary branch (V_2) of the trigeminal and facial (VII) nerves. The facial nerve provides taste fibers over most of the tongue and, of course, touch sensation for the lips and face. The superior laryngeal nerve of the vagus contains sensory fibers for the posterior larynx, base of tongue, and hypopharynx.

Optimal stimuli that elicit swallowing show regional variation [2]. For example, the most effective stimulus is light touch at the fauces, and water in hypopharynx and aditus of the larynx. Taste sensation is a weak stimulus for swallowing. Authorities believe that coded sensory information of a given pattern and intensity from a receptive field of the orad cavity, tongue, and pharynx serves as the major trigger for swallowing. Stimuli, such as the conscious intent to swallow, are thought to facilitate existing input stimuli that are already present as background stimuli. Sensory pharyngeal signals that differ from the code needed to evoke a swallow may elicit a gag, cough, or other patterned responses that use the same muscles as swallowing.

Brainstem Swallowing Centers

Paired swallowing centers reside in the hindbrain. Studies in the dog suggest that only one intact center is needed for normal swallowing [6]. The swallowing centers are not discrete focal areas (Fig. 2), but rather, consist of poorly defined broad areas comprising the nucleus tractus solitarius and ventromedial reticular formation. Input sensory fibers from the cranial nerves and higher cerebral centers synapse within the nucleus tractus solitarius or reticular formation. Thus, each swallow center consists of an elaborate array of interneurons, or neuropil, that processes incoming information, generates a preprogrammed swallowing response, and distributes the appropriate signals to cranial nerve motor nuclei and their axons, which then deliver neural signals to the many muscles involved in swallowing.

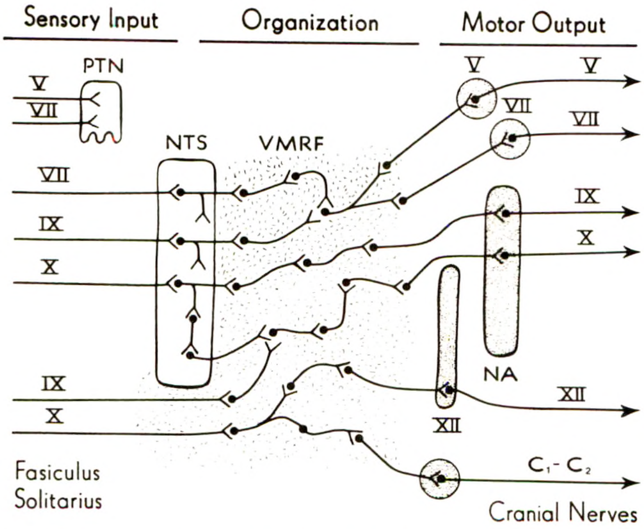

Fig. 2.—Schematic representation of brainstem swallowing center. Swallowing centers are paired, but only one is shown. Sensory input from V_2, VII, IX, and X nerves that trigger swallowing is carried mainly to nucleus tractus solitarius (NTS). Afferent input from V_2 and VII also synapse in primary trigeminal nucleus (PTN) and some fibers reach NTS. An area comprising ipsilateral NTS and ventral medial reticular formation (VMRF), a neuropil with multiple interneurons and synaptic connections, constitutes each of the paired swallowing centers. When swallowing center receives appropriate afferent information from periphery or from higher cranial centers (*not shown*), preprogrammed swallowing response is triggered. Muscle machinery of swallowing response is driven by motor neurons that leave swallowing center and synapse in cranial nerve nuclei on ipsilateral side. Lower motor neurons to muscles that execute swallowing run in cranial nerves V_3, VII, IX, X, and XII as well as in ansa cervicalis (C_1–C_2).

Two major hypotheses have been proposed to describe the neural control mechanism that executes the oral and pharyngeal phases of swallowing: (1) the reflex-chain hypothesis and (2) the central pattern generator hypothesis. According to the reflex-chain hypothesis, a bolus moving through the mouth and pharynx stimulates sensory receptors that sequentially trigger the next step in the swallowing sequence. Even in the absence of a bolus, the posterior excursion of the tongue is thought to stimulate faucial or pharyngeal mechanoreceptors that trigger the pharyngeal swallow. In practical terms the concept of "pharyngeal triggering" is widely used as an operational definition by swallow therapists who treat patients with abnormal swallowing.

The second hypothesis suggests that once swallowing is initiated, it is programmed in a stereotyped manner by the network of nerves in the brainstem swallowing centers, which function independently of any sensory feedback. Currently, evidence exists to support elements of both the reflex-chain and central pattern generator hypotheses. We believe that swallowing occurs as a basic medullary program that may be modified by certain bolus variables, such as volume and consistency [7–10], or in some instances, by voluntary control. For example, swallowed bolus volume alters many of the variables of the swallow sequence, such as the timing and duration of upper esophageal sphincter (UES) opening, but it does not alter other variables such as the magnitude of pharyngeal contraction.

Radiologic Examination

The specific methods used to evaluate the oral and pharyngeal phases of swallowing vary among examiners and whether the examination is being done by a radiologist for a diagnostic evaluation alone, or by a radiologist and speech therapist for diagnosis and assessment of therapy for a "safe swallow" without aspiration. The radiologic examination should include an evaluation of oral and pharyngeal morphology as well as function. Both types of examinations require posteroanterior as well as lateral views [11]. The esophagus should also be elevated. The optimal filming method for oral and pharyngeal morphology is the spot film, whereas imaging for function requires rapid filming, such as videofluorography or cineradiography. We prefer videofluorography to alternative methods because of its lower cost and level of radiation as well as better playback capabilities. In general, optimal examination for morphology is obtained with double-contrast images made with high-density barium (250% wt/vol), and examination for function is done with thin barium (30% wt/vol), thick barium (250% wt/vol), and paste barium. For studies of function, more than one bolus volume is desirable (e.g., 2–10 ml). Of interest is the fact that the radiologic evaluation of oral-pharyngeal function is an extension of the neurologic function of specific cranial nerves.

The sequencing and filming method requires careful consideration by each examiner. For initial swallows, we prefer a small 2- to 3-ml barium bolus in case the patient exhibits substantial aspiration; a small amount of aspiration does not necessarily terminate the examination and allows additional swallows, to increase the sample size of observation. If the patient tolerates a small 2- to 3-ml bolus, then we proceed to larger bolus sizes, such as 5 and 10 ml and, occasionally, 20 ml. In the search for suspected aspiration, we always use a thin barium preparation and a large barium bolus (e.g., 10 ml) when aspiration is not observed for a 2-ml bolus. When laryngeal penetration or aspiration occurs, we test thick barium, a paste barium bolus, and often different head positions and other therapeutic maneuvers that may prevent aspiration. The examination is terminated if the patient aspirates a substantial amount of barium with each swallow or if the aspirated barium passes below the sternal notch.

After completion of the oral and pharyngeal examinations, the esophagus also should be examined by conventional methods. A limited examination of the esophagus should be attempted even when the delivery of barium to the esophagus is difficult in patients with severe aspiration. A careful search is done for obstructing esophageal lesions (e.g., strictures or rings), abnormal esophageal motor function, and gastroesophageal reflux.

Characteristics of Normal Oral-Pharyngeal Swallowing on the Lateral Projection

A series of images from normal oral-pharyngeal swallowing of a 10-ml bolus of thin barium is shown in Figure 3. The entire swallowing sequence lasts about 1.0–1.5 sec (oral phase about 0.5 sec and pharyngeal phase about 0.7 sec). The oral-pharyngeal swallow is quicker than the eye. Therefore, even rapid filming with 105 images is skimpy because its practical frame rate of 4–6/sec is marginal for adequate coverage of the swallowing sequence. However, imaging at a frame rate of 30/sec by videofluorography or cineradiography is sufficient. These methods allow subsequent slow-motion playback and frame-by-frame analysis.

Bolus Preparation

As part of the bolus preparation, an oral liquid bolus is generally positioned on the dorsum of the tongue, with the tongue tip pressed against the posterior aspect of the maxillary incisors or maxillary alveolar ridge [12]. This initial bolus position leads to the common tipper-type swallow (Fig. 4A). Most of the bolus is located within the midline groove of the tongue (Fig. 5A) and in a spoonlike depression of the mid tongue (Fig. 4A). The posterior part of the tongue elevates against the soft palate, which pushes downward to keep the bolus from escaping from the mouth with premature bolus entry into the pharynx. Thus, closure of the posterior tongue against the soft palate [13, 14] functions as a glossopalatal sphincter.

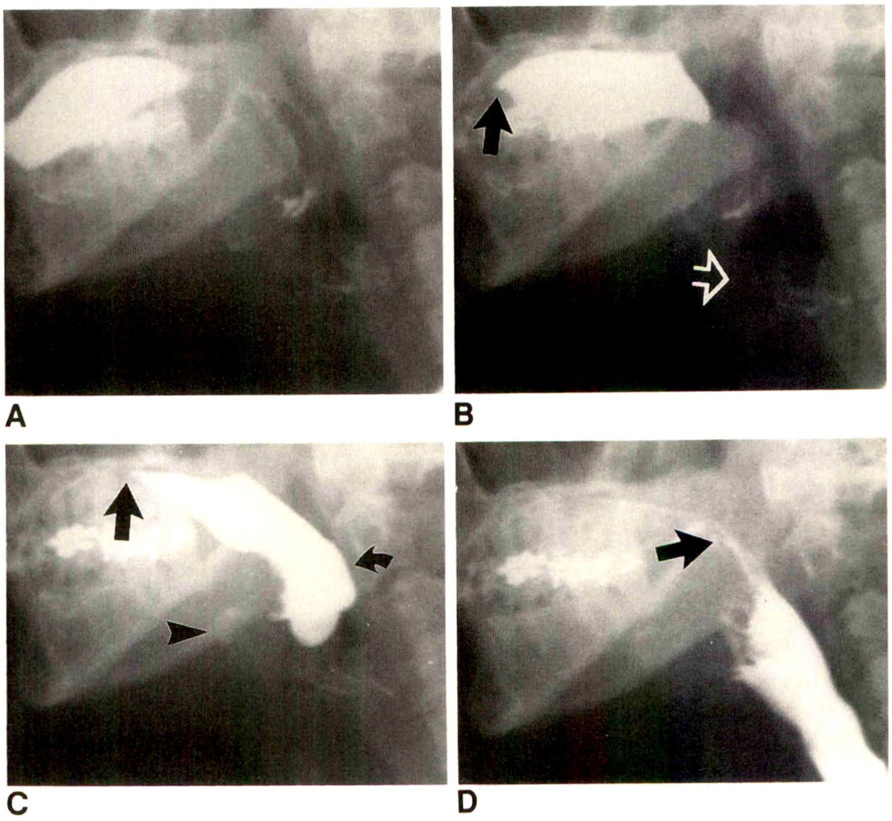

Fig. 3.—Overview of oral and pharyngeal swallowing sequence in a normal subject. Four images taken 0.03 sec apart during swallowing sequence of 10-ml barium bolus.

A, Bolus is positioned in supralingual position with tongue tip against maxillary incisors. Posterior oral cavity is sealed off from oropharynx by approximation of posterior tongue and soft palate.

B, With initiation of swallowing, superior surface of tongue makes sequential contact (*solid arrow*) with hard palate in peristaltic sequence that begins to propel bolus into oropharynx. Bolus head is just reaching fauces. Air is seen in open laryngeal vestibule (*open arrow*).

C, Small amount of air still remains in laryngeal vestibule. As glossopalatal sphincter opens, tongue base moves forward and palate moves upward and backward to make contact with posterior pharyngeal wall (*curved arrow*), thereby sealing off nasopharynx. Hyoid (*arrowhead*) is well into its orad excursion and now overlaps posterior mandible. Little air is seen in laryngeal vestibule. Head of bolus fills valleculae. Tail of bolus (*straight arrow*).

D, Mouth is now empty of barium, and peristaltic stripping wave is seen at bolus tail (*arrow*) in oropharynx. Hyoid has moved further orad, and closed vestibule is now devoid of air. Valleculae are empty. Upper esophageal sphincter is fully open, and barium flows freely across sphincter into cervical esophagus.

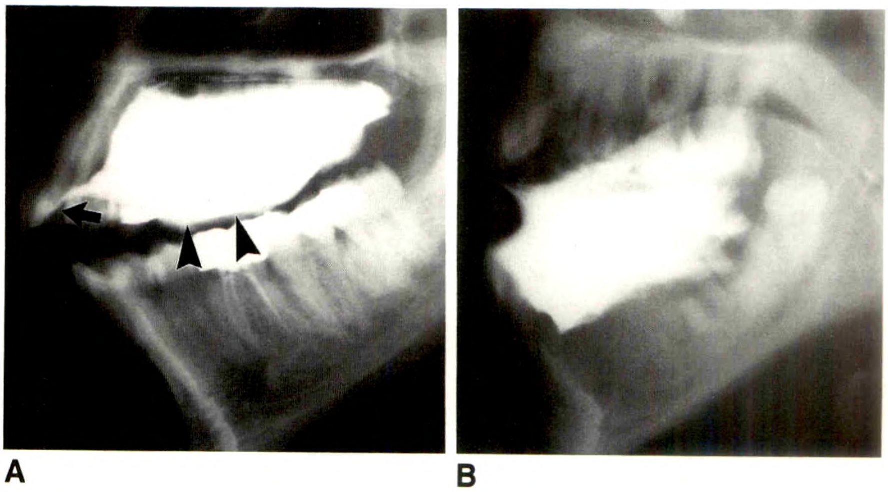

Fig. 4.—Initial bolus and tongue position for two major types of normal oral swallow. Both examples are with 10-ml bolus of barium.

A, Tipper swallow. Tip of tongue (*arrow*) is positioned immediately behind and in contact with maxillary incisors and maxillary alveolar ridge. Bolus is stored in spoonlike depression (*arrowheads*) on dorsum of tongue. With onset of swallowing, tongue tip sweeps posteriorly with powerful peristaltic motion to deliver bolus into oropharynx.

B, Dipper swallow. At onset of swallowing, major part of bolus is beneath tongue tip in anterior sublingual meatus (tongue tip obscured by barium). With onset of swallowing, tongue tip must dip beneath bolus in a scooping motion to elevate bolus to a supralingual position. Then tongue motion proceeds as in tipper-type swallow.

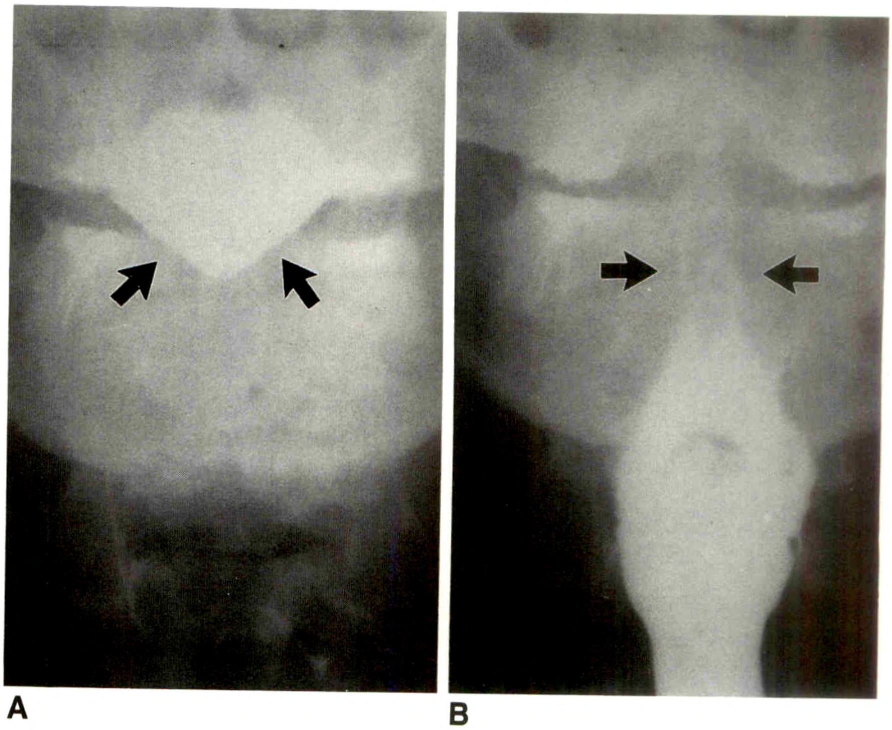

Fig. 5.—Posteroanterior projections of barium swallow in normal subject.

A, Just before swallowing begins, barium is seen nestled in deep midline groove (*arrows*) on posterior half of tongue.

B, During early pharyngeal phase of swallowing, barium has entered oropharynx. Superior constrictors approximate one another (*arrows*) in coronal plane.

Oral Phase of Swallowing

As a variant of normal, some subjects exhibit a dipper-type swallow wherein the bolus is initially located beneath the anterior tongue, within the anterior sublingual sulcus (Fig. 4B). With the bolus in this position, the tongue at the onset of swallowing must dive beneath the bolus to scoop it to a supralingual position. With this motion, the tongue tip reaches the posterior aspect of the maxillary incisors and the dipper- and tipper-type swallows then proceed in the same manner [12]. The anterior two-thirds of the tongue elevates as a globular mass to make sequential peristaltic contact with the hard palate to impart a V-shaped configuration [15, 16] to the bolus tail (Fig. 6B).

The tongue rolls posteriorly in pistonlike motion to thrust the bolus into the oropharynx. Concurrently, the base of the tongue moves downward and forward to expand the hypopharynx and provide a chute down which the bolus flows into the pharynx (Fig. 6C). Simultaneously, the palate moves upward to open the zone of the glossopalatal sphincter, thereby further facilitating flow between the oral and pharyngeal cavities (Fig. 6C). Concurrently, the palate contacts the posterior pharyngeal wall to seal off the nasopharynx from the oropharynx and thereby prevent nasal regurgitation. This sealing movement of the palate is more than simply an upward swing of a trap door. Rather, the side walls of the nasopharynx, comprising the superior pharyngeal constrictors, also oppose one another (Fig. 5B) to make a forceful circular closure.

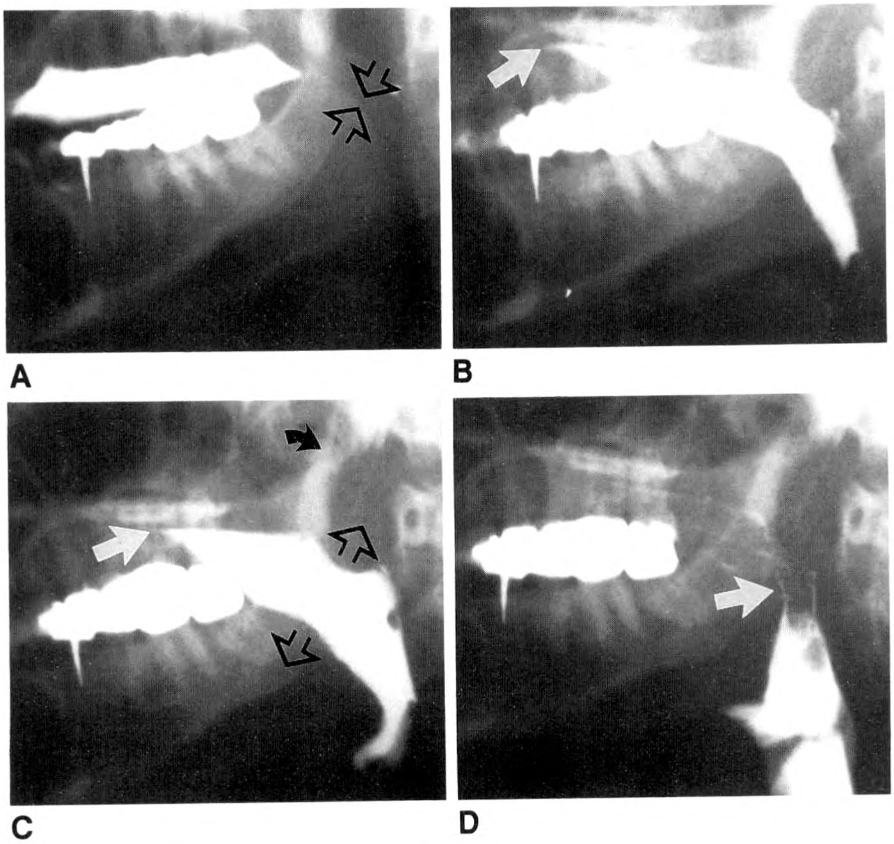

Fig. 6.—Opening of glossopalatal sphincter during 10-ml barium swallow in normal subject. *Straight solid arrows* indicate tail of barium bolus, which is propelled by peristaltic sequence of tongue against palate or against pharyngeal constrictors.

A, Bolus positioned in mouth. Glossopalatal sphincter (*open arrows*) is closed and thereby prevents barium from spilling prematurely into pharynx.

B, Oral swallow initiated. Glossopalatal sphincter has opened and barium begins to enter oropharynx.

C, Glossopalatal sphincter now fully open (*between open arrows*) and barium flows down chute into pharynx. Tongue base (*lower open arrow*) has moved forward to expand pharynx. Soft palate (*upper open arrow*) has moved posteriorly to open oral-pharyngeal junction and also seal off nasopharynx. Prominent posterior bulge or buckle (*curved arrow*) of soft palate is caused by contraction of levator veli palatini.

D, Tail of bolus (*arrow*) is in oropharynx, and glossopalatal sphincter has closed as tongue base moves backward to contact posterior pharyngeal wall.

In addition to elevation of the soft palate, several other events occur that make room for the swallowed bolus to enter the oropharynx. The posterior tongue (Fig. 6), hyoid, and larynx move upward and forward to expand the pharynx in the sagittal plane. In effect, the bolus slides down the ramp, or chute, created by the flattening and forward movement of the posterior tongue (Figs. 6B and 6C). Additionally, shortening of the pharyngeal levators (e.g., stylopharyngeus) serves to expand the transverse diameter of the pharynx (Fig. 7B).

Pharyngeal Phase of Swallowing

As the bolus enters the oropharynx, the posterior tongue makes a rapid posterior pistonlike motion to drive the bolus through the oropharynx into the hypopharynx (Fig. 6D). The posterior chamber for the posterior lingual piston is formed by the posterior pharyngeal wall, which stiffens because of the sequential contraction of its three constrictors (superior, middle, and inferior). Thus, bolus pulsion through the pharynx is a combination of posterior tongue thrust and sequential caudally oriented contraction of the pharyngeal constrictors [17]. Similar to its appearance in the oral cavity (Fig. 6), the bolus tail in the pharynx has a V-shaped configuration [15, 18]. Because the bolus head moves faster than the bolus tail, the bolus elongates in the pharynx, acts as a force that contributes to UES opening, and rapidly enters the proximal esophagus. Normal UES opening occurs in a generous unrestricted fashion (Fig. 3D). The diameter of sphincter opening depends directly on the volume of the swallowed barium bolus [19].

Normally, the oral phase and pharyngeal phases of swallowing are coupled so tightly together that the first oral phase blends in smoothly with the second pharyngeal phase. Some believe that the oral phase of swallowing triggers the pharyngeal phase when the posterior tongue compresses the tonsillar pillars or delivers a bolus into the oropharynx. An alternative possibility is that the relationship between the oral and pharyngeal phases of swallowing is mainly programmed by the brainstem swallowing center.

The normal pharyngeal phase of swallowing involves (1) palatal closure, (2) bolus transport through the pharynx, (3) glottal closure to prevent aspiration, and (4) UES opening and transsphincteric fluid flow. We propose that normal UES opening involves four elements: (1) transient relaxation, about 0.5 sec, of a tonically contracted UES; (2) low compliance, or easy stretchability, of the relaxed UES; (3) forward traction on the relaxed compliant UES by anterior movement of the hyoid, which acts on the larynx; and (4) radial pressure forces within an oncoming bolus that fully distend the relaxed UES, once it is opened initially by hyoid traction [19]. Manometric studies demonstrate that the resting UES exhibits a high-pressure zone that is higher posteriorly and anteriorly than laterally because of the cricopharyngeal configuration [20]. Pullthroughs of pressure sensors across the UES indicate that the cricopharyngeus is the major muscle element of the UES [19, 21]. During swallowing the UES high-pressure zone

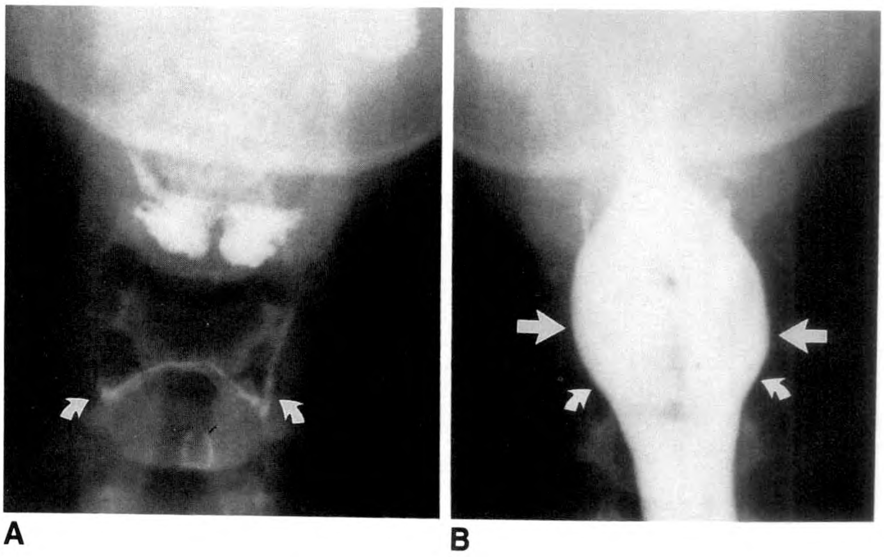

Fig. 7.—Posteroanterior view. Effacement of piriform sinuses during barium swallow in normal subject.

A, Before swallowing begins, piriform sinuses (*arrows*) are seen outlined with barium.

B, During pharyngeal phase of swallowing, piriform sinuses (*curved arrows*) have moved upward and are effaced. Coronal diameter of pharyngeal side walls (*straight arrows*) has increased. Upper esophageal sphincter is at junction of funnel-shaped pharynx and straight tube of cervical esophagus.

as well as its underlying electromyographic activity relax. In fresh anatomic specimens, the atonic compliant cricopharyngeus is readily stretched by gentle traction.

At the onset of swallowing, the hyoid, because of contraction of the suprahyoid muscles, begins an orad excursion that has superior and anterior components (Fig. 8). The larynx moves with the hyoid because of interconnections (Fig. 1) of the thyrohyoid membrane, and paired thyrohyoid muscles. Therefore, the larynx moves forward along with the anterior movement of the hyoid. Thus, the hyoid exerts traction on the larynx, which imparts anterior traction on the cricoid, which in turn exerts forward traction on the UES. This anterior traction force causes an initial opening (about 6 mm) of the relaxed UES [19].

Once the UES is open, the swallowed barium bolus begins to enter the sphincter segment. When the sphincter segment is penetrated by the barium bolus, pressure forces within the bolus serve to further expand the UES segment. In some instances, a faint transient bulge of the cricopharyngeus is seen during the swallowing sequence. This slight indentation of the cricopharyngeus is normally transient and rapidly disappears (Fig. 9). Generally, however, the UES segment opens fully without a trace of a cricopharyngeal indentation. The duration of UES opening and UES diameter depend directly on bolus volume and viscosity [10, 19]. Superior hyoid movement lasts about 1.2 sec, straddles the oral and pharyngeal phases of swallowing, and persists from the onset of the swallow until the end of the swallow. UES opening and closing occur while the hyoid and larynx are near or at the apogee of their oral excursion (Fig. 8).

During the pharyngeal phase of swallowing, the laryngeal vestibule closes for about 0.6–0.7 sec, beginning just before UES opening (Fig. 10). Closure of the vestibule depends largely on movement of the epiglottis, which is governed mainly by contraction of the thyrohyoid muscles (Figs. 11 and 12). Deglutitive epiglottal movement occurs as a two-step process [22]. First, the epiglottis moves from an upright to a horizontal position, caused mainly by elevation of the hyoid and larynx as well as by contraction of the paired thyrohyoid muscles. The flip of the free margin, or tongue, of the epiglottis is accomplished mainly by the aryepiglottic and thyroepiglottic muscles once the epiglottis is horizontal, by using the approximated arytenoids as a fulcrum. Contraction of these muscles also acts as a sphincter at the laryngeal introitus. The elastic epiglottis rapidly flips downward. In some cases, however, an elongated epiglottis is mechanically blocked from flipping downward by the posterior pharyngeal cervical wall, cervical spine, or indwelling nasogastric tube. The beginning of vestibular closure corresponds to horizontal movement of the epiglottis, which acts in a bellowslike movement to empty gas rapidly from the vestibule. Thus, initial vestibular closure ejects a puff of gas into the pharynx; this tends to help prevent swallowed material from entering the airway. Vestibular closure alone, however, does not guarantee a lack of barium penetration. In some normal subjects slight barium penetration of the vestibule is seen on one or two barium swallows, particularly the initial swallow (Fig. 9). Such penetrations are generally cleared rapidly during the swallow.

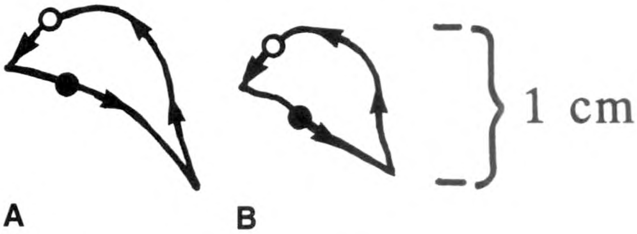

Fig. 8.—*A* and *B*, Oral excursion loops made by hyoid in normal subject during swallowing 10-ml (*A*) and 1-ml (*B*) boluses of barium. *Arrows* indicate direction of movement. *Open circles* indicate upper esophageal sphincter opening; *solid circles* indicate closure. Note that hyoid makes a greater superior and anterior excursion for 10-ml bolus than for 1-ml bolus.

To this point, we have discussed the evaluation of the normal oral and pharyngeal swallow nearly entirely in qualitative terms. During the past several years, however, considerable effort has developed to quantify swallowing [7, 18, 23,

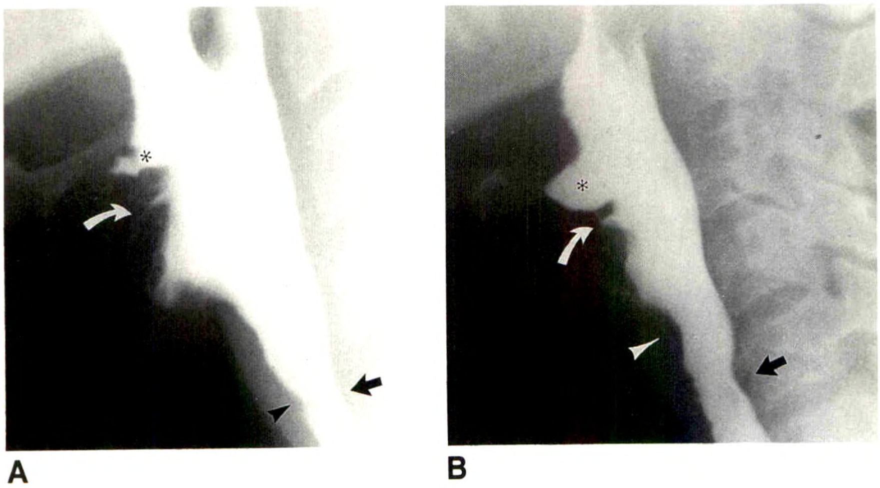

Fig. 9.—Examples of mild posterior bulge (*straight arrows*) of cricopharyngeus during pharyngeal phase of 10-ml barium swallow in two young healthy volunteers. Also seen in both examples is a postcricoid impression (*arrowheads*) and mild penetration (*curved arrows*) of laryngeal vestibule. Valleculae (*asterisks*).

A, 22-year-old man. Mild cricopharyngeal impression disappeared later during pharyngeal swallow of laryngeal vestibule.

B, 25-year-old man. Mild cricopharyngeal impression was not seen during 15-ml barium swallow. Ventricular penetration of barium was eliminated later during pharyngeal swallow.

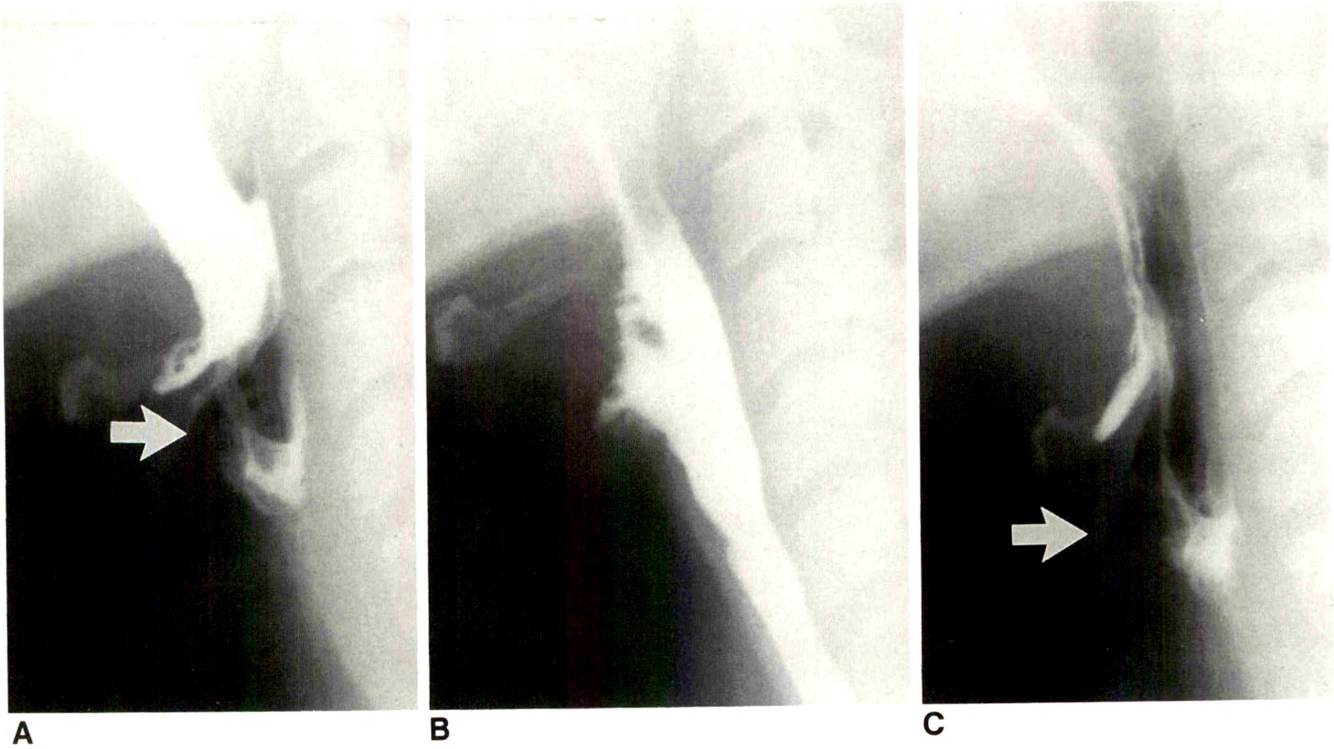

Fig. 10.—Closure and opening of laryngeal vestibule during 10-ml barium swallow in a normal subject.

A, Head of bolus has just reached valleculae and free margin of epiglottis is upright. Air is seen in open laryngeal vestibule (*arrow*).

B, Laryngeal vestibule is now closed and devoid of air. Barium flows freely across open upper esophageal sphincter.

C, Pharyngeal swallowing now complete. Laryngeal vestibule has reopened and is refilled with air (*arrow*).

24]. Such efforts involve assessment of the relative timing of events in the swallowing sequence, for example, timing of events (e.g., vestibular closure), calculation of durations (e.g., UES opening), and measurement of distances (e.g., hyoid movement). Initially, these measurements were done entirely by hand, but recently have been aided by computer methods [24].

The two primary functions of pharyngeal swallowing are to transport a swallowed bolus through the pharynx while protecting the airway from aspiration. A number of mechanisms converge to achieve airway protection. Many mechanisms that contribute to airway protection also contribute to bolus transport. For example, during hyoid elevation and thyrohyoid shortening, the glottis becomes locked to the hyoid as a single unit so that the angle of the laryngeal introitus tilts forward and downward so that it is protected by the overhanging epiglottis. Additionally, elevation of the larynx and UES shorten the distance that a bolus must travel and, therefore, the interval for potential aspiration. Opening of the UES by a liquid bolus requires only a low intrabolus pressure

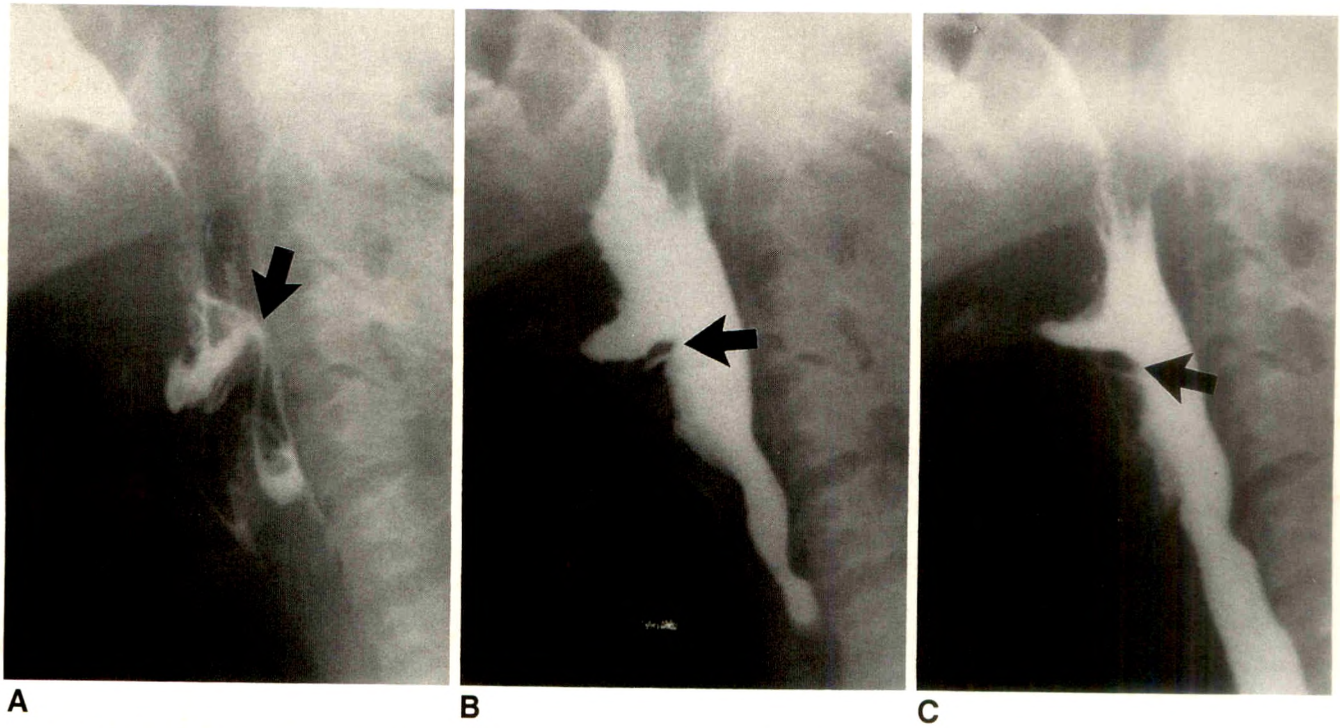

Fig. 11.—Epiglottal movement during swallowing of 10-ml barium bolus in normal subject. Images separated by 0.03-sec intervals.
A, Bolus head is just leaving mouth. Epiglottis (*arrow*) is obliquely upright.
B, Bolus head has just entered region of upper esophageal sphincter. Epiglottis (*arrow*) is now horizontal.
C, Upper esophageal sphincter is now fully open, although there is a slight impression from cricopharyngeus. Barium flows freely into cervical esophagus. Free margin, or tongue, of epiglottis (*arrow*) has flipped caudally. Laryngeal vestibule (not well seen) is closed.

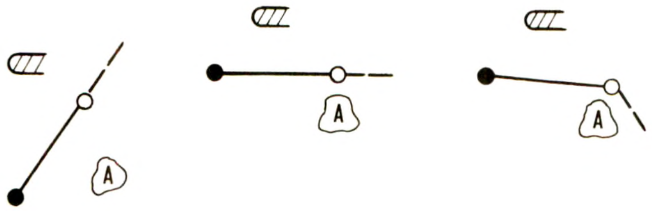

Fig. 12.—Schematic representation of normal epiglottal movement during swallowing. Hyoid is marked by hatching. A = Arytenoid cartilage. Body of epiglottis is attached to hyoid cartilage at *solid circles*, and *open circles* indicate junction of body and tongue of epiglottis. During resting conditions (*left*) epiglottis exhibits a vertical oblique position. During swallowing, hyoid (middle) epiglottis and larynx all move superiorly. Epiglottis acquires a horizontal orientation. During middle phase of pharyngeal swallow (right), arytenoid cartilages have approximated one another to close vocal cords (*not shown*) and moved forward to contact the body of epiglottis. In this position, arytenoids (A) act as a fulcrum to give a mechanical advantage over which free margin of epiglottis bends to flip caudad. This flip is executed mainly by contraction of aryepiglottic and lateral thyroepiglottic muscles.

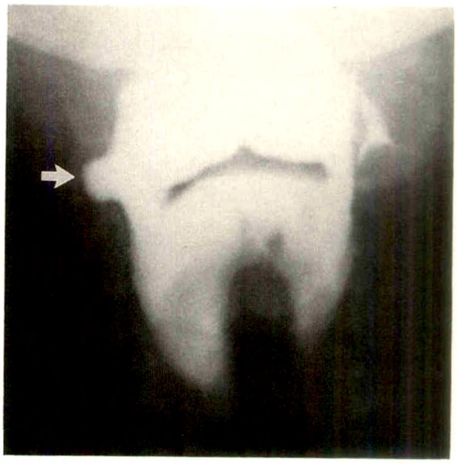

Fig. 13.—Posteroanterior image of 5-ml barium swallow in asymptomatic subject. Smooth right-sided pharyngeal pouch (*arrow*) appeared early during pharyngeal phase of swallowing (i.e., 0.5 sec after onset of swallowing) and disappeared by middle part of pharyngeal phase (i.e., by 0.8 sec). Barium is seen to split at horizontal free margin of epiglottis (horizontal filling defect in the barium column) and flow mainly down lateral side channels of pharynx.

in the pharynx so that only a low-pressure gradient exists between the bolus and larynx [19]. Intrinsic muscles of the glottis forcefully approximate the true vocal cords. Effacement of the piriform sinuses creates lateral food channels so that the bolus generally deviates laterally around the epiglottis (Fig. 13), thereby making minimal contact with the closed vestibule. Any residual fluid trapped in the piriform sinus after the swallow is normally at a lower level than the laryngeal vestibule, thereby retarding aspiration after the swallow. Overall, the larynx closes from below upward: first, the vocal cords, then the false cords (in some cases), then the lower vestibule (approximation and forward movement of the arytenoids), and then the upper vestibule (horizontal position of

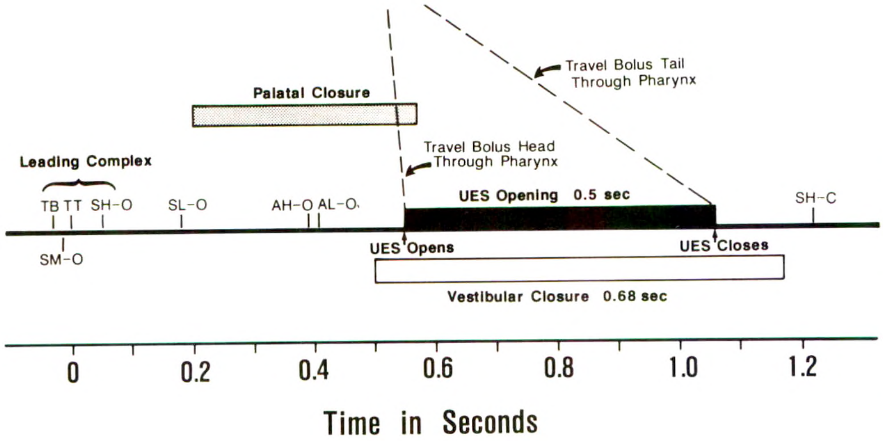

Fig. 14.—Time line of 5-ml barium bolus swallow in normal subject. Reference time of zero is used as onset of propulsive tongue tip (TT) movement at maxillary incisors. This movement begins to propel bolus toward pharynx. Other notations include tongue base movement (TB), onset of superior hyoid movement (SH-O), onset of submental electric activity (SM-O), onset of superior laryngeal movement (SL-O), onset of anterior hyoid movement (AH-O), onset of anterior laryngeal movement (AL-O), and completion of superior hyoid movement (SH-C). Palatal closure occurs as barium bolus flows from mouth into oropharynx. *Broken lines* indicate flow of bolus head and tail, respectively, through pharynx. Upper esophageal sphincter (UES) opening occurs when bolus head reaches UES; UES closes when bolus tail reaches sphincter. In this example, closure of laryngeal vestibule straddles the interval that the bolus is in the pharynx. Entire swallowing sequence lasted about 1.2 sec.

the epiglottis contacts closed arytenoids). Opening of the larynx proceeds from above downward.

One useful method for quantifying swallow-related events is the time line (Fig. 14). The initial events in swallowing include onset of superior hyoid movement, onset of submental electromyographic activity [18], and vocal cord closure. These events form the leading complex of swallowing. In most swallows, vocal cord closure is the first event and vocal cord opening the last event. Events in the leading complex generally occur within 0.1–2.0 sec of one another. Next, the onset of palatal closure occurs at about 0.35 sec before UES opening. The onset of anterior hyoid movement occurs about 0.15 sec before UES opening. UES opening with transsphincteric flow for a 5-ml barium bolus last about 0.5 sec. UES closure occurs as the pharyngeal peristaltic wave reaches the UES. Oral transit time (tail of bolus at maxillary incisors until it reaches the fauces) measured by videofluoroscopy is the equivalent of that measured by manometry because passage of the barium tail by a manometric sensor corresponds to the upstroke onset of the manometric pressure complex [16]. Because of the way it is measured, oral transit, about 0.5 sec, equals oral clearance time [18]. Pharyngeal transit, about 0.7 sec, is measured in the same manner as oral transit. However, pharyngeal transit (entry bolus head into pharynx until tail reaches UES) is faster than pharyngeal clearance because the bolus head enters the pharynx before the bolus tail. These distinctions need to be recognized when making such measurements and comparing measurements between studies.

Appearance of Normal Swallow on Frontal Projection

For assessment of the first two phases of swallowing, the mouth and pharynx should be viewed in the frontal as well as in the lateral projection. With the bolus positioned in the mouth awaiting swallowing, the midline tongue groove is often evident (Fig. 5A). Some of the bolus may be positioned within the buccal pouches, which are cleared during the oral phase of swallowing, or, in some instances, part of the oral bolus may escape into the buccal pouches during oral swallowing. In some subjects, midline apposition of the superior pharyngeal walls at the nasopharynx is seen during swallowing (Fig. 5B). The valleculae generally disappear during swallowing as the epiglottis moves to a horizontal position and its free margin flips downward. The valleculae normally evert and evacuate (Figs. 3 and 6). Small amounts of residual barium within normal-sized valleculae are a normal variant. As the free margin of the epiglottis becomes horizontal, its free margin is often seen as a transverse defect within the horizontal column (Fig. 13). Later, in the pharyngeal phase, the epiglottis projects an inverted V, or chevron configuration, within the barium column. During pharyngeal swallowing, the piriform sinuses make a brisk upward movement, largely governed by the four levator muscles of the pharynx. During their superior excursion, the piriform sinuses normally invert and evacuate their contents into the pharynx (Fig. 7B). Inversion of the piriform sinuses is caused by contraction of the levator muscles of the pharynx. At the onset of swallowing, the vocal cords begin to close and move upward with the larynx. The posteroanterior view is also useful for evaluating the vocal cord approximation during phonation (e.g., "ee") and for examining for unilateral cord paralysis. In many subjects, barium flows around the closed glottis as two lateral channels (Fig. 13) that meet 1–2 cm above the UES (Fig. 7B). The pharynx projects as a funnel. The level of the UES is readily identified as the junction of the pharyngeal funnel and the cervical esophagus, where slight wasting may be transiently present. At the completion of the posteroanterior examination for pharyngeal motor function, the pharyngeal walls are generally well coated with barium, and several spot films may be obtained for an evaluation of pharyngeal morphology. A Valsalva maneuver with an open glottis or having the patient pronounce the sound "ooo" will expand the piriform sinuses for better imaging. Slightly oblique images (15–20°) are often helpful for better imaging of the piriform sinuses and aryepiglottic folds.

From the preceding description, it is clear that an oral-pharyngeal swallow comprises a number of component elements that are synchronized in a fluid sequence. Each element needs to be evaluated in the assessment of swallowing function. When rapid-filming recording methods with slow-motion playback capability are available, each component can be evaluated fluoroscopically during the same swallowing sequence. Otherwise, each component needs to be evaluated during separate swallows because the swallowing sequence is too complex to focus on all of the components during a single swallow.

Normal Morphologic Variants

Morphologic variants that may be observed in normal asymptomatic subjects include a postcricoid impression, pharyngeal outpouches (Fig. 13), small cervical web, and slight posterior impression of the cricopharyngeus during swallowing. Several decades ago the postcricoid impression (Fig. 9) was commonly diagnosed as a neoplasm until it became recognized that this impression was a frequent finding during the pharyngeal phase of swallowing. Initially, the impression was attributed to a postcricoid plexus of veins [25]. In our opinion, however, the postcricoid impression is simply a mucosal plication because large-sized veins are not located behind the cricoid lamina. Thin mucosal webs about 1–2 mm in height, usually located on the anterior wall of the cervical esophagus, are a common incidental finding of no clinical significance [26, 27]. More pronounced and extensive webs that are hemispheric or circumferential may cause sufficient luminal narrowing to result in dysphagia for solids. Most pharyngeal outpouches are a transient incidental finding in asymptomatic subjects. Such pharyngeal pouches generally appear and disappear early during the pharyngeal phase of swallowing [28]. Another morphologic aberration seen commonly in asymptomatic individuals is a slight impression by the cricopharyngeus that may occur early, late, or during the interval of UES opening and transsphincteric flow of barium (Fig. 9). Such mild impressions may be effaced by a large bolus of barium (e.g., 15 or 20 ml). Some believe that any impression by the cricopharyngeus is abnormal [29, 30]. Our bias is that a mild cricopharyngeal impression is within the range of normal and does not cause clinical symptoms. Further investigation is needed, however, to resolve this issue.

Swallowing in Infants and Children

Although a full discussion of swallowing in children and infants is beyond the scope of the present discussion, some mention of infantile-type swallowing is warranted. In infants, the tongue is oversized and fills the mouth; the hyoid has a high position at the level of the mandible. During nursing, the mouth is filled by an oral suckle consisting of compression of the nipple and oral suction. Fluid from each suckle is pumped back into the pharynx, which when full, triggers a pharyngeal swallow. Normally, two or three suckles precede every pharyngeal swallow. During the pharyngeal swallow, the hyoid moves only forward because it is already located in a high superior position. Because of the high resting position of the hyoid, epiglottis, and larynx, infants are alleged to suckle and swallow while they breathe through their nose. During maturation, the hyoid descends and the pharynx becomes larger and the tongue relatively smaller because of differential growth of the mandible and tongue. These developments are accompanied by the ability to chew and manipulate food in the mouth. These developmental changes enable delivery of larger boluses into the pharynx and resonatation of speech in the pharynx. Interestingly, the adult pattern of swallowing recapitulates that of the infant in that the hyoid and larynx transiently assume a high superior position during swallows.

REFERENCES

1. Logemann JA. *Manual for the videofluorographic study of swallowing*. San Diego: College-Hill Press, **1986**
2. Miller AJ. Deglutition. *Physiol Rev* **1982**;62:129–184
3. Dodds WJ. The physiology of swallowing. *Dysphagia* **1989**;3:171–178
4. Dent J, Dodds WJ, Friedman RH, Sekiguichi T, Hogan WJ, Arndorfer RC. Mechanisms of lower gastroesophageal reflux in recumbent asymptomatic human subjects. *J Clin Invest* **1980**;65:256–267
5. Lichter I, Muir RC. The pattern of swallowing during sleep. *Electroencephalogr Clin Neurophysiol* **1975**;38:427–432
6. Doty RW, Bosma JF. An electromyographic analysis of reflex deglutition. *J Neurophysiol* **1956**;19:44–60
7. Dodds WJ, Man KM, Cook IJ, Kahrilas PJ, Stewart ET, Kern MK. Influence of bolus volume on swallow-induced hyoid movement in normal subjects. *AJR* **1988**;150:1307–1309
8. Kahrilas PJ, Dodds WJ, Dent J, Logemann JS, Shaker R. Upper esophageal sphincter function during deglutition. *Gastroenterology* **1988**;95:52–62
9. Dantas RO, Dodds WJ, Massey BT, Kern MK. The effect of high- vs low-density barium preparations on the quantitative features of swallowing. *AJR* **1989**;153:1191–1195
10. Dantas RO, Kern MK, Massey BT, et al. Effect of swallowed bolus variables on the oral and pharyngeal phases of swallowing. *Am J Physiol* (in press)
11. Jones B, Donner MW. Examination of the patient with dysphagia. *Radiology* **1988**;167:319–326
12. Dodds WJ, Taylor AJ, Stewart ET, Kern MK, Logemann JA, Cook IJ. Tipper and dipper types of oral swallows. *AJR* **1989**;153:1197–1199
13. Rubesin SE, Jones B, Donner MW. Radiology of the adult soft palate. *Dysphagia* **1987**;2:8–17
14. Dantas RO, Dodds WJ, Massey BT, Shaker R, Cook IJ. Manometric characteristics of the glossopalatal sphincter. *Dig Dis Sci* (in press)
15. Sokol EM, Heitmann P, Wolf BS, Cohen BR. Simultaneous cineradiographic and manometric study of the pharynx, hypopharynx and cervical esophagus. *Gastroenterology* **1966**;51:960–974
16. Shaker R, Cook IJS, Dodds WJ, Hogan WJ. Pressure-flow dynamics of the oral phase of swallowing. *Dysphagia* **1988**;3:79–84
17. Ramsey GH, Watson JS, Gramiak R, Weinberg SA. Cinefluorographic analysis of the mechanism of swallowing. *Radiology* **1955**;64:498–518
18. Cook IJ, Dodds WJ, Dantas RO, et al. Timing of videofluoroscopic, manometric events and bolus transit during the oral and pharyngeal phases of swallowing. *Dysphagia* **1989**;4:8–15
19. Cook IJ, Dodds WJ, Dantas RO, et al. Opening mechanisms of the human upper esophageal sphincter. *Am J Physiol* **1989**;20:G748–G759
20. Dodds WJ, Kahrilas PJ, Dent J, Hogan WJ. Considerations about pharyngeal manometry. *Dysphagia* **1987**;1:209–214
21. Asoh R, Goyal RD. Manometry and electromyography of the upper esophageal sphincter in opossum. *Gastroenterology* **1978**;74:514–520
22. Curtis DJ, Sepulveda GU. Epiglottic motion: video record of muscular dysfunction. *Radiology* **1983**;148:473–477
23. Curtis DJ, Cruess DF, Dachman AH, Maso E. Timing in the normal pharyngeal swallow. *Invest Radiol* **1984**;19:523–529
24. Logemann JA, Kahrilas PJ, Begelman J, Dodds WJ, Pauloski BR. Interactive computer program for biomechanical analysis of videoradiographic studies of swallowing. *AJR* **1989**;153:277–280
25. Pitman RG, Fraser GM. The post-cricoid impression on the oesophagus. *Clin Radiol* **1965**;16:34–39
26. Clements JL Jr, Cox GW, Torres WE, Weens HS. Cervical esophageal webs—a roentgen-anatomic correlation. Observations on the pharyngoesophagus. *AJR* **1974**;121:221–231
27. Nosher JL, Campbell WL, Seaman WB. The clinical significance of cervical esophageal and hypopharyngeal webs. *Radiology* **1975**;117:45–47
28. Curtis DJ, Cruess DF, Crain M, Sivit C, Winters C Jr, Dachman AH. Lateral pharyngeal outpouchings: a comparison of dysphagic and asymptomatic patients. *Dysphagia* **1988**;2:156–161
29. Asherson N. Achalasia of the cricopharyngeal sphincter. *J Laryngol Otol* **1950**;64:747–758
30. Sutherland HD. Cricopharyngeal achalasia. *J Thorac Surg* **1962**;43:114–126

Videotape Review

RSNA Today, Vol. 3, No. 4. Oak Brook, IL: The Radiological Society of North America, 1989. $75; by subscription, 4 issues annually at $225 for RSNA members and $275 for nonmembers

This videotape consists of three segments, all from the exhibits and refresher courses presented at the 1988 annual meeting of the Radiological Society of North America (RSNA). The first segment is on nonsurgical catheterization of the fallopian tube. Amy S. Thurmond and Josef Rosch from Portland, OR, give a filmed example, and RSNA editorial board member Stanley S. Siegelman asks appropriate questions. After discussing the prevalence of proximal tubular disease and the infertility related thereto in the United States, Dr. Thurmond reviews the accepted surgical procedures for the correction of these problems, their inherent disadvantages, and the technique she and others are using for nonsurgical catheterization of the fallopian tube. The pitfalls, complications, and success rates are discussed and seem to compare favorably with the more expensive and time-consuming surgical alternatives. The experience with 98 patients is reviewed. In the most important subset of 19 patients chosen according to specific criteria, 33 of 36 fallopian tubes were reopened, and 40% of these patients conceived in an average time of 2 months after the procedure. The preparation necessary for the procedure and the pathophysiology of the diseases responsible for obstruction of the fallopian tube are discussed. As with many procedure-oriented topics, the videotape mechanism is used ideally to demonstrate each detail of the performance of the procedure.

The second segment is a discussion between Harley C. Carlson of the Mayo Medical School and Dean D. T. Maglinte of Indiana University on barium examination of the small bowel. Dr. Carlson gives a detailed review of the fluoroscopic examination with vigorous manual compression, his preferred method of small-bowel examination, and Dr. Maglinte discusses enteroclysis, which he prefers. Their slight disagreements as to the efficacy and usefulness of either examination are more than offset by their agreement on the lack of efficacy of the classic barium-meal method of small-bowel examination. The techniques, advantages, and disadvantages of both types of examinations are discussed, and there seems to be at least one important area of complete agreement: the need for careful fluoroscopic examination throughout the procedure along with compression and imaging in oblique positions. With the expected increased use of enteroscopy, the necessity of increasing the usefulness and accuracy of radiologic imaging of the small intestine is discussed. As an aside, during demonstration of these procedures, many interesting cases of pathologic changes of the small bowel are shown.

The third segment is a presentation of the first videotape accepted in response to the notice in *Radiology*. Sjirk J. Westra from the University of Amsterdam, the Netherlands, presents his tape on ultrasound evaluation of gastroesophageal reflux and hiatus hernia in young children. The advantages of ultrasound examination over classic barium studies, such as a longer observation time and a more physiologic observation, are stressed, and the technique is described and demonstrated simultaneously. Normal sonographic anatomy of the gastroesophageal junction is reviewed, and the criteria for diagnosing reflux and hernias are presented. The facility and usefulness of the procedure in competent hands is demonstrated clearly.

Overall, this tape contains three interesting and informative segments that might be of interest to the general radiologist in terms of general information and to the appropriate subspecialist in terms of more specific educational objectives.

Hano A. Siegel
Mercy Hospital
San Diego, CA 92103

Review Article

Radiologic Assessment of Abnormal Oral and Pharyngeal Phases of Swallowing

Wylie J. Dodds,[1] Jeri A. Logemann,[2] and Edward T. Stewart[1]

In our companion report [1], we reviewed the normal physiology and radiologic appearance of the oral and pharyngeal phases of swallowing. Our purpose here is to review abnormalities of the first two phases of swallowing.

The most frequent symptoms of abnormal oral or pharyngeal swallowing include difficulty initiating swallowing, cervical dysphagia, nasal regurgitation, coughing, and choking. Generally, abnormal oral or pharyngeal swallowing function is associated with high cervical dysphagia in the upper neck, whereas the abnormal esophageal motor function or obstructive morphology may be in the retrosternal area or lower neck. The symptoms of persistent sore throat or pain with swallowing are suggestive of neoplasm or infection.

On clinical examination, abnormalities of liquid bolus preparation for swallowing include drooling from the lips due to facial muscle weakness and failure to gather the bolus normally within the mouth. Disorders in the pharyngeal phase may not be obvious by observing the patient swallow. Contrary to a widely held opinion, the efficacy of the pharyngeal swallow does not correlate with an intact gag reflex. Additionally, "silent aspiration" may go undetected on clinical examination. For these reasons, swallow function is optimally evaluated by radiologic examination.

Preparation for Swallowing

Functional abnormalities in the preparatory and oral phases of swallowing are listed in Table 1. The majority of these abnormalities are caused by abnormal tongue movement and, occasionally, by a soft-tissue defect of the tongue or oral cavity. Problems in motor function or reduced bulk of the anterior two-thirds of the tongue cause abnormalities in lifting, shaping, and propelling oral boluses; paresis, restricted movement, or loss of bulk of the posterior tongue impairs function of the glossopalatal sphincter and bolus pulsion.

Abnormalities of the preparatory phase for the oral swallow demonstrated radiologically include an inability to shape the bolus or hold it above the tongue. The latter circumstance must be distinguished from a normal dipper-type swallow in which the bolus is initially positioned in the anterior lingual sulcus [2]. Inability to segregate the bolus from the oropharynx by elevation of the posterior tongue and approximation to the soft palate may lead to premature spilling of the bolus into the oropharynx (Fig. 1).

Oral Phase of Swallowing

In some instances, an impairment of the oral phase of swallowing is seen as a repetitive attempt at initiating swallowing, piecemeal swallows, or rolling movements of the tongue (Table 1). Occasionally, some patients who are capable of normal pharyngeal swallowing may have difficulty initiating oral swallowing because of problems in cooperation, cognition, or oral sensation (Fig. 2). Abnormalities in the oral phase of swallowing generally lead to delayed oral transit and clearance of the oral bolus with retained residual in the mouth.

Received October 30, 1989; accepted after revision December 14, 1989.

[1] Department of Radiology, the Medical College of Wisconsin, Froedtert Memorial Lutheran Hospital, 9200 W. Wisconsin Ave., Milwaukee, WI 53226. Address reprint requests to W. J. Dodds.

[2] Department of Communication Sciences and Disorders, Neurology and Otolaryngology–Head and Neck Surgery, Northwestern University, Evanston, IL 60208.

AJR 154:965–974, May 1990 0361–803X/90/1545–0965 © American Roentgen Ray Society

TABLE 1: Abnormalities in the Preparatory and Oral Phases of Swallowing

Radiologic Findings	Type of Impairment
Preparatory Phase	
Cannot hold barium in mouth anteriorly	Reduced lip closure
Cannot form bolus	Reduced range or coordination of tongue movement
Cannot hold bolus posteriorly (premature spill)	Reduced tongue shaping
Cannot chew	Reduced tongue lateralization
Oral Phase	
Hesitancy initiating swallow	Impaired cognitive function, neural function, or oral sensation
Tongue moves forward at onset of swallow	Forward tongue thrust
Stasis in sulci	Reduced labial or buccal tension
Stasis in floor mouth	Reduced tongue shaping
Stasis in midtongue depression	Tongue scarring
Abnormal lingual peristalsis	Impaired tongue motion
Poor tongue to palate contact	Reduced tongue elevation
Repetitive tongue rolling	Parkinson disease
Premature spill of bolus	Reduced tongue or palatal control
Piecemeal deglutition	Abnormal neural control
Slow oral transit	Impaired tongue movement

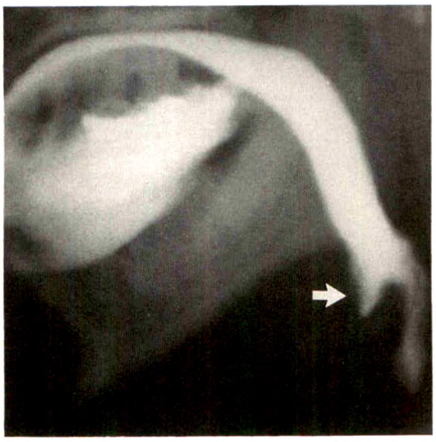
1

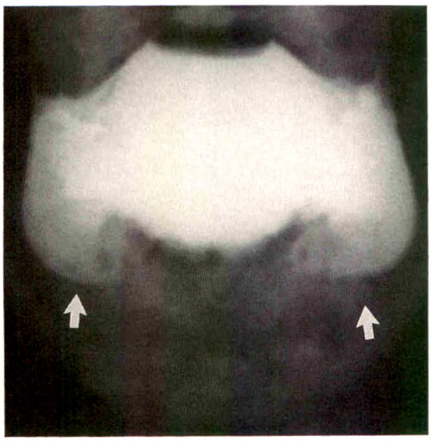
2

Fig. 1.—Premature spill of barium from oral cavity into pharynx of elderly patient after a stroke. Barium fills valleculae (*arrow*) and spills over free margin of epiglottis. Also noted is dipper-type bolus preparation near tongue with barium in lateral and anterior sublingual sulci.

Fig. 2.—Posteroanterior view in elderly patient who had difficulty initiating swallowing. On initial efforts to swallow, patient stored liquid barium in buccal pouches (*arrows*) and did not initiate swallowing. Patient was then given applesauce with barium, which he swallowed normally. Patient liked taste of applesauce but not regular barium. He then swallowed liquid barium normally with only slight storage of barium in buccal pouches, which is a normal variant in some subjects.

Impaired lingual movement or conditions such as a soft-tissue defect lead to barium stasis in the mouth. Premature spilling of barium into the pharynx may be accompanied by failed transition into normal pharyngeal peristalsis or aspiration or both. Impaired oral function is commonly associated with abnormal pharyngeal swallowing, but one may be abnormal while the other is normal. Normally, the oral phase of swallowing undergoes a smooth transition to a brisk pharyngeal phase, with vigorous transport of the swallowed bolus into and through the pharynx. In some patients, however, the pharyngeal phase is delayed, but once initiated is normal. In the presence of severe oral impairment, the pharyngeal phase may be triggered by injecting a small barium bolus directly into the pharynx through a soft tube passed into the pharynx through either the mouth or nose. Such techniques, however, are used only for examination and not for feeding.

Radiation may cause an impaired oral phase as well as a pharyngeal phase of swallowing for several reasons: (1) decreased salivation that helps initiate swallowing, (2) fibrosis with restrictive tongue or hyoid movement, (3) damage to lingual nerves, and (4) damage to tongue muscles with accompanying atrophy. Additionally, the pharyngeal phase is delayed or impaired in some radiated patients. Such delays may arrest or retard pharyngeal bolus transport or lead to aspiration.

Pharyngeal Phase of Swallowing

Abnormalities of the pharyngeal phase of swallowing are listed in Table 2. Nasal regurgitation of fluid and nasal speech may occur when the soft palate does not make a good seal against the posterior pharyngeal wall or the superior pharyngeal constrictors do not contract normally. The generic causes include impaired neurologic function, disease of striated muscle, or a structural abnormality, such as a palatal defect. In some instances, the palatal sealing appears normal when the patient is upright and regurgitation is not seen until the patient is positioned horizontally or in a slightly head-down position (Fig. 3). In some patients, nasal regurgitation can be caused

TABLE 2: Abnormalities in the Pharyngeal Phase of Swallowing

Radiologic Findings	Generic Impairment
Absent or decreased hyoid movement	Feeble contraction, suprahyoid muscle
Absent or decreased laryngeal movement	Abnormal contraction, thyrohyoid
Poor palatal movement	Impaired function of velopharngeal closure mechanism
Delayed or absent pharyngeal phase	Impaired sensation; damage to neural programming in the brainstem
Increased unilateral residual valleculae and/or piriform sinus	Unilateral impairment of pharyngeal peristalsis
Abnormal movement, epiglottis	Impaired function of thyrohyoids, cervical spur, mass
Laryngeal penetration/aspiration	Early: premature oral spill; during: impaired laryngeal closure; late: pharyngeal residue
Abnormal opening of upper esophageal sphincter (UES)	Impaired UES relaxation; decreased UES compliance; feeble hyoid movement; feeble pharyngeal transport

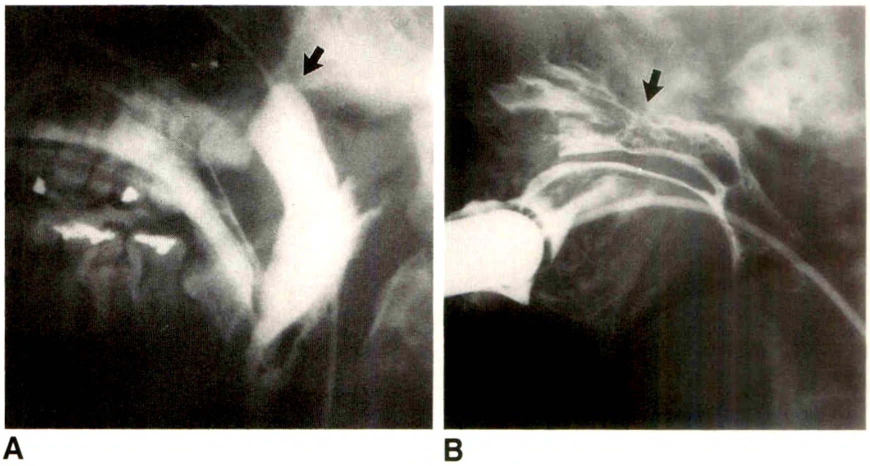

Fig. 3.—Two examples of nasal regurgitation due to feeble palatal contraction during swallowing. Regurgitation occurred only while patients were recumbent.

A, Elderly man several weeks after a stroke. Nasogastric tube is present. Substantial amount of barium (*arrow*) has regurgitated into nasopharynx.

B, 6-month-old infant with neuromuscular dysfunction and respiratory symptoms. Oral esophageal tube is present to search for tracheoesophageal fistula. Regurgitated barium is visible in nasopharynx and nasal cavity (*arrow*).

by disorders of pharyngeal transport and accompanying residual when swallowed material refluxes into the nasopharynx after palatal closure and reopening.

A number of factors may contribute to impaired pharyngeal bolus transport. A feeble or disorganized posterior tongue thrust will weaken the tongue driving force that is so important in initiating bolus transport into the oropharynx. Such impaired tongue movement may be caused by neurologic disease, muscle disease, fibrosis, or a surgical defect. In the hypopharynx, bolus transport is achieved largely by peristalsis of the pharyngeal constrictors. In some instances, impaired constrictor function, often neurologic in origin, may be limited to a single constrictor, for example, the middle constrictor. The bolus will lose its sharp tail and move slowly through the area of involvement. In other instances, constrictor weakness is unilateral and seen only on frontal imaging. The abnormal side bulges, compared with the normal contralateral side (Fig. 4), and retains residual swallowed material. The cardinal feature of impaired pharyngeal transport is increased residual volume, generally in the piriform sinuses but also in the valleculae (Fig. 5). With unilateral pharyngeal paresis the residual in the hypopharynx is on the ipsilateral side.

Another abnormality that may be observed during the oral and pharyngeal phases of swallowing is a diminished superoanterior excursion of the hyoid and larynx, which normally becomes maximal during the pharyngeal swallow. Diminished movement of these structures is generally related to impairment of the neural program that drives the muscles that move the structures or to tissue fibrosis (e.g., from surgery or radiation). Decreased hyoid and laryngeal movement may contribute to impaired oropharyngeal filling, impaired bolus transport, aspiration, or abnormal upper esophageal sphincter (UES) opening.

Yet another abnormality that may be observed during the pharyngeal swallowing phase is impaired movement of the epiglottis. As discussed earlier, normal epiglottic movement is a major factor in closure of the laryngeal vestibule. On lateral videofluoroscopy, bilateral impairment of thyrohyoid contraction is seen as a lack of laryngeal-hyoid approximation accompanied by absent or only partial vestibular closure. Such impairments are generally neurologic in origin. On posterolateral projection, unilateral thyrohyoid impairment causes upward epiglottic tilting (Fig. 6) to the ipsilateral side [3]. Other causes of epiglottic tilting include cervical spurs or a mass on the ipsilateral side, such as a mass of the aryepiglottic fold that mechanically prevents normal epiglottic closure.

Perhaps the most significant abnormality sought during radiologic examination of pharyngeal function is aspiration [4]. We define aspiration as barium penetration into the laryngeal vestibule with passage below the vocal cords. The term penetration is applied to barium entry into the laryngeal vestibule without passage below the cords. Penetration alone occurs more commonly than penetration with aspiration. Often the penetrated barium is cleared during the course of the same swallow as the laryngeal elevation increases (Fig. 7) or during a subsequent cough. Penetration occurs most commonly with swallows of thin barium and may be seen as a "finger" of barium extending into the vestibule. On posteroanterior views, penetration is seen as a thin vertical line of barium in the midline (Fig. 4). Severe penetrations are often

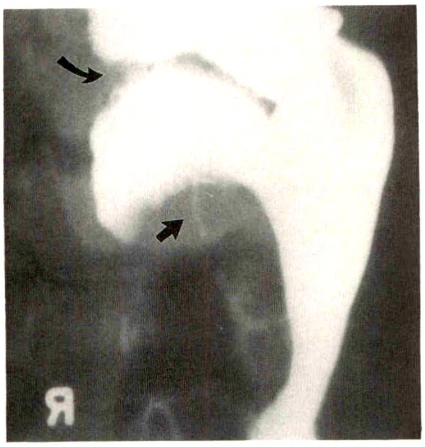

Fig. 4.—Posteroanterior view. Bulging of left pharynx in patient with left-sided paralysis of pharyngeal peristalsis. All of swallowed barium flowed down left pharynx and none through right pharynx. Trace amount of penetration into laryngeal vestibule is seen in midline (*straight arrow*). Slightly oblique defect is caused by epiglottis (*curved arrow*). When patient's head was turned to right, swallowed barium flowed mainly down right side of pharynx and vestibular penetration did not occur.

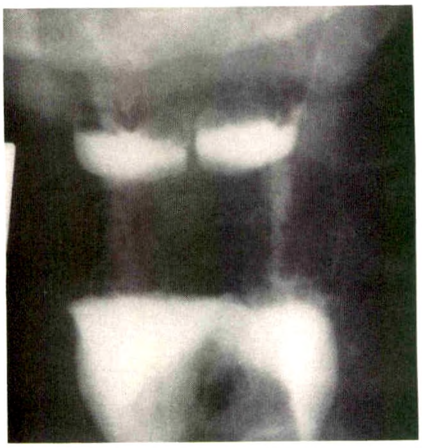

Fig. 5.—Posteroanterior view. Substantial barium residue in valleculae and piriform sinuses after 10-ml barium swallow in a patient in whom pharyngeal peristalsis was absent after a stroke.

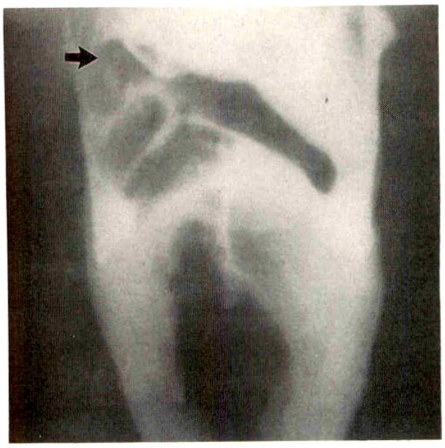

Fig. 6.—Example of epiglottic tilt during pharyngeal phase of 10-ml barium swallow in 45-year-old man with amyotonia dystrophy. Free margin of epiglottis is tilted upward on right (*arrow*). Gas bubble is trapped beneath right side of epiglottis. Barium is seen to stream down side channels of pharynx. Epiglottic tilt in this patient is attributed to impaired contraction of right thyrohyoid muscle. There was no evidence of a cervical spur or pharyngeal mass.

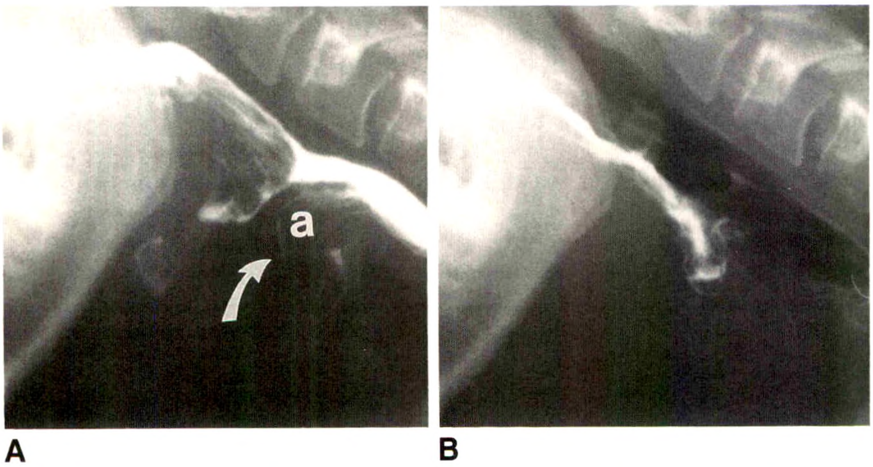

Fig. 7.—Laryngeal penetration during swallowing of 5-ml barium bolus by patient who had undergone cranial surgery and radiation for craniopharyngioma.

A, During pharyngeal phase of swallowing, thin finger of barium (*arrow*) has penetrated laryngeal vestibule. Epiglottis is bowed over arytenoids (a); its free margin has flipped caudad.

B, By completion of swallowing sequence, most of penetrated barium has been "kicked out" of laryngeal vestibule, which is now open, and only a thin coating of barium remains to be seen.

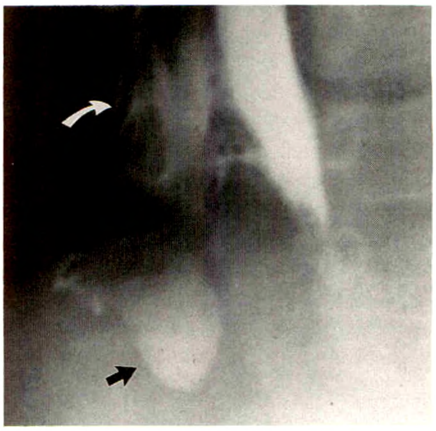

Fig. 8.—Tracheal aspiration in patient with dermatomyositis. Barium is seen in laryngeal vestibule (*curved arrow*) and also in trachea (*straight arrow*). Pharyngeal bolus transport was impaired because of weakness of pharyngeal constrictors. High residuals of barium remained in pharynx and piriform sinuses. Aspiration occurred both during and after a swallow.

accompanied by aspiration and are seen as a substantial extension of barium on the lateral view (Fig. 8) and as a thick vertical line, or wedge, on the posteroanterior view (Fig. 9B). On the posteroanterior view, the inner margin of the aryepiglottic folds often becomes well coated with barium (Fig. 9A). On the lateral view the arytenoids may remain vertical and split the barium column (Fig. 10), with some barium going into the larynx and the remainder filling the hypopharynx or crossing the UES [5]. In such cases, there is severe impairment of vocal cord closure. We believe that mild penetration is generally caused by a feeble or dyssynergic contraction of one or both of the thyrohyoid muscles, thereby showing laryngeal elevation. Aspiration has several general causes and may occur (1) early, before the pharyngeal swallow; (2) during the pharyngeal swallow; or (3) late, after the pharyngeal swallow. Early aspiration is caused by premature spill of fluid from the mouth and is related to impaired lingual or lingual-palatal function. Aspiration during a swallow is usually related to impaired function of the intrinsic laryngeal muscles, generally from a neural cause or surgical ablation. Late aspiration is generally related to increased pharyngeal residual of any cause, for example, impaired bolus transport; abnormal UES opening; or, occasionally, esophagopharyngeal regurgitation. Other types of conditions in the differential diagnosis of aspiration include a cleft epiglottis or tracheoesophageal fistula. This last condition may simulate aspiration when barium abruptly appears in the upper trachea and larynx and is coughed through the vestibule into the pharynx. The key point with a tracheoesophageal fistula is that the barium does not enter the trachea via the larynx, but rather enters the upper trachea from below. The therapy for aspiration depends on its generic type. Some patients exhibit more than one type and cause of aspiration.

Incomplete UES opening during the pharyngeal phase of

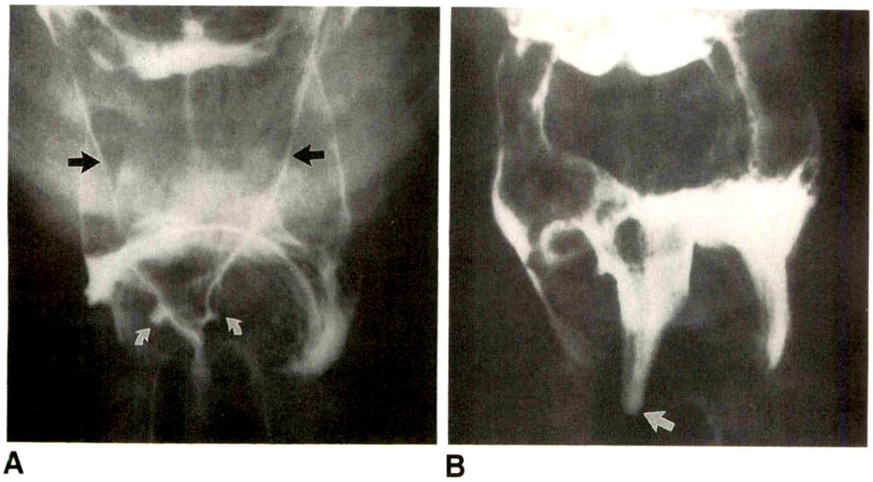

Fig. 9.—Posteroanterior views. Two examples of severe aspiration.

A, Elderly woman after a stroke. Laryngeal vestibule and glottis are widely patent. Barium outlines aryepiglottic folds (*straight arrows*) and laryngeal ventricles (*curved arrows*). Barium is also seen in trachea.

B, Elderly man with nodular carcinoma in right piriform sinus that involves base of right aryepiglottic fold. Large vertical wedge of barium fills laryngeal ventricle and extends into trachea (*arrow*).

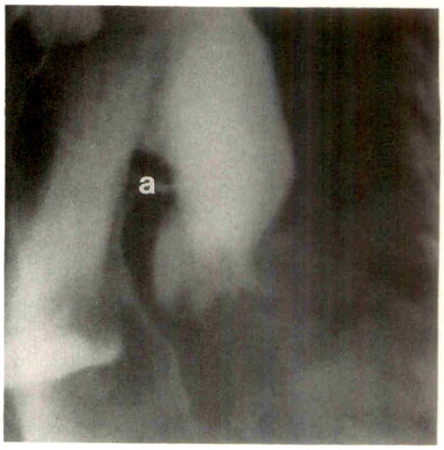

Fig. 10.—Severe aspiration. Elderly senile man who exhibited absent pharyngeal peristalsis, aspiration, and a large amount of residual barium in pharynx. Upper esophageal sphincter did not open normally. Arytenoid (a) cartilages remained vertical and split barium column.

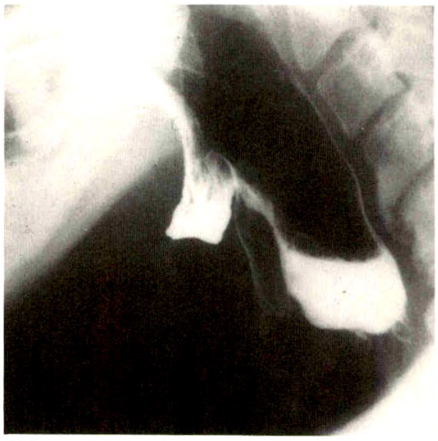

11

Fig. 11.—Failed opening of upper esophageal sphincter (UES) in 51-year-old man with abrupt onset of difficulty in swallowing. Patient was hypertensive but without CT or clinical evidence of stroke. Radiologic examination showed absent pharyngeal peristalsis and failed UES opening. Oral phase of swallowing was normal. Patient did not aspirate but held his breath and coughed residual barium out of his pharynx. A substantial residue of barium is present in valleculae and piriform sinuses. On manometry, UES did not relax with swallowing. During a 2-month period, pharyngeal swallows, peristalsis, and UES relaxation returned to normal. This patient's condition was attributed to lacunar infarcts of brainstem.

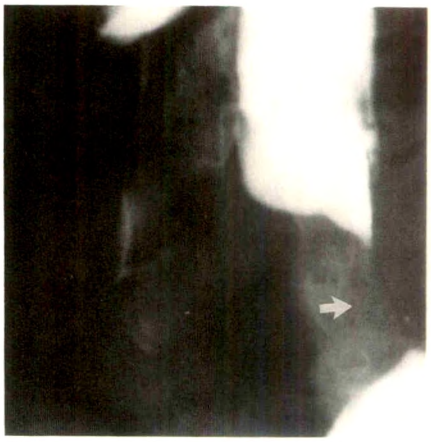

12

Fig. 12.—Abnormal opening of upper esophageal sphincter (UES) in elderly man with oculopharyngeal dysphagia. Radiologic examination demonstrated normal oral phase of swallowing with feeble pharyngeal contractions, high residual in pharynx, and aspiration. On some swallows, UES opened partially or, as in this example, not at all (*arrow*); however, UES relaxed normally on manometry.

swallowing may impair pharyngeal bolus transport, lead to excessive pharyngeal residual, and cause late aspiration. Impaired UES opening is caused by an abnormality in one or more of the four factors associated with normal sphincter opening.

Failure of UES relaxation is most commonly caused by neurologic disease, such as stroke or head trauma, and is generally accompanied by abnormalities in pharyngeal bolus transport (Fig. 11). Thus, impaired UES (cricopharyngeus) relaxation rarely occurs as an isolated abnormality. Intraluminal manometry is the only satisfactory clinical laboratory method for validating impaired UES relaxation [6, 7]. Simply observing absent or incomplete UES (cricopharyngeal) opening radiologically does not establish impaired sphincter relaxation (Fig. 12). Some patients exhibit a pronounced cricopharyngeal indentation (Fig. 13) that has often been judged, simply on the basis of its radiologic appearance, to represent isolated impaired UES relaxation; this has been termed cricopharyngeal achalasia [8, 9]. In our experience, such patients generally exhibit normal UES relaxation on manometry and the underlying abnormality is decreased compliance of the relaxed UES. Decreased stretchability of the relaxed cricopharyngeus is probably caused by fibrosis. A subset of patients with Zenker diverticulum exhibit the same abnormality. Feeble anterior movement of the hyoid may contribute to incomplete UES opening but seldom occurs as an isolated finding. The most common cause of incomplete UES opening seems to be decreased intrabolus pressure related to impaired bolus transport through the pharynx (Fig. 12). The underlying cause may be neurologic or muscular.

A useful concept has been suggested for evaluating and understanding abnormalities of the oral and pharyngeal phases of swallowing. This concept stresses the relationship between specific functional impairments, adaptive compensation, and decompensation [10]. For example, glossopalatal closure and tongue thrust control fluid flow from the mouth to the pharynx. In some patients, weakness of the posterior tongue may be compensated for by increased downward movement of the soft palate. Decompensation consists of premature escape of fluid from the mouth (Fig. 1), often associated with aspiration. Weakness of the soft palate may be associated with prominence of Passavant ridge as a compensation to seal off the nasopharynx. This compensation seems especially common in children. Decompensation consists of nasal regurgitation during swallowing (Fig. 3). A third example is weakness of the intrinsic laryngeal muscles. Compensation against aspiration may be achieved by flexion of the head, which tucks the larynx beneath the epiglottis. Decompensation consists of aspiration.

Radiation therapy is believed to contribute to abnormalities in the pharyngeal phase of swallowing. Such functional abnormalities include pharyngeal paresis, delayed pharyngeal clearance, epiglottic dysfunction, and aspiration [11].

As stressed earlier, the examination for cervical dysphagia is incomplete without a careful examination of esophageal function and motility. Findings of significance may include esophageal motor dysfunction, esophageal stricture, esophageal neoplasm, reflux esophagitis, and reproducible gastroesophageal reflux. Morphologic abnormalities in the pharynx or proximal esophagus include tumor, circular webs (Fig. 14), or Zenker diverticulum (Fig. 15). Generally, small incomplete webs or transient pharyngeal pouches are of no clinical significance. Recently, however, Curtis et al. [12] reported that pharyngeal pouches that appear late and persist late into the swallowing sequence are associated with cervical dysphagia (Fig. 16), whereas pharyngeal pouches in asymptomatic subjects appear and disappear earlier in the sequence. Persistent pharyngeal diverticula are commonly associated with clinical symptoms.

During the past decade numerous claims have emerged that the symptoms of globus or cervical dysphagia are associated with gastroesophageal reflux disease. Many of these claims have been based on the notion that gastroesophageal acid may cause spasm or dysfunction of the UES. In our experience, however, we have been unable to document that intraesophageal infusion of acid or spontaneous episodes of acid gastroesophageal reflux cause any alteration of normal UES function [13]. Nevertheless, in occasional patients with reflux disease, regurgitated acid may cause pharyngitis or aspiration laryngitis. To our knowledge, however, acid regur-

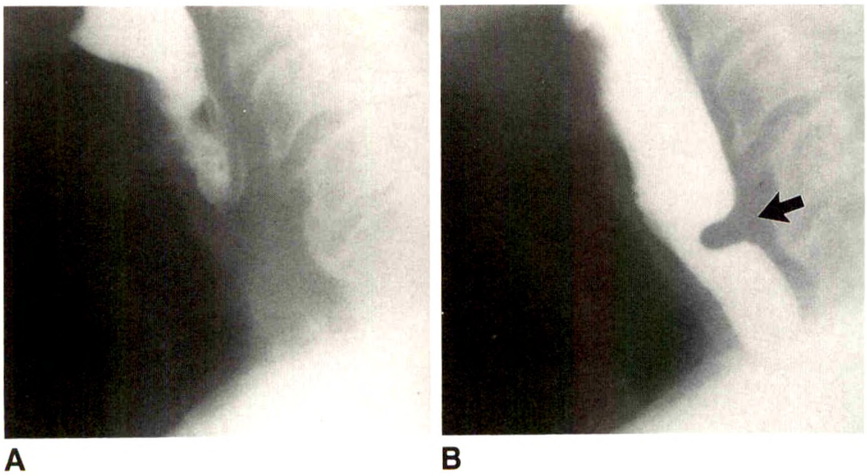

Fig. 13.—Prominent cricopharyngeal (CP) bar in elderly patient with mild cervical dysphagia. Swallows of 10-ml barium bolus.

***A*, Head of barium bolus is just reaching upper margin of upper esophageal sphincter (UES).**

***B*, Prominent restrictive CP bar (*arrow*) is seen at level of UES. This bar persisted throughout entire interval of barium flow into cervical esophagus and narrowed aperture of open UES did not change in dimension. On pharyngeal manometry, pharyngeal peristalsis and UES relaxation were normal. We attribute prominent CP bar to reduced compliance, or stiffness, of CP muscle, even when relaxed [7]. Reduction in CP compliance is probably related mainly to idiopathic fibrosis or muscle contracture.**

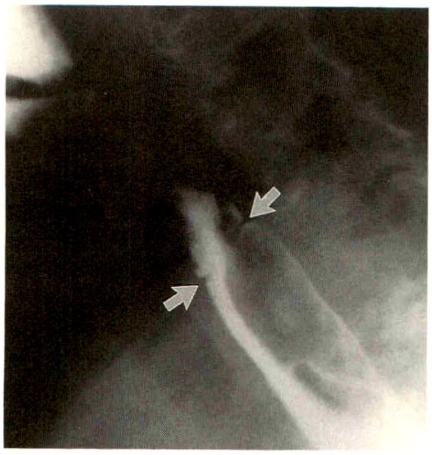

Fig. 14.—Circumferential web (*arrows*) in cervical esophagus in a patient with dysphagia for solids. Half of a marshmallow was caught at web and produced clinical symptoms.

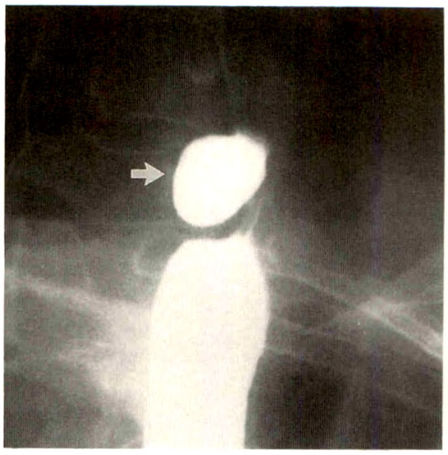

Fig. 15.—Lateral oblique view of Zenker diverticulum (*arrow*) in elderly man with cervical dysphagia. Pharyngeal peristalsis and clearance were normal.

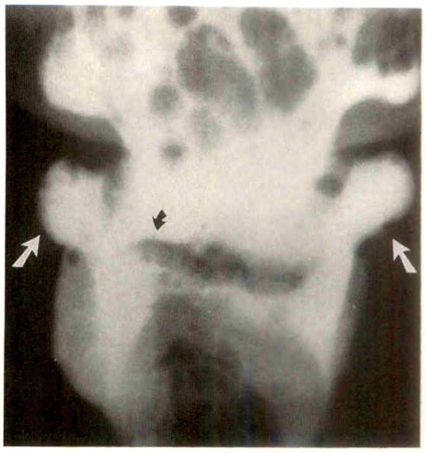

Fig. 16.—Bilateral pharyngeal pouches (*straight arrows*) in patient with unexplained cervical dysphagia. Pouches appeared during middle of pharyngeal swallow and lasted until late in pharyngeal swallow. Curtis et al. [12] suggest this timing is abnormal. Also noted is slight tilting of epiglottis (*curved arrow*), caused by cervical osteophyte. All other components of swallowing appeared normal.

gitation is rarely associated with any overt change in the oral-pharyngeal function detectable on videofluoroscopy, or pharyngeal manometry. For this reason, we believe that although a relationship may exist between acid gastroesophageal reflux disease and cervical symptoms in some patients, this association is overstated and poorly substantiated. In fact, only a minority of patients with acid reflux disease have acid reflux into the proximal esophagus and regurgitation into the pharynx. Therefore, the finding of a hiatal hernia or isolated episodes of gastroesophageal reflux on radiologic examination do not establish a reflux cause for globus or cervical dysphagia.

Value of Radiologic Examination

Thorough radiologic evaluation of each component of the oral and pharyngeal phases of swallowing leads to two beneficial circumstances: (1) the judgment that swallowing function is normal is a highly accurate one, rather than signifying that abnormal function simply has not been noticed and (2) an accurate complete description is obtained of the normal and abnormal features of oral or pharyngeal swallowing. Such descriptions are essential even when a specific cause is not apparent. For example, a given patient may exhibit impaired tongue movement with difficulty forming a bolus and a delay in initiating swallowing while pharyngeal function is entirely normal. Another patient may exhibit normal oral and pharyngeal function in the presence of weak palatal function and nasal regurgitation. Virtually unlimited combinations of impaired and normal function of the different components of swallowing may be observed in individual patients. This phenomenon is especially true in patients who have suffered a sudden neurologic event such as a stroke or head injury.

Accurate description of swallow function forms the basis for patient management and the design of therapy, where appropriate. A partial list of possible causes of impaired oral or pharyngeal swallowing is given in Table 3. It must be emphasized, however, that an accurate description of the constellation of impairments during oral and pharyngeal swallowing often does not lead to a specific diagnosis. Nevertheless, the radiologic diagnosis provides critical information relative to the patient's swallowing function and management. A specific diagnosis is generally provided mainly by the clinical history alone, or the clinical history in combination with the radiologic findings.

The most common cause of neurologic dysfunction is cerebral vascular disease. Commonly, abnormalities of swallowing related to stroke are reversible over weeks to months. Primary muscle disorders tend to affect the pharyngeal phase of swallowing more than the oral phase, but this pattern is variable and nonspecific. Deteriorating swallow function with repetitive swallows suggests a diagnosis of myasthenia gravis. Such changes may be reversed with IV administration of edrophonium (Tensilon), which should be given with caution.

In some instances, pharmacologic therapeutic agents may cause abnormalities in swallowing. For example, many drugs, such as thorazine, have an anticholinergic effect that impairs salivation and thereby may lead to difficulty in initiating swallows. Other drugs, such as metoclopramide, may cause rhythmic protrusion of the tongue. For these reasons, examination of swallowing should include a comprehensive clinical history of drug therapy.

Neoplasms in the mouth or pharynx may cause abnormalities in swallowing function. For example, a neoplasm in the anterior or middle tongue may impair bolus preparation or oral clearance, and a neoplasm of the tongue base may compromise delivery of the oral bolus into the pharynx or cause premature spill into the oropharynx (Fig. 17). A lesion of the pharyngeal wall may impair pharyngeal bolus transport and lead to an increased residual in the pharynx. As discussed earlier, a tumor of the aryepiglottic fold or medial wall of the piriform sinus may cause tilting of the epiglottis during the pharyngeal swallow [3]. Such lesions may also lead to aspiration (Fig. 18).

The effect of aging on swallowing is controversial. Although aging per se probably causes subtle quantitative changes in the oral and pharyngeal phases of swallowing, such changes remain to be fully elucidated and measured.

TABLE 3: Causes of Abnormal Oral or Pharyngeal Swallowing

- Neurologic disease
  - Cerebrovascular
  - Posttraumatic
  - Degenerative (e.g., Alzheimer)
  - Parkinsonism
  - Amyotrophic lateral sclerosis/motor neuron disease
  - CNS neoplasm
  - Bulbar poliomyelitis
  - Pseudobulbar palsy
  - Friedreich spastic ataxia
  - Familial dysautonomia
  - Postoperative CNS tumor
- Muscle disease
  - Muscular dystrophy
  - Oculopharyngeal dystrophy
  - Myotonic dystrophy
  - Dermatomyositis
  - Myasthenia gravis
- Radiation injury
- Gastroesophageal reflux disease?
- Pharmacologic agents (e.g., atropine, thorazine)
- Malignancy
  - Tongue
  - Pharynx
  - Larynx
- Postoperative
  - Tongue
  - Pharynx
  - Larynx

Postoperative Studies

As with the general examination for patients with a suspected abnormality of oral or pharyngeal swallowing, the radiologic examination in patients who have undergone surgery for oral, pharyngeal, or laryngeal malignancies involves a careful evaluation of morphology [14] as well as function [15]. Such surgeries include resection for primary malignancies of the tongue, pharynx, and larynx. In many cases, the patient may also undergo a radical lateral neck dissection and/or subsequent irradiation.

The aim of surgical resection is to include a 1-cm margin free of tumor. Therefore, even a small tongue lesion of 2 cm would require resection of a 4-cm block of tissue, probably with a primary closure. Such surgery might not be expected by the surgeon to cause a severe abnormality with swallowing. However, difficulty may be caused by loss of tongue mass or restrictive tongue movement because of fibrosis [16]. Loss of normal tongue movement often leads to difficulty shaping a bolus, difficulty initiating swallowing, and increased residual in the mouth following the oral swallow. The pharyngeal phase of swallowing is generally normal.

Tumors involving the alveolar ridge, tongue base, tonsil, lateral pharyngeal wall, or palate require wider resection than simple tumors confined to the tongue. The large defect may be dealt with by primary closure or a skin flap. These patients may have a substantial tissue defect, abnormal pharyngeal bolus transport, nasal regurgitation, or aspiration [17].

Carcinoma of the larynx may be focal, for example, limited to a vocal cord or aryepiglottic fold. However, such carcinomas may extend to multiple sites, such as both supraglottic and glottic areas or the subglottic region or even beyond the glottis into the piriform sinus. The type of treatment is determined by the extent of the tumor. Lesions limited to one vocal fold are commonly treated by radiation alone. Types of surgical procedure include a hemilaryngectomy, supraglottic laryngectomy, and total laryngectomy with tracheostomy. Hemilaryngectomies are seldom performed. With a supraglottic laryngectomy, the hyoid and epiglottis and aryepiglottic folds are removed [17, 18]. On lateral view, the vocal cords and infraglottic larynx are pulled up to the base of the tongue.

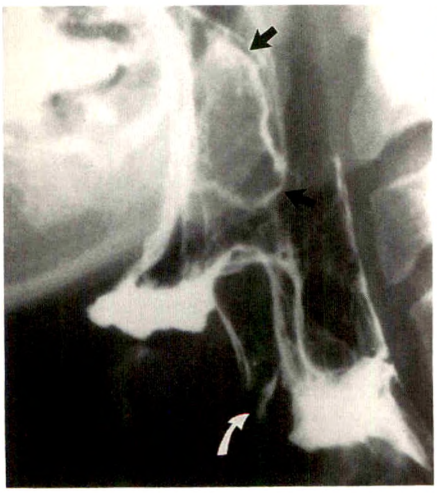

17

Fig. 17.—Bulky carcinoma (*straight arrows*) involving right posterior tongue and right pharyngeal wall. Tumor caused premature spill of barium from mouth, impaired posterior tongue thrust, impaired pharyngeal bolus transport, and increased residual barium in the valleculae and piriform sinuses and barium penetration into laryngeal vestibule (*curved arrow*).

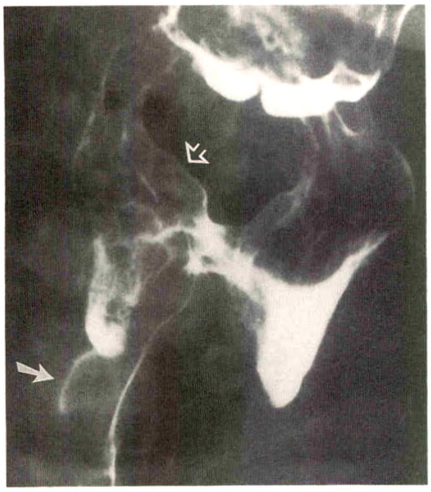

18

Fig. 18.—Posteroanterior view of nodular carcinoma originating in right piriform sinus. Carcinoma causes constriction of right piriform sinus (*solid arrow*), invades right side of glottis, and causes flat mass on aryepiglottic fold (*open arrow*). During swallowing, barium was aspirated into trachea.

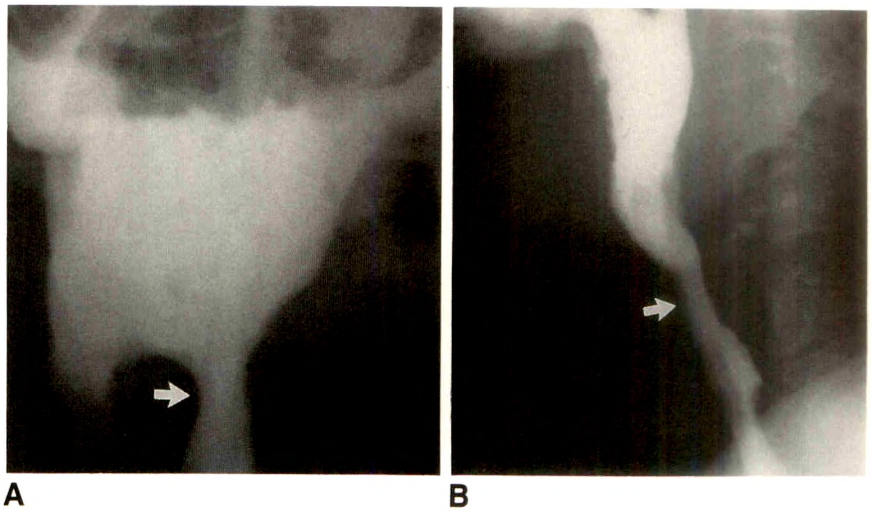

Fig. 19.—Patient after partial pharyngectomy and total laryngectomy for carcinoma of larynx and left piriform sinus. Hyoid and larynx are absent.

A, Anteroposterior view. Left piriform sinus is absent. Stricturelike narrowing (*arrow*) exists in region of upper esophageal sphincter (UES).

B, Lateral view. Stricture seen at level of UES (*arrow*). Also seen is substantial regurgitation of barium into nasopharynx.

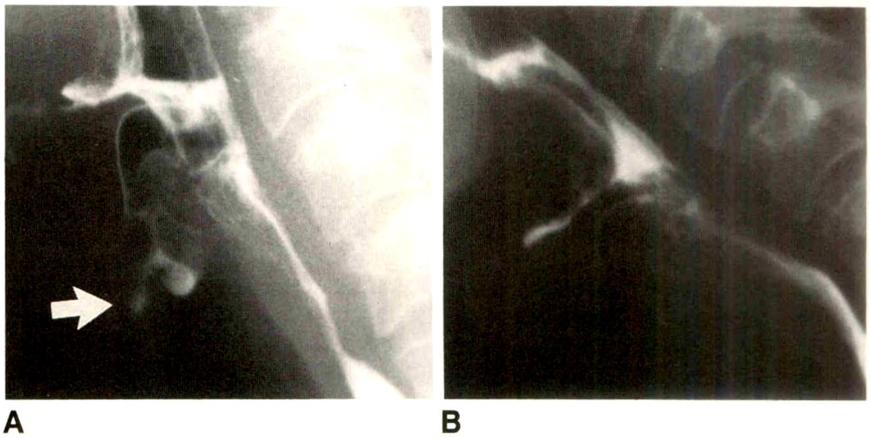

Fig. 20.—Value of head flexion in prevention of aspiration.

A, Head in neutral position. With barium swallow, barium is seen to have been aspirated below glottis (*arrow*). Aspiration also occurred with thick barium and barium paste.

B, Head in flexed position. During this swallow, barium penetrated laryngeal vestibule, but aspiration did not occur. On other swallows with head flexed, there was no vestibular penetration. Vestibular penetration did not occur with thick barium or barium paste.

Although closure of the cords alone is generally sufficient to prevent aspiration during the swallow, some aspiration of pharyngeal residue may occur after the swallow when the vocal folds open for respiration. Oral swallowing and pharyngeal bolus transport are generally normal. With total laryngectomy, an effort is made to reconstruct an upper esophageal sphincter by attaching the free ends of the cricopharyngeus or filling in the gap of the resected cricoid with soft tissue. Therefore, some narrowing or stricture of the reconstructed UES may be present (Fig. 19) with increased residual in the pharynx, or the patient may have a pseudoepiglottis at the tongue base [17]. The oral phase of swallowing is usually normal. In some patients, laryngectomy is accompanied by a cricopharyngeal myotomy.

Evaluation of Therapeutic Maneuvers

Videofluorography is not only a useful method for the diagnostic evaluation of oral-pharyngeal swallowing disorders but can be used to search for a "safe swallow" without aspiration accompanied by satisfactory pharyngeal bolus transport [4]. Therapeutic maneuvers include (1) manipulations of bolus variables such as volume and consistency, (2) variation of head position, and (3) use of certain specific therapeutic maneuvers such as supraglottic swallow [19]. Some patients exhibit aspiration with a small barium bolus (e.g., 2 ml), while others require a larger bolus (e.g., 10 ml). For this reason, at least several volumes should be used during the diagnostic examination. Examination with several bolus consistencies is critical. In some patients, aspiration occurs most commonly with thin barium (e.g., 30% wt/vol), but may not occur at all with thick barium or paste material (e.g., barium paste, applesauce, or pudding). Head position can be very important. Head flexion often prevents aspiration by reducing premature spill from the mouth and also by tucking the larynx anteriorly beneath the epiglottis (Fig. 20). Tilting the head backward can enhance oral transit. Turning of the head directly to the contralateral side may compensate for unilateral pharyngeal weakness (Fig. 4). Bending the head laterally directs swallowed liquid to the ipsilateral side and may also be useful therapeutically to enhance pharyngeal bolus transport and prevent aspiration.

Two special maneuvers that may be evaluated during videofluoroscopy include the supraglottic swallow and the Mendelsohn maneuver. The supraglottic swallow is done for patients with aspiration before or during a pharyngeal swallow.

The subject is instructed to take a deep breath and then swallow during breath-holding. A cough immediately following the swallow clears the larynx of aspirated material. The Mendelsohn maneuver is done to facilitate UES opening and, therefore, enhance pharyngeal emptying and reduce aspiration. For the Mendelsohn maneuver, the subject is instructed to produce a sustained hyoid-laryngeal elevation during a swallow. Placing a finger on the subject's hyoid or having the patient look at the video monitor may help in the completion of this maneuver. This maneuver puts sustained traction on the UES and prolongs its opening, thereby facilitating sphincter opening and pharyngeal emptying.

REFERENCES

1. Dodds WJ, Stewart ET, Logemann JA. Physiology and radiology of the normal oral and pharyngeal phases of swallowing. *AJR* **1990**;154: 953-963
2. Dodds WJ, Taylor AJ, Stewart ET, Kern MK, Logemann JA, Cook IJ. Tipper and dipper types of oral swallows. *AJR* **1989**;153:1197–1199
3. Curtis DJ, Sepulveda GU. Epiglottic motion: video record of muscular dysfunction. *Radiology* **1983**;148:473–477
4. Logemann JA. Treatment for aspiration related to dysphagia: an overview. *Dysphagia* **1986**;1:34–38
5. Curtis DJ, Hudson T. Laryngotracheal aspiration: analysis of specific neuromuscular factors. *Radiology* **1983**;149:517–522
6. Dodds WJ. The physiology of swallowing. *Dysphagia* **1989**;3:171–178
7. Cook IJ, Dodds WJ, Dantas RO, et al. Opening mechanism of the human upper esophageal sphincter. *Am J Physiol* **1989**;20:G748–G759
8. Asherson N. Achalasia of the cricopharyngeal sphincter. *J Laryngol Otol* **1950**;64:747–758
9. Sutherland HD. Cricopharyngeal achalasia. *J Thorac Cardiovasc Surg* **1962**; 43:114–126
10. Buchholz DW, Bosma JF, Donner MW. Adaptation, compensation, and decompensation of the pharyngeal swallow. *Gastrointest Radiol* **1985**;10:235–239
11. Ekberg O, Nylander G. Pharyngeal dysfunction after treatment for pharyngeal cancer with radiotherapy. *Gastrointest Radiol* **1983**;8:97–104
12. Curtis DJ, Cruess DF, Crain M, Sivit C, Winters C Jr, Dachman AH. Lateral pharyngeal outpouchings: a comparison of dysphagic and asymptomatic patients. *Dysphagia* **1988**;2:156–161
13. Vakil NB, Kahrilas PJ, Dodds WJ, Vanagunas A. Absence of an upper esophageal sphincter response to acid reflux. *Am J Gastroenterol* **1989**; 84:606–610
14. Balfe DM, Heiken JP. Contrast evaluation of structural lesions of the pharynx. *Curr Probl Diagn Radiol* **1986**;15:73–160
15. Jones B, Kramer SS, Donner MW. Dynamic imaging of the pharynx. *Gastrointest Radiol* **1985**;10:213–224
16. Logemann J. *Evaluation and treatment of swallowing disorders*. San Diego: College-Hill Press, **1983**
17. Balfe DM, Koehler RE, Setzen M, Weyman PJ, Baron RL, Ogura JH. Barium examination of the esophagus after total laryngectomy. *Radiology* **1982**;143:501–508
18. McConnel FMS, Mendelsohn M. The effects of surgery on pharyngeal deglutition. *Dysphagia* **1987**;1:145–151
19. Logemann JA. *Manual for the videofluorographic study of swallowing*. San Diego: College-Hill Press, **1986**

Comparison of Biello, McNeil, and PIOPED Criteria for the Diagnosis of Pulmonary Emboli on Lung Scans

Milo M. Webber[1]
Antoinette S. Gomes[2]
Denise Roe[3]
Richard L. La Fontaine[4]
Randall A. Hawkins[1]

The McNeil, Biello, and newly proposed PIOPED (from the National Institutes of Health–sponsored study, *Prospective Investigation of Pulmonary Embolism Detection*) interpretive methods for detection of pulmonary embolism on lung scans were compared in 96 patients who also underwent pulmonary angiography. Segmental findings on ^{99m}Tc perfusion and aerosol ventilation scans, chest radiographs, and pulmonary angiograms obtained within 48 hr of each other were encoded along with other information into a data base to facilitate analysis. The McNeil, Biello, and PIOPED criteria were applied to the encoded data. Although the PIOPED set of criteria yielded the most favorable likelihood ratio for predicting an angiogram showing pulmonary emboli and a favorable likelihood ratio for predicting an angiogram not showing pulmonary emboli, it had the highest number of indeterminate studies. The McNeil criteria demonstrated the least favorable likelihood for predicting pulmonary emboli on an angiogram. The Biello and McNeil criteria showed the most favorable likelihood ratio for predicting an angiogram not showing pulmonary emboli. Analysis of receiver-operating-characteristic (ROC) curves yielded the greatest area under the ROC curve for the Biello criteria, but there were no statistically significant differences among the three sets of criteria.

This study suggests that the Biello scheme represents the best compromise of the sets of criteria studied.

***AJR* 154:975–981, May 1990**

The diagnosis of pulmonary embolism by clinical or laboratory findings is often inaccurate [1, 2]. Although the pulmonary angiogram is the most accurate study available to confirm the diagnosis of pulmonary embolism [3, 4], it is invasive; therefore, noninvasive pulmonary perfusion and ventilation scans are the primary screening techniques used [5]. Although a normal perfusion scan has been found to very reliable in excluding pulmonary embolism [6], opinions differ regarding the overall reliability, usefulness, methodology, and interpretation of radionuclide studies [7].

Several diagnostic schemes have been suggested for the interpretation of radionuclide scans [8–10], with the goal of increasing the accuracy of the radionuclide studies for predicting the findings on the pulmonary angiogram. In this study, schemes patterned after those developed by McNeil [8], Biello [9], and the Nuclear Medicine Working Group of the Prospective Investigation of Pulmonary Embolism Detection (PIOPED) study [10] were applied to a group of consecutive patients who underwent pulmonary radiography, angiography, and radionuclide pulmonary studies in a recent 3-year period. Although McNeil [8] did not explicitly set forth a set of criteria, we derived such a set from the data in the McNeil article, as did Sullivan et al. [11] in their report. All sets of criteria used in this study are outlined in Table 1.

Materials and Methods

A total of 1064 patients underwent radionuclide lung scanning during a recent 3-year period. One hundred seventeen (11%) of these had pulmonary angiograms and chest

Received October 2, 1987; accepted after revision December 12, 1989.

[1] Department of Radiological Sciences, Division of Nuclear Medicine and Biophysics, Rm. BL428, CHS, University of California, Los Angeles, School of Medicine, Los Angeles, CA 90024. Address reprint requests to M. M. Webber.

[2] Department of Radiological Sciences, Division of Diagnostic Radiology, Rm. BL428, CHS, University of California, Los Angeles, School of Medicine, Los Angeles, CA 90024.

[3] School of Public Health, University of California, Los Angeles, Los Angeles, CA 90024. Present address: 1515 N. Campbell, Tucson, AZ 85724.

[4] Department of Radiology, Naval Hospital, San Diego, CA 92134.

0361–803X/90/1545–0975
© American Roentgen Ray Society

TABLE 1: Sets of Criteria Used to Assess Radionuclide Scans for the Probability of Pulmonary Embolism on Angiograms

Category	McNeil [8]	Biello [9]	PIOPED [10]
Normal	1. Normal perfusion	1. Normal perfusion	1. Normal perfusion
Very low probability	–	–	2. One to three small[a] perfusion defects; normal chest radiograph; ventilation irrelevant
Low probability	2. Single ventilation/perfusion mismatch, segmental or subsegmental; chest radiograph clear 3. Ventilation/perfusion match(es) alone 4. Multiple ventilation/perfusion mismatches, subsegmental; chest radiograph clear	2. Small[a] ventilation/perfusion mismatch(es) 3. Ventilation/perfusion matches without corresponding changes on chest radiograph 4. Perfusion defect substantially smaller than chest film density	3. Nonsegmental perfusion defects[b] 4. Single moderate[c] perfusion defect; chest radiograph normal; ventilation irrelevant 5. Any perfusion defect substantially smaller than chest film defect; ventilation irrelevant 6. Ventilation/perfusion match ≤50% of lung including ≤75% of one lung zone[d] with normal or almost normal chest radiograph 7. More than three small[a] perfusion defects; chest film and ventilation irrelevant 8. Three or fewer small perfusion/chest film matches; ventilation irrelevant
Indeterminate or intermediate	5. Mixed ventilation/perfusion match and mismatch 6. Perfusion defect with matched density on chest radiograph	5. Severe diffuse obstructive pulmonary disease with perfusion defects 6. Perfusion defect same size as change on chest film 7. Single medium[e] ventilation/perfusion mismatch	9. Abnormality that is not defined clearly by other criteria
High probability	7. Single ventilation/perfusion mismatch, lobe or larger, with normal chest film 8. Multiple ventilation/perfusion mismatches, segmental or larger; chest film normal	8. Single large[e] ventilation/perfusion mismatch 9. Perfusion defect substantially larger than density on chest film 10. Multiple medium or large[e] ventilation/perfusion mismatches without matched density on chest film	10. Two or more large[f] perfusion defects; ventilation and chest film normal 11. Two or more large[f] perfusion defects in which perfusion defect is substantially larger than either matching ventilation or chest film defect 12. Two or more moderate[c] perfusion defects and one large[f] perfusion defect; ventilation and chest film normal 13. Four or more moderate[c] perfusion defects; ventilation and chest film normal

Note.—PIOPED = Prospective Investigation of Pulmonary Embolism Detection.

[a] Biello and PIOPED: Small is 25% or less of an anatomic segment.

[b] PIOPED: Nonsegmental means very small effusion, cardiomegaly, hila, etc.

[c] PIOPED: Moderate means >25% and <75% of a segment.

[d] PIOPED: Lung zone means upper, middle, or lower third of the lung.

[e] Biello: Medium is 25–90%; large is more than 90% of a segment.

[f] PIOPED: Large means >75% of a segment.

radiographs within 48 hr of the lung scan. Of the patients studied, 22 did not undergo ventilation scanning. One of the 22 was included in this report because the perfusion scan was normal and a ventilation scan was not needed for interpretation. The other 21 cases in which a ventilation scan was not obtained were excluded. Ninety-six patients constituted the study group.

Pulmonary perfusion scanning was performed after injecting 1 mCi (37 MBq) of commercially obtained ^{99m}Tc-labeled macroaggregates of albumin. Images (300,000 counts) were made in six views: anterior, posterior, right anterior oblique, left anterior oblique, right posterior oblique, and left posterior oblique.

The ventilation studies were done with the use of ^{99m}Tc-DTPA aerosol. Although several reports have correlated angiography, pulmonary perfusion, and xenon ventilation scan studies [5, 8, 12–14], we are unaware of any similar report on the results of a pulmonary scanning technique that used aerosol ventilation scanning, except for phase II in the study of Hull et al. [5]. The technique of pulmonary ventilation scanning with an aerosol was originally described by Hayes et al. [15] and more recently by Ramanna et al. [16] and Alderson et al. [17]. Patients were given ^{99m}Tc-DTPA by inhalation according to the method of Hayes et al. [15] until the amount of activity in their lungs had increased to at least four times the level at the end of the perfusion lung scan. The interpretive criteria were not significantly modified because of the use of the aerosol technique, even though the xenon gas technique was originally used when the McNeil and Biello criteria were developed. The Biello criteria require identification of the presence or absence of chronic obstructive pulmonary disease. This diagnosis was made on the basis of the chest radiograph when signs of overexpansion, increased diameters, flattened diaphragms, and increased lucency were present. The aerosol ventilation scan was almost always confirmatory of this diagnosis, demonstrating a patchy ventilation pattern with excessive central deposition and/or diffuse punctate deposition of the radiotracer within the lung fields. Equipment used and views obtained were the same used for perfusion imaging.

Either posteroanterior or anteroposterior and lateral chest radiographs were obtained. The majority of patients had standard chest radiographs, with the patient in an upright position; 20% of patients had portable anteroposterior radiographs of the chest.

Pulmonary angiography was performed by using conventional angiographic techniques. Selective right and left pulmonary artery injections were performed in anteroposterior and oblique or lateral projections. Both nonmagnification and magnification views were obtained. The site or sites of abnormality on the chest radiographs and lung scans were generally known at the time of pulmonary angiography; however, angiographic positioning was based primarily on the findings of the initial selective anteroposterior injection into the right and left pulmonary arteries.

Each radionuclide pulmonary study, chest radiograph, and angiogram was analyzed by two observers. Any disagreement was resolved by consensus. The analysis was on a segment-by-segment basis, and results were recorded for each imaging technique. There was no consideration of information relating to the patient's history or of any of the risk factors for pulmonary embolism. Results from each patient were tabulated on a work sheet and then entered into a computer data base. Each patient's data were then compared with each criterion of each of the three diagnostic schemes (Table 1). The purpose of the computer-assisted technique was twofold: (1) to facilitate analysis of the data and (2) to improve the objectivity of the application of various sets of criteria to the data.

As more than one criterion may be satisfied owing to differing findings in various areas of the lungs, each patient's scan was categorized on the basis of the highest probability category found in any lung area: (1) high probability, (2) intermediate or indeterminate, or (3) low probability.

A "normal" scan category was considered determinative because such a scan virtually eliminates the possibility of an occlusive pulmonary embolism.

The final diagnosis established for each set of criteria was then compared with the findings on the pulmonary angiogram. The pulmonary angiogram was considered as showing pulmonary embolism when or more filling defects or vessel cutoffs were identified in the branch pulmonary arteries or proximal pulmonary arteries. Angiograms showing other abnormal findings were classified as abnormal but without evidence of pulmonary embolism.

Receiver-operating-characteristic (ROC) curves were generated for the three interpretative criteria sets. As shown in Table 1, the three sets of criteria were subdivided into the four categories of normal, low and very low probability, intermediate or indeterminate, and high probability; these were assigned ranks of 1–4, respectively. Each of the four categories yielded three points on an ROC curve. The computer program RSCORE II [18], developed by Dorfman and Alf [19], was used to calculate the area under the ROC curve and the corresponding standard error. Statistical analysis of the difference in area between ROC curves was done by the method of Hanley and McNeil [20] for data obtained from matched images. This method involves calculating a critical ratio z from the equation,

$$z = (A_1 - A_2)/(SE_1^2 + SE_2^2 - 2r\ SE_1\ SE_2)^{1/2}, \tag{1}$$

where A and SE are the observed areas under the ROC curves and the estimated standard errors of the curves being compared, respectively, and r is the estimated correlation between areas calculated using Kendall's tau. The values of z were compared with tables of the normal distribution [21]; values of z above 1.96, corresponding to a probability of less than 5% that the observed difference would arise by chance given no underlying difference ($p < .05$), were accepted as evidence that the true ROC areas were different. A two-tailed test was used for this study.

Results

A data table was constructed for the three schemes on the basis of the findings on the angiograms. Patients with an angiogram showing pulmonary embolism were considered to have pulmonary embolism. Patients with a pulmonary angiogram that did not show pulmonary embolism were considered not to have pulmonary embolism. Following the method described by McNeil [8], overall likelihood ratios of having pulmonary embolism for the three sets of criteria were determined. For each possible pattern (set of criteria), the frequency of that pattern in patients whose angiogram showed emboli was divided by the frequency of the same pattern in patients whose angiogram did not show thromboembolism (Table 2). The PIOPED criteria for high probability had a greater likelihood of predicting an angiogram showing emboli than the McNeil or Biello criteria for high probability; however, the PIOPED criteria for low probability showed less likelihood

TABLE 2: Ability of Radionuclide Scans to Predict Pulmonary Embolism on Angiograms

Finding	Set of Criteria Used		
	McNeil [8]	Biello [9]	PIOPED [10]
Prediction from radionuclide scan[a]			
High probability	23/8	28/4	13/1
Low probability	4/14	6/21	7/22
Normal	0/4	0/4	0/4
Indeterminate	15/28	8/25	22/27
Likelihood ratio			
High probability	3.70	9.00	16.70
Low probability	0.37	0.37	0.41
Fraction indeterminate			
Overall	0.45	0.34	0.51
Positive on angiogram	0.35	0.24	0.45
Fraction low probability plus normal scan; positive on angiogram	0.18	0.19	0.21

Note.—PIOPED = Prospective Investigation of Pulmonary Embolism Detection.

[a] No. of cases showing embolism on angiogram/no. of cases not showing embolism on angiogram. Total no. of cases = 96 (42/54).

than (was not as good as) the McNeil and Biello low-probability criteria for predicting a normal angiogram.

The likelihood ratios of each of the specific individual criteria (from McNeil, Biello, and PIOPED) appearing in any patient study when it was determinative are shown in Table 3. High probability, low probability, and negative criteria likelihood ratios are listed. Indeterminate criteria are also listed for interest. Noteworthy is the high likelihood of predicting an angiogram showing emboli with McNeil criterion 7; Biello criteria 8–10; and PIOPED criterion 10. Criterion 7 of the McNeil scheme, with a likelihood ratio of 5.15, appeared in 19% of patients who had angiograms showing emboli. Criterion 10 of the Biello scheme, with a likelihood ratio of 9.65, appeared in 36% of patients who had an angiogram showing emboli. Biello criterion 8, with a likelihood ratio of 6.44, appeared in 24% of such cases. As for the PIOPED data, the angiograms showing emboli were best predicted by criterion 10, with an infinite likelihood ratio; criterion 10 identified 26% of patients with angiograms showing emboli. Criteria 13 and 11 (also infinite) appeared in only 2.4% of the patients with angiograms showing emboli.

Lower ratios indicate greater ability to predict a normal angiogram. The likelihood ratio of predicting normal angiograms by using the negative criterion for all these schemes was perfect (0.00). However, the low probability criteria were not as good. McNeil criterion 2, with a likelihood ratio of 0.00, was the best but appeared in only 7% of the patients with a normal angiogram. Biello criterion 5, with a likelihood ratio of 0.26, appeared in 9% of normal angiogram cases. Biello criterion 3, with a likelihood ratio of 0.30, appeared in 31% of patients with normal angiograms. PIOPED criterion 2 had the best likelihood (0.26) of the PIOPED criteria for predicting a normal angiogram, and appeared in 19% of patients with a normal angiogram.

TABLE 3: Likelihood Ratios for Criteria Studied When Criteria for Pulmonary Embolism Were Determinative

Source/ Criterion	No. of Patients		Frequency of Pattern[a]		Likelihood Ratio
	Angio +	Angio −	Angio +	Angio −	
McNeil [8]					
1	0	4	0	0.0741	0.00
2	0	4	0	0.0741	0.00
3	4	11	0.0952	0.2037	0.47
4	0	0	0	0	—
5	4	4	0.0952	0.0741	1.28
6	15	26	0.3571	0.4815	0.74
7	8	2	0.1905	0.0370	5.15
8	16	6	0.3810	0.1111	3.43
9	3	2	0.0714	0.0370	1.93
Biello [9]					
1	0	4	0	0.0741	0.00
2	1	3	0.0238	0.0556	0.43
3	4	17	0.0952	0.3148	0.30
4	4	6	0.0952	0.1111	0.86
5	1	5	0.0238	0.0926	0.26
6	6	15	0.1429	0.2778	0.51
7	1	4	0.0238	0.0741	0.32
8	10	2	0.2381	0.0370	6.44
9	4	0	0.0952	0	—
10	15	2	0.3571	0.0370	9.65
PIOPED [10]					
1	0	4	0	0.0741	0.00
2	2	10	0.0476	0.1852	0.26
3	0	0	0	0	—
4	2	3	0.0476	0.0556	0.86
5	4	7	0.0952	0.1296	0.73
6	0	2	0	0.0370	0.00
7	0	1	0	0.0185	0.00
8	2	3	0.0476	0.0556	0.86
9	22	27	0.5238	0.5000	1.05
10	11	0	0.2619	0	—
11	1	0	0.0238	0	—
12	1	1	0.0238	0.0185	1.29
13	1	0	0.0238	0	—

Note.—More than one criterion in any category may be determinative in any single patient. Therefore, the number of determinative criteria listed in a specific category in this table may not be the same as the number of patients in the same category. Criteria are defined in Table 1. Angio + = pulmonary emboli were confirmed on angiogram; Angio − = pulmonary emboli were not confirmed on angiogram; — = undefined; PIOPED = Prospective Investigation of Pulmonary Embolism Detection.

[a] Pattern of finding on radionuclide scan.

The areas under the ROC curves and associated standard errors for the three sets of criteria are contained in Table 4. The Biello criteria had the greatest area (0.852 ± 0.086), followed by PIOPED (0.793 ± 0.104) and McNeil (0.778 ± 0.104), which had areas that were approximately equal. Intervals on the areas under the ROC curves represent the 95% confidence level (±2 SD), which has been shown to be approximately symmetric for these types of ROC curves [22]. The areas were compared with each other, and a critical ratio was calculated for each of the three possible comparisons by using the method of Hanley and McNeil [20]. A critical ratio of 1.96 or larger was considered statistically significant ($p < .05$).

Critical ratios of the differences in area under the ROC curves and correlation coefficients between the three criteria are contained in Table 5. None of the comparisons yielded a critical ratio equal to or greater than 1.96, and therefore no statistical difference was shown between areas under the ROC curves. The difference between the Biello and McNeil criteria ROC curve areas has a critical value of 1.83, which is significant at the $p < .07$ level, but this can only be said to be suggestive of a true difference between areas.

Discussion

We compared schemes of interpreting ventilation-perfusion scans that might enable us to use the noninvasive scanning procedures to predict the finding on the invasive pulmonary angiogram. Even though a variety of factors limit the accuracy of pulmonary angiography (e.g., clot resolution between the onset of symptoms and obtaining the angiogram) [3, 12, 23], angiography is widely accepted as a "gold standard" and often follows a lung scan in the sequence of diagnostic tests. It is obviously useful to statistically profile the results of ventilation-perfusion scans relative to angiograms.

At this institution, we have used the aerosol ventilation scan technique since its development [15]. In contrast to the usual one-view ^{133}Xe gas study, ^{99m}Tc-DTPA aerosol scans permit an excellent comparison of multiple views with the perfusion scans. Although "washout" data are not available with the aerosol scan, and it has been stated that it might be difficult to see small ventilation defects, Ramanna et al. [16] concluded that the aerosol technique detects all parenchymal abnormalities associated with significant perfusion defects.

As stated earlier, 11% of patients undergoing lung scan studies in the period of the study underwent pulmonary angiography. In order to understand better why only 11% of the patients had angiography, the pulmonary medicine attending staff members at this institution were polled about their criteria for requesting that a pulmonary angiogram be obtained in a patient suspected of having pulmonary embolism. The results were surprisingly nonuniform. Sixty percent would obtain angiograms in patients at high risk for receiving anticoagulants who had a high-probability scan outcome, regardless of prior clinical probability of the patient having pulmonary embolism. Another 20% would obtain an angiogram in any patient only if the patient had moderate or greater prior clinical probability of pulmonary embolism. Most would obtain an angiogram if the scan were indeterminate in a patient with high or moderate prior probability for pulmonary embolism. In the case of low-probability scans, 20% would not order an angiogram; others would if there was high prior clinical probability. Because of the diversity of responses to the poll, it is difficult to determine the actual reasons for requesting an angiogram. However, it appears that the perception of most of the pulmonologists is that an angiogram is generally necessary unless the patient has a normal scan and/or a low prior clinical probability of having pulmonary embolism.

TABLE 4: Areas Under Receiver-Operating-Characteristic Curve

Criteria Set	Area Under Curve[a]	Standard Error
Biello [8]	0.852 ± 0.086	0.043
PIOPED [10]	0.793 ± 0.104	0.052
McNeil [9]	0.778 ± 0.104	0.052

Note.—PIOPED = Prospective Investigation of Pulmonary Embolism Detection.

[a] Area ± 95% confidence interval.

TABLE 5: Critical Ratios of Differences in Area Under Receiver-Operating-Characteristic Curves

Comparison	Critical Ratio	*p* Value	Correlation Coefficient (r)
Biello [8] > McNeil [9]	1.83	.07	.65
Biello > PIOPED [10]	1.34	.18	.59
PIOPED > McNeil	0.30	.77	.52

Note.—PIOPED = Prospective Investigation of Pulmonary Embolism Detection.

A prior analysis [23] of the discharge diagnoses in a sampling of 300 of the 1064 patients having lung scan studies during the period of our study revealed that 80% of those patients with a scan diagnosis of high probability of pulmonary embolism were diagnosed at discharge as having pulmonary embolism. Thirty percent of those with an indeterminant outcome of the scan were discharged with the diagnosis of pulmonary embolism. Only 3% of those with a low-probability reading of the scan were discharged as having pulmonary embolism. One percent of those with a normal scan had a discharge diagnosis of pulmonary embolism. These data give some idea as to how the pulmonary scan relates to the perceived diagnosis of pulmonary embolism.

Our results (Table 2) suggest that when all cases including those in the intermediate category are considered, the Biello criteria represent the best compromise of the schemes studied, with 34% indeterminate. The fraction of indeterminate results was the lowest among the three schemes and the fraction of the indeterminate group found to have angiograms showing pulmonary embolism was 24%, which is also the lowest fraction of the three schemes. Including the patients in the indeterminate category, the Biello scheme classified the largest number of patients with an angiogram showing pulmonary embolism as high probability: 28 of 42. The McNeil scheme identified 23 of 42 and the PIOPED identified 13 of 42. Although the PIOPED scheme was the most successful in identifying those patients whose angiogram did not show pulmonary embolism, by combining normal and low-probability categories (26 of 54), Biello was a very close second, identifying 25 of 54. McNeil identified 18 of 54.

The area under an ROC curve obtained by the rating method has been shown to represent the probability that a randomly chosen diseased subject will be correctly rated or ranked with greater suspicion than a randomly chosen nondiseased subject [24]. By using a two-tailed test, however, no criterion demonstrated a statistically significant improvement in area ($p < .05$) when compared with the other two criteria. Lack of statistically significant results in this study may be due to the small sample size of only 42 cases with angiograms showing emboli and 54 cases with angiograms not showing emboli, resulting in a type II statistical error, that is, failure to show a difference between two areas when it exists. The probability of making a type II error can be quantified by an analysis of the statistical power of the hypothesis test. The statistical power of this study was estimated using the methodology of Hanley and McNeil [22]. In order to apply this methodology, the unequal numbers of abnormal and normal cases were pooled to yield an equally divided case size of 48, and the paired cases were converted to equivalent unpaired cases using the relationship [20]:

$$n(u) = n(p)/(1 - r), \qquad (2)$$

where n(u) and n(p) are the unpaired and paired sample sizes, respectively, and r is the estimated correlation between areas listed in Table 5. The probability, $Z(\alpha)$, of a type II error can

TABLE 6: Comparison of Various Studies by Using Biello [9] or Similar Criteria

Study/Criterion	No. of Patients		Frequency of Pattern[a]		Likelihood Ratio
	Angio +	Angio −	Angio +	Angio −	
This study					
High probability	28	4	0.6667	0.0741	9.00
Low probability + negative	6	25	0.1429	0.4630	0.31
Biello et al. [27]					
High probability	37	4	0.6981	0.0412	16.94
Low probability + negative	2	53	0.0377	0.5464	0.07
Sullivan et al. [11]					
Reader 1					
High probability	15	7	0.5000	0.1029	4.86
Low probability + negative	3	28	0.1000	0.4118	0.24
Reader 2					
High probability	13	12	0.4333	0.1905	2.27
Low probability + negative	3	21	0.1000	0.3333	0.32
Carter et al. [14]					
Reader 1					
High probability	10	4	0.4545	0.0870	5.22
Low probability + negative	1	22	0.0455	0.4783	0.10
Reader 2					
High probability	14	1	0.4516	0.0256	17.64
Low probability + negative	7	17	0.2258	0.4359	0.52
Reader 3					
High probability	16	4	0.6400	0.0888	7.21
Low probability + negative	4	24	0.1600	0.5333	0.30
Rosen et al. [26]					
High probability	10	1	0.3333	0.0227	14.68
Low probability + negative	1	16	0.0333	0.3636	0.09
Spies et al. [28]					
High probability	34	4	0.4789	0.0580	8.26
Low probability + negative	1	28	0.0141	0.4058	0.03
Sostman et al. [25]					
High probability	3	3	0.1765	0.0750	2.35
Low probability + negative	1	7	0.0588	0.1750	0.34
Hull et al. [5]					
Aerosol					
High probability	21	3	0.4375	0.0682	6.42
Low probability + negative	24	32	0.5000	0.7272	0.69
Xenon-127					
High probability	30	5	0.7500	0.1163	6.45
Low probability + negative	8	28	0.2000	0.6512	0.31

Note.—Angio + = pulmonary emboli were confirmed on angiogram; Angio − = pulmonary emboli were not confirmed on angiogram.

[a] Pattern of finding on radionuclide scans.

then be calculated from equation 3 of Hanley and McNeil [20] using $Z(\beta)$ equal to 1.96 for a 5% two-sided test of significance. (Although pooling introduces a small uncertainty, it does not alter the conclusion that the statistical power of this study is low.)

Computation of $Z(\beta)$ yields values of −0.10, −0.57, and −1.66 for the three comparisons of Biello/McNeil, Biello/PIOPED, and PIOPED/McNeil, respectively. These values correspond to a statistical power of probability of 0.46, 0.28, and 0.05, respectively, that the test of significance would yield a statistically significant difference. Conversely, the probability of making a type II error for the three comparisons is 0.54, 0.72, and 0.95, respectively. Therefore, even if underlying differences exist between the ROC areas of the three criteria, the chance of demonstrating statistically significant differences for a 5% two-sided test of significance was less than 50% for each of the three comparisons in this study because of the small sample size. For that reason, the lack of statistically significant findings in this study cannot be taken as conclusive that underlying differences between the areas under the ROC curves do not exist.

The likelihood ratios arising from our data were compared with the data of other reports (Table 6). Several published reports [11, 14, 25–28] that used the Biello or a similar set of criteria were studied and the likelihood ratios were determined. Although some of the reports indicate likelihood ratios of 14 or more, many are comparable to our data.

Recently, interest has been stirred by the data of Hull et al. [5]. Their prospective study showed that over 40% of the low-probability group had angiographic evidence of pulmonary embolism, which is substantially greater than the percentages of Biello et al. [27] and others [11, 14, 25, 26, 28]. The value of 19% reported in this study (see Biello criteria, Table 2) is more comparable to the results of others [14, 25, 29] than to the results of Hull et al. [5].

Use of computer data base techniques as reported here permits rapid, more objective correlation of a large amount of data. It also provides a method by which future proposed criteria can be evaluated retrospectively, without reevaluation of the images themselves.

REFERENCES

1. Wigton RS, Hoellerich VL, Patil KD. How physicians use clinical information in diagnosing pulmonary embolism: an application of conjoint analysis. *Med Decis Making* **1986**;6:2–11
2. Sostman HD, Rapoport S, Gottschalk A, Greenspan RH. Imaging of pulmonary embolism. *Invest Radiol* **1986**;21(6):443–454
3. Murphy JL, Bullock RT. Factors influencing the restoration of blood flow as determined by angiography and scanning. *Circulation* **1968**;38:1116–1126
4. Mills SR, Jackson DC, Sullivan DC, et al. Angiographic evaluation of acute pulmonary embolism. *Radiology* **1980**;136:301–308
5. Hull RD, Hirsh J, Carter CJ, et al. Diagnostic value of ventilation-perfusion lung scanning in patients with suspected pulmonary embolism. *Chest* **1985**;88(6):819–828
6. Kipper MS, Moser KM, Kortman KE, Ashburn WL. Longterm followup of patients with suspected pulmonary embolism and a normal lung scan. *Chest* **1982**;82:411–415
7. Braun SD, Newman GE, Ford K, Miller GA, Coleman RE, Dunnick NR. Ventilation-perfusion scanning and pulmonary angiography: correlation in clinical high-probability pulmonary embolism. *AJR* **1984**;143:977–980
8. McNeil BJ. Ventilation-perfusion studies and the diagnosis of pulmonary embolism: concise communication. *J Nucl Med* **1980**;21:319–323
9. Biello DR. Radiological (scintigraphic) evaluation of patients with suspected pulmonary embolism. *JAMA* **1987**;257(23):3257–3259
10. PIOPED Data and Coordination Center. *Prospective investigation of pulmonary embolism detection*. Baltimore: Maryland Medical Research Institute, **1986**:7:7–8
11. Sullivan DC, Coleman RE, Mills SR, Ravin CE, Hedlund LW. Lung scan interpretation: effect of different observers and different criteria. *Radiology* **1983**;149:803–807
12. Sautter RD, Fletcher FW, Emanuel DA, Lawton BR, Olsen TG. Complete resolution of a massive pulmonary thromboembolism. *JAMA* **1964;**189:948–949
13. Simon M, Sasahara A. Observations on the angiographic changes in pulmonary thromboembolism. In: Sasahara A, Stein M, eds. *Pulmonary embolic disease*. New York: Grune & Stratton, **1965**:214–224
14. Carter WD, Brady TM, Keyes JW, et al. Relative accuracy of two diagnostic schemes for detection of pulmonary embolism by ventilation-perfusion scintigraphy. *Radiology* **1982**;145:447–451
15. Hayes M, Taplin GV, Chopra SK, Knox DE, Elam D. Improved radioaerosol administration system for routine inhalation lung imaging. *Radiology* **1979**;131:256–258
16. Ramanna L, Alderson PO, Waxman AD, et al. Regional comparison of technetium-99m DTPA aerosol and radioactive gas ventilation (xenon and krypton) studies in patients with suspected pulmonary embolism. *J Nucl Med* **1986**;27(9):1391–1396
17. Alderson PO, Biello DR, Kumar B, et al. ^{99m}Tc-DTPA aerosol and radioactive gases compared as adjuncts to perfusion scintigraphy in patients with suspected pulmonary embolism. *Radiology* **1984**;153:515–521
18. Swets JA, Pickett RM. *Evaluation of diagnostic systems.* New York: Academic Press, **1982**
19. Dorfman DD, Alf E. Maximum likelihood estimation of parameters of signal theory and determination of confidence intervals-rating-method data. *J Math Psychol* **1969**;6:487–496
20. Hanley JA, McNeil BJ. A method of comparing the areas under receiver operating characteristics curves from the same cases. *Radiology* **1983**;148:839–843
21. Armitage P. *Statistical methods in medical research.* Oxford: Blackwell Scientific Publications, **1971**
22. Hanley JA, McNeil BJ. The meaning and use of the area under a receiver operating characteristic (ROC) curve. *Radiology* **1982**;143:29–36
23. Wong WS, Makuno DH, Hawkins RA, Webber MM, Roe DJ. A diagnostic scheme for work-up of pulmonary embolism in young women. *J Nucl Med* **1982**;23:P43
24. Fred HL, Azelrod MA, Lewis JM, Alexander JK. Rapid resolution of pulmonary thromboemboli in man: an angiographic study. *JAMA* **1966**;196:1137–1139
25. Sostman HD, Ravin CE, Sullivan DC. Use of angiography for suspected pjulmonary embolism: influence of scintigraphic diagnosis. *AJR* **1982**;139:673–677
26. Rosen JM, Biello DR, Siegel BA, Sedlin DW, Alderson PO. ^{81m}Kr imaging: clinical utility in suspected pulmonary embolism. *Radiology* **1985**;154:787–790
27. Biello DR, Mattar AG, McKnight RC, Siegel BA. Ventilation-perfusion studies in suspected pulmonary embolism. *AJR* **1979**;133:1033–1037
28. Spies WG, Burstein SP, Dellehay GL, Vogelzang RL, Spies SM. Ventilation-perfusion scintigraphy in suspected pulmonary embolism: correlation with pulmonary angiography and refinement of criteria for interpretation. *Radiology* **1986**;159:383–390
29. Davis RB, Schauwecker DS, Siddiqui AR, et al. Indeterminant lung imaging: can the number be reduced? *Clin Nucl Med* **1986;**11:577–582

Book Review

CT and Sonography of the Acute Abdomen. By R. Brooke Jeffrey, Jr. New York: Raven, 303 pp., 1989. $98

The authors of this text have succeeded admirably in providing a concise, readable review of the role of CT and sonography in common abdominal and pelvic conditions. They have achieved their purpose in writing "a practical clinical guide emphasizing the diagnostic strengths and weaknesses" of CT and sonography in the diagnosis and management of those problems most likely to be encountered by the radiology resident or other house officer on call in the acute care setting. The scope of this book is actually greater than the acute abdomen. It includes trauma; iatrogenic injuries; postoperative complications; and other conditions such as acute rejection of renal transplants, urinary and gastrointestinal obstruction, and inflammatory diseases. Another useful feature is the discussion of the expanding role of CT- and sonography-guided percutaneous procedures as alternatives to surgery. With few exceptions, the images are superb. The authors have culled some of the best images from the recent literature. Unfortunately, the layout is somewhat distracting in that the illustrations are frequently several pages removed from the relevant text.

The book has eight chapters that cover the liver; gallbladder and bile ducts; spleen; pancreas; kidney and adrenal glands; gastrointestinal tract; pelvis; and, finally, the aorta, inferior vena cava, and psoas compartments. The common pathologic entities in each organ or region are presented with the assumption that the reader is familiar with cross-sectional anatomy and normal findings. Unusual entities covered in larger reference texts are not included. The format in each chapter is consistent. Each entity is introduced with an "imaging overview" paragraph. This is followed by a detailed discussion of the clinical and imaging features. The role and relative usefulness of CT and sonography are considered in each case. Because of this format, the text is often redundant, but this organization also facilitates the use of the book as a quick reference source. Each chapter has an extensive bibliography, with many references published as recently as 1987 and 1988. Of considerable help to the novice is the detailed technical information provided, such as when and how contrast material is administered in CT examinations and ideal positioning of the patient in sonography tailored to a specific clinical problem. Although color Doppler imaging is not discussed, the applications of deep Doppler sonography in the abdomen are included. Common diagnostic pitfalls are demonstrated.

Some topics, such as acute pancreatitis, are presented in great depth, with a lengthy discussion of pathogenesis and clinical and pathologic aspects. However, the chapter on the pelvis has fewer than 15 pages and is a superficial presentation of a few topics. In the section on pelvic inflammatory disease, the authors indicate that "sonography is the imaging modality of choice in evaluating patients with suspected acute pelvic inflammatory disease." The discussion that follows is somewhat misleading because it fails to point out that sonography does not have a significant role in the evaluation of most patients with this disorder. It is important for the reader to understand the appropriate indications for sonography, that is, to evaluate for complications, such as tuboovarian abscess and hydrosalpinx. For several other entities, it would have been helpful to clarify what the specific indications for imaging are, in addition to presenting the relative value of CT vs sonography.

Although several large reference texts on cross-sectional body imaging are available, this excellent book satisfies an important need. It is much more readable, practical, and current than another recent publication, *Diagnostic Imaging of the Acute Abdomen*, edited by Beyer and Modder. Jeffrey's book will be a valuable resource for radiology residents and others with little experience in cross-sectional imaging who are learning the value of using CT and sonography in specific acute abdominal and pelvic problems.

Anna S. Lev-Toaff
Temple University
Philadelphia, PA 19140

Bronchiolitis Obliterans Organizing Pneumonia: CT Features in 14 Patients

Nestor L. Müller[1]
Catherine A. Staples[2]
Roberta R. Miller[3]

Bronchiolitis obliterans organizing pneumonia is a disease characterized by the presence of granulation tissue within small airways and the presence of areas of organizing pneumonia. We retrospectively reviewed the chest radiographs, CT scans, and biopsy specimens in 14 consecutive patients with proved bronchiolitis obliterans organizing pneumonia. Six patients were immunocompromised because of leukemia or bone-marrow transplantation. In all patients, 10-mm collimation CT scans were available. In 11 of the 14 patients, select 1.5-mm scans were obtained. The CT findings included patchy unilateral (*n* = 1) or bilateral air-space consolidation (*n* = 9), small nodular opacities (*n* = 7), irregular linear opacities (*n* = 2), bronchial wall thickening and dilatation (*n* = 6), and small pleural effusions (*n* = 4). All patients had areas of air-space consolidation, small nodules, or both. A predominantly subpleural distribution of the air-space consolidation was apparent on the radiographs of two patients and on CT scans of six. Pathologically, the nodules and the consolidation represented different degrees of inflammation in bronchioles, alveolar ducts, and alveoli.

Although most of the findings were apparent on the radiographs, the CT scans depicted the anatomic distribution and extent of bronchiolitis obliterans organizing pneumonia more accurately than did the plain chest radiographs.

***AJR* 154:983–987, May 1990**

Bronchiolitis obliterans organizing pneumonia is characterized pathologically by the presence of granulation tissue within the lumens of bronchioles and alveolar ducts and by the presence of associated patchy areas of organizing pneumonia [1]. Most cases are idiopathic. The radiologic findings include unilateral or bilateral patchy areas of air-space consolidation and small rounded and irregular linear opacities [1–4]. To the best of our knowledge, the conventional CT findings of bronchiolitis obliterans organizing pneumonia have been reported for only two patients and high-resolution CT findings, for one patient [4, 5]. The CT appearance of bronchiolitis obliterans organizing pneumonia in immunocompromised patients has not been described before.

The aims of the present study were to determine the appearance of bronchiolitis obliterans organizing pneumonia on conventional and high-resolution CT scans and to correlate the radiologic and pathologic findings.

Materials and Methods

Fourteen consecutive patients (eight women and six men) with biopsy-proved bronchiolitis obliterans organizing pneumonia and CT scans of the chest were included in the study. Their age range was 20 to 77 years (mean, 44 years). Six patients were immunocompromised because of leukemia (*n* = 3) or bone-marrow transplantation (*n* = 3). The other eight had normal immunological status.

CT scanning was performed on a GE 9800 scanner (General Electric, Milwaukee, WI). All scans were obtained at end-inspiration by using 1-cm collimation at 1-cm intervals. They

Received November 3, 1989; accepted after revision January 2, 1990.

[1] Department of Radiology, University of British Columbia and Vancouver General Hospital, 855 W. 12th Ave., Vancouver, B.C., Canada V5Z 1M9. Address reprint requests to N. L. Müller.

[2] Department of Radiology, St. Paul's Hospital, 1081 Burrard St., Vancouver, B.C., Canada V6Z 1Y6.

[3] Department of Pathology, University of British Columbia and Vancouver General Hospital, 855 W. 12th Ave., Vancouver, B.C., Canada V5Z 1M9.

0361–803X/90/1545–0983
© American Roentgen Ray Society

were photographed at window and level settings designed to optimize the display of parenchymal (level −600 to −700 H; window width, 1000–2000 H) and mediastinal soft-tissue (level, 30–50 H; width, 350–500 H) detail. In 11 patients, additional 1.5-mm collimation scans were obtained at the level of the aortic arch, the tracheal carina, and 1 cm above the dome of the right hemidiaphragm. The high-resolution CT scans were obtained by using 120 kVp and 360 to 420 mAs and were targeted retrospectively by using a 20- to 25-cm field of view and a high-spatial-resolution algorithm (bone algorithm). IV contrast medium was used in two patients. The CT scans were obtained within 1–10 days of the chest radiograph (median, 1 day) and within 1–14 days (median, 2 days) of the lung biopsy.

The radiographs and CT scans were assessed independently by two chest radiologists for the presence and distribution of pulmonary, pleural, hilar, and mediastinal abnormalities. Mediastinal nodes were considered enlarged if the short axis was longer than 10 mm. Final decisions were reached by consensus.

Thirteen patients had open-lung biopsy and one patient had transbronchial biopsy. The site of lung biopsy was chosen on the basis of the pattern and distribution of CT findings. Virtually all scans were reviewed preoperatively with the thoracic surgeons by one of the authors. The areas chosen for lung biospy were those most easily accessible to the surgeon that would provide a representative sample on the basis of the CT findings. An attempt was made to match the abnormalities on CT to the specific anatomic region in which the lung biopsy samples were obtained. All pathologic specimens were reviewed by a pathologist, and the presence and relative extent of involvement of proximal and distal respiratory bronchioles and alveolar ducts was noted, as was the presence and extent of organizing pneumonia components. Other features such as acute inflammation, fibrinous exudate, and eosinophilia were noted also. The viral, bacterial, and fungal tissue cultures in 12 patients were normal. *Legionella pneumophila* was grown from the biopsy material of a leukemic patient and *Enterococcus* from the biopsy material of another patient with leukemia. Both patients were included because their pathologic findings were otherwise indistinguishable from bronchiolitis obliterans organizing pneumonia. In two patients who had bronchiolitis obliterans organizing pneumonia after bone-marrow transplantation, the clinical and pathologic findings were thought to be due to graft-vs-host disease. In the other two immunocompromised patients and in all eight immunologically intact patients, the lesions were idiopathic.

Results

On the frontal and lateral radiographs of the chest, nine patients had bilateral, patchy air-space consolidation, and one patient had two ill-defined rounded areas of consolidation (1.5–2.0 cm diameter) in the right upper lobe (Table 1). The latter was diffuse in two patients, involved mainly the lower lung zones in three patients, mid lung zones in two patients, and upper lung zones in two patients. A subpleural distribution of air-space densities was apparent on the chest radiographs in two patients. One of the nine patients with bilateral air-space consolidation also had bilateral nodular opacities 1–10 mm in diameter. Four of the 14 patients had only nodular opacities on the radiograph and no other abnormalities were seen. The nodules were bilateral, and most were 3–5 mm in diameter (range, 1–10 mm).

The pattern and distribution of air-space consolidation were similar on CT scans and radiographs except that a subpleural predominance of the consolidation was apparent on CT scans in six patients (Fig. 1). In three of these patients, the consolidation was limited almost entirely to the subpleural and peribronchovascular regions of the lungs. Four patients had no subpleural predominance. Two of these four patients had extensive consolidation centrally, almost completely sparing the subpleural lung regions, and in two patients, the subpleural involvement was similar to that in the remaining lung (Fig. 2). Air bronchograms were present on CT scans in all patients with air-space consolidation. In all patients, the lung biopsy site was determined by the distribution of disease as assessed preoperatively on the CT scans. Pathologically, examination of the open-lung biopsy specimens in all but one patient with air-space consolidation showed variable degrees of organizing pneumonia. The other patient had overlapping features of bronchiolitis obliterans and chronic eosinophilic pneumonia.

CT confirmed the impression of nodular opacities seen on the radiograph in five patients as described earlier. In addition,

TABLE 1: Radiographic and CT Findings in Bronchiolitis Obliterans Organizing Pneumonia

Patient[a]	Age (yr)	Sex	Radiograph				CT			
			Consolidation			Nodules	Consolidation			Nodules
			Present	Bilateral	Subpleural		Present	Bilateral	Subpleural	
1	20	M	+	−	−	−	+	−	+	−
2	29	F	+	+	−	−	+	+	−	−
3	22	M	+	+	−	−	+	+	+	+
4	21	F	−	−	−	+	−	−	−	+
5	40	F	−	−	−	+	−	−	−	+
6	24	M	−	−	−	+	−	−	−	+
7	47	F	+	+	−	+	+	+	−	+
8	77	M	+	+	−	−	+	+	−	−
9	52	F	+	+	−	−	+	+	−	−
10	60	F	+	+	−	−	+	+	+	−
11	64	F	+	+	−	−	+	+	+	+
12	47	F	+	+	+	−	+	+	+	−
13	48	M	−	−	−	+	−	−	−	+
14	61	M	+	+	+	−	+	+	+	−

[a] Patients 1–6 were immunocompromised, and patients 7–14 were not immunocompromised.

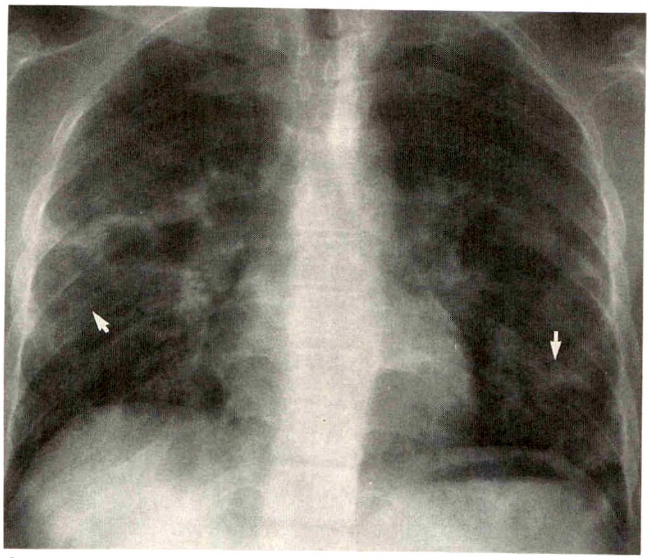

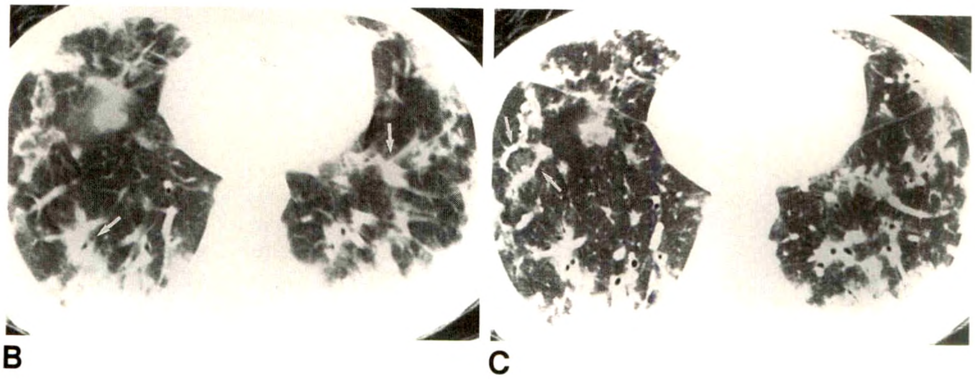

Fig. 1.—22-year-old man in whom bronchiolitis obliterans organizing pneumonia developed, presumably because of graft-vs-host disease, 1 year after bone marrow transplantation.

A, Chest radiograph shows patchy bilateral air-space consolidation mostly in middle and lower lung zones. A subpleural predominance is not apparent. A few ill-defined nodules 3–10 mm in diameter are present (*arrows*).

B, 10-mm collimation CT scan at level of dome of right hemidiaphragm shows consolidation is mostly along bronchovascular bundles (*arrows*) and in subpleural lung regions.

C, 1.5-mm collimation CT scan better delineates areas of consolidation from normal parenchyma and shows mildly dilated bronchi with thickened walls and thickening of interlobular septa (*arrows*).

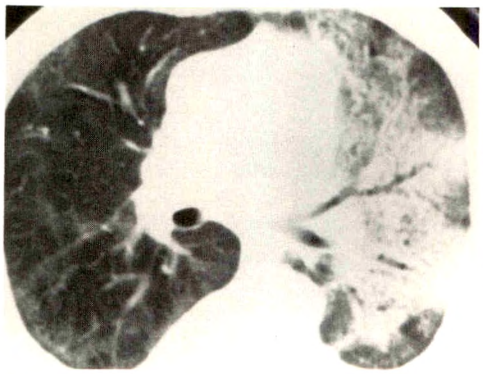

Fig. 2.—10-mm collimation CT scan in 77-year-old nonimmunocompromised man shows asymmetric bilateral air-space consolidation with air bronchograms. Although consolidation on left side is extensive, subpleural regions are relatively spared.

2

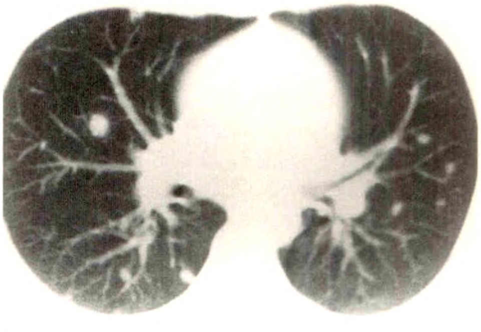

Fig. 3.—10-mm collimation CT scan in 21-year-old woman with leukemia shows bilateral nodules 2–10 mm in diameter. Most have smooth margins.

3

a few nodules 1–5 mm in diameter that had not been apparent on the radiograph were seen in two other patients. In two of the seven patients, the nodules were situated predominantly along the bronchovascular bundles. Most of the nodules had well-defined smooth margins (Figs. 3 and 4). A few nodules 5–10 mm in diameter with poorly defined margins ("air-space nodules") also were seen. Pathologically, the nodules represented focal areas of organizing pneumonia around areas of bronchiolitis obliterans (Fig. 4).

A few irregular linear opacities were apparent on CT scans in two patients with air-space consolidation. Small unilateral pleural effusions were present in two patients, and bilateral effusions were noted in another two patients. Mediastinal adenopathy was present in two patients (position 7 node in one and positions 10R and 5 in the other). Bronchial wall thickening and dilatation were seen in five patients in association with areas of air-space consolidation and in one patient with nodules only 1–3 mm in diameter.

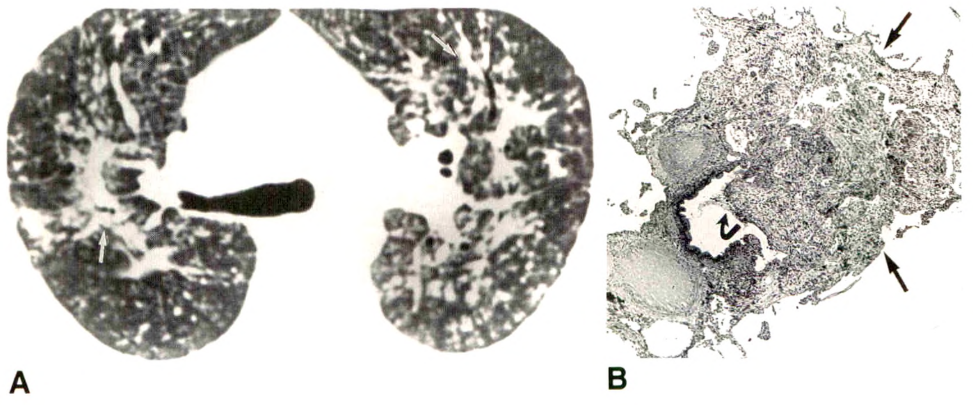

Fig. 4.—*A*, 1.5-mm collimation CT scan in 47-year-old nonimmunocompromised man shows numerous bilateral nodules 1–10 mm in diameter. Confluence is present in several areas. Nodules are more numerous along bronchovascular structures (*arrows*).

B, Photomicrograph of nodules shows localized areas of organizing pneumonia (*straight arrows*) around bronchiolitis obliterans (*curved arrow*). This type of lesion is separated from other involved bronchioles by a zone of relatively normal lung, which explains nodular appearance.

High-resolution CT allowed easier distinction of normal from abnormal parenchyma and better definition of the areas with bronchial wall thickening and dilatation (Fig. 1). It also allowed assessment of the secondary pulmonary lobule (Fig. 1). In three patients, a few smoothly thickened interlobular septa were seen on high-resolution CT. In two patients, areas of consolidation were bound by interlobular septa, and in both, this impression was confirmed pathologically. Otherwise, the distribution of the areas of consolidation and the nodules had no relationship to the secondary pulmonary lobules.

Three of our patients had mild peripheral eosinophilia. In two of these, eosinophils were present in the areas of organizing pneumonia. In one of the patients who had eosinophils in the pulmonary parenchyma, a marked peripheral predominance of the air-space consolidation was noted that simulated the distribution of consolidation seen in patients with chronic eosinophilic pneumonia. However, most of the consolidation in this patient was distributed asymmetrically in the left lower lobe and lingula, which is more in keeping with bronchiolitis obliterans organizing pneumonia than with chronic eosinophilic pneumonia. On open-lung biopsy, this patient had overlapping features of both conditions. This case has been previously published [6]. The second patient also had asymmetric distribution of consolidation, mostly in the lower lung zones. Pathologically, occasional collections of eosinophils were present in the inflammatory intraalveolar infiltrate, but the tissue eosinophilia was minor compared with the bronchiolitis obliterans.

Discussion

Bronchiolitis obliterans is a disorder characterized by the presence of tufts of loose connective tissue within the lumen of bronchioles and alveolar ducts. In most cases, lipid-laden macrophages accumulate in alveolar spaces and a mononuclear cell alveolitis occurs, which is the "organizing pneumonia" component of the lesion [1]. Bronchiolitis obliterans may be due to a variety of causes, including inhalation of toxic gases, connective tissue disorders, infection, and bone-marrow and heart-lung transplantation [1, 2, 7–19]. However, in most cases of bronchiolitis obliterans organizing pneumonia, no cause is found.

The plain film features of bronchiolitis obliterans organizing pneumonia are well known [1–4, 19]. They consist of patchy unilateral or bilateral areas of air-space consolidation with no particular lung-zone predominance. In a small percentage of patients, the consolidation may be peripheral, a pattern similar to that seen with chronic eosinophilic pneumonia. Small nodular or irregular linear opacities may be seen in 10–50% of patients. The lung volume is decreased in approximately half of the patients.

Müller et al. [4] reported the CT appearance in two patients with bronchiolitis obliterans organizing pneumonia. The findings consisted of areas of consolidation predominantly in the lung periphery. Miki et al. [5] described the conventional and high-resolution CT findings in one patient with bronchiolitis obliterans organizing pneumonia. They reported segmental areas of consolidation with air bronchograms. A follow-up CT scan after steroid therapy showed almost complete resolution.

In the present study, CT scans showed air-space consolidation in 10 patients, ranging from two localized areas of consolidation 1.5–2.0 cm in diameter to extensive bilateral disease. The consolidation was usually bilateral and asymmetric. The consolidation was patchy throughout the three lung zones, but predominant involvement of upper, middle, or lower lung zones was seen in most of the patients. A subpleural predominance was present in six patients, but in two patients with extensive disease centrally, the lung periphery was almost completely spared. Pathologically, the consolidation usually corresponded to areas of organizing pneumonia.

Nodular opacities 1–10 mm in diameter were seen in 50% of patients. In two patients, these were more numerous along the bronchovascular bundles. On pathologic examination, the parenchymal nodules were found to be involved bronchioles surrounded by a localized zone of organizing pneumonia but separated from other involved areas by relatively normal parenchyma.

Bronchial wall thickening and dilatation were seen on high-resolution CT in most patients with extensive consolidation and were usually restricted to these areas. These are nonspecific findings and can be seen with many inflammatory and fibrotic processes. Follow-up CT scans were not obtained, and therefore it is not known whether these changes are reversible or whether they represent cylindrical bronchiectasis.

Six of our patients were immunocompromised, and eight had no underlying disease. Bronchiolitis obliterans organizing pneumonia appeared the same on both CT and pathologic examination in this small series. The relatively large number of immunocompromised patients and the severity of the radiologic abnormalities in the nonimmunocompromised patients in our series probably are due to patient selection. Patients who are immunocompromised and those with more severe disease are the ones most likely to be referred to our institution for open-lung biopsy.

The CT and the plain film findings of bronchiolitis obliterans are nonspecific and may be seen in a variety of infections and neoplastic diseases. We were unable to determine any single finding or combination of findings on CT that could be considered diagnostic of bronchiolitis obliterans organizing pneumonia and that could not be seen on a radiograph. However, CT gave a better assessment of disease pattern and distribution than did the chest radiograph and was used routinely as a guide to optimal biopsy site in patients undergoing open-lung biopsy.

REFERENCES

1. Epler GR, Colby TV, McLoud TC, Carrington CB, Gaensler EA. Bronchiolitis obliterans organizing pneumonia. *N Engl J Med* **1985**;312:152–158
2. Gosink BB, Friedman PJ, Liebow AA. Bronchiolitis obliterans: roentgenographic-pathologic correlation. *AJR* **1973**;117:816–832
3. Chandler PW, Shin MS, Friedman SE, Myers JL, Katzenstein AL. Radiographic manifestations of bronchiolitis obliterans with organizing pneumonia vs usual interstitial pneumonia. *AJR* **1986**;147:899–906
4. Müller NL, Guerry-Force ML, Staples CA, et al. Differential diagnosis of bronchiolitis obliterans with organizing pneumonia and usual interstitial pneumonia: clinical, functional, and radiologic findings. *Radiology* **1987**;162:151–156
5. Miki Y, Hatabu H, Takahashi M, Sadatoh N, Kuroda Y. Case report: computed tomography of bronchiolitis obliterans. *J Comput Assist Tomogr* **1988**;12:512–514
6. Mayo JR, Müller NL, Road J, Sisler J, Lillington G. Chronic eosinophilic pneumonia: CT findings in six cases. *AJR* **1989**;153:727–730
7. Cornelius EA, Betlach EH. Silo-filler's disease. *Radiology* **1960**;74:232–235
8. Charan NB, Myers CG, Lakshminarayan S, Spencer TM. Pulmonary injuries associated with acute sulfur dioxide inhalation. *Am Rev Respir Dis* **1979**;119:555–560
9. Laraya-Cuasay LR, DeForest A, Huff D, Lischner H, Huang NN. Chronic pulmonary complications of early influenza virus infection in children. *Am Rev Respir Dis* **1977**;116:617–625
10. Nikki P, Meretoja O, Valtonen V, et al. Severe bronchiolitis probably caused by varicella-zoster virus. *Crit Care Med* **1982**;10:344–346
11. Geddes DM, Corrin B, Brewerton DA, Davies RJ, Turner-Warwick M. Progressive airway obliteration in adults and its association with rheumatoid disease. *Q J Med* **1977**;46:427–444
12. Epler GR, Snider GL, Gaensler EA, Cathcart ES, Fitzgerald MX, Carrington CB. Bronchiolitis and bronchitis in connective tissue disease. *JAMA* **1979**;242:528–532
13. Schwarz MI, Matthay RA, Sahn SA, Stanford RE, Marmorstein BL, Scheinhorn DJ. Interstitial lung disease in polymyositis and dermatomyositis: an analysis of six cases and review of the literature. *Medicine* **1976**;55:89–104
14. Herzog CA, Miller RR, Hoidal JR. Bronchiolitis and rheumatoid arthritis. *Am Rev Respir Dis* **1979**;119:555–560
15. Ostrow D, Buskard N, Hill RS, Vickars L, Churg A. Bronchiolitis obliterans complicating bone marrow transplantation. *Chest* **1985**;87:828–830
16. Roca J, Granena A, Rodriguez-Roisin J, Alvarez P, Agusti-Vidal A, Rozman C. Fatal airway disease in an adult with chronic graft-versus-host disease. *Thorax* **1982**;37:77–78
17. Stein-Streilen J, Lipscomb MF, Hart DA, Darden A. Graft-versus-host reaction in the lung. *Transplantation* **1981**;32:38–44
18. Burke CM, Theodore J, Dawkins KD, et al. Post transplant obliterative bronchiolitis and other late lung sequellae in human heart-lung transplantation. *Chest* **1984**;86:824–829
19. McLoud TC, Epler GR, Colby TV, Gaensler EA, Carrington CB. Bronchiolitis obliterans. *Radiology* **1986**;159:1–8.

Book Review

Clinical Pelvic Imaging. CT, Ultrasound, and MRI. Edited by Arnold C. Friedman, Paul D. Radecki, Anna S. Lev-Toaff, and Pamela L. Hilpert. St. Louis: Mosby, 531 pp., 1990, $98

Nobody beats this new book. Nobody. It is a veritable dictionary of pelvic pathology. All systems are covered with a wide-angle view and in the usual pathologic method (neoplastic, inflammatory, congenital, and traumatic), albeit unequally weighted. Everything is included, from polycystic ovary disease and testicular ectopia to vesicoureteral reflux, prune-belly syndrome, and Hirschprung disease.

The book has a wonderful all-inclusive review of basic sciences and a few words on physical principles. The bibliography is exhaustive and generally encompasses the current literature. For example, chapter 3 has 34 pages of text and illustrations and 244 references. An abundance of quality illustrations is integrated meticulously with an easily understandable and comprehensive narrative. Key charts and classifications dealing with clinical topics are available. The index is accurate and adequate. Basically, this is a textbook of pathology as seen through imaging procedures.

The authors are quick to point out the far-reaching advantages of transvaginal sonography in their discussions of female infertility, problems of early gestation, and diseases of the endometrium. There are, however, concurring and contrary opinions as to the role of this technique in the early workup of the patient (Arger and Coleman, *Diagnostic Imaging*, 1989; Tessler, *Radiology*, 1989). Newer indications (Tessler et al., *AJR*, 1989) and further refinements are being reported continually (the *New York Times*, December 5, 1989, discusses transvaginal color flow imaging for the early detection of ovarian carcinoma).

Arguably, the strength of the book lies with discussions of the efficacy of CT, sonography, and MR imaging individually and collectively with regard to specific pelvic diseases. In this regard as well, the book is an excellent source of references. Specifically, the discussions on the detection and staging of carcinoma of the cervix, urinary bladder, and prostate; the anticipated role of transrectal sonography in the screening of tumors of the prostate; and guided needle biopsy offer a sensible perspective. The capacity of imaging techniques for detection of lymph node involvement, pelvic side-wall extension of tumor, encroachment of the muscle wall or capsule, and invasion of the adjacent pelvic organs and for evaluation of tumor mass is covered thoroughly for the aforementioned malignancies. Recent reports agree with the authors that MR is more effective than CT in conjunction with the clinical examination for the detection and staging of early cancer of the cervix (Rubens, *AJR*, 1988). The discussions of the role of transrectal sonography, present and future, in differentiating cancer of the prostate from benign prostatic hypertrophy and in staging and screening are most informative, particularly when the limitations of transabdominal sonography, CT (Platt, *AJR*, 1987), and MR imaging (Schiebler, *Radiology*, 1989) are recognized. As indicated by the authors and others (Rifkin, *Radiology*, 1989), the consensus varies. Will transrectal sonography become the "mammogram" for screening of cancer of the prostate? This controversial topic merits the attention given. Caution appears to prevail at this time, certainly with respect to substitution for the digital examination as well as cost-effectiveness (Torp-Pedersen, *Radiology*, 1988). The sections on inflammatory diseases, obstetric imaging, and pelvic trauma make this comprehensive work even more complete.

One day last week, at a major municipal hospital, not a single excretory urogram was requested or performed. As newer technologies replace old standbys, we will need timely and responsible information for practitioners and students. Surely, *Clinical Pelvic Imaging* is a paradigm of this genre.

Murray A. Rosenberg
Easton, CT 06612

MR Imaging of Thoracic and Abdominal Wall Infections:

Comparison with Other Imaging Procedures

Hassan S. Sharif[1]
David C. Clark
Mohamed Y. Aabed
Osarugue A. Aideyan
Maurice C. Haddad
Tor A. Mattsson

Infections of the chest and abdominal wall are rare but potentially fatal disorders that can occur spontaneously or in association with diabetes mellitus, immunosuppression, or trauma. The condition (either in the form of necrotizing fasciitis and/or pyomyositis) is difficult to diagnose clinically because of poor localizing signs. Prognosis depends on early recognition, extent of disease, and type of causative organism. Pathologically, the infections can manifest as cellulitis, abscess, and/or granulation tissue formation. To determine the value of MR imaging in the assessment of these infections, we compared the findings of MR with those of CT, sonography, scintigraphy, and plain radiography in 13 patients with proved thoracic and/or abdominal wall infection. The imaging findings were correlated with microbiological, pathologic, and/or surgical data. The isolated pathogens were *Staphylococcus aureus* ($n = 6$), *Klebsiella pneumoniae* ($n = 1$), *Mycobacterium tuberculosis* ($n = 4$), and *Streptomyces somaliensis* ($n = 2$). In 10 of 13 patients, MR imaging and CT were comparable and proved accurate in detecting the nature and extent of the inflammatory process. In seven of the patients, CT also was useful in guiding percutaneous biopsy and/or partial drainage procedures. Coronal and sagittal MR images were helpful for planning surgery. Rib osteomyelitis was missed with both techniques in one patient; in two other patients who did not have CT, MR imaging missed osteomyelitis of the ribs, the spinous process of a vertebral body, and the iliac bone. Sonography underestimated the extent of the disease in all 13 patients, but detected fluid collections in six. Findings on scintigraphy and plain radiography were the least contributory to the diagnosis and treatment of these patients.

Our results suggest that MR imaging and CT are the best methods for detecting thoracoabdominal wall infection. CT appears to be the technique of choice whenever percutaneous biopsy and/or drainage are required.

***AJR* 154:989–995, May 1990**

Infection of the chest and abdominal wall is an uncommon but serious condition that can occur spontaneously or in association with diabetes mellitus, immunosuppression, sepsis, surgery, trauma, atherosclerosis, alcoholism, obesity, and malnutrition [1–3]. Clinical recognition of such lesions can be difficult and patients may present with fever, pain, and skin changes ranging from minor discoloration to frank cutaneous necrosis [1]. The extent of underlying tissue involvement is frequently underestimated by physical examination, and at surgery abscesses are often found to extend far beyond the visualized area of cutaneous abnormality [1, 3].

The advantages and limitations of plain radiography, sonography, and CT scanning in these cases have been addressed [3–8]. The role of MR imaging in assessing these lesions has not been evaluated.

To determine the relative merit of MR imaging in detecting the presence and extent of thoracoabdominal wall infection, we compared the findings of MR with those of other imaging techniques (CT, sonography, scintigraphy, and plain radiography) in 13 patients with proved infections. We also correlated the imaging findings with microbiological, pathologic, and surgical data.

Received August 4, 1989; accepted after revision November 20, 1989.

Presented in part at the annual meeting of the Society of Magnetic Resonance Imaging, Boston, February 1988.

[1] All authors: Department of Radiology, Riyadh Armed Forces Hospital, P.O. Box 7897 (979), Riyadh 11159, Kingdom of Saudi Arabia. Address reprint requests to H. S. Sharif.

0361–803X/90/1545–0989

© American Roentgen Ray Society

TABLE 1: Summary of Imaging Findings in Patients with Thoracic and/or Abdominal Wall Infection

Case No.	Radiography	Bone Scintigraphy	Sonography	CT and/or MR Imaging[a]
1	No abnormality	No abnormality	No abnormality	**L:** Midline posterior abdominal wall collection; **E:** L1–S1; **O:** subcutaneous tissue posterior to spine
2	Increased bone density of T12 and L1 on left; loss of psoas shadow on left	Minimal increased uptake in T12, L1	Small hypoechoic mass in left psoas	**L:** Left-sided posterolateral thoracoabdominal wall; **E:** T8–L4; **O:** diaphragm, muscles, two vertebrae, epidural space, subcutaneous tissue (Fig. 2)
3	Extrapleural mass in right thoracic cavity	Minimal increased uptake in pedicle of T11 on right	Small hypoechoic collection posterior to liver	**L:** Right-sided posterolateral thoracoabdominal wall; small amount of gas seen on CT; **E:** T4–L3; **O:** pleura, diaphragm, muscles, epidural space, subcutaneous tissue (Fig. 1)
4	No abnormality	Minimal increased uptake of 10th, 11th ribs on left	No abnormality	**L:** Left-sided posterolateral thoracoabdominal wall; **E:** T8–L2; **O:** diaphragm, muscles, subcutaneous tissue
5	No abnormality	No abnormality	Not done	**L:** Midline posterior thoracoabdominal wall; gas seen best on CT; **E:** T4–T8; **O:** subcutaneous tissue posterior to spine
6	No abnormality	No abnormality	No abnormality	**L:** Midline posterior abdominal wall; **E:** T12–coccyx; **O:** subcutaneous tissue posterior to spine (Fig. 3)
7	No abnormality	No abnormality	Small hypoechoic collection posterior to liver	**L:** Right-sided posterolateral abdominal wall; **E:** T12–L4; **O:** intercostals, psoas, subcutaneous tissue
8	No abnormality	Increased uptake C6–T7; right sternoclavicular joint and right sixth and seventh ribs anteriorly and L1–L3	No abnormality	**L:** Right-sided anterior chest wall; CT not done; **E:** T8–T12; **O:** intercostals, subcutaneous tissue
9	Small area of bone destruction, right iliac bone	Minimal increased uptake in right iliac bone	Large hypoechoic collection in right psoas and iliac fossa	**L:** Midline and right-sided posterolateral abdominal wall; CT not done; **E:** L3–midshaft of right femur; **O:** psoas, iliacus, glutei, thigh muscles, subcutaneous tissue (Fig. 4)
10	No abnormality	No abnormality	No abnormality	**L:** Midline posterior abdominal wall; CT not done; **E:** L1–S1; **O:** subcutaneous tissue posterior to spine
11	No abnormality	No abnormality	Small hypoechoic collection in posterior thoracic wall	**L:** Left-sided posterolateral thoracic abdominal wall; **E:** T8–L3; **O:** pleura, diaphragm, abdominal wall muscles, subcutaneous tissue

TABLE 1: Continued

Case No.	Radiography	Bone Scintigraphy	Sonography	CT and/or MR Imaging[a]
12	Large posterior mediastinal mass at T4–T12; irregular lower ribs; slender vertebral osteophytes	Minimal increased uptake from lower three ribs bilaterally	Not done	**L:** Midline posterior thoracoabdominal wall; **E:** T4–coccyx; **O:** posterior mediastinum, epidural space, all posterior thoracoabdominal wall muscles, glutei, upper muscles of thighs, subcutaneous fat (Fig. 6)
13	Multiple rounded calculi in right renal bed; excretory urography: nonfunctioning right kidney	No abnormality	Small hypoechoic collections in region of renal bed on right	**L:** Right-sided posterolateral thoracoabdominal mass; **E:** T11–L5; **O:** kidney and adrenal, muscles of posterolateral abdominal wall, subcutaneous tissue (Fig. 5)

[a] CT and MR imaging findings were comparable (CT was performed in 10 cases). Findings are presented with respect to location (**L**), extent (**E**), and organ involvement (**O**). CT enhancement did not occur in cases 1, 6, and 7; all pyogenic and tuberculous abscesses were hypo- or isodense relative to muscle and showed rim enhancement after IV contrast. On MR, pyogenic and tuberculous abscesses were isointense relative to muscle on short TR/TE and hyperintense on long TR/TE and STIR sequences. The most appropriate planes of imaging were the coronal and sagittal.

Materials and Methods

Images obtained by various radiologic methods in 13 patients with microbiologically and/or pathologically verified thoracoabdominal wall infection were analyzed retrospectively and correlated with surgical findings ($n = 12$). All patients were examined and treated at the Riyadh Armed Forces Hospital between January 1987 and May 1989.

The patient group comprised 10 men and three women 18–75 years old (mean age, 42 years). The pathogens were *Staphylococcus aureus* ($n = 6$), *Klebsiella pneumoniae* ($n = 1$), *Mycobacterium tuberculosis* ($n = 4$), and *Streptomyces somaliensis* ($n = 2$). Signs, symptoms, and duration of symptoms were different for the different types of pathogens; those with pyogenic infections ($n = 7$) had a more acute course. Skin changes suggestive of an underlying infection were detected in two patients with pyogenic infection, one patient with tuberculosis, and two patients with mycetoma. Four of the seven patients with pyogenic infections had diabetes mellitus and one was on immunosuppressive therapy.

In all 13 patients, frontal and lateral chest radiographs and frontal and lateral radiographs of the affected body region had been obtained on the basis of the clinical signs and symptoms. Two patients were examined further with excretory urography. Real-time sonography of the abdomen was performed with special emphasis on areas in the thoracoabdominal wall that produced clinical signs and symptoms. On the sonograms, areas of abnormal echogenicity in the thoracic or abdominal wall were identified and were labeled as cystic if they were echo free with increased through transmission and a thin rim, as abscesses if they were relatively echo free with debris and a thick wall, and as a solid mass if they were echogenic.

Single-phase static bone scintigraphy was done in all 13 patients by using a gamma camera with a low-energy high-resolution collimator and 600 MBq of ^{99m}Tc methylene diphosphonate given IV. Anterior and posterior views (500,000 counts/image) of the entire skeleton were obtained 3 hr after injection.

Ten patients were examined with CT by using a G.E. 9800 scanner (General Electric, Milwaukee, WI). Contiguous sections (10 mm) were scanned through what was suspected as the affected body region from the clinical signs and symptoms and with the guidance of earlier imaging findings. When spinal involvement was suspected, additional contiguous sections (3 mm) were scanned. The CT studies of seven patients were repeated after IV injection of 100 ml (300 mg I/ml) of Omnipaque (Nyegaard, Oslo, Norway). Appropriate sagittal and coronal reconstructed images were obtained from the 3-mm-thick slices in the spine. All images were evaluated on bone and soft-tissue windows.

All 13 patients underwent MR imaging on a 0.5-T whole-body superconductive unit (Gyroscan, Philips, Best, the Netherlands). Images were obtained in sagittal and coronal planes, and seven patients were imaged in the axial plane also. Sections 7-mm thick with a gap of 1 mm in a 256 × 256 matrix were obtained in the affected region. Eight patients had MR imaging studies repeated during the course of therapy.

The following scanning parameters were used: (1) spin-echo (SE) multislice sagittal and coronal images were obtained in four to six acquisitions at 500/30 (TR/TE); (2) SE multislice coronal, sagittal, and/or axial images in two acquisitions at 2000/50,100; and (3) multislice coronal and sagittal images for two patients with short-tau inversion recovery (STIR), 1500/120/30 (TR/TI/TE), with two measurements.

The area of the body evaluated by the MR study was determined on the basis of clinical findings as well as from the abnormalities detected on previous imaging studies. Patchy or diffuse loss of signal from subcutaneous fat and muscle planes on the short TR/TE sequence was considered evidence of involvement. Anatomic distortion of skin, muscles, and other organs (in comparison with a normal contralateral side) was also considered evidence of involvement on this sequence. High signal on long TR/TE and STIR sequences in these or other areas was considered indicative of inflammation.

All initial radiologic investigations were done within 10 days of admission to the hospital; all were done preoperatively.

Percutaneous drainage of abscess under CT guidance, attempted in seven patients, was unsuccessful because the abscesses were invariably loculated. Complete surgical drainage of the abscesses (containing 70–1500 ml of pus) and removal of necrotic infected tissue were achieved in all pyogenic and tuberculous lesions. Only partial resection was possible in one of the mycetoma cases because of adherence of the inflammatory mass to the inferior vena cava and aorta. The patient with the more extensive mycetoma had several skin biopsies that showed characteristic histopathologic changes.

The different studies were evaluated separately and independently by three radiologists blinded to the final diagnosis. For each imaging technique and for every patient, the following points were assessed: location and extent of the lesion, organ involvement, and type of pathology (example, inflammatory vs neoplastic). Whenever there was disagreement, the consensus opinion was accepted.

All imaging findings were subsequently correlated with surgical data with regard to the size (estimated volume), number (loculations), and extent of the abscesses. The findings at surgery of bone, muscle, and abdominal organ involvement also were compared with those of imaging.

Results

The imaging findings are summarized in Table 1.

On MR images the signal behavior of the abscess collections was similar for all the 11 patients with pyogenic and tuberculous infections. The abscesses were isointense relative to skeletal muscle on the short TR/TE SE images and became hyperintense on the long TR/TE and STIR images (Figs. 1–4). Epidural extension and associated vertebral osteomyelitis were detected in two of these patients (areas of high signal intensity on long TR/TE images), but pathologically proved osteomyelitis was missed with MR imaging in three ribs, a spinous process, and an iliac bone (Fig. 4).

In the two patients with mycetoma, the inflammatory tissue appeared isointense relative to muscle on short TR/TE images and exhibited only moderate increase in signal on long TR/TE images (Figs. 5 and 6). The cystic lesions replacing the right kidney (Fig. 5) showed behavior similar to that of pyogenic abscesses. Extensive epidural extension in the second case (Fig. 6) was not associated with vertebral body or disk involvement.

On CT, pyogenic and tuberculous abscesses were better visualized on postcontrast scans and appeared as areas of low attenuation surrounded by an enhancing rim (Figs. 1 and 2). Vertebral osteomyelitis was detected in only one of the two patients with epidural extension, and rib osteomyelitis was missed in one patient (Fig. 2). A small amount of gas was seen in the abscesses of two patients (Fig. 1).

In the patient with the right-sided mycetoma, changes in the renal bed similar to those of pyogenic abscesses were seen (Fig. 5). The affected areas in both mycetoma patients enhanced minimally after administration of contrast material. Destruction of the muscles and replacement by fat were extensive, and, despite severe epidural extension, no vertebral body or disk involvement was detected (Fig. 6).

MR imaging and CT findings were comparable and correlated well with surgery, particularly with respect to the abscess collections. In patients who were explored by large incisions for better drainage, surgical and pathologic proof of muscle group involvement correlated with the MR and CT appearances. The presence of osteomyelitis in flat bones (ribs, spinous process, iliac bone) was missed by CT in one and by MR in three cases. Epidural extension in two patients, clearly noted by both techniques, could not be verified surgically because the area was not explored (Figs. 1 and 2).

Two radiologists correctly identified the nature of the disease as being inflammatory on both CT ($n = 10$) and MR. The third was in doubt about the MR study of two patients (unilateral mycetoma, anterior chest wall tuberculosis), as to whether the changes were caused by a neoplastic process. No attempts were made by the three radiologists to suggest the possible pathogen except in the case of the unilateral

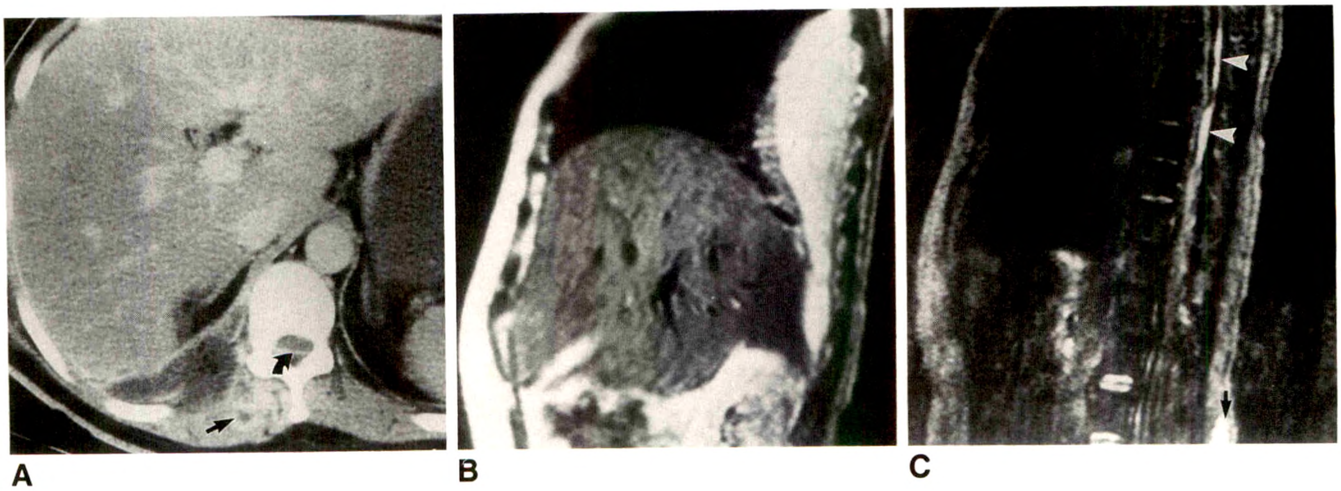

Fig. 1.—Case 3: 50-year-old diabetic man with fever, right flank pain, and *Staphylococcus aureus* septicemia.

A, Postcontrast axial CT scan shows small fluid collection extending from extrapleural space and dissecting posterior to diaphragm. This is in continuity with large extrapleural collection starting from level of T4. Note gas within collection, small abscesses within erector spinae muscles (*straight arrow*), and inflamed dura suggesting epidural extension (*curved arrow*).

B, Right parasagittal MR image (SE 2000/50) shows extrapleural collection extending from thoracic down to abdominal cavity. Pleura, lung, diaphragm, and liver are displaced anteriorly.

C, Midsagittal MR image (SE 2000/100) shows epidural extension (*arrowheads*) posterior to spinal cord. Signal is higher than that of CSF, presumably because of higher protein content of pus and/or because of its limited mobility. Note high signal intensity in subcutaneous tissue (*arrow*).

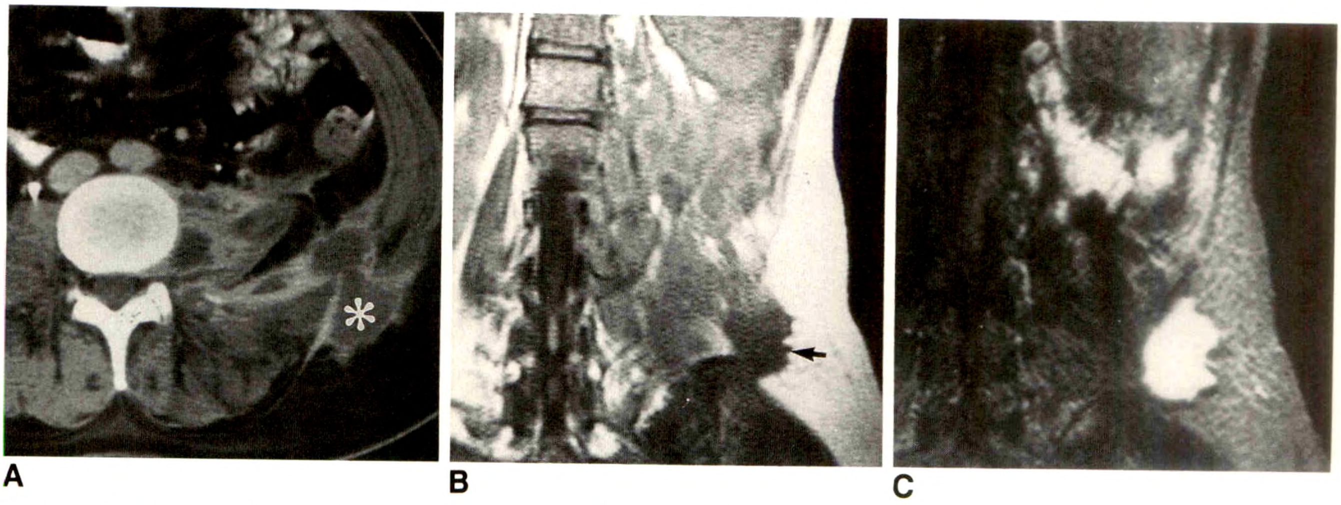

Fig. 2.—Case 2: 47-year-old man with fever and left flank pain of 12 days duration.

A, Axial postcontrast CT scan at level of inferior endplate of L3 shows multiloculated abscess involving left psoas muscle extending into neural foramen and involving lateral abdominal wall muscles and subcutaneous fat (*asterisk*). *Staphylococcus aureus* was isolated from pus obtained by CT-guided percutaneous biopsy.

B, Coronal MR image (SE 500/30) at level of kidneys shows replacement of left perinephric fat by isointense collection that extends into subcutaneous fat (*arrow*).

C, Coronal MR image (SE 2000/100) at same level as *B* shows multiple hyperintense collections corresponding to isointense areas in *B*.

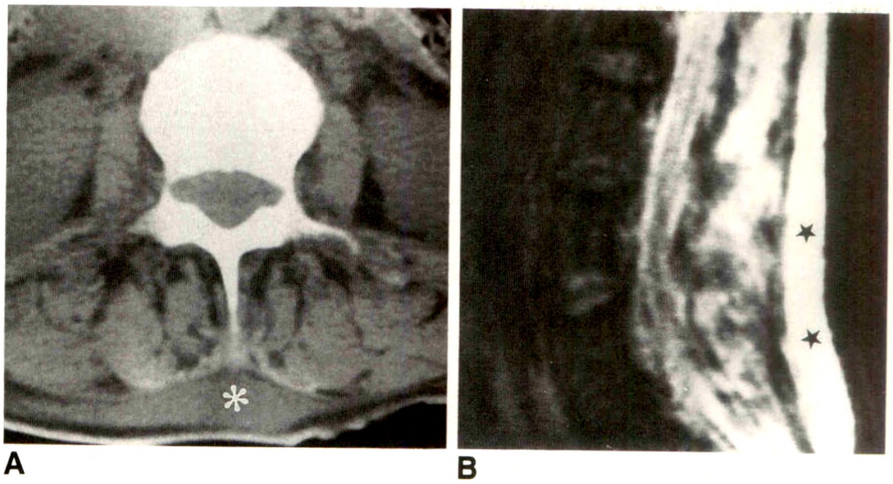

Fig. 3.—Case 6: 70-year-old diabetic man with fever and low back pain.

A, Axial CT scan at level of L3 shows isodense collection between latissimus dorsi muscle and skin (*asterisk*).

B, Midsagittal MR image (SE 2000/50) shows marked increase in signal of soft tissues posterior to spinous processes (*stars*). *Staphylococcus aureus* was isolated from removed subcutaneous collection.

mycetoma, where two radiologists thought the changes were compatible with tuberculous autonephrectomy (Fig. 5).

On sonography, abnormal fluid collections were detected in six patients, but delineation of the extent was obscured by neighboring bone. On scintigraphy, moderate increased uptake of radionuclide was detected in six patients from ribs, the transverse process, vertebrae, and an iliac bone. The spinous process of L5, which was involved by the infection, showed normal activity. Plain radiographs showed abnormal bone changes in three patients and abnormal soft-tissue shadowing in two.

Discussion

Infections of the thoracic and abdominal wall are potentially fatal. The prognosis depends on early clinical recognition, the type of causative organism (pyogenic infections being the more severe), and the extent of tissue involvement [1–3]. The 11 cases in this series with pyogenic and tuberculous infections had quick and complete recovery because of early diagnosis and adequate therapy.

In this study, CT and MR examinations provided the most useful information about the nature and extent of the infections. Findings with both techniques were similar and correlated well with surgery. MR offered the advantage of direct multiplanar imaging without ionizing radiation and the use of IV contrast agents; CT helped in guiding percutaneous biopsy and/or partial drainage procedures in seven patients. Abscess loculation prevented complete percutaneous drainage.

Of the different planes used, sagittal and coronal MR images were found to be most helpful for surgical planning because they clearly displayed the extent and communication sites of the different abscess loculations (Figs. 1–4). The MR signal of the pyogenic and tuberculous abscesses was com-

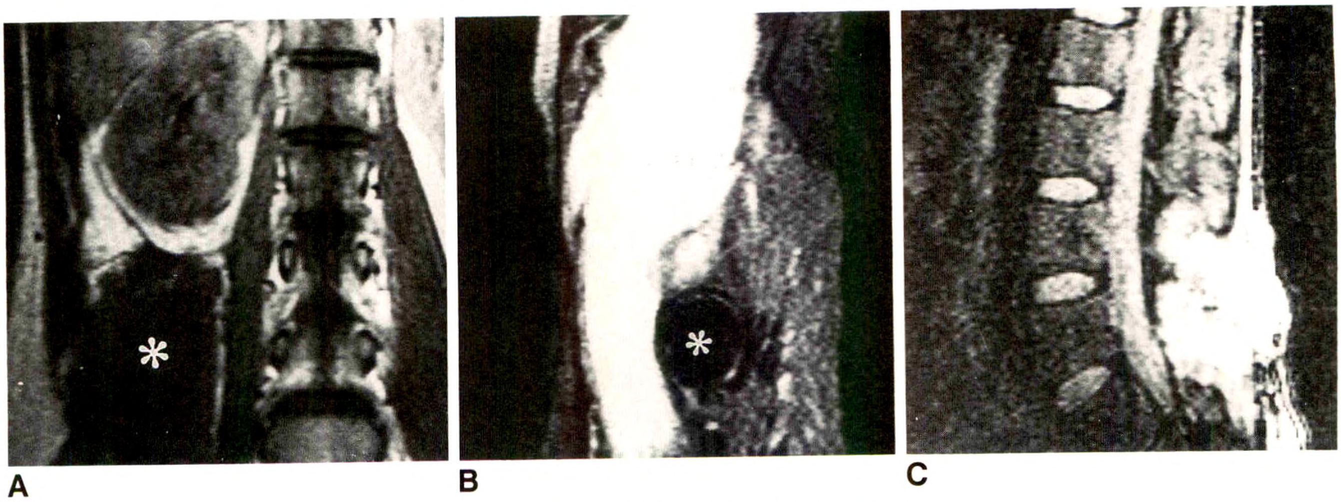

Fig. 4.—Case 9: 23-year-old man with back pain of 6 months duration radiating to right lower extremity.

A, Coronal MR image (SE 500/30) shows large mass inferior to kidney, isointense relative to psoas muscle (*asterisk*).

B, Right parasagittal MR image (STIR 1500/120/30) at level of femoral head (*asterisk*) shows psoas collection extending from iliopsoas muscle into upper thigh muscles.

C, Midsagittal MR image (STIR 1500/120/30) shows large collection involving skin, subcutaneous tissue, and posterior elements but sparing spinal canal. At surgery, acid-fast bacilli were isolated together with 1500 ml of pus. Spinous process of L5 also was removed because of involvement.

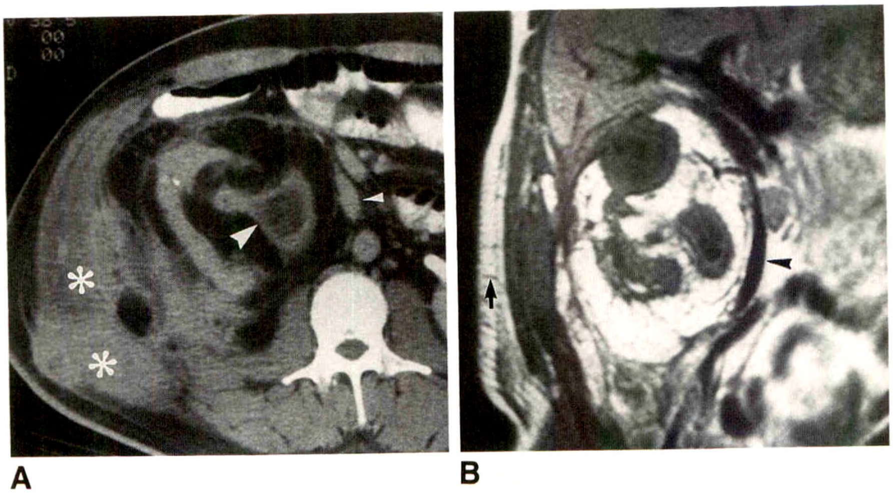

Fig. 5.—Case 13: 43-year-old man with fullness in right upper abdominal quadrant of a few years duration.

A, Postenhancement axial CT scan at level of L3 shows inflammatory process affecting lateral and posterior abdominal wall (*asterisks*). Note loss of demarcation between abdominal wall muscles and extension into subcutaneous fat. There is enhancement in residual tissue of destroyed right kidney with rim enhancement around small collection (*large arrowhead*). Inferior vena cava is displaced to left (*small arrowhead*).

B, Coronal MR image (SE 500/30) shows destroyed right kidney with inflamed perinephric fat displacing inferior vena cava to left (*arrowhead*). Note thickened lateral abdominal wall together with subcutaneous fat, which has multiple linear areas of echo void, probably representing subcutaneous edema (*arrow*).

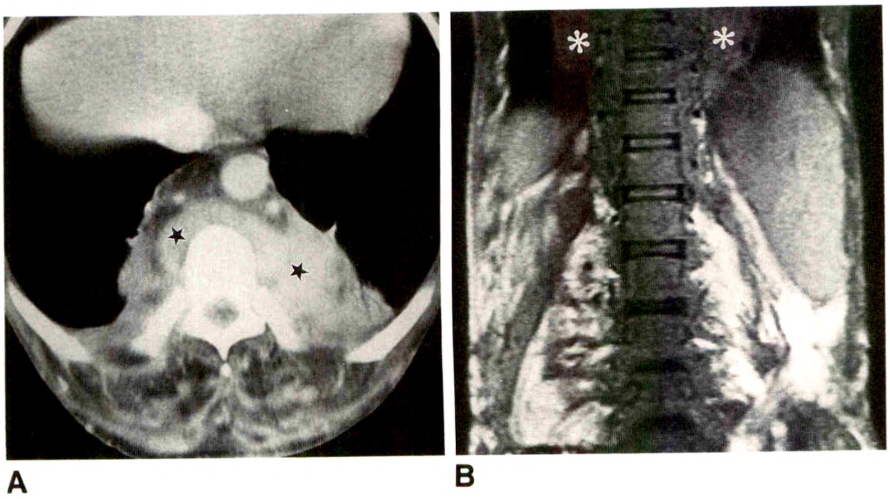

Fig. 6.—Case 12: 34-year-old man with extensive mycetoma involving entire posterior thoracoabdominal wall.

A, Axial postcontrast CT scan at level of T11 shows large posterior mediastinal mass displacing aorta anteriorly (*stars*). Mass extends posteriorly to involve all muscles of back. Patient was scanned in prone position because he was unable to lie supine.

B, Coronal MR image (SE 500/30) shows posterior mediastinal mass (*asterisks*) extending paraspinally into abdominal cavity. There is almost complete destruction of psoas muscles, but vertebrae and disks appear normal. Spleen is markedly enlarged.

parable to what has been described for abdominal collections [9–11]. The abscesses appeared hypointense on short TR/TE SE pulse sequences and became hyperintense on the long TR/TE and STIR sequences (Figs. 1–4). Although the short TR/TE study provided optimal contrast for differentiating normal from abnormal structures in the thoracoabdominal wall, it was the long TR/TE and STIR images that helped in better delineation of the location and extent of the abscesses. This concurs with observations made by others in relation to musculoskeletal infections and other types of disease affecting this anatomic region [12–15]. Rib osteomyelitis was missed with CT and MR imaging, probably because of the relatively small size of these flat bones and also because of the difficulty of imaging the ribs in one plane with either technique. Furthermore, MR imaging failed to depict the presence of osteomyelitis in a spinous process of a vertebral body and in the iliac bone of the patient with the extensive tuberculous abscess, presumably because they were obscured by the hyperintense signal of the overlying abscesses (Fig. 4).

Sonography, bone scintigraphy, and radiography provided limited help in the overall assessment of these lesions.

Infections of the thoracoabdominal wall are usually divided into necrotizing fasciitis if localized to the subcutaneous fat and superficial fascia and pyomyositis if they involve the muscles alone. Such a differentiation could be made in only four of our cases where the disease was localized to the skin and superficial fascia (Fig. 3). The rest of the patients had involvement of the skin, subcutaneous fat, superficial fascia, and muscles.

Tuberculous abscesses predominantly affecting the soft tissues are infrequent but nevertheless well recognized [7, 16, 17]. In the four patients with thoracoabdominal wall tuberculosis, imaging findings were indistinguishable from those in the cases of pyogenic infections (Fig. 4).

Mycetoma is a chronic exogenous granulomatous infection that affects the skin and extends to involve deeper tissue [18, 19]. True fungi and aerobic actinomycetes are the causative agents, introduced into the skin after trauma usually by a sharp thorn [18]. Both types of organisms tend to induce an identical histopathologic picture; diagnosis is achieved by isolation of the organism and/or by characteristic histologic findings [19]. The foot is the most frequently affected site, but in endemic countries the hand, the back, and the retroperitoneum can be involved [18–20]. The two cases in this study with actinomycotic mycetoma represent a severe form of this complication (Figs. 5 and 6). The long duration of the illness is not unusual in this disease.

In conclusion, this study has shown that MR imaging and CT are equally adequate for evaluating patients with thoracoabdominal wall infection. They both provide useful information about the nature and extent of these lesions, and hence have important impact on their management. CT is the preferred technique whenever percutaneous biopsy and/or drainage is required. MR imaging can be used for the initial diagnosis and is most appropriately used in follow-up after therapy because it offers direct multiplanar imaging in the absence of ionizing radiation and IV contrast agents.

ACKNOWLEDGMENTS

We thank the Departments of Medical Administration and Medical Studies of the Riyadh Al Kharj Hospital Programme for encouragement and support; George Green for reading the manuscript; our radiologic colleagues for cooperation; our clinical colleagues for referring their cases; and the Department of Medical Illustration, Kathleen Harrison, and Julie Moore for assistance in the preparation of this manuscript.

REFERENCES

1. Stamenkovic I, Lew PD. Early recognition of potentially fatal necrotizing fasciitis. *N Engl J Med* **1984**;310:1689–1693
2. Cave DR, Robinson WR, Brotschi EA. Necrotizing fasciitis following percutaneous endoscopic gastrostomy. *Gastrointest Endosc* **1986**;32:294–296
3. Fisher JR, Conway MJ, Takeshita RT, Sandoval MR. Necrotizing fasciitis, importance of roentgenographic studies for soft tissue gas. *JAMA* **1979**;241:803–806
4. Weiner CI, Diaconis JN. Primary abdominal wall abscess diagnosed by ultrasound. *Arch Surg* **1975**;110:341–342
5. Yeh HC, Rabinowitz JG. Ultrasonography and computed tomography of inflammatory abdominal wall lesions. *Radiology* **1982**;144:859–863
6. Gibson RK, Resenthal SJ, Lukert BP. Pyomyositis, increasing recognition in temperate climates. *Am J Med* **1984**;77:768–772
7. Coppola J, Muller NL, Connell DG. Computed tomography of musculoskeletal tuberculosis. *J Can Assoc Radiol* **1987**;38:199–203
8. Pandolfo I, Balandino A, Gaeta M, Racchiusa S, Chirico G. CT findings in palpable lesions of the anterior abdominal wall. *J Comput Assist Tomogr* **1986**;10:629–633
9. Wall SD, Fisher MR, Amparo EG, Hricak H, Higgins CB. Magnetic resonance imaging in the evaluation of abscesses. *AJR* **1985**;144:1217–1221
10. Beltran J, Noto AM, McGhee RB, Freedy RM, McCalla MS. Infections of the musculoskeletal system. High-field strength MR imaging. *Radiology* **1987**;164:449–454
11. Beltran J, McGhee RB, Shaffer PB, et al. Experimental infections of the musculoskeletal system. Evaluation with MR imaging and Tc-99m MDP and Ga-67 scintigraphy. *Radiology* **1988**;167:167–172
12. Weinreb JC, Cohen JM, Maravilla KR. Iliopsoas muscles: MR study of normal anatomy and disease. *Radiology* **1985**;156:435–440
13. Lee JK, Glazer HS. Psoas muscle disorders: MR imaging. *Radiology* **1986**;160:683–687
14. De Roos A, Van Meerten EP, Bloem JL, Bluem RG. MRI of tuberculous spondylitis. *AJR* **1986**;146:79–82
15. Haggar AM, Pearlberg JL, Froelich JW, et al. Chest wall invasion by carcinoma of the lung: detection by MR imaging. *AJR* **1987**;148:1075–1087
16. Chafetz N, Genant HK, Hoaglund FT. Ischiogluteal tuberculous bursitis with progressive bony destruction. *J Can Assoc Radiol* **1982**;33:119–120
17. Butorac R, Littlejohn GO, Hooper J. Mycobacterial disease in the musculoskeletal system. *Med J Aust* **1987**;147:388–391
18. Mariat F, Desfombes P, Segretain G. The mycetomas: clinical features, pathology, etiology and epidemiology. *Contrib Microbiol Immunol* **1977**;4:1–39
19. Lewall DB, Ofale S, Bendl B. Mycetoma. *Skeletal Radiol* **1985**;14:257–262
20. Gumaa SA, Mahgoul ES, El Sid MA. Mycetoma of the head and neck. *Am J Trop Med Hyg* **1986**;35:594–600

Radiology Outreach Foundation

The Radiology Outreach Foundation (ROF) is a nonprofit corporation whose goal is to help disadvantaged countries improve their health care by providing radiology equipment, books, consultation, education, and training to their practitioners. This assistance is on an application basis that is independent of political, ethnic, or religious orientation of the grantee. It depends on the need of the people and the ability of the ROF to meet that need. The ROF is approved by the U.S. Internal Revenue Service as a tax-exempt organization. It is endorsed by the following radiologic societies:

American Association of Women Radiologists
American College of Radiology
American Roentgen Ray Society
Association of University Radiologists
Radiological Society of North America
Society of Chairmen of Academic Radiology Departments
Society for Pediatric Radiology
European Society of Pediatric Radiology

All donations to the ROF are tax deductible. Persons who would like to contribute financially to the ROF, would be interested in being a visiting professor, would like to send books or journals to any of the institutions supported by the ROF, or would like further information about the ROF should write to

Charles A. Gooding, M.D.
President
Radiology Outreach Foundation
3415 Sacramento St.
San Francisco, CA 94118 USA

Case Report

Laryngeal Chondrosarcoma: CT Findings in Three Patients

Alberto Muñoz,[1] L. Peñarrocha,[2] F. Gallego,[2] G. Olmedilla,[3] and J. Poch-Broto[4]

Cartilaginous tumors of the larynx are rare lesions, usually of the chondroma type. Forty-six cases of chondrosarcoma of the larynx have been documented in the English-language literature [1]. In the world literature, Ferlito [2] reviewed 149 reported cases, and recently Neis et al. [3] described four additional cases.

Chondrosarcomas are slow-growing, locally aggressive tumors. The diagnosis is suggested when calcification is identified in a laryngeal tumor. CT is the best noninvasive technique for imaging the lesion [4, 5]. We report three cases, emphasizing the CT features.

Case Reports

CT scans of the larynx were obtained preoperatively on three patients with pathologically proved larynx chondrosarcomas by using a GE 8800 CT scanner (General Electric, Milwaukee, WI). Contiguous slices (5 mm thick from the subglottic level to the tongue) were made during quiet breathing. No contrast material was administered. Images were recorded at bone and soft-tissue settings. Biopsy and surgery were performed; pathologic studies showed low-grade chondrosarcoma in all three cases. No lymphadenopathy was identified on CT or during surgery.

The first case was in a 72-year-old male smoker who was admitted because of acute airway obstruction. Attempts at oral intubation were unsuccessful, and a tracheostomy was performed. Pathologic examination of cartilaginous fragments taken from the tracheostomy tube showed low-grade chondrosarcoma.

A CT scan (Fig. 1) showed a mass involving two thirds of the cricoid ring that was occluding the subglottic lumen. A total laryngectomy was performed. The patient was discharged after a complicated postoperative period. There is no evidence of relapse 2 years later.

The second case was in a 57-year-old male nonsmoker who had undergone excision of a thyroid chondroma 12 years earlier. The patient complained of hoarseness, and a hard mass (3 × 3 cm) was present in the thyroid cartilage. Direct laryngoscopy showed a mass protruding into the left false vocal cord, which was causing partial stenosis of the laryngeal vestibule. CT findings are shown in Fig. 2. One year after partial laryngectomy, the patient has no evidence of recurrent tumor.

The third case was in a 70-year-old male smoker who complained of cough and hemoptysis for 2 months. Direct laryngoscopy revealed a small subglottic mass. CT findings are shown in Figure 3. The tumor was removed and the base of the cricoid was curetted.

Discussion

Laryngeal chondrosarcomas are slow-growing tumors that are much less aggressive than similar tumors elsewhere in the body. The male-to-female ratio is three or four to one [6]. The average age of patients at presentation is 59 years.

Laryngeal chondrosarcomas usually arise from hyaline cartilage. Seventy percent begin in the cricoid cartilage, usually in the posterior cricoid lamina. Twenty percent arise from the thyroid cartilage [6]. Chondrosarcomas also may arise from arytenoid, epiglottic, or corniculate cartilage and from the true vocal cord [3]. Symptoms of larynx chondrosarcomas are those of any mass growing slowly inside the larynx. These include hoarseness, dyspnea, and dysphagia.

Received October 31, 1989; accepted after revision January 2, 1990.

[1] Departamento de Radiodiagnóstico, Hospital Universitario de San Carlos, Ciudad Universitaria, 28040 Madrid, Spain. Address reprint requests to A. Muñoz.
[2] Servicio de Otorrinolaringología, Hospital Militar "Gómez Ulla," Glorieta del Ejercito s/n 28047 Madrid, Spain.
[3] Servicio de Radiodiagnóstico, Hospital Militar "Gómez Ulla," Glorieta del Ejercito s/n 28047, Madrid Spain.
[4] Departamento de Otorrinolaringología, Hospital Universitario de San Carlos, Madrid, Spain.

AJR **154:997–998, May 1990** 0361–803X/90/1545–0997 © American Roentgen Ray Society

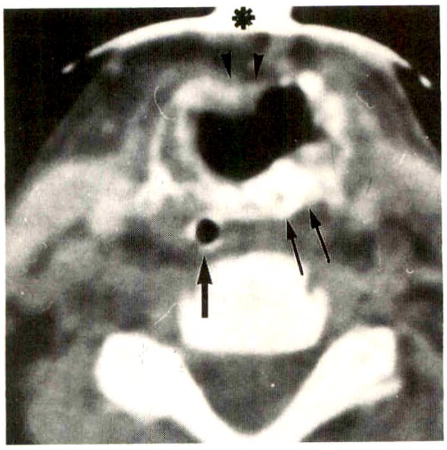

Fig. 1.—Unenhanced CT scan shows destruction of cricoid cartilage (*arrowheads*), calcification, and subtle mass (*thin arrows*). *Thick arrow* = nasogastric tube; *asterisk* = end tracheal tube.

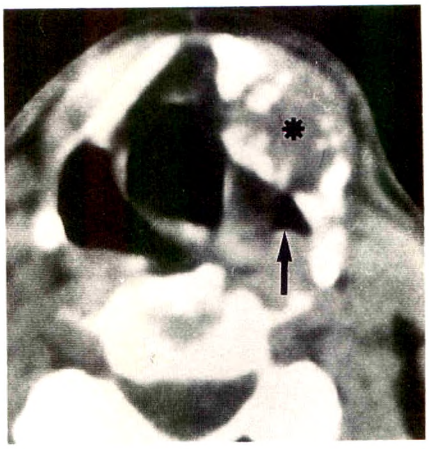

Fig. 2.—Unenhanced CT scan shows a mass with coarse calcification involving left thyroid wing (*asterisk*). Lumen of pyriform sinus is partially occluded by mass (*arrow*).

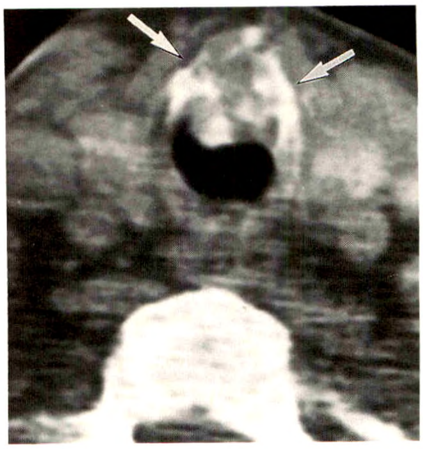

Fig. 3.—Unenhanced CT scan shows a calcified mass involving lamina of cricoid cartilage (*arrows*). Note narrowing of subglottic airway.

Chondrosarcomas can be extremely difficult to diagnose pathologically and are often misinterpreted as benign chondromas. Ninety-five percent of cases have low-grade malignancy and rarely metastasize [7]. The prognosis is generally good. A complete laryngotomy may be required for high-grade malignant tumors, recurrent lesions, or in patients in whom total excision by conservative laryngeal surgery is not feasible [1, 7].

The detection of calcification in the tumor is an important diagnostic feature [6]. Calcification that is not visible on conventional radiographs can be seen on CT scans. CT images do not superimpose adjacent structures and allow calcification in the neck to be distinguished from bone or normal cartilage [4, 5]. CT scans are useful for determining the extent of the tumor and the best operative approach.

REFERENCES

1. Lavertu P, Tucker HM. Chondrosarcoma of the larynx: case report and management philosophy. *Ann Otol Rhinol Laryngol* **1984**;93:452–456
2. Ferlito A. Secondary tumors of the larynx. In: Ferlito A, ed. *Cancer of larynx*, Vol. 2, Chap. 2. Boca Raton, FL: CRC Press, **1985**
3. Neis PR, McMahon MF, Norris CW. Cartilaginous tumors of the larynx. *Ann Otol Rhinol Laryngol* **1989**;98:31–36
4. Mancuso AA, Hanafee WN. Larynx and hypopharynx. In: Mancuso AA, Hanafee WH, eds. *Computed tomography and magnetic resonance imaging of the head and neck*, 2nd ed., Chap. 9. Baltimore: Williams & Wilkins, **1984**
5. Van Holsbeeck MT, Stresseus RC, Oyen RH, Wilms GE, Baest AL. CT diagnosis of larynx chondrosarcoma. *Eur J Radiol* **1985**;5:297–299
6. Chambers RG, Fried W. Chondrosarcoma of the larynx. *Laryngoscope* **1975**;85:713–717
7. Cantrell RW, Jahrsdoerfer RA, Reibel JF, Jhous ME. Conservative surgical treatment of chondrosarcoma of the larynx. *Ann Otol* **1980**;89:567–571

Wooden Foreign Body in the Lung Parenchyma

Alison R. Spouge,[1] Gordon L. Weisbrod,[1] Steven J. Herman,[1] and Dean W. Chamberlain[2]

Pulmonary parenchymal foreign bodies are a rare cause of chronic lung disease and infrequently are considered in a differential diagnosis of pulmonary opacities on chest radiographs. We report an unusual case of a parenchymal wooden foreign body diagnosed 12 years after chest trauma.

Case Report

A 29-year-old pregnant woman came to the emergency department because of sudden shortness of breath. She had a history of intermittent respiratory tract infections that she attributed to smoking.

A remote history of left chest trauma was obtained. The patient was unable to remember details of the incident but recalled that, while sledding supine on a piece of cardboard 12 years earlier, she had suddenly experienced severe chest discomfort. She was taken to a local hospital. A chest radiograph was obtained, and she was sent home to convalesce for 1 week. She was informed that she had residual "scarring" in the left lung.

Physical examination at the current admission showed pronounced clubbing of the fingers and decreased breath sounds over the left hemithorax. A scar was noted at the inferior aspect of the left chest posteriorly, which the patient claimed was the result of the remote sledding accident. A chest radiograph showed a 50% hydropneumothorax. The chest radiographs made 12 years earlier were not available for comparison.

The pneumothorax was treated by percutaneous aspiration. A follow-up chest radiograph showed complete resolution of the pneumothorax, a residual faint tubular density in the left upper lobe, mild volume loss of the left lung, and blunting of the left costophrenic angle (Figs. 1A and 1B).

During the ensuing months, the patient complained of intermittent cough with purulent sputum, hemoptysis, and left-sided chest discomfort.

A CT scan of the chest obtained 16 months after discharge from the hospital showed a cylindrical cavity in the left upper lobe containing a calcific density. This was interpreted as a calcified hematoma in a posttraumatic cyst (Fig. 1C). The thickness of the wall of the cavity varied, up to 7 mm. Linear parenchymal densities surrounded the lesion, and localized bronchiectasis extended from the hilum.

A transthoracic needle biopsy of the abnormality was performed. The lesion was described as "rock hard," and the aspirate was "scanty"; Gram stain and cultures were negative. Because the patient had no clinical improvement after a long-term course of antibiotics, an inferior lingular segmentectomy and wedge excision of the anterior segment of the left lower lobe were performed.

The excision specimen contained a wedge-shaped piece of wood 8 × 1.6 × 1 cm (Fig. 2), which was enveloped in granulation tissue with fibrosis. Immediately adjacent to this in the lung was localized postobstructive bronchiectasis and organizing obstructive pneumonia.

Discussion

Although asymptomatic aspiration of a foreign body into the tracheobronchial tree is not unusual [1], occult pulmonary parenchymal foreign bodies are rare. Most parenchymal foreign bodies are introduced as a result of trauma, and the diagnosis is made on the basis of the history and physical examination at the time of presentation. Our patient was unaware of the magnitude of her injury until pathologic ex-

---

Received November 8, 1989; accepted after revision December 19, 1989.

[1] Department of Diagnostic Imaging, Toronto General Hospital, 200 Elizabeth St., Toronto, Ontario, Canada M5G 2C4. Address reprint requests to G. L. Weisbrod.

[2] Department of Pathology, Toronto General Hospital, Toronto, Ontario, Canada M5G 2C4.

AJR 154:999–1001, May 1990 0361–803X/90/1545–0999 © American Roentgen Ray Society

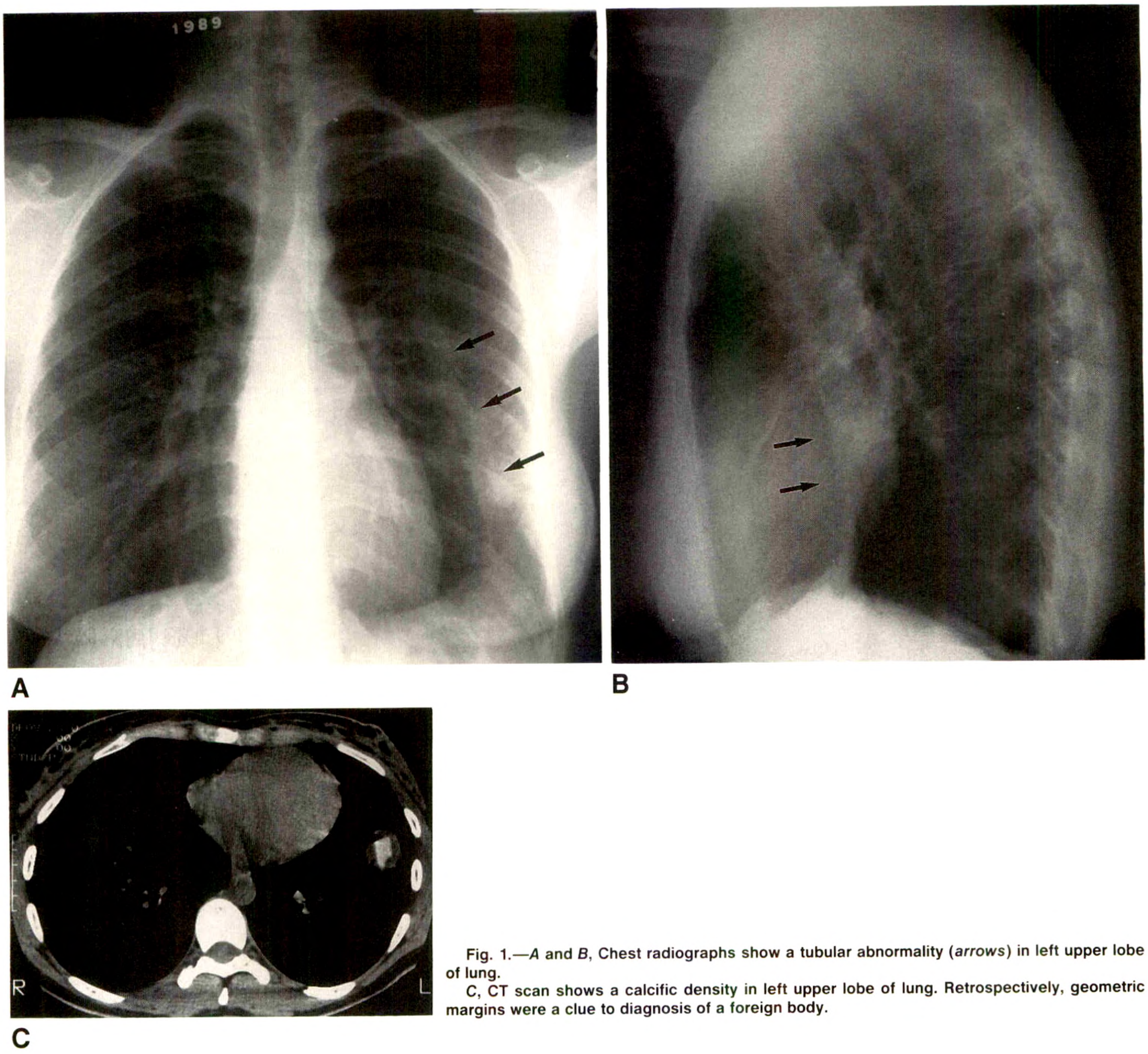

Fig. 1.—*A* and *B*, Chest radiographs show a tubular abnormality (*arrows*) in left upper lobe of lung.

C, CT scan shows a calcific density in left upper lobe of lung. Retrospectively, geometric margins were a clue to diagnosis of a foreign body.

amination of the resected pulmonary specimen obtained 12 years after the traumatic episode confirmed the presence of a wooden foreign body in the lung parenchyma. The injury most likely occurred while the patient accelerated down a slope lying supine on a cardboard sled and the apex of a wooden fragment that was lying on the ground impaled her left chest.

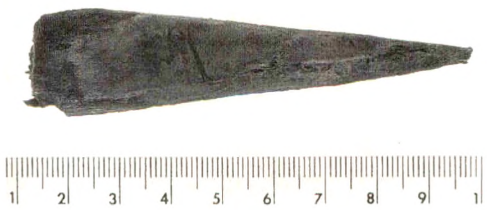

Fig. 2.—Surgical specimen contained a wedge-shaped piece of wood.

Wood accounts for the largest proportion of retained foreign bodies after trauma to the human body [2]. It is the most difficult foreign body to detect on plain film radiographs because of its low-density chemical composition. It is less dense than soft tissues initially and, with time, becomes isodense. Occasionally, it is detected only as a result of secondary inflammatory change [2].

It is not certain whether the abnormality on the chest radiograph in this case was caused by the foreign body itself or by the surrounding soft-tissue response. The former is more likely, as evidenced by the CT appearance of the specimen in a water bath, which confirmed that the wood had the density of calcium. Although the diagnosis was not made preoperatively in this patient, the CT scan showed that the abnormality had square margins and tubular geometry, which in retrospect suggests a foreign body.

The high attenuation value of the wood on CT is unexpected in view of its low density on plain radiographs. However, Bodne et al. [3] cited three cases of wooden foreign bodies of the extremities imaged on CT with various attenuation values, ranging from extremely low (close to air) in acute cases to high (close to calcium) in chronic cases. They suggested the difference may be due to superimposed inflammatory changes. Louis et al. [4] also noted that wooden foreign bodies retained in soft tissue for a long time may become calcified. Brewer and Leonard [5] stated that CT scans are the most sensitive tool available for the detection of wooden foreign bodies in lacerations or puncture wounds. Finally, Kuhns et al. [6], in a cadaver study, noted toothpicks to be detectable on CT and to be isodense with "clotted blood" in adjacent tissues.

REFERENCES

1. Thomas V, Chandy G, Rolston DK. Foreign body in the lung for 45 years without symptoms. *Br J Dis Chest* **1986**;80:292–294
2. Anderson MA, Newmeyer WL, Kilgore ES. Diagnosis and treatment of retained foreign bodies in the hand. *Am J Surg* **1982**;144:63–67
3. Bodne D, Quinn SF, Cochran CF. Imaging foreign glass and wooden bodies of the extremities with CT and MR. *J Comput Assist Tomogr* **1988**;12:608–611
4. Louis D, Green TL, Poznanski AK. Burns, frostbite, foreign bodies and other traumatic lesions of the hand. In: Poznanski AK, ed. *The hand in radiologic diagnosis: with gamuts and pattern profiles*, vol. 2, 2nd ed. Philadelphia: Saunders, **1984**:722
5. Brewer TE, Leonard RB. Detection of retained wood following trauma. *N C Med J* **1986**;47:575–577
6. Kuhns LR, Borlaza GS, Seigel RS, Paramagul C, Berger PE. An in vitro comparison of computed tomography, xeroradiography, and radiography in the detection of soft-tissue foreign bodies. *Radiology* **1979**;132:218–219

Book Review

ERCP Atlas. By Gerhard Pott and Bernhard Schrameyer. (Translated from the German by Gertrude Graubert Champe.) Philadelphia: Decker, 227 pp., 1989. $79.50

This is a true atlas in that it contains an extensive series of endoscopic retrograde cholangiopancreatograms supplemented by minimal descriptive text. The only exception is the first chapter, which by text and drawings provides preliminary information on the definition of ERCP, preparatory information for patient and physician, and a short description of the technique of performing ERCP and endoscopic sphincterotomy. This is followed by a discussion of contraindications, complications, and causes of failure. The subsequent chapters portray the normal ERCP appearance, the pathologic pancreatogram, the pathologic cholangiogram, and papillary stenosis. A chapter of color photographs shows the endoscopic appearance of the papilla of Vater.

The radiographic and endoscopic reproductions are of generally good quality although some suffer from annoying reproduction of artifacts from the original radiographs and endoscopic images. Some of the radiographs are printed as dark images, occasionally compromising their diagnostic usefulness. The line drawings are excellent and provide important support for the radiographs. A particularly useful series of drawings illustrates the grading of chronic pancreatitis, and another shows the pancreatographic findings of pancreatic carcinoma.

The atlas provides broad coverage of a variety of pathologic entities. There is, however, room for disagreement in interpretation of some of the images. For instance, images attributed to types of Caroli syndrome easily could be interpreted as typical choledochal cysts, sclerosing cholangitis, or ductal obstruction due to choledocholithiasis. Because of the limited descriptions of the illustrations, the fine points of differential diagnosis are not discussed in detail. Frequently, however, helpful interpretive tips and comments on treatment are provided.

The sequence of presentation of the illustrations will be unfamiliar to many readers. In a multicomponent figure, the first illustration is presented on the right-hand page, and subsequent illustrations are presented on the left-hand page. This requires modification of the approach to reading the text, and until this adjustment is made, the format can be somewhat irritating. Similarly, the translation to English will require flexibility on the part of the reader, especially when the sizes of lesions are related to vegetables of unfamiliar or variable size, such as peas, lentils, hazelnuts, and tomatoes.

Some of the sections, such as those dealing with pancreatograms and congenital biliary abnormalities, could be strengthened by increasing the number of illustrations. Other sections provide outstanding and, in many cases, unique examples of abnormalities such as the Mirizzi syndrome, sclerosing cholangitis, and biliary calculus disease.

This atlas has many admirable features that should make it an important resource for endoscopists and radiologists facing the difficult challenge of interpreting endoscopic retrograde cholangiograms and pancreatograms.

Charles A. Rohrmann, Jr.
Scott J. Schulte
University of Washington Medical Center
Seattle, WA 98195

Percutaneous Gastrostomy with Gastropexy: Experience in 125 Patients

Sanjay Saini[1]
Peter R. Mueller[1]
Jochen Gaa[1,2]
Susan E. Briggs[3]
Peter F. Hahn[1]
Bruce H. Forman[1]
Glen A. Tung[1]
Stuart G. Silverman[1,4]
Michael J. Lee[1]
Mary C. Morrison[1]
Alan T. Brown[1,5]
Joseph T. Ferrucci, Jr.[1]

We report our experience with radiologically guided percutaneous tube gastrostomy in 125 patients by using a gastropexy technique in which the anterior gastric wall is nonsurgically sutured to the anterior abdominal wall with percutaneously placed T-fasteners before catheter insertion. Short-term follow-up of up to 2 weeks was available in all patients. In 63 patients, long-term follow-up (>4 weeks; average, 3.5 months; maximum, 1 year) was available. Catheter placement was successful in 124 (99%) of 125 patients, including three patients with anatomic changes after Billroth II hemigastrectomy and two patients with failed endoscopic attempts. There were no deaths related to the procedure, and no patients required surgical intervention for complications attributable to the gastrostomy procedure. The 30-day mortality rate was 11% (*n* = 7). These deaths were due to cardiorespiratory arrest and were not attributable to the gastrostomy procedure. Major complications occurred in 1.6% (*n* = 1) and minor complications in 9.5% (*n* = 6).

These results indicate that percutaneous gastrostomy with gastropexy is a safe and effective technique for placement of catheters in the stomach.

***AJR* 154:1003–1006, May 1990**

Radiologically guided percutaneous placement of a gastrostomy tube in patients requiring nutritional support or enteric decompression is often used as an alternative to surgical and endoscopic techniques [1–5]. Although percutaneous gastropexy techniques for radiologic placement of gastrostomy tubes are available [6, 7], in the reports published to date, gastrostomies were performed without gastropexy [1–5]. Conversely, in surgical or endoscopic gastrostomy, the anterior wall of the stomach is sutured (Stamm surgical gastrostomy with gastropexy) or fixed (percutaneous endoscopic gastrostomy) to the anterior abdominal wall, or the gastrostomy tube is encased in a seromuscular tunnel as it enters the stomach (Witzel gastrostomy without gastropexy), in order to prevent spillage of gastric contents into the peritoneal cavity. As the complication rates for the radiologic techniques without gastropexy are comparable to those reported in literature for surgical and endoscopic placement of gastrostomy tubes, gastropexy during radiologically guided placement of a gastrostomy tube has been thought to be unnecessary [1, 2].

In an earlier report, we described a method for a fluoroscopically guided percutaneous gastrostomy in which, before catheter insertion, the anterior wall of the stomach is nonsurgically sutured to the anterior abdominal wall by using specially designed T-fasteners (Meditech, Watertown, MA) [8]. Our experience with this technique is expanded from 10 patients in the original report to 125 patients in this report. We emphasize the absence of procedure-related deaths, tube extrusion into the peritoneal space, or any other major complication necessitating surgical intervention in gastrostomies performed with the gastropexy technique.

Received November 13, 1989; accepted after revision January 11, 1990.

[1] Division of Gastrointestinal Radiology, Department of Radiology, Massachusetts General Hospital and Harvard Medical School, 32 Fruit St., Boston, MA 02114. Address reprint requests to S. Saini.

[2] Present address: Städtische Klinik Darmstadt, Grafenstrasse 9, 6100 Darmstadt, West Germany.

[3] Department of Surgery, Massachusetts General Hospital and Harvard Medical School, 32 Fruit St., Boston, MA 02114.

[4] Present address: Brigham and Women's Hospital, Boston, MA 02114.

[5] Present address: Baystate Medical Center, Springfield, MA 01199.

0361–803X/90/1545–1003
© American Roentgen Ray Society

Subjects and Methods

Population of Patients

From 1985 to 1989, radiologically guided gastrostomy, or indirect small-bowel enterostomy (gastrostomy with catheter tip placed beyond the pylorus) was attempted in 125 patients. Short-term (up to 2 weeks) follow-up was available in all patients. In 63 (50%) patients, follow-up was possible for more than 4 weeks (average, 3.5 months; maximum, 1 year). These patients ranged in age from 29 to 90 years; 37 were men and 26 were women. In five patients, the catheter tip was placed beyond the pylorus. All but two gastrostomies were performed exclusively under fluoroscopic guidance [8]. In two patients, a nasogastric tube could not be passed and gastric distension was achieved with an 18-gauge needle that was advanced percutaneously into the stomach under CT guidance. Feeding gastrostomies were performed in 21 patients because of poor nutritional intake due to esophageal obstruction from a variety of causes. These included neck cancer ($n = 10$), esophageal carcinoma ($n = 4$), paraesophageal metastases ($n = 6$), and benign esophageal stricture ($n = 1$). In 33 patients, inability to eat resulted from neurologic disorders; this included patients with strokes ($n = 18$), primary or metastatic cancer of the CNS ($n = 4$), subdural hematoma ($n = 2$), Parkinson disease ($n = 2$), and a variety of miscellaneous conditions ($n = 7$) such as encephalitis, amyotrophic lateral sclerosis, and Alzheimer disease. Nine patients had various miscellaneous conditions necessitating percutaneous gastrostomy, including cachexia ($n = 3$), cystic fibrosis ($n = 1$), tracheal trauma ($n = 1$), and systemic lupus erythematosus ($n = 1$).

Complications

Patients' charts were reviewed for immediate and long-term complications associated with placement of gastrostomy tubes as defined by Shellito and Malt [9]. Major complications were defined as deep wound infection, inadvertent tube extrusion requiring repetition of the procedure, early aspiration pneumonia due to feeding, significant external or internal leak around the tube requiring reoperation or tube change, gastric hemorrhage requiring transfusion, gastroparesis, failure of tube to function for feeding, persistent gastrocutaneous fistula after tube removal, and deep vein thrombosis after the procedure. Gastrocolic fistula formation and exploratory laparotomy after percutaneous tube gastrostomy were added to this list.

Minor complications were defined as tube migration producing bowel obstruction, failure to function as a decompressive device, early (<2 weeks) inadvertent tube removal with replacement at bedside, subcutaneous abscess formation, and internal leak after removal of a decompressing gastrostomy tube. Failure to feed, necessitating tube repositioning, and self-limited peritonitis with no demonstrable internal leak and treated only with IV antibiotics were added to the list of minor complications. Late (>2 weeks) inadvertent tube removal with replacement at bedside was not considered a complication of the procedure nor were any late mechanical problems such as tube occlusion or catheter breakdown. Similarly, indirect medical problems such as those associated with enteral feedings (e.g., diarrhea) were excluded.

Gastrostomy Technique

Details of the procedure used in all 125 patients have been published [8]. Only the gastropexy portion of this technique is described here (Fig. 1). The anterior wall of the stomach was nonsurgically affixed (by gastropexy) to the anterior abdominal wall with four Brown-Mueller T-fasteners (Meditech, Watertown, MA). Each T-fastener was introduced into the air-distended stomach with a specially designed 18-gauge needle. The T-fastener was released into the stomach only when air could be freely aspirated into a syringe attached to this needle. When no air could be aspirated, the T-fastener–loaded needle was simply withdrawn and repositioned. After releasing the T-fastener into the stomach, the needle was withdrawn and with gentle traction on the suture of the T-fastener, the anterior gastric wall was apposed to the anterior abdominal wall. The suture was then secured with a metal clamp to prevent slippage of the T-fastener into the gastric lumen. The T-fasteners were positioned 1.0–1.5 cm apart in the form of a square, and at the center of this square the gastrostomy catheter (12 French–18 French) was inserted by using the Seldinger technique. If the catheter tip needed to be placed beyond the pylorus (because of a history of aspiration pneumonia or if gastroesophageal reflux was noted at the time of the procedure) the guidewire was manipulated into the duodenum and/or proximal jejunum before tract dilatation and catheter insertion. Catheter position was confirmed with an injection of contrast material before securing the tube. No prophylactic IV antibiotics were administered.

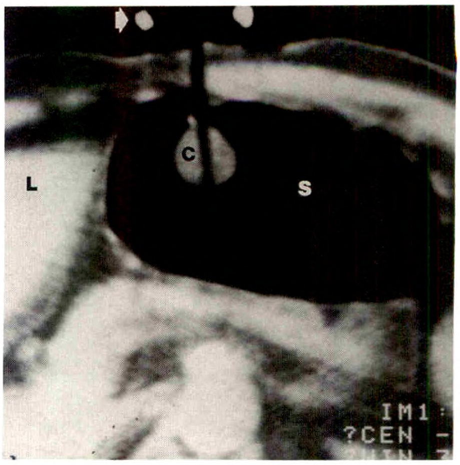

Fig. 1.—CT scan obtained immediately after percutaneous gastrostomy shows fixation of stomach to anterior abdominal wall. Adherence of two layers facilitates gastrostomy tract dilatation and prevents tube extrusion or leakage of gastric contents into peritoneum. L = liver; C = catheter; S = stomach; *arrow* = T-fastener.

Catheters used as enterostomy tubes ranged from 12- to 18-French. Forty-four (44/63 = 70%) of the catheters used as gastrostomy tubes were 16-French ($n = 22$) or 18-French ($n = 22$). This included one gastrostomy that was converted into an indirect small-bowel enterostomy when gastroesophageal reflux was noted during the procedure. Nineteen (19/63 = 30%) gastrostomy tubes (including four indirect small-bowel enterostomies for gastroesophageal reflux) were 12-French ($n = 4$) or 14-French ($n = 15$).

The nasogastric tube was removed immediately after the percutaneously placed catheter was documented to be in proper intraluminal position. Catheters were left to gravity drainage for the first 12–18 hours, although small aliquots of medications were often administered sooner. Feedings were initiated the morning after placement of the enterostomy tube. No follow-up radiography (plain film or contrast injection) was performed before initiation of feeding. T-fasteners were cut at the skin surface after 14–21 days, allowing adequate time for adhesion of the gastric wall to the abdominal wall.

Results

Tube gastrostomies were performed successfully in 124 (99%) of 125 patients. This included two patients in whom endoscopic gastrostomy tube placement failed and three patients who had a partial gastrectomy with a Bilroth II anastomosis. Catheter placement was not possible in a patient with neurologic disorder (stroke) in whom the transverse colon overlaid the stomach and no direct access route was available. This was recognized before radiologic intervention, and the patient underwent a surgical gastrostomy.

Complications

Major complications (1/63 = 1.6%).—No patients required surgery for any complications associated with tube gastrostomy. Similarly, no patients had complications of significant internal leakage, extraluminal catheter placement, early aspiration pneumonia, gastric hemorrhage, deep wound infection, inadvertent tube removal requiring laparotomy for replacement, or creation of a gastrocolic fistula. External (pericatheter) leakage, classified as a major complication by Shellito and Malt [9], occurred in one patient in whom a catheter was placed for nutritional support.

Minor complications (6/63 = 9.5%).—Superficial (subcutaneous) wound infections developed in one patient even though prophylactic IV antibiotics were not used routinely. One patient had signs of peritonitis that lasted 24–36 hr. This may have resulted from a transient and limited leak of gastric contents into the peritoneal cavity although no pneumoperitoneum or leak could be shown on contrast enhanced images. The patient's symptoms were successfully treated with a 1-week course of IV antibiotics. No patients experienced bleeding from the gastrostomy tube, although one patient had melena 5 days after catheter placement, which was subsequently shown to arise from a gastric ulcer located 8 cm distal to the gastrostomy site. In one patient, the gastrostomy tube was advanced into the jejunum 10 days after the initial gastrostomy because of recurrent episodes of aspiration (without pneumonia). In two patients, the gastrostomy catheters were subsequently advanced into the jejunum because of poor gastric emptying. In one patient, catheter migration from the stomach into the duodenum produced bowel obstruction from the inflated balloon. This was corrected by exchanging the Foley catheter for a Levine tube.

30-Day Mortality Rate

The 30-day mortality rate was 11% ($n = 7$). All patients died of cardiorespiratory arrest. Three autopsies were performed and in all three cases the gastrostomy tube was well secured and without complication. The cardiorespiratory arrests occurred at 4 days ($n = 1$; subdural hematoma), 5 days ($n = 2$; amyotrophic lateral sclerosis; metastatic thyroid carcinoma), 8 days ($n = 1$; metastatic gastric carcinoma), 10 days ($n = 1$; metastatic esophageal carcinoma), 14 days ($n = 1$; Alzheimer disease) and 18 days ($n = 1$; metastatic lung carcinoma).

Tube Complications (7/63 = 11%)

A variety of mechanical problems resulting in catheter malfunction (kinking, blockage, etc.) occurred. All ($n = 7$) were late and were related to the long-term gastrostomy tube therapy. These included catheter occlusion ($n = 3$) and catheter disintegration ($n = 2$). These catheters were exchanged at bedside, without radiologic guidance. Inadvertent tube removal occurred in two patients, but the catheter was reinserted at bedside without radiologic guidance.

Discussion

The combined radiologic experience reported to date suggests that radiologically guided percutaneous gastrostomy can be performed safely in a large majority of referred patients, including those with partial gastrostomies. However, comparison of complication rates associated with competing (radiologic or endoscopic or surgical) techniques is difficult because reported series have used differing definitions of minor and major complications. In their review of 424 of 3359 surgical gastrostomies, Shellito and Malt [9] developed comprehensive and specific definitions of major and minor complications associated with tube gastrostomies. Thus, we have adopted their criteria and have modified them only to add complications not seen with surgical gastrostomies, such as transgression of the colon and inadvertent catheter placement into the peritoneal cavity.

The radiologic technique used here replicates a Stamm surgical gastrostomy in all respects. As the steps involved in inserting the four T-fasteners are simple and do not significantly prolong the procedure time, we think that this form of gastropexy can be adopted readily by others. In addition to safety issues, additional advantages exist, such as facilitating dilatation of the gastrostomy tract to permit insertion of large-bore catheters (which are less likely to occlude). Thus, for example, most (120/124 = 97%) catheters inserted in this series were larger than 12-French, whereas the usual catheter size used for feeding in the percutaneous techniques without gastropexy has been 9- to 12-French [1, 3–5]. As tract dilatation after gastropexy is relatively straightforward, the procedure can be adopted readily by radiologists who might perform feeding gastrostomies infrequently. Fixation of the stomach to the anterior abdominal wall also may assist in preventing gastric hemorrhage [10] because the pierced stomach is tightly attached to the abdominal wall, resulting in a tamponade of any vascular injury. Further advantages, including absence of inadvertent tube migration into the peritoneum or leakage of gastric contents into the peritoneum, are obvious and are the major reasons that we prefer to fix the stomach to the abdominal wall (Fig. 1). Gray et al., for example, reported that such complications necessitated a laparotomy in two (2.8%) of 72 patients [3] and stimulated the design of a "safer" feeding catheter [11]. Similarly, Halkier et al. [1] reported that five (2%) of 252 gastrostomies were complicated with peritoneal leakage and that three of these patients needed surgical exploration. We have encountered no such sequela in our entire series of 124 gastrostomies, which is particularly relevant because all catheters were placed by residents and fellows under staff supervision.

Interference with gastric peristalsis resulting in gastroparesis has been reported to be a potential disadvantage of gastropexy [12]. Indeed in this series, two patients did not tolerate feedings infused into the stomach and the catheters were manipulated into the jejunum. These patients have been included in our list of patients with minor complications. However gastroparesis was not noted on enhanced radiographs, and in both these patients with strokes, poor gastric emptying was attributed to their supine position, which caused the feedings to pool in the dependent gastric fundus. Although in the technique without gastropexy jejunal feedings may be preferred because of concerns with gastric leakage, we do not routinely infuse feedings into the jejunum but, whenever possible, prefer to maintain physiologic function by instilling feedings directly into the stomach.

Although the rates for major complications reported in this and other radiologic series are slightly lower than those reported in endoscopy journals [13, 14], the differences are small and could be related to differences in patient populations. However, the principal advantage of the radiologic technique over endoscopic gastrostomies is that the radiologic technique specifically permits identification of patients in whom the bowel (colon) may lie anterior to the stomach. In this small but important group of patients, the radiologic percutaneous approach can, under fluoroscopic guidance, allow selection of a gastrostomy site that specifically avoids the colon, or if no safe route is available, triage of the patient to surgery. Thus, no instances of gastrocolic fistula formation in this series or in any of the other large radiologic series have been reported to date.

The radiologic techniques also manifest several advantages over surgical gastrostomies. These include elimination of the risk of general anesthesia and the absence of postoperative ileus, which permits feedings to be started within a few (6–12) hours after gastrostomy tube insertion. A significant advantage over surgical and endoscopic gastrostomies is that, if necessary, the tube placed by means of radiologic gastrostomy with gastropexy can be converted into a jejunal feeding catheter at any time. In comparison, patients undergoing surgical and endoscopic gastrostomies must wait 7–10 days before the gastrostomy tract can be manipulated, and surgical gastrostomies that have been created by using the Witzel canal are extremely difficult to convert under radiologic guidance into jejunal catheters because the Witzel canal is oriented toward the gastric fundus and redirecting a catheter toward the pylorus is very difficult and often impossible.

Our experience and that of others have shown that radiologically guided tube gastrostomy is an extremely low-risk procedure. Indeed, because of the simplicity and ease of this procedure, in our practice the threshold for radiologically guided tube placement has been lowered. Marginally malnourished patients with cystic fibrosis and terminally ill patients with malignant bowel obstruction have benefitted from this technique (bowel decompression in the latter group). Furthermore, as gastrostomy is performed with widely available fluoroscopic equipment it remains an inexpensive procedure that can be adopted by virtually any radiologic facility worldwide. It also permits wide flexibility in selection of catheter size, which can be selectively left in the stomach or the small bowel.

REFERENCES

1. Halkier BK, Ho CS, Yee ACN. Percutaneous feeding gastrostomy with the Seldinger technique: review of 252 patients. *Radiology* **1989**;171:359–362
2. O'Keeffe F, Carrasco CH, Charnsangavej C, et al. Percutaneous drainage and feeding gastrostomies in 100 patients. *Radiology* **1989**;173:276–278
3. Gray RR, St. Louis EL, Grossman H. Percutaneous gastrostomy and gastro-jejunostomy. *Br J Radiol* **1987**;60:1067–1070
4. Willis JS, Oglesby JT. Percutaneous gastrostomy. *Radiology* **1988**;167:41–43
5. van Sonnenberg E, Wittich GR, Brown LK, et al. Percutaneous gastrostomy and gastroenterostomy. II. Clinical experience. *AJR* **1986**;146:581–586
6. Brown AS, Mueller PR. Controlled percutaneous gastrostomy: nylon T-fastener for fixation of the anterior gastric wall (letter). *Radiology* **1986**:160:278
7. Cope C. Suture anchor for visceral drainage. *AJR* **1986**;146:160–161
8. Brown AS, Mueller PR, Ferrrucci JT Jr. Controlled percutaneous gastrostomy: nylon T-fastener for fixation of the anterior gastric wall. *Radiology* **1986**;158:543–545
9. Shellito PC, Malt RA. Tube gastrostomy: techniques and complications. *Ann Surg* **1985**;201:180–185
10. Rose DB, Wolman SL, Ho CS. Gastric hemorrhage complicating percutaneous transgastric jejunostomy. *Radiology* **1986**;161:835–836
11. Gray RR, St. Louis EL, Grossman H. Modified catheter for percutaneous gastrojejunostomy. *Radiology* **1989**;173:276–278
12. Johnston WD, Lopez MJ, Kraybill WG, Bricker EM. Experience with a modified Witzel gastrostomy without gastropexy. *Ann Surg* **1982**;195:692–699
13. Mamel JJ. Percutaneous endoscopic gastrostomy. *Am J Gastroenterol* **1989**;84:703–710
14. Larson DE, Burton DD, Schroeder KW, DiMagno EP. Percutaneous endoscopic gastrostomy: indications, success, complications, and mortality in 314 consecutive patients. *Gastroenterology* **1987**;93:48–52

Angioplasty for Long-Term Treatment of Patients with Budd-Chiari Syndrome

Louis G. Martin[1]
J. Michael Henderson[2]
William J. Millikan, Jr.[2]
William J. Casarella[1]
Stephen L. Kaufman[1]

The goal of radiologic intervention in patients with Budd-Chiari syndrome is to control portal hypertension and prevent further hepatocellular damage until collateral hepatic venous outflow channels can develop. Percutaneous balloon angioplasty was used to treat six patients with this syndrome who were followed up for an average of 43 months (range, 12–92 months). Standard interventional radiologic techniques were used to dilate the hepatic veins (two patients), inferior vena cava (three patients), and proximal anastomosis of a mesoatrial shunt (one patient). Angioplasty was the only invasive treatment in three patients, whereas the remaining three patients had previous portosystemic shunts. Clinical and hemodynamic improvement occurred after each angioplasty. Multiple dilatations were required in all patients (average, 3.2; range, 2–5) because of restenosis at the angioplasty site and ongoing hepatocyte necrosis shown by biopsy. Long-term benefit occurred in five patients despite ultimate caval occlusion in two patients and restenosis in one patient. One patient who was almost free of symptoms for 36 months developed gastrointestinal bleeding caused by portal hypertension.

This experience suggests that balloon angioplasty is a safe and effective treatment for patients with Budd-Chiari syndrome. The therapy is not definitive, but serves to moderate the severity of the disease until collateral venous pathways develop. Multiple angioplasties are required for the long-term care of these patients.

***AJR* 154:1007–1010, May 1990**

Budd-Chiari syndrome is an uncommon, but by no means rare, disease. Symptomatic hepatic venous occlusion is seen in 0.05% of necropsies [1]; asymptomatic hepatic venous occlusion occurs in 0.183% [2]. More than 500 cases have been reported in the world literature.

Interventional radiologic procedures have a significant role in treating some patients with Budd-Chiari syndrome. These include (1) percutaneous transluminal angioplasty of occlusions or stenoses of the hepatic vein or inferior vena cava (IVC), (2) percutaneous transluminal angioplasty to preserve the function of surgically created shunts; (3) hepatic arterial embolization to treat hepatocellular carcinoma, and (4) transhepatic embolization of varices. In this paper, we review our experience with angioplasty in the long-term treatment of six patients with Budd-Chiari syndrome.

Subjects and Methods

Between 1980 and 1989 we performed percutaneous transluminal angioplasty on six patients with Budd-Chiari syndrome. Conventional angioplasty techniques, which have been described elsewhere [3, 4], were used in two patients with hepatic vein stenoses, one patient with a 1-cm occlusion of the hepatic portion of the IVC (Fig. 1), two patients with stenoses of the hepatic portion of the IVC that compromised the function of infrahepatic portosystemic shunts, and one patient with stenosis of the proximal anastomosis of a mesoatrial shunt. In the last patient, who had lost an estimated liter of blood because of bleeding esophageal

Received September 25, 1989; accepted after revision January 3, 1990.

[1] Department of Radiology, Emory University Hospital, 1364 Clifton Rd., N.E., Atlanta, GA 30322. Address reprint requests to L. G. Martin.

[2] Department of Surgery, Emory University Hospital, 1364 Clifton Rd., N.E., Atlanta, GA 30322.

0361–803X/90/1545–1007
© American Roentgen Ray Society

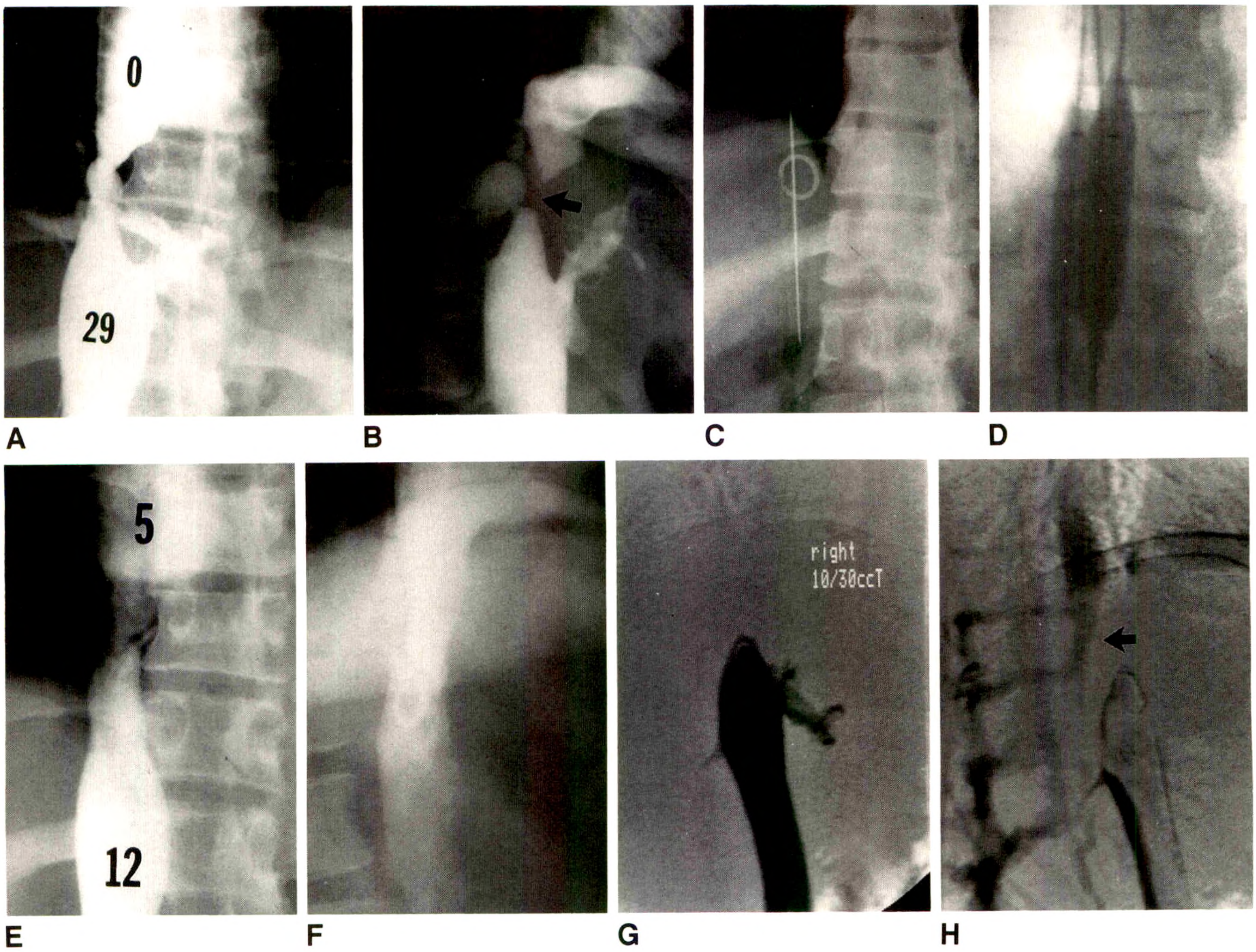

Fig. 1.—Patient no. 3. 31-year-old man with an occlusion of inferior vena cava (IVC) caused by trauma incurred when his fall from a tree was abruptly stopped by a safety belt he was wearing around his waist. The patient improved clinically and histologically despite ultimate occlusion of angioplasty site.

***A* and *B*, Anteroposterior (*A*) and lateral (*B*) views of a biplane inferior venacavogram after simultaneous injections of contrast material through catheters placed above and below a complete occlusion of IVC (*arrow*).**

***C*, A transeptal needle has been placed through occlusion into lower IVC.**

***D*, Simultaneous inflation of angioplasty balloons with 7-, 10-, and 12-mm diameters.**

***E* and *F*, Anteroposterior (*E*) and lateral (*F*) views of a biplane venacavogram after percutaneous transluminal angioplasty.**

***G* and *H*, Early (*G*) and late (*H*) lateral digital inferior venacavograms show reocclusion of IVC. Collateral perispinous and epidural veins reconstituted flow in IVC above obstruction (*arrow*).**

Numerals indicate mean pressure measurements in millimeters of mercury in right atrium and IVC.

varices treated by endoscopic sclerosis, the coronary vein was embolized with Gelfoam pledgets (Upjohn, Kalamazoo, MI) and three 8-mm Gianturco coils (Cook, Bloomington, IN) introduced through the mesoatrial shunt. Demographic information is included in Table 1.

Patients were periodically readmitted for follow-up evaluation, which included live function tests, liver-spleen volume determination, biopsy, and angiography. Patients and their physicians were also contacted directly for follow-up information. The angioplasty was considered a technical success if the pressure gradient across the area of stenosis was reduced and a greater than 50% enlargement of the vessel lumen was seen angiographically. The patient was considered *improved* clinically if symptoms lessened and a trend was seen toward normalization of liver function tests, liver volume, hepatic blood flow, and biopsy. The patient was not considered *cured* unless all test results returned to normal and the patient was free of symptoms. Postprocedural morbidity was considered significant if any alteration in the patient's condition prolonged hospitalization or required specific treatment such as blood transfusion or antibiotics.

Results

The clinical, hemodynamic, and pathologic findings on the six patients who were treated are summarized in Table 1. Clinical and hemodynamic improvement occurred after each angioplasty; however, multiple dilatations were required in each patient (average, 3.2; range, 2–5) because of restenosis at the angioplasty site and the presence of ongoing hepatocellular congestion and necrosis shown by percutaneous biopsy. Only patient 4, who is free of symptoms 84 months after his last angioplasty, is considered cured. Long-term

TABLE 1: Summary Data of Patients with Budd-Chiari Syndrome Included in This Study

Patient Number	Age (yr)	Sex	Associated Condition	Site of PTA	Type of Lesion	PTA Dates	Pressure Gradient Before/After (mm Hg)	Months FU Since Last PTA	Condition on last FU		Anticoagulation
									Vessel	Clinical	
1[a]	37	F	PRV	IVC	Stenosis	Nov. '85	17/5	25	Restenosed	Improved	None
						Feb. '86	23/5				
						Feb. '87	17/10				
2[b]	22	F	Postpartum	IVC	Stenosis	Feb. '85	17/4	29	Occluded	Improved	None
						Feb. '85[c]	8/2				
						Sept. '85	14/3				
						Feb. '86	30/6				
						May '86	17/4				
3	31	M	Abdominal trauma	IVC	1 cm occlusion	Jan. '86	29/7	23	Occluded	Improved	Coumadin
						Mar. '86	15/6				
						June '86	25/12				
						Aug. '86	18/8				
4	50	M	None	RHV	Web	Sept. '80	24/0	84	Patent	Cured	Coumadin
						Dec. '80	23/6				
						Aug. '81	?				
5[d]	30	M	None	2 RHVs	Stenosis	Feb. '85	28/15 and 27/15	36	Patent	Gastrointestinal bleeding due to portal hypertension	None
						Aug. '85	16/4 and 20/7				
6[e]	24	M	PRV	Mesoatrial shunt	Stenosis of proximal shunt anastomosis	Aug. '88	28/4	6	Patent	Improved	None
						Feb. '89	?/11				

Note.—PTA = percutaneous transluminal angioplasty, FU = follow-up, PRV = polycythemia rubra vera, IVC = inferior vena cava, RHV = right hepatic vein, ? = information unknown.

[a] Mesoatrial shunt, Sept. '84; meso–left renal vein shunt, June '85.

[b] Mesoatrial shunt, Sept. '82; portocaval shunt, Feb. '83.

[c] Four days after first PTA.

[d] Awaiting liver transplant.

[e] Coronary vein embolized through shunt, Sept. '85.

benefit was seen in four patients. This occurred despite ultimate caval occlusion in patients 2 and 3 and restenosis in patient 1. Patient 5, who was almost free of symptoms for 36 months, had recurrent gastrointestinal bleeding from esophageal varices and is now awaiting liver transplantation.

Discussion

Focal areas of stenosis affecting the hepatic veins or IVC have been reported in 60–80% of Orientals with Budd-Chiari syndrome but in fewer than 5% of non-Oriental patients. In the non-Oriental population, surgical efforts are mainly directed at decompressing the obstructed sinusoids, which is achieved by using the portal vein as the venous outflow tract of the liver. Surgeons prefer to perform a portosystemic shunt below the diaphragm because it is technically easier, short in length, and has better patency than the longer mesoatrial shunt or other procedures that shunt blood above the diaphragm. The type of shunt performed depends on the condition of the IVC and the relative pressure gradients between the portal vein, IVC, and right atrium. High caval pressures preclude successful shunting below the diaphragm. Percutaneous transluminal angioplasty was used to prolong the effectiveness of portosystemic shunts in patients 1, 2, and 6. This differs from our remaining patients and those reported by others [4–20], in whom the angioplasty was the only interventional procedure performed. In all of our cases and those reported in the literature, balloon angioplasty successfully enlarged the hepatic vein or IVC lumens, resulting in initial physiologic and symptomatic improvement. Restenosis was the rule rather than the exception in these patients. An average of 3.2 percutaneous transluminal angioplasties (range, 2–5) were required in the patients we treated. Twenty-three additional patients with Budd-Chiari syndrome treated by percutaneous transluminal angioplasty have been reported in the literature. They required an average of 1.7 percutaneous transluminal angioplasties each. It is likely that this average would be higher if longer follow-up were available, as was true of patient 4 in our series, who was originally reported by Meier et al. [3] in 1983 and returned for his third percutaneous transluminal angioplasty after publication of their report.

The efficacy of any therapy for Budd-Chiari syndrome is measured by its ability to stop hepatocyte necrosis, which will continue to occur if hepatic venous outflow obstruction is too great. Ultimately, liver biopsy is the only test sensitive enough to determine whether the disease has been arrested [21]. We think that it is very important to monitor patients with Budd-Chiari syndrome by serial biopsies and to use the results to direct therapeutic efforts. Patients 1, 2, and 3 remain clinically and histologically improved despite caval restenosis. The temporary luminal improvement due to percutaneous transluminal angiography may be sufficient to prevent further hepatocellular damage until collateral venous outflow channels have developed to decompress the liver or IVC.

Although balloon angioplasty can be considered an effective treatment, it may not be the best percutaneous therapy. The percutaneous transluminal angioplasty itself most likely contributes to the high rate of restenosis. It is well established that the cellular response after intimal and medial disruption causes further degeneration and a stenotic response. This mechanism in a patient who is already hypercoagulable predisposes the vessel toward reocclusion. Factors responsible for restenosis also include the fibrotic nature of the obstructing bands and external compression by swollen or regenerating hepatic tissue. Shioyama et al. [20] recently used a percutaneous atherectomy catheter successfully to treat a patient with restenosis of the IVC after balloon angioplasty. They report no evidence of restenoses at 6-month follow-up. Spiral spring prostheses have been surgically implanted in patients with Budd-Chiari syndrome to maintain IVC patency [22, 23]. Thus far, no cases of percutaneous insertion of stents in patients with Budd-Chiari syndrome have been reported; however, balloon expandable and self-expanding metallic stents will most certainly be used in these patients in the near future. Laser energy was used by Furui et al. [7] to recanalize the IVC in three patients. The lumina of these patients had to be enlarged by balloon angioplasty; however, future improvements in laser design and directability may permit ablation of webs and diaphragms without the need for supplementary balloon angioplasty.

In conclusion, percutaneous transluminal angioplasty is a safe and effective treatment for some patients with Budd-Chiari syndrome. It is unlikely to be a definitive therapy, but it can be useful in moderating the severity of the disease until collateral venous pathways develop to decompress hepatic congestion. Multiple treatments most likely will be required during the long-term care of these patients. We think that the liver biopsy is the only test that is sensitive enough to determine whether the disease has been arrested and that biopsy should be performed to determine whether further treatment is necessary.

ACKNOWLEDGMENTS

We thank Dana Hall and Thadeus Gardocki for their assistance in the preparation of this manuscript.

REFERENCES

1. Gall EA, Mostofi FK, eds. *The liver*. The International Academy of Pathology Monograph, no. 13. Baltimore: Williams & Wilkins **1973**:406–430
2. Parker RGF. Occlusion of the hepatic veins in man. *Medicine* **1959**;38: 369–402
3. Meier WL, Waller RM III, Sones PJ Jr. Budd-Chiari web treated by percutaneous transluminal angioplasty. *AJR* **1981**;137:1257–1258
4. Yamada R, Sato M, Kawabata M, Nakatsuka H, Nakamura K, Kobayashi N. Segmental obstruction of the hepatic inferior vena cava treated with transluminal angioplasty. *Radiology* **1983**;149:91–96
5. Sparano J, Chang J, Trasi S, Bonanno C. Treatment of the Budd-Chiari syndrome with percutaneous transluminal angioplasty: case report and review of the literature. *Am J Med* **1987**;82:821–828
6. Lois JF, Hartzman S, McGlade CT, et al. Budd-Chiari syndrome: treatment with percutaneous transhepatic recanalization and dilation. *Radiology* **1989**;170:791–793
7. Furui S, Yamauchi T, Ohtomo K, Tsuchiya K, Makita K, Takenaka E. Hepatic vena cava obstructions: clinical results of treatment with percutaneous transluminal laser-assisted angioplasty. *Radiology* **1988**;166: 673–677
8. Hosie KB, Bolia A, Watkin DFL. Treatment of Budd-Chiari syndrome by percutaneous transluminal angioplasty. *Lancet* **1988**;2:158–159
9. Ida M, Arai K, Yoshikawa J, et al. Therapeutic hepatic vein angioplasty for Budd-Chiari syndrome. *Cardiovasc Intervent Radiol* **1986**;9:187–190
10. Grippon P, Duche M, Aboulker C, Tubiana J-M, Levy V-G. Syndrome de Budd-Chiari et obstruction membraneuse de la veine cave inferieure sus-hepatique: traitement par angioplastie intra-luminale percutanée. *Gastroenterol Clin Biol* **1985**;9:70–74
11. Swada S, Oshima T, Kato T, Kubota Y, Tanaka Y. Budd-Chiari syndrome treated by percutaneous transluminal angioplasty: report of a case. *Acta Radiol [Diagn]* (Stockh) **1985**;26:25–27
12. Eguchi S, Takeuchi Y, Asano K. Successful balloon membranotomy for obstruction of the inferior vena cava. *Surgery* **1974**;76:837–840
13. Yamada R, Tsumura M, Itami K. Non-surgically treated long segmental obstruction of the hepatic inferior vena cava by means of transluminal angioplasty using a Gruntzig balloon catheter. *Nippon Igaku Hoshasen Gakkai Zasshi* **1981**;41:101–107
14. Case records of the Massachusetts General Hospital. *N Engl J Med* **1982**;307:236–242
15. Nishikawa M, Miyoshi S, Imai Y, et al. Treatment of the Budd-Chiari syndrome in polycythemia vera by repeated percutaneous transluminal angioplasty of a hepatic vein stenosis. *Postgrad Med J* **1982**;58:511–514
16. Taguchi M. A case of Budd-Chiari syndrome treated by percutaneous transluminal angioplasty. *Rinsho Hoshasen* **1983**;28:615–617
17. Jeans WD, Bourne JT, Read AE. Treatment of hepatic vein and inferior vena caval obstruction by balloon dilatation. *Br J Radiol* **1983**;56:687–689
18. Bar-Meir S, Rubinstein S, Miller H, et al. Failure of balloon membranotomy of the inferior vena cava. *Isr J Med Sci* **1984**;20:618–621
19. Uflacker R, Francisconi C, Rodriquez M, Amaral M. Percutaneous transluminal angioplasty of the hepatic veins for treatment of Budd-Chiari syndrome. *Radiology* **1984**;153:641–642
20. Shioyama Y, Satoh M, Tanaka H, et al. A case report of Budd-Chiari syndrome treated with PTA: usefulness of peripheral atherectomy catheter. *Nippon Igaku Hoshasen Gakkai Zasshi* **1988**;48:154–160
21. Millikan WJ Jr, Henderson JM, Sewell CW, et al. Approach to the spectrum of Budd-Chiari syndrome: which patients require portal decompression? *Am J Surg* **1985**;149:167–176
22. Bransky G, Ernest C, Jenni R, Zollikofer C, Burger HR, Senning A. Treatment of Budd-Chiari syndrome by dorsocranial liver resection and direct hepatoatrial anastomosis. *J Hepatol* **1986**;2:101–112
23. Maass D, Zollikofer Ch L, Largiader F, Senning A. Radiological follow-up of transluminally inserted vascular endoprostheses: an experimental study using expanding spirals. *Radiology* **1984**;152:659–663

CT of the Abdomen After the Whipple Procedure: Value in Depicting Postoperative Anatomy, Surgical Complications, and Tumor Recurrence

Robert J. Coombs[1]
Jacob Zeiss[1]
John M. Howard[2]
Neil R. Thomford[2]
Hollis W. Merrick[2]

We performed a retrospective study of CT scans in 29 patients who had undergone the Whipple procedure (radical pancreaticoduodenectomy) to study the CT appearance of the postsurgical anatomy and assess the use of CT in the evaluation of early postoperative complications and recurrent tumor. In the postoperative period, the scans from 15 patients revealed seven transient fluid collections; four deep abscesses, three of which were successfully drained under CT guidance; three superficial abscesses; and five cases of ascites. In 19 patients, CT scans were obtained up to 4 years after surgery to search for recurrent tumor. The most frequent site of recurrence was the liver. CT correctly identified liver metastases in six of seven patients and was falsely positive in one. Recurrence also was found twice in retroperitoneal lymph nodes; one time each in the mesenteric root, spleen, and lung base; and twice causing afferent loop blockage. Surgical proof of recurrence was obtained in eight cases.

Our experience suggests that an understanding of the normal postoperative anatomy following the Whipple procedure is essential in evaluating postoperative CT scans. Scans obtained for detection of tumor recurrence should be optimized for imaging the liver because this was the most frequent site of recurrence.

***AJR* 154:1011–1014, May 1990**

The Whipple procedure is performed for the treatment of malignancy of the pancreatic head, duodenum, ampulla of Vater, and occasionally for chronic pancreatitis or trauma. The purpose of this article is to describe the postoperative CT anatomy of the upper abdomen after the Whipple procedure and to investigate the efficacy of CT evaluation for detection of postoperative complications and recurrent tumor.

The Whipple procedure consists of radical resection of the pancreatic head, duodenum, gastric antrum, and usually a short segment of proximal jejunum [1, 2]. In order to restore the continuity of the gastrointestinal tract, a series of anastomoses to the jejunum must be performed, namely, pancreaticojejunostomy, choledochojejunostomy, and gastrojejunostomy. The sequence of the anastomoses and the placement of the anastomotic loop in either a retrocolic or antecolic position vary depending on the clinical situation and the surgeon's preference. Cholecystectomy also may be performed.

Materials and Methods

Ninety CT scans were obtained in 29 patients in whom a Whipple procedure had been performed. The patients included 14 men and 15 women 27–83 years old (mean age, 59 years). All patients undergoing the Whipple procedure and having subsequent CT scans at our institution between 1985 and 1989 were included. Of the 29 patients, 16 underwent surgery for adenocarcinoma of the head of the pancreas; three for adenocarcinoma of the papilla of Vater; three for chronic pancreatitis; two for cholangiocarcinoma; two for nonampullary duodenal carcinoma; and one each for malignant carcinoid of the pancreatic head,

Received October 16, 1989; accepted after revision January 8, 1990.

[1] Department of Radiology, Medical College of Ohio, P.O. Box 10008, Toledo, OH 43699. Address reprint requests to R. J. Coombs.

[2] Department of Surgery, Medical College of Ohio, Toledo, OH 43699.

0361–803X/90/1545–1011
© American Roentgen Ray Society

melanoma in the distal common bile duct, and blunt trauma of the right upper quadrant.

In 15 patients, 35 CT scans were obtained prior to discharge to detect postoperative complications. In 19 patients, 53 CT scans were obtained after discharge and up to 4 years after surgery to evaluate for evidence of recurrent tumor. Seven patients were included in both groups. Two additional patients who underwent surgery for chronic pancreatitis and received one scan each after discharge were included as examples of normal anatomy.

The scans were interpreted independently by two radiologists; a consensus of opinion was obtained if there were any disagreements. Findings specifically recorded included the presence of contrast material in the afferent loop; the presence of abscesses, ascites, or bile duct obstruction; as well as the presence of recurrent tumor in the pancreatic bed, liver, retroperitoneal lymph nodes, or other locations. The accuracy of these interpretations was determined by comparing them to the officially recorded interpretations and by reviewing the patients' subsequent clinical course and biopsy, surgical, or autopsy findings.

CT scanning was performed on GE 8800 and 9800 Quick scanners. Scans were routinely obtained first through the liver at 20-mm intervals (10-mm slice thickness) without contrast material, and then enhanced scans were obtained from the diaphragm to the iliac crest at 10-mm intervals (10-mm slice thickness). Often, additional 5-mm cuts were obtained through the pancreatic region. Oral contrast material was given routinely. Our contrast protocol calls for the injection of 150 ml of iohexol (Omnipaque 300, Winthrop-Breon, New York, NY) via power injector at a rate of 0.4 ml/sec, with scanning beginning at the diaphragm after the first 50 ml have been injected. Scans were most commonly obtained with a 3-sec scanning time and an 18-sec interscan delay.

Results

Normal Anatomy

Because the pancreatic head, duodenum, and gastric antrum have been resected, these structures are absent on CT scans obtained through the upper abdomen. Air in the biliary tree is a common finding after choledochojejunostomy and was present on at least one scan in 16 of 29 patients. The afferent loop can be positively identified in the right upper quadrant when it is filled with oral contrast material (53% of our scans). With contrast material in the afferent loop, the gastrojejunostomy (Fig. 1A) and pancreaticojejunostomy (Fig. 1B) can be located. The origin of the portal vein at the junction of the superior mesenteric and splenic veins was clearly visible on scans of 16 of 29 patients. Because the head of the pancreas is no longer present, the superior mesenteric vein/portal vein junction lies to the right of the pancreatic remnant rather than posterior to it. On 88 of 90 scans, the retroperitoneum was seen sufficiently to evaluate retroperitoneal adenopathy; however, on 11 of 90 scans, the bed of the pancreatic head was obscured by artifacts from surgical clips and patient motion.

In three patients who had retrocolic anastomoses, additional jejunal loops migrated through the transverse mesocolon filling the porta hepatis and pancreatic bed (Fig. 1C). In three other patients with retrocolic anastomoses, the jejunal loop was tunneled to the right upper quadrant through the duodenal bed, posterior to the superior mesenteric vessels [2]. When this bowel segment is filled with oral contrast material, it may suggest that the duodenum has been retained (Fig. 2). When it is not filled, it may simulate adenopathy.

Five patients had an antecolic anastomosis. This can be identified on CT if the gastrojejunostomy is seen anterior to the splenic flexure and transverse colon (Fig. 3).

Postoperative Complications

Thirty-five CT scans in 15 patients were obtained prior to discharge for evaluation of postoperative complications. Abnormalities were present on the initial scan in 14 patients.

Seven patients had fluid collections in the pancreatic bed,

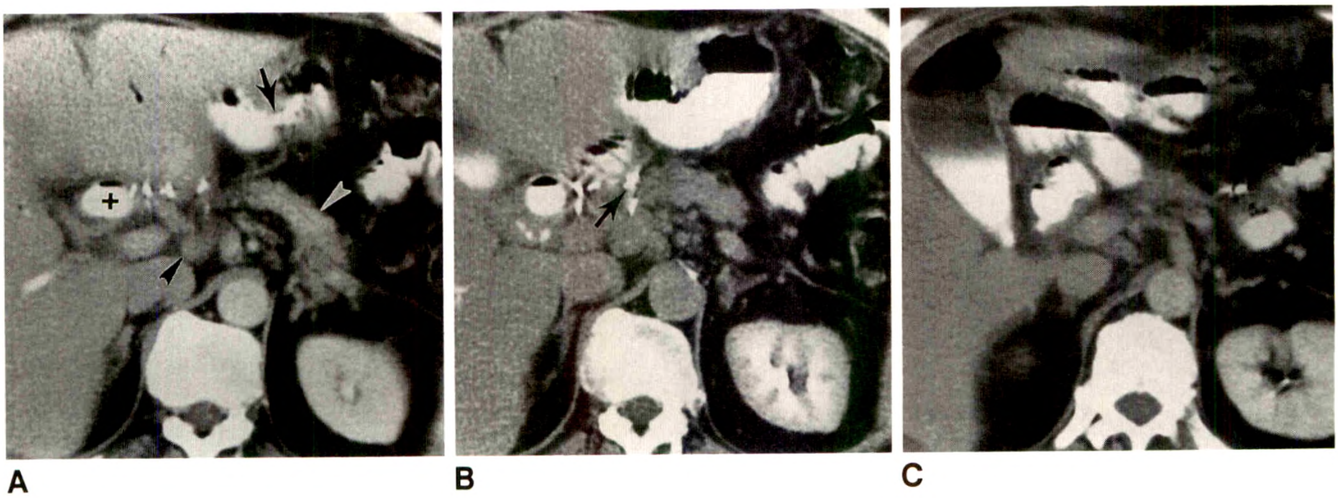

Fig. 1.—Normal anatomy after Whipple procedure.

A, CT scan shows gastrojejunostomy (*arrow*) and pancreatic remnant (*white arrowhead*). Oral contrast material in porta hepatis (+) identifies choledochojejunostomy. Equivocal-sized lymph node (*black arrowhead*) is present between superior mesenteric vein and inferior vena cava.

B, CT scan shows pancreaticojejunostomy (*arrow*).

C, CT scan shows multiple jejunal loops in right upper quadrant after retrocolic anastomosis. Oral contrast material has reached gallbladder.

Morrison pouch, or right paracolic gutter that resolved or improved without any specific intervention. Generalized ascites was found on CT scans in five patients. Three of these patients, all with malignant disease, died, two with multiple organ failure and one suddenly while awaiting discharge. Deep abscesses in four patients were identified and subsequently drained under CT guidance (Fig. 4). Three were drained successfully but the fourth patient died with sepsis. Superficial wound abscesses were identified in three additional patients and treated surgically. Four patients had two complications each.

Recurrent Tumor

Fifty-three CT scans obtained in 19 patients after discharge and up to 4 years after surgery were evaluated for recurrent tumor. CT evidence of recurrence was present in 12. The liver was the most common site of recurrence. CT was able to correctly identify liver metastases in six of seven cases in which they were present. Histologic proof was obtained at surgery in four of these cases. A hyperdense metastasis identified on CT in one patient could not be found at surgery and represents the only false-positive case.

By using 1.5 cm as the upper limit for normal-sized abdominal lymph nodes, only two patients were diagnosed with definite nodal recurrence. These two patients had nodes of 4.0 and 2.5 cm, respectively; disease in both was confirmed surgically (Fig. 5).

In two patients, surgically confirmed recurrent malignant neoplasm caused blockage of the afferent loop. The recurrence was not visualized directly on CT scans but was inferred in one patient by increasing dilatation of the intrahepatic bile ducts and in the other by dilatation of the bile ducts as well as dilatation of the afferent loop itself (Fig. 6).

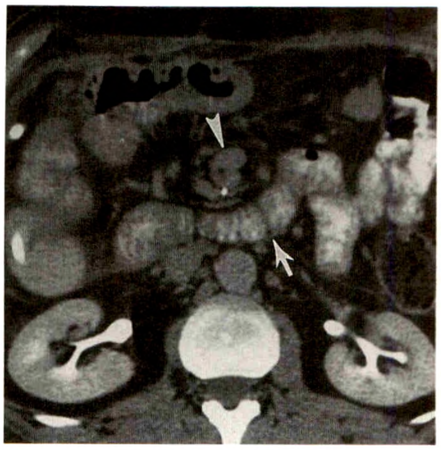

2

Fig. 2.—CT scan obtained after Whipple procedure in patient with retrocolic anastomosis. Jejunum is filled with contrast material (*arrow*) and can be seen behind superior mesenteric vessels (*arrowhead*). This appearance simulates normal duodenum.

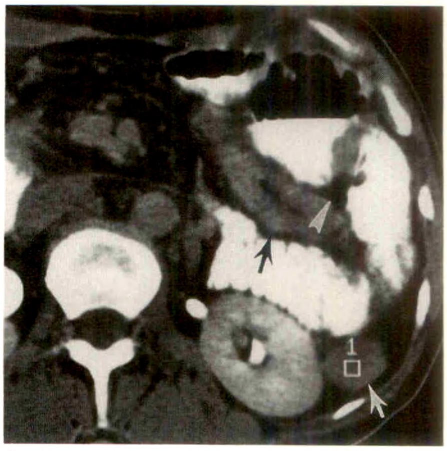

3

Fig. 3.—CT scan obtained after Whipple procedure in patient with anticolic anastomosis. Jejunum passes anterior to colon (*arrows*) at level of gastrojejunostomy (*arrowhead*).

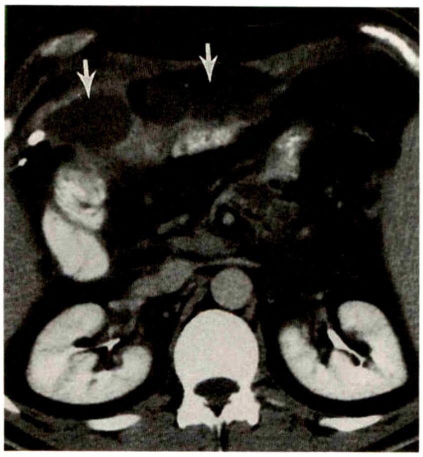

Fig. 4.—CT scan obtained 26 days after Whipple procedure shows two intraperitoneal abscesses (*arrows*) between anterior abdominal wall and contrast-filled afferent loop.

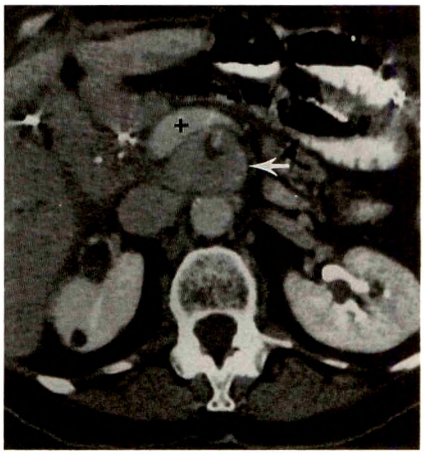

Fig. 5.—CT scan obtained 30 months after Whipple procedure shows recurrent tumor (*arrow*) in retroperitoneal lymph nodes. Primary tumor was malignant carcinoid in head of pancreas. Tumor has recurred at level of origin of portal vein (+). Superior mesenteric artery is surrounded by tumor.

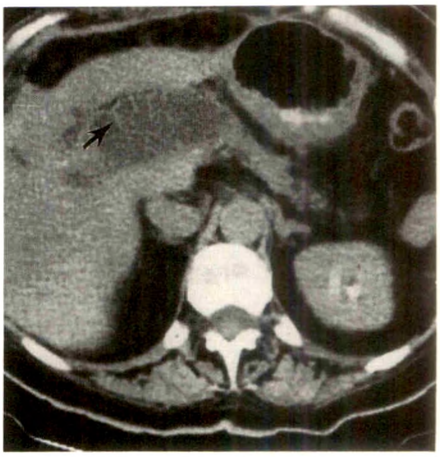

Fig. 6.—CT scan obtained 4 months after Whipple procedure in patient with recurrent jaundice. Dilatation of afferent loop is only CT manifestation of tumor recurrence. Disease obstructed jejunum between gastrojejunostomy and the other two anastomoses, causing afferent loop to distend with bile. Note valvulae conniventes (*arrow*) within jejunal lumen.

Other recurrences shown on CT scans include a metastasis to the left lung base found 4 years after surgery. Recurrence to the mesenteric root in one patient and to the spleen in another were found on CT and confirmed surgically. These two patients also had CT evidence of hepatic recurrence. At this time, seven patients have not yet been diagnosed as having recurrence. One patient was lost to follow-up after 1 year; however, the other six have been followed for an average period of 17 months.

Discussion

In order to evaluate a postoperative Whipple patient with CT scanning, an understanding of the normal postoperative anatomy is required. Anastomotic jejunal loops are present in the porta hepatis and bed of the pancreatic head. These loops can easily be mistaken for either abscesses or recurrence. This misinterpretation can best be avoided if the loops are filled with oral contrast material. The use of 1 mg of IV glucagon has been recommended to facilitate afferent loop filling [3]. Recognition of the afferent loop certainly is easier in the presence of oral contrast material, but even when it is not filled, the afferent loop can be identified by its valvulae conniventes. When the jejunum is brought into the right upper quadrant via a retrocolic approach, it is sometimes placed posterior to the superior mesenteric vessels, simulating the normal position of the duodenum. When it is not filled with contrast material, it may be mistaken for lymph-node metastases. Caution, therefore, is advised in diagnosing adenopathy if this variant of the procedure is used.

Scans obtained in the early postoperative period are unlikely to show recurrent tumor but may be indicated for evaluation of surgical complications. The clinical complications suspected in the early postoperative period are usually persistent fever or elevated serum bilirubin. In seven of 15 patients, early CT scans showed fluid collections in or around the pancreatic bed. Although these seven collections improved spontaneously, and therefore are believed to represent postoperative serum collections, their CT appearance was not altogether dissimilar to that of true abscesses. Percutaneous aspiration of these collections should be performed when the patient's clinical course suggests sepsis. Generalized ascites was present in five patients. In two, it appeared to be associated with multiple organ failure, including acute renal failure and respiratory distress syndrome. Deep abscesses were found in four patients, and CT-guided percutaneous drainage was used successfully in three of them [4, 5].

The most common site of recurrent malignant tumor identified on CT scans was the liver. Because of this, we think that scans obtained for long-term follow-up of pancreatic and duodenal cancer patients should accentuate evaluation of the liver. In this retrospective series, this was achieved by obtaining a combination of unenhanced and enhanced scans through the liver [6]. Hepatic lesions are delineated best when contrast material is given in a rapid bolus followed by incremental dynamic scanning through the liver [7, 8]. Scans obtained with dynamic enhancement of the liver will also deliver a large contrast bolus to the pancreatic bed and residual pancreas. It should be noted that the only scan that was falsely negative for hepatic disease was obtained without enhancement because of a patient history of contrast sensitivity. In patients who cannot receive contrast material, another hepatic imaging technique such as MR imaging should be used [9].

CT evaluation of tumor in retroperitoneal lymph nodes has always relied on arbitrary measurements of lymph-node size [10]. Nodes less than 1.0 cm are considered normal, whereas those between 1.0 and 1.5 cm are called equivocal. Only two patients studied had unequivocal CT evidence of lymph-node recurrence. In four other patients, nodes of equivocal size were encountered; however, the surgeons elected to follow these nodes with serial CT scans rather than subject the patients to biopsy or reexploration. At this time, none of these nodes has gotten larger nor has there been CT evidence of recurrence in other organs. If available, a preoperative CT scan can be used as a baseline for comparison of lymph-node size in the postoperative period. Because recurrence can occur rapidly in patients with pancreatic or duodenal malignant tumors, we think follow-up CT scans at 3- to 6-month intervals after surgery are justified.

ACKNOWLEDGMENTS

We thank Faye Keen and Randy Morris for photographs and manuscript preparation.

REFERENCES

1. Whipple AO, Parsons WB, Mullins CR. Treatment of carcinoma of the ampulla of Vater. *Ann Surg* **1935**;102:763–779
2. Howard JM, Jordan GL, Reber HA. *Surgical disease of the pancreas*. Philadelphia: Lea & Febiger, **1987**:670–682
3. Heiken JP, Balfe DM, Picus D, Scharp DW. Radical pancreatectomy: postoperative evaluation by CT. *Radiology* **1984**;153:211–215
4. Aeder MI, Wellman JL, Haaga JR, Hau T. Role of surgical and percutaneous drainage in the treatment of abdominal abscesses. *Arch Surg* **1983**;118: 273–280
5. Halasz NA, vanSonnenberg E. Drainage of intraabdominal abscesses: tactics and choices. *Am J Surg* **1983**;146:112–115
6. Moss AA, Schrumpf J, Schnyder P, Korobkin M, Shimshak RR. Computed tomography of focal hepatic lesions: a blind clinical evaluation of the effect of contrast enhancement. *Radiology* **1979**;131:427–430
7. Foley WD, Berland LL, Lawson TL, Smith DF, Thorsen MK. Contrast enhancement technique for dynamic hepatic computed tomographic scanning. *Radiology* **1983**;147:797–803
8. Foley WD. Dynamic hepatic CT. *Radiology* **1989**;170:617–622
9. Chezmar JL, Rumancik WM, Megibow AJ, Hulnick DH, Nelson RC, Bernardino ME. Liver and abdominal screening in patients with cancer: CT versus MR imaging. *Radiology* **1988**;168:43–47
10. Korobkin M. Computed tomography of the retroperitoneal vasculature and lymph nodes. *Semin Roentgenol* **1981**;16:251–267

Case Report

Hepatic Subcapsular Hematoma: An Unusual Complication of Biliary Lithotripsy

Frank P. McGrath,[1] Stephen H. Lee, Robert G. Gibney, and H. Joachim Burhenne

Biliary extracorporeal shock-wave lithotripsy (BESWL) is now widely available in North America and Europe and is becoming an increasingly common noninvasive means for treating symptomatic gallstones. To our knowledge, this is the first report of a hepatic subcapsular hematoma occurring after such treatment.

Case Report

Clinical and sonographic features of a large subcapsular hematoma of the liver developed in a 49-year-old man within 24 hr of extracorporeal shock-wave lithotripsy for symptomatic gallstones. Prelithotripsy coagulation factors were normal. The procedure was performed with a second-generation lithotripter (Lithostar Plus, Siemens, Erlangen, W. Germany). An intercostal approach [1] was used to target the shock-wave beam because of the retrocostal position of the gall bladder. Analgesia was required, and the patient was given IV fentanyl citrate 50 μg and diazepam 2.5 mg in addition to transcutaneous electrical nerve stimulation. After 770 shocks over a period of 15 min at 66% of the maximal focal pressure, the procedure was discontinued by the supervising radiologist because of development of excessive pain deep to the intercostal targeting window and increasing difficulty in visualizing the gallbladder. Findings on sonography of the liver were normal at this time.

Twenty-four hours later, the patient was admitted with acute pain in the right upper quadrant. Sonography revealed a 15 × 11 × 6 cm hepatic subcapsular collection (Fig. 1). The hemoglobin level had dropped from 160 to 140 g/l and an elevation in alkaline phosphatase (140 U/l), total bilirubin (40 μmol/l), and aspartate aminotransferase (201 U/l) levels occurred. The symptoms resolved during 3 days of conservative treatment, and the patient was discharged. Follow-up sonography 2 weeks and 2 months later showed organization and slight decrease in size of the hematoma. The patient remains well.

Discussion

Complications as a result of the energy/trauma of BESWL with the newer second-generation lithotripsy machines have been relatively minor [2–4]. The reported frequencies of these side effects vary [2, 4] and include biliary colic (33–54%), mild pancreatitis (1–2%), transient microscopic hematuria (3–5%), and skin petechiae (14–80%). To date, over 250 patients with symptomatic gallstones have been treated at our institution without significant side effects. Malone et al. [1] reported no adverse effects in 22 patients in whom the intercostal approach was used for targeting and shock-wave delivery.

A large perisplenic hematoma as a result of ESWL for urinary calculi has recently been reported by Lanctin et al. [5], who used the second-generation Siemens Lithostar. Left flank and shoulder tip pain developed in their patient some hours after an uneventful lithotripsy session. In retrospect, it was felt that the shoulder tip pain was an important diagnostic sign suggesting the development of this complication. The overriding feature in our patient was the excessive pain deep to the targeting site that developed early during BESWL, which persisted despite relocating the intercostal position of the shock-wave head. We are aware of one other case of subcapsular hematoma after BESWL with the second-generation Dornier HM-4 lithotripsy unit (L. Greiner, personal communication). This patient also had experienced severe

---

Received November 15, 1989; accepted December 14, 1989.

[1] All authors: Department of Radiology, University of British Columbia and Vancouver General Hospital, 855 W. 12th Ave., Vancouver, B.C. Canada V5Z 1M9. Address reprint requests to H.J. Burhenne.

AJR **154:1015–1016, May 1990** 0361–803X/90/1545–1015 © American Roentgen Ray Society

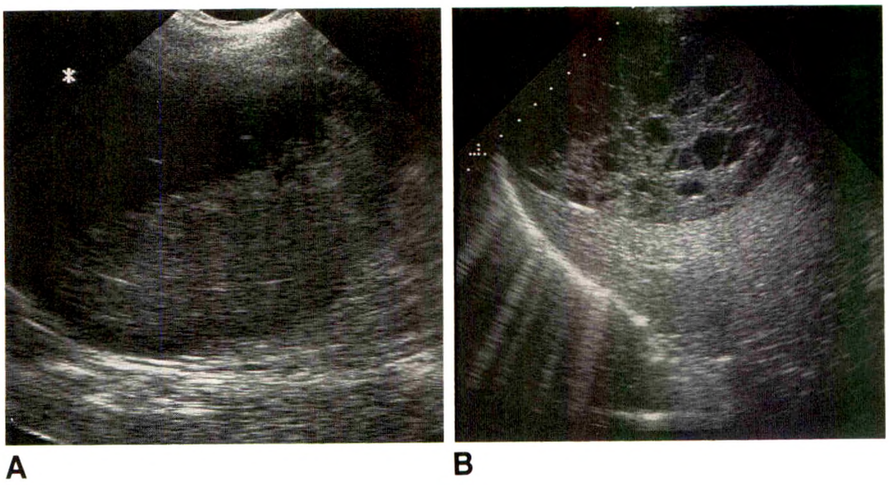

Fig. 1.—Sonograms through right lobe of liver. Sonogram obtained before biliary extracorporeal shock-wave lithotripsy (BESWL) was normal (*not shown*).

***A*, Sonogram obtained 24 hr after BESWL shows 15 × 11 × 6 cm subcapsular collection.**

***B*, Sonogram obtained 2 weeks later shows organization.**

deep pain during BESWL that had necessitated discontinuation of the treatment.

The severity of soft-tissue damage from ESWL is directly related to the mean pressure at the focal point of the shock waves, the total number of shock waves administered, and the frequency with which shock waves are administered [2, 6]. It is important to note that this complication developed after the first lithotripsy treatment and only 770 shock waves at 66% of the maximum focal pressure had been given. (Most of our first-time BESWL patients receive more than 2000 shock waves at 70% of maximum focal pressure.)

It is therefore of the utmost importance to have a supervising physician in attendance at all times during treatment, both to ensure accurate targeting and to monitor the patient's response in an attempt to recognize any early signs that may indicate the development of a complication.

Since preparing this manuscript, we have become aware of a case of fatal retroperitoneal hemorrhage that occurred after renal lithotripsy with a Dornier machine [7].

REFERENCES

1. Malone DE, Rawat B, Fache JS, Quenville NF, Burhenne HJ. The intercostal pathway for biliary extracorporeal shockwave lithotripsy. *Radiology* **1990**;174:349–351
2. Sackmann M, Delius M, Sauerbruch T, et al. Shock-wave lithotripsy of gallbladder stones: the first 175 patients. *N Engl J Med* **1988**;318:393–397
3. Malone DE, Becker CD, Reich KD, Quenville NF, Burhenne HJ. Soft-tissue effects of biliary extracorporeal shockwave lithotripsy in swine. *Br J Radiol* **1989**;62:843–848
4. Rawat B, Fache JS, Malone DE, Burhenne HJ. Biliary lithotripsy without oral chemolitholysis: the Vancouver experience. In: Burhenne HJ, Paumgartner G, Ferrucci JT (eds.). *Biliary lithotripsy*, vol. 2. Chicago: Year Book Medical, **1990**
5. Lanctin HP, Futter NG, McKay DE, Herringer R, Faucher R. Splenic injury with extracorporeal shock wave lithotripsy: case report. *Lithotripsy Stone Dis* **1989**;1:308–310
6. Sauerbruch T, Delius M, Paumgartner G, et al. Fragmentation of gallstones by extracorporeal shock waves. *N Engl J Med* **1986**;314:818–822
7. Stoller ML, Litt L, Salazar RG. Severe hemorrhage after extracorporeal shock-wave lithotripsy. *Ann Intern Med* **1989**;111:612–613

Adult Ankle Fractures: Comparison of Plain Films and Interactive Two- and Three-Dimensional CT Scans

Donna Magid[1,2]
James D. Michelson[2]
Derek R. Ney[1]
Elliot K. Fishman[1]

Thirteen patients with 15 ankle fractures potentially requiring surgical reduction according to plain film criteria were studied with transaxial CT, from which static and animated interactive two-dimensional (2-D) images and animated volumetric three-dimensional (3-D) images were generated. CT criteria believed to parallel well-accepted plain film criteria for triage of ankle fractures were developed and applied. The tibiofibular, talofibular, and tibiotalar articulations were characterized and, where possible (nine cases), compared with the (presumably normal) contralateral ankle. Talocrural angle measurements were made on interactive coronal measurements and compared with standard plain film measurements. Fracture fragment displacement, rotation, and impaction were noted. Posterior tibial lip disruption was quantified. Information derived from the 2-D/3-D CT study led to cancellation of proposed surgery in three of the distal fibular fractures and in two distal tibial fractures. There was far less variation than anticipated between the talocrural angles of the injured and normal ankles, and both injured and normal ankles deviated significantly from the accepted standard of 84°. Displacement at the level of the fibular fracture was a poor predictor of more distal disruption.

Two-dimensional CT was found to provide anatomic detail and information superior to either plain film or 3-D CT; 3-D CT was preferred by the surgeons for final surgical planning and for integration of the 2-D data. CT altered management in five of the 13 patients studied, supporting our belief that 2-D/3-D CT can be of significant value in assessing ankle fractures.

***AJR* 154:1017–1023, May 1990**

The extent and severity of ankle fractures, like fractures elsewhere in the body, may be underestimated by conventional radiographs. In the traumatized ankle, equal consideration is given to the integrity of the articulating tibia, talus, and fibula, and to the maintenance of the normal mortise and joint space they define. Transaxial CT gives better bone and soft-tissue detail than plain films do. However, in the ankle, the primary weight-bearing structures—the tibial plafond, the superior mortise, and the talar dome—are essentially horizontally oriented and may be incompletely assessed by transaxial CT alone. We developed an integrated interactive Orthotool workstation (HipGraphics Inc, Baltimore, MD) [1] that allows us to review transaxial images in conjunction with coronal and sagittal reformatted images. These two-dimensional (2-D) image series are combined with animated volumetric simulated three-dimensional (3-D) images when surgery is anticipated or planned. Since all commercially available CT scanners now offer coronal and sagittal reformatting, at least part of our approach could be used on any CT scanner, if clinically warranted.

Subjects and Methods

Thirteen adult patients 18–64 years old who were potential surgical candidates for treatment of known or suspected displaced ankle fractures were studied with conventional

Received September 27, 1989; accepted after revision December 26, 1989.

Presented at the annual meeting of the American Roentgen Ray Society, New Orleans, May 1989.

[1] Russell H. Morgan Department of Radiology and Radiological Science, The Johns Hopkins Medical Institutions, Baltimore, MD 21208. Address reprint requests to D. Magid.

[2] Department of Orthopaedic Surgery, The Johns Hopkins Medical Institutions, Baltimore, MD 21208.

0361–803X/90/1545–1017
© American Roentgen Ray Society

radiographs (anteroposterior, lateral, mortise views), transaxial CT, static multiplanar reformatted coronal and sagittal images, and animated integrated Orthotool 2-D and 3-D image rendering. Patients were admitted to the study after an initial plain film was obtained and interpreted independently by one radiologist and one orthopedic surgeon, the latter of whom generated a tentative treatment plan. The findings on the plain films were graded by using Lauge-Hansen class fixation guidelines [2], with quantification of talar shift, talocrural angle, and fibular displacement.

A CT study was then obtained for each patient following the established protocol: field of view to encompass both ankles, in anatomic position; 125 kVp; 280 mAs; 3 sec; and 4-mm collimation at 3-mm intervals. CT scans were obtained on a Siemens Somatom DRH or DR3 unit (Siemens Medical Systems, Iselin, NJ). Conventional static coronal and sagittal reconstructions were generated by using the multiplanar reconstruction and display (MPR/D) software, as has been previously described [3]. The average ankle study required 35–50 transaxial slices (varying with patient height and cephalocaudal extent of fractures) and generated similar numbers of coronal and sagittal static images, which were displayed as 2:1, 4:1, or 6:1 hard-copy sequences.

Transaxial CT data were transferred via ½-in. magnetic tape to a Sun 3/180 or Sun 3/280 workstation (Sun Microsystems, Mountain View, CA), which provided the operator interaction interface with a PIXAR Image Computer (PIXAR, Inc., San Rafael, CA). This Sun/PIXAR computer system has been described [1, 4, 5]. The PIXAR is a high-speed parallel architecture computer system with large (24 megabyte) image memory, high-resolution (1024 × 768) color display, and four parallel bit-section processors processing up to 40 million instructions per second. We used the 2-D/3-D Orthotool software to generate animated interactive 2-D and 3-D image series.

Once the transaxial CT sections were transferred, a z axis (cephalocaudal) bicubic interpolation algorithm was used to produce cubic voxels (x = y = z). This procedure takes less than 10 sec. This interpolated data set is used for subsequent 2-D and 3-D image rendering. The Orthotool software accepts up to 192 contiguous CT sections (vs 49 for the standard MPR/D program) and preserves the entire data set (full field of view vs 127 × 127 matrix, or approximately one-quarter of the field of view). The original and reformatted CT images are stored as a volume in the frame buffer, permitting real-time display in any plane. The Orthotool display screen presents the three orthogonal planar series (transaxial, coronal, and sagittal) simultaneously, with three reference 3-D images representing patient orientation for each corresponding planar series. Each 2-D image has two "cross-haired" axes that indicate the level from which concurrently displayed orthogonal images are selected (the transaxial image shows one reference axis for the displayed coronal image and one for the displayed sagittal image; the coronal image has one transaxial and one sagittal reference axis, and so on). The standard display can be rotated and regenerated to get three new image sets orthogonal to any desired oblique section within 10 sec. As the primary structures of interest in the ankle are approximately parallel or perpendicular to the standard transaxial plane, this option was not routinely exercised once review of three cases demonstrated that little additional information was gained. Images were archived on ¾-in. videotape.

A score sheet was generated for the Orthotool image sequences. Landmarks, measurements, and observations were respectively consensually chosen, performed, and made by one radiologist and one orthopedic surgeon at the Orthotool workstation screen. Parameters were recorded for the traumatized and for the contralateral, allegedly normal, ankle.

The distal fibula and tibiofibular space were assessed for width, contour, and deviation from the contralateral side on the first transaxial image cephalad to the cortical tibial plafond that appeared to be showing all central cancellous bone rather than partial-volumed cortical articular bone; this was four to six interpolated images proximal to the reference plafond slice depending on patient height. The talofibular space was assessed in a similar manner on the first transaxial image clearly distal to the talar dome cortex, usually six interpolated images distal to the selected reference dome cortex slice. At these two measurement levels, the distal fibula was assessed for rotation, lateral displacement, and posterior displacement as judged by alterations in the tibiofibular and fibulotalar relationships and in comparison with the normal side. Review of the coronal images confirmed the presence or absence of impaction; the coronal and sagittal image series confirmed the degree of angulation at the fracture site, where present.

The talocrural angle was measured via coronal image landmarks believed to duplicate the plain film measurement landmarks: the perpendicular to a line drawn through the articular central plafond was established with the Orthotool Measurement/Angle option. Points at the most distal tips of the medial and lateral malleoli were chosen after reviewing the coronal series in real time and were connected. The superolateral angle formed by this line and the original perpendicular is the talocrural angle [6], which was measured three times on each side with consensual landmarks chosen "from scratch" for each of the three measurements.

The distal tibia and posterior tibial lip were assessed for percentage of articular surface involvement, fracture fragment distraction, and impaction or displacement creating an articular step-off or discontinuity. Fracture lines, distraction, and percentage of involvement were reviewed and measured on transaxial and sagittal images primarily; articular congruity and continuity were reviewed on the coronal and sagittal series.

The interpolated data set was then edited, where necessary, to remove cast material and (where desired) the normal ankle before 3-D reconstruction. This has been described in detail elsewhere [4, 5]. We generated two series of animated rotating simulated 3-D views: one around the spinning or spinal axis and one in a somersaulting direction. It was consensually noted whether these views added any information not available on the 2-D study or whether they altered the proposed surgical management.

Results

In 13 patients with ankle trauma there were nine distal fibular fractures (Figs. 1 and 2), two medial malleolar fractures (Fig. 3), one posterior tibial lip fracture (Fig. 4), two pylon fractures (Fig. 5), and one talar dome fracture. All patients had plain films and/or clinical findings suggesting a displaced fracture potentially requiring surgical repair; the average plain film displacement of the fibula at the level of the fracture was 3 mm laterally and 3 mm posteriorly. CT findings revealed far less displacement, with the distal talofibular articulation often normal even with minor alterations in the more proximal tibiofibular articulation. Similarly, mild apparent fibular rotation on transaxial CT images (wedge-shaped opening of the normally symmetric articulation, rotation of the triangular cross-sectional appearance of the fibula) proximally was not associated with distal talofibular disruption (Fig. 2).

The average talocrural angle in the normal contralateral ankles was 77 ± 4° and averaged 1.9° (±1.9° SD) difference from the traumatized ankle even in those patients requiring surgery. CT and plain film measurements of the talocrural angle on average agreed to within 0.5° (±2.1° SD).

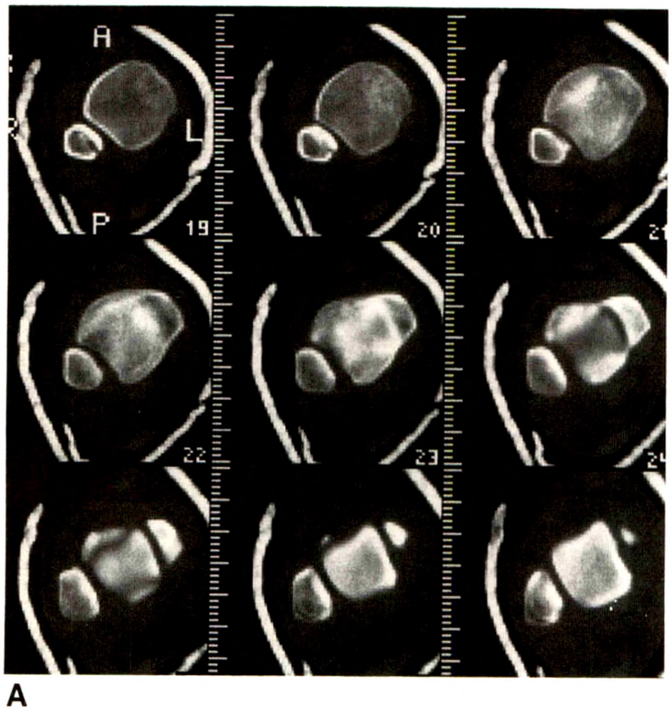

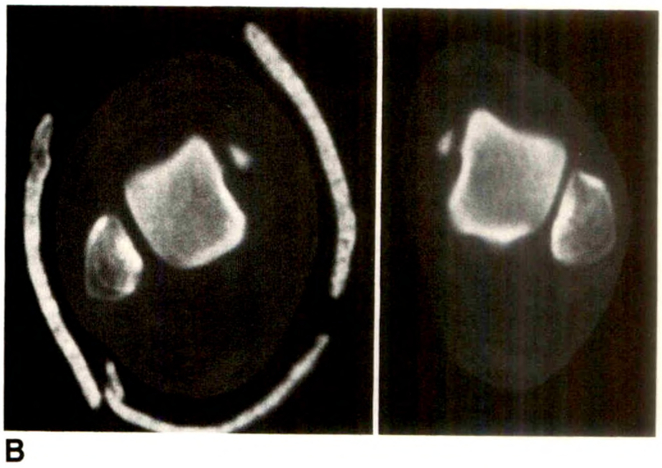

Fig. 1.—22-year-old man with acute oblique distal fibular fracture.

A, Sequential transaxial CT images characterize fibular articulations just proximal (tibiofibular, images 19 and 20) and distal (talofibular, images 26 and 27) to central ankle joint. Distal extent of fracture is seen on images 19–21.

B, Comparison with contralateral ankle at same level reinforces impression of talofibular joint integrity.

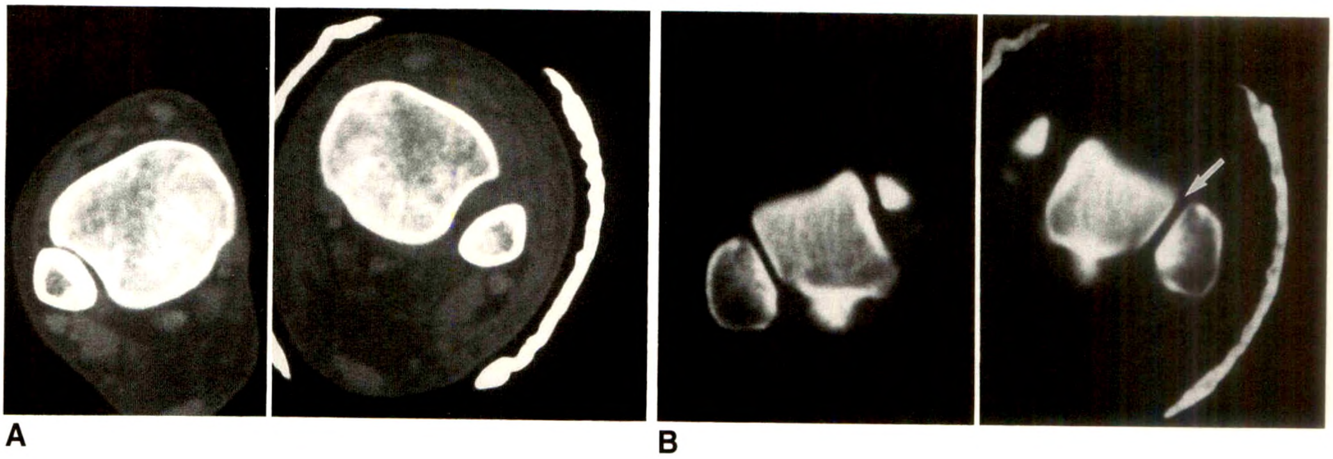

Fig. 2.—31-year-old man with acute oblique distal fibular fracture.

A, Symmetrically positioned transaxial CT images show marked widening of left tibiofibular space compared with nontraumatized right. There is subtle external rotation of left fibula at this level.

B, Transaxial CT image just distal to talar dome, while showing subtle left talofibular widening (*arrow*), shows less loss of integrity of distal fibular articulation than had been anticipated. Talocrural angle averaged 75° on left and 72.3° on right.

For tibial pylon and posterior lip fractures, 2-D CT was more accurate and detailed in determining percentage of surface involvement, displacement, distraction, or impaction of fracture fragments (Figs. 4 and 5). One unsuspected posterior tibial lip fracture was detected only with CT.

The 2-D/3-D CT studies led to cancellation or marked alteration of proposed surgery in three of the nine distal fibular fracture cases (Fig. 2), in one of the medial malleolar fracture cases, and in one of the two pylon fractures (Fig. 5). In one additional distal fibular fracture, surgery was called for in light of the CT findings but could not be performed because of other clinical problems.

Discussion

Determination of a treatment regimen for the acutely traumatized ankle depends on the assessment of the instability produced by the injury. The existence of either static or dynamic instability or of joint incongruity is a primary cause of long-term degenerative articular changes.

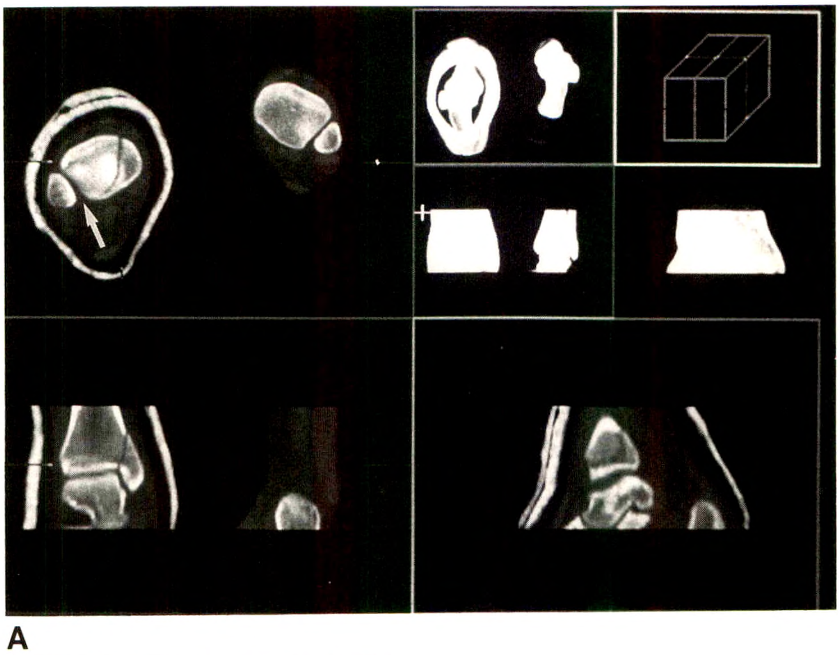

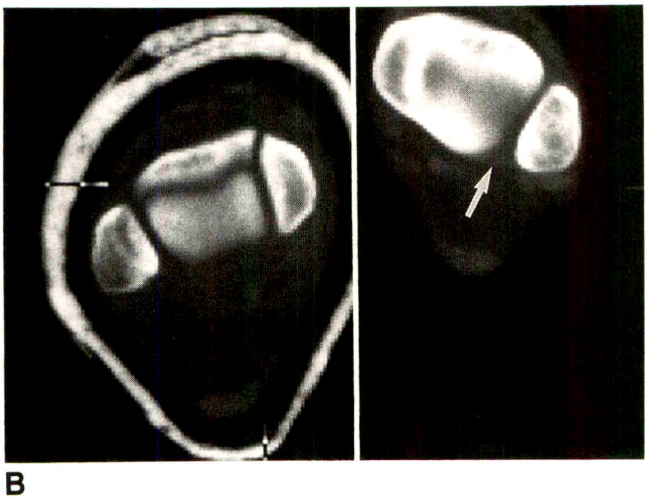

Fig. 3.—18-year-old man with acute nondisplaced medial malleolar fracture.

***A*, Orthotool CT image displays fracture in transaxial (top left), coronal (bottom left), and sagittal (bottom right) planes. Coronal and sagittal images confirmed preservation of articular surfaces and proximal extent of fracture.**

***B*, Comparison of nontraumatized left ankle on transaxial slice just proximal to tibial plafond (right) with traumatized right ankle at same level (*A*, top left) shows symmetry and integrity of tibiofibular space (*arrows*).**

If enough fibular fracture displacement occurs to create incongruity at the fibulotalar joint, surgical intervention is indicated. In part, this is a derivative of studies that have shown the key role of the lateral malleolus in maintaining stability of the ankle mortise [6–8]. It has been shown, for instance, that a lateral malleolar fracture that allows a 1-mm shift of the talus underneath the tibia leads to a 42% reduction in tibiotalar contact area [9]. This presumably would predispose the ankle to subsequent degeneration because of the higher contact pressures. However, in the absence of gross medial malleolar or deltoid ligament disruption, it is not clear that such dramatic alterations in contact area occur [10].

As the displacement of the distal fibula in ankle fractures involves rotation and axial shortening, as well as posterior displacement, plain radiographs do not completely visualize the fracture pathology nor the possible talofibular incongruity. In the absence of obvious tibiotalar instability, CT would be expected to allow more precise surgical decision making on the basis of its superior multiplanar representation of the fracture pattern.

On transaxial CT, the normal tibiofibular joint is defined by a concentric and regular relationship of the convex cortex of the fibula paralleling the slightly concave tibial cortex (Fig. 1). Fibular rotation would produce widening either anteriorly (external rotation) or posteriorly (internal rotation) and is best appreciated when an initial impression of anteroposterior asymmetry is confirmed by comparison with the nontraumatized (and it is hoped normal) contralateral ankle. Lateral or posterior fibular displacement also alters the contours of this space, and again, in subtle cases, can be confirmed in comparison with the normal ankle. With careful attention to patient positioning during the CT study, both ankles will be available and symmetrically presented on each 2-D image; even with positional asymmetry, however, the interactive nature of the

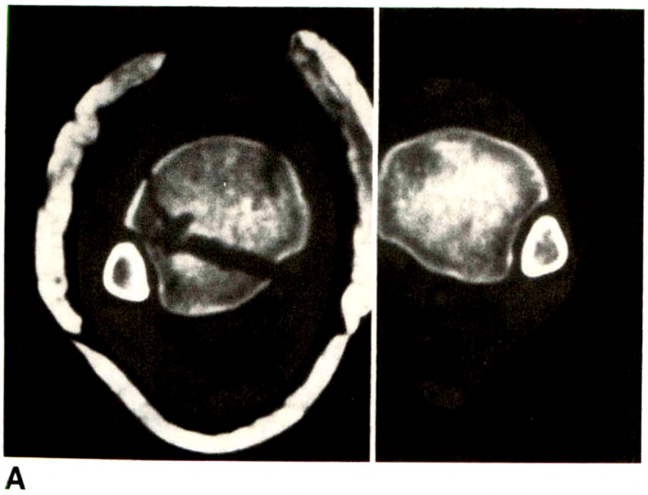

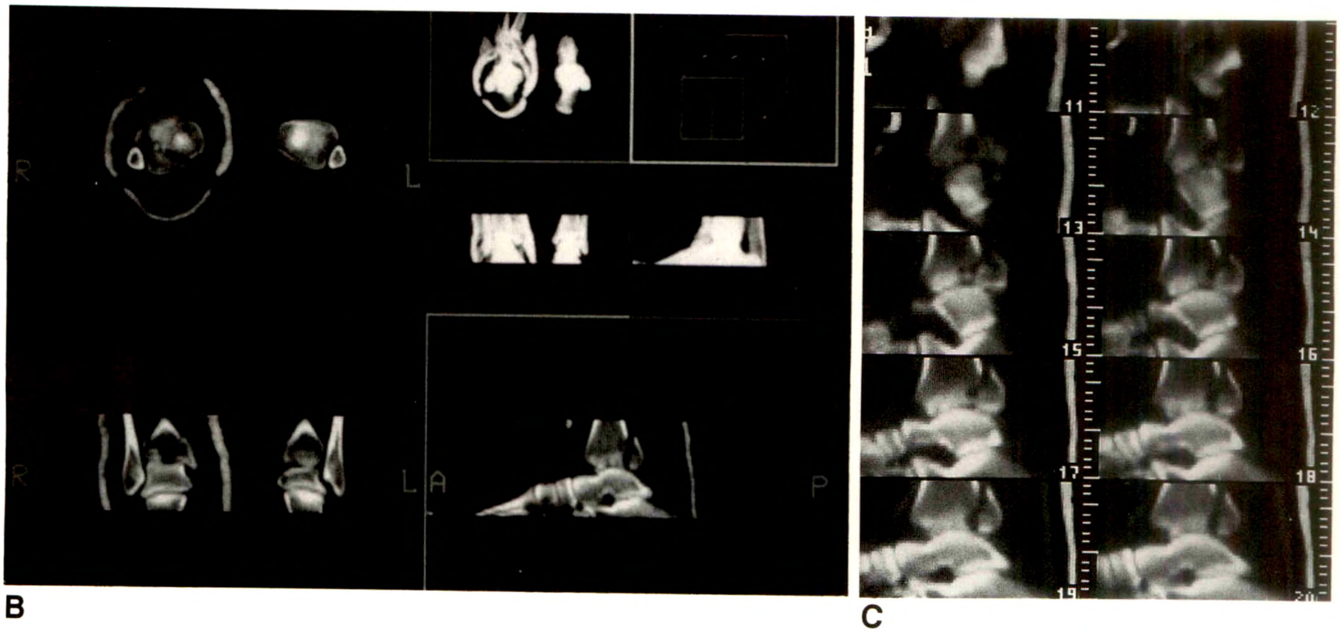

Fig. 4.—36-year-old man with acute pylon fracture and moderately comminuted right distal tibia.

A, Transaxial CT image shows posterolateral distraction of fragments. Comparison with normal left ankle confirms that fibula is not rotated.

B, Orthotool image displays right central plafond disruption on coronal plane (bottom left) and posterior tibial lip distraction on sagittal plane (bottom right).

C, Serial multiplanar reformatted sagittal images document posterior tibial surface involvement approximating 50% in lateral parasagittal sections (images 14–16): significant gap is due to distraction, which required surgical fixation.

Fig. 5.—25-year-old man with acute, markedly comminuted, impacted pylon fracture of distal articular tibia.

A, Multiplanar reformatted image displays stellate fragmentation and distraction on transaxial section just proximal to joint (left, in box); coronal (top right) and sagittal (bottom right) views show extensive loss of central articular surface, impaction of several large fragments, and proximal continuation of fracture lines into metadiaphyseal tibia. Coronal and sagittal images displayed are from levels marked by right and left (R and L) and anteroposterior (A and P) axes, respectively.

B, Animated volumetric 3-D image gives less articular surface detail from this perspective, but was used preoperatively to study fragment displacement while planning operative approach. From plain films, initial surgical plan had been to use open reduction and internal fixation, but extent of comminution seen on CT indicated that it would be preferable to use external fixation instead.

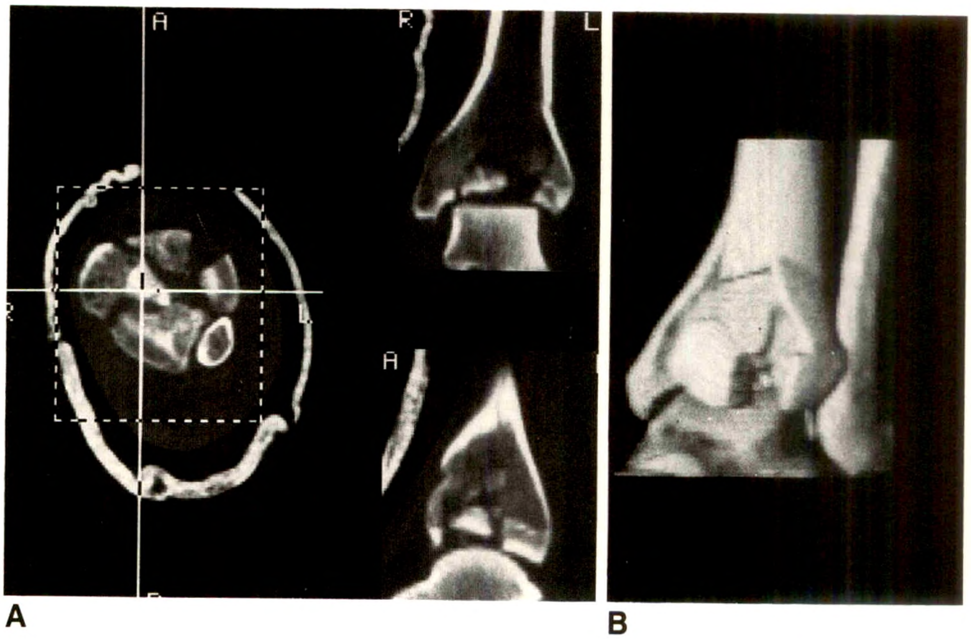

Orthotool system allows simple and rapid travel through the image stacks to allow the right and left ankles to be compared at the same level for each feature.

The coronal 2-D images confirm lateral displacement, both absolutely and relative to the contralateral fibula. The sagittal images confirm distal posterior displacement relative to the proximal fibular fragment, but are less useful in directly visualizing the altered tibiofibular relationship, because the sagittal plane does not allow the tibia and fibula to be seen together. We compared 2-D analysis of the distal fibula on the Orthotool to static multiplanar reformatted images because multiplanar reformatting of some kind is available on any commercial scanner whereas the Orthotool system has not yet become widely adopted. A static series of transaxial, coronal, and sagittal images would be more awkward to manipulate, involving many sheets of film, and would require additional operator and machine time to generate a 2-D series for the contralateral (normal) ankle. As performed at our institution with the MPR/D software, static 2-D images are at a slight disadvantage in terms of image quality, but are just as clinically useful for lateral malleolus and tibiofibular assessment. One of the chief differences between Orthotool and MPR/D, in assessing this subset of criteria or in assessing any anatomic region, is the presence of mobile cross-haired reference axes on the former, allowing instant reorientation to exact position in three planes. This may be of importance in pinpointing focal abnormalities (such as chip fractures tentatively scheduled for arthroscopic repair) (Fig. 6) and in choosing landmarks for measurements, because any selected landmark can be simultaneously confirmed in three planes before use.

The accepted width for the tibiofibular joint is 2–3 mm; the size of most CT cursors precludes sufficiently accurate measurements at this width. Experience with the reference measuring unit included on each hard-copy transaxial image, and with a series of normal ankles, helps assess this space. However, it was far more important, and less experience- and viewer-dependent, to use the relative guideline of the contralateral ankle rather than an absolute measurement. Our experience suggests there may be more normal variability than the literature suggests, probably reflecting differences in age, height, and activity. Assuming the contralateral ankle to be normal, of course, runs the risk of comparison with old traumatic or arthritic changes rather than a true normal baseline for that patient. In taking a history from an acutely injured patient, remote minor trauma may be forgotten.

Assessment of the posterior tibial lip fragment was found to be more comprehensive and precise on 2-D (Orthotool or MPR/D) images than on plain films. Transaxial slices just proximal to the plafond depicted fracture lines and gave an estimation of surface area involvement and distraction, which was then confirmed by review of the sagittal series. Surgery is suggested in those fractures involving over 25% of the articular surface, those with more than 2-mm distraction if the surface remains congruous, and/or those with a significant step-off [11]. Each of these posterior fragment criteria was best assessed on the sagittal images; coronal images were less helpful.

From plain film measurements, the normal talocrural angle is accepted to be 84 ± 4° [6]. Alterations in this angle are produced by displaced fractures and/or ligamentous injury, resulting in bony shifts. Our initial series, although small (nine normal contralateral ankles measured in 13 patients), suggests that the absolute measurement may be smaller than the literature suggests; the contralateral side in our patients averaged 77 ± 4°.

It is probably more reliable, and more clinically meaningful, to consider the relative measurement (i.e., the difference between the traumatized and asymptomatic ankle) in looking for indicators of ankle instability. Although a side-to-side difference of less than 3° or 4° may not rule out significant instability, a larger difference may prove to be a meaningful indicator of surgical instability. Until the contralateral side routinely is included in plain film assessment, the true range of normal or of right-left variation will be uncertain. However, with no additional patient time or cost, transaxial CT routinely includes both sides, allowing a built-in standard of comparison without bias. One of the chief advantages of the Orthotool workstation, as mentioned earlier, is its capacity to process the full data set from the outset, presenting both ankles automatically. Static multiplanar reconstruction would require a second reconstruction series of the normal ankle. We considered initially that an alternate source for the variation between 2-D and plain film measurements was a failure to compare apples with apples; that is, for some reason, the angle measured on interactive 2-D images was not the same as that on the plain film angle. The very close (±0.5°) agreement of these two angles in our series precluded that possibility. Both sets of measurements (2-D and plain film) were performed blinded, without knowledge of the results of measurements done with the other imaging method.

This series included only one talar fracture. However, the utility of multiplanar CT in depicting talar trauma and subsequent alignment is easily extrapolated from our experience with the distal tibia and fibula. The utility of reformatted CT in assessing the essentially horizontal talar dome articulation also is self-explanatory; even transaxial CT alone may surpass plain films in documenting small abnormalities in this region [12].

Overall symmetry of the mortise is best reviewed on the serial coronal views and, again, benefits from comparison with the contralateral ankle. This can be done as readily on static multiplanar reformatted images, once both the left and right sides have been reformatted. Either dynamic or static coronal review will be less position-dependent than plain films.

Although our experience here and in studying other anatomic regions [4, 5, 13, 14] suggests that 3-D images, animated or static, cannot be used as easily for size or angle measurements, and do not resolve fracture lines in as much detail as 2-D CT, the role of 3-D imaging in the total assessment should not be underestimated. In this anatomic area as in others, the final step in communicating the findings to the referring clinician is review of the animated 3-D rotations. This provides an integration of the planar image findings to formulate an improved diagnostic and therapeutic overview. The surgeons report in virtually all cases that both the 2-D and 3-D images were critical in establishing all the findings, planning

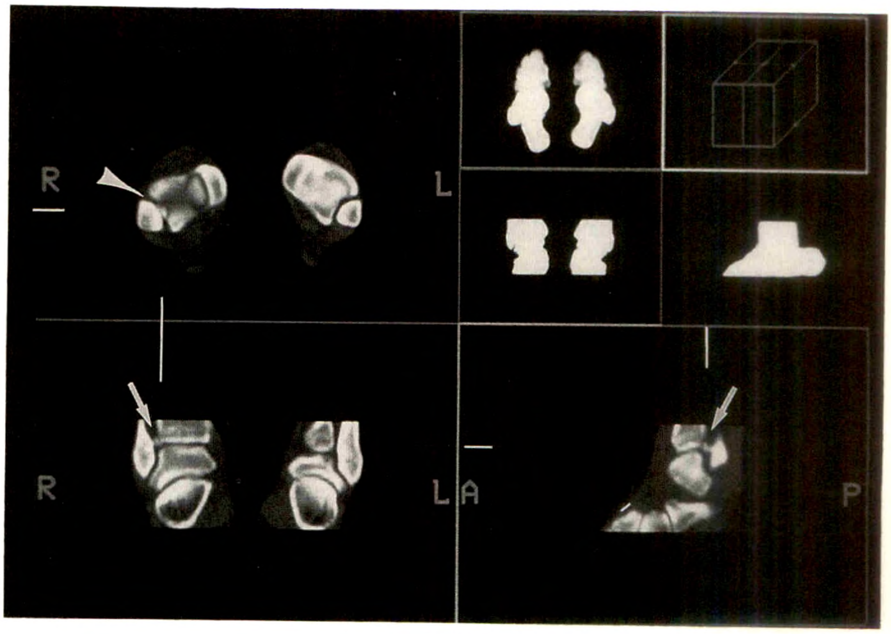

Fig. 6.—28-year-old man with several weeks of ankle pain after minor trauma. History and physical examination suggested a loose body, which could not be confirmed by conventional radiography. Transaxial Orthotool CT image (top left) suggests a small fragment in tibiofibular space (*arrowhead*), but at a level where partial-volume effect can interfere with interpretation. Coronal and sagittal axes were centered to obtain cross-hair views; coronal (bottom left) and sagittal (bottom right) images were thus obtained, both clearly showing small chip off lateral tibia (*arrows*). If necessary, this technique would localize this finding for arthroscopic or minimal incision removal.

surgery, and assessing the existing status of reduction. In this series, interactive 2-D imaging established the presence or absence of fractures, and were used to measure fragment displacement and rotation. Three-dimensional images were used to synthesize the relations of these structures, completing surgical triage and preoperative planning. In the same vein, it is difficult to quantify what we believe is another major benefit of the Orthotool workstation, that is, the ease with which it routinely encourages the radiologist and surgeon to review each case together and to jointly review diagnostic findings and proposed therapeutic plans.

ACKNOWLEDGMENTS

We thank Nancy Lawrence for secretarial assistance and George P. Saba II for encouragement and support.

REFERENCES

1. Ney DR, Fishman EK, Magid D, Kuhlman JE. Interactive real-time multiplanar CT imaging. *Radiology* **1989**;170:275–276
2. Lauge-Hansen N. Fractures of the ankle: combined experimental-surgical and experimental-roentgenologic investigations. *Arch Surg* **1950**;60:957–985
3. Fishman EK, Magid D, Mandelbaum BR, et al. Multiplanar (MPR) imaging of the hip. *RadioGraphics* **1986**;6:7–54
4. Fishman EK, Drebin RA, Magid D, et al. Volumetric rendering techniques: applications for three-dimensional imaging of the hip. *Radiology* **1987**;163:737–738
5. Fishman EK, Ney DR, Magid D, Drebin RA. Volumetric rendering in three dimensional CT reconstruction: clinical applications in pelvic trauma. *Medicamundi* **1988**;33:143–147
6. Phillips WA, Schwartz HS, Keller CS, et al. A prospective, randomized study of the management of severe ankle fractures. *J Bone Joint Surg [Am]* **1985**;67-A:67–78
7. Yablon IG, Heller FG, Shouse L. The key role of the lateral malleolus in displaced fractures of the ankle. *J Bone Joint Surg [Am]* **1977**;59-A:169–173
8. Mak KH, Chan KM, Leung PC. Ankle fracture treated with the AO principle—an experience with 116 cases. *Injury* **1985**;16:265–272
9. Ramsey PL, Hamilton W. Changes in tibiotalar area of contact caused by lateral talar shift. *J Bone Joint Surg [Am]* **1976**;58-A:356–357
10. Clarke H, Michelson JD, Jinnah R. Tibio talar stability and bimalleolar ankle fractures: a dynamic in vitro contact area study. *J Bone Joint Surg [Am]* (in press)
11. Wilson FC. Fractures and dislocations of the ankle. In: Rockwood CA Jr, Green DP, eds. *Fractures in adults*, vol. 2. Philadelphia: Lippincott, **1984**:1665–1701
12. Zinman C, Wolfson N, Reis ND. Osteochondritis dissecans of the dome of the talus. *J Bone Joint Surg [Am]* **1988**;70-A:1017–1019
13. Fishman EK, Magid D, Ney DR, Drebin RA, Kuhlman JE. Three-dimensional imaging and display of musculoskeletal anatomy. *J Comput Assist Tomogr* **1988**;12:465–467
14. Magid D, Fishman EK. Two and three-dimensional imaging in musculoskeletal trauma. *Radiol Clin North Am* **1989**;27:945–956

Book Review

Positron Emission Tomography in Clinical Research and Clinical Diagnosis. Tracer Modelling and Radioceptors. Edited by C. Beckers, A. Goffinet, and A. Bol. (Vol. 15 of the series Developments in Nuclear Medicine.) Boston: Kluwer, 292 pp., 1989. $86.50

This book is the proceedings of a workshop held at the University of Louvain Medical School, Brussels, October 20–22, 1988. The workshop focused on details of modeling data from receptor and metabolism studies with positron emission tomography (PET).

The book has two sections, "Receptors" and "Energy Metabolism," and contains 21 papers. In an introductory paper, Puech reviews elementary concepts of treating neuropsychiatric disorders and suggests using PET for detection of receptor abnormalities, validation of current hypotheses on drug effects, and development of drugs. This basic discussion sets the stage for subsequent papers.

The section on receptors has some excellent summaries on tracer kinetic modeling, a dynamic model for reversible ligand binding for dopamine receptors, a D_2 dopamine antagonist, and a benzodiazepine antagonist. Other papers deal with the kinetics of and a method for obtaining rate constants for L-^{18}F-fluorodopa by using Patlak plots, the kinetics of fluoroethylspiperone and fluoro-deoxyglucose (FDG) in patients with neuropsychiatric disorders involving the dopaminergic trasmitter-receptor system, and kinetic parameters from time-activity data obtained by applying a two-compartment blood-brain barrier–crossing model in dogs. The biochemistry of noradrenaline, the related anatomy, the corresponding adrenergic receptors and their localization and specific ligands, and the CNS pharmacology of α_2-adrenergic agents are presented in two excellent papers.

The second day of the workshop was devoted to energy metabolism. Complex whole-body, multicompartmental models requiring multitracer/sampling procedures, are described by one group, but with few data for glucose and amino acid metabolism. Another group studied gliomas and meningiomas, using a standard FDG transport model. They showed that better contrast is achieved in statistically optimized postreconstruction spatial averaging of pixels, giving functional images.

Other papers dealt with problems of stationarity in kinetic tracer modeling and steady-state and dynamic (i.e., sequential activities vs time) applications of simple brain and myocardial flow models. Another group studied the function of the blood-brain barrier by performing 3-O-^{11}C-methylglucose and FDG analyses and found improved influx and efflux rates by using the simpler model of methylglucose.

Approximately 80% of the text is devoted to neuropsychiatric disorders. The limited coverage of potential PET applications in cancer or coronary artery disease probably reflects the history of PET rather than the intentions of the authors. Some PET applications in neoplasms or coronary artery disease are discussed in the last 50 pages of the book.

The mathematical approach for computing FDG transport constants is described, and a linearized procedure used in assessing therapy response of small-cell carcinomas of the lung gave the best results. Another group reviewed amino acids and PET in oncology and offered an immediate, practical application of PET that uses methionine rather than FDG for grading human brain tumors.

The final two presentations of the workshop dealt with technical details in modeling of tracer kinetics in the heart, quantification of regional myocardial consumption of glucose, and a review of the Sokoloff model and the Patlak method. A simple approach for assessing viability of the myocardium that is based on the glucose uptake over perfusion ratio is offered.

Many of the papers are well worth reading for the suggested techniques they propose or describe for obtaining improved results from PET studies. Interesting data are given in some papers; a few show differences between control subjects and patients with various disorders. The roundtable discussions are excellent additions and make it clear that many things are still in flux and preliminary in PET clinical research and diagnosis; more research is needed to validate some proposed models. PET is a good tool for clarifying receptor-ligand interactions, but practical applications are not quite here yet. This book has much valuable information for research-oriented radiologists who use PET, but clinicians should not be misled: This volume does not contain much that is of immediate diagnostic use. Nevertheless, the book is an extremely useful compendium on how to take advantage of PET in tracer kinetic modeling.

The book has numerous typographic errors. Those in words do not affect comprehension, but garbled mathematical expressions can be interpreted only by experts who are willing, in some cases, even to rederive the model mathematics. None should be used without some form of mathematical verification. The illustrations and reproduction of PET images are good, and the many references provided by most of the authors are a valuable asset.

For readers who do not have time to read every paper, two improvements would have been worthwhile: abstracts for all the papers and a better grouping into more general topics. For example, neuropharmacology and general mathematical modeling are intermixed in the first half of the book. Despite some of its shortcomings, the book is well worth reading and should be of interest to physiologists, physicians, mathematicians involved in PET, and clinicians who expect valid answers from PET procedures.

Karl F. Hubner
The University of Tennessee, Medical Center at Knoxville
Knoxville, TN 37920-6999

Insufficiency Fracture of the Sternum Caused by Osteopenia:

Plain Film Findings in Seven Patients

Clement Chen[1]
Vijay Chandnani[1]
Heung Sik Kang[1]
Jean P. Schils[1]
Donald Resnick[1]
Ann G. Bjorkengren[2]
Phoebe Kaplan[3]

Sternal insufficiency fractures, whether nonbuckling (displaced or nondisplaced) or buckling, are rare and have been described in elderly osteopenic patients with accentuated kyphosis of the thoracic spine. We retrospectively analyzed the radiographs and clinical records in seven osteopenic patients with sternal insufficiency fractures and correlated the type of insufficiency fracture with the presence and degree of dorsal kyphosis, as well as the presence of chest pain, soft-tissue mass, and osteolysis. We found that displaced or nondisplaced nonbuckling fractures (five patients) may be associated with chest pain localized to the sternum (three patients), and may be present with (three patients) or without (two patients) associated thoracic kyphosis. This type of insufficiency fracture also may be accompanied by a soft-tissue mass and osteolysis (three patients), findings simulating pathologic fractures. All buckling insufficiency fractures (two patients) were associated with thoracic kyphosis and were asymptomatic.

Our findings suggest that sternal insufficiency fractures may occur with or without exaggerated dorsal kyphosis. The fractures are an uncommon complication of osteopenia and may resemble pathologic fractures when osteolysis and soft-tissue swelling are present.

***AJR* 154:1025–1027, May 1990**

Acute fractures of the sternum have been described as resulting from blunt trauma to the anterior portion of the chest or from flexion-compression injury of the upper thorax [1]. Normal stress related to spinal flexion and extension applied to the sternum in osteopenic patients with accentuated thoracic kyphosis also has been reported to cause insufficiency fractures, either nonbuckling (displaced or nondisplaced) or buckling [2, 3].

We retrospectively analyzed radiographs and conventional tomograms of sternal insufficiency fractures in seven osteopenic patients to determine if there is a correlation between the fractures and thoracic kyphosis, sternal pain, osteolysis, and soft-tissue mass.

Materials and Methods

We retrospectively reviewed the lateral radiographs (seven patients) and conventional tomograms (one patient) of five women and two men, aged 50–85 years (mean, 68 years) with sternal insufficiency fractures. The diagnosis of a pathologic fracture was excluded by the clinical history and absence of radiologic criteria of osteolysis or associated soft-tissue mass (five patients) or sternal biopsy (two patients). Review of the patients' clinical records revealed that none had a history of sternal trauma and three patients had mild pain, localized to the sternum.

The sternal fractures were classified as nonbuckling (nondisplaced or displaced) and buckling. Displaced fractures were arbitrarily defined as having an offset at the fracture site of greater than 25% of the thickness of the sternum in the lateral projection. Buckling sternal fractures were defined as a sternal deformity in which the upper portion of the sternum was located posterior to the lower portion, and in which there was no cortical disruption, focal

Received August 3, 1989; accepted after revision December 29, 1989.

This work was supported in part by Veterans Administration grant #SA306.

[1] Department of Radiology, Veterans Administration Medical Center, San Diego, CA 92161, and University of California Medical Center, San Diego, CA 92103. Address reprint requests to D. Resnick, V.A. Medical Center, 3550 La Jolla Village Dr., San Diego, CA 92161.

[2] Department of Radiology, Stanford University Medical Center, Stanford, CA 94305-2114.

[3] Department of Radiology, University of Nebraska Medical Center, 42nd and Dewey Aves., Omaha, NE 68105.

0361–803X/90/1545–1025
© American Roentgen Ray Society

bone resorption, or callus formation. We also evaluated the radiographs for the presence of an associated soft-tissue mass or osteolysis at the fracture site.

We analyzed the lateral chest radiographs for the presence and location of compression fractures of the thoracic vertebrae. Using Cobb's method [4], we measured the dorsal kyphotic angle in six patients (the angle formed by the intersection of the lines parallel to the superior and inferior vertebral endplates most tilted on the lateral chest radiograph). Abnormal thoracic kyphosis was considered present when this angle was greater than 45 degrees [4]. The lateral radiograph of the seventh patient was unavailable, although no kyphosis or compression fractures were noted on the report and the patient did not appear to be kyphotic when sternal biopsy was done. We then correlated the type of fracture with the pattern of thoracic kyphosis and the presence of clinical symptoms.

Results

Nonbuckling fractures were present in five patients (displaced in three and nondisplaced in two), and buckling fractures were present in two patients (Fig. 1). One patient had two buckling fractures, one in the upper and another in the lower portion of the sternum. Three patients with nonbuckling fractures (two with a displaced fracture and one with a nondisplaced fracture) (Fig. 2) had chest pain localized to the sternum. Neither of the patients with buckling fractures had chest pain; in these patients, the fractures were discovered on routine chest radiographs.

Moderate to severe thoracic kyphosis was present in five patients (kyphotic angle, 63–103°), resulting from compression fractures of one or more of the following vertebral bodies: T1–T4 (four patients); T5–T8 (three patients); T9–T12 (three patients). The remaining two patients, both with nonbuckling fractures, showed normal configuration of the dorsal spine, aside from osteopenia. No evidence was found of compression fractures of thoracic vertebrae. The kyphotic angle measured 38° in one of these two patients, which is considered within the normal range of thoracic curvature.

Mild to extensive osteolysis with adjacent soft-tissue swelling was identified in three patients with sternal fractures, simulating the appearance of a pathologic fracture. A sternal biopsy was performed in two patients to exclude a pathologic fracture (Figs. 2 and 3). Mild osteolysis was present in a third patient. In this patient, a pathologic fracture was excluded on the basis of clinical findings and the unchanged appearance of follow-up radiographs.

Discussion

Insufficiency fractures of the sternum, although uncommon, have been reported in patients with generalized osteoporosis,

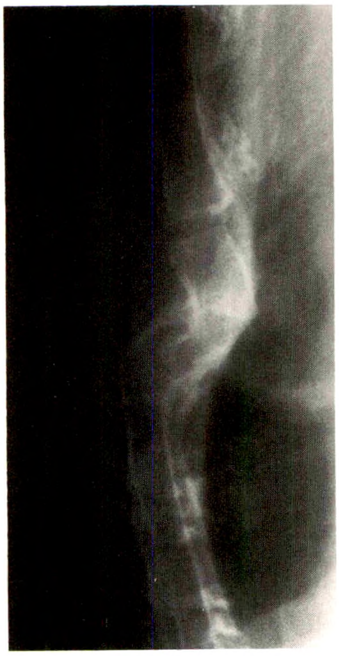

Fig. 1.—Lateral chest radiograph of an 85-year-old woman shows buckling fracture of upper body of sternum. Previous radiograph obtained 6 years earlier showed normal appearance of sternum although thoracic kyphosis (kyphotic angle = 66°) due to compression fractures of thoracic vertebrae had been evident. Patient denied a history of trauma or chest pain.

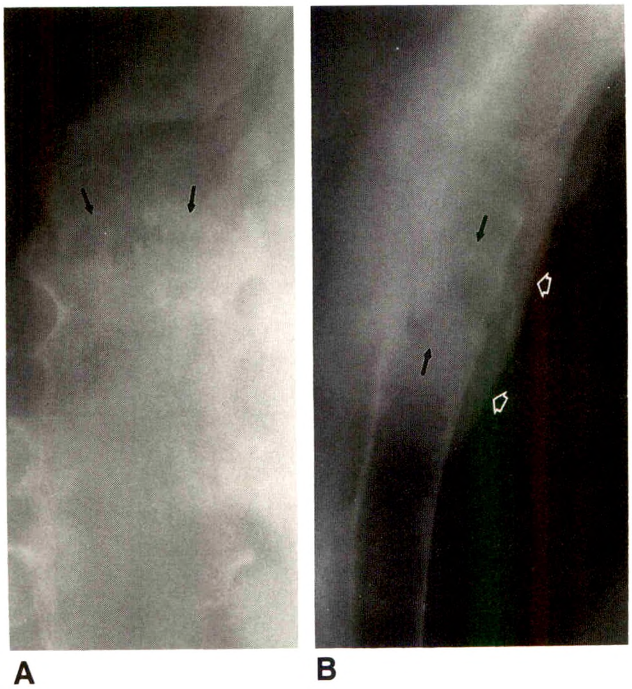

Fig. 2.—*A* and *B*, Conventional frontal (*A*) and lateral (*B*) tomograms of sternum of a 55-year-old woman reveal a nondisplaced fracture (*solid arrows*) of upper body of sternum. Moderate bony resorption and soft-tissue swelling (*open arrows*) around fracture suggest a pathologic fracture. Biopsy confirmed a healing fracture. No evidence is seen of abnormal thoracic kyphosis (kyphotic angle = 38°).

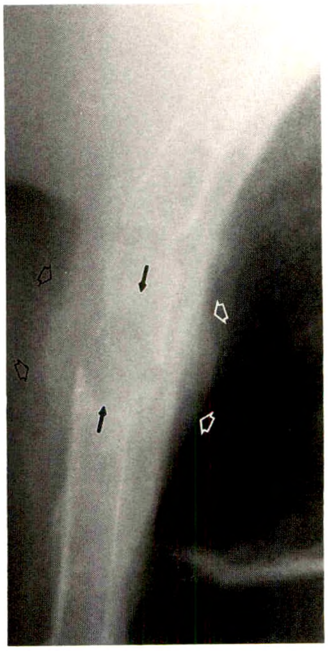

Fig. 3.—Lateral chest radiograph of a 50-year-old woman with a history of alcoholism and osteomalacia shows a displaced insufficiency fracture of upper body of sternum. Thoracic spine is osteopenic but otherwise normal. Extensive osteolysis (*solid arrows*) and adjacent soft-tissue swelling (*open arrows*) suggest a pathologic fracture. Biopsy confirmed a healing fracture.

particularly elderly women [1, 2]. These fractures or deformities have been attributed to chronically applied flexion-compression stress to the sternum caused by accentuated dorsal kyphosis. This combination of accentuated dorsal kyphosis and sternal insufficiency fracture was encountered in five of seven patients in our series. No clear relationship was found between the location of the thoracic compression fracture and the presence of sternal fracture.

Displaced or nondisplaced insufficiency fractures of the sternum also were evident in two additional patients who did not have any compression fractures of the thoracic or lower cervical vertebrae. The sternal fractures in these patients presumably result from acute flexion-compression stress applied to the weakened sternum, particularly during forward bending.

Patients with buckling sternal insufficiency fractures were asymptomatic, the sternal lesions being incidentally discovered on routine lateral chest radiographs. Displaced and nondisplaced nonbuckling fractures, however, may be associated with pain and, therefore, might be confused with acute cardiopulmonary emergencies such as myocardial infarction [5] or pulmonary embolism [6].

Posttraumatic osteolysis is well documented after injury of the distal portion of the clavicle, pubic or ischial rami, and femoral neck [7]. Extensive osteolysis, especially when associated with soft-tissue swelling, may simulate a pathologic fracture resulting from multiple myeloma, other primary neoplasms, skeletal metastasis [8], or infection. In our series, three sternal fractures were accompanied by mild to extensive osteolysis and adjacent soft-tissue swelling, and in two patients, bone biopsy was required for exclusion of a pathologic fracture.

In summary, our observations confirm that sternal insufficiency fractures may occur with or without exaggerated thoracic kyphosis, may be symptomatic or asymptomatic, and sometimes may be confused with a pathologic fracture.

REFERENCES

1. Park WM, McCall IW, McSweeney T, Jones BF. Cervicodorsal injury presenting as sternal fracture. *Clin Radiol* **1980**;31:49–53
2. Itani M, Evans GA, Park WM. Spontaneous sternal collapse. *J Bone Joint Surg [Br]* **1982**;64-B:432–434
3. Cooper KL. Insufficiency fractures of the sternum: a consequence of thoracic kyphosis? *Radiology* **1988**;167:471–472
4. Winter RB, Hall JE. Kyphosis in childhood and adolescence. *Spine* **1978**;3:285–308
5. Rutledge DI. Spontaneous fracture of the sternum simulating myocardial infarction. *Postgrad Med* **1962**;32:502–504
6. Vassalo L. Spontaneous fracture of the sternum simulating pulmonary embolism. *Br J Clin Pract* **1969**;23:288–289
7. Resnick D, Niwayama G. Posttraumatic osteolysis. In: Resnick D, Niwayama G, eds. *Diagnosis of bone and joint disorders*, 2nd ed. Philadelphia: Saunders, **1988**:4143–4146
8. Urovitz EPM, Fornasier VL, Czitrom AA. Sternal metastases and associated pathological fractures. *Thorax* **1977**;32:444–448

Book Review

Emergency Interventional Radiology. Edited by M. Pinson Neal, Jr., Jaime Tisnado, and Shao-Ru Cho. Boston: Little, Brown, 433 pp., 1989. $85

This book contains 23 chapters on interventional radiologic techniques for diagnosing and treating emergent or urgent traumatic and iatrogenic conditions as well as life- or limb-threatening conditions associated with various disease processes. The entire body is covered, from transcatheter embolization of vascular lesions in the CNS to therapy of acute arterial occlusions and venous thrombosis in the lower extremities. In the chest, embolization of bronchial arteries in patients with hemoptysis, catheter pulmonary embolectomy, and thrombolytic therapy and angioplasty for acute coronary artery occlusion are addressed. In the abdomen, the management of bleeding esophageal varices, gastrointestinal bleeding, visceral ischemia, and percutaneous biliary and uroradiologic techniques are discussed in detail. Embolotherapy for posttraumatic bleeding in the head and neck, abdomen, pelvis, and extremities is covered also. Other topics include percutaneous unknotting and repositioning of intravascular catheters and percutaneous retrieval of embolized catheter fragments and other iatrogenic foreign bodies; these chapters are illustrated profusely with helpful diagrams. Rounding out the book are chapters on percutaneous abscess drainage and management of emergency situations in infants and children.

Rather than being a basic "how to do it" book for the neophyte, this volume often is geared to the practicing interventional radiologist or angiographer who is generally familiar with percutaneous and transluminal techniques. In other words, in several chapters it is assumed that the reader is familiar with superselective angiographic techniques, whereas in others, the more basic approach to the problem is reviewed. Reference lists vary from adequate to extensive, and most include current articles through 1988. These minor inconsistencies are typical of texts that have more than one contributor, and they do not detract from the usefulness of this book. The illustrations are generally of high quality and show typical radiologic findings for the cases under discussion.

Although several excellent texts currently are available on interventional techniques, this book attempts to establish its uniqueness by concentrating on the area of emergency situations. It succeeds in this regard, but, in all fairness, these techniques can be found in other texts. However, it deserves a place in interventional radiology libraries as a succinct reference when review is necessary or desirable before interventional therapy takes place. It also will be of particular use as a ready source of information for emergent situations for those radiologists who perform interventional or angiographic procedures infrequently.

E. Stephen Amis, Jr.
Columbia-Presbyterian Medical Center
New York, NY 10032

Pictorial Essay

The Neer Classification of Displaced Proximal Humeral Fractures: Spectrum of Findings on Plain Radiographs and CT Scans

R. F. Kilcoyne,[1] William P. Shuman,[2] Frederick A. Matsen III,[3] Michael Morris,[4] and Charles A. Rockwood[5]

In 1934, Codman [1] described fractures of the proximal humerus and classified them as occurring in the head, shaft, or greater or lesser tuberosity. He indicated that surgical treatment is needed if these fractures are displaced. In 1970, Neer [2] described a classification system of displaced proximal humeral fractures that clarified and expanded on the

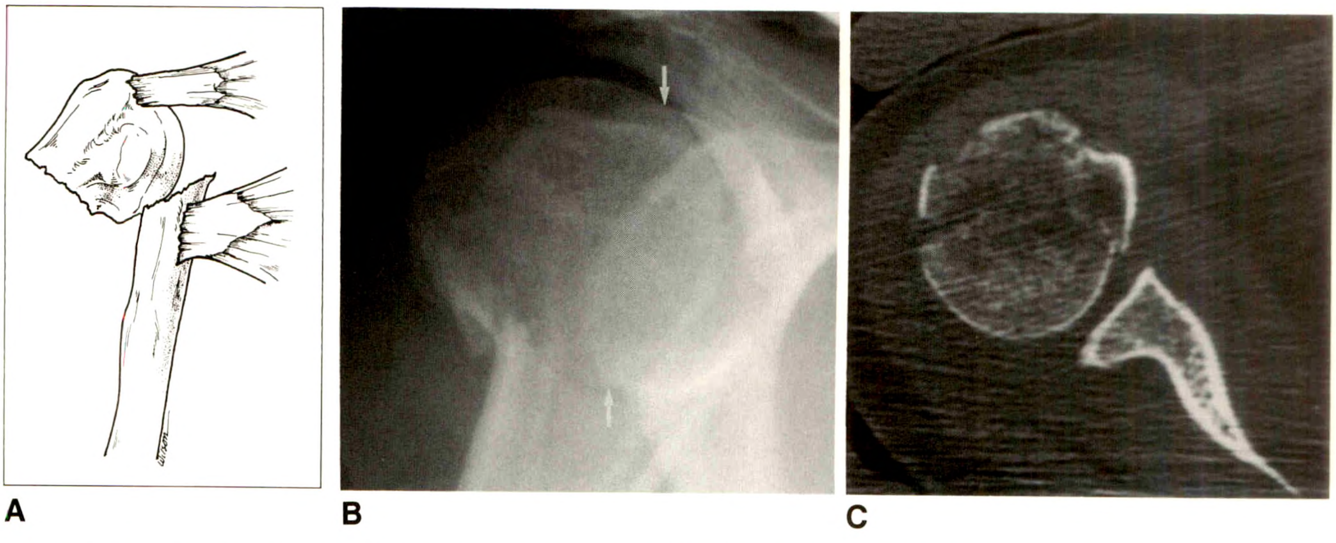

Fig. 1.—Two-part surgical neck fracture (displaced subtuberous fracture). Rotator cuff attachment is intact, which allows humeral head to remain in neutral position or be abducted by pull of supraspinatus tendon. Distal segment is pulled medially and usually anteriorly by action of pectoralis major.

***A*, Anatomic drawing.**

***B*, Anteroposterior radiograph shows medial displacement of humeral shaft. There is also a suggestion of fracture of anatomic neck in region of tuberosities (*arrows*).**

***C*, CT scan shows that humeral head is intact. Fractures of greater and lesser tuberosities are nondisplaced.**

Received October 25, 1989; accepted after revision December 6, 1989.

Presented in part at the annual meeting of the American Roentgen Ray Society, San Francisco, May 1988.

[1] Department of Radiology, University of Texas Health Science Center at San Antonio, and Veterans Administration Medical Center, 7400 Merton Minter Blvd., San Antonio, TX 78284. Address reprint requests to R. F. Kilcoyne.

[2] Department of Radiology, University of Washington, Seattle, WA 98115.

[3] Department of Orthopaedic Surgery, University of Washington, Seattle, WA 98115.

[4] Department of Orthopaedic Surgery, The Mason Clinic, 904 Seventh Ave., Seattle, WA 98104.

[5] Department of Orthopaedic Surgery, University of Texas Health Science Center at San Antonio, San Antonio, TX 78284.

AJR **154:1029–1033, May 1990** 0361–803X/90/1545–1029 © American Roentgen Ray Society

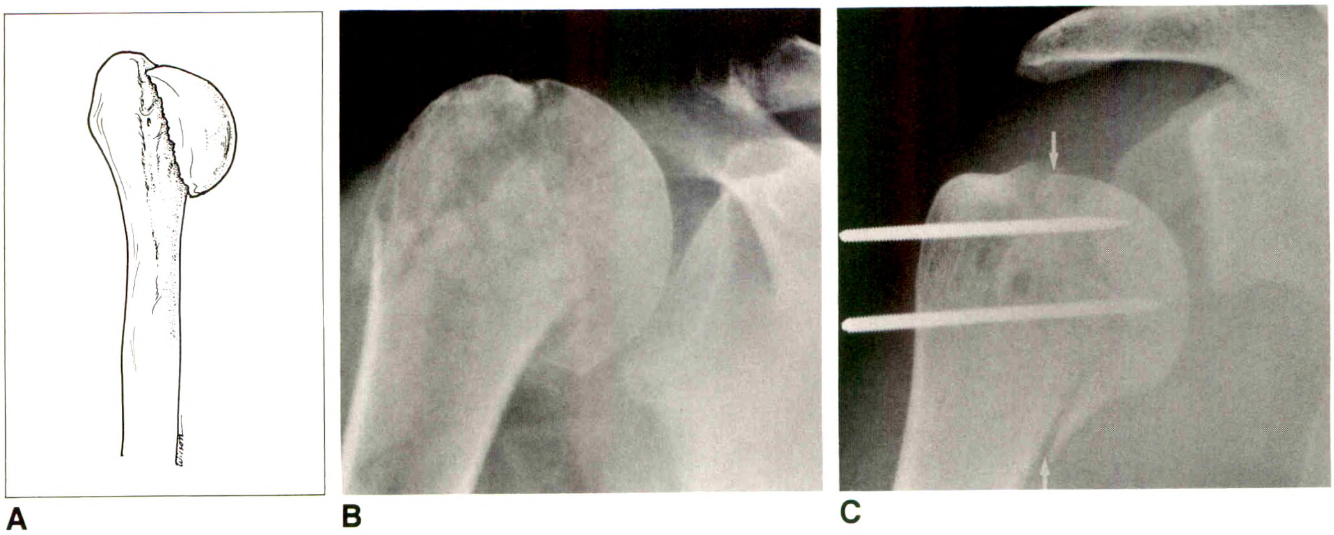

Fig. 2.—Two-part anatomic neck fracture (articular segment fracture). This uncommon injury may cause disability from malunion or osteonecrosis of humeral head. Displacement is easily seen on anteroposterior radiograph, and CT may not be needed. Distal segment is pulled superiorly by deltoid.

A, Anatomic drawing.

B, Anteroposterior radiograph with superior migration of humeral shaft due to muscle pull.

C, Postoperative radiograph in a different patient shows reduction of fracture (*arrows*).

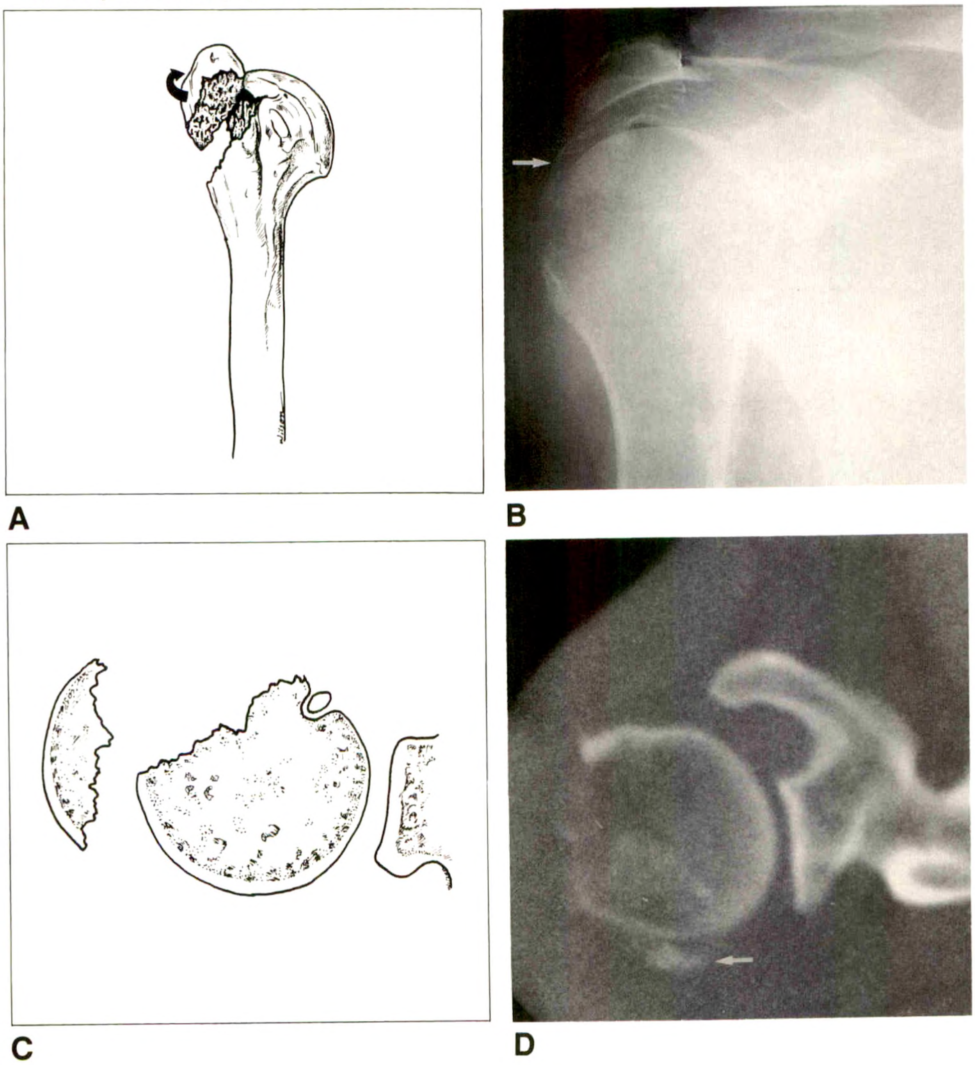

Fig. 3.—Two-part greater tuberosity fracture. Greater tuberosity is pulled superiorly and posteriorly by supraspinatus muscle and external rotators (infraspinatus and teres minor). CT is helpful in showing degree of posterior displacement of fracture fragments.

A, Anatomic drawing. Direction of displacement (*arrow*).

B, Plain film shows fracture site (*arrow*).

C, Anatomic drawing shows appearance of displaced greater tuberosity on cross-sectional view.

D, CT scan shows posterior displacement of greater tuberosity, which is difficult to appreciate on plain film (*arrow*).

Fig. 4.—Two-part lesser tuberosity fracture. In these rare fractures, lesser tuberosity is pulled medially by subscapularis muscle. This displacement may be seen better on CT than on plain films.

***A*, Anatomic drawing. Direction of displacement (*arrow*).**

***B*, Anatomic drawing shows appearance of displaced lesser tuberosity on cross-sectional view.**

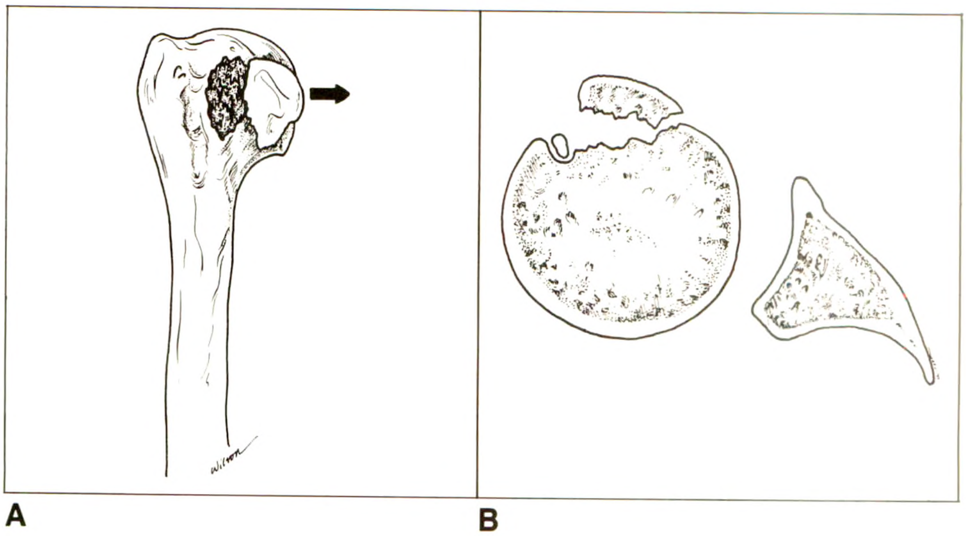

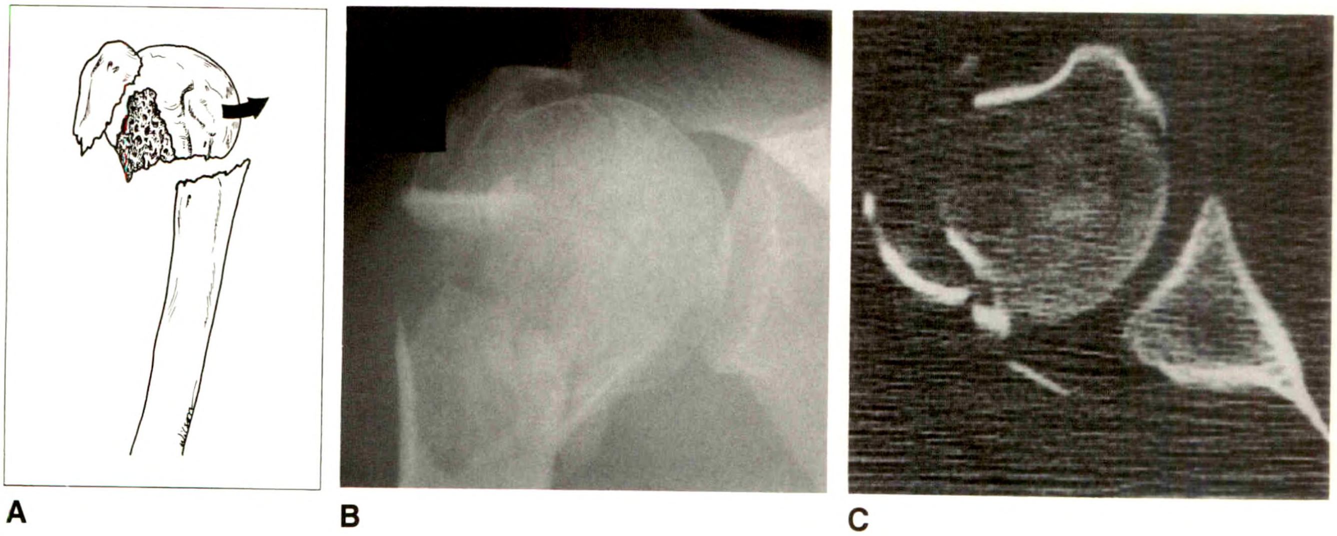

Fig. 5.—Three-part surgical neck and greater tuberosity fracture. More complex fractures show more displacement. Humeral head is rotated internally by pull of subscapularis muscle.

***A*, Anatomic drawing. Direction of displacement (*arrow*).**

***B*, Plain film shows surgical neck displacement but underestimates displacement of greater tuberosity fragment.**

***C*, CT scan shows displacement of greater tuberosity fragment.**

earlier work of Codman. Radiologists should be aware of this classification so that they can recognize the various fracture patterns and the significance of displacement of proximal humeral fractures. Proper treatment of these fractures depends on the ability to show radiologically whether or not the fragments are displaced.

In the Neer classification, one fragment or part is the humeral shaft, so the simplest displaced fracture is called a "two-part" fracture. The classification includes two-part fractures (Figs. 1–4); three-part fractures (Figs. 5 and 6); four-part fractures (Fig. 7); and fracture-dislocations, including head-splitting fractures (Fig. 8). Malunited fractures may lead to pain or limitation of motion (Fig. 9).

According to Neer [2], displacement of a fracture fragment by more than a centimeter or angulation of more than 45° is considered significant. Neer estimated that over 85% of proximal fractures are not displaced. In those cases no operation is required. However, if the fractures are substantially displaced, surgery is necessary to preserve shoulder function [2].

In the preoperative evaluation of patients with proximal humeral fractures, we routinely obtain an anteroposterior and an axillary or scapular lateral radiograph [2]. Sometimes it is difficult to see the exact position of the fracture fragments, or the patient may be difficult to position. Kristiansen et al. [3] found wide interobserver variation in the classification of

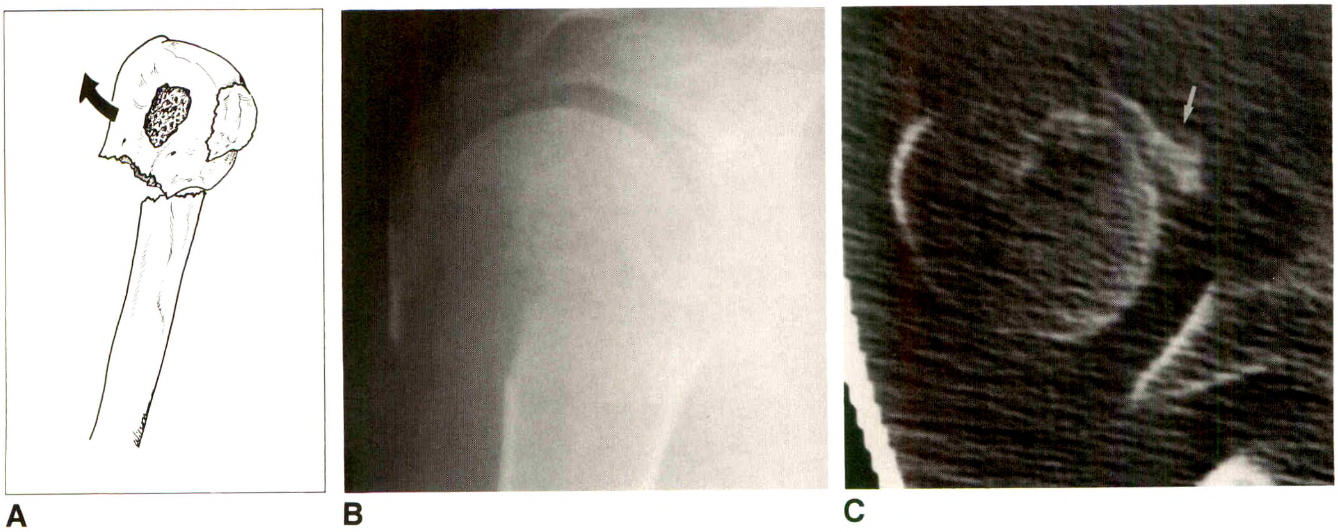

Fig. 6.—Three-part surgical neck and lesser tuberosity fracture. With these uncommon injuries humeral head is rotated externally by pull of infraspinatus and teres minor muscles.

A, Anatomic drawing. Direction of displacement (*arrow*).

B, Plain film shows displacement of surgical neck, but not of lesser tuberosity.

C, CT scan shows rotation of head and displacement of lesser tuberosity (*arrow*).

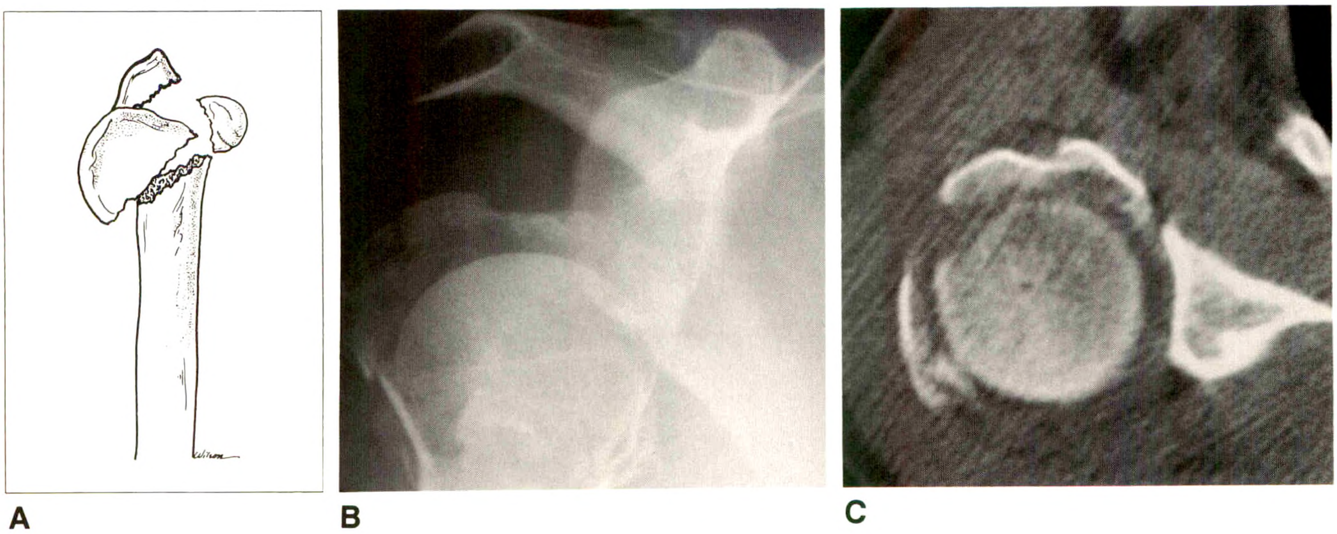

Fig. 7.—Four-part fracture of surgical neck and lesser and greater tuberosities. With four-part fractures or fracture-dislocations, blood supply is disrupted and may lead to osteonecrosis. Humeral head is free of its ligamentous attachments and frequently rotates 90° superiorly, laterally, and anteriorly or posteriorly.

A, Anatomic drawing.

B, Plain film shows superior displacement of tuberosity fragments.

C, CT scan shows that displaced tuberosities will cause severe impairment of rotatory motion.

proximal humeral fractures when only plain radiographs were used. Accuracy of assessment improved with more experience in the use of the Neer classification. We have found that CT can be useful in these difficult cases where the amount of displacement or rotation of fragments is difficult to determine on plain radiographs.

Specific cases in which the plain films may underestimate displacement include greater or lesser tuberosity fractures, impression fractures of the humeral head, head-splitting fractures, or loose bodies in the shoulder joint. In those instances CT can be helpful in showing the abnormality. CT is also useful for the evaluation of malunion, in which case impingement by displaced healed fragments on the glenoid or arthritic changes in the humeral head can be seen [4].

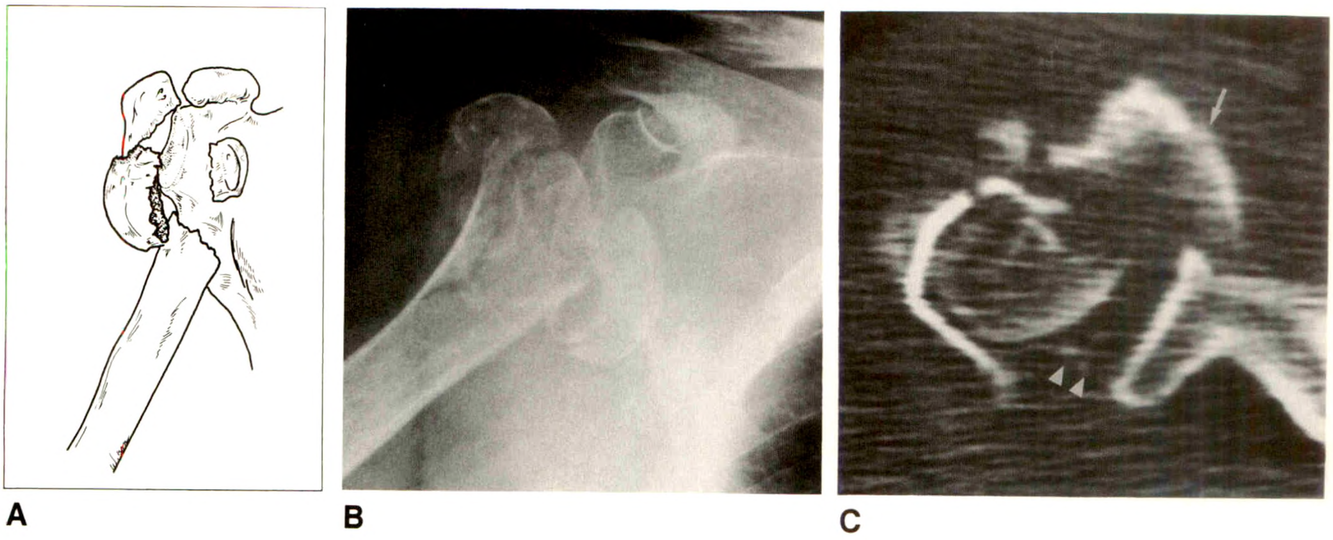

Fig. 8.—Dislocated head-splitting fracture. Plain films may suffice to detect severity of this injury. CT is helpful if there is question about presence of head-splitting fracture and location of head fragments.

A, Anatomic drawing.

B, Plain film shows fracture-dislocation.

C, CT scan shows dislocated head fragment (*arrow*) and loose bodies in joint (*arrowheads*).

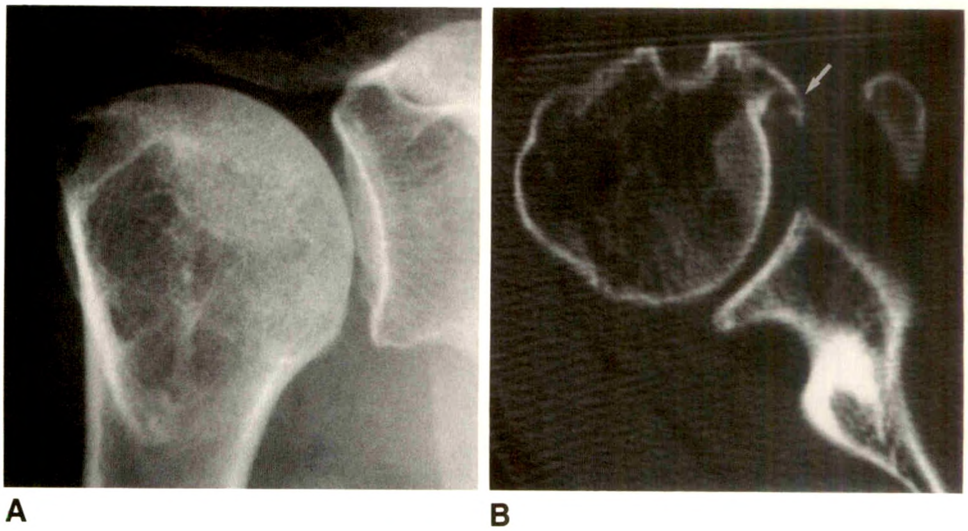

Fig. 9.—Healed, malunited lesser tuberosity fracture.

A, Anteroposterior radiograph shows healed fracture of proximal humerus.

B, CT scan shows that cause of limitation of internal rotation is healed bone fragment medial to its normal attachment (*arrow*).

ACKNOWLEDGMENT

We thank Dinah Wilson for the anatomic drawings.

REFERENCES

1. Codman EA. *The shoulder: rupture of the supraspinatus tendon and other lesions in or about the subacromial bursa.* Brooklyn, NY: Miller, **1934**: 262–287
2. Neer CS. Displaced proximal humeral fractures. Part I: Classification and evaluation. *J Bone Joint Surg [Am]* **1970**;52-A:1077–1089
3. Kristiansen B, Andersen LS, Olsen CA, Vasmarken JE. The Neer classification of fractures of the proximal humerus: an assessment of interobserver variation. *Skeletal Radiol* **1988**;17:420–422
4. Castagno AA, Shuman WP, Kilcoyne RF, Haynor DR, Morris ME, Matsen FA. Complex fractures of the proximal humerus: role of CT in treatment. *Radiology* **1987**;165:759–762

Book Review

Basic Atlas of Sectional Anatomy with Correlated Imaging, 2nd ed. By Walter J. Bo, Neil T. Wolfman, Wayne A. Krueger, and Isadore Meschan. Philadelphia: Saunders, 380 pp., 1990. $75

The first edition of this book filled a critical need for a well-labeled, high-quality cross-sectional atlas to serve as a reference in the burgeoning clinical CT and sonographic arenas of the early 1980s. It became a frequently used "classic," a benchmark against which subsequent atlases were compared. In the 10 years since, cross-sectional imaging capabilities have increased significantly, with a correspondingly dramatic need and expectation for equally high-caliber atlases with superb imaging correlation.

The second edition has been revamped and expanded, with some, but not all, positive results. The basic organization remains unchanged. The core of the atlas is still its high-quality, well-labeled anatomic sections logically divided into chapters illustrating axial slices in the head and neck, thorax, abdomen, male and female pelvis, and lower and upper extremities. Interspersed appropriately are sections and images in sagittal planes; there are no coronal sections. Sections through the head at a 30° angle to Reid's line (corresponding to the customary CT head scanning angle) are appended.

As in the first edition, the right-hand pages show the anatomic sections, and the opposite pages contain line drawings depicting the anatomic level and plane of the sections; xeroradiographs of the sections to highlight the tissue planes; and correlated MR, CT, or sonographic images. The anatomic sections, line drawings, and xeroradiographs are taken unaltered from the first edition. The descriptive text outlining anatomic and clinical considerations has been deleted, and the relatively infrequent CT correlative scans have been replaced by improved CT scans, numerous MR images, and a few sonograms. The introduction, detailing the basics of cross-sectional imaging techniques, has been altered substantially, with updated, brief, superficial descriptions of current CT and sonographic technology and an introduction to MR imaging.

The purpose of the first edition was to "present cross-sectional anatomy in a meaningful manner to students of gross anatomy and to clinicians and technologists who are interested in correlations between cross-sectional anatomy and computed tomography and ultrasonography." The first edition succeeded in this task. The second edition is intended to be an atlas of detailed anatomy presented by section, and the authors chose images "in order to display the breadth of anatomy seen with CT, US, and MRI." To the extent that the second edition uses the same general format and organization as the first edition, it fills its designated niche: the demonstration of anatomy by anatomic cross-sections and correlated images. Unfortunately, the practically oriented text that accompanied the sections in the first edition has been deleted and, I anticipate, will be missed by those readers for whom this atlas has the greatest benefit. Even though the text would have required revision, its exclusion and replacement by correlated images that are neither state of the art nor carefully matched to the anatomic sections are disappointing. The MR images are particularly disappointing as they suffer from poor contrast and poor resolution; they would not be considered optimal, much less adequate, for any current imaging journal. The CT scans would have benefited from dynamic scanning with excellent contrast enhancement; they are satisfactory at best. The sonograms are adequate, though few.

Although this atlas is useful as an occasional reference, it is insufficiently detailed for the experienced cross-sectional radiologist. For example, the chapters on the head and neck are not adequately detailed for the student or practitioner of neuroradiology. Similarly, in this era of segmental hepatic resections, the segments of the liver and their anatomic landmarks are neither labeled nor described. More effective, albeit more expensive, atlases are available now that will become the reference "atlases of choice" for the experienced cross-sectional radiologist.

This atlas will continue to fill an important role in the education of, and as a reference for, students, technologists, and clinical colleagues. As it is perhaps better suited for this group than other atlases available, and as its price is relatively modest, it should be on the library reference shelf in any department in which cross-sectional imaging is done.

H. Esterbrook Longmaid III
New England Deaconess Hospital
Boston, MA 02215

Review Article

Differentiation of Child Abuse from Osteogenesis Imperfecta

Deborah S. Ablin,[1] Adam Greenspan,[1] Michael Reinhart,[2] and Arthur Grix[2]

In cases of suspected child abuse, the possibility of abnormal bone fragility and fractures due to osteogenesis imperfecta (OI) is considered in the differential diagnosis. These issues are also frequently raised by defendants in judicial proceedings concerning child abuse or by other involved or interested persons during documentation of child abuse in care proceedings to arrange for proper protection of the child. Recently, more emphasis has been placed on documenting abuse, rather than seeking retribution of the abuser, protecting the abused child, and attempting to rehabilitate the family by addressing the reasons and causes for the family violence. The radiologist must accurately distinguish child abuse from OI for the protection of the child in question and for recognition of other children at risk in the environment. This situation emphasizes the crucial importance of being familiar with the recent reclassification of OI and with features that distinguish it from child abuse.

Osteogenesis imperfecta is an inherited disorder of connective tissue resulting from abnormal quality and/or quantity of type I collagen. Depending on the type of OI, the inheritance of the disorder can be autosomal dominant, autosomal dominant with new mutation, or autosomal recessive [1–12]. The incidence of OI is estimated to be between 1/15,000 and 1/60,000 births [13–15]. The effects of the disorder can be seen in the bones, ligaments, skin, sclerae, and dentin [4, 5, 15–17]. In general, four major features characterize OI: (1) abnormal bone fragility with osteoporosis, (2) blue sclerae, (3) defective dentition (dentinogenesis imperfecta), and (4) presenile onset of hearing impairment [16, 18]. Other clinical features also may be seen, among them, ligamentous laxity and hypermobility of joints, short stature, easy bruising, hyperplastic scars, abnormal temperature regulation, constipation, mitral and/or aortic valvular disease [7, 15], premature vascular calcifications [7], and inappropriate euphoria [16]. The earlier classification of OI into congenita and tarda types fails to reflect the complexity and heterogeneous nature of this disorder. The new classification proposed by Silence and colleagues in 1979 [13] is based on phenotypic features and mode of inheritance and is widely described in the literature [2, 19–25]. This classification was the basis for the revision and reclassification of OI by the Seventh International Congress of Human Genetics in 1986 [26] and its publication in 1988 [22]. The Third International Conference on Osteogenesis Imperfecta was held in 1987, and the proceedings were published in 1988 [27]. They reflect further changes in the modes of genetic patterns of inheritance [9, 11, 12, 28–32]. The four major types of OI and their subtypes are described in the following sections; their crucial features are summarized in Table 1 [1–10, 12, 13, 15–17, 19–26, 31, 33–41]. In approximately 80% of patients, OI is autosomal dominant and the patients have blue sclerae (OI type I) [14]. Only the rarer types III and IV may be confused with child abuse.

Most of the features associated with OI result from abnormal quantity and/or quality of type I collagen in body tissues. The genetic, biochemical, and molecular biology of type I collagen is quite complex [1–5, 7–13, 15, 17, 24, 28–32, 36,

---

Received September 5, 1989; accepted after revision December 19, 1989.

[1] Department of Radiology, University of California, Davis Medical Center, Sacramento, CA 95817. Address reprint requests to D. S. Ablin in the Division of Diagnostic Radiology (Research) FOLB II-D.

[2] Department of Pediatrics, University of California, Davis Medical Center, Sacramento, CA 95817.

AJR 154:1035–1046, May 1990 0361–803X/90/1545–1035 © American Roentgen Ray Society

TABLE 1: Classification of Osteogenesis Imperfecta[a]

Classification	Clinical Features	Sclerae	Inheritance
Type I			
Subtype A: normal teeth	Osseous fragility: variable (mild to moderately severe)	Blue: all ages	Autosomal dominant [3–5, 7, 9]
Subtype B: dentinogenesis imperfecta	Normal or near-normal stature; presenile hearing loss or impairment (or family history); most common type		
Type II			
Subtypes (radiologic) [24]	Lethal in fetal or perinatal period	Blue	Autosomal dominant–new mutation[b] [3–5, 7, 9–12]; Autosomal recessive (rare) [7, 9–11]
Subtype A: long bones—broad, crumpled; ribs—broad with continuous beading	Osseous fragility: extremely severe; intrauterine growth retardation		
Subtype B: long bones—broad, crumpled; ribs—discontinuous or no beading			
Subtype C: long bones—thin, fractured; ribs—thin, beaded			
Type III	Osseous fragility: moderately severe to severe; progressive deformity of long bones and spine; marked short stature and severe growth retardation; hearing impairment less frequent than type I	Normal or pale blue/gray in infancy progressing to normal	Autosomal dominant–new mutation [4, 9]; Autosomal recessive (rare) [2, 4, 6, 8, 9, 11]
Type IV			
Subtype A: normal teeth	Osseous fragility: variable (mild to moderately severe)	Normal	Autosomal dominant [4, 5, 7, 9]
Subtype B: dentinogenesis imperfecta	Variable deformity of long bones and spine Hearing impairment less frequent than in type I		

[a] Modified from Byers et al. [41], Beighton et al. [22], and Silence [7]

[b] Recurrence risk 6–7% on the basis of parental germ-line mosaicism [9, 10].

37, 40–52], and this complexity on the molecular level often is reflected in the disorder's clinical heterogeneity. Type I collagen is formed from procollagen consisting of two pro $\alpha 1$(I) chains and one pro $\alpha 2$(I) chain. These proteins are coded on chromosomes number 7 and 17; their gene loci are referred to as COL1A2 ($\alpha 2$-chain) and COL1A1 ($\alpha 1$-chain), respectively [4, 5, 15, 29]. Abnormalities in the gene loci of chromosome 7 and/or 17 produce decreased or abnormal synthesis of pro $\alpha 2$(I) and pro $\alpha 1$(I) proteins, procollagen, and collagen; they may also result in abnormalities in the subsequent triple-helix formation of the proteins [4, 10, 12, 15, 17, 29, 31, 32, 41, 51].

The previous clinical delineation of OI was based on the age of onset and the severity of bony changes. The congenita form in the old terminology referred to a severe type of disorder that was fatal before or around the time of birth; the tarda form, on the other hand, encompassed a range of milder skeletal anomalies with longer survival or a normal life expectancy. Today, the terms *congenita* and *tarda* refer simply to the age at presentation [13, 16]. Congenita is reserved for patients with osseous deformities and/or bowing present at birth, and tarda, for patients with acquired bowing or osseous deformity and no bowing at birth [16, 34, 35]. Currently, patients with any type of OI may present with bowing or fractures at birth [13, 19, 20]. The first fractures in types I, III, and IV may manifest at any time during childhood [19, 20]. The severity of bowing correlates with the severity of the disease, and deformities increase with the rise in the number of fractures [16]. The better the bone morphology and mineralization are at birth or at the time of first fracture, the longer the survival [1].

Classification of Osteogenesis Imperfecta

Osteogenesis Imperfecta, Type I

Type I OI is the most common form of the disorder. Of all patients with OI in the Victoria, Australia, study [13], 71% of patients had OI type I and the minimum incidence was 3.5/100,000 live births. Type I is a relatively mild form of OI with autosomal dominant inheritance [3–5, 7, 9, 12, 13, 22, 31, 40, 41, 53]. Sporadic cases due to new dominant mutation also have been reported [13]. Bone fragility is mild to moderate (variable), less than with types II and III, and osteoporosis is present (Figs. 1 and 2); sclerae are distinctly blue [12, 41]. Presenile hearing loss or impairment (35–40% of patients) or a family history of hearing loss or impairment is a common feature [7, 12, 13, 19, 39, 40]. Stature is normal or near normal [4, 12, 40, 41]; although short stature may occur, it is not as severe as in types II and III [7, 13]. Wormian bones are present [40]. The two subtypes of OI type I are distinguished by the presence of normal teeth (subtype IA) or dentinogenesis imperfecta (subtype IB) [19, 39, 41].

Fractures present at birth have been observed in 8–10% of patients with OI type I [13, 19], 6% with subtype IA, and 25% with subtype IB [7, 39]. In the majority of cases, however, fractures begin in the preschool period [7, 13] and may be seen at the time of birth or at any time during childhood. Fractures heal at a normal rate [7], and their frequency declines after puberty. In 10% of patients, no fractures develop [7]. Bowing deformities, especially anterior and lateral bowing of femora and tibiae (as opposed to the physiologic bowing) [13], and angulation of the long bones are characteristic radiologic features (see Fig. 1). Patients with dentinogenesis imperfecta (subtype IB) exhibit more growth retardation and a higher fracture rate; moreover, they are most likely to have their first fracture at birth than patients with normal teeth (subtype IA) [7, 39]. Mild to moderate progressive kyphoscoliosis is present in 20% of adults with OI type I [7, 13]. The head is often large [7, 13]. Ligamentous laxity and joint hypermobility may occur [7] (see Figs. 2A and 2B). Easy bruising, caused by capillary fragility due to abnormal collagen in vessels, is seen in 75% of patients. Functional impairment due to bony deformity is mild in most cases, and severe functional impairment can be prevented or limited by treatment. Most patients were able to walk unaided, with only three of 127 patients requiring crutches or wheelchair and seven of 127 patients having gait disturbance or limited mobility [13].

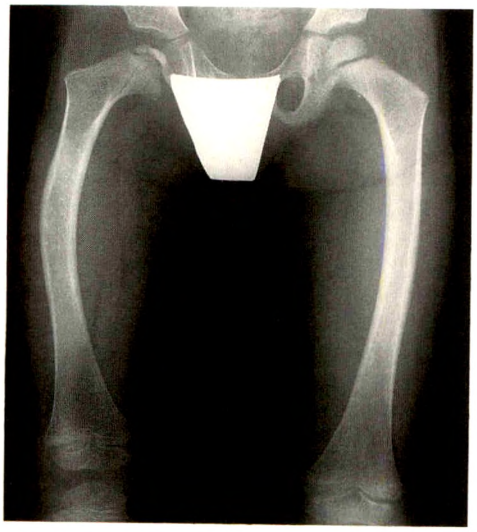

Fig. 1.—Mild osteogenesis imperfecta type I. 5-year-old boy with light blue sclera, ligamentous laxity, and history of recurrent left tibial fractures. Anteroposterior radiograph of both femora shows lateral bowing, mild osteoporosis, and osteonecrosis of right femoral head and right coxa vara.

Osteogenesis Imperfecta, Type II

Type II OI is the fetal or perinatal lethal form of the disorder. Of all patients with OI in the Victoria, Australia, study, 9% of patients had type II and the minimum incidence was 1.6/100,000 live births [13, 24]. This form results from an autosomal dominant new mutation [1–5, 7, 9–13, 22, 24, 41]. This mode of inheritance differs from the earlier classification by Silence et al. [24]. It has a recurrence risk of 6–7% on the basis of parental germ-line mosaicism [1, 3, 9, 10]. Rarely, inheritance may be autosomal recessive [2, 3, 7, 9–11]. Within this group there is biochemical, molecular, and genetic heterogeneity [1–5, 9–13, 22, 24, 28, 42, 51, 52].

The very severe nature of generalized osteoporosis, bone fragility, and severe intrauterine growth retardation result in death in the fetal or early perinatal period [10, 13, 24]. Of those who survive, 80–90% die by 4 weeks of age [1, 7, 10, 54]. Of these survivors, all have radiologic features typical of OI.

Sclerae are blue/black [7, 41]. Facies have a triangular shape, caused by soft craniofacial bones, and a beaked nose

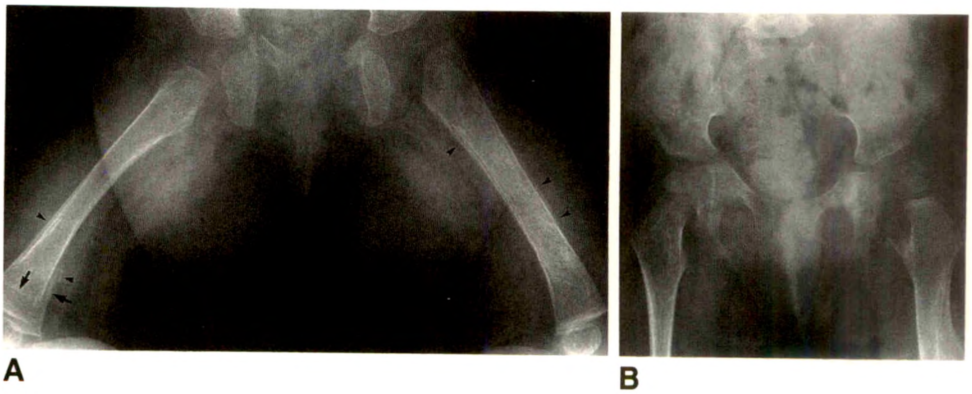

A

B

Fig. 2.—Osteogenesis imperfecta type I. Girl with dark blue sclerae, short stature (10%), joint laxity, and history of fractures of tibiae and left humerus.

***A*, At 4 months old, frontal and frog-leg lateral radiograph shows moderate osteoporosis, thin cortices, and periosteal reaction (*arrowheads*). Femoral diaphyses are widened. Left femoral head is unossified, but superolateral dislocation due to ligamentous laxity is obvious. Right distal femoral metaphysis has acute transverse fracture (*arrows*).**

***B*, At 1 year 3 months old, anteroposterior radiograph of pelvis shows osteoporosis and left hip dislocation. Note deformity of left femur due to multiple previous fractures.**

[19]. The calvarium is large relative to the face, and the skull shows a marked lack of mineralization [1, 10, 13, 24], as well as wormian bones [7, 10]. Platyspondyly may be present; the chest is small [7, 41]. Thighs are usually held in abduction and external rotation. These infants have very severe skeletal deformity, multiple fractures, and osteopenia at birth [1, 7, 10, 13, 19, 20, 24]. Limbs are short, bowed, and angulated. Three radiologic subtypes based on Silence's work [7, 13, 19, 24] and modified for international classification [22] have been identified. In both subtypes IIA and IIB, long bones are short, broad, and crumpled; in subtype IIA, however, ribs are broad with continuous beading, whereas beading is absent or discontinuous in subtype IIB (Fig. 3). Long bones are thin and fractured in subtype IIC, and ribs are thin and beaded (see Table 1).

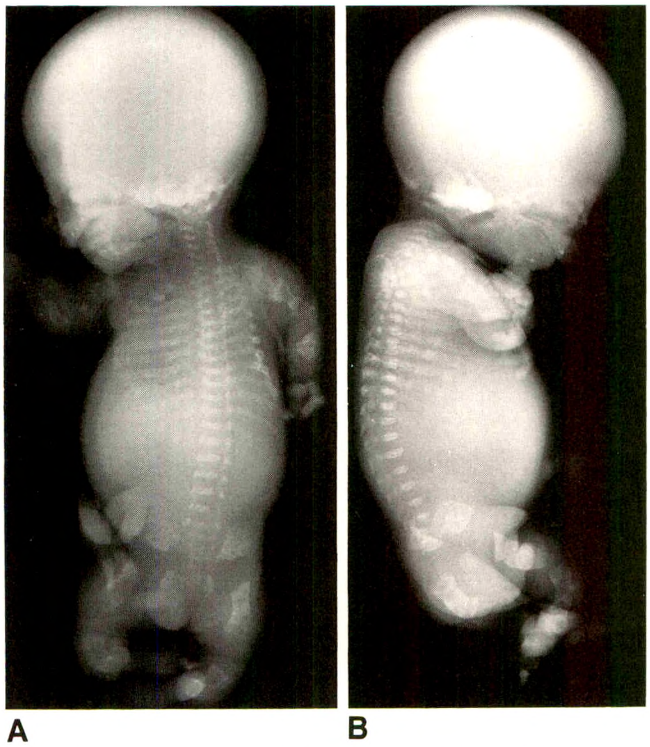

Fig. 3.—Osteogenesis imperfecta subtype IIB. Stillborn baby.
***A* and *B*, Anteroposterior (*A*) and lateral (*B*) radiographs of stillborn baby show severe osteopenia of calvarium and bony skeleton. Long bones are short, broad, and crumpled; ribs are broad with discontinuous beading. Platyspondyly is present.**

Osteogenesis Imperfecta, Type III

Type III OI is a progressive severe form. Of all patients with OI in the Victoria, Australia, study, 15% of patients had type III and the minimum incidence was 1.45/100,000 live births [13].

Type III OI, which is rare, originally was thought to be autosomal recessive in inheritance [2, 4, 6–9, 11, 13]. Autosomal recessive inheritance is rare, however, except in certain populations, such as South African blacks [2, 4, 6–9, 11]. At present, OI type III is thought to be due to sporadic autosomal dominant new mutation [1, 2, 4, 9, 13] with genetic heterogeneity [1, 2, 4, 9, 12, 13].

Bone fragility and osteopenia are severe, leading to multiple fractures and severe progressive deformity of the long bones (Fig. 4) and spine with age [1, 4, 13, 19, 41]. Bone abnormalities are generally less severe than in type II OI and more severe than in types I or IV. Fractures at birth are present in two thirds of patients [2, 16, 33], and patients have multiple fractures by age 1–2 years [7]. Most often they present with multiple rib and long bone fractures [2, 13], together with shortening, bowing, deformity, and angulation of the long bones (Fig. 5, see also Fig. 4). The frequency of fractures decreases with age, but bowing and angulation of long bones and moderate to severe kyphoscoliosis are progressive [2, 7, 13]. This leads to a most severe form of growth retardation and dwarfism in longer-surviving OI type III patients [7, 13]. Early in the process the long bones are broad, but by puberty the diaphyses become thin (Fig. 6A and 6B). Later, popcorn-type calcifications (see Fig. 4) may develop in the region of the growth plate of long bones [2, 13, 55, 56].

Sclerae are normal, pale blue, or gray at birth, but the color changes through infancy and early childhood until it is normal by adolescence or adulthood [2, 4, 13, 19]. The calvarium is large, thin, and poorly ossified, and wormian bones (Figs. 6C

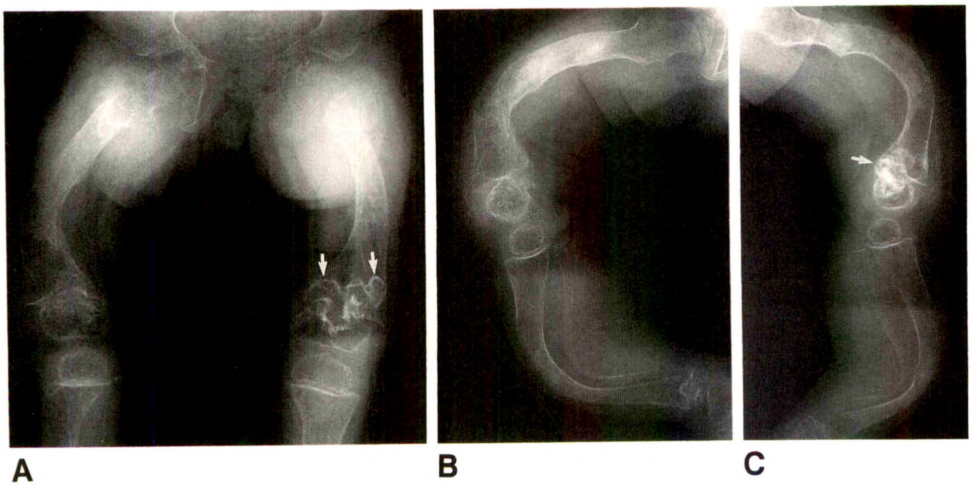

Fig. 4.—Severe osteogenesis imperfecta (OI) type III. 4-year 10-month-old girl with white sclera, wormian bones, and severe short stature. No family history of OI.
***A–C*, Anteroposterior (*A*) and lateral (*B* and *C*) radiographs of lower extremities show severe osteoporosis and thin cortices. Femora are short and broad with marked anterolateral bowing. Popcorn calcifications are seen in left distal femur (*arrows*). Thinning of diaphyses and anterior bowing of tibiae and fibulae are marked. Note healing fracture of right femur.**

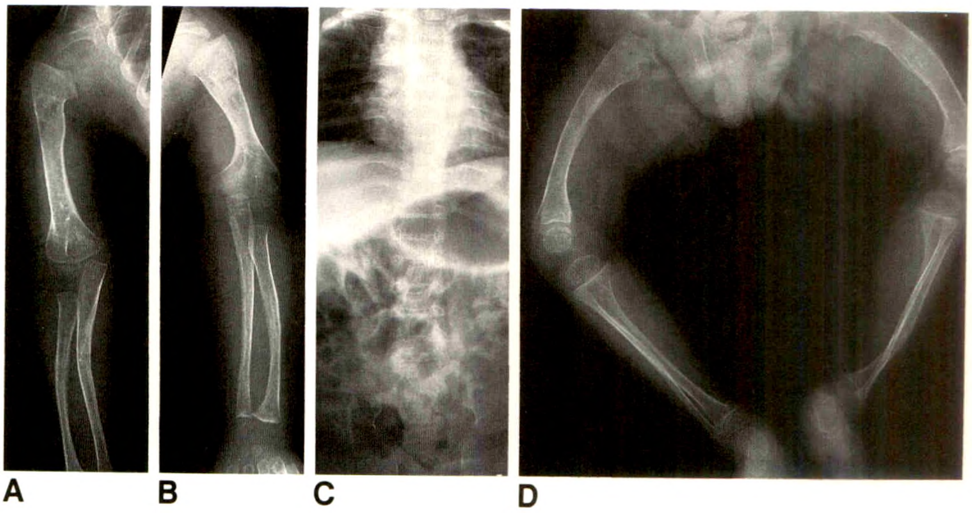

Fig. 5.—Osteogenesis imperfecta type III. 1-year 10-month-old boy with mottled teeth and blue sclera in newborn period. Sclera later changed to white. History of multiple recurrent fractures.

A and *B*, Anteroposterior radiographs of upper extremities show severe osteoporosis and shortening with deformity of both humeri. Humeral shafts are broadened; left humerus and both radii and ulnae show mild lateral bowing.

C, Anteroposterior radiograph of thoracic and lumbar spine shows severe generalized osteoporosis, platyspondyly, and thin ribs.

D, Anteroposterior radiograph of lower extremities shows lateral bowing, deformity, and shortening of both femora. Note anterolateral bowing of left tibia and thin tibial diaphyses. Cortices are thin; osteoporosis is marked.

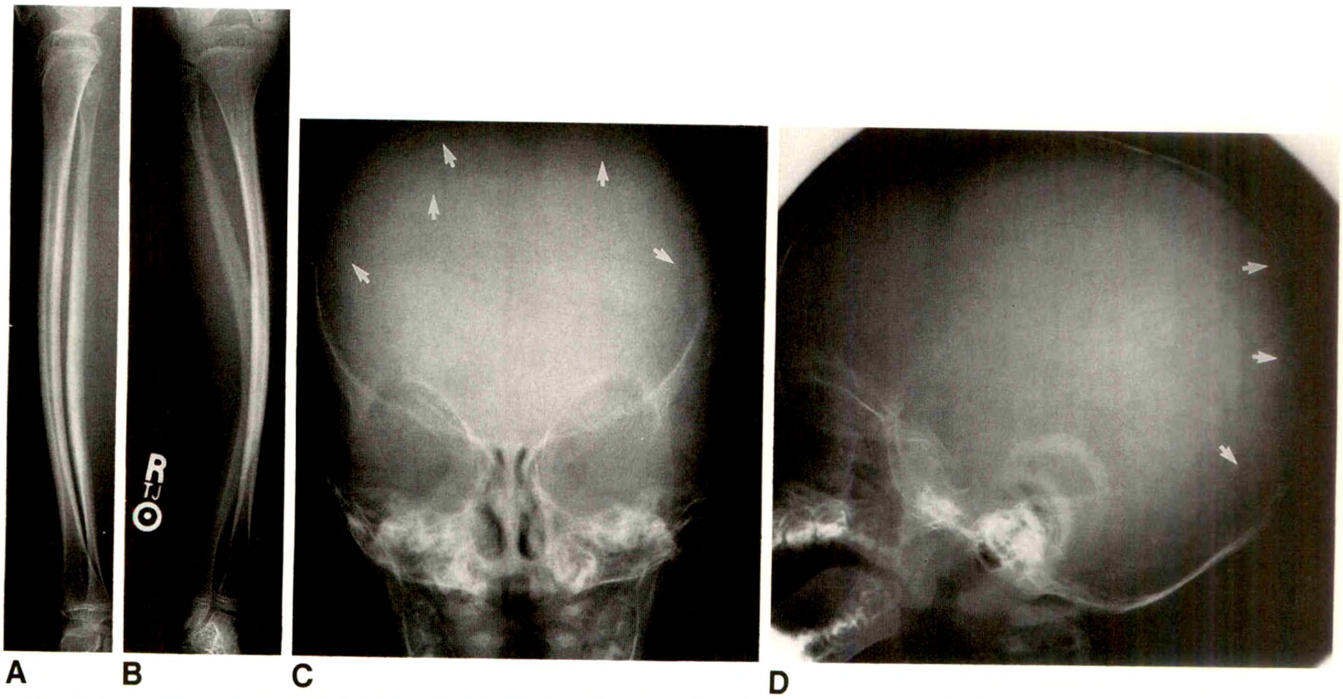

Fig. 6.—Osteogenesis imperfecta (OI) type III. 12-year 10-month-old girl with slightly blue sclerae and short stature (3%) at age 5 months. Sclera were later normal. Patient had history of multiple fractures of ribs and long bones of upper and lower extremities. Severe scoliosis was present. No family history of OI was elicited.

A and *B*, Anteroposterior (*A*) and lateral (*B*) radiographs of right tibia and fibula show long bones to be thin and gracile. Tibia and fibula show mild osteopenia and anteromedial bowing.

C and *D*, Anteroposterior (*C*) and lateral (*D*) radiographs of skull at 5 months of age show multiple wormian bones (*arrows*). Osteoporosis of calvarium is pronounced.

and 6D) are present [2, 7, 13]. Triangular facies (Fig. 7), due to soft craniofacial bones and relative frontal and temporal bossing, occur in 85% of patients [7, 13]. Although this feature is seen in OI, it is not specific enough to be diagnostic for this condition. Fontanelles and sutures may be abnormally wide [7]. Patients die because of associated cardiopulmonary complications and pulmonary hypertension related to severe kyphoscoliosis and severe bone fragility [2, 4, 7, 13]. In a study by Silence et al. [2] of 17 patients with OI type III, 41% (7/17) were surviving long term (four at preschool age, two in the third decade, and one in the fourth decade), 53% (9/17) died (four in first year, and five in the second and third decades), and 6% (1/17) were aborted in utero. Eighty-eight percent of patients with OI type III in Silence's study were handicapped or had severe difficulty in walking [13]. Other common features include ligamentous laxity (50% of patients) [13], dentinogenesis imperfecta (45%) [13], easy bruising (26%) [13], and hearing loss 5% [2, 4, 13].

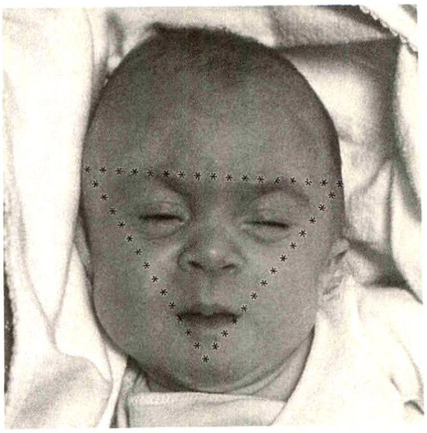

Fig. 7.—Osteogenesis imperfecta type III. 1-year 3-month-old girl with white sclera, osteoporosis, bowed femora and tibiae, history of multiple fractures, deformed chest due to old rib fractures and scoliosis, and mitral regurgitation due to mitral valve prolapse. Photograph shows triangular facies due to soft craniofacial bones with relative temporoparietal bossing and small chin. Nasal root is underdeveloped and nose slightly upturned. Left ear is posteriorly rotated and lower than right ear.

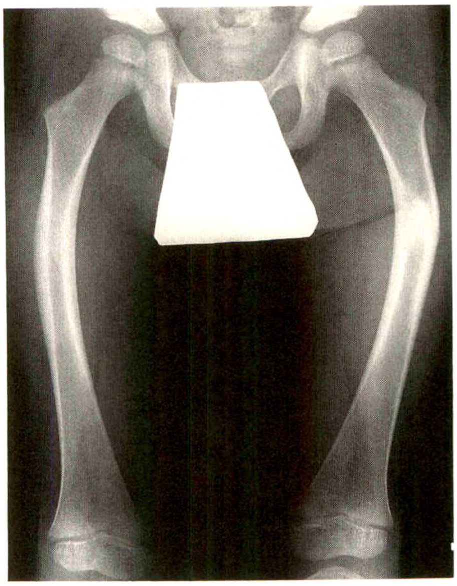

Fig. 8.—Mild osteogenesis imperfecta type IV. 4-year-old boy with white sclerae, hyperextensible joints, discolored teeth, wormian bones, and history of previous femoral, clavicular, and skull fractures. In infancy, his mother had blue sclera and fractures. Inheritance was autosomal dominant. Skin biopsy showed abnormal type I collagen in patient and mother. Anteroposterior radiograph of both femora shows mild anterolateral bowing. Cortex is normal in thickness but trabeculae are prominent because of mild osteopenia. A band of sclerosis reflects an old healed fracture of proximal left femur.

Osteogenesis Imperfecta, Type IV

Type IV OI is a rare type of osteogenesis imperfecta [13, 19, 20, 23, 32, 36, 37]. Of all patients with OI in the Victoria, Australia, study, 5% of patients had type IV and the minimum incidence was not indicated [13]. Type IV OI is inherited as an autosomal dominant trait [4, 5, 7, 9, 13, 19, 20, 23, 29, 37, 53]; only a few families with the disorder have been documented [7, 13, 20, 23, 36, 37]. Sporadic cases due to new dominant mutations also have been reported [1, 9, 19, 23]. The type IV phenotype is genetically heterogeneous [9, 12, 29, 31, 32, 36, 40, 53]. Characteristically, osteoporosis [7, 13], bone fragility, and deformity are present (Fig. 8); however, bone fragility and deformity vary in severity from mild to moderate [7, 12, 13, 20, 23, 36]. Fractures at birth are present in 28–32% of patients (compared with 12% in OI type I) [20, 23, 34]. The total number and frequency of fractures vary widely at specific ages but decrease markedly after puberty [7, 20, 23]. History of fracture may or may not be present [13]. Bones may be normal if no fracture has occurred [23] and may be normal (with minimal or no osteoporosis) at the time of first fracture [7, 20, 23]. Demineralization, bowing deformities, and thinning of cortex occur later at various ages, resulting from fractures [8] and immobilization [20, 23]. Fractures heal at a normal rate [7]. Rarely, a severe form of OI type IV may mimic a relatively mild form of OI type III, and in these cases skeletal manifestations are obvious. The bony changes in mild OI type IV and mild OI type I (see Figs. 1 and 8) may be similar, but these types of OI should be easily distinguished by correlating the sclera color.

Sclerae most frequently are normal [13, 23, 36], but they may be pale blue (not gray or distinctly blue) in early childhood and become normal in adolescence or adulthood [7, 20, 23]. It is worthwhile to note that pale blue sclerae may be seen in some normal children up to 3–4 months old. The incidence of hearing impairment is low [7, 13, 20, 23] and is lower than it is in OI type I. In one study of OI type IV, deafness in patients more than 30 years old was 29% [20]. Two subtypes of OI type IV have been identified on the basis of normal dentition (subtype IVA) and the presence of dentinogenesis imperfecta (subtype IVB) [7, 20, 23, 41]. Abnormal dentition is more common in type IV than in type I [4, 20]. Mild to moderate short stature is common [4, 7, 12, 23, 36, 41]. In the majority of patients, wormian bones are present [7]. Basiliar impression has been reported in OI types I, III, and IV, but it is rare [7, 57, 58]. The incidence of nosebleeds and bruising is much less common than in type I [7].

The clinical features, as evaluated by Paterson and colleagues [23] through questionnaires completed by parents in 78 patients with OI subtype IVA from a total of 834 patients with OI, are given in Table 2. However, his methodology has several scientific flaws.

In a study by Paterson et al. [23] of OI subtype IVA, the number of fractures between birth and 5 years ranged from zero to more than 20; fracture-free periods also occurred. Fractures at birth were present in 32% of patients with OI subtype IVA (compared with 12% in OI type I) [20, 23], and 75% had their first fracture by age 2 years. Eighty-nine percent of patients were less than 5 years old at the time of the first fracture [23]; 99% experienced their first fracture by age 9. The number of fractures declined after puberty [7, 20, 23].

Paterson et al. [20] examined radiographs of 11 (23%) of 48 patients with OI type IV that apparently showed no osteoporosis at the time of first fracture. However, only one radiograph with classic bowing of the tibiae and fibulae characteristic of OI was included in their paper. No further systematic

TABLE 2: Clinical Features of Osteogenesis Imperfecta Subtype IVA[a]

Feature	Frequency (%)
Height	
<2 SD	68
<4 SD	41
Fractures	
Ribs	40
Skull	28
Sclerae	
White	56
White but earlier pale blue	30
Pale blue	13
Teeth	
No or few fillings	88
Crumbling and/or more than average decay	12
Nosebleeds	30
Easy bruising	32
Deafness	13
Hernia	10
Excessive sweating	60
Dislocated joints	27
Double jointedness	51

[a] Modified after Paterson et al. [23]

description of radiographs (including skulls) was given. Also, systematic description of associated abnormalities was not detailed, and all data were obtained from questionnaires filled out by patients and/or parents.

From the total of 78 patients with OI subtype IVA, Paterson et al. [23] investigated only 17 sets of radiographs (22%), which included only 11 skull radiographs (14%). Of these, 9% had significant (>10) wormian bones, 45.5% had one to 10 wormian bones, and 45.5% had no wormian bones. No comment was made on association of wormian bones with osteoporosis. Metaphyseal fractures were shown in 24% (4/17) of examined radiographs, normal bones at the time of first fracture were shown in 59% (10/17), but in 18% (3/17) osteoporosis developed later. No comment was made regarding the remaining patients. As in his earlier work [20], no further detailed data were given. No radiographs of patients with OI subtype IVA are presented in his paper to verify his radiologic findings [23]. In this study, the prevalence of skull fractures was unusually high (28%). The reason for this was questioned by Carty and Shaw [59], who raised the possibility of misdiagnosis of OI for actual child abuse.

Obviously, Paterson's studies are flawed and incomplete because only a small percentage of radiographs of patients with OI type IV [20] and subtype IVA [23] were reviewed. Also, only sporadic comments were made on associated radiologic and clinical features of individual patients [23, 59]. Radiologic documentation to support his findings is lacking. Further detailed information about these cases of OI type IV is needed to make an accurate assessment and conclusion. The validity of Paterson's work has been questioned before [59]. Paterson and colleagues did not explain how they diagnose OI subtype IVA with neither radiologic confirmation nor progressive deformity (except fractures), without family history, with normal sclera and teeth, and without fracture recurrence in protective environment [14, 59–62]. It would indeed be difficult to diagnose OI without at least some other definite feature of OI. The rarity of sporadic (without family history) type IV OI can be appreciated from understanding that the probability of encountering a child with this type of OI in a large city (population 500,000) is estimated by Taitz to be between 1/1,000,000 and 1/3,000,000 births [14]; thus, one case might occur every 100 to 300 years. These numbers are based on a study by Silence et al. [13] in which nine of 180 patients with OI had OI type IV; only one of those instances was a sporadic case with no family history. Paterson and coworkers' studies [20, 23] of OI type IV are also sources of these estimates.

Distinguishing Osteogenesis Imperfecta from Child Abuse

Patient and family history, physical examination, diagnostic imaging, and the clinical course all contribute to the distinction of OI from child abuse. The major features of OI are discussed in the preceding sections and are summarized in Table 3. The features in clinical history and physical examination that are helpful to the radiologist in diagnosing child abuse [63–65] are listed in Table 4, and the salient radiologic features of child abuse [33, 64–68] are summarized in Table 5. The keys to distinguishing OI from abuse are the presence of blue sclera or abnormal teeth; investigation of clinical and family

TABLE 3: Summary of the Salient Features of Osteogenesis Imperfecta

1. Bone fragility, fractures, osteoporosis
2. Blue sclerae
3. Deafness or hearing impairment
4. Dentinogenesis imperfecta
5. Wormian bones
6. Positive family history of hearing impairment, dentinogenesis imperfecta, osteogenesis imperfecta, and/or history of fractures or bone deformity
7. Ligamentous laxity and hypermobility of joints
8. Abnormal temperature regulation (heat intolerance, excessive sweating)
9. Easy bruising
10. Fragile skin
11. Short stature, growth retardation
12. Progressive scoliosis
13. Fractures continue in protected environment

TABLE 4: Features in Clinical History and Physical Examination Helpful to the Radiologist in Diagnosing Child Abuse

1. Injury with cause or extent not compatible with a given history
2. Inconsistent or conflicting history
3. Lack of history of significant trauma in patient with fractures
4. Lack of or delay in seeking appropriate medical attention for an injury
5. Retinal hemorrhages
6. Specific bruises (e.g., palmprints, fingerprints, strap marks), bruises in unusual places (perineum), human bites, and cigarette burns
7. Lack of blue sclera
8. Lack of clinical features or family history of osteogenesis imperfecta (see Table 3)

TABLE 5: Radiologic Features of Child Abuse[a]

1. Bucket-handle and metaphyseal corner fractures
2. Multiple rib fractures, especially posterior rib fractures
3. Multiple fractures and/or multiple fractures showing different stages of healing
4. Scapular, acromial, or sternal fractures
5. Transverse, oblique, or spiral fractures of long bones in nonambulatory infants in the absence of significant accidental trauma or fracture inconsistent with given history
6. Fracture separations of distal humeral epiphysis or distal femoral epiphysis (suggestive but nondiagnostic of abuse)
7. Unsuspected fractures found in patient without history of trauma
8. Unexplained fractures associated with normal bone mineralization
9. Lack of repeated fractures in a protective environment
10. Visceral injuries such as duodenal or jejunal hematomas
11. Head injuries not compatible with mechanism of injury or unexplained, such as subdural hematoma, subarachnoid hemorrhage, diffuse cerebral edema, intracerebral hematoma, and skull fracture; although head injuries can be the result of child abuse, they are not distinctive and look like abnormalities of other cause

[a] Adapted from Silverman [33], Kleinman [64], Hilton [65], Kleinman et al. [66], Radkowski et al. [67], and Kirks [68].

history; physical examination; and radiologic examination for detection of wormian bones, osteoporosis, metaphyseal corner fractures and bucket-handle fractures or other fractures typical of abuse. Metaphyseal corner fractures and bucket-handle fractures (Fig. 9A) are virtually pathognomonic and highly specific features of child abuse [64–66]. They both result from the same pathologic injury and are simply variations in appearance due to different radiographic projections [64, 66]. These types of fractures occur in relatively young infants, usually less than 1 year old, and are highly specific for abuse. The pattern of injury is different from more extensive metaphyseal fractures that may involve the growth plate in older children or metaphyseal fractures in OI, which correspond to type II fractures of the Salter classification. These fractures should be clearly distinguished from abuse-specific metaphyseal lesions in young infants. It must be stressed that the presence of multiple rib fractures (Fig. 9B), especially posterior rib fractures [64, 65, 69] near or at the costovertebral junction (Fig. 10); multiple fractures and/or multiple fractures showing different stages of healing (Fig. 11, see also Fig. 9); and sternal or scapular fractures, especially acromial (see Figs. 11B and 11C), are highly specific of child abuse [64–66]. Transverse, oblique, or spiral fracture of a long bone with normal mineralization (see Fig. 9C) in the absence of significant accidental trauma or fracture inconsistent with given history, especially in a nonambulatory infant, are also highly suggestive of child abuse [64–67].

Blue Sclerae and Osteoporosis

Types I and II of OI easily are distinguished from child abuse simply by the presence of blue sclerae. Of 392 OI patients in a pedigree of 60 families, 370 had blue sclerae [14, 70]. In addition to the child, the parents of OI type I patients should be examined for the presence of blue sclerae. Furthermore, most children with OI type II are stillborn or die in the perinatal period and are easily recognized by the severe radiologic skeletal deformities and osteopenia [1, 13, 14, 20, 24] (Fig. 3).

Most cases of OI type III with normal sclerae cannot be confused with child abuse because of the severe nature of skeletal deformities [1, 14], marked dwarfism, and the presence of osteoporosis (Figs. 4–6). However, a mild case of type III with normal sclerae initially may cause problems in diagnosis if the skeletal manifestations are not correlated with clinical history, family history, and physical examination. Family history and medical records of family members should always be reviewed for features of OI.

Wormian Bones

Cremin et al. [71] defined significant wormian bones, as opposed to normal developmental variants, as "sutural bones which are 6 mm by 4 mm (in diameter) or larger, in excess of 10 in number, with a tendency to arrangement in a mosaic pattern." The presence of significant wormian bones on skull radiographs (see Figs. 6B and 6C), a feature absent in normal skulls [71], is a strong indicator of OI [63] or other abnormal conditions as listed below. In the study of Cremin et al. [71], 88% of 81 patients with proved OI had significant wormian bones. The absence of this feature is strong evidence against osteogenesis imperfecta [14, 63], although Paterson and McAllion [23, 60] state that the absence of wormian bones does not exclude OI. The neonatal period may present some difficulties because the skull may be insufficiently ossified or too small to evaluate for wormian bones [71]. Cremin et al. [71] found that essentially all patients with OI except some neonates (6/81) and adults (4/81) with technically poor radiographs had wormian bones. Thus, good-quality skull radiographs (lateral, frontal, and Towne views) later in infancy may be helpful for further evaluation for wormian bones. Consistent significant wormian bones are not unique to OI; they may also be seen in cleidocranial dysostosis, cretinism, pachydermoperiostosis, Jansen-type metaphyseal dysplasia, Menkes syndrome, acroosteolysis, Prader-Willi syndrome, and trisomy F translocation. Inconsistent significant wormian bones may be seen in pyknodysostosis, sclerosteosis, hydrocephalus, osteopetrosis, aminopterin-induced syndrome, Down syndrome, Hallerman-Strieff syndrome, otopalatodigital syndrome, rickets, hypophosphatasia, and progeria [68, 71, 72].

Metaphyseal Corner Fractures

Metaphyseal corner fractures and bucket-handle fractures (see Figs. 9A, 11B, 11C, and 11D) are virtually pathognomonic and highly specific for child abuse [33, 63, 64, 66, 68]. In OI, this feature is extremely rare and fractures are seen primarily in the diaphyses of long bones [63]. Metaphyseal corner fractures have been reported by Astley [73] in 17% of patients with OI and by Paterson et al. [23] in 23% of patients with OI subtype IVA. In all of Astley's patients [73], metaphyseal corner fractures invariably were seen together with generalized bone disease, including osteoporosis, abnormal bone modeling, deformities or fractures, and wormian bones in the

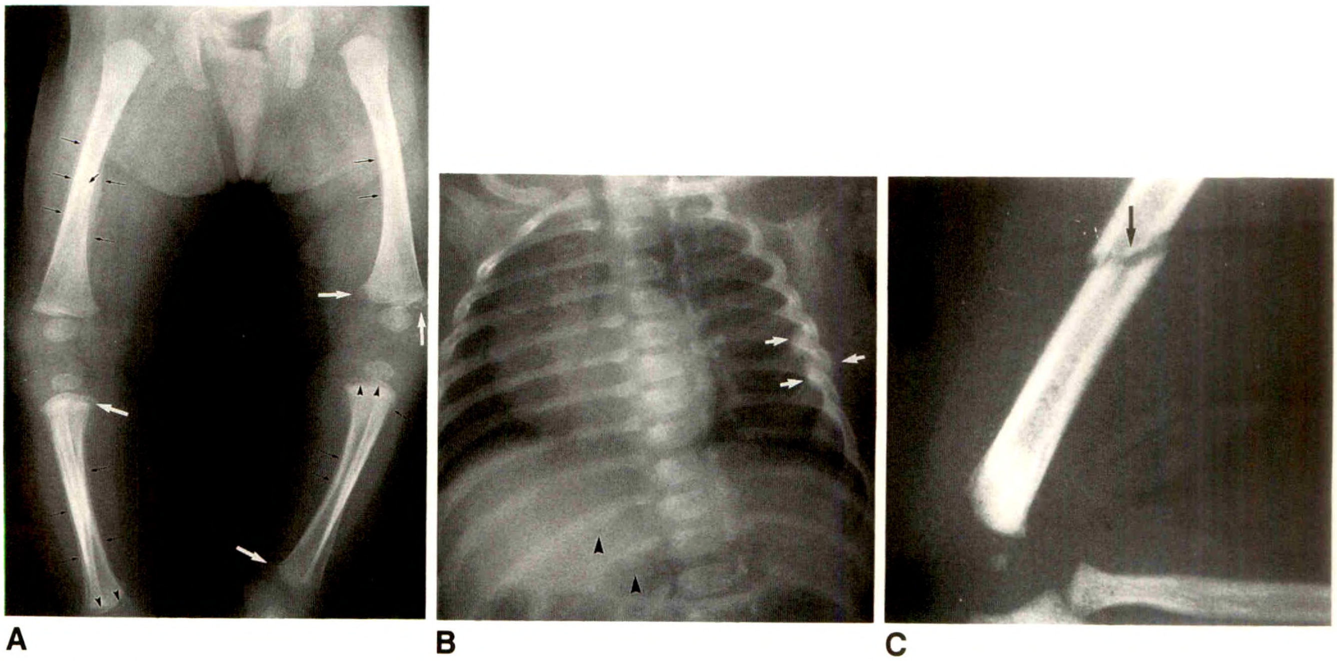

Fig. 9.—Child abuse. 1-month 10-day-old girl.

A, Anteroposterior radiograph of lower extremities shows metaphyseal corner fractures (*white arrows*) and bucket-handle fractures (*arrowheads*), virtually pathognomonic and highly specific of child abuse. Note healing spiral fracture of right femur (*short black arrow*) with surrounding periosteal reaction (*long black arrows*). Fractures are at different stages of healing. Periosteal reaction is also seen along shafts of left femur and both tibiae (*long black arrows*). Bone mineralization is normal.

B, Anteroposterior radiograph of chest and abdomen shows healing fractures of the left fifth to seventh ribs (*arrows*) and right posterior 10th and 11th ribs (*arrowheads*) with surrounding callus, typical of child abuse. Rib fractures are at an older stage of healing than fractures of proximal tibiae in *A*.

C, Lateral radiograph of left elbow of same patient at 21 days old shows an acute fracture of midshaft of left humerus (*arrow*). This fracture cannot be related to birth trauma because there is no visible periosteal reaction. Bones are of normal mineralization.

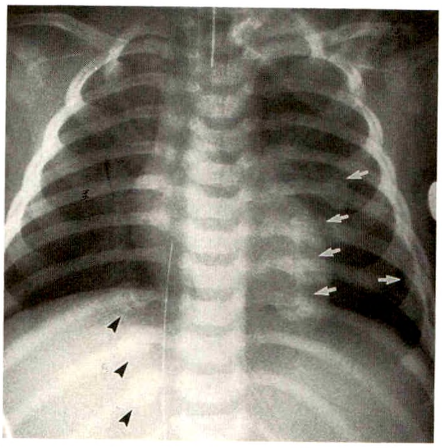

Fig. 10.—Child abuse. 2-month-old boy. Anteroposterior chest radiograph shows multiple fractures with surrounding callus of left posteromedial sixth–ninth ribs and lateral sixth rib (*arrows*), and right posterior ninth to 11th ribs (*arrowheads*) at or near costovertebral junctions, highly specific for child abuse.

skull. In the study of Paterson et al. [23], no comment is made on whether the metaphyseal corner fractures were associated with osteoporosis, deformities, or wormian bones in individual patients. This study [23], as mentioned earlier, is limited by the fact that only 22% of the radiographs of the patients with OI subtype IVA were reviewed. The presence of metaphyseal corner fractures or bucket-handle fractures without osteoporosis and/or wormian bones is diagnostic of child abuse [63–67].

Potentially Difficult Cases

The most difficulty in distinguishing OI from child abuse might occur in patients with mild cases of OI type III or OI type IV, especially in patients with OI subtype IVA and normal teeth [1, 14, 23, 74]. In both instances, patients and parents may have normal sclerae, and with autosomal dominant new mutation there may be no family history; moreover, radiographs may be evaluated without the benefit of pertinent clinical history. Yet, in mild OI type III and severe type IV, osteoporosis and/or wormian bones should be present, as should at least some other associated features of OI. The patient's physical examination and clinical history also must be correlated with regard to features of OI for proper diagnosis.

Mild OI type IV, on the other hand, might present more difficulty if mild osteoporosis is not observed carefully, or if osteoporosis is minimal or absent at the time of the first fracture. Family history may be absent in rare autosomal dominant new mutation. In sporadic cases of the rare form of mild OI type IV, theoretically a patient could present with normal sclerae, one or more fractures or no fracture, minimal or no osteoporosis, no family history, no hearing impairment,

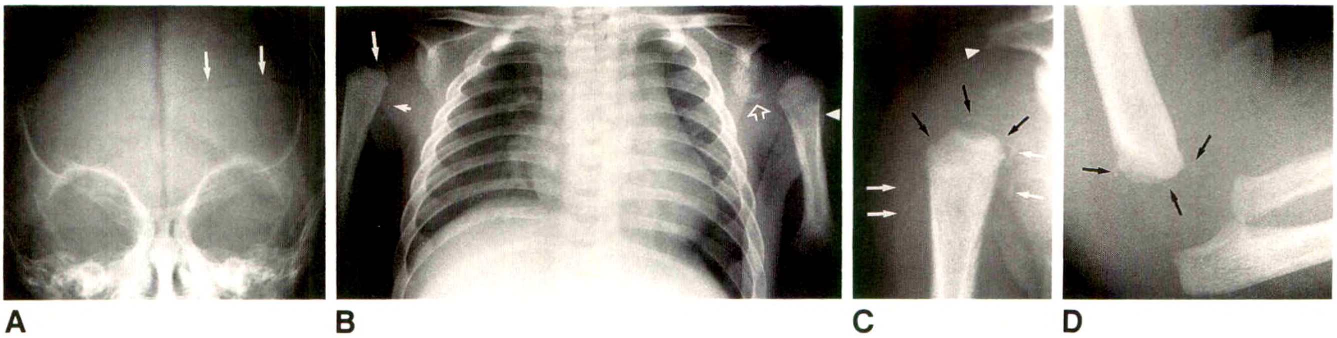

Fig. 11.—Child abuse. 4-month-old boy.

A, Anteroposterior radiograph of skull shows a linear left parietal skull fracture (*arrows*) associated with mild diastasis of sagittal suture. Skull is well mineralized with no evidence of wormian bones.

B, Anteroposterior radiograph of chest shows a healing fracture of inferior glenoid of left scapula with callus (*open arrow*). A bucket-handle fracture of proximal right humerus (*long solid arrow*), virtually pathognomonic and highly specific for child abuse, is associated with elevated medial periosteal reaction (*short solid arrow*) due to subperiosteal hematoma. Periosteal reaction is present along lateral shaft of left proximal humerus (*arrowhead*).

C, Magnified anteroposterior radiograph of right humerus seen in *B* better shows bucket-handle fracture of the proximal right humerus (*black arrows*) with elevated periosteal reaction indicating subperiosteal hematoma (*white arrows*) and a small right acromion avulsion fracture (*arrowhead*), highly specific of child abuse. Bone mineralization is normal.

D, Magnified lateral view of left elbow shows a bucket-handle fracture (*arrows*) of distal humerus, virtually pathognomonic of child abuse. Bones are normally mineralized.

normal teeth (if subtype IVA), and no fracture recurrence after removal from home (fracture-free period) [14]. The combination of all these events together, however, would be very rare, as detailed earlier. Thus, only the sporadic case representing an uncommon mild form of OI type IV might create difficulty in being distinguished from child abuse [14]. However, if clinical and historical features are scrutinized along with the radiographs, this should not create a significant problem in the majority of patients. Sporadic occurrence of OI type IV is rare, as detailed earlier, whereas child abuse is common. In otherwise normal bones and in the absence of features typically associated with OI, unexplained fractures are much more likely to represent child abuse than this rare form of OI [14, 59, 62, 63, 74, 75].

On the other hand, Acland [61] speculates that approximately 1% of parents of children with bone disease (15 cases a year) may be convicted unjustly of abuse of children when injuries actually were due to bone disease [74]. There have been sporadic reports in the literature of children diagnosed as victims of abuse and kept in protective care who later were found to have OI type IV [20, 38, 60]. Unfortunately, several publications pertaining to osteogenesis imperfecta and child abuse have been written by Paterson and colleagues [20, 23, 38, 39, 60]. Paterson is active in the field of abuse and is a member of the Department of Biochemical Medicine, Ninewells Hospital and Medical School at the University of Dundee. Paterson's work, as detailed earlier under type IV OI, has a weak scientific basis. His work, although partially based on radiologic assessments, lacks strong radiologic support. Taitz [62] reports that a court was not convinced by Paterson's evidence that an abused child had OI, a judge rejected Paterson's testimony in a wardship case, and another court case rejected his evidence. Despite this fact, writings of Paterson et al. provide potential ammunition for aggressive lawyers seeking to undermine clear-cut cases of child abuse.

If, after a complete clinical history and family history have been obtained and a careful physical examination and proper skeletal survey have been performed, confusion remains as to the proper diagnosis of OI vs child abuse, a punch biopsy of the skin for collagen analysis may be helpful. With the use of local anesthesia, a small, 2- to 3-mm biopsy specimen can be obtained and placed in a standard tissue-culture medium. This can be sent to a cell-culture facility and then to a principal investigator of type I collagen abnormalities for collagen analysis [10, 12, 31, 32, 52]. This can be facilitated through a regional genetic counseling center or the sample can be shipped directly after contacting the research laboratory for handling instructions. The amounts of collagen synthesized from this cell culture can be assessed, looking for defects in the production of the proα1(I) chains or the proα2(I) chain. If such defects are found, the biochemical diagnosis of osteogenesis imperfecta is confirmed. In a few cases of OI type III, a biochemical defect has not been found, but the clinical and radiologic findings are usually severe and allow an appropriate diagnosis.

When entertaining the possibility of OI in a case of suspected child abuse, the pediatrician, orthopedist, geneticist, and radiologist must work together in a coordinated effort to arrive at the proper diagnosis. Thus, in the presence of unexplained fractures or fractures typical for child abuse, the possibility of OI is unlikely without the presence of some other associated clinical features of OI: blue sclerae, osteoporosis, dentinogenesis imperfecta, hearing loss or impairment, joint laxity or hypermobility, wormian bones, short stature, excessive sweating, easy bruising and nosebleeds, or family history of hearing impairment, dentinogenesis imperfecta, OI, or fractures (see Table 3). The key to the distinction is the correlation of clinical history, physical examination, family history, and radiologic findings.

ACKNOWLEDGMENT

We gratefully acknowledge the expert assistance of Shirley Ellis in the preparation of the manuscript.

REFERENCES

1. Thompson EM, Young ID, Hall CM, Pembrey ME. Recurrence risks and prognosis in severe sporadic osteogenesis imperfecta. *J Med Genet* **1987**;24:390–405
2. Silence DO, Barlow KK, Cole WG, Dietrich S, Garber AP, Rimoin DL. Osteogenesis imperfecta type III: delineation of the phenotype with reference to genetic heterogeneity. *Am J Med Genet* **1986**;23:821–832
3. Young ID, Thompson EM, Hall CM, Pembrey ME. Osteogenesis imperfecta type IIA: evidence for dominant inheritance. *J Med Genet* **1987**;24:386–389
4. Byers PH. Osteogenesis imperfecta: an update. In: Blizzard RM, ed. *Growth, Genetics and Hormones* (newsletter). New York: Biomedical Information Corp., **1988**;4:1–5
5. Smith R. The molecular genetics of collagen disorders. *Clin Sci* **1986**;71:129–135
6. Beighton P, Versfeld GA. On the paradoxically high relative prevalence of osteogenesis imperfecta type III in the black population of South Africa. *Clin Genet* **1985**;27:398–401
7. Silence DO. Osteogenesis imperfecta nosology and genetics. *Ann NY Acad Sci* **1988**;543:1–15
8. Beighton P, Wallis G, Viljoen D, Versfeld G. Osteogenesis imperfecta in southern Africa. *Ann NY Acad Sci* **1988**;543:40–46
9. Byers PH, Bonadio JF, Cohn DH, Starman BJ, Wenstrup RJ, Willing MC. Osteogenesis imperfecta: the molecular basis of clinical heterogeneity. *Ann NY Acad Sci* **1988**;543:117–128
10. Byers PH, Tsipouras P, Bonadio JF, Starman BJ, Schwartz RC. Perinatal lethal osteogenesis imperfecta (OI type II): a biochemically heterogeneous disorder usually due to new mutations in the genes for type I collagen. *Am J Hum Genet* **1988**;42:237–248
11. Steinmann B, Superti-Furga A, Royce PM. Imperfect collagenesis in osteogenesis imperfecta: the consequences of cysteine-glycine substitutions upon collagen structure and metabolism. *Ann NY Acad Sci* **1988**;543:47–61
12. Cohn DH, Byers PH. Osteogenesis imperfecta and other inherited disorders of the structure and synthesis of type I collagen: models for the analysis of mutations that result in inherited chondrodysplasias. *Pathol Immunopathol Res* **1988**;7:132–138
13. Silence DO, Senn A, Danks DM. Genetic heterogeneity in osteogenesis imperfecta. *J Med Genet* **1979**;16:101–116
14. Taitz LS. Child abuse and osteogenesis imperfecta. *Br Med J* **1987**;295:1082–1083
15. Sykes B, Ogilvie D, Wordsworth P, Anderson J, Jones N. Osteogenesis imperfecta is linked to both type I collagen structural genes. *Lancet* **1986**;2:69–72
16. Goldman AB. Collagen diseases, epiphyseal dysplasias and related conditions. In: Resnick D, Niwayama G, eds. *Diagnosis of bone and joint disorders*, 2nd ed., vol. 5. Philadelphia: Saunders, **1988**:3374–3441
17. Prockop DJ. Osteogenesis imperfecta: a model for genetic causes of osteoporosis and perhaps several other common diseases of connective tissue. *Arthritis Rheum* **1988**;31:1–8
18. Thalmann I, Thallinger G, Thalmann R. Otosclerosis: a local manifestation of a generalized connective tissue disorder? *Am J Otolaryngol* **1987**;8:308–316
19. Silence D. Osteogenesis imperfecta: an expanding panorama of variants. *Clin Orthop* **1981**;159:11–25
20. Paterson CR, McAllion S, Miller R. Osteogenesis imperfecta with dominant inheritance and normal sclerae. *J Bone Joint Surg [Br]* **1983**;65-B:35–39
21. Byers PH, Bonadio JF, Steinman B. Osteogenesis imperfecta: update and perspective (invited editorial comment). *Am J Med Genet* **1984**;17:429–435
22. Beighton P, dePaepe A, Danks D, et al. International nosology of heritable disorders of connective tissue, Berlin, 1986. *Am J Med Genet* **1988**;29:581–594
23. Paterson CR, McAllion SJ, Shaw JW. Clinical and radiological features of osteogenesis imperfecta type IVA. *Acta Paediatr Scand* **1987**;76:548–552
24. Silence DO, Barlow KK, Garber AP, Hall JG, Rimoin DL. Osteogenesis imperfecta type II: delineation of the phenotype with reference to genetic heterogeneity. *Am J Med Genet* **1984**;17:407–423
25. Maroteaux P, Frézal J, Cohen-Solal L. The differential symptomatology of errors of collagen metabolism: a tentative classification. *Am J Med Genet* **1986**;24:219–230
26. Harper PS. Osteogenesis imperfecta (editorial). *J Med Genet* **1987**;24:385
27. Cetta G, Ramirez F, Tsipouras P. Third International Conference on Osteogenesis Imperfecta. *Ann NY Acad Sci* **1988**;543:1–187
28. Ramirez F, DeWet W. Molecular biology of human fibrillar collagen genes. *Ann NY Acad Sci* **1988**;543:109–116
29. Cohn DH, Wenstrup RJ, Willing MC, Bonadio JF, Byers PH. General strategies for isolating the genes encoding type I collagen and for characterizing mutations which produce osteogenesis imperfecta. *Ann NY Acad Sci* **1988**;543:129–135
30. Thompson EM, Young D, Hall CM, Pembrey ME. Genetic counselling in perinatally lethal and severe progressively deforming osteogenesis imperfecta. *Ann NY Acad Sci* **1988**;543:142–156
31. Cohn DH, Apone S, Eyre DR, et al. Substitution of cysteine for glycine within the carboxyl-terminal telopeptide of the α1 chain of type I collagen produces mild osteogenesis imperfecta. *J Biol Chem* **1988**;263:14605–14607
32. Wenstrup RJ, Cohn DH, Cohen T, Byers PH. Arginine for glycine substitution in the triple-helical domain of the products of one α2(I) collagen allele (COL1A2) produces the osteogenesis imperfecta type IV phenotype. *J Biol Chem* **1988**;263:7734–7740
33. Silverman FN. *Caffey's pediatric x-ray diagnosis*, 8th ed. Chicago: Year Book Medical, **1985**:617–621,780–785
34. Falvo KA, Root L. Osteogenesis imperfecta tarda. *J Hosp Special Surg* **1975**;1:44–51
35. Falvo KA, Root L, Bullough PG. Osteogenesis imperfecta: clinical evaluation and management. *J Bone Joint Surg [Am]* **1974**;56-A:783–793
36. Wenstrup RJ, Tsipouras P, Byers PH. Osteogenesis imperfecta type IV. *J Clin Invest* **1986**;78:1449–1455
37. Tsipouras P, Schwartz RC, Goldberg JD, Berowitz RL, Ramirez F. Prenatal prediction of osteogenesis imperfecta (OI Type IV): exclusion of inheritance using a collagen gene probe. *J Med Genet* **1987**;24:406–409
38. Paterson CR. Osteogenesis imperfecta in the differential diagnosis of child abuse. *Child Abuse Negl* **1977**;1:449–452
39. Paterson CR, McAllion SJ, Miller R. Heterogeneity of osteogenesis imperfecta type I. *J Med Genet* **1983**;20:203–205
40. Wallis G, Beighton P, Boyd C, Mathew CG. Mutations linked to the pro α2(I) collagen gene are responsible for several cases of osteogenesis imperfecta type I. *J Med Genet* **1986**;23:411–416
41. Byers PH, Wenstrup RJ, Bonadio JF, Starman B, Cohn DH. Molecular basis of inherited disorders of collagen biosynthesis: implications for prenatal diagnosis. *Curr Probl Dermatol* **1987**;16:158–174
42. Maroteaux P, Cohen-Solal L, Bonaventure J. Clinical and genetical heterogeneity of osteogenesis imperfecta. *Ann NY Acad Sci* **1988**;543:16–29
43. Pontz BF, Stoss H, Spranger J. Heterogeneity in osteogenesis imperfecta: clinical and morphological findings. *Ann NY Acad Sci* **1988**;543:30–39
44. Hollister DW, Gaudette ND, Rao VH. Collagen studies in an osteogenesis imperfecta type III family. *Ann NY Acad Sci* **1988**;543:62–72
45. Tenni R, Cetta G, Dyne K, Valli M, Zanaboni G, Castelliani A. Severe nonlethal osteogenesis imperfecta: biochemical heterogeneity. *Ann NY Acad Sci* **1988**;543:73–82
46. Royce PM, Superti-Furga A, Rao VH, Steinmann B. Normal thermal stability of an overmodified type I collagen despite a structural mutation within the triple helical region in a case of osteogenesis imperfecta type IVB. *Ann NY Acad Sci* **1988**;543:83–84
47. Superti-Furga A, Royce PM, Pistone FM, Romano C, Steinmann B. Delayed triple-helix formation of abnormal type I collagen is corrected by reduced temperature. *Ann NY Acad Sci* **1988**;543:85–92
48. Van der Rest M, Machan J, Dufour L. Defining structural defects in type I collagen by protein analysis? *Ann NY Acad Sci* **1988**;543:93–94
49. Bateman JF, Chan D, Lamande S, Mascara T, Cole WG. Biochemical heterogeneity of type I collagen mutations in osteogenesis imperfecta. *Ann NY Acad Sci* **1988**;543:95–105
50. Brenner RE, Vetter U, Wörsdorfer O, Nerlich A, Teller WM, Müller PK. Biochemical analysis of bone compacta in osteogenesis imperfecta. *Ann NY Acad Sci* **1988**;543:106–108
51. Willing MC, Cohn DH, Starman B, Holbrook KA, Greenberg CR, Byers PH. Heterozygosity for a large deletion in the α2(I) collagen gene has a dramatic effect on type I collagen secretion and produces perinatal lethal osteogenesis imperfecta. *J Biol Chem* **1988**;263:8398–8404
52. Bonadio JF, Byers PH. Subtle structural alterations in the chains of type I procollagen produce osteogenesis imperfecta type II. *Nature* **1985**;316:363–366
53. Tsipouras P, Børresen A, Dickson LA, Berg K, Prockop DJ, Ramirez F. Molecular heterogeneity in the mild autosomal dominant forms of osteo-

genesis imperfecta. *Am J Med Genet* **1984**;36:1172–1179
54. Goldfarb AA, Ford D. Osteogenesis imperfecta congenita in consecutive siblings. *J Pediatr* **1954**;44:264–268
55. Bullough PG. Osteogenesis imperfecta. In: Taveras JM, Ferrucci JT, eds. *Radiology—diagnosis, imaging, intervention*, vol 5. Philadelphia: Lippincott, **1986**:1–8
56. Goldman AB, Davidson D, Pavlov H, Bullough PG. "Popcorn" calcifications: a prognostic sign in osteogenesis imperfecta. *Radiology* **1980**;136: 351–358
57. Rush PJ, Berbrayer D, Reilly BJ. Basilar impression and osteogenesis imperfecta in a three-year-old girl: CT and MRI. *Pediatr Radiol* **1989**;19: 142–143
58. Pozo JL, Crockard HA, Ransford AO. Basiliar impression in osteogenesis imperfecta. *J Bone Joint Surg [Br]* **1984**;66-B:233–238
59. Carty H, Shaw DG. Child abuse and osteogenesis imperfecta (letter). *Br Med J* **1988**;296:292
60. Paterson CR, McAllion SJ. Child abuse and osteogenesis imperfecta (letter). *Br Med J* **1987**;295:1561
61. Acland PR. Child abuse and osteogenesis imperfecta (letter). *Br Med J* **1987**;295:1346
62. Taitz LS. Child abuse and osteogenesis imperfecta (letter). *Br Med J* **1988**;296:292
63. Carty H. Brittle or battered. *Arch Dis Child* **1988**;63:350–352
64. Kleinman PK. *Diagnostic imaging of child abuse.* Baltimore: Williams and Wilkins, **1987**
65. Hilton SvW. The accidentally injured and abused child. In: Hilton SvW, Edwards DK, Hilton JW. *Practical pediatric radiology.* Philadelphia: Saunders, **1984**:443–485
66. Kleinman PK, Marks SC, Blackbourne B. The metaphyseal lesion in abused infants: a radiologic-histopathologic study. *AJR* **1986**;146:895–905
67. Radkowski MA, Merten DF, Leonidas JC. The abused child: criteria for the radiologic diagnosis. *RadioGraphics* **1983**;3:262–297
68. Kirks D. *Practical pediatric imaging.* Boston: Little, Brown, **1984**:43: 281–285
69. Kleinman PK, Marks SC, Adams VI, Blackbourne BD. Factors affecting visualization of posterior rib fractures in abused infants. *AJR* **1988**; 150:635–638
70. Warkany J. Osteogenesis imperfecta (osteopsathyrosis). In: *Warkany J. Congenital malformations: notes and comments.* Chicago: Year Book Medical, **1971**:824–836
71. Cremin B, Goodman H, Spranger J, Beighton P. Wormian bones in osteogenesis imperfecta and other disorders. *Skeletal Radiol* **1982**;8: 35–38
72. Reeder MM, Felson B. *Gamuts in radiology.* Cincinnati: Audiovisual Radiology of Cincinnati, **1975**:Gamut A-31
73. Astley R. Metaphyseal fractures in osteogenesis imperfecta. *Br J Radiol* **1979**;52:441–443
74. Taitz LS. Child abuse and osteogenesis imperfecta (letter). *Br Med J* **1987**;295:1346
75. Holt KS. Child abuse and osteogenesis imperfecta (letter). *Br Med J* **1987**;295:1345–1346

Commentary

Differentiation of Child Abuse and Osteogenesis Imperfecta: Medical and Legal Implications

Paul K. Kleinman[1]

In 1946, Caffey [1] described the association of long-bone fractures with subdural hematomas in young infants. A concept of inflicted injury in children gradually evolved and culminated in 1962 with the landmark article by Kempe et al. [2], entitled "The battered-child syndrome." Not long after Caffey's original description, an article by Astley [3], "Multiple metaphyseal fractures in small children (metaphyseal fragility of bone)," appeared in the *British Journal of Radiology*. Astley suggested that the multiple unrecognized fractures of the long bones, spine, and ribs in the infants and toddlers in his study were, in fact, due to underlying osseous metaphyseal fragility. This report was the first to suggest that naturally occurring conditions might result in injuries that could simulate those of child abuse. Although time has failed to provide support for Astley's views, numerous articles have been published that draw attention to conditions that could mimic child abuse. In the great majority of cases, differentiation of naturally occurring conditions from child abuse is easily accomplished on clinical, laboratory, and radiologic grounds.

The concept of nonaccidental injury has undergone a natural evolution from initial descriptions, to further definition and characterization, and ultimately to a critical analysis designed to avoid confusion with other diseases. In general, this process has occurred in response to the natural forces at work in the field of scientific investigation. However, heightened awareness of the social implications, and a growing involvement of the legal community in the field of child abuse, have intensified the focus on potential imitators of child abuse and the consequences of a missed diagnosis.

Increasingly, physicians are caught between their obligations to suspect and report child abuse and their fear of an inappropriate diagnosis of inflicted injury. Although laws exist in all 50 states that generally hold professionals free from civil and criminal liability in the reporting of child abuse cases, lawsuits have been initiated against expert witnesses testifying about the presence of abuse, and indications strongly suggest that innovative attempts will be made to use the civil legal apparatus to seek recourse from consulting physicians in cases of unsubstantiated alleged child abuse. More than ever, a compelling need exists for the education of physicians about the characteristics of child abuse and their differentiation from those of naturally occurring disease and accidental injury.

The article in this issue by Ablin et al. seeks to provide a scientific approach to differentiate child abuse from osteogenesis imperfecta (OI) [4]. The authors have systematically reviewed the scientific literature and have provided us with the necessary data to determine the likelihood of OI given a constellation of clinical and radiologic findings. Specifically, they provide us direction in differentiating OI from child abuse.

Types I and II of OI should not be confused with child abuse, because the characteristic blue sclerae are present. Problems may arise, according to Ablin et al., in types III and IV. The rare type III has normal sclera, but bone fragility and osteopenia are usually severe, leading to multiple fractures and severe progressive deformity of the long bones and spine. In the occasional mild case, wormian bones are usually present in association with osteoporosis and other clinical features

---

This article is a commentary on the preceding article by Ablin et al.

[1] Department of Radiology, University of Massachusetts Medical Center, 55 Lake Ave. N., Worcester, MA 01655. Address reprint requests to P. K. Kleinman.

AJR 154:1047–1048, May 1990 0361–803X/90/1545–1047 © American Roentgen Ray Society

of OI. Cases of type IV OI may pose greater problems, because involvement tends to be less severe than it is in type III. However, family history, wormian bones, bony deformity and demineralization, dentinogenesis imperfecta, and other clinical findings are frequently present.

Unfortunately, solid radiologic data in reported cases of type IV OI are lacking, and as Ablin et al. have pointed out, this problem has led to publication of unjustified conclusions. Although the potential for misdiagnosis exists, the probability is minute, given the relative prevalences of nonaccidental injury and type IV OI in the community. The authors quote the work of Taitz, which estimates the probability of encountering sporadic cases of type IV OI to be between one in a million to one in three million births; or one case in a large city every 100–300 years [5].

Radiologic practices vis-à-vis the diagnosis of child abuse vary widely, and although overzealousness in making this diagnosis may occur rarely, in general, the tendency is to underdiagnose. To best facilitate accurate diagnosis, radiologists must be fully versed in the radiologic manifestations of abuse, as well as its imitators. Although certain radiologic findings carry a high specificity for abuse, in particular osseous lesions in young infants, they are frequently lacking, and the findings must be assessed in the context of other clinical and laboratory indicators. Similarly, the diagnosis of OI, particularly in its milder forms, must use clinical data.

Ultimately, the radiologist may be required to draw conclusions regarding the diagnosis of abuse vs the possibility of OI. It should be understood that in certain instances of long-bone fractures in childhood, it may be impossible to absolutely exclude the possibility of OI before the development of demineralization. However, even the most stringent legal criteria do not demand 100% certainty. The radiologist is asked daily to make diagnoses to the best of his ability at a reasonable level of medical certainty. Frequently, these decisions form the basis for therapy that may pose real risks to the patient. Similarly, the remote possibility always exists that the radiologist may be incorrect in excluding the diagnosis of OI. The thorough and critical analyses of the existing data on the subject in the article by Ablin et al. should go a long way toward minimizing the chances of this occurrence. Similar work with other potential radiologic imitators of child abuse should be encouraged [6].

REFERENCES

1. Caffey J. Multiple fractures in the long bones of infants suffering from chronic subdural hematoma. *AJR* **1946**;56:163–173
2. Kempe CH, Silverman FN, Steele BF, Droegemueller W, Silver HK. The battered-child syndrome. *JAMA* **1962**;181:105–112
3. Astley R. Multiple metaphyseal fractures in small children (metaphyseal fragility of bone). *Br J Radiol* **1953**;26:577–583
4. Ablin DS, Greenspan A, Reinhart M, Grix A. Differentiation of child abuse from osteogenesis imperfecta. *AJR* **1990**;154:1035–1046
5. Taitz LS. Child abuse and osteogenesis imperfecta. *Br Med J* **1987**; 295:1082–1083
6. Chapman S. Child abuse or copper deficiency? A radiologic review. *Br Med J* **1987**;294:1370

Case Report

Prenatal Detection of an Abdominal Mass by MR Imaging Performed While the Fetus is Immobilized with Pancuronium Bromide

Paolo Tomá,[1] Giorgio Lucigrai,[1] Paolo Dodero,[2] and Mario Lituania[3]

We report a case in which a renal mass in a 37-week-old fetus was identified on prenatal MR images made after injection of pancuronium bromide into the umbilical vein to prevent fetal motion. After birth, a left nephrectomy was performed, and the pathologic diagnosis was a Wilms tumor.

Case Report

A 32-year-old woman was referred for evaluation in the 37th week of pregnancy because of a fetal abdominal mass suspected on the basis of sonographic findings.

Repeated sonography (Ansaldo AU 450, Genoa, Italy; 3-MHz convex scanner) confirmed the presence of a solid inhomogeneous mass in the left upper quadrant of the fetal abdomen, arising from the renal fossa (Fig. 1A). The left kidney was not visualized.

For the MR imaging, fetal motion was prevented by the injection of pancuronium bromide (a neuromuscular blocking agent, 0.08 mg/kg) into the umbilical vein via a 20-gauge spinal needle inserted under continuous sonographic guidance. No changes in fetal heart rate were evident. Images were made with a 0.5-T Esaote 5000 MR scanner (Genoa, Italy). Slice thickness was 7 mm, with a 3-mm interslice gap. Spin-echo sequences with repetition/echo times (TR/TE) of 500/20 and 2000/100 were made in the transverse and coronal planes of the fetal abdomen. In addition, images were made by using a gradient-echo pulse sequence (180/20, $\alpha = 20°$) in the transverse plane. The examination lasted about 55 min. Fetal movements reappeared about 90 min after the pancuronium bromide injection was stopped.

MR images showed a solid mass in the left renal fossa. The mass was hypointense relative to the liver parenchyma on T1-weighted images and hyperintense on T2-weighted and gradient-echo images. The left kidney was not visualized (Figs. 1B and 1C).

Sonographic examination (Acuson 128, Mountain View, CA; 5-MHz sector scanner) of the neonate showed a solid mass 9 × 7.5 × 7 cm arising from the left kidney. CT scanning, performed 2 days later, confirmed the presence of the renal tumor. Twelve days after birth, a left nephrectomy was performed. The pathologic diagnosis was capsulated Wilms tumor (150 g) without involvement of lymph nodes or the renal capsule.

Discussion

Congenital renal tumors are rare; the most common is mesoblastic nephroma. Prenatal visualization of these tumors by use of sonography has been reported on several occasions [1]. No description was found of fetal renal tumors diagnosed by using MR imaging. The sonographic findings of mesoblastic nephroma and of Wilms tumor in the newborn are similar; the distinction can be made only postoperatively.

We performed MR imaging prenatally to acquire further information about the tumor and possibly to improve postpartum management. MR imaging was better than sonogra-

---

Received November 8, 1989; accepted after revision December 26, 1989.

[1] Department of Radiology, "Giannina Gaslini" Children's Hospital, Largo G. Gaslini, 5, 16100 Genoa, Italy. Address reprint requests to P. Tomá.

[2] Department of Surgery, "Giannina Gaslini" Children's Hospital, 16100 Genoa, Italy.

[3] Department of Obstetrics and Gynecology, "Giannina Gaslini" Children's Hospital, 16100 Genoa, Italy.

AJR 154:1049–1050, May 1990 0361–803X/90/1545–1049 © American Roentgen Ray Society

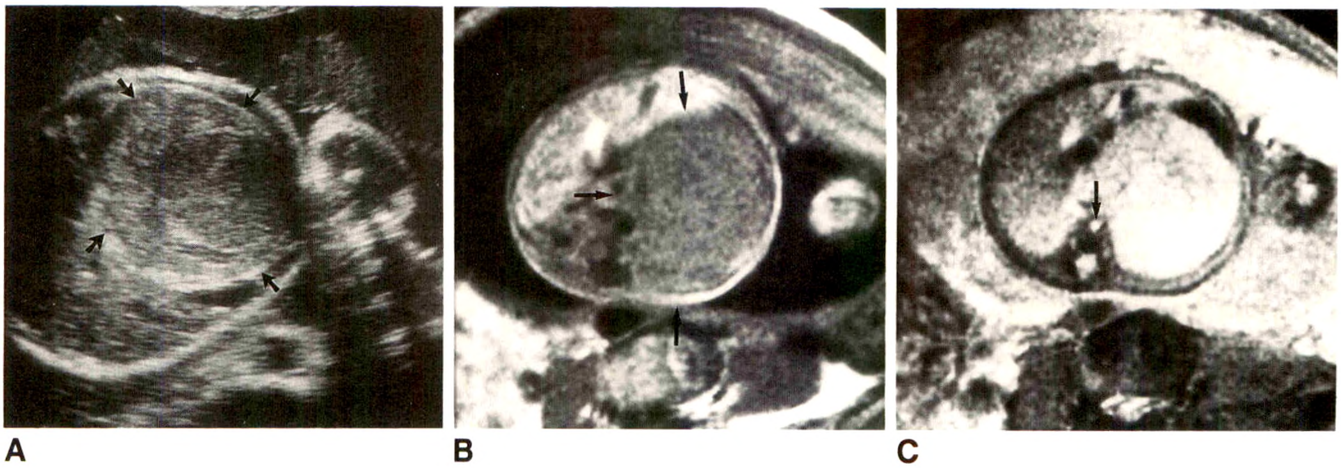

Fig. 1.—*A*, Transverse sonogram of fetus at 37th week of pregnancy shows an echogenic mass with well-demarcated borders arising from left renal fossa (*arrows*).

B, Transverse T1-weighted MR image obtained with pancuronium bromide at 37th week of pregnancy confirms solid mass (*arrows*) on left side. Mass is hypointense relative to liver.

C, Gradient-echo MR image obtained at same time as *B* shows mass is hyperintense and separated from aorta (*arrow*).

phy for defining the relation of the tumor to the vessels, but was not more useful for determining the origin of the mass.

The lack of visualization of the left kidney suggested the renal origin of the tumor. We suspected renal neoplasm (particularly a mesoblastic nephroma), but a large neuroblastoma could not be excluded.

Fetal movement is a major drawback in prenatal MR imaging. To overcome this, maternal sedation has been proposed [2]. Neuromuscular blockade obtained by intramuscular curarization of the fetus has been reported [3, 4]. Daffos et al. [5, 6] described direct intravascular fetal curarization by vecuronium bromide.

In our case, the fetus was immobilized for 90 min with an IV injection of pancuronium bromide. A decrease in fetal heart rate as reported by Pielet et al. [7] did not occur, but our observations were limited to 15 min before and after MR imaging.

REFERENCES

1. Walter JP, McGahan JP. Mesoblastic nephroma: prenatal sonographic detection. *JCU* **1985**;13:686–689
2. Weinreb JC, Lowe T, Cohen JM, Kutler M. Human fetal anatomy: MR imaging. *Radiology* **1985**;157:715–720
3. Moise KJ, Carpenter RJ, Deter RL, Kirshon B, Diaz SF. The use of fetal neuromuscular blockade during intrauterine procedures. *Am J Obstet Gynecol* **1987**;157:874–879
4. Seeds JW, Corke BC, Spielman FJ. Prevention of fetal movement during invasive procedures with pancuronium bromide. *Am J Obstet Gynecol* **1986**;155:818–819
5. Daffos F, Cappella-Pavlovsky M, Forestier F. Fetal blood sampling during pregnancy with use of a needle guided by ultrasound: a study of 606 consecutive cases. *Am J Obstet Gynecol* **1985**;153:655–660
6. Daffos F, Forestier F, MacAleese L, et al. Fetal curarization for prenatal magnetic resonance imaging. *Prenat Diagn* **1988**;8:311–314
7. Pielet BW, Socol ML, MacGregor SN, Dooley SL, Minogue J. Fetal heart rate changes after fetal intravascular treatment with pancuronium bromide. *Am J Obstet Gynecol* **1988**;159:640–643

Case Report

Castleman Disease in the Neck: Atypical Appearance on CT

John C. Chaloupka,[1] Mauricio Castillo, and Patricia Hudgins

Castleman disease is a rare lymphoproliferative disorder of uncertain cause characterized by a distinctive pattern of hypervascular lymphoid hyperplasia. Since its original description [1], it has been reported under a variety of headings that reflect various theories of pathogenesis. Most cases occur as mediastinal tumors, although involvement of other anatomic sites has been reported [2–6]. Recent reports [4–9] have noted that on CT these tumors show homogeneous enhancement of moderate to marked intensity after administration of IV contrast material. We present a case of Castleman disease of the neck in which the appearance of the tumor on CT was distinctly different from previous descriptions and thus was mistaken for another disorder.

Case Report

A 16-year-old boy was admitted with a 6-month history of a painless mass in the left side of the neck. He denied constitutional symptoms, hoarseness, dysphagia, and dyspnea. The only notable finding on physical examination was a 10-cm firm and nontender mass extending from the left supraclavicular triangle to the level of the angle of the mandible. Routine laboratory data were normal.

Contrast-enhanced CT of the neck (Fig. 1) was performed by using a combined bolus and rapid infusion technique. A large, multilobular mass was seen within the left anterior triangle of the neck. The mass extended medially to the parapharyngeal space and carotid sheath and posteriorly deep to the sternocleidomastoid muscle. Multicentric "ring enhancement" of the mass was prominent. These findings were thought most likely to represent necrotic lymphadenopathy caused by lymphoma or metastatic neoplasm. Suppurative and tuberculous lymphadenitis were considered less likely diagnoses.

At surgery, a well-encapsulated, solitary, hypervascular tumor was completely excised. Histologic examination revealed characteristic features of the hyaline vascular variant of Castleman disease throughout the entire lesion without evidence of central necrosis.

Discussion

Castleman disease is a rare benign tumor of lymphoid tissue. It has been described under a variety of headings, including angiomatous lymphoid hamartoma, giant lymph node hyperplasia, giant hemolymph node, angiofollicular hyperplasia, and follicular lymphoreticuloma. This variable terminology reflects its uncertain cause, although the most tenable theories of pathogenesis are that Castleman disease is either a hamartomatous or inflammatory process [2, 10].

The disease has two histologic variants. The most common is the hyaline vascular variant (80–90%), which consists of small lymphoreticular follicles distributed within a hypervascular hyalinized stroma. The plasma cell variant is less common (10%) and consists of larger lymphoreticular nodules that are separated by sheets of plasma cells and somewhat less vascular stroma [2, 3].

Castleman disease most frequently manifests as an asymptomatic, solitary mediastinal tumor (40–70% of cases) [2, 6]. Additional sites of occurrence include the axilla, retroperitoneum, mesentery, vulva, pancreas, pelvis, and neck [4–6]. Less than 10% of cases occur in the neck [4]. Recently, a multicentric form of the disease has been described [9]. Patients with the plasma cell variant and multicentric form are more likely to have constitutional symptoms, anemia, and

---

Received October 23, 1989; accepted after revision December 12, 1989.

[1] All authors: Department of Radiology, Emory University Hospital, 1364 Clifton Rd., N.E., Atlanta, GA 30322. Address reprint requests to J. C. Chaloupka.

AJR 154:1051–1052, May 1990 0361–803X/90/1545–1051 © American Roentgen Ray Society

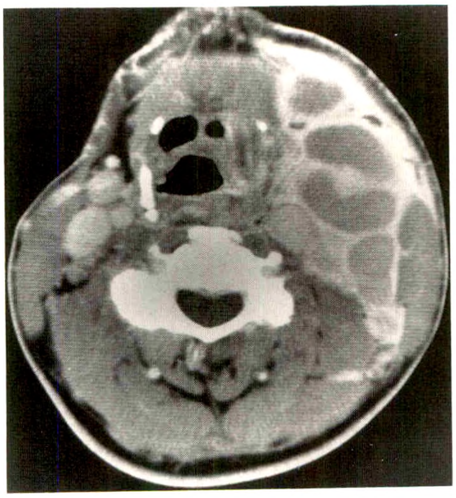

Fig. 1.—CT scan of neck shows a large lobular mass lateral to left carotid sheath. Note multicentric ring enhancement.

hypergammaglobulinemia [3, 9]. Complete surgical resection is usually curative, although systemic immunosuppressive therapy may be necessary for the multicentric type [10].

Only a few reports [4–9] have described the CT appearance of Castleman disease. In all of these, both histologic variants, regardless of location, had a similar pattern of homogeneous, moderate to marked contrast enhancement. The hyaline vascular variant tends to show more prominent enhancement on CT, most likely because of its greater vascularity [4, 7, 9, 11].

To our knowledge, only one report [4] of the CT appearance of Castleman disease of the neck (hyaline vascular variant) describes the characteristic enhancement pattern in a solitary mass lateral to the carotid sheath. The lateral location of the tumor also has been noted in the surgical literature [10]. In our case, although the tumor occurred in a similar location, multicentric ring enhancement was observed. Consequently, alternative diagnoses were considered, such as necrotic lymphadenopathy from lymphoma or various metastatic neoplasms and suppurative or tuberculous lymphadenitis. Unfortunately, no ready explanation exists for the observed pattern of enhancement, as the tumor was homogeneous in composition and had not undergone central necrosis.

Castleman disease should be considered in the differential diagnosis of solitary neck masses that occur along the major lymphatic chains of the anterior triangle, particularly if the mass is lateral to the carotid sheath and shows homogeneous, moderate to marked contrast enhancement. As seen in our patient, ring enhancement of the mass does not exclude the diagnosis of Castleman disease, thus making it indistinguishable from necrotic lymphadenopathy of various neoplastic or infectious causes.

REFERENCES

1. Castleman B, Iverson L, Menender VP. Localized mediastinal lymph-node hyperplasia resembling thymoma. *Cancer* **1956**;9:822–830
2. Abell MR. Lymphoid hamartoma. *Radiol Clin North Am* **1968**;1:15–24
3. Keller AR, Hochlalzer L, Castleman B. Hyaline vascular and plasma cell types of giant lymph node hyperplasia of the mediastinum and other locations. *Cancer* **1972**;29:670–683
4. Koslin DK, Berland LL, Sekar BC. Cervical Castleman disease: CT study with angiographic correlation. *Radiology* **1986**;160:213–214
5. Joseph N, Vogelzang RL, Hidvegi D, Neiman HL. Computed tomography of retroperitoneal Castleman disease (plasma cell type) with sonographic and angiographic correlation (case report). *J. Comput Assist Tomogr* **1985**;9:570–572
6. Iida E, Kohno A, Mikami T, Kumekawa H, Akimoto S, Hamano K. Mesenteric Castleman tumor (case report). *J Comput Assist Tomogr* **1983**;7:338–340
7. Onik G, Goodman PC. CT of Castleman disease. *AJR* **1983**;140:691–692
8. Fiore D, Bionodetti PR, Calabro F, Rea F. CT demonstration of bilateral Castleman tumors of the mediastinum (case report). *J Comput Assist Tomogr* **1983**;7:719–720
9. Ferreiros J, Gomez-Leon N, Mata MI, Casanova R, Pedrosa CS, Cuevas A. Computed tomography in abdominal Castleman's disease. *J Comput Assist Tomogr* **1989**;13:433–436
10. Johnson JT, Oral A, Nalesnik M, Roscoe GJ, Whiteside TL. Giant lymph node hyperplasia: clinical and immunohistologic correlation of an intermediate variant. *Ear Nose Throat J* **1985**;64:63–70
11. Greenstein S, Fishman EK, Kaufman SL, Kadir S, Siegelman SS. Castleman disease of the retroperitoneum: CT demonstration. *J Comput Assist Tomogr* **1986**;10:547–548

1989 ARRS Executive Council Award

The Role of Ferritin and Hemosiderin in the MR Appearance of Cerebral Hemorrhage: A Histopathologic Biochemical Study in Rats

Keith R. Thulborn[1]
A. Gregory Sorensen[1]
Neil W. Kowall[2]
Ann McKee[2]
Albert Lai[1]
Robert C. McKinstry[1]
John Moore[1]
Bruce R. Rosen[1]
Thomas J. Brady[3]

A rat model of cerebral hemorrhage using stereotaxic injection of blood into the right basal ganglia was developed to investigate the influence of iron metabolism on the appearance of cerebral hemorrhage on MR images. Images of in vitro fixed brain sections stained specifically for different iron-storage substances, ferritin and hemosiderin, created by digitization of the pathology sections using an Eikonix CCD camera, were compared with the in vivo MR images of late-phase hematomas. Areas of the pathologic and MR features of the lesions were quantitatively correlated. The single-slice MR images were obtained with the use of T1- and T2-weighted spin-echo pulse sequences, as well as T2-weighted spin-echo pulse sequences in which the 180° refocusing pulse was offset from the center of the echo time; this was termed an asymmetric spin-echo pulse sequence. The symmetric and asymmetric T2-weighted images allowed the calculation of line-width images, which emphasize line broadening from intravoxel magnetic field inhomogeneities that arise from the presence of iron-containing substances.

From biochemical and histochemical staining, we conclude that at least two iron-storage substances are present in the late phase of resolving cerebral hematomas. Ferritin has a wider distribution than hemosiderin, showing a similar distribution to the MR signal changes of the calculated line-width images. Line-width mapping is a sensitive means of detecting magnetic field inhomogeneities caused by the magnetic susceptibility differences introduced by the aggregation of these iron-storage substances.

***AJNR* 11:291–297, March/April 1990; *AJR* 154:1053–1059, May 1990**

The temporally varying appearance of cerebral hemorrhage observed by MR imaging has been well documented over the full range of magnetic field strengths available for clinical studies [1–8]. Because of the great variability in appearance, hemorrhage has received considerable attention in the clinical literature. The current model developed to rationalize this behavior is that of Gomori and Grossman [1], in which the major features of resolving intraparenchymal cerebral hematoma have been attributed to iron metabolism and integrity of the erythrocyte, as well as to vasogenic edema and structural changes around the site of hemorrhage. This model is an excellent summary of the MR features of cerebral hemorrhage and allows the formulation of several hypotheses that can be tested readily. Specifically pertinent to this investigation, the model states that the signal loss of late-phase hemorrhage on T2-weighted MR images is due to the magnetic susceptibility effects of hemosiderin, an iron-storage substance in macrophages in the periphery of resolving hematomas. Hemosiderin is readily demonstrated by Perls Prussian blue iron stain, used routinely to demonstrate the presence of iron in pathologic specimens. However, on the basis of the biochemistry of iron metabolism, iron storage in the form of ferritin would be expected to be present [9–13]. The purpose of this study was to determine if ferritin makes a contribution to the magnetic susceptibility effects that dominate the MR appearance of resolving hemorrhage in a rat model and to examine the application of line-width mapping, as determined

Received May 14, 1989; revision requested May 23, 1989; final revision received September 5, 1989; accepted September 8, 1989.

Presented at the annual meeting of the American Roentgen Ray Society, New Orleans, May 1989.

This work was supported by U.S. Public Health Service grants 1PO1CA48729, R01CA40303, and T32CA09502 and the General Electric Corp.

[1] Department of Radiology, Massachusetts General Hospital, Fruit St., Boston, MA 02114. Address reprint requests to K. R. Thulborn, Massachusetts General Hospital MR Imaging Center, Second Floor, 13th St., Bldg. 149, Charlestown, MA 02129.

[2] Department of Pathology, Massachusetts General Hospital, Boston, MA 02114.

[3] Department of Medicine, Massachusetts General Hospital, Boston, MA 02114.

0361–803X/90/1545–1053
© American Roentgen Ray Society

from symmetric (SE) and asymmetric (ASE) spin-echo pulse sequences, for detection of such magnetic susceptibility effects. Although magnetic susceptibility effects are detected by changes on T2-weighted images, as discussed in detail elsewhere [12, 14, 15], line-width maps have not been used extensively for in vivo studies [16]. The significance of this study is that the magnetic susceptibility effects in the model of Gomori and Grossman [1] of late-phase resolving cerebral hematomas should include ferritin and hemosiderin, thereby bringing the model into agreement with current concepts of iron metabolism.

Materials and Methods

Rat Model of Cerebral Hemorrhage

Three series of rats were prepared in an identical fashion; each series was divided between blood-injected and plasma-injected groups. The two groups of animals were used to isolate the effects attributable to the presence of the injected erythrocytes from effects due to the trauma of injection. The first series was used for MR imaging (blood-injected, $n = 8$; plasma-injected, $n = 2$), the second series for biochemical assays (blood-injected, $n = 14$; plasma-injected, $n = 10$), and the third series for histochemical staining (blood-injected, $n = 9$; plasma-injected, $n = 9$).

Sprague-Dawley male rats (200–250 g, Charles River Breeding Labs., Inc., Wilmington, MA) were placed under general anesthesia by intraperitoneal injection of pentobarbital (60 mg/kg). Animals were numbered by tattoos on entry into the study to identify subsequent MR data files, biochemical samples, and histopathologic specimens. A left carotid arterial or femoral venous catheter was placed in a donor animal using standard cutdown procedures and aseptic technique. The recipient animal was positioned in a stereotaxic frame, and, using aseptic technique, a longitudinal skin incision was made along the dorsal cranium exposing the bregma of the calvarium. A burr hole over the right caudate nucleus (0.5 mm anterior, 3.5 mm lateral) was drilled with an electric drill mounted on the stereotaxic frame [17]. The drill was cooled with sterile lidocaine solution (1%). Care was taken not to penetrate deeper than the inner table of the skull. The stereotaxically mounted sterile syringe (1-ml, 27-gauge needle) was then lowered through the burr hole to the appropriate depth (4.5 mm) [17].

Injection of blood or plasma (0.05 ml) was made at 100 mm Hg pressure by a reproducible mechanical pressure delivered by a weight falling from a constant precalibrated height. This pressure is the mean arterial blood pressure, mimicking arterial hemorrhage. The blood was obtained from the arterial or venous catheter and used within 2 min without heparinization. Hematocrits were determined on all samples of blood to ensure no hemodilution occurred among injected samples (40–45%). The reproducibility of the injection technique was verified initially by the similar histopathologic appearances and sizes of the acute lesions in animals sacrificed within 12 hr after production of the lesions and by physiologic stability among animals ($n = 6$). Plasma was obtained as the supernatant after centrifugation of heparinized arterial blood (2000 rpm, 3 min, bench centrifuge) and was injected under conditions identical to that of the whole blood. The needle was removed slowly and the burr hole was plugged with bone wax. The scalp incision was closed with sutures after topical administration of bacitracin.

The recipient animals were permitted to recover from anesthesia under warming lights and returned to the animal housing facilities until the imaging procedure. Animals were housed with access to fresh water and rat chow ad lib until sacrifice at 10–100 days. Immediately before imaging, a small glass disk (3 mm diameter × 1 mm thick) containing gadolinium-doped water (1 mmol/l) was glued over the burr hole in the cranium of the rat to allow the lesion to be readily located on the MR images. Imaging was performed within several hours after placement of the marker. Animals were sacrificed by lethal dose of pentobarbital immediately after imaging; the brains were removed intact for further processing, depending on the series. The authors complied with the National Institutes of Health guidelines for use of laboratory animals.

MR Imaging

Procedure.—The blood-injected ($n = 8$) and plasma-injected ($n = 2$) animals in the MR group were imaged 10–15 weeks after injection. Each rat was placed in the prone position within a custom-designed, air-warmed Plexiglas animal cradle; the head was in the homogeneous B_1 field of an RF coil (copper foil, 4 cm diameter × 4 cm length, mounted on Pyrex glass) [18]. General anesthesia was maintained by delivering nitrous oxide:oxygen gas (1:4 vol/vol, 2 l/min) via face mask to the animal within the Isolette. The cradle allowed the RF coil to be easily and reproducibly located within the most uniform B_0 field of the superconducting horizontal bore magnet (2.0 T). The RF coil at the proton resonance frequency with the animal in position was matched to the impedance of the spectrometer by minimizing the reflected power. Homogeneity of the B_0 field was maximized by prior shimming on a doped water phantom using the air temperature shim gradient coils and the DC offset of the three orthogonal imaging gradient coils. Homogeneity was routinely better than 1 ppm across the head of a rat.

Images were recorded on a Technicare prototype broadband spectrometer equipped with imaging hardware and software. The instrument did not have multislice capabilities. Single-slice coronal images (1.0 mm thick) were obtained after localizing the lesion with the marker over the burr hole on an initial sagittal projectional image. The lesion was located in the coronal plane by moving the whole animal cradle by 1-mm steps until the largest diameter of the lesion was located. Subsequent imaging was performed in this plane. After data acquisition, images were reconstructed, recorded on magnetic tape, and transferred to a Sun Microsystems model 4/260c workstation for production of synthetic images (T1, T2, and line-width) using software developed in our laboratory.

Protocols.—Imaging was performed on rats with lesions of 10–15 weeks in duration. Each animal was imaged with five pulse sequences: (1) SE 2000/50/4 (TR/TE/excitations), (2) ASE 2000/50/5/4 (TR/TE/τ/excitations), (3) SE 400/25/20 (TR/TE/excitations), (4) SE 2000/25/4, and (5) SE 2000/100/4. τ represents the refocusing 180° pulse offset time; the number of acquisitions was varied to maintain equal total acquisition times for all sequences (20 min). A complete description of the implementation of sequence 2 is given elsewhere [16]. The data were acquired as 256 × 128 matrices but displayed as 256 × 256 matrices by interpolation of the phase-encoding data.

In addition to the T2- and T1-weighted images obtained from the above sequences, synthetic images based on line width, T1, and T2 were calculated on a pixel-by-pixel basis by using the following algorithms. These calculated parameters are readily compared between different animals and at different times, whereas signal intensities obtained directly from the initial images are subject to variation on different days and between different animals due to variation in the sensitivity of the imaging system.

Line-width (LW) images were calculated from SE and ASE images assuming Lorentzian line shape (of the general form of $y = 1/$

$[1 + x^2]$) and TE >> τ, using the algorithm discussed in detail elsewhere [16]:

$$LW = [1/(\pi T_2^*)] = (1/\pi\tau)\ \ln(S2/S1) \quad (1)$$

where S1 and S2 are the pixel signal intensities from sequences 1 and 2, respectively. The line width of a pixel is a measure of the spread of resonance frequencies of protons within the pixel. If the pixel corresponds to an area of tissue that shows variation in magnetic susceptibility, such as may arise from the presence of paramagnetic iron storage products, then the resultant magnetic field gradients within the tissue cause dispersion of resonance frequencies of the protons within the pixel. Thus, a large line width means a wide dispersion of frequencies within a pixel, implying the presence of paramagnetic substances and resultant magnetic susceptibility effects.

T1 images were calculated assuming a steady-state solution to the linearized Bloch equations for the saturation recovery SE experiment [19] with a correction for the effect of gaussian slice selection [20] using the equation:

$$SI \propto M_0 e^{-(TE/T2)}(1 - 2e^{-(TR-TE/2)/T1} + e^{-(TR/T1)})(1 - 0.279e^{-(0.78TR/T1)}) \quad (2)$$

This expression for signal intensity, SI, was used to generate a look-up table of the ratio of signal intensities for sequences 3 and 4 for T1 values within physiologic ranges ($0 < T1 < 3000$ msec). Sequences 3 and 4 were used, as the TE is the same for both short and long TRs, respectively. Cubic spline interpolation, a routine mathematical method of interpolating between data points using a cubic polynomial [21], was performed to improve the precision of the look-up table. The images were then processed by computing the ratio of signal intensities from sequence 3 and sequence 4 on a pixel-by-pixel basis and using that value to determine T1 from the look-up table.

T2 images were computed from pixel signal intensities and the TEs, TE(4) and TE(5), respectively, of images obtained from sequences 4 and 5 (S4 and S5), respectively, assuming a single exponential decay and using the equation:

$$T2 = [TE(5) - TE(4)]/[\ln(S5/S4)] \quad (3)$$

The calculations were performed on a Sun Microsystems workstation (model 4/260c) using software designed to take data from corresponding pixels of any two designated images and calculate the desired parameter using one of the above equations. The result is recorded in an identical-sized matrix that is then displayed as the synthetic image.

Histopathology

Tissue preparation.—For the histochemical staining series, rats were sacrificed at about 1-week intervals from 2 to 15 weeks and the brains removed in toto and fixed overnight at 4°C in a solution of 10% neutral buffered formalin. After cryoprotection in 20% glycerol and 2% dimethyl sulfoxide, each brain was blocked and sectioned in the coronal plane at 50-μm intervals on a freezing microtome. Standard surface landmarks were used to select serial sections spanning the entire basal ganglia. These were collected in sets for storage at 4°C in 0.1 mol/l of phosphate buffer until staining.

Staining procedures.—Alternate sections from each rat brain were stained using the two stains for each iron-storage protein. Although counterstains were used in initial studies, they were not used in the studies employing digitization.

For Perls Prussian blue, the serial sections in the set were mounted on chrome alum–gelatin covered slides and air-dried, followed by immersion in a fresh incubating solution consisting of equal parts of 2% potassium ferrocyanide and 2% hydrochloric acid for 10–60 min [22]. After the reaction was completed, the slides were washed in water and dehydrated, cleared, and applied with cover glasses.

For ferritin immunocytochemistry, free-floating sections were treated in 0.3% hydrogen peroxide in absolute methanol for 30 min followed by 3- to 10-min washes in 0.1 mol/l phosphate-buffered solution (PBS, pH 7.3). After incubation in 10% normal goat serum in PBS to saturate nonspecific antibody binding sites, sections were placed in primary antiserum diluted in PBS with 0.3% Triton-X 100 at room temperature (1:1000, Boehringer Mannheim, rabbit anti-human ferritin). After further PBS washes, the sections were incubated in goat anti-rabbit peroxidase complex (antibody to the rabbit ferritin-specific antibody that is linked to the enzyme peroxidase used to produce the color reaction) for 3 hr (1:200 in PBS, Boehringer Mannheim) followed by further washes and disclosure using 3-3′-diaminobenzidine as the chromogen.

Digitization.—Pathology sections were digitized by using an Eikonix CCD camera (model 1000, 4096 diodes in a linear array × 4096 lines of resolution for a maximum of 4096 × 4096 resolution) interfaced to an IBM PC XT 286 computer that was connected to a network of Sun workstations using PC/NFS software. Images of complete brain sections were obtained through a standard 50-mm camera lens using diffused uncollimated incandescent light transmitted through the slide. Calibration of the camera exposure settings was performed with software supplied by the manufacturer, with 0 corresponding to zero light and 255 (the maximum on the eight-bit scale of the camera) corresponding to full transmission of white light.

Counterstains usually applied for direct visualization were not applied to sections used for digitization because, although of different color, they are still digitized to a gray-scale level. This increases the average background signal in a pathology section, decreasing the discrimination of the lesion from the background in the gray-scale image. Such digitized imaging measures the amount of uncollimated polychromatic light transmitted through the pathology specimen. The quantitative relationship between staining characteristics and transmission of light is complex, and is assumed to be a monotonically increasing function. Different stains can be expected to show different responses depending on the absorbance wavelength and filtering properties of the histologic structures detected by each stain. Because of the complexity of these response functions, it was not possible to quantify the amount of a particular substance present but only to delineate its distribution.

Image Analysis

Both MR and histologic images were analyzed with custom-designed software on the Sun Microsystems model 4/260c workstation. After choosing a background signal intensity over the contralateral hemisphere of the brain (be it an MR or pathology image), signal means and standard deviations were calculated. Contours for signal intensities at a given number of standard deviations (2 SD contour data are presented) from the background mean were then selected over the whole brain, including the ipsilateral hemisphere containing the lesion. The areas of the lesion from the different images of the same brain were then compared by using the two-tailed t test for the mean of differences of paired observations. Differences in areas at the $p < .05$ confidence limit for the two-tailed t test were required for statistical significance. Corrections for the differences in pixel sizes between the MR images (0.2 × 0.1 mm) and pathologic images (0.025 × 0.025 mm) and for changes in size of the brain from in vivo to after fixation (28%, $n = 25$) were applied to allow the areas of signal abnormalities in the various images to be compared directly. Because more data were available for the separate cohorts of animals used for MR and pathology studies, measurements of area of lesions defined by MR images (synthetic line-width and T1-weighted and T2-

weighted images) and pathology images (based on different iron stains) were compared by using the two-tailed t test based on the means of the groups of such unpaired observations with the requirement that statistical significance be reached at the $p < .05$ confidence limit. Registration of thin pathologic sections with considerably thicker MR images makes multiple pathologic sectioning essential for statistical reliability. Pathology sections with maximum lesion size were used for digitization and correlation.

Biochemistry

Tissue preparation.—To ensure that the iron products observed by the histochemical stains were due to injected blood and not just the result of the trauma of injection, and to determine the rate of removal of iron-storage products from the lesion area, iron assays were performed on the series of rats underoing biochemical assay. The concentration of iron remaining in the brains was determined at about 7-day intervals from 3 to 15 weeks after injection of blood (n = 1 or 2 for each interval; total, n = 14) and plasma (n = 1 or 2 for each interval; total, n = 10). After sacrifice under general anesthesia, the intact brain was rapidly removed and the lesion was removed in a 3-mm-thick coronal section using standard brain landmarks for localization. The tissue (≈60 mg) around the lesion and that from the corresponding contralateral caudate nucleus (used as an internal control) were harvested separately, washed in cold normal saline, homogenized in phosphate buffer (1 ml, 10 mmol/l, pH 7.2) using a Dounce homogenizer (0.75 or 0.40 ml, 20 plunges), and stored in sealed vials at −5°C prior to assay.

Assays.—Iron analyses were performed by standard colorimetric methods (Sigma Chemical Co. kit #565). Acid digestion (perchloric acid:homogenate:buffer, 0.02:0.050:0.10 ml at 110°C overnight) was required to release protein-bound iron. All assays were performed by using three-point standard curves in triplicate. The total protein of the samples was determined by using standard protein assay techniques (Sigma Chemical Co. kit #690), with five-point standard curves in triplicate. Results were recorded as micromoles iron per mg protein.

Results

Representative contiguous pathology sections for the ferritin and Perls stains at the same magnification in the chronic phase of hematoma resolution (10 weeks) in the same rat demonstrated the presence of two iron-storage substances, hemosiderin and ferritin (Fig. 1). Examination of the distribution of the injected blood in the tissue indicated that the blood dissected along white-matter tracts and along the injection tract extending away from the injection site. This resulted in the elongated distribution observed in Figure 1. Whereas the hemosiderin was localized to macrophages along the injection tract, ferritin appeared not only in macrophages but also in glial cells with a wider distribution from the lesion. The differences in distribution were apparent visually; lesion areas from contiguous sections for the two stains that were 2 SD above background in the digitized pathology images (Fig. 2) are analyzed in Table 1. Because no statistically significant differ-

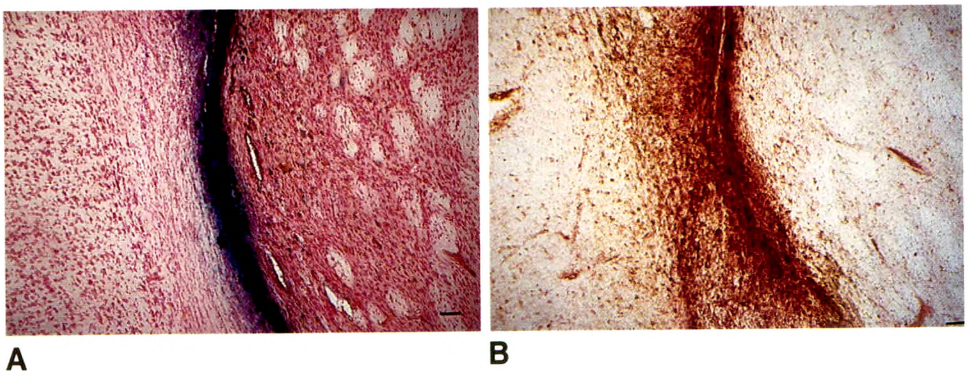

Fig. 1.—Representative pathology stains of contiguous coronal sections at same magnification in same rat brain 10 weeks after injection of blood into right basal ganglia. Scale bar = 0.05 mm.

***A*, Perls Prussian blue stain shows hemosiderin as very dark blue, linear region confined to center of field on lighter background.**

***B*, Immunochemical stain for ferritin shows ferritin as brown on pale background.**

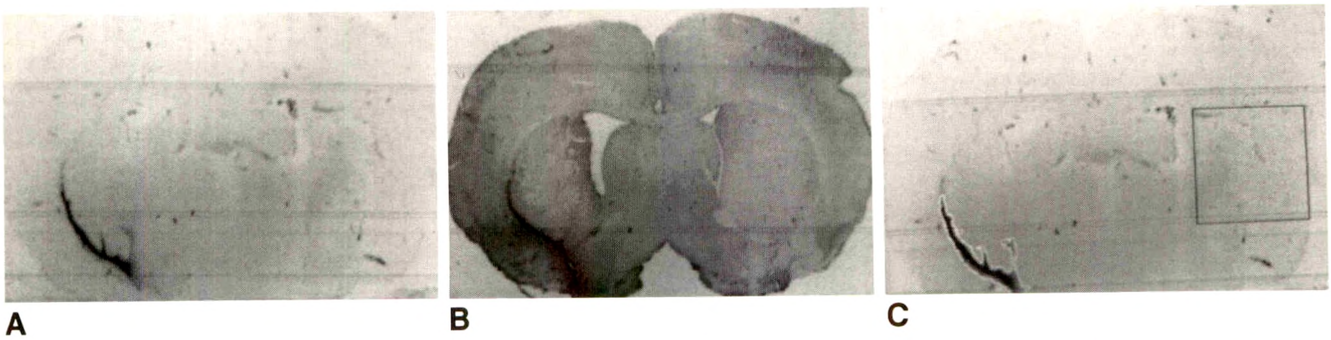

Fig. 2.—*A* and *B*, Digitized images of contiguous coronal brain sections stained for hemosiderin (Perls stain) (*A*) and ferritin (immunochemical stain) (*B*).

***C*, Contour analysis of image in *A* shows region of interest over normal left hemisphere (*black box*) and 2-SD contour about hematoma in right basal ganglia (*white border*). Lesion area is determined from number of pixels within contour multiplied by pixel size and corrected for shrinkage during processing.**

ences could be detected between smaller groups of lesions aged 1–4, 5–9, and 10–15 weeks, these data are pooled in Table 1. Similarly, no difference between venous and arterial blood was detected on MR or pathology images over this time period; thus, these groups were combined for subsequent statistical analysis. Ferritin detected by immunochemical reactivity showed a statistically significant ($p < .01$ for blood injection, $p < .05$ for plasma injection) broader distribution than hemosiderin detected by Perls stain positivity for contour thresholds of 2 SD above background. The lesions created by plasma injection contained significant iron-storage products, as detected by the stains, but the area of hemosiderin distribution was statistically greater in the blood-injected lesions ($p < .01$).

Biochemical analysis of the concentration of total iron as summarized in Table 2 demonstrated that both the plasma- and blood-injected lesions showed a statistically significant increased level of iron above the background in the contralateral hemisphere ($p < .01$) and that the blood-injected lesions contained more iron than the plasma-injected lesions ($p < .01$). No statistically significant variation in the quantity of iron was found from 1 to 15 weeks, suggesting that iron recycling away from the lesion was very slow over this time period.

Comparison of areas of lesions on T1- and T2-weighted SE images demonstrated that the areas of signal change at contour thresholds of 2 SD above background are significantly greater for T2- than for T1-weighted images ($p < .01$), with no statistical difference between the blood- and plasma-injected groups.

Representative SE, ASE, and line-width images are presented in Figure 3. The larger area of signal loss in the right basal ganglia on the ASE image (Fig. 3B) relative to the SE

TABLE 1: Comparison Among Areas of Late-Phase Hematomas Detected by Line-Width MR Images and Measured from Digitized Pathology Images of Brain Sections Stained for Ferritin Immunoreactivity and Perls Positivity

Lesion Group	Mean Area (mm^2)			Significance (p)		
	Ferritin (n)	Perls Stain (n)	Line Width (n)	Ferritin–Perls	Line Width–Ferritin	Line Width–Perls
Blood	16 ± 7 (9)	6 ± 2 (9)	12 ± 8 (8)	<.01	NS	<.05
Plasma	11 ± 8 (9)	3 ± 2 (9)	9 ± 2 (2)	<.05	NS	<.01
Significance (blood-plasma)	NS	<.01	NS	–	–	–

Note.—Areas were determined within contour thresholds of 2 SD above backgrounds. Statistical significance was determined by two-tailed t test for the paired ferritin-Perls observations and for means of separate cohorts of rats for the unpaired observations. NS = not significant at the .05 confidence limit.

TABLE 2: Biochemical Analysis of Iron in Ipsilateral (Right) and Contralateral (Left) Basal Ganglia of Rats with Late-Phase Hematomas Produced in Right Basal Ganglia

Lesion Group	Mean Iron Content (μg/mg protein)		Right-Left Significance (p)
	Right Hemisphere	Left Hemisphere	
Blood ($n = 14$)	0.8 ± 0.4	0.3 ± 0.1	<.01
Plasma ($n = 10$)	0.4 ± 0.2	0.2 ± 0.1	NS
Significance (blood-plasma)	<.01	NS	–

Note.—Statistical significance was determined by two-tailed t test for means of unpaired observations. NS = not significant at the .05 confidence limit.

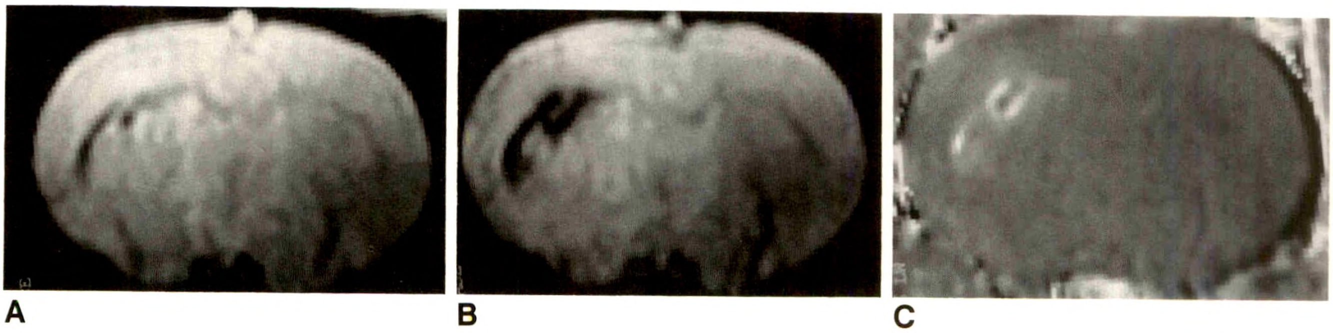

Fig. 3.—Representative in vivo coronal images of rat brain 10 weeks after production of hematoma.
***A*, Symmetric SE 2000/50/4 sequence.**
***B*, Asymmetric SE 2000/50/4 sequence ($\tau = 5$).**
***C*, Synthetic line-width image calculated from symmetric and asymmetric SE images with the use of equation 1 in text.**

image (Fig. 3A) was due to the greater sensitivity of the ASE image to magnetic susceptibility effects, as is discussed elsewhere [16]. The area of increased line width on the line-width image reflected the areas of both the SE and ASE images, and hence shows an area similar to that on the ASE image. The line widths of individual pixels at the center of the lesion were as high as 3–4 ppm, as compared with less than 0.2 ppm in normal tissue. This indicates significant magnetic susceptibility effects in the area of the lesion. Because line-width images are based on signal ratios, systematic changes in signal intensities across the images (caused by B_1 inhomogeneities) are corrected, thereby making contour mapping more reliable. Therefore, the contour analysis of lesions on line-width maps allowed more straightforward comparisons with pathology images than did the T1- or T2-weighted images obtained directly from the SE 400/25/20 and SE 2000/50/4 sequences, respectively. The areas of change in line width on line-width images, and ferritin stain immunoreactivity and Perls stain positivity on pathology images, are compared in Table 1 for blood and plasma lesions. Whereas the areas determined from line-width changes and ferritin immunoreactivity were not statistically different, the area of Perls positivity was significantly smaller ($p < .05$ for blood, $p < .01$ for plasma). These data showed no difference in areas in line-width changes and ferritin immunoreactivity between plasma- and blood-injected lesions, whereas the area of Perls positivity increased with blood injection ($p < .01$).

The signal-to-noise ratio of the synthetic T1 and T2 images was of insufficient quality to permit reliable contour analysis of lesion areas. However, our visual inspection of representative images showed that T1 changes were not readily detected, whereas T2 changes were observed in the area of the lesion.

Discussion

The lesions produced in the rat model of late hematoma showed stability in biochemical forms and area of distribution of iron-storage products within the statistical limits measured in this study over the 2- to 15-week period. Such stability may reflect the rapid establishment of the blood-brain barrier after initial traumatic disruption with consequently slow recycling of iron back to the reticuloendothelial system. The long-term deposition of hemosiderin in human cerebral hemorrhage is well documented and is in marked contrast to extraaxial lesions not contained by a blood-brain barrier [1]. As iron products were detected in both blood- and plasma-injected lesions, some of the iron must arise from local bleeding caused by the trauma of the injection. This is not surprising, as morphologic changes showed that the injected fluid dissected along white-matter tracts of the internal capsule rather than forming a discrete spherical hematoma. Such patterns are observed in arterial putaminal hemorrhages in humans. As heparin was used in the preparation of the plasma, traumatic bleeding may have been more pronounced in the plasma-injected lesions. Nevertheless, based on the distribution analysis of this study, the excess iron introduced by injection of blood rather than plasma increased the area of hemosiderin but not of ferritin. This suggests that this deposited blood may constitute a localized iron overload state, overloading the supply of apoferritin with concomitant formation of hemosiderin. Although the wider distribution of ferritin relative to hemosiderin may reflect the increased sensitivity of the immunochemical ferritin stain over that of the Perls stain, the differential increase in area of hemosiderin without change in ferritin between blood and plasma groups cannot be explained by stain sensitivity. Similarly, although the background of the ferritin stain is greater than that of the Perls stain, the analysis of digitized pathology images at statistically well-defined contour thresholds above background ensures that background bias is avoided.

Comparison of the areas of line broadening from magnetic susceptibility effects of the iron-storage substances on line-width MR images with areas of lesions defined by the pathology images suggests that the area of significant line broadening matches the wider distribution of ferritin rather than hemosiderin. Similarly, the constancy of the distribution of ferritin and line-width changes for blood and plasma injections, in contrast to the corresponding increase in the area of hemosiderin, supports this contention. However, quantitative biochemical fractionation of ferritin and hemosiderin is still required to determine the relative contributions of these two substances to the heterogeneity of tissue magnetic susceptibility.

This study suggests that the current explanation for the MR appearance of late-phase cerebral hematoma proposed by Gomori and Grossman [1] may require modification to include the role of ferritin in addition to hemosiderin as a source of magnetic susceptibility effects, as summarized in Figure 4. Human studies are essential to establish the relevance of this finding to clinical studies.

The marked signal changes on T2-weighted and T2 images, which are not readily apparent on T1-weighted and T1 images, demonstrate the presence of magnetic susceptibility–induced T2 relaxation with minimal relaxivity effects from dipole-dipole–induced T1 relaxation. Lack of the short-range relaxivity effects is expected for aggregates of iron-storage proteins such as ferritin and hemosiderin within subcellular compartments in which water is restricted from close approach to the paramagnetic and perhaps superparamagnetic

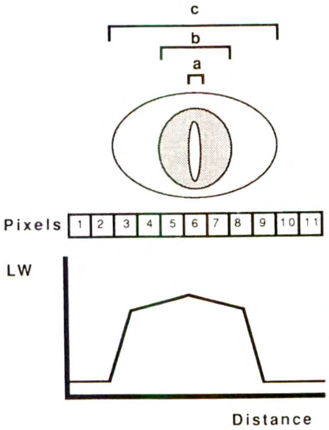

Fig. 4.—Schematic diagram of late phase of resolving hematoma as determined in rat model in which central cavitation (a) is variably present and surrounded by inner area of macrophages containing ferritin and hemosiderin (b) and wider area of ferritin in glial cells (c). Line width (LW) is increased in pixels (3 to 9) covering distribution of ferritin (c) but remains within normal limits (<0.2 ppm) outside this area.

ferric ions. However, diffusion of water through the magnetic field inhomogeneities induced by the volumes of different magnetic susceptibility, such as paramagnetic iron aggregates in surrounding diamagnetic tissue within a single imaging voxel, is significant during the TE time of T2-weighted imaging. Such diffusion results in signal attenuation. This mechanism is verified directly by the increase in line width on the line-width images.

As predicted from the known pathways of iron metabolism, at least two iron-storage substances are present in the late phase of resolution of cerebral hematoma. Ferritin in glial cells and macrophages has a wider distribution than hemosiderin in macrophages around the lesion. The rat model has provided a simple model for comparison of histopathology, biochemistry, and MR imaging data. The use of digitized histopathology provides an objective means of quantifying lesion size as depicted by specific stains for comparison with areas of signal changes on MR images. The use of line-width images in addition to T1- and T2-weighted images allows signal changes in late-phase hematomas to be attributed to intravoxel magnetic field inhomogeneities that show a distribution similar to that of ferritin. The late phase of hemorrhage described by the model of Gomori and Grossman [1] should be modified to include the role of ferritin in the magnetic susceptibility–induced signal changes observed in MR images. Determination of the relative contributions of ferritin and hemosiderin to such magnetic susceptibility effects awaits quantitative biochemical fractionation of these substances.

ACKNOWLEDGMENTS

We thank Edward P. Richardson for his enthusiasm and encouragement and Richard B. Buxton for his method of calculating T1 values.

REFERENCES

1. Gomori JM, Grossman RI. Head and neck hemorrhage. In: Kressel HY, ed. *Magnetic Resonance Annual 1987*. New York: Raven, **1987**:71–112
2. Sipponen JT, Sepponen RE, Silvula A. Nuclear magnetic resonance (NMR) imaging of intracerebral hemorrhage in the acute and resolving phases. *J Comput Assist Tomogr* **1983**;7:954–960
3. DeLaPaz RL, New PFJ, Buonanno FS, et al. NMR imaging of intracranial hemorrhage. *J Comput Assist Tomogr* **1984**;8:599–607
4. Di Chiro G, Brooks RA, Girton ME, et al. Sequential MR studies of intracerebral hematomas in monkeys. *AJNR* **1986**;7:193–199
5. Gomori JM, Grossman RI, Goldberg HI, Zimmerman RA, Bilaniuk LT. Intracranial hematomas: imaging by high-field MR. *Radiology* **1985**;157: 87–93
6. Gomori JM, Grossman RI, Hackney DB, Goldberg HI, Zimmerman RA, Bilaniuk LT. Variable appearances of subacute intracranial hematomas on high-field spin-echo MR. *AJNR* **1987**;8:1019–1026
7. Gomori JM, Grossman RI, Hackney DB, et al. Acute intracranial hemorrhage: intensity changes on sequential MR scans at 0.5 T. *AJNR* **1988**;9:47–57
8. Edelman RR, Johnson KA, Buxton RB, et al. MRI of hemorrhage: a new approach. *AJNR* **1986**;7:751–756
9. Trump BF, Valigorsky JM, Arstila AU, Mergner WJ, Kinney TD. The relationship of intracellular pathways of iron metabolism to cellular iron overload and iron storage diseases. *Am J Pathol* **1973**;72:295–324
10. Hill JM, Switzer RC. The regional distribution and cellular localization of iron in the rat brain. *Neuroscience* **1984**;11:595–603
11. Deizel PB. Iron in the brain: a chemical and histochemical examination. In: Waelsch H, ed. *Biochemistry of the developing nervous system*. London: Academic Press, **1955**:145–152
12. Drayer B, Burger P, Darwin R, Riederer S, Herfkens R, Johnson GA. Magnetic resonance imaging of brain iron. *AJNR* **1986**;7:373–380
13. Matsuno T, Mori M, Awai M. Distribution of ferritin and hemosiderin in the liver, spleen and bone marrow of normal, phlebotomized and iron overloaded rats. *Acta Med Okayama* **1985**;39:347–360
14. Lauffer RB. Paramagnetic metal complexes as water proton relaxation agents for NMR imaging: theory and design. *Chem Rev* **1987**;87:901–927
15. Thulborn KR, Brady TJ. Iron in magnetic resonance imaging of cerebral hemorrhage. *Magn Reson Q* **1989**;5:23–38
16. Wismer GL, Buxton RB, Rosen BR, et al. Susceptibility induced magnetic resonance line broadening: applications to brain iron mapping. *J Comput Assist Tomogr* **1988**;12:259–265
17. Konig JRF, Klippel RA. *The rat brain: a stereotaxic atlas of the forebrain and lower parts of the brain stem*. Baltimore: Williams & Wilkins, **1963**
18. Hoult DH. The NMR receiver: a description and analysis of design. *Prog NMR Spectra* **1978**;12:41–77
19. Farrar TC, Becker ED. *Pulse and Fourier transform NMR*. New York: Academic Press, **1971**:1–65
20. Buxton RB, Wismer GL, Brady TJ, Rosen BR. Quantitative proton chemical shift imaging. *Magn Reson Med* **1986**;3:881–900
21. Press WH, Flannery BP, Teukosky SA, Vetterling WT. *Numerical recipes in C. The art of scientific computing*. Cambridge, England: Cambridge University, **1988**:94–98
22. Luna L. *Manual of histologic staining methods of the armed forces institute of pathology*. New York: McGraw-Hill, **1968**

Book Review

Textbook of Color Doppler Echocardiography. Edited by Navin C. Nanda. Philadelphia: Lea & Febiger, 347 pp., 1989. $110

The development of color Doppler flow mapping in the early 1980s was a major enhancement of the instrumentation available for study of the heart. Shortly after its advent, this technique burst onto the clinical field of noninvasive cardiology, both in the literature and in the practicing cardiology community. Many texts, articles, and abstracts have been published on the capabilities and problems of color flow mapping. Navin Nanda, the editor of this text, was one of the pioneers in the introduction of color flow imaging in the United States, and this textbook is one of the first major works on the topic that is not in an atlas format.

The text consists of 32 chapters and an appendix and was written by well-recognized authorities in the field of color Doppler echocardiography. The first chapter summarizes the history of color flow mapping. It is followed by three chapters that describe comprehensively the physical principles of color flow imaging. They are organized in an easy-to-understand systematic approach and omit the complex mathematical relationships. The next three chapters explain how color flow imaging is incorporated into a sonographic system, principles of color flow imaging when an annular array is used, and the value of color Doppler imaging in study of the peripheral vascular system. Chapter 8 discusses limitations of color flow imaging. Chapter 9 presents the similarities and differences of the currently available color Doppler systems, enabling readers to understand more about their own sonographic instruments.

Chapter 10 offers a practical approach to the two-dimensional and conventional Doppler examination. This is one of the most valuable sections of the text, especially for readers who do not have much experience with the basic pulsed- and continuous-wave Doppler techniques.

Chapters 12 through 16 discuss the flow abnormalities caused by different types of valve lesions. These are competently and comprehensively presented, reflecting the wide experience of the authors. Chapter 17 provides data on surgery without cardiac catheterization for rheumatic valve lesions. Chapters 18 and 19 discuss color Doppler assessment of prosthetic valve functions and aortic aneurysms, respectively. Chapters 20 and 21 discuss congenital cardiac anomalies and include a nicely illustrated section on the morphologic basis of these disorders. The text also contains two chapters on the role of color flow imaging in assessing heart disease in the fetus and in evaluating the fetal circulation in general. Chapters 24 and 25 discuss intraoperative and transesophageal echocardiography, respectively. Chapter 25 lacks a comprehensive discussion of instrumentation and different planes of viewing and is not as well illustrated as other chapters.

Finally, chapters 26 through 32 contain interesting but exhaustive details about the recent applications of color flow imaging, namely, digital collection and analysis of Doppler flow data, the semiquantitative aspects of color flow imaging, computer quantification of color flow mapping, the use of laser Doppler anemometry in velocity mapping of prosthetic aortic valves, in vitro evaluation of prosthetic mitral valves, experimental laboratory use of color flow imaging, and three-dimensional reconstruction of cardiac blood flow by means of color flow mapping (called four-dimensional imaging). The appendix defines terms commonly used in color flow imaging. The text lacks chapters on ischemic heart diseases, cardiomyopathies, and pericardial diseases, but the new color flow techniques have less impact on these areas.

This book is richly invested with illustrations (362) in the form of schematic diagrams, photographs of autospy specimens, and color and conventional Doppler images. The editor has tried to avoid some of the technical defects of his previously published atlas (e.g., illustrations of different qualities and wasted space in the illustrations taken up by alphanumerics and nonessential information).

This is a major and comprehensive textbook, but sometimes it delves into more esoteric research areas. It should be extremely worthwhile for technicians, clinicians, and echocardiographers at all levels of expertise. This book is probably a better investment dollar for dollar than the recently published *Atlas of Color Doppler Echocardiography* (Lea & Febiger, 1989) by the same editor.

Taher A. F. Elkadi
David J. Sahn
University of California, San Diego
La Jolla, CA 92093

Carotid Artery Disease Assessed by Color Doppler Flow Imaging:

Correlation with Standard Doppler Sonography and Angiography

Wolfgang Steinke[1]
Christof Kloetzsch[1]
Michael Hennerici[1,2]

Carotid artery disease was assessed in 180 patients by means of color Doppler flow imaging. Color Doppler findings in 360 carotid arteries were compared with the results of standard Doppler sonography, and color Doppler findings in 60 bifurcations were compared with the results of intraarterial angiography. The sensitivity of color Doppler for the detection of carotid disease was 100% when compared with angiography. The accuracy of color Doppler in classifying minor (40–60%), moderate (61–80%), and severe (81–90%) stenosis ranged from 91.3% to 97.8% vs standard Doppler sonography, and from 91.7% to 95.8% vs angiography. Whereas all occlusions were identified correctly by both color Doppler and angiography, four pseudoocclusions of the carotid artery were misdiagnosed as occluded. Characteristic features providing reliable criteria of the degree of stenosis are (1) intensity, extent, and duration of color fading; (2) postprocessed systolic peak frequency; (3) plaque extent on serial sonograms; and (4) poststenotic flow patterns. Display of hemodynamic disturbances induced by less pronounced plaques showed highly variable patterns that could not be anticipated from the plaque morphology alone. Thus, color Doppler preserves the advantages of standard Doppler and duplex sonography but provides additional information about otherwise anechoic necrotic and thrombotic material that often causes cerebral embolisms.

With atherogenesis, repair mechanisms may be sustained or progression be stopped by reducing the risk factors and instituting medical treatment; thus, the application of this noninvasive technique is important.

***AJNR* 11:259–266, March/April 1990; *AJR* 154:1061–1068, May 1990**

For more than a decade various sonographic techniques have been used for the assessment of carotid arterial disease. Of these, continuous-wave Doppler and single-gate pulsed wave Doppler sonography incorporated in duplex systems are reported to be highly accurate relative to angiography for the detection and classification of the degree of obstruction producing a narrowing of the lumen greater than 50% [1–10]. In addition, the use of high-resolution B-mode real-time sonography makes it possible to identify small, nonstenotic (<50%) plaques and to describe their echo morphology [11–14]. Because standard duplex analysis involves difficulty in detecting local alterations in flow patterns near small plaques, and in separating these from complex blood-flow variants in the normal carotid bifurcation, its general application is limited. Apart from the advantage of standard noninvasive tests for the evaluation of carotid disease, the lack of a simultaneous display of the morphologic-hemodynamic interaction of carotid lesions is a major handicap in carrying out prospective follow-up investigations.

With the sonographic technique of color Doppler flow imaging (CDFI), the spatial and temporal distribution of the color-coded Doppler signal can be visualized in realtime and superimposed on a high-resolution gray-scale image of tissue and vessel morphology. A few studies using CDFI have examined flow patterns in the normal carotid bifurcation and confirmed previous in vitro investigations about its unique and complex nature of physiologic hemodynamics; in particular, these

Received June 22, 1989; revision requested August 30, 1989; revision received September 27, 1989; accepted September 29, 1989.

This work was supported in part by the Deutsche Forschungsgemeinschaft SFB 200/D2.

[1] Department of Neurology, Heinrich Heine University of Düsseldorf, Düsseldorf, West Germany.

[2] Present address: Neurologischen Klinik im Klinikum Mannheim der Universität Heidelberg, 6800 Mannheim 1, Theodor-Kutzer-Ufer, FRG. Address reprint requests to M. Hennerici.

0361–803X/90/1545–1061
© American Roentgen Ray Society

studies illustrate a large interindividual variability of secondary slow-flow phenomena separated from the laminar mainstream flow in the carotid bulb, where atherogenesis starts [15–17]. The inability to separate normal from abnormal flow conditions induced by carotid plaques has represented another obstacle for conventional sonographic techniques [18, 19].

The capacity of CDFI vs standard duplex sonography was investigated in a recent study [20], but the prototype used in this series provided a less than optimal image quality. The current study was undertaken to determine the advantages and limitations of CDFI in the assessment of carotid atherosclerosis and to establish characteristic features for various degrees of stenosis. CDFI was compared with standard Doppler sonography in 180 patients and with angiography in 60 carotid systems.

Subjects and Methods

Between July and September 1988, 180 patients, 128 men 43–87 years old (mean age, 62 years) and 52 women 41–88 years old (mean age, 63 years), were selected for the study. In all cases, evidence of arterial disease of either one or both carotid systems had been provided by conventional continuous-wave Doppler sonography (MDV Delalande D-480/K, Rauenberg, W. Germany; operating frequency, 4 MHz) and by Doppler sonography from duplex-system analysis with a single-gate 5-kHz pulsed-wave Doppler probe (DRF 400, Diasonics Inc., Milpitas, CA). Both systems were used because the spatial resolution of pulsed-wave Doppler for local flow analysis is superior to that of continuous-wave Doppler, whereas continuous-wave Doppler compensates for the limited capacity of pulsed-wave Doppler to display very high and low Doppler shifts. Patients were admitted for follow-up examination of asymptomatic extracranial arterial disease (46%), for cerebrovascular events (28%), for peripheral and/or coronary artery diseases (15%), or prior to vascular surgery of abdominal or peripheral arteries (11%). Classification of the degree of stenosis by means of standard Doppler sonography was consistent with criteria defined previously [2, 3, 6, 8].

CDFI examinations were performed in a total of 360 carotid systems on a Quantum angiodynograph (HQAD PV, Philips Medical System, Hamburg, FRG) using a 7.5-MHz linear transducer for simultaneous display of a gray-scale tissue image (B mode) and the superimposed color-coded Doppler information. Blood flow away from the transducer is coded in red and toward the transducer in blue; color saturation indicates the velocity of the moving target. Each pixel represents the peak frequency in a given space and time; this allows a two-dimensional display of the spatial distribution of intra-arterial flow, whereas conventional Doppler spectrum analysis summarizes the various frequencies in a larger sample volume lacking similar spatial resolution. Doppler maximum shift frequencies could be measured between 150 Hz and 16 kHz. The technical details of the instrument and results from normal carotid arteries have been reported [15].

The examinations were performed in two steps: First, multiple longitudinal and transverse B-mode sonograms were assessed for analysis of the plaque extent and morphology; then, the color-coded blood flow was superimposed for the evaluation of the hemodynamic situation at the lesion site. Stenoses with greater than 40% lumen narrowing were graded according to the following criteria: (1) degree, extent, and duration of the fading color-coded Doppler signal; (2) systolic peak frequency, obtained from postprocessing of the color signal (green tag); (3) plaque extent on the longitudinal and cross-sectional B-mode sonogram; (4) presence and characteristics of poststenotic flow pattern; and (5) pre- and poststenotic reduction in flow velocity compared with that in the contralateral carotid artery (Table 1). CDFI quality was classified as good if the high-resolution B-mode sonogram clearly demonstrated normal or pathologic vascular morphology of the bifurcation on longitudinal and cross-sectional images, and if the intensity of the real-time color-coded Doppler signal allowed a reliable distinction of normal blood flow from various abnormal hemodynamic conditions.

Biplane intraarterial angiography was performed in 38 patients (60 carotid arteries) because of transient or persistent focal neurologic symptoms in the carotid territory with a view to possible carotid endarterectomy. Carotid surgery was performed in 13 patients with a recent recurrence of events associated with severe stenosis. In all cases the extent of the lesion and tissue characteristics as revealed by CDFI were confirmed by the pathologic findings, for example, suspected thrombosis and wall hemorrhage could be correlated with anechoic, nonflow areas.

Two sonographic examinations were performed on the same day in each patient, the investigators being blinded to the results of the other studies. Similarly, angiographic findings were graded without knowledge of the CDFI result. The degree of stenosis was determined by caliper measurements of the stenotic and normal segments of the lumen.

Results

Performance

Display quality depended largely on the experience of the examiner and improved during the course of the study: initially it was unsatisfactory in 24%, reasonably good in 52%, and excellent in 24%. After 3 months of experience it was poor in only 11% and satisfactory or excellent in 89% of the patients examined. A high location of the bifurcation, an inability to hyperextend the neck, or a very deeply located carotid system were the main reasons for poor image quality. The longitudinal configuration of the large transducer certainly contributed to these difficulties. The display of the carotid bifurcation was frequently easier when the approach was from a posterolat-

TABLE 1: Classification of Internal Carotid Artery Stenosis by Color Doppler Flow Imaging

Classification	Description
Low grade (40–60%)	Color fading (>4 kHz) only during systole; long segment of increased flow velocity; minor plaque extent on B-mode image; minimal poststenotic turbulence
Medium grade (61–80%)	Color fading (>4 kHz) more circumscribed; increased diastolic flow velocity; moderate lumen narrowing on B-mode image; turbulent and reversed poststenotic flow
High grade (81–90%)	Short segment of marked color fading (>8 kHz); severe poststenotic flow reversal and mixed turbulence; severe lumen narrowing on B-mode scan; reduced prestenotic flow velocity in common carotid artery

eral position with the internal jugular vein located in front of the carotid artery.

Doppler Sonography vs CDFI

CDFI detected 72 small, nonstenotic plaques and eight minor stenoses (lumen narrowing, 40–60%) of the internal carotid artery (ICA) in 159 vessels classified as normal on conventional Doppler sonography (Table 2). In 16 cases, local abnormalities of the Doppler audio signal were related to 10 nonstenotic plaques and six minor stenoses identified by CDFI. Five suspected low-grade stenoses of the ICA could not be confirmed by CDFI. The number of misclassifications of CDFI as compared with that of standard Doppler sonography was small throughout various classes of obstruction. However, one high-grade and all four subtotal stenoses were misclassified as occlusion by CDFI. One moderate and one minor common carotid artery (CCA) stenosis, which were assessed by CDFI alone, and two common carotid occlusions are not included in Table 2. The overall accuracy of CDFI vs standard Doppler sonography in the classification of stenosis (lumen narrowing greater than 40%) and occlusions, not including nine cases with poor CDFI quality, was 89.2%.

Angiography vs CDFI and Standard Doppler Sonography

Compared with intraarterial angiography, CDFI was more accurate in classifying various grades of stenosis, whereas standard Doppler sonography showed a tendency to underestimate the degree of obstruction, leading to misclassification of one moderate and two severe stenoses (Table 3). The four subtotal stenoses detected by standard Doppler sonog-

TABLE 2: Comparison of Doppler Sonography and Color Doppler Flow Imaging of the Internal Carotid Artery

Conventional Doppler Study	Color Doppler Flow Image						
	Normal	Plaque	Minor Stenosis (40–80%)	Moderate Stenosis (61–80%)	Severe Stenosis (81–90%)	Occlusion	Poor Quality
Normal	79	72	8	0	0	0	0
Local signal abnormalities	0	10	6	0	0	0	0
Minor stenosis	4	2	65	2	0	0	4
Moderate stenosis	0	0	4	51	2	0	4
Severe stenosis	0	0	0	0	7	1	1
Subtotal stenosis	0	0	0	0	0	4	0
Occlusion	0	0	0	0	0	34	0
Total	83	84	83	53	9	39	9

TABLE 3: Correlation of Conventional Doppler Sonography and Color Doppler Flow Imaging with Intraarterial Angiography of the Internal Carotid Artery

Doppler Study	Angiogram						
	Normal	Plaque	Minor Stenosis (40–60%)	Moderate Stenosis (61–80%)	Severe Stenosis (81–90%)	Subtotal Stenosis	Occlusion
Color							
Normal	7	1	1	0	0	0	0
Plaque	1	9	1	0	0	0	0
Minor stenosis	0	3	7	0	0	0	0
Moderate stenosis	0	0	0	7	1	0	0
Severe stenosis	0	0	0	0	7	0	0
Subtotal stenosis	0	0	0	0	0	0	0
Occlusion	0	0	0	0	0	4	10
Poor display	0	0	1	0	0	0	0
Total	8	13	10	7	8	4	10
Conventional							
Normal	4	10	1	0	0	0	0
Plaque	3	1	1	0	0	0	0
Minor stenosis	1	2	6	1	0	0	0
Moderate stenosis	0	0	1	6	2	0	0
Severe stenosis	0	0	0	0	6	0	0
Subtotal stenosis	0	0	0	0	0	4	0
Occlusion	0	0	0	0	0	0	10
Poor display	0	0	1	0	0	0	0
Total	8	13	10	7	8	4	10

raphy but not displayed by CDFI were confirmed by angiography. CDFI identified nine nonstenotic plaques corresponding to the angiographic findings, but in three of 13 plaques CDFI demonstrated increased blood-flow velocity at the lesion site and hence suggested a low-grade stenosis. Standard Doppler sonography, however, failed to diagnose 10 of the small plaques. Overall accuracy of CDFI compared with angiography was 80%; the total sensitivity for the detection of carotid artery lesions was 100%. Statistical evaluation of the CDFI and conventional Doppler results vs angiography showed that CDFI also had a higher sensitivity, specificity, and accuracy for minor, moderate, and severe stenoses (Table 4).

TABLE 4: Sensitivity, Specificity, and Accuracy of Color Doppler (CDFI) vs Conventional Doppler Study and Angiography and Conventional Doppler Study vs Angiography of Minor (40–60%), Moderate (61–80%), and Severe (81–90%) Stenoses

Comparison	% Sensitivity	% Specificity	% Accuracy
CDFI vs conventional Doppler (n = 360)			
Minor	89.0	93.8	91.3
Moderate	89.5	97.5	94.2
Severe	87.5	98.5	97.8
CDFI vs angiography (n = 60)			
Minor	77.8	100	91.7
Moderate	100	94.1	95.8
Severe	87.5	100	95.8
Conventional Doppler vs angiography (n = 60)			
Minor	66.7	93.3	83.3
Moderate	85.7	82.3	83.3
Severe	75.0	100	91.7

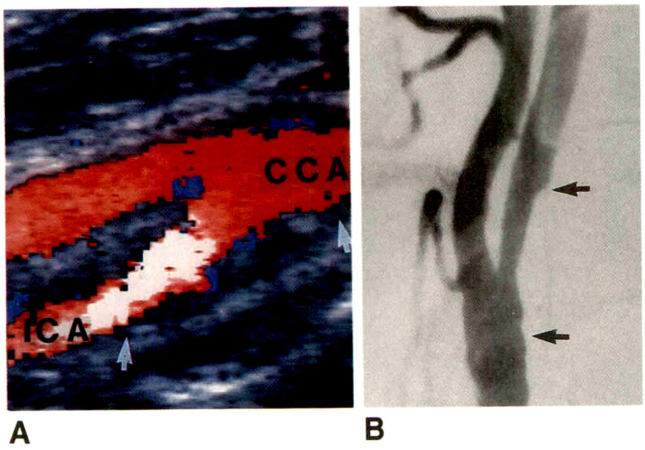

Fig. 1.—*A*, Color Doppler flow image of minor internal carotid artery (ICA) stenosis (Doppler, 40% lumen narrowing) due to long-segment plaque at posterior wall of bifurcation extending into ICA (*arrows*). Marked color fading indicates increased flow velocity. CCA = common carotid artery.

B, Corresponding angiogram shows smooth atheroma (*arrows*) producing minor lumen narrowing.

According to the criteria for ICA stenosis (Table 1), Figures 1–3 illustrate typical CDFI findings in different degrees of stenosis. In total occlusion, a late systolic short blue Doppler signal was frequently observed, indicating flow reversal in the residual stump of the ICA (Fig. 4).

Interaction of Plaque Morphology and Hemodynamics

Longitudinal and transverse B-mode sonograms of nonstenotic lesions (<40% lumen narrowing) in the CCA, ICA, and external carotid artery (ECA) (n = 154) demonstrated a smooth surface in 47%, irregular surface structures in 32%, ulcerations in 13%, and thornlike plaques in 8%. In contrast to what might have been suspected, the actual hemodynamic

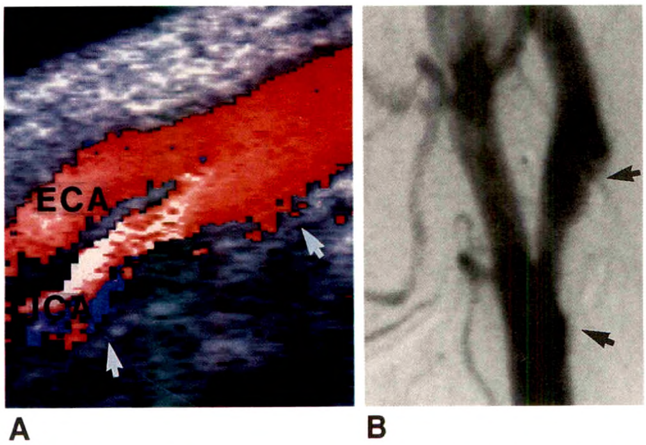

Fig. 2.—*A*, Color Doppler flow image shows minor stenosis in internal carotid artery (ICA) (Doppler, 60% lumen narrowing) with moderate poststenotic turbulence. *Arrows* indicate extent of heterogeneous plaque. ECA = external carotid artery.

B, Angiogram shows minor poststenotic dilatation (*arrows*), corresponding to site of turbulent flow displayed by color Doppler.

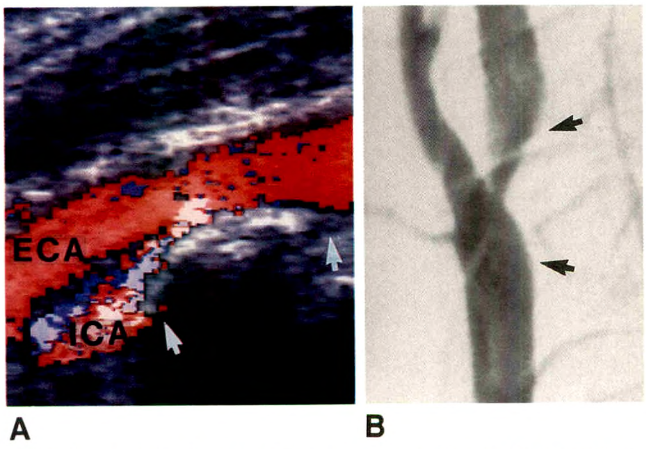

Fig. 3.—*A*, Color Doppler flow image shows high-grade stenosis in internal carotid artery (ICA) (Doppler, 80% lumen narrowing) due to large calcified plaque (*arrows*) with short-segment maximum color fading and mixed-color poststenotic turbulence and flow reversal. ECA = external carotid artery.

B, Angiogram shows circumscribed high-grade ICA stenosis with smooth surface (*arrows*).

situation at the lesion site could not be predicted from the plaque echo pattern, surface characteristics, or location alone (Table 5): in about half of the cases, smooth plaques revealed laminar flow (Fig. 5A), but detectable flow disturbances were seen in 51%. For irregular plaques, turbulence was found in only 36% (Fig. 5B); usually it was quite marked. If high-resolution B-mode images demonstrated ulcerative lesions, a turbulent flow pattern within the niche was observed more often (Fig. 5C); turbulence was present in two-thirds with small thornlike plaques (Fig. 5D). Independent of the associated surface structures, hemodynamic disturbances were observed more often if the plaque bulged into the vessel lumen.

With regard to cerebrovascular events, moderate or severe turbulence was associated with otherwise inconspicuous flat plaques and regular surfaces in seven of 23 symptomatic patients. On the other hand, despite a significant association of disturbed flow and ulcerative lesions (Table 5), flow reversal could not be assessed in nine of 11 asymptomatic subjects with irregularly surfaced plaques. This observation is of clinical interest but is not statistically significant because of the small number of cases studied. At the carotid sinus it was always possible to differentiate turbulent flow in the presence of atherosclerotic plaques from physiologic zones of secondary flow in the absence of adjacent echogenic areas. In some cases the plaque extent was underestimated owing to the anechoic appearance, or plaques were not detected even on the B-mode sonogram without intravascular color-coded

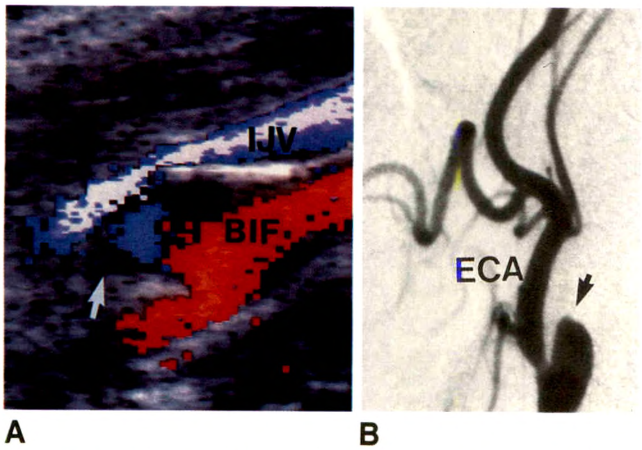

Fig. 4.—*A*, Color Doppler flow image shows total occlusion of internal carotid artery (*arrow* indicates occluded vessel) with blue-coded Doppler signal in residual stump of internal carotid artery directly above bifurcation (BIF). External carotid artery leaves insonation plane. IJV = internal jugular vein.

B, Angiogram confirms occlusion of internal carotid artery. ECA = external carotid artery.

TABLE 5: Interaction of Plaque Surface Characteristics and Hemodynamics in Nonstenotic Lesions (Lumen Narrowing <40%)

Plaque Surface	No.	Associated Turbulence (%)		
		Absent	Moderate	Marked
Smooth	72	49	19	32
Irregular	50	64	14	22
Ulcerative	20	20	20	60
Thornlike	12	33	33	33
Total	154	49	20	31

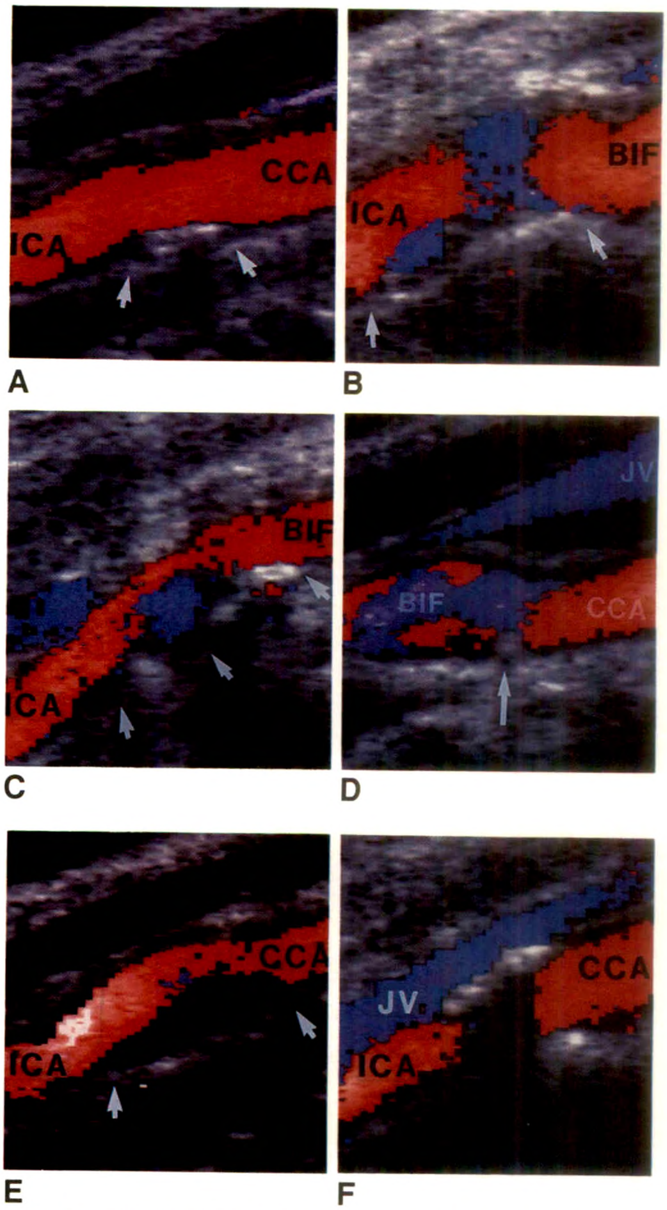

Fig. 5.—Color Doppler flow images in various types of nonstenotic carotid artery plaques.

A, Smooth echodense, partially calcified lesion (*arrows*) without associated flow disturbances.

B, Large, heterogeneous plaque (*arrows*) with irregular surface producing marked flow disturbances.

C, Partially calcified ulcerative plaque at posterior wall of internal carotid artery (*arrows*) shows marked turbulence (blue color) within ulcer niche.

D, Very small, homogeneous, thornlike plaque (*arrow*) with associated severe turbulence and flow reversal.

E, Large, anechoic plaque at posterior wall of bifurcation (*arrows*), detectable only because of spared color signal.

F, Calcified plaque at anterior vessel wall shadows opposite wall structures and extinguishes color Doppler signal.

ICA = internal carotid artery; CCA = common carotid artery; BIF = bifurcation; JV = jugular vein.

blood flow (Fig. 5E). Calcified plaques at the anterior vessel wall not only shadowed structures of the posterior wall but also extinguished the Doppler signal (Fig. 5F).

CCA

Pathologic findings in the CCA were easily assessed by CDFI. In patients with a dilative arteriopathy, hemodynamic alterations due to the altered vessel geometry were characterized by reduced blood-flow velocity, turbulence, and marked flow reversal near the vascular wall (Fig. 6). The narrowing of a long segment of the CCA lumen up to the bifurcation with diffuse thickening of the vessel wall, detected in one patient with histologically confirmed Takayasu disease, produced a high blood-flow velocity indicating stenotic lumen narrowing (Fig. 7). In cases of total CCA occlusion, CDFI was useful in determining whether or not the ICA and ECA were still patent (Fig. 8).

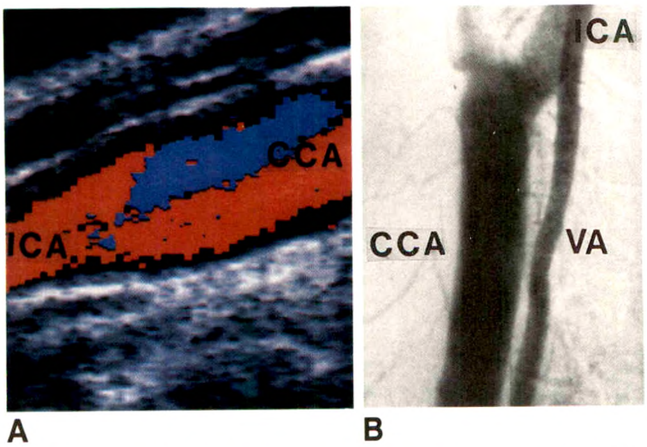

Fig. 6.—*A*, Color Doppler flow image of common carotid artery (CCA). Dilative arteriopathy produces turbulence and flow reversal at vessel wall (blue color) in CCA. ICA = internal carotid artery.

B, Angiogram shows dilated CCA up to bifurcation. VA = vertebral artery.

Discussion

CDFI is the most recent technical development in the noninvasive evaluation of carotid artery disease. In order to determine the capacity of this system for the detection and classification of different degrees of carotid disease, we correlated both the two-dimensional flow information and the echo pattern of the plaque with the results of angiography and conventional Doppler sonography. The latter had proved to be a reliable method for assessing and grading ICA stenoses in large studies published during the last decade [3, 5, 6, 8]. Because single-gate and multigate pulsed-wave Doppler sonography provide discontinuously selected information only, according to the geometry and location of the sample volume within the vessel lumen, continuous-wave Doppler sonography was used in addition for comparison with CDFI.

Characteristic abnormalities of the color-coded Doppler signal in different grades of stenosis (>40%) and measurements of the plaque extent allowed a highly accurate classification. In contrast to CDFI, conventional Doppler sonography tended to underestimate the degree of stenosis revealed by angiography. This may partly be due to the difficulty of displaying the true morphology of the obstructive lesion on angiography when only two dimensions are shown, but it also results from the limited spatial resolution of the Doppler method. In particular, classification of different degrees of stenosis with CDFI is better than has been reported in studies using pulsed-wave Doppler sonography: Zwiebel et al. [21] over- or undergraded 31% of carotid stenoses, and Hennerici and Freund [8] misclassified 37% of obstructive lesions with lumen narrowings of greater than 50% when using a proto-

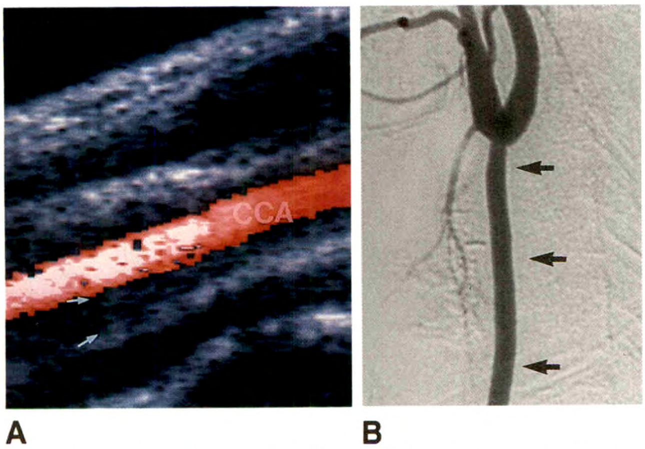

Fig. 7.—*A*, Color Doppler flow image shows long-distance lumen narrowing of common carotid artery (CCA) due to diffuse thickening of vascular wall (*arrows*) with increased velocity of blood flow (color fading) in patient with Takayasu disease.

B, Angiogram shows lumen narrowing of CCA (*arrows*). Internal and external carotid arteries are not involved.

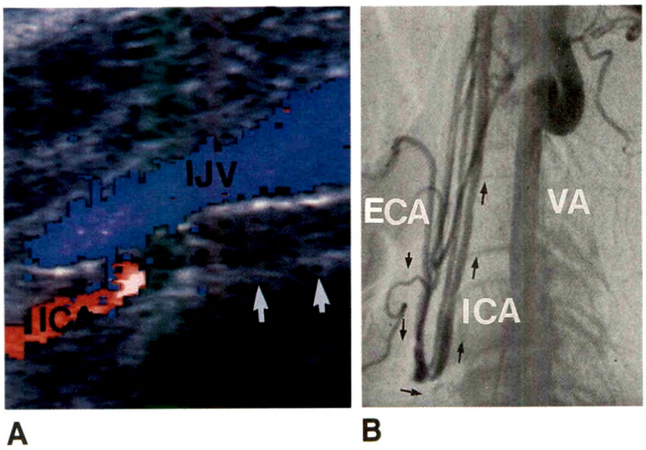

Fig. 8.—Occlusion of common carotid artery.

A, Color Doppler flow image shows patent internal carotid artery (ICA) and atrophy of occluded common carotid artery (*arrows*). IJV = internal jugular vein.

B, Corresponding angiogram proves patency of bifurcation branches (*arrows* indicate flow direction from external carotid artery [ECA] into ICA). Common carotid artery is occluded at bifurcation. VA = vertebral artery.

type duplex scanner with a multigate pulsed-wave Doppler system. Similarly, Fell et al. [22] found a correct estimation in only 72% of 50–99% stenoses. Glover et al. [23] classified the grade of lumen narrowing in accordance with the angiogram in 54% of the 30–70% stenoses; Roederer et al. [24] reported a concordance of 86% for the 50–79% stenoses but only 71% for the 80–99% stenoses. In the latter studies the B-mode image was used mainly as a guide for the positioning of the pulsed-wave Doppler sample volume. In only a few studies was the accuracy of duplex sonography vs angiography as high as in the present series. Jacobs et al. [25] found that the overall accuracy of duplex scanning improved during the course of the study; after 6 months 89% of 51–90% stenoses were classified correctly.

Angiography has been the gold standard in the definition of carotid lesions, and the availability of IV and intraarterial digital subtraction angiography encourages outpatient studies. A disadvantage of angiography, however, is that it tends to overestimate the degree of the lumen narrowing because it visualizes the lumen as opaque in two planes only. The arterial wall remains a negative contour, and no information is available on its morphologic structure. In addition, aortic arch angiograms alone may be insufficient for correct diagnosis. Thus, for the noninvasive estimation of carotid obstruction, the classification of the degree of stenosis may preferentially be based on the abnormal features of the color-coded Doppler signal and the various structural alterations of the plaque as revealed by the B-mode sonogram.

The level of accuracy in the assessment of different degrees of stenosis is far lower if B-mode scans are used without continuous- or pulsed-wave Doppler sonography [13, 21, 26]. In a large multicenter validation study, Ricotta et al. [26] reported a sensitivity between 36% and 43% for different types of stenosis vs angiography. On the other hand, high-resolution B-mode sonograms may detect early nonstenotic atherosclerotic lesions even better, and may to some extent provide useful information about the plaque configuration and composition [11, 13, 14, 27]. Our present experience shows that CDFI contributes important additional information to the B-mode and Doppler-mode analysis already available in the assessment of carotid plaques:

1. The color-coded Doppler signal at the lesion site improves the evaluation of the extent of carotid plaques by the simultaneous two-dimensional display of tissue structure and the flow-velocity profile. One reason for this is the ability of this method to directly assess anechoic plaque components such as necrotic and thrombotic material, which now can be identified adjacent to the vessel wall, and the atherosclerotic plaque by sparing the color-flow signal in the absence of any tissue reflection.

2. Differentiation of smooth and irregular surface structures and identification of ulcerative niches are improved. Both are of great clinical importance, since most cerebrovascular events today are suspected to be of embolic origin, and the vascular source of many hitherto undetectable ones thus may be identified. In addition, repair mechanisms as well as progression of minor and moderate plaques can be followed prospectively [28], which may finally influence risk factor adjustment and medical treatment in individual patients.

3. Prospective studies on the characteristics of hemodynamic disturbances associated with various forms of carotid plaques can now be performed to investigate whether dangerous plaques are to be separated from benign ones. This important problem has not been solved unanimously by means of any available conventional sonographic technique.

4. With regard to conventional duplex sonography, the additional use of a simultaneous display of hemodynamic aspects in two dimensions facilitates the detection and evaluation of the degree and extent of carotid lesions considerably. This will improve the reproducibility of findings and compensate for one of the major obstacles of conventional techniques, that is, interobserver disagreement.

At present, CDFI still has limitations, some of which are temporary. In our series it failed to identify reliably four cases of subtotal stenoses, although they had been detected by conventional continuous-wave Doppler sonography. Intraarterial aortic arch digital subtraction angiography alone similarly misdiagnosed these "pseudoocclusions" of the internal carotid artery, a condition that is characterized by (1) flow velocities equal to zero distal to a very tight stenosis or (2) segmental occlusion with retrograde filling from the siphon [29–32]. Until recently the detection of this vascular condition was restricted to the use of special angiographic techniques of transfemoral subtraction angiography with selective carotid and sometimes vertebral catheterization, and occasionally long serial imaging runs of reduced flow rates and increased injection bolus. However, CDFI now may offer an improved diagnosis: we recently identified two similar cases with the use of refined software with the facility to assess very-slow-flow Doppler-shift frequencies (<150 Hz).

Although the rate of good or fair display quality increased during the course of our study, 11% of the examinations in the second half of the study population were unsatisfactory when using strict criteria for adequate visualization of color-coded blood flow and vascular structures. Because only a few studies using B-mode imaging and duplex sonography give data on image quality [12, 21, 25], comparison with our results is difficult, but it can be assumed that CDFI provides more technically good examinations compared with other sonographic techniques, owing to easier vessel identification and data acquisition with the color-coded Doppler display.

The results of the present study demonstrate that CDFI not only preserves the advantages of conventional Doppler sonography and duplex sonography, but also provides important additional diagnostic information. Part of its clinical relevance is the improved assessment of carotid atherogenesis from its early onset in as much detail as is currently possible. This may be useful in prospective trials on the natural history of carotid artery diseases. These studies can form the basis for better knowledge about the pathogenesis of ischemic cerebral events.

REFERENCES

1. Barnes RE, Rittgers SE, Putney WW. Real-time Doppler spectrum analysis. *Arch Surg* **1982**;117:52–57
2. Blackshear WM, Phillips DJ, Thiele BL, et al. Detection of carotid occlusive

disease by ultrasonic imaging and pulsed Doppler spectrum analysis. *Surgery* **1979**;86:698–706

3. Hennerici M, Aulich A, Sandmann W, Freund HJ. Incidence of asymptomatic extracranial arterial disease. *Stroke* **1981**;12:750–758
4. Johnston KW, Baker WH, Burnham SJ, Hayes AC, Kupper CA, Poole MA. Quantitative analysis of continuous-wave Doppler spectral broadening for the diagnosis of carotid disease: results of a multicenter study. *J Vasc Surg* **1986**;4:493–504
5. Reneman RS, Spencer MP. Local Doppler audio spectra in normal and stenosed carotid arteries in man. *Ultrasound Med Biol* **1979**;5:1–11
6. Trockel U, Hennerici M, Aulich A, Sandmann W. The superiority of combined continuous wave Doppler examinations over periorbital Doppler for the detection of extracranial carotid disease. *J Neurol Neurosurg Psychiatry* **1984**;47:43–50
7. Arbeille P, Lapierre F, Patat F, et al. Evaluation du degre des stenoses carotidiennes par l'analyse spectrale du signal Doppler. *Arch Mal Coeur* **1984**;77:1097–1107
8. Hennerici M, Freund HJ. Efficacy of cw-Doppler and duplex system examinations for the evaluation of extracranial carotid disease. *JCU* **1984**;12:155–161
9. Keagy BA, Pharr WF, Thomas D, Bowles DE. A quantitative method for the evaluation of spectral analysis patterns in carotid artery stenosis. *Ultrasound Med Biol* **1982**;8:625–630
10. Rittgers SE, Thornhill BM, Barnes RW. Quantitative analysis of carotid artery spectral waveforms: diagnostic value of parameters. *Ultrasound Med Biol* **1983**;9:255–264
11. Bluth EI, Kay D, Merritt CRB, et al. Sonographic characterization of carotid plaque: detection of hemorrhage. *AJR* **1986**;146:1061–1065
12. Comerota AJ, Cranley JJ, Cook SE. Real-time B-mode carotid imaging in diagnosis of cerebrovascular disease. *Surgery* **1981**;89:718–729
13. Hennerici M, Reifschneider G, Trockel U, Aulich A. Detection of early atherosclerotic lesions by duplex scanning of the carotid artery. *JCU* **1984**;12:455–464
14. Reilly LM, Lusby RJ, Hughes L, Ferrell LD, Stoney RJ, Ehrenfeld WK. Carotid plaque histology using real-time ultrasonography. *Am J Surg* **1983;**146:188–189
15. Middleton WD, Foley WD, Lawson TL. Flow reversal in the normal carotid bifurcation: color Doppler flow imaging analysis. *Radiology* **1988**;167:207–210
16. Steinke W, Kloetzsch C, Hennerici M. Variability of flow patterns in the normal carotid bifurcation. *Atherosclerosis* (in press)
17. LoGerfo FW. Hemodynamics and the arterial wall. *J Vasc Surg* **1989**;9:380–381
18. Nicholls SC, Phillips DJ, Primozich JF, et al. Diagnostic significance of flow separation in the carotid bulb. *Stroke* **1989**;20:175–182
19. Middleton WD, Foley WD, Lawson TL. Color-flow Doppler imaging of carotid artery abnormalities. *AJR* **1988**;150:419–425
20. Hallam MJ, Reid JM, Cooperberg PL. Color-flow Doppler and conventional duplex scanning of the carotid bifurcation: prospective, double-blind, correlative study. *AJR* **1989**;152:1101–1105
21. Zwiebel WJ, Austin CW, Sackett JF, Strother CM. Correlation of high-resolution B-mode and continuous-wave Doppler sonography with arteriography in the diagnosis of carotid stenosis. *Radiology* **1983**;149:523–532
22. Fell G, Phillips DJ, Chikos PM, Harley JD, Thiele BL, Strandness DE Jr. Ultrasonic duplex scanning for disease of the carotid artery. *Circulation* **1981**;64:1191–1195
23. Glover JL, Bendick PJ, Jackson VP, Becker GJ, Dilley RS, Holden RW. Duplex ultrasonography, digital subtraction angiography and conventional angiography in assessing carotid atherosclerosis. *Arch Surg* **1984**;119:664–669
24. Roederer GO, Langlois YE, Jager KA, et al. The natural history of carotid arterial disease in asymptomatic patients with cervical bruits. *Stroke* **1984**;15:605–613
25. Jacobs NM, Grant EG, Schellinger D, Byrd MC, Richardson JD, Cohan SL. Duplex carotid sonography: criteria for stenosis, accuracy, and pitfalls. *Radiology* **1985**;154:385–391
26. Ricotta JJ, Bryan FA, Bond G, et al. Multicenter validation study of real-time (B-mode) ultrasound, arteriography, and pathologic examination. *J Vasc Surg* **1987**;6:512–520
27. O'Donnell TF, Erdoes L, Mackey WC, et al. Correlation of B-mode ultrasound imaging and arteriography with pathologic findings at carotid endarterectomy. *Arch Surg* **1985**;120:443–449
28. Hennerici M, Rautenberg W, Trockel U, Kladetzky RG. Spontaneous progression and regression of small carotid atheroma. *Lancet* **1985**;1:1415–1419
29. Countee RW, Vijayanathan T. Reconstruction of "totally" occluded internal carotid arteries. Angiographic and technical considerations. *J Neurosurg* **1979**;50:747–757
30. Heros RC, Sekhar LN. Diagnostic and therapeutic alternatives in patients with symptomatic "carotid occlusion" referred for extracranial-intracranial bypass surgery. *J Neurosurg* **1981**;54:790–796
31. Gabrielsen TO, Seeger JF, Knake JE, Burke DP, Stilwill EW. The newly occluded internal carotid artery. A diagnostic trap. *Radiology* **1981;**138:611–618
32. Ringelstein EB, Zeumer H, Angelou D. The pathogenesis of strokes from internal carotid artery occlusion. Diagnostic and therapeutical implications. *Stroke* **1983**;14:867–874

Pseudoatrophy of the Cervical Portion of the Spinal Cord on MR Images: A Manifestation of the Truncation Artifact?

David M. Yousem[1]
Peter A. Janick[1]
Scott W. Atlas[1]
David B. Hackney[1]
Scott A. Glasser[2]
Felix W. Wehrli[1]
Robert I. Grossman[1]

Routine evaluation of axial MR images of the cervical spine with high-intensity CSF (long TR/TE spin-echo or gradient-echo images) revealed apparent narrowing of the cord's anteroposterior diameter when these images were compared with corresponding postmyelography CT scans. This discrepancy was believed to be due to the truncation artifact at the CSF-cord boundary. To examine the truncation effect, we compared cord diameters in 12 patients on postmyelography CT scans and MR images and then compared these with MR scans of normal volunteers and of an agar-saline spine phantom. There was an artifactual diminution of the cord diameter in the 128-step phase-encoding axis of the 128 × 256-matrix MR scan as compared with the diameter of the cord in the patients' postiohexol CT scans and in the 256 phase-encoded axis MR scan in the volunteer study. A similar discrepancy was noted in the spine phantom study, in which the cord diameter in the 256-step phase-encoded MR scan, the CT scan, and direct measurement exceeded that in the 128-step phase-encoded axis MR scan. The range of differences between the measurements was as large as 2.3 mm (patients), 1.7 mm (volunteers), and 1.8 mm (phantom) for the three studies. In all three studies, varying the photographic window width and level produced variation in the apparent cord diameter of up to 1.5 mm. To eliminate this effect, the cord diameters in the phantom and the normal control subjects were measured at identical window levels.

The truncation artifact, coupled with standard window settings used in photography, may lead to inaccurate display of the diameter of the cervical spinal cord.

AJNR **11:373–377, March/April 1990;** ***AJR*** **154: 1069–1073, May 1990**

During routine evaluation of MR images of the cervical spine obtained with either conventional spin-echo or 3D Fourier transformation (3DFT) gradient-echo sequences in which CSF was hyperintense, a discrepancy was noted in the apparent size of the anteroposterior (AP) diameter of the cervical spinal cord compared with postmyelography axial CT scans obtained in the same patient (Fig. 1). The spinal cord appeared smaller on the MR images. It was hypothesized that the truncation artifact at the interface of hyperintense CSF and hypointense spinal cord was responsible for the misrepresentation of the cord size. By comparing the MR images with postintrathecal contrast CT scans and examining the effects of matrix size and phase-encoding direction in normal volunteers and in a spine phantom, we developed an explanation for the mechanism for the incongruity of the measured cervical spinal cord dimensions.

Subjects and Methods

Clinical Patients

The axial scans of 12 consecutive patients who had an MR scan with hyperintense CSF (i.e., either a long TR/TE spin-echo or a low flip angle gradient-echo MR scan) and a postmyelography CT scan with the same scan angulation within a period of 6 weeks were retrospectively reviewed by three neuroradiologists. The MR scans were obtained on a 1.5-

Received May 22, 1989; revision requested July 27, 1989; revision received October 2, 1989; accepted October 10, 1989.

Presented at the annual meeting of the American Society of Neuroradiology, Orlando, March 1989.

[1] Department of Radiology, Neuroradiology Section, Hospital of the University of Pennsylvania, 3400 Spruce St., Philadelphia, PA 19104. Address reprint requests to S. W. Atlas.

[2] Department of Radiology, Albert Einstein Medical Center, Philadelphia, PA 19141.

0361–803X/90/1545–1069
© American Roentgen Ray Society

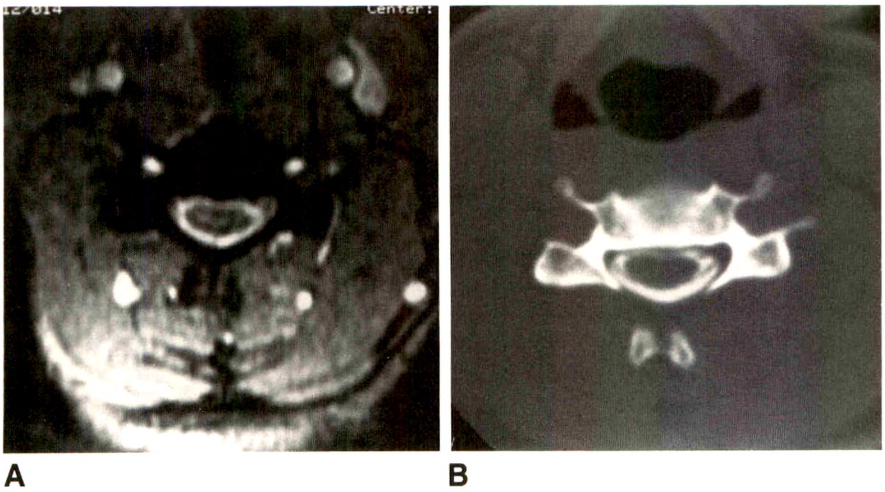

Fig. 1.—MR vs postmyelography CT of C5 AP diameter.

***A*, Axial gradient-echo 3DFT MR image.**

***B*, Axial CT scan after intrathecal contrast administration.**

The gradient-echo image (*A*) demonstrates a 1.3-mm difference in AP cord diameter as compared with postmyelography CT scan (*B*) taken 2 weeks later at the same plane and angulation. Cord atrophy might have been suspected on the MR study if one had not been cognizant of the truncation artifact in the 128 AP axis.

T GE imaging system employing a 5-in. round surface coil. Long TR/TE spin-echo scans had TRs greater than 2000, TEs of 50 or greater, 3–5-mm slice thicknesses, and 16–24-cm fields of view (FOV). The MR gradient-echo 3DFT gradient-recalled acquisition in the steady state (GRASS) volumetric sequences were obtained with flip angles of 5° with 50/15/1 (TR/TE/excitations), 1.5-mm contiguous slices, a 128 × 256 matrix (the 128-phase axis in the AP direction), 64 slice encodings, and a 24-cm field of view. Velocity compensation (first-order gradient moment nulling) was employed on all sequences. The CT scans were obtained on a GE 9800 scanner after the intrathecal administration of iohexol (240–300 mg/dl). Slice thickness was 3 mm, and scans were photographed at soft-tissue and bone-window settings.

Measurements of the cervical spinal cord were obtained in the AP dimension for equivalent levels on the CT and MR images. Thirty levels in 12 patients were independently evaluated by three radiologists. Direct measurements from hard copy images were made with calipers and were rounded to the nearest 0.5 mm.

Normal Volunteers

To corroborate the conjecture that the truncation artifact was responsible for the discrepancy in cord dimensions on MR images, we compared MR scans on three normal volunteers obtained with a gradient-echo 3DFT volumetric sequence with a 128 × 256 and a 256 × 256 matrix. Pixel sizes were 1.875 mm and 0.9375 mm when 128 and 256 encoding steps were used, respectively, with this 24-cm FOV sequence. Additionally, 3DFT scans were obtained in which the orientation of the 128 axis of the 128 × 256 matrix was designated AP and then right-left. AP cord diameters were measured at random slice sections. The results of the cord dimensions on the three separate sequences, as measured by a single radiologist using electronic calipers on the viewing screen, were then compared.

Phantom Study

A phantom consisting of a 7.3-mm inner core of agar in dialysis tubing surrounded by an outer concentric tube of normal saline and floating in tap water was used to simulate the intensity characteristics of the CSF and spinal cord. This phantom was scanned with identical MR parameters used for the normal volunteer study. The number of phase-encoding steps, and the orientation of the 128-step phase and frequency axes, were varied in a similar fashion to the volunteer study described above. AP diameters were again measured by one radiologist at 16 random levels. The phantom was also scanned by CT to ascertain CT dimensions of the concentric tubes. Direct measurement of the diameter was also performed at the corresponding levels.

Results

Table 1 provides a summary of the results described in this section.

Clinical Patients

In 52 of 90 patient levels (30 levels measured by three radiologists), the AP diameter of the cervical cord as measured on MR was less than that measured on CT. In these 52 instances in which the CT scan diameter was greater than the MR diameter, the average difference was 1.04 mm, with an average CT cord diameter of 7.25 mm. The range of differences in these 52 pairs of measurements was 0.17 to 2.3 mm (SD = 1.02 mm) (Fig. 1). The MR diameter exceeded the CT diameter in 18 instances. In 20 levels examined, the AP cord diameter was the same on CT and MR. When all 90 levels were averaged, the mean CT diameter exceeded the mean MR diameter by 0.5 mm (7.25 mm vs 6.75 mm). The difference between the mean CT diameter and the mean MR diameter was statistically significant with a p value of .026 on the Student's t test.

Normal Volunteers

Of 28 random sections measured in the normal volunteers' cervical spines, the AP diameter of the cord was larger in 23 sections employing a 256 × 256 matrix compared with the 128 × 256 scan with the 128-phase axis oriented in the AP direction (128 AP). The average difference between the measurements was 0.77 mm for all 28 levels measured. In just those levels in which the 256 × 256 scan diameter exceeded that of the 128 AP scan, the average difference was 1.02 mm. The difference between the two measurements ranged from 0.3 to 1.5 mm (SD = 0.50 mm).

TABLE 1: Comparison of AP Diameter of Cord Among Different Imaging Techniques

Study Type	No. of Levels
Patient study	
CT postiohexol AP diameter > 128 AP × 256 right-left MR	52*
CT postiohexol AP diameter = 128 AP × 256 right-left MR	20
CT postiohexol AP diameter < 128 AP × 256 right-left MR	18
MR volunteer study (different matrices)	
1. 256 AP × 256 right-left AP diameter > 128 AP × 256 right-left MR	23*
256 AP × 256 right-left AP diameter = 128 AP × 256 right-left MR	5
256 AP × 256 right-left AP diameter < 128 AP × 256 right-left MR	0
2. 256 AP × 128 right-left AP diameter > 128 AP × 256 right-left MR	21*
256 AP × 128 right-left AP diameter = 128 AP × 256 right-left MR	5
256 AP × 128 right-left AP diameter < 128 AP × 256 right-left MR	2
MR phantom study (different matrices)	
1. 256 AP × 256 right-left AP diameter > 128 AP × 256 right-left MR	13*
256 AP × 256 right-left AP diameter = 128 AP × 256 right-left MR	3
256 AP × 256 right-left AP diameter < 128 AP × 256 right-left MR	0
2. 256 AP × 128 right-left AP diameter > 128 AP × 256 right-left MR	11*
256 AP × 128 right-left AP diameter = 128 AP × 256 right-left MR	3
256 AP × 128 right-left AP diameter < 128 AP × 256 right-left MR	2

Note.—AP = anteroposterior.

* Our comparisons show that the scan with the 128 phase-encoding steps in the AP direction produces a diminution in measured cord diameter. The magnitude of the difference can be as high as 2.3 mm in a 7.5-mm-wide cord.

The AP cord diameter of the 128 × 256 scan with the 128-phase axis oriented right-left (128 right-left) was greater than the AP diameter of the corresponding section in the 128 × 256 scan with the 128-phase axis oriented in the AP direction in 21 of 28 instances. When all 28 sections were examined, the scan cord diameter in the 128 right-left matrix exceeded the 128 AP matrix scan diameter by an average of 0.71 mm. However, the average difference was 0.94 mm in just those 21 instances in which the 128 right-left matrix measurement exceeded the 128 AP matrix. The range of differences in these 21 levels was 0.3 to 1.7 mm (SD = 0.64 mm) (Fig. 2).

Phantom Study

The 256 × 256 matrix AP diameter of the cord phantom was greater in 13 of 16 levels and equal in three levels compared with the 128 × 256 study with the 128-phase axis in the AP direction. The average overall diameter of the phantom cord was greater by 0.56 mm in the 256 matrix study (average 256 × 256 phantom dimension of 7.3 mm) when all 16 levels were examined. In those 13 levels in which the 256 × 256 measurement exceeded the 128 AP diameter, the average difference was 0.73 mm, with a range of 0.3 to 1.8 mm (SD = 0.48 mm).

When the 128 matrix was right-left, the overall phantom diameter was greater than the 128 AP image in 11 of 16 measurements by an average of 0.50 mm. In just those 11 levels in which the 128 AP scan's diameter was smaller than the 128 right-left study, the average difference was 0.78 mm, with a range of 0.3 to 1.6 mm (SD = 0.56 mm) (Fig. 3). The average CT AP phantom measurement and the direct measurement were within 0.2 mm of the 256 × 256 matrix dimensions, ranging from 7.1 to 7.5 mm.

When the window levels and widths were changed on the same 128 AP matrix MR image, it was noted that one could

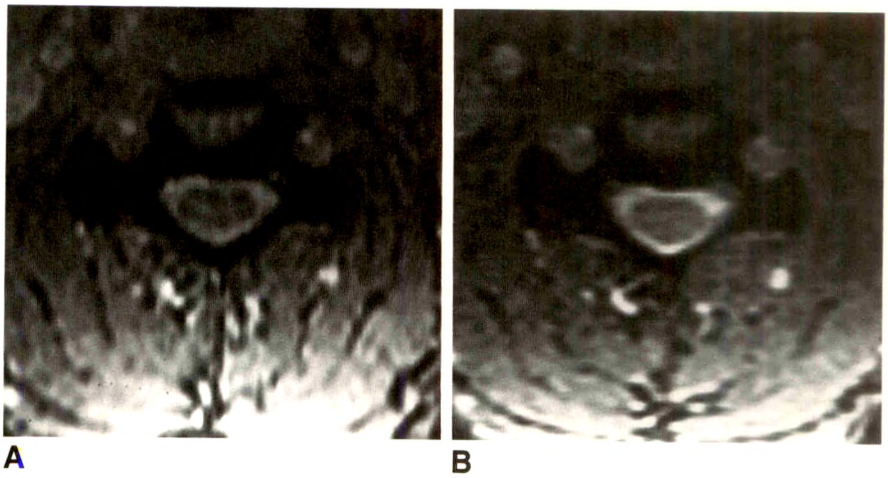

Fig. 2.—Effect of matrix size on apparent cord dimensions.

***A*, Gradient-echo volumetric 3DFT scan (50/15/1), 128 (AP) × 256 (right-left).**

***B*, Gradient-echo volumetric 3DFT scan (50/15/1), 256 (AP) × 256 (right-left).**

The scan with the 128 axis of a 128 × 256 matrix in the AP direction (*A*) demonstrates a narrower AP diameter than does the scan at same level with exact same parameters but a 256 × 256 matrix (*B*). This is due to truncation artifact and photographic windowing to achieve the bright CSF effect. The difference is 1 mm anteroposteriorly between the two scans, but less than 0.1 mm transversely. When the 128 axis is in the right-left direction, the same reduction in diameter is produced in the transverse measurement.

alter the measured cord width by up to 1.5 mm before severe image distortion was produced. This finding was reproducible in the normal volunteer study (Fig. 4).

Discussion

Although the truncation artifact has been well described with respect to its pseudosyrinx appearance on sagittal images of the cervical spinal cord, the impact on spinal cord size on axial images of the spine, and in low flip angle gradient-echo scans, has not been emphasized [1–6].

Truncation artifacts occur at sharp, high-contrast interfaces [1–6]. Whereas the Fourier transformation used in image reconstruction assumes an infinite set of data, in reality, only a finite number of k-space samples are available. The result of this raw data truncation is an oscillatory intensity pattern manifested as a series of alternating bands of low and high signal intensity parallel to the high-contrast interface [1–7]. These intensity bands, appearing in the substance of the cervical spinal cord, create the pseudosyrinx appearance described by previous investigators [2–4, 6]. The characteristic features of this artifact are its regular, periodic spacing and the noticeable drop-off in intensity with successive side lobes/bands [1, 4, 5, 8]. The Gibbs phenomenon refers to the first undershoot and overshoot intensity waves of the interface, approximately 9% below and above the actual intensity differences of the two structures being examined [1, 3, 4, 8].

The second implication of the truncation artifact and the subject of this paper is the apparent change in the dimensions of objects being imaged when high-contrast interfaces exist. This effect is caused by the sloping of the intensity profile, schematically shown in Figure 5 and evident in the profile calculations in the article by Bronskill et al. [2], which assume rectangular high-contrast objects [3, 9] (Fig. 5). The sloping line of intensity plotted against the distance axis is reinforced when the 128 scanning matrix is interpolated onto a 512 imaging matrix for photography [3, 4, 8, 10]. The sloping line may extend over a minimum of one pixel width (1.875 mm in a 128-matrix scan with a 24-cm FOV) or may extend over more than one pixel in an apodized (filtered) scan [3, 8]. The use of a low-pass, high-frequency filter to attenuate the repetitive side lobes of the signal profile tends to blur high-contrast edges, allowing more potential distortion of cord dimensions by decreasing the slope of the intensity profile through the interface [3, 4, 6, 8]. One may photograph at window settings to create an apparent interface anywhere

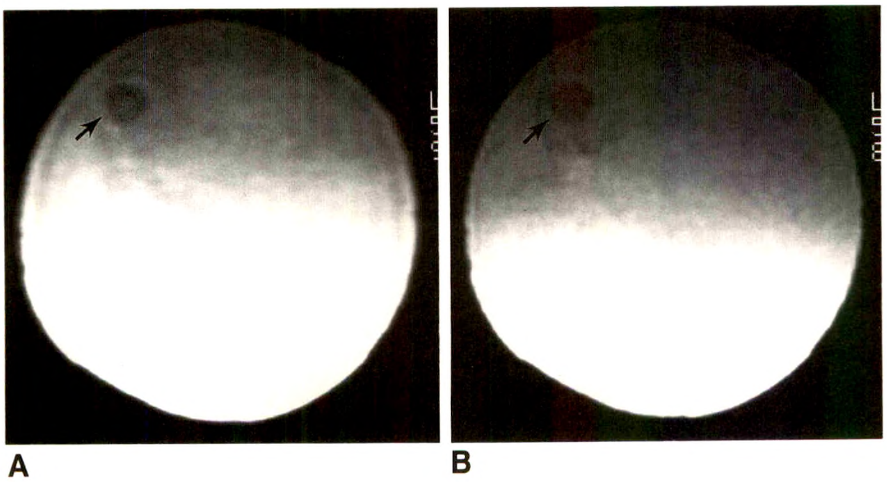

Fig. 3.—Transverse diameter distortion in spine phantom with 128 axis right-left.

A, **Gradient-echo volumetric 3DFT scan (50/15/1), 128 (right-left) × 256 (AP).**

B, **Gradient-echo volumetric 3DFT scan (50/15/1), 256 (AP) × 256 (right-left).**

The transverse diameter of the agar spinal cord phantom (*arrow*) in a water bath is truncated in the 128 × 256 scan when the 128 plane is transverse (*A*) compared with a 256 × 256 scan (*B*) through same level. The phenomenon is not an AP or right-left factor, but dependent on the direction of the 128 axis. A CT scan through the phantom confirmed the accuracy of the 256 × 256 dimensions.

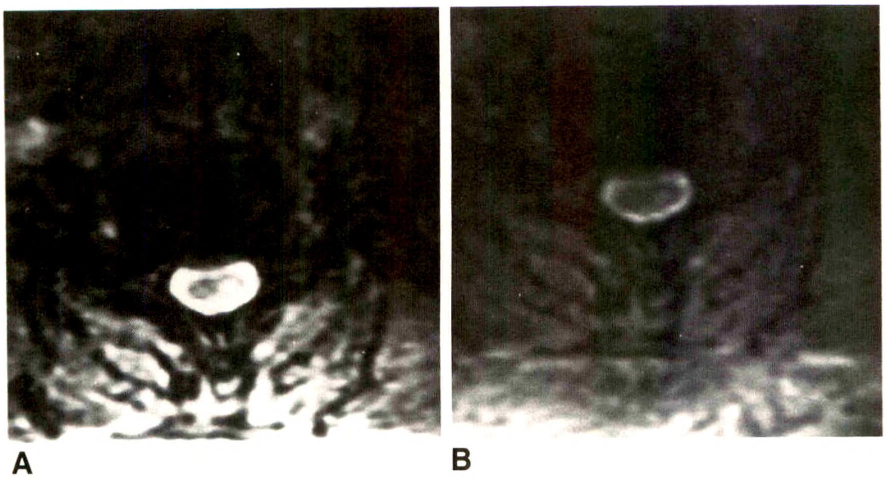

Fig. 4.—Effect of photographic windowing on apparent cord size.

A, **Gradient-echo volumetric 3DFT scan (50/15/1), 128 (AP) × 256 (right-left), narrow window settings.**

B, **Gradient-echo volumetric 3DFT scan (50/15/1), 128 (AP) × 256 (right-left), with wide window settings.**

These two images (*A* and *B*) are at exact same level with exact same scanning parameters, but are photographed with a narrow window and level (*A*) or a wide window and level (*B*). Note apparent increase in cord diameter in the darker image (*B*) and pseudoatrophic appearance in the scan with the more hyperintense CSF (*A*). Anatomic detail is lost with wider windowing.

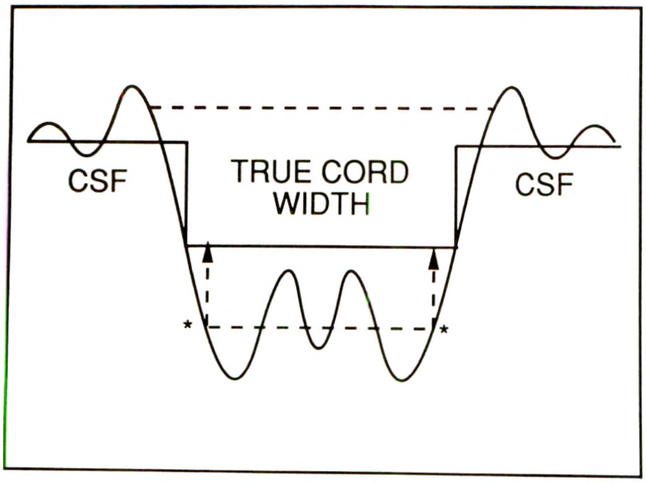

Fig. 5.—Diagrammatic representation of mechanism of pseudoatrophy. The sloping line of the Fourier transformation intensity profile between CSF and spinal cord will extend across at least one pixel width. In a scan with a 24-cm FOV and a 128 × 256 matrix, one pixel width is 1.875 mm, producing a flatter slope than if a 256 × 256 matrix (0.9375 mm pixel) were used. The cord may be photographed within the range of intensity levels shown as *dotted lines*, which inaccurately display the true cord width. To produce the bright CSF intensity desired for a myelographic effect, one usually photographs at the lower window level (*asterisks*), thereby producing an underestimation of cord diameter.

along this sloping line, leading to misrepresentation of true cord width. The potential for misrepresentation of cord size is lessened with the use of a 256 × 256 matrix scan owing to the sampling of higher spatial frequencies; however, it does persist and its magnitude is dependent on operator-determined photographic window settings.

The methods for reducing truncation artifacts include decreasing the pixel diameter by increasing the matrix size or decreasing the field of view [1–6, 8, 9]. Alternatively, one may change frequency and phase-encoding axes to divert the artifact to a less confusing plane with the smaller sampling frequency [2, 4, 6, 7]. Although this artifact is exaggerated on long TR/TE and short flip angle gradient-echo images of the spinal cord, it is expected to occur on short TR/TE images as well. The presence of a pseudosyrinx on sagittal short TR/TE spin-echo scans attests to the truncation artifact's persistence on these sequences. Even if the 128 phase-encoding steps were able to be represented perfectly as a perpendicular step function at the cord-CSF interface, the interpolation of points between the two high-contrast intensity points during conversion of the data onto a standard 512 × 512 display format will create the potential for misrepresentation of absolute cord measurements through photographic windowing on the monitors.

In summary, the truncation artifact creates the potential for misrepresenting the cord-CSF interface because of the sloping of the intensity profile. This sloping line of intensity is perpetuated by interpolation of 128 matrix points onto a 512 photographic matrix. By attempting to achieve high-contrast images of the spine, window settings may be selected at which the apparent spinal cord size is reduced.

It is critically important to recognize the truncation effect in the axial examination of the cervical spine. Because the cord's dimensions may be inaccurately depicted on these MR images, the potential exists for overdiagnosing spinal cord atrophy or compression. The neuroradiologist must therefore be wary of conclusions based on spinal cord measurements or cord morphology obtained while using a relatively small matrix scan.

REFERENCES

1. Wood ML, Henkelman RM. Truncation artifacts in magnetic resonance imaging. *Magn Reson Med* **1985**;2:517–526
2. Bronskill MJ, McVeigh ER, Kucharczyk W, Henkelman RM. Syrinx-like artifacts on MR images of the spinal cord. *Radiology* **1988**;166:485–488
3. Levy LM, Di Chiro G, Brooks RA, Dwyer AJ, Wener L, Frank J. Spinal cord artifacts from truncation errors during MR imaging. *Radiology* **1988**;166:479–483
4. Czervionke LF, Czervionke JM, Daniels DL, Haughton VM. Characteristic features of MR truncation artifacts. *AJNR* **1988**;9:815–824
5. Curtin AJ, Chakeres DW, Bulas R, Boesel CP, Finneran M, Flint E. MR imaging artifacts of the axial internal anatomy of the cervical spinal cord. *AJNR* **1989**;10:19–26
6. Henkelman RM, Bronskill MJ. Artifacts in magnetic resonance imaging. *Rev Magn Reson Med* **1987**;2:1–126
7. Haacke EM. The effects of finite sampling in spin-echo or field-echo magnetic resonance imaging. *Magn Reson Med* **1987**;4:407–421
8. Lufkin RB, Pusey E, Stark DD, Brown R, Leikind B, Hanafee WN. Boundary artifact due to truncation errors in MR imaging. *AJR* **1986**;147:1283–1287
9. Breger RK, Czervionke LF, Kass EG, et al. Truncation artifact in MR images of the intervertebral disk. *AJNR* **1988**;9:825–828
10. Gellad F, Rao KCVG, Joseph PM, Vigorito RD. Morphology and dimensions of the thoracic cord by computer-assisted metrizamide myelography. *AJNR* **1983**;4:614–617

Book Review

Cerebral and Spinal Computerized Tomography, 2nd ed. By Sebastian Lange, Thomas Grumme, Wolfgang Kluge, Kurt Ringel, and Wolfgang Meese. (Translated by Joseph H. Long.) New York: Karger, 267 pp., 1989. $54.75

It can be quite a lot of fun to read textbooks on one's specialty that are written by authors from other countries. Anatomic nomenclature can be surprising, pathologic terms might change, and sometimes the tenor of practice is quite different. This is the primary strength of *Cerebral and Spinal Computerized Tomography*. The next best feature of this book is the attempt to map out functional pathways on axial CT. Particularly good diagrams are found regarding the major motor and sensory pathways as well as another showing the location of the most common berry aneurysms. In the brief spinal section, an attempt has been made to correlate signs, symptoms, and lesion location. A particularly clear explanation of this type is seen regarding cervical radiculopathies.

Other drawings are not as well executed. For example, the optic radiations are diagramed improperly. It is important to know that those fibers placed more ventrally first turn forward and descend into the temporal lobe, spreading out over the temporal horn. The illustrations do not show this. Annotation on the sagittal diagram in Figure 25 apparently has slipped upward over the drawing, causing gross misidentification of structures. It may be difficult for North American readers to be comfortable with the left-right reversal used in this book. Other limitations include simplistic anatomic diagrams, annotation of sketches of CT images instead of the images themselves, lack of appropriate discussion of techniques superior to CT in certain imaging algorithms, unnecessary complication of certain diagrams (e.g., those on the imaging characteristics of primary brain neoplasms), and generally extremely superficial handling of normal and disease states.

I have the impression that this work was put together for advertising purposes. The copyright is held by Schering AG of West Germany. Accordingly, the primary design of this work may have been as a complimentary promotion. If a superficial review of modern neuroimaging is desired, *Introduction to Neuroimaging*, by William W. Orrison, Jr. (Little, Brown), would be a better choice. A true reference source for brain, head and neck, and spinal imaging would require a multivolume text such as *Radiology: Diagnosis, Imaging, Intervention*, edited by Juan M. Taveras and Joseph T. Ferrucci (Lippincott), or multiple, separate texts.

Stephen S. Gebarski
University of Michigan Hospitals
Ann Arbor, MI 48109-0030

The Diagnosis of Acromegaly:
Value of Inferior Petrosal Sinus Sampling

John L. Doppman[1]
Donald L. Miller[1]
Nicholas J. Patronas[1]
Edward H. Oldfield[2]
George R. Merriam[3]
Stuart J. Frank[4]
Mary R. Flack[3]
Bruce D. Weintraub[5]
Phillip Gorden[6]

The early diagnosis of acromegaly may be difficult when serum levels of growth hormone are minimally elevated and imaging of the pituitary gland fails to show an adenoma. However, transsphenoidal surgery has the greatest chance of cure at this stage. We therefore investigated the value of sampling petrosal sinuses for measurement of growth hormone in this group of patients. Simultaneous bilateral sampling of the inferior petrosal sinuses to measure serum concentrations of growth hormone was performed in five patients suspected of having acromegaly but with nondiagnostic CT scans ($n = 5$) and MR images ($n = 3$) of the pituitary gland. Levels of growth hormone from the petrosal sinuses were five to 36 times greater than levels in the peripheral veins in all five patients, and three of four showed a marked response to growth hormone–releasing hormone. During transsphenoidal surgery, growth hormone–producing microadenomas were resected completely in four patients. In the fifth patient, a left-sided microadenoma had invaded the cavernous sinus and could not be resected completely. Lateralization of the adenomas within the pituitary gland on the basis of differences in levels of growth hormone between the two petrosal sinuses was not completely reliable.

Elevated levels of growth hormone in selective samples from the inferior petrosal sinuses can help support an early diagnosis of acromegaly when peripheral growth hormone levels and imaging are not diagnostic.

AJR **154:1075–1077, May 1990**

Simultaneous bilateral sampling of blood from the inferior petrosal sinuses for the determination of serum concentrations of adrenocorticotrophic hormone (ACTH) reliably distinguishes Cushing disease from ectopic ACTH syndrome [1–5]. Sampling of the petrosal sinuses also may indicate the side of the pituitary gland harboring the adenoma [3–5]. Because at least 80% of ACTH-producing pituitary tumors are microadenomas (<10 mm) [6], and results of CT [7] and MR [8, 9] imaging studies are often normal, such lateralizing information has been helpful to the neurosurgeon during transsphenoidal exploration [5].

Unlike ACTH-producing adenomas, few growth hormone–producing adenomas are microadenomas [10–12]. In a review from the Mayo Clinic [6], only three (13%) of 23 growth hormone–producing adenomas were less than 10 mm in diameter. However, mixed growth hormone/prolactin–producing adenomas, which also may be associated with acromegaly, presented as microadenomas in nine (26%) of 35 cases. In addition, the diagnosis of acromegaly often is suspected nowadays at an earlier stage, when serum levels of growth hormone, as measured by radioimmunoassay, are in the borderline range. Under such circumstances, imaging studies (CT and MR) of the pituitary gland also may be normal or equivocal.

We recently performed bilateral sampling of the petrosal sinuses in five patients with acromegaly and normal or equivocal imaging studies of the pituitary gland. Our purpose was to evaluate the role of petrosal sinus sampling in acromegalic patients with less advanced symptoms and in whom imaging studies of the pituitary gland did not clearly indicate the presence or site of an adenoma.

Received November 21, 1989; accepted after revision December 26, 1989.

[1] Department of Diagnostic Radiology, Warren G. Magnuson Clinical Center, National Institutes of Health (NIH), Bethesda, MD 20892 and Department of Radiology, Georgetown University Medical Center, Washington, DC 20007. Address reprint requests to J. L. Doppman, Diagnostic Radiology Department, Bldg. 10, Rm. 1C660, National Institutes of Health, Bethesda, MD 20892.

[2] Surgical Neurology Branch, National Institute of Neurological and Communicative Disorders and Stroke, NIH, Bethesda, MD 20892.

[3] Developmental Endocrinology Branch, National Institute of Child Health and Human Development, NIH, Bethesda, MD 20892.

[4] Cell Biology and Metabolism Branch, National Institute of Child Health and Human Development, NIH, Bethesda, MD 20892.

[5] Molecular, Cellular and Nutritional Endocrinology Branch, National Institute of Diabetes and Digestive and Kidney Diseases, National Institutes of Health, Bethesda, MD 20892.

[6] Diabetes Branch, National Institute of Diabetes and Digestive and Kidney Diseases, NIH, Bethesda, MD 20892.

0361–803X/90/1545–1075
© American Roentgen Ray Society

TABLE 1: Petrosal Sinus Sampling in Acromegalic Patients

Case No.	Sex	Age (yr.)	Pituitary Imaging		Petrosal Sinus Sampling: Growth Hormone in ng/ml (After GHRH)			Findings at Surgery	Miscellaneous
			CT	MR	Right Sinus	Peripheral Vein	Left Sinus		
1	F	68	Normal	Not performed	166	19	17.5	3-mm adenoma to right of midline	3 months after surgery, GH was 13 ng/ml
2	M	43	Normal	Not performed	164 (175)	7.1 (8.7)	18.8 (21.7)	8-mm left-sided adenoma invading left cavernous sinus	
3	M	50	Prominent right side	Prominent right side; no focal defect	3.6 (9.9)	3.7 (7.6)	63.5 (561)	7-mm right-sided adenoma	Also had left-sided ACTH gradient
4	M	27	Normal	Normal (Gd-DTPA)	116 (567)	3.2 (9.2)	30.8 (255)	6-mm midline adenoma	Cured
5[a]	M	44	Normal	Normal	21.7 (25.6)	3.1 (4.4)	71 (235)	10-mm left-sided adenoma	Cured

Note.—GH = growth hormone, GHRH = growth hormone–releasing hormone, ACTH = adrenocorticotrophic hormone.

[a] Previously reported in Frank et al. [13].

Subjects and Methods

Four men and one woman 27 to 68 years old (mean age, 46 years) with mild features of acromegaly and minimal elevation of serum levels of growth hormone were studied. All patients had CT scans (GE 9800, Milwaukee, WI) in the coronal projection with 3-mm-thick sections at 2-mm intervals during the rapid infusion of 150 ml of 60% meglumine diatrizoate (Squibb Pharmaceuticals, Princeton, NJ). Three patients had MR imaging of the pituitary gland in the coronal and sagittal projections on a 0.5-T scanner (Picker International, Highland Heights, OH) or a 1.5-T scanner (Signa, General Electric, Milwaukee, WI) as previously described [8, 9]. One patient received Gd-DTPA (Berlex Laboratories, Cedar Knolls, NJ).

The inferior petrosal sinuses were catheterized bilaterally [3, 4], and samples were obtained simultaneously from the right and left inferior petrosal sinuses and from a peripheral vein. In four patients, growth hormone–releasing hormone (GHRH) (1 μg/kg) was administered as an IV bolus, and samples were obtained at −10, 0, 2, 5, 10, 15 or 20, and 30 min from both petrosal sinuses and a peripheral vein. All patients underwent transsphenoidal surgery for resection of a growth hormone–producing adenoma.

Results

Findings on CT examination of the pituitary gland were normal in four patients. One patient (Case 3) with a 7-mm right-sided adenoma confined to the pituitary gland had a down-sloping sellar floor on the right side but no focal defect on CT. Another patient (Case 5) with a 10-mm left-sided adenoma had a gland at the upper limits of normal in height (10 mm), but no focal defects on either CT or MR. MR of the pituitary gland was normal in two patients (Cases 4 and 5) and equivocal in one patient (Case 3) (Table 1) [13].

In all patients, samples from the inferior petrosal sinuses had elevated levels of growth hormone (Table 1). The levels in samples from the petrosal sinuses ranged from fivefold to 36-fold above the levels in samples from a peripheral vein. Three of four patients who received an infusion of GHRH showed a rapid increase of growth hormone levels in the petrosal sinuses; peak values were seen in the 10- or 15-min sample (Tables 2 and 3). The increase of growth hormone levels from the petrosal sinuses above growth hormone levels in a peripheral vein in response to GHRH stimulation ranged from 53-fold to 74-fold. One patient (Case 2) had no response to GHRH.

Discussion

Because of the subtle progression of symptoms and signs, the diagnosis of acromegaly often is delayed. Growth hormone–producing adenomas of the pituitary gland are usually macroadenomas (>10 mm) and often are locally invasive at the time of initial diagnosis [6, 11, 12]. Complete surgical excision of the adenoma with permanent restoration of normal growth hormone levels may be impossible at this stage. If 5 ng/ml is accepted as the normal adult level of growth hormone, cure rates of acromegaly in recent surgical series have varied from 26% to 62% [14, 15]. In all series [6, 14, 15], microadenomas, as opposed to macroadenomas, are associated with a more favorable outcome. In the Mayo Clinic series [6], none of the growth hormone–producing microadenomas were locally invasive at the time of surgery, and complete resection was possible. On the other hand, 18 (40%) of the 46 growth hormone–producing macroadenomas were locally invasive. Although radiation therapy is effective, a complete remission may require 2 to 3 years to develop and ultimately may progress to panhypopituitarism [16, 17]. Because of this, the goal of therapy in acromegaly should be early diagnosis and complete resection of growth hormone–producing adenomas. The more widespread availability of reliable assays for growth hormone may facilitate earlier diagnosis.

Although acromegaly can be diagnosed when the adenoma producing growth hormone is smaller than 10 mm, it is unlikely that microadenomas in the 2-mm to 4-mm range, as are common with ACTH-producing tumors, will be encountered frequently in acromegalic patients. All growth hormone–producing microadenomas in our patients were in the 6-mm to

TABLE 2: Growth Hormone Levels (ng/ml)

Timing of Measurement	Right Petrosal Sinus	Left Petrosal Sinus	Peripheral Vein
Baseline	21.7	71.0	3.1
Post-GHRH			
2 min	21.0	92.0	2.9
5 min	43.0	160.0	3.4
10 min	18.5	182.0	4.1
15 min	25.6	235.0	4.4
30 min	76.0	180.0	7.1

Note.—GHRH = growth hormone–releasing hormone.

TABLE 3: Growth Hormone Levels (ng/ml)

Timing of Measurement	Right Petrosal Sinus	Left Petrosal Sinus	Peripheral Vein
Baseline	116.0	30.8	3.2
Post-GHRH			
2 min	309.0	126.0	3.3
5 min	510.0	272.0	5.0
10 min	567.0	255.0	9.2
20 min	282.0	450.0	15.4
30 min	230.0	220.0	15.9

Note.—GHRH = growth hormone–releasing hormone.

10-mm range and easily visualized during transsphenoidal exploration. In two of our five patients (Cases 2 and 3), the highest gradients were on the side contralateral to the adenoma. For these reasons, lateralization of the adenoma by petrosal sinus sampling will play a less important role in acromegaly than it does in Cushing disease [5].

Crock et al. [18] have recently published their results with petrosal sinus sampling for growth hormone in five patients with acromegaly and equivocal or negative findings on CT scans of the pituitary gland. All patients demonstrated petrosal/peripheral gradients of growth hormone, but the intrasinus gradients incorrectly lateralized the tumor in four of five patients. Although four of five tumors were microadenomas (<10 mm), the average diameter of the microadenomas was 7 mm, and only one tumor was smaller than 4 mm in diameter. These results confirm our impression that even when preoperative imaging studies are negative, growth hormone–producing adenomas tend to be in the 6–10 mm range, and false lateralization is common. However, such large microadenomas are easily found by the neurosurgeon (all patients had adenomas successfully resected in the Crock series), so lateralization by petrosal sampling is not critical.

In addition, ectopic production of growth hormone by nonpituitary tumors is rarer than ectopic production of ACTH by nonpituitary tumors (15–20% of patients with Cushing syndrome) [19]. For this reason, the role of petrosal sinus sampling in differential diagnosis is less important in acromegaly than in Cushing syndrome. A few cases of ectopic production of GHRH have been reported. It might be anticipated that petrosal sinus sampling in these patients would show a central to peripheral gradient of growth hormone due to excessive GHRH stimulation, but petrosal sinus sampling in this situation has not been reported.

Our analysis is limited by the lack of data on petrosal sampling in normal adults. Although we have a large experience with petrosal sinus sampling in Cushing disease, these patients cannot be used to establish normal adult values of growth hormone in petrosal samples because elevated cortisol levels suppress growth hormones. Controlled studies are needed to determine the minimal gradient of growth hormones that would be necessary to diagnose a growth hormone–producing pituitary tumor. In defining such a minimal gradient, a role for petrosal sinus sampling as a sensitive diagnostic procedure in early acromegaly might be established.

REFERENCES

1. Corrigan DF, Schaaf M, Whaley RA, Czerwinski CL, Earll JM. Selective venous sampling to differentiate ectopic ACTH secretion from pituitary Cushing's syndrome. *N Engl J Med* **1977**;296:861–862
2. Findling JW, Aron DC, Tyrrell JB, et al. Selective venous sampling for ACTH in Cushing's syndrome: differentiation between Cushing's disease and the ectopic ACTH syndrome. *Ann Intern Med* **1981**;94:647–652
3. Doppman JL, Oldfield E, Krudy AG, et al. Petrosal sinus sampling for Cushing syndrome: anatomical and technical considerations. *Radiology* **1984**;150:99–103
4. Doppman JL, Krudy AG, Girton ME, Oldfield EH. Basilar venous plexus of the posterior fossa: a potential source of error in petrosal sinus sampling. *Radiology* **1985**;155:375–378
5. Oldfield EH, Chrousos GP, Schulte HL, et al. Preoperative lateralization of ACTH-secreting pituitary microadenomas by bilateral and simultaneous inferior petrosal venous sampling. *N Engl J Med* **1985**;312:100–103
6. Sheithauer BW, Kovacs KT, Laws ER Jr, Randall RV. Pathology of invasive pituitary tumors with special reference to functional classification. *J Neurosurg* **1986**;65:733–744
7. Saris SC, Patronas NJ, Doppman JL, et al. Cushing syndrome: pituitary CT scanning. *Radiology* **1987**;162:775–777
8. Dwyer AJ, Frank JA, Doppman JL, et al. Pituitary adenomas in patients with Cushing disease: initial experience with Gd-DTPA-enhanced MR imaging. *Radiology* **1987**;163:421–426
9. Doppman JL, Frank JA, Dwyer AJ, et al. Gadolinium DTPA enhanced MR imaging of ACTH-secreting microadenomas of the pituitary. *J Comput Assist Tomogr* **1988**;12:728–735
10. Horvath E, Kovacs K. Pathology of the pituitary gland. In: Ezrin C, Horvath E, Kaufman B, et al., eds. *Pituitary diseases*. Boca Raton, FL: CRC Press, **1980**:1–84
11. Sheithauer BW. Surgical pathology of the pituitary and sellar region. In: Laws ER Jr, Randall RV, Kern EB, et al., eds. *Management of pituitary adenomas and related lesions with emphasis on transsphenoidal microsurgery*. New York: Appleton-Century-Crofts, **1982**:129–218
12. Melmed S, Braunstein GD, Horvath E, Ezrin C, Kovacs K. Pathophysiology of acromegaly *Endocrinol Rev* **1983**;4:271
13. Frank SJ, Gesundheit N, Doppman JL, et al. Preoperative lateralization of pituitary microadenomas by petrosal sinus sampling: utility in two patients with non-ACTH secreting tumors. *Am J Med* (in press)
14. Roelfsema F, Van Dulken H, Frolich M. Long-term results of transsphenoidal pituitary microsurgery in 60 acromegalic patients. *Clin Endocrinol* **1985**;23:555–565
15. Baskin DS, Baggon JE, Wilson CB. Transsphenoidal microsurgical removal of growth hormone-secreting pituitary adenomas. *J Neurosurg* **1982**;56:634–641
16. Eastman RC, Gorden P, Roth J. Conventional supervoltage irradiation is an effective treatment for acromegaly. *J Clin Endocrinol Metab* **1979**;48:931–940
17. Gorden P, Glatstein E, Oldfield EH, Roth J. Conventional supervoltage radiation in the treatment of acromegaly. Serono symposium on acromegaly: A century of scientific and clinical progress. In: Robbins RJ, Melmed S., eds. *Acromegaly*. New York: Plenum, **1987**:211–220
18. Crock PA, Gilford ET, Henderson JK, et al. Inferior petrosal sinus sampling in acromegaly. *Aust NZ J Surg* **1989**;19:244–247
19. Doppman JL, Nieman L, Miller DL, et al. Ectopic adrenocorticotropic hormone syndrome: localization studies in 28 patients. *Radiology* **1989**;172:115–124

Book Review

Tomographic Methods in Nuclear Medicine: Physical Principles, Instruments, and Clinical Applications. Edited by Bhagwat D. Ahluwalia. Boca Raton, FL: CRC, 239 pp., 1989. In United States, $124.96; outside United States, $147

This book consists of 11 chapters, three of which are written by the editor. Chapter 1 is a brief two-page essay on the future of imaging techniques. Chapter 2 presents a fairly thorough treatment of different theories of tomographic reconstructions. Chapters 3 and 4 cover computer and hardware requirements, imaging systems, and quality control for single-photon emission tomography (SPECT). These chapters are somewhat dated as the most recent reference appeared in 1984–1985.

Chapter 5, the longest chapter, deals with clinical applications and protocols of SPECT. It gives 185 references and covers the available information as of 1985 on brain, myocardium, liver, spleen, lung, kidneys, adrenal gland, thyroid, bones, and pituitary gland. Of course, the brain and myocardial images are the prevailing topics. Positron emission tomography is discussed in chapter 6. Both focal-plane dual-head longitudinal and limited-angle slant-hole tomographies are discussed in chapters 7 and 8. Chapters 9 and 10 discuss seven-pinhole tomography and its reconstruction algorithm. The last chapter covers coded aperture tomography.

The editor claims that no other volume in print deals with different tomographic methods for nuclear medicine. This book does serve that purpose well. One major concern is that almost all the references were published before 1985.

SPECT has grown in recent years and with its decreasing cost has been accepted as a clinical imaging technique, even in smaller community hospitals. This book provides a resource volume of general interest to medical physics students, nuclear medicine scientists and physicians, and researchers in organ imaging and image processing techniques. For practicing nuclear medicine physicians, this book may be difficult to read and comprehend. They might find another book, *Single Photon Emission Computed Tomography* by Barbara Y. Croft (Chicago: Yearbook Medical, 1986), a more readable reference for SPECT.

Hing-Har Lo
University of Virginia
Charlottesville, VA 22908
Montgomery Radiology Associates
Blacksburg, VA 24060

CT Evaluation of Anaplastic Thyroid Carcinoma

Shodayu Takashima[1]
Shizuo Morimoto[1]
Junpei Ikezoe[1]
Shinichirou Takai[2]
Tetsurou Kobayashi[2]
Hiroki Koyama[3]
Kinji Nishiyama[1]
Takahiro Kozuka[1]

CT findings in 19 patients with anaplastic thyroid carcinoma were compared retrospectively with pathologic findings and the results of palpation. The carcinoma appeared as a large mass of low attenuation accompanied by dense calcification in 58% of the patients; there was necrosis in 74%. Often, adjacent structures were infiltrated. CT correctly showed tumor invasion of the carotid artery (7/7), internal jugular vein (9/10), larynx (5/6), trachea (8/10), esophagus (4/5), mediastinum (5/5), and regional lymph nodes (14/16). Seven patients (50%) had necrotic nodes. CT was superior to palpation in the detection of a primary tumor in one patient and of metastatic nodes in seven patients. It suggested a suitable place for biopsy in two patients, leading to a correct diagnosis. CT altered surgical planning in five patients with intrathoracic extension of the thyroid tumor, and in three patients with laryngeal or esophageal invasion of the tumor.

CT can increase diagnostic accuracy in patients with anaplastic thyroid carcinoma by suggesting a likely diagnosis and by indicating an appropriate site for biopsy. It is indispensable in the planning of surgery for patients with this disorder.

***AJNR* 11:361–367, March/April 1990; *AJR* 154: 1079–1085, May 1990**

Anaplastic carcinoma of the thyroid gland accounts for 4–15% of all thyroid malignancies; it affects women slightly more often than men [1–5]. The peak occurrence of this disorder is during the seventh decade of life. Most patients with the disease have a rapidly enlarging thyroid mass and symptoms of obstruction such as dyspnea and dysphagia. Hoarseness due to recurrent laryngeal nerve palsy is often seen. Such clinical features are very similar to those of primary thyroid lymphoma [6–8]. Primary thyroid lymphoma accounts for 4% of all thyroid malignancies [6], and secondary thyroid gland involvement is found incidentally in 15% of patients with systemic malignant lymphoma at autopsy [9]. Thyroid lymphoma in the early stages has a relatively good prognosis [6, 8]. Burke et al. [10] mentioned that the 5-year survival rate for patients with stage IE lymphoma is as high as 89%, and that the 5-year survival rate for those with stage IIE disease is 27%. Patients in whom thyroid lymphoma is confined to the neck are treated with radiation therapy, with or without chemotherapy; surgery is not the treatment of choice [6, 10].

In early reports, the outcome of patients with anaplastic thyroid carcinoma was almost invariably fatal within a year from diagnosis; the median survival from the time of diagnosis was 3–6 months [1–5]. The survival period in recent reports, however, has been improved as a result of a combination of surgery, hyperfractionated radiotherapy, and chemotherapy [11–13]. Werner et al. [13] reported that patients with distant metastases and/or vocal cord paralysis had a median survival time from diagnosis of 7 months, and that patients with less advanced disease survived on average 12 months with the use of such multimodal therapy. Many authorities think that tumor resection can extend the survival time and that, when possible, radical removal of the tumor should be performed [2–4, 13–15]. Therefore,

Received May 11, 1989; revision requested August 2, 1989; revision received September 12, 1989; accepted September 21, 1989.

[1] Department of Radiology, Osaka University Medical School, 1-1-50 Fukushima, Fukushima-ku, Osaka 553, Japan. Address reprint requests to S. Takashima.

[2] Second Department of Surgery, Osaka University Medical School, Osaka 553, Japan.

[3] Department of Surgery, Center for Adult Diseases, Osaka, 3 Nakamichi 1-chome, Higashinari-ku, Osaka 537, Japan.

0361–803X/90/1545–1079
© American Roentgen Ray Society

it is important to establish a final diagnosis promptly, to define the tumor extent, and to identify the site and extent of metastatic lymph nodes preoperatively. We studied whether there are any features of anaplastic thyroid carcinoma seen on CT that distinguish it from primary thyroid lymphoma. The CT findings were compared with those of surgery, pathology, and palpation, and the role of CT in the management of the patients with the disease was studied.

Materials and Methods

We retrospectively analyzed the clinical data and CT findings in 19 patients with anaplastic thyroid carcinoma who underwent CT for diagnosis or staging of the cancer between June 1983 and November 1988. Histologic diagnosis was by surgical specimens in 17 patients and by autopsy in two. The 11 women and eight men were 35–87 years old (mean, 65 years). CT was performed with an 8800 CT/T or 9800 CT scanner (General Electric, Milwaukee) or a CT 8600 scanner (Yokogawa, Tokyo). Scans were obtained through the neck and thyroid masses principally with contiguous 5-mm-thick sections. Nine patients were studied with both plain and contrast-enhanced scanning. The other 10 patients were studied with contrast-enhanced scanning only. Contrast enhancement was always required to distinguish enlarged lymph nodes from vascular structures; it also provided important information about the presence or absence of necrosis in the masses and their relationship to surrounding structures. Contrast enhancement was attained with a rapid drip infusion of 100 ml of 65% iodinated contrast material administered IV. Special attention was paid to the tumor extent in the thyroid gland, tumor invasion of surrounding structures, site and extent of metastatic lymph nodes, and presence of calcification or necrosis in the tumor.

The CT findings were compared with pathologic or surgical findings, and also with those of palpation, which was performed by a surgeon specializing in the head and neck to detect primary tumors and metastatic lymph nodes. On CT images, lymph nodes in the submandibular and jugulodigastric regions of the internal jugular chain that were larger than 1.5 cm in their greatest diameter were considered to have a metastasis [16]. For the other nodes in the neck and those in the mediastinum, a diameter of more than 1 cm was considered to show metastasis. Any nodes with central necrosis, regardless of size, were also considered to be metastatic. Picus et al. [17] found that if the esophageal carcinoma was in contact with 90° or more of the aortic circumference on CT, aortic invasion by the tumor was very likely. Mancuso [18] used the same criteria to predict the carotid invasion by the cervical nodal metastases. We modified the same rule to define tumor invasion of adjacent structures. Tumor invasion of surrounding structures such as the common carotid artery, internal jugular vein, larynx, trachea, and esophagus was diagnosed if the tumor was in contact with one-half or more of the circumference of such organs, and if the plane between them was lost. When ossified cartilage invasion of the larynx was present, tumor invasion was diagnosed also.

Results

Goiter had been present in nine patients (47%) for 3 months to 30 years before the diagnosis of anaplastic carcinoma. Five patients had had surgery for thyroid tumors before the diagnosis of anaplastic carcinoma was established: three for papillary carcinoma and two for thyroid adenoma. Fourteen patients (74%) had had a rapidly enlarging neck mass. Symptoms of obstruction were reported by 17 patients (89%),

TABLE 1: CT Findings in Anaplastic Thyroid Carcinoma

Case No.	Age	Sex	Primary Site			Metastatic Lymph Nodes				Intrathoracic Extension/ Location
			Extent	Necrosis	Calcification	Palpation	CT	Pathology	Necrosis	
1	80	F	Both lobes, isthmus	Yes	Yes	No	No	Yes	–	No
2	63	F	Both lobes, isthmus	Yes	Yes	No	Yes	Yes	Yes	No
3	71	M	One lobe, isthmus	No	Yes	Yes[a]	Yes	Yes	No	No
4	60	M	One lobe, isthmus	Yes	Yes	Yes[a]	Yes	Yes	No	No
5	70	M	Both lobes, isthmus	Yes	Yes	Yes[a]	Yes	Yes	Yes	Yes/middle mediastinum
6[b]	64	F	–	–	–	Yes	Yes	Yes	Yes	No
7	80	F	One lobe, isthmus	Yes	Yes	No	No	Yes	–	No
8	57	F	Both lobes, isthmus	No	No	No	No	No	–	No
9	61	M	One lobe	No	No	No	No	No	–	Yes/middle mediastinum
10	72	F	One lobe, isthmus	Yes	No	Yes[a]	Yes	Yes	No	No
11	35	M	One lobe[c]	No	No	No	Yes	Yes	No	No
12	59	F	Both lobes[c]	Yes	No	Yes	Yes	Yes	Yes	No
13	57	M	One lobe	Yes	No	Yes	Yes	Yes	Yes	No
14	85	F	One lobe, isthmus	Yes	Yes	No	No	No	–	No
15	65	F	One lobe, isthmus	Yes	Yes	No	Yes	Yes	No	Yes, middle mediastinum
16	87	F	One lobe, isthmus	Yes	Yes	Yes	Yes	Yes	Yes	No
17	57	F	Both lobes, isthmus	Yes	Yes	No	Yes	Yes	No	Yes/anterior mediastinum
18	48	M	One lobe	Yes	No	Yes[a]	Yes	Yes	Yes	No
19	65	M	One lobe	Yes	Yes	Yes[a]	Yes	Yes	No	Yes/posterior mediastinum

[a] More metastatic nodes were detected by CT than by palpation.

[b] This patient had had a total thyroidectomy.

[c] Multiple lesions were found on pathologic studies.

recurrent nerve palsy by seven (37%), and neck pain by nine (47%). Fifteen patients had normal serum thyroid hormone levels; the other four were taking thyroid hormone after thyroidectomies. Antithyroid autoantibodies were positive at low titers in four of the 11 patients tested.

Fifteen patients underwent needle aspiration cytology preoperatively. Ten patients (67%) were diagnosed as having or as suspected of having anaplastic carcinoma. In two of these 10 patients, the correct diagnosis was made by repeated aspiration biopsies after CT examinations that indicated appropriate sites for sampling. One patient was falsely diagnosed as having squamous cell carcinoma, one as having adenocarcinoma, and one as having an unspecified malignancy; two had negative results. Later, two of these patients underwent needle biopsy; one had open biopsy. The correct diagnosis was then obtained in all three. Histologic study showed seven cases of spindle cell tumor, five of giant cell tumor, and three of pleomorphic cell tumor. For the remaining four tumors, the type of anaplastic carcinoma was not identified. Eleven patients (58%) had other thyroid cancers, either in the thyroid gland or in the metastatic lymph nodes: papillary carcinoma (10 patients), follicular carcinoma (three patients), and squamous cell carcinoma (one patient).

Table 1 summarizes the CT findings of anaplastic carcinoma in comparison with those of pathology and palpation. Eighteen patients had a solitary mass on CT that was palpated as a hard mass; in one of these patients, another small nodule of anaplastic carcinoma measuring 4 mm in diameter was found in the thyroid on pathologic examination but not on palpation. In the remaining patient, multiple small nodules that were not palpable were depicted on CT. Tumors were generally identified as inhomogeneous isodense or slightly hyperdense areas relative to skeletal muscle on CT; contrast enhancement was not necessary to depict the site of the primary tumor. Tumor necrosis was identified as areas of lower attenuation than that of the skeletal muscle; areas of necrosis did not enhance with contrast material (Figs. 1, 2, 3B, 3C, 4B, and 4C). Calcification (Figs. 1A and 4C) and necrosis (Figs. 1B, 2A, and 3B) in the primary tumors were detected in 10 (58%) and 14 (74%) patients, respectively. All calcification was of the dense, amorphous type. Necrosis of the tumor was extensive in four cases (21%) (Fig. 2A).

Regional lymphadenopathy was found on CT in 14 patients (74%). Of these 14 patients, seven had central necrosis in the involved nodes; the remaining seven had nonnecrotic nodes (Figs. 2 and 3A). CT detection of metastatic nodes in each anatomic region was compared with that by palpation and pathology (Table 2). In four patients, histologically proved metastatic nodes were detected by neither palpation nor CT: two patients (cases 1 and 7) had normal-sized lymph nodes with microscopic tumor deposits; the other two had enlarged nodes containing tumor deposits in the middle or inferior internal jugular chains or both. Metastasis was not found by palpation but was found by CT in 10 cases: eight nodes in the tracheoesophageal groove or in the superior mediastinum, three in the inferior internal jugular chain, two in the middle internal jugular chain, and two in the spinal accessory chain. One node with metastasis on CT and without metastasis by palpation was found to be reactive.

Table 3 summarizes the CT detection of tumor infiltration into adjacent structures. Tumor invasion of the common carotid artery was predicted by CT in eight patients (Fig. 2). Of these, one patient (case 2) had a false-positive result. Tumor invasion of the internal jugular vein was predicted in nine cases (Figs. 3A and 3B); one result (in case 15) was false negative (Fig. 3C). Laryngeal invasion was seen on CT in five patients (Figs. 3B and 4A). Of these, four patients had tumor invasion of ossified cartilage of the larynx. The result was a false negative in one patient. Laryngectomy was performed in one of the patients with laryngeal invasion of the tumor. Tracheal invasion was detected by CT in 10 patients (Fig. 1); false-positive (Fig. 4B) and false-negative (Fig. 2B) results were obtained in two cases each. Invasion of the esophagus was seen on CT in five patients (Figs. 1 and 4A); the results were false negative and false positive in one patient each. Partial esophagectomy was done in two of the patients with esophageal invasion of the tumor. Intrathoracic extension of the thyroid tumor was detected in five patients (Fig. 4C).

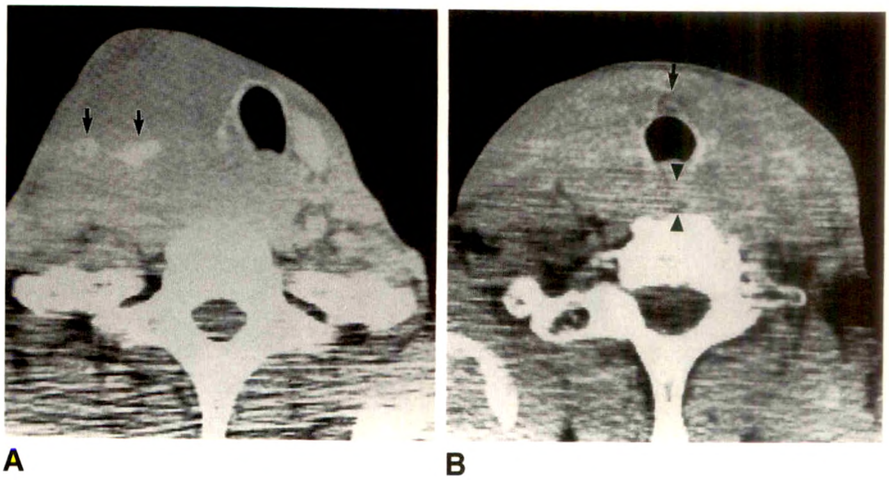

Fig. 1.—Anaplastic thyroid carcinoma with and without necrosis.

A, Primary site without necrosis in case 3. Contrast-enhanced CT scan shows large mass of low attenuation with amorphous calcifications (*arrows*); mass replaces entire right lobe of thyroid gland. Necrosis cannot be seen. Trachea is displaced to the left, and tumor is in contact with more than half of circumference of trachea, with loss of tissue plane between them. Discrimination between tumor and esophagus is difficult, because tumor encroaches on it. Tumor infiltration of trachea and esophagus predicted by CT was found during surgery.

B, Primary site with small area of necrosis in case 5. Contrast-enhanced CT scan shows low-attenuation mass replacing entire thyroid gland. Small necrotic portion (*arrow*) is seen in thyroid isthmus. Trachea and esophagus (*arrowheads*), surrounded by tumor on more than three sides, were found to be infiltrated by tumor during surgery.

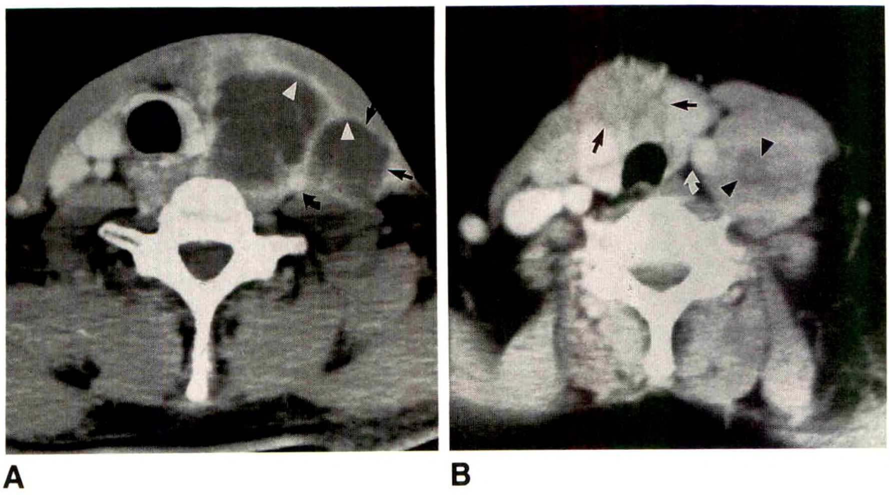

Fig. 2.—Tumor invasion of common carotid artery.

A, True-positive diagnosis in case 18. Contrast-enhanced CT scan shows rim-enhancing mass with extensive necrosis in left lobe of thyroid gland and necrotic nodal mass (*straight arrows*) in inferior internal jugular chain. Interface between tumor and sternocleidomastoid muscle (*arrowheads*) is irregular. Tumor encircles left common carotid artery (*curved arrow*) on more than half of its circumference with loss of plane between them. Left internal jugular vein has been obliterated. Tumor invasion of these structures predicted by CT was confirmed by pathologic or surgical studies.

B, False-positive diagnosis in case 2. Low-attenuation mass (*straight arrows*) and nodal mass with small area of necrosis (*arrowheads*) in inferior internal jugular chain are seen on contrast-enhanced CT. CT suggested that tumor had invaded left common carotid artery (*curved arrow*) but not trachea. However, surgical findings showed that tumor had infiltrated trachea but not carotid artery.

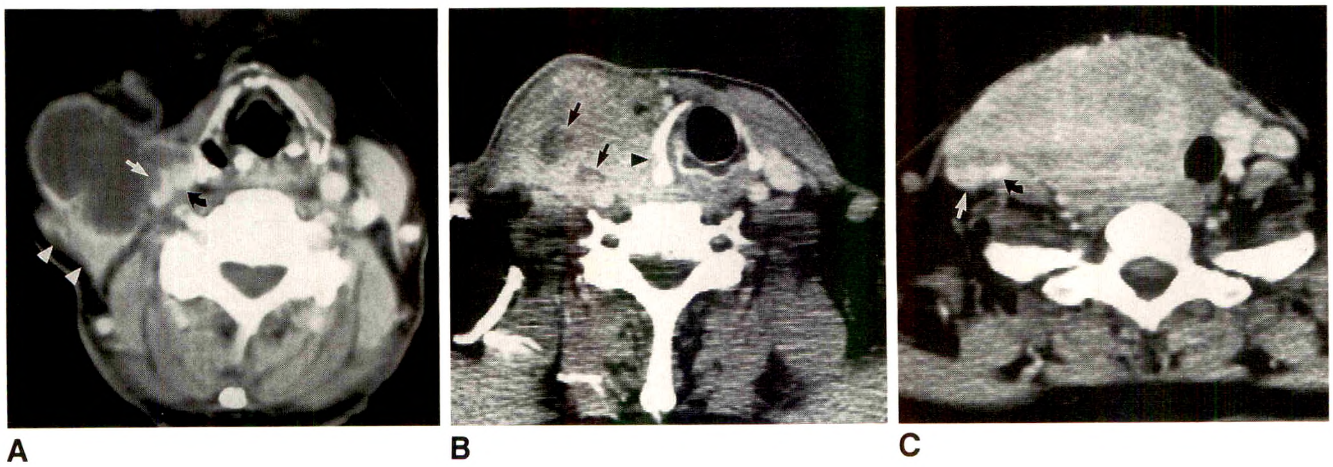

Fig. 3.—Tumor invasion of internal jugular vein.

A, True-positive diagnosis in case 16. Contrast-enhanced CT scan shows large necrotic node in middle internal jugular chain on right. Border between tumor and internal jugular vein (*straight arrow*) is irregular. Ipsilateral sternocleidomastoid muscle (*arrowheads*) is posteriorly displaced and deformed. Pathologic studies confirmed tumor invasion of internal jugular vein and muscle; common carotid artery (*curved arrow*) was dissected free during surgery.

B, True-positive diagnosis in case 4. Large, low-attenuation mass with few foci of necrosis (*arrows*) is seen in right lobe of thyroid gland on contrast-enhanced CT. Ipsilateral internal jugular vein has been obliterated, and tumor invasion of ossified thyroid cartilage (*arrowhead*) is seen. Tumor infiltration of internal jugular vein and thyroid cartilage was confirmed by pathologic or surgical studies, findings compatible with those on CT.

C, False-negative diagnosis in case 15. Contrast-enhanced CT scan shows low-attenuation mass in right lobe and isthmus of thyroid gland. Tumor invasion of adjacent vessels was not predicted by CT. However, pathologic specimens from surgery showed tumor infiltration of internal jugular vein (*straight arrow*); common carotid artery (*curved arrow*) was easily separated from tumor during surgery.

Thoracotomy was performed in these five patients; contiguous spreading of the thyroid tumor was found in all.

Discussion

The clinical features in our patients are similar to those of patients previously reported [1–5, 11, 14, 15]. In this series, thyroid function tests were normal in all but the patients who had had thyroidectomies. Antithyroid antibodies were positive in four patients, but at low titers. Such results were different from those reported previously for primary thyroid lymphoma [7]. Patients with thyroid lymphoma usually have antimicrosomal antibodies at high titers because superimposed Hashimoto thyroiditis is always present; these patients often have hypothyroidism.

Many researchers think that anaplastic thyroid carcinoma results from the transformation of preexisting well-differentiated thyroid carcinoma, and that, in most cases, the areas of well-differentiated carcinoma can be identified if sufficient tissue is available for pathologic examination [2–5, 14, 19]. Aldinger et al. [5] reported that 89% of their cases showed elements of well-differentiated carcinoma. The relatively low frequency of coexisting well-differentiated carcinoma in our series may have resulted from the fact that only small portions of the resected specimen were used for pathologic examination. However, the presence or absence of well-differentiated carcinoma will not affect surgical planning.

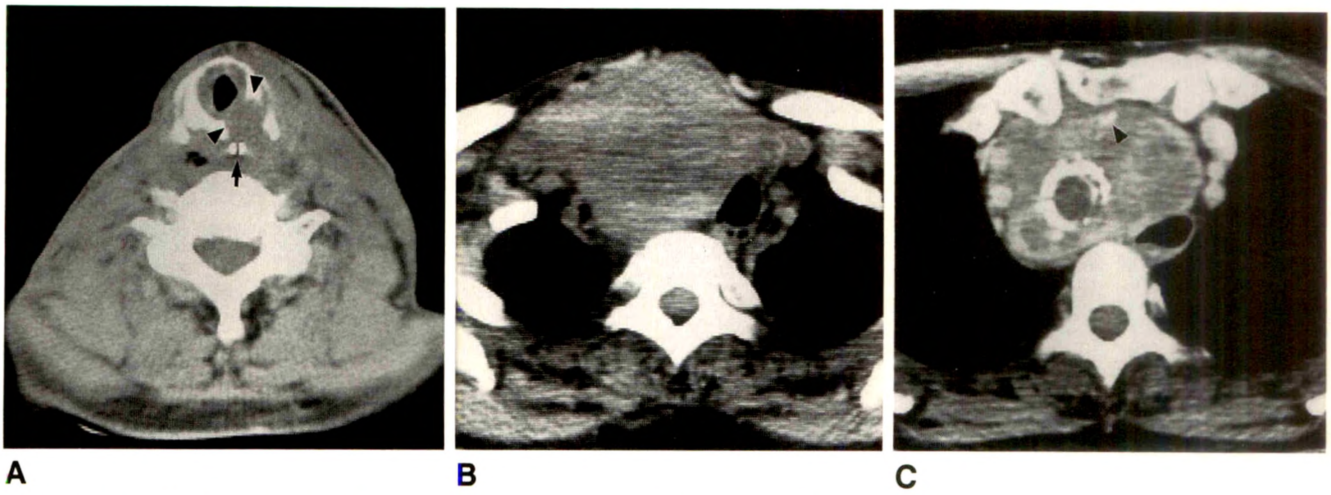

Fig. 4.—*A*, Laryngeal invasion in case 13. Laryngeal invasion by tumor was diagnosed by CT, because ossified cricoid cartilage (*arrowheads*) had been partly destroyed by tumor. Nasogastric tube (*arrow*) is seen in esophagus, which has been encroached on by tumor. Pathologic studies showed tumor invasion of larynx and esophagus.

B, False-positive diagnosis of tracheal invasion in case 15. Trachea has been displaced to the left and is compressed by large mass. Tumor surrounds trachea on more than half of its circumference. Tumor invasion of trachea was predicted by CT, but trachea was dissected free from tumor during surgery.

C, Intrathoracic extension of thyroid tumor in case 15. Tumor extension into mediastinum is seen. Dense amorphous calcifications (*arrowhead*) are present in mass. Thoracotomy was performed in this patient for total removal of tumor.

TABLE 2: Detection of Metastatic Nodes by CT and Palpation Compared with Pathology

Palpation/CT	Pathology	
	Positive	Negative
Palpation negative		
CT negative	4	3
CT positive	10	1
Palpation positive		
CT positive	10	0
CT negative	0	0

TABLE 3: CT Detection of Tumor Invasion of Adjacent Structures vs Surgical or Pathologic Findings

Structure	CT Finding			
	True Positive	True Negative	False Positive	False Negative
Common carotid artery	7	11	1	0
Internal jugular vein	9	9	0	1
Larynx	5	13	0	1
Trachea	8	7	2	2
Esophagus	4	13	1	1
Mediastinum	5	14	0	0

In our series, anaplastic carcinoma of the thyroid was manifested by relatively large masses that were isodense or slightly hyperdense relative to skeletal muscle; calcification (53%) and necrosis (74%) usually were present, and often were extensive. One-half of the patients had necrotic nodes. Calcification of the tumors was invariably dense. Such calcification is seen in both benign and malignant tumors, but is more common in benign masses [20]. Precise correlation of CT findings with pathology in four patients in our study revealed that well-differentiated carcinoma surrounded the calcification in the masses, while anaplastic carcinoma was relatively remote from the calcification; however, CT could not discriminate between these tumors. Because 47% of our patients had had goiters for a long time, this condition may have caused the calcification. Meanwhile, primary thyroid lymphoma appeared as large, homogeneous masses that were isodense or hyperdense relative to skeletal muscle on CT; contrast enhancement was usually required to better detect the primary tumor site because Hashimoto thyroiditis was always present (Fig. 5) [7, 8]. Moreover, thyroid lymphoma is rarely calcified (7%) or necrotic (7%), and lymphomatous nodes are rarely necrotic [7, 8]. Even if the primary tumor develops an area of necrosis, its proportion to the total tumor size is small.

As already reported [1, 3, 15], anaplastic thyroid carcinoma in our study often invaded neighboring structures such as the carotid artery (37%), internal jugular vein (53%), larynx (32%), trachea (53%), esophagus (26%), and regional lymph nodes (84%), as judged by pathologic or surgical findings. CT accurately showed tumor spread to the vascular structures and regional lymph nodes, but prediction of tumor invasion of the trachea or esophagus by CT was not reliable. Primary thyroid lymphoma also invades adjacent vascular and visceral structures [7, 8, 10]. Burke et al. [10] reported that 18 (51%) of 35 cases showed invasion into the surrounding tissues and that five (14%) involved the regional lymph nodes. In our previous study of 16 patients with primary thyroid lymphoma [8], surgically proved carotid invasion was present in three patients (19%), laryngeal invasion in one (6%), regional lymph-node involvement in seven (44%), and intrathoracic extension of the thyroid tumor in two (13%). Thus, we suggest that

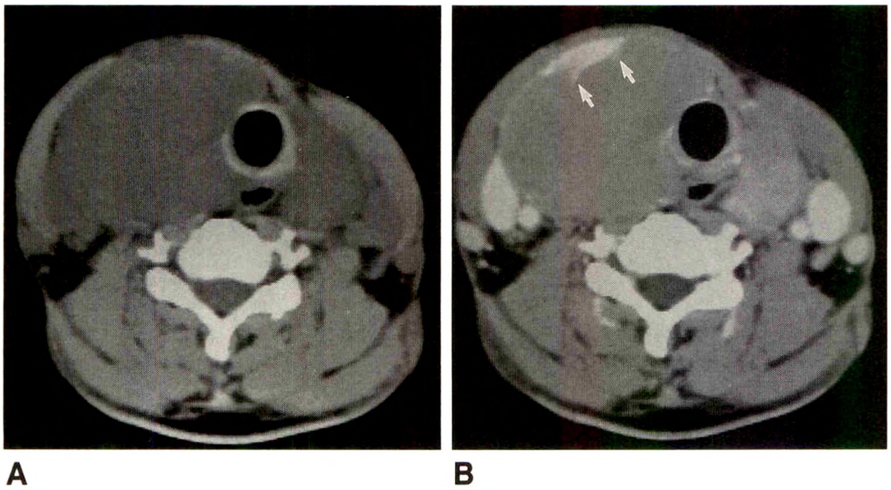

Fig. 5.—Primary thyroid lymphoma.

A, Plain CT scan shows enlarged thyroid gland with generally reduced attenuation and displacement of larynx and esophagus to left. Discrimination between unaffected areas and lymphoma is impossible.

B, Contrast-enhanced CT scan shows homogeneous masses to be isodense relative to skeletal muscle in both lobes and isthmus of thyroid gland. Small unaffected thyroid tissue is seen (*arrows*) in anterior portion of right lobe of thyroid gland. Anterior portion of left lobe of thyroid gland is replaced by tumor, but interface between posterior portion of tumor in left lobe and residual thyroid tissue is indistinct.

anaplastic thyroid carcinoma more frequently invades the surrounding structures and more often involves the regional lymph nodes than primary thyroid lymphoma does.

Benign and malignant conditions overlap on CT images [21–23]. Multinodular goiter appears on CT as multiple regions of decreased density often accompanied by dense calcifications randomly scattered throughout the thyroid gland [21]. The multiplicity of this nodule should be useful in differentiating it from anaplastic thyroid carcinoma. In their report of CT findings in 67 patients with various thyroid tumors, Shibakiri et al. [23] mentioned that an inhomogeneous solid pattern, one of their seven CT patterns, was found in 11 of 23 follicular carcinomas, nine of 19 papillary carcinomas, two of two medullary carcinomas, and two of two anaplastic carcinomas. We believe that primary thyroid lymphoma can be reliably discriminated from other conditions if the clinical and CT criteria described in our previous report [7] are followed. Seven recent patients with thyroid lymphoma were strongly suspected of having the disorder on the basis of CT and clinical data, and, after histologic diagnosis made with biopsy procedures, unnecessary surgery was avoided. We also suggest that, with our criteria, a probable diagnosis of anaplastic thyroid carcinoma can be ventured. If CT scans show invasive isodence or hyperdense masses in the thyroid of patients who have either symptoms of obstruction or a rapidly enlarging neck mass, if there is no evidence of Hashimoto thyroiditis, and if additional features such as calcification or necrosis are present, then the most likely diagnosis is anaplastic carcinoma. The final diagnosis, however, must depend on the results of a biopsy. Nonetheless, the tentative CT diagnosis will contribute to an early final diagnosis.

Several authors have reported that the diagnosis of anaplastic thyroid carcinoma can be made by needle aspiration cytology [13, 24, 25]. Ten (67%) of 15 cases in our series were correctly diagnosed with this procedure. In two of these patients, CT information was useful in establishing the definite diagnosis. Three patients were diagnosed as having well-differentiated carcinoma or a malignancy, and two patients in whom the diagnosis was negative on the basis of needle aspiration cytology were found by CT to have extensive necrosis in the tumor. Thus, we believe that when anaplastic thyroid carcinoma is suspected, multiple aspirates should be sampled from different parts of the remaining solid portion of the tumor that is remote from the calcification; this tumor often is necrotic and frequently there is coexisting well-differentiated carcinoma. Radiologic information on the extent and location of tumor necrosis and site of calcification in the tumor will lower the prevalence of false-negative diagnoses. No patient in our study was studied by this technique, but image-guided biopsy should increase the accuracy of the diagnosis in the head and neck region [26, 27].

CT and palpation were nearly comparable in the detection of primary tumors; however, CT was superior to physical examination in one patient in whom small nodules in the thyroid gland were identified by CT but not by palpation. Moreover, CT defined the extent of the masses in the thyroid gland more exactly than physical examination did, and CT discriminated between primary tumors and adjacent enlarged nodes; this could not be done by palpation. In eight patients (42%), surgical planning was modified in light of CT findings: in five, the mediastinal approach was chosen because of intrathoracic extension of the thyroid tumor; in three, partial esophagectomy or laryngectomy was added.

Mancuso et al. [28] reported that 5% of metastatic nodes from head and neck cancer will not be palpable but will be detected by CT because these nodes lie deep under the sternocleidomastoid muscle or in areas that are not accessible on physical examination, such as in the regions of the retropharyngeal or tracheoesophageal grooves. In 53% of our cases (10 patients), more information about the metastatic nodes was obtained by CT than by palpation. Our detection rate of such nodes by palpation was lower than generally reported in the literature [28, 29], possibly because the nodes frequently were in areas beyond the limits of palpation or because the nodes in the middle, inferior internal jugular chain or in the spinal accessory chain were behind the large primary tumors. Information about the presence of metastatic nodes alone did not considerably alter the surgical plan, but the detection of involved nodes, especially those in the superior mediastinum, and the discovery of their extent were useful in planning.

Thus, our study has shown that a likely diagnosis of anaplastic thyroid carcinoma can be obtained by the combination of CT and clinical findings. CT can improve diagnostic accuracy in the disease by suggesting an appropriate site for biopsy; it is indispensable in the planning of surgery.

ACKNOWLEDGMENTS

We thank Fumio Matsuzuka, Kuma Hospital, for clinical data; Hitoshi Yamamoto for advice; Chieko Watanabe for secretarial assistance; and Miwako Takashima for help in manuscript preparation.

REFERENCES

1. Woolner LB, Beahrs OH, Black BM, McConahey WM, Keating FR Jr. Classification and prognosis of thyroid carcinoma: a study of 885 cases observed in a thirty year period. *Am J Surg* **1961**;102:354–387
2. Ibanez ML, Russell WO, Albores-Saavedra J, Lampertico P, White EC, Clark RL. Thyroid carcinoma—biologic behavior and mortality: postmortem findings in 42 cases, including 27 in which the disease was fatal. *Cancer* **1966**;19:1039–1052
3. Rafla S. Anaplastic tumors of the thyroid. *Cancer* **1969**;23:668–677
4. Nishiyama RH, Dunn EL, Thompson NW. Anaplastic spindle-cell and giant-cell tumors of the thyroid gland. *Cancer* **1972**;30:113–127
5. Aldinger KA, Samaan NA, Ibanez M, Hill CS Jr. Anaplastic carcinoma of the thyroid: review of 84 cases of spindle and giant cell carcinoma of the thyroid. *Cancer* **1978**;41:2267–2275
6. Souhami L, Simpson WJ, Carruthers JS. Malignant lymphoma of the thyroid gland. *Int J Radiat Oncol Biol Phys* **1980**;6:1143–1147
7. Takashima S, Ikezoe J, Morimoto S, et al. Primary thyroid lymphoma: evaluation with CT. *Radiology* **1988**;168:765–768
8. Takashima S, Morimoto S, Ikezoe J, et al. Primary thyroid lymphoma: comparison of CT and US assessment. *Radiology* **1989**;171:439–443
9. Walfish PG. Miscellaneous tumors of the thyroid. In: Ingbar SH, Braverman LE, eds. *The thyroid*, 5th ed. Philadelphia: Lippincott, **1986**:1363–1376
10. Burke JS, Butler JJ, Fuller LM. Malignant lymphoma of the thyroid: a clinical pathologic study of 35 patients including ultrastructural observations. *Cancer* **1977**;39:1587–1602
11. Simpson WJ. Anaplastic thyroid carcinoma: a new approach. *Can J Surg* **1980**;23:25–27
12. Kim JH, Leeper RD. Treatment of anaplastic giant and spindle cell carcinoma of the thyroid gland with combination Adriamycin and radiation therapy: a new approach. *Cancer* **1983**;52:954–957
13. Werner B, Abele J, Alberyd A, et al. Multimodal therapy in anaplastic giant cell thyroid carcinoma. *World J Surg* **1984**;8:64–70
14. Thomas CG Jr, Buckwalter JA. Poorly differentiated neoplasms of the thyroid gland. *Ann Surg* **1973**;177:632–642
15. Lindahl F. Anaplastic thyroid carcinoma in Denmark 1943–1968. *Dan Med Bull* **1976**;23:120–128
16. Som PM. Lymph nodes of the neck. *Radiology* **1987**;165:593–600
17. Picus D, Balfe DM, Koehler R, Roper CL, Owen JW. Computed tomography in the staging of esophageal carcinoma. *Radiology* **1983**;146:433–438
18. Mancuso AA. The neck. In: Stamathis G, Eckhart C, Nolley CS, eds. *Computed tomography and magnetic resonance imaging of the head and neck*, 2nd ed. Baltimore: Williams & Wilkins, **1985**:169–191
19. Jao W, Gould VE. Ultrastructure of anaplastic (spindle and giant cell) carcinoma of the thyroid. *Cancer* **1975**;35:1280–1292
20. Reichelt HG, Brase A, Hundeshagen H, Stender HS. Xeroradiographic studies in 150 patients with solitary scintigraphically nonfunctioning nodules of the thyroid gland. *Radiology* **1977**;125:689–692
21. Silverman PM, Newman GE, Korobkin M, Workman JB, Moore AV, Coleman RE. Computed tomography in the evaluation of thyroid disease. *AJR* **1984**;141:897–902
22. Takahashi M, Matsumoto M, Saitoh Y, et al. Computed tomographic diagnosis of thyroid nodules. *Rinsho Hoshasen* **1984**;29:257–261
23. Shibakiri I, Cho K, Takemoto H, et al. Computed tomographic diagnosis of thyroid tumors: a new attempt to classify the pattern of thyroid tumors. *Rinsho Hoshasen* **1985**;30:17–20
24. Walfish PG, Hazani E, Strawbridge HTG, Miskin M, Rosen IB. Combined ultrasound and needle aspiration cytology in the assessment and management of hypofunctioning thyroid nodule. *Ann Intern Med* **1977**;87:270–274
25. Schneider V, Frable WJ. Spindle and giant cell carcinoma of the thyroid. Cytologic diagnosis by fine needle aspiration. *Acta Cytol* (Baltimore) **1980**;24:184–189
26. Gatenby RA, Mulhern CB Jr, Richter WP, Moldofsky PJ. CT-guided biopsy for the detection and staging of tumors of the head and neck. *AJNR* **1984**;5:287–289
27. Sutton RT, Reading CC, Charboneau JW, James EM, Grant CS, Hay ID. US-guided biopsy of neck masses in postoperative management of patients with thyroid cancer. *Radiology* **1988**;168:769–772
28. Mancuso AA, Harnsberger HR, Muraki AS, Stevens MH. Computed tomography of cervical and retropharyngeal lymph nodes: normal anatomy, variants of normal, and applications in staging head and neck cancer. Part II. Pathology. *Radiology* **1983**;148:715–723
29. Gatenby RA, Mulhern CB Jr, Strawitz J, Moldofsky PJ. Comparison of clinical and computed tomographic staging of head and neck tumors. *AJNR* **1985**;6:399–401

Memorial

Robert James Borgerson, 1919–1989

Robert J. Borgerson died August 12, 1989, in Fort Collins, CO. "Borgy" was born in Devil's Lake, ND, September 9, 1919. He attended both the University of North Dakota and the University of Illinois, graduating from the University of Illinois with an M.D. in December 1943.

After completing an internship at Cook County Hospital, he served in the U. S. Army from 1944 through 1946. He practiced medicine as a general practitioner in Richland Center, WI, from 1947 through 1949. He then entered a radiology residency at Hines Veterans Administration Hospital in Hines, IL, finishing in 1952. He became a diplomat of the American Board of Radiology in 1953. Borgy was chairman of the department of radiology at St. Joseph Hospital in Chicago from 1954 through June 30, 1988. He was on the clinical faculty of Loyola University School of Medicine and Northwestern University School of Medicine. He was a member of the American Medical Association, the American College of Radiology, the Radiological Society of North America, and the Chicago Radiological Society.

Borgy was a well-respected physician and administrator. His 34-year tenure as chairman of radiology at St. Joseph Hospital is an impressive, unprecedented accomplishment. He prided himself on his relationships with other physicians and his ability to provide a "country doctor" approach to medicine. Borgy was a devoted husband and father. He is survived by his wife, Pat, and his daughter, Lisa. He surely will be missed by all who knew him.

Gregory D. Moss
Chicago, IL 60631

Nonsurgical Treatment of Primary Hyperparathyroidism with Sonographically Guided Percutaneous Injection of Ethanol:

Results in a Selected Series of Patients

Steen Karstrup[1]
H. H. Holm[1]
A. Glenthøj[2]
L. Hegedüs[3]

Twelve patients with primary hyperparathyroidism were treated with sonographically guided percutaneous injection of ethanol (96%) into solitary parathyroid tumors verified by biopsy. The patients were all selected for nonoperative chemical parathyroid ablation either because of acute severe hypercalcemic symptoms (four patients), a high surgical risk or an advanced age (four patients), or refusal of a surgical intervention (four patients). Before treatment, the serum concentration of ionized calcium ranged from 1.38 to 2.39 mmol/l (median, 1.59 mmol/l), and after the last treatment the serum concentration ranged from 0.80 to 1.47 mmol/l (median, 1.32 mmol/l) ($p < .001$). Normocalcemia was achieved in eight patients, and evident clinical improvement was seen in seven patients. The only complication was a permanent unilateral vocal cord paralysis due to involvement of the recurrent laryngeal nerve. The present study confirms the possibility of percutaneous treatment of hyperactive parathyroid glands. However, the treatment was not found to be beneficial to all patients and hypercalcemia recurred.

On the basis of our experience with these patients, we conclude that sonographically guided chemical parathyroidectomy should be considered an alternative treatment to surgery in patients who are not suited for surgical intervention.

***AJR* 154:1087–1090, May 1990**

The ability to place needles precisely in parathyroid tumors under sonographic guidance provides new possibilities of percutaneous treatment [1–4]. On the basis of earlier investigations, we have found it possible to inactivate hyperactive parathyroid glands by sonographically guided percutaneous injection of 96% ethanol [1–3]. As a result, we are now offering nonsurgical ablation of parathyroid tumors to highly selected patients in whom the surgical risk is increased.

The present study reports the initial results of sonographically guided chemical parathyroidectomy in a highly selected series of patients with primary hyperparathyroidism (PHPT).

Subjects and Methods

Selection of Patients

Twelve patients (10 women and two men) with hypercalcemia due to primary hyperparathyroidism were selected for sonographic examination and sonographically guided chemical parathyroidectomy. Four of the patients were admitted because of severe hypercalcemic symptoms, four because of a high surgical risk or advanced age, and four because they refused surgical treatment. The median age was 65 years (range, 45–85 years).

Design of Study

Ninety-six percent ethanol was used. The dose was estimated individually depending on the intraglandular dissemination. However, the dose never exceeded half of the volume of the parathyroid tumor (half of the product of maximum length, width, and depth). In principle,

Received October 26, 1989; accepted after revision January 3, 1990.

[1] Department of Ultrasound, Herlev Hospital, University of Copenhagen, DK-2730 Herlev, Denmark. Address reprint requests to S. Karstrup.

[2] Department of Pathology, Herlev Hospital, University of Copenhagen, DK-2730 Herlev, Denmark.

[3] Department of Internal Medicine and Endocrinology, Herlev Hospital, University of Copenhagen, DK-2730 Herlev, Denmark.

0361–803X/90/1545–1087
© American Roentgen Ray Society

a maximum of three treatments, separated by no more than 1 week, were given. Additional treatments were given depending on the biochemical results and the clinical condition.

Routine blood tests including measurements of ionized calcium were performed before biopsy, before treatment, between treatments, and during the follow-up period.

Informed consent was obtained from all patients except one who was in a hypercalcemic coma.

Technique for Examination and Treatment

The sonographic examinations were performed with a 7-MHz sector scanner (Brüel & Kjær, Nærum, Denmark) mounted with a needle-steering device for precise sonographically guided punctures. Tissue diagnoses were obtained by using fine-needle (0.6 mm) aspirations for immunochemical parathyroid hormone (PTH) measurements [5, 6] and cytologic examinations [7]. Diagnoses were verified histologically by examining tissue samples obtained with a 0.8-mm cutting needle (Sure-cut, TSK Laboratory, Tokyo, Japan) [8]. All the fine-needle biopsies were performed under local anesthesia and in the same setting according to principles previously described [6]. Generally, biopsies were performed in a separate session before treatment. However, in two patients treatment was started immediately after biopsy because of the patients' life-threatening clinical condition.

The alcohol injection was performed under local anesthesia and continuous sonographic guidance. Initially an outer guide needle (1.2 mm) was introduced into the skin and neck muscle. A 0.6-mm fine needle was inserted through the guide needle. When the needle-tip echo was seen inside the parathyroid tumor, ethanol was injected slowly (Fig. 1).

Statistical analysis was performed with Wilcoxon's test for paired data. Probability values less than .05 were regarded as significant.

Results

The sonographic findings and the serum concentrations of ionized calcium before and after last treatment are indicated in Table 1 and Figure 2, respectively. The follow-up period after the last treatment ranged from 7 days to 12 months (median, 6 months). The number of treatments given to each patient ranged from one to five (median, three). In three patients, additional (more than three) treatments were given because of recurrence of hypercalcemia. During follow-up, a significant decrease in serum concentrations of ionized calcium was found ($p < .001$). Before treatment, the serum concentrations of ionized calcium ranged from 1.38 to 2.39 mmol/l (median, 1.59 mmol/l; normal range, 1.15–1.35 mmol/l), and after the last treatment the serum concentrations

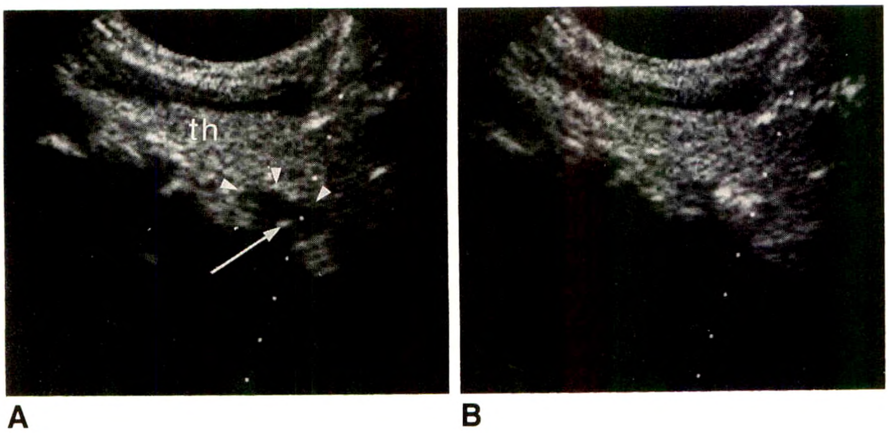

Fig. 1.—Longitudinal sonograms of neck show a parathyroid tumor (*arrowheads*).

***A*, Echo of needle tip is seen inside parathyroid tumor (*arrow*). th = thyroid gland.**

***B*, Parathyroid tumor has become echogenic after ethanol injection.**

TABLE 1: Sonographic and Biopsy Findings in 12 Patients with Primary Hyperparathyroidism

Case No.	Age	Sex	Sonographic Findings		Biopsy Findings		
			Size (cm)	Site	PT Tissue	PT Cells	PTH-Gradient PT/TH (μg/l)
1	65	F	1.8 × 1.2 × 1.0	LS	+	+	26/0.3
2	51	F	1.5 × 1.2 × 1.0	RI	None	+	—
3	45	F	2.0 × 2.0 × 1.0	LI	+	+	2.7/0.3
4	85	F	1.7 × 1.0 × 1.0	RI	+	+	22/0.3
5	78	F	2.5 × 1.0 × 1.0	LI	+	+	2.9/0.3
6	64	F	2.0 × 1.0 × 1.0	LS	+	+	38/0.3
7	58	F	0.8 × 0.6 × 0.5	RI	None	+	1.3/0.3
8	78	F	1.6 × 1.5 × 1.5	RI	None	+	—
9	57	M	1.2 × 0.5 × 0.5	RI	+	+	4.0/0.3
10	65	F	0.8 × 0.8 × 1.6	RS	+	?	2.5/0.3
11	50	F	2.0 × 1.6 × 1.0	LS	+	+	39/0.3
12	69	M	2.0 × 1.6 × 1.6	LI	+	+	2300/0.3

Note.—PT = parathyroid, PTH = C-terminal parathryoid hormone, TH = thyroid, LS = left superior, + = positive verification, RI = right inferior, None = no tissue for examination, — = procedure was not performed, LI = left inferior, RS = right superior, ? = inconclusive examination.

ranged from 0.80 to 1.47 mmol/l (median, 1.32 mmol/l). In eight patients, normocalcemia was achieved (Fig. 2).

In seven patients, the reduction in serum levels of ionized calcium was paralleled by an obvious clinical improvement, namely, disappearance of dyspepsia and anorexia, proximal neuromuscular weakness, fatigue, and/or depression. All of these symptoms had caused hospitalization. Unspecific physical or mental well-being was not regarded as clinical improvement. Two patients were of special interest. One (case 8) was in a coma and suffered from gastrointestinal bleeding of unknown origin. Although the patient was treated intensively with IV infusion of calcium-lowering agents, the serum levels of ionized calcium stayed unchanged and the patient remained in a life-threatening coma. After two treatments 4 days apart, the serum concentration of ionized calcium and the clinical condition normalized. The patient has now been followed up as an outpatient for 10 months and is healthy.

The other patient of special interest (case 12) had severe hypercalcemia and was precomatose. Three months earlier a pulmonary carcinoma had been diagnosed and the patient had been treated with chemotherapy. Before admission, the serum level of calcium increased dramatically. Initially, this condition was thought to be due to his pulmonary carcinoma. However, a large parathyroid adenoma was detected sonographically. After one treatment, the patient became normocalcemic and even hypocalcemic. However, the patient died from sudden diffuse gastrointestinal bleeding. At autopsy, a parathyroid adenoma was found in accordance with the sonographic finding. The adenoma was found to be totally necrotic within its capsule. No signs of extraglandular involvement were seen.

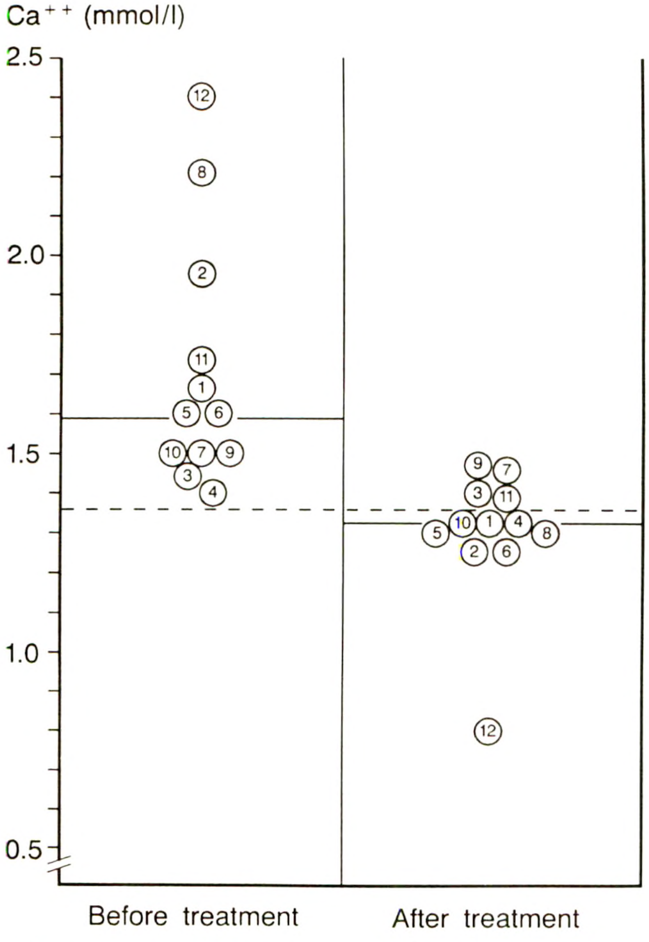

Fig. 2.—Serum levels of ionized calcium (Ca^{++}) before treatment and after last treatment. Dotted line indicates upper limit of normal range. Solid lines indicate median values.

Complications After Treatment

Only one complication occurred after treatment. In one patient (case 3), unilateral vocal cord paralysis occurred immediately after alcohol injection during the second treatment. Nothing was done differently in this patient and she did not have any unusual pain. The condition is still present (1 year later) and seems to be permanent. However, the patient does not presently have any symptoms of this complication. Generally, during the ethanol injection the patients complained of moderate pain extending unilaterally toward the jaw.

Patients Who Had Surgery

Two patients (cases 3 and 7) underwent neck surgery. In both patients, a solitary parathyroid adenoma was found in accordance with the sonographic findings. Both adenomas were found to contain an unusual amount of fibrosis on the microscopic examination. Furthermore, in one patient (the patient with permanent paralysis of a vocal cord) the parathyroid tumor and the recurrent laryngeal nerve were surrounded by fibrosis, making surgery difficult.

Discussion

The ability to use sonographic guidance to place needles in parathyroid tumors has formed the basis of percutaneous treatment [1–4]. The conventional treatment of symptomatic patients with PHPT is neck surgery [9, 10]. The surgical treatment is generally safe, with a high cure rate [9]. However, increased morbidity and mortality after surgical intervention have been described in elderly patients, in patients with other concurrent chronic diseases, and in patients with severe hypercalcemic symptoms [11–16]. In patients belonging to the last group, a life-threatening hypercalcemic crisis may develop, for which surgical intervention, although associated with a high morbidity rate [17], is the only definitive treatment. In the present study, three out of four patients with severe hypercalcemia were treated, resulting in marked biochemical and clinical improvement.

A prerequisite for this kind of treatment is that a tissue diagnosis can be secured. Sonography of the neck, combined with fine-needle biopsies, seems to be useful in this respect.

The present study was prompted by promising preliminary results [1, 2] and observations from a previous study of sonographically guided chemical parathyroidectomy in a consecutive (unselected) group of patients with PHPT [3]. The results are generally comparable. That not all patients are cured or experience symptomatic relief after this treatment should be stressed. In the present study, no signs of biochemical or clinical improvement were observed in three of 12 patients. The reasons for stopping further treatment attempts (more than three) in these patients were a complication in one of the patients and a suspicion of parathyroid hyperplasia in the other two patients.

Patients with hyperplasia of the parathyroid glands constitute 10–15% of patients with PHPT [10]. Furthermore, it might be difficult sonographically to visualize small hyperplastic parathyroid glands and thus be able to exclude the patients from the treatment. Consequently, a suspicion of a parathyroid hyperplasia is unavoidable, whether it is true or not, in a patient with a sonographically detected small parathyroid tumor and no signs of improvement after percutaneous treatment [3].

The treatment implies a risk of vocal cord paralysis. In particular, two circumstances are important for the increased risk of recurrent laryngeal nerve involvement. First, progressive fibrosis of the parathyroid tumor after each injection probably increases the chance of ethanol escaping from the tumor [3]. Furthermore, the run of the recurrent laryngeal nerve is unpredictable, as it is not visualized sonographically. The patient with the permanent vocal cord paralysis was found, during surgery, to have the nerve running just anterior to the parathyroid tumor. The nerve was probably punctured during treatment.

In principle, a wide variety of agents can be introduced through the needle into the tumor. Absolute alcohol has been reported to be an extremely powerful ablation agent that causes permanent tissue destruction and vascular occlusion [18]. Therefore, in order to reduce the risk of extraglandular spread, injections should be performed only when the echo from the needle tip is seen inside the parathyroid tumor. The intraglandular dissemination should be visualized under continuous sonographic control and injections should be stopped in the following situations: (1) A maximum of intraglandular dissemination has been reached, that is, whenever echoes from the alcohol injection have spread over the entire gland or no more spread can be produced from a limited area of the tumor (Fig. 1). (2) Echoes are seen escaping along the needle tract during injections. (3) The calculated maximum dose (half the product of the volume of the parathyroid tumor) has been reached.

The follow-up period is too short to decide how long the clinical or biochemical improvements will persist. Recurrence of hypercalcemia does not seem to be uncommon, and the patients should therefore be followed up regularly with blood tests. In patients not well suited for surgical intervention, we find it reasonable to give additional treatments. However, in any other patient, we believe surgery should be considered.

Sonographically guided chemical parathyroidectomy seems to be a useful alternative to surgery. However, the treatment should only be considered in selected patients with PHPT, that is, especially in patients with severe and life-threatening hypercalcemia and in other patients who are not good candidates for surgery.

REFERENCES

1. Karstrup S, Holm HH, Torp-Pedersen S, Hegedüs L. Ultrasonically guided percutaneous inactivation of parathyroid tumours. *Br J Radiol* **1987**; 60:667–670
2. Karstrup S, Lohela P, Apaja Sarkinnen M, Borgmästers H, Holopeinen O. Non-operative inactivation of a parathyroid tumour in a patient with hypercalcaemic crisis. *Acta Med Scand* **1988**;224:187–188
3. Karstrup S, Transbøl I, Holm HH, Glenthøj A, Hegedüs L. Ultrasound-guided chemical parathyroidectomy in patients with primary hyperparathyroidism: a prospective study. *Br J Radiol* **1989**;62:1037–1042
4. Solbiati L, Giangrande A, De-Pra L, Belotti E, Cantu P, Ravetto C. Percutaneous ethanol injection of parathyroid tumors under US-guidance: treatment of secondary hyperparathyroidism. *Radiology* **1985**;155: 607–610
5. Doppman JL, Krudy AG, Marx SJ, et al. Aspiration of enlarged parathyroid glands for parathyroid hormone assay. *Radiology* **1983**;148:31–35
6. Karstrup S, Glenthøj A, Torp-Pedersen S, Hegedüs L, Holm HH. Ultrasonically guided fine needle aspiration of suggested enlarged parathyroid glands. *Acta Radiol* **1988**;29:213–216
7. Glenthøj A, Karstrup S. Parathyroid identification by ultrasonically guided aspiration cytology: is correct cytological identification possible? *APMIS* **1989**;97:497–502
8. Karstrup S, Glenthøj A, Hainau B, Hegedüs L, Torp-Pedersen S, Holm HH. Ultrasonically guided histological fine needle biopsy from suspect parathyroid tumours: success-rate and reliability of histological diagnosis. *Br J Radiol* **1989**;62:981–985
9. Grandberg OP, Cedermark B, Farnebo OV, Hamberger B. Surgery for primary hyperparathyroidism: indications, intraoperative decision-making and results. *Prog Surg* **1986**;18:93–105
10. Kristofferson A, Grandstrand B, Järhult J. Primary hyperparathyroidism in Northern Sweden. *Surg Gynecol Obstet* **1987**;164:119–123
11. Christensen P, Hessov I, Mosekilde L, Melsen F. Operative treatment of primary hyperparathyroidism. *Ugeskr Laeger* **1988**;150:2527–2530
12. Cowie AGA. Morbidity in adult parathyroid surgery. *J R Soc Med* **1982**;75:942–945
13. Fitzpatrick A, Bilezikan PJ. Acute hyperparathyroidism. *Am J Med* **1987**;82:275–282
14. Hoff VW, Ballardie WF, Bicknell JE. Primary hyperparathyroidism: the case for medical management. *Br Med J* **1983**;287:1605–1608
15. Lafferty WF, Hubay AC. A review of the long-term surgical and non-surgical morbidities as a basis for a rational approach to treatment. *Arch Intern Med* **1989**;149:789–796
16. Pearson MW. Asymptomatic primary hyperparathyroidism in the elderly: a review. *Age Ageing* **1984**;13:1–5
17. Maselly JM, Lawrence MA, Brooks M, et al. Hyperparathyroid crisis: successful treatment of ten comatose patients. *Surgery* **1981**;90:741–746
18. Uflacker R, Paolini MR, Nobrega M. Ablation of tumor and inflammatory tissue with absolute ethanol. *Acta Radiol* **1986**;27:131–138

A Solution to the Problem of High-Flow Jets from Miniature Angiographic Catheters

Timothy B. Daniel[1]
E. William Akins
Irvin F. Hawkins, Jr.

In this study we evaluated methods for reducing high-flow jets from 5-French catheters that occur when injection pressures approach catheter tolerance (1000 psi [6.9 MPa]). This "jet effect" has been responsible for subintimal extravasation of contrast material in patients. We designed a physical model that accurately measures flow rates through the end hole and each side hole of 5-French high-flow catheters under simulated physiologic arterial pressure. When a standard catheter commonly used for injection of contrast material was studied, flow of contrast material was 34% through the end hole and 31% through the distal side-hole pair at high injection pressures (1000 psi). We examined the effect of altering the size and configuration of catheter side holes and end hole in an effort to create an improved flow profile, and thus a safer angiographic catheter. End-hole flow rate was reduced by 73% to 9% of total flow by tapering the 5-French catheter to 0.018 in. (0.046 cm) and by using smaller 0.015-in. (0.038-cm) side holes for even flow distribution.

The high-flow jets present with standard high-flow 5-French catheters do not occur when flow-restrictive end holes and side holes are used. A uniform flow profile can be obtained without sacrificing delivery of contrast material through small catheters.

AJR **154:1091–1095, May 1990**

Extravasation of contrast material during angiography can be a serious complication. The likelihood of extravasation is increased when high-pressure jets of contrast occur. Early angiographers used larger catheters to reduce the risks of extravasation, but patients suffered the complications of thrombosis and hematoma at the puncture site [1–4]. In an effort to reduce catheter-related thrombosis, smaller high-flow catheters are now widely used. At the high injection pressures (1000–1200 psi [6.9–83 MPa]) required for delivery of contrast material, extravasation may occur from end holes and distal side holes. On the basis of our previous work [4], we think that small catheters could be modified to improve their flow delivery.

In the current study, flow rates were partitioned and measured at the end hole and each side hole of 5-French catheters under simulated physiologic arterial pressure. Graphic representation of these values creates a "flow profile" that correlates the jet effect with a particular catheter design. By using this model, the size and configuration of the ports of exit were varied to attempt to create a catheter with an improved flow profile.

Materials and Methods

A model was constructed that allowed us to measure the flow through the end holes and individual side holes of 5-French high-flow catheters under simulated arterial pressure. A 5-French high-flow catheter was threaded through 0.045-in. (0.114-cm) holes punched into Tygon plastic tubing (internal diameter, $^{3}/_{32}$ in. [0.09 cm]) so that the side holes of the catheter were contained completely within the lumen of the plastic tubing. The catheter was placed

Received October 20, 1989; accepted after revision December 27, 1989.

[1] All authors: Department of Radiology, University of Florida College of Medicine, Box J-374, JHMHC, Gainesville, FL 32610-0374. Address reprint requests to I. F. Hawkins, Jr.

0361–803X/90/1545–1091
© American Roentgen Ray Society

so that the flow through the side holes (two per site and directly opposite each other) was parallel to the lumen of the plastic tubing (Fig. 1). The two free ends of the plastic tubing were connected to a glass column (1.5 cm in diameter and 100 cm in height) through a nonrestricting plastic Y connector. The top of the column was open to atmospheric pressure; a plastic cup was attached to catch overflow and thus allow measurement of the flow through that side-hole pair. Duplicating this system for each pair of side holes allowed measurement of flow through each side-hole pair and end hole.

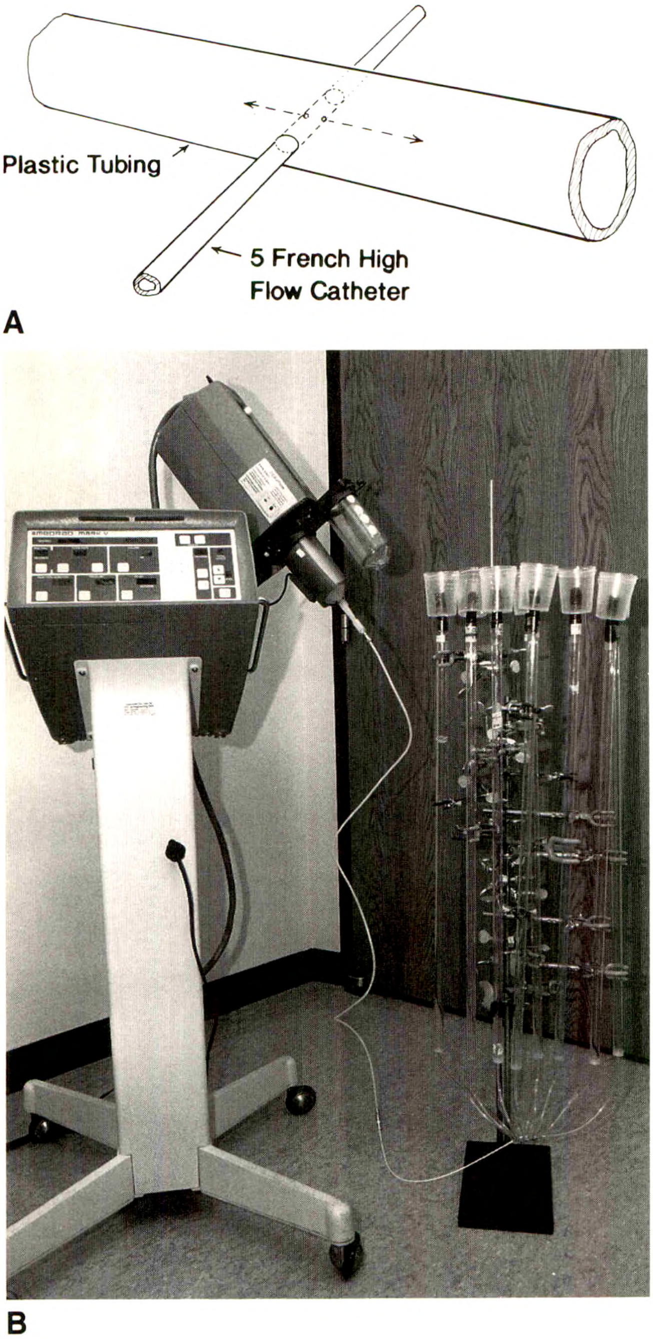

Fig. 1.—*A*, Drawing shows 5-French catheter threaded through 0.045-in. (0.114-cm) holes punched through plastic tubing. Seal between catheter and tubing was watertight but nonrestrictive. Flow through side hole was measured easily.

B, Photograph shows model with all side holes and end hole attached to columns for measurements of flow. Flow rate, injection pressure, duration of injection, and total volume were displayed by injector.

The complete system was filled with Hypaque 76 (Winthrop Breon, New York, NY), the contrast material used for injection. A MEDRAD V injector (Pittsburgh, PA) was used, allowing actual volume, flow rate, duration of injection, and pressure to be recorded for each injection. Two injections of 100 ml each were performed and averaged to produce each injection representation on the graph.

The model used for the experiment was validated by examining the effect of injecting Hypaque 76 under simulated physiologic arterial pressure vs atmospheric pressure (that is, without the columns of pressure) and by determining if resistance to flow was imposed by the Tygon plastic tubing around the catheter. First, injections were performed under simulated arterial pressure (100 ml of Hypaque 76) and full resistance (Tygon tubes covering all nine holes). Second, injections were performed under atmospheric pressure and full resistance. Third, injections were performed under atmospheric pressure, but minimal resistance (that is, only one set of side holes was covered with a Tygon tube, allowing measurement of flow through a pair of side holes with no distal or proximal resistance to contrast flow).

After validation of the model, flow rates for individual side holes and end holes were measured for the standard 5-French catheter and proposed modified catheters with variations in the size and numbers of end holes and side holes. Five-French high-flow catheters 50 cm long were used throughout this experiment. Side holes were carefully hand-punched by using Cook (Bloomington, IN) hole punches. The end holes were tapered by hand, and their internal diameters were gauged carefully by using standard hypodermic needles.

As the standard for comparison, a catheter was constructed that was similar to commercially available 5-French high-flow pigtail catheters. This catheter had a 0.035-in. (0.089-cm) end hole and three pairs of 0.035-in. side holes situated 4 cm proximal to the end hole and 5 mm apart.

Results

The model was validated by showing that no significant change in the relative flow rates of end holes and side holes occurred when different degrees of potential restriction from the model were imposed on the catheter (Fig. 2). Only a slight change in the relative flow rates of end holes and side holes was noted under simulated physiologic arterial pressure vs atmospheric pressure. This would be expected because of the tremendous difference between injection measure (1000 psi) and simulated arterial pressure (100 mm Hg). The model simulating arterial pressure was used for the rest of the experiment.

Testing of the standard reference catheter was performed at low and high flow rates. This catheter had a relatively uniform flow profile at low injection pressures (300 psi [2.1 MPa]; flow rate, 10 ml/sec), but at high injection pressures (1000 psi; flow rate, 25 ml/sec) a marked increased in flow occurred at the end hole (34% of total flow) and distal pair of side holes (31% of total flow) (Fig. 3). We think this exaggerated flow through the end hole at high injection pressure produces the potentially dangerous complication of extravasation in patients.

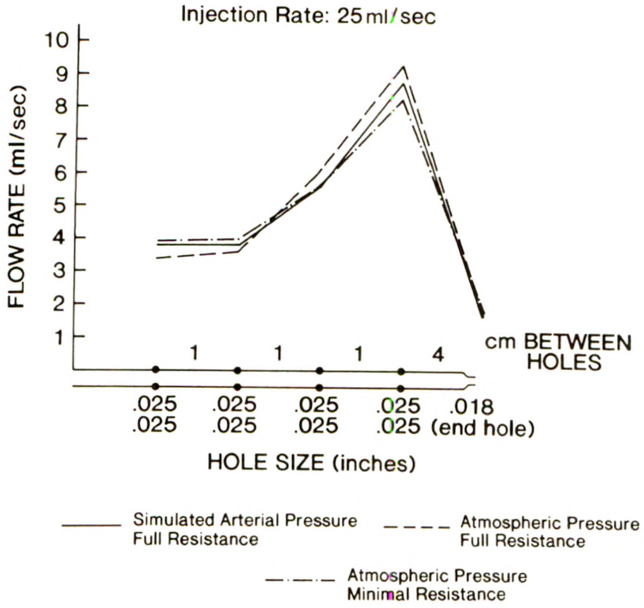

Fig. 2.—Model was validated as nonrestrictive and representative of intraarterial events by injecting at varied degrees of resistance and pressure in column.

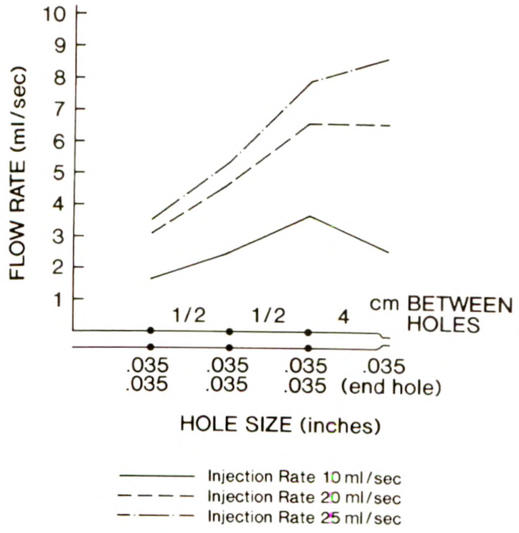

Fig. 3.—Catheter similar to commercially available 5-French catheters was tested. Flow rate is plotted against side hole of catheter. X axis is schematic representation of catheter tested. At low injection rates, this catheter had a relatively uniform flow profile, but at higher injection rates, 25 ml/sec at 970 psi (6.7 MPa), flow through distal side hole and end hole increased markedly.

To overcome this problem, we examined the effect of varying catheter design. Increasing the number of 0.035-in. side holes from six to 10 created only a slight decrease in distal-port flow rates (32% end hole, 26% distal side-hole pair) (Fig. 4). Decreasing the size of the side hole alone without altering the 0.035-in. end hole produced high flow rates of the end hole (32%) and at the distal side-hole pair (21%) (Fig. 5). This phenomenon also was not affected substantially by increasing the number of side holes. Decreasing the end hole to 0.018 in. (0.046 cm) while keeping the side holes at 0.035 in. decreased the flow rate at the end hole to 11%, but at the expense of creating exaggerated flow in the distal side-hole pair of 43% (Fig. 6).

The modified catheter that performed most favorably had an end hole of 0.018 in. and a side hole of 0.015 in. (0.038 cm) (Fig. 7). As shown graphically, the catheter was improved further by increasing the number of side holes from six to 10. The flow profile of this catheter was quite uniform; the flow rate was only 9% at the end hole and 23% at the distal side-hole pair. This modified catheter with one 0.018-in. end hole and ten 0.015-in. side holes delivered 73% less flow from the end hole, and a 28% reduction of flow from the distal side-hole pair, relative to the standard reference catheter. Overall delivery of contrast material was not affected by this modification, allowing between 23 and 25 ml/sec of Hypaque 76 to be delivered at 970 psi (6.7 MPa). Our preliminary clinical experience with catheters of this design in more than 20 patients has revealed no extravasation and excellent delivery of contrast material to the region of interest. These catheters do not have a pigtail design but are tapered straight catheters.

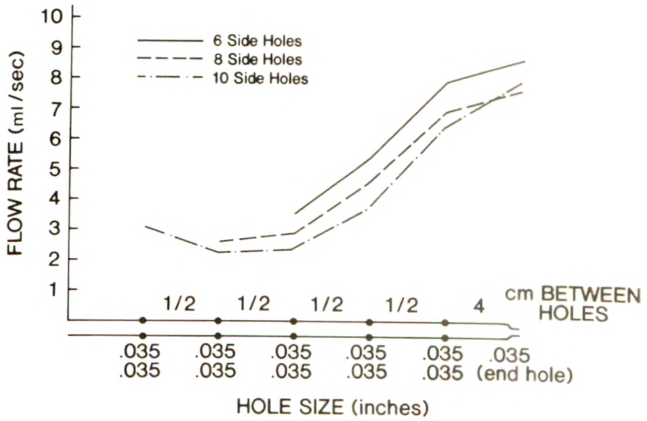

Fig. 4.—Graph shows that increasing number of 0.035-in. (0.089-cm) side holes in standard reference catheter mildly decreased overall flow rates of port of exit, but flow from end hole and distal side holes was still high.

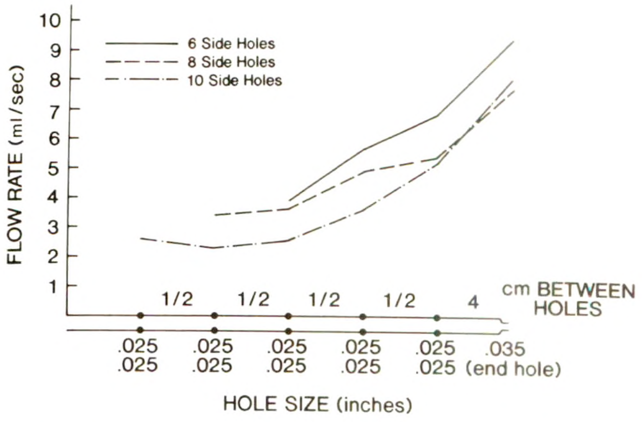

Fig. 5.—Graph shows that decreasing the size of side hole alone without altering 0.035-in. (0.089-cm) end hole produced even greater exaggeration of flow at end hole.

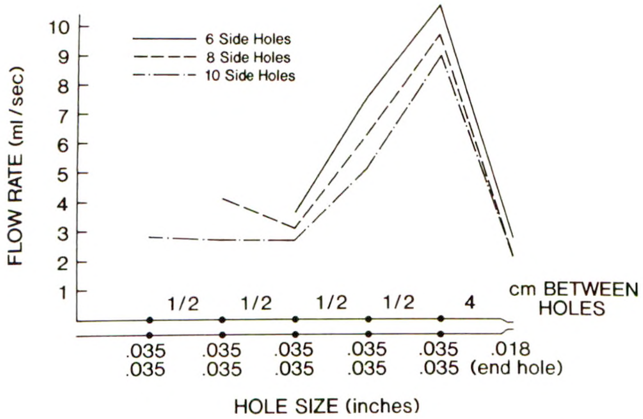

Fig. 6.—Graph shows that decreasing end hole to 0.018 in. (0.046 cm) while keeping the size of side hole at 0.035 in. (0.089 cm) decreased flow at end hole substantially, but at expense of markedly increasing flow at distal side hole.

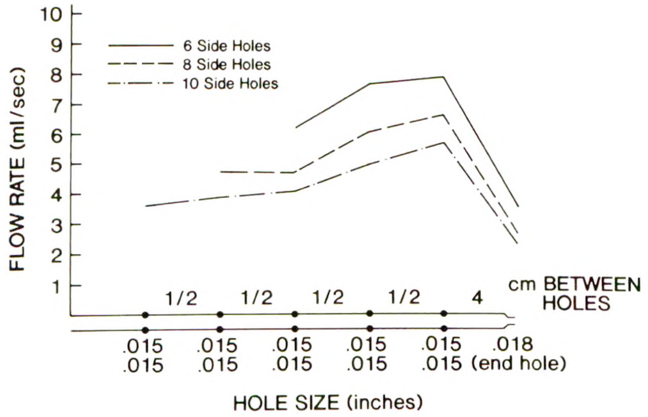

Fig. 7.—Graph shows flow profile was improved markedly by reducing end hole to 0.018 in. (0.046 cm) and side holes to 0.015 in. (0.038 cm). Further improvement was achieved by increasing number of side holes from six to 10.

Discussion

It has been recognized for many years that using large-diameter catheters for high-flow angiographic studies results in less traumatizing whip, less recoil, and lower injection pressures than when smaller, more flexible catheters are used. In the 1960s, both Nebesar and Polard [2] and Melnick and Gilbert [3] advised using larger catheters to minimize these effects, despite the recognized risk of local thrombosis and spasm at the puncture site. Recently, however, many leading angiographers have tended toward smaller-diameter, more flexible catheters and have shown that use of these catheters is relatively safe, allowing angiography to be performed on an outpatient basis [5, 6].

Five-French catheters can tolerate pressures up to and above 1000 psi and deliver at 20–25 ml/sec, but at these pressures vascular damage may occur because of the jet force of contrast material flowing from the catheter ports of exit. This problem is manifested as subintimal extravasation of contrast material, dissection, vascular perforation, and rupture, which has been reported to contribute to the immediate death of the patient [7–13]. Although arguments have been made that these complications follow damage to the intima from the catheter tip or guidewire, Lipton et al. [14] showed clearly that the jet effect by itself is a mechanism of vascular damage. Despite the potential consequences of catheter-induced complications, methods of solving the jet effect problem associated with use of miniature catheters have not been reported by others.

The physical properties of angiographic catheters under high injection pressure have been reviewed by Hansen et al. [4]. The Bernoulli equation predicts that flow out of a nontapered end hole will be greater than that out of individual side holes. Hansen et al. determined that tapered end holes and variably-sized side holes would produce nearly equal flow of contrast material out of the exit ports and create a "cloud effect." Our data agree with those of Hansen et al. and suggest that reasonably good flow characteristics can be achieved with simple catheter modifications, that is, smaller side holes and end hole.

In this experiment, the model created to test catheter flow rates was reproducible and nonrestrictive. It allowed measurement of the flow rate from the end hole and individual pairs of side holes of standard and modified catheter designs.

The flow profile of the standard reference catheter (5-French pigtail with a 0.035-in. end hole and six 0.035-in. side holes) showed clearly that this catheter design produced an unbalanced flow profile that appears to be responsible for jet effects from the end hole and distal side holes causing extravasation of contrast material. This unbalanced flow profile cannot be overcome by adding more side holes to the standard catheter, by decreasing the size of the side holes alone, or by decreasing the size of the end hole alone. Of the catheters tested in this experiment, the one that showed the best flow characteristics had the sizes of both the end hole and the side holes decreased (to 0.018 and 0.015 in., respectively) and the number of side holes increased from six to 10. These smaller holes did not decrease the overall flow rate of the catheter, which remained at 25 ml/sec.

This catheter with end-hole–restrictive properties does require insertion over 0.018-in. guidewires. Some radiologists may object to the use of 0.018-in. guidewires, preferring to use the standard 0.035-in. wires. Cope [5] has extensive experience inserting 5-French catheters over 0.018-in. mandril wires with few complications and little difficulty. This also allows a smaller entry needle to be used (20 or 21 gauge). At our institution, routine angiography is conducted with miniature 3- to 5-French catheters and small 20- to 22-gauge entry needles by radiology residents without difficulty. It does require a change in attitude to adopt miniature techniques, but the trend now seems to be favoring reduction in lumen size of angiographic and balloon catheters [15, 16]. It is unlikely that optimal flow characteristics can be achieved from 5-French catheters with 0.035-in. end holes, but further work in the design of side holes will be needed.

In summary, the standard minicatheters now commonly used for high-flow angiographic procedures create high-flow jet forces of contrast material flowing through distal side holes and end hole, which we have observed to cause extravasation in many cases. The jet forces can be modulated by altering the catheter design, that is, size and configuration of the end hole and side holes. When a catheter with a tapered 0.018-in. end hole and 10 0.015-in. side holes was used, flow distribution was improved without sacrificing overall flow delivery.

REFERENCES

1. Bove AA, Gimenez JL. Computer analysis of flow characteristics of injection catheters. *Invest Radiol* **1968**;3:427–432
2. Nebesar RA, Polard JJ. Catheter recoil and whipping in aortography: a potentially serious hazard. *Radiology* **1967**;89:845–847
3. Melnick GS, Gilbert GJ. Mechanical hazards in catheter aortography. *Circulation* **1965**;32:876–877
4. Hansen E, Akins EW, Collela J, Hawkins M, Hawkins IF Jr. New high-flow "cloud" catheter for safer contrast delivery. *Radiology* **1990** (in press)
5. Cope CC. Minipuncture angiography. *Radiol Clin North Am* **1986**;24:359–367
6. Hawkins IF, Haseman MK, Gelfand PN. Single mini-catheter technique for abdominal aortography and selective injection. *Radiology* **1979**;132:755–757
7. Talner LB, McLaughlin AP, Bookstein JJ. Renal artery dissection: a complication of catheter arteriography. *Radiology* **1975**;117:291–295
8. Laberge JM, Jeffrey RB. Aortic lacerations: fatal complications of thoracic aortography. *Radiology* **1987**;165:367–369
9. Soo CS, Wallace S, Chuang VP, Charnsangavej C, Bowers TA. Injury to the intima of the hepatic artery. *Radiology* **1982**;143:373–378
10. O'Reilly GV, Naheedy MH, Colucci VM, Hammerschlag SB. The 5-French catheter in cerebral angiography. *Radiology* **1981**;141:411–414
11. Hessel SJ, Adams DF, Abrams HL. Complications of angiography. *Radiology* **1981**;138:273–281
12. Long JA, Krudy A, Dunnick NR, et al. False aneurysm formation following arteriographic intimal dissection. *Radiology* **1980**;135:323–326
13. Mani RL, Eisenberg RL, McDonald EJ, Pollock JA, Mani JR. Complications of catheter cerebral arteriography: analysis of 5,000 procedures. 1. Criteria and incidence. *AJR* **1978**;131:861–865
14. Lipton MJ, Abbott JA, Kosek JC, et al. Cardiovascular trauma from angiographic jets: validation of a theoretical concept in dogs. *Radiology* **1978**;129:363–370
15. Becker GJ, Katzen BT, Dake MD. Noncoronary angioplasty. *Radiology* **1989**;170[SCVIR Suppl]:921–940
16. Hicks ME, Kreipke DL, Becker GJ, et al. Cerebrovascular disease: evaluation with transbrachial intra-arterial digital subtraction angiography using a 4-French catheter. *Radiology* **1986**;161:545–546

Book Review

Clinical Renal Imaging. By W. R. Cattell, Judith A. W. Webb, and A. J. W. Hilson. New York: Wiley, 218 pp., 1989. $137.50

This book is the distillation of questions, arguments, and conclusions acquired from weekly joint conferences attended by nephrologists, urologists, and radiologists. It is a critical assessment of the renal imaging procedures available placed in the context of the diagnostic problem posed by the clinician. The authors are a nephrologist, a diagnostic radiologist, and a nuclear medicine physician. The focus is clearly more nephrologic than urologic and is confined almost exclusively to adults rather than to infants and children.

The book is divided into three parts. The first section summarizes the various techniques available for renal imaging. The chapter on nuclear medicine techniques is especially useful, with an excellent review of diuretic scintigraphy and of the use of provocation studies that use angiotension-converting-enzyme inhibitors. The chapter on CT is far too short, given its relative importance in renal imaging and in comparison with the other chapters. The chapter on sonography includes only one small paragraph on duplex Doppler studies of the kidney—probably because much of the exciting work in this area has occurred since this book was written. The final chapter nicely outlines the strengths and weaknesses of IV urography, nuclear medicine, sonography, and CT and wisely points out that the factors of availability, local expertise, and cost must always enter the question of which study to perform.

The second section discusses the role of imaging in the evaluation of patients who have the most common findings confronting the nephrologist: proteinuria, hematuria, pyuria, flank pain, hypertension, and renal failure. For most patients with hematuria, persistent pyuria, or flank pain, IV urography remains the first imaging procedure to perform. The authors emphasize that if the results of urography are normal, but flank pain and gross hematuria are intermittent, a repeat urogram is useless unless it is performed *during* any repeat episodes. Although sonography is highly accurate in detecting pelvicaliceal dilatation, the problem of false-positive and false-negative sonographic findings in the assessment of possible urinary tract obstruction is emphasized. Occasionally, only minor degrees of dilatation may be observed in some cases of severe obstructive uropathy—especially with retroperitoneal fibrosis and some cases of ureteric calculi. Conversely, some dilated systems can be due to anatomic variants or to previous disease such as reflux nephropathy, calculus disease, or obstruction.

The third section of the book discusses in some detail the specific renal disorders that require imaging evaluation, the findings on each pertinent imaging technique, and the most cost-effective choice of imaging for diagnosis and subsequent management. The chapter on urinary tract obstruction emphasizes the distinction between obstruction and dilatation (hydronephrosis) and clarifies the role and limitations of imaging procedures in making the distinction. Observations reported since this book's publication suggest that the vascular resistive index derived from duplex Doppler studies of the cortical arteries may permit a noninvasive sonographic distinction between obstructive and nonobstructive hydronephrosis. In the chapter on stone disease, the authors remind us how meticulous the technique and interpretation of urography must be to avoid the common misdiagnosis of urinary tract calculi. The controversial and confusing questions on the necessity for and choice of renal imaging in known or suspected urinary tract infection are discussed lucidly in the chapter on infections. The chapter on renal masses contains the standard information available in other sources, but I disagree with two recommendations: I do not think that all septated renal cysts require cyst puncture, and I do not agree that sonography is adequate to exclude venous extension, liver metastases, and contralateral renal tumors in patients with renal cell carcinoma. The chapter on renal cystic diseases includes a useful summary of our knowledge about acquired cystic kidney disease in patients with chronic renal disease, the associated risk of renal adenocarcinoma, and the controversy about possible screening of these patients.

As the authors point out, this is not a comprehensive or exhaustive text. The subtleties and nuances of imaging for diagnosis or therapy are ignored or glossed over. No attempt is made to place things in a historical context, and a more detailed discussion of renal imaging can be found in other texts. Still, the most significant and widely accepted clinical and imaging features of renal disease are described in this book, and a sense of confident authority is apparent in every section and on every page. The choice and order of imaging tests for each disease or each clinical finding are offered boldly and with explicit rationale. The authors are somewhat tentative only when they discuss the use of IV contrast agents for urography in patients with mild or moderate renal failure. They acknowledge this is a controversial subject but claim that urography can be used safely in renal failure if the patient is well hydrated and the "minimum" dose of contrast medium is used "consistent with a diagnostic result."

The book has no citations or bibliographic references, although a small list of general references is included at the end. The advantages of this approach are obvious: The volume is shorter, the text looks less cluttered, and it is obviously quicker and easier to write a text without having to provide specific citations. It is also frustrating for the reader not to know when a statement or recommendation is based on published data or on personal opinion or experience.

The book is a model of clear and concise language, well organized and easy to read. The quality of the printing and binding is good, and the reproductions are almost uniformly excellent. Great care and skill obviously were used in the selection, cropping, and labeling of the illustrations. Useful tables of clinical and imaging topics, such as classifications of disorders or clinical features, imaging features, and differential diagnoses, are scattered throughout several chapters.

This book can be a useful handbook for physicians involved in the care and imaging of patients with suspected renal disease. I recommend it for nephrologists, urologists, and those radiologists who have a specific interest in urinary tract disease. It will be a useful introduction to renal imaging for the beginning radiology resident and an excellent review of the field in preparation for certification examinations.

Melvyn Korobkin
University of Michigan Medical Center
Ann Arbor, MI 48109-0030

Case Report

Transcatheter Thrombosis of a Leaking Saccular Aneurysm of the Main Renal Artery with Preservation of Renal Blood Flow

William D. Routh,[1] Frederick S. Keller,[1] and Gary M. Gross[2]

Percutaneous techniques have been used in the treatment of aneurysms and pseudoaneurysms in a variety of anatomic locations, including the kidney. An elderly patient with a leaking saccular aneurysm of the main left renal artery was considered a poor operative risk. We were able to embolize and thrombose the aneurysm selectively by using a combination of coil springs, guidewire, thrombin, and bucrylate without occluding the renal artery.

Case Report

A 79-year-old man with a history of hypertension, angina pectoris, and ethanol abuse was admitted to his local hospital with abdominal pain. CT scan revealed a cystic-appearing mass near the pancreatic tail that at first was interpreted as a pancreatic pseudocyst. At laparotomy, however, the lesion was thought to be a leaking suprarenal abdominal aortic aneurysm, and the patient was transferred emergently to this hospital.

On arrival, his blood pressure was 150/76 mm Hg and his serum creatinine level was 1.3 mg/dl. Review of the CT scan raised the question of a left renal artery aneurysm with adjacent hemorrhage (Fig. 1A). Abdominal aortography and selective left renal angiography confirmed the presence of a saccular renal artery aneurysm 3 cm in diameter having a narrow neck and arising from the left main renal artery near its bifurcation (Fig. 1B). The right renal artery and kidney appeared normal.

Because of the patient's age, history of symptomatic coronary artery disease, recent surgery, and ventilator dependency, the attending vascular surgeon considered the risk of emergent operative repair excessive. He therefore recommended transcatheter embolotherapy, accepting the associated risk of renal artery occlusion. A 5-French end-hole polyethylene catheter inserted via the right femoral approach was positioned with its distal end coiled within the aneurysm. The position of the catheter within the aneurysm was judged to be stable because it did not change during forceful manual saline injection or during passage of a movable core guidewire until its J-tip exited the catheter into the aneurysm. Initially, six 8-mm Gianturco coils (Cook, Bloomington, IN) and 130 cm of stainless steel movable core 0.035-in. (0.889 mm) diameter guidewire devoid of its mandrel were soaked in thrombin and then carefully deposited inside the aneurysm (Fig. 1C). The guidewire was inserted into the aneurysm in two separate fragments (100-cm and 30-cm long, respectively). The entire length of each guidewire fragment was intially wrapped tightly around the barrel of a 10-ml plastic syringe to form a large coil-spring configuration. The coiled guidewire was reloaded onto the stainless steel mandrel to facilitate insertion into the embolization catheter. The guidewire was then advanced off the mandrel until it was completely within the embolization catheter, then it was pushed completely through the catheter into the aneurysm with another 0.035-in.-diameter movable-core J-tipped guidewire. Because thrombosis of the aneurysm was incomplete, 1000 units of thrombin in a volume of 1 ml of normal saline and then 0.3 ml of isobutyl 2-cyanoacrylate (bucrylate) mixed with iophendylate (to retard polymerization) were

---

Received November 14, 1989; accepted after revision December 15, 1989.

[1] Department of Radiology, University of Alabama at Birmingham School of Medicine, 619 S. 19th St., Birmingham, AL 35233. Address reprint requests to W. D. Routh.

[2] Department of Surgery, University of Alabama at Birmingham School of Medicine, 619 S. 19th St., Birmingham, AL 35233.

AJR 154:1097–1099, May 1990 0361–803X/90/1545–1097 © American Roentgen Ray Society

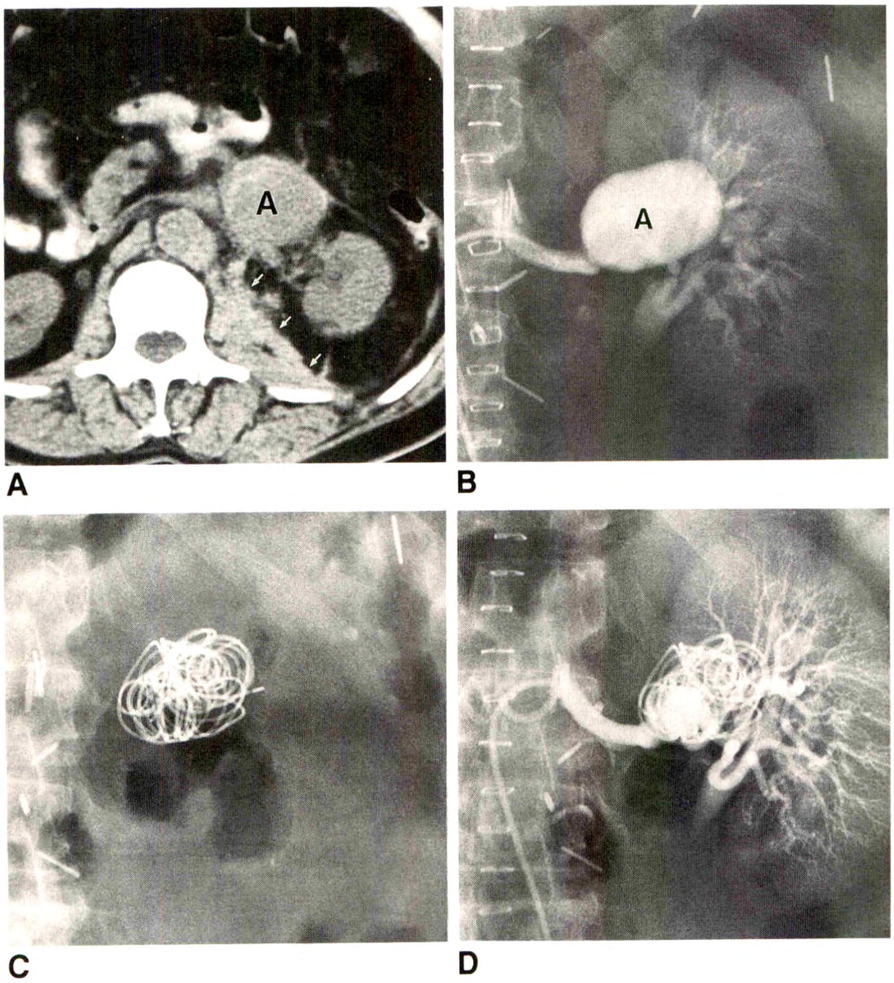

Fig. 1.—*A*, Abdominal CT scan depicts left renal artery aneurysm (A). Note abnormal relatively high-attenuation density infiltrating left perirenal fat and extending along psoas muscle (*arrows*), indicating recent retroperitoneal bleeding.

B, Selective left renal arteriogram confirms presence of a saccular aneurysm (A) of main renal artery.

C and *D*, Plain film (*C*) and repeated selective left renal arteriogram (*D*) after embolization show steel coils and guidewire within thrombosed aneurysm and persistent patency of left renal artery and its branches.

injected. Immediate follow-up angiography showed complete thrombosis of the aneurysm with continued patency of the left renal artery and all of its intrarenal branches. Slight fusiform dilatation of the main left renal artery was seen near its bifurcation (Fig. 1D).

The patient was weaned gradually from the ventilator and discharged on the 12th day after embolization. At that time, his serum creatinine level was 1.5 mg/dl, and his blood pressure was 128/72 mm Hg. He was receiving nifedipine and a thiazide diuretic. He was not placed on anticoagulant therapy. A radionuclide renogram obtained at 7 months follow-up showed 30% of total renal blood flow to the left kidney. Repeated left renal angiography at 9 months confirmed persistent thrombosis of the saccular aneurysm and patency of the renal artery. Slight enlargement of the previously noted fusiform segment of the left renal artery had occurred. The serum creatinine level had increased to 2.1 mg/dl. Two days later he was admitted to his local hospital for acute lower gastrointestinal bleeding and had a left hemicolectomy for a presumed diverticular hemorrhage. He died on the 14th hospital day of multiple postoperative complications. Permission for an autopsy was not granted by his family.

Discussion

Suggested indications for surgery in patients with renal artery aneurysm include rupture, expansion, erosion into adjacent structures (renal vein, renal collecting system, lumbar vertebrae), and pain attributable to the aneurysm. Surgery also has been advocated for women in their childbearing years, for aneurysm size greater than 1.5–2 cm (especially if rim calcification is absent), and for evidence of distal embolization. Indications for aneurysm surgery to control hypertension are more controversial [1–3]. In recent years, the operative mortality rate has ranged from 0% to 4% in series including elderly patients with generalized vascular disease when significant coronary and/or cerebrovascular disease is corrected first [4].

Percutaneous embolization has been used in the treatment of renal artery aneurysms [5–7]. Small intrarenal aneurysms have been thrombosed successfully by embolization with gelatin sponge or occlusion of feeding arteries with steel coils or detachable balloons [6, 7]. In general, these procedures compromise flow to at least a portion of the kidney because of embolic occlusion of intrarenal arterial branches. Resultant partial renal ischemia or infarction could manifest itself by worsening hypertension or deterioration of renal function.

We are unaware of previous reports of successful embolotherapy of an aneurysm of the main renal artery without compromising blood flow to the involved kidney. This procedure allowed the patient to avoid a high-risk surgical repair and removed the potential for further bleeding of the aneurysm. This patient's postoperative death 9 months after the embolization procedure underscores his high operative risk.

Persistent patency of the renal artery preserved function of the left kidney and avoided the possibility of worsening hypertension due to renal ischemia or a postembolization syndrome due to renal infarction.

Steel coils and guidewire initially were injected into the aneurysm to slow flow and provide a structural matrix for thrombus formation. Thrombin and bucrylate were injected subsequently to accelerate thrombosis. The presence of a narrow aneurysm neck was an important anatomic factor in preventing reflux of embolic material into the main renal artery. In a case of transcatheter thrombosis of a mycotic pseudoaneurysm of the renal artery to a nonfunctioning kidney, Lammert et al. [8] used an occlusion balloon that was inflated within the aneurysm and drawn back against its neck. This slowed flow within the lesion and facilitated thrombosis while helping prevent reflux of embolic material. The follow-up aortogram included in their case report did not show a patent renal artery distal to the pseudoaneurysm and the patient reportedly had a mild postembolization syndrome.

Our case demonstates the potential feasibility of transcatheter thrombosis of a saccular renal artery aneurysm with preservation of renal blood flow and maintenance of a functional nonischemic kidney. Embolotherapy may therefore play a role in the treatment of this entity in patients who are poor operative risks.

REFERENCES

1. Ortenberg J, Novick AC, Straffon RA, Stewart BH. Surgical treatment of renal artery aneurysms. *Br J Urol* **1983**;55:341–346
2. Youkey JR, Collins GJ, Orecchia PM, Brigham RA, Salander JM, Rich NM. Saccular renal artery aneurysm as a cause of hypertension. *Surgery* **1985**;97:498–501
3. Hageman JH, Smith RF, Szilagyi DE, Elliott JP. Aneurysms of the renal artery: problems of prognosis and surgical management. *Surgery* **1978**; 84:563–572
4. Olin JW, Vidt DG, Gifford RW Jr, Novick AC. Renovascular disease in the elderly: an analysis of fifty patients. *J Am Coll Cardiol* **1985**;5:1232–1238
5. Almgård LE, Fernström I. Embolic occlusion of an intrarenal aneurysm: a case report. *Br J Urol* **1973**;45:485–486
6. D'Souza VJ, Glass TA, Velasquez G, Formanek AG. Nonsurgical treatment of childhood hypertension: embolization of an intrarenal aneurysm. *Cardiovasc Intervent Radiol* **1984**;7:229–231
7. Kadir S, Marshall FF, White RI Jr, Kaufman SL, Barth KH. Therapeutic embolization of the kidney with detachable balloons. *J Urol* **1983**;129: 11–13
8. Lammert GK, Merine D, White RI Jr, Fishman EK, Porterfield JK. Embolotherapy of a high-flow false aneurysm by using an occlusion balloon, thrombin, steel coils, and a detachable balloon. *AJR* **1989**;152:383–384

Book Review

Urologic Pathology with Clinical and Radiologic Correlations. By Ayten Someren. New York: MacMillan, 768 pp., 1989. $125

No specialist can afford to operate in a vacuum, and this applies to pathologists as well as to everyone else. This book, which is intended for pathologists, is the first on uropathology that provides extensive correlations between clinical, radiologic, and pathologic findings. In order to achieve this end, the volume's 28 contributors include pathologists, urologists, and radiologists. All the contributors were originally from the Emory University School of Medicine, though some have since moved on.

The book is a single compact volume of 768 pages and is intended to be a basic practical review, not a comprehensive reference book. It has seven chapters, on the kidneys, urinary passages, renal transplants, the prostate and seminal vesicles, the testis and paratesticular structures, the penis and scrotum, and the adrenal glands. Each chapter is organized in exactly the same way: normal development and structure; radiologic evaluation, including normal radiologic findings; general guidelines for pathologic evaluation; congenital anomalies; inflammatory and other nonneoplastic disorders; and neoplasms. For each lesion, the clinical features, radiologic appearance, pathologic features, and treatment and prognosis are discussed.

The book is heavily illustrated. Rather than having the illustrations labeled with arrows, numbers, or letters, the labels conveniently are printed out in full, with an accompanying arrow. This makes the illustrations fast and easy to digest. The references are limited to key articles and books, but this volume clearly meets its advertised goal, and does so quite well.

The radiologic descriptions are generally equal to what would be found in a small general radiologic textbook. Transrectal sonography for prostate cancer, for example, is given a couple of lines acknowledging that the technique exists, but no further discussion is included. Rare entities, such as Cowper syringocele, are not mentioned at all. However, these limitations are appropriate, given the scope of the book. That scope is quite different from, for example, David Hartman's *Renal Cystic Disease: AFIP Atlas of Radiologic-Pathologic Correlations, Fascicle I* in which the radiologic aspects are discussed in much greater depth.

All in all, this is an excellent work. It is well written and easy to read, it achieves its stated goal, and no other book is quite like it. As with any such book, it has numerous minor points about which I might disagree. The most serious problems involve the performance characteristics of the imaging examinations, which are not based on the latest literature. This means that the reports of performance characteristics are often far too optimistic. Many illustrations, such as Figure 2-26, are too dark, suggesting that the book may have been overinked at printing.

Although the book is intended mainly for pathologists, it could serve as a reference book for urologists, nephrologists, and students. It would be a useful book to have in a radiologic library. It would be of interest to the general radiologist, to residents in radiology, and, of course, to uroradiologists, who may wish to purchase it for the discussion of pathology it provides.

Gerald W. Friedland
Stanford University, School of Medicine
Stanford, CA 94305

Technical Note

Use of the Hawkins-Hunter Rocket Wire in the Biliary System

Dennis W. W. Shaw,[1] Douglas M. Coldwell, Michael Kimmey, and Martin L. Goldman

The Hawkins-Hunter rocket wire (Cook Inc., Bloomington, IN), developed for retrograde placement of percutaneous nephrostomy catheters by forming a tract through soft tissues via sharp dissection, also can be used in the biliary tract. We present a case that demonstrates the use of the Hawkins-Hunter wire coaxial system to perform sharp dissection necessary for the percutaneous treatment of complete obstruction of the biliary system due to surgical transection of the common bile duct.

Case Report

A 56-year-old man had a bile leak into a surgical wound after a Billroth I hemigastrectomy performed 3 months earlier to treat peptic ulcer disease. An initial ^{99m}Tc-diisopropyliminodiacetic acid biliary scan showed nonfilling of the small bowel due to obstruction of the distal common bile duct. This was subsequently confirmed when contrast medium injected into an indwelling cholecystotomy tube showed filling of the common bile duct and the distal pancreatic duct. Contrast material was not evident in the duodenum, but was seen to pool around a Jackson-Pratt drain in the abdominal wound. Endoscopic catheterization of the common bile duct was unsuccessful. A percutaneous transhepatic cholangiogram showed normal intrahepatic ducts and pancreatic duct. Contrast material spilled from the common bile duct into the surgical wound (Fig. 1A). A catheter was advanced into the distal common bile duct and several unsuccessful attempts were made to pass a guidewire into the duodenum. No tract was present between the end of the common bile duct and the duodenum, a distance of approximately 2 cm. An endoscope was positioned in the duodenum adjacent to the papilla of Vater. The angiographic catheter was oriented so that its tip was aimed at the portion of the endoscope that identified the papilla. A Hawkins-Hunter rocket wire was passed through the angiographic catheter and into the duodenum by using the endoscope as a landmark (Fig. 1B). The rocket wire was seen endoscopically to enter the duodenum approximately 1 cm posterior to the papilla. The wire was snared and stabilized against the endoscope while a transhepatic catheter was passed into the duodenum. The endoscope was then removed.

The next day, the patient was examined again endoscopically and a long exchange wire was passed transhepatically through the catheter, snared by the endoscope, and the end pulled through the patient's mouth. One end of the wire was stabilized at the patient's right flank and the other at the patient's mouth. Over this, an 11.5-French stent was placed endoscopically between the distal common bile duct and the duodenum, establishing internal biliary drainage (Fig. 1C). After 10 days, the bile leak into the drainage tubes stopped, and all drains were removed. The patient died 3 weeks later of a massive pulmonary embolus.

Discussion

The development of instruments such as the Hawkins-Hunter wire has made it possible to perform procedures that require sharp dissection beyond the reach of the percutaneous needle [1, 2].

The Hawkins-Hunter "rocket" wire set includes both sharp- and round-tipped 0.018-in. (0.46 mm) stiff guidewires and an assortment of catheters. The stiff guidewire is passed through a catheter and then advanced through the tissue desired. As the wire has a small diameter, it may be deflected by the tissues. Hence, its effectiveness is limited to within a few centimeters of the guiding catheter tip. The catheter providing

---

Received November 9, 1989; accepted after revision January 3, 1990.

[1] All authors: Department of Radiology (SB-05), University of Washington, Seattle, WA 98195. Address reprint requests to D. M. Coldwell.

AJR **154:1101–1102, May 1990** 0361–803X/90/1545–1101 © American Roentgen Ray Society

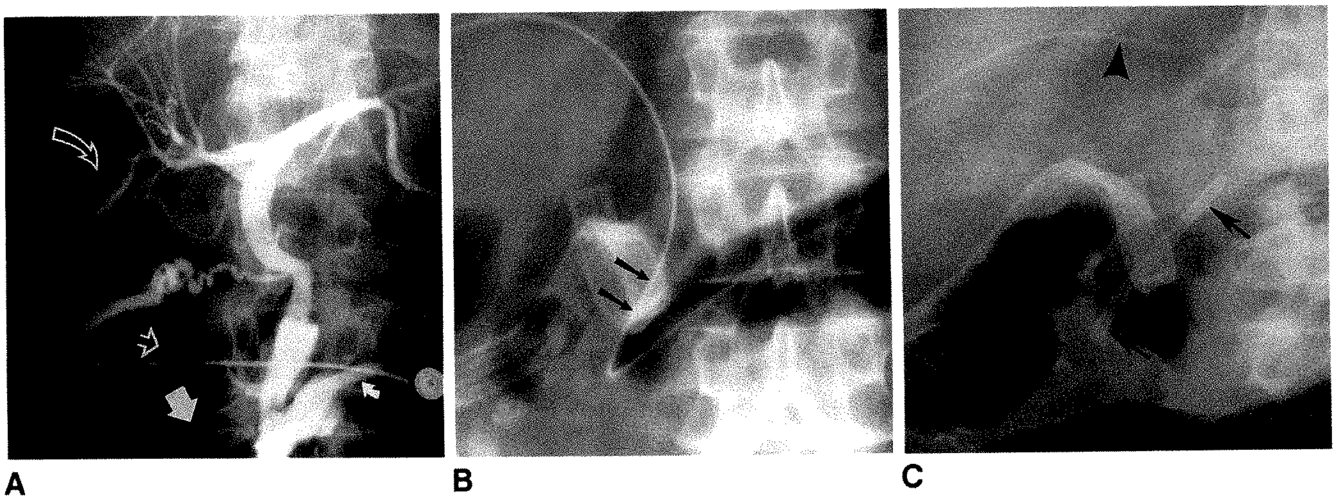

Fig. 1.—*A*, Percutaneous cholangiogram shows leak of contrast material from distal common bile duct, along a Jackson-Pratt drain (*solid straight arrow*). Pancreatic duct is partly filled (*solid curved arrow*). A transhepatic cholangiogram catheter (*open curved arrow*) and indwelling cholecystotomy tube (*open straight arrow*) are also evident.

B, Radiograph shows Hawkins-Hunter rocket wire advanced through avulsed end of common bile duct (*arrows*) into duodenum, where it was snared endoscopically and placed in stomach.

C, A stent (*arrows*) has now been placed via endoscope, bridging defect between duodenum and distal common bile duct. Percutaneous transhepatic cholangiogram catheter has been withdrawn (*arrowhead*).

directional control of the wire must be able to attain the desired direction and to be stable in that configuration while the rocket wire is advanced.

The Hawkins-Hunter rocket wire is exceedingly sharp and will pass through any soft tissues. Consequently, the anatomy through which the wire passes must be known in detail. The following catheter, which is usually 5-French in diameter, must not be advanced over the "rocket" wire until the wire tip is in the correct position and the route traveled is not across vital structures. If the wire punctures an artery, it can easily be withdrawn without complication. Such may not be the case if the 5-French catheter is advanced. This technique should not be used in areas containing large vessels. Surgeons should be readily available to treat complications (hemorrhage, perforation of a viscus, or spillage of bile).

In our case, the reestablishment of internal biliary drainage by this procedure was important because reoperation was not feasible. The common bile duct was encased in fibrotic tissue, making it exceedingly difficult to identify and isolate surgically.

We used this technique in another patient in whom an undrained lobule remained after routine percutaneous drainage of a pelvic abscess. In this case, no other approaches for additional catheter placement were necessary. Radical pelvic surgery was subsequently performed.

REFERENCES

1. Hunter PT, Hawkins IF, Finlayson B, Nanni G, Senior D. Hawkins-Hunter retrograde transcutaneous nephrostomy: a new technique. *Urology* **1983**;22:583-587
2. Hawkins IF, Hunter PT, Leal G, Hawkins M, Finlayson B, Senior D. Retrograde nephrostomy for stone removal: combined cystoscopic/percutaneous technique. *AJR* **1984**;143:299-304

Technical Note

Complications from 0.018-in. Floppy Platinum-Tip Guidewires

Stephen F. Quinn[1] and Steven Morse[2]

Introduction sets for drainage procedures that use 0.018-in. (0.045 cm) floppy platinum-tip guidewires have become popular interventional radiologic systems [1-3]. A variety of systems use these guidewires, including the Accu-Stick and One-Stick Introducer systems (Medi-tech, Watertown, MA). The primary advantage of these systems is the safety afforded by the 21-gauge needle that is used to gain system access. If multiple insertions are necessary, the 21-gauge needle has the theoretical advantage of being safer than an 18-gauge sheath-needle system. The 0.018-in. (0.045 cm) floppy platinum-tip guidewire is passed through the 21-gauge needle and coaxially dilated to accommodate a larger 0.038-in. (0.096 cm) working wire.

The floppy platinum tip is a 7.5-cm distal segment welded to a stiffer proximal portion made of stainless steel. The platinum tip aids in fluoroscopic visualization and the stiffer proximal portion facilitates coaxial dilatations. Although this system ordinarily allows safe system access, we have encountered instances in which the floppy platinum tip has detached from the stainless steel portion of the guidewire. In this report, we review the complications and discuss why detachments occur.

Technique

The One-Stick introducer system consists of a 21-gauge diagnostic needle and stylet, a 0.018-in. extra-stiff stainless steel guidewire with a floppy platinum tip, a 6.5-French introducer with stiffening cannula, and a 0.038-in. (0.096 cm) working guidewire. The initial puncture is made with the 21-gauge diagnostic needle, which is used to localize and opacify the cavity or system to be drained. Through this needle, the 0.018-in. (0.045 cm) guidewire is passed to the desired location. The 6.5-French introducer and stiffening cannula are passed coaxially over the 0.018-in. (0.045 cm) guidewire. The stiffening cannula is removed, and the 0.038-in. (0.046 cm) working guidewire is exchanged for the 0.018-in. (0.045 cm) working guidewire.

Two percutaneous nephrostomies and one percutaneous renal abscess drainage were performed in three patients at two institutions during an 18-month period. The nephrostomies were performed under fluoroscopic guidance, and the renal abscess drainage was performed with sonographic guidance. In two cases, the 0.018-in. (0.045 cm) guidewire was withdrawn through the stiffening cannula while within the 6.5-French introducer. In both instances, when minimal force was used, the platinum tip was severed at the point where it was welded to the proximal stainless steel portion of the guidewire. In one case, the 0.018-in. (0.045 cm) guidewire was withdrawn through the 6.5-French introducer cannula, and with minimal force the platinum tip was severed at the weld. In one case, the platinum tip was retrieved with a loop snare through the nephrostomy tract under fluoroscopic guidance. In both cases, the platinum tips were in the renal pelvis and perirenal soft tissues (Fig. 1), respectively, with no untoward effects at 19 months and 2 months of follow-up.

Close inspection of the 0.018-in. (0.045 cm) floppy platinum-tip guidewire reveals that the distal 5.5 cm of the stainless steel guidewire gradually tapers from 0.018 in. (0.045 cm) to 0.014 in. (0.035 cm). The distal platinum tip and weld, which measure 0.018 in. (0.045 cm), are larger than the proximal stainless steel segment of guidewire, and this gives the platinum tip a relatively high profile (Fig. 2).

Received October 4, 1989; accepted after revision December 12, 1989.

[1] Department of Radiology, Good Samaritan Hospital, 1015 N. W. 22nd Ave., Portland, OR 97210 and Oregon Health Sciences University, 3181 S. W. Sam Jackson Park Rd., Portland, OR 97201. Address reprint requests to S. F. Quinn at Good Samaritan Hospital.

[2] Department of Radiology, H. Lee Moffitt Cancer Center, P. O. Box 280179, Tampa, FL 33612.

AJR 154:1103-1104, May 1990 0361-803X/90/1545-1103 © American Roentgen Ray Society

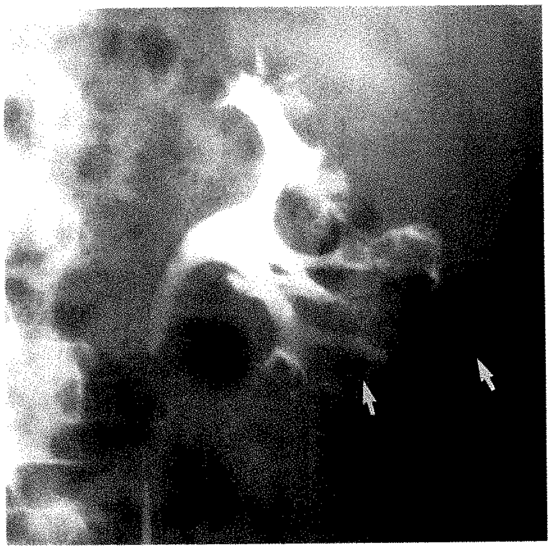

1

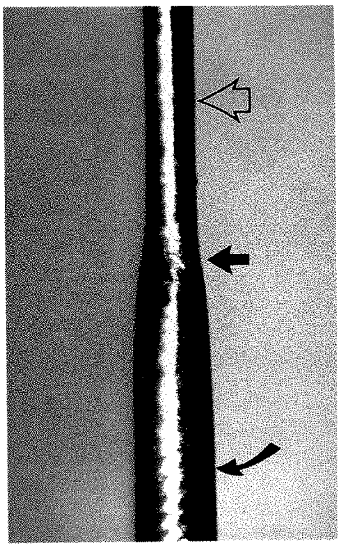

2

Fig. 1.—Radiograph shows detached platinum tip (*arrows*) in soft tissues adjacent to left kidney. Tip detached at weld of 0.018-in. (0.045 cm) guidewire during drainage of a left renal abscess.

Fig. 2.—Weld of 0.018-in. (0.045 cm) guidewire (*straight solid arrow*) has a bond strength of approximately 3 lb. (1.36 kg). Platinum tip (*curved arrow*) has a higher profile than does distal portion of stainless steel segment (*open arrow*), which creates a point of high friction during guidewire withdrawal and predisposes to detachment.

Discussion

The welds broke when seemingly slight amounts of tension were being used. The manufacturer does print a warning on the packages of the One-Stick introducer system: "Caution: withdrawal of 0.018-in. wire should be smooth and without resistance. If resistance is felt, remove 0.018-in. wire, one-stick dilator and stiffening cannula as a unit." The manufacturer acknowledges reports of platinum-tip detachments but all of these occurred during breaches of proper technique, and to their knowledge, there were no significant sequelae of these detachments (L. Jasinski, Medi-tech Manager, personal communication).

The breaks at the weld are probably due in part to the larger 0.018-in. (0.045 cm) diameter of the platinum tip relative to the tapered distal stainless steel portion, which measures 0.014 in. (0.035 cm). This change in caliber gives the platinum tip a relatively high profile (Fig. 2) and provides a potential site of resistance when the guidewire is withdrawn. The manufacturer claims a 3-lb. (1.36 kg) bond strength at the weld of the floppy tip (L. Jasinski, Medi-tech Manager, personal communication), which, compared with the strength of standard 0.038-in. (0.096 cm) working guidewires, is relatively tenuous.

The 0.018-in. (0.045 cm) floppy platinum-tip guidewire, when used according to the manufacturer's guidelines, should be safe and effective. To avoid platinum-tip detachments, the 0.018-in. (0.045 cm) guidewire should never be withdrawn through the 21-gauge needle or stiffening cannula. If resistance is felt while withdrawing through the 6.5-French introducer, then the 0.018-in. (0.045 cm) guidewire should be advanced and/or the 6.5-French introducer manipulated under fluoroscopic guidance until the guidewire can be removed with little or no resistance. If these maneuvers fail, then the introducer and guidewire should be removed together.

REFERENCES

1. Cope C. Conversion from small (0.018-in.) to large (0.039-in.) guidewires in percutaneous drainage procedures. *AJR* **1982**;138:170–171
2. Greenwood LH, Yrizarry JM, Brown SB. Observations on the use of the Cope introduction set. *AJR* **1984**;144:257–258
3. Vogelzang RL. A modified Cope introducing dilator to allow straight guidewire introduction. *AJR* **1986**;146:381–382

Case Report

Phlegmasia Cerulea Dolens, a Complication After Placement of a Bird's Nest Vena Cava Filter

John E. Aruny[1] and Krishna Kandarpa

Phlegmasia cerulea dolens (PCD) is the descriptive term coined by Gregorie [1] in 1938 to denote the unusual occurrence of venous thrombosis, painful ischemia with loss of distal pulses, and purple ecchymosis. This entity should be distinguished from the relatively more common and less serious phlegmasia alba dolens or "milk leg," which is caused by thrombosis of the common femoral vein above the junction with the deep femoral vein [2].

The clinical findings of PCD are impressive, with the rapid formation of massive edema. The limb feels cold, tense, and indurated. A deep cyanosis begins distally and eventually involves the entire limb. PCD involves thrombosis of the deep and superficial collateral venous channels, occluding venous return within the involved extremity. The iliofemoral venous system is completely thrombosed, the terminal vena cava is usually involved, and the cross-pelvic collaterals are obstructed [3]. Ischemia develops from arterial collapse when the arterial closing pressure is exceeded by rising interstitial tissue pressure. Distal arterial pulses are palpable in only 17% of the afflicted extremities [2].

PCD has occurred after placement of a Greenfield inferior vena cava filter (Medi-tech, Watertown, MA) [4]. To our knowledge, bilateral PCD after femoral placement of a Gianturco-Roehm "Bird's Nest Vena Cava Filter" (Cook Co., Bloomington, IN) has not been described before. We present a recent case in which caval obstruction, PCD, and death occurred after the uneventful placement of a bird's nest vena cava filter.

Case Report

A 50-year-old man with adenocarcinoma of the lung with brain metastases and a newly discovered neck mass was admitted because of upper gastrointestinal bleeding. One week after admission, shortness of breath and pleuritic chest pain developed suddenly. The patient had been treated for thrombophlebitis and pulmonary embolism 14 years ago. A nuclear medicine ventilation-perfusion lung scan gave a high probability pattern for pulmonary embolism. The patient was treated first with heparin but continued to have marked hematochezia with full systemic anticoagulation. The degree of hematochezia, along with a left frontal lobe intracranial metastasis, prompted the discontinuation of heparin therapy and placement of a bird's nest vena cava filter.

An inferior venacavogram performed before placement of the filter showed no evidence of luminal thrombus. The origins of the renal veins were well seen. The filter was placed in the infrarenal vena cava without difficulty (Figs. 1A and 1B). Twenty-four hours later, bilateral lower extremity weakness associated with lower back pain developed. An excerpt from the medical intern's notes gave the classic description of PCD: "Extremely swollen legs, blue and cold with no palpable pulses in either leg."

The patient died approximately 36 hr after placement of the filter. An autopsy revealed thrombosis of the inferior vena cava with extension into the popliteal veins bilaterally. Metastatic disease was widespread throughout the thorax and abdomen, including the liver, mediastinum, omentum, small bowel, and contralateral lung. Retroperitoneal and parapancreatic metastatic lymphadenopathy were present. Multiple pulmonary emboli of various ages were identified. A primary follicular carcinoma of the thyroid, previously undiagnosed,

---

Received October 30, 1989; accepted after revision December 26, 1989.

[1] Both authors: Department of Radiology, Brigham and Women's Hospital, Harvard Medical School, 75 Francis St., Boston, MA 02115. Address reprint requests to K. Kandarpa.

AJR 154:1105–1106, May 1990 0361–803X/90/1545–1105 © American Roentgen Ray Society

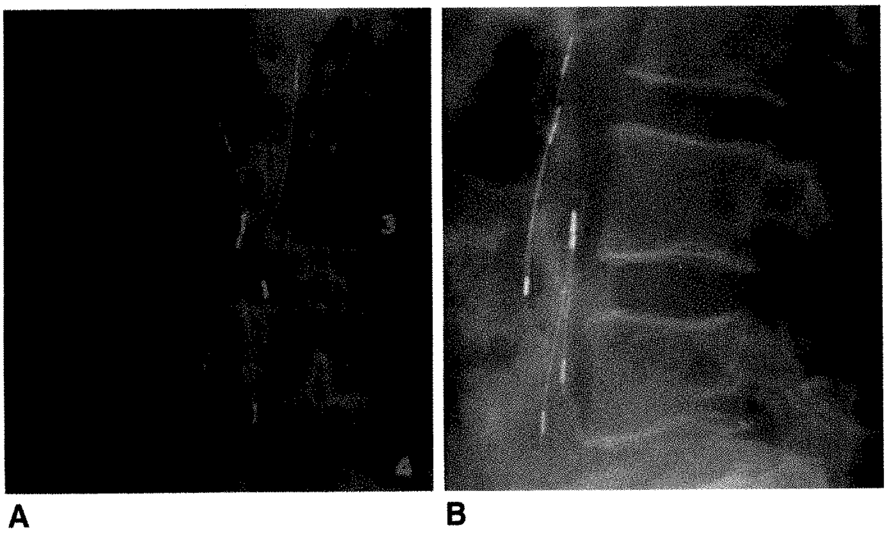

Fig. 1.—Phlegmasia cerulea dolens after placement of a bird's nest filter.

***A* and *B*, frontal (*A*) and lateral (*B*) radiographs show bird's nest filter in situ.**

was discovered directly adjacent to a metastatic adenocarcinoma in the neck.

The bird's nest filter was found in the position of original placement with no evidence of caval perforation.

The cause of death was massive venous thrombosis in the setting of widespread metastatic lung adenocarcinoma.

Discussion

The use of vena cava filters has found widespread application as protection against pulmonary thromboembolism in patients who cannot undergo systemic anticoagulation. Reported complications after placement of the bird's nest filter include caval obstruction (2.9%); recurrent pulmonary thromboembolism (2.7%); movement of the filter, which is a change in the position of one or more filter elements (0.2%); and migration of the filter, which is a change in the position of the filter assembly (1.1%) [5].

Placement of the filter in our patient was uneventful. Autopsy results disclose that caval perforation or filter migration had no role in the development of PCD. However, the temporal relationship between placement of the filter and the development of PCD is clear. Close scrutiny of radiographs in this patient obtained after placement of the filter shows that the mesh was coiled tightly within the inferior vena cava. We theorize that several factors of unknown relative importance may have contributed to the occurrence of PCD. The tight mesh configuration may have allowed effective trapping of a large thrombus fragment. The blockage of the filter, in the presence of the hypercoagulable state caused by the malignant neoplasm, resulted in caval thrombosis and retrograde extension of the thrombus into the deep and superficial venous system of both lower extremities. Likewise, the tight mesh configuration may have decreased the blood flow velocity in a vessel in which flow velocity was already slowed by the presence of deep venous thrombosis distally.

Of unknown significance, but of interest, is the coexistence of primary thyroid carcinoma in our patient and in the patient reported by Feinman and Meltzer [4], in whom PCD developed after placement of a Kimray-Greenfield filter.

REFERENCES

1. Gregorie R. La phlebite bleue (phlegmatia caerulea dolens). *Presse Med* **1938**;46:1313–1315
2. Strandness DE Jr, Summer DS. *Hemodynamics for surgeons.* New York: Grune and Stratton, **1975**:428–431
3. Haller JA Jr. *Deep thrombophlebitis, pathophysiology and treatment.* Philadelphia: Saunders, **1967**
4. Feinman LJ, Meltzer AJ. Phlegmasia cerulea dolens as a complication of percutaneous insertion of a vena caval filter. *J Am Osteopath Assoc* **1989**;89:63–68
5. Roehm JOF Jr, Johnsrude IS, Barth MH, Gianturco C. The bird's nest inferior vena cava filter: progress report. *Radiology* **1989**;168:749

Evaluation of Radiographs Developed by a New Ultrarapid Film Processing System

Robert A. Schmidt[1]
Kunio Doi[1]
Masaru Sekiya[1, 2]
Xin-Wei Xu[1]
Maryellen L. Giger[1]
Chien-Tai Lu[1]
Saeid Mojtahedi[1]
Heber MacMahon[1]

The image quality of radiographs developed by a new ultrarapid processor was evaluated to determine if faster processing causes degradation in the image. The processor used was the Konica Super-Rapid SRX-501 model. Two films designed for this processor (Konica MGH-SR and MGL-SR) were processed in 45 sec and were compared with standard rapid processing in 90 sec of corresponding conventional films (Kodak TMG and OC). Rare-earth screens (Kodak Lanex Regular and Lanex Medium) used with the new and conventional films interleaved during angiographic studies or for phantom images were assessed for image quality. The basic imaging properties of the screen-film systems were examined by measuring (1) Hurter and Driffield curves, (2) modulation transfer functions by using the slit method, and (3) noise Wiener spectra. Subjective clinical assessment showed that the images obtained with ultrarapid processing were acceptable, with increased contrast and graininess. Hurter and Driffield curve measurements confirmed higher gradients. Modulation transfer function measurements were the same as for the conventional films. Noise Wiener spectrum measurements showed a 10% increase in noise for MGH-SR vs TMG film and a 30% increase for MGL-SR vs OC film.

We conclude that acceptable image quality can be obtained using ultrarapid processing, with processing time approximately 60% that of conventional rapid processing. Potential applications include all areas in which rapid availability of the radiograph for interpretation is important. Although the processor studied was the first of its kind available, our evaluation indicates that the technology is available for a new class of ultrarapid processors.

AJR **154:1107–1110, May 1990**

The introduction of rapid processing systems for radiographic film development approximately 20 years ago had a major impact on the practice of radiology. Current rapid processors generally have a total processing time of approximately 90 sec and have almost completely replaced manual development in general practice. The recent availability of processors with even shorter processing times raises the question of whether compromises are made in image quality when ultrarapid processing is used. We addressed the issue by studying the physical image characteristics and clinical diagnostic quality of radiographs processed in this manner. The processor studied was the first of its type available, but several other manufacturers are developing machines for ultrarapid processing.

Materials and Methods

Two Konica (Konica Corp., Tokyo, Japan) superrapid processors (SRX-501) were installed side-by-side in the angiography darkroom of our institution. The SRX-501 processor has variable processing times of 45 sec, 90 sec, and 3.5 min, instantly switchable if developer temperatures are not changed. Temperature can be changed, with 15–20 min of stabilization time required for a 5°C temperature change. The processor uses conventional developer and fixer chemistry, with a temperature stability of ±0.1°C. We examined two types of films

Received September 5, 1989; accepted after revision January 3, 1990.

[1] Kurt Rossmann Laboratories for Radiologic Image Research, Department of Radiology, Box 429, University of Chicago, 5841 S. Maryland Ave., Chicago, IL 60637. Address reprint requests to R. A. Schmidt.

[2] Present address: College of Biomedical Technology, Niigata University, Niigata, Japan.

0361-803X/90/1545-1107
© American Roentgen Ray Society

suitable for rapid processing: Konica MGH-SR, a general-purpose film; and MGL-SR, a wide-latitude film. These films have a clear base with a thin emulsion, and have speeds comparable to those of conventional ortho film, when used with green-emitting rare-earth screens.

These SR films were compared with corresponding conventional films: Kodak (Eastman Kodak Co., Rochester, NY) TMG processed at 90 sec vs MGH-SR at 45 sec, and Kodak OC at 90 sec vs MGL-SR at 45 sec. All films were exposed with standard angiographic changers or cassettes and Kodak Lanex screens (Lanex regular for MGH-SR and TMG; Lanex medium for MGL-SR and OC). The SR films were processed at a development temperature of 37°C in order to match the speed of the conventional screen-film system processed at our standard setting of 35.5°C. Although 37°C is higher than the optimal 35°C development temperature recommended by the manufacturer, no difference was seen in the fog density of the films developed at the two different temperatures. This permitted similar exposures on the same patient, or interleaved films in the case of angiographic studies, without any change in technical factors.

Basic imaging properties [1–4] of screen-film systems for each processing condition were evaluated by obtaining (1) Hurter and Driffield curves by X-ray sensitometry [3], (2) modulation transfer functions (MTFs) by the slit method [4], and (3) noise Wiener spectra [1, 2]. Exposures were made at 80 kVp. Clinical assessment of images was based on phantom images with matched optical density (±0.03 at selected points); direct comparison images on the same patient made by interleaving conventional and SR films in an angiographic changer and processing them separately; and films taken in routine examinations of individual patients by using SR film only, with subjective assessment by the subspecialist radiologist in the appropriate area. Comparison films using both SR and conventional systems from the same patient were generated from selected gastrointestinal examinations. SR films also were deliberately processed at 90 sec, and conventional films at 45 sec, to determine the effects.

Results

Hurter and Driffield curve measurements show that both MGH-SR and MGL-SR films have higher gradients than their conventional counterparts in the midrange of optical densities used in radiologic practice, as shown in Figure 1. The base plus fog densities were comparable. The SR films tend to saturate at a somewhat lower maximum optical density.

MTF measurements (Fig. 2) do not show any significant difference, as would be expected for the MTFs of screen-film systems, which are dependent primarily on the screen used rather than the film used. At least two measurements were averaged for each MTF curve. The accuracy and precision of MTF measurements in our laboratory are ±0.02 [4].

Noise Wiener spectrum measurements show increased noise for the SR systems (Fig. 3). The noise is approximately 10% and 30% higher for MGH-SR vs TMG films and MGL-SR vs OC films, respectively. These increases in noise are due to the increased contrast of SR films, as the Wiener spectrum of quantum mottle in a screen-film system is proportional to the square of the gradient (or gamma) of the system used [1, 2].

Both phantom images (Fig. 4) and clinical radiographs showed increased contrast with the SR films and a visual impression of increased sharpness, probably due to the increased contrast. Radiographically dense areas were some-

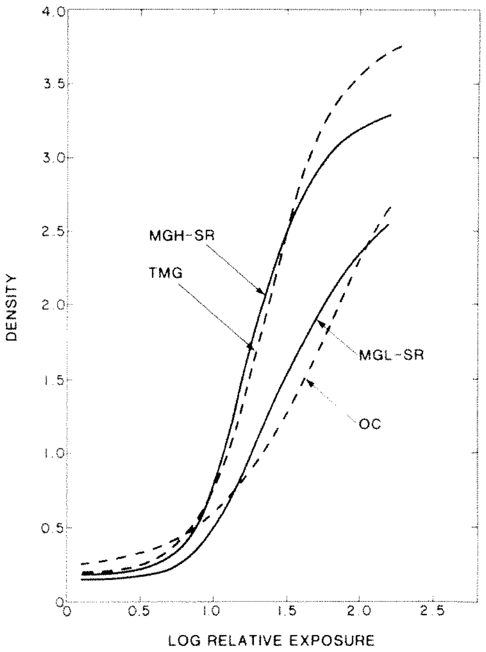

Fig. 1.—Hurter and Driffield curves for MGH-SR and TMG films with Lanex regular screens, and MGL-SR and OC films with Lanex medium screens.

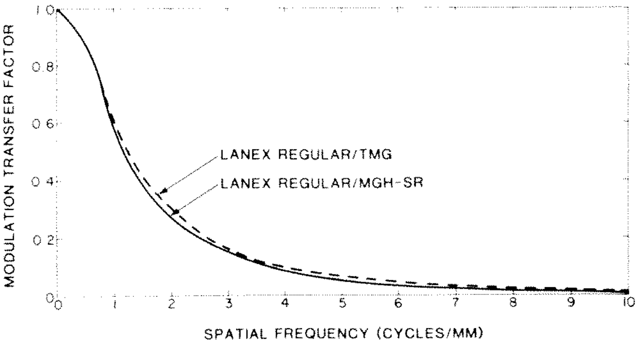

Fig. 2.—Modulation transfer function of Lanex regular screens with MGH-SR and TMG films.

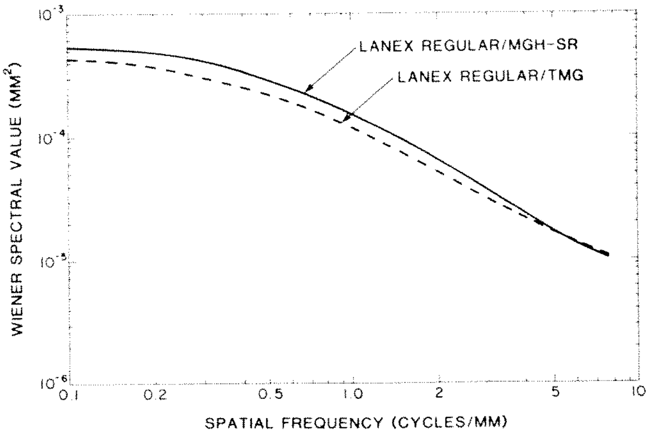

Fig. 3.—Wiener spectra of Lanex regular screens with MGH-SR and TMG films.

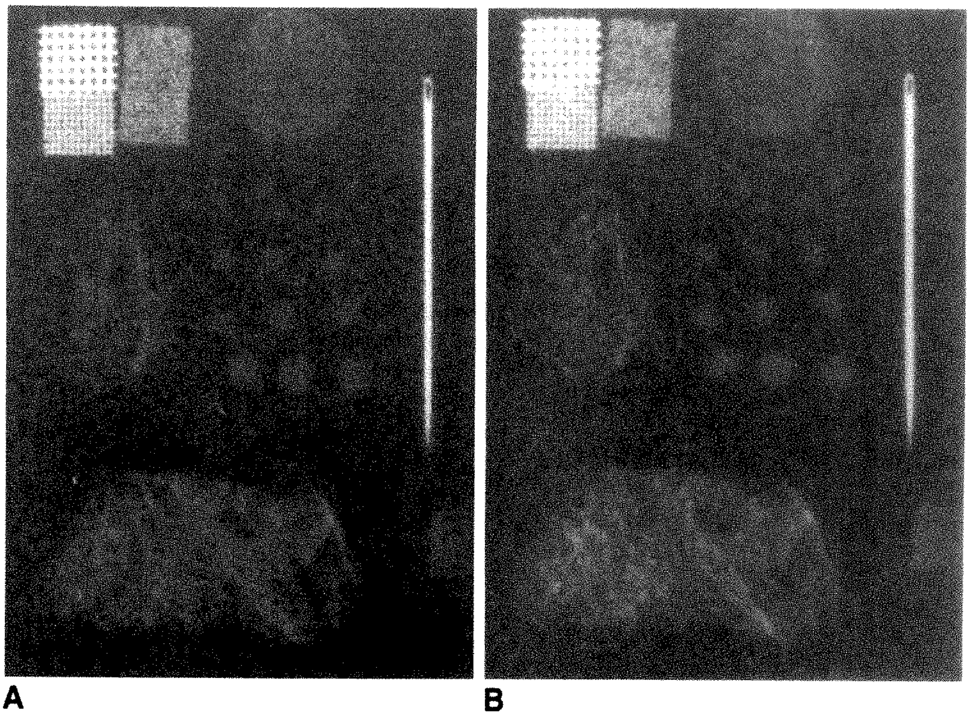

Fig. 4.—*A* and *B*, Test phantom images of TMG (*A*) vs MGH-SR (*B*) films.

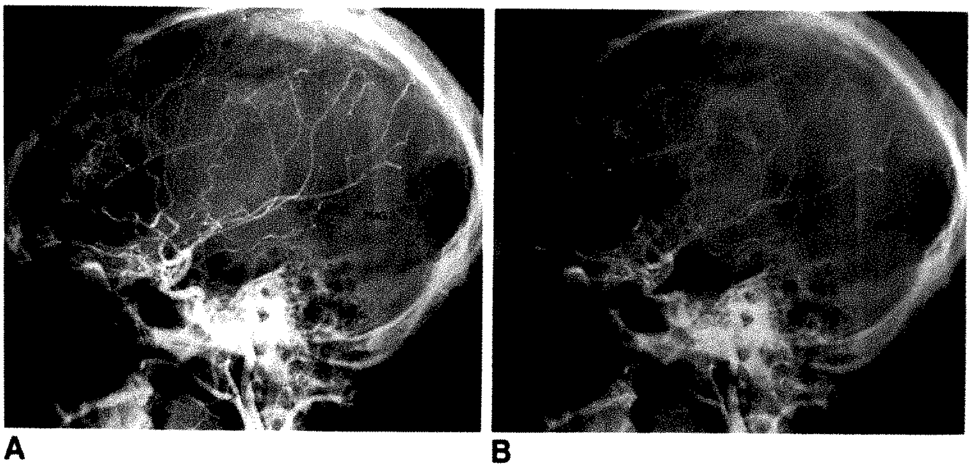

Fig. 5.—*A*, Neuroangiogram, TMG film.
B, Next frame of neuroangiogram, MGH-SR film.

times noted to have suppression of detail, for example, vessels overlying the bones at the base of the skull in neuroangiography (Fig. 5). Clinically, the SR images showed increased graininess. Although some clinicians had distinct preference for the tinted base and decreased graininess of the conventional films, diagnostic quality was considered to be within the range of routine clinical practice in our department. Spot films taken during fluoroscopic upper gastrointestinal examinations produced comparable images (Fig. 6). The wide-latitude MGL-SR film, when used for chest imaging, produced acceptable mediastinal detail. However, the OC film provided lower contrast (and thus wider latitude) than the MGL-SR film. SR films produce images that are still usable when processed at conventional 90-sec processing times. Conversely, conventional film images are usable when processed at 45 sec, with the chief disadvantage being that the film is incompletely dried.

Discussion

While some differences between the SR films and the conventional films routinely used in our department were observed, both objective physical measurements and subjective clinical assessment indicate acceptable image quality for both systems. The preference of an individual radiologist for greater contrast or increased latitude would probably be the most important determinant for any specific radiologic examination or practice. For example, the wider latitude of OC film was preferred in our department over MGL-SR for chest radiography.

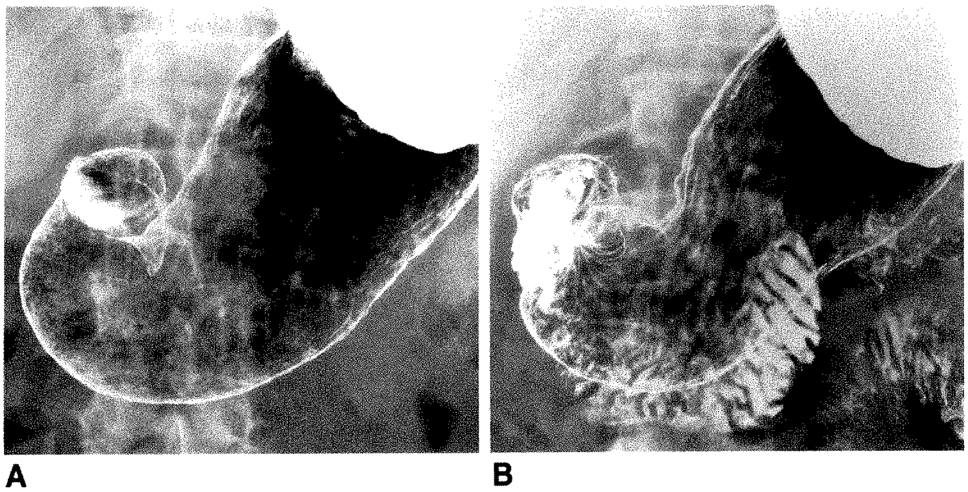

Fig. 6.—*A*, Double-contrast upper gastrointestinal examination, TMG film.
***B*, Film obtained immediately after *A*, MGH-SR film. (The reproduction process does not adequately demonstrate small differences seen in the original radiograph.)**

The SR system uses a faster film transport speed through the developer, fixer, and dryer. The time intervals between films fed in rapid succession to the processor were measured at 11.5 sec for the ultrarapid processor operated in the 45-sec processing mode and 18.5 sec for our conventional (Kodak M-6) 90-sec processor. The times are not different by precisely the ratio of the nominal processing times because of differences in the methods manufacturers use to measure transport times. The key factor is how quickly the processor is ready to accept another film. For a 40-film biplane angiographic run, this difference results in saving 5-min for the entire run (8.5 vs 13.5 min). The chief potential benefit of ultrarapid processing therefore is increased throughput and more efficient patient care. Such a system would be most applicable to areas in which speed is important or volume is high, such as angiography or interventional procedures, where large numbers of images are generated rapidly. Although the time saved for a single film processed on a patient is modest, approximately 0.5 min, areas where time is critical are potential applications, such as intraoperative studies and emergency department trauma cases. In very busy departments, more rapid patient throughput can be achieved for general radiologic procedures. Approximately 370 14- by 17-in. (36- by 43-cm) films can be processed per hour in the SR system, as opposed to 220 films per hour with conventional rapid processing. The variable-speed processing feature allows other possibilities, for example, processing of screening mammograms by using extended development (3.5-min processing time). Although the change in processing speed is instantaneous, a short time is needed for restabilization of development temperature, if the selected temperature is changed. This is about 15–20 min for a 5°C change.

The current ultrarapid processing does require special films. Currently, no subtraction film is available for 45-sec processing, which is a limitation in angiographic practice. However, conventional subtraction film can be processed by switching to 90-sec processing when performing subtractions, once the subtraction exposure condition is adjusted so that no temperature change is needed.

Conclusions

Instantaneous image acquisition and display represents the ideal goal in many areas of clinical radiology. Currently this is most closely approximated in digital subtraction angiography, and improvements in non-film-based digital detectors hold the promise of achieving this goal in many other areas in the foreseeable future. The SR processing system evaluated in this study offers a step in the direction of more rapid image availability for diagnosis, with conventional screen-film–based technology. Image quality observed is acceptable compared with that obtained by using conventional 90-sec processing.

ACKNOWLEDGMENTS

We thank Michael Carlin and Harold Tyler for technical assistance, Leslie Cleveland for secretarial help, and Elizabeth Lanzl for editing the manuscript.

REFERENCES

1. Doi K, Holje G, Loo LN, et al. *MTF's and Wiener spectra of radiographic screen-film systems.* Washington, DC: Health and Human Services, **1982**:1–77. HHS publication no. FDA 82-8187
2. Doi K, Kodera Y, Loo LN, Chan HP, Higashida Y. *MTF's and Wiener spectra of radiographic screen-film systems*, vol. 2. Washington, DC: Health and Human Services, **1986**:1–100. HHS publication no. FDA 86-8257
3. Doi K. *Basic imaging properties in radiographic systems and their measurements.* In: Orton C, ed. *Progress in medical radiation physics*, vol. 2. New York: Plenum, **1985**:181–298
4. Doi K, Bunch PC, Holje G, Pfeiler M, Wagner RG. *Modulation transfer function of screen-film systems.* Bethesda, MD: International Commission on Radiological Units. **1986**:1–56. ICRU report 41

Perspective

The Radiology Manpower Equation: A New Look

B. G. Brogdon[1]

Perception of, and response to, the problem of radiologic manpower in the United States is at best cyclic, at worst schizophrenic, and always erratic when viewed in historical perspective. Alarms of surplus and warnings of shortage have leapfrogged their way through the last three decades or more. Changes in the specialty have occurred more quickly than we are able to respond to them.

For many years the American College of Radiology (ACR) has monitored the manpower issue sporadically. Its attention to the problem has become more intense in the past decade. Recently acquired data offer an opportunity to evaluate the current status of radiologic manpower as the specialty enters an era of unprecedented technologic capability amid prodigious pressure from socioeconomic and political change.

Materials and Methods

The Supply Side

Since 1984 the ACR's Committee on Manpower has attempted to assess the supply of new radiologists entering the work force. Small postcard survey forms were sent to radiologists certified by the American Board of Radiology (ABR) in 1984, 1985, 1986, and 1987, requesting information on their training background and employment status and opportunities. Radiologists certified by the ABR in 1984 were mailed a questionnaire in April of 1985 (referred to as the 1984 survey); those certified in 1985 were mailed a questionnaire in October of 1985 (referred to as the 1985 survey); and those certified in 1986 and 1987 were mailed questionnaires in August of 1986 and 1987, respectively (referred to as the 1986 and 1987 surveys). The survey elicited 666 (76%) usable responses in 1984, 715 (80%) in 1985, 843 (81%) in 1986, and 768 (79%) in 1987. Usable responses are those completed surveys received from ABR diplomates who were trained and who practice in the United States and who were certified by the ABR for the first time in the year surveyed.

Since 1988 (largely through the efforts of Manpower Committee member Daniel F. Flynn), the ACR has been able to establish and maintain an accurate directory of all United States residents and fellows currently training in radiology. Consequently, in June of 1988 and 1989, the postcard survey was sent to all residents who were completing their training that month. Hence, the groups surveyed before and after 1988 are similar but not identical. There were 540 responses (81%) obtained in 1988 and 650 (70%) in 1989. Not all respondents completed every question on the card.

In both 1988 and 1989, the median age of responding residents was 31 years. In 1988, 20% of respondents were women, rising to 21% in 1989. The majority of residents (74% in 1988 and 81% in 1989) planned to take the ABR certification examination in the field of diagnostic radiology. In both 1988 and 1989, 3% of residents had prepared for diagnostic radiology with special competence in nuclear medicine. In 1988, 23%, and in 1988, 16% of residents had trained in therapeutic radiology.

Approximately 60% of the residents finishing their training had trained in one of 10 states (Table 1); location of training is shown later to be a significant factor in selection of postresidency practice.

The Demand Side

A 12-page questionnaire was sent to 1164 ABR-certified radiologists who were active members of the ACR and to 212 noncertified radiologists who were associate members of the ACR. The survey instrument addressed basic demographic items, including sex, age, year of residency completion and board certification, radiology sub-

---

Received November 27, 1989; accepted after revision December 26, 1989.
From the American College of Radiology Committee on Manpower, 1891 Preston White Dr., Reston, VA 22091.
Presented in part at the annual meeting of the American College of Radiology, Seattle, WA, September 1989.

[1] Department of Radiology, University of South Alabama Medical Center, 2451 Fillingim St., Mobile, AL 36617. Address reprint requests to B. G. Brogdon.

AJR 154:1111–1115, May 1990 0361–803X/90/1545–1111 © American Roentgen Ray Society

TABLE 1: Top 10 States Chosen by Residents for Training

State	1988 No. (%)	1989 No. (%)
New York	55 (10)	84 (13)
California	52 (10)	67 (11)
Texas	49 (9)	38 (6)
Pennsylvania	39 (7)	42 (7)
Ohio	27 (5)	28 (4)
Illinois	26 (5)	23 (4)
Michigan	24 (5)	28 (4)
Florida	21 (4)	17 (3)
Massachusetts	19 (4)	25 (4)
North Carolina	19 (4)	21 (3)
Total	331 (61)	373 (57)

specialty, and compensation arrangements. Respondents were asked to estimate their practice's needs for additional radiologists in the future and to evaluate the importance of various applicant qualities in final hiring decisions. Respondents over the age of 50 were asked to reveal their retirement plans or other future career intentions. Women were queried about pregnancy and its effect on their residency and/or practice. Opinions were solicited on practice satisfaction and other indicators of happiness.

The mailing list was randomized by zip code to virtually exclude the sampling of two or more members of the same practice group. Responses were returned by 648 active members (56%), of whom 47 were women and three did not state their sex. Seventy-seven associates (36%), of whom seven were women, returned the questionnaires. The returns are representative, geographically, of the population sampled. The ACR is a voluntary membership organization that prides itself on representing all of radiology; however, the ACR sample does not precisely match the universe of radiologists in the American Medical Association (AMA) data base.

In 1986, 24,679 radiologists were entered in the AMA data base [1] by self-designation as practitioners of that discipline (a somewhat less stringent qualification than that met by ACR members or associates). Of those, 24% were not board-certified (vs 11% of the ACR survey sample), and 12% were women (as opposed to only 7.5% of the ACR survey respondents). However, extrapolation of AMA projections [2], which estimate that women will account for 22% of all radiologists in the year 2010, corresponds with the number of women now finishing radiology training according to the current ACR annual surveys.

The average age of the 725 respondents to the 1988 ACR questionnaire was 47 years (average age of radiologists in the AMA data base was 46 years).

When asked to characterize their major activity in caring for patients, 11% identified themselves as therapeutic radiologists, 2% as general radiologists (both diagnostic and therapeutic), and 86% as practicing diagnostic radiology or one of its subspecialty areas. No response was obtained from 2%.

Some respondents were in solo practice, and others were members of large groups. The typical respondent, however, represents a median group size of five radiologists.

Results

The Supply Side

Postresidency plans.—The proportion of residents finishing their fourth year who were choosing to enter a radiology practice and the proportion choosing a fellowship were the same (46%) in 1988 and 1989. This reflects a pronounced increase in the number of postresidency fellows since 1984, when the residency training program in diagnostic radiology was extended from 3 to 4 years long (Fig. 1). The result is an effective prolongation of some 18 to 30 months between commencing a residency and entering a practice. This has resulted in some irregularity of flow through the manpower pipeline, but a steady stream of radiologists entering practice should be reestablished within a year or two if the current situation is not further modified.

Fellowships.—Fellowships in radiologic subspecialty areas are 1 or 2 years long, but the distribution of fellows in 1- or 2-year programs is not known. Current ABR regulations forbid the incorporation of fellowship training within the residency training period.

Practice types.—Of those residents who accepted positions in radiology practices, a substantial majority opted for group practice in a hospital and/or office setting. The next largest proportion joined a group practice in a university or teaching hospital. Other practice options attracted relatively small numbers of residents. There are proportional differences between the practice selections of radiation therapists and diagnostic radiologists (Table 2).

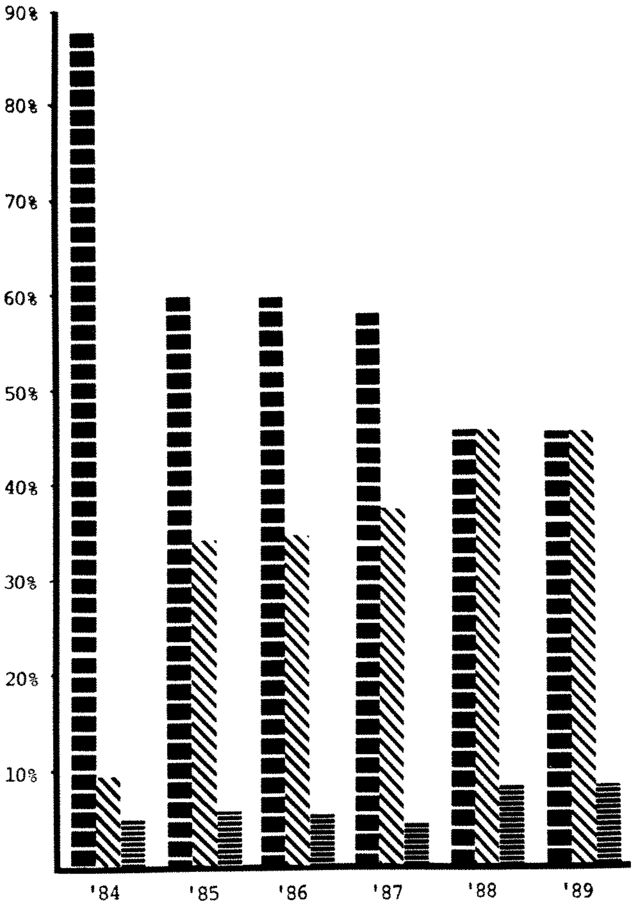

Fig. 1.—Graph shows changing trends in selection of first postresidency position by finishing residents since 1984. Thick bands = practice; diagonal bands = fellowship; thin bands = locums, military or government service.

TABLE 2: Type of Practice Selected by Residents, by Specialty Category

Practice	Diagnostic		Therapeutic	
	1988	1989	1988	1989
Group radiologic				
Office and/or hospital	78	77	44	54
University/teaching hospital	13	15	37	26
Multispecialty group	2	4	7	7
Solo radiologic				
Office and/or hospital	3	2	3	10
Multispecialty group	0	0	2	0
Government, military, or other	3	2	6	2

Note.—Numbers are percentages of respondents.

Since 1984 there has been a slight trend in favor of group practice (Table 3).

Practice location.—A quarter of those residents entering a practice do so at the location of their residency; about half of those remain in the university practice setting.

The top 10 states selected by residents as their first practice location (Table 4) vary only slightly from the top 10 states for location of residency training (Table 1). Only 13 states can encompass half or more of residents in training and residents beginning their first practice; a "balance of trade" can be identified by comparing Tables 1 and 4: some states are importers, others exporters, of residents.

Half of the residents choose practice positions outside of their state of residency (Table 5). A significantly higher percentage of women choose practices in the same state as their residency site.

The Demand Site

Effort allocation.—The ACR questionnaire asked practicing radiologists to allocate the approximate percentage of time spent in various professional activities. The 725 respondents reported 85% of their effort was devoted to care of patients, 6% to teaching, 2% to research, and 1% to other professional activities including practice management and administration.

Self-assessed competency.—The decision to add another radiologist to the practice or group may be based not only on work load, but also on the need to bring certain skills or knowledge into the practice. Radiologists were asked to indicate the two fields of radiology practice in which they felt most and least competent, in the belief that this might be indicative of the capabilities sought in a new associate.

For "most competent" fields, 64% of respondents selected diagnostic radiology alone or in combination with another option. The five most frequent combinations with general diagnostic radiology were, in order, mammography, CT, sonography, nuclear radiology, and interventional radiology. Consistent with the practice characteristics of the sample population, 10% selected therapeutic radiology, alone or in combination with another option, as their most competent area(s) of practice. One hundred eighty respondents (25%) selected options that included neither general diagnostic nor therapeutic radiology; they, presumably, practice principally in one or more diagnostic subspecialty fields.

In indicating the two fields of radiologic practice in which they felt least competent, many diagnosticians listed therapeutic radiology, of course. Omitting therapy, the most frequent combinations included interventional radiology, MR, and cardiac radiology.

Attrition.—Many factors cause attrition in the ranks of practicing radiologists, and attrition rates are difficult to obtain and substantiate.

Radiologists responding to the ACR questionnaire represent an average group size of five full-time members. That average group size has not changed since 1981. The 10-year average group size for 1978–1987 is 4.7 full-time radiologists. Respondents were asked how many members of the group died, retired, left the field of radiology, or left the practice for a radiologic practice elsewhere.

Calculations from the data supplied indicate that within the groups reported, during a 10-year period, the death rate of practicing radiologists was 0.42%. Another 1.56% retired (at average age, 65 years), and 0.48% left the field of radiology, presumably for some activity other than retirement; this may include part-time work, which was reported by 22 (3%), or locum tenens, reported by nine (1.2%) of the total 725 respondents. Thus the annual attrition rate for full-time practicing radiologists appears to be about 2.5%. If applicable to nationwide figures, then about 600 radiologists are lost each year from full-time practice.

It is striking that 3.4% of radiologists apparently leave one practice for another each year. Again, if applicable to the entire specialty group, this would amount to more than 800 radiologists changing practices annually—a figure almost equal to the number of radiologists newly certified each year.

TABLE 3: Types of Practices Selected by Residents

Practice	1984	1985	1986	1987	1988	1989
Group radiologic						
Office and/or hospital	53	53	54	54	68	70
University/teaching hospital	28	22	25	25	24	19
Multispecialty group	5	5	3	4	4	5
Solo radiologic						
Office and/or hospital	5	5	4	4	3	5
Multispecialty group	0	1	1	0	1	0
Government, military, or other	10	14	14	12	5	1

Note.—Numbers are percentage of respondents.

TABLE 4: Top 10 States in Which Residents Enter Their First Practice

State	1988 No. (%)	1989 No. (%)
California	19 (8)	18 (6)
Florida	18 (7)	23 (8)
Pennsylvania	18 (7)	14 (5)
New York	15 (6)	20 (7)
Texas	10 (4)	14 (5)
Virginia	10 (4)	8 (3)
Massachusetts	9 (4)	12 (4)
North Carolina	9 (4)	12 (4)
Tennessee	9 (4)	12 (4)
Wisconsin	9 (4)	10 (4)
Total	126 (51)	143 (49)

Retirement.—Respondents to this survey reported that associates has retired from the practice at an average age of 65 years. According to this survey, the average age of American radiologists is only 47 years. Interpolation of existing actuarial tables [3] predicts an expected life span of 33 more years, with an expected work-life span of 25.5 years, for a radiologist aged 47. Only a minority can be expected to take advantage of such longevity, however. As previously reported [4], given a choice, 30% would retire at the regular time, 20% would retire early, 14% would go part-time now, another 14% picked other combinations or failed to answer. Only 19% of respondents would like to "keep doing what I'm doing forever."

Recruiting.—Four hundred thirty-three (60%) of the respondents had added a new first-time practice member to their groups in the years 1985–1988.

Demand for radiologists.—Radiologists were asked to indicate their needs for adding to their group in each calendar year from 1988 through 1997 and to estimate how the new associate's professional activities would be divided between specialty areas.

The 725 respondents anticipated a need for 727 new associates in the years 1988 and 1989 (Fig. 2). There obviously is difficulty in making long-term projections, but a requirement for an additional 487 radiologists for the years 1990 and beyond was recorded. It is not known whether expected attrition in groups was considered in making estimates of future needs.

As each of the 725 respondents can be estimated to represent on average a five-person group, 3625 radiologists anticipate an immediate need for 727 new associates (or 0.2 full-time new associates for each practicing radiologist) in 1988 and 1989. An additional 487 new associates (0.13 per practitioner) were believed needed before the turn of the century. Thus, if one makes the uncertain assumption that these factors can be applied to the total radiology manpower pool, a need for almost 5000 additional radiologists immediately, and another 3200 within the decade, can be projected. Actually, although all the assessments of need for 1988 and 1989 have a confidence level of .95, the estimated needs for the years beyond are undependable and probably on the low side of reality.

Type of radiologists needed.—If one takes the estimated division of labor predicted for new members of groups and converts them to full-time-equivalent (FTE) radiologists, a table of proportional specialty needs is derived (Table 6). Although the requirement for general diagnostic radiology is five times larger than that for any one subspecialty area, the sum of those subspecialty areas is greater. This may justify the trend toward subspecialization manifested by the increasing pursuit of fellowship training.

Discussion

This study refutes the commonly held belief of recent years that there is an incipient surplus of radiologists in this country. Although there may be statistical weaknesses in the survey data, its interpretation, and predictions based on the data, the evidence is clear that an immediate and substantial shortage of radiologists exists today and may persist. If the present annual insertion of about 900 newly trained radiologists into the practice community continues, and if the projected future need is accurate, *and* if those projections allowed for an annual attrition of 600 radiologists, then the radiology manpower supply-demand equation may balance by the end of this century. It is likely, however, that projected needs beyond the early 1990s will prove to be inaccurate—and low.

Many other factors may affect the radiology manpower equation in the next decade. Most would seem to increase the requirement for new radiologists, or diminish the productivity of existing ones: for example, more technologic advances that are labor-intensive for the radiologist, a shortage of technologists, a reversal of the urban concentration of physicians, changing physician life-styles with shorter hours and fewer days worked, the aging of the baby boom generation, changing population life-styles and diseases (e.g., AIDS), an increasing proportion of women in radiology, shorter practice span because of later entry (longer training) and earlier retirement, increasing involvement of physicians in activities not involving care of patients, increasing subspecialization with consequent diminished overall productivity.

TABLE 5: First Practice State Same as Residency State

Response	Men		Women		All	
	1988	1989	1988	1989	1988	1989
Yes	45	50	61	61	48	52
No	55	50	39	39	52	48

Note.—Numbers are percentage of respondents.

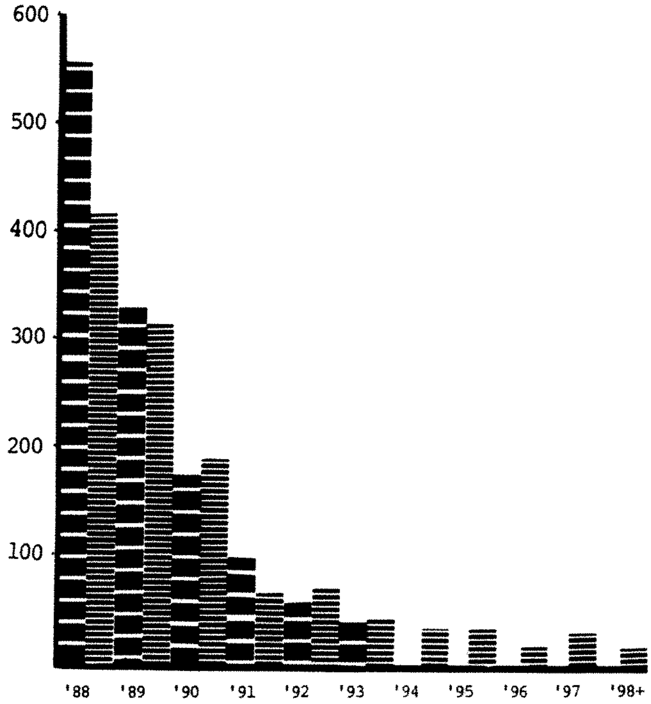

Fig. 2.—Graph shows number of respondents indicating number of additional radiologists needed in practice groups, by year. Thick bands = number of respondents, thin bands = number of radiologists needed.

There is no easy solution to a shortage of radiologists. There is not, nor is there likely to be, any significant increase in institutionally or government-funded residency positions. Unfortunately, in the long term, inability of the discipline to meet service demands may lead to loss of "turf" to other specialists in order to reduce workload requirements to manageable levels for available radiologic manpower.

TABLE 6: Percentage Distribution of Effort Anticipated for Additional Radiologists Needed Within the Decade, by Specialty or Subspecialty Area

Specialty	Percentage
Therapeutic radiology	8
General radiology	3
General diagnostic radiology	38
Cardiovascular radiology	1
CT	6
Interventional radiology	7
Mammography	4
MR imaging	7
Neuroradiology	6
Nuclear radiology	4
Pediatric radiology	4
Sonography	7
Vascular radiology	4
Other	2

ACKNOWLEDGMENTS

The assistance of Eileen D. Heveron, James J. Diamond, and Pamela J. Kassing, from the American College of Radiology, and Donald E. Herbert, from the University of South Alabama, in the collection, processing, and analysis of the survey data on which this paper is based is most gratefully acknowledged.

REFERENCES

1. Radiology. In: *Specialty profiles*, 1988 ed. Chicago: American Medical Association, **1988**:733–766
2. *Women in medicine: data source 1989* (pamphlet). Chicago: American Medical Association, **1989**
3. *Physicians supply and utilization by specialty: trends and projections*. Chicago: AMA Center for Health Policy Research, **1988**:42
4. Brogdon BG, Heveron ED, Diamond JJ. Attitudes of American radiologists toward practice: present and future. AJR **1990**;154:867–869

Radiology Outreach Foundation

The Radiology Outreach Foundation (ROF) is a nonprofit corporation whose goal is to help disadvantaged countries improve their health care by providing radiology equipment, books, consultation, education, and training to their practitioners. This assistance is on an application basis that is independent of political, ethnic, or religious orientation of the grantee. It depends on the need of the people and the ability of the ROF to meet that need. The ROF is approved by the U.S. Internal Revenue Service as a tax-exempt organization. It is endorsed by the following radiologic societies:

American Association of Women Radiologists
American College of Radiology
American Roentgen Ray Society
Association of University Radiologists
Radiological Society of North America
Society of Chairmen of Academic Radiology Departments
Society for Pediatric Radiology
European Society of Pediatric Radiology

All donations to the ROF are tax deductible. Persons who would like to contribute financially to the ROF, would be interested in being a visiting professor, would like to send books or journals to any of the institutions supported by the ROF, or would like further information about the ROF should write to

Charles A. Gooding, M.D.
President
Radiology Outreach Foundation
3415 Sacramento St.
San Francisco, CA 94118 USA

Perspective

Quality Improvement in Diagnostic Radiology

Philip N. Cascade[1]

> *Grant me strength, time, and opportunity always to correct what I have acquired, always to extend its domain; for knowledge is immense and the spirit of man can extend infinitely to enrich itself daily with new requirements. Today he can discover his errors of yesterday, and tomorrow he may obtain new light on what he thinks himself sure of today.*
>
> Maimonides, *Oath and Prayer*

That we have entered a new and revolutionary phase in our system of health care delivery is indisputable. Dr. Paul Ellwood, in his Shattuck Lecture of 1988 [1], describes the current health care environment as consisting of "uninformed patients, skeptical payors, concerned politicians, frustrated physicians and besieged healthcare executives." Stimulated by questions raised in studies such as Wennberg's [2], which describes wide variations in practice patterns in different geographic settings without demonstrable differences in health care outcomes, government and private sector payers have begun to question the ability and motivation of physicians to resolve issues of cost-effectiveness in health care quality. They are thus becoming more adamant that the medical profession either monitor itself or have it done by others. Unfortunately, as we head into this new era of assessment and accountability [3], this new function of monitoring has resulted in physicians being introduced to new, and at times confusing, concepts and terminology. It is my intent in this article to discuss important aspects of quality improvement programs and to pose a challenge to the discipline of radiology.

Quality: Assessment, Improvement, and Assurance

To evaluate the quality of health care, we must first define exactly what we mean by quality. To do otherwise is to invite miscommunication, disagreement, and conflict. There are as many definitions of health care quality as there are organizations with an interest in quality. An example that reflects the basic elements of current definitions is that espoused by the Joint Commission of Accreditation of Healthcare Organizations (JCAHO). The JCAHO defines health care quality as "the degree to which patient care services increase the probability of desired patient outcomes and reduce the probability of undesired outcomes given the current state of knowledge." Basically, one can then say that individuals or organizations that achieve more desirable outcomes compared with the norms have a higher quality of care and vice versa, and that such comparisons should be made on a continual basis as scientific advances are introduced.

The process of *quality assessment*, then, involves comparing the performance of organizations and individual practitioners with established norms. The ultimate goal, however, is not just to undertake an assessment of performance but to introduce feedback mechanisms that will allow the introduction of changes, which in turn would lead to an improvement in the quality of care. The continuous feedback of comparative performance information and the introduction of changes for improving performance are referred to as *quality improvement* programs [4]. The question of whether the cost of care should enter into the measurement of quality seems reasonable in that inefficiency and low quality often go hand in hand, either directly, by delaying diagnoses or treatments and by the introduction of complications from medical interventions, or

---

Received October 23, 1989; accepted after revision December 14, 1989.

[1] Department of Diagnostic Imaging/Radiology, Sinai Hospital of Detroit and Wayne State University, 6767 W. Outer Dr., Detroit, MI 48235-2899. Address reprint requests to P. N. Cascade.

AJR 154:1117–1120, May 1990 0361–803X/90/1545–1117 © American Roentgen Ray Society

indirectly by unnecessarily absorbing resources that otherwise could be directed toward more appropriate care. This is the rationale for including assessment of appropriateness as part of quality assessment programs.

One brief comment about the term *quality assurance*. The word assurance may instill an image of confidence and certainty, misleading lay organizations and the public into thinking that all outcomes should or can be positive for any given medical intervention. This is certainly not the case.

Indicators, Thresholds, Standards of Care

When the definition of health care quality is examined, the basic elements extracted are those related to the measurement of quality and the subsequent comparison with established norms. Measures of quality, so-called *indicators*, should be objective, quantifiable, and statistically reliable, and norms should, whenever possible, be based on carefully conducted and scientifically controlled clinical studies. Proper development of each requires considerable time and financial investment.

To attempt to develop indicators and study every aspect of care related to the practice of diagnostic radiology would be an enormous endeavor, virtually impossible. It is therefore necessary to focus attention and direct available quality-assessment resources toward high-volume and high-risk activities that are problem prone and that have the most direct impact on outcome. By way of example, broad aspects of care deserving of indicators that might be developed include radiation safety, performance of personnel, and efficacy of operations. Correspondingly, specific indicators might include patient exposure doses during mammography, technical success rates of percutaneous transluminal angioplasty, and the timeliness of performance of emergent CT in the evaluation of head trauma.

Once indicators are developed and data are being collected, comparisons should be made to establish the relative quality of care. In some instances, relative performance will be high, whereas in others it will be lower. In these circumstances, it seems reasonable to establish *thresholds*. When these thresholds are crossed, an in-depth study should be undertaken to determine a cause. In a few instances, data will reveal results of such a negative nature that acceptable *standards* of practice will be considered breached and immediate corrective action will be warranted. It is extremely important the standards be equitable, reasonable, applicable to all settings in which care is delivered, and always have the best interest of the patient in mind. Whenever possible, standards of care should be developed by explicit methodology based on properly conducted scientific studies or by implicit methods that use consensus panel techniques. In either case, the standards should be acceptable to the majority of those individuals to be assessed.

Quality Assessment and Quality Improvement as a Science

The American College of Utilization Review Physicians was established in 1973 to encourage and maintain academic excellence among physicians engaged in the many facets of utilization review and the assessment of the quality of medical care. Under the sponsorship of the College, the American Board of Quality Assurance and Utilization Review Physicians was founded in 1978. Certification in this specialty is now being granted pending successful completion of a certification examination. The examination is comprehensive, covering quality, timeliness, economics, appropriateness of care, techniques of care review, sociology, and demography.

Most research in radiology today is directed toward the advancement of diagnostic and therapeutic knowledge and the comparative assessment of technology. Our research experts, with some exceptions, are not sufficiently trained or motivated in the study of medical care components or consequences. Knowledgeable researchers in the fields of economics, statistics, computer science, public health administration, and psychology and behavioral sciences could ideally coordinate their efforts with clinical research scientists to provide optimal quality assessment and improvement programs. A coordinated group such as this could improve on proposed and existing computer data bases, which are developed and maintained primarily by payers and the government. These data bases have been focused on the determination of the cost/benefit implications of patterns of practice and have not been used for identifying factors directly affecting the outcome of health care. Improved national data bases developed with the input of physicians, including radiologists, could allow analysis of the impact of physician interventions on clinical outcomes and the appropriateness of care. The information provided would assist patients, payers, and physicians in making correct decisions on health care delivery. One model of such a data base is being developed by the JCAHO as part of its "Agenda for Change." National indicators are under study in obstetrics, anesthesiology, cardiology, cardiac surgery, oncology, trauma, and organization management. Additional areas will be considered in the near future. Indicator development for imaging services is scheduled to begin in 1990.

Although incomplete in design and detail, an example of a radiology-oriented clinical data base that could provide an assessment of diagnostic outcome was described recently by Bird [5]. He used information provided by a computerized tumor registry to assess the diagnostic accuracy of more than 21,000 consecutive screening mammograms. By using similar techniques, it seems feasible that sophisticated data bases could be developed to provide continuous feedback loops of the outcome of procedures to those wishing to participate. Specific areas of concern, such as the early diagnosis of colorectal, breast, and lung neoplasms, could be evaluated more effectively by extending data collection and feedback beyond specific health care organizations to broader communities. This might help us to answer serious questions about the costs and benefits of new technology and procedures raised by skeptical patients, payers, and the medical community. For example, the place of lasers and atherectomy devices in interventional radiology might be determined by objective results, rather than by ego, public promotion, and turf battles. Before such programs can be successful, however, serious questions need to be addressed, including those related to maintaining physician and patient confidentiality, as well as cost-effectiveness.

Research is now being conducted in an attempt to extend our knowledge of the factors responsible for so-called missed diagnoses. Studies of the psychophysiologic mechanism involved in optical information gathering, image perception and formulation of false images, and failure to recognize disease patterns are now under way [6]. A natural extension of accumulation of this basic science information will be to develop means to improve these operating characteristics to make them clinically useful. Further studies to identify variables related to diagnostic accuracy and the means to improve on these variables are largely unexplored. Only a few studies related to the necessity for seclusion, privacy, and time for analysis have been performed. Psychological tests could be formulated to identify prospective radiology residents for inborn physiologic capacity to recognize patterns. These variables can best be tested by outcome analysis of an objective nature, with the assistance of large data bases and automatic feedback processes.

Physician Performance, Necessary Fallibility, Peer Review

Evaluation of the cognitive performance of the diagnostic radiologist is a difficult task. Whereas indicators of performance related to technical procedures are relatively easy to develop, accurate and cost-effective methods of data gathering and setting standards of diagnostic accuracy are difficult to design and implement. Attempts to judge the overall capabilities of an individual are thwarted by the lack of knowledge of the complexity of an individual practice. Double reading and determination of disagreements on retrospective review of relatively small samples of cases, a method often used by radiology departments to pass external reviews by the JCAHO, cannot be expected to reflect accurately the capabilities of a typical general diagnostic radiologist who may interpret more than 10,000 studies annually, a total consisting of variable numbers and types of studies that use multiple imaging techniques. What is required then, is the development of indicators and systematic methods that will more accurately determine when an incorrect diagnosis has been made. Development of computer data bases and feedback loops, particularly focused on disease categories or outcomes, would be advantageous and justified.

Three factors should be considered when a false-positive or false-negative interpretation has been made. The first two, scientific ignorance and negligence, are obvious. The third factor, unrelated to ineptitude, has been well described by Gorovitz and MacIntyre in their article "Toward a Theory of Medical Fallibility" [7]. Not even the most experienced, studious, and intelligent physician deeply involved in research at the cutting edge of medical knowledge can ever reach the goal of infallibility. Each patient has his or her own distinct and unique characteristics, and it is the infinite number of particulars that lead to fallibility. Patients, payers, government, and even physicians need to understand that patient injury or failure to diagnose is not proof of culpability. Evaluation of missed diagnoses by peer review can be used to ascertain to the best degree whether a particular incorrect diagnosis was unavoidable or should have been made correctly after reviewing all of the particulars of a given case. The objective is to take action as a group to commend, reeducate, proctor, or change privilege delineations.

Political and Psychological Issues

Why is it then, that portions of the medical community have resisted the monitoring and evaluation of physician performance, peer review, the development of standards of practice, and periodic reaccreditation of physicians after completing initial training programs? Many physicians have expressed the opinion that such efforts are bureaucratic, time consuming, costly endeavors that are unnecessary and infringe on the independent practice of medicine. Furthermore, the malpractice climate has instilled defensive attitudes, particularly as they relate to the establishment of standards for fear of encouraging and aiding plaintiff attorneys, although the opposite is as likely to occur, that is, setting up legal defenses based on national accepted norms.

For these reasons and others, the process of developing quality improvement programs has not been well received by many radiologists. Behavioral patterns that are rather consistent in nature have arisen and have been well described by Miller and Flanagan [8]. First there is the "infantile stage," in which physicians have little knowledge and much resistance to change, reacting with anger and ridicule; this is followed by an "adolescent phase," in which the physician accepts what is imposed but with passive resistance and an unwillingness to participate; the subsequent "phase of maturity" is reached when the process of quality improvement is understood and accepted and participation is active. The final phase, "adulthood," is reached when creativity, innovation, research, and active contributions take place and there is true motivation to improve the quality of care.

The Challenge

The challenge now is for the discipline of diagnostic radiology to mature into the phase of adulthood—to develop its own quality improvement programs rather than them imposed by others. What group of people, other than radiologists and allied health personnel, is better prepared, more knowledgeable, or better suited to do so? Should not our scientific societies, in conjunction with the American College of Radiology, work together to determine which aspects of care are most important, which factors are the best indicators of quality, and exactly what standards and thresholds should be put into place?

Should not the radiologic community, which has struggled long and hard with the subject of mandatory reaccreditation, finally reach consensus by developing a cost-effective mechanism of certification that reflects the unique, everyday functions of each radiologist and satisfies the ever-increasing expectations of government and the public? Perhaps the solution will be found in the development of quality assessment programs based on generic indicators of performance monitored and evaluated on an ongoing basis. Locating adequate funding to support a national program of generic indicator development, stimulating research in the field of outcome improvement, and creating extensive data bases with sufficient detail to provide continuous feedback loops to radiologists is one of the most significant challenges of all. Although volunteerism will still be sought and applauded, a full time staff of experts is necessary if these goals are to be reached. And finally, by achieving these goals it will be possible not only to make the statement but to provide objective proof to the public, payers, the government, and accreditating agencies, such as the Joint Commission, that "radiology is best practiced by radiologists."

REFERENCES

1. Ellwood PM. Shattuck lecture. Outcomes management: a technology of patient experience. *N Engl J Med* **1988**;318:1549–1556
2. Wennberg J. Which rate is right? *N Engl J Med* **1986**;314:310–311
3. Relman AS. Assessment and accountability: the third revolution in medical care. *N Engl J Med* **1988**;319:1220–1222
4. Berwick DM. Sounding board: continuous improvement as an ideal in health care. *N Engl J Med* **1989**;320:53–56
5. Bird RE. Low-cost screening mammography report on finances and review of 21,716 consecutive cases. *Radiology* **1989**;171:87–90
6. Hendee WR, Wells PNT. Visual perception as an opportunity for radiologic research. *Invest Radiol* **1989**;24:575–576
7. Gorovitz S, MacIntyre A. Toward a theory of medical fallibility. *Hastings Cent Rep* **1975**;5:13–23
8. Miller ST, Flanagan E. Growth and development of physicians in quality assurance: an ontogeny for quality assurance managers. *QRB* **1988**; 14:358–362

Letters

Perception of Radiologic Images

Radiographs of the pelvis almost invariably are interpreted with the image in the "anatomic" position, that is, transversely. This causes one view box to be occupied and another partly overlapped, which is often a nuisance. One day when faced with a pile of radiographs, I placed a pelvic radiograph vertically, and I was struck by the increase in my perception of the image. I found that this effect also was useful for views of the spine and ribs. I was struck particularly with the apparent increase in my perception of, for example, the spinous processes of the vertebrae in the lateral views of the spine, especially in the lumbar region, and with how well fractures and other bony lesions could be detected.

I wondered if this effect occurs, in part, because the eye makes more horizontal movements than vertical ones, all of which are outside voluntary control [1]. Kundel and Wright [2] studied the eye motions in visual search strategies. They described three patterns of eye movement: circumferential, localized, and complex. A disproportionate amount of time also is spent sampling strong edges. Kundel, in another paper [3], discussed the perception of form, which is not yet well understood at a fundamental level. However, if perception is based, in part, on connecting boundaries to define objects and structures, this is more probable in the horizontal mode because of the scanning along this preferred plane. Also, placing radiographs at an unusual angle may increase the "interest" [4].

It is tempting to speculate that our primordial water-dwelling ancestors had to protect themselves against enemies from all directions of a surrounding sphere. As these ancestors evolved and climbed onto land surfaces, the range of danger became hemispherical, but mainly from a horizontal level, and, because of natural selection, those who were best adapted to protect themselves in this plane were able to survive. The ability to protect oneself depends on the ability to react to a change in the horizontal plane, which may be caused by an enemy. The greater the deformation, the greater is the stimulus, which poses a threat accompanied by "fear."

Even a small vertical line interrupting a horizontal line is seen easily, as exemplified by a view of rib lesions (Fig. 1). To bring the idea into a life situation, consider the example of the two snakes (Fig. 2). The rearing (vertical) snake appears to be more threatening than the horizontal one.

Frank I. Jackson
Cross Cancer Institute
Edmonton, Alberta, Canada T6G 1Z2

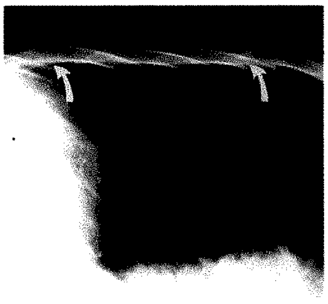

1

Fig. 1.—Radiograph shows subtle fractures of ribs (*arrows*) are seen best when fracture line interrupts horizontal plane.

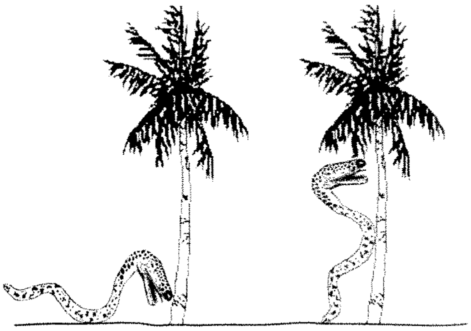

2

Fig. 2.—Horizontal and vertical snakes are same size, but vertical snake appears more aggressive and threatening than its companion.

REFERENCES

1. Thomas EL. Search behaviour. *Radiol Clin North Am* **1969**;7:403–416
2. Kundel HL, Wright DJ. The influence of prior knowledge on visual search strategies during the viewing of chest radiographs. *Radiology* **1969**;93:315–320
3. Kundel HL. Visual perception and image display terminals. *Radiol Clin North Am* **1986**;24:69–78
4. Thomas EL. Movements of the eye. *Sci Am* **1968**;279:88–95

Please Be Specific

Dr. Harris [1] has pointed out that incorrect use of statistical terminology has become frequent in the radiologic literature. We note that this trend is continued in recent articles by Hann et al. [2] and Brenner [3], both of which state that mammography has low specificity, whereas in fact it is the positive predictive value of mammography

	CANCER		
	PRESENT	ABSENT	
MAMMOGRAM +	TP	FP	PV (+) = $\frac{TP}{TP+FP}$
MAMMOGRAM —	FN	TN	PV (-) = $\frac{TN}{TN+FN}$
	SENS = $\frac{TP}{TP+FN}$	SPEC = $\frac{TN}{TN+FP}$	PR = $\frac{TP+FN}{TP+FP+TN+FN}$

Fig. 1.—Two-by-two table used to calculate statistical results of a mammographic audit. MAMMOGRAM + = biopsy recommended, TP = true positive, FP = false positive, PV (+) = predictive value of a positive test, FN = false negative, TN = true negative, PV (−) = predictive value of a negative test, SENS = sensitivity, SPEC = specificity, and PR = prevalence.

that the data show is low. Unfortunately, such misuse of terminology is likely to cause misunderstanding about the success of mammography screening programs.

Primarily because breast cancer is rare in a screened population, screening mammograms are interpreted with high specificity, but their positive predictive value is relatively low [4]. Several recent papers [5–7] have described the procedures that should be used in a mammographic audit. Calculation of results is performed most easily in terms of a two-by-two table that summarizes data obtained from follow-up of the screened population (Fig. 1). With a prevalence of five cancers per 1000 patients examined, a hypothetical mammographer who recommends biopsies in 5% of patients and fails to detect a single cancer would have a specificity of 95% but a positive predictive value of 0% (true positive [TP] = 0, false positive [FP] = 50, true negative [TN] = 945, false negative [FN] = 5 in Fig. 1). As a contrasting extreme example, an ideal mammographer whose sensitivity is 100% and who does biopsies on only 0.5% of patients would have a specificity of 100% and a positive predictive value of 100% (TP = 5, FP = 0, TN = 995, FN = 0). More realistically, a good mammographer with a sensitivity of 80% who does biopsies on 1% of patients would have a specificity of 99.4% and a positive predictive value of 40% (TP = 4, FP = 6, TN = 989, FN = 1). Because few patients have cancer in screening mammography, the specificity associated with a particular biopsy rate is determined primarily by the overwhelming predominance of actually negative cases and will vary little from 100%, regardless of the ability of the mammographer, as long as biopsy rates are kept small.

In comparing published sensitivities, specificities, and predictive values, it is important to note that all of these calculated results depend on the criterion used for a "positive" mammogram. Because the chief decision in breast imaging is whether to perform a biopsy to determine if cancer is present, we and most other authors take a positive mammogram to be one that resulted in a recommendation of biopsy. Alternatively, a positive mammogram might be taken as one in which the initial interpretation suggested any abnormality. These two definitions of a "positive" mammogram produce different combinations of sensitivity and specificity, which correspond to different points on a single receiver-operating-characteristic curve [8] and different predictive values. The specificity calculated from any given data set is generally high with either definition, however. Using the second definition of a positive mammogram, Sickles [7] found that the specificity of screening mammography was 94.2%, with a positive predictive value of 10%, for example.

Target values for positive predictive value as a barometer of a mammographic practice are not uniformly agreed on, but Hall et al. [9] have argued that 40% is a reasonable goal when a positive mammogram is defined as one that results in a recommendation of biopsy. Although this is far from controversial [10], even higher predictive values have been achieved routinely in screening centers in Sweden (Falun, Uppsala, Vesteros) that deal with large numbers of patients [11].

Robert A. Schmidt
Charles E. Metz
The University of Chicago
Chicago, IL 60637

REFERENCES

1. Harris RD. Diagnostic specificity: proper use (letter). *AJR* **1989**;153:653
2. Hann L, Ducatman BS, Wang HH, Fein V, McIntire JM. Nonpalpable breast lesions: evaluation by means of fine-needle aspiration cytology. *Radiology* **1989**;171:373–376
3. Brenner RJ. Medicolegal aspects of screening mammography. *AJR* **1989**; 153:53–56
4. Moskowitz M. Screening for breast cancer: how effective are our tests? A critical review. *CA* **1983**;33:26–39
5. Spring DB, Kimbrell-Wilmot K. Evaluating the success of mammography at the local level: how to conduct an audit of your practice. *Radiol Clin North Am* **1987**;25:983–992
6. Bird RE. Low-cost screening mammography: report on finances and review of 21,716 consecutive cases. *Radiology* **1989**;171:87–90
7. Sickles E, Ominsky SH, Sollitto RA, Galvin HB, Monticciolo DL. Medical audit of a rapid -throughput mammography screening program; methodology and results of 27,114 examinations. *Radiology* (in press)
8. Metz CE. ROC methodology in radiologic imaging. *Invest Radiol* **1986**; 21:720–733
9. Hall FM, Storella JM, Silverstone DZ, Wyshak G. Nonpalpable breast lesions: recommendations for biopsy based on suspicion of carcinoma at mammography. *Radiology* **1988**;167:353–358
10. Moskowitz M. Predictive value, sensitivity, and specificity in breast cancer screening. *Radiology* **1988**;167:576–578
11. Tabar L. International Teaching Seminar in Mammography. Presented in Falun, Sweden, June 3–10, **1989**

Reply

I thank Drs. Schmidt and Metz for their thoughtful letter, which confirms my premise that there is a significant problem with incorrect use of statistical terminology in the radiologic literature. Mammographic screening, in particular, is an area in which proper use of statistics is meaningful and appropriate for both radiologists and referring physicians.

Robert D. Harris
Dartmouth-Hitchcock Medical Center
Hanover, NH 03756

Tracheal Rupture

I read with interest the paper by Unger et al. [1], "Tears of the Trachea and Main Bronchi Caused by Blunt Trauma: Radiologic Findings," in the December 1989 *AJR*. Although I realize that space limitations preclude authors from quoting and including all possible references, I find it an oversight on the part of the authors and reviewers to omit pertinent and current references in a review article. In particular, the authors failed to refer to the April 1987 *AJR* article [2] by Rollins and Tocino, "Early Radiographic Signs of Tracheal Rupture," in which new signs of tracheal rupture are described. Figure 6 in the paper by Unger et al. illustrates findings first reported in the 1987 paper.

Tracheal rupture is not a common entity, and thus available literature is not overwhelming and 1987 not such a distant date as to neglect such a reference.

Irena M. Tocino
LDS Hospital
Salt Lake City, UT 84143

REFERENCES

1. Unger JM, Schuchmann GG, Grossman JE, Pellett JR. Tears of the trachea and main bronchi caused by blunt trauma: radiologic findings. *AJR* **1989**;153:1175–1180
2. Rollins RJ, Tocino I. Early radiographic signs of tracheal rupture. *AJR* **1987**;148:695–698

Reply

My colleagues and I sincerely regret the inadvertent omission of the excellent paper by Rollins and Tocino [1] from the list of references of our paper [2]. Despite what we had considered an exhaustive search of the literature, including a Medline search, we somehow missed this important contribution. It would have been a valuable addition, as it contains information on the importance of the appearance of the endotracheal tube and balloon cuff in tracheal rupture and a discussion of tracheal damage as a function of cuff-to-tracheal wall pressure, rather than absolute cuff volume. Our apologies to Drs. Rollins and Tocino for this oversight.

June M. Unger
University of Wisconsin, Clinical Science Center
Madison, WI 53792

REFERENCES

1. Rollins RJ, Tocino I. Early radiographic signs of tracheal rupture. *AJR* **1987**;148:695–698
2. Unger JM, Schuchmann GG, Grossman JE, Pellett JR. Tears of the trachea and main bronchi caused by blunt trauma: radiologic findings. *AJR* **1989**;153:1175–1180

Hydrostatic Reduction of Intussusception

I would like to clarify certain points on the advisability of attempting hydrostatic reduction of intussusception, a topic recently discussed in the excellent article by Franken et al. [1]. The subject is, indeed, controversial, as the available information is incomplete. The diagnosis of gangrenous intussusception cannot be made preoperatively. When evidence of small-bowel obstruction is present on radiographs, the probability of gangrenous intussusception increases, and that of hydrostatic reducibility decreases. In the article quoted by Franken et al. "Treatment of Intussusception with Small Bowel Obstruction: Application of Decision Analysis [2], I used pooled data to arrive at some numerical conclusions. Published articles indicate that the reducibility of intussusception in the presence of small-bowel obstruction is only about 40%. This figure is obviously not a "hard" statistic. Nevertheless, the 95% confidence interval indicates that with existing data, the projected reducibility in a theoretically infinite number of attempts should range from 33% to 49% (i.e., much higher than the estimate of 10–20% quoted by Franken et al.). Moreover, my estimates were subjected to sensitivity analysis so that room could be left for variation of the data. The cutoff point regarding the lowest possible mortality from treatment of intussusception was a 50–60% rate of reduction. In other words, at least 50–60% of intussusceptions with small-bowel obstruction should be able to be reduced to achieve the best survival rate. This figure is higher than anyone's published experience. Franken et al. are, therefore, correct about survival, which is indeed a prime consideration. No recent publications, however, have reported the occurrence of any deaths associated with surgery for perforation caused by hydrostatic reduction, which is the main source of differences in mortality for surgery vs. hydrostatic reduction as the primary treatment. Because mortality is extremely low for either mode of treatment, I looked at other aspects of each option, such as overall complication rates and costs. The latter value progressively is assuming a cardinal role in the thinking of health care planners, administrators, insurers, the government, and, eventually, our own. Sensitivity analysis indicates a break-even point for reducibility rates as low as 10–15%.

In conclusion, as I indicated in the article [2], establishing a policy of always operating or always attempting hydrostatic reduction when small-bowel obstruction is present is difficult, and it may be necessary to tailor the treatment for the patient; estimates are not always sound. This applies to my estimates as well as those of others, including Franken et al. Radiologists, if they attempt hydrostatic reduction more aggressively, will have to use their experience regarding their rate of success when small-bowel obstruction is present. This figure is essential in using my estimates. My article simply provided some guidelines so that those who attempt hydrostatic reduction will have rational data to fit their own experience.

John C. Leonidas
Schneider Children's Hospital
New Hyde Park, NY 11042

REFERENCES

1. Franken EA Jr, Kao SCS, Smith WL, Sato Y. Imaging of the acute abdomen in infants and children. *AJR* **1989**;153:921–928
2. Leonidas JC. Treatment of intussusception with small bowel obstruction: application of decision analysis. *AJR* **1985**;145:665–669

Reply

We thank Dr. Leonidas for his astute comments on the advisability of attempting hydrostatic reduction of intussusception, which was discussed in our review article, "Imaging of the Acute Abdomen in Infants and Children" [1]. We have no argument with his emphasizing a need to individualize each decision. His points on minimizing morbidity are equally valid. The situation is one in which we are all looking at the same elephant from different aspects and with incomplete information.

One of our reasons for quoting Leonidas's article [2] on the use of decision making in the treatment of intussusception was to introduce the reader to that important technique of diagnostic radiology by citing such a well-done study. Our own anecdotal experience is that successful hydrostatic reduction of intussusception in the presence of bowel obstructions occurs in about only 10% of cases. Using this figure as our own individual result and applying Leonidas's decision tree indicates increased mortality and morbidity with hydrostatic reduction compared with surgery. Thus, our recommendation to the radiologist who is not particularly expert at this procedure is to be conservative.

E. A. Franken, Jr.
Simon C. S. Kao
Wilbur L. Smith
Yutaka Sato
The University of Iowa
Iowa City, IA 52242

REFERENCES

1. Franken EA Jr, Kao SCS, Smith WL, Sato Y. Imaging of the acute abdomen in infants and children. *AJR* **1989**;153:921–928
2. Leonidas JC. Treatment of intussusception with small bowel obstruction: application of decision analysis. *AJR* **1985**;145:665–669

Bile Duct Necrosis After Partial Hepatectomy and Transcatheter Hepatic Arterial Embolization

The effectiveness of transcatheter arterial embolization in the treatment of malignant hepatic tumors has been reported [1]. Side effects are minimal and usually require only conservative treatment. The selective ischemic effect of transcatheter arterial embolization on hepatic tumors compared with normal hepatic parenchyma plays a major role in the success of the treatment. Necrosis of the main bile duct usually does not occur after proximal transcatheter arterial embolization [2] because of the dual blood supply to the biliary tree from the hepatic and gastroduodenal arteries. We came to this conclusion after encountering a case of extensive necrosis of the bile duct in a patient whose blood supply to the intrahepatic bile ducts was totally dependent on a branch of the left hepatic artery because of previous radiologic interventions and surgery.

The patient had had transcatheter arterial embolization twice and transcatheter portal embolization and laparotomy for hepatocellular carcinoma. Finally, he had surgery to remove the right lobe containing the main tumor and an intrahepatic metastasis in the lateral segment. During the operation, the liver was skeletonized completely, and the common bile duct in the hepatoduodenal ligament was dissected completely free from adjacent tissue. The right hepatic artery also was ligated. Severe fibrosis of the bile duct in the liver hilus was observed. In an attempt to control the remaining intrahepatic metastases, transcatheter arterial embolization of the left lobe was done on the 16th day after surgery by using a catheter that had been inserted through the right gastroepiploic artery during the operation. High fever, nausea, and vomiting developed 11 days after the embolization.

An arteriogram performed via the indwelling arterial catheter showed extravasation of contrast medium into the biliary tree (Fig. 1A). CT scan showed a large biloma in the right subphrenic and hilar space of the remaining left lobe. Percutaneous transhepatic biliary drainage was performed. Injection of contrast medium showed extensive necrosis of the bile duct that began just above the fibrotic hilar bile duct recognized at surgery (Fig. 1B). The capillary network from the gastroduodenal artery was assumed to have ended in this portion, and the intrahepatic biliary tree was completely dependent on the blood flow from the left hepatic artery. This extensive necrosis of the bile duct was comparable with that occurring after hepatic arterial thrombosis in liver allografts in patients who lack blood flow from the gastroduodenal artery [3]. The condition of the hilar biliary tree in our patient shows the importance of arterial blood flow from the gastroduodenal artery.

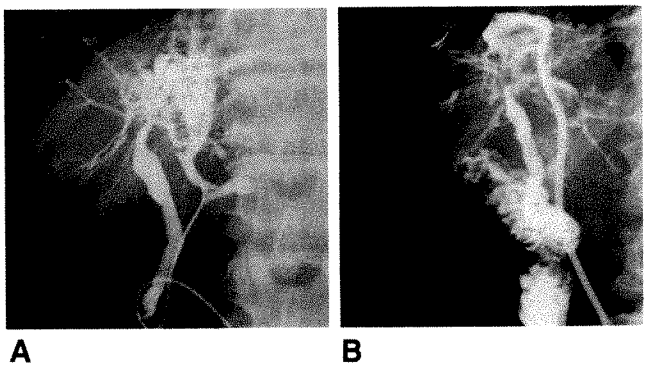

Fig. 1.—Bile duct necrosis after partial hepatectomy and transcatheter hepatic arterial embolization.

***A*, Arteriogram shows contrast medium injected through indwelling arterial catheter has extravasated into biliary tree.**

***B*, Cholangiogram obtained after injection of contrast medium through percutaneous transhepatic biliary drainage tube shows extensive necrosis of bile duct.**

Mitsukazu Gotoh
Morito Monden
Masato Sakon
Toshio Kanai
Koji Umeshita
Wakio Endoh
Jun Okamura
Kenichi Wakasa
Masami Sakurai
Tarou Marukawa
Chikazumi Kuroda
Takesada Mori
Osaka University Medical School
Osaka 553, Japan

REFERENCES

1. Chuang VC, Wallace S. Hepatic artery embolization in the treatment of hepatic neoplasms. *Radiology* **1981**;140:51-58
2. Makuuchi M, Sukigara M, Mori T, et al. Bile duct necrosis: complication of transcatheter hepatic arterial embolization. *Radiology* **1985**;156:331-334
3. Zajko AB, Campbell WL, Logsdon GA, et al. Cholangiographic findings in hepatic artery occlusion after liver transplantation. *AJR* **1987**;149:485-489

Periportal Lymphedema in Trauma Patients

Previous reports have described zones of low attenuation ascribed to dilated hepatic lymphatics surrounding portal venous radicles in patients with rejection of liver transplants, [1, 2], hepatic or perihepatic hematomas, upper abdominal lymphadenopathy, congestive heart failure [3], and constrictive pericarditis [4].

Over 9 months, we found hepatic perivascular lymphedema in five (20, 21, 23, 45, and 62 years old) of 540 patients who had abdominopelvic CT because of trauma (Fig. 1). None of the five patients with periportal collars had any other CT evidence of abdominal trauma; all had extremity injuries. All five patients were hypotensive when they arrived in the emergency department and received large volumes of IV fluids as part of routine posttrauma resuscitation immediately before the CT scan was performed.

Although we did not review the records of the other 535 patients to determine how much IV fluid they received, we suspect that

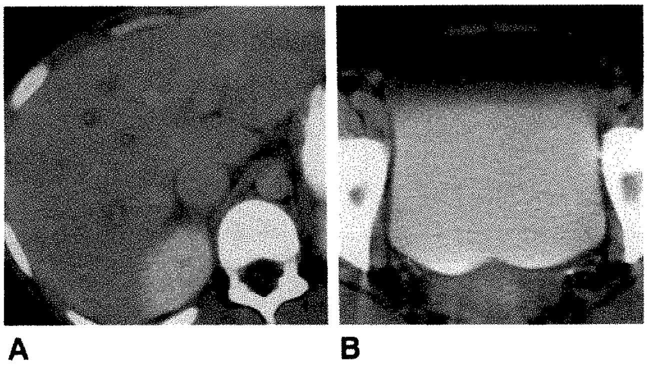

Fig. 1.—*A* and *B*, Contrast-enhanced CT scans of abdomen and pelvis of a trauma patient who had received 2 l of IV fluids show ring lucencies (*A*) due to periportal lymphedema surrounding portal vein branches and distension of bladder (*B*). Bladder dome was at level of umbilicus.

vigorous hydration can cause distension of the periportal lymphatics and periportal collars even in patients with normal cardiac output. Thus, in patients with hepatic injuries, periportal collars may be caused by vigorous hydration rather than by the trauma itself.

John F. Cox
Arnold C. Friedman
Paul D. Radecki
Anna S. Lev-Toaff
Dina F. Caroline
Temple University Hospital
Philadelphia, PA 19140

REFERENCES

1. Wechsler RJ, Munoz SJ, Needleman L, et al. The periportal collar: a CT sign of liver transplant rejection. *Radiology* **1987**;165:57–60
2. Marincek B, Barbier PA, Becker CD, Mettler D, Ruchti C. CT appearance of impaired lymphatic drainage in liver transplants. *AJR* **1986**;147:519–523
3. Koslin DB, Stanley RJ, Berland LL, Shin MS, Dalton SC. Hepatic perivascular lymphedema: CT appearance. *AJR* **1988**;150:111–113.
4. Goldstein L, Mervis SE, Kostrubiak IS, Turney SZ. CT diagnosis of acute pericardial tamponade after blunt chest trauma. *AJR* **1989**;152:739–741

Confusing Similarities Between Peripancreatic Retroperitoneal Lymphangioma and Other Lesions

We recently observed a case that not only emphasizes the important similarities between retroperitoneal lymphangioma and other benign cystic or vascular tumors but also illustrates the difficulty of radiologically distinguishing those lesions arising in the pancreas itself from those merely arising in the contiguous extrapancreatic retroperitoneum.

A renal sonogram of an asymptomatic 58-year-old woman incidentally showed a well-demarcated cystic mass in the pancreatic head containing multiple internal septa (Fig. 1A). CT of the mass showed that it had a density near that of water, with internal septa less clearly defined than on sonography. Spin-echo MR imaging of the mass showed low signal intensity on T1-weighted images (300/20) and high signal intensity on T2-weighted images (Fig. 1B). The initial diagnosis was primary cystic neoplasm of the pancreas. On exploratory laparotomy, however, it was found that the mass arose from the retroperitoneal soft tissues; the pancreas itself was normal. A frozen section of the mass was interpreted originally as a microcystic (glycogen-rich) adenoma of the pancreas, but final histologic study showed instead a cavernous retroperitoneal lymphangioma.

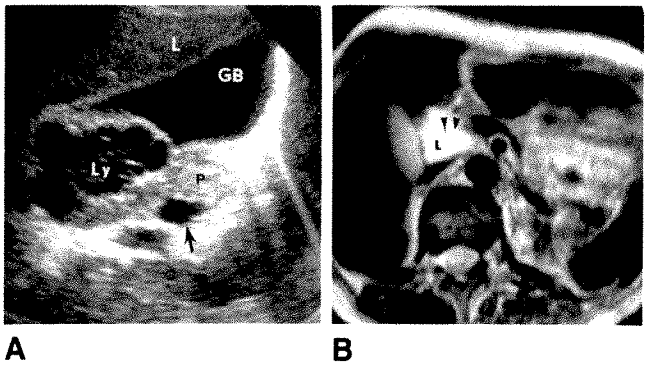

Fig. 1.—Cavernous retroperitoneal lymphangioma.
***A*, Oblique transverse real-time sonogram of right upper quadrant shows multiseptated cystic lymphangioma (Ly) sharply demarcated from adjacent pancreatic head (P). *Arrow* = superior mesenteric vein, L = liver, GB = gallbladder.**
***B*, Axial T2-weighted MR image, 2000/60 (TR/TE), shows hyperintense peripancreatic lymphangioma (L) with faint internal septation (*arrowheads*).**

Retroperitoneal lymphangiomas and microcystic pancreatic adenomas are both benign, often asymptomatic, and found only incidentally. Both lesions also are composed of multiple small cysts lined with a single layer of cells and separated by thin fibrous septa [1, 2]. On CT, both appear well demarcated and hypodense [3, 4]. On MR, both tumors are hypointense on T1-weighted images and hyperintense on T2-weighted images; the internal septa usually are visualized better on the latter [4]. Nevertheless, sonography of an adenoma usually shows a hypoechoic, solid-appearing lesion in which individual small cysts cannot be resolved [3]. Lymphangiomas, on the other hand, may have prominent solid components, but their cystic character is usually more evident [5] (Fig. 1). Additionally, the microcystic pancreatic adenoma often contains a distinctive central stellate or partially calcified scar [3].

The clinical, histologic, sonographic, CT, and MR characteristics of hemangiomas and lymphangiomas also may be quite similar. CT of hemangiomas, however, usually shows a distinctive pattern of contrast enhancement different from that observed with lymphangiomas. Also, on sonography, hemangiomas usually are more solid and less cystic than lymphangiomas.

In essence, therefore, the differentiation between a retroperitoneal lymphangioma and a comparable cystic or vascular intrapancreatic or extrapancreatic mass may require close scrutiny of subtle radiologic differences. Biopsy or percutaneous aspiration might still be necessary for a conclusive diagnosis.

H. Richard Parvey
Ronald L. Eisenberg
Don M. Morris
Warren D. Grafton
Peter C. Meyers
Louisiana State University Medical Center
Shreveport, LA 71130

REFERENCES

1. Murao T, Toda K, Tomiyama Y. Lymphangioma of the pancreas: a case report with electron microscopic observations. *Acta Pathol Jpn* **1987**;37:503–510
2. Compagno J, Oertel JE. Microcystic adenomas of the pancreas (glycogen-rich cystadenomas): a clinicopathologic study of 34 cases. *Am J Clin Pathol* **1978**;69:289–298
3. Friedman AC, Lichtenstein JE, Dachman AH. Cystic neoplasms of the pancreas: radiological-pathological correlation. *Radiology* **1983**;149(1):45–50
4. Minami M, Itai Y, Ohtomo K, Yoshida H, Yoshikawa K, Iio M. Cystic neoplasms of the pancreas: comparison of MR imaging with CT. *Radiology* **1989**;171(1):53–56
5. Blumhagen JD, Wood BJ, Rosenbaum DM. Sonographic evaluation of abdominal lymphangiomas in children. *J Ultrasound Med* **1987**;6(9):487–495

Renal Imaging in Long-term Dialysis Patients: A Comparison of CT and Sonography

The significant difference that Taylor et al. [1] found between CT (59%) and sonography (18%) in the detection of cysts in patients with end-stage kidneys makes me wonder if part or all of the reason for the poorer detection rate with sonography is not related to the equipment used. Thirty-six of the patients were examined on a GE R/T 3600 scanner (General Electric Medical Systems, Milwaukee, WI), whereas only five were examined on an Acuson 128 scanner (Acuson, Mt. View, CA).

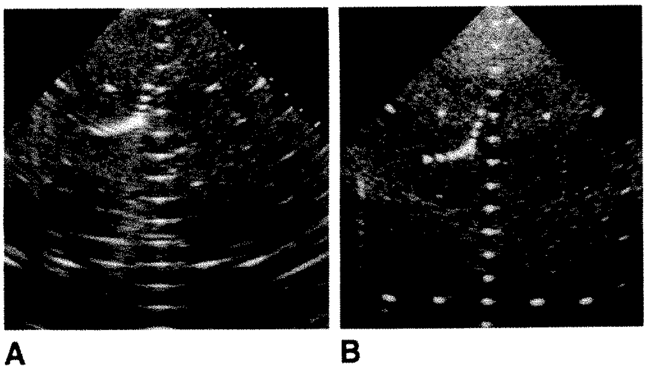

Fig. 1.—*A* and *B*, Comparison of images of a phantom (ATS mode 539) obtained on GE 3600 (*A*) and Acuson 128 (*B*) 3.5-MHz phased-array scanners with probes. Multizone focus used with both scanners. Lateral resolution in far field of GE unit is much worse than in region of best focus (5 cm depth), whereas lateral resolution in Acuson is uniform and tightly focused from about 5 to 16 cm.

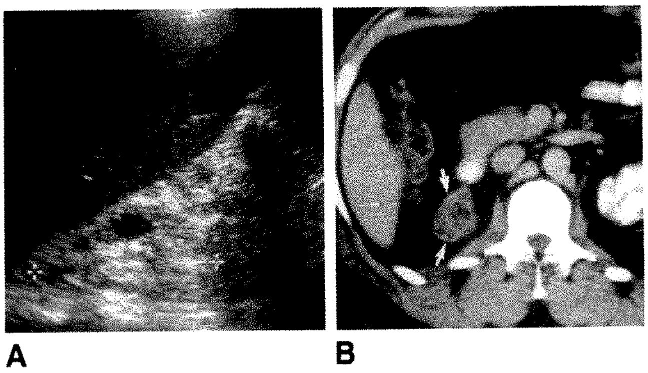

Fig. 1.—Comparison of sonography with Acuson 128 and contrast-enhanced CT with GE CT 8800 in imaging acquired cystic kidney disease.

***A*, Longitudinal sonogram of right kidney (*cursors*) shows a 1.5-cm cyst in interpolar segment and no discernible cysts in lower pole.**

***B*, Contrast-enhanced CT scan of a slice 1 cm thick shows numerous cysts in lower pole of right kidney (*arrows*).**

The GE R/T 3600 scanner has a significantly poorer beam pattern, especially in the deeper regions of the sector image where the kidneys usually lie, than the Acuson 128 (compare phantom images of a 3.5-MHz phased-array probe scan of GE and Acuson, Fig. 1). Thus, although I agree with the authors that cysts less than 1 cm may be difficult to visualize with the GE scanner, it may be because of the poor lateral beam resolution that fills in cysts with echoes or cannot even resolve small ones. I suspect that cysts as small as 0.5 cm could be detected with the Acuson because of its better lateral resolution.

It would be helpful if the authors could elaborate on why they think cysts were missed on sonography. Were the cysts not seen at all, or were they confused with other structures because they were not echo-free? How did the detection rate and size of cysts compare between those patients studied with the GE scanner vs the Acuson?

Leon Skolnick
University of Pittsburgh, School of Medicine
Pittsburgh, PA 15213

REFERENCE

1. Taylor AJ, Cohen EP, Erickson SJ, Olson DL, Foley WD. Renal imaging in long-term dialysis patients: a comparison of CT and sonography. *AJR* **1989**;153:765–767

Reply

Dr. Skolnick raises the possibility that our results [1] in the imaging of acquired cystic kidney disease might be skewed because of our available sonographic equipment (i.e., 36 patients were examined on the GE R/T 3600 scanner [General Electric Medical Systems, Milwaukee, WI], whereas only five were examined on the Acuson 128 [Acuson, Mountain View, CA]). Reviewing the data obtained from the institution that uses the Acuson 128 and the GE CT 8800 scanner might be helpful. At that institution, a total of nine kidneys in five patients were imaged. CT showed a greater grade of cystic change in all nine kidneys. With CT, five kidneys in three patients were shown to have changes indicative of acquired cystic kidney disease (i.e., five or more cysts per kidney); sonography showed one patient (or two kidneys) that met the requirements.

We certainly agree that the technical considerations for imaging are important. However, we think that the marked difference in our study shows the inherent greater capacity of CT compared with sonography in defining the diminutive cysts associated with acquired cystic kidney disease (Fig. 1).

Andrew J. Taylor
Eric P. Cohen
Scott J. Erickson
David L. Olson
W. Dennis Foley
Medical College of Wisconsin
Milwaukee, WI 53226

REFERENCE

1. Taylor AJ, Cohen EP, Erickson SJ, Olson DL, Foley WD. Renal imaging in long-term dialysis patients: a comparison of CT and sonography. *AJR* **1989**;153:765–767

Multiple Hydatid Cysts

A 23-year-old man had signs and symptoms that suggested progressive spinal compression at L3. Contrast-enhanced CT of the abdomen showed numerous cysts (Fig. 1). They included a cyst in the right kidney, a paraspinal cyst involving the multifidus muscle and extending to the erector spinae muscle, an epidural cyst, a retroperitoneal cyst within the pararenal space, a cyst within the psoas muscle, and a cyst in the innominate bone causing marked expansion of the iliac wing. Attenuation values of the cysts ranged from 8 to 25 H. The liver was normal. Chest radiographs and head CT scans showed no abnormalities. Serologic tests for hydatid disease were positive. The lesion in the epidural space was resected, and a germinative membrane and scoleces were shown. The diagnosis of *Echinococcus granulosus* infestation was established histologically. All the other cysts were left in place, and chemotherapy with mebendazole was started.

Echinococcosis, or hydatid disease, is a parasitic infestation caused by the larval stage of the tapeworms *E. granulosus* and *Echinococcus multilocularis*. The nematode is swallowed in the egg form. In the stomach, the egg dissolves, and the embryo gains access to the body by penetrating the intestinal wall and entering the portal circulation. Most of the embryos lodge in the liver and lung (approximately 60% in the liver and 25% in the lung), and the remainder are spread throughout the rest of the body [1–4]. Our case is unique

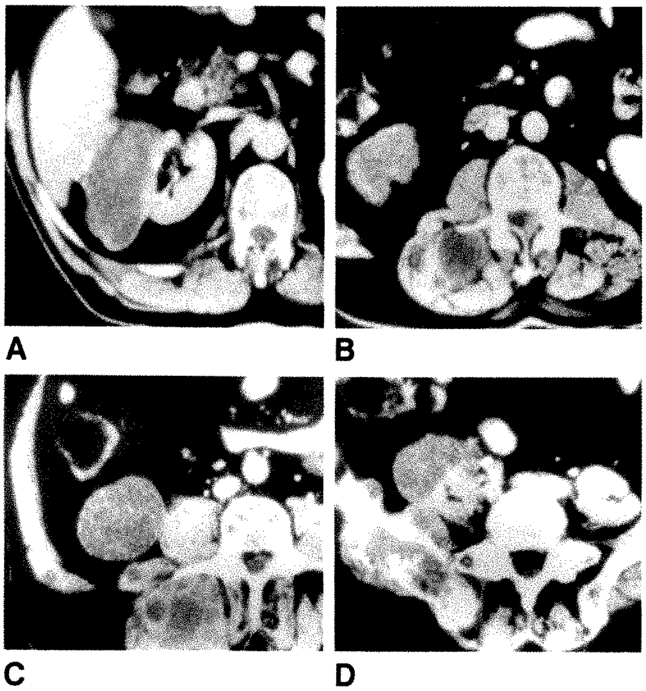

Fig. 1.—CT scans show multiple hydatid cysts in a 23-year-old man.
***A*, Cyst in right kidney originating from lateral cortex. Walls are partially calcified.**
***B*, Epidural cyst to right of L3 and another cyst originating from right multifidus muscle. Lower part of renal cyst shown in *A* is seen also.**
***C*, Cyst in right pararenal space adjacent to psoas muscle. Cyst affecting erector spinae muscle and a small cyst in right quadratus lumborum muscle are visible also.**
***D*, Cysts originating from right psoas muscle and right iliac wing.**

because of the multiple sites of involvement with sparing of the liver and lung.

R. Nuri Sener
Utku Ozcan
Vedat Isik
Ali Demirci
Private Hospital of Isparta
Isparta, Turkey

REFERENCES

1. Haaga JR, Alfidi RJ. *Computed tomography of the brain, head, and neck.* St. Louis: Mosby, **1985**:128–129
2. Clements R, Bowyer FM. Hydatid disease of the pelvis. *Clin Radiol* **1986**;37:375–377
3. Braithwaite PA, Lees RF. Vertebral hydatid disease: radiological assessment. *Radiology* **1981**;140:763–766
4. Missas S, Gouliamos A, Kourias E, Kalovidouris A. Primary hydatid disease of the pancreas. *Gastrointest Radiol* **1987**;12:37–38

CT of the Wrist: What Is Abnormal?

Hindman et al. [1] concisely underlined the technique of CT of the wrist. They showed the beautiful detail obtained with CT in an area complicated on plain films by overlapping structures. Undoubtedly CT will reveal significant occult fractures in the wrist. However, perspective and a note of caution need to be introduced. It soon becomes obvious that CT also shows the multiple accessory ossicles that may be present normally in the wrist [2, 3]. A clean fracture line that heals is unequivocal. However, a corticated ossicle that does not unite cannot blithely be called a nonunited fracture. Imaging both sides does not avoid this problem if ossicles are unilateral. Resolution of signs and symptoms with therapy directed to the ossicle certainly does not resolve the debate. The natural resolution of signs and symptoms with "a tincture of time" is a long held adage.

As indicated by Hindman et al., the significance of findings in light of the patient and the patient's problems always must be questioned. If doubt exists then in this situation, clinical and radiologic follow-up studies or an isotopic bone scan may be helpful.

Mark E. Pierce
Canberra Imaging
Belconnen Act 2617, Australia

REFERENCES

1. Hindman BW, Kulik WJ, Lee G, Avolio RE. Occult fractures of the carpals and metacarpals: demonstration by CT. *AJR* **1989**;153:529–532
2. Kohler A, Zimmer EA. *Borderlands of the normal and early pathologic in skeletal roentgenology*, 3rd ed. New York: Grune & Stratton, **1968**: 79–117
3. Keats TE. *Atlas of normal roentgen variants that may simulate disease*, 3rd ed. Chicago: Year Book Medical, **1984**:399–439

Reply

We appreciate Dr. Pierce's interest and constructive comments. We agree that a risk exists of sometimes showing fragments of bone that are normal variants or partial-volumned ridges and prominences and that care must be taken to avoid this possibility. In our study [1], of the 16 patients with 21 fractures, 11 patients with 13 occult fractures showed evidence of fracture healing or marked improvement with surgical removal of the fracture fragment or fusion of the fractured bone to the adjacent carpal bone. Five patients with six fractures, including all of the lunate fractures and one fracture of a metacarpal and one scaphoid fracture, failed to show evidence of fracture healing or clinical improvement, and this type of patient deserves careful clinical, radiologic, and scintigraphic follow-up. Two of these patients had healing of one of their fractures, and two declined to have a recommended surgical procedure. Although the diagnosis of fracture in some of these six instances may be debated, we think the importance of this study is underscored by the diagnosis of the 13 fractures that otherwise would have gone unrecognized, and possibly undertreated.

B. W. Hindman
W. J. Kulik
G. Lee
R. E. Avolio
Flower Imaging Medical Group
Los Angeles, CA 90007

REFERENCE

1. Hindman BW, Kulik WJ, Lee G, Avolio RE. Occult fractures of the carpals and metacarpals: demonstration by CT. *AJR* **1989**;153:529–532

Bone Scan Screening for Occult Fractures of Carpals and Metacarpals

Chronic joint pain despite normal radiographs is a frequent occurrence. As the imaging center for a large sports medicine clinic, we encounter many patients with chronic posttraumatic bone pain, particularly about the ankle but also in the wrist. The recent article by Hindman et al. [1] on the CT demonstration of occult carpal and metacarpal fractures is most informative. This retrospective review, however, did not mention use of ^{99m}Tc-MDP bone scanning as a

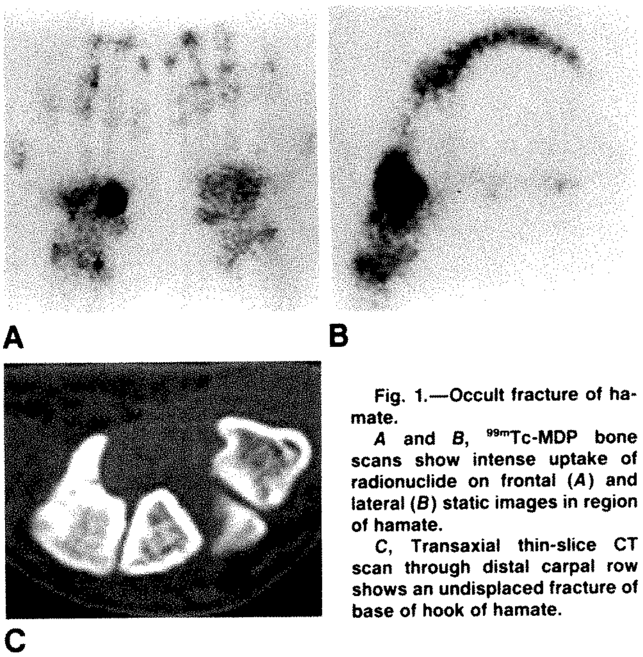

Fig. 1.—Occult fracture of hamate.
***A* and *B*, ^{99m}Tc-MDP bone scans show intense uptake of radionuclide on frontal (*A*) and lateral (*B*) static images in region of hamate.**
***C*, Transaxial thin-slice CT scan through distal carpal row shows an undisplaced fracture of base of hook of hamate.**

screening method. The efficacy of the initial bone scan after preliminary normal radiographs is well established [2, 3]. At our institution at least, and I suspect elsewhere, bone scanning tends to be readily available and of much lower cost than CT. A simple scanning routine has been established [4], and we have found no abnormal CT scans after initial normal bone scans. The following typical case outlines this approach.

A 21-year-old man saw his family physician because of a 1-year history of pain in the ulnar aspect of the wrist after fisticuffs. Clinical examination showed tenderness over the pisiform and hamate. Radiographs were unremarkable. The tentative clinical diagnosis was a tear of the fibrocartilage.

Because the pain persisted, arthrography was performed, which was also unrevealing. Two months later, a bone scan was obtained that showed normal dynamic images with immediate mild increased uptake of radionuclide at the ulnar aspect of the wrist on the blood-pool study. Static images (Fig. 1) showed an intense area of focal uptake in the region of the hamate. The clinical diagnosis in conjunction with the bone scan was therefore probable fracture of the hook of the hamate. Eight days later, high-resolution thin-slice CT scans were obtained. The transaxial images were most revealing, showing an undisplaced fracture through the base of the hook of the hamate.

Radionuclide bone scanning is an inexpensive study with a high capacity for detection of occult fractures. Patients who have abnormal scans then have directed CT examinations at our institution, and the rate of detection of fractures is high. It would be interesting to know how many of the 200 wrist CT scans reviewed by Hindman et al. [1] were obtained after screening bone scans. The use of a simple standardized approach to chronic joint pain has decreased the imaging costs and limited the number of CT scans performed.

W. J. Sisler
University Hospital
University of British Columbia
Vancouver, B.C., Canada

REFERENCES

1. Hindman BW, Kulik WJ, Lee G, Avolio RE. Occult fractures of the carpals and metacarpals: demonstration by CT. *AJR* **1989**;153:529–532
2. Hopkins SR, Ammann W. Isolated fractures of the capitate: use of nuclear medicine as an aid to diagnosis. *Int J Sports Med* (in press)
3. Young MRA, Lowry JH, Laird JD, Ferguson WR. ^{99m}Tc-MDP bone scanning of injuries of the carpal scaphoid. *Injury* **1988**;19:14–17
4. Sisler WJ. Imaging assessment of post-traumatic tarsal pain. *Can J Sports Med* (in press)

Reply

We appreciate Dr. Sisler's comments and agree that technetium bone scanning is an excellent screening technique for patients with chronic posttraumatic joint pain. We also think that his experience of no abnormal CT scans after normal results on scintigraphy is probably universal and that a fracture diagnosed on the basis of CT findings obtained after normal results on scintigraphy may be subject to question. We support the position of our hand surgeons that CT, because of its greater accuracy in detecting fractures, is essential in the management of chronic joint pain. The decision to remove a fracture fragment surgically or to allow the fracture to heal with immobilization can be made readily on the basis of CT. This information is particularly useful in fractures of the hamate because fractures of the tip are treated differently than fractures at the base of the hook. These surgeons go directly to CT when other findings are highly suggestive of fracture. Few of the 200 patients studied with CT [1] had initial screening bone scans. In most of these cases, CT was performed to show a second process or to evaluate a fracture for healing or incorporation of a bone graft. In cases in which the process is uncertain, we agree that radionuclide scintigraphy followed by CT is a cost-effective and accurate imaging sequence.

B. W. Hindman
W. J. Kulik
G. Lee
R. E. Avolio
Flower Imaging Medical Group
Los Angeles, CA 90007

REFERENCE

1. Hindman BW, Kulik WJ, Lee G, Avolio RE. Occult fractures of the carpals and metacarpals: demonstration by CT. *AJR* **1989**;153:529–532

Letters are published at the discretion of the Editor and are subject to editing.

Letters to the Editor must not be more than two *double-spaced*, typewritten pages. One or two figures may be included. Abbreviations should not be used. See Author Guidelines, page A5.

Material being submitted or published elsewhere should not be duplicated in letters, and authors of letters must disclose financial associations or other possible conflicts of interest.

Letters concerning a paper published in the *AJR* will be sent to the authors of the paper for a reply to be published in the same issue. Opinions expressed in the Letters to the Editor do not necessarily reflect the opinions of the Editor.

Review of Current Literature

Initials and addresses of corresponding authors are provided in parentheses for each article so that the reader can obtain reprints directly. Abstracts are printed verbatim from each journal.

The New England Journal of Medicine

Peritoneovenous shunting as compared with medical treatment in patients with alcoholic cirrhosis and massive ascites. Stanley MM, Ochi S, Lee KK, et al. (MMS, VA Medical Center, P. O. Box 23, Hines, IL 60141). *N Engl J Med* 321:1632–1638, Dec. 1989

The optimal management of severe ascites in patients with alcoholic cirrhosis has not been defined. In a 5½-year study, we randomly assigned 299 men with alcoholic cirrhosis, who had persistent or recurrent severe ascites despite a standard medical regimen, to receive either intensive medical treatment or peritoneovenous (LeVeen) shunting. We identified three risk groups: Group 1 had normal or mildly abnormal results on liver-function tests. Group 2 had more severe liver dysfunction or previous complications, and Group 3 had severe prerenal azotemia without kidney disease.

For the patients who received the medical treatment and those who received the surgical treatment combined, the median survival times were 1093 days in Group 1, 222 days in Group 2, and 37 days in Group 3 ($P \leq 0.01$ for all comparisons). For all the groups combined, the median time to the resolution of ascites was 5.4 weeks for medical patients and 3.0 weeks for surgical patients ($P < 0.01$). Within each risk group, mortality during the initial hospitalization and median long-term survival were similar among patients receiving either treatment. However, the median time to the recurrence of ascites in Group 1 was 4 months in medical patients, as compared with 18 months in surgical patients ($P = 0.01$); in Group 2 it was 3 months in medical patients as compared with 12 months in surgical patients ($P = 0.04$). The median duration of hospitalization was longer in medical patients than in surgical patients (6.1 vs. 2.4 weeks in Group 1 [$P < 0.001$] and 5.0 vs. 3.1 weeks in Group 2 [$P < 0.01$]). Group 3 was too small to permit a meaningful comparison. During the initial hospitalization, the incidence of infections, gastrointestinal bleeding, and encephalopathy was similar among the medical and surgical patients.

We conclude that peritoneovenous shunting alleviated disabling ascites more rapidly than medical management. However, survival was closely related to the severity of the illness at the time of randomization and was not altered by shunting.

Prevalence of *Helicobacter pylori* infection and histologic gastritis in asymptomatic persons. Dooley CP, Cohen H, Fitzgibbons PL, et al. (CPD, Section of Gastroenterology, Dept. of Medicine, USC School of Medicine, 2025 Zonal Ave., Los Angles, CA 90033). *N Engl J Med* 321:1562–1566, Dec. 1989

We estimated the prevalences of *Helicobacter pylori* (formerly called *Campylobacter pylori*) infection and histologic gastritis in 113 asymptomatic persons, using endoscopic biopsy of the gastric antrum and corpus.

Unsuspected lesions, mainly mucosal erosions, were revealed at endoscopy in 16 subjects (14 percent). Gastritis was found in 42 subjects (37 percent), of whom 36 (32 percent of the total) were found to be infected with *H. pylori* on the basis of hematoxylin–eosin staining. *H. pylori* was not found in any of the 71 subjects with normal histologic features. Gastritis and *H. pylori* were noted in both the antrum and corpus in 75 percent of those infected ($n = 27$). The prevalence of *H. pylori* infection increased from 10 percent (2 of 20 subjects) in those between the ages of 18 and 29, to 47 percent (7 of 15) in those between the ages of 60 and 69, but the effect of age did not reach statistical significance. The prevalence of gastritis increased significantly with advancing age. Stepwise logistic regression analysis revealed that the relative risk for *H. pylori* infection associated with recent (within six months) antibiotic use was 5.8 (95 percent confidence interval, 1.5 to 22.1), whereas the relative risk was 6.5 (95 percent confidence interval, 1.4 to 29.2) for those who had never used bismuth compounds.

We conclude that histologic gastritis and *H. pylori* infection commonly occur in the stomach of apparently normal persons and increase in prevalence with advancing age. All the subjects with *H. pylori* infection had gastritis, suggesting a possible etiologic role for the bacterium in the histologic lesion.

Leukemia following chemotherapy for ovarian cancer. Kaldor JM, Day NE, Pettersson F, et al. (JMK, International Agency for Research on Cancer, 150 cours Albert-Thomas, 69372 Lyon Cédex 08, France). *N Engl J Med* 322:1–6, Jan. 1990

An international collaborative group of cancer registries and hospitals identified 114 cases of leukemia following ovarian cancer. We investigated the possible etiologic role of chemotherapy, radiotherapy, and other factors, using a case–control study design, with three controls matched to each case of leukemia.

Chemotherapy alone was associated with a relative risk of 12 (95 percent confidence interval, 4.4 to 32), as compared with surgery alone, and patients treated with both chemotherapy and radiotherapy had a relative risk of 10 (95 percent confidence interval, 3.4 to 28). Radiotherapy alone did not produce a significant increase in risk, as compared with surgery alone. The risk of leukemia was greatest four or five years after chemotherapy began, and the risk was elevated for at least eight years after the cessation of chemotherapy.

The drugs cyclophosphamide, chlorambucil, melphalan, thiotepa, and treosulfan were independently associated with significantly increased risks of leukemia, as was the combination of doxorubicin hydrochloride and cisplatin. Chlorambucil and melphalan were the most leukemogenic drugs, followed by thiotepa; cyclophosphamide and treosulfan were the weakest leukemogens, and the effect per gram was substantially lower at high doses than at lower doses. The extent to which the relative risks of leukemia are offset by differences in chemotherapeutic effectiveness is not known.

Leukemia following Hodgkin's disease. Kaldor JM, Day NE, Clarke A, et al. (JMK, International Agency for Research on Cancer, 150 cours Albert-Thomas, 69372 Lyon Cédex 08, France). *N Engl J Med* 322:7–13, Jan. 1990

To investigate the effect of different treatments for Hodgkin's disease on the risk of leukemia, we used an international collaborative group of cancer registries and hospitals to perform a case–control study of 163 cases of leukemia following treatment for Hodgkin's disease. For each case patient with leukemia, three matched controls were chosen who had been treated for Hodgkin's disease but in whom leukemia did not develop.

The use of chemotherapy alone to treat Hodgkin's disease was associated with a relative risk of leukemia of 9.0 (95 percent confidence interval, 4.1 to 20) as compared with the use of radiotherapy alone. Patients treated with both had a relative risk of 7.7 (95 percent confidence interval, 3.9 to 15). After treatment with more than six cycles of combinations including procarbazine and mechlorethamine, the risk of leukemia was 14-fold higher than after radiotherapy alone. The use of radiotherapy in combination with chemotherapy did not increase the risk of leukemia above that produced by the use of chemotherapy alone, but there was a dose-related increase in the risk of leukemia in patients who received radiotherapy alone.

The peak in the risk of leukemia came about five years after chemotherapy began, and a large excess persisted for at least eight years after it ended. After adjusting for drug regimen, we found that patients who had undergone splenectomy had at least double the risk of leukemia of patients who had not, and an advanced stage of Hodgkin's disease carried a somewhat higher risk of leukemia than Stage I disease.

We conclude that chemotherapy for Hodgkin's disease greatly increases the risk of leukemia and that this increased risk appears to be dose-related and unaffected by concomitant radiotherapy. In addition, the risk is greater for patients with more advanced stages of Hodgkin's disease and for those who undergo splenectomy.

Cocaine-induced coronary-artery vasoconstriction. Lange RA, Cigarroa RG, Yancy CW Jr, et al. (LD Hillis, Rm. 1.5.134, University of Texas Southwestern Medical Center, 5323 Harry Hines Blvd., Dallas, TX 75235). *N Engl J Med* 321:1557–1562, Dec. 1989

Intranasal cocaine is used frequently as a local anesthetic during many rhinolaryngologic procedures. Although its "recreational" use in high doses has been associated with chest pain and myocardial infarction, this association has not been established when cocaine is used in low doses as a topical anesthetic, and its effect on the coronary vasculature of humans is unknown.

We studied the effects of intranasal cocaine (10 percent cocaine hydrochloride; 2 mg per kilogram of body weight) on the blood flow in and dimensions of the coronary arteries and on myocardial oxygen demand in 45 patients (34 men and 11 women, 36 to 67 years of age) who were undergoing cardiac catheterization for the evaluation of chest pain. Heart rate, arterial pressure, blood flow in the coronary sinus (measured by thermodilution), and the dimensions of the epicardial left coronary artery (measured by quantitative arteriography) were measured before and 15 minutes after the intranasal administration of saline (in 16 patients) or cocaine (in 29).

No variables changed after the administration of saline. After cocaine was administered, the heart rate and arterial pressure rose, the coronary-sinus blood flow fell (from a mean [±SD] of 149 ± 59 ml per minute to 124 ± 53 ml per minute), and the diameter of the left coronary artery decreased by 8 to 12 percent ($P < 0.01$ for all comparisons). No patient had chest pain or electrocardiographic evidence of myocardial ischemia after the administration of cocaine. Subsequently, the administration of the alpha-adrenergic blocking agent phentolamine caused all these values to return to base-line levels. There was no difference in response between the patients found to have disease of the left coronary artery ($n = 28$) and those without such disease ($n = 17$).

We conclude that the intranasal administration of cocaine near the dose used for topical anesthesia causes vasoconstriction of the coronary arteries, with a decrease in the coronary blood flow, despite an increase in myocardial oxygen demand, and that these effects are mediated by alpha-adrenergic stimulation. It is reasonable to assume that these effects would be more pronounced at the much higher doses associated with the recreational use of cocaine.

Cancer

Pathogenesis of vertebral metastasis and epidural spinal cord compression. Arguello F, Baggs RB, Duerst RE, Johnstone L, McQueen K, Frantz CN (FA, Dept. of Pediatrics, Box 777, University of Rochester School of Medicine and Dentistry, 601 Elmwood Ave., Rochester, NY 14642). *Cancer* 65:98–106, 1990

The authors have studied the sequential events in the process of vertebral metastasis that result in spinal cord compression. Different tumor cell lines were injected into the systemic arterial circulation of syngeneic or nude mice, and they were killed at timed intervals after injection or when they became paraplegic. The following observations were made. The tumor cells lodged and grew in the hematopoietic bone marrow of the vertebrae. Cancer cells in the vertebral marrow cavity invaded into the spinal canal through the foramina of the vertebral veins rather than destroying the cortical bone. Tumor cell lines that grew in an infiltrative fashion migrated toward a posterior location in the spinal canal, and compressed the spinal cord from a posterior direction. Tumor cell lines that grew as compact tumors formed a tumor mass at the same location from which the cells emerged from the vertebra, and compressed the cord predominantly from an anterior direction. Radiographic evidence of vertebral metastasis was a late event, and commonly associated with significant compression of the cord and extraosseous tumor. These experimental findings may help to establish better diagnostic and treatment strategies for patients with metastatic disease of the spine.

Reprinted by permission from the American Cancer Society.

Fine needle aspiration diagnosis of intraabdominal and retroperitoneal lymphomas by a morphologic and immunocytochemical approach. Cafferty LL, Katz RL, Ordonez NG, Carrasco CH, Cabanillas FR (RLK, Dept. of Pathology, M. D. Anderson Cancer Center, 1515 Holcombe Blvd., Houston, TX 77030). *Cancer* 65:72–77, 1990

We reviewed 238 fine needle aspiration biopsies (FNA) of intraabdominal or retroperitoneal (IA/RP) masses in 192 patients with known or suspected lymphoma. A limited battery of immunocytochemical stains, including kappa (k) and lambda (l) light chains and Leu-4, was performed in 104 aspirates. One hundred twenty-eight of the FNA were diagnostic of or consistent with lymphoma, and three were diagnostic of carcinoma. Twenty-eight were considered negative for malignancy and 79 were suspicious for lymphoma or were nondiagnostic. For 135 of the FNA, a histologic biopsy specimen was available for comparison purposes. Overall, only one false-positive result was seen in a specimen lacking immunocytochemical data. The sensitivity of FNA lymphoma diagnosis was 66%. False-negative results due to sampling error were not uncommon, giving a predictive value of a negative result as 42%. The classification of the lymphomas by FNA was identical to that of the surgical biopsy in 86% of specimens and concurrently discrepant in 6%. We conclude that the routine performance of immunocytochemical studies on FNA of IA/RP masses is a feasible and valuable technique. Whereas suboptimal sensitivity and sampling error may make a negative diagnosis unreliable, lymphoma marker studies (combined with morphology) allow for an accurate and confident diagnosis and subclassification of lymphoma in the majority of cases.

Reprinted by permission from the American Cancer Society.

Chest

Postoperative evaluation of ascending aortic prosthetic conduits by magnetic resonance imaging. Pucillo AL, Schechter AG, Moggio RA, Kay RH, Tenner MS, Herman MV (ALP, Westchester Medical Center, Valhalla, NY 10595). *Chest* 97:106–110, 1990

Operative repair of ascending thoracic aortic dissection and aneurysm often involves the placement of prosthetic aortic conduits and stents with wrapping of the native aorta around the prosthetic device. Postoperative assessment has been clinical because of the absence of an adequate noninvasive imaging modality and a reluctance to perform invasive contrast aortography. Magnetic resonance imaging was performed on ten patients after operative placement of a prosthetic ascending aortic graft. The MR images were reviewed and a grading system was devised based on appearance of the operative site. An increase in MR signal was noted in some patients between the graft and wrapped native vessel. In 20 percent of patients vascular lumen compromise was noted. Magnetic resonance imaging offers a noninvasive technique to assess postoperative complications and offers a viable alternative to invasive contrast aortography.

Gastroenterology

Early gallstone recurrence rate after successful shock-wave therapy. Sackmann M, Ippisch E, Sauerbruch T, Holl J, Brendel W, Paumgartner G (MS, Dept. of Medicine II, Klinikum Grosshadern, Ludwig-Maximilian-University, Munich, F. R. G.). *Gastroenterology* 98:392–396, 1990

Extracorporeal shock-wave lithotripsy combined with adjuvant bile-acid dissolution therapy results in complete clearance of stone fragments in a high percentage of selected patients with radiolucent gallbladder calculi. With the gallbladder in situ, these patients are at risk of stone recurrence. Therefore, the early rate of stone recurrence after successful lithotripsy was evaluated. Fifty-eight of the first 60 consecutive patients who became stone free underwent follow-up examinations at least 1 yr (range, 12–37 mo; mean ±SD, 18 ± 6) after discontinuation of adjuvant bile-acid therapy. Five patients reported recurrent biliary pain within 1 yr after lithotripsy, and recurrent gallstones were detected. Fifty-three patients were asymptomatic during the first yr, and no recurrence was detected. Thus, the rate of gallstone recurrence was 9% within 1 yr. The rate of gallstone recurrence up to 3 yr was estimated by actuarial analysis. The probability of stone recurrence was 11% (±4%) at 1.5 yr, and no further increase was observed up to 3 yr. Gallstone recurrence within 1 yr after successful shock-wave therapy has to be expected in approximately the same percentage of patients as has been reported in earlier postdissolution trials. It causes recurrent biliary pain in most cases.

Reprinted with permission by the American Gastroenterological Association.

Reflux esophagitis in patients with Zollinger-Ellison syndrome. Miller LS, Vinayek R, Frucht H, Gardner JD, Jensen RT, Maton PN (LSM, Digestive Diseases Branch, National Institute of Diabetes and Digestive and Kidney Diseases, National Institutes of Health, Bethesda, MD). *Gastroenterology* 98:341–346, 1990

The incidence of ulcers of the stomach and duodenum and their response to medical therapy, in patients with Zollinger-Ellison syndrome is well described. However, reflux esophagitis is less well recognized. In this study we determined the frequency of reflux esophagitis in 122 patients with Zollinger-Ellison syndrome and examined their response to medical therapy. Esophageal symptoms, endoscopic abnormalities, or both were present in 61% of patients. Forty-five percent of patients had esophageal symptoms consisting of heartburn, dysphagia, or both. Forty-three percent of patients had endoscopic abnormalities of the esophagus, and 23% demonstrated moderate or severe disease. When sufficient antisecretory medication was administered to lower gastric acid secretion to <10 mEq/h in the last hour before the next dose of drug, 67% of the patients with reflux esophagitis responded with complete disappearance of symptoms and normalization of the endoscopic abnormalities. The other 33% of patients required an increase in medication to lower acid output to <5 mEq/h in 7% and <1 mEq/h in the other 26% to resolve symptoms and signs completely. We conclude that reflux esophagitis occurs in the majority of patients with Zollinger-Ellison syndrome and responds well to medical therapy, although one third of patients require intensive antisecretory medication.

Reprinted with permission by the American Gastroenterological Association.

Digestive Diseases and Sciences

Sphincter of Oddi manometry in healthy volunteers. Guelrud M, Mendoza S, Rossiter G, Villegas MI (MG, Policlinica Metropolitana, Urb. Caurimare, Caracas, Venezuela). *Dig Dis Sci* 35(1):38–46, Jan. 1990

In this study we describe in detail the characteristics of sphincter of Oddi motor function in a large group of healthy subjects. Studies were obtained in 50 healthy volunteers. The findings showed a sphincter of Oddi segment that had a basal pressure of 14.8 ± 6.3 mm Hg (*X* ± SD). Phasic contractions were superimposed on the basal pressure. They had an amplitude of 119.7 ± 32 mm Hg, a duration of 4.7 ± 1 sec, and a frequency of 5.7 ± 1.2 contractions/min. In 40 subjects the propagation sequence of phasic contractions could be evaluated and were simultaneous in 53%, antegrade in 35%, and retrograde in 11% of the waves. In 20 subjects, pressure measurements done at the common bile duct sphincter were similar to those obtained at the pancreatic duct sphincter. In 10 subjects, pressure values obtained at the common bile duct sphincter within a week were similar. Our study should help to establish standards for normal manometric values of the sphincter of Oddi and emphasizes the importance of having a healthy volunteer group from which to obtain the normal values of sphincter of Oddi motor function.

The Journal of Bone and Joint Surgery

The fate of acetabular allografts after bipolar revision arthroplasty of the hip: a radiographic review. Wilson MG, Nikpoor N, Aliabadi P, Poss R, Weissman BN (BNW, Dept. of Radiology, Brigham and Woman's Hospital, 75 Francis St., Boston, MA 02115). *J Bone Joint Surg [Am]* 71-A(10):1469–1479, Dec. 1989

We reviewed the radiographs of thirty-one patients (thirty-two hips) who had had revision of the acetabular component of a total hip arthroplasty with a bipolar socket supplemented by allograft and were followed for twenty-four to forty-eight months. The grafts were categorized according to their consistency (solid or crushed bone), the location of the acetabular defect (peripheral [rim] or central), and the extent of the acetabular defect (contained—the medial part of the acetabular wall was intact, or non-contained—it was deficient). We recorded the time to incorporation of the graft, the amount of migration of the socket in the superior and medial axes, and the percentage of graft remaining at the time of the most recent follow-up.

The time to healing was similar for all categories of grafts. The central, contained, solid grafts had less resorption than did the central, contained, crushed-bone grafts, as evidenced by less migration of the socket during follow-up. The non-contained grafts, in both peripheral and central locations, were associated with high rates of migration and of instability of the socket.

Clinical Orthopaedics and Related Research

Prognostic accuracy of preoperative and postoperative scintimetry after femoral neck fracture. Alberts KA (KAA, Dept. of Orthopedic Surgery, Karolinska Hospital, S-104 01 Stockholm, Sweden). *Clin Orthop* 250:221–225, Jan. 1990

Forty patients with fresh femoral neck fractures treated with closed reduction and internal fixation were included in a prospective study of nonunion and osteonecrosis by preoperative and postoperative scintimetry. Correlated roentgenographic follow-up studies were continued for two years postoperatively. The aim of the study was to determine the relative prognostic accuracy of preoperative versus postoperative scintimetry. A ratio between the radionuclide uptake over the femoral head on the fracture side and the contralateral side exceeding 1.9 at the preoperative scintimetry and 1.2 at the postoperative scintimetry was associated with a high incidence of union, whereas a lower ratio often predicted subsequent complications (redisplacement, nonunion, or late segmental collapse). Prognostic accuracy was higher for scintimetry of fractures treated with closed reduction and internal fixation (0.70) than for untreated fractures (0.53). These results suggest that scintimetry is useful postoperatively to complement roentgenographic examination in assessing the prognosis of femoral neck fractures.

The Journal of Urology

Abdominal radiograph and renal ultrasound versus excretory urography in the evaluation of asymptomatic patients after extracorporeal shock wave lithotripsy. Coughlin BF, Risius B, Streem SB, Lorig RJ, Siegel SW (BR, Dept. of Diagnostic Radiology, Cleveland Clinic Foundation, 9500 Euclid Ave., Cleveland, OH 44195-5103. *J Urol* 142:1419–1424, Dec. 1989

A prospective study was done to compare the relative efficacy of an abdominal radiograph and renal ultrasound to excretory urography for the evaluation of asymptomatic patients 1 month after extracorporeal shock wave lithotripsy.

We evaluated 101 renal units in 84 asymptomatic patients who had undergone extracorporeal shock wave lithotripsy 1 month previously with abdominal radiography, excretory urography and ultrasonography to evaluate the presence of retained stone fragments, dilatation of the collecting system and intrarenal or perirenal fluid collections or masses. The combination of abdominal radiography and ultrasonography identified retained fragments in 62 renal units, while excretory urography identified them in 54. Ultrasonography was less specific in identifying dilatation of part or all of the collecting system; proving falsely positive in 7 renal units and falsely negative in 14 compared to excretory urography. However, the case of obstruction was diagnosed correctly by both modalities. Finally, ultrasound appeared to be more specific and more sensitive in the evaluation of the presence of intrarenal or perirenal abnormalities.

We conclude that a combination of abdominal radiography and ultrasonography is as good or better than excretory urography in identifying residual stone fragments and intrarenal or perirenal abnormalities. However, the finding of dilatation of all or part of the collecting system by ultrasonography is nonspecific and probably is better evaluated by excretory urography. We suggest that the routine radiological evaluation of asymptomatic patients 1 month after extracorporeal shock wave lithotripsy could be limited routinely to abdominal radiography and ultrasonography. However, when abnormalities of the collecting system are visualized on these studies excretory urography should be performed.

Pediatrics

Readability of pediatric biomedical research informed consent forms. Tarnowski KJ, Allen DM, Mayhall C, Kelly PA (KJT, Dept. of Pediatrics Core A451, Case Western Reserve University, Cleveland Metropolitan General Hospital, 3395 Scranton Rd., Cleveland, OH 44109). *Pediatrics* 85(1):58–62, Jan. 1990

Informed consent forms are used in biomedical research as a mechanism to convey study information to potential subjects so that they may arrive at a decision concerning their willingness to participate. Although the Department of Health and Human Services Regulations for the Protection of Human Subjects require the presentation of specific study information at a level that is easily understood, according to research concerning adult biomedical consent forms, the typical form is not readily comprehensible. Unfortunately, no data exist concerning the readability of informed consent forms that are used in the context of pediatric biomedical research. In the present study, readability analyses were conducted on a large sample (N = 238) of pediatric biomedical informed consent forms obtained during a 10-year period from a large midwestern children's hospital. For the entire sample, results derived from two readability estimates (Fry grade equivalent and Flesch Reading Ease methods) indicated that the consent forms were written at the college graduate level. Although there was a linear increase in the length of the consent document during the 10-year period evaluated, expanded length was not associated with improved readability. According to analyses, a differential pattern of reading difficulty was associated with specific sections of the informed consent document. Findings are highly consistent with those from studies of adult biomedical consent forms and document that the purpose of the informed consent form is being compromised, in part, by a readability factor. Suggestions for solving this critical problem are advanced.

Reprinted by permission of PEDIATRICS © 1990.

The Journal of Pediatrics

Congenital rubella syndrome associated with calcific epiphyseal stippling and peroxisomal dysfunction. Pike MG, Applegarth DA, Dunn HG, et al. (HGD, Division of Neurology, Dept. of Pediatrics, British Columbia's Children's Hospital, 4480 Oak St., Vancouver, B.C., Canada V6H 3V4). *J Pediatr* 116:88–94. Jan. 1990

An infant girl had the clinical and immunologic findings of congenital rubella syndrome but also had arthrogryposis multiplex and calcific epiphyseal stippling. Spastic quadriparesis developed, and both physical and behavioral development were slow. Increased spasticity of the legs at 5½ years was related not to progressive rubella encephalomyelopathy but to spinal cord compression by abnormal cartilaginous tissue. The presence of a peroxisomal disorder was demonstrated by a greatly increased level of phytanic acid and slightly increased levels of hexacosanoate in serum and by reduced activity of peroxisomal dihydroxyacetone phosphate acyltransferase and a slightly increased ratio of cytosolic to peroxisomal catalase activity in cultured fibroblasts. A reduction in the number and size of peroxisomes was demonstrated in cultured fibroblasts, and a needle biopsy specimen of the liver also showed the peroxisomes to have a smaller diameter than usual. We recommend that any child with epiphyseal stippling be assessed for peroxisomal disease and that the potential for spinal cord compression by dysplastic bone or cartilage be recognized. The association of peroxisomal dysfunction with congenital rubella has not been described previously. The interaction between rubella virus infection and peroxisomal function may need further investigation.

Effects of exogenous surfactant therapy on dynamic compliance during mechanical breathing in preterm infants with hyaline membrane disease. Couser RJ, Ferrara B, Ebert J, Hoekstra RE, Fangman JJ (RJC, Minneapolis Children's Medical Center, 2525 Chicago Ave. S., Minneapolis, MN 55404). *J Pediatr* 116:119–124, Jan. 1990

In a prospective, randomized, controlled clinical trial, the immediate and the longitudinal effects of exogenous surfactant therapy on pulmonary mechanics were evaluated in extremely premature infants during mechanical respiration. Ninety-four infants weighing between 600 and 1250 gm received either exogenous surfactant or sham (air) therapy in the delivery room and up to three additional doses in the first 48 hours of life if they were ventilator-dependent, had fractional inspiratory oxygen requirements $\geq$0.30, and radiographic findings consistent with hyaline membrane disease. Each infant underwent pulmonary mechanics assessment (dynamic compliance, total pulmonary resistance, tidal volume) immediately before and 1 hour after each dose, and at 24, 48, and 72 hours and 7 days of age. There were no significant differences in dynamic compliance, total pulmonary resistance, and tidal volume in the surfactant (n = 47) and control (n = 47) groups before and 1 hour after each dose. However, dynamic compliance was 50% greater in the surfactant group at 24 hours of age ($p \leq 0.009$); this difference steadily increased to 94% at 7 days of age ($p \leq 0.009$). Oxygenation, assessed by the ratio of alveolar to arterial oxygen pressure, was significantly greater in the surfactant group during the first 72 hours of life; the greatest difference was noted at 24 hours ($p \leq 0.001$). Mean airway pressure requirements in the surfactant group were significantly less than in the control group at all times during the first week. We conclude that exogenous surfactant therapy, administered at birth and during the first 48 hours of life in extremely premature infants with hyaline membrane disease, improves dynamic compliance and gas exchange during mechanical breathing.

Journal of Thoracic Imaging

Newer imaging methods in chest radiography. Wandtke JC (JCW, Dept. of Radiology, University of Rochester Medical Center, P. O. Box 648, Rochester, NY 14642). *J Thorac Imaging* 5(1):1-9, 1990

In recent years the application of computers to chest radiography has resulted in a wide variety of innovative research. Major research efforts have resulted in the development of new types of x-ray detectors, such as storage phosphor technology, for use with computers. Storage phosphor imaging is one of the most promising new techniques, and almost 100 systems have been installed worldwide. Radiologists are quickly evaluating the image quality provided by this new detector system, which has the potential to improve image quality. It has wide latitude and is coupled with a computer to perform image processing. Another promising technology, originally studied in the form of scan equalization radiology, is now commercially available in the form of advanced multiple-beam equalization radiography. This film technique uses computers to modulate the x-ray exposure to take maximum advantage of the imaging capabilities of radiographic film. Digital solid-state detectors have been studied in conjunction with computerized image enhancement systems. These currently show improvement in nodule detection and quantification of the calcium content of a lesion. Application of large image intensifiers to a digital image system is being studied, but there are currently limitations on spatial resolution.

Journal of Ultrasound in Medicine

A prospective comparison of transabdominal and transvaginal ultrasound with surgical findings in gynecologic disease. Andolf E, Jörgensen C (EA, Dept. of Obstetrics and Gynecology, University Hospital, S-221 85 Lund, Sweden). *J Ultrasound Med* 9:71-75, Feb. 1990

Eighty-five patients underwent transabdominal (TAU) and transvaginal ultrasound (TVU) 24 hours before elective surgery for gynecologic disease. No obstetric cases were included. The diagnostic outcome of TVU was not significantly better than that of TAU in spite of a better image quality. The evaluation of large ovarian cysts and sizeable fibroids was difficult with TVU due to the limited field of view. Endometrial pathology was clearly diagnosed by TVU. We recommend using TVU in combination with TAU, especially in cases of unclear pelvic pathology or when larger masses are present.

Reprinted with permission by the American Institute of Ultrasound in Medicine.

Journal of Computer Assisted Tomography

MR characterization of hepatic lesions by t-null inversion recovery sequence. Patrizio G, Pavone P, Testa A, Marsili L, Tettamanti E, Passariello R (GP, Departimento di Radiologia, Ospedale Santa Maria di Collemaggio, 67100 L'Aquila, Italy). *J Comput Assist Tomogr* 14(1):96-101, Jan./Feb. 1990

Tissue characterization of focal hepatic lesions was performed employing an inversion recovery sequence with short repetition time and short inversion time (TI) values. Different and specific TI values, correlated to the in vivo measured TI relaxation times, were used to null the signal intensity of each type of lesion. In 40 patients studied, we observed the nulling effect of normal liver in 10 of 10 cases with a TI of 136 ms, of metastases in 7 of 8 cases with a TI of 175 ms, of hemangiomas in 15 of 16 cases with a TI of 200 ms, and of cysts in 6 of 7 cases with a TI of 235 ms. A quantitative analysis of the nulled signal was performed by measuring the signal/noise values. A further qualitative and quantitative characterization was carried out by evaluating the signal intensity of hepatic lesions at the null point of normal liver. The method provided the possibility of discriminating different focal lesions with specificity values of 83-94%, according to the type of lesion.

Magnetic Resonance Imaging

Assessment of mitral regurgitation by magnetic resonance imaging. Glogar D, Globits S, Neuhold A, Mayr H (DG, Kardiologische Univ. Klinik, University of Vienna, Garnisongasse 13, A-1090 Vienna, Austria). *Magn Reson Imaging* 7:611-617, 1989

To evaluate the potential of magnetic resonance imaging (MRI) in detection and quantification of mitral regurgitation, 26 pts. with echocardiographically or angiographically documented mitral regurgitation were examined using a 0.5 Tesla superconducting magnet. In each patient a multislice-multiphase study in a sagittal-coronal double angulated projection (four-chamber view equivalent) was performed to assess left and right ventricular volumes, ejection fraction and regurgitant fraction. Additionally a blood flow sensitive cine-study (fast field echo: FFE) was done to visualize direction and area of regurgitant jet. MRI data were compared with quantitative and qualitative assessment of mitral regurgitation by angiography, 2D echocardiography, Doppler sonography and color flow mapping. Using the FFE mode MRI was able to detect the regurgitant jet as a typical signal loss within the left atrium in all patients. The ratio of regurgitant jet area/left atrium area as determined by MRI showed a correlation with a comparable ratio from color Doppler sonography of $R = 0.87$ ($p < 0.001$). There was also good agreement in semiquantitative grading of mitral regurgitation between MRI and angiography ($R = 0.77, p < 0.001$). The determination of left and right ventricular stroke volume allowed the calculation of the regurgitant fraction, which showed a correlation with invasively determined regurgitation fraction of $R = 0.84$ ($p < 0.001$). These data provide additional information that MRI may be useful as a noninvasive technique to detect and quantify mitral regurgitation.

FORTHCOMING ARTICLES

SPECIAL ARTICLE

Medical decision making: practical points for practicing radiologists. *Phillips WC Jr, Scott JA*

EXPERT ADVICE

Radiologic investigation of dysphagia. *Levine MS, Rubesin SE*

REVIEW ARTICLE

Pitfalls in the radiologic diagnosis of lung cancer. *Woodring JH*

CHEST RADIOLOGY

Pulmonary blastomycosis: chest radiographic findings in 63 patients. *Sheflin JR, Campbell JA, Thompson GP*

Percutaneous biopsy of thoracic lesions: value of sonography for needle guidance. *Ikezoe J, Morimoto S, Arisawa J, Takashima S, Kozuka T, Nakahara K*

Case report. Whipple disease of the mediastinum. *Samuels T, Hamilton P, Shaw P*

Case report. Bilateral internal mammary artery aneurysms: a previously unreported cause of an anterior mediastinal mass. *Giles JA, Sechtin AG, Waybill MM, Moser RP Jr*

BREAST RADIOLOGY

Stereotactic fine-needle aspiration for cytologic diagnosis of nonpalpable breast lesions. *Löfgren M, Andersson I, Lindholm K*

Commentary. Stereotactic fine-needle aspiration biopsy for nonpalpable breast lesions. *Jackson VP, Bassett LW*

GASTROINTESTINAL RADIOLOGY

The value of sonography for the diagnosis of acute diverticulitis of the colon. *Wilson SR, Toi A*

Pictorial essay. CT of the abdominal wall. *Goodman P, Raval B*

Technical note. Common bile duct biopsy with the Simpson atherectomy catheter. *Kim D, Porter DH, Siegel JB, Mowschenson PM, Steer ML*

Case report. Obstructing villous adenoma and papillary adenomatosis of the bile ducts. *Harshfield DL, Teplick SK, Stanton M, Tunuguntla K, Diner WC, Read RC*

Case report. Combined systemic and portal venous gas: sonographic and CT detection in two cases. *Kriegshauser JS, Reading CC, King BF, Welch TJ*

GENITOURINARY RADIOLOGY

Intrarenal arterial Doppler sonography in patients with nonobstructive renal disease: correlation between the resistive index and biopsy findings. *Platt JF, Ellis JH, Rubin JM, DiPietro MA, Sedman AB*

Heating of the scrotum by high-field-strength MR imaging. *Shellock FG, Rothman B, Sarti D*

MUSCULOSKELETAL RADIOLOGY

Jogging causes acute changes in the knee joint: an MR study in normal volunteers. *Kursunoglu-Brahme S, Schwaighofer B, Gundry C, Ho C, Resnick D*

MR imaging of the knee: pseudotear of the lateral meniscus caused by the meniscofemoral ligament. *Vahey TN, Bennett HT, Arrington EL, Shelbourne KD, Ng J*

Pictorial essay. Intracapsular osteoid osteoma of the proximal femur: plain film and CT findings. *Schlesinger AE, Hernandez RJ*

MR imaging of the temporomandibular joint: a cadaver study of the value of coronal images. *Schwaighofer BW, Tanaka TT, Klein MV, Sartoris DJ, Resnick D*

PEDIATRIC RADIOLOGY

Hodgkin disease in children: comparison of staging with CT, lymphography, and laparotomy. *Baker LL, Parker BR, Donaldson SS, Castellino RA*

Case report. Arterial embolization to control life-threatening hemorrhage from a Meckel's diverticulum. *Okazaki M, Higashihara H, Yamasaki S, Akita Y, Toriya H, Shirai Z*

NEURORADIOLOGY

Diagnosis of tumors of the parotid gland with anti-CEA immunoscintigraphy. *Kairemo KJA, Hopsu EVM*

Pictorial essay. MR imaging of the cranial nerves. *Lanzieri CF*

MR findings in patients with subacute necrotizing encephalomyelopathy (Leigh syndrome): correlation with biochemical defect. *Medina L, Chi TL, DeVivo DC, Hilal SK*

Intracranial chemical-shift artifacts on MR images of the brain: observations and relation to sampling bandwidth. *Smith AS, Weinstein MA, Hurst GC, DeRemer DR, Cole RA, Duchesneau PM*

MR signal abnormalities in memory disorder and dementia. *Bowen BC, Barker WW, Loewenstein DA, Sheldon J, Duara R*

Posttraumatic cerebral infarction diagnosed by CT: prevalence, origin, and outcome. *Mirvis SE, Wolf AL, Numaguchi Y, Corradino G, Joslyn JN*

Neuroimaging of disseminated germ cell neoplasms. *Mathews VP, Broome DR, Smith RR, Bognanno JR, Einhorn LH, Edwards MK*

CONTRAST MATERIAL

Case report. The excretion of Gd-DTPA in human breast milk. *Schmiedl U, Maravilla KR, Gerlach R, Dowling CA*

MEETING NEWS

The Society of Gastrointestinal Radiologists: 19th Annual Meeting, January 1990. *Whalen E*

CASE OF THE DAY

Introduction. *Stull MA*

Chest case of the day. *Stull MA, Clark LR, Reagan K, et al.*

Abdominal case of the day. *Silverman PM, Hayes WS, Cooper CJ, et al.*

Musculoskeletal case of the day. *Stull MA, Glass-Royal MW*

Neuroradiology case of the day. *Deveikis JP, Cammarata CA, Reid WM, et al.*

News

Diagnostic Imaging of the Eye and Orbit

The Dept. of Ophthalmology, The New York Hospital-Cornell University Medical College, New York City, is sponsoring the 17th annual ophthalmology course, Diagnostic Imaging of the Eye and Orbit: Ultrasound, CT and MRI, June 1–2. Course director: D. Jackson Coleman. Category 1 credit: 14 hr. Information: Suzanne Woods, R.N., Dept. of Ophthalmology, The New York Hospital, 525 E. 68th St., New York, NY 10021; (212) 746-2504.

Annual Pittsburgh Breast Imaging Seminar

The 10th annual Pittsburgh Breast Imaging Seminar will be held July 13–15 at the Westin William Penn Hotel, Pittsburgh. Course codirectors: Kathleen M. Harris, Ellen B. Mendelson, Ingrid E. Naugle, and William R. Poller. Information: Pittsburgh Breast Imaging Seminar, c/o Pittsburgh Radiology Associates, 3471 5th Ave., Ste. 301, Pittsburgh, PA 15213; (412) 648-6043.

International Meeting on Topics of Interventional Radiology

The 2nd International Meeting on Topics of Interventional Radiology—The Progress will be held Sept. 20–22 at the Hotel Oranje Noordwyk, the Netherlands. The meeting is designed especially for interventional radiologists and vascular surgeons and cardiologists who have an interest in interventional radiology. Topics to be covered include angioplasty recanalization methods; stenting; laser-assisted treatment; gynecologic, gastrointestinal, and biliary interventions; Doppler duplex diagnosis; fibrinolysis; and lithotripsy. Program director: Peter Bylsma. Faculty: Arina van Breda, Mike Kellett, Rolf Guenther, Barry Katzen, Eric Martin, Klaus Mathias, Manuel Maynar, Gordon McLean, Herbert Geschwind, Jean Marco, Plinio Rossi, Donald Schwarten, Thomas Sos, Ernst-Peter Strecker, Charles Tegtmeyer, Mark Wholey, and Eberhard Zeitler. Fee: physicians, $225; residents, $150. Information: International Meeting Office, Ravenswade 94,3439 LD Nieuwegein, the Netherlands; telephone: (030) 893245; fax: (030) 899399.

Radiology in Britain and Brussels

The University of Connecticut; the Royal Marsden Hospital, London; and the Royal Belgium Society of Radiology are cosponsoring Radiology in Britain and Belgium, Sept. 23–30, in Eastbourne, Sussex, England, and Brussels, Belgium. Program chairman: Thomas J. Spackman. Program director: D. Beatty Crawford. Faculty: G. Bydder, A. Hasso, C. Helms, J. Husband, P. Fritzsche, B. Kendall, T. McLoud, and H. Meire. Fee: physicians, $700; residents and technicians, $350. Information: D. Beatty Crawford, M.D., Dept. of Radiology, University of Connecticut Health Center, Farmington, CT 06032; telephone: (203) 679-3322; fax: (203) 679-3145.

Practical Radiology

The University of Virginia will offer its 13th annual postgraduate course, Practical Radiology, Oct. 8–11, at the Boar's Head Inn, Charlottesville, VA. Faculty: Gerald Friedland, Igor Laufer, P. R. Ros, and R. L. Teele. Category 1 credit: 20 hr. Fee: $400. Information: Theodore E. Keats, M.D., Professor and Chairman, Dept. of Radiology, University of Virginia School of Medicine, Charlottesville, VA 22908; (804) 924-2781.

Magnetic Resonance Imaging 1990: Back to the Future

The University of Cincinnati, College of Medicine, is sponsoring Magnetic Resonance Imaging 1990: Back to the Future, Oct. 10–13, at the Westin Cincinnati Hotel, Cincinnati. The course is designed to educate radiologists and clinicians in the use of state-of-the-art MR technology for the evaluation of commonly encountered clinical problems in neuroradiology, orthopedics, and body imaging. Conference directors: Robert R. Lukin, Jonathan S. Moulton, and George S. Bisset III. Category 1 credit: 20 hr. Information: Lynne K. Tiras, CMP, International Meeting Managers, Inc., 4550 Post Oak Pl., Ste. 248, Houston, TX 77027; telephone: (713) 965-0566; fax: (713) 960-0488.

Advances in Color Doppler Sonography

The Dept. of Radiology and Radiological Sciences and the Division of Continuing Medical Education, Vanderbilt University, Medical Center, will offer Advances in Color Doppler Sonography, Nov. 1–3, at The Greenbriar, White Sulphur Springs, WV. The purpose of the meeting is to provide medical imaging specialists with an update on clinical applications of color Doppler sonography. Category 1 credit: 7 hr. Fee: physicians, $250; sonographers, $200. Information: Brenda Boner, Course Coordinator, Vanderbilt Division of CME, CCC-5326 MCN, Nashville, TN 37232-2337; (615) 322-4030.

Symposium on Bone and Soft-Tissue Tumors

The School of Medicine, University of California, Davis, is offering the 2nd annual symposium, Bone and Soft-Tissue Tumors—Diagnostic Imaging Modalities, Pathology, and Surgery, Nov. 9–10, at the Hyatt Regency Hotel, Sacramento, CA. Category 1 credit: 13 hr. Fee: physicians, $345; residents, $175; others, $215. Information: Office of Continuing Medical Education, UC Davis, School of Medicine, 2701 Stockton Blvd., Sacramento, CA 95817; (916) 734-5390.

International Congress of Radiation Research

The 9th International Congress of Radiation Research will be held July 7–12, 1991, at the Sheraton Centre, Toronto, Canada. Tentative deadlines are Oct. 15, 1990, for Junior Investigators Awards and Jan. 15, 1991, for abstracts. Information: 9th International Congress of Radiation Research, 1891 Preston White Dr., Reston, VA 22091; (703) 648-3780.

American Association of Women Radiologists Officers

The American Association of Women Radiologists elected the following officers at the meeting of their executive committee on Nov. 26, 1989, in Chicago: president, Peggy J. Fritzsche; president-elect, Cheryl Hicks; vice-president, Kay Shaffer; secretary, Lynne Steinbach; treasurer, Ellann McCrory; newsletter editor, Sandra Fernbach; past-president, Dixie Anderson; member at large, Sheila Moore; membership committee, chair, Kathryn Evers; ACR councilor, Kay Vydareny; ACR alternate councilor, Carol Rumack; and executive director, Ann Wieseneck.

The American Board of Radiology Examinations

Written examinations for the American Board of Radiology (ABR) are scheduled for Sept. 27–28, 1990, and Oct. 3–4, 1991. Oral examinations will be held at the Executive West Hotel in Louisville, KY, June 4–8, 1990, and June 3–7, 1991. The ABR will accept applications for admission to the examinations after July 1, but not later than Sept. 30, in the year *preceding* the year in which the examination is to be taken. For application forms and further information: Office of the Secretary, The American Board of Radiology, 300 Park, Ste. 440, Birmingham, MI 48009.

Meeting and Course Review

For the reader's convenience, a summary of upcoming meetings and courses is provided. Detailed listings are given in the *AJR* issue given in parentheses.

Visiting Fellowship in Interventional Radiology, times arranged, Baltimore (Sept 1989)
Visiting Fellowships at UCSF, times arranged, San Francisco (Sept 1989)
Preceptorships in Transrectal Ultrasound of the Prostate, Ann Arbor, MI (Sept 1989)
Radiology Review Course, April 29–May 4, Miami, FL (Feb)
Mid-Pacific Diagnostic Ultrasound Conference, May 1–5, Kauai, HI (Feb)
Advances in CT and MRI, May 2–4, Ann Arbor, MI (Feb)
The Leading Edge in Diagnostic Ultrasound, May 2–4, Atlantic City, NJ (April)
Fellowships in Biliary Lithotripsy, May 3–5 and June 7–9, Baltimore, MD (Dec 1989)
Symposium in Diagnostic Ultrasound, May 4–6, New York City (Feb)
Congress of the European Federation of Societies for Ultrasound in Medicine and Biology, May 6–11, Jerusalem, Israel (May 1989)
Biliary Calculus Disease, May 7–9, Boston (Nov 1989)
Surgical Neuroangiography, May 7–11, New York City (April)
Diagnostic Imaging in Musculo-Skeletal Radiology, May 10–11, Glasgow, Scotland (Dec 1989)
Pulsed Lasers in Angioplasty, May 11–12, Tübingen, F. R. G. (April)
Cardiovascular and Interventional Radiology, May 13–18, Brussels, Belgium (Dec 1989)
27th Congress of the European Society of Paediatric Radiology, May 14–18, Munich, West Germany (Jan)
Blood Vessel Imaging Using Ultrasound Techniques, May 16–18, Southampton, Hampshire, United Kingdom (March)
Clinical Magnetic Resonance Imaging, May 21–23, New Haven, CT (March)
Mammography for the General Radiologist, May 21–24, Sept. 10–13, and Oct. 22–25, Boston (March)
Clinical MRI: 1990 Update, May 23–26, Boston (March)
Sonography Symposium, May 25–26, Nashville, TN (April)
Musculoskeletal MRI for Orthopedists and Radiologists, May 28–June 1, Sonesta Beach Hotel (Dec 1989)
Emergency Radiology 1990, May 29–June 1, Boston (March)
Italian Society of Radiology and Nuclear Medicine, May 30–June 3, 1990, Turin, Italy (Nov 1989)
Contemporary Medical Imaging VII, May 30–June 3, Hilton Head Island, SC (April)
American Society of Emergency Radiology Annual Meeting, June 2, Boston (Feb)
American College of Medical Physics Annual Meeting, June 7–10, Austin, TX (Dec 1989)
Abdominal Ultrasound, June 11–14, Philadelphia (Jan)
Prostate Ultrasound, June 15, Philadelphia (Jan)
Advanced Techniques in MRI, June 16–22, Kiawah Island, SC (March)
Radiology in Scandinavia and the Soviet Union, June 16–30, Copenhagen, Malmo, Stockholm, Helsinki, and Leningrad (Feb)
Diagnostic Radiology, June 17–22, Myrtle Beach, NC (March)
Pediatric Nuclear Medicine Categorical Seminar, June 18, Washington, DC (March)
Liver Imaging, June 25–27, Boston (March)
International Course in Cardiovascular Interventional Radiology, July 11–13, Leeds, United Kingdom (Dec 1989)
Mammography and the Search for Breast Cancer, July 13–14, Rochester, NY (April)
Advances in Radiation Oncology Physics, July 16–20, Lawrence, KS (March)
American Association of Physicists in Medicine Annual Meeting, July 22-26, St. Louis (Feb)
Napa Valley Imaging Update—MRI 1990, July 22-26, Napa, CA (April)
Musculoskeletal Imaging, July 23–25, Laguna Niguel, CA (March)
Symposium on Magnetic Resonance Imaging, July 26–29, Laguna Niguel, CA (March)
Annual Northern Imaging Meeting, Aug. 4–8, Winnipeg, Manitoba (March)

Copenhagen Symposium on Uroradiology, Aug. 27–30, Herlev, Denmark (Feb)

Uroradiology Postgraduate Course, Sept. 1–14, Vancouver, B.C. (April)

European Society of Head and Neck Radiology Annual Meeting, Sept. 12–15, Bresica (Lake of Garda), Italy (Feb)

Applied Ultrasound: Accent on Doppler, Sept. 12–15, Naples, FL (April)

Musculoskeletal Disorders, Sept. 12–15, Salzburg, Austria (April)

Interventional Radiology/2nd Marmara Medical Days, Sept. 19–21, Haydarpasa-Istanbul, Turkey (March)

Nuclear Medicine Technology Certification Examination, Sept. 22; application deadline, July 21 (Nov 1989)

International Conference on Ultrasound Angiography, Sept. 25–28, London, United Kingdom (Feb)

Royal Australasian College of Radiologists Annual Meeting, Oct. 5–11, Perth, Western Australia (April)

American Lithotripsy Society Annual Meeting, Oct. 11–14, San Diego (March)

MR Imaging Course in Riyadh, Saudi Arabia, Oct. 14–17, Riyadh, Saudi Arabia (April)

AJR carries announcements of courses, symposia, and meetings of interest to its readers if received a minimum of 5 months before the event. There is no charge; receipt of items by the *AJR* Editorial Office is not acknowledged. Submit items for publication typed double-spaced. Provide title, date, location, brief description, sponsor, course directors, fees, category I credit, and address and telephone number for additional information. Faculty from the host institution will not be listed. Guest faculty names will appear **only** if initials are provided. Mail news items to *AJR* Editorial Office, 2223 Avenida de la Playa, Suite 200, La Jolla, CA 92037-3218.

Information and Application for Membership in the American Roentgen Ray Society

General Information

The American Roentgen Ray Society, founded in 1900, has been a forum for progress in radiology since shortly after the discovery of x-rays. From its beginning and continuing to today, the ARRS has been guided by dedication to the goal of the advancement of medicine through the science of radiology and its allied sciences.

The goal of the ARRS is maintained through an annual scientific and educational meeting, and through publication of the *American Journal of Roentgenology*.

The annual meeting consists of instructional courses, scientific sessions, a symposium, scientific exhibits, and commercial exhibits. A special categorical course is also offered. Category I CME credits are available on an hour-for-hour basis.

The monthly *American Journal of Roentgenology* is a highly respected peer review journal with a worldwide subscription base. For over 75 years the *AJR* has been accepted as one of the best specialty journals available in the world, and this reputation grows each month.

A recently developed quarterly ARRS newsletter keeps members informed of events and general Society news.

Application Instructions

Candidates for Active Membership

1. An Active member must be a graduate of an approved medical school or hold an advanced degree in one of the physical, chemical or biological sciences and be certified by the American Board of Radiology, the American Osteopathic Board of Radiology, the Royal College of Physicians of Canada, or document training and credentials that are adequate to qualify for membership. Active members shall actively practice radiology or one of its branches in the United States or Canada. Such members are eligible to participate in all activities of the Society, including membership on committees, and have full voting privileges.
2. Application must be on an official form, signed by the applicant and at least two members of the American Roentgen Ray Society, active or emeritus, in good standing, who endorse the applicant.
3. Application fee is $50 (payable when billed for dues).
4. Annual dues are $125, payable on January 1 of each year following the initial year. First year dues will be invoiced following candidate election at the annual meeting. Of this amount, $50 is for a 1-year subscription to the *American Journal of Roentgenology*, beginning with the July issue following election to membership.
5. Application must be received by February 1 for action during the current year's meeting.

Candidates for In-Training Membership

1. In-training members must be serving in a radiology residency program approved by the Radiology Residency Review Committee, the American Osteopathic Board of Radiology, or the Royal College of Physicians of Canada, or in an approved post-residency fellowship, or be a postgraduate student in an allied science. Training status must be verified by the program director. In-training members have special consideration in fees and subscription rates to the Society journal. Such members cannot hold Society offices or vote.
2. Application must be on an official form and signed by the applicant and by the applicant's training or residency program director.
3. In-training status is limited to a maximum of five years starting with the entrance date into the radiology residency. In the last year, each in-training member will receive an application for active membership from the Society. Those who do not apply for transfer to active membership shall be dropped from membership at the end of the fifth year, but can later apply as a new member through the process outlined for active status.
4. There is no application fee. Annual dues are $25. Membership includes a subscription to the *American Journal of Roentgenology* and admission to the annual meeting without payment of the registration fee.
5. Membership applications will be acted on when received.

Corresponding Membership

A corresponding member must meet the qualifications of active membership, but reside and practice in a foreign country. Corresponding members shall pay dues and fees, but shall not have the privileges of voting nor of holding elective office.

All Applicants

1. **Do not remit application fee or dues until requested.**
2. **Send completed forms to: American Roentgen Ray Society**

1891 Preston White Drive
Reston, Virginia 22091

For ARRS
Office Use
Date Rec'd ______
I.D.# ______

AMERICAN ROENTGEN RAY SOCIETY
APPLICATION FOR MEMBERSHIP

Date: ______

Category of Membership: (Check One)
☐ Active
☐ Corresponding
☐ In-Training

Name (Please Print) ______ First Initial Last

Degree(s) ______

Mailing Address ______ Street/Box

______ City/State/Country Zip Code

Date of Birth ______

Telephone (   ) ______

A. Education: (List name of institution, years attended, and degree and type received.)

Undergraduate: ______

Graduate (Medical School, Graduate School, etc.): ______

Postgraduate (Internship, Residency, Fellowship, etc.): ______

B. Licensure:

Licensed to practice ______ (Type) in ______ (State, Province, etc.) since ______

C. Appointments/Memberships: (In-Training applicants: skip to Section F on reverse.)

Present Appointments: Academic ______

Hospitals ______

Memberships in Scientific Societies: ______

Offices or Committee Assignments: ______

Government Service (Military or Civilian) ______ (Position) (Years)

Continued on Reverse Side

D. Credentials:

I hereby certify that I was issued a certificate of qualification in ______________________ (Specialty)

in ______________ (Year) by the ______________________ (Name of Qualifying Board)

Other Credentials: ______________________

Signature: ______________________

E. References:

We, active or emeritus members in good standing of the American Roentgen Ray Society, and acquainted with the applicant, do recommend him/her for membership in the Society. (Two references are required.)

Name (Please Print) 1. ______________________ 2. ______________________

Address ______________________ ______________________

______________________ ______________________

Signatures: ______________________ ______________________

F. IN-TRAINING APPLICANTS MUST COMPLETE THIS SECTION

Credentials:

I certify that I am serving as a Resident/Fellow in ______________________ (Specialty)

at ______________________ (Name of Institution). Date program began (begins): ______________________;

date program to end: ______________________. I understand that in-training membership is limited to a maximum of 5 years.

Applicant Signature: ______________________

Verification: (Program Director or Department Chairman *only*)

I certify that the applicant is in training at the institution named and qualifies for enrollment as a member-in-training of the American Roentgen Ray Society.

Name (Please Print) ______________________

Address: ______________________

____

Signature ______________________

Send completed form to: **American Roentgen Ray Society**
1891 Preston White Drive
Reston, Virginia 22091

American Roentgen Ray Society:

Officers, Committees, and Membership Information

Officers

President: Ronald G. Evens
President-elect: M. Paul Capp
1st Vice-president: John A. Kirkpatrick, Jr.
2nd Vice-president: A. Everette James, Jr.
Secretary: Glen W. Hartman
Treasurer: Beverly P. Wood

Executive Council: R. J. Alfidi, R. N. Berk, B. G. Brogdon, M. P. Capp, W. J. Casarella, R. G. Evens, J. T. Ferrucci, Jr., R. A. Gagliardi, G. W. Hartman, J. A. Kirkpatrick, Jr., A. Landry, Jr., G. R. Leopold, J. E. Madewell, A. A. Moss, L. F. Rogers, J. H. Thrall, K. H. Vydareny, B. P. Wood, A. K. Poznanski, chairman

Committees

Editorial Policy: R. N. Berk, M. M. Figley, S. V. Hilton, M. S. Huckman, C. A. Rohrmann, Jr., S. S. Sagel, R. J. Stanley, N. O. Whitley, W. J. Casarella, chairman

Education and Research: C. B. Higgins, B. J. Hillman, R. A. McLeod, W. M. Thompson, B. G. Brogdon, chairman

Finance and Budget: R. J. Alfidi, R. C. Gedgaudas-McClees, G. R. Leopold, J. R. Thornbury, J. Thrall, chairman

Nominating: R. A. Gagliardi, N. O. Whitley, R. J. Alfidi, chairman

Publications: C. A. Rohrmann, Jr., S. S. Sagel, R. J. Stanley, N. O. Whitley, W. J. Casarella, chairman

Membership: R. J. Alfidi, A. A. Moss, K. H. Vydareny, G. R. Leopold, chairman

Representatives to Other Organizations

American Board of Radiology: J. A. Kirkpatrick, Jr., E. C. Klatte, L. F. Rogers

American College of Radiology: R. A. Gagliardi, G. A. Kling, J. E. Madewell, L. F. Rogers

American Medical Association House of Delegates: S. F. Ochsner, K. L. Krabbenhoft, alternate

American National Standards Institute: M. Haskin

National Council on Radiation Protection and Measurements: H. L. Friedell, E. L. Saenger

Meeting Arrangements

Annual Meetings: May 13–18, 1990, Sheraton Washington, Washington, DC; May 5–10, 1991, Sheraton Boston, Boston

Annual Meeting Committee: H. C. Carlson, J. K. Crowe, G. P. Janetos, R. R. Lukin, A. Landry, Jr., chairman

Instructional Courses: R. J. Stanley, associate chairman, J. T. Ferrucci, Jr., chairman

Scientific Program: R. J. Alfidi, E. Buonocore, D. O. Davis, K. B. Hunter, T. C. McLoud, W. A. Murphy, Jr., A. E. Robinson, L. B. Talner, J. H. Thrall, M. P. Capp, chairman

Scientific Exhibits: R. J. Churchill, A. A. Moss, R. G. Ramsey, J. E. Madewell, chairman

ARRS Membership

An application form is printed in this issue of the Journal. For consideration at the 1991 ARRS meeting, send completed forms before February 1, 1991, to American Roentgen Ray Society, 1891 Preston White Dr., Reston, VA 22091. Active members are graduates of an approved medical or osteopathic school or hold an advanced degree in an allied science. They must practice radiology or work in an associated science in the United States or Canada and be certified by the American Board of Radiology, American Osteopathic Board of Radiology, or Royal College of Physicians of Canada or otherwise adequately document training and credentials. Corresponding members are foreign radiologists or scientists who are active in radiology or an allied science. Members-in-training are residents or fellows in radiology or postgraduate students in an allied science. Additional application forms can be obtained from the ARRS offices in Reston, VA.

Business Office

Paul Fullagar, Executive Director, American Roentgen Ray Society, 1891 Preston White Dr., Reston, VA 22091; (703) 648-8900

Classified Advertisements

Positions Available

KEARNEY, NE, A BUSTLING COLLEGE TOWN Excellent opportunity for a BE/BC diagnostic radiologist to join a progressive, expanding, 3-person radiology group. 197-bed, community hospital-based practice with all imaging modalities. Presently have busy interventional practice; assistance needed with angiography. Prefer someone with neuroradiology interest. Other areas considered would be CT, MRI, and ultrasound. Above-average salary and fringe benefits. Rapid pathway to full partnership. Inquire at (308) 234-7555, or write to Great Plains Radiology, P. O. Box 2051, Kearney, NE 68848. 5–6ap

FLORIDA DIAGNOSTIC CENTER (east central coast) seeks a board-eligible/certified radiologist with recent training in nuclear medicine, ultrasound, CT scanning, and skeletal imaging. Must be personable. Send CV and salary requirements to Administrator, P. O. Box 693, Melbourne, FL 32902. 5ap

SUMMIT, NJ—Excellent opportunity for diagnostic radiologist with special interest in mammography to join private-practice group of 13 radiologists. University-affiliated, 600-bed community hospital with a radiology residency, located in a pleasant suburban setting 25 mi. from New York City. State-of-the-art equipment including Acuson with color Doppler, Siemens Somatom Plus CT, and a 1.5-T Magnetom. Competitive salary leading to partnership. Please send CV to A. Salomon, M.D., 151 Summit Ave., Summit, NJ 07901. 5–8ap

NORTHERN NEW JERSEY DIAGNOSTIC RADIOLOGIST—Half- or full-time position available for BC/BE radiologist to join established group in hospital and expanding outpatient practice. Applicant should be interested and experienced in all modalities of diagnostic radiology, except nuclear medicine, including MRI. Send letter and CV to Box A17, *AJR* (see address this section). 5–6ap

TEN-PERSON RADIOLOGY GROUP located in Corpus Christi is seeking a new associate to start July 1990, or as late as July 1991. Must be board-certified or eligible. Will perform all diagnostic studies, including interventional, CT, MRI, nuclear medicine, and ultrasound. Please send CV to Search Committee, P. O. Box 5608, Corpus Christi, TX 78465-5608. 5–6ap

MAINE—Excellent opportunity for BC/BE, MRI or neuroradiology fellowship-trained radiologist for general diagnostic position with progressive, well-established, small group. Live and work in college community in southern region close to coast, mountains, and lakes. Competitive compensation package leading to partnership. Affiliate with 200-bed, modern community hospital. Send CV to New England Health Search, 63 Forest Ave., Orono, ME 04473; (207) 866-5680 or (207) 866-5685. 5–6ap

BC/BE IN RADIOLOGY—Excellent opportunity to join 5-member group based at MacNeal Hospital, a 427-bed, progressive teaching facility with university affiliation, in western suburb of Chicago. All state-of-the-art modalities including 2 GE 9800 CT scanners, ultrasound, nuclear medicine with SPECT, mammography, and interventional radiology suite, all located in the newly rebuilt, modern replacement facility of the hospital. MRI located in free-standing adjacent facility. Ideal candidate should be BC/BE in radiology, energetic, and progressive, with an interest in general diagnostic radiology. Competitive salary and benefits leading to equal parity. Send CV to Jeanette Simons, Division of Physician Affairs, MacNeal Hospital, 3249 S. Oak Park Ave., Berwyn, IL 60402. 5–6a

THE DEPT. OF RADIOLOGY AT NEW ENGLAND MEDICAL CENTER HOSPITALS has a new staff position available. Time will be divided evenly between the 2 sections of CT/MRI and ultrasound. Both of these areas are active clinically and academically. The hospital (450 beds) is the major teaching site of Tufts University School of Medicine. Any interested candidate should contact either Mark S. Bankoff, M.D., CT/MRI, or Frederick J. Doherty, M.D., Director of Ultrasound, New England Medical Center Hospitals, 750 Washington St., Boston, MA 02111; (617) 956-0043 CT/MRI, (617) 956-6340 ultrasound. 5ap

WESTERN MARYLAND—Radiologist needed to join a very successful, 3-person group in a hospital-based practice with separate billing. This group is very progressive and has a varied practice, performing procedures that range from diagnostic studies to MRI. They are affiliated with a 240-bed hospital in a highly rated city in beautiful western Maryland. An extremely attractive salary and benefits package is offered for a board-certified or eligible radiologist. Contact Bill Lowderman, 3939 Roswell Rd., N.E., Ste. 100, Marietta, GA 30062; (800) 759-3020. 5ap

DIAGNOSTIC RADIOLOGIST, TEXAS—Position available immediately for BC radiologist with competency in MRI, CT, and ultrasound. Eight radiologists, 6 with fellowships, in 30-yr-old partnership. Well-diversified practice with 2 hospitals, 2 offices, and an imaging center. Early partnership; excellent salary and benefits. Mild, dry climate, strong economy, 4-yr university, and friendly people add up to a great quality of life. Interested parties send CV to Todd Samuels, M.D., Lubbock Radiology Associates, 3707 21st St., Lubbock, TX 79410. 5ap

NEURORADIOLOGIST—Immediate faculty opening for a fellowship-trained neuroradiologist to join an evolving neuroimaging center at the University of Oklahoma Health Sciences Center, Oklahoma City, OK. Academic rank determined by previous experience. Salary and benefits are highly competitive. Strong commitment to teaching and research desired. Must be board-certified and eligible for senior membership in the ASNR. Send cover letter and CV to Don A. Wilson, M.D., MR Center of Oklahoma (BMR-10), P. O. Box 26307, Oklahoma City, OK 73126. Affirmative action/equal opportunity employer. 5–10a

IMMEDIATE OPENING—Four board-certified radiologists seek a 5th for a dynamic diagnostic and interventional practice in a multispecialty clinic attached to a 200-bed hospital. All imaging modalities are represented. Excellent benefit package includes health, life, disability and malpractice insurance, profit-sharing plan, and continuing medical education. Fargo is on the Minnesota-North Dakota state line, 30 mi. from the Minnesota lake country, 250 mi. from both Minneapolis-St. Paul, MN, and Winnipeg, Canada. Contact Douglas Landers, M.D., Dakota Clinic, Ltd., Box 6001, Fargo, ND 58108; (701) 280-3321. 5–10a

CHALLENGING LOCUM TENENS POSITIONS AVAILABLE NOW—Work at your convenience, full- or part-time. Competitive compensation. No hassles, politics, or paperwork. Paid malpractice insurance, housing, and transportation. Put an experienced leader to work for you! Contact LOCUM Medical Group, 30100 Chagrin Blvd., Cleveland, OH 44124; (800) 752-5515. 5–8xap

NORTHWEST WASHINGTON—Progressive, 7-person group seeks a BC radiologist preferably with a fellowship in body imaging or nuclear medicine. Complete imaging including CT, MR, angio/interventional, ultrasound, nuclear medicine, and mammography provided at 2 hospitals and 3 offices. Excellent salary and benefits with potential for early partnership. Reply Box A13, *AJR* (see address this section). 5–7a

PEDIATRIC RADIOLOGISTS—Vacancies are available in various parts of the pediatric radiology dept. at The Hospital for Sick Children, Toronto. The hospital is a 560-bed, tertiary-care pediatric center situated in downtown Toronto and affiliated with the University of Toronto. Staff includes 17 full-time pediatric radiologists and 7 fellows; 100,000 exams are performed each yr. Positions are available in general pediatric radiology areas and in more specialized areas such as neuroradiology. The dept. is equipped with state-of-the-art equipment. Applicants must have had previous pediatric radiology experience including 1- and preferable 2-yr fellowship. Staff radiologists with greater experience are certainly most welcome. For further information, please contact A. Daneman, M.D., Radiologist-in-Chief, Dept. of Radiology, The Hospital for Sick Children, 555 University Ave., Toronto, Ontario, M5G 1X8, Canada; (416) 598-6026. 5–6a

NUCLEAR MEDICINE—Excellent opportunity for diagnostic radiologist with special interest in nuclear medicine, special competency preferred, to join private-practice group of 13 radiologists. University-affiliated, 600-bed community hospital with a radiology residency, located in a pleasant suburban setting 25 mi. from New York City. State-of-the-art equipment including Acuson with color Doppler, Siemens Somatom Plus CT, and 1.5-T Magnetom. Competitive salary leading to partnership. Please send CV to A. Salomon, M.D., 151 Summit Ave., Summit, NJ 07901. 5–8ap

CHAIRPERSON, DEPT. OF RADIOLOGY, STATE UNIVERSITY OF NEW YORK AT BUFFALO—Applications are being accepted for the position of professor and chairperson of the Dept. of Radiology, State University of New York at Buffalo. Applicants should have an M.D. degree, should have successfully completed a residency in radiology approved by the ACGME, and should be certified by the American Board of Radiology or have equivalent qualifications. Applicants should demonstrate evidence of leadership and achievement in academic radiology with significant accomplishments in clinical, educational, administrative, managerial, and investigative endeavors. Candidates must qualify as professor with tenure. Please send letter of application and CV to Gerald Sufrin, M.D., Chairman, Radiology Search Committee, State University of New York at Buffalo, 100 High St., Buffalo, NY 14203. Application deadline is June 30, 1990. SUNY at Buffalo, AA/EEOC. 5a

RADIOLOGIST—BC/BE to join a group of 4 radiologists at the university/county hospital complex in El Paso, TX. Should be skilled in all forms of imaging and general diagnostic radiology including pediatrics. The hospital is a major trauma center with a busy emergency room and obstetrical practice. The work is interesting and challenging. The candidate will have time for clinical research and will have the support of the Texas Tech School of Medicine, including a large library and complete audiovisual facilities. Compensation is negotiable depending on the candidate's qualifications and experience. El Paso is a city of 500,000 people with yr-round sunny and warm weather. Contact Lloyd K. Mark, M.D., Professor and Associate Chairman, Dept. of Radiology, Texas Tech University HSC, 4800 Alberta St., El Paso, TX 79905; (915) 545-6845. 5–7a

SOUTHERN OREGON—Opportunity for BC/BE, general diagnostic radiologist to join group of 5 board-certified radiologists. Experience in all modalities desired. Practice includes 2 hospitals and own private office. Competitive starting salary with early full partnership. Excellent lifestyle with many outdoor activities from Pacific Coast to Oregon Cascades. Send CV to Larry Strickland, Administrator, Roseburg Radiologists, P.C., P. O. Box 1547, Roseburg, OR 97478. 5–10ap

WANTED—Full- and/or part-time BE/BC diagnostic radiologist, with MRI experience and interventional training desirable, to join 4-person group in 200-bed community hospital and private office setting doing 50,000 exams per yr. All imaging modalities offered. Located in Reading, PA, with population in metropolitan area of 300,000. Family-oriented suburban life with excellent schools, recreation, and cultural activities. One hr to Philadelphia, 2½ hr to New York City or Washington, and 2 hr to the Poconos or seashore. Competitive salary and benefits leading to partnership for full-time position. Write with CV to Jonathan L. Stolz, M.D., Director, Dept. of Radiology, Community General Hospital, 145 N. Sixth St., Reading, PA 19601. 5–6ap

CONNECTICUT—BC/BE radiologist needed for general radiology, mammography, and ultrasound in private office practice. All replies confidential. Reply to Box A15, *AJR* (see address this section). 5ap

DIAGNOSTIC RADIOLOGIST/GASTROINTESTINAL IMAGING, Yale New Haven Medical Center, Yale University School of Medicine. Superb opportunity for a person interested in the highest quality practice combining the best of academic and clinical resources. Applicant should be an enthusiastic person interested in all aspects of gastrointestinal imaging including conventional barium radiography and CT. An effort will be made to accommodate additional interests. Salary and rank are most competitive and commensurate with experience, in addition to an excellent fringe package. Please send inquiries along with CV to Morton Burrell, M.D., Professor of Radiology, Director of Gastrointestinal Radiology, Yale University School of Medicine, 333 Cedar St., New Haven, CT 06510. Yale University is an equal opportunity/affirmative action employer; applications from women and minority groups are encouraged. Application deadline is June 30, 1990. 5–6a

WANTED, JULY 1991—Young, outgoing, BC/BE general radiologist to work in 120-bed community medical center (1 of 2 Missoula, MT, hospitals) covered by 6-person group. We seek someone with special interest in ultrasound and mammography, but also experienced in angiography, CT, and MRI. Position leads to directorship of dept. in 3 yr. One yr to full partner income, 2 yr to full partnership. Missoula, in mountainous western Montana, is the home of the University of Montana and offers a progressive medical environment with over 150 physicians, as well as abundant recreational opportunities including skiing, fishing, hunting, and backpacking. Send CV to Missoula Radiology, Inc., P. O. Box 2039, Missoula, MT 59806. 5–9ap

ACADEMIC HEAD, CANADA—Applications are invited for the position of head of the Dept. of Diagnostic Radiology at Queen's University. The qualified applicant shall hold certification in radiology, have a relevant background in teaching and research, and be eligible for licensure in Ontario, Canada. Candidates of either sex are equally encouraged to apply. Nominations and applications, including CV, should be directed to D. G. Sinclair, M.D., Vice-Principal, Health Sciences and Dean, Faculty of Medicine, Queen's University, Kingston, Ontario, Canada K7L 3N6. This position is now open. 5a

BC DIAGNOSTIC RADIOLOGIST—Private office imaging center. Five-day work wk, no call. MRI (GE 1.5), CT (GE 9800), ultrasound, nuclear medicine, SPECT, mammography, routine radiography, and fluoroscopy. First yr salary and benefits, $175,000. Send CV to Desmond Fischer, M.D., 1301 McCallie Ave., Chattanooga, TN 37404; (615) 622-7212. 5–8ap

RADIOLOGIST—An excellent opportunity to work in the beautiful Rocky Mountains of British Columbia in the Columbia Valley. A fully qualified diagnostic radiologist with ultrasound qualifications is required by 2 rural hospitals 120 km apart; Golden and District General Hospital and Windermere District Hospital. Golden Hospital does a variety of general radiologic procedures and provides ultrasound. The Windermere Hospital is similar without ultrasound at present. Golden and District General Hospital has 25 acute beds, 8 extended beds, and a freestanding, 29-bed, intermediate-care facility. Windermere has 27 acute beds and 4 extended beds. Each community hospital serves an area population of approximately 8500 (this population grows during the summer and winter months). Six GPs at Golden with 1 pediatrician, 4 GPs and 1 surgeon at Windermere. An excellent recreational area, skiing, hiking, golf, and swimming. Please write, phone, or fax Ms. L. Ritchie, Administrator, Golden and District General Hospital, P. O. Box 1260, Golden, B.C., Canada V0A 1H0; Phone (604) 334-5271; Fax (604) 344-2511. 4–5a

MINNEAPOLIS-ST. PAUL, INTERVENTIONAL NEURORADIOLOGIST—Incumbent interventional neuroradiologist needs help in handling rapidly expanding interventional neuro case load. Present full-time, 3-member neuroradiology section is a growing and active component of a 21-member practice based in 800-bed, tertiary-care facility in Minneapolis-St. Paul. Private practice with academic affiliation and appointments. This practice currently operates 2 MRI and 7 CT scanners. Three additional MRI scanners will be installed in the near future. Excellent starting salary and benefits. Short track to full partnership. Minneapolis-St. Paul consistently places in the top 10 of the most livable U.S. cities and recently was ranked #1 in the country as a place to raise children. Outstanding cultural, outdoor, and athletic activities immediately accessible. The opening represents an outstanding and unique practice opportunity for the right person. Please submit all inquires with CV to Philip Murray, M.D., Dept. of Radiology, Abbott Northwestern Hospital, 800 E. 28th St., Minneapolis, MN 55407. 4–5a

NUCLEAR MEDICINE/IMAGING—Twelve-person radiology practice has an opening for a diagnostic radiologist with experience/expertise in nuclear medicine. Practice is hospital-based with full range of equipment. Will share duties with 1 other fellowship-trained nuclear medicine radiologist. Cardiac nuclear imaging experience required. Please send letter of inquiry and CV to Richard D. Herman, M.D., Chairman, Dept. of Radiology, St. Luke's Hospital, Bethlehem, PA 18015. 4–6ap

TWO BOARD-CERTIFIED/ELIGIBLE GENERAL DIAGNOSTIC RADIOLOGISTS to join expanding, 11-person group covering 2 hospitals and 2 MR sites. Ideal private practice in a stable midwest community using all imaging modalities and interventional techniques. Can start immediately or wait until July 1990. Excellent opportunity with excellent salary and benefits. Send CV to Joseph F. Norfray, M.D., MR Center of Springfield, 319 E. Madison, Springfield, IL 62701. 4–7ap

PEDIATRIC RADIOLOGIST—William Beaumont Hospital is a modern, tertiary-care medical center with a strong residency and fellowship program in diagnostic radiology. We are seeking a pediatric radiologist to join the full-time pediatric radiologist on our staff. The medical center is located in southeastern Michigan, with nearby desirable living areas and summer and winter resort activities. Compensation and benefits are generous and very competitive. Send CV to Jalil Farah, M.D., Chairman, Diagnostic Radiology, William Beaumont Hospital, 3601 W. 13 Mile Rd., Royal Oak, MI 48072. 4–5a

NEURORADIOLOGIST—The University of Texas Health Science Center at San Antonio is seeking a qualified academic neuroradiologist to fill an immediate opening. Send cover letter and CV to John R. Jinkins, M.D., Director of Neuroradiology, The University of Texas Health Science Center, 7703 Floyd Curl Dr., San Antonio, TX 78284-7800. 3–8ap

PRACTICE IN THE COASTAL PLAIN OF NORTH CAROLINA at a well-established 100-bed hospital seeks third radiologist. 23,000/24,000 procedures/yr. General radiology including mammography, CT, ultrasound, and nuclear medicine. No angio, interventional, or MRI. Compensation and benefits competitive. Available immediately. Contact Roanoke-Chowan Radiology Associates, Inc., P. O. Box 459, Ahoskie, NC 27910; (919) 332-6011. 3–6ap

BC/BE RADIOLOGIST, preferably with training and experience in neuroradiology, to join 5-member radiology group in Savannah, GA. Practice includes coverage of 300-bed, acute-care hospital and new private office. Excellent facilities with state-of-the-art CT, nuclear medicine with SPECT, general and vascular ultrasonography, mammography, fluoroscopy, neuro/angio/interventional, and MRI. Generous salary and benefits with early partnership. Savannah is an attractive coastal community with expanding economy and outstanding year-round recreational resources. Send CV with letter of inquiry to Thomas H. Philbrick, M.D., Savannah Radiologists, P. O. Box 14444, Savannah, GA 31499. 3–5ap

RADIOLOGIST—Associate diagnostic radiologist to join a 4-radiologist group in Massachusetts. Hospital and private practice. All diagnostic modalities. Interest in angiography and interventional radiology preferred. Reply Box Y54, *AJR* (see address this section). 3–5ap

NUCLEAR MEDICINE—Immediate opening in large, progressive radiology group in the Central New Jersey/Bucks County, PA, region for recently trained person with a nuclear medicine fellowship with emphasis on cardiac imaging. Must be willing to do all other facets of noninvasive radiology. Four-hospital group has 8 cameras and 3 SPECT units. Send letter and CV to L. Ratner, M.D., 838 W. State St., Trenton, NJ 08618. 4–6a

DARTMOUTH-HITCHCOCK MEDICAL CENTER, DEPT. OF RADIOLOGY is offering 2 permanent positions for BC/BE, GI/GU radiologists at the Mary Hitchcock Memorial Hospital. This is a 400-bed hospital with 80 radiology personnel who perform 55,000 inpatient and 45,000 outpatient exams/yr. The dept. consists of 13 staff and 9 residents covering the full range of modern radiologic practice. Become a member of the 200-physician, academic, multispecialty group that forms the clinical faculty of Dartmouth Medical School. Position has responsibility for a full scope of general diagnostic procedures. Interest in teaching essential, research desirable. Interested candidates should write to P. K. Spiegel, M.D., Dartmouth-Hitchcock Medical Center, Dept. of Radiology, 2 Maynard St., Hanover, NH 03756. AA/EOE. 5xa

ORTHOPEDIC RADIOLOGIST—A position is available at the University of Rochester Medical Center, Strong Memorial Hospital, Dept. of Radiology, a 750-bed, tertiary-care facility. An appointment as assistant professor or higher is available at a level appropriate to experience. Research and teaching opportunities are available in a strong academic dept. with state-of-the-art radiologic equipment. Send CV to Robert E. O'Mara, M.D., Professor and Chair, Diagnostic Radiology, Box 648, University of Rochester Medical Center, Rochester, NY 14642. EO/AA/M-F employer. 3–6ap

RADIOLOGIST—Full-time; nice, small, well-located North Carolina town. Join active, hospital-based, service-oriented practice. General diagnostic, nuclear medicine, ultrasound, CT, and mobile MRI. No arteriography. Reply with CV to Box Y50, *AJR* (see address this section). 3–5ap

IMMEDIATE OPENING—BC/BE radiologist to join medium-sized group in Austin, TX. Special interest, expertise, or fellowship training in body imaging and/or interventional radiology is necessary. Practice covers major trauma center and outpatient radiology facility. In addition to general diagnostic services, outpatient facility also provides CT and MRI services on 2 GE 9800 scanners and on GE 1.5-T and 0.5-T MR units. Applicants are requested to contact Drs. Gray, Lava, or Boyd at 711 W. 38th St., Ste. B-8, Austin, TX 78705; (512) 454-8718. 3–5ap

FULL-TIME BC RADIOLOGIST needed to staff outpatient women's diagnostic center in suburban Dallas. Experience in mammography and OB/GYN sonography preferred. No call responsibilities. Attractive compensation package. Send CV to Box Y56, *AJR* (see address this section). 5xa

OPPORTUNITY FOR YOUNG, WELL-TRAINED, AGGRESSIVE RADIOLOGIST to join 5-person group in a small, midwestern city near St. Louis. Excellent equipment including mobile MRI. Competitive salary leading to early partnership. Reply to Box U40, *AJR* (see address this section). 5xa

ISRAEL, DIAGNOSTIC RADIOLOGY. Opportunities for 3–4 week or longer working vacations in a number of Israeli medical centers, on a volunteer basis. Positions varied, arrangements flexible. For information contact: Jonathan H. Fish, M.D., 1844 San Miguel Dr., #302, Walnut Creek, CA 94596; (415) 947-0560. 5–7xa

NEURORADIOLOGIST/MRI—Two positions available; Fellowship training a necessity. Group of 7 radiologists seek BC colleague in multihospital practice. Must be capable as general diagnostic radiologist as well. Position available July 1990. Send letter and CV to Neel E. Bennett, M.D., Medical Director and Chairman, Dept. of Radiology, Holy Cross Hospital, 1050 E. South Temple, Salt Lake City, UT 84102; (801) 350-4636. 5xa

NEURORADIOLOGIST—The Dept. of Diagnostic Imaging/Radiology of Sinai Hospital of Detroit is seeking an individual with appropriate training and interest in performing and interpreting neuroradiologic exams. The hospital is about to open an off-site imaging center with MRI and CT capabilities. The person hired will be the Medical Director of this center but also will have responsibilities in neuroradiology at the main hospital. The hospital is a tertiary-care, university-affiliated institution with a thriving residency program. The dept. consists of 13 radiologists in private practice on a fee-for-service, separate billing arrangement. Candidates should have an interest in teaching and research. Apply to Philip N. Cascade, M.D., Chairman, Dept. of Diagnostic Imaging/Radiology, Sinai Hospital of Detroit, 6767 W. Outer Dr., Detroit, MI 48235-2899; (313) 493-5906. 4–5ap

LAKES REGION, CENTRAL NEW HAMPSHIRE A predominantly hospital-based practice of 3 radiologists seeks an additional recently trained radiologist with expertise in all imaging modalities. State-of-the-art equipment available in recently expanded/renovated hospital. Potential to become full partner in 1-1/2 yr with no buy-in. Practice located in Laconia, NH, in the "Lakes Region" at southern border of White Mountains. Lake Winnipesaukee and several major ski facilities nearby. For more information, please contact Benjamin Tuttle, M.D., Chairman, Dept. of Medical Imaging, Lakes Region General Hospital, Elliot St., Laconia, NH 03246; (603) 527-2900. 4–5ap

FACULTY POSITIONS AVAILABLE IN DIAGNOSTIC RADIOLOGY—The University of Miami School of Medicine is currently recruiting a 4th full-time vascular and interventional radiologist. The interventional section provides radiologic services at Jackson Memorial Medical Center and Veterans Administration Medical Center. We perform approximately 3000 exams/yr in the section. The vascular and interventional section performs all angiographic procedures except for cardiac and neuroradiologic studies. These include all diagnostic and interventional vascular procedures. We also have an active nonvascular service involving thoracic and abdominal intervention. This includes all percutaneous liver procedures, percutaneous nephrostomies, abscess drainages, and percutaneous gastrostomy placements. The section currently consists of 3 staff members and 4 fellows. Residents rotate through the service on a monthly basis. Please submit CV to Jose M. Yrizarry, M.D., University of Miami School of Medicine, Dept. of Radiology (R-109), P. O. Box 016960, Miami, FL 33101; (305) 549-6894. 4–5ap

OREGON—Group of 12 radiologists in Salem, OR, seeks BC/BE radiologist with general radiology skills. Special competence in nuclear medicine desirable, but not mandatory. Practice includes 450-bed community hospital, large office, and a multispecialty clinic. Send CV to John Eyre, M.D., c/o Salem Radiology, 919 Oak St. S.E., Salem, OR 97301. 4–6ap

VIRGINIA'S CHESAPEAKE BAY—BC/BE general radiologist for 100-bed, full-service rural hospital. All modalities including mobile MRI, no angio currently. Closely associated with regional medical center and multispecialty group for backup. Wonderful waterfront lifestyle possibilities. Available July 1, 1990. Send CV to Box Z82, *AJR* (see address this section). 4–5ap

UNIQUE OPPORTUNITY—Permanent part-time position for diagnostic radiologist to work weekends, or more if desired, in exciting Las Vegas at a university-affiliated hospital with a large private group. Ample time to enjoy the many regional recreational activities. Candidates should be well-trained general radiologists with basic skills in ultrasound and CT. Angiography not required. Generous salary and fringe benefits. Contact Brent Birkin, M.D., 3848 Pima Ln., Las Vegas, NV 89109; (702) 384-5210 (7 a.m. to 5 p.m.) or (702) 732-0559 (after 6 p.m.). 4–6ap

ABDOMINAL RADIOLOGIST—The Dept. of Radiology at the Albany Medical College has an immediate opening for a faculty position in abdominal imaging. The candidate should have fellowship training or demonstrated experience in cross-sectional imaging. Clinical duties will be in ultrasound, body CT, body MR, and GI/GU. The candidate also will participate in medical student and postgraduate education and be able to pursue clinical and basic research interests. Academic rank and salary are commensurate with experience. The dept. has 23 attending staff, 3 fellows, and 16 residents. Please contact James C. Peters, M.D., Interim Chairman, Dept. of Radiology, Albany Medical College, 43 New Scotland Ave., Albany, NY 12208; (518) 445-3277. Albany Medical College is an equal opportunity/affirmative action employer. 3–5ap

RADIOLOGIST—This 52-physician, multispecialty clinic is seeking a second radiologist for general radiologic procedures excluding CT and MRI. Experience or formal training in mammography required. Located in western Montana, abundant 4-season recreational opportunities. Offered salary and benefits generous. Send CV to Administrator, Western Montana Clinic, P. O. Box 7609, Missoula, MT 59807. 4–5ap

ANGIOGRAPHY/INTERVENTIONAL RADIOLOGIST—Position available at the New Jersey Medical School, Newark, NJ, July 1, 1990. Academic position will include resident supervision, scholarly activity, and clinical practice. Excellent equipment. Rapidly developing institution and dept. Recent completion of fellowship in angio/interventional and board-certification, or current faculty member in current academic section in angio/interventional would be considered. Compensation starting at $150,000 for entry level. Please contact Gail Eliot, M.D., Acting Chairperson, Dept. of Radiology, NJMS, University Hospital, C-320, 150 Bergen St., Newark, NJ 07103; (201) 456-5188 or 5189. 3–5ap

BE/BC GENERAL DIAGNOSTIC RADIOLOGIST, experienced in CT, ultrasound, mammography, and nuclear medicine, wanted for established 2-person practice at 150-bed community hospital in rural southeastern Virginia. Opening July 1990. Competitive salary, benefits. Send CV to Box Y70, *AJR* (see address this section). 3–5ap

DIAGNOSTIC RADIOLOGIST WITH SPECIAL INTEREST IN ANGIOGRAPHY AND INTERVENTIONAL RADIOLOGY—The Dept. of Radiology at the University of Texas Medical School at Houston has an immediate opening at the Hermann Hospital, and an opening for July 1, 1990, at the Lyndon Baines Johnson General Hospital, for an experienced interventionist/angiographer with strong interest in patient care and teaching. Research interest and experience are important, but not essential. Although the principal responsibilities will be in intervention/angiography, there will be an opportunity to be involved in other clinical areas of the candidate's interest. The position will include teaching at the medical student and resident levels. Candidate must be a diplomate of the ABR and have completed at least a 1-yr interventional/angiography fellowship, have a Texas state medical license, and have had at least 1 yr postfellowship experience. Candidates with the qualifications for a senior assistant professor or associate professor appointment are preferred. Academic rank will be commensurate with qualifications. Compensation will be based on the most recent AAMC survey and the candidate's qualifications and experience. Please submit CV, along with the names and addresses of 3 references, to John H. Harris, Jr., M.D., D. Sc., Professor and Chairman, Dept. of Radiology, The University of Texas Medical School at Houston, 6431 Fannin, Ste. 2.132, Houston, TX 77030. The University of Texas Health Science Center at Houston is an equal opportunity employer. Women and minorities are encouraged to apply. 1–6a

ASSISTANT, ASSOCIATE, OR FULL PROFESSOR OF THORACIC RADIOLOGY—The University of Texas Medical School at Houston has an opening for a thoracic radiologist to perform clinical thoracic radiology exams and procedures and participate in resident and medical student teaching. Candidates should have completed an approved residency in diagnostic radiology and must have postresidency experience or training in thoracic radiology. Candidates must be board-certified by the ABR, or equivalent, and must have a Texas medical license. Compensation will be based on the most recent AAMC survey and the candidate's qualifications. Applicants should send a CV, along with the names and addresses of 3 references, to John H. Harris, Jr., M.D., D.Sc., Professor and Chairman, Dept. of Radiology, The University of Texas Medical School at Houston, 6431 Fannin St., Ste. 2.132, Houston, TX 77030. The University of Texas Health Science Center at Houston is an equal opportunity employer and encourages women and minority candidates to apply. 1–6a

FACULTY POSITIONS AVAILABLE IN DIAGNOSTIC RADIOLOGY—On July 1, 1990, the faculty of the University of Texas Medical School at Houston (UTMSH) will assume clinical practice, teaching, and research at the Lyndon Baines Johnson (LBJ) General Hospital, newly constructed by the Harris County Hospital District, in Houston, TX. LBJ General will be a principal medical student teaching affiliation of the UTMSH, is certified for 300 beds (with expansion capabilities to approximately 500 beds) and is projected to perform approximately 130,000 imaging procedures the first yr. The Dept. of Radiology at LBJ is fully equipped with new, state-of-the-art GE equipment, including a 9800 Quick CT scanner with 3-D software and an LU angiographic unit, and comparable routine, R&F, ultrasound, and nuclear equipment. Full-time UTMSH faculty positions exist for 5 associate professors and 10 assistant professors with clinical, teaching, and research interests in all aspects of diagnostic imaging. Residents who have just completed training and are board-certified will be offered the rank of assistant professor at an annual salary of $90,000. Fellows who have completed training and are board-certified will be offered the rank of assistant professor at an annual salary of $100,000. These salaries may be increased depending on the candidate's education and experience beyond either residency or fellowship, and in addition to base salary, total fringe benefits of approximately 20% of the base salary will be provided. Associate professor compensation will be based on the most recent AAMC survey and the candidate's qualifications. Candidates must be diplomates of the ABR, or its equivalent, and must have a Texas medical license. Applicants are requested to send their CV to John H. Harris, Jr., M.D., D.Sc., Professor and Chairman, Dept. of Radiology, The University of Texas Medical School at Houston, 6431 Fannin St., Ste. 2.132, Houston, TX 77030. The University of Texas Health Science Center at Houston is an equal opportunity employer. Women and minorities are encouraged to apply. 1–6a

ASSISTANT OR ASSOCIATE PROFESSOR OF NEURORADIOLOGY—The University of Texas Medical School at Houston has openings for neuroradiologists at the Lyndon Baines Johnson General Hospital and the Hermann Hospital to perform clinical neuroradiology and participate in resident and medical student teaching. Candidates must have completed an approved residency in diagnostic radiology and a 2-yr neuroradiology fellowship. Candidates must be board-certified by the ABR, or equivalent, and must have a Texas medical license. Compensation will be based on the most recent AAMC survey and the candidate's qualifications. Applicants should send a CV, along with the names and addresses of 3 references, to John H. Harris, Jr., M.D., D.Sc., Professor and Chairman, Dept. of Radiology, The University of Texas Medical School at Houston, 6431 Fannin St., Ste. 2.132, Houston, TX 77030. The University of Texas Health Science Center at Houston is an equal opportunity employer and encourages women and minority candidates to apply. 1–6a

GENERAL RADIOLOGIST needed July 1, 1990, or sooner to replace retiring member of 3-person group servicing a small but busy hospital in scenic area of western Pennsylvania; also own private outpatient office. Necessary skills: general, CT, ultrasound, mammography, and nuclear medicine. Generous salary with early advancement to partnership available. Contact Alan Stankiewicz, M.D., 623 Lang Ave., Patton, PA 16668; (814) 674-8508. 12–5ap

PART-TIME RADIOLOGIST wanted to do routine diagnostic work in central western Pennsylvania, near Pittsburgh. No specials. Apply to Box R14, *AJR* (see address this section). 5ap

DIRECTOR OF CLINICAL MAGNETIC RESONANCE—The Dept. of Radiology at the University of Texas Medical School at Houston has an opening for a radiologist at the assistant, associate, or full professor level, who will direct clinical activities, medical student and resident teaching, and clinical research in the university MRI center at Hermann Hospital. Candidate will be expected to conduct or direct clinical or basic research in MR leading to grant support. Candidates must have demonstrated experience in direction of a clinical MRI unit, teaching, research, writing, and obtaining grant support, and have a strong publication background. Candidate must be board-certified by the ABR and must have a Texas medical license. Compensation will be based on the most recent AAMC survey and candidate's qualifications. Please forward a CV, and the names and addresses of 3 references, to John H. Harris, Jr., M.D., D. Sc., Professor and Chairman, Dept. of Radiology, The University of Texas Medical School at Houston, 6431 Fannin, Ste. 2.132, Houston, TX 77030. The University of Texas Health Science Center at Houston is an equal opportunity employer and encourages women and minority candidates to apply. 1–6a

NORTHERN CALIFORNIA/SAN FRANCISCO BAY AREA—The Permanente Medical Group is seeking a BC radiologist with multimodality interests and fellowship training in MR or interventional radiology to join a 10-person group serving a 337-bed acute-care hospital and 2 outpatient clinics. Teaching opportunities are available with residents of subspecialty services on rotation from Stanford University Hospital and our own medical residents. We are currently siting a GE 1.5-T MRI system and installing a new LU arm. Competitive salary and excellent benefits. Please send inquiries and CV to Bruce Baker, M.D., Chief, Dept. of Radiology, Kaiser-Permanente Medical Center, 900 Kiely Blvd., Santa Clara, CA 95051; (408) 236-4444. EOE. 5–7a

THE RADIOLOGY DEPT., University of Massachusetts Medical Center, is seeking a full-time radiologist with interest in trauma, emergency room, and musculoskeletal radiology. The Medical Center is a 370-bed university hospital and medical school located in Worcester, MA, approximately 40 mi. west of Boston. The dept. consists of 19 clinical staff, 12 residents, and 3 fellows and soes approximately 120,000 exams/yr. The dept. is well-equipped with 2 fourth-generation CT scanners, two 1.5-T GE MR scanners, and a 2.0-T small-bore unit for animal research. The hospital is a major traums center and is serviced by 2 Life Flight helicopters. The candidate must be board-eligible/certified and have a clinical background in skeletal radiology. Please send CV/requests to Dr. Edward H. Smith, Chair, Dept. of Radiology, University of Massachusetts Medical Center, 55 Lake Ave. N., Worcester, MA 01655. The University of Massachusetts Medical Center is an equal opportunity employer. 3–5a

ULTRASOUND/CT/MRI—Opportunity for board-certified radiologist specializing in ultrasound, body CT, and body MRI to pursue academic career at The New York Hospital-Cornell Medical Center. Dept. provides state-of-the-art equipment, including Acuson ultrasound, GE 9800 CT, and GE Signa 1.5-T MR. Wide variety of ultrasound exams include abdominal, OB-GYN, color Doppler, small parts, neonatal head, transvaginal, and transrectal. Prefer candidate with prior fellowship in sectional imaging or ultrasound. Responsibilities include clinical practice, teaching, and research. Position available 7/1/90 or earlier. Please send CV to Elias Kazam, M.D., Dept. of Radiology, The New York Hospital-Cornell Medical Center, 525 E. 68th St., New York, NY 10021. 4–6ap

ASSISTANT, ASSOCIATE, OR FULL PROFESSOR OF DIAGNOSTIC RADIOLOGY—The University of Texas Medical School at Houston has an opening for a general diagnostic radiologist to perform clinical radiologic exams and procedures and to participate in resident and medical student teaching. Candidates should have completed an approved residency in diagnostic radiology. Postresidency experience or training would be preferable, but not mandatory, at the assistant professor level. Candidates must be board-certified by the ABR, or equivalent, and must have a Texas medical license. Compensation will be based on the most recent AAMC survey and the candidate's qualifications. Applicants should send a CV, along with the names and addresses of 3 references, to John H. Harris, Jr., M.D., D.Sc., Professor and Chairman, Dept. of Radiology, The University of Texas Medical School at Houston, 6431 Fannin St., Ste. 2.132, Houston, TX 77030. The University of Texas Health Science Center at Houston is an equal opportunity employer and encourages women and minority candidates to apply. 1–6a

SEATTLE AREA—Opening for a BC general diagnostic radiologist with basic angio and interventional skills. Washington license not required. Teaching hospital, regular hours, limited call, and 5-yr contract. Call G. Bernstein, M.D.; (206) 840-9652. 4–6xa

SITKA, ALASKA—Challenging diagnostic radiology practice, JCAHO-accredited Alaska Native Indian Health Service Hospital. Includes ultrasound and mammography. Close professional association with primary-care physicians. Requires acceptance in USPHS Commissioned Corps. Send inquiries, CV, and references to S. Carlson, M.D., Clinical Director, Mt. Edgecumbe Hospital, 222 Tongass Dr., Sitka, AK 99835; (907) 966-8310. 1–5ap

ULTRASOUND RADIOLOGIST—The University of Tennessee, Memphis/University Physicians Foundation has an opening for a radiologist in ultrasound at the instructor or assistant professor level. Applicant must be board-certified/eligible in diagnostic radiology. Additional training in ultrasound is highly desirable and the applicant should be particularly conversant with obstetric ultrasonography. Blacks, women, handicapped, and other minorities are encouraged to apply. The University of Tennessee, Memphis/University Physicians Foundation is an equal employment opportunity/affirmative action/Title IX/Section 504 employer. Send CV to Barry Gerald, M.D., Chairman, Dept. of Radiology, University of Tennessee, Memphis, 800 Madison Ave., Memphis, TN 38163. 5xa

PEDIATRIC RADIOLOGIST—The University of Tennessee, Memphis/University Physicians Foundation has an opening for a pediatric radiologist. Faculty rank of assistant or associate professor based on experience. Applicant must be board-certified/eligible in diagnostic radiology. At least 1 yr of postgraduate training in a recognized program in pediatric radiology is required. Primary work sites will be LeBonheur Children's Medical Center and St. Jude Children's Research Hospital. Blacks, women, handicapped, and other minorities are encouraged to apply. The University of Tennessee, Memphis/University Physicians Foundation is an equal employment opportunity/affirmative action/Title IX/Section 504 employer. Address inquiries to Barry Fletcher, M.D., Chairman, Diagnostic Imaging Dept., St. Jude Children's Research Hospital, 332 N. Lauderdale, Memphis, TN 38101, or Robert A. Kaufman, M.D., Director, Dept. of Radiology, The University of Tennessee, Memphis/LeBonheur Children's Medical Center, 800 Madison Ave., Memphis, TN 38163. 5xa

RADIOLOGIST, TYLER, TX—The University of Texas Health Center at Tyler, Dept. of Radiology, Tyler, TX, invites applications for a faculty position at the level of assistant or associate professor, to open July 1, 1990. Interest in teaching and/or research is desired but not required. Progressive, 4-person dept. practices general radiology including interventional, with a total of 27,000 exams/yr. The University of Texas Health Center at Tyler, the state's designated chest disease hospital, is located just outside of Tyler on a beautiful, 600-acre campus amid the forests and lakes of East Texas. The dept. also supports a rapidly growing, dynamic research group located on campus in a new, state-of-the-art research facility. Year-round tennis, golf, and boating are available in addition to excellent schools. Competitive first-yr salary and an unsurpassed benefits package are offered. Send CV to J. R. Shepherd, M.D., University of Texas Health Center at Tyler, P. O. Box 2003, Tyler, TX 75710; (214) 877-7100. The University of Texas Health Center at Tyler is an affirmative action, equal opportunity employer. Minorities are encouraged to apply. 12-5a

DIAGNOSTIC RADIOLOGIST—The University of Tennessee, Memphis/University Physicians Foundation has an opening for a radiologist at the instructor or assistant professor level. Applicant must be board-certified/eligible in diagnostic radiology. Subspecialty interests are encouraged but not required. Blacks, women, handicapped, and other minorities are encouraged to apply. University of Tennessee, Memphis/University Physicians Foundation is an equal employment opportunity/affirmative action/Title IX/Section 504 employer. Send CV to Barry Gerald, M.D., Chairman, Dept. of Radiology, University of Tennessee, Memphis, 800 Madison Ave., Memphis, TN 38163. 5xa

VASCULAR/INTERVENTIONAL RADIOLOGIST The University of Maryland is seeking an additional faculty member, with fellowship training, for its Section of Vascular and Interventional Radiology. The medical center is an 800-bed, acute-care hospital and tertiary referral center with an active and varied interventional practice. A new 324-bed VA hospital is now under construction and will be adjacent to and connected to the university. The duties of the new faculty member will be limited to vascular and interventional radiology. Interested persons should contact Gerald S. Johnston, M.D., Dept. of Diagnostic Radiology, 22 S. Greene St., Baltimore, MD 21201; (800) 866-8667, ext. 3477. Affirmative action/equal opportunity employer. 3&5ap

DIAGNOSTIC RADIOLOGIST—BC/BE to join 2 radiologists in 50-physician, multispecialty clinic. Fellowship in body imaging preferred. Practice includes general radiography, CT, ultrasound, MRI, and film-screen mammography. Excellent first yr salary leading to partnership. Send CV to Michael D. Lavine, M.D., 333 Dixie Hwy., Chicago Heights, IL 60411. 5-7ap

DIAGNOSTIC RADIOLOGY, PACIFIC NORTHWEST, MRI, CT AND ULTRASOUND—Progressive group of 4 radiologists seeks board-certified radiologist with subspecialty interest and expertise in MRI, CT, and ultrasound. Busy, dynamic practice in regional medical center hospital, privately owned MRI center (presently mobile unit—planning for fixed site in spring 1990), plus private outpatient office. Located in beautiful recreation area in the inland Northwest. World-class lakes for boating and sailing. Excellent skiing, hunting, and fishing. Family-oriented environment 30 min from Spokane. Competitive starting salary with full partnership in 1 yr. Send CV to Richard Hehn, M.D., Radiology Associates of North Idaho, 1104 Ironwood Dr., Coeur d'Alene, ID 83814; (208) 667-0686- 5-7ap

Positions Desired

JULY 1990 PGY-3 RADIOLOGY RESIDENCY SOUGHT—Current PGY-2 radiology resident seeking PGY-3 position. Have training in plain film, CT, ultrasound, nuclear medicine, and angiography. Reply to Box A9, *AJR* (see address this section). 5-7bp

GENERAL DIAGNOSTIC RADIOLOGIST—Board-certified, MRI fellowship. Four yr angio/interventional experience in busy practice. Prefer general diagnostic with some subspecialization. Competent in nuclear medicine and ultrasound. Desire partnership opportunity. Impeccable references. Available July 1990. Reply Box Y52, *AJR* (see address this section). 3-6bp

Fellowships and Residencies

FELLOWSHIPS AT THOMAS JEFFERSON UNIVERSITY HOSPITAL—The Dept. of Radiology at Thomas Jefferson University Hospital in Philadelphia offers the following fellowship programs each yr. Ultrasound/CT/MRI—Jefferson has 1 of the largest and most modern ultrasound facilities in the world, performing 40,000 exams of all types per yr. This includes obstetrical, vascular, lithotripsy, invasive, endoluminal, etc. We also operate 3 CT scanners and 4 GE 1.5-T MRI units. Contact Barry Goldberg, M.D., regarding this program. Cardiovascular/interventional—This division is housed in a new suite with state-of-the-art Philips units with digital subtraction angiography, and performs the full range of both vascular and nonvascular interventional procedures. Contact Geoffrey Gardiner, Jr., M.D. Neuro/ENT radiology—Very active clinical services supply a wealth of material to this division, which is housed in a Neurosciences Imaging Center containing all imaging modalities in a single comprehensive facility. Contact Carlos Gonzalez, M.D. Chest/breast imaging—Jefferson's new Breast Imaging Center performs approximately 85 studies/day. Contact Stephen Feig, M.D., or Robert Steiner, M.D. MRI—This is a dedicated body MRI program and includes excellent research opportunities, in addition to a large clinical caseload. Contact Matthew Rifkin, M.D. Musculoskeletal—This program includes MRI of the musculoskeletal system. Contact David Karasick, M.D. All program directors listed above can be contacted at the Dept. of Radiology, Thomas Jefferson University Hospital, Philadelphia, PA 19107. Jefferson is an equal opportunity/affirmative action employer. 5xc

FELLOWSHIP IN MR IMAGING at Central Massachusetts Magnetic Imaging Center, July 1991 through June 1992. CMMIC is a consortium of 3 area teaching hospitals, including a university hospital with a mixture of clinical and research responsibilities, dedicated to furthering the applications and addressing the educational requirements of MRI. CMMIC currently uses 2 clinical 1.5-T GE Signa systems capable of multifaceted imaging as well as a 2.0-T GE Fremont CSI research system. The fellowship will include thorough training in MRI physics, imaging principles, clinical applications, and image interpretation. Duties will include image interpretation of neurologic, musculoskeletal, pediatric, and cardiac studies; daily supervision of scanning; teaching file maintenance; and participation in CMMIC's numerous teaching and research responsibilities. Requirements include satisfactory completion of a 4-yr accredited radiology training program and board-eligibility or certification. Please send inquiries to Ronald Ragland, M.D., Medical Director, CMMIC, Inc., 367 Plantation St., Worcestor, MA 01605. 5-6cp

BODY IMAGING FELLOWSHIP, JULY 1990—CT/ultrasound/MRI. Clinical and research activities in all areas tailored to the fellow's and dept. goals. Should have interest in teaching and research. GE 9800 CT, GE 1.5-T Signa MRI, Acuson and Diasonics ultrasound. Full resident complement. Four body-imaging faculty. Send CV to Fred W. Flickinger, M.D., Body Imaging Section, Dept. of Radiology, Medical College of Georgia, 1120 15th St., Augusta, GA 30912-3900. 5-7c

FELLOWSHIP POSITIONS—Applications are invited now for July 1991. Positions are available in neuroradiology, vascular/interventional radiology, and body imaging (CT/ultrasound/MRI). For information, contact James R. Schmidgall, M.D. or Richard W. Katzberg, M.D., Chairman, Dept. of Radiology, L-340, Oregon Health Sciences University, 3181 S. W. Sam Jackson Park Rd., Portland, OR 97201. 7-6c

CARDIOVASCULAR-INTERVENTIONAL RADIOLOGY FELLOWSHIP—Available July 19, 1989. One-year fellowship program at a 750-bed teaching hospital. Extensive clinical experience involving all aspects of cardiovascular imaging, interventional vascular and nonvascular procedures, and availability for clinical or animal research. Send CV and Inquiries to Oscar H. Gutierrez, M.D., Dept. of Radiology, Box 648, University of Rochester Medical Center, Rochester, NY 14642. An equal opportunity employer (M/F). 1-6c

NEURORADIOLOGY FELLOWSHIP, THOMAS JEFFERSON UNIVERSITY HOSPITAL—An unexpected opening for a neuroradiology fellow is available in the Dept. of Radiology at Thomas Jefferson University Hospital, beginning July 1990. The Division of Neuroradiology has close clinical and research relationships with Jefferson's very active neurology, neurosurgery, orthopedic surgery, and otolaryngology depts. Complete training in ENT radiology is part of this program. Five full-time faculty members currently staff this division. Clinical facilities include 2 dedicated CT scanners, a myelography room, a biplane angiography room with DSA, and a GE 1.5-T MRI unit. Two more MRI units will be operational by the summer of 1990. Contact Carlos Gonzalez, M.D., Director of Neuroradiology, 1009 Main Bldg., Thomas Jefferson University Hospital, Philadelphia, PA 19107; (215) 928-5447. Jefferson is an affirmative action/equal opportunity employer. 5xc

FELLOWSHIP IN PEDIATRIC RADIOLOGY—LeBonheur Children's Medical Center/St. Jude Children's Research Hospital/The University of Tennessee, Memphis/University Physicians Foundation, Inc. combined program in pediatric radiology offers a 1- or 2-yr fellowship in pediatric radiology. There are approximately 75,000 pediatric exams performed annually by 10 full-time radiologists. Two fellowship positions are available annually. Training includes all aspects of pediatric imaging, including neonatal, neuro, nuclear, oncologic, cardiovascular, special and interventional procedures, ultrasound, CT, and MRI. Facilities include Doppler ultrasound, CT, and MRI. Opportunity to participate in MRI and other imaging research. Blacks, women, handicapped, and other minorities are encouraged to apply. The University of Tennessee, Memphis/University Physicians Foundation, Inc. is an equal employment opportunity/affirmative action/Title IX/Section 504 employer. Address inquiries to Barry D. Fletcher, M.D., Chairman, Diagnostic Imaging Dept., St. Jude Children's Research Hospital, 332 N. Lauderdale, Memphis, TN 38101 or Robert A. Kaufman, M.D., Director, Dept. of Radiology, LeBonheur Children's Medical Center/The University of Tennessee, Memphis, 800 Madison Ave., Rm. 114C Chandler, Memphis, TN 38163. 5xc

FELLOWSHIPS IN PEDIATRIC RADIOLOGY, JULY 1991—The Dept. of Radiology, Children's Hospital Medical Center, Cincinnati, OH, offers 1- or 2-yr fellowships in pediatric radiology beginning July 1991. Children's Hospital Medical Center is a 355-bed institution where approximately 100,000 radiological exams are performed annually by 13 full-time faculty radiologists. Four fellowship positions are available annually. Training includes all aspects of pediatric imaging: neonatal radiology, neuroimaging, musculoskeletal radiology, cardiovascular and thoracic imaging, abdominal imaging, oncologic imaging, ultrasonography, nuclear medicine, CT, MRI, and vascular/interventional techniques. Facilities include digital fluoroscopy, Acuson and ATL ultrasound units with Doppler and color-flow Doppler capabilities, Gamma and SPECT tomographic nuclear cameras, GE 9800 Quick CT scanner, 1.5-T GE MRI, and cardiac catheterization/angiographic suite with digital vascular imaging. Numerous opportunities to participate in both clinical and basic research. Salary and fringe benefits are highly competitive. Candidates must be board-certified or board-qualified in diagnostic radiology and must be able to obtain an Ohio medical license. Children's Hospital Medical Center and the University of Cincinnati College of Medicine are affirmative action/equal opportunity employers. Address inquiry and CV to Donald R. Kirks, M.D., Director, Dept. of Radiology, Children's Hospital Medical Center, Elland and Bethesda Aves., Cincinnati, OH 45229-2899; (513) 559-8058. 1–12cp

IMAGING FELLOWSHIP (CT, ULTRASOUND, MRI)—William Beaumont Hospital, a 970-bed, modern, tertiary-care, teaching and academic institution in southeast Michigan, offers a 1-yr fellowship in sectional body imaging. The fellowship will provide extensive clinical experience in body CT, ultrasound, and MRI, including CT- and ultrasound-guided procedures, conventional and color flow Doppler exams, prostatic and endovaginal sonography. Ample elective time is also provided for other rotations of interest to fellow. Candidates must be board-certified or board-eligible in diagnostic radiology and have a valid Michigan medical license. Four positions are available for July 1991. Salary and fringe benefits are highly competitive. For further information, write to Ali Shirkhoda, M.D., Chief of Imaging Division, William Beaumont Hospital, 3601 W. 13 Mile Rd., Royal Oak, MI 48073; (313) 551-1001. 4–6c

MRI FELLOWSHIP AT THOMAS JEFFERSON UNIVERSITY HOSPITAL—A new MRI fellowship position has been created in the Dept. of Radiology of Thomas Jefferson University Hospital, Philadelphia. This 1-yr position encompasses a full range of clinical and research activities. The MRI division includes 6 staff physicians, 2 MRI physicists, and 3 Signa systems (1.5T). The position is available as of Jan. 1990, but applications will also be taken for the academic year beginning in July 1990. Send inquiries to Matthew Rifkin, M.D., Dept. of Radiology, Thomas Jefferson University Hospital, Philadelphia, PA 19107. Jefferson is an equal opportunity/affirmative action employer. 9–6c

FELLOWSHIP IN ULTRASOUND AND BODY CT/MRI—July 1, 1991 to June 30, 1992, at the New York Hospital/Cornell Medical Center. Dept. provides state-of-the-art equipment, including Acuson ultrasound, GE 9800 CT, and GE Signa 1.5-T MR. Wide variety of ultrasound exams include abdominal, OB-GYN, color Doppler, small parts, neonatal head, transvaginal, and transrectal. Applicants should be ABR eligible or certified. Send CV to Elias Kazam, M.D., Dept. of Radiology, The New York Hospital/Cornell Medical Center, 525 E. 68th St., New York, NY 10021. 4–6cp

FELLOWSHIPS IN ABDOMINAL IMAGING—The Dept. of Radiology at the University of Texas Medical School at Houston has openings for 2 abdominal imaging fellowships to begin July 1991. Under faculty direction and supervision, candidates will further their training in the specialty of abdominal imaging including CT, ultrasound, and MRI through 4-mo rotations in each service. Candidate will participate in teaching in each section at the medical student and resident levels, will have the opportunity to conduct basic or clinical research, and will be expected to prepare and submit at least 1 scientific article to an appropriate refereed journal. Candidate must be a graduate of an approved U.S. medical school or its equivalent, must have completed an approved residency in diagnostic radiology, must be a diplomate of the ABR, and must have a Texas medical license. Please submit CV, along with the names and addresses of 3 references, to John H. Harris, Jr., M.D., D.Sc., Professor and Chairman, Dept. of Radiology, The University of Texas Medical School at Houston, 6431 Fannin St., Ste. 2.132, Houston, TX 77030. The University of Texas Health Science Center at Houston is an equal opportunity employer. Women and minorities are encouraged to apply. 1–6c

THE UNIVERSITY OF PITTSBURGH offers fellowships in angiography/interventional radiology, abdominal imaging (CT/ultrasound/MRI), neuroradiology, pediatric radiology, and MRI. Positions in all of these areas are available to begin July 1991. A fellowship position in pediatric radiology and 1 in abdominal imaging are also available to begin July 1990. Interested applicants should send letters of inquiry and CV to Lawrence A. Cooperstein, M.D., Dept. of Radiology, Presbyterian-University Hospital, DeSoto at O'Hara Sts., Pittsburgh, PA 15213. 3–7cp

FELLOWSHIPS IN NEURORADIOLOGY—The Dept. of Radiology at the University of Texas Medical School at Houston has openings for 1- and 2-yr neuroradiology fellowships to begin July 1990 and July 1991. Under faculty supervision, candidates will be responsible for neuroradiologic exams and procedures (i.e., angiograms, myelograms, CT, MR imaging, and in vivo spectroscopy). The candidate will participate in teaching at the medical student and resident levels and will conduct basic or clinical research. Candidate must be a graduate of an approved U.S. medical school or its equivalent, must have completed an approved residency in diagnostic radiology, must be a diplomate of the ABR, and must have a Texas medical license. Please submit CV, along with the names and addresses of 3 references, to John H. Harris, Jr., M.D., D.Sc., Professor and Chairman, Dept. of Radiology, The University of Texas Medical School at Houston, 6431 Fannin St., Ste. 2.132, Houston, TX 77030. The University of Texas Health Science Center at Houston is an equal opportunity employer. Women and minorities are encouraged to apply. 1–6c

Tutorials/Courses

WORKSHOP—NATO Advanced Study Institute (ASI), Picture Archiving and Communication System (PACS) in Medicine, Evian, France, Oct. 14–26, 1990. The aim of this ASI workshop is to bring 80 participants for intensive presentation and probing discussions on PACS. The theme of this meeting is to emphasize "how to." Cost per person including room and board for the full duration is $645 single, $585 double. No registration fee is required. There is limited funding to support participation. For more information, please contact Professor H. K. Huang, M.D., Division of Medical Imaging, Dept. of Radiological Sciences, UCLA School of Medicine, Los Angeles, CA 90024-1721, U.S.A.; (213) 206-1045. FAX: (213) 206-2967. 5–8d

INTERNATIONAL SYMPOSIUM & COURSE, LIVER IMAGING—Present and future trends in MRI, CT, and ultrasound. Presented by Massachusetts General Hospital, Dept. of Radiology, at The Westin Hotel, Copley Place, Boston, June 25–27, 1990. Program Director: Joseph T. Ferrucci, M.D., Co-Director: David D. Stark, M.D. A distinguished international faculty with pioneering experience will present up-to-date results with new clinical imaging techniques. Invited lecturers and discussions will be complemented by proferred scientific papers, technical exhibits by manufacturers, and original syllabus material. The program will be directed to radiologists as well as academic and industrial researchers in the imaging sciences. Contact Dept. of Cont. Medical Ed., Harvard Medical School, Boston, MA 02115; (617) 432-1525 or P. O. Box 825, Boston, MA 02117. $450/$350 Residents. 21 hr of category I credit. 5d

5th ANNUAL IMAGING SEMINAR—Topnotch at Stowe, VT. October 5–8, 1990. Category I accreditation. For information, contact Carol McClure, Coordinator, Dept. of Radiology, Medical Center Hospital of Vermont, 111 Colchester Ave., Burlington, VT 05401; (802) 656-3592. 4–5d

SIXTH ANNUAL LONDON-PARIS ULTRASOUND CONGRESS, SEPTEMBER 15–22, 1990—Category I accreditation followed by OPTIONAL LOIRE VALLEY BICYCLE TOUR. For information contact Medical Seminars International, Inc., 9800 D Topanga Canyon Blvd., Ste. 232, Chatsworth, CA 91311; (818) 700-9821. 3–8d

ALASKA 90—CRUISE THE INLAND PASSAGE, July 6–13, 1990. Patrick Colletti, M.D., University of Southern California. MRI tutorial and course. Category I CME credits. For information, contact Medical Seminars International, Inc., 9800 D Topanga Canyon Blvd., Ste. 232, Chatsworth, CA 91311; (818) 700-9821. 1–6d

Other

X-RAY FILM FOR SALE FROM NATIONWIDE DISTRIBUTOR—Very attractive prices and excellent service. Freight prepaid and no sales tax. Orders phoned in before noon are shipped out by UPS the same day. We ship anywhere in the world. No minimum order necessary. For information, prices, and free samples, please contact Dacco Enterprises, 7350 S.W. 48th St., Miami, FL 33155; USA (800) 222-8242. 5–8ep

VISITING PROFESSORSHIP, THOMAS JEFFERSON UNIVERSITY HOSPITAL—The Dept. of Radiology at Thomas Jefferson University Hospital in Philadelphia offers a visiting professorship in our Division of General Diagnostic Radiology. The position commences July 1990 and will be available for 2 yr, while several of our faculty members are on sabbatical leave. Funding for the position is appropriate for a senior faculty member from another institution on sabbatical with partial funding or for a junior faculty member. In addition to working in the General Diagnostic Division, the visiting radiologist will have access, for research or educational purposes, to state-of-the-art MRI, CT, and ultrasound units, and to well-equipped physics and physiology research laboratories. Liberal research time will be available. Interested individuals should contact David C. Levin, M.D., Chairman, Dept. of Radiology, Thomas Jefferson University Hospital, Philadelphia, PA 19107. Jefferson is an equal opportunity/affirmative action employer. 11–10e

AJR Classified Advertisements Information

Box Responses and Address for Ad Placement

Write Box ______, AJR, 2223 Avenida de la Playa, Suite 200, La Jolla, CA 92037-3218; (619) 459-2229; FAX: (619) 459-8814.

How to Place an Ad

AJR accepts classified advertising for Positions Available, Positions Desired, Fellowships and Residencies, and Tutorials/Courses. Ads are accepted by mail or FAX.

Rates: $6.00/line with a $30 minimum charge. Box service is $10 additional for each month the ad appears. There are discounts for multiple insertions: 10% for 2–3 insertions; 20% for 4 or more. To estimate lines, count all words and divide by 7.

Billing: Ads *must* be prepaid, or advertisers will be billed after the ad appears *providing* a purchase order number is submitted with the advertising copy. Terms are net 30 days.

Deadlines: 6 weeks prior to issue date. For specific deadlines, telephone the AJR editorial office.

Estimating Ad Charges

Line charge: divide total words by 7 and multiply by $6.00 . . . . . $ ______
Multiple insertions? If so, multiply by number . . . . × ______
Subtotal . . . . $
Discount applies to two or more insertions. Subtract 10% if ad appears 2–3 months, 20% if 4 months or more . . . . − ______
Subtotal . . . . $
Box response requested? If so, multiply number of months by $10.00 . . . . + ______
Approximate advertising charge . . . . $

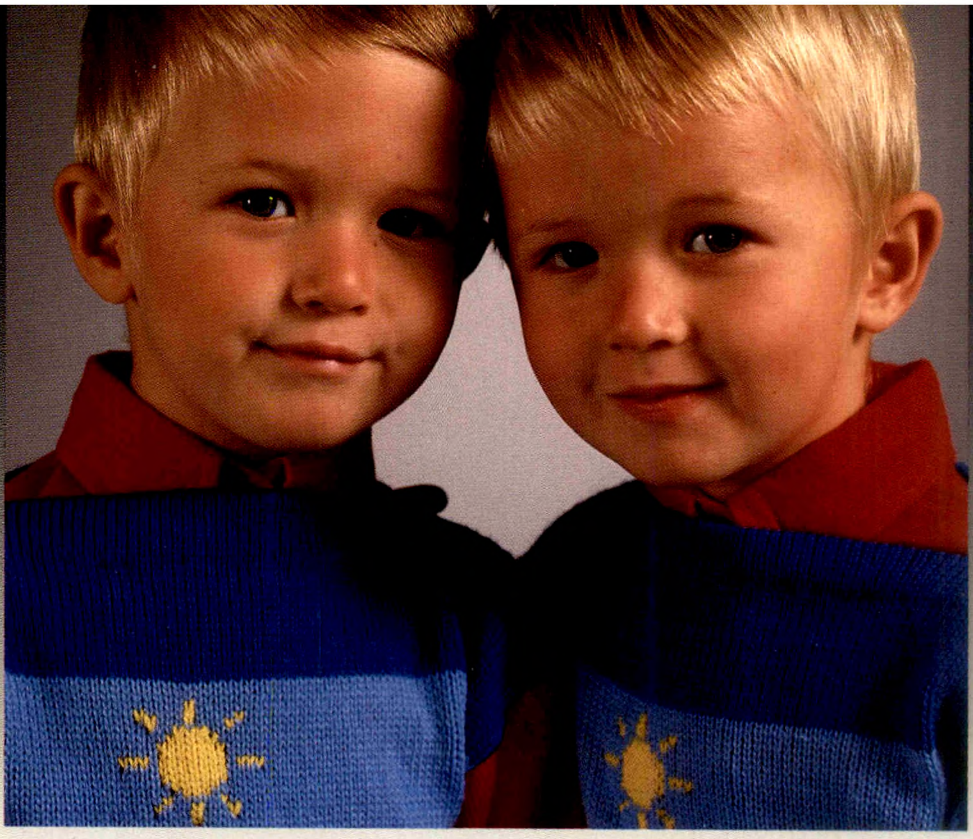

When is the duplicate as good as the original?

In nature the "twin" is almost always as good as the original, but in medical radiography . . . rarely. That's why Fuji developed a superior duplicating film which will consistently give faithful reproductions with contrast and image values right up there with the original.

Frankly, nature still has us beat . . . but that's as it should be. For the next best duplicating process, call your Fuji representative or 800-431-1850.

CIRCLE 7 ON READER SERVICE CARD

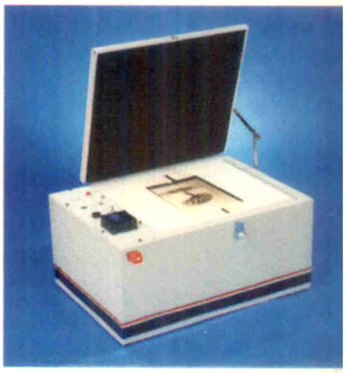

Fuji's high quality Radiographic Duplicato
provides reliable and convenient original

The Reason for Change!

Burbank – Chicago – Stamford CT.

Volume 154

American Journal of Roentgenology

May 1990

HANSON LECTURE

927 **Adrenal imaging: current status.** *Dunnick NR*

PROGRESS IN RADIOLOGY

937 **MR angiography.** *Edelman RR, Mattle HP, Atkinson DJ, Hoogewoud HM*
947 **Percutaneous ethanol injection therapy for the treatment of hepatocellular carcinoma.** *Shiina S, Tagawa K, Unuma T, Terano A*

REVIEW ARTICLES

953 **Physiology and radiology of the normal oral and pharyngeal phases of swallowing.** *Dodds WJ, Stewart ET, Logemann JA*
965 **Radiologic assessment of abnormal oral and pharyngeal phases of swallowing.** *Dodds WJ, Logemann JA, Stewart ET*

CHEST RADIOLOGY

975 **Comparison of Biello, McNeil, and PIOPED criteria for the diagnosis of pulmonary emboli on lung scans.** *Webber MM, Gomes AS, Roe D, La Fontaine RL, Hawkins RA*
983 **Bronchiolitis obliterans organizing pneumonia: CT features in 14 patients.** *Müller NL, Staples CA, Miller RR*
989 **MR imaging of thoracic and abdominal wall infections: comparison with other imaging procedures.** *Sharif HS, Clark DC, Aabed MY, Aideyan OA, Haddad MC, Mattsson TA*
997 **Case report. Laryngeal chondrosarcoma: CT findings in three patients.** *Muñoz A, Peñarrocha L, Gallego F, Olmedilla G, Poch-Broto J*
999 **Case report. Wooden foreign body in the lung parenchyma.** *Spouge AR, Weisbrod GL, Herman SJ, Chamberlain DW*

GASTROINTESTINAL RADIOLOGY

1003 **Percutaneous gastrostomy with gastropexy: experience in 125 patients.** *Saini S, Mueller PR, Gaa J, et al.*
1007 **Angioplasty for long-term treatment of patients with Budd-Chiari syndrome.** *Martin LG, Henderson JM, Millikan WJ Jr, Casarella WJ, Kaufman SL*
1011 **CT of the abdomen after the Whipple procedure: value in depicting postoperative anatomy, surgical complications, and tumor recurrence.** *Coombs RJ, Zeiss J, Howard JM, Thomford NR, Merrick HW*
1015 **Case report. Hepatic subcapsular hematoma: an unusual complication of biliary lithotripsy.** *McGrath FP, Lee SH, Gibney RG, Burhenne HJ*

MUSCULOSKELETAL RADIOLOGY

1017 **Adult ankle fractures: comparison of plain films and interactive two- and three-dimensional CT scans.** *Magid D, Michelson JD, Ney DR, Fishman EK*
1025 **Insufficiency fracture of the sternum caused by osteopenia: plain film findings in seven patients.** *Chen C, Chandnani V, Kang HS, et al.*
1029 **Pictorial essay. The Neer classification of displaced proximal humeral fractures: spectrum of findings on plain radiographs and CT scans.** *Kilcoyne RF, Shuman WP, Matsen FA III, Morris M, Rockwood CA*

PEDIATRIC RADIOLOGY

1035 **Review article. Differentiation of child abuse from osteogenesis imperfecta.** *Ablin DS, Greenspan A, Reinhart M, Grix A*
1047 **Commentary. Differentiation of child abuse and osteogenesis imperfecta: medical and legal implications.** *Kleinman PK*
1049 **Case report. Prenatal detection of an abdominal mass by MR imaging performed while the fetus is immobilized with pancuronium bromide.** *Tomá P, Lucigrai G, Dodero P, Lituania M*
1051 **Case report. Castleman disease in the neck: atypical appearance on CT.** *Chaloupka JC, Castillo M, Hudgins P*

NEURORADIOLOGY

1053 **The role of ferritin and hemosiderin in the MR appearance of cerebral hemorrhage: a histopathologic biochemical study in rats.** *Thulborn KR, Sorensen AG, Kowall NW, et al.*
1061 **Carotid artery disease assessed by color Doppler flow imaging: correlation with standard Doppler sonography and angiography.** *Steinke W, Kloetzsch C, Hennerici M*
1069 **Pseudoatrophy of the cervical portion of the spinal cord on MR images: a manifestation of the truncation artifact?.** *Yousem DM, Janick PA, Atlas SW, et al.*

ENDOCRINE RADIOLOGY

1075 **The diagnosis of acromegaly: value of inferior petrosal sinus sampling.** *Doppman JL, Miller DL, Patronas NJ, et al.*
1079 **CT evaluation of anaplastic thyroid carcinoma.** *Takashima S, Morimoto S, Ikezoe J, et al.*
1087 **Nonsurgical treatment of primary hyperparathyroidism with sonographically guided percutaneous injection of ethanol: results in a selected series of patients.** *Karstrup S, Holm HH, Glenthøj A, Hegedüs L*

ANGIOGRAPHY AND INTERVENTIONAL RADIOLOGY

1091 **A solution to the problem of high-flow jets from miniature angiographic catheters.** *Daniel TB, Akins EW, Hawkins IF Jr*
1097 **Case report. Transcatheter thrombosis of a leaking saccular aneurysm of the main renal artery with preservation of renal blood flow.** *Routh WD, Keller FS, Gross GM*
1101 **Technical note. Use of the Hawkins-Hunter rocket wire in the biliary system.** *Shaw DWW, Coldwell DM, Kimmey M, Goldman ML*
1103 **Technical note. Complications from 0.018-in. floppy platinum tip guidewires.** *Quinn SF, Morse S*
1105 **Case report. Phlegmasia cerulea dolens, a complication after placement of a bird's nest vena cava filter.** *Aruny JE, Kandarpa K*

RADIOLOGIC TECHNOLOGY

1107 **Evaluation of radiographs developed by a new ultrarapid film processing system.** *Schmidt RA, Doi K, Sekiya M, et al.*

PERSPECTIVES

1111 **The radiology manpower equation: a new look.** *Brogdon BG*
1117 **Quality improvement in diagnostic radiology.** *Cascade PN*

OTHER CONTENT

952 **Memorial, Glen W. Hartman**
Book and videotape reviews 964, 982, 988, 1002, 1024, 1028, 1034, 1060, 1074, 1078, 1096, 1100
1086 **Memorial, Robert James Borgerson**
1121 **Letters**
1129 **Review of current literature**
1134 **Forthcoming articles**
1135 **News**
1138 **ARRS membership information and application**
1141 **American Roentgen Ray Society Information**
1142 **Classified advertisements**
A3 **Guidelines for authors**
A8 ***AJR* business and subscriber information**

1990 ARRS Meeting: May 13–18, Washington, DC

Ame
Jou
Roe

Jun

544-4624.

may be attached as an option
imize cross-contamination.

Excellent coa
even in a wet

12. 4. 91

Official Journal of the American Roentgen Ray Society

AJR

American Journal of Roentgenology
Diagnostic Imaging and Related Sciences

Editor-In-Chief Robert N. Berk, *La Jolla, California*
University of California, San Diego
School of Medicine and Medical Center

Editor Emeritus Melvin M. Figley, *Seattle, Washington*

Associate Editor Saskia von Waldenburg Hilton, *San Diego, California*

Consulting Editor Michael S. Huckman, *Chicago, Illinois*

Statistician Charles C. Berry, *San Diego, California*

Editorial Board

John R. Amberg
Itamar Aviad
Mark E. Baker
Lawrence W. Bassett
Michael A. Bettmann
Felix S. Chew
N. Reed Dunnick
David K. Edwards
Ronald G. Evens
David S. Feigin
Sandra K. Fernbach
Richard H. Gold
William R. Hendee
John R. Hesselink
Charles B. Higgins
Melvyn T. Korobkin
Faye C. Laing
Thomas L. Lawson
Robert G. Levitt
Bruce L. McClennan
Richard P. Moser
Albert A. Moss
Jeffrey H. Newhouse
Donald L. Resnick
Stewart R. Reuter
Charles A. Rohrmann, Jr.
Peter M. Ronai
Sjef H. J. Ruijs
Stuart S. Sagel
David J. Sartoris
Stefan C. Schatzki
William P. Shuman
Edward A. Sickles
Barry A. Siegel
David D. Stark
Edward T. Stewart
Murali Sundaram
Eric vanSonnenberg
Robert K. Zeman

Editorial Staff: Margaret Levene, *managing editor*; Katie L. Spiller, Barbara Rose, Barbara L. Halliburton, and Janine Anderson, *manuscript editors*; Nancy Rydbeck, *office manager*; Sheri Smith, *administrative assistant*; Sandra L. Griffin, *administrative secretary*.

AJR, AMERICAN JOURNAL OF ROENTGENOLOGY (ISSN 0361 803X) is the official journal of the American Roentgen Ray Society and is published monthly by Williams & Wilkins, 428 E. Preston St., Baltimore, MD 21202. Annual dues include $50 for journal subscription. Second-class postage paid at Baltimore, MD, and at additional mailing offices. Postmaster, send address changes (Form 3579) to AJR, 428 E. Preston St., Baltimore, MD 21202. Subscription rates $110 ($155 foreign, $244 Japan); institutions $120 ($165 foreign, $254 Japan); in training $25 ($70 foreign, $159 Japan); single copy $16 ($19 foreign). Japanese rates include airfreight. Japanese yen price is available from our sole agent USACO Corporation, 13-12, Shimbashi 1-Chome, Minato-Ku, Tokyo 105, Japan, telephone 03-502-6471. Airmail rates furnished on request. Indexed by *Current Contents* and *Index Medicus*. Copyright © 1990 by American Roentgen Ray Society.
0361-803X/90$2.00

You learn from your experience with

CONTEMPORARY DIAGNOSTIC RADIOLOGY

Editor: **Robert E. Campbell, M.D.**

A Biweekly Review of Clinical Radiologic Practice—26 issues a year!

One of your toughest jobs is keeping up with the many new developments that affect radiology. That's why you want **Contemporary Diagnostic Radiology**... an effective and convenient way to perfect your skills and maintain your professional status.

Contemporary Diagnostic Radiology is designed as a continuing education program that lets you work at your own pace. Every two weeks you'll receive an issue that covers a single topic or procedure in detail. Read the information and study the clearly reproduced radiographs—and then, if you choose, respond to a comprehensive examination in the strictest confidence. You set the pace.

Each biweekly lesson brings you pertinent review of the basics in bone radiology... gastrointestinal radiology... pediatric radiology... genitourinary radiology... MR imaging... and all of the topics you want to know more about.

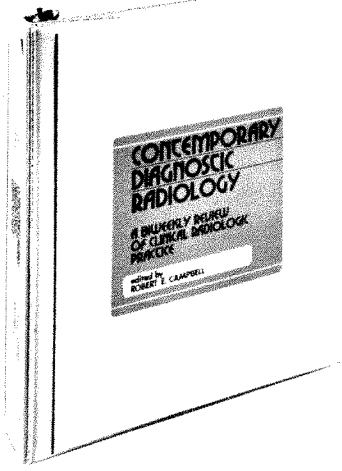
CONTEMPORARY
DIAGNOSTIC
RADIOLOGY
A BIWEEKLY REVIEW OF CLINICAL RADIOLOGIC PRACTICE
edited by ROBERT E. CAMPBELL

Contemporary Diagnostic Radiology works *two ways*. You may choose to subscribe to the non-scoring version, receiving every issue as an important element of your professional reading. The scoring version, however, supplements your reading and computer-coded examinations with confidential result responses, making you eligible for Continuing Medical Education credits co-sponsored by the University of Pennsylvania School of Medicine.

"As an organization for continuing medical education, the University of Pennsylvania School of Medicine designates this continuing medical education activity as meeting the criteria for 1 credit hour per bi-weekly issue in Category I for Educational Materials for the Physician's Recognition Award of the American Medical Association provided it has been completed according to instructions."

You can begin this ongoing program **today**. **Contemporary Diagnostic Radiology** is a year-round program, so you can join at any time. To begin your lessions, just fill out the enclosed card and return it to us. Or call **FREE** 1-800-638-6423. In Maryland call 1-800-638-4007. You'll find that **Contemporary Diagnostic Radiology** is the most efficient and inexpensive way to keep up with your dynamic field.

Williams & Wilkins

P.O. Box 23291
Baltimore, Maryland 21203-9990

Broadway House
2-6 Fulham Broadway
London SW6 1AA England

clip & mail

CONTEMPORARY DIAGNOSTIC RADIOLOGY

☐ **Yes!** I want to keep pace in my field! Begin my 26-issue subscription:
☐ Send me the scoring version ($230)
☐ Send me the non-scoring version ($187)
☐ Send me the resident non-scoring version* ($115)
(add $45 for optional airmail delivery outside the U.S.)
☐ new subscription
☐ renewal

name

address

city/state/zip

payment options
☐ payment enclosed ☐ bill me
☐ American Express ☐ MasterCard ☐ VISA

card # expiration date

signature/P.O. #

Maryland residents add 5% sales tax. Subscriptions outside the U.S. must be prepaid in U.S. dollars only. Rates valid through October 31, 1990. Please allow 8 weeks for delivery of your first issue, up to 16 weeks for surface delivery outside the U.S. Optional airmail rates add $45 per subscription.

***Residents** are eligible for the special in-training rate for up to three years. When requesting this rate, please include training status and institution.

☎ Don't forget: you can order with a **FREE** phone call at 1-800-638-6423. In Maryland, call 1-800-638-4007.

Williams & Wilkins

P.O. Box 23291
Baltimore, Maryland 21203-9990

Broadway House
2-6 Fulham Broadway
London SW6 1AA England

printed in USA

CDR 52079

J0091S01

AJR Guidelines for Authors

Address new and revised manuscripts, correspondence, and classified ads to the Editor:

AJR Editorial Office
2223 Avenida de la Playa, Suite 200
La Jolla, CA 92037-3218
Telephone: (619) 459-2229; FAX: (619) 459-8814

Inquiries regarding subscriptions, display advertising, reprints, or permission to republish *AJR* material should be addressed to the publisher:

The Williams & Wilkins Co.
428 E. Preston St.
Baltimore, MD 21202 Telephone: 1-800-638-6423

The *AJR* publishes original contributions to the advancement of medical diagnosis and treatment. Submitted manuscripts should not contain previously published material and should not be under consideration for publication elsewhere. Papers dealing with neuroradiology should be addressed to: American Journal of Neuroradiology, Dept. of Diagnostic Radiology, 1653 W. Congress Pkwy., Chicago, Il 60612. At the discretion of the *AJR* Editor, *AJNR* articles that are of interest to the general reader may be republished in the *AJR*. Neuroradiologic papers sent to the *AJR* will be forwarded to the Editorial Office of the *AJNR*.

Manuscript decisions are based on peer review. Reviewers receive manuscripts without title pages to ensure an unbiased review. Statements made in the article, including changes made by the Editor or manuscript editor, are the responsibility of the author and not of the *AJR* or its publisher. Authors will be sent the edited manuscript, galley proof, and proofs of illustrations. If the corresponding author will be unavailable to review galleys, arrangements should be made for a coauthor or colleague to read and return the proof.

The following guidelines are based on instructions set forth in the **Uniform Requirements for Manuscripts Submitted to Biomedical Journals** (*Ann Intern Med* **1988;**108:258–265). Articles will be edited, however, to conform to the individual style of AJR.

General Guidelines for Major Papers

Abstract. Clearly state (in 200 words or less) the purpose, methods, results, and conclusions of the study. Include actual data.

Introduction. Briefly describe the purpose of the investigation and explain why it is important.

Methods. Describe the research plan, the materials (or subjects), and the methods used, in that order. Explain in detail how disease was confirmed and how subjectivity in observations was controlled.

Results. Present results in a clear, logical sequence. If tables are used, do not duplicate tabular data in text, but do describe important trends and points.

Discussion. Describe the limitations of the research plan, materials (or subjects), and methods, considering both the purpose and the outcome of the study. When results differ from those of previous investigators, explain the discrepancy.

AUTHOR'S CHECKLIST

For priority handling, complete the following checklist, sign the copyright form on the reverse side of this page, and include both with the manuscript.

________ Two copies of the manuscript (the original and a photocopy) and two complete sets of figures are submitted. One copy has been retained by the author.

________ If appropriate, *AJR* Guidelines for case reports, technical notes, pictorial essays, or letters to the Editor have been followed. (See page A5.)

________ The manuscript, including references, figure legends, and tables, is typed double-spaced on 8½ × 11 in. (21.6 × 27.9 cm) *nonerasable* paper. Right-hand margins are not justified.

________ All manuscript pages are numbered consecutively beginning with the abstract. Authors' names do not appear on the manuscript pages.

________ The manuscript is organized as follows: title page, blind title page (title only), abstract, introduction, methods, results, discussion, acknowledgments, references, tables, figure legends, and figures.

________ Informed consent has been obtained from patients who participated in clinical investigations. If experiments were performed on animals, authors complied with NIH guidelines for use of laboratory animals.

________ Use of unfamiliar acronyms and abbrevations is kept to a minimum. When abbreviations are used they are defined at first mention, followed by the abbreviation in parentheses.

________ Metric measurements are used throughout, or the metric equivalent is given in parentheses.

________ Names and locations (city and state only) of manufacturers are given for equipment and nongeneric drugs.

Title Page

________ The following information is given: title of article; names and complete addresses (including zip code) of all authors; current addresses of authors who have moved since study; acknowledgment of grant or other assistance. The corresponding author is clearly identified, and a current address, phone number, and FAX number are given.

________ A blind title page is included in each copy of the manuscript, giving only the title (without the authors' names) for use in the review process.

Abstract

________ An abstract of approximately 200 words concisely states the purpose, methods, and results of the study in one paragraph. Actual data are included. Conclusions are stated in a second, summary paragraph.

________ No abbreviations or reference citations are used.

References

________ References (not to exceed 35) are typed double-spaced starting on a separate page and are **numbered consecutively in the order in which they appear in the text.**

________ All references are cited in the text and are enclosed in brackets and typed on line with the text (not superscript).

________ Unpublished data are not cited in the reference list, but are cited parenthetically in the text, for example, (Smith DJ, personal communication), (Smith DJ, unpublished data). This includes papers submitted, but not yet accepted, for publication.

________ Papers presented at a meeting are not cited in the reference list, but are cited parenthetically in the text (e.g., Smith DJ et al., presented at the annual meeting of the American Roentgen Ray Society, May 1990). After first mention, use (Smith DJ et al., ARRS meeting, May 1990).

________ Inclusive page numbers (e.g., 333–335) are given for all references.

________ Journal names are abbreviated according to *Index Medicus*.

________ Style and punctuation of references follow the format illustrated in the following examples (all authors are listed when six or fewer; when seven or more authors, the first three are listed, followed by "et al."):

Journal article

1. Long RS, Roe EW, Wu EU, et al. Membrane oxygenation: radiographic appearance. *AJR* **1986**;146:1257–1260

Book

2. Smith LW, Cohen AR. *Pathology of tumors*, 6th ed. Baltimore: Williams & Wilkins, **1977**:100–109

Chapter in a book

3. Breon AJ. Serum monitors of bone metastasis. In: Clark SA, ed. *Bone metastases*. Baltimore: Williams & Wilkins, **1983**:165–180

Tables

________ Each table is typed double-spaced on a separate page without vertical or horizontal rules; each has a short, descriptive title. Tables do not exceed two pages in length and contain at least four lines of data.

________ Tables are numbered in the order in which they are cited in the text.

________ Abbreviations are defined in an explanatory note below each table.

________ Tables are self-explanatory and do not duplicate data given in the text or figures.

________ All arithmetic (percentages, totals, differences) has been double checked for accuracy, and tabular data agree with data given in the text.

Figures and Legends

________ Two complete sets of original figures are submitted unmounted in labeled envelopes.

________ Figures are clean, unscratched, 5 × 7 in. (13 × 18 cm) glossy prints with **white borders.** A separate print is submitted for each figure *part*.

________ All figure parts relating to one patient have the same figure number.

________ Each figure is labeled on the back with the figure number and an arrow indicating "top." For black-and-white figures, labeling is done on a gummed label, which is then affixed to the back of the print. *Never* use labels on color figures, but write figure number on the back lightly in pencil. *Never* use ink on front or back of any figures.

________ Author's names are *not* written on the backs of figures.

________ Only removable (rub-on) arrows and letters are used on the figures. Symbols are uniform in size and style and are not broken or cracked.

________ Images are uniform in size and magnification.

________ Line drawings are done in black ink on a white background. They are professional in quality, and all use the same size type. (Only glossy prints are acceptable.)

________ Written permission has been obtained for use of all previously published illustrations (and copies of permission letters are included), and an appropriate credit line is given in the legends.

________ Legends are typed double-spaced, and figure numbers correspond with the order in which the figures are cited in the text.

Transfer of Copyright Agreement, Conflict of Interest Acknowledgment, Certification of Coauthors, and Exclusive Publication Statement

Complete copyright to the article entitled: ____

____

is hereby transferred to the American Roentgen Ray Society (for United States government employees to the extent transferable), effective if and when the article is accepted for publication in the *American Journal of Roentgenology*. In the case of the authors who are officers or employees of the United States government, the American Roentgen Ray Society recognizes that works prepared by officers or employees of the United States government as part of their official government duties are in the public domain.

Authors reserve all proprietary rights other than copyright, such as patent rights and the right to use all or part of this article in future works of their own. The authors retain the right of replication, subject only to crediting the original source of publication and receiving written permission from the publisher.

Authors guarantee that this manuscript contains no matter that is libelous or otherwise unlawful, invades individual privacy, or infringes any proprietary rights.

Authors understand that they will receive no royalty or other compensation from the American Roentgen Ray Society or the publisher.

Authors guarantee that the editor has been or will be informed of any proprietary or commercial interest or conflicts of interest the authors may have that relate directly or indirectly to the subject of this article.

All authors certify that they have made substantive and specific intellectual contributions to the article and assume public responsibility for its content.

Finally, the authors certify that none of the material in this manuscript has been published previously or is currently under consideration for publication elsewhere.

____________________	____________________	____________________
First author/date	Second author	Third author
____________________	____________________	____________________
Fourth author	Fifth author	Sixth author

This agreement must be signed by all authors in order for the manuscript to be published.

Case Reports

A case report is a brief description of a special case that provides a message that transcends the individual patient.

Format. There is no abstract. The introduction should be a short paragraph giving the general background and the specific interest of the case. No more than one case should be described in detail (similar ones can be mentioned briefly in the discussion). Emphasis should be on the radiologic aspects; clinical information must be limited to that necessary to provide a background for the radiology. The discussion should be succinct and should focus on the specific message and relevance of radiologic methods. A review of the literature is not appropriate.

Length. Maximum of five double-spaced, typewritten pages, including the references but not the title page or figure legends.

References. Maximum of eight.

Figures. Maximum of four, unless the text is shortened accordingly. Legends must not repeat the text.

Tables and Acknowledgments. Not appropriate in case reports.

Pictorial Essays

A pictorial essay is an article that conveys its message through illustrations and their legends. Unlike other *AJR* articles, which are based on original research, pictorial essays serve primarily as teaching tools, like exhibits at a scientific meeting. They are not encyclopedic book chapters. The abstract should be a short, introductory paragraph.

Length. Maximum of four double-spaced, typewritten pages, including the references but not the title page or figure legends.

References. Maximum of four.

Figures. Maximum of 30 figure *parts*. Number should be as few as necessary to convey the message of the paper.

Tables and Acknowledgments. Not appropriate in pictorial essays.

Opinions, Commentaries, and Perspectives

Opinions, commentaries, and perspectives are special articles dealing with controversial topics or issues of special concern to radiologists.

Format. Include a title page but no abstract. Headings may be used to break up the text.

Length. Maximum of five double-spaced, typewritten pages.

References. Maximum of five.

Tables and Figures. Maximum of four.

Technical Notes

A technical note is a brief description of a specific technique or procedure, modification of a technique, or equipment of interest to radiologists.

Format. No abstract, headings, or subheadings are required. If headings are used, they should be a combination of "Case Report," "Materials and Methods," "Results," and "Discussion." A brief one-paragraph introduction should be included to give the general background. Discussion should be limited to the specific message, including the uses of the technique or equipment. Literature reviews and lengthy case reports are not appropriate.

Length. Maximum of five double-spaced, typewritten pages, including the references but not the title page or figure legends.

References. Maximum of eight.

Figures. Maximum of two, unless the text is shortened accordingly.

Tables and Acknowledgments. Not appropriate in technical notes.

Letters to the Editor and Replies

Letters to the Editor and Replies should offer objective and constructive criticism of published articles. Letters may also discuss matters of general interest to radiologists. Do not end a letter with a hand-written signature.

Format. All letters should be typed double-spaced on nonletterhead paper, with no greeting or salutation. Name and affiliation should appear at the end of the letter. Titles for letters should be short and pertinent. The title for a reply is simply "Reply."

Length. Maximum of two double-spaced, typewritten pages, including references.

References. Maximum of four.

Figures. Maximum of two.

Tables and Acknowledgments. Not appropriate in Letters to the Editor and Replies.

Computer Page Articles

Articles published on the computer page deal with practical computer applications to radiology.

Format. Include a title page and an abstract.

Length. Maximum of eight double-spaced, typewritten pages.

References. Maximum of five.

Figures and Tables. Maximum of five. Computer printouts are not acceptable. Figures must be submitted as 5 × 7 in. glossy prints.

All submissions to the *AJR* must be accompanied by a completed copy of the Author's Checklist and the signed Copyright Agreement.

PICKER
IQ
PICKER

Outstanding CT Image Quality at an Affordable Price.

Performance this good has always had its price. Now Picker provides performance at a price you won't believe. Until you see it. Responsive to your needs, designed at your request, the result of four years of intensive R&D effort. The new I.Q.™ CT system delivers throughput, image quality and simplicity of operation, unequalled by any other scanner in its class. For first time CT buyers, as a replacement for mobile service, free standing clinics, or as an add-on CT for your busy department, I.Q. is your smartest answer.

Technology

Based on the proven principle of 4th generation performance, the I.Q. delivers new technology at an affordable price. Combining new PRISM data handling and distributed processing architecture, along with slip ring rotation and compact CT-tuned solid state generator, the I.Q. is so compact it can fit into a 260 square foot room.

Speed

The I.Q. user-friendly control center represents human engineering at its finest. Viewing can be done simultaneously with either scanning or reconstruction. A touch panel and simplified menu software guide the technologist through the studies in a matter of seconds.

Image Quality

Compare the quality of I.Q. images with any other CT on the market and you'll quickly conclude that I.Q. is in a class by itself. Advanced electronics provide the best low contrast resolution and lowest noise levels of any scanner in its class. The result is superior image quality for all head, body, and spine exams.

Simplicity

From patient positioning, through set-up and operation, your department will work faster, studies will run more smoothly, diagnoses will be more accurate. Installation and training on the I.Q. can be accomplished in as little as five days. Basic operating procedures can be learned in minutes. The net effect on the department efficiency, patient throughput and the bottom line will be perfectly clear to you.

I.Q. means image quality and investment quality. Call 1-800-543-4331, in Ohio (216) 473-3364.

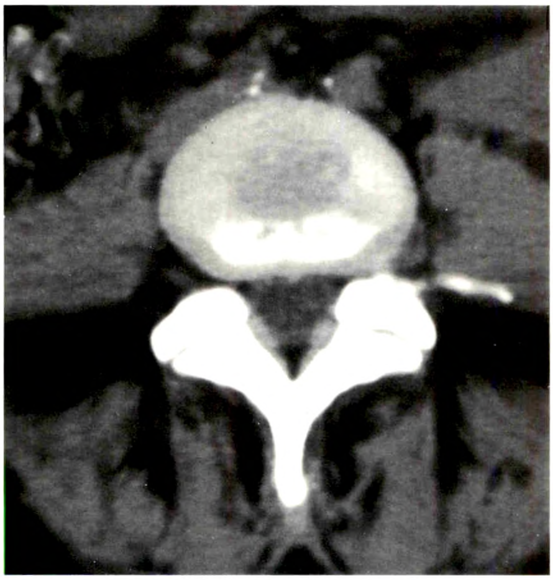

Lumbar spine, 420 mAs

It only acts expensive.

AJR Business and Subscriber Ir

The American Roentgen Ray Society

AJR, American Journal of Roentgenology, is published monthly to disseminate research on current developments in the radiologic sciences and commentary on topics related to radiology. It is published by the American Roentgen Ray Society, 1891 Preston White Dr., Reston, VA 22091; (703) 648-8992. Inquiries regarding society business, the annual ARRS meeting, and membership should be addressed to the Society at the above address.

Correspondence Concerning the *AJR*

Correspondence regarding display (not classified) advertising, subscriptions, address changes, reprints, and permission requests should be addressed to Williams & Wilkins, 428 E. Preston St., Baltimore, MD 21202; (301) 528–4000.

Correspondence regarding editorial matters and classified advertising should be addressed to Editorial Office, AJR, 2223 Avenida de la Playa, Ste. 200, La Jolla, CA 92037-3218; telephone (619) 459-2229; FAX (619) 459-8814. For information on manuscript submission, see Guidelines for Authors, pages A3–A5.

Subscriber Information

Subscription requests and inquiries should be sent to Williams & Wilkins, 428 E. Preston St., Baltimore, MD 21202. ARRS annual dues include $50 for journal subscription. Subscription rates are as follows: nonmembers, $110/year ($155 foreign, $244.00 Japan); institutions, $120 ($165 foreign, $254.00 Japan); nonmember in-training, $25 ($70 foreign, $159.00 Japan). Single copies of the Journal may be purchased for $16 ($19 foreign). Airmail rates will be furnished on request.

Japanese rates include airfreight. Ja
available from our sole agent, USACO
Shimbashi 1-Chome, Minato-Ku, Toky
phone 03-502-6471.

Call toll-free, 1-800-638-6423 (in Mar
4007), with subscription questions or pı
the mailing label from your latest issue
call.

If a subscriber receives a damaged cc
to receive an issue, the subscriber shc
Wilkins (428 E. Preston St., Baltimore,
days of publication (90 days for foreign
issue will be replaced.

Change of address information shoul
& Wilkins, 428 E. Preston St., Baltimo
90 days for address changes.

Copyrights, Permissions, and Reprint

The American Roentgen Ray Society
for all material published in the *AJR*. No p
may be reproduced without permission
quests for such permission should be a
& Wilkins, 428 E. Preston St., Baltimore

For reprints of a particular article, plea
designated in the footnotes for that artic

Indexes

The *AJR* provides volume and yearly
author) in the June and December iss
articles are also indexed in *Current Cont*
and the cumulative index published by

There's nothing like a great contrast to make a great picture.

©1990 Abbott & Costello enterprises under license by Curtis Management Group, Indpls., IN. USA. ©1990 W.C. Fields Productions, Inc., LA., ©1990 Receivership Estate of Mae West, ©1990 Gable Estates & Co., ©1990 S. Farrington, all represented by The Roger Richman Agency, Beverly Hills, CA.

Optiray® works

Great contrasts have always produced better results on film.

Take OPTIRAY. It produced diagnostic-quality images in more than 99% of the cases in clinical trials.[1] In fact, OPTIRAY 320 (ioversol injection 68%) produced a significantly higher percentage of excellent-quality urograms than did diatrizoate-292 in a comparative study.[2]

OPTIRAY also offers a very low incidence of individual drug-related adverse reactions: less than 1% in clinical trials involving 1,186 patients.[3]

Hydrophilicity may be one reason for the safety of OPTIRAY. While all of the recently introduced nonionics are hydrophilic, OPTIRAY is the most hydrophilic.[4] And although nonionic media haven't been as extensively investigated as conventional ionic media, preliminary evidence suggests an association between increased hydrophilicity and decreased neurotoxicity.[5-8]

With an iodine concentration of 32%, OPTIRAY 320 is flexible enough to use across a broad range of imaging procedures. In IVP and CT procedures, OPTIRAY 320 delivers more iodine per milliliter than either iohexol-300 or iopamidol-300. And when OPTIRAY 320 was compared with diatrizoate-370 or iopamidol-370 in coronary arteriography, no differences were observed in radiographic quality.[9,10]

the same principle

Now you can find OPTIRAY in the Ultraject™ prefilled syringe for safe, more cost-effective contrast media delivery. Each prelabeled syringe contains a single dose of contrast medium. That can mean improved aseptic technique, as well as time saved on each procedure.

All of which means OPTIRAY is ideal for a supporting role in your diagnostic imaging procedures. Please contact your Mallinckrodt representative for more information, or call us toll free at (800) 325-3688.

All nonionic iodinated contrast media currently available inhibit blood coagulation, *in vitro,* less than ionic contrast media. Clotting has been reported when blood remains in contact with syringes containing nonionic contrast media. Therefore, meticulous intravascular administration technique is necessary to minimize thromboembolic events.

References:

1. Data on file, Mallinckrodt Medical, Inc. **2.** Spataro R. Data on file (Study No. 204), Mallinckrodt Medical, Inc. **3.** Benamor M, et al. Ioversol clinical safety summary. *Invest Radiol.* 1989;24 (suppl 1):S67-S72. **4.** Ralston WH, et al. Acute and subacute toxicity of ioversol (Optiray) in laboratory animals. *Invest Radiol.* 1989;24 (suppl 1):S2. **5.** Castel JC, et al. Penetration of the brain by nonionic water soluble tri- and hexaiodinated contrast media. *Neuroradiology.* 1987;29:206-220. **6.** Hilal DK, et al. Development and evaluation of a new water-soluble iodinated myelographic contrast medium with markedly reduced convulsive effects. *Radiology.* 1978;126:417-422. **7.** Sovak M, et al. Concepts in design of improved intravascular contrast agents. *Ann Radiol.* 1978;21:283-289. **8.** Speck U, Mutzel W, Weinman HJ. Physiochemistry and pharmacology of known and new contrast media for angiography, urography and CT enhancement. In: Taenszer V, Zeitler E, eds. *Contrast Media in Urography, Angiography, and Computerized Tomography.* Stuttgart, Germany: Georg Thieme Verlag; 1983:2. **9.** Hirshfeld J, et al. Hemodynamic and electrocardiographic effects of ioversol during cardiac angiography: comparison with iopamidol and diatrizoate. *Invest Radiol.* 1989;24:138-144. **10.** Reagan K, et al. Double-blind study of a new nonionic contrast agent for cardiac angiography. *Radiology.* 1988;167:409-413.

Nonionic
OPTIRAY®
(ioversol)

%

THE PERCENTAGES ARE IN YOUR FAVOR

Caution must be used to avoid drawing clinical conclusions based solely upon nonclinical data. Please see the following page for a brief summary of presc

OPTIRAY® 160 240 320
(Ioversol Injection)

DESCRIPTION: Each milliliter of OPTIRAY 160 (ioversol injection 34%) provides 339 mg of ioversol with 3.6 mg of tromethamine as a buffer and 0.2 mg of edetate calcium disodium as a stabilizer. OPTIRAY 160 provides 16% (160 mg/mL) organically bound iodine.

Each milliliter of OPTIRAY 240 (ioversol injection 51%) provides 509 mg of ioversol with 3.6 mg of tromethamine as a buffer and 0.2 mg of edetate calcium disodium as a stabilizer. OPTIRAY 240 provides 24% (240 mg/mL) organically bound iodine.

Each milliliter of OPTIRAY 320 (ioversol injection 68%) provides 678 mg of ioversol with 3.6 mg of tromethamine as a buffer and 0.2 mg of edetate calcium disodium as a stabilizer. OPTIRAY 320 provides 32% (320 mg/mL) organically bound iodine.

CONTRAINDICATIONS: None.

WARNINGS: Nonionic iodinated contrast media inhibit blood coagulation, in vitro, less than ionic contrast media. Clotting has been reported when blood remains in contact with syringes containing nonionic contrast media.

Serious, rarely fatal, thromboembolic events causing myocardial infarction and stroke have been reported during angiographic procedures with both ionic and nonionic contrast media. Therefore, meticulous intravascular administration technique is necessary, particularly during angiographic procedures, to minimize thromboembolic events. Numerous factors, including length of procedure, catheter and syringe material, underlying disease state and concomitant medications may contribute to the development of thromboembolic events. For these reasons, meticulous angiographic techniques are recommended including close attention to guidewire and catheter manipulation, use of manifold systems and/or three-way stopcocks, frequent catheter flushing with heparinized saline solutions and minimizing the length of the procedure. The use of plastic syringes in place of glass syringes has been reported to decrease but not eliminate the likelihood of in vitro clotting.

Serious or fatal reactions have been associated with the administration of iodine-containing radiopaque media. It is of utmost importance to be completely prepared to treat any contrast medium reaction.

As with any contrast medium, serious neurologic sequelae, including permanent paralysis, can occur following cerebral arteriography, selective spinal arteriography and arteriography of vessels supplying the spinal cord. A cause-effect relationship to the contrast medium has not been established since the patients' pre-existing condition and procedural technique are causative factors in themselves. The arterial injection of a contrast medium should never be made following the administration of vasopressors since they strongly potentiate neurologic effects.

Caution must be exercised in patients with severely impaired renal function, combined renal and hepatic disease, severe thyrotoxicosis, myelomatosis, or anuria, particularly when large doses are administered.

Intravascularly administered iodine-containing radiopaque media are potentially hazardous in patients with multiple myeloma or other paraproteinemia, particularly in those with therapeutically resistant anuria. Myeloma occurs most commonly in persons over age 40. Although neither the contrast agent nor dehydration has been proved separately to be the cause of anuria in myelomatous patients, it has been speculated that the combination of both may be causative. The risk in myelomatous patients is not a contraindication to the procedure; however, special precautions, including maintenance of normal hydration and close monitoring, are required. Partial dehydration in the preparation of these patients prior to injection is not recommended since this may predispose the patient to precipitation of the myeloma protein.

Administration of radiopaque materials to patients known or suspected of having pheochromocytoma should be performed with extreme caution. If, in the opinion of the physician, the possible benefits of such procedures outweigh the considered risks, the procedures may be performed; however, the amount of radiopaque medium injected should be kept to an absolute minimum. The blood pressure should be assessed throughout the procedure, and measures for treatment of a hypertensive crisis should be available.

Contrast media may promote sickling in individuals who are homozygous for sickle cell disease when administered intravascularly.

Reports of thyroid storm following the intravascular use of iodinated radiopaque agents in patients with hyperthyroidism or with an autonomously functioning thyroid nodule, suggest that this additional risk be evaluated in such patients before use of any contrast medium.

PRECAUTIONS: *General:* Diagnostic procedures which involve the use of iodinated intravascular contrast agents should be carried out under the direction of personnel skilled and experienced in the particular procedure to be performed. A fully equipped emergency cart, or equivalent supplies and equipment, and personnel competent in recognizing and treating adverse reactions of all types should always be available. Since severe delayed reactions have been known to occur, emergency facilities and competent personnel should be available for at least 30 to 60 minutes after administration.

Preparatory dehydration is dangerous and may contribute to acute renal failure in patients with advanced vascular disease, diabetic patients, and in susceptible non-diabetic patients (often elderly with pre-existing renal disease). *Patients should be well hydrated prior to and following the administration of OPTIRAY.*

The possibility of a reaction, including serious, life-threatening, fatal, anaphylactoid or cardiovascular reactions, should always be considered (See ADVERSE REACTIONS). Increased risk is associated with a history of previous reaction to a contrast medium, a known sensitivity to iodine and known allergies (i.e., bronchial asthma, hay fever and food allergies) or hypersensitivities.

The occurrence of severe idiosyncratic reactions has prompted the use of several pretesting methods. However, pretesting cannot be relied upon to predict severe reactions and may itself be hazardous to the patient. It is suggested that a thorough medical history with emphasis on allergy and hypersensitivity, prior to the injection of any contrast medium, may be more accurate than pretesting in predicting potential adverse reactions. A positive history of allergies or hypersensitivity does not arbitrarily contraindicate the use of a contrast agent when a diagnostic procedure is thought essential, but caution should be exercised. Premedication with antihistamines or corticosteroids to avoid or minimize possible allergic reactions in such patients should be considered. Reports indicate that such pretreatment does not prevent serious life-threatening reactions, but may reduce both their incidence and severity.

General anesthesia may be indicated in the performance of some procedures in selected patients; however, a higher incidence of adverse reactions has been reported in these patients, and may be attributable to the inability of the patient to identify untoward symptoms or to the hypotensive effect of anesthesia which can prolong the circulation time and increase the duration of exposure to the contrast agent.

In angiographic procedures, the possibility of dislodging plaques or damaging or perforating the vessel wall should be considered during catheter manipulations and contrast medium injection. Test injections to insure proper catheter placement are suggested.

Angiography should be avoided whenever possible in patients with homocystinuria because of the risk of inducing thrombosis and embolism.

Patients with congestive heart failure should be observed for several hours following the procedure to detect delayed hemodynamic disturbances which may be associated with a transitory increase in the circulating osmotic load.

Selective coronary arteriography should be performed only in selected patients and those in whom the expected benefits outweigh the procedural risk. The inherent risks of angiocardiography in patients with chronic pulmonary emphysema must be weighed against the necessity for performing this procedure.

Extreme caution during injection of a contrast medium is necessary to avoid extravasation. This is especially important in patients with severe arterial or venous disease.

Drug Interactions: Renal toxicity has been reported in a few patients with liver dysfunction who were given oral cholecystographic agents followed by intravascular contrast agents. Administration of any intravascular contrast agent should therefore be postponed in patients who have recently received a cholecystographic contrast agent.

Other drugs should not be mixed with ioversol injection.

Drug Laboratory Test Interactions: The results of PBI and radioactive iodine uptake studies, which depend on iodine estimation, will not accurately reflect thyroid function for up to 16 days following administration of iodinated contrast media. However, thyroid function tests not depending on iodine estimations, e.g., T3 resin uptake and total or free thyroxine (T4) assays are not affected.

Carcinogenesis, Mutagenesis, Impairment of Fertility: No long term animal studies have been performed to evaluate carcinogenic potential. However, animal studies suggest that this drug is not mutagenic and does not affect fertility.

Pregnancy Category B: No teratogenic effects attributable to ioversol have been observed in teratology studies performed in animals. There are, however, no adequate and well controlled studies in pregnant women. It is not known whether ioversol crosses the placental barrier or reaches fetal tissues. However, many injectable contrast agents cross the placental barrier in humans and appear to enter fetal tissue passively. Because animal teratology studies are not always predictive of human response, this drug should be used during pregnancy only if clearly needed. X-ray procedures involve a certain risk related to the exposure of the fetus.

Nursing Mothers: It is not known whether ioversol is excreted in human milk. However, many injectable contrast agents are excreted unchanged in human milk. Although it has not been established that serious adverse reactions occur in nursing infants, caution should be exercised when intravascular contrast media are administered to nursing women because of potential adverse reactions, and consideration should be given to temporarily discontinuing nursing.

Pediatric Use: Safety and effectiveness in children have not been established.

ADVERSE REACTIONS: Adverse reactions following the use of OPTIRAY formulations are usually mild to moderate, of short duration and resolve spontaneously (without treatment). However, serious, life-threatening and fatal reactions, mostly of cardiovascular origin, have been associated with the administration of iodine-containing contrast media.

Injections of contrast media are often associated with sensations of warmth and pain. In controlled double-blind clinical studies, significantly less warmth and pain were associated with the injection of OPTIRAY than with iothalamate meglumine, diatrizoate meglumine, and diatrizoate meglumine and diatrizoate sodium.

When OPTIRAY 320 is used for coronary arteriography and ventriculography in double-blind clinical trials, electrocardiographic and hemodynamic changes occur with less frequency and severity with ioversol injection than with diatrizoate meglumine and diatrizoate sodium.

Following coronary artery and left ventricular injection, electrocardiographic parameters were affected less with OPTIRAY (ioversol injection) than with diatrizoate meglumine and diatrizoate sodium injection. These parameters included the following: bradycardia, tachycardia, T-wave amplitude, ST depression and ST elevation.

OPTIRAY has also been shown to cause fewer changes in cardiac function and systemic blood pressure than conventional ionic media. These include cardiac output, left ventricular systolic and end-diastolic pressure, right ventricular systolic and pulmonary artery systolic pressures and decreases in systolic and diastolic blood pressures.

The following table of incidence of reactions is based upon clinical trials with OPTIRAY formulations in over 1100 patients. This listing includes all adverse reactions which were coincidental to the administration of ioversol regardless of their direct attributability to the drug or the procedure. Adverse reactions are listed by organ system and in decreasing order of occurrence. Significantly more severe reactions are listed before others in a system regardless of frequency.

Adverse Reactions

System	> 1%	≤ 1%
Cardiovascular	none	angina pectoris hypotension vascular spasm bradycardia conduction defect false aneurysm hypertension transient arrhythmia vascular trauma
Digestive	none	nausea vomiting
Nervous	none	cerebral infarct headache blurred vision vertigo lightheadedness vasovagal reaction disorientation dysphasia paresthesia visual hallucination
Respiratory	none	laryngeal edema nasal congestion sneezing coughing hypoxia
Skin	none	periorbital edema urticaria facial edema flush pruritus
Miscellaneous	none	extravasation shaking chills bad taste general pain

Regardless of the contrast medium employed, the overall incidence of serious adverse reaction is higher with coronary arteriography than with other procedures. Cardiac decompensation, serious arrhythmias, myocardial ischemia or myocardial infarction may occur during coronary arteriography and left ventriculography.

General Adverse Reactions to Contrast Media

The following adverse reactions are possible with any parenterally administered iodinated contrast medium. Severe life-threatening reactions and fatalities, mostly of cardiovascular origin, have occurred. Most deaths occur during injection or 5 to 10 minutes later; the main feature being cardiac arrest with cardiovascular disease as the main aggravating factor. Isolated reports of hypotensive collapse and shock are found in the literature. Based upon clinical literature, reported deaths from the administration of conventional iodinated contrast agents range from 6.6 per 1 million (0.00066 percent) to 1 in 10,000 patients (0.01 percent).

The reported incidence of adverse reactions to contrast media in patients with a history of allergy is twice that of the general population. Patients with a history of previous reactions to a contrast medium are three times more susceptible than other patients. However, sensitivity to contrast media does not appear to increase with repeated examinations.

Adverse reactions to injectable contrast media fall into two categories: chemotoxic reactions and idiosyncratic reactions.

Chemotoxic reactions result from the physicochemical properties of the contrast medium, the dose and the speed of injection. All hemodynamic disturbances and injuries to organs or vessels perfused by the contrast medium are included in this category.

Idiosyncratic reactions include all other reactions. They occur more frequently in patients 20 to 40 years old. Idiosyncratic reactions may or may not be dependent on the dose injected, the speed of injection, the mode of injection and the radiographic procedure. Idiosyncratic reactions are subdivided into minor, intermediate and severe. The minor reactions are self-limited and of short duration; the severe reactions are life-threatening and treatment is urgent and mandatory.

In addition to the adverse reactions reported for ioversol, the following additional adverse reactions have been reported with the use of other contrast agents and are possible with any water soluble, iodinated contrast agent.

Nervous: muscular spasm, convulsions, aphasia, syncope, paralysis, visual field losses which are usually transient but may be permanent, coma and death.

Cardiovascular: angioneurotic edema, peripheral edema, vasodilation, thrombosis and rarely thrombophlebitis, disseminated intravascular coagulation and shock.

Skin: maculopapular rash, erythema, conjunctival symptoms, ecchymosis and tissue necrosis.

Respiratory: choking, dyspnea, wheezing which may be an initial manifestation of more severe and infrequent reactions including asthmatic attack, laryngospasm and bronchospasm, pulmonary edema, apnea and cyanosis. Rarely these allergic-type reactions can progress into anaphylaxis with loss of consciousness, coma, severe cardiovascular disturbances and death.

Miscellaneous: hyperthermia, temporary anuria or other nephropathy.

Other reactions may also occur with the use of any contrast agent as a consequence of the procedural hazard; these include hemorrhage or pseudoaneurysms at the puncture site, brachial plexus palsy following axillary artery injections, chest pain, myocardial infarction, and transient changes in hepatorenal chemistry tests. Arterial thrombosis, displacement of arterial plaques, venous thrombosis, dissection of the coronary vessels and transient sinus arrest are rare complications.

In cerebral arteriography, cardiovascular reactions that may occur with some frequency are bradycardia and either an increase or decrease in systemic blood pressure. Neurological reactions that may occur are: seizures, drowsiness, transient paresis, and mild disturbances in vision.

Central nervous system reactions with OPTIRAY in controlled clinical studies in cerebral arteriography that occurred with frequencies greater than 1% were: vertigo (4%) and blurred vision (3%).

In aortography, depending on the technique employed, the risks of this procedure also include the following: injury to the aorta and neighboring organs, pleural puncture, renal damage including infarction and acute tubular necrosis with oliguria and anuria, retroperitoneal hemorrhage from the translumbar approach and spinal cord injury and pathology associated with the syndrome of transverse myelitis. Under conditions of slowed aortic circulation there is an increased likelihood for aortography to cause muscle spasm. Occasional serious neurologic complications, including paraplegia, have also been reported in patients with aortoiliac obstruction, femoral artery obstruction, abdominal compression, hypotension, hypertension, spinal anesthesia, and injection of vasopressors to increase contrast. In these patients the concentration, volume, and number of repeat injections of the medium should be maintained at a minimum with appropriate intervals between injections. The position of the patient and catheter tip should be carefully monitored.

Entry of a large aortic dose into the renal artery may cause, even in the absence of symptoms, albuminuria, hematuria, and an elevated creatinine and urea nitrogen. Rapid and complete return of function usually follows.

Cardiovascular system reactions with OPTIRAY in controlled clinical studies in coronary arteriography with left ventriculography that occurred with frequencies greater than 1% were: angina (1.2%) and nausea (1.2%).

PRECAUTIONS FOR SPECIFIC PROCEDURES:

Cerebral Arteriography

Extreme caution is advised in patients with advanced arteriosclerosis, severe hypertension, cardiac decompensation, senility, recent cerebral thrombosis or embolism, and migraine.

Peripheral Arteriography

Pulsation should be present in the artery to be injected. In thromboangiitis obliterans, or ascending infection associated with severe ischemia, angiography should be performed with extreme caution, if at all.

Coronary Arteriography and Left Ventriculography

Mandatory prerequisites to the procedure are specialized personnel, ECG monitoring apparatus and adequate facilities for immediate resuscitation and cardioversion. Electrocardiograms and vital signs should be routinely monitored throughout the procedure.

Venography

Special care is required when venography is performed in patients with suspected thrombosis, phlebitis, severe ischemic disease, local infection or a totally obstructed venous system. In order to minimize extravasation during injection, fluoroscopy is recommended.

OVERDOSAGE: The adverse effects of overdosage are life-threatening and affect mainly the pulmonary and cardiovascular system. Treatment of an overdosage is directed toward the support of all vital functions, and prompt institution of symptomatic therapy.

Ioversol does not bind to plasma or serum protein and is therefore, dialyzable.

The intravenous LD_{50} values (g/kg) for ioversol in animals were: 17 (mice), and 15 (rats).

DOSAGE AND ADMINISTRATION: Details on dosage are provided in the package insert. CONSULT FULL PACKAGE INSERT BEFORE USE.

MALLINCKRODT®

Changing the look of medicine.™

© 1990 Mallinckrodt Medical, Inc.

MI22316

PICTURE PERFECT

IF YOUR MAMMOGRAPHY EQUIPMENT ISN'T THE "PICTURE" OF EFFICIENCY,

YOUR PRODUCTIVITY AND PERFORMANCE WILL BE OUT OF FOCUS!

For over 40 years, specially-dedicated S & S x-ray equipment and accessories have been improving Radiologists' efficiency and productivity. Specially-dedicated mammography equipment includes:

MOBILE *MOTORIZED VIEWERS*

Hold *Mammography* radiographs for random access recall and viewing within 7 seconds! Individual on-off light switches control divided viewing areas.

MODELS:

MV810-170: 10 viewing areas for 170 8 x 10" films

MV 1824-272: 16 viewing areas for 272 18 x 24cm films

MV2430-204: 12 viewing areas for 204 24 x 30cm films

S & S MAMMOGRAPHY ILLUMINATORS:

The standard for illumination excellence. Surface or recessed mounting is available for 1 to 6 banks — 1 over 1 up to 6 over 6. Individual on-off light controls for ***each*** viewing section reduce glare and prevent spill-over. Single or two tier models for straight or angulated viewing include:

MODELS:

147000: Series for 8x10/18x24cm films

146000: Series for 24 x 30cm films

MAMMOGRAPH-SIZED VERTIFILE:

Doubles capacity over conventional drawer files. Adjustable partitions. Available with or without sliding door closures.

MODELS:

871: 1 shelf (2 doors) 14 x 30 x 13½"

873: 3 shelves (6 doors) 14 x 30 x 37¾"

876: 6 shelves (12 doors) 14x30x74½"

ADD-ON *MOVING GRID BUCKY SYSTEM:*

Converts existing non-Bucky mammography equipment. Improves contrast and micro-calcification visibility. Eliminates grid lines. Reduces scattered radiation.

MODELS:

MB-12: for 18 x 24cm film

MB-24: for 24 x 30cm film

See your local x-ray dealer or call S & S directly for *Picture Perfect* mammography equipment and our expanded line of radiological equipment and accessories.

S.&S.

S & S X-RAY PRODUCTS, INC.
1101 Linwood Street, Brooklyn, NY 11208
TOLL FREE: 800/347-XRAY ■ **NY STATE:** 718/649-8500 ■ **FAX:** 718/257-0219

CIRCLE 9 ON READER SERVICE CARD

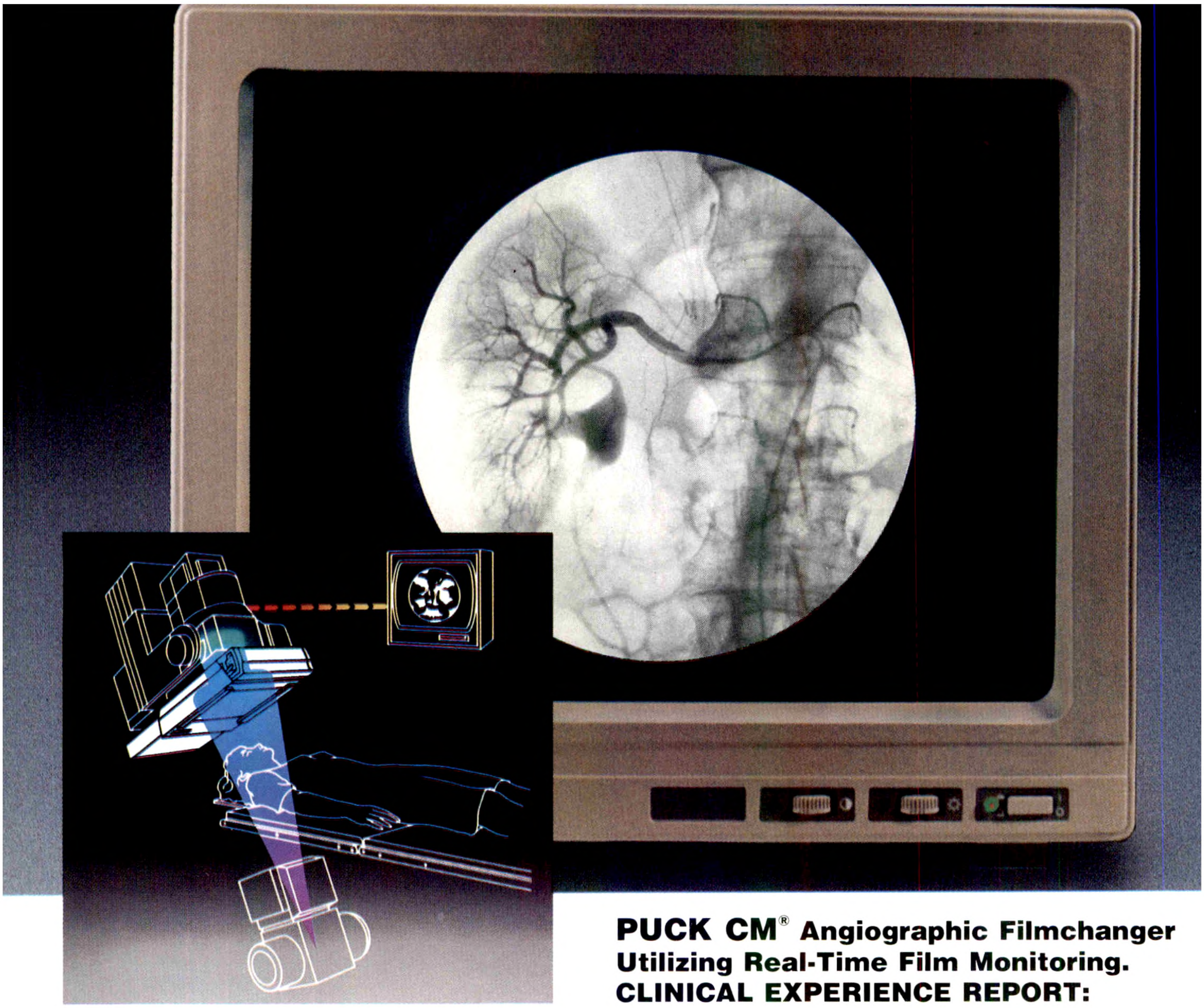

PUCK CM® Angiographic Filmchanger Utilizing Real-Time Film Monitoring. CLINICAL EXPERIENCE REPORT:

“Immediate verification of stable catheter position… catheter time in patient reduced… possible increase in the number of daily examinations… control of procedures enhanced.”

PUCK CM angiographic exposure monitoring… real-time viewing of each film exposure… is now in use at a number of institutions. This new capability is available in PUCK CM Filmchangers as part of an appropriate X-ray system. Dr. Holton cites the adjacent benefits of the system to both patient and radiologist.

'Monitor image and quotation courtesy of Jerry C. Holton, M.D., of Radiology Associates, St. Vincents Infirmary Medical Center, Little Rock, Arkansas.

89213

PUCK CM Filmchanger

Elema-Schonander, Inc.
2360 N. Palmer Drive
Schaumburg, IL 60173-3887
Phone: (708) 397-5900 Telefax (708) 397-5943

Summary of Benefits, the PUCK® CM/C Filmchanger System

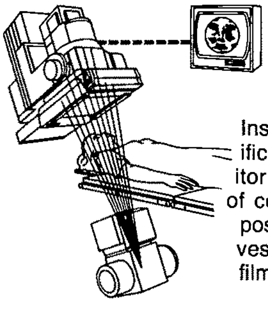

PERMITS EXPOSURE MONITORING CAPABILITY
Instantaneous verification on a monitor and recording of correct cathether position and proper vessel filling while filmchanger series is in progress.

100 CHARACTER FILM MARKING:

Fiber-optic marking is always correctly displayed for normal film reading. Programmed from SEP-3 Program Control.

PUCK CM for POSITION-INDEPENDENT PROJECTIONS:
Features a light, compact receiving cassette which attaches and detaches left, right or back away from patient.

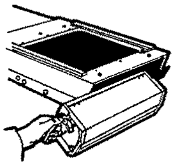

PUCK C for R&F, LATERAL and a.p. APPLICATIONS:

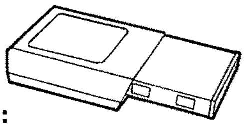

Offers all other PUCK CM advantages except exposure monitoring. Multi-Directional M4/20 Universal Loading Magazine for ALL PUCK changers.

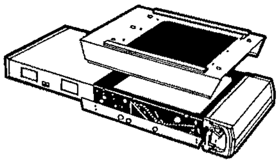

OPTIMUM IMAGE QUALITY:
Easy, rapid screen plate removal encourages frequent filmchanger screen cleaning. This feature helps extend screen surface life, maintaining high image quality and filmchanger performance.

REAL-TIME DISPLAY with SEP-3:
Shows pertinent events second-by-second, for easy visualization of program progression during the run. Exposure rates up to 4 exp./sec. Interfaces with two generators, injector, table stepper and other devices. Stores up to 20 programs. Enters film marking data. 89212

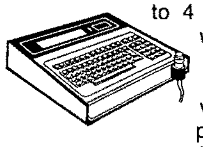

Elema-Schonander, Inc.
2360 N. Palmer Drive, P.O. Box 94517
Schaumburg, IL 60173-3887
Phone: (708) 397-5900
Telefax (708) 397-5943

Circle 4 on the Reader Service Card

UNIVERSITY OF
Miami
SCHOOL OF MEDICINE

Department of Radiology is recruiting faculty for the UM/Jackson Memorial Medical Center, a 1300 bed tertiary care referral center. Positions available to meet expanding clinical and academic programs in:

ABDOMINAL IMAGING
MUSCULOSKELETAL IMAGING
NUCLEAR MEDICINE
PEDIATRIC RADIOLOGY
THORACIC IMAGING

Candidates must be Board certified or eligible, with fellowship training or equivalent experience. Rank and salary commensurate with qualifications. Send C.V. to:

C.A. Poole, M.D.
Professor and Chairman
Department of Radiology (R-130)
University of Miami
School of Medicine
P.O. Box 016960
Miami, Florida 33101

An Affirmative Action/Equal Opportunity Employer

CHIEF OF DIAGNOSTIC IMAGING

Hawaii Permanente Medical Group, Inc., a large multi-specialty group practice, is seeking a radiologist with management experience to direct the professional activities of diagnostic imaging for Kaiser Permanente on the island of Oahu.

Approximately 120,000 procedures are performed annually at the 200-bed medical center and detached clinics. CT, ultrasound, nuclear medicine, angiography, and other standard modalities are provided. MRI is planned for 1991.

Contact:
Michael Chaffin, M.D.
at 808-834-9112 or send
curriculum vitae to
3288 Moanalua Road
Honolulu, HI 96819.

An equal opportunity employer

SIEMENS

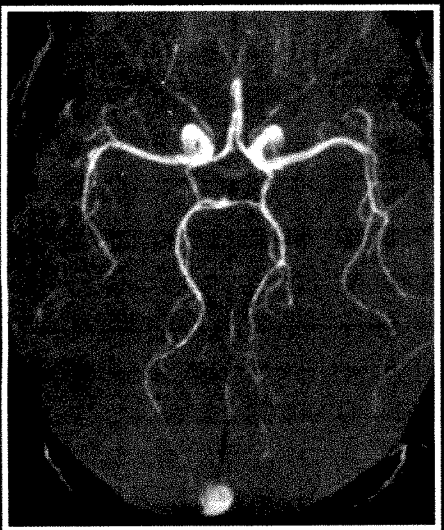

The Circle of Willis: *Axial MIP*
Note excellent delineation of the fine Posterior Communicating Arteries.
11 minute acquisition

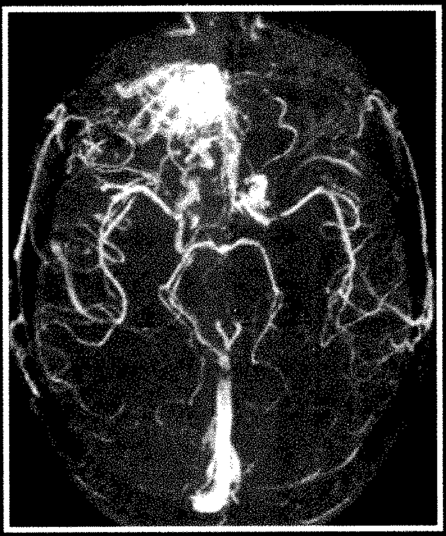

Arteriovenous Malformation:
6 minute acquisition
(courtesy of U.Z. Leuven Radiologie)

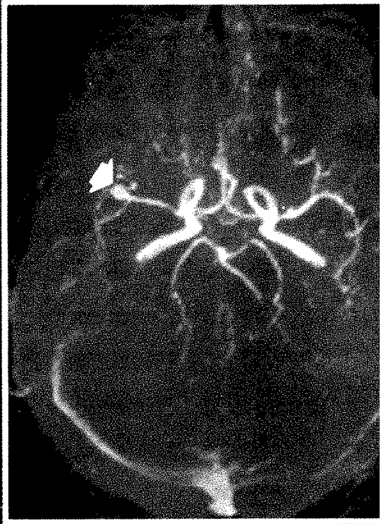

Middle Cerebral Artery Aneurysm:
5 mm, 11 minute acquisition
(courtesy of Parkside MRI)

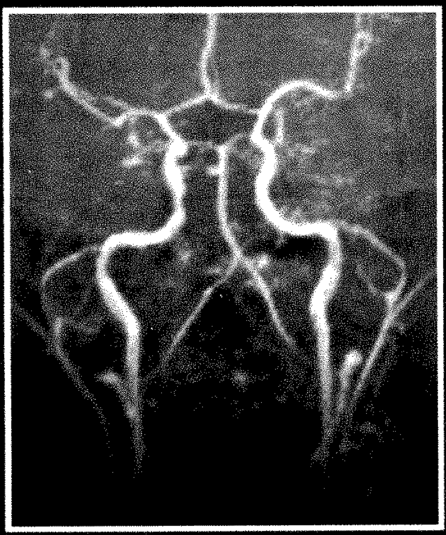

The Carotid Siphon: *Coronal MIP*
Very short echo times and refocusing pulses minimize phase dispersion and associated signal loss in the torturous Carotid Siphon.
11 minute acquisition

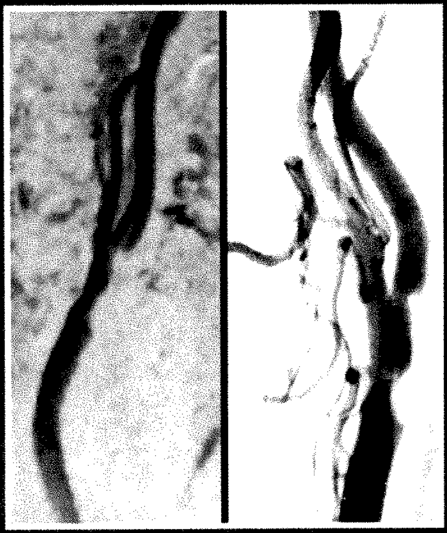

Carotid Ulceration:
MRA left, DSA right.
7 minute bilateral acquisition
(courtesy of University Hospitals of Cleveland)

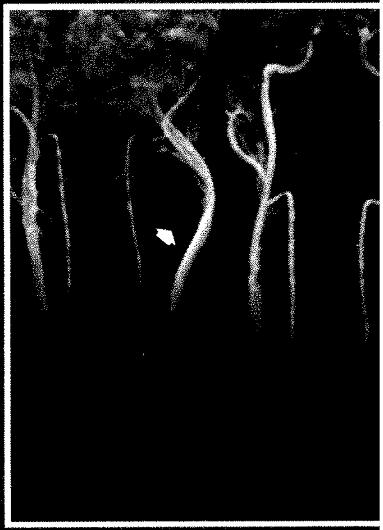

Glomus Tumor:
Before (left) and after (right) surgery.
11 minute acquisition
(courtesy of University of Muenster)

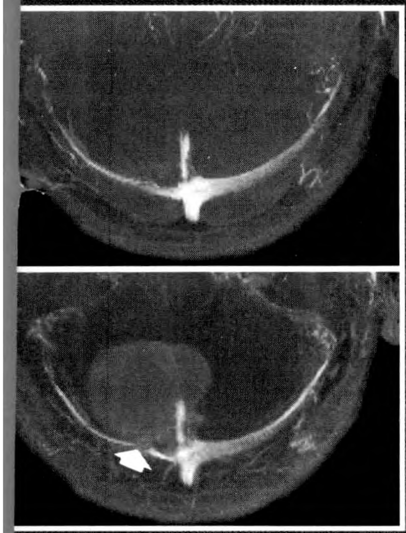

ıor Pre/Post Gadolinium:
Gadolinium study reveals tumor invasion
Transverse Sinus. 11 minute acquisition
rtesy of Loma Linda Univ. Medical Center)

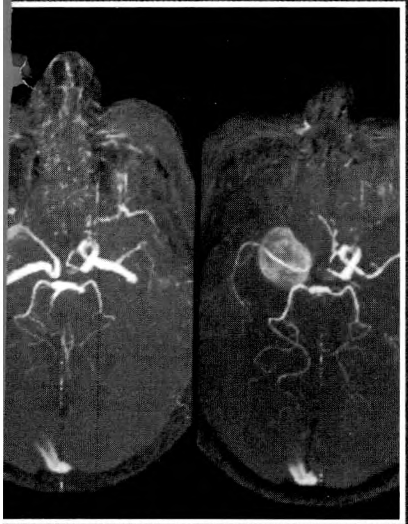

ernal Carotid Aneurysm: *(Pre/Post*
loon Embolization) Methemoglobin within
ombosed vessel (right) provided high signal
ne 3D data, and therefore excellent
neation of thrombus. MCA is still filling post
olization. 11 minute acquisition
urtesy of Abbott Northwestern Hospital)

MG/5000-244 3528 © Siemens Medical Systems, Inc. 1990

What you can do today...

MRI's sensitivity to flow presents a unique opportunity to produce high resolution "MR Angiograms" without the application of contrast agents.

MRA: Magnetic Resonance Angiography

It's simple to perform MRA...if you have a MAGNETOM®. Our robust 10 mT/m gradient system provides all the power and flexibility that is required.

With the MAGNETOM SP user interface, it's as easy as a click of the mouse. No transfer time to separate workstations. No after-hours data crunching. Only one system, the MAGNETOM SP does it all - *fast.*

You won't want to put off 'til next year...when you see what you can do today.

Now, who has the advantage?

The third of a series of informative posters by Siemens discusses effective techniques for achieving clinically superior "MR Angiograms."

Write for our informative posters.
38" x 24", mailed in protective mailing tubes.

Please send me:
☐ MRA ☐ MR Myelogram ☐ MR: The Knee

Name: ______
Affiliation: ______
Address: ______
City: ______ State: ______ Zip: ______

Siemens Medical Systems, Inc.
Marketing Services
186 Wood Avenue South
Iselin, NJ 08830
(201) 321-4500

Circle 8 on the Reader Service Card

Siemens...
technology in caring hands.

Fifteenth Annual International

BODY IMAGING CONGRESS

HYATT REGENCY MAUI · MAUI, HAWAII

October 6-13, 1990

*This multimodality imaging conference will offer an integrated course presenting topics in **Magnetic Resonance Imaging, Computed Tomography, Ultrasonography and Interventional Radiology**, as well as offer a special section on **Breast Imaging.** The meeting will offer participants Category I CME credits.*

*Congress sessions will end at mid-day Thursday allowing optional extensions which can include the fabulous new **Hyatt Regency Waikoloa Hotel** and the just-opened **Hyatt Regency Kauai Hotel** in the Poipu Beach region of Kauai.*

Invited faculty include Drs. D. Adler, University of Michigan Hospital; L. W. Bassett, University of California School of Medicine; T. Berquist, Mayo Clinic; G. Borkowsky, Cleveland Clinic Foundation; W. Boswell, University of Southern California; P. Burns, Thomas Jefferson Memorial Hospital; R.J. Friedman, University of Southern California; B. Goldberg, Thomas Jefferson Memorial Hospital; H. Kressel, Hospital of the University of Pennsylvania; G. Leopold, University of California, San Diego; A. Lurus, Holy Family Hospital, Spokane; E.A. Lyons, Winnipeg Health Sciences Center; M. Manco-Johnson, University of Colorado Health Sciences Center; C. Merritt, Oschner Clinic, New Orleans; M. Modic, Cleveland Clinic; S. Moore, Stanford University Medical Center, T. Silver, University of Michigan Hospital and J. Weinreb, New York University Medical Center.

Ronald J. Friedman, M.D., Meeting Coordinator, University of Southern California

For Registration or Information:

ANNUAL BODY IMAGING CONFERENCE
c/o Medical Seminars International, Inc.
9800 D Topanga Canyon Blvd., Suite 232
Chatsworth, CA 91311
TEL: (818) 700-9821 FAX: (818) 881-6062

Join The Leading Group Medical Provider In An Exceptional Locale.

Radiologists who choose Kaiser Permanente excel with the largest and most experienced prepaid group medical practice in America. As a premier medical provider we can offer some very distinctive career pluses, including some of health care's most advanced Radiology environments. You will also find immediate significant responsibility plus a highly collegial atmosphere that emphasizes professional development. Currently, we have excellent opportunities for board certified/eligible Radiologists.

RADIOLOGY DEPT. CHAIRMAN

This key position will assume broad clinical, administrative and executive responsibilities. Demonstrated leadership skills are required.

STAFF RADIOLOGISTS

Will perform services in all imaging modalities.

ANOTHER DISTINCTIVE ADVANTAGE

...is our location in northeastern Ohio. Here, you will enjoy a thriving major metropolitan city • an ideal housing market • an acclaimed symphony orchestra • theatre • ballet • Great Lakes recreation • and a growing service base of some 210,000 Kaiser members in the Cleveland-Akron area. Relocation assistance programs are available. In addition, we offer attractive salary, superb benefits, shareholder status, paid retirement plans, and full malpractice coverage. For further details simply contact: **Ronald G. Potts, M.D., Medical Director, Ohio Permanente Medical Group, Inc., Dept. HRAJR, 1300 E. 9th Street, Suite 1100, Cleveland, OH 44114. Or call us at 1-800-837-OPMG/(216) 623-8770.** EOE.

KAISER PERMANENTE

Good People. Good Medicine.

Help us to serve you better.....

USE
YOUR
ZIP
CODE

Remember, your zip code provides faster, more direct delivery of your journals. Use it on all correspondence, too.

Review Article

Medical Decision Making: Practical Points for Practicing Radiologists

Warren C. Phillips, Jr.[1] and James A. Scott[2]

The concepts of medical decision making are an important part of the scientific evaluation of imaging methods and equipment. We attempted to explain these concepts several years ago [1], and we think that the principles should be emphasized again because expanding technology is presenting practicing radiologists with more imaging choices than ever before. Each choice is coupled with advantages and disadvantages with respect to utility, safety, and cost. The scientific evaluation of these methods is critical to their appropriate application, and the concepts of medical decision making have been developed for this purpose.

The major emphasis of the following discussion is

1. definition of terms, with a discussion of their interrelationships
2. the role of prevalence of disease in clinical practice
3. the rationale behind multiple tests for the same condition
4. how the term "accuracy" should be used.

The Basics

The principles of medical decision making are simple, representing little more than formalized common sense. The mathematics is essentially that of ratio and proportions. However these ratios interact with each other in ways that the uninitiated may find surprising.

In order to evaluate the efficacy of any test, one needs to compare it with a standard of "acceptable infallibility" so that the "truth" can be established. This allows a given patient or specimen to be classified as "normal" or "abnormal." This standard is often based on pathologic results, long-term follow-up, or comparison with other tests/procedures with an established track record. For example, the results of carotid duplex sonography could be compared with results of angiography or surgery. The standard reference test is often called the "gold standard."

One of the most confusing aspects of medical decision making is the large number of terms (a short list of important terms can be found in the glossary at the end of this article). Let us define a few of the more important ratios now:

sensitivity: probability of a positive test given the presence of disease

specificity: probability of a negative test given the absence of disease

prevalence of disease: proportion of patients in the test population with disease

positive predictive value (PV+): probability of the presence of disease given a positive test

negative predictive value (PV−): probability of the absence of disease given a negative test

accuracy: proportion of correct results.

Received November 30, 1989; accepted after revision February 6, 1990.

[1] Department of Radiology, Milford Memorial Hospital, Milford, DE 19963.

[2] Department of Radiology, Harvard Medical School, Massachusetts General Hospital, Boston, MA 02114. Address reprint requests to Radiology Research Office.

AJR **154:1149–1155, June 1990** 0361–803X/90/1546–1149 © American Roentgen Ray Society

Results from Inpatient Ward

Let us now apply these definitions to a hypothetical situation (Table 1). Suppose that 50 chest films from an inpatient infectious disease ward are available for interpretation. These are interpreted by a radiologist who we assume makes no perceptual errors on this set of films. We wish to determine how good chest radiographs are for detecting lung infections. All patients are subjected to bronchial washings and/or biopsy so that the "truth" is known. Before looking at Table 1, cover up the footnote and try to determine the value of each of the ratios defined in the preceding paragraph.

The data show that among diseased patients the "test" was correct 84% (21/25) of the time. Among disease-free patients, the results were slightly better at 88% (22/25). Thus, the sensitivity and specificity were 84% and 88%, respectively. Of the 50 patients in the study, 25 had the disease; thus prevalence was 50% (25/50). A positive test was correct in 88% (21/24); a negative test correct in 85% (22/26). Finally the overall results were correct in 86% of patients ([21 + 22]/50); this is the accuracy.

False-positive/negative ratios also may be determined from Table 1. For example, there were 24 positive tests and three were incorrect; the false-positive ratio (FP) is 3/24 or 12%. Similarly the false-negative (FN) ratio is 4/26 or 15%.

The terms sensitivity, specificity, false-positive and false-negative occur in the medical literature with varying usage. Please see glossary and Harris [2] for additional information.

Results from Outpatients and Screening Clinics

After interpreting the cases summarized in Table 1, the radiologist proceeds to interpret cases from the outpatient infectious disease ward, and again we assume that no perceptual errors are made (Table 2). Finally, a similar but much larger set of cases from a screening clinic is interpreted (Table 3). Again try to determine the value of the ratios before looking at the table footnote.

How were the three tables constructed? The sensitivity and specificity were held constant, and the prevalence of disease was varied to reflect a decreasing number of patients who were abnormal as we proceeded from an inpatient population to an outpatient screening clinic. These two steps will determine *all* of the numbers in the tables. Then one need only calculate the values of the six ratios according to their definitions.

TABLE 1: Inpatients, Representative of High Prevalence

Test	Disease		Total
	Present	Absent	
Positive	21	3	24
Negative	4	22	26
Total	25	25	50

Note.—Prevalence of disease (25/50) = 0.50; sensitivity (21/25) = 0.84; specificity (22/25) = 0.88; positive predictive value (21/24) = 0.88; negative predictive value (22/26) = 0.85; accuracy ([21 + 22]/50) = 0.86.

For example, when comparing Tables 1 and 2, the numbers reflecting diseased patients were held constant at 21 and four, whereas the numbers referring to disease-free patients were increased arbitrarily tenfold from 3 and 22 to 30 and 220 to reflect an increasing proportion of normal patients (i.e., lower prevalence of disease). Calculations are based on these data. The numbers at the bottom of the columns and at the end of the rows were determined by addition of the two figures of the corresponding column/row. The number at the extreme lower right reflects the sum of the corresponding column/row and represents the total number of patients examined. Finally, the six ratios are calculated according to their definitions.

Analysis of Terms

The ratios for all three tables are summarized in Table 4. The values of false-positive/negative ratios also have been

TABLE 2: Outpatients, Representative of Intermediate Prevalence

Test	Disease		Total
	Present	Absent	
Positive	21	30	51
Negative	4	220	224
Total	25	250	275

Note.—Prevalence of disease (25/275) = 0.09; sensitivity (21/25) = 0.84; specificity (220/250) = 0.88; positive predictive value (21/51) = 0.41; negative predictive value (220/224) = 0.98; accuracy ([21 + 220]/275) = 0.88.

TABLE 3: Inpatients, Representative of Low Prevalence

Test	Disease		Total
	Present	Absent	
Positive	21	300	321
Negative	4	2200	2204
Total	25	2500	2525

Note.—Prevalence of disease (25/2525) = 0.01; sensitivity (21/25) = 0.84; specificity (2200/2500) = 0.88; positive predictive value (21/321) = 0.07; negative predictive value (2200/2204) = 0.99; accuracy ([21 + 2200]/2525) = 0.88.

TABLE 4: Summary of Values

Ratio	Inpatients	Outpatients	Screening
Prevalence	0.50	0.09	0.01
Sensitivity	0.84	0.84	0.84
Specificity	0.88	0.88	0.88
Positive predictive value (PV+)	0.88	0.41	0.07
False-positive	0.12	0.59	0.93
Negative predictive value (PV−)	0.85	0.98	0.99
False-negative	0.15	0.02	0.01
Accuracy	0.86	0.88	0.88

Note.—The relationships between positive/negative predictive values and false-positive/negative values are as follows: (PV+) + FP = 1 and (PV−) + FN = 1.

included. Sensitivity and specificity have not changed at all, and accuracy has changed only slightly. The values of the other parameters have changed considerably, however. Let us discuss each ratio in more detail now.

Sensitivity and Specificity

These terms represent the inherent characteristics of the test. We need two ratios because we are dealing with two groups of patients—diseased and nondiseased. When the test is used on the diseased patients, the sensitivity will be defined—it is simply the proportion of correct results. Similarly when used on the nondiseased or "control" group the specificity also will be defined—it too is the proportion of correct responses in this group of patients.

Thus the sensitivity tells how "accurate" the test is among diseased patients, and specificity tells how "accurate" the test is among nondiseased patients. The sensitivity was held constant in order to ensure that the proportion of correct responses among diseased patients did not change. Similarly, the specificity was held constant to ensure that the proportion among nondiseased patients did not change. Thus, sensitivity and specificity are not affected by the ratio of the two groups of patients—that is, they do not depend on the prevalence of disease. However, the prevalence of disease will have a major effect on how the test will work for you! We will come back to this point shortly.

The values of sensitivity and specificity are very important because they represent the inherent strengths of the test. There are some problems that must be addressed before these ratios can be determined. Two that seem important enough to mention now are the gold standard and the selection of the population of patients. Let us consider each of these briefly:

1. Gold standard. It was mentioned that there are two groups of patients—diseased and nondiseased. The gold standard is used to define these groups. Therefore, the gold standard is used to define the "truth." Some common methods are long-term follow-up, surgical results, and comparison with other tests. Often the reference standards are not infallible, and thus the two groups of patients cannot be accurately defined.

One good example of this problem concerns the comparison of endoscopy with barium studies. Often endoscopic criteria are used to evaluate the merits of barium exams. This is clearly skewed because endoscopic results are used to define the truth—hence they are perfect by definition! Therefore, these comparisons will always show that endoscopy is superior to radiologic analysis. What would be a better way to define the "truth"? Good question—there really is not a suitable alternative in this case.

Furthermore suppose that one is evaluating a new fluoroscopic technique by using prior test results as a gold standard. One might look very hard for disease in those patients with a prior positive test and less diligently when the prior tests were negative. Generally the harder you look, the more you will find. If this is true, then you will find more abnormalities in patients with prior positive tests—thus artificially raising the sensitivity. Conversely, a "quick look" in patients with prior negative tests will yield a high specificity.

The bottom line is that the gold standard often is not infallible, thus causing the values of sensitivity and specificity to be less than ideal.

2. Test population. Another problem that may arise when defining sensitivity and specificity relates to the type of patients found in the two groups. If the diseased group contains obvious disease, then the test will frequently yield positive results—resulting in a high sensitivity. This may happen in a major referral hospital, where the majority of investigations are conducted. For example, suppose that we wish to evaluate a new MR contrast agent for the detection of liver metastasis, and we examine patients who all have multiple large lesions. The chances of a positive result would most likely be higher than if the patients had early disease, a situation that more nearly approximates the situation in a community hospital. Therefore, a local radiologist will often be unable to reproduce the results reported in the literature.

Conversely if the nondiseased or "control group" consisted of young healthy adults, then a high specificity would be obtained. The control group should consist of patients who are in the same general age group and who have conditions that may be confused with liver metastasis. For example, some should have cirrhosis, benign liver lesions, or a history of hepatitis.

The bottom line here is that the population of patients used to define sensitivity and specificity should mirror as closely as possible the population of patients where the test will be used in routine clinical practice.

Prevalence of Disease

This term represents the number of patients in the test population who actually have the disease. The only difference between the inpatient/outpatient/screening clinics is prevalence, which was purposely altered. Knowledge of sensitivity, specificity, and prevalence permits the calculation of other factors such as PV+/PV− (or FP/FN), which tell you how the test will work for you.

In routine clinical practice, the value of prevalence must be estimated. It will vary among referring doctors. For example, the chance of a ventilation-perfusion lung scan being positive for pulmonary embolism might be higher if the patient were referred from an inpatient orthopedic service rather than from an outpatient clinic. It would also be higher if the patient were postoperative, immobile, and had a markedly decreased arterial oxygen saturation. Thus, prevalence refers to the population of patients actually examined and not to the general population walking the streets of your community.

Additionally "clinical intuition" is often used to estimate "prevalence" in an individual patient. In Bayesian analysis, this individualized connotation of prevalence is called the "prior probability" [3]. We will return to this subject in the section entitled "predictive values."

Surprisingly, prevalence or "prior probability" has a major effect on the reliability of a test's performance. Let us see why.

Predictive Values

The positive/negative predictive values allow one to specify how often a positive/negative result is correct. These values vary widely because of the effect of disease prevalence. For example, Table 4 shows that PV+ changes from 88% to 7% as prevalence decreases from 50% to 1%. This means that of 100 patients from the inpatient service (50% prevalence) who have a positive test, 88 will actually have a lung infection, whereas of 100 patients from the screening clinic (1% prevalence) with a positive test, only seven will have an infection. Note that we could not have determined this value without knowing three parameters: sensitivity, specificity, and prevalence. In general, as prevalence decreases, PV+ decreases and PV− increases. This indicates that as prevalence drops, an increasing proportion of patients with either positive or negative tests will be true-negative.

Let us return to consideration of a single patient by using Bayesian analysis. Look again at Table 4. Mentally change the word "prevalence" to "prior probability" (PP). If a clinician estimates the chance of disease is 50% (PP = 0.50), Table 4 tells us that a positive result raises the chance of disease to 88% (i.e., PV+ = 0.88). Using Bayesian terminology, we would say that the "posterior probability" is 0.88. A negative test implies that the chance of "no disease" is 85% (PV− = 0.85); therefore the chance of disease is 15%. In other words, a negative test has lowered the chance of disease from 50% to 15%.

However if PP is only 1%, Table 4 tells us that a positive result only raises the chance of disease to 7% (PV+ = 0.07). Conversely, a negative result has a 99% chance of being correct (PV− = 0.99). Therefore the chance of disease remains at 1%. If PP is 99%, further analysis shows that the chance of disease given a positive result is 99% and given a negative result is 95%. These results are summarized in Table 5.

In general, prevalence (or prior probability) has a major effect on the likelihood of disease. The results of any test are most useful when the status of the patient is unclear before the test is performed. With a low or high prevalence (or PP), an unexpected negative or positive result is not very helpful. To avoid prejudice, the estimation of PP should be made before the test results are known.

False-Positive/Negative Ratios

These ratios are closely related to predictive values. Given a positive result, PV+ tells how often you are correct, whereas the FP depicts the likelihood of being wrong. Because any positive result is either right or wrong, these two values always add up to unity (Table 4). An analogous situation exists for PV− and FN ratios.

TABLE 5: Effect of Prior Probability on Chance of Disease

Prior Probability (%)	Chance of Disease (%)	
	Positive Test	Negative Test
1	7	1
50	88	15
99	99	95

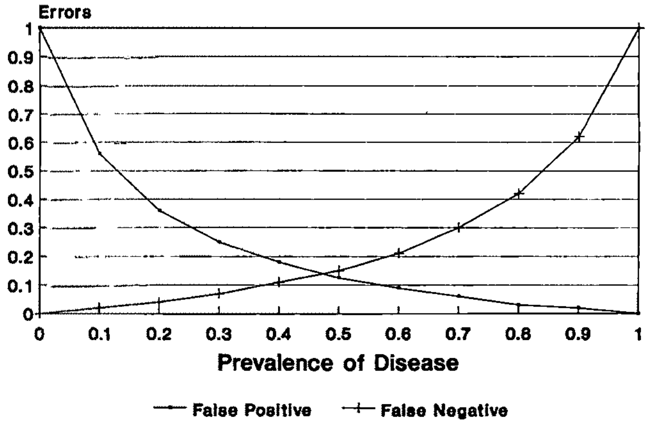

Fig. 1.—Relationship between false-positive (FP) errors, false-negative (FN) errors, and prevalence of disease. In most clinical settings, prevalence is less than 0.5, where graph shows that FP errors predominate. When prevalence is very high or very low, either FP or FN error ratios can approach 100%, resulting in poor test performance. NOTE: Curves were drawn assuming a sensitivity of 0.84 and a specificity of 0.88, same values used in Tables 1–4.

Like predictive values, the FP/FN ratios vary widely because of changes in disease prevalence. Note in Table 4 that the FP ratio increased from 12% to 59% to 93% as prevalence decreases. The 93% figure means that of 100 positive tests in the screening clinic, 93 are wrong!

Before going on, let us look further at the outpatient clinic with an FP ratio of 59%. This poor result is due to the prevalence of only 9%. If we perform a second test that is independent of the first on only those patients with a positive test, the new prevalence will be much higher at 21/51, or 41%. If CT has a sensitivity/specificity of 90%/90% in these circumstances, the new FP ratio would be 14%, much better than the 59% that we started with. As the FN ratio is only 2%, no further testing is needed on those patients with a negative test. Thus, the common practice of performing additional confirmatory tests in unclear situations has a sound quantitative basis. Figure 1 shows graphically how FP/FN ratios vary with prevalence. Note that either the FN or the FP ratio will approach 100% when prevalence is very high or low. Under these conditions, almost any test will perform poorly.

The practice of performing additional tests is often referred to as "two-phase testing." If both tests are positive, then the uncertainty regarding the true condition of the patient is reduced. Conversely if they are not both positive, then the amount of uncertainty regarding the patient's disease increases. Furthermore, the characteristics of each test are important. The first "screening" test should be very "accurate" in the diseased group so that as many as possible will be detected. A highly accurate test in the diseased group implies a high sensitivity. However, the price for a high sensitivity often is a high false-positive ratio. The second "confirmatory test" should work well in the nondiseased group—that is, have high specificity. Those nondiseased patients (i.e., the false-positives) will thus be detected and eliminated from further consideration. Usually a patient is considered "positive for disease" only if both tests are positive. Radiologic studies are often used for screening purposes (e.g., mammograms and chest radiographs). Those patients with a positive or equivocal result often are subjected to a more definitive examination such as bronchoscopy or lung or breast biopsy.

Accuracy

The last term to be discussed is accuracy. The values of PV+/− (or FP/FN) show that the test will perform very differently as prevalence changes. But the accuracy has not changed very much (Table 4). Why? Consider the following: If you issued negative reports on all of the patients in the screening clinic without ever looking at any of the films, you would be right in 2500/2525, or 99%, of the time. This is actually better than the 88% obtained by reading the films! Thus accuracy is not a useful term when applied to the results of tests in clinical patients. This is because this term tries to describe the test's reliability in two groups of patients—diseased and nondiseased—at the same time. Unfortunately this just is not possible. Also this term does not indicate the relative balance between FP and FN errors. We think that scientific journals should not permit improper use of this term (see the glossary for other definitions of "accuracy").

Related Topics

There are two topics that are very closely related to the concepts explained earlier. One has already been introduced—Bayesian analysis. This presents the same information using somewhat different terminology [1, 3]. Also it is possible to evaluate more than one test or disease simultaneously. For example, one could evaluate the merits of CT vs MR imaging for the early detection of cerebral contusion or hemorrhage.

The second topic is the receiver-operating-characteristic (ROC) curve [4, 5]. In this article, we have assumed that the test was always performed and interpreted in the same way, thus holding sensitivity/specificity constant. Suppose a second radiologist interpreted the same films in such a way as to minimize false-negatives by reading the chest films "very closely," whereas a third felt that the false-positive ratio should be minimized and called results positive only if they were clear-cut. Assuming that the radiologists have equal interpretive skills, each would obtain a different set of values for sensitivity/specificity, and all would be valid. If these were plotted on a suitable graph, one would obtain an "ROC curve." This graph allows one to determine the strengths of the test independent of decision-threshold effects. The FP/FN tradeoffs could be evaluated quantitatively, and direct comparisons between the ROC curves of other tests would be possible. However, these considerations are outside the scope of this article.

Conclusion and Comments

Medical decision making is a quantitative tool that is useful when data can be classified into two distinct groups. Its widespread use in radiology arises from the desire of patients and doctors who prefer and often expect a positive or negative report. The reliability of these reports is related not only to the inherent strengths of the test and the skill of the radiologist but also strongly to prevalence of disease. Both radiologists and referring clinicians should be aware of these facts in order to avoid skewed expectations that could result from direct transfer of information from the literature. A surgeon who reads that sonography is 95% "accurate" for liver metastasis or that the false-positive ratio is less than 5% should not expect the local radiologist to reproduce these results. However, it appears that referring clinicians often do expect these results. This could lead to a lack of confidence in the radiologist, causing strained work relationships and perhaps encouraging some clinicians to provide radiologic services themselves. We hope that awareness of the effects of disease prevalence on test performance will help to avoid this situation.

When reading the literature, one should focus on the inherent test characteristics: sensitivity and specificity. Then one needs to estimate prevalence or prior probability of disease and use these data to define positive/negative predictive values (or FP/FN errors). Two ways to do this would be to use the formulas in the appendix or to use the graph in Figure 1, realizing that it was constructed for sensitivity/specificity values of 0.84/0.88. However, these values approximate those of many radiologic tests with sensitivity/specificity values of 80–90%.

For interested readers, a short list of references [6–8] and an appendix have been provided.

Appendix: Application of Principles

Think about the following situation to see whether you fully understand the preceding discussion.

Problem: A radiologist whose referral base is a suburban outpatient population reads an article describing a study comparing a new bone scanning agent whose accuracy in the detection of osteomyelitis (88%) is reported to exceed the accuracy of the standard agent (83%). The radiologist begins using the new agent but soon finds that his referring physicians detect no difference in the quality of his readings and some even suspect that they may be less accurate than when he was using the old scanning agent. He angrily writes a letter to the editor. What could be the explanation?

Answer: Remember accuracy is a misleading term because it is population-dependent. Closer reading of the article shows an improved sensitivity for the new agent of 95% compared with 85% for the old agent and a decrease in specificity from 75% for the old agent to 65% for the new agent. Further investigation reveals that the paper was written at an institution where there was a high incidence of osteomyelitis in a diabetic population. In fact, the population of patients on whom the article was based included 80 patients, 75% of whom had documented osteomyelitis. As the radiologist's referral base is a suburban outpatient population with a much lower incidence of osteomyelitis (only 15%), let us see what comparative results will be obtained.

We will need to find the FP and FN rates, remembering that FP + PV+ = 1, and FN + PV− = 1. PV+/− can be directly calculated by using the following relationships, which can be derived from the definitions of the relevant terms and some algebra:

$$PV+ = \frac{PS}{PS + (1 - P)(1 - s)} \qquad PV- = \frac{s(1 - P)}{s(1 - P) + P(1 - S)}$$

where P is prevalence of disease, S is sensitivity, and s is specificity.

We substitute as follows:

	old bone scan agent	new bone scan agent
P	0.15 and 0.75	0.15 and 0.75
S	0.85	0.95
s	0.75	0.65

and obtain these results, which show how the FP/FN rates change when switching from the old agent to the new one:

Prevalence	0.75	0.15
FP(%)	9 → 11	63 → 68
FN(%)	38 → 19	3 → 1

When the prevalence is high at 75%, the FP rate increases only 2% (9% to 11%), whereas the FN rate drops in half from 38% to 19%, a 19% change. In other words, the small increase in FP is offset by a big drop in FN. Therefore, the new agent has significant advantages in this setting.

However, when prevalence is lower at 15%, the radiologist sees a 5% increase in FP and only 2% decrease in FN. Therefore, the radiologist actually does better with the old test, which has a higher specificity, better suited to his population of patients with a lower prevalence of disease.

This example shows how it can be difficult to transfer information directly from the literature to routine clinical practice. Here are two other issues that should be addressed:

1. Are the changes in FP/FN due to chance or are they real? In other words, are the differences statistically significant? For example, the results could be invalid if the sample size were too small [9].
2. The sensitivity/specificity values used assumed that the bone scans were interpreted in the same way. Suppose that the criteria for interpretation were altered? Then ROC curves for both agents would have to be constructed and compared. This would be the best way to compare these two agents.

Glossary

accuracy 1. proportion of correct results; not scientifically correct in medical decision making, where prevalence of disease is a factor. 2. area under receiver-operating-characteristic curve.

Bayes' theorem method used to revise probability of disease given additional information, such as a positive or negative test.

conditional probability probability that something is true given that something else is true (e.g., sensitivity, specificity, and positive and negative predictive values).

control group nondiseased group.

cutoff point boundary between what is defined as "diseased" vs "nondiseased" or what is normal vs abnormal. In ROC analysis, this is varied to produce a graph.

false-negative 1. total number of negative results that were incorrect. (In Table 2, there were four false-negative cases.) 2. individual test result that is negative but incorrect. 3. the proportion of patients with a negative result that was incorrect. (In Table 2, this is 4/224 or 0.02.) It is equal to 1− negative predictive value. Varies with prevalence of disease. In routine clinical practice indicates likelihood that a negative result is wrong. 4. proportion of patients with disease who have a negative test. (In Table 2, this is 4/25 or 0.16.) It is equal to 1− sensitivity. Does not vary with prevalence of disease. Used in receiver-operating-characteristic analysis.
Note: When third or fourth definition of "false negative" is used, modifiers (decisions, fraction, percentages, rate, ratio, response, etc.) may be used differently by various authors. Example: "false-negative rate."

false-positive 1. total number of positive results that were incorrect. (In Table 2, there were 30 false-positive cases.) 2. individual test result that is positive but incorrect. 3. proportion of patients with a positive result that was incorrect. (In Table 2, this is 30/51 or 0.59.) It is equal to 1− positive predictive value. Varies with prevalence of disease. In routine clinical practice, indicates likelihood that a positive result is wrong. 4. proportion of patients with no disease that have a positive test. (In Table 2, this is 30/250 or 0.12.) It is equal to 1 − specificity. Does not vary with prevalence of disease. Used in receive-operating-characteristic analysis.
Note: When third or fourth definition of "false positive" is used, modifiers (decisions, fraction, percentages, rate, ratio, response, etc.) may be used differently by various authors. Example: "false-positive rate."

gold standard reference examination used to categorize subjects as diseased or nondiseased.

likelihood ratio probability of a certain test result given disease divided by same result given no disease. If result is positive, then Table 2 shows that it would equal 21/25 divided by 30/250, or 7.00. This means that a positive result is seven times more likely in a diseased patient than in a nondiseased one.

predictive value probability of disease/no disease given a positive/negative test.

pretest probability *same as* prior probability

prevalence proportion of patients in test population who are diseased

posterior probability in Bayesian analysis, likelihood of disease after test is done.

posttest probability *same as* posterior probability.

prior probability in Bayesian analysis, likelihood of disease before test is done. Represents individualized connotation of prevalence, but often is more accurate than prevalence because referring clinicians know more about an individual patient than is generally known about test population as a whole.

receiver-operating-characteristic curve (ROC curve) graphic relationship between sensitivity and 1− specificity that allows evaluation of test performance by using a variety of cutoff points. It is independent of disease prevalence. Also allows comparison of one test with another [4, 5].

screening test test used to find as many cases as possible in a given population, usually associated with low prevalence of disease. Should have high sensitivity.

sensitivity 1. medical decision-making term: probability of positive test given presence of disease. 2. nonmedical decision-making term: likelihood of finding a disease if it is present. Example: MR has a higher sensitivity than does CT for brain lesions in the posterior fossa.

specificity 1. medical decision-making term: probability of negative test given no disease. 2. nonmedical decision-making term: likelihood of determining the exact nature of any abnormality found. Example: MR has a low specificity for determining the exact nature of brain lesions [2].

true-negative fraction (TNF) *same as* specificity (first definition).

true-positive fraction (TPF) *same as* sensitivity (first definition).

REFERENCES

1. Phillips WC, Scott JA, Blasczcynski G. Statistics for diagnostic procedures. 1. How sensitive is "sensitivity"; how specific is "specificity"? *AJR* **1983**;140:1265–1270
2. Harris RD. Diagnostic specificity: proper usage (letter). *AJR* **1989**;153:653
3. Chang PJ. Bayesian analysis revisited: a radiologist's survival guide. *AJR* **1989**;152:721–727
4. Metz CE. Basic principles of ROC analysis. *Semin Nucl Med* **1978**;8:283–298
5. Swets JA. R.O.C. analysis applied to the evaluation of medical imaging techniques. *Invest Radiol* **1979**;14:109–121
6. Patton DD. Introduction to clinical decision making. *Semin Nucl Med* **1978**;8:273–282
7. Feinstein AR. Clinical biostatistics XXXI: on the sensitivity, specificity, and discrimination of diagnostic tests. *Clin Pharmacol Ther* **1975**;17:104–116
8. McNeil BJ, Keeler E, Adelstein SJ. Primer on certain elements of medical decision making. *N Engl J Med* **1975**;293:211–215
9. Phillips WC, Scott JA, Blasczcynski G. Statistics for diagnostic procedures. II. The significance of "no significance." What a negative statistical result really means. *AJR* **1983**;141:203–206.

Book Review

Videofluoroscopic Studies of Speech in Patients with Cleft Palate. By M. Leon Skolnick and Ellen R. Cohn. New York: Springer-Verlag, 186 pp., 1989. $95

The authors have written a valuable book that codifies more than 14 years of personal practical clinical experiences with multiview videofluoroscopy. It contains 119 figures in 429 parts that excellently demonstrate, mostly in line drawings, the videofluoroscopic findings relative to speech in patients with cleft palate. The drawings from videotape images are used rather than still photographs of actual video frames because the authors contend that line drawings convey concepts more clearly and rapidly. Performance and interpretation of videofluoroscopy are as much an art as they are a science. The book is organized in 17 chapters that include the following: the why and how of imaging the velopharyngeal portal; equipment and techniques for multiview videofluoroscopy; anatomy of the velopharyngeal portal and Passavant ridge; interpretation, readings, and report writing; congruence of portal dimensions among multiviews; patterns of velopharyngeal closure in patients with and without pharyngeal flaps; fundamental principles of normal speech production; speech patterns of velopharyngeal dysfunction; the speech protocol; and preparing the patient and obtaining cooperation.

In patients with speech evidence of velopharyngeal insufficiency, velopharyngeal videofluoroscopy furnishes information that helps the clinician improve the patients' quality of speech. The velopharyngeal portal is imaged in motion and with simultaneous speech recording in three planes—lateral, frontal, and base—by using barium and air as contrast media. The authors offer good reasons for preferring videofluoroscopy over cinefluoroscopy, specifically, the 10 times lower dose of radiation and the facility for synchronous recording of speech with morphologic and functional images. Although they refer to the advantages of C-arm fluoroscopy for this examination, the practicality of its use for this examination in most radiology departments is questionable. Usually, the C-arm fluoroscope is not readily available in the main department.

Of particular importance is the chapter on the cleft palate team because the videofluoroscopic examination of the velopharyngeal portal is an unfamiliar procedure to most radiologists. Basic knowledge of speech pathology and familiarity and ease in working with children are necessary for the radiologist to do this procedure well. The American Cleft Palate Association has specified that the minimal staff for a cleft palate team comprises a plastic surgeon, a speech-language pathologist, and a dentist. However, an expanded team may include an orthodontist, an otolaryngologist, a prosthodontist, a pediatrician, a psychologist, a radiologist, a geneticist, and a social worker or pediatric nurse practitioner. When craniofacial surgery is necessary, a neuroradiologist, a neurosurgeon, and an ophthalmologist also may serve. The authors appropriately emphasize that the radiologist should be involved with the meetings of the team to gain better understanding of velopharygneal behavior while assisting others in learning the limitations and the advantages of videofluoroscopy.

The chapter on ethical concerns is also noteworthy, and the recommendation of the authors that the following questions be addressed before requests are made for the "clinically necessary" videofluoroscopic velopharyngeal examination is appropriate: (1) the clinical need question: "Is it strongly anticipated that the data supplied by the videofluoroscopic examination will potentially alter the course of clinical treatment?" (2) the alternative methods question: "Are there equally effective means by which to obtain the needed information which involve less or no radiation?" and (3) the so what question: "What will be done if velopharyngeal insufficiency is detected?" The book ends with a nice touch for the patient and the patient's family: an appendix that includes a story orientation to videofluoroscopy for young children.

Overall this is an extremely informative book about the specialized velopharyngeal examination by videofluoroscopy in patients with cleft palate. The book has no serious weaknesses, and I have no serious criticisms of it. I recommend it to all potential members or members of a cleft palate team, especially the radiologists.

Lionel W. Young
Children's Hospital Medical Center of Akron
Akron, OH 44308

Expert Advice

Radiologic Investigation of Dysphagia

Marc S. Levine[1] and Stephen E. Rubesin

Dysphagia is defined as the subjective awareness of swallowing difficulty during passage of a solid or liquid bolus from the mouth to the stomach. This symptom may be caused by abnormalities of the oral cavity, pharynx, esophagus, or cardia of the stomach. A barium study is often requested to elucidate the underlying abnormality. In the best circumstances, this examination should include videofluoroscopic evaluation of the oral cavity, pharynx, and cervical esophagus; upright double-contrast views of the pharynx and esophagus; recumbent double-contrast views of the gastric cardia and fundus; prone single-contrast and mucosal relief views of the esophagus; and evaluation of esophageal motility. In practice, however, the examination usually is tailored to individual patients on the basis of the clinical history. Our radiologic techniques for evaluating these patients at the Hospital of the University of Pennsylvania have evolved considerably during the past decade. On the basis of our experience, we have devised a practical approach for the radiologic investigation of dysphagia.

Clinical Perspective

Many patients with dysphagia subjectively can localize a sensation of blockage or discomfort to the throat or chest. Patients with pharyngeal dysphagia typically complain of a "lump in the throat" or of food "sticking in the throat" during swallowing. Pharyngeal dysphagia may be caused by a functional abnormality such as cricopharyngeal dysmotility or by a morphologic abnormality such as a Zenker diverticulum or pharyngeal tumor. Other pharyngeal symptoms include coughing or choking during swallowing due to laryngeal penetration and a nasal-quality voice or nasal regurgitation due to soft-palate insufficiency. An abnormal oral phase of swallowing may be manifested by food dribbling from the mouth, difficulty in chewing, or difficulty in initiating the swallow. Whether an abnormality is suspected in the oral cavity or pharynx, a dynamic examination should be performed in all patients with pharyngeal symptoms [1, 2].

Other patients with dysphagia have a sensation of blockage at the level of the suprasternal notch or thoracic inlet. This symptom raises the possibility of a cervical esophageal web or tumor or of extrinsic compression of the cervical or upper thoracic esophagus by an enlarged thyroid, mediastinal lymphadenopathy, or other mass lesion. The videofluoroscopic examination of the pharynx therefore should include views of the cervical or upper thoracic esophagus in these patients.

Other patients have substernal dysphagia with a sensation of blockage or discomfort anywhere from the thoracic inlet to the xiphoid process. As in the pharynx, this symptom may be caused by a functional abnormality in the esophagus such as achalasia or by a structural abnormality such as a ring, stricture, or tumor. Carcinoma of the gastric cardia or fundus may produce similar symptoms. Therefore, a careful radiologic examination of the esophagus and cardia should be performed as the initial study in all patients with substernal dysphagia.

Unfortunately, the ability of the radiologist to perform a tailored examination is complicated by the fact that the patient's subjective assessment of the site of dysphagia does not always correlate with the site of the pathologic finding. Not infrequently, abnormalities of the mid or distal esophagus or even the gastric cardia may cause referred dysphagia to

---

Received December 11, 1989; accepted after revision February 1, 1990.

[1] Both authors: Department of Radiology, Hospital of the University of Pennsylvania, 3400 Spruce St., Philadelphia, PA 19104. Address reprint requests to M. S. Levine.

AJR 154:1157-1163, June 1990 0361-803X/90/1546-1157 © American Roentgen Ray Society

the pharynx or upper thorax. As a result, the esophagus and cardia also must be examined radiographically in patients with pharyngeal symptoms, particularly if the pharyngeal study fails to explain the patient's dysphagia. At the same time, pharyngeal abnormalities almost never cause referred dysphagia below the level of the thoracic inlet, so a careful pharyngeal study is unnecessary in patients whose dysphagia is localized to the region of the mid or lower sternum. Thus, a combined radiologic examination of the pharynx, esophagus, and gastric cardia should be performed primarily in patients who have pharyngeal or upper esophageal symptoms [3].

Other patients may have odynophagia (pain on swallowing) without a sensation of blockage. Odynophagia is the classic symptom in patients with opportunistic (i.e., fungal or viral) esophagitis. However, this symptom also may be caused by mucosal ulceration associated with other types of esophagitis or esophageal tumors. Still other patients may have chest pain unrelated to swallowing. The presence of episodic substernal burning or pain exacerbated by lying down or bending over is highly characteristic of gastroesophageal reflux disease. Chest pain or dysphagia also may be a symptom of diffuse esophageal spasm or other esophageal motor disorders. Thus, the radiologic examination should include both functional and morphologic evaluation of the esophagus in patients with substernal symptoms.

In summary, a rational approach for examining the patient with dysphagia requires a clear understanding of the nature and location of the underlying symptoms.

Examination Technique

Preparation

The pharynx, esophagus, and stomach should be as free of fluid and secretions as possible to permit optimal mucosal coating during the barium study [4]. The patient is instructed to fast overnight before having the examination. The patient also should avoid smoking or chewing gum, as these activities may stimulate salivary and/or gastric secretions and impair mucosal coating [4].

Routine Examination of the Pharynx

The pharyngeal study requires both a dynamic examination (either cineradiography or videofluoroscopy) to evaluate motility and a series of double-contrast spot films to evaluate morphology. Cine or video recordings of swallowing permit a frame-by-frame or slow-motion analysis of the parameters of deglutition, including tongue movement, soft-palate elevation, epiglottic tilt, laryngeal closure, cricopharyngeal opening, and pharyngeal peristalsis. At the same time, double-contrast spot films of the pharynx are important for detecting pharyngeal tumors or other morphologic abnormalities [5–7]. The radiologist's challenge is to integrate the dynamic and static images in a way that minimizes examination time without compromising diagnostic value. The following is a step-by-step approach for examining the pharynx:

Step 1.—Standing in a right lateral position (all radiographic projections are indicated with respect to the table top), the patient takes a mouthful (i.e., 8–10 ml) of high-density barium (E-Z-HD, E-Z-EM Co., Westbury, NY) and swallows the barium as a video recording is obtained on a full-field lateral view of the oral cavity and pharynx to show both the oral and pharyngeal phases of swallowing. After the fluoroscopic image is columnated and centered on the pharynx, a second swallow is videotaped in the lateral projection.

Step 2.—One set of two-on-one vertically split spot films of the pharynx is obtained in a lateral projection, centering the image so that it includes the region extending inferiorly

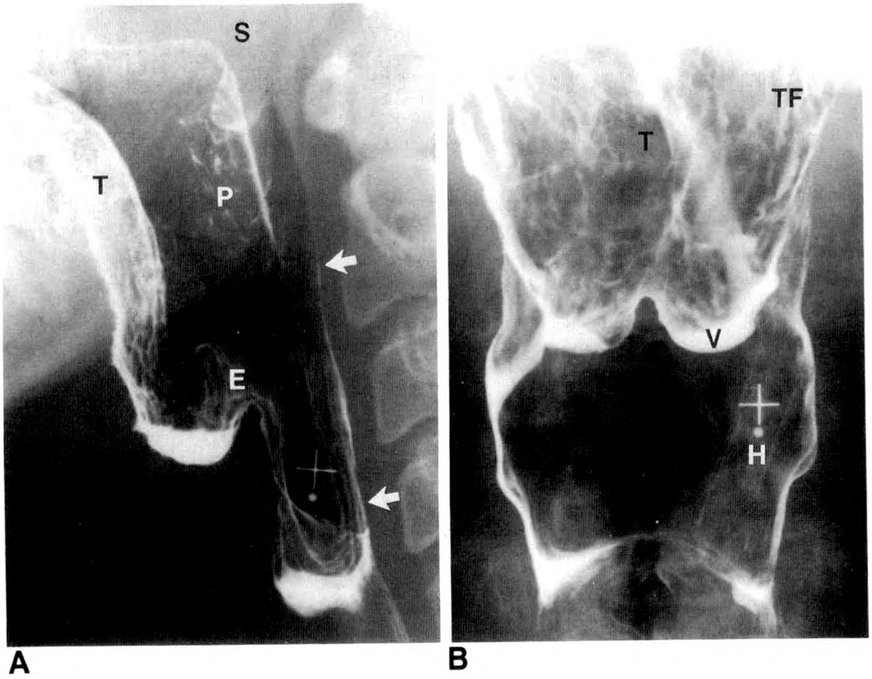

Fig. 1.—Spot films of normal pharynx.

***A*, Lateral view during phonation shows normal contours of soft palate (S), base of tongue (T), epiglottis (E), posterior pharyngeal wall (*arrows*), and palatine tonsil en face (P).**

***B*, Frontal view shows normal contours of tonsillar fossae (TF), valleculae (V), lateral walls of hypopharynx (H), and base of tongue en face (T).**

from the soft palate to the cricopharyngeus. One film is exposed during suspended respiration and the other during phonation. For the latter view, the patient is instructed to say "Eeeee ... " to expand the pharynx and permit optimal visualization of pharyngeal structures (Fig. 1A) [8]. These spot films should be obtained rapidly, and the patient should be instructed to avoid swallowing saliva between exposures to prevent deterioration of mucosal coating. Lateral views are best for showing abnormalities of the base of the tongue, posterior pharyngeal wall, anterior hypopharyngeal wall, epiglottis, and cricopharyngeus (Fig. 2) [8].

Step 3.—The patient is placed in a frontal position with the head tilted until the mandible is superimposed over the occiput, so that the pharynx is not obscured by these bony structures. Two separate swallows are videotaped to evaluate the pharynx in this projection. If esophageal compression by an enlarged thyroid or other cervical esophageal abnormalities are suspected, one or two additional swallows should be videotaped in a frontal projection with the image centered more distally at the level of the clavicles.

Step 4.—A second set of two-on-one vertically split spot films of the pharynx is obtained in a frontal projection (Fig. 1B). One film is taken during suspended respiration and the other during a modified Valsalva maneuver (i.e., the patient puffs out the cheeks against closed lips to optimally distend the pharynx) [9]. The frontal views are best for showing abnormalities of the valleculae, tonsillar fossae, and lateral walls of the hypopharynx (Fig. 3).

Tailored Examination of the Pharynx

Although scout films are not obtained routinely, frontal and lateral plain films of the neck may be helpful in cases of suspected foreign body, abscess, or fistula formation. In other patients who have an equivocal abnormality on the initial video recordings or spot films, additional swallows may be obtained to better delineate the area in question. Oblique views of the pharynx sometimes may be helpful in these patients. Flexion or extension of the neck under fluoroscopic guidance also may permit better visualization of anatomic structures such as the uvula, epiglottic tip, and hypopharynx [4].

In patients who have neuromuscular disorders resulting in laryngeal penetration (i.e., aspiration just before or during swallowing), the pharyngeal study may be performed with the assistance of a swallowing therapist from rehabilitation medicine or speech pathology. These patients may be asked to ingest barium of different viscosity or barium-impregnated substances (i.e., marshmallows or bread) so that swallowing can be evaluated better. They also may be asked to modify the position of the head or their breathing technique during swallowing to prevent or decrease laryngeal penetration or other types of swallowing dysfunction.

If the soft palate moves abnormally or nasopharyngeal regurgitation occurs during the routine pharyngeal study, intranasal barium may be given for a more detailed examination of this region [10]. Approximately 1–2 ml of high-density barium are instilled into the nares via a small syringe as the patient tilts the head up and swallows. This technique also permits better delineation of tumors or other abnormalities involving the superior surface of the soft palate (Fig. 4).

Routine Examination of the Esophagus and Cardia

As in the pharynx, the radiologic examination of the esophagus and cardia is performed to assess both morphologic and functional abnormalities. Double-contrast radiographs of upright patients are best for providing morphologic informa-

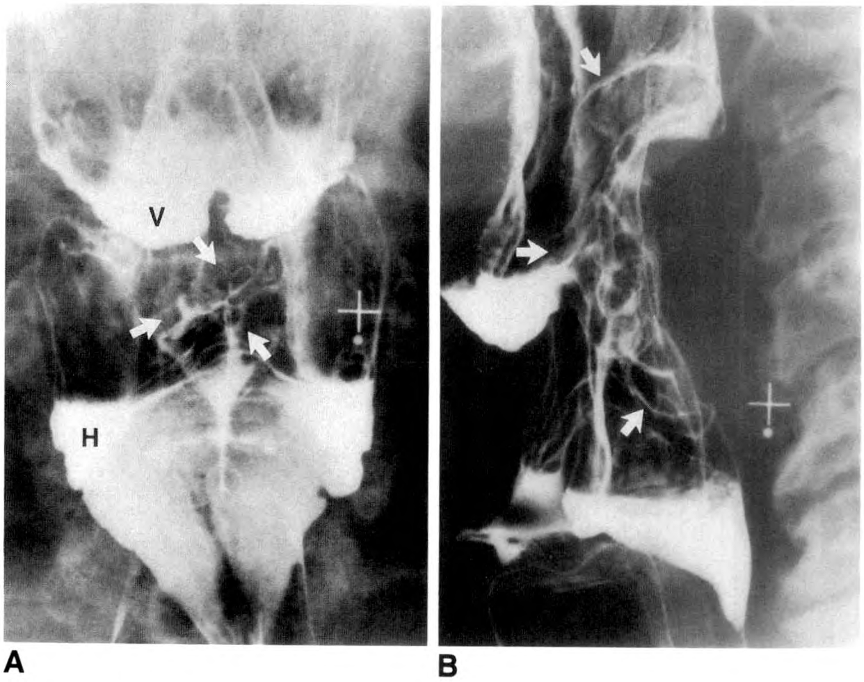

Fig. 2.—Spot films show pharyngeal carcinoma best on lateral view.

_A_, Frontal view shows retention of barium in valleculae (V) and hypopharynx (H) with aspirated barium in larynx. Note nodular mucosa (_arrows_) below level of valleculae.

_B_, Lateral view during phonation shows large, lobulated mass (_arrows_) on posterior pharyngeal wall that is poorly seen on frontal view.

(Reprinted with permission from Rubesin and Glick [4].)

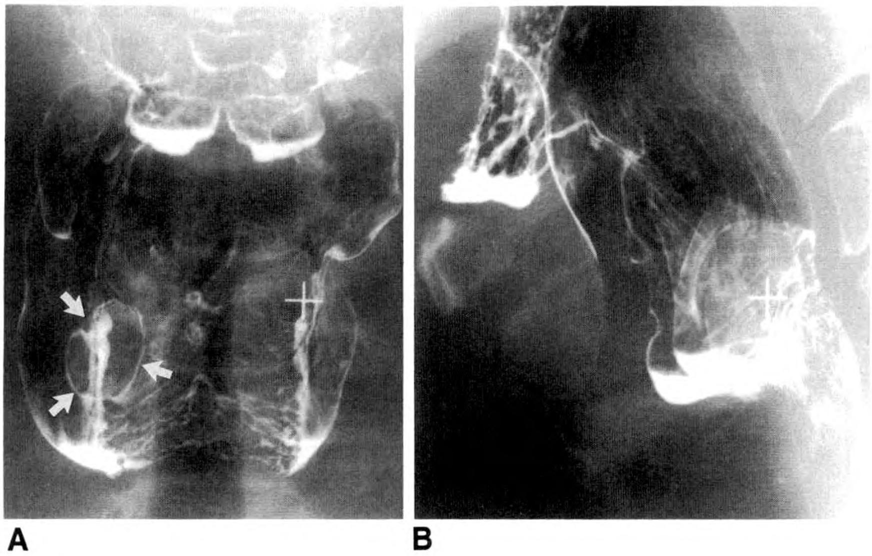

Fig. 3.—Spot films show aryepiglottic fold cyst best on frontal view.

A, Frontal view during modified Valsalva maneuver shows smooth, ovoid, 2-cm mass (*arrows*) in right hypopharynx. (Reprinted with permission from Rubesin and Glick [4].)

B, Mass is difficult to identify on lateral view during phonation.

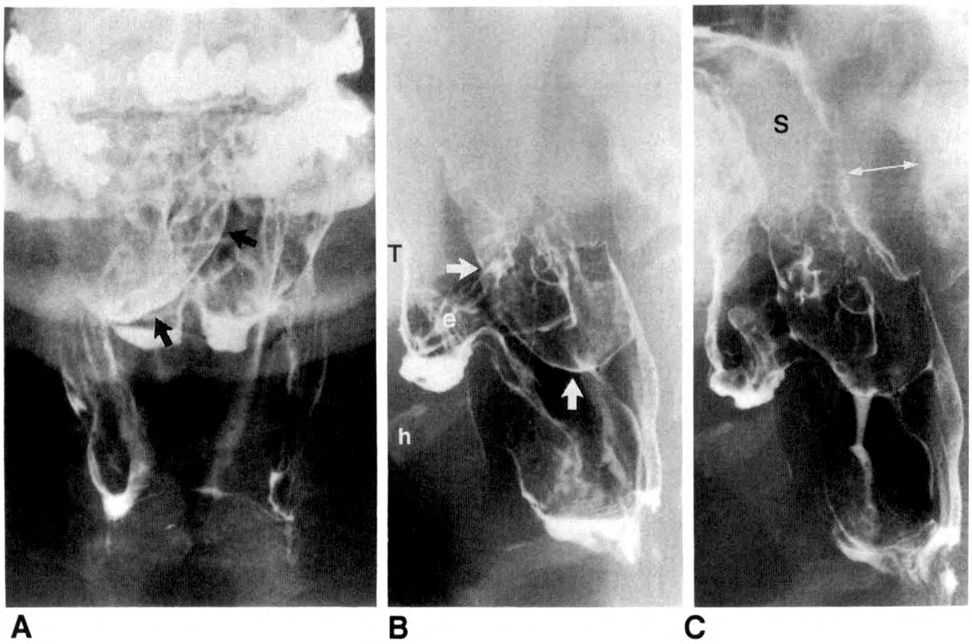

Fig. 4.—Spot films show value of intranasal barium for delineating tumor involving soft palate.

A, Frontal view of pharynx shows 6-cm mass (*arrows*) in region of right tonsillar fossa.

B, Lateral view during phonation shows centrally ulcerated mass (*arrows*) in palatine fossa. T = base of tongue; e = epiglottis; h = hyoid bone.

C, Lateral view after intranasal instillation of 2 ml of high-density barium shows enlarged, lobulated soft palate (S). Note irregular contour of posterior pharyngeal wall and widening of retropharyngeal space (*double arrow*). Biopsies revealed non-Hodgkin lymphoma.

tion about the esophagus. Double-contrast radiographs of the cardia are also important for detecting tumors or other abnormalities in this region that may cause dysphagia. At the same time, single-contrast radiographs of prone patients with the esophagus and gastroesophageal junction fully distended are best for detecting webs, rings, or strictures that can be missed on double-contrast views of an inadequately distended esophagus and gastroesophageal junction. Finally, single swallows of barium in the prone position are important for evaluating esophageal motility without the effects of gravity. Thus, a combination of techniques is required for optimal radiologic evaluation of the esophagus and cardia [11]. The following is a step-by-step approach for examining the esophagus and cardia:

Step 1.—The patient swallows a packet of effervescent granules (Baros, Lafayette Pharmacal, Lafayette, IN) and then 10 ml of water.

Step 2.—The patient rapidly gulps a cup (120 ml) of high-density barium (E-Z-HD) as one three-on-one or two two-on-one upright spot films of the esophagus are obtained in a left posterior oblique projection (Fig. 5A). Two exposures should be centered on the upper or mid esophagus and two on the distal esophagus. Although most patients swallow enough air to produce a double-contrast effect in the esophagus, subsequent peristalsis causes the esophagus to collapse almost immediately after passage of the barium bolus into the stomach. The fluoroscopist therefore must time the exposures to capture the esophagus during a relatively brief period of

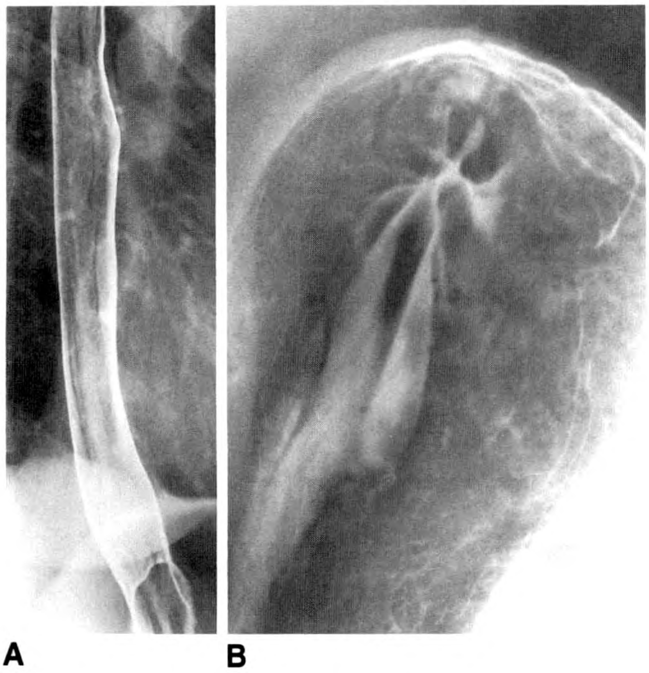

Fig. 5.—Spot films of normal esophagus and cardia.
***A*, Upright left posterior oblique view of esophagus.**
***B*, Right lateral view of gastric cardia and fundus. Note stellate folds radiating toward gastroesophageal junction.**

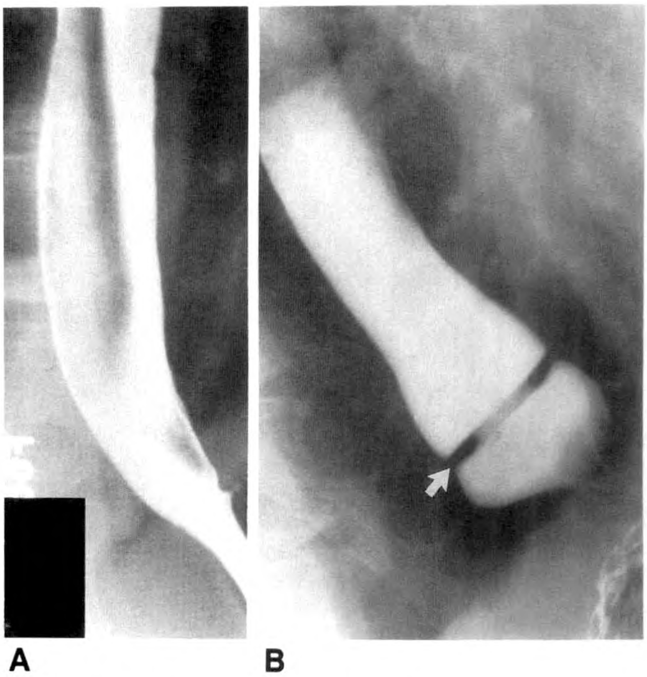

Fig. 6.—Radiographs of lower esophageal ring.
***A*, Double-contrast radiograph of distal esophagus in upright patient shows no definite ring.**
***B*, Single-contrast radiograph of prone patient shows unequivocal Schatzki ring (*arrow*) above sliding hiatal hernia.**
(Reprinted with permission from Laufer [11].)

optimal distension and coating. With some experience, it is possible to obtain satisfactory double-contrast views of the esophagus in 75–85% of patients [12, 13].

Step 3.—The table is brought to the horizontal position, and the patient turns to a right lateral position for a double-contrast view of the gastric cardia and fundus (Fig. 5B). The normal cardia usually appears en face as a stellate collection of folds radiating to a central button or dimple at the gastroesophageal junction (the esophageal "rosette") [14].

Step 4.—The patient drinks a low-density barium suspension (Solopake, E-Z-EM Co.) while in a prone right anterior oblique position. The patient takes two to five separate swallows of barium so that esophageal motility can be evaluated at fluoroscopy. During the initial swallow, the pharynx also should be observed fluoroscopically. If esophageal motility appears abnormal, a video recording of additional swallows should be obtained to document the abnormality. Then, one three-on-one or two two-on-one spot films of the esophagus are obtained while the patient continuously drinks low-density barium for optimal distension of the distal esophagus and gastroesophageal junction. This technique permits detection of lower esophageal rings and strictures that are not visible on double-contrast radiographs (Fig. 6) [15, 16].

Step 5.—The patient is turned onto the left side and then onto the back, so that barium pools in the gastric fundus. The gastroesophageal junction then is monitored fluoroscopically as the patient turns slowly to the right in order to show spontaneous gastroesophageal reflux. The patient also can perform a straight-leg-raising maneuver or Valsalva maneuver to increase intraabdominal pressure and elicit reflux.

Tailored Examination of the Esophagus and Cardia

When mucosal disease is suspected fluoroscopically on the double-contrast portion of the study, the patient may be turned 90° to the right and asked to swallow additional high-density barium in a right posterior oblique position in order to show protruded or depressed lesions both en face and in profile. Double-contrast radiographs in various projections are particularly helpful for showing plaques or ulcers associated with reflux disease, opportunistic infection, and other types of esophagitis (Fig. 7) [17–20]. If the initial double-contrast radiographs are inadequate, mucosal relief views of the collapsed or partially collapsed esophagus may provide additional information by showing abnormalities of the longitudinal folds that are due to varices, tumor, or esophagitis (Fig. 8).

In other patients who have equivocal abnormalities on the routine double-contrast study, a tube esophagogram may be obtained for a more detailed examination [21]. The tube esophagogram is obtained by passing a small red rubber catheter through the patient's mouth into the proximal thoracic esophagus. The patient then swallows high-density barium as air is gently insufflated through the catheter. The tube esophagogram is particularly helpful when the initial double-contrast examination is inconclusive because of in-

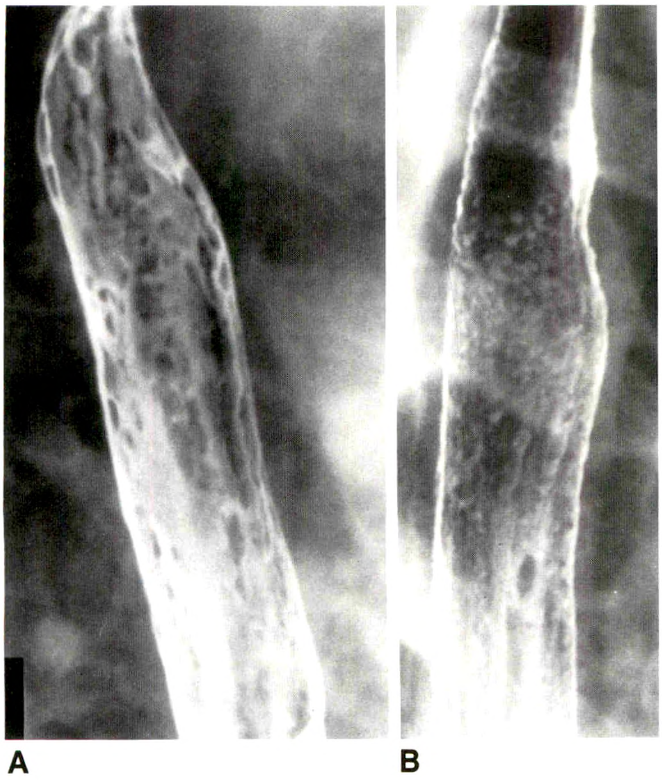

Fig. 7.—Infectious esophagitis diagnosed on basis of double-contrast esophagograms.

A, *Candida* esophagitis with multiple discrete plaquelike lesions.

B, Herpes esophagitis with numerous punctate ulcers. (Reprinted with permission from Levine et al. [19].)

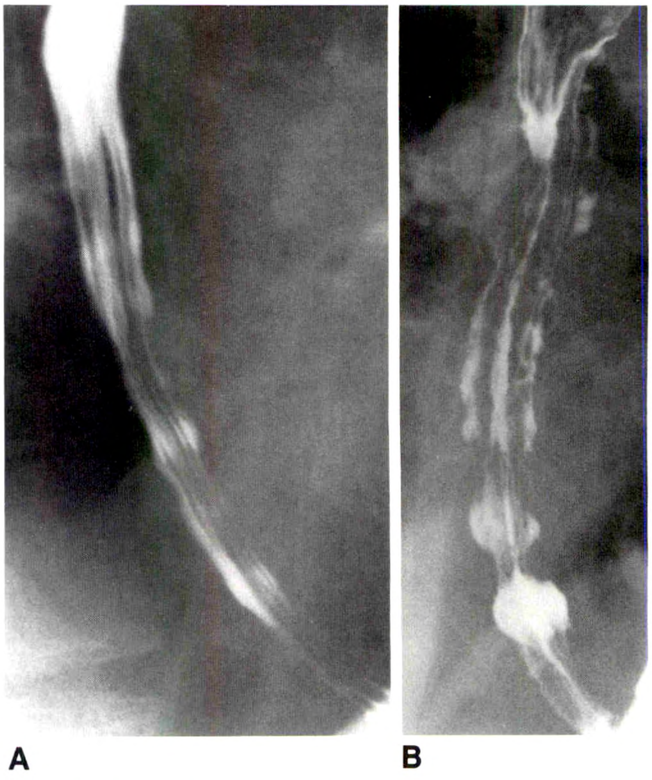

Fig. 8.—Mucosal relief esophagograms.

A, Normal appearance of collapsed esophagus. Longitudinal folds are thin, delicate structures several millimeters in diameter.

B, Marked thickening of longitudinal folds due to *Candida* esophagitis. (Reprinted with permission from Levine et al. [18].)

adequate distension or pooling of barium in the distal esophagus that obscures mucosal detail in this region (Fig. 9).

Double-contrast views of the gastric cardia are important for detecting malignant tumors or other abnormalities involving the cardia. Some patients with carcinoma of the cardia have an obvious mass lesion in the fundus; others have distortion or obliteration of the normal landmarks at the cardia with irregular areas of ulceration in this region (Fig. 10) [14, 22, 23]. Occasionally, it may be unclear whether a suspected mass at the cardia is a true lesion or normal invagination of the cardia into the fundus. In such cases, the patient should swallow additional barium in a recumbent right lateral position with the cardia visualized en face. The normal defect associated with the cardia should disappear as the lower esophageal sphincter relaxes and barium enters the stomach, whereas a true mass lesion at the cardia should be recognized as a persistent finding as barium streams past this region.

Recommended Approach

Patients with pharyngeal dysphagia or other symptoms localized to the pharynx, neck, or suprasternal notch should undergo a careful radiologic examination of the pharynx with videofluoroscopic recordings and double-contrast spot films. If the patient aspirates a substantial amount of barium, the examination should be terminated. If marked swallowing dysfunction (i.e., aspiration or nasopharyngeal regurgitation) occurs, particularly in stroke patients, a detailed study of the esophagus is unwarranted. Instead, one or two additional swallows with the patient in a recumbent or semiupright position are probably adequate to rule out gross esophageal disease. However, patients with pharyngeal carcinomas have a significantly increased risk of synchronous esophageal carcinomas [24, 25]. Therefore, a double-contrast examination of the esophagus should be performed when there is evidence of tumor in the pharynx. Finally, a normal pharyngeal study should always be followed by a careful examination of the esophagus and cardia to rule out more distal abnormalities causing referred dysphagia to the pharynx. A complete radiologic examination of the pharynx, esophagus, and cardia can be performed in reasonably cooperative patients in less than 10 min (including 2–4 min of fluoroscopy).

Conversely, patients with substernal dysphagia or odynophagia, reflux symptoms, or nonspecific chest pain should first undergo a detailed radiologic examination of the esophagus and cardia. A double-contrast esophagogram (done as a biphasic study, as described) can be obtained in most patients, although some debilitated or elderly individuals are able to tolerate only a limited single-contrast examination. When double- and single-contrast techniques are used to evaluate morphology and function, it generally is possible to show esophagitis, tumors, webs, rings, or strictures in the

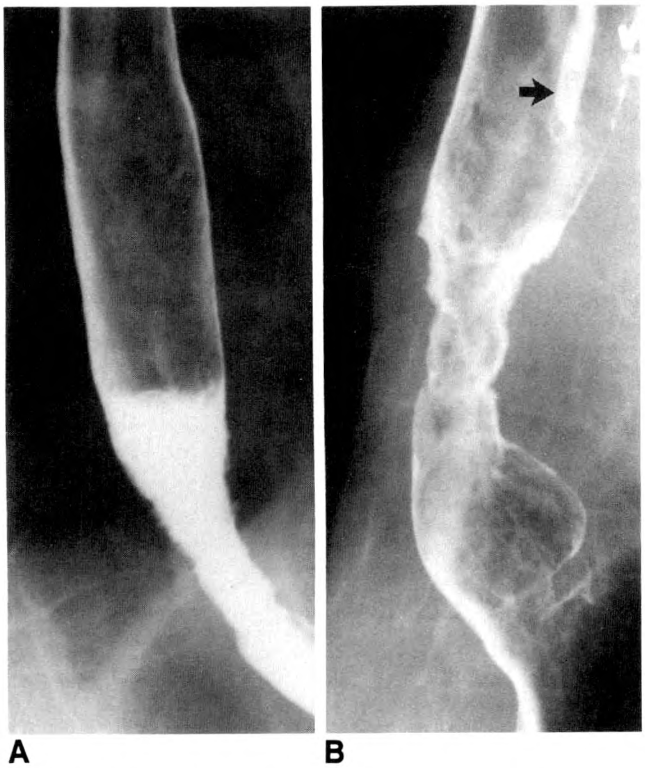

Fig. 9.—Value of tube esophagogram.

***A*, Initial double-contrast esophagogram shows distal esophageal narrowing with fine marginal serrations, suggesting benign peptic stricture with associated reflux esophagitis. However, distal esophagus is not distended optimally, and pooling of barium in this region obscures mucosal detail.**

***B*, Tube esophagogram permits better distension of distal esophagus, revealing infiltrating lesion with shelflike upper borders due to esophageal carcinoma (*arrow* shows tip of tube).**

(Reprinted with permission from Levine et al. [21].)

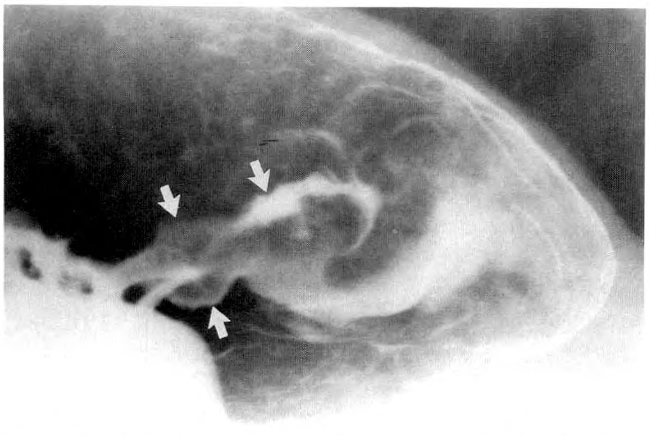

Fig. 10.—Double-contrast radiograph shows carcinoma of gastric cardia with obliteration of normal anatomic landmarks at cardia and irregular areas of ulceration (*arrows*) due to tumor in this region.

esophagus or esophageal motor abnormalities responsible for the patient's symptoms. Some esophageal disorders such as achalasia and gastroesophageal reflux disease may be associated with pharyngeal or cricopharyngeal dysfunction [26]. However, pharyngeal abnormalities virtually never cause referred dysphagia below the level of the thoracic inlet, so a limited pharyngeal study may be performed in patients with substernal symptoms.

REFERENCES

1. Curtis DJ, Hudson T. Laryngotracheal aspiration: analysis of specific neuromuscular factors. *Radiology* **1983**;149:517–522
2. Jones B, Kramer SS, Donner MW. Dynamic imaging of the pharynx. *Gastrointest Radiol* **1985**;10:213–224
3. Jones B, Ravich WJ, Donner MW, Kramer SS, Hendrix TR. Pharyngoesophageal interrelationships: observations and working concepts. *Gastrointest Radiol* **1985**;10:225–233
4. Rubesin SE, Glick SN. The tailored double-contrast pharyngogram. *CRC Crit Rev Diagn Imaging* **1988**;28:133–179
5. Ekberg O, Nylander G. Double contrast examination of the pharynx. *Gastrointest Radiol* **1985**;10:263–271
6. Balfe DM, Heiken JP. Contrast evaluation of structural lesions of the pharynx. *Curr Probl Diagn Radiol* **1986**;15:73–160
7. Rubesin SE, Jessurun J, Robertson D, Jones B, Bosma JF, Donner MW. Lines of the pharynx. *RadioGraphics* **1987**;7:217–237
8. Rubesin SE, Jones B, Donner MW. Contrast pharyngography: the importance of phonation. *AJR* **1987**;148:269–272
9. Jing BS. The pharynx and larynx: roentgenographic technique. *Semin Roentgenol* **1974**;9:259–265
10. Rubesin SE, Rabischong P, Bilaniuk LT, Laufer I, Levine MS. Contrast examination of the soft palate with cross sectional correlation. *RadioGraphics* **1988**;8:641–665
11. Laufer I. Technique and normal anatomy. In: Levine MS, ed. *Radiology of the esophagus*. Philadelphia: Saunders, **1989**:1–14
12. Balfe DM, Koehler RE, Weyman PJ, Baron RL, Reinus WR. Routine air-contrast esophagography during upper gastrointestinal examinations. *Radiology* **1981**;139:739–741
13. Maglinte DDT, Schultheis TE, Krol KL, Caudill LD, Chernish SM, McCune WM. Survey of the esophagus during the upper gastrointestinal examination in 500 patients. *Radiology* **1983**;147:65–70
14. Herlinger H, Grossman R, Laufer I, Kressel HY, Ochs RH. The gastric cardia in double-contrast study: its dynamic image. *AJR* **1980**;135:21–29
15. Chen YM, Ott DJ, Gelfand DW, Munitz HA. Multiphasic examination of the esophagogastric region for strictures, rings, and hiatal hernia: evaluation of the individual techniques. *Gastrointest Radiol* **1985**;10:311–316
16. Ott DJ, Chen YM, Wu WC, Gelfand DW, Munitz HA. Radiographic and endoscopic sensitivity in detecting lower esophageal mucosal ring. *AJR* **1986**;147:261–265
17. Laufer I. Radiology of esophagitis. *Radiol Clin North Am* **1982**;20:687–699
18. Levine MS, Macones AJ, Laufer I. *Candida* esophagitis: accuracy of radiographic diagnosis. *Radiology* **1985**;154:581–587
19. Levine MS, Loevner LA, Saul SH, Rubesin SE, Herlinger H, Laufer I. Herpes esophagitis: sensitivity of double-contrast esophagography. *AJR* **1988**;151:57–62
20. Bova JG, Dutton NE, Goldstein HM, Hoberman LJ. Medication-induced esophagitis: diagnosis by double contrast esophagography. *AJR* **1987**;148:731–732
21. Levine MS, Kressel HY, Laufer I, Herlinger H, Goren R. The tube esophagram: a technique for obtaining a detailed double-contrast examination of the esophagus. *AJR* **1984**;142:293–298
22. Freeny PC, Marks WM. Adenocarcinoma of the gastroesophageal junction: barium and CT examination. *AJR* **1982**;138:1077–1084
23. Levine MS, Laufer I, Thompson JJ. Carcinoma of the gastric cardia in young people. *AJR* **1983**;140:69–72
24. Goldstein HM, Zornoza J. Association of squamous cell carcinoma of the head and neck with cancer of the esophagus. *AJR* **1978**;131:791–794
25. Thompson WM, Oddson TA, Kelvin F, Daffner R, Postelthwait RW. Synchronous and metachronous squamous cell carcinomas of the head, neck, and esophagus. *Gastrointest Radiol* **1978**;3:123–127
26. Jones BJ, Donner MW, Rubesin SE, Ravich JJ, Hendrix TR. Pharyngeal findings in 21 patients with achalasia of the esophagus. *Dysphagia* **1988**;2:87–92

Book Review

Procedures in Diagnostic Radiology. By Terence Doyle, William S. C. Hare, Kenneth Thomson, and Brian Tress. New York: Churchill Livingstone, 235 pp., 1989. $29, softcover

This relatively short, softcover book describes many of the most common radiologic techniques. It is intendeded for residents who are learning the procedures or as a refresher for radiologists who are in private practice. The explanations are relatively brief and mainly present the authors' preferred methods. For each examination, the indications, equipment, technique, and complications are given. Practical ways to avoid complications are included and are helpful.

Chapter 3, which describes gastrointestinal and biliary system radiology, is a good example of the coverage. First, barium sulfate preparations are discussed. Subsequently, esophagograms and upper gastrointestinal studies that use the double-contrast technique are described. Then the methods of hypotonic duodenography, small-bowel series, and small-bowel enema are discussed briefly. Both the diagnostic (double contrast and a modified seven-pump method) and the therapeutic barium enema are handled succinctly. The short section on barium studies in the patient who has a colostomy is helpful. Next, oral cholecystography, IV cholangiography, operative cholangiography, and T-tube cholangiography are covered. Endoscopic retrograde cholangiopancreatography is described in terms of the role of the radiologist and not that of the endoscopist. The chapter ends with fairly detailed coverage of biliary calculus extraction and percutaneous transhepatic cholangiography, which is quite informative.

The main topics are assessment of patients, sedation and emergencies, urinary tract, gastrointestinal and biliary tract, vascular radiology, cerebral angiography, and arthrography. Invasive procedures receive the most emphasis. The book is well organized and easy to understand, with much of it presented in a practical format. It has a moderate number of good-quality diagrams but only a few reproductions of radiographs. This book is not all-inclusive, but most examinations are included. Nuclear medicine, sonography, CT, and MR imaging are not included.

The book is up to date. I found it interesting and helpful. Most residents need more detailed explanation as they develop their expertise, and their departments probably have different approaches to many of the examinations. Most practicing radiologists already know this information, but the book may be helpful if a new technique is encountered by the practitioner. Because the price is inexpensive and the topics are easy to find, the book has moderate value in one's library.

Harris Newmark III
Linda Vista Community Hospital
Los Angeles, CA 90049

Review Article

Pitfalls in the Radiologic Diagnosis of Lung Cancer

John H. Woodring[1]

Pitfalls in the radiologic diagnosis of lung cancer can be roughly grouped into three broad categories: (1) errors in the detection of subtle lung cancers; (2) errors in the analysis of solitary pulmonary nodules, including miscalculation of the growth of nodules and unusual growth patterns of lung cancer; and (3) lack of familiarity with uncommon manifestations of lung cancer. It is hoped that, through an increased understanding of these problems, radiologists will avoid some of the pitfalls that may be encountered in initially detecting and diagnosing lung cancer.

Pitfalls in the Detection of Subtle Lung Cancers

Perceptual Errors

The generally accepted error rate for the detection of early lung cancer is between 20% and 50%, and little improvement has been noted over the last few decades (Fig. 1) [1–3]. The results of several studies designed specifically to screen patients for the radiologic detection of early lung cancer suggest that the error rate for subtle lung cancers may be much higher. Heelan et al. [4], in a study of 168 patients with "incidence non-small-cell lung cancers" screened by yearly chest radiographs, detected 102 of the lung cancers by the routine annual screening process. Seventy-eight of these patients had had chest radiographs from the previous year; in retrospect, 51 (65%) of these had evidence of the cancer on the previous film. Similarly, Muhm et al. [5] detected 92 cases of lung cancer by routine radiologic screening at 4-month intervals. In retrospect, 90% of cases with peripheral lung cancers and 65% of cases with hilar cancers had tumor present on previous radiographs dating back months or years. This occurred despite adequate radiographic technique, routine double reading to avoid perceptual errors, and a high index of suspicion of the presence of the disease [4, 5]. In retrospect, Muhm et al. were very self-critical in the assessment of their results. Although 90% of the cancers were present on previous radiographs, many of the early cancers were extremely small and vague [5]. It is doubtful that very many of these early cancers could have been diagnosed as cancer prospectively. Still, their study does point out the limitation of plain film radiology in detecting early lung cancer.

A number of problems in the detection of subtle lung cancers, primarily related to the visual detection of lung nodules, have been enumerated in the literature. These problems can be categorized as being related to faulty visual search patterns and inadequate search duration, intentional and unintentional underreading of chest radiographs, contrast differences between the nodule and the surrounding areas, image noise, the complexity of the area surrounding the nodule, size and shape, and improper viewing conditions [1, 6–10].

Many think that errors in nodule detection are caused by correctable mistakes such as lapses of attention or failure to view all of the radiograph [6]. Those with this point of view assume that the nodule would have been reported if only it had been searched for properly and identified [6]. Of course, we are all aware of how obvious a missed nodule may seem once it is pointed out by someone else. It often is assumed that such errors would be eliminated if a more systematic approach to viewing the radiograph were developed and if more time were spent viewing the radiograph. When an

---

Received November 6, 1989; accepted after revision December 12, 1989.

[1] Department of Diagnostic Radiology, University of Kentucky Medical Center, 800 Rose St., Lexington, KY 40536-0084.

AJR 154:1165–1175, June 1990 0361-803X/90/1545-1165 © American Roentgen Ray Society

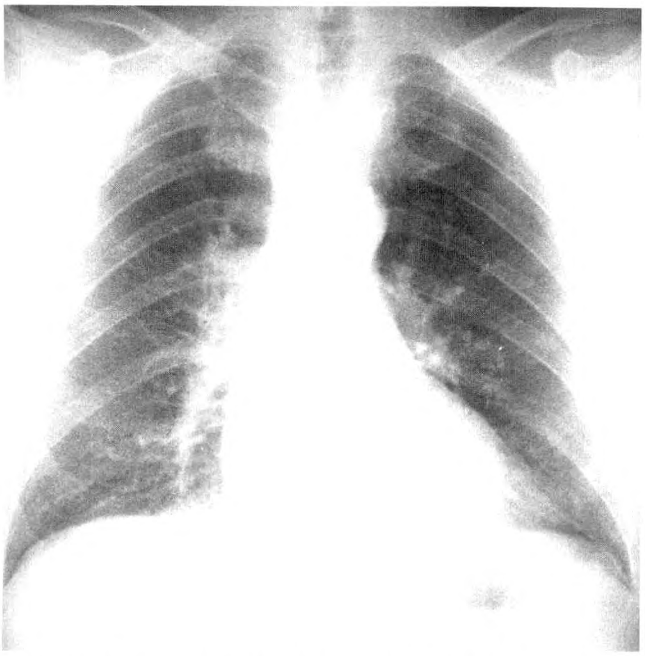

Fig. 1.—Chest radiograph in 41-year-old man with lower extremity weakness for 2 weeks. Do you see an abnormality? View the image for a few moments before proceeding. There is a 2.5 × 2.5-cm large-cell carcinoma in the superior pole of the right hilum and a 2.0 × 2.5-cm lung-to-lung metastasis posterior to the left subclavian artery. The patient also had spine, liver, and brain metastases. This case illustrates how subtle even an advanced case of lung cancer may be.

untrained observer views a radiograph, substantial portions of the image are neither searched nor recognized, and with specific training the search pattern is improved [10]. Still, studies of well-trained radiologists' eye movements during interpretation confirm that large areas of the film are never examined by foveal vision [6]. Kundel et al. [8] have shown that the probability that an observer will detect a subtle nodule during discovery scanning depends on four factors: nodule contrast, average distance between visual fixations, location of the nodule in the visual field during a single fixation, and search duration. Although it might appear that nodule detection could be improved by altering the visual search pattern so that the radiologist made systematic, closely spaced visual sweeps back and forth across the radiograph over a prolonged period of time until the entire film was searched exhaustively, studies in human visual scanning indicate that this cannot be accomplished [8]. When humans are searching for inconspicuous targets, they try to use the smallest possible visual field to cover the maximal area in minimal time [8]. As a result, the human visual search pattern is semisystematic at best with some areas never being studied [8]. It is apparent that, through the evolutionary process, humans have been provided with a visual search system that is best adapted for scanning in the real world, where reaction time is often crucial for survival [8]. In other words, in human visual scanning, accuracy has been sacrificed for speed [8]. Although this real-world situation does not apply to the interpretation of medical images, where reaction time is not important, human scanning behavior cannot be significantly altered [8].

The majority of obvious lung cancers are detected with flash viewing of the radiograph (0.2 sec) [8, 11]. Although the detection of subtle lung cancers is impaired severely by reducing viewing time to less than 4 sec [11], prolonged viewing time is of little or no value. By 10 sec, 85% of the lung is studied, and all of the nodules that will be reported have been seen [8]. If discovery viewing time is prolonged much beyond that length of time, the number of true-positive readings is unaffected, whereas the number of false-positive readings increases [10]. Kundel et al. [9] have shown that areas of the chest radiograph interpreted as falsely positive or suspicious receive prolonged visual attention; more than 90% of false-positive decisions are related to some perturbation in the image that the viewer cannot resolve [9]. Double reading of radiographs by two separate observers is very beneficial in reducing perceptual errors, particularly in forcing decisions on areas for which the readers lack confidence [5, 9]. Although the results of the lung cancer screening studies indicate that a substantial percentage of early cancers will still be missed by double reading [4, 5], comparison of single and double reading clearly shows the superiority of double reading [5, 9]. The false-negative rate for detecting early lung cancer may be reduced without an increase in the false-positive rate by double reading [5, 9]. A single observer also may place the films aside and reinterpret them at a later time, thus simulating double reading [8].

The human decision-making process plays a role in the failure to detect subtle lung cancers. Studies of radiologists' eye movements show that missed nodules are often adequately scanned by the fovea, and then rescanned after comparison eye movements, before the nodules are reported as negative [7]. In these cases the viewer is never consciously aware of having seen the nodule, of having made the comparison eye movements, or of having decided to ignore the nodule [7]. In fact, many missed nodules receive prolonged visual attention [9]. This suggests that there is an active, unconscious, mental process not to perceive a nodule [7]. This unconscious limitation of nodule perception may not be correctable [7].

Still, evidence indicates that intentional underreading also plays a role. Despite the fact that radiologists often state that false-negative errors are more important than false-positive errors, their performance indicates that they take false-positive errors much more seriously [7]. This may stem from subliminal or overt peer pressure from other radiologists and clinicians to drive the false-positive rate for the chest radiograph as low as possible. Swensson et al. [6] had a group of radiologists interpret a series of difficult chest radiographs under free search conditions, in which the pretest probability of abnormality was unknown, and report them as they would in the usual clinical setting. Subsequently, the same cases were interpreted in a focused search condition that directed readers to pay attention to specific anatomic regions on the chest radiograph and to report the pathologic findings (if any) [6]. The focused search did not improve the readers' ability to perceive the abnormalities, but did focus their attention on certain areas suggesting that the likelihood of abnormality might be greater in those regions [6]. As a result, the true-positive rate increased from 49% under free search conditions to 68% under focused search conditions, whereas the false-positive rate increased only from 4.6% to 10.6% [6]. Swensson et al. [6] concluded that the reduced omissions in the focused search scheme were the result of less stringent criteria for reporting the presence of abnormalities on the part of the radiologist when the pretest probability of abnormality was high. Therefore, the pretest probability of abnormality is important in the decision-making process related to the reporting of subtle radiologic findings; as the prevalence of cancer in the population from which the patient is drawn increases, a decision to report a small nodule as cancer is more likely to be correct [6, 7]. In the clinical setting, the patient's history, clinical symptoms, and even the specialty of the referring doctor, when combined with experience, can roughly be used to assign patients to prevalence groups [6, 7]. In general, the failure to report a significant finding would be of greater significance than the overinterpretation of a radiologic study, which might only lengthen the patient's diagnostic workup [6]. In order to help reduce the number of missed subtle lung cancers, deliberate overreading of chest radiographs may be justified, especially when the clinical information suggests a high likelihood of abnormality [6, 7].

The contrast difference between a nodule and the surrounding area is another major factor in the detectability of the nodule. If the contrast difference is great, detectability is enhanced; however, if the contrast difference is small, detectability is impaired [1, 8, 10]. The energy of the X-ray beam has a profound effect on the quality of the image [12]. Increasing energies cause a striking decrease in contrast between bone and soft tissue; with decreasing contrast between bone and soft tissue, the image of the bones becomes less conspicuous, and the bones are less likely to obscure the underlying pulmonary structures [12]. The same magnitude of energy change also decreases the contrast between water and air, but to a lesser degree [12]. Thus, even though the contrast between the intrapulmonary structures is diminished, they are easier to see because the overlying bones interfere less [12]. As a result, nodule detection is enhanced by high-kilovoltage technique, at the expense of hindering evaluation of the ribs and detection of calcification [12]. Studies comparing high-kilovoltage techniques found no diagnostic advantage with films obtained at 300–350 kVp over those obtained at lower energies [12, 13]. Christensen et al. [12], however, did find that nodule detection improved with increasing energies up to 200 kVp. In this country, 140 kVp is the most readily available "high" kilovoltage; therefore, chest radiographs routinely should be obtained at or near this level [12, 14]. The use of grids for elimination of scatter radiation is essential with high-kVp techniques [2, 15]. The use of long-scale radiographic film has also been shown to further improve nodule detection [15, 16].

Despite the advantages of modern high-kilovoltage, long-scale film chest radiography over the older low-kilovoltage technique for detecting subtle soft-tissue lesions in the lung, a substantial false-negative diagnosis rate persists, and the technique is not well suited to differentiate between calcified and noncalcified nodules, often requiring additional studies to identify calcification [16]. Furthermore, in the poorly penetrated areas of the lung (subpleural, retrodiaphragmatic, retrocardiac, paramediastinal), the contrast difference between lung nodules and the surrounding area is low, greatly hindering nodule detection [2, 3, 17, 18]. A number of techniques, although not used widely, increase contrast differences and nodule detection, especially in these poorly penetrated areas of the lung, and improve detection of calcification within nodules. These include optical unsharp masking [2, 15, 18], scanning equalization radiography [7, 19–21], and digital radiography of the chest [11, 16, 22–25].

The presence of superimposed structures (anatomic image noise) and the complexity of the area surrounding a nodule adversely affect nodule detection [1, 7, 9, 10]; this is particularly true in the apical and perihilar areas of the lungs [3]. End-on vessels and overlapping vessels and ribs commonly are encountered on chest radiographs and may simulate or camouflage a nodule [1, 6, 7, 9, 10]. These opacities cause confusion and compete for the radiologist's attention [1, 6, 7, 9, 10]. If the image contains a great deal of anatomic noise, a nodule is less likely to be perceived [7]. The radiologist must decide whether or not to report all questionable opacities resembling a nodule as suspicious or positive, resulting in a high false-positive rate, or to ignore such opacities, resulting in a high false-negative rate [6]. Shifted, stereoscopic, posteroanterior films have been shown to improve overall performance in nodule detection, both by clarifying end-on vessels and overlapping shadows and by confirming true nodules [3, 7, 9, 26]. The stereoscopic view does not have to be viewed stereoscopically to be effective [26] and does not have to be obtained simultaneously with the initial posteroanterior view.

Although the human eye is capable of detecting a single nodule as small as 3 mm [7], it is quite unusual for a solitary neoplasm less than 1 cm in diameter to be seen [2, 7]. Although 1 cm has generally been accepted as the size threshold of detectability for peripheral lung cancers [2], Heelan et al. [4] have suggested that for the prospective analysis of chest radiographs the threshold size of detectability may be much larger. In their series [4], the size of peripheral lung cancers at the initial time of prospective detection during routine screening ranged from 0.7 to 9.4 cm, with an average size of 2.4 cm.

The shape of a nodule also plays a significant role in its detectability. If a peripheral lung cancer is spherical and sharply marginated, its edge will be enhanced by a negative Mach band [10, 27]. The presence of the negative Mach band will greatly increase the detectability of the nodule [10]. In fact, in the poorly penetrated areas of the lung, nodules may be perceived solely because of their associated negative Mach band [27]. Unfortunately, many lung cancers are poorly defined or spiculated in nature and cannot produce a surrounding negative Mach band [10, 27]. Thus, these poorly defined lung cancers may be difficult or impossible to perceive until they become quite large [10].

Although pitfalls in the detection of lung cancers arising in the hilum have not been studied extensively, it is apparent that the detection of hilar cancers is hindered by similar technical and perceptual limitations (Fig. 1). Muhm et al. [5] found that 65% of lung cancers arising in the hilum were missed initially during routine screening and were usually more than 3 cm in diameter by the time they were discovered. Furthermore, detection of hilar cancers frequently is limited by a surprising lack of familiarity with normal and abnormal hilar anatomy on the part of those who interpret chest radiographs. A number of articles [28–37] have addressed plain film hilar anatomy and the radiologic signs of subtle hilar abnormality that may greatly improve the detection of early hilar cancers. Unfortunately, early tumors that are limited to the bronchial lumen and have not caused bronchial obstruction are usually not detectable on plain films.

It is apparent that there are a number of factors that limit the ability of the radiologist to detect early or subtle lung cancers. Although faulty search patterns and carelessness on the part of the radiologist are always potential pitfalls, the majority of limitations are either inherent to the human visual system or decision-making process, are related to the limitations of the plain film method itself, are related to the complexity of the image of the lungs, or are due to the location and edge characteristics of the tumor itself. The radiologist should take steps to reduce detection errors whenever possible; however, it is obvious that the failure to detect an early lung cancer on plain radiographs is well within an accepted, normal standard of care and does not constitute negligence or malpractice [5].

Improper Viewing Conditions

By paying attention to a few simple precautions concerning the viewing of the chest radiographs, the radiologist can improve the detection of subtle lung cancers. Chest radiographs should be checked routinely, immediately after processing, for technical quality and should be repeated if necessary [3]. They should always be read in side-to-side comparison with previous studies when these studies are available [3]. Preferably, at least one set of films more remote than the most recent set of previous radiographs should also be compared with the current study. Ideally, interpretation of radiographs should occur in a calm environment free of constant interruption or severe time pressure [6]. Light coming from the view box around the film causes light flooding of the eye from intraocular scattering and decreases the sensitivity of the eye for detecting subtle changes in contrast in the denser portion of the image [10]. This veiling glare should be blocked out [10]. Viewing distance also should be varied routinely [10]. Routine use of a reducing lens (Edmund Scientific Co., Barrington, NJ) greatly improves the evaluation of radiographs by reducing the number of visual fixations needed to search the image adequately, enhancing the visibility of large, poorly defined lesions, increasing the luminance gradient of threshold images, allowing previously subliminal images to be perceived, and facilitating comparison of two films [19, 38]. Increasing the use of scotopic vision by glancing at the radiograph from the side also may improve detection of subtle lesions [38].

Pitfalls Related to the Analysis of Solitary Pulmonary Opacities

Size and Shape of Solitary Pulmonary Opacities

The division of solitary pulmonary opacities into two categories, based simply on size, is important. A solitary pulmonary mass (defined as being more than 3 cm in diameter) is almost always malignant [39]. Furthermore, if serial films show growth of a solitary pulmonary mass, the suspicion of malignancy is even greater [39, 40]. For a solitary pulmonary nodule (defined as 3 cm or less in diameter), the distinction between benignity and malignancy is based on features of the nodule other than size [39]. Edge characteristics are useful in assessing solitary nodules. The findings of lobulation (notch sign), spiculation (corona radiata), and pleural retraction (tail sign) suggest that a solitary pulmonary nodule is malignant [39, 41–43], although some benign nodules have these features and some malignant nodules remain sharply circumscribed and spherical [39]. The growth of a solitary pulmonary nodule is also important in assessing whether it is benign or malignant.

Growth of a Solitary Pulmonary Nodule

Assessment of the growth of a solitary pulmonary nodule can provide great insight into the nature of the nodule; comparison with previous chest radiographs remains of fundamental importance in this task [39, 40]. Unfortunately, it is not possible to assess the growth of a pulmonary nodule accurately by visual inspection alone; the growth of a pulmonary nodule always should be judged with the aid of a measuring instrument [10]. If it can be shown that no growth at all has occurred over a minimum of 2 years, the nodule is almost certainly benign [39].

If a solitary pulmonary nodule grows, malignancy is more likely. Assessment of the doubling time of the volume of a nodule that is growing may be of diagnostic value [39]. It must be remembered, however, that doubling time refers to volume and not diameter [39]; doubling of the diameter of a nodule represents an eightfold increase in volume. The volume of a sphere (Vs) is determined by the equation,

$$Vs = 4/3(\pi r^3) = 4.1866 r^3,$$

where r is the radius of the sphere [44]. If a nodule 1 cm in diameter ($r = 0.5$) increases in diameter to 1.26 cm ($r = 0.63$), the nodule has doubled in volume as indicated in the following:

$$Vs = 4.1866 (0.5 \text{ cm})^3 = 0.52 \text{ cm}^3$$

and

$$Vs = 4.1866 (0.63 \text{ cm})^3 = 1.04 \text{ cm}^3.$$

A simplified method also may be used. Assuming that a nodule is spherical, multiply its diameter by 1.26 to obtain the diameter of a sphere whose volume has doubled. The doubling time in lung cancer has been shown to be between 30 and

490 days; if the doubling time falls outside this range the nodule is most likely benign [39].

Still, it is well known that some lung cancers may change little in size over a long time only to disseminate widely in a short time, or alternatively, some may show rapid growth and spread in the first few weeks after initial presentation [40]. In addition, hemorrhage in or around lung cancer may be associated with dramatic changes in the size of the lesion that may mimic benign disease (Fig. 2) [39]. Therefore, absolute reliance on measurements of doubling time is not recommended [40].

Cummings et al. [45] have provided mathematical formulas that may be used to estimate the likelihood that a given nodule is malignant. By using the likelihood ratio form of Bayes' theorem to combine individual odds into an overall estimate of the odds favoring malignancy, they developed a simple formula for estimating the likelihood that a solitary pulmonary nodule is malignant based on the diameter of the nodule, the patient's age and history of cigarette smoking, and data on the overall prevalence of malignancy in solitary nodules [45]. This method improves the accuracy of estimating the likelihood of malignancy for individual patients with solitary pulmonary nodules and may be very helpful in deciding how to manage the patient. The article is highly recommended to anyone interested in the evaluation and management of solitary pulmonary nodules.

Pitfalls Related to Unusual Radiologic Manifestations of Lung Cancer

Calcification

Visible calcification within a solitary pulmonary nodule generally is considered good evidence of a benign lesion if the calcification is of the diffuse, popcorn, laminated, or central-core types [39, 40, 46]. However, unlike the solitary pulmonary nodule, the presence of calcification within a solitary pulmonary mass is not a reliable sign of benignity [39]. Although the presence of calcification within lung cancer is common histologically [40, 46–48], demonstration of such calcification on plain radiographs or conventional tomograms is exceedingly rare [40].

The demonstration of calcification within lung cancer by CT is apparently more common and has been reported in adenocarcinoma, bronchioloalveolar carcinoma, and large-cell carcinoma (Fig. 3) [46–49]. The metastases from calcium-producing lung cancers also may contain calcium [46, 48, 49]. CT features of a calcified lung nodule or mass that suggest malignancy include poorly defined, spiculated, or lobulated margins; size larger than 3 cm; and continued growth [46].

Thin-Walled Cavitation

Cavitation in lung cancer is common and occurs in 2–16% of cases [39, 40]. Typically, the cavity will have thick walls; nodular extensions of tumor (mural nodules) projecting into the lumen of the cavity are common [40, 50–52]. Occasionally, a cavitated lung cancer will have smooth, thin walls (Fig. 4) [39, 50–52]. In a retrospective and prospective analysis of 126 patients with solitary cavities of the lung, Woodring et al. [50, 51] found that 94% (29 of 31) of solitary cavities with a maximal wall thickness of 4 mm or less were benign; however, two (6%) of 31 were malignant. These two cases had smooth walls with a maximal wall thickness of 2 mm [50, 51]. Carcinoma always should be considered seriously in the diagnosis of any cavitary lesion of the lung, especially if the patient is

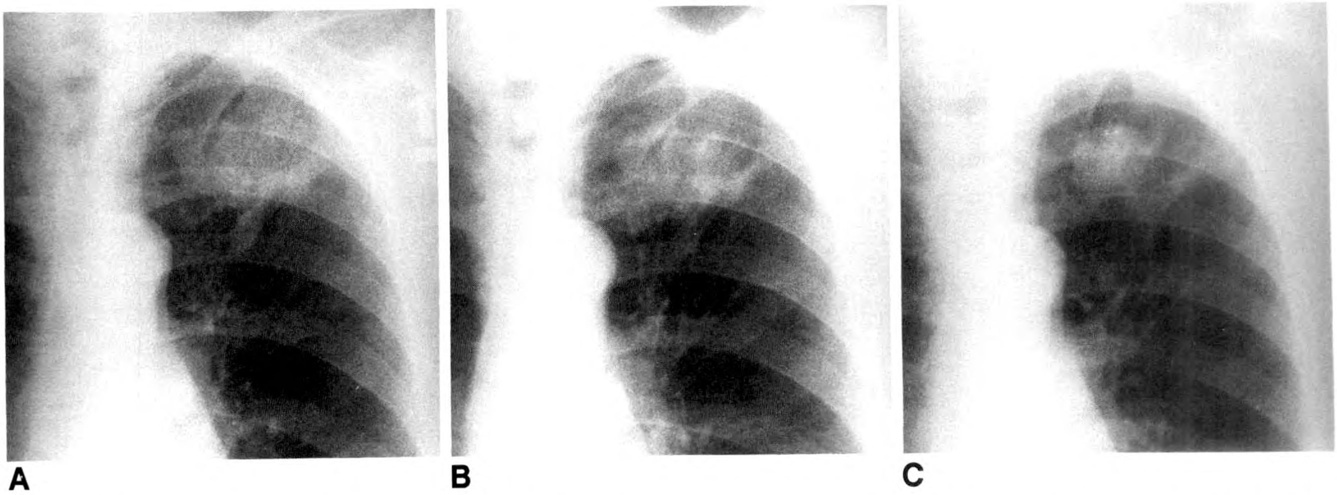

Fig. 2.—Rapid resolution of hemorrhage surrounding lung cancer mimicking benign disease in a 45-year-old woman with hemoptysis; she had no other symptoms.

***A*, Radiograph shows poorly defined opacity of approximately 5 × 6 cm in left upper lobe. Skin tests, sputum cultures, serology, and fiber-optic bronchoscopy were negative.**

***B*, Radiograph obtained 8 days later. Opacity has decreased to approximately 3.5 × 5 cm. Hemoptysis has ceased.**

***C*, Radiograph obtained 22 days after *A*. Opacity has decreased to 3 × 4 cm, but it appears more masslike. Surgical resection revealed poorly differentiated adenocarcinoma.**

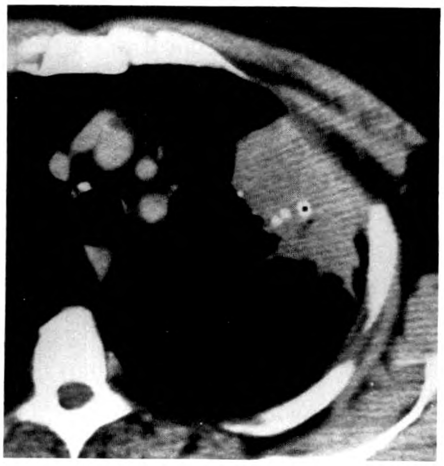

Fig. 3.—Adenocarcinoma of left upper lobe with intrinsic calcification. CT scan shows spiculated mass 4.5 × 7.0 cm in left upper lobe containing calcification (cursor reading from largest calcification was 515 H). Malignancy is indicated by large size (more than 3 cm) and by spiculated lung-tumor interface.

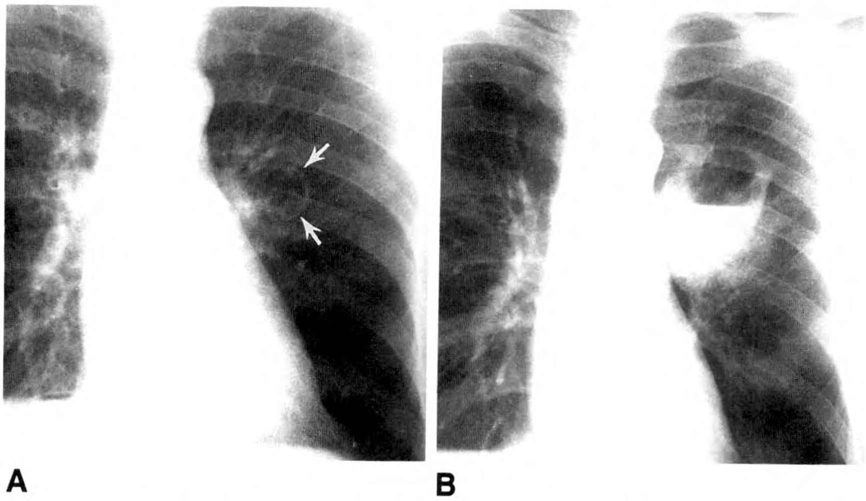

Fig. 4.—Lung cancer with thin-walled cavity in asymptomatic 43-year-old man.

A, Radiograph shows 3 × 3 cm thin-walled cavity (*arrows*) with maximal wall thickness of 2 mm in superior segment of left lower lobe.

B, Radiograph obtained 11 months later shows more typical thick-walled cavity with air-fluid level. Final diagnosis was squamous cell carcinoma.

more than 35 years old [52]. Although a wall thickness of 4 mm or less strongly favors a benign lesion [50, 51], close follow-up is indicated. If subsequent radiographs show that the cavity has enlarged or that the wall has thickened, carcinoma is suggested [40].

Cystic Appearance

Occasionally, a necrotic lung cancer may not develop a communication with a bronchus. In this situation, the necrotic tumor still will appear as a solid mass on plain films; however, on CT it will appear as a fluid-filled mass that may resemble a bronchogenic cyst, hydatid cyst, lung abscess, or infected bulla [53]. The presence of thick, lobular walls and a size larger than 3 cm should suggest the possibility of carcinoma in such a cystic lesion [53].

Air-Crescent Sign

Rarely, a meniscus or air-crescent sign may be seen in association with a cavitated lung cancer (Fig. 5) [40]. This may occur because of an intracavitary tumor mass, aspergilloma, or other formed debris within the cavity [40, 54]. Unfortunately, such a lesion may be mistaken for a fungus ball in a preexisting benign cavity. The presence of thick, nodular cavity walls; size larger than 3 cm; continued growth; or lack of a preexisting benign cavity should suggest malignancy.

Air-Space Filling Pattern

Usually lung cancer is thought of as a nodule or mass lesion. Although most lung cancers do present in this way, adenocarcinoma, especially the bronchioloalveolar form, may present as an air-space filling process with an alveolar pattern on radiographs (Fig. 6) [40, 55–61]. This occurs because the tumor may grow and spread within the lumen of the distal air spaces, using the existing stroma of the peripheral lung tissue as its support [59, 60]. Bronchioloalveolar carcinoma may present as focal segmental or nonsegmental consolidation, lobar consolidation, or a diffuse air-space filling process that may involve both lungs extensively [55, 56, 58–60]. The alveolar consolidation produced by bronchioloalveolar carcinoma usually is chronic [57] but may show rapid progression and mimic acute air-space diseases such as pneumonia, edema, or hemorrhage [56, 60]. Air bronchogram formation is common (Fig. 6) [40, 55, 58]. Im et al. [58] have shown that CT of lobar bronchioloalveolar carcinoma may show stretching, spreading, and uniform narrowing of the involved bronchi without obstruction. This is the CT equivalent of the classic bronchographic features of bronchioloalveolar carcinoma reported by Zheutlin et al. [62] in 1954. The air-filled bronchi in chronic pneumonic consolidation usually show some degree of tortuosity and ectasia because of fibrosis and atelectasis of the involved lung [58]. These bronchial findings then would differ from those of bronchioloalveolar carcinoma [58]. Unfortunately, the characteristic bronchial findings of bronchioloalveolar carcinoma on CT may be absent (Fig. 6).

Kuriyama et al. [43] have shown that air bronchograms frequently are identified in small peripheral lung cancers on thin-section CT. Although the presence of air bronchograms within a solitary pulmonary opacity on plain radiographs classically has been considered as evidence against lung cancer, their presence within peripheral lung nodules on thin-section CT should not be used as evidence of benign disease.

Satellite Nodules

Multiple small pulmonary nodules clustered together in proximity, often in association with a larger peripheral nodule, are termed satellite nodules [63]. These nodules often are said to be characteristic of inflammatory disease, particularly tuberculosis, and have been reported in about 10% of cases of tuberculoma and 8% of cases of tuberculosis [63]. Unfortunately, satellite nodules also have been reported in 1% of cases of primary lung cancer [63].

Bronchial Abnormalities

Focal bronchial wall thickening is an early sign of lung cancer that may precede the development of an obvious mass lesion by several years [33, 39, 64]. The bronchial cuff sign, also termed the anterior bronchus sign, consists of two components: (1) an increase in the thickness of the soft-tissue compartment surrounding an end-on bronchus, often with partial or complete obliteration of the normal curvilinear demarcation of the bronchial wall; and (2) partial or complete envelopment of the adjacent artery by the increased soft-tissue component, causing partial or complete obscuration of the artery [39]. On plain films the sign is seen best in the end-on perihilar bronchi, particularly the anterior segmental bronchi of the upper lobes (Fig. 7) [33, 39]. Early endobronchial tumor occasionally may be identified on CT as focal thickening of the bronchial wall limited to the lumen of the involved bronchus (Fig. 8) [64].

Obstructive hyperinflation is an uncommonly imaged manifestation of lung cancer. Obstruction of the larynx or trachea by tumor can act as a check valve and can result in obstructive hyperinflation of both lungs [40, 65]. The lungs become markedly overinflated; both diaphragms are low; respiratory excursion is diminished markedly on expiration; and the heart, which may appear small on expiration, paradoxically will enlarge on inspiration [40, 65]. A history of stridor should evoke close scrutiny of the trachea and larynx on the chest radiograph. Obstructive hyperinflation also may develop distal to obstructing tumors of the main bronchi (Fig. 9), lobar bronchi, or segmental bronchi [65]. A history of unilateral

Fig. 5.—Intracavitary tumor mass with meniscus sign in a 44-year-old man with sudden onset of massive hemoptysis. Chest radiograph shows oval cavity of 4.5 × 6.0 cm with irregular walls in anterior segment of right upper lobe. Mass is present inferiorly in cavity, causing meniscus sign. Surrounding lung is opacified by pulmonary hemorrhage. Surgical resection revealed cavitary adenocarcinoma containing necrotic tumor tissue.

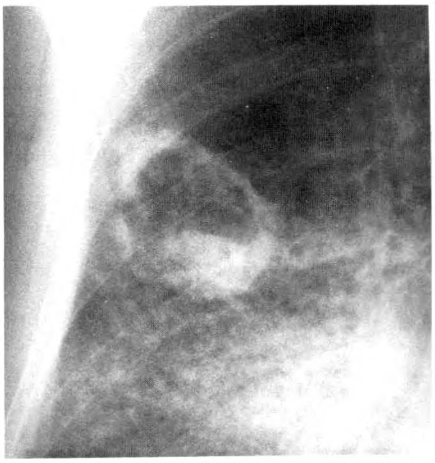

5

Fig. 6.—CT scan shows bilateral air-space opacification from bronchioloalveolar carcinoma. Note prominent air bronchogram in lingula of left upper lobe (*arrowheads*).

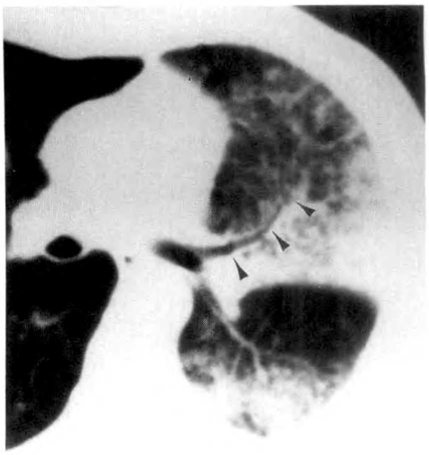

6

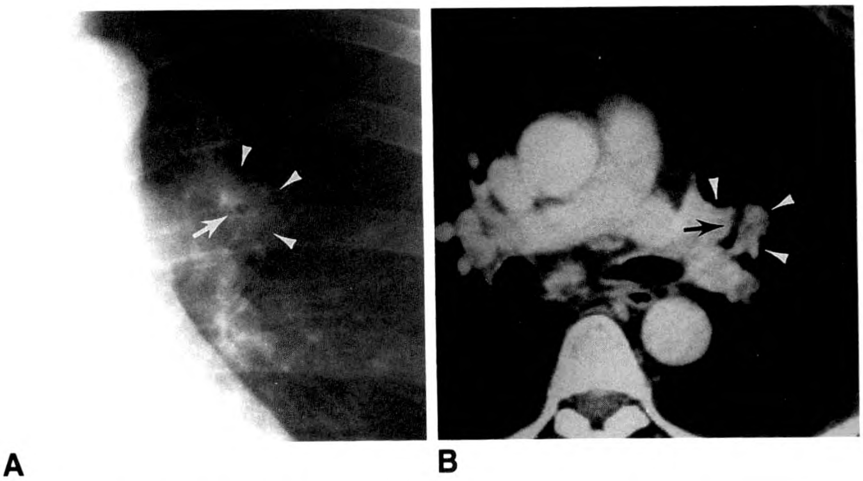

Fig. 7.—Anterior bronchus sign of hilar cancer.

***A*, Radiograph shows soft tissue (*arrowheads*) surrounding and extending laterally to anterior segmental bronchus (*arrow*) of left upper lobe.**

***B*, CT scan shows how anterior bronchus sign is formed: a cuff of tumor tissue (*arrowheads*) completely surrounds anterior segmental bronchus (*arrow*) of left upper lobe. Biopsy revealed poorly differentiated non-small-cell carcinoma.**

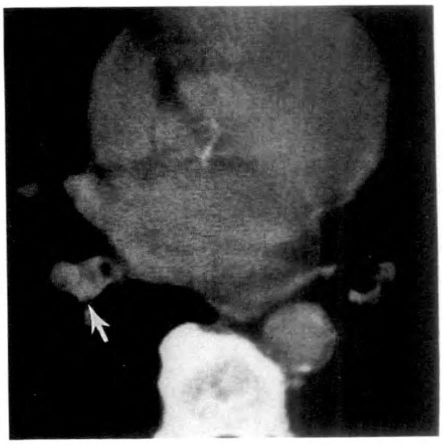

Fig. 8.—Lung cancer limited to bronchial lumen. CT scan through right-lower-lobe bronchus below origin of superior segmental bronchus shows small squamous cell carcinoma (*arrow*) limited to lumen of bronchus and causing focal narrowing of bronchial lumen.

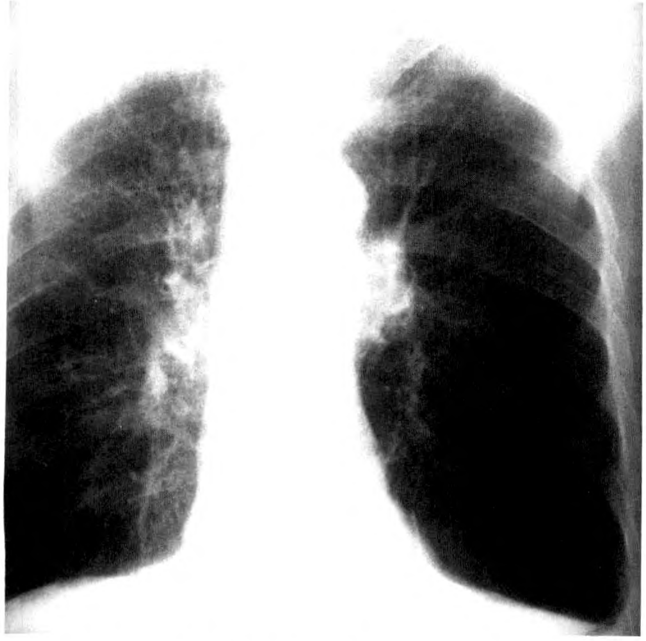

Fig. 9.—Radiograph shows postobstructive hyperinflation of left lung associated with endobronchial tumor in left main bronchus causing check-valve-type obstruction. Left lung is enlarged, hyperlucent, and underperfused compared with right.

wheezing is highly suggestive of the condition [40]. The hyperinflation may be missed on full inspiration; an expiratory view is often necessary to demonstrate the air trapping [65].

Mucoid impaction of bronchi refers to the accumulation of inspissated secretions within the bronchial lumen usually associated with bronchial dilatation or bronchiectasis [40, 66, 67]. Lung cancer is by far the most common cause of mucoid impaction caused by bronchial obstruction [66, 67]. Radiologically, mucoid impaction of the bronchi distal to an obstructing tumor often is obscured by postobstructive pneumonia or collapse. However, if collateral ventilation occurs, so that the lung distal to the obstruction remains aerated, mucoid impaction may be visible on plain films or CT scans [40, 66, 67]. The plain film or CT appearance of mucoid impaction usually consists of one or more fusiform, branching structures with their long axes directed toward the hilum [40, 66, 67]. If the tumor obstructing the bronchus is large enough, a central tumor mass may be identified proximal to the mucoid impaction; however, if the obstructing tumor is small and limited to the bronchial lumen, mucoid impaction may be the only radiologic indication of an obstructing bronchial tumor (Fig. 10) [40, 66, 67]. Visible mucoid impaction commonly is seen in lung cancer obstructing a segmental bronchus [66] and may be seen distal to carcinoma of a lobar or main bronchus [67].

The "double lesion sign," considered strong evidence against lung cancer, is defined as lobar or segmental atelectasis in two different lobes that cannot be explained easily by a single bronchial abnormality [40]. The sign does fail rarely, and the exceptions have various explanations, including multiple primaries, atelectasis in one lobe from a primary tumor and in another from a metastasis, extension of the primary tumor through a fissure to obstruct a major bronchus in an adjacent lobe, carcinoma in one lobe and inflammatory disease in another, variations in bronchial anatomy, and a channel situated through the bronchial tumor so that the lumen to one lobar bronchus is patent while the other lobar bronchi are occluded [40].

Pleural Involvement

Pleural involvement in primary lung cancer is not uncommon, occurring in about 8–15% of cases [68]. Usually this is manifested by pleural effusion. Typically a hilar or parenchymal mass is visible on the radiograph; however, a subtle hilar mass or small peripheral tumor may be relatively inapparent on the initial radiographs, especially when the effusion is large, leaving the impression that the pleural effusion is an isolated finding [68]. It has been my experience that the majority of massive, unilateral pleural effusions ultimately are proved to be malignant (lymphoma, lung cancer, mesothelioma, or metastatic disease). However, the presence of smaller unilateral or bilateral pleural effusions, with a normal-sized heart, should always raise the possibility of a malignant process [68].

Pulmonary Artery Involvement

Invasion of one or more of the pulmonary arteries is common in lung cancer. This may result in decreased perfusion of the involved lung [69]. Occasionally, invasion of the pulmonary artery will cause pulmonary infarction; this may be seen as a dumbbell-shaped opacity with the central mass representing the tumor and the peripheral mass representing the infarct (Fig. 11) [69]. When an approach for percutaneous needle biopsy is planned in such a case, the central lesion representing the tumor should be sampled rather than the more easily accessible peripheral infarct [39].

Esophageal Involvement

Dysphagia is occasionally the presenting symptom in patients with lung cancer [39, 70]. Metastatic enlargement of the subcarinal or posterior mediastinal lymph nodes may compress the esophagus, or lung cancer may invade the esophagus directly, causing dysphagia [39, 70]. The extrinsic pressure effect of the lung tumor on the esophagus may be subtle and may be easily missed on chest radiographs, barium studies, or endoscopy [70].

Pericardial and Cardiac Involvement

Approximately 8–10% of lung tumors metastasize to the heart [71]. Metastatic disease to the heart may follow three pathways: hematogenous or lymphangitic spread to the pericardium or myocardium, direct invasion across the pleura and pericardium, or extension into the right or left atrium by continuity through the vena cava or pulmonary veins [71–74]. Pericardial effusion is the most common manifestation of metastatic lung cancer and may be the presenting feature of the disease; generalized or localized neoplastic pericardial thickening or nodular masses also may be seen [73].

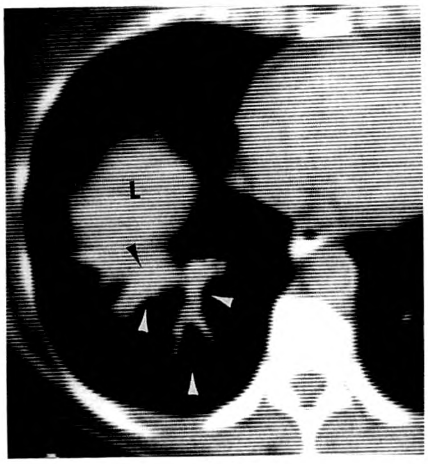

Fig. 10.—CT scan shows mucoid impaction of right-lower-lobe bronchi caused by obstructing endobronchial adenocarcinoma of right-lower-lobe bronchus. Note branching V- and Y-shaped opacity (*arrowheads*) representing inspissated mucus in distended bronchi distal to tumor. No central mass effect was evident on higher cuts. L = apex of liver.

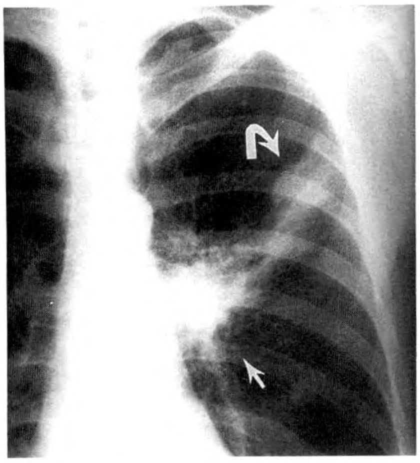

Fig. 11.—Radiograph shows poorly defined squamous cell carcinoma of 4.5 × 5.0 cm arising in left hilum (*straight arrow*). Invasion of left pulmonary artery by this tumor resulted in peripheral pulmonary infarct in left upper lobe (*curved arrow*). This produces typical dumbbell-shaped opacity seen in this condition.

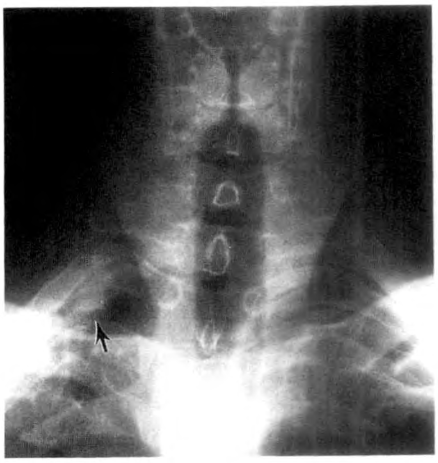

Fig. 12.—Pancoast tumor. Cervical radiograph in 47-year-old man with weakness in right upper extremity for 2 weeks shows subtle, asymmetric opacity (*arrow*) 12 mm thick at extreme lung apex on right. Subsequent needle biopsy revealed large-cell carcinoma of lung.

Pancoast Syndrome

Pancoast syndrome is caused by a tumor, usually primary to the lung, occurring at the extreme lung apex, that invades the neck, brachial plexus, and shoulder, causing pain in the distribution of the eighth cervical and first and second thoracic nerves, wasting of the muscles of the hand, and Horner syndrome [75, 76]. Radiologically, Pancoast described "small homogeneous shadows at the extreme lung apex associated with more or less rib destruction and often with vertebral infiltration" [77]. In retrospect, it is now apparent that all of Pancoast's cases were diagnosed at a late, advanced stage of disease; most patients diagnosed today have only one or two components of the syndrome, and Horner syndrome now is quite rare [75–77]. It is now also known that the radiologic findings of a Pancoast tumor may be quite subtle, consisting of only slight asymmetric apical thickening with or without bone destruction [77]. In the series reported by O'Connell et al. [77], old films in two-thirds of the patients in whom they were available showed evidence of apical thickening on the side of abnormality before the development of clinical signs and symptoms, a finding that carries considerable significance. Certainly, any degree of apical asymmetry in a symptomatic patient should raise the suspicion of a superior sulcus cancer and elicit an appropriate workup [77]. An asymptomatic patient who has not received prior cervical lymph-node irradiation, with a unilateral or asymmetric apical cap of greater than 5 mm, or a patient with an enlarging apical cap, merits further investigation [77]. Unfortunately, because of the vague nature of the shoulder and arm pain, and the similarity with other clinical conditions, Pancoast tumor may not be suspected clinically and the radiologic workup may be focused on the cervical spine or shoulder (Fig. 12).

Conclusions

Perceptual problems account for a large proportion of missed lung cancers. Although it is apparent that we are limited to a certain extent by the inherent limitations of the human visual system and often by the nature of the lung cancer itself, perceptual errors can be reduced by the use of modern high-kilovoltage, long-scale radiographic technique, meticulous attention to proper viewing conditions and procedures, assimilation of the patient's history and clinical symptoms in the decision-making process, close scrutiny of known trouble spots on the radiographs (apical, hilar, paramediastinal, retrocardiac, retrodiaphragmatic, and subpleural regions), double reading of radiographs, and the use of a reducing lens. Conscious awareness of our tendency to deliberately underread chest radiographs, coupled with a willingness to freely obtain shifted views or repeat radiographs to clarify questionable opacities, also will improve our performance.

Still, the radiologist may perceive a nodule or mass, report its presence, and misinterpret the radiologic features of the cancer as indicating benign disease. Any solitary pulmonary opacity larger than 3 cm in size should be viewed as malignant. Pulmonary nodules less than 3 cm in size should be considered malignant if the pretest probability of cancer is high; if they grow; or if their edge is spiculated, notched, or there is a pleural tail sign. Assessment of nodule growth should be made with the assistance of a measuring device, and calculation of doubling time should consider doubling of the volume of the nodule rather than doubling of the diameter of the nodule. The presence of calcification within a pulmonary opacity, especially one larger than 3 cm, should not be considered evidence of benignancy. Occasionally lung cancer may show thin-walled cavitation, an air-crescent sign, and cyst formation. Although these findings usually indicate benign disease, focal wall thickening, size larger than 3 cm, and growth of the lesion suggest cancer. Bronchioloalveolar carcinoma should be considered as a possible cause for chronic alveolar disease. Satellite nodules that grow also suggest the possibility of lung cancer. Focal bronchial wall thickening, obstructive hyperinflation, and mucoid impaction are subtle signs of lung cancer that suggest an underlying malignancy. The presence of the double lesion sign should not be considered as absolute evidence of a benign process. Pleural effusion, pulmonary infarction, dysphagia, and pericardial effusion are not uncommon in lung cancer. When these are the presenting findings, the possibility of cancer should be considered, especially when the pretest probability of cancer is high. Pancoast tumor may be present on the radiographs of asymptomatic patients and may be suspected by the presence of unilateral or asymmetric apical thickening of 5 mm or greater. Any patient with a growing apical cap, or any patient with signs of Pancoast syndrome, should be viewed as possibly harboring a superior sulcus carcinoma. It is hoped that through increased awareness of the growth patterns of lung cancer and of some of the more uncommon manifestations of lung cancer, radiologists may escape some of the avoidable pitfalls in the detection and diagnosis of lung cancer.

REFERENCES

1. Revesz G, Kundel HL. Psychophysical studies of detection errors in chest radiology. *Radiology* **1977**;123:559-562
2. Sorenson JA, Mitchell CR, Armstrong JD II, et al. Effects of improved contrast on lung-nodule detection: a clinical ROC study. *Invest Radiol* **1987**;22:772-780
3. Hayabuchi N, Russell WJ, Murakami J, Nishitani H. Screening for lung cancer in a fixed population by biennial chest radiography. *Radiology* **1983**;148:369-373
4. Heelan RT, Flehinger BJ, Melamed MR, et al. Non-small-cell lung cancer: results of the New York screening program. *Radiology* **1984**;151:289-293
5. Muhm JR, Miller WE, Fontana RS, Sanderson DR, Uhlenhopp MA. Lung cancer detected during a screening program using four-month chest radiographs. *Radiology* **1983**;148:609-615
6. Swensson RG, Hessel SJ, Herman PG. Omissions in radiology: faulty search or stringent reporting criteria? *Radiology* **1977**;123:563-567
7. Kundel HL. Predictive value and threshold detectability of lung tumors. *Radiology* **1981**;139:25-29
8. Kundel HL, Nodine CF, Thickman D, Toto L. Searching for lung nodules: a comparison of human performance with random and systematic scanning models. *Invest Radiol* **1987**;22:417-422
9. Kundel HL, Nodine CF, Krupinski EA. Searching for lung nodules: visual dwell indicates locations of false-positive and false-negative decisions. *Invest Radiol* **1989**;24:472-478
10. Jaffe CC. Medical imaging, vision, and visual psychophysics. *Med Radiogr Photogr* **1984**;60:1-48
11. Oestmann JW, Greene R, Kushner DC, Bourgouin PM, Linetsky L, Llewellyn HJ. Lung lesions: correlation between viewing time and detection. *Radiology* **1988**;166:451-453
12. Christensen EE, Dietz GW, Murry RC, Moore JG, Stokely EM. Effect of kilovoltage on detectability of pulmonary nodules in a chest phantom. *AJR* **1977**;128:789-793
13. Herman PG, Drummey J, Swensson RG, Hessel SJ, Balikian JP. 350 kV chest radiography has no diagnostic advantage: a comparison with 140 kV technique. *AJR* **1982**;138:485-489
14. Revesz G, Shea FJ, Kundel HL. The effects of kilovoltage on diagnostic accuracy in chest radiography. *Radiology* **1982**;142:615-618
15. Sorenson JA, Mitchell CR. Evaluation of optical unsharp masking and contrast enhancement of low-scatter chest radiographs. *AJR* **1987**;149: 275-281
16. Oestmann JW, Greene R, Rhea JT, et al. "Single-exposure" dual energy digital radiography in the detection of pulmonary nodules and calcifications. *Invest Radiol* **1989**;24:517-521
17. Plewes DB, Wandtke JC. A scanning equalization system for improved chest radiography. *Radiology* **1982**;142:765-768
18. Armstrong JD II, Sorenson JA, Nelson JA, et al. Clinical evaluation of unsharp masking and slit scanning techniques in chest radiography. *Radiology* **1983**;147:351-356
19. Wandtke JC, Plewes DB. Exposure equalization radiography of the chest: clinical comparison of slit and raster scanning techniques. *AJR* **1985**;144: 1171-1181
20. Wandtke JC, Plewes DP, Vogelstein E. Scanning equalization radiography of the chest: assessment of image quality. *AJR* **1985**;145:973-978
21. Wandtke JC, Plewes DB. Improved chest disease detection with scanning equalization radiography. *AJR* **1985**;145:979-983
22. Ishigaki T, Sakuma S, Ikeda M. One-shot dual-energy subtraction chest imaging with computed radiography: clinical evaluation of film images. *Radiology* **1988**;168:67-72
23. Sherrier RH, Chiles C, Wilkinson WE, Johnson GA, Ravin CE. Effects of image processing on nodule detection rates in digitized chest radiographs: ROC study of observer performance. *Radiology* **1988**;166:447-450
24. Fraser RG, Breatnach E, Bearnes GT. Digital radiography of the chest: clinical experience with a prototype unit. *Radiology* **1983**;148:1-5
25. Fraser RG, Sanders C, Barnes GT, et al. Digital imaging of the chest. *Radiology* **1989**;171:297-307
26. Kelsey CA, Moseley RD Jr, Mettler FA Jr, Briscoe DE. Cost-effectiveness of stereoscopic radiographs in detection of lung nodules. *Radiology* **1982**;142:611-613
27. Lane EJ, Proto AV, Phillips TW. Mach bands and density perception. *Radiology* **1976**;121:9-17
28. Vix VA, Klatte EC. The lateral chest radiograph in the diagnosis of hilar and mediastinal masses. *Radiology* **1970**;96:307-316
29. Chang CH(J), Zinn TW. Roentgen recognition of enlarged hilar lymph nodes: an anatomical review. *Radiology* **1976**;120:291-296
30. Schnur MJ, Winkler B, Austin JHM. Thickening of the posterior wall of the bronchus intermedius: a sign on lateral chest radiographs of congestive heart failure, lymph node enlargement, and neoplastic infiltration. *Radiology* **1981**;139:551-559
31. Don C, Hammond DI. The vascular converging points of the right pulmonary hilus and their diagnostic significance. *Radiology* **1985**;155:295-298
32. Webb WR. Radiologic imaging of the pulmonary hila. *Postgrad Radiol* **1986**;6:145-168
33. Spizarny DL, Cavanaugh B. The anterior bronchus sign: a new clue to hilar abnormality. *AJR* **1985**;145:265-267
34. Genereux GP. Conventional tomographic hilar anatomy emphasizing the pulmonary veins. *AJR* **1983**;141:1241-1257
35. Chasen MH, Yrizarry JM. Tomography of the pulmonary hili: anatomical reassessment of the conventional 55° posterior oblique view. *Radiology* **1983**;149:365-369
36. Proto AV, Speckman JM. The left lateral radiograph of the chest. *Med Radiogr Photogr* **1979**;55:30-74
37. Proto AV, Speckman JM. The left lateral radiograph of the chest. *Med Radiogr Photogr* **1980**;56:38-64
38. Stark P, Harle T. The reducing lens: an important but underused tool. *Invest Radiol* **1989**;24:721-722
39. Fraser RG, Paré JAP, Paré PD, Fraser RS, Genereux GP. *Diagnosis of diseases of the chest*, vol. II, 3rd ed. Philadelphia: Saunders, **1989**:1367-1442
40. Felson B, Wiot JF. Some less familiar roentgen manifestations of carcinoma of the lung. *Semin Roentgenol* **1977**;12:187-206
41. Heitzman ER. Bronchogenic carcinoma: radiologic-pathologic correlations: *Semin Roentgenol* **1977**;12:165-174
42. Theros EG. Varying manifestations of peripheral pulmonary neoplasms: a radiologic-pathologic correlative study. *AJR* **1977**;128:893-914
43. Kuriyama K, Tateishi R, Doi O, et al. CT-pathologic correlation in small peripheral lung cancers. *AJR* **1987**;149:1139-1143
44. Moise EE, Downs FL Jr. *Geometry*. Reading, MA: Addison-Wesley, **1964**: 562-568

45. Cummings SR, Lillington GA, Richard RJ. Estimating the probability of malignancy in solitary pulmonary nodules: a bayesian approach. *Am Rev Respir Dis* **1986**;134:449–452
46. Kelly RB, Mahoney PD, Johnson JF. A calcified carcinoma of the lung and intracerebral metastasis. *J Comput Tomogr* **1987**;11:389–391
47. Goldstein MS, Rush M, Johnson P, Sprung CL. A calcified adenocarcinoma of the lung with very high CT numbers. *Radiology* **1984**;150:785–786
48. Mallens WMC, Nijhuis-Heddes JMA, Bakker W. Calcified lymph node metastases in bronchioloalveolar carcinoma. *Radiology* **1986**;161: 103–104
49. Austin JHM, Grimes MM, Carberry D. CT detection of calcified nodal metastases of lung adenocarcinoma. *J Comput Assist Tomogr* **1988**; 12:314–316
50. Woodring JH, Fried AM, Chuang VP. Solitary cavities of the lung: diagnostic implications of cavity wall thickness. *AJR* **1980**;135:1269–1271
51. Woodring JH, Fried AM. Significance of wall thickness in solitary cavities of the lung: a follow-up study. *AJR* **1983**;140:473–474
52. Good CA, Holman CB. Cavitary carcinoma of the lung: roentgenologic features in 19 cases. *Dis Chest* **1960**;37:289–293
53. Hebert C, George RB. Large fluid-filled thoracic mass in a young man. *South Med J* **1988**;81:1322–1323
54. Torpoco J, Yousuffiddin M, Pate JW. Aspergilloma within a malignant pulmonary cavity. *Chest* **1976**;69:561–563
55. Berkmen YM. The many faces of bronchioloalveolar carcinoma. *Semin Roentgenol* **1977**;12:207–214
56. Epstein DM, Gefter WB, Miller WT. Lobar bronchioloalveolar cell carcinoma. *AJR* **1982**;139:463–468
57. Heitzman ER. *The lung: radiologic-pathologic correlations*, 2nd ed. St. Louis: Mosby, **1984**:70–79
58. Im J-G, Choi BI, Park JH, et al. CT findings of lobar bronchioloalveolar carcinoma. *J Comput Assist Tomogr* **1986**;10:320–322
59. Liebow AA. Bronchiolo-alveolar carcinoma. *Adv Intern Med* **1960**;10: 329–358
60. Ludington LG, Verska JJ, Howard T, Kypridakis G, Brewer LA III. Bronchiolar carcinoma (alveolar cell), another great imitator: a review of 41 cases. *Chest* **1972**;61:622–628
61. Woodring JH, Stelling CB. Adenocarcinoma of the lung: a tumor with a changing pleomorphic character. *AJR* **1983**;140:657–664
62. Zheutlin N, Lasser EC, Rigler LG. Bronchographic abnormalities in alveolar cell carcinoma of the lung: a new diagnostic sign. *Dis Chest* **1954**;25: 542–549
63. Fraser RG, Paré JAP, Paré PD, Fraser RS, Genereux GP. *Diagnosis of the chest*, vol I, 3rd ed. Philadelphia: Saunders, **1988**:578
64. Foster WL Jr, Roberts L Jr, McLendon RE, Hill RC. Localized peribronchial thickening: a CT sign of occult bronchogenic carcinoma. *AJR* **1985**; 144:906–908
65. Rabin CB, Baron MG. *Radiology of the chest*, 2nd ed. Baltimore: Williams & Wilkins, **1980**:128–132
66. Felson B. Mucoid impaction (inspissated secretions) in segmental bronchial obstruction. *Radiology* **1979**;133:9–16
67. Woodring JH, Bernardy MO, Loh FK. Mucoid impaction of the bronchi. *Australas Radiol* **1985**;29:234–239
68. Fraser RG, Paré JAP. *Diagnosis of diseases of the chest*, vol. III, 2nd ed. Philadelphia: Saunders, **1979**:1759
69. Marriott AE, Weisbrod G. Bronchogenic carcinoma associated with pulmonary infarction. *Radiology* **1982**;145:593–597
70. Heater K, Macmahon H, Vybomy CJ. Occult lung carcinoma presenting with dysphagia: the value of computed tomography. *Clin Imaging* **1989**; 13:122–126
71. Dore R, Alerci M, D'Andrea F, Di Giulio G, De Agostini A, Volpato G. Intracardiac extension of lung cancer via pulmonary veins: CT diagnosis. *J Comput Assist Tomogr* **1988**;12:565–568
72. Koo BC, Woldenberg LS, Kim C-T. Pulmonary vein tumor thrombosis and left atrial extension in lung carcinoma. *J Comput Tomogr* **1984**;8:331–336
73. Posniak HV, Olson MC, Moncada R. Pericardial diseases: still a radiologist's province? *Postgrad Radiol* **1988**;8:122–136
74. Borts FT, Rohatgi PK, Sehgal E. Bronchogenic cavoatrial tumor thrombus: CT demonstration. *J Comput Assist Tomogr* **1985**;9:1115–1117
75. Johnson DH, Hainsworth JD, Greco FA. Pancoast's syndrome and small cell lung cancer. *Chest* **1982**;82:602–606
76. Rockoff SD. Apical lung cancer masquerading as a Pancoast tumor. *AJR* **1982**;139:163–165
77. O'Connell RS, McLoud TC, Wilkins EW. Superior sulcus tumor: radiographic diagnosis and workup. *AJR* **1983**;140:25–30

Robert D. Pugatch, Sixth Distinguished Scientist, Armed Forces Institute of Pathology

Richard P. Moser, Jr.[1]

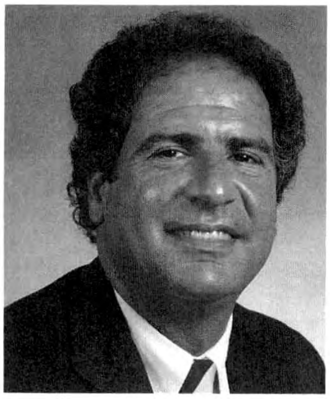

Robert D. Pugatch is the sixth Distinguished Scientist in the Department of Radiologic Pathology, Armed Forces Institute of Pathology (AFIP), for the academic year July 1, 1990, through June 30, 1991.

Dr. Pugatch received a bachelor of arts degree in 1967 from the Johns Hopkins University, Baltimore, MD. He received the degree of doctor of medicine from George Washington University School of Medicine, Washington, DC, in 1971. Dr. Pugatch took a surgical internship, and then a residency in diagnostic radiology, at the New England Medical Center, Boston, MA. This was followed by a fellowship in vascular/neuroradiology at the Boston Veterans Administration Medical Center, where he remained from 1976 to 1983 as staff radiologist and head of pulmonary radiology. Since 1983, Dr. Pugatch has been the director of thoracic radiology at Brigham and Women's Hospital, Boston, MA. During this same time, he has also been an associate professor of radiology at Harvard Medical School.

Dr. Pugatch has studied, written, and lectured extensively, primarily in the area of chest radiology. He is a member of nine radiologic societies and is currently president-elect of the New England Roentgen Ray Society. He is the author of approximately 60 scientific papers, abstracts, and book chapters. In addition, Dr. Pugatch is a much sought after lecturer and has been a visiting professor or invited speaker at more than 100 major medical meetings. His major research interests include the use of CT in evaluating and staging bronchogenic carcinoma, the use of high-resolution CT in evaluating the pulmonary parenchyma, and the radiologic assessment of septic pulmonary emboli.

The Distinguished Scientist program in the Department of Radiologic Pathology was established in 1985 through the efforts of the director of the AFIP, the American Registry of Pathology, the Conjoint Committee on Radiology at the AFIP, and the chairman and registrar of the Department of Radiologic Pathology, AFIP. The representatives of the four major radiologic societies that make up the Conjoint Committee on Radiology at the AFIP are John E. Madewell, American Roentgen Ray Society; Mark M. Mishkin, chairman, American College of Radiology; Robert E. Campbell, Radiological Society of North America; and Thomas S. Harle, Association of University Radiologists. Otha Linton, associate executive director of the American College of Radiology, is the liaison between the committee and the AFIP.

The first five Distinguished Scientists were William W. Olmsted (1985–1986), professor of radiology at the George Washington University Medical Center, Washington, DC, and current editor of *RadioGraphics*; Alan J. Davidson (1986–1987), who currently holds a joint appointment as senior scientist at the AFIP and professor of radiology at Johns Hopkins University; Roger K. Harned (1987–1988), professor of radiology at the University of Nebraska Medical Center, Omaha, NE; Terry M. Hudson (1988–1989), professor of radiology, Emory University, Atlanta, GA; and Anne G. Osborn (1989–1990), professor of radiology at the University of Utah, School of Medicine, Salt Lake City, UT.

The efforts of the members of the Conjoint Committee on Radiology at the AFIP and the financial support of the societies they represent have been the foundation for the Distinguished Scientist Program. As the sixth Distinguished Scientist, Dr. Robert D. Pugatch is certain to continue in the successful tradition established by his predecessors.

The opinions or assertions contained herein are the private views of the author and are not to be construed as official or as reflecting the views of the Department of Army or the Department of Defense.

[1] Department of Radiologic Pathology, Armed Forces Institute of Pathology, Washington, DC 20306-6000. Address reprint requests to R. P. Moser, Jr.

Pulmonary Blastomycosis: Findings on Chest Radiographs in 63 Patients

John R. Sheflin[1]
John A. Campbell[2]
Gregory P. Thompson[2]

Posteroanterior and lateral chest radiographs of 63 patients with proved pulmonary blastomycosis were evaluated to determine the most common findings. Included in the analysis were the location of the pulmonary infiltrates, the distribution and parenchymal patterns of disease, and the prevalence of adenopathy, pleural effusions, and/or cavity formation. Blastomycosis pneumonitis involved more than one pulmonary lobe in 21 patients and a single upper lobe in 27 of 63 patients. Forty-eight of the 63 patients had air-space consolidation. In nine of the 63 patients, a pulmonary mass was the major abnormality seen on radiographs. Approximately one fifth of the patients had associated pleural effusions and/or mediastinal or hilar adenopathy. Twenty-three patients (37%) had cavitation within the area of pulmonary consolidation.

These findings suggest that blastomycosis should be considered when chest radiographs show air-space infiltrate in the upper lobes or in more than one lobe of the lung, especially when the infiltrate is associated with pleural effusions, cavitation, lymphadenopathy, and/or a paramediastinal mass.

AJR **154:1177–1180, June 1990**

North American blastomycosis is a pyogranulomatous fungal infection caused by *Blastomyces dermatitidis*. The disease is endemic in major areas of the central, north-central, and southeastern portions of the United States [1].

The organism appears to enter humans by inhalation, and pulmonary manifestations are most common, although the disease may affect the skin, CNS, bones and joints, or reproductive organs [2].

Many of the radiologic features of blastomycosis have been described in previous reports [1–7]. However, most of the analyses have been exclusively or primarily a review of patients from the southeastern or central portions of the United States. The purpose of the present study was to evaluate the radiologic appearance of the disease in patients from the north-central portion of the United States and to attempt to identify characteristic features of the disease seen on chest radiographs.

Materials and Methods

Eighty patients with proved blastomycosis were seen at the Marshfield Clinic; all but one were seen between 1974 and 1988. The clinic is located in central Wisconsin, in the north-central portion of the United States. The clinical records of these patients were evaluated, and the chest radiographs were reviewed.

The most frequent complaints included coughing (46%), fever (35%), and chest pain (22%). The procedures used for establishing the diagnosis of blastomycosis included sputum analysis with cytology and culture (31 patients), bronchoscopy with washing (36 patients), open-lung biopsy (20 patients), and fine needle aspiration of the lung (seven patients).

Sixty-three of the 80 patients had adequate chest radiographs that had been obtained at the time of presentation to the clinic. The radiographs were reviewed to evaluate the anatomic location and pattern of parenchymal disease and the presence of other findings, such as pulmonary cavitation, mediastinal or hilar adenopathy, or pleural effusion.

Received December 12, 1989; accepted after revision January 30, 1990.

[1] Department of Radiology, Marshfield Clinic, 1000 N. Oak St., Marshfield, WI 54449. Address reprint requests to J. R. Sheflin.

[2] Department of Internal Medicine, Marshfield Clinic, 1000 N. Oak St., Marshfield, WI 54449.

0361–803X/90/1546–1177
© American Roentgen Ray Society

Classification of location of disease was based on commonly recognized lobar anatomy. Lingular disease was considered to be within the left upper lobe. Infiltrates involving more than one lobe were considered multilobar unless the disease involved the majority of all pulmonary lobes, in which case they were classified as diffuse.

Lobar involvement was considered to be present when the major portion of a lobe was involved with infiltrate and the disease did not cross lobar borders. Nonlobar patterns included infiltrates involving segments of lung and parenchymal disease not corresponding to segmental distribution and/or crossing usual segmental boundaries.

Pleural effusions were considered to be present if abnormal pleural density that changed in size or volume over a short period of time was present.

An attempt was made to differentiate incomplete pneumonic consolidation from cavity formation. However, an identifiable air-fluid level was not required for a diagnosis of cavitation.

Results

Location of Disease

Pulmonary parenchymal infiltrate involving multiple lobes or a single upper lobe was the most common feature seen on radiographs (Table 1). Twenty-one (33%) of the 63 patients had multilobar disease. When only one lobe was involved, the upper lobes were affected in 27 patients (43%) and the lower lobes were involved in 12 patients (19%). Disease was isolated in the right upper lobe in 15 patients (24%); this was the most frequent single site. The right middle lobe was affected in only three (5%) of the 63 patients.

Distribution of Disease

The most frequent appearance was nonlobar (segmental or nonsegmental) disease, which occurred in 37 (59%) of the 63 patients (Table 2). Twelve (19%) of the patients showed a lobar distribution. Only five (8%) of the 63 patients had diffuse disease.

Pattern on Radiographs

Air-space consolidation with an alveolar pattern occurred in 48 patients (76%) (Table 2). The pulmonary infiltrate was seen as a patchy or homogeneous alveolar pneumonitis with poorly marginated borders and was occasionally accompanied by well-defined air bronchograms. Interstitial disease, presenting as linear, reticular, or reticulonodular infiltrate, occurred in five patients (8%).

The second most frequent manifestation on radiographs was a mass or masslike infiltrate. Nine (14%) of the 63 patients had mass effect as the primary or sole finding on radiographs.

TABLE 1: Anatomic Location of Pulmonary Infiltrate

Location	No. of Patients
Multiple lobes	21
Right upper lobe	15
Right lower lobe	7
Right middle lobe	3
Left upper lobe	12
Left lower lobe	5

TABLE 2: Findings on Radiographs in Pulmonary Blastomycosis

Finding	No. of Patients
Distribution	
Nonlobar	37
Lobar	12
Diffuse	5
Parenchymal pattern	
Air space	48
Interstitial	5
Mass	9
Miliary	1
Other	
Effusions	13
Adenopathy	14
Cavitation	23

Other Findings on Radiographs

Pleural effusions were identified in 13 (21%) of the 63 patients, and the fluid usually caused only mild to moderate blunting of the costophrenic sulci (Table 2). Fourteen (22%) of the 63 patients had lymphadenopathy. This occurred at multiple sites, including hilar, paratracheal, and aortopulmonary locations. Twenty-three (37%) of the patients had cavitation within the parenchymal infiltrate.

Discussion

Pulmonary blastomycosis is caused by *Blastomyces dermatitidis*, which is thought to be a primary pathogen rather than an opportunistic organism [3]. It originally was described as a dermatologic disease by Gilchrist in 1894 and only subsequently was associated with systemic manifestations including lesions of the pulmonary and musculoskeletal systems [4]. The current study was designed to evaluate the appearance of blastomycosis on chest radiographs of patients selected from a region in which the disease is endemic.

The primary manifestation of pulmonary blastomycosis on radiographs is a focal parenchymal infiltrate. Several authors have studied the anatomic location of the disease in the lungs. Halvorsen et al. [5] noted that blastomycosis was a predominantly upper-lobe disease. Rabinowitz et al. [6] identified disease restricted to the upper lobes in 38 (75%) of 51 patients, with right-upper-lobe disease in 21 (41%) and multilobar disease in 13 (25%) of the patients. Our result show that infiltrates involving multiple lobes (33% of patients) were more common than specific single-lobe involvement. However, when only a single lobe was affected, the upper lobes were involved over twice as often as the lower lobes (43% vs 19% of patients). The right upper lobe was the most frequently involved single lobe (24%).

The distribution of disease within the lung has been reported to be segmental, nonsegmental, or lobar [3, 5]. The most frequent appearance of the infiltrate in our series was a

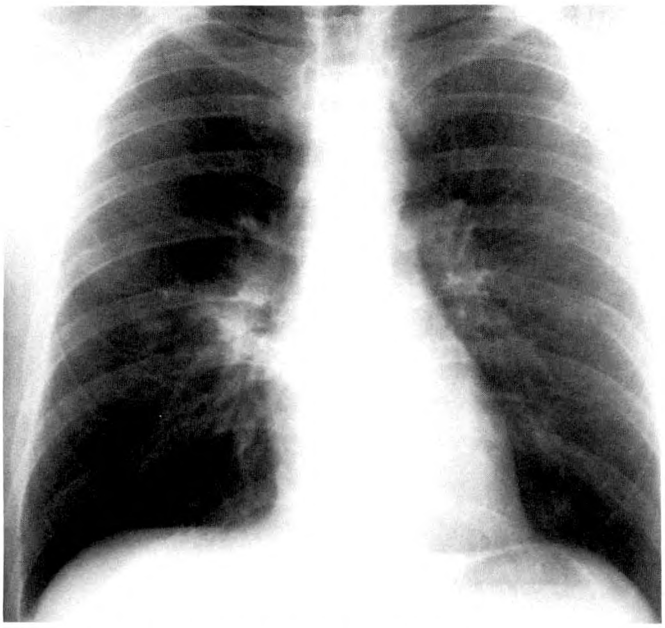

Fig. 1.—Chest radiograph of 38-year-old man with pulmonary blastomycosis shows nonlobar right perihilar air-space infiltrate.

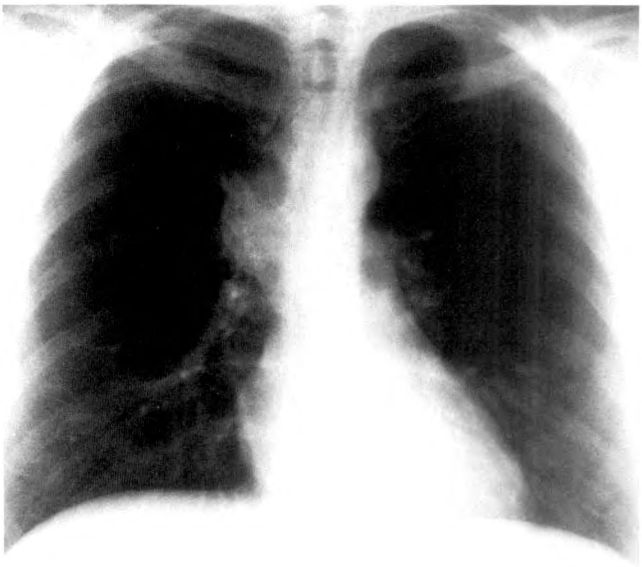

Fig. 2.—Chest radiograph of 42-year-old woman shows right paramediastinal mass infiltrate, subsequently proved to be blastomycosis at thoracotomy.

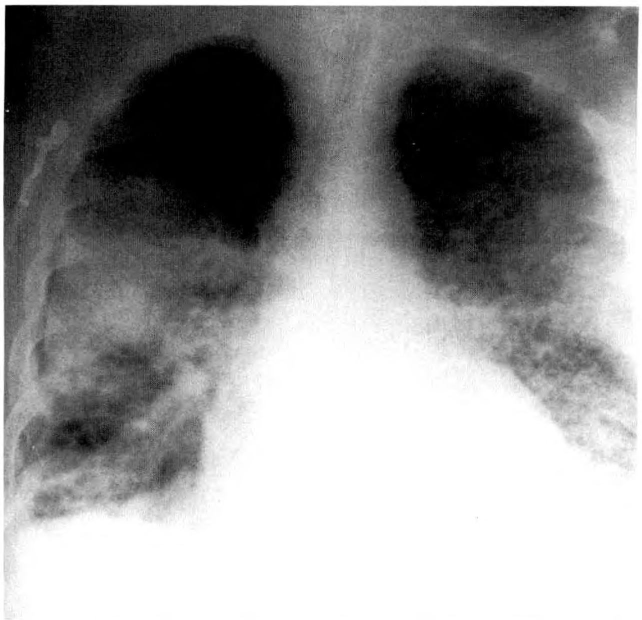

Fig. 3.—Portable chest radiograph of 77-year-old man with blastomycosis shows diffuse alveolar infiltrate and right-sided pneumothorax.

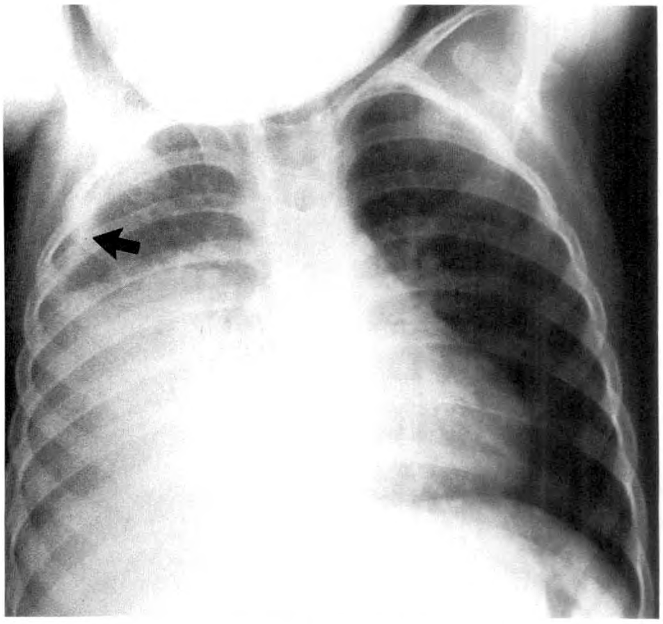

Fig. 4.—Obtained in right lateral decubitus position, chest radiograph of a child with blastomycosis shows small mobile pleural effusion (*arrow*) and lobar consolidation.

moderately confluent area of consolidation with relatively poorly defined margins. The pneumonitis frequently was not confined to usual lobar or segmental borders or did not occupy a major portion of a segment or lobe.

Air-space consolidation, rather than interstitial disease, was the usual appearance of pulmonary parenchymal disease (Fig. 1). This is generally in agreement with other studies [3, 5, 6], although some analyses [7] have shown an equal distribution of alveolar and interstitial patterns. Mass or masslike infiltrate was seen on chest radiographs in nine (14%) of our 63 patients. Several of these patients had thoracotomy for evaluation of possible neoplasm. The reported prevalence of mass

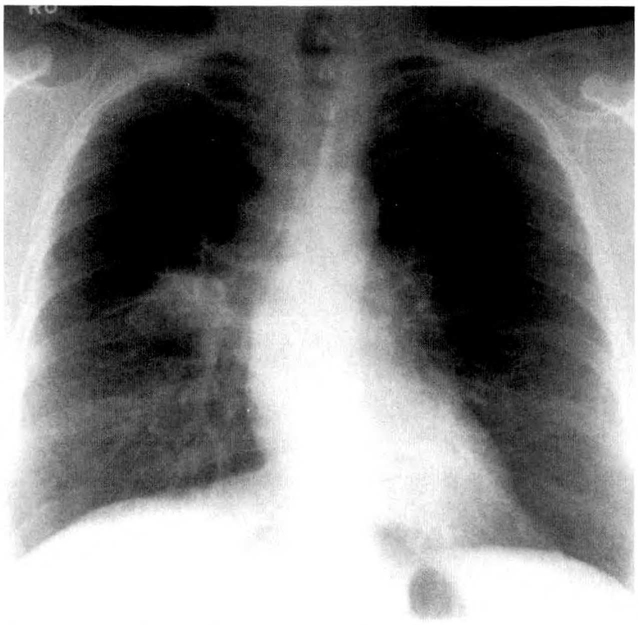

Fig. 5.—Chest radiograph of 45-year-old woman with pulmonary blastomycosis shows right paratracheal adenopathy associated with right perihilar infiltrate.

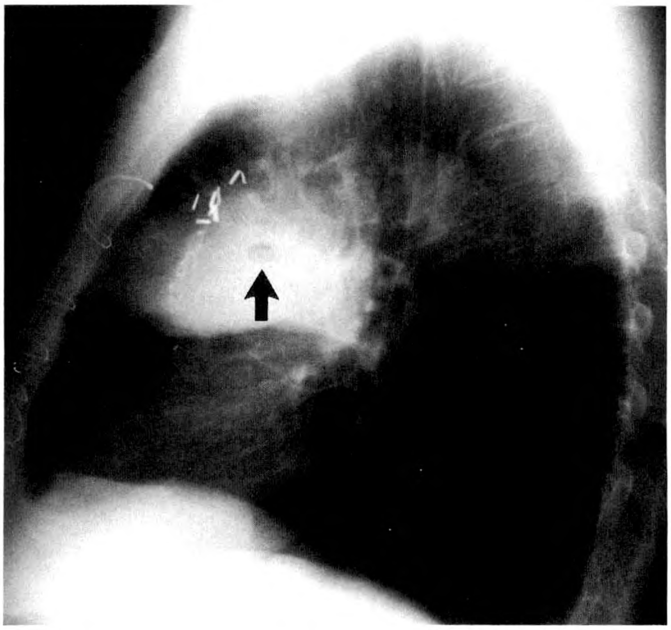

Fig. 6.—Lateral chest radiograph shows region of air-space consolidation with small central cavity and air-fluid level (*arrow*) in 54-year-old man with blastomycosis.

effect in other studies varies from less than 4% [7] to 26% [5]. Rabinowitz et al. [6] noted that the mass lesions in their series occurred in the upper lobes, a pattern seen also in our patients. In addition, the masses observed in our series were frequently central or paramediastinal rather than peripheral (Fig. 2).

Five (8%) of our patients showed diffuse disease (Fig. 3). Only one of our patients had a miliary pattern. This appearance has been noted in other studies; Stelling et al. [1] noted miliary disease in four of their 46 patients.

The Veterans Cooperative study [4] found evidence of pleural fluid in only four of 118 patients. Kinasewitz et al. [7] studied various types of pleural involvement in blastomycosis and determined that 23 (88%) of 26 patients had pleural disease, although the findings usually consisted of "minor pleural reaction adjacent to the parenchymal infiltrate." Assessment of pleural involvement in our series was limited to evaluation for basilar pleural effusions. One fifth of our patients had findings on radiographs that were compatible with pleural fluid, usually evident as blunting of costophrenic sulci but occasionally larger in extent (Fig. 4).

Approximately one fifth of the patients in our series also had enlarged lymph nodes (Fig. 5). This prevalence of adenopathy is significantly higher than 6% in both the Veterans Cooperative Study [4] and the study by Rabinowitz et al. [6]. Halvorsen et al. [5] reported no adenopathy in their series of 27 patients.

Pulmonary parenchymal cavitation was present in 23 (37%) of 63 patients. This prevalence is also greater than the 10% to 25% reported in other series [4–6]. Many of the cavities were small and centrally located in the infiltrate (Fig. 6), although several were relatively large and well demarcated.

Our review of chest radiographs in 63 patients does not identify a specific feature that characterizes blastomycosis as the cause of a particular infiltrate. However, our patients showed a greater prevalence of adenopathy, pleural effusion, and/or cavitation than seen in previous studies [4–6]. When one or more of these findings are present in a patient from an endemic area with upper lobe or multilobar air-space infiltrate, blastomycosis should be strongly considered.

REFERENCES

1. Stelling CB, Woodring JH, Rehm SR, Hopper DW, Noble RC. Miliary pulmonary blastomycosis. *Radiology* **1984**;150:7–13
2. Murphy PA. Blastomycosis. *JAMA* **1989**;126:3159–3162
3. Fraser RG, Paré JA, Paré PD, Fraser RS, Genereux GP. *Diagnosis of diseases of the chest*. 3rd ed. Philadelphia: Saunders, **1989**:968–974
4. Busey JF, Baker R, Birch L, et al. Blastomycosis cooperative study of the Veterans Administration. *Am Rev Respir Dis* **1964**;89:659–672
5. Halvorsen RA, Duncan JD, Merten DF, Gallis HA, Putman CE. Pulmonary blastomycosis: radiologic manifestations. *Radiology* **1984**;150:1–5
6. Rabinowitz JG, Busch J, Buttram WR. Pulmonary manifestations of blastomycosis. *Radiology* **1976**;120:25–32
7. Kinasewitz GT, Penn RL, George RB. The spectrum and significance of pleural disease in blastomycosis. *Chest* **1984**;86:580–584

Percutaneous Biopsy of Thoracic Lesions: Value of Sonography for Needle Guidance

Junpei Ikezoe[1]
Shizuo Morimoto[1]
Jun Arisawa[1]
Shodayu Takashima[1]
Takahiro Kozuka[1]
Kazuya Nakahara[2]

Fluoroscopy and CT are widely used to guide percutaneous needle biopsy of thoracic lesions. However, some lesions are not sufficiently visible on fluoroscopy and others are dangerous to access on CT without real-time monitoring. When these are the circumstances, sonographic guidance may be helpful. Real-time sonography was used to guide percutaneous needle biopsy in 124 patients with thoracic lesions. The indications for sonographic guidance included pulmonary, pleural, or mediastinal lesions in contact with the chest wall, including lesions near the heart or great vessels ($n = 12$); lesions in the apical region ($n = 5$); lesions in a juxtadiaphragmatic location ($n = 6$); small lung nodules adjacent to the chest wall ($n = 16$); and peripheral tumors with adjacent pleural effusion ($n = 4$). A diagnosis was made in 74 (90%) of 82 malignant lesions and in 24 (67%) of 36 benign lesions. Complications included pneumothorax ($n = 5$), hemoptysis ($n = 1$), and hemothorax ($n = 1$). The advantages of sonographic guidance are that the sonographic equipment is mobile and real-time monitoring makes the procedure safer. Its limitations are that it cannot be used when aerated lung or free air (pneumothorax) lies between the chest wall and the lesion and that cavitary lesions are difficult to sample by biopsy.

Our results show that the use of sonographic guidance considerably expands the number of thoracic lesions amenable to percutaneous biopsy.

***AJR* 154:1181–1185, June 1990**

Transthoracic needle biopsy for thoracic lesions is a well-established method of obtaining cytologic and histologic material [1–5]. Since the description of fluoroscopically guided transthoracic needle biopsy by Dahlgren and Nordenström [6, 7], many improvements have been made in the needle itself [8–13] and in its guidance [14–16].

CT and sonography are newer methods to guide needle aspiration [14–21]. Although CT is widely used for guiding percutaneous needle biopsy, sonography offers the advantage that the needle position can be followed in real time. We reported a preliminary study of sonographically guided needle biopsy in 1984 [19]; we now describe our experience in 124 cases.

Materials and Methods

Sonographically guided needle biopsy was performed in over 200 cases of intrathoracic lesions from September 1981 through March 1989. In the first 124 consecutive patients in whom biopsies were performed with sonographic guidance through June 1986, clinical data were adequate for evaluation of the cases in which a definitive diagnosis was not made by biopsy. The results in those 124 cases were analyzed. All lesions could be visualized with sonography via the chest wall.

In the first 38 patients, sonographically guided biopsy was performed when definitive diagnosis could not be established by serial sputum cytology, bronchial brushing, or transbronchial biopsy. In the last 86 patients, this method was performed, when possible (i.e., when the lesion was in contact with the chest wall), before other diagnostic measures.

Received November 17, 1989; accepted after revision January 8, 1990.

[1] Department of Radiology, Osaka University Medical School, 1-1-50, Fukushima, Fukushima-ku, Osaka, Japan. Address reprint requests to J. Ikezoe.

[2] First Surgical Department, Osaka University Medical School, Fukushima-ku, Osaka, Japan.

0361-803X/90/1546–1181
© American Roentgen Ray Society

The 124 patients comprised 92 with pulmonary masses adjacent to the chest wall, 14 with mediastinal masses, eight with chest wall masses, and 10 with pleural diseases.

Final diagnoses were established by examination of specimens, autopsy material, or clinical follow-up. There were 82 malignant and 36 benign lesions. The remaining six cases were lost to follow-up and therefore are unconfirmed. Malignant lesions consisted of 60 bronchogenic carcinomas; 14 metastatic pulmonary tumors; five malignant mediastinal tumors; and one each of malignant lymphoma of the lung, mesothelioma, and hemangioendothelioma. Benign lesions consisted of nine tuberculous lung nodules; three mediastinal tumors (one each of thymoma, neurofibroma, and ganglioneuroma); and one each of hamartoma, mesothelioma, *Cryptococcus,* and 21 other nonneoplastic lesions.

The aspiration needle was made of steel and consisted of an inner stylet and an outer sheath (19 or 21 gauge, 1.06- or 0.8-mm outer diameter). It was 20 cm long and the tip was sharpened at an 18 or 30 bevel. For cutting biopsy, our initial experience was with a Tru-cut needle (Travenol Labs, Inc., Deerfield, IL), but during the last 5 years we have used the Sure-cut needle (Modified Menghini needle, Cutter Japan Ltd., Kobeshi, Japan) in various lengths, but almost exclusively of 18 or 22 gauge.

A commercially available sonographic unit (Model RT-100, RT-2000, or RT-3600, Yokogawa Medical Systems, Tokyo, Japan) with an electronic linear-array scanner (3.5 or 5 MHz) was used. The biopsy probe was sterilized in 1% chlorhexidine gluconate before the procedure. The puncture site was disinfected and anesthetized. Povidone-iodine gel was used as the coupling medium. The needle was inserted through a small skin incision. Respiration was suspended during manipulation of the needle. The echo from the needle tip was monitored as a round spot or short line.

When the aspiration needle tip was in place, suction was applied with a 50-ml syringe while the needle was moved back and forth in the lesion. When a Tru-cut or Sure-cut needle was used, the most suitable biopsy site within the lesion could be selected sonographically after the placement of the needle tip in the mass. Both aspiration and cutting biopsies were performed, when possible. If the mass was small or the patient was in poor condition, only aspiration biopsy was performed. Usually two needle passes were made for aspiration biopsy, and one or two cutting biopsies were performed for each patient.

Aspirated specimens were placed on glass slides and fixed for cytology or dried in air for bacteriologic study. The needle was then immersed in saline solution, which was used for the examination of centrifuged cells or for cell culture. Tissue specimens from Tru-cut biopsies were fixed in formalin.

Results

Of the 82 malignant lesions, 74 (90%) were diagnosed by sonographically guided biopsy and eight were false-negatives. Of the 36 benign lesions, 24 (67%) were diagnosed by this method; a specific benign diagnosis was made in 17, and a nonspecific benign diagnosis was made in the other seven. The specific benign diagnoses were tuberculous or cryptococcal granuloma (eight cases), organizing pneumonia (one), chronic pleuritis (two), ganglioneuroma (one), neurofibroma (one), thymoma (one), hamartoma (one), and bacterial pneumonia (two). The nonspecific benign diagnoses were granuloma (type not specifiable), localized fibrosis of the lung, and fibrous thickening of the pleura.

In the remaining 11 of the 36 benign lesions, cytologic diagnosis for malignancy was Papanicolaou class I or II, and the bacteriologic diagnosis was negative. In three of these, the lesions disappeared in the course of antibiotic therapy; in the others, the lesions showed no change in size or shape after more than 2 years of follow-up. One false-positive diagnosis of malignancy occurred; this case proved surgically to be a benign mesothelioma but had been diagnosed as a small-cell carcinoma of the lung.

Complications occurred in seven (5.6%) of the 124 cases, including five cases of pneumothorax and one each of transient hemoptysis and hemothorax. In one of these cases, a minimal pneumothorax occurred during the first puncture, but it could not be verified by fluoroscopy because of its small size. However, the biopsy procedure had to be discontinued because the small pneumothorax made the lesion invisible on sonography.

Discussion

Biplane fluoroscopically guided needle biopsy of thoracic lesions is well established [1–5, 12, 13, 22]. It is quick and easy to perform [1] and has no major disadvantages. Nevertheless, not all kinds of pulmonary lesions are amenable to this method [23]. For example, extremely peripheral and very small lesions may not be detectable on lateral fluoroscopy; juxtadiaphragmatic and small apical lesions often are not visible on lateral images because of overlying structures; with paracardiac, mediastinal, and apical lesions it is dangerous to perform needle insertion under fluoroscopic guidance alone, and a preliminary CT scan may be necessary to map adjacent cardiovascular structures. In such cases, CT-guided or sonographically guided biopsy may be useful [23].

CT-guided biopsy is helpful in some cases, but the lack of real-time monitoring of the needle position and the relatively high frequency of large pneumothoraces are major disadvantages [14–16].

In 1984, we reported our preliminary experience with sonographically guided needle biopsy in 38 thoracic lesions [19]. Our current analysis of the results in 124 patients shows more clearly the indications, advantages, disadvantages, and value of this method.

Real-time sonographically guided needle biopsy can be performed easily and safely for diagnosis of thoracic lesions when fluoroscopic guidance is ineffective. The procedure is suitable for apical tumors, juxtadiaphragmatic or small nodules adjacent to the chest wall (Fig. 1); peripheral lung tumors with adjacent pleural effusion; and anterior mediastinal masses.

The advantages of sonographic guidance include the following: (1) No radiation is required. (2) The procedure can be performed at the patient's bedside. (3) The needle inserted under sonographic guidance passes through the chest wall directly into the lesion without traversing aerated lung, so the occurrence of pneumothorax is low. (4) Real-time monitoring makes the procedure safe and allows the operator to work with confidence. (5) In the case of a large mass lesion, specimens can be obtained from different regions of the lesion (often showing different echogenicity) (Fig. 2). (6) If a sonographic window can be obtained, any plane of section can be chosen and the direction and course of the needle can be selected freely (Fig. 3).

Fig. 1.—Lung metastasis from breast cancer.

A, CT scan shows small pulmonary nodule (*arrow*) adjacent to anterior chest wall.

B, Sonographically guided aspiration biopsy of lesion (*arrows*) revealed metastatic breast carcinoma (Papanicolaou class V). + = pleural surface.

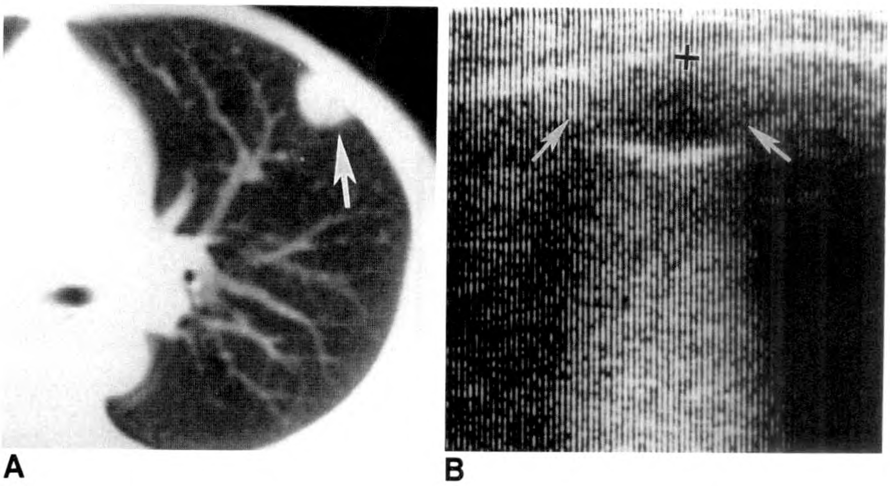

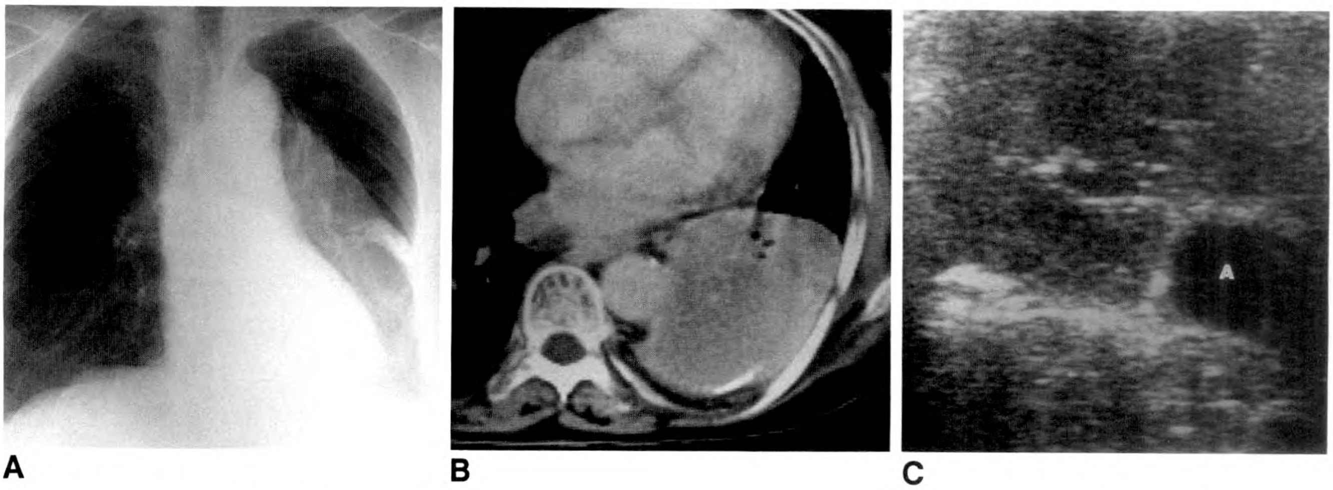

Fig. 2.—Non-Hodgkin lymphoma in lung.

A, Radiograph shows homogeneous opacity in middle and lower left hemithorax, resembling pleural effusion or pleural thickening.

B, CT scan shows large left-lower-lobe mass.

C, Sonogram reveals inhomogeneous solid mass. Descending aorta (A) is clearly visible as round anechoic region. Pathologic diagnosis of non-Hodgkin lymphoma was obtained from deepest hyperechoic layer of mass.

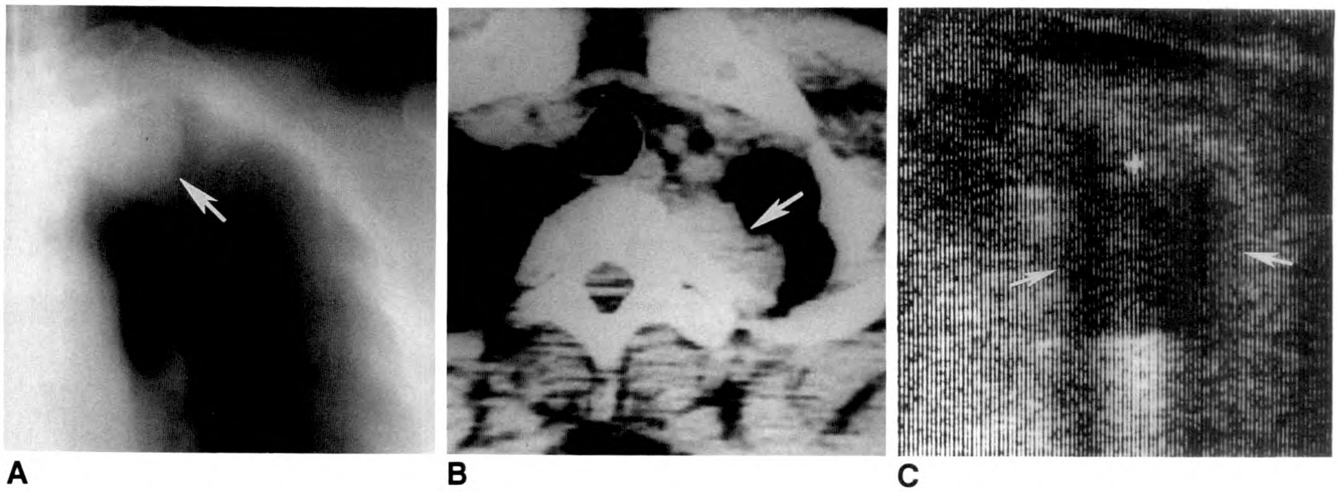

Fig. 3.—Left apical lung cancer.

A, Radiograph shows apical mass (*arrow*).

B, Contrast-enhanced CT scan shows mass (*arrow*) adjacent to spine. Findings on serial sputum cytology and transbronchial biopsy were normal. Fluoroscopic biopsy was difficult because of trouble identifying lesion on lateral view.

C, Prebiopsy sonogram shows lesion (*arrows*). + = pleural surface.

Sonographically guided biopsy was performed without complication through left posterior surface of neck with cephalocaudal insertion of needle. Needle tip, lesion, and vessels were easily identified during procedure. Tru-cut biopsy revealed small-cell lung carcinoma.

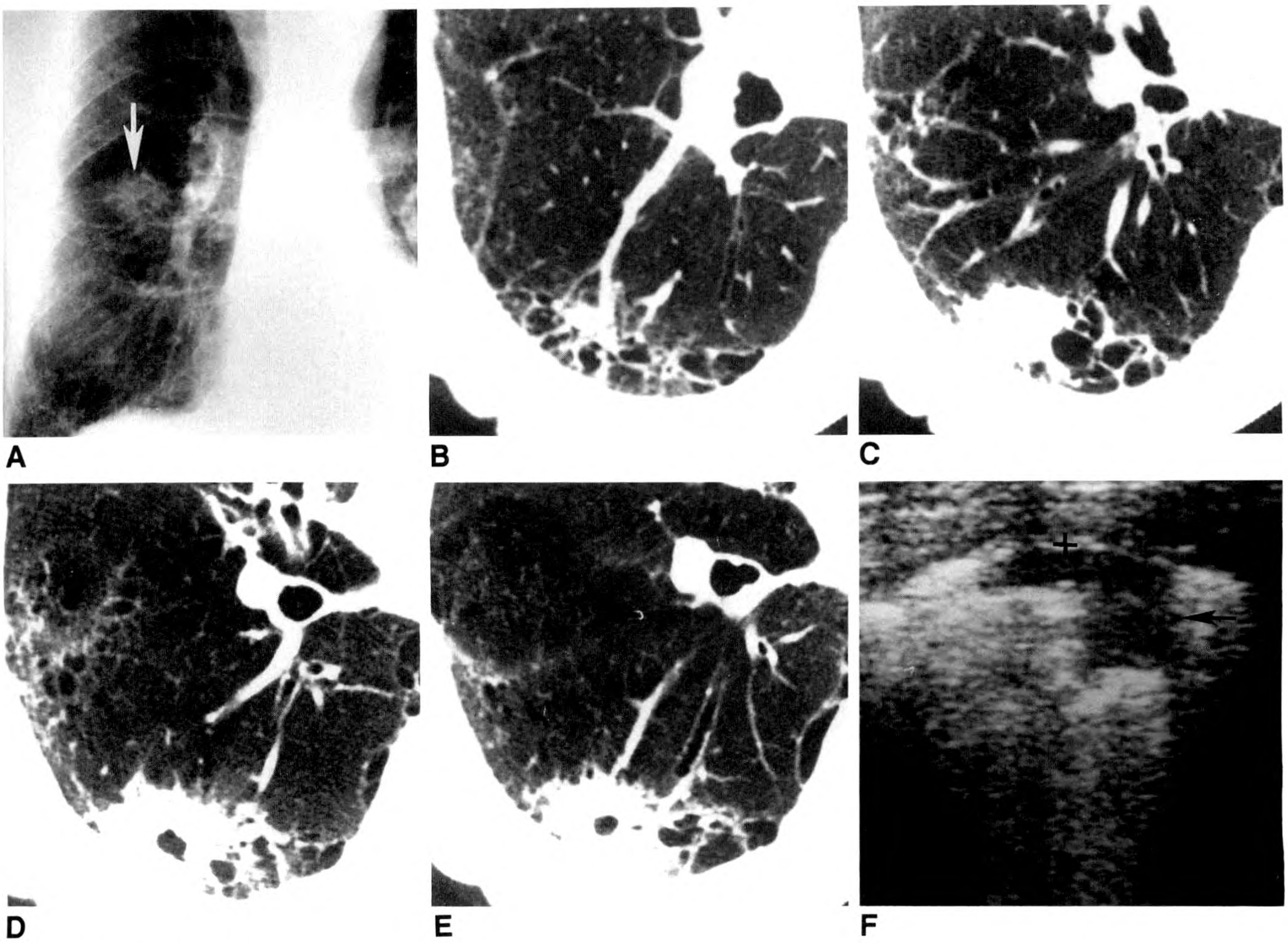

Fig. 4.—Cavitary right-lower-lobe mass.

A, Radiograph shows small cavitary lesion (*arrow*).

B–E, CT scans reveal irregular mass near chest wall with many small bullae around lesion. Note that medial wall is thin and lateral wall is thick.

F, Sonogram delineates posterior and lateral (*arrow*) walls of cavity. Air in cavity prevents visualizing thin medial wall and anterior wall of lesion. + = posterior pleural surface.

Sonographically guided biopsy was performed through posterior chest wall and squamous cell carcinoma was diagnosed by histology. Needle did not pass through aerated lung or bullae, and no pneumothorax or other complication occurred.

Sonographic guidance has some disadvantages: (1) If aerated lung or free air lies between the chest wall and the lesion, sonography cannot delineate the lesions, and biopsy cannot be performed; therefore the lesion must be in contact with the chest wall. (2) Cavitary mass lesions, especially those with thin walls, are difficult to biopsy (Fig. 4) because air in the cavity prevents visualizing the entire lesion. (3) If a pneumothorax develops during the procedure, sonographic guidance will not be sufficient. In this case and in the case of a cavitary mass, we use sonography to determine the site of needle insertion and we monitor the needle position by fluoroscopy (sonographically assisted fluoroscopically guided biopsy). (4) Some technical skill and experience are required.

When peripheral pulmonary mass lesions are found in our clinical practice, we choose among sonographically guided needle biopsy, fluoroscopically guided needle biopsy, or transbronchial biopsy. We do not use CT for guidance of needle biopsy because of the lack of real-time monitoring of the needle position and relatively high frequency of pneumothorax. The ratio of sonographic to fluoroscopic to transbronchial biopsy of such peripheral lesions during the past 7 years is as follows. Sonographically guided biopsy was performed in 195 (30%) of 647 cases, fluoroscopically guided biopsy in 132 (20%), and transbronchial biopsy in 320 (50%). Although sonographically guided biopsy is limited to lesions adjacent to the chest wall, the data show that a larger number of cases than expected are good candidates.

In conclusion, sonographically guided needle biopsy can be performed safely and easily, taking advantage of real-time monitoring of needle position for thoracic masses located adjacent to the chest wall, even when fluoroscopic guidance is not effective.

REFERENCES

1. Jereb M, Us-Krasovec M. Thin-needle biopsy of chest lesions: time-saving potential. *Chest* **1980**;78:288–290
2. Westcott JL. Direct percutaneous needle aspiration of localized pulmonary lesions: results in 422 patients. *Radiology* **1980**;137:31–35

3. Herman PG, Hessel SJ. The diagnostic accuracy and complications of closed lung biopsies. *Radiology* **1977**;125:11–14
4. Lalli AF, McCormack LJ, Zelch M, Reich NE, Belovich D. Aspiration biopsies of chest lesions. *Radiology* **1978**;127:35–40
5. Tao LC, Pearson FG, Delarue NC, Langer B, Sanders DE. Percutaneous fine-needle aspiration biopsy. *Cancer* **1980**;45:1480–1485
6. Nordenström B. A new technique for transthoracic biopsy of lung changes. *Br J Radiol* **1965**;38:550–553
7. Dahlgren SE, Nordenström B. *Equipment and biopsy technique.* Chicago: Year Book Medical, **1966**:29–41
8. Zornoza J, Snow J Jr, Lukeman JM, Libshitz HI. Aspiration biopsy of discrete pulmonary lesions using a new thin needle. *Radiology* **1977**; 123:519–520
9. House AJS, Thomson KR. Evaluation of a new transthoracic needle for biopsy of benign and malignant lung lesions. *AJR* **1977**;129:215–220
10. Poe RH, Tobin RE. Sensitivity and specificity of needle biopsy in lung malignancy. *Am Rev Respir Dis* **1980**;122:725–729
11. Zavala DC, Schoell JE. Ultrathin needle aspiration of the lung in infections and malignant disease. *Am Rev Respir Dis* **1981**;123:125–131
12. Nahman BJ, Van Aman ME, McLemore WE, O'Toole RV. Use of the Rotex needle in percutaneous biopsy of pulmonary malignancy. *AJR* **1985**; 145:97–99
13. Greene R, Szyfelbein WM, Isler RJ, Stark P, Jantsh H. Supplementary tissue-core histology from fine-needle transthoracic aspiration biopsy. *AJR* **1985**;144:787–792
14. vanSonnenberg E, Casola G, Ho M, et al. Difficult thoracic lesions: CT-guided biopsy experience in 150 cases. *Radiology* **1988**;167:457–461
15. Gobien RP, Skucas J, Paris BS. CT-assisted fluoroscopically guided aspiration biopsy of central hilar and mediastinal masses. *Radiology* **1981**; 141:443–447
16. Fink I, Gamsu G, Harter LP. CT-guided aspiration biopsy of the thorax. *J Comput Assist Tomogr* **1982**;6:958–962
17. Chandrasekhar AJ, Reynes, CJ, Churchill RJ. Ultrasonically guided percutaneous biopsy of peripheral pulmonary masses. *Chest* **1976**;70:627–630
18. Izumi S, Tamaki S, Natori H, Kira S. Ultrasonically guided aspiration needle biopsy in disease of the chest. *Am Rev Respir Dis* **1982**;125:460–464
19. Ikezoe J, Sone S, Higashihara T, Morimoto S, Arisawa J, Kuriyama K. Sonographically guided needle biopsy for diagnosis of thoracic lesions. *AJR* **1984**;143:229–234
20. Cinti D, Hawkins HB. Aspiration biopsy of peripheral pulmonary masses using real-time sonographic guidance. *AJR* **1984**;142:1115–1116
21. Pederson OM, Aasen TB, Gulsvik A. Fine needle aspiration biopsy of mediastinal and peripheral pulmonary masses guided by real-time sonography. *Chest* **1986**;89:504–508
22. Khouri NF, Stitik FP, Erozan YS, et al. Transthoracic needle aspiration biopsy of benign and malignant lung lesions. *AJR* **1985**;144:281–288
23. Greene R. Transthoracic needle aspiration biopsy. In: Athanasoulis CA, ed. *Interventional radiology.* Philadelphia: Saunders, **1982**:587–634

American Roentgen Ray Society
Residents' Award Papers, 1991

The ARRS announces competition for the 1991 President's Award and two Executive Council Awards for the best papers concerning the clinical application of the radiologic sciences.

Awards

The winner of the President's Award will receive a certificate and a $2000 prize. The winners of the two Executive Council Awards will each be given a certificate and a prize of $1000. The winners will be announced on March 15, 1991. Winning papers will be presented at the ARRS annual meeting at the Sheraton Boston Hotel, Boston, MA, May 5–10, 1991. Winning papers will be submitted for early publication in the *American Journal of Roentgenology*. All other papers will be returned to the authors.

Regulations

Eligibility is limited to residents or fellows in radiology who have not yet completed 4 years of approved training in a radiologic discipline. A letter from the resident's department chairman attesting to this status must accompany the manuscript. The resident must be the sole or senior author and be responsible for all or most of the project.

Submitted manuscripts must not exceed 5000 words and have no more than 10 illustrations. Four copies of the manuscript and illustrations are required. Submitted manuscripts should not contain previously presented or published material and should not be under consideration for publication elsewhere.

Deadline for submissions is February 15, 1991. Send papers to

Nancy O. Whitley, M.D.
Chairman, Committee on Education & Research
American Roentgen Ray Society
Department of Radiology
University of Maryland Medical Systems Hospital
22 South Greene St.
Baltimore, MD 21201

Case Report

Whipple Disease of the Mediastinum

T. Samuels,[1] P. Hamilton,[1] and P. Shaw[2]

Whipple disease is a rare systemic disorder that usually affects the small bowel but may affect extraintestinal sites such as the CNS, liver, kidney, bone, heart and coronary arteries, lungs, serosal surfaces, and pulmonary arteries [1, 2]. Peripheral lymphadenopathy occurs in half the cases. Central lymphadenopathy typically occurs in the retroperitoneum and mesentery. Mediastinal lymphadenopathy was described in two previous articles [3, 4], but both reviews were written before the era of CT, and neither provided ultrastructural analysis. We report an unusual case of mediastinal widening, seen on a chest radiograph and chest CT scan, caused by an inflammatory infiltrate and adenopathy associated with Whipple disease. Electron microscopy was used to identify the rod-shaped bacilli diagnostic of this entity. To our knowledge, the CT appearance of mediastinal Whipple disease has not been described.

Case Report

A 24-year-old man, profoundly retarded and institutionalized since early childhood, suffered an acute respiratory arrest necessitating intubation and ventilation. A chest film showed a widened mediastinum (Fig. 1A), and bronchoscopy revealed extrinsic compression of the trachea and bronchial collapse with active expiration.

Limited physical examination revealed cachexia, severe contractures, and skin pigmentation over the upper anterior chest. Because of the rapidly deteriorating respiratory status, a thoracic CT study could not be performed before emergent thoracotomy. The patient was managed aggressively at the parents' request.

A sample of tissue encasing the right side of the mediastinum showed extensive replacement of fatty tissue and lymph nodes by a diffuse inflammatory infiltrate. Strongly PAS-positive and diastase-resistant foamy macrophages were the preponderant cell type. PAS-positive material also was present extracellularly. Electron microscopy showed numerous rod-shaped bacteria in intracellular and extracellular locations. Macrophages contained intact bacilliform microorganisms (Fig. 1C) and bacteria in various stages of degradation.

A postoperative chest CT scan showed mediastinal widening (Fig. 1B). Results of small-bowel biopsy were negative for bacilli.

Despite some decrease in the mediastinal widening after 5 months of antibiotic treatment, the patient has remained chronically ill with progressive right ventricular failure related to congenital heart disease.

Discussion

To most radiologists, the diagnosis of Whipple disease (intestinal lipodystrophy) suggests a rare clinical syndrome typically occurring in middle-aged men, characterized by diarrhea, weight loss, and arthritis and associated with PAS-positive material in macrophages of the intestinal submucosa and lymph nodes. The entity is considered in the differential diagnosis of malabsorption when the characteristic radiologic finding of a thickened mucosal fold pattern is observed in the small bowel. Treatment with antibiotics results in clinical and radiologic improvement [1].

Since Whipple's original description in 1907 [5], the diagnosis of the disease is more likely to be made on the basis of peroral biopsy of small bowel than on the basis of autopsy. Whatever the affected organ, the histologic hallmark of the disease is the presence of numerous macrophages containing strongly PAS-positive, diastase-resistant glycoprotein. Be-

---

Received November 28, 1989; accepted after revision January 11, 1990.

[1] Department of Radiology, Sunnybrook Medical Centre, University of Toronto, 2075 Bayview Ave., Toronto, Ontario, Canada M4N 3M5. Address reprint requests to T. Samuels.

[2] Department of Pathology, Sunnybrook Medical Centre, University of Toronto, 2075 Bayview Ave., Toronto, Ontario, Canada M4N 3M5.

AJR 154:1187–1188, June 1990 0361–803X/90/1546–1187 © American Roentgen Ray Society

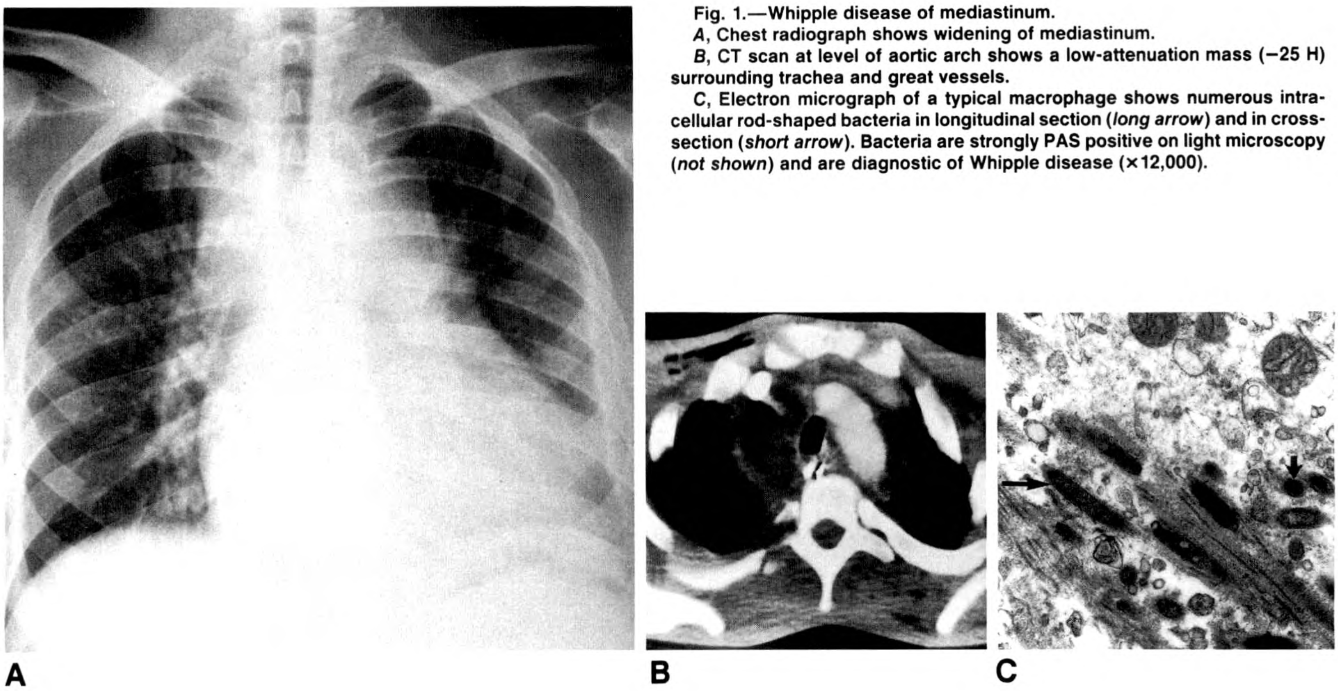

Fig. 1.—Whipple disease of mediastinum.

_A_, Chest radiograph shows widening of mediastinum.

_B_, CT scan at level of aortic arch shows a low-attenuation mass (−25 H) surrounding trachea and great vessels.

_C_, Electron micrograph of a typical macrophage shows numerous intracellular rod-shaped bacteria in longitudinal section (_long arrow_) and in cross-section (_short arrow_). Bacteria are strongly PAS positive on light microscopy (_not shown_) and are diagnostic of Whipple disease (×12,000).

cause the elusive bacillus is not infectious in laboratory animals and has not been cultured in vitro, and because on light microscopy a PAS-positive reaction is nonspecific, the diagnosis of Whipple disease depends on identifying the characteristic structural appearance on electron microscopy (Fig. 1C).

The microscopic features form the basis for the gross findings: when enlarged nodes are sectioned, a cystic and spongy appearance with an oily exudate can be seen [2]. This in turn explains the low-density appearance of nodes and masses described on abdominal CT [6]. A similarly affected mediastinum would account for the low-density mass observed in our case.

Other thoracic manifestations reported in Whipple disease include parenchymal bibasilar interstitial infiltrates, "nodular shadows," and reduced lung volumes. Pleural and pericardial effusions and thickening reflect the polyserositis [7]. The respiratory manifestations may be caused by an inflammatory reaction to locally deposited immune complexes containing bacterial antigens rather than solely due to primary invasion by the bacilli [1].

Exclusive involvement of an extraintestinal site has been reported previously [8], but no author has described only mediastinal disease.

The differential diagnosis of a widened mediastinum in a retarded patient with skin pigmentation suggested neurofibromatosis, possibly a plexiform neurofibrosarcoma. The low CT number of the mass (−25 H) eliminated a variety of mediastinal masses that may appear cystic on contrast-enhanced CT studies. A thymolipoma was also considered. Steroid-induced mediastinal fat was not a diagnosis that could be supported by the patient's history.

Although Whipple disease is a rare entity, it should be considered in the differential diagnosis of a low-attenuation mediastinal mass because if left untreated, the disease is usually fatal.

REFERENCES

1. Keren DF. Whipple's disease: a review emphasizing immunology and microbiology. *CRC Crit Rev Clin Lab Sci* **1981**;14:75–108
2. Enzinger FM, Helwig EB. Whipple's disease: a review of the literature and report of fifteen patients. *Virchows Arch [A]* **1963**;336:238–269
3. Eyler WR, Doub HP. Extraintestinal roentgen manifestations of intestinal lipodystrophy. *JAMA* **1956**;160:534–536
4. Sieracki JC, Fine G. Whipple's disease: observations on systemic involvement. II. Gross and histologic observations. *Arch Pathol* **1959**;67:81–93
5. Whipple GH. A hitherto undescribed disease characterized anatomically by deposits of fat and fatty acids in the intestinal and mesenteric lymphatic tissues. *Johns Hopkins Med J* **1907**;18:382–391
6. Li DKB, Rennie CS. Abdominal computed tomography in Whipple's disease. *J Comput Assist Tomogr* **1981**;5:249–252
7. Fraser RG, Paré JAP, Paré PD, Fraser RS, Genereux GP. *Diagnosis of diseases of the chest*, 3rd ed. Philadelphia: Saunders, **1989**:872–873
8. Romanul FCA, Radvany J, Rosales RK. Whipple's disease confined to the brain: a case studied clinically and pathologically. *J Neurol Neurosurg Psychiatry* **1977**;40:901–909

Case Report

Bilateral Internal Mammary Artery Aneurysms: A Previously Unreported Cause for an Anterior Mediastinal Mass

John A. Giles,[1] Alan G. Sechtin,[1] Mary M. Waybill,[1,2] and Richard P. Moser, Jr.[1,3]

Although anterior mediastinal masses have many causes, vascular causes are among the most important and must always be excluded. Vascular causes usually include aneurysms of the thoracic aorta, the brachiocephalic arteries, the intercostal arteries or, rarely, of the innominate vein [1–6]. We report a case of a 39-year-old woman with bilateral internal mammary artery aneurysms, an unusual (and, to the best of our knowledge, previously unreported) cause for an anterior mediastinal mass.

Case Report

A 39-year-old woman had cough and hemoptysis of 2 months duration. Her medical history was significant for suspected polyarteritis nodosa and end-stage renal disease, the latter diagnosed histologically 1 year earlier after percutaneous renal biopsy, which showed crescentic glomerulonephritis and extensive glomerulosclerosis. During this earlier workup, chest radiographs were unremarkable. Hemodialysis was begun and, 6 months later, moderate hypertension developed. Posteroanterior and lateral chest radiographs (Figs. 1A and 1B), obtained during the current admission for the assessment of cough and hemoptysis, showed a well-circumscribed, anterior mediastinal mass that had not been apparent on the films obtained approximately 10 months earlier.

Further radiologic evaluation of the anterior mediastinal mass included contrast-enhanced CT, which showed that the mass represented bilateral internal mammary artery aneurysms (Figs. 1C and 1D), with a moderate amount of associated peripheral thrombus. Superior venacavography showed normal bronchocephalic veins. An arch aortogram and selective internal mammary angiograms (Figs. 1E and 1F) clearly showed bilateral fusiform aneurysms of the internal mammary arteries, without evidence of arteriovenous fistula.

On the basis of combined clinical and radiologic findings, the patient underwent thoracotomy and bilateral aneurysmectomy. She made an uneventful postoperative recovery and continues on hemodialysis.

Pathologic examination of the resected internal mammary artery aneurysms revealed thrombus formation overlying an eroded, fibrotic vessel wall. Additional findings included loss of elastic tissue and sparse lymphocytic and eosinophilic infiltrates. Although nonspecific, these features are consistent with a healed vasculitis as may be encountered in polyarteritis nodosa.

Discussion

For unknown reasons, the internal mammary arteries are remarkably resistant to typical (nontraumatic) abnormalities. Previous isolated reports of internal mammary artery diseases include posttraumatic arteriovenous fistulas, mycotic aneurysms, fibromuscular hyperplasia and, rarely, atherosclerotic disease [2–4].

To the best of our knowledge, there have been no previous reports of bilateral internal mammary artery aneurysms or of diseased internal mammary arteries presenting as a mediastinal mass. In this 39-year-old woman, possible preoperative causes for the internal mammary artery aneurysms included trauma, infection, and atheroma, but these were all deemed unlikely in the absence of appropriate history or laboratory or echocardiographic findings.

Although the precise cause of these aneurysms remains unclear, vasculitis is favored because of the underlying renal disease, recent onset of hypertension, abnormal level of antinuclear antibody (1:640), and supportive histologic findings. This case of bilateral internal mammary artery aneurysms represents an unusual and, to the best of our knowledge, previously unreported cause of an anterior mediastinal mass.

Received January 12, 1990; accepted February 2, 1990.

The opinions and assertions contained herein are the private views of the authors and do not reflect the views of the Department of the Army or of the Department of Defense.

[1] Department of Radiology, Penn State University, The Milton S. Hershey Medical Center, Hershey, PA 17033.
[2] Department of Internal Medicine, Penn State University, The Milton S. Hershey Medical Center, Hershey, PA 17033.
[3] Department of Radiologic Pathology, Armed Forces Institute of Pathology, Washington, DC 20306-60000. Address reprint requests to R. P. Moser, Jr.

AJR **154:1189–1190, June 1990** 0361–803X/90/1546–1189

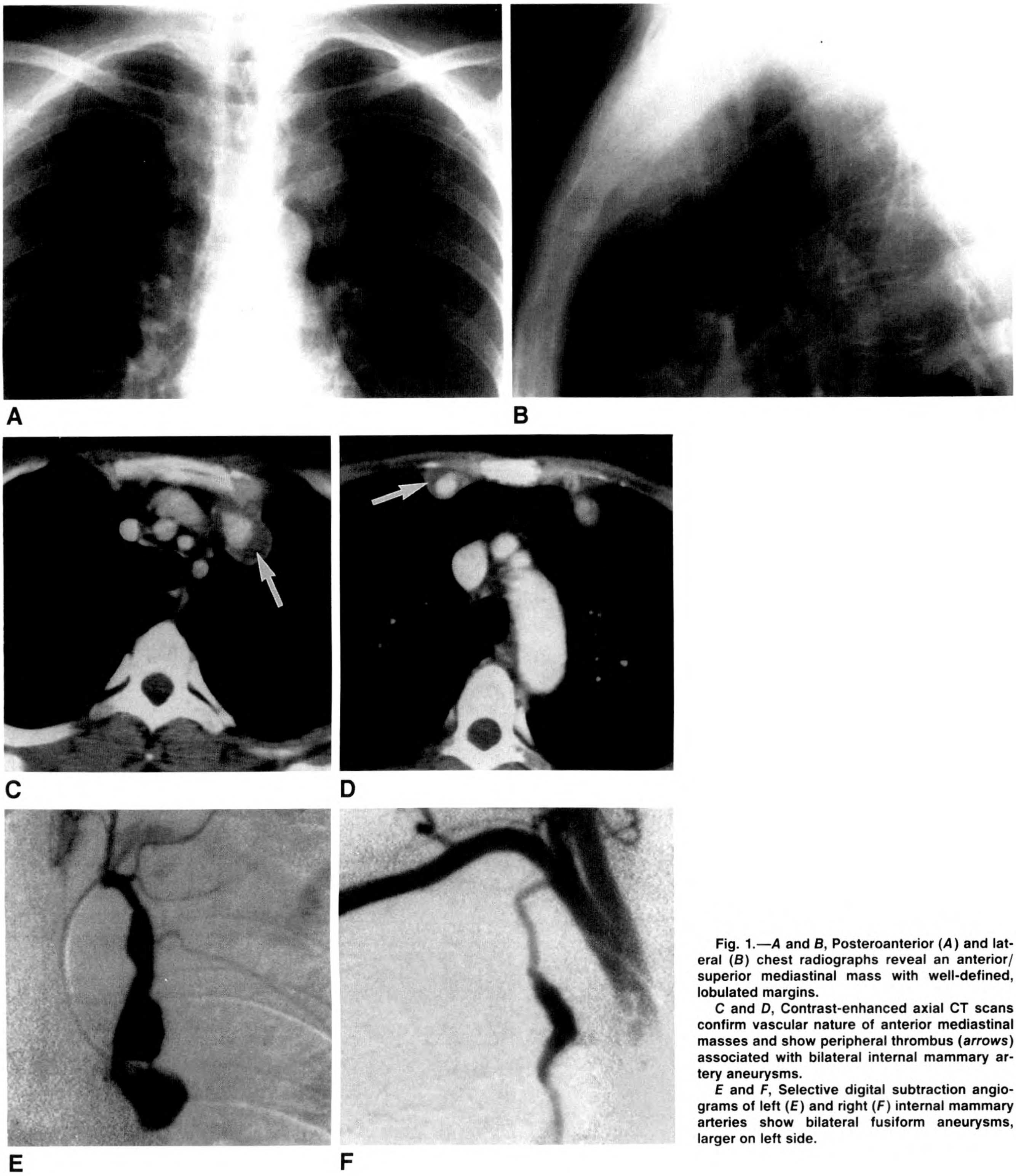

Fig. 1.—*A* and *B*, Posteroanterior (*A*) and lateral (*B*) chest radiographs reveal an anterior/superior mediastinal mass with well-defined, lobulated margins.

C and *D*, Contrast-enhanced axial CT scans confirm vascular nature of anterior mediastinal masses and show peripheral thrombus (*arrows*) associated with bilateral internal mammary artery aneurysms.

E and *F*, Selective digital subtraction angiograms of left (*E*) and right (*F*) internal mammary arteries show bilateral fusiform aneurysms, larger on left side.

REFERENCES

1. Den Otter G, Stam J. Aneurysm of internal mammary artery. *Thorax* **1978**;33:526–557
2. Ishikawa T, Brown GR. Traumatic arteriovenous fistula of the internal mammary artery. *J Trauma* **1977**;17:978–980
3. Sanchez FW, Freeland, PN, Bailey GT, et al. Embolotherapy of a mycotic pseudoaneurysm of the internal mammary artery in chronic granulomatous disease. *Cardiovasc Intervent Radiol* **1985**;8:43–45
4. Shelton ME, Mervyn FB, Virmani R. A comparison of morphologic and angiographic findings in long-term internal mammary artery and saphenous vein bypass grafts. *J Am Coll Cardiol* **1988**;11:297–307
5. Marmolya G, Yagan R. Computed tomographic diagnosis of left innominate vein aneurysm mimicking an anterior mediastinal mass on plain films: a case report. *J Thorac Imaging* **1989**;4:77–78
6. Glassberg RM, Sussman SK. Life-threatening hemorrhage due to percutaneous transthoracic intervention: importance of the internal mammary artery. *AJR* **1990**;150:47–49

Stereotactic Fine-Needle Aspiration for Cytologic Diagnosis of Nonpalpable Breast Lesions

Marianne Löfgren[1]
Ingvar Andersson[1]
Karin Lindholm[2]

Fine-needle aspiration for cytologic diagnosis was performed on 219 nonpalpable breast lesions by using a stereotactic localization technique. Cytologic results were correlated with mammographic findings, and therapeutic decisions were based on the results of both procedures. Representative cytologic material was obtained in 74% of the lesions. Strict criteria of representativeness were observed. If only cases with representative cytologic yield are considered, the sensitivity was 93% and the specificity was 97%. The predictive values were high except for the predictive value of a negative cytologic finding in a spiculated lesion (50%). Sampling errors caused by abundant fibrosis, needle deviation, and difficulty in defining the lesion on the stereoscopic views are discussed. Another source of sampling error may be the mixed nature of some lesions consisting of benign and malignant components.

Fine-needle aspiration of 219 nonpalpable breast lesions by using a stereotactic localization device yielded representative cytologic samples in 74% of the lesions.

***AJR* 154:1191–1195, June 1990**

With the more widespread use of mammography, especially for screening of asymptomatic women, an increasing number of nonpalpable breast lesions will be detected. Accordingly, an additional diagnostic technique for further characterization of such lesions is needed to minimize the number of surgical biopsies and to allow definitive preoperative planning of surgical procedures. We have previously reported our experience with the coordinate grid technique for localization of nonpalpable breast lesions [1]. This report deals with the results of fine-needle aspiration biopsy guided by stereotactic localization.

Material and Methods

From September 1985 to the end of March 1987, 219 lesions in 215 patients were examined by means of stereotactically guided fine-needle aspiration biopsy performed in the radiology department at Malmö General Hospital in Sweden. Seventy-four patients were referred from an ongoing mammographic screening program [2], and 141 patients were referred because of breast symptoms, which usually were unrelated to the lesion being aspirated. Physical findings were either normal or equivocal.

The indications for stereotactically guided fine-needle aspiration were identical with those described in our earlier study [1] on coordinate-grid aspiration biopsies and can be summarized as clustered small calcifications (83 lesions, 38%), tumors with irregular or spiculated borders (39 lesions, 18%), solitary or new tumors with mainly smooth margins (73 lesions, 33%), and asymmetric densities or parenchymal distortion (24 lesions, 11%). The lesions seen on mammograms were put into the following categories: probably benign, suspicious for carcinoma, and definitive carcinoma.

Clusters of five or more small (0.1–1 mm) calcifications of various sizes and forms were considered suspicious for carcinoma. If numerous, and/or in the presence of ductal arrangement or branching pattern, the mammographic diagnosis of carcinoma was made. The size of a cluster was not considered important. Rounded calcifications of relatively uniform size

Received July 17, 1989; accepted after revision December 19, 1989.

[1] Department of Diagnostic Radiology, Malmö General Hospital, University of Lund, S-214 01 Malmö, Sweden. Address reprint requests to M. Löfgren.

[2] Department of Cytology, Malmö General Hospital, University of Lund, S-214 01 Malmö, Sweden.

0361–803X/90/1546–1191
© American Roentgen Ray Society

were considered probably benign. Clearly benign calcifications such as those associated with secretory disease, fibroadenoma, microcystic adenosis, and fat necrosis were not included in the study [3, 4].

Solitary tumors with mainly smooth margins were classified on the basis of whether the entire border or only part of it was well circumscribed. If part of the border was irregular, the degree of irregularity was considered, as was the possibility that the irregularity was caused by superimposition of adjacent normal tissue. Furthermore, high density of a circumscribed tumor was thought to suggest malignancy. Also, the appearance of a tumor since an earlier examination increased the index of suspicion.

A spiculated lesion was classified radiologically as suspicious or definitively malignant depending on how clearly a spiculation could be seen. If no tumor density could be identified in the center of the spiculation, the lesion was classified as architectural distortion. This latter group also included abnormal, nonspecific densities, usually not present on an earlier examination and lacking any characteristics of the other mammographic groups.

The equipment used (Stereotix, General Electric CGR/NRT, Aarhus Denmark) is easily attached to newer or modified versions of mammography units made by the same manufacturer. It consists of a measuring unit and a module with a compression plate, needle holder, and film holder. The compression plate has a rectangular opening 53 × 43 mm. With the patient seated in front of the mammography unit, the breast is compressed moderately with the area of interest under the opening in the compression plate (Fig. 1). The stereotactic technique involves taking two views of the lesion with the X-ray tube angled plus and minus 15°. This gives two different projections of the lesion, making it possible to calculate its x, y, and z coordinates. The position of two reference lines and the positions of the lesion in the two views are fed into a preprogrammed computer that automatically computes the necessary adjustment of the needle holder for a given needle length.

An 80-mm long, 0.8-mm needle (21 gauge) was used for most of the aspirations. In order to avoid needle deviation that might be caused by the bevelled tip, the needle was rotated during insertion. When the appropriate depth was reached, a new pair of films was made to check the position of the needle in relation to the lesion being punctured (Fig. 2). A syringe and a grip were then attached, and the needle was moved up and down within the lesion to improve the yield. Usually three different parts of the lesion were aspirated. Local anesthesia was not used. Most aspirations were carried out with the breast compressed for the craniocaudal projection, although sometimes oblique and lateral approaches were used for lesions in the lower quadrants.

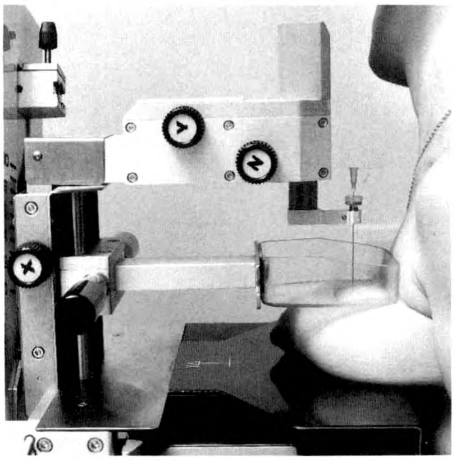

Fig. 1.—Patient positioned for aspiration. Needle holder has been adjusted with knobs (X, Y, Z). An 80-mm needle (outer diameter, 0.8 mm) has been introduced. In this situation, another pair of stereotactic views will be obtained to check needle's position. Then syringe and a handle are attached and aspiration is performed.

The aspirations were performed by the radiologist, and the material was processed immediately by an experienced cytotechnologist who gave a preliminary report on representativeness on ethanol-fixed material stained by a quick hematoxylin-eosin method. On the average, three passes were made (range, one–five). In many cases, the macroscopic appearance of the material (e.g., clear cystic fluid, mucoid or dry necrotic material) gave enough information to judge representativeness. In most cases, both alcohol-fixed and air-dried smears for hematoxylin-eosin and May-Grunwald-Giemsa staining, respectively, were prepared. Cyst fluids were filtered (5-μm filter) and then examined. For this report, the cytologic specimens were reexamined without knowledge of mammographic findings, or of primary or final diagnosis, and classified as follows: 0 = unsatisfactory or insufficient material (this group included specimens with a few normal epithelial cells regarded as a "contamination" from the needle track); 1 = benign lesion (this group was reserved strictly for clearly proliferative and reactive lesions and cysts); 2 = slight atypia without evidence of malignancy (this group of atypia was judged to represent reactive or degenerative changes that were not severe enough to require surgery); 3 = atypia suspicious of malignancy requiring surgical biopsy for definitive diagnosis; 4 = definitive malignancy (this group consisted only of cases in which the cytologic picture was considered clear enough for a recommendation of definitive cancer surgery).

Every case was discussed in a weekly multidisciplinary conference with cytologists, radiologists, surgeons, oncologists, and pathologists. In general, surgical biopsy was recommended for patients with a mammographic grade of 2 (suspicious) unless the aspiration revealed a simple cyst or fibroadenoma. Surgical biopsy also was recommended for all patients who had mammographic grade 3 (definitive carcinoma) lesions, even if cytologic findings indicated benignity. The surgical procedures were planned to be therapeutic as well as diagnostic.

Patients who did not undergo surgical biopsy were followed up with mammography, with a minimal follow-up of 10 months except for patients with simple cysts, who were not followed up. All surgical specimens were radiographed.

Results

A total of 219 lesions were aspirated (Table 1). One hundred three patients had surgical biopsy, and 63 specimens turned out to be carcinoma, 49 invasive and 14 ductal carcinoma in situ. Forty lesions could be dismissed immediately as simple cysts. The remaining 76 were followed up by mammography and physical examination for a median of 21 months (range, 10–40 months) without evidence of malignancy. Only lesions that were classified as benign or with a low suspicion of malignancy in combination with negative cytologic findings were followed up. Thus, clusters containing mainly rounded and relatively uniform calcifications were followed up with mammography, and clusters with more irregular calcifications were recommended for surgical biopsy. Accordingly, circumscribed tumors with well-defined borders all around and low density relative to the parenchyma were followed up if cytologic findings were negative whereas those with partly irregular borders or higher density were recommended for surgical

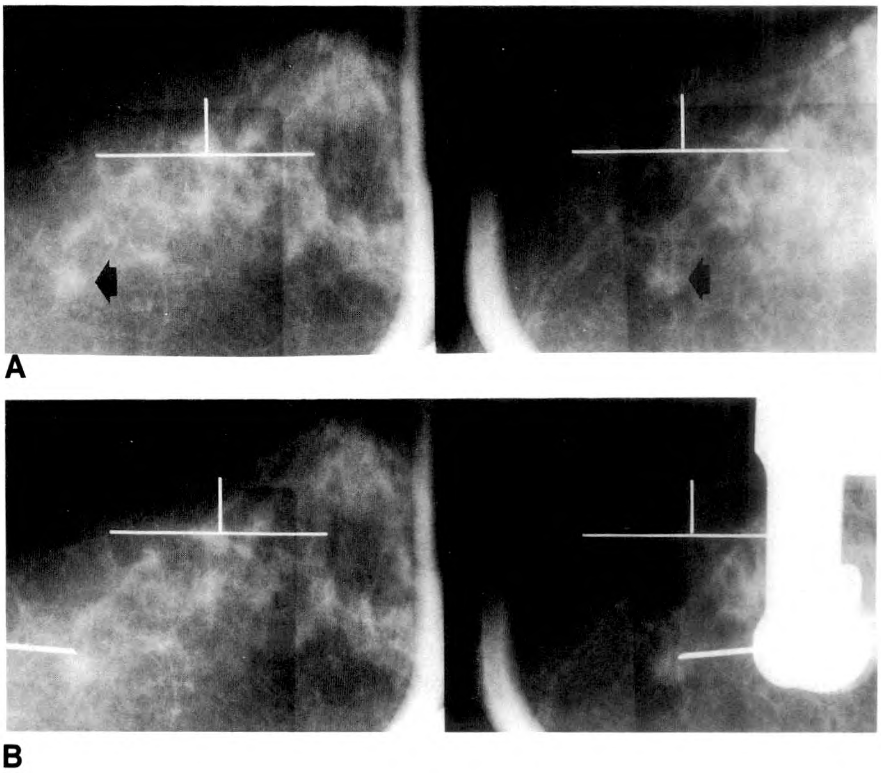

Fig. 2.—Mammograms show two stereotactic pairs of views. Cytologic diagnosis was carcinoma, which was confirmed on microscopic examination of surgically resected specimen.

***A*, 4-mm tumor (*arrow*) is visible in aperture of compression plate.**

***B*, Images obtained to check position of needle.**

TABLE 1: Findings and Procedures by Mammographic Type of Abnormality in 219 Aspirated Nonpalpable Breast Lesions

Mammographic Abnormality	No. of Lesions	Simple Cyst at Aspiration	Follow-up Mammogram	Surgical Biopsy	Histopathologic Type	
					Benign	Malignant
Microcalcifications	83	0	34	49	33	16
Spiculated tumor	39	0	1	38	2	36
Circumscribed tumor	73	40	23	10	4	6
Abnormal density or distortion	24	0	18	6	1	5
Total	219	40	76	103	40	63

biopsy. The median size of these lesions was 7 mm (range, 5–24 mm). Spiculated lesions were recommended for surgical biopsy except in one patient in whom a mastitis was diagnosed clinically. The lesion disappeared on treatment with antibiotics. Abnormal densities or distortion were followed up if the index of mammographic suspicion was low and in the presence of clearly benign cytology.

Out of 40 biopsies with benign histopathologic findings, all but eight were suspicious mammographically. Two of these eight patients wanted their lesions removed despite benign cytologic findings; another lesion was diagnosed at autopsy (nonrepresentative cytology). These three lesions were fibroadenomas. The remaining five (one with insufficient cytology, three benign, one slight atypia) were operated on after a recommendation in the breast conference. Among the 40 lesions, three were suspicious for malignancy cytologically, eight showed slight atypia, 17 were clearly benign, and 12 smears were insufficient.

The most common mammographic abnormalities were microcalcifications and circumscribed tumors; they accounted for 38% and 33% of the total number of lesions. More than half of the circumscribed tumors were simple cysts; only 8%

TABLE 2: Mammographic Grading of Malignancy by Different Mammographic Abnormalities in 219 Aspirated Nonpalpable Breast Lesions

Mammographic Abnormality	Probably Benign	Suggestive of Malignancy	Definitive Carcinoma	Total
Microcalcifications	15	67 (15)	1 (1)	83 (16)
Spiculated tumor	0	24 (21)	15 (15)	39 (36)
Circumscribed tumor	60 (1)	13 (5)	0	73 (6)
Abnormal density or architectural distortion	8 (1)	16 (4)	0	24 (5)

Note.—Figures in parentheses are numbers of carcinomas found at surgery.

TABLE 3: Cytologic Classification by Mammographic Abnormality in 219 Aspirated Nonpalpable Breast Lesions

Cytologic Classification	Microcalcification	Spiculated Tumor	Circumscribed Tumor	Abnormal Density or Distortion	Total
Not representative material	24 (1)	3 (2)	17	12 (1)	56 (4)
Benign lesion	33	0	48	6	87
Slight atypia	10 (2)	4 (2)	2	2	18 (4)
Severe atypia	5 (2)	3 (3)	1 (1)	2 (2)	11 (8)
Definitive malignancy	11 (11)	29 (29)	5 (5)	2 (2)	47 (47)
Total	83 (16)	39 (36)	73 (6)	24 (5)	219 (63)

Note.—Figures in parentheses are numbers of carcinomas found at surgery.

represented carcinoma, unlike the spiculated tumors, of which 92% represented carcinoma. Surgical biopsy was performed on a larger proportion of spiculated tumors and microcalcifications (97% and 59%, respectively) than on circumscribed tumors and parenchymal distortion (30% and 25%, respectively, cysts excluded). The reason for this was a higher grading of findings suggestive of malignancy for spiculated tumors and microcalcifications (Table 2).

Satisfactory material was obtained in 74% of all aspirations (Tables 3 and 4). A definitive diagnosis of carcinoma was made in 47 (75%) of 63 patients with histologically proved cancer. If cases of severe atypia are included, either a definitive or probable carcinoma was diagnosed cytologically in 87% of the cancers demonstrated during subsequent surgery. The group with severe atypia contained three benign lesions (false-positives). However, no false-positive diagnosis of carcinoma occurred in cytologic group 4.

In the group classified as slight atypia, four of the aspirated specimens were falsely diagnosed as benign (false-negatives). Another four breast cancers were found among patients with aspirated material classified as insufficient.

In comparison with the primary cytologic diagnosis, 10 more specimens were classified as insufficient on review; all were nonmalignant on follow-up. Some of these cases actually were cysts. However, information on aspiration of a small amount of cystic fluid was not available at the review. Among the infiltrating carcinomas, five were classified as definitely malignant on review, whereas the primary cytologic classification was "suspicious for carcinoma."

The overall sensitivity and specificity of the biopsies were high (Table 5). The data were calculated on the basis of cases with sufficient cytologic material. The predictive value of a negative finding on aspiration cytology was low (50%) for spiculated lesions. The positive predictive value of cytology was lower for microcalcifications than for other types of lesions. The three false-positive aspirates were sclerosing adenosis, duct ectasia with nonspecific inflammation, and intraductal epithelial proliferations. These aspirates all showed relatively severe atypia.

The positive predictive value of the combined mammographic and cytologic procedures can be calculated from Table 1. If the recommendation of surgical biopsy is taken as an expression of the combined positive diagnoses (all recommended biopsies were performed). The positive predictive value was lowest for microcalcifications (16/49, 33%) and highest for spiculated tumors (36/38, 95%).

Frozen sections were examined in only one patient. In 44 malignant lesions, the primary surgery also was the definitive therapeutic surgery. Eighteen lesions needed supplementary surgery, 12 because of nonconclusive preoperative cytologic findings and six because tumor was found at the margins of the resected tissue or because of the unexpected finding of invasive carcinoma in addition to a primarily suspected noninvasive malignant neoplasm. In the latter cases, the primary procedure had to be supplemented with axillary biopsy. No patient was overtreated (according to our treatment protocol) because of the bimodal preoperative radiologic-cytologic diagnosis.

Discussion

There are basically two different techniques for localizing nonpalpable breast lesions under radiologic guidance. The two-dimensional coordinate-grid technique has been described by Mühlow [5] and Novak [6]. We recently published our results with the coordinate-grid technique [1].

The three-dimensional stereotactic technique was described by Nordenström [7], who designed a unit completely dedicated to stereotactic localization of breast lesions. Good results have been reported for this instrument [8, 9]. The stereotactic device used in the current series is a smaller instrument that can be attached to the regular mammography machine in less than a minute.

The main problem with the two-dimensional technique is that it does not give the depth of the lesion. This problem is overcome by the stereotactic technique. Accordingly, lesions seen in only one projection can be localized.

It may be difficult to define exactly corresponding points on the two stereotactic images. Small lesions, including cancers, often vary in appearance because of the superimposition of normal breast tissue or the irregular form of the lesion [10]. This may result in false values of one or more of the coordinates.

TABLE 4: Cytologic Classification by Mammographic Grading in 219 Aspirated Nonpalpable Lesions

Cytologic Classification	Mammographic Classification			
	Probably Benign	Suggestive of Malignancy	Definitive Carcinoma	Total
Not representative material	24 (1)	32 (3)	0	56 (4)
Benign lesion	54	33	0	87
Slight atypia	4	14 (4)	0	18 (4)
Severe atypia	1 (1)	10 (7)	0	11 (8)
Definitive malignancy	0	31 (31)	16 (16)	47 (47)

Note.—Figures in parentheses are numbers of carcinomas found at surgery.

TABLE 5: Stereotactic Fine-Needle Aspiration Biopsy: Cytologic Accuracy Calculated from 163 Lesions with Satisfactory Yields

Mammographic Abnormality	Sensitivity (%)	Specificity (%)	Positive Predictive Value	Negative Predictive Value
Microcalcifications	87	93	81	95
Spiculated tumor	94	100	100	50
Circumscribed tumor	100	100	100	100
Abnormal density or distortion	100	100	100	100
All abnormalities	93	97	95	96

Note.—A cytologic grade of 1 or 2 was considered negative, whereas a grading of 3 or 4 was considered positive for malignancy. The 163 cases represent 74% of all lesions in this series.

Needle deviation is another source of error. Relatively long needles (usually 80 mm) are used. Because of the bevelling of the tip, the needle may deviate from an accurate course. This problem can be reduced by rotating the needle while inserting it. This is also important for minimizing the risk of pushing the lesion aside or in front of the needle.

Other factors may influence the probability of getting representative material. A needle with a stylet has been suggested as a means of reducing the risk of contamination when the needle is passed through the tissue above the lesion. This may be true when passing through several organs on the way to the target or if thicker needles are used. We do not think that this is a significant problem in breast aspiration. Abundant reactive fibrosis reduces the chance of getting representative material in a breast lesion. Highly cellular cancers give a better yield in general than cancers of the scirrhous type, which was reflected in the predictive value of a negative aspirate of circumscribed and spiculated tumors, respectively. A potential pitfall [1] is the complex structure of many breast lesions that have benign, atypical, as well as malignant proliferation.

Finally, the number of aspirations, the histologic sampling procedure, the complex breast pathologic changes, and the subjectivity of the histologic diagnosis of some borderline breast lesions may influence the apparent accuracy of the cytologic diagnosis.

Compared with the coordinate-grid technique, stereotactic fine-needle aspiration provided representative cytologic material in a significantly higher proportion of the cases, 64% and 74%, respectively (χ^2 $p = .02$). Also, the proportion of smears providing either a definite or suspicious diagnosis of cancer was greater when this technique was used.

The greatest advantage of fine-needle aspiration biopsy is that various therapeutic options can be discussed with the patient preoperatively. Cancer surgery can be performed in one stage rather than two stages in most patients (44 of 63 malignant lesions in this series). Axillary biopsy is not performed routinely for ductal noninvasive carcinoma according to the treatment protocol at this hospital. The mammographic and cytologic appearance of ductal noninvasive carcinoma is often characteristic, but the extension of the ductal noninvasive carcinoma in the breast and the coexistence of invasive cancer are more difficult to evaluate. This is reflected in the need for supplementary surgery in six of 63 malignant lesions.

Finally, the number of surgical biopsies for benign disease can be reduced by the use of aspiration cytology. In our study, 33 mammographically suspicious lesions were clearly benign cytologically (Table 4). In such cases surgical biopsy often can be averted. Also, in the group classified as probably benign mammographically, clearly benign cytologic findings provided further support of expectations in 54 cases. A large proportion of lesions in this group (34) were simple cysts. From a mammographic point of view, however, many of the lesions classified as probably benign were borderline. Practices in recommendations for surgical biopsy may vary among countries, and it is not certain that all lesions subjected to fine-needle aspirations in the current series would have been recommended for surgical biopsy in the United States. Also, our current practice does not routinely include sonography in the evaluation of breast lesions. Clearly, sonography could have differentiated most of the cysts from solid lesions. However, we believe that cytology contributes to appropriate treatment of patients and results in less unnecessary surgery, follow-up, and anxiety.

For these principles to be valid, the cytologist and the radiologist must be fairly experienced. Decisions on treatment of patients must be based on the combined information from cytology and mammography, preferably in multidisciplinary conferences.

REFERENCES

1. Löfgren M, Andersson I, Bondeson L, Lindholm K. X-ray guided fine-needle aspiration for the cytologic diagnosis of nonpalpable breast lesions. *Cancer* **1988**;61:1032–1037
2. Andersson I, Aspegren K, Janzon L, et al. Mammographic screening and mortality from breast cancer: the Malmö mammographic screening trial. *Br Med J* **1988**;297:943–948
3. Sigfusson B, Andersson I, Aspegren K, et al. Clustered breast calcifications. *Acta Radiol [Diagn]* (Stockh) **1983**;24:273–281
4. Sickles E. Breast calcifications: mammographic evaluation. *Radiology* **1986**;160:289–293
5. Mühlow A. A device for precision needle biopsy of the breast at mammography. *AJR* **1974**;121:843–845
6. Novak R. A method for control of the target at aspiration biopsy of nonpalpable breast lesions. *Acta Radiol [Diagn]* (Stockh) **1986**;27:65–70
7. Nordenström B. Stereotaxic screw needle biopsy of nonpalpable breast lesions. In: Logan W, ed. *Breast carcinoma: the radiologist's expanded role.* New York: Wiley, **1977**:313–318
8. Svane G, Silfverswärd C. Stereotaxic needle biopsy of non-palpable breast lesions: cytologic and histopathologic findings. *Acta Radiol [Diagn]* (Stockh) **1983**;24:283–288
9. Dowlatshahi K, Gent HJ, Schmidt R, Jokich PM, Bibbo M, Sprenger E. Nonpalpable breast tumors: diagnosis with stereotaxic localization and fine-needle aspiration. *Radiology* **1989**;170:427–433
10. Sickles EA. Mammographic features of 300 consecutive nonpalpable breast cancers. *AJR* **1986**;146:661–663

The reader's attention is directed to the commentary on this article, which appears on the following pages.

Commentary

Stereotactic Fine-Needle Aspiration Biopsy for Nonpalpable Breast Lesions

Valerie P. Jackson[1] and Lawrence W. Bassett[2]

Dr. Löfgren and associates have reported their experience with fine-needle aspiration biopsy of 219 nonpalpable breast lesions by using a stereotactic device to guide needle placement [1]. This is an exciting technology that could reduce the number of unnecessary excisional breast biopsies. Good results also have been reported in other studies [2-4], mostly performed in Europe. Although it is tempting to immediately adapt this technology for widespread clinical practice, we must proceed cautiously because this manuscript originating in Europe may not be applicable to the United States. Satisfactory results with stereotactically guided fine-needle aspiration biopsy have yet to be verified in the United States, where case selection and medical practice are different. In addition, this method has not been tested in our medicolegal arena, which, for better or worse, influences the practice of medicine in this country.

Several manufacturers of mammography equipment are marketing stereotactic devices. Each of these devices has its own strengths and weaknesses. The costs range from $35,000 for systems that attach to existing mammography units, to more than $120,000 for free-standing equipment designed specifically for stereotactic needle placement. Thus, a sufficiently large number of nonpalpable breast lesions must be detected mammographically to justify its purchase. Most of the stereotactic devices provide accurate guidance for fine-needle aspiration biopsy when properly installed, calibrated, and used. However, stereotactic systems for mammography are in a relatively early stage of development, and mammographers have had significant problems with them.

To date, the only proved role for stereotactic mammography devices is for fine-needle aspiration biopsy. They have occasionally been used to guide pneumocystography of nonpalpable cysts (a procedure not widely used in the United States) and to localize suspicious lesions seen in only one mammographic view. Use of a stereotactic system for improving routine preoperative needle localization has been reported once [5]. However, when compared with the use of fenestrated compression plates for preoperative needle localization, the stereotactic devices generally require more time and a larger radiation dose. In addition, stereotactic hookwire placement is sometimes unreliable. This is because, until recently, most stereotactic systems did not allow repositioning of the breast for biplane confirmation of needle placement before removal of the needle. Thus, the wire was placed without the benefit of adjusting its depth on an orthogonal view. With stereotactic placement from a single plane, the wire and lesion may move apart on the release of breast compression, leaving the hook of the wire too deep (suboptimal) or too superficial (unacceptable). When using a biplane method (fenestrated compression plate or even freehand technique), the relationship of the needle and lesion can be evaluated from two directions before the wire is loaded through the needle.

It is difficult to evaluate and compare the data from many of the reports on stereotactic fine-needle aspiration biopsy because study designs, techniques, and case selection differ significantly. Although Löfgren et al. [1] do elaborate on the mammographic features of the lesions in their series, other

---

This article is a commentary on the preceding article by Löfgren et al.

This work was supported in part by grant #R01 CA48004-01A1 of the National Cancer Institute of the National Institutes of Health.

[1] Department of Radiology, Indiana University School of Medicine, Wishard Memorial Hospital, 1001 W. 10th St., Indianapolis, IN 46202. Address reprint requests to V. P. Jackson.

[2] Iris Cantor Center for Breast Imaging, University of California, Los Angeles, School of Medicine, Los Angeles, CA 90024-1721.

AJR 154:1196-1197, June 1990 0361-803X/90/1546-1196 © American Roentgen Ray Society

investigators do not. Many reports, including that by Löfgren et al. [1], include many cysts among the nonpalpable lesions. The inclusion of cysts, which are readily diagnosed by aspiration, exaggerates the sensitivity and specificity of fine-needle aspiration biopsy because in the United States most cysts would be diagnosed by sonography alone and thus would not be selected for fine-needle aspiration biopsy.

The categorization of data on fine-needle aspiration biopsy has been inconsistent in published reports. For example, cases with insufficient fine-needle aspiration biopsy specimens have been distributed among normal, negative, and positive categories in different studies. Similar inconsistencies are encountered with "atypical" or "suspicious" lesions, those not clearly benign or malignant by cytology. However, only some of these suspicious lesions will turn out to be malignant at excisional biopsy. If such lesions are included in the positive category, the false-positive rate is increased. Conversely, if they are listed as "negative," the false-negative rate is increased.

It is imperative that investigators report their data more clearly so that radiologists can make well-informed judgments of the usefulness of fine-needle aspiration biopsy in their practices. Optimally, standard nomenclature and methodology should be adopted so that data from different sources can be pooled to clarify rather than confuse this issue.

Is a stereotactic system essential for fine-needle aspiration biopsy of nonpalpable breast lesions? Two reports showed good results with a coordinate-grid fenestrated compression plate to guide fine-needle aspiration biopsy [6, 7]. The disadvantage of using a modified compression plate is less precise needle guidance, increasing the possibility of missing the lesion. Using a fenestrated compression plate, Löfgren et al. [6] reported a 36% insufficient specimen rate, identical to the rate reported by Hann et al. [7] with the same method of guidance. Using the stereotactic system, Löfgren et al. [1] reported an insufficient specimen rate of only 26%, and most other investigators report insufficiency rates of less than 25% for this method [2–4]. Does this small, yet statistically significant, difference in the yield of diagnostic specimens justify the purchase of a stereotactic system? The answer to this question depends on the number of procedures performed and how an insufficient specimen result is handled. A failed fine-needle aspiration biopsy might be followed by another attempt at fine-needle aspiration or by excisional biopsy. For many of us who are not skilled at fine-needle aspiration biopsy with fenestrated compression plates, the improved precision of stereotactic guidance could be a welcome luxury or even an essential ingredient for fine-needle aspiration biopsy of nonpalpable lesions.

We cannot overemphasize the benefits of the team approach used by Löfgren et al. Their successful stereotactic fine-needle aspiration biopsy program uses a compulsive mammographer, a pathologist experienced in breast cytology, and a supportive surgeon who works closely with the radiologist and pathologist. However, many breast surgeons in the United States remain skeptical about the role of fine-needle aspiration biopsy in their practices. They argue that if cytologic findings are positive, they must still remove the lesion, and if cytologic findings are not definitely benign (e.g., fibroadenoma or lymph node), or there is a possibility that the lesion has been missed, excisional biopsy is still performed. Undoubtedly, results will improve when decisions are based on joint input from the mammographer, the cytopathologist, and the surgeon. Unfortunately, this is not the way cases are usually managed in the United States, where the approach is frequently disjointed. In such a setting, fine-needle aspiration biopsy for nonpalpable breast lesions is unlikely to fulfill its potential.

Stereotactic fine-needle aspiration biopsy should not be used as just another step in a costly "multimodality" workup. Optimally, it should make a useful and cost-effective contribution to the management of nonpalpable breast lesions. It can decrease the need for excisional biopsies by identifying (1) definite benign lesions that do not require excisional biopsy and (2) definite malignant lesions that will necessitate only one operation (for treatment), instead of two operations (one for diagnosis and one for treatment). Another potential benefit is the immediate determination of the nature of equivocal mammographic findings, eliminating the need for anxiety-provoking 4- to 6-month follow-up mammograms. By increasing the specificity of mammographic workups, we can improve our own image with referring physicians who have come to believe that our indecisions outnumber our decisions.

Despite the need for further refinements of stereotactic instruments and the paucity of data from the United States, we should not underestimate the impact that this technology could have on mammography. The large number of unnecessary biopsies that result from false-positive and equivocal mammograms is a major deterrent to referring physicians for recommending screening mammography. Hopefully, mammographically guided fine-needle aspiration biopsy will reduce the number of unnecessary surgical biopsies, and thus we believe that this method will become increasingly important in the management of nonpalpable breast lesions. However, we caution readers to critically evaluate published studies in relation to their own setting, and, as suggested by Kopans [8], perform their own pilot studies before implementing this technology in their clinical practice. Stereotactic fine-needle aspiration biopsy is best suited to high-volume practices where many biopsies are performed and where experienced mammographers, cytopathologists, and breast surgeons use a team approach to manage each case.

REFERENCES

1. Löfgren M, Andersson I, Lindholm K. Stereotactic fine-needle aspiration for cytologic diagnosis of nonpalpable breast lesions. *AJR* **1990**; 154:1191–1195
2. Ciatto S, Del Turco MR, Bravetti P. Nonpalpable breast lesions: stereotaxic fine-needle aspiration cytology. *Radiology* **1989**;173:57–59
3. Dowlatshahi K, Gent HJ, Schmidt R, Jokich PM, Bibbo M, Sprenger E. Nonpalpable breast tumors: diagnosis with stereotaxic localization and fine-needle aspiration. *Radiology* **1988**;170:427–433
4. Azavedo E, Svane G, Auer G. Stereotactic fine-needle biopsy in 2594 mammographically detected non-palpable lesions. *Lancet* **1989**;1:1033–1036
5. Merritt CRB, Bergeron RB, Sullivan MA, et al. Stereotactic guidance for breast biopsy localization and aspiration. *Radiology* **1989**;173(P):457
6. Löfgren M, Andersson I, Bondeson L, Lindholm K. X-ray guided fine-needle aspiration for the cytologic diagnosis of nonpalpable breast lesions. *Cancer* **1988**;61:1032–1037
7. Hann L, Ducatman BS, Want HH, Fein V, McIntire JM. Nonpalpable breast lesions: evaluation by means of fine-needle aspiration cytology. *Radiology* **1989**;171:373–376
8. Kopans DB. Fine-needle aspiration of clinically occult breast lesions. *Radiology* **1989**;170:313–314

Book Review

Gastrointestinal Radiology. A Pattern Approach, 2nd ed. By Ronald L. Eisenberg. Philadelphia: Lippincott, 1053 pp., 1990. $125

As stated by the author in the preface, this book attempts to combine the best features of a list of gamuts with an extensive disease-oriented textbook. This combination of the two approaches is most successful. The text is well organized and concise in spite of its almost encyclopedic proportions.

The book is divided into nine chapters (called parts): "Esophagus," "Diaphragm," "Stomach," "Duodenum," "Small Bowel," "Ileocecal Valve and Cecum," "Colon," "Biliary System," and "Miscellaneous." Each part is subdivided into a number of sections, each of which describes a specific radiologic pattern or gamut. The organization is the same as that of the first edition, which was published in 1983. I would have enjoyed seeing chapters on the liver, pancreas, and spleen in view of the newer techniques that have become widely applied in gastrointestinal radiology, but the author has maintained his focus on the hollow viscera and the use of barium studies. The addition of CT scans and occasionally sonograms and nuclear medicine studies has enhanced presentation of the disease processes that are covered in this book. For a full understanding of their impact, however, another textbook, such as *Computed Tomography of the Gastrointestinal Tract,* by Megibow and Balthazar, should be consulted.

Although the number of pages has been increased only slightly compared with the previous edition, the size of the page has been expanded, and this volume is a full pound heavier. Although not every entity in the differential diagnosis introducing each section is illustrated subsequently, the text has been enriched by new entities and radiographs—often from cases published since 1983—and a few illustrations from the previous edition have been eliminated. Occasionally, radiographs from the previous edition have been replaced by better examples, usually from a technically superior study. Illustrations of similar radiologic findings have been juxtaposed, whereas they were scattered throughout the text in the first edition. The bibliography has been updated with references through 1987. Only in a couple of chapters have the references been arranged by topics; otherwise they are arranged alphabetically and not cited in the text. This approach poses no problem in the shorter sections, but it can be somewhat difficult for readers to follow up a point made in the text if they must look through more than 40 listings at the end of a longer section.

Repetition in a book of this nature is unavoidable because many entities manifest themselves with different patterns in different organs (more than 20 patterns for a rare condition like amyloidosis). Such repetition is of no concern to the reader who is looking up a particular pattern, and it does reinforce information for the novice, who may read the book cover to cover. The text is well written, well organized, comprehensive yet concise, and profusely illustrated with good-quality radiographs. All of the relevant information about radiologic manifestations of disease is discussed, and frequently the author explains the pathophysiologic basis of the condition with elaboration of its clinical features when pertinent.

I recommend this text without reservation for every radiology resident and practicing radiologist or gastroenterologist who performs gastrointestinal fluoroscopic procedures. This book has become the bible of gastrointestinal radiology for senior residents studying for the oral examination of the American Board of Radiology, which, correctly or not, is perceived by them to emphasize the differential diagnosis of radiologic patterns. I further recommend this new edition for purchase as part of the core collection of every radiology departmental library as one of the most practical books in the radiologic literature.

Herbert F. Gramm
New England Deaconess Hospital
Harvard Medical School
Boston, MA 02215

The Value of Sonography in the Diagnosis of Acute Diverticulitis of the Colon

Stephanie R. Wilson[1]
Ants Toi

To assess the value of sonography as the initial imaging procedure in patients suspected of having acute diverticulitis of the colon, we evaluated the sonograms of 71 patients who had clinical signs and symptoms of the disease. Identification of diverticula on sonograms was taken as evidence of acute diverticulitis. Fifty-four patients had sonographic findings consistent with this diagnosis. These included gut wall thickening (53), diverticula (34), pericolic (21) and intramural (two) fluid collections, edema of the pericolic fat (22), and intramural sinus tract (one). The final diagnosis was based on the clinical impression (all cases); pathologic interpretation of a surgical specimen (33 cases); findings on contrast enema (40 cases), CT scan (14 cases), and colonoscopy (18 cases); and a favorable clinical outcome in the absence of therapy (17 cases). Forty-six of the 54 patients with positive sonograms had acute diverticulitis, six had pericolic inflammatory masses caused by other colonic diseases, and two had surgically confirmed diverticulosis without active inflammation. All 17 patients with normal sonograms were treated conservatively. Diverticulitis was not confirmed in any of these patients.

Our study suggests that sonography is a valuable imaging technique in the patient with signs and symptoms of acute diverticulitis.

***AJR* 154:1199–1202, June 1990**

The role of imaging in the evaluation of patients with suspected acute diverticulitis is twofold. First, those patients with acute diverticulitis must be distinguished from those in whom other diseases account for their symptoms. Second, patients with mild diverticulitis limited to the colon must be distinguished from those in whom pericolic extension might necessitate surgery or percutaneous intervention. We studied the usefulness of sonography as the initial imaging technique for these purposes in 71 patients suspected of having the disease.

Materials and Methods

From January 1987 to August 1988, all patients with a working diagnosis of acute diverticulitis who were referred for sonography as the initial imaging procedure were included in the study. Patients were referred from the emergency department (46 cases), from the inpatient wards (11 cases), and from private physicians (14 cases). The charts of these patients were reviewed and the following information was noted: patient characteristics; presenting signs and symptoms; sonographic findings; CT, contrast enema, and colonoscopic findings, when performed; and the final diagnosis.

The ultimate diagnosis in the patients was based on the clinical impression (all cases); pathologic reports of surgical specimens (33 cases); and findings on CT scans (14 cases), contrast enemas (40 cases), and colonoscopies (18 cases).

Seventy-one patients were seen during the study period. There were 38 men and 33 women 16–78 years old (mean, 52). Sixty-two patients had at least two of the following: left lower quadrant pain, fever, and elevated WBC count. Six patients had left lower quadrant pain alone, six a change in bowel habit, and two urinary tract symptoms. The final diagnosis

Received November 2, 1989; accepted after revision January 22, 1990.

[1] Both authors: Department of Radiology, Division of Ultrasound, Toronto General Hospital and University of Toronto, 200 Elizabeth St., Toronto, Ontario, Canada M5G 2C4. Address reprint requests to S. R. Wilson.

0361–803X/90/1546–1199

© American Roentgen Ray Society

in our 71 patients was acute diverticulitis in 46 patients, probable diverticulosis with spasm in 19, and other diseases in six: carcinoma of the sigmoid colon with perforation and abscess (two patients); ischemic gangrene of the left colon with abscess (one); pericolonic, cryptogenic abscess (one); Crohn colitis with abscess (one); and *Salmonella* gastroenteritis with thickening of the bowel and free intraperitoneal fluid (one).

In addition, all charts of patients with a discharge diagnosis of acute diverticulitis during our study period were obtained to determine any utilization or patient selection bias. For example, were only mild cases of diverticulitis referred for sonography? Review of these charts indicated there were at least 12 additional patients who were admitted to our hospital in whom sonography was not performed as the initial imaging procedure. None of these patients required surgery or percutaneous intervention.

All sonograms were obtained with 3.5- and 5-MHz sector or convex linear transducers on commercially available equipment (Siemens Sono 2, Erlangen, West Germany, or Aloka 630 or 650, Tokyo, Japan). Routine thorough scanning of the abdomen and pelvis was performed along with compression sonography of abnormal gut by using a modification of the technique described by Puylaert [1]. Abnormal bowel was specifically sought in all patients in view of the clinical suspicion of acute diverticulitis. Scans were obtained by a qualified ultrasound technologist and reviewed by a physician. The examination routinely required at least 30 min.

Sonographic diagnosis of diverticulitis was made if two of the following were present: focal gut-wall thickening, inflamed diverticula, inflammatory changes in the pericolic fat, intramural or pericolic inflammatory mass, and intramural fistulas. The segment of bowel involved was determined by its anatomic position and morphology. The most lateral loop of gut running lengthwise in the right and left flanks was typical of the ascending and descending colon, respectively. An oblique loop of gut in the left lower quadrant above the bladder dome in continuity with the descending colon and the rectum was interpreted as the sigmoid colon. Haustral pattern and valvulae conniventes suggested large and small bowel, respectively. Bowel-wall thickness greater than 4 mm was considered abnormal. Echogenic shadowing foci seen in outpouches of the thickened colon wall or beyond in the pericolonic soft tissues were interpreted as inflamed diverticula. Poorly defined zones of hypoechogenicity in the pericolic fat were interpreted as evidence of inflammatory extension to the fat. As these areas became more sharply defined, our interpretation was inflammatory mass. The presence of fluid or air in the mass was interpreted as evidence of abscess formation. Linear echogenic foci, frequently with a "ring-down artifact," within the gut wall but outside of the gut lumen were considered intramural fistulas. All sonograms were interpreted at the time of the procedure, with knowledge of the clinical indication for the study. CT was recommended after sonography if we were not confident about the character or extent of an identified pericolic inflammatory mass.

Contrast enemas were performed with either diatrizoate sodium (Hypaque, Winthrop, Aurora, Ontario) or barium at the discretion of the radiologist. A diagnosis of diverticulitis required the demonstration of at least two of the following: localized extravasation of contrast material, marked and distorted colonic fold thickening, localized mass effect, and mucosal tethering. Contrast enemas were not necessarily interpreted without prior knowledge of the results of sonography.

Of the 65 patients with diverticular disease, 40 had contrast enemas. Thirty-eight of the 40 had acute diverticulitis; the results of the contrast enema supported this diagnosis in 30 examinations. Smooth-muscle hypertrophy was diagnosed in four and severe spasm in two; the other two studies were indeterminate owing to total obstruction of the flow of barium. In two patients with true-negative sonograms, contrast enemas performed electively 10 and 14 days later revealed sigmoid diverticula with no evidence of inflammation.

The CT technique was not standardized in this retrospective study. CT scans were interpreted as consistent with diverticulitis when bowel-wall thickening equal to or greater than 4 mm, diverticula, and mesenteric or fascial soft-tissue stranding were present. The scans were interpreted as diagnostic of diverticulitis if abnormal, adjacent, pericolic fluid or gas collections suggesting abscess were found. CT scans were not necessarily interpreted without prior knowledge of the results of the sonographic examination or the contrast enema.

CT scans were obtained in eight patients who had true-positive sonograms; all sonograms suggested pericolic inflammatory mass or abscess. In seven, the scans suggested diverticulitis with significant extraluminal disease; in the eighth patient, the CT scan showed evidence of gut-wall thickening and diverticula. A small undetected abscess was found at surgery, performed 2 days later. An additional two patients with acute diverticulitis had CT confirmation of thick gut wall and diverticula.

CT scans in four of six patients with colonic pathologic changes other than diverticular disease were all abnormal. They showed thick gut with pericolic inflammatory masses. No diverticula were shown. Interpretation included acute diverticulitis in the differential diagnosis, but it was not the preferred diagnosis in any case.

Eighteen patients underwent colonoscopy, all with a final diagnosis of diverticulitis. Seven had diverticula, 12 had severe spasm, two showed evidence of diverticulitis, and one revealed no abnormality.

Thirty-three patients in our study group had surgical resection. Twenty-six of the 46 patients with a final diagnosis of acute diverticulitis underwent surgery 1–31 days after the initial diagnosis. In all 26, the surgical specimen confirmed the preoperative diagnosis. In two additional patients, with a preoperative diagnosis of acute diverticulitis, smooth-muscle hypertrophy and diverticula were found at surgery, but no active inflammation was present in the surgical specimen. In five patients with false-positive sonograms who underwent surgical resection, gut-wall thickening and a pericolic inflammatory mass were found, but there was no evidence of diverticulitis.

Results

Sonographic abnormalities in the patients with acute diverticulitis were localized to the left colon or sigmoid in 44 of the 46 patients and to the right colon in the other two. Thickening of the gut wall was seen in 45 patients (Fig. 1), and 32 had diverticula that were also occasionally thick-walled (Figs. 2 and 3). Changes in the pericolic fat were seen in 22 patients (Fig. 4). Eighteen had abnormal inflammatory masses, two intramural and 16 pericolic (Fig. 5). In one, an intramural fistulous tract was seen as air in a linear distribution in the gut wall (Fig. 6). Additional findings included focal thickening of the bladder wall (two patients), air in the bladder with a fistulous connection to the gut (two), hydronephrosis (one), liver abscess (one), and free intraperitoneal air and fluid (one). The last finding occurred in a patient who had had a double-lung transplant and developed perforation postoperatively from acute diverticulitis.

Seventeen of the 19 patients ultimately considered to have diverticulosis showed no definite sonographic abnormality. The other two had positive sonograms consistent with acute diverticulitis. Both demonstrated gut-wall thickening and diverticula. At surgery, performed for presumed acute diverticulitis, neither patient had active inflammation.

All six patients with false-positive examinations had pathologic changes in the colon with gut-wall thickening in the left and sigmoid colon, five with a pericolic inflammatory mass.

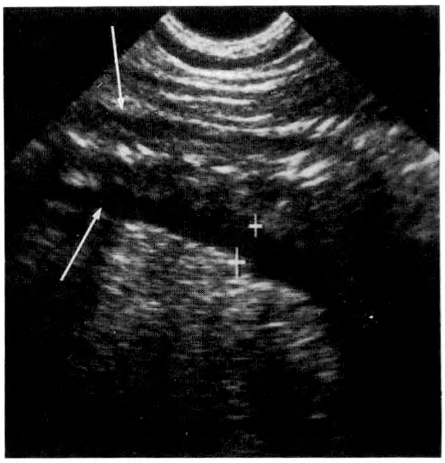

1

Fig. 1.—63-year-old woman with left lower quadrant pain. Sagittal sonogram shows thick loop of gut (*arrows*) with typical thick muscularis propria (*cursors*). Inflamed diverticulum was seen on other views. Contrast enema confirmed acute diverticulitis.

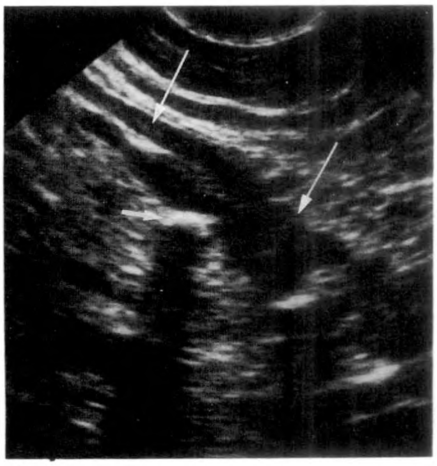

2

Fig. 2.—57-year-old woman with acute left lower quadrant pain and fever. Sagittal sonogram shows mildly thickened loop of gut (*long arrows*) with bright shadowing echogenic focus (*short arrow*) protruding beyond margin of gut wall; this was interpreted as inflamed diverticulum. Contrast enema confirmed acute diverticulitis.

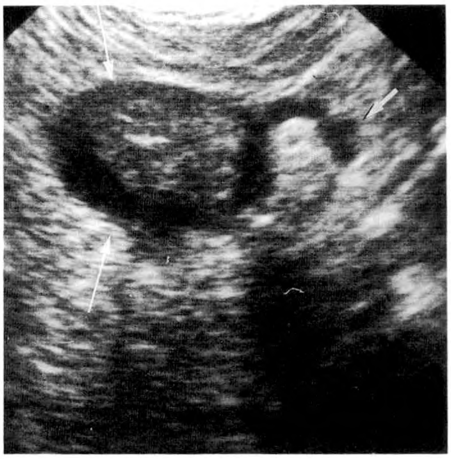

3

Fig. 3.—52-year-old man with left lower quadrant pain, fever, and elevated WBC count. Cross-sectional sonogram shows thickened loop of gut (*long arrows*) with large, inflamed diverticulum (*short arrow*) that has thickened wall protruding beyond margin of gut wall. Contrast enema confirmed acute diverticulitis.

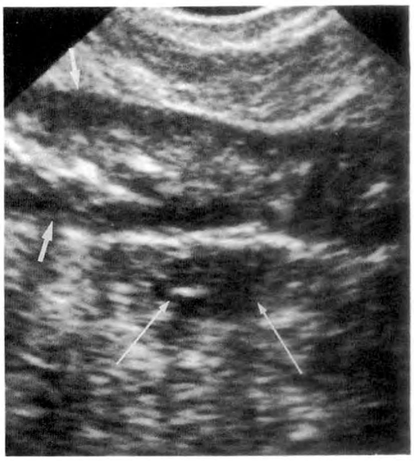

4

Fig. 4.—52-year-old man with acute left lower quadrant pain and fever. Sagittal sonogram shows thickened loop of gut (*short arrows*) and edema of pericolic fat producing poorly defined hypoechoic zone (*long arrows*). Contrast enema confirmed acute diverticulitis. The patient responded to conservative therapy.

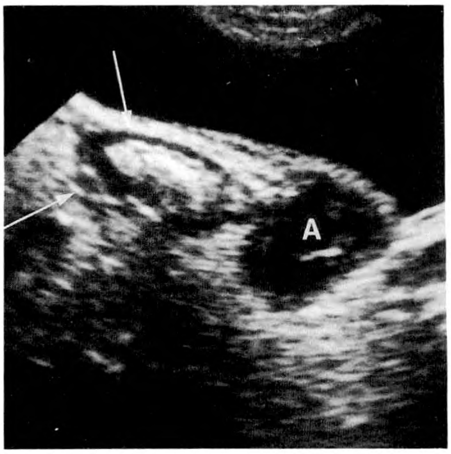

Fig. 5.—41-year-old man with recurrent severe pelvic pain, fever, and elevated WBC count. Oblique sonogram shows abscess (A) adjacent to mildly thickened loop of gut (*arrows*). CT scan and surgery confirmed acute diverticulitis with abscess formation.

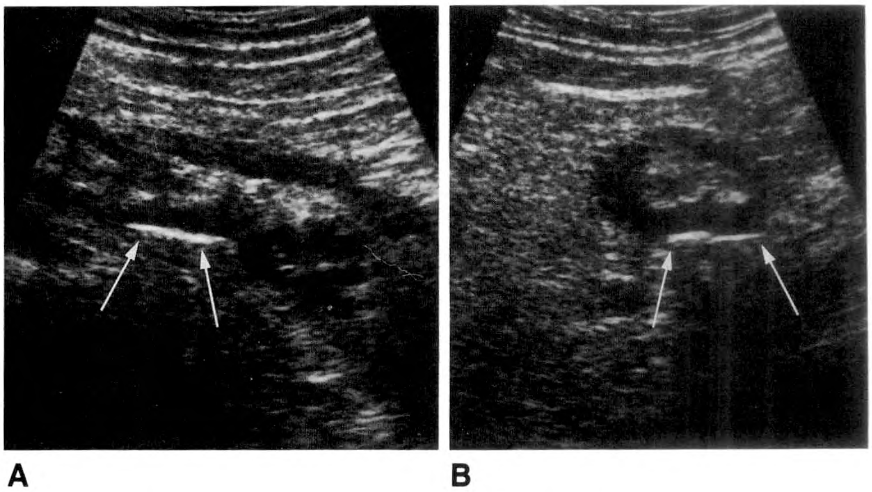

Fig. 6.—35-year-old man with recurrent left lower quadrant pain and fever.

A and *B*, Sagittal (*A*) and cross-sectional (*B*) sonograms show loop of thickened gut with intramural sinus tract seen as linear echogenic line (*arrows*) deep to muscularis propria. Surgery confirmed acute diverticulitis.

One had free intraperitoneal fluid. No diverticula were seen in this group. These cases were sonographically indistinguishable from the true-positive cases for diverticulitis with formation of pericolic abscess.

Discussion

Smooth-muscle hypertrophy and diverticula are present in all patients with acute diverticulitis. Although diverticula of the colon occur in about 50% of adults [2], we find that they are rarely noticeable on sonograms of an asymptomatic person. Presumably, the events associated with acute diverticulitis allow their detection: We believe that spasm, edema, and inflammation of the gut wall enhance evaluation of the thickened segment of gut, and inflammation of the diverticular wall accentuates the diverticulum. On sonography, inflamed diverticula are seen as outpouchings protruding beyond the lumen of the gut into or beyond the thickened wall. They generally contain shadowing echogenic material that may be related to calcified fecaliths, microabscess formation, or merely fecal material and air. Thickening of the diverticular wall may also be seen with active inflammation.

Diverticula were observed in 32 of our 46 patients with proven diverticulitis and in the two patients operated on for acute diverticulitis in whom inflammation was not present in the surgical specimen. Diverticula were not seen in a man with a free intraperitoneal perforation or in 13 of the 16 patients with pericolic inflammatory masses or abscesses. In the latter patients, presumably the diverticulum was incorporated in the adjacent inflammatory process, making its identification difficult. We did not see diverticula in any of our false-positive cases, five of which also had pericolic abscess; nor did we see diverticula in 17 of the 19 patients with presumed acute diverticulosis.

Smooth-muscle hypertrophy, the underlying abnormality in patients with diverticular disease, is not seen often on sonography in the absence of symptomatology. In seven patients with acute diverticulitis, in whom initial scans showed gut-wall thickening, follow-up scans, obtained 4–7 days after presentation to confirm a clinical impression of improvement, showed the thickening was substantially reduced in five. We believe this rapid change was more likely related to relief of spasm and resolution of edema and inflammation than to decreased smooth-muscle hypertrophy.

The lack of specificity of the gut-wall thickening shown on sonography is exemplified by our six false-positive cases. Five of these patients had thickening of the colon with an adjacent inflammatory mass. Their sonograms were virtually identical to those of the patients who had acute diverticulitis with abscess formation in whom inflamed diverticula were not identified. We now interpret segmental colon-wall thickening with an adjacent inflammatory mass as consistent with, rather than diagnostic of, acute diverticulitis.

The clinical distinction between acute diverticulitis and spastic colon disease with diverticulosis may be difficult [3]. Surgical specimens from patients with a classical clinical presentation who undergo colon resection for "acute diverticulitis" frequently show no evidence of active inflammation [4, 5], as in two of our patients. The use of CT and contrast-enema examinations in establishing the correct diagnosis of acute diverticulitis has been discussed often in the imaging literature [6, 7]. The proponents of the contrast enema claim that it is a safe, excellent first step to confirm the clinical impression of diverticulitis, whereas the supporters of CT scanning praise its greater delineation of bowel-wall thickness and its sensitivity in detecting the extent of extraluminal disease. Sonographic descriptions of patients with diverticular disease are limited to a few case reports [8, 9] of cecal diverticulitis studied with compression sonography and a descriptive article by Parulekar [10], who noted the sonographic features of colonic diverticulitis in 16 patients. He described concentric hypoechoic gut-wall thickening in aperistaltic segments and occasional diverticula.

Our study attempted to establish the clinical value of sonography in the preliminary evaluation of patients with a classical presentation of acute diverticulitis. No patient in whom significant pericolic disease was shown by another technique or at surgery was missed by sonography in our study period. However, interloop abscesses, abscesses filled with gas, and poor-quality sonograms are potential pitfalls; we recommend CT scanning be performed if an abscess is highly suspect but undetected or if poor visualization of the area of concern is encountered on sonography. In our experience, sonography readily detected gut-wall thickening and inflamed diverticula. Because of the urgency of diagnosis often associated with these patients, as well as the clinical importance of differentiating acute diverticulitis from other diseases, we believe that the ready availability and accuracy of sonography make it an excellent initial imaging tool.

ACKNOWLEDGMENTS

We thank Gina Sciortino for manuscript preparation and Carla Salvador for critical appraisal.

REFERENCES

1. Puylaert JBCN. Acute appendicitis: an ultrasound evaluation using graded compression. *Radiology* **1986**;158:355–360
2. Dreyfuss JR, Janower ML, eds. *Radiology of the colon.* Baltimore: Williams & Wilkins, **1980**
3. Janower ML. Diverticulitis and the contrast enema. *AJR* **1987**;149: 861–862
4. Fleischner FG, Ming SC, Henken EM. Revised concepts on diverticular disease of the colon. I. Diverticulosis: emphasis on tissue derangement and its relation to the irritable colon syndrome. *Radiology* **1964**;83: 859–871
5. Fleischner FG, Ming SC. Revised concepts on diverticular disease of the colon. II. So-called diverticulitis: diverticular sigmoiditis and perisigmoiditis; diverticular abscess, fistula, and frank peritonitis. *Radiology* **1965**;84: 599–609
6. Hulnick DH, Megibow AJ, Balthazar EJ, Naidich DP, Bosniak MA. Computed tomography in the evaluation of diverticulitis. *Radiology* **1984**; 152:491–495
7. Johnson CD, Baker ME, Rice RP, Silverman P, Thompson WM. Diagnosis of acute colonic diverticulitis: comparison of barium enema and CT. *AJR* **1987**;148:541–546
8. Townsend RR, Jeffrey RB Jr, Laing FC. Cecal diverticulitis differentiated from appendicitis using graded-compression sonography. *AJR* **1989**;152: 1229–1230
9. Puylaert JBCM. Graded compression ultrasound in acute disease of the right lower quadrant. *Semin US CT MR* **1987**;4:385–402
10. Parulekar SG. Sonography of colonic diverticulitis. *J Ultrasound Med* **1985**;4:659–666

CT of Hilar Cholangiocarcinoma:
Late Contrast Enhancement in Six Patients

Kenichi Takayasu[1]
Shinichi Ikeya[1]
Kiyoshi Mukai[2]
Yukio Muramatsu[1]
Masatoshi Makuuchi[3]
Hiroshi Hasegawa[3]

Hilar cholangiocarcinoma usually appears on CT scans as a low-density or isodense mass that abruptly obstructs converging dilated bile ducts. In four of six patients with histopathologically proved hilar cholangiocarcinoma who had late enhanced CT 8–15 min after dynamic CT, the lesion was seen as a high-density mass instead of the low-density lesion seen earlier on unenhanced and dynamic CT scans. The other two patients had ring enhancement with evidence of a thickened wall of the bile duct both on early and late enhanced CT scans. In the first four patients, carcinoma invaded the neighboring hepatic parenchyma and produced a mass, whereas in the last two, carcinoma was localized in the wall of the bile duct. Histopathologically, all lesions consisted of adenocarcinoma associated with a dense fibrotic tissue.

As late enhanced CT shows hilar cholangiocarcinoma as a high-density mass, the exact location of the tumor and its relation to neighboring vessels can be determined, especially in relatively small tumors, and differentiation from sclerosing cholangitis is possible.

***AJR* 154:1203–1206, June 1990**

Hilar cholangiocarcinoma (HC) is defined as a carcinoma arising in the bifurcation of the hepatic ducts [1], but after the carcinoma invades the liver parenchyma, it is difficult to determine whether the mass is intrahepatic or extrahepatic [2]. This tumor is known to have poor prognosis because of aggressive local invasion [3, 4]. On CT, HC is usually detected as a relatively large low-density or isodense mass that abruptly obstructs the proximal portions of the dilated bile ducts. Only a minority of these carcinomas are detected with enhanced CT [5], and the location and size of the lesion, especially when it is small and does not cause any symptoms, are difficult to identify in most cases. We report examples of HC in which late enhanced CT scans showed a high-density mass.

Subjects and Methods

Twenty-one patients with histopathologically proved HC were studied with CT during the past 5 years. Of them, six consecutive patients undergoing dynamic CT (Toshiba 60A or 900s, Tokyo) followed by late enhanced CT were selected for this study; the remaining 15 were excluded because late enhanced CT was not performed. We injected 100–120 ml of contrast medium (65% meglumine diatrizoate, Schering, Kenilworth, NJ) into the antecubital vein at a speed of 2–3 ml/sec and early enhanced CT was performed on sections in a cranial to caudal direction with a table incrementation method. Late enhanced CT was performed 8–10 min after the start of systemic injection of contrast medium. Slice thickness and slice interval were 10 mm in all cases.

There were four men and two women whose ages ranged from 58 to 71 years (average, 55 years). The main location of the cholangiocarcinoma (diagnosed by means of sonography, percutaneous transhepatic cholangiography, endoscopic retrograde cholangiography, and angiography) was the left hepatic duct in four patients; in one patient carcinoma extended to the right hepatic duct and in two patients, to the common hepatic duct. The diameter of the

Received October 26, 1989; accepted after revision December 27, 1989.

This work was supported in part by a Grant-in-Aid for Cancer Research (62s-1) from the Ministry of Health and Welfare.

[1] Department of Diagnostic Radiology, National Cancer Center Hospital, 5-1-1, Tsukiji, Chuo-ku, Tokyo 104, Japan. Address reprint requests to K. Takayasu.

[2] Pathology Division, National Cancer Center Research Institute, Tokyo 104, Japan.

[3] Department of Surgery, National Cancer Center Hospital, Tokyo 104, Japan.

0361–803X/90/1546–1203
© American Roentgen Ray Society

mass in the left hepatic duct ranged from 1.7 to 4.5 cm (average, 3.2 cm) and the depth of carcinoma in the common hepatic duct was 0.4 and 0.6 mm. Five of six masses were measured in the resected specimen and the other one was measured by using CT and sonography.

Five patients underwent surgery: extended left bisegmentectomy was performed in two, left trisegmentectomy in one, extended right lobectomy in one, and right lobectomy in one. In the remaining patient, diagnosis was made on the basis of biopsy findings. The mean interval between CT study and surgery or biopsy was 19 days (range, 4–36 days).

Histopathologically, all tumors were moderately or well-differentiated adenocarcinoma with an abundant stroma that consisted of scirrhous tissue in all patients.

Results

In all cases, dilated intrahepatic bile ducts were observed on both unenhanced and enhanced CT scans, in the left lobe in three patients and in both lobes in three patients. Histopathologically, the extent of carcinoma invasion in the hepatic ducts was found to be wider than that assessed by means of CT in all cases. Four patients with an exophytic mass mainly located in the left hepatic duct and invading the liver parenchyma had characteristic findings, in which the mass was shown as a low-density area on both unenhanced and early enhanced CT scans and was recognized as a high-density area on late enhanced CT scans (Figs. 1 and 2). By contrast,

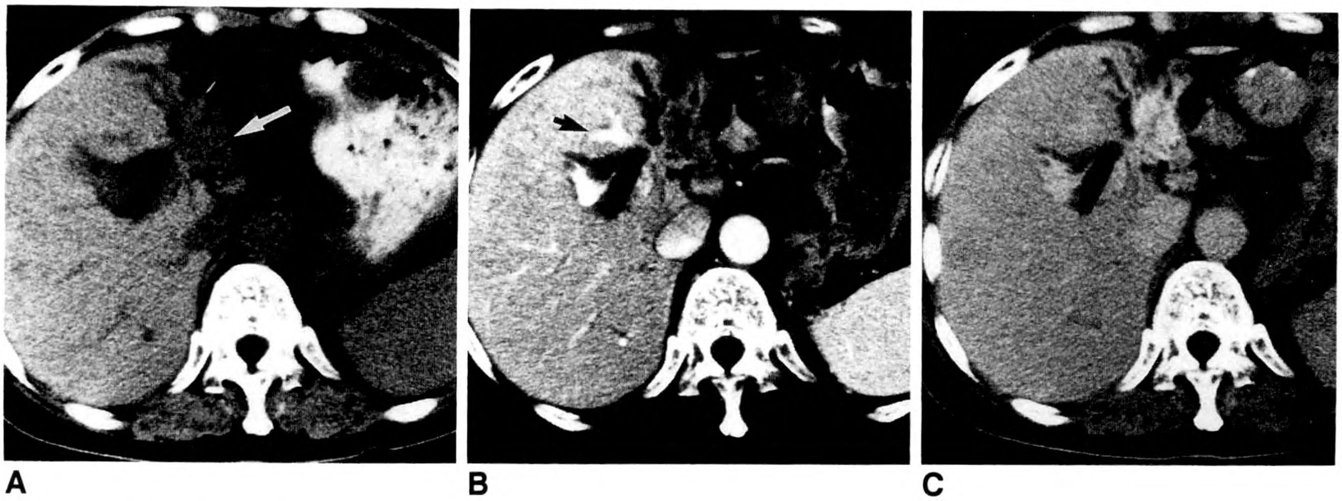

Fig. 1.—63-year-old man with cholangiocarcinoma in left hepatic duct.

***A*, Unenhanced CT scan of porta hepatis shows an oblong low-density mass (*arrow*).**

***B*, In early phase of dynamic CT, margin of an oblong mass is slightly enhanced. Dilatation of bile ducts is clearly seen both in left medial and right anterior areas of liver. Arrow indicates middle hepatic vein.**

***C*, Late enhanced CT scan obtained 10 min later shows a high-density oblong mass.**

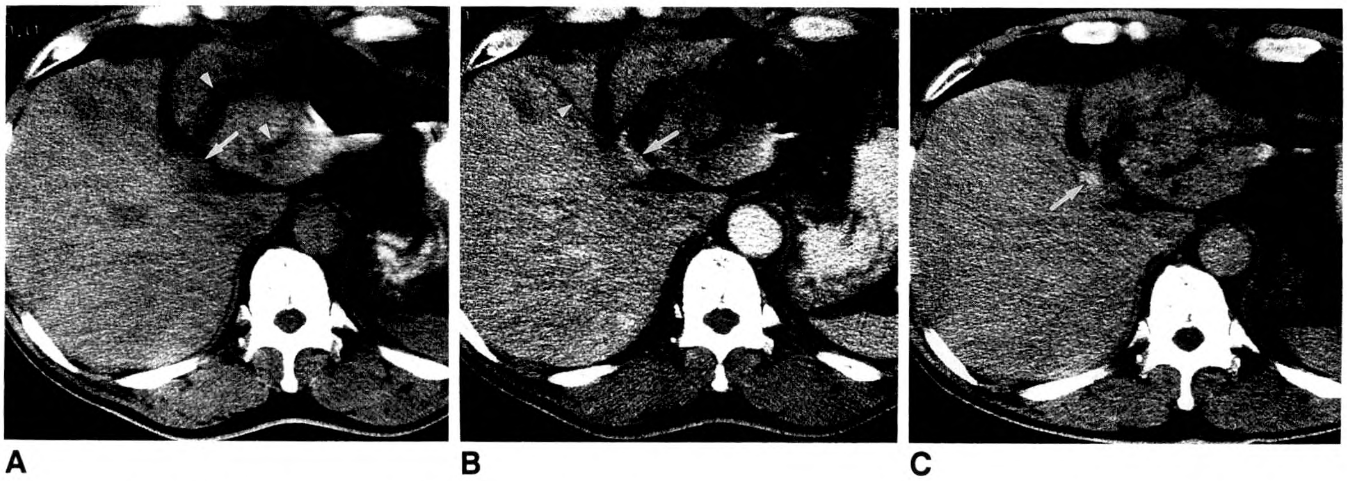

Fig. 2.—62-year-old man with cholangiocarcinoma in left hepatic duct.

***A*, Unenhanced CT scan shows biliary dilatation of left lateral segment of liver (*arrowheads*). A protruding small low-density area is also shown (*arrow*), but exact extent of mass is unclear.**

***B*, Dynamic CT in early phase shows umbilical portion of portal vein (*arrow*) running medially to low-density area. Dilatation of bile duct in left medial area is also shown (*arrowhead*).**

***C*, Late enhanced CT scan obtained 10 min later shows a change from low density to high density in this area (*arrow*). Portal veins are not shown in this phase.**

hilar carcinoma localized within the bile duct wall without invasion into liver parenchyma in the common hepatic duct in the remaining two cases was recognized as a low-density area on unenhanced CT scans and as a ringlike enhancement on both early and late enhanced CT scans (Fig. 3).

Discussion

For the diagnosis of HC, CT can show only the dilated bile ducts whose proximal portions are abruptly obstructed near the porta hepatis and the extent of carcinomatous involvement in the hepatic parenchyma. The carcinoma is usually shown as a low-density or isodense lesion on unenhanced and enhanced CT scans, even though a few HCs have appeared as hypervascular lesions on enhanced CT scans [5]. Only one case of choledochal cyst with hilar carcinoma has been described as a high-density mass [6], with no pathologic details. In those two studies, late enhanced CT was not performed. A recent study reported that only 40% of HCs were detected and six (43%) of them were high-density masses on conventional CT scans [7]. If they had used late enhanced CT, the frequency of high-density masses would have been higher. The number of patients evaluated in our study was small because late enhanced CT was not always performed. Therefore, further study is necessary to determine how frequently HC is seen as a high-density area on late enhanced CT scans.

As most HCs are composed of few cancer cells and abundant fibrous tissue within the central portion (with many viable cancer cells in the margin of the tumor), tumor is not usually enhanced in the early phase of enhanced CT, nor is it enhanced by angiography except for thin marginal enhancement around the mass (Fig. 1B). This finding coincides with the doughnutlike ring enhancement in intrahepatic cholangiocarcinoma [8] and/or metastatic adenocarcinoma in the liver.

On late enhanced CT scans, contrast medium was seen to have remained in the center of the tumor, the same finding that is seen in metastatic adenocarcinoma in the liver [9]. This phenomenon is thought to occur in the abundant fibrous connective tissue of cancer masses and perhaps also in inflammatory lesions. Water-soluble contrast medium diffuses depending on the difference in concentration of contrast medium between tissues and vessels. Therefore, in the early phase, the margins of well-vascularized carcinomas are well enhanced and their inner, poorly vascularized portions are poorly enhanced. Once contrast medium moves into the abundant fibrous tissues with scanty blood supply in the late phase, it remains there, staining the inner portion of the mass for a long time [9, 10]. In our four patients with a mass, scirrhous cancer with abundant fibrous tissue was histopathologically confirmed.

In order to diagnose HC as a high-density mass on late enhanced CT scans, a tumor-forming mass that invades the neighboring liver parenchyma from the original site in the bile duct seems to be necessary. Four patients with lesions ranging from 1.7 to 4.5 cm in diameter that invaded liver parenchyma had this finding, but the other two patients in whom cancer was localized in the bile duct without parenchymal invasion did not have the same feature except for enhancement of the bile duct wall. Cholangiocarcinoma arising from the hepatic duct may be difficult to diagnose at an early stage because there are no symptoms, such as jaundice and a compressed feeling due to the mass, whereas carcinoma in the common hepatic duct usually causes jaundice in the early stage even though the tumor is small [11]. Thus, a carcinoma arising from the hepatic duct may develop into a mass without any clinical signs.

Our method for late enhanced CT is simple and saves time, as only 8–15 min are needed to make late enhanced CT scans. These findings are useful in determining the real location and size of HCs, especially of small HCs (Fig. 2), and in differential diagnosis of a mass-forming hilar cholangiocarcinoma from sclerosing cholangitis, and perhaps from hilar lymph-node metastasis of a digestive cancer. Sclerosing cholangitis usually does not form a mass, and the majority of lymph-node metastases are seen as unenhanced masses even on late enhanced CT scans. However, differential diagnosis of HC localized in the bile duct without invasion into liver parenchyma and sclerosing cholangitis may remain difficult because both are shown as an enhancement of the bile duct wall (Fig. 3) [12].

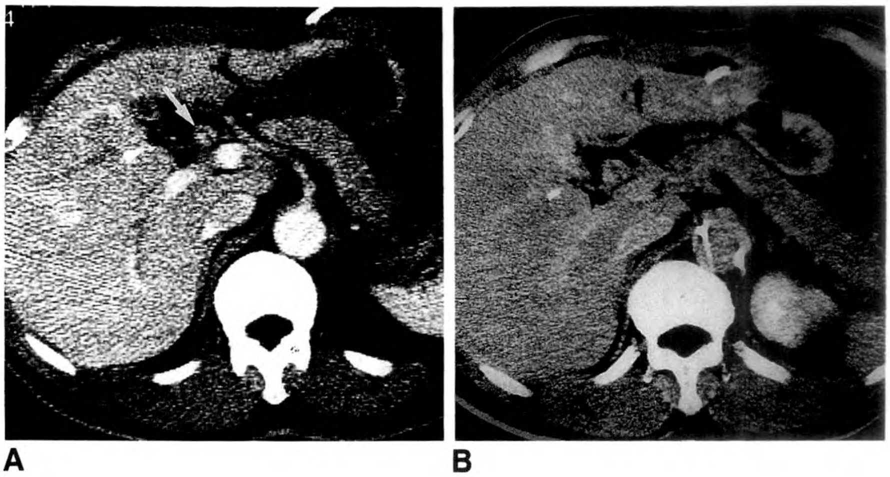

Fig. 3.—61-year-old man with cholangiocarcinoma in common hepatic duct.

A, Dynamic CT scan in early phase shows common hepatic duct proximal to bifurcation of hepatic ducts as a ringlike enhancement (*arrow*); it was seen as a low-density area on unenhanced CT scan (*not shown*).

B, Common hepatic duct on late enhanced CT scan looks almost same as in *A*. Invasion of entire circumference of bile duct and its wall, measuring 4 mm in depth, was confirmed histopathologically.

ACKNOWLEDGMENTS

The authors thank K. Okuda of Chiba University School of Medicine for his review.

REFERENCES

1. Klatskin G. Adenocarcinoma of the hepatic duct at its bifurcation within the porta hepatis: an unusual tumor with distinctive clinical and pathological features. *Am J Med* **1965**;38:241-256
2. Okuda K, Kubo Y, Okazaki N, et al. Clinical aspects of intrahepatic bile duct carcinoma including hilar carcinoma: a study of 57 autopsy-proven cases. *Cancer* **1977**;39:232–246
3. Iwasaki Y, Okamura T, Ozaki A, et al. Surgical treatment for carcinoma at the confluence of the major hepatic ducts. *Surg Gynecol Obstet* **1986**; 162:457-464
4. Tsuzuki T, Uekusa M. Carcinoma of the proximal bile ducts. *Surg Gynecol Obstet* **1978**;146:933–943
5. Carr DH, Hadjis NS, Banks LM, Hemingway AP, Blumgart LH. Computed tomography of hilar cholangiocarcinoma: a new sign. *AJR* **1985**;145: 53-56
6. Araki T, Itai Y, Tasaka A. CT of choledochal cyst. *AJR* **1980**;135:729–734
7. Choi BI, Lee JH, Han MC, Kim SH, Yi JG, Kim C-W. Hilar cholangiocarcinoma: comparative study with sonography and CT. *Radiology* **1989**;172: 689–692
8. Numata K, Takayasu K, Muramatsu Y, et al. Clinico-pathological study of cholangiocellular carcinoma (in Japanese). *Jpn J Gastroenterol Surg* **1989**; 22:2375–2382
9. Muramatsu Y, Takayasu K, Moriyama N, et al. Peripheral low-density area of hepatic tumors: CT-pathologic correlation. *Radiology* **1986**;160:49–52
10. Itai Y, Ohtomo K, Kokubo T, et al. CT of hepatic masses: significance of prolonged and delayed enhancement. *AJR* **1986**;146:729–733
11. Takayasu K, Muramatsu Y, Shima Y, Moriyama N, Yamada T, Makuuchi M. Hepatic lobar atrophy following obstruction of the ipsilateral portal vein from hilar cholangiocarcinoma. *Radiology* **1986**;160:389–393
12. Teefey SA, Baron RL, Rohrmann CA, Shuman WP, Freeny PC. Sclerosing cholangitis: CT findings. *Radiology* **1988**;169:635–639

Pictorial Essay

CT of the Abdominal Wall

Philip Goodman[1, 2] and Bharat Raval[1]

CT is an excellent method for evaluating the abdominal wall. Various abnormalities including hernia, hematoma, abscess, tumor, and neuromuscular disease are easily detected and assessed by CT. Examples of common and uncommon diseases illustrate the value of CT in the diagnosis of abdominal wall diseases.

Normal Anatomy

The abdominal wall consists of skin, subcutaneous tissues, and a muscular layer that is divided into anterior, anterolateral, and posterior groups (Fig. 1). The anterior group consists of rectus abdominis muscles lying within the rectus sheath. The anterolateral group is formed by external and internal oblique and transversus abdominis muscles. Latissimus dorsi, quadratus lumborum, and paraspinal muscles make up the posterior group. The abdominal wall is separated from the peritoneum by the transversalis fascia and extraperitoneal fat [1].

Hernia

Abdominal wall hernias may be difficult to diagnose clinically in obese patients or in those who have acute abdominal pain and distension or when the hernia is located in an uncommon site. CT readily detects the size, location, and content of paraumbilical, incisional, spigelian, and lumbar hernias (Figs. 2–4) [2]. CT may be used in the symptomatic patient for preoperative planning.

Hematoma

Abdominal wall hematomas may be associated with trauma, anticoagulation therapy, or blood dyscrasia or may occur spontaneously because of muscular strain. These commonly involve the anterior or anterolateral muscle groups and may dissect along fascial planes or involve the muscle itself. Acute hematomas are hyperdense because of clot formation, and attenuation values decrease with time as breakdown of blood products occurs (Figs. 5 and 6) [3].

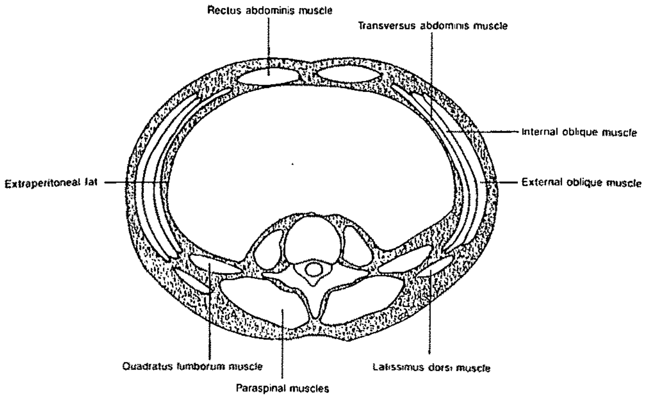

Fig. 1.—Drawing shows axial section of normal anatomy of abdominal wall.

Received December 11, 1989; accepted after revision January 22, 1990.

[1] Department of Radiology, The University of Texas Medical School at Houston, 6431 Fannin, 2134 MSMB, Houston, TX 77030.

[2] Present address: Department of Radiology, University of Texas Medical Branch, Galveston, TX 77550. Address reprint requests to P. Goodman.

AJR **154:1207–1211, June 1990** 0361-803X/90/1546-1207 © American Roentgen Ray Society

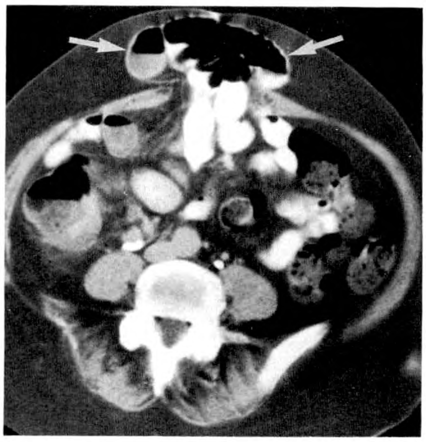

Fig. 2.—Large incisional ventral hernia containing opacified bowel loops (*arrows*).

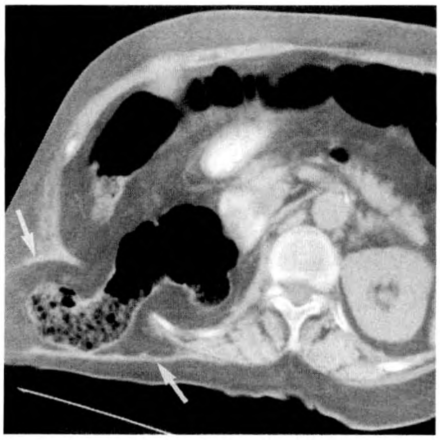

Fig. 3.—Herniation of colon through right posterolateral abdominal wall incisional hernia (*arrows*).

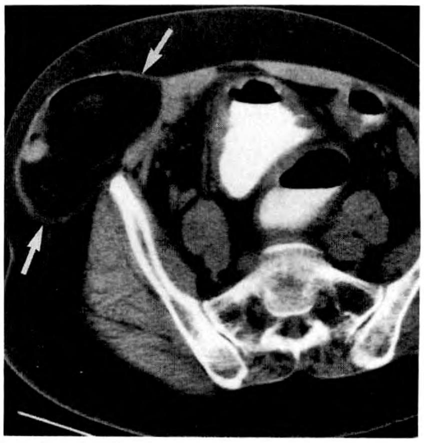

Fig. 4.—Large spigelian hernia containing bowel and intraperitoneal fat (*arrows*), adjacent to inferolateral aspect of right rectus abdominis muscle.

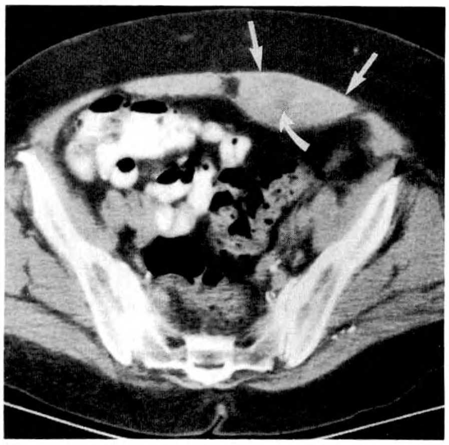

5

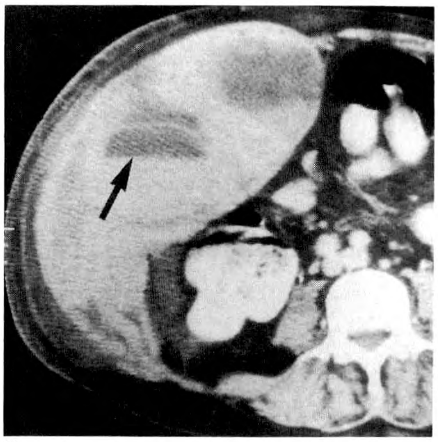

6

Fig. 5.—Left rectus abdominis hematoma (*straight arrows*) in patient whose hemoglobin level dropped after cardiopulmonary resuscitation. Low-density area within hematoma represents clot lysis (*curved arrow*).

Fig. 6.—Large abdominal wall hematoma occurred spontaneously in this patient on anticoagulant therapy. Fluid-fluid level representing "hematocrit" effect is present within hematoma (*arrow*).

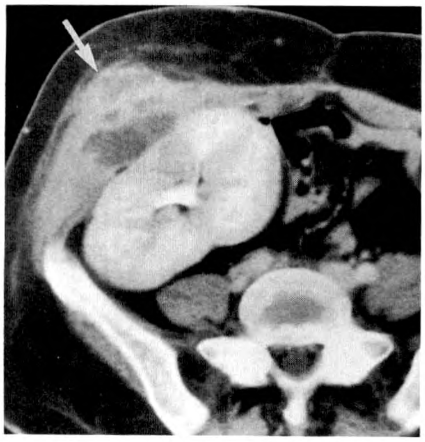

Fig. 7.—Large complex mass (*arrow*) is present adjacent to transplanted kidney. Patient had fever and chills that resolved after pus was drained from abdominal wall abscess.

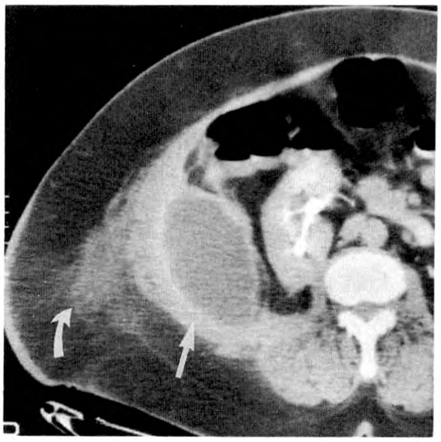

Fig. 8.—Low-density abscess (*straight arrow*) in right flank displaces right kidney. Increased density in adjacent subcutaneous fat represents inflammatory edema (*curved arrow*).

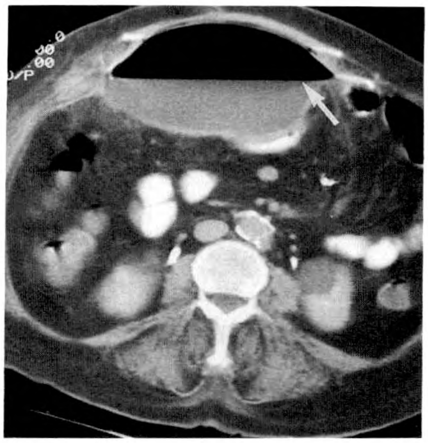

Fig. 9.—Long gas-fluid level (*arrow*) lies just deep to mesh graft in patient with postsurgical abscess after ventral hernia repair.

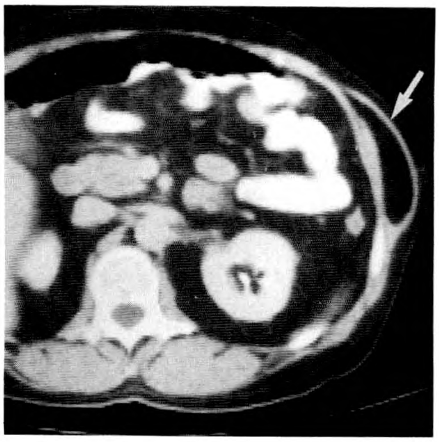

Fig. 10.—Well-defined low-density mass between left external and internal oblique muscles is a lipoma (*arrow*).

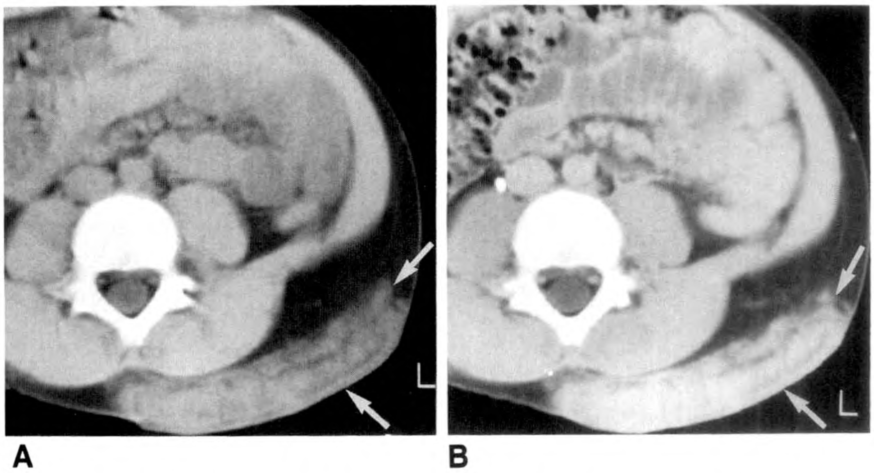

Fig. 11.—*A* and *B*, CT scans before (*A*) and after (*B*) administration of contrast material show enhancing soft-tissue mass (*arrows*) extending deep into subcutaneous tissues in child with hemangioma of the back.

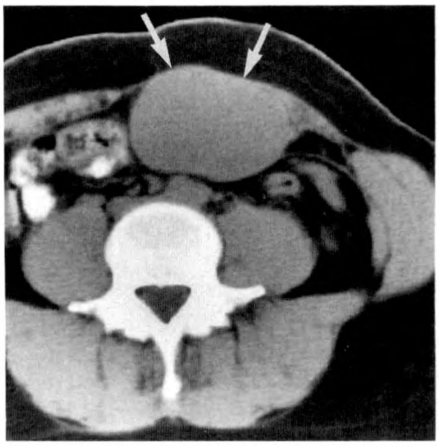

12

Fig. 12.—Diffuse infiltration of left rectus abdominis muscle by desmoid tumor (*arrows*).

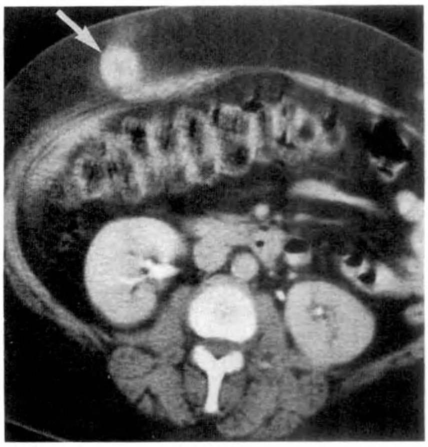

13

Fig. 13.—Metastatic subcutaneous nodule in anterior abdominal wall from adenocarcinoma of the lung (*arrow*).

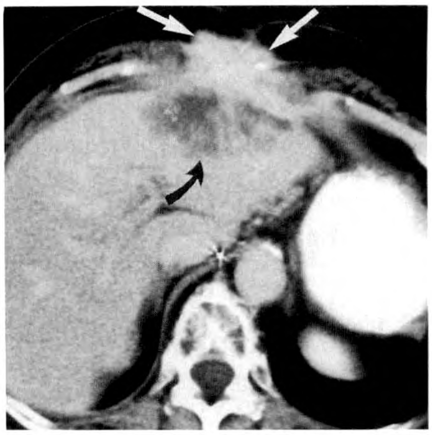

14

Fig. 14.—Irregular soft-tissue mass (*straight arrows*) in anterior abdominal wall adjacent to low-density area in liver (*curved arrow*). Subxiphoid mass resected from this area 1 year earlier was metastatic colonic carcinoma.

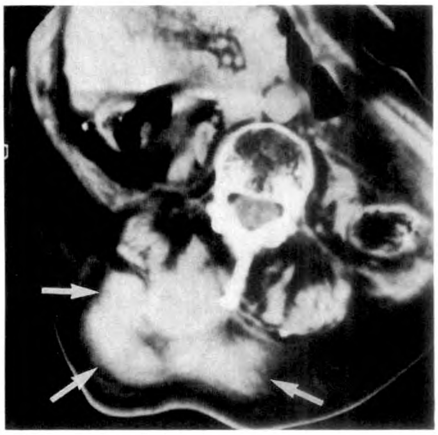

15

Fig. 15.—Diffuse soft-tissue mass involving subcutaneous tissues and right paraspinal muscles is direct extension of sacral chordoma (*arrows*).

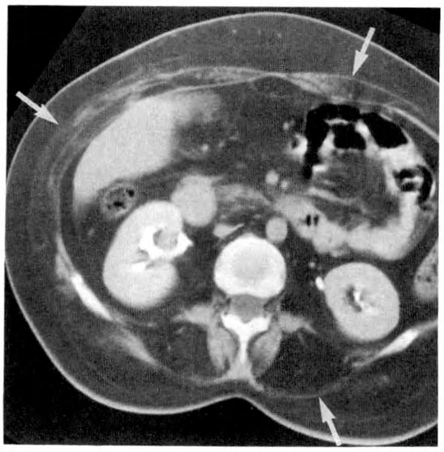

Fig. 16.—Diffuse muscular atrophy with fatty replacement (*arrows*) in patient with long history of limb-girdle muscular dystrophy.

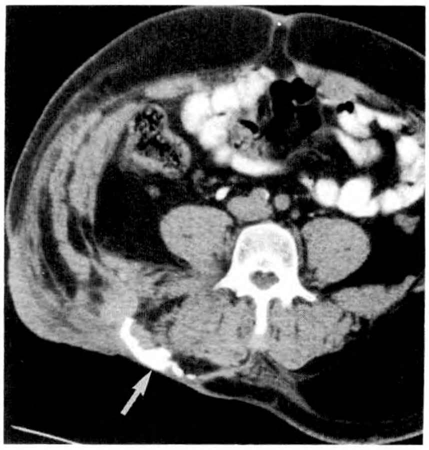

Fig. 17.—Marked asymmetry of right flank in patient with previous massive soft-tissue injury of the right flank and subsequent reconstructive surgery. Irregular posttraumatic calcifications involve posterior abdominal wall (*arrow*).

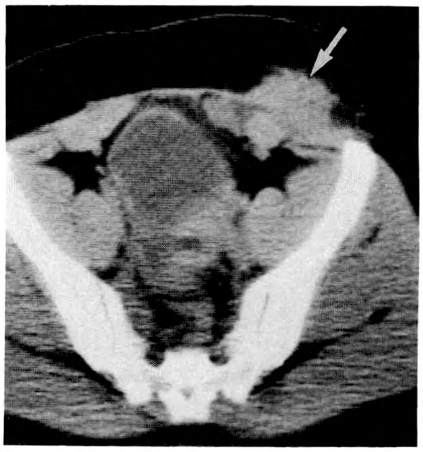

Fig. 18.—Irregular soft-tissue mass of left rectus sheath and adjacent subcutaneous tissue is endometriosis in a surgical scar (*arrow*).

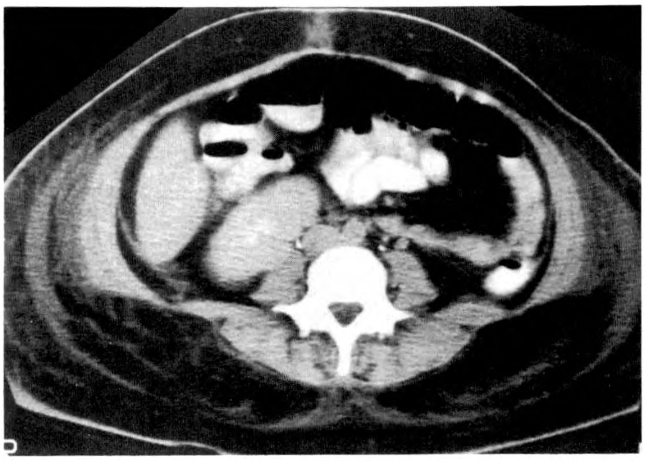

Fig. 19.—Diffuse streaky soft-tissue densities indicate edema in subcutaneous tissues associated with congestive heart failure.

Abscess

Inflammatory disease of the abdominal wall commonly results from postsurgical wound infection or extension of an intraabdominal abscess. Usually it involves the subcutaneous tissues or the muscular layer. When the usefulness of physical examination is limited, particularly in obese patients, CT is the method of choice to evaluate suspected abdominal wall infection. The CT findings include diffuse edema with cellulitis or discrete fluid collections when abscess formation has occurred (Figs. 7–9). Gas or gas-fluid levels have been reported to be present in approximately 30% of abscesses [3, 4].

Tumor

Commonly encountered benign neoplasms of the abdominal wall include lipoma, hemangioma, and neurofibroma (Figs.

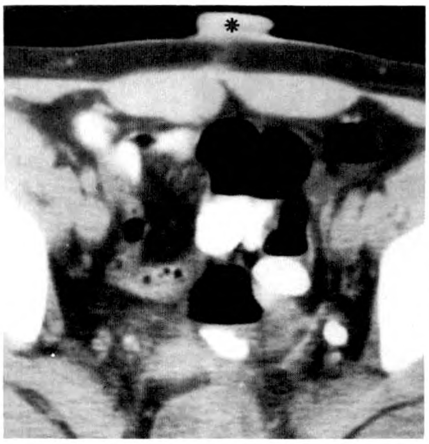

20

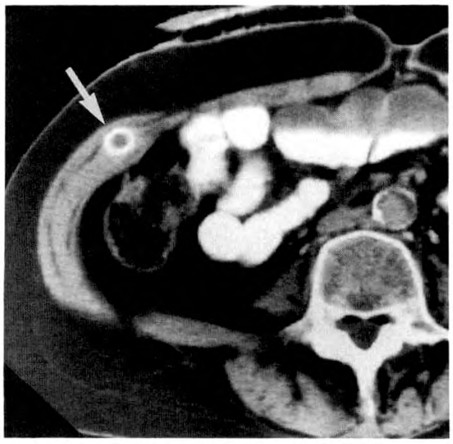

21

Fig. 20.—Midline anterior abdominal wall keloid (*asterisk*).

Fig. 21.—Tubular structure (*arrow*) in right anterolateral muscle group is axillofemoral bypass graft (confirmed by digital angiogram).

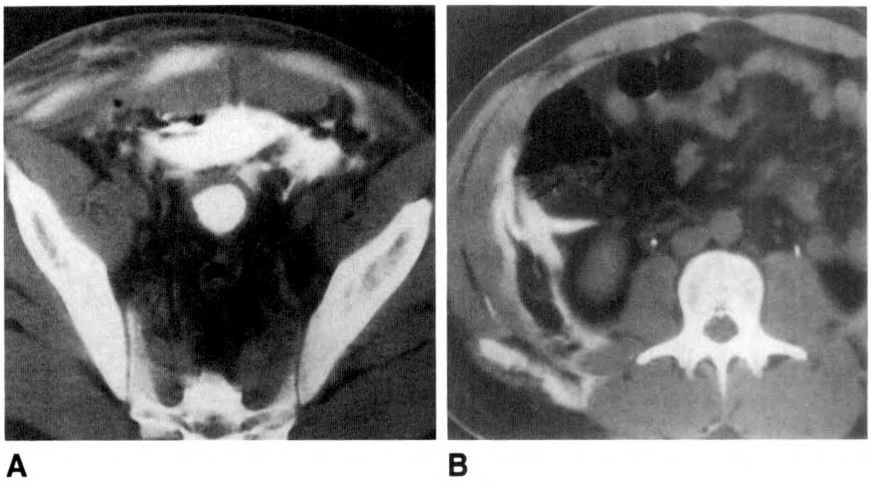

Fig. 22.—*A* and *B*, Extravasation of contrast material deep and superficial to abdominal wall muscles from extraperitoneal rupture of bladder.

10 and 11). Primary malignant lesions are rare and include soft-tissue sarcoma and lymphoma. Desmoid tumor, though histologically benign, is often locally aggressive (Fig. 12).

Secondary malignancies of the abdominal wall occur as subcutaneous nodules by hematogenous spread. These are well visualized on CT because of contrast with adjacent fat (Fig. 13). Contiguous spread of a primary or metastatic lesion to the abdominal wall may cause infiltration of muscles and loss of adjacent fat planes (Figs. 14 and 15). These tumors usually arise in superficial organs such as the transverse colon, gallbladder, urinary bladder, and omentum. This is sometimes difficult to distinguish from extension of an intraabdominal abscess and may require percutaneous biopsy.

CT is the method of choice for staging and follow-up of malignancies involving the abdominal wall and for directing percutaneous biopsy and placing radiotherapy ports [3, 4].

Miscellaneous

Other abnormalities of the abdominal wall detected by CT are shown in Figures 16–22.

REFERENCES

1. Fisch AE, Brodey PA. Computed tomography of the anterior abdominal wall: normal anatomy and pathology. *J Comput Assist Tomogr* **1981**; 5:728–733
2. Wechsler RJ, Kurtz AB, Needleman L, et al. Cross-sectional imaging of abdominal wall hernias. *AJR* **1989**;153:517–521
3. Heiken JP. Abdominal wall and peritoneal cavity. In: Lee JKT, Sagel SS, Stanley RJ, eds. *Computed body tomography with MRI correlation*. New York: Raven, **1989**:661–705
4. Pandolfo I, Blandino A, Gaeta M, Racchiusa S, Chirico G. CT findings in palpable lesions of the anterior abdominal wall. *J Comput Assist Tomogr* **1986**;10:629–633

Radiology Outreach Foundation

The Radiology Outreach Foundation (ROF) is a nonprofit corporation whose goal is to help disadvantaged countries improve their health care by providing radiology equipment, books, consultation, education, and training to their practitioners. This assistance is on an application basis that is independent of political, ethnic, or religious orientation of the grantee. It depends on the need of the people and the ability of the ROF to meet that need. The ROF is approved by the U.S. Internal Revenue Service as a tax-exempt organization. It is endorsed by the following radiologic societies:

American Association of Women Radiologists
American College of Radiology
American Roentgen Ray Society
Association of University Radiologists
Radiological Society of North America
Society of Chairmen of Academic Radiology Departments
Society for Pediatric Radiology
European Society of Pediatric Radiology

All donations to the ROF are tax deductible. Persons who would like to contribute financially to the ROF, would be interested in being a visiting professor, would like to send books or journals to any of the institutions supported by the ROF, or would like further information about the ROF should write to

Charles A. Gooding, M.D.
President
Radiology Outreach Foundation
3415 Sacramento St.
San Francisco, CA 94118 USA

Common Bile Duct Biopsy with the Simpson Atherectomy Catheter

Ducksoo Kim,[1] David H. Porter,[1] Jeffrey B. Siegel,[1] Peter M. Mowschenson,[2] and Michael L. Steer[2]

The Simpson AtheroCath (Devices for Vascular Intervention, Inc., Redwood City, CA) was originally designed for treatment of atherosclerotic occlusive disease by means of percutaneous atheroma removal [1, 2]. We recently used this atherectomy catheter for biopsy of common bile duct lesions via transhepatic tracts of indwelling percutaneous biliary drainage catheters in two patients. Both had recurrent obstructive jaundice after Whipple procedures for pancreatic carcinoma.

Conventional brush (Geenen replacement brush, 3-mm diameter, Wilson-Cook Medical, Inc., Winston-Salem, NC) biopsy of each lesion was performed before atherectomy catheter biopsy. Adequate brush specimens were obtained and were negative for malignant cells on immediate cytologic interpretation.

Atherectomy catheter biopsy in each patient provided satisfactory pieces of tissue from the common bile duct for histologic examination, the results of which were positive for malignant cells in the first patient and suspicious in the second. Follow-up CT of the abdomen after biopsy in each patient revealed metastatic lesions in the liver and no hemorrhage or perforation at the atherectomy catheter biopsy sites.

Technique

A cholangiogram is first performed via an indwelling biliary drainage catheter. A guidewire is passed through the drainage tube and the obstructing lesion of the common bile duct into the jejunum. The biliary catheter is exchanged over the wire for an 8-French, thin-wall catheter positioned in the stricture of the common bile duct. The biopsy brush is introduced through the 8-French catheter and positioned in contact with the stricture by unsheathing the 8-French outer catheter. The lesion is then brushed with multiple to-and-fro motions. If immediate cytologic interpretation is negative, biopsy of the lesion is performed with the atherectomy catheter.

The atherectomy catheter consists of a flexible catheter shaft, a stiff metal cutter housing, a collection chamber, and a short 0.018-in. (0.46-mm) fixed platinum floppy guidewire tip. For bile duct biopsy, the atherectomy catheter requires an introducer sheath as with vascular atherectomy. A long (24-cm), 9-French introducer sheath (C.R. Bard, Covington, GA) is used to facilitate passing the stiffer distal part of the atherectomy catheter through acute angulations in the bile ducts and into position within the stricture (Figs. 1A and 1B). After the atherectomy catheter is positioned, the introducing sheath is withdrawn above the lesion (Fig. 2). The biopsy is then performed in a fashion similar to a vascular atherectomy, with tissue samples obtained from various portions of the stricture. The atherectomy catheter is then removed through the introducing sheath, and an internal-external biliary drainage catheter or endoprosthesis is introduced.

Case Reports

Case 1

A 72-year-old man was admitted for evaluation of recurrent jaundice, abdominal pain, and fever 4 months after having a Whipple procedure for treatment of pancreatic carcinoma. A percutaneous transhepatic cholangiogram showed a severe obstruction of the common bile duct at the anastomosis with the jejunal loop.

Received December 26, 1989; accepted after revision February 6, 1990.

[1] Department of Radiology, Beth Israel Hospital and Harvard Medical School, 330 Brookline Ave., Boston, MA 02215. Address reprint requests to D. Kim.

[2] Department of Surgery, Beth Israel Hospital and Harvard Medical School, 330 Brookline Ave., Boston, MA 02215.

AJR **154:1213–1215, June 1990** 0361–803X/90/1546–1213 © American Roentgen Ray Society

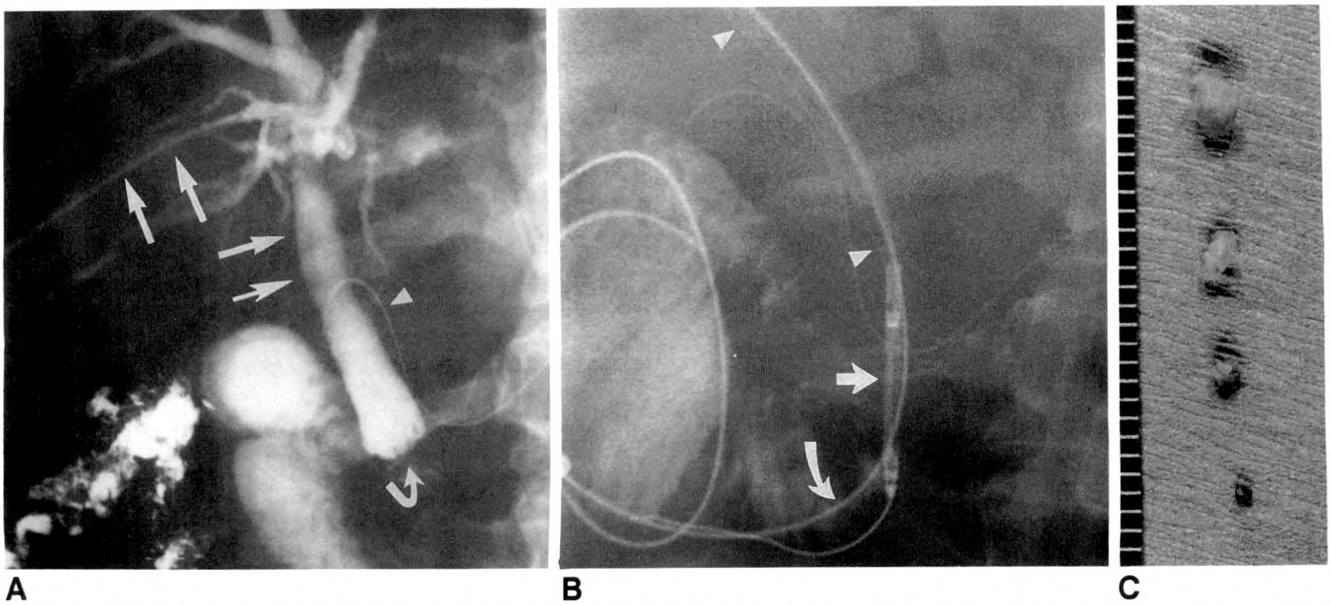

Fig. 1.—*A*, Percutaneous transhepatic cholangiogram shows severe stricture of common bile duct at jejunal anastomosis (*curved arrow*) and typical acute angulation of bile ducts at porta hepatis (*arrows*). A surgical pancreatic duct stent (*arrowhead*) is noted.

B, An AtheroCath (*straight arrow*) is positioned through an introducing sheath (*arrowheads*) at stricture of common bile duct. A safety wire (*curved arrow*) is also placed through introducing sheath with its tip in jejunum.

C, Gross specimen from atherectomy catheter biopsy.

An 8.3-French internal-external biliary drainage catheter was subsequently placed. Six days later, the common bile duct stricture was brushed with two separate biopsy brushes. Immediate cytologic interpretations of both brush biopsy samples showed only normal mucosal cells. A 7-French atherectomy catheter was then introduced through a long 9-French sheath and positioned at the site of the obstruction, where multiple samples were taken circumferentially. Four soft yellowish-white tissue cores (1.0–1.5 mm wide, 20 mm long) were obtained. After the biopsy, a 10.2-French internal-external biliary drainage catheter was placed. There were no procedural complications.

Histologic examination of the atherectomy catheter biopsy specimen revealed recurrent adenocarcinoma. Four days later, CT of the abdomen also revealed multiple metastatic lesions in the liver. Thereafter, the patient underwent placement of a 12-French Miller double-mushroom biliary endoprosthesis (Cook, Inc., Bloomington, IN).

Case 2

A 58-year-old man was admitted for evaluation of painless jaundice and weight loss. Sonography and CT showed dilatation of the extrahepatic bile ducts but no masses in the abdomen. A presumptive diagnosis of malignant extrahepatic biliary obstruction was made. The patient underwent a Whipple procedure for a small carcinoma in the head of the pancreas discovered during surgery. The surgical margins and regional lymph nodes were free of tumor. The patient was treated postoperatively with radiation therapy and chemotherapy.

The patient did well until 8 months after surgery when a fever (103.4°F) developed. CT revealed no evidence of recurrent tumor or dilated bile ducts. The patient underwent percutaneous transhepatic cholangiography, which showed a severe focal narrowing of the common bile duct at the jejunal anastomosis (Fig. 1A). Subsequently, an 8.3-French internal-external biliary drainage catheter was placed. Six months after placement of the biliary drainage tube, the stricture of the common bile duct was brushed with two separate biopsy brushes. Both of the brush biopsies were negative for malignant cells on immediate cytologic interpretation. An 8-French atherectomy catheter was then introduced via a long 9-French sheath and placed at the site of anastomotic narrowing for biopsy (Fig. 1B). Four tan to dark red soft-tissue fragments (1–2 mm wide, 1–3 mm long) were obtained after four cuts (Fig. 1C). Histologic examination of these specimens revealed atypical cells suspicious for malignancy. The patient tolerated the procedure well without complications. A 10-French biliary drainage catheter was then placed with its tip in the jejunum for internal drainage. CT of the abdomen 1 month after the biopsy showed interval development of metastatic lesions in the liver, but still no mass around the common bile duct at the level of obstruction.

Discussion

Postoperative stricture of the common bile duct after a Whipple procedure occurs at the anastomotic site to the intestine either because of benign postsurgical scarring or recurrent malignant tumor. These causes can be difficult to distinguish from each other. Results of percutaneous transhepatic cholangiography or ERCP are usually not diagnostic. Metastases or recurrent mass lesions at the surgical site can be evaluated with CT or sonography, but these findings are often absent even in the presence of obstructive jaundice. Percutaneous needle aspiration can be performed but is extremely difficult when no obvious masses are present, as in our patients [3–5]. Brush biopsy of the obstruction of the bile duct can be performed through the existing biliary drain-

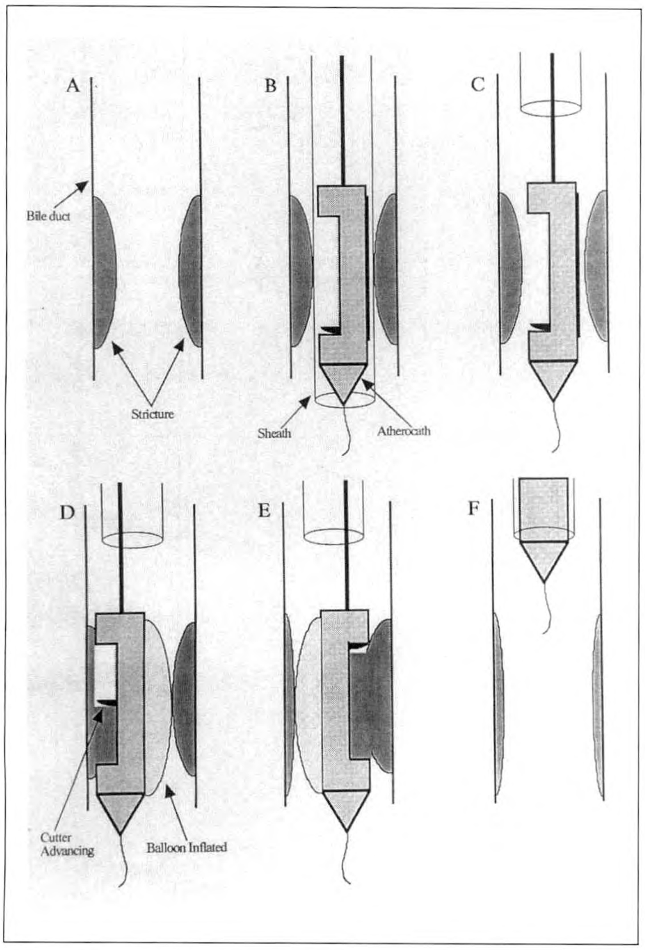

Fig. 2.—*A* and *B*, Atherectomy catheter is introduced through a long sheath and positioned at stricture of common bile duct.

C, Introducing sheath is withdrawn to unsheath atherectomy catheter in contact with stricture in common bile duct.

D and *E*, After inflation of atherectomy catheter balloon, cutter is advanced and multiple samples are taken circumferentially.

F, Atherectomy catheter is withdrawn.

age catheter tract [4, 6]. However, its sensitivity is not high, ranging from 57% to 67% [4, 6], because only the mucosal layer of the bile duct is usually sampled, and often the tumor grows predominantly in the submucosal layers without intraluminal invasion [4, 6]. Thus, we used the atherectomy catheter to obtain deeper biopsy specimens from the lesions of the common bile duct, including the submucosal layers. The atherectomy catheter biopsies in our two patients provided histologic specimens, one of which was diagnostic and one of which was highly suspicious, whereas the brush biopsy results in both patients were false-negative.

Without a long introducer sheath, considerable technical difficulties can occur: (1) in advancing the rigid distal part of the atherectomy catheter, by itself, through the acutely angled branches of the biliary ducts and (2) in positioning the atherectomy catheter within the severe irregular luminal narrowing at the lesion. The biliary drainage catheter course often changes acutely from transverse to longitudinal at the porta hepatis, as in our case 2 (Fig. 1). This acutely angled course can offer significant resistance to or prevent smooth advancement of the rigid cutter housing/collection chamber assembly. With resultant buckling and kinking of the leading frail floppy guidewire tip, further atherectomy catheter advancement may risk trauma to the bile ducts, including potential perforation by the stiff end of the atherectomy catheter. We found long (24-cm) introducer sheaths (C.R. Bard, Covington, GA) very helpful for allowing smooth passage of the stiffer distal part of the atherectomy catheter through angulations of the bile ducts and through distal obstructions in the common bile duct.

In conclusion, this small experience indicates that the Simpson atherectomy catheter can be used successfully for percutaneous biopsy through drainage catheter tracts, yielding material sufficient for histologic analysis. Because the atherectomy catheter is expensive and involves more manipulation, we still use brush biopsy as our first approach. We reserve atherectomy catheter biopsy only for patients in whom our initial brush biopsy is negative. We do not recommend that atherectomy catheter biopsy be performed routinely. Although we did not have any complications associated with our two procedures, we recognize the potential for injury to the bile ducts during passage of the rigid metal cutter housing. The use of a long sheath for introducing and positioning the atherectomy catheter appears to facilitate this procedure and make it safer.

REFERENCES

1. Schwarten DE, Katzen BT, Simpson JB, Cutcliff WB. Simpson catheter for percutaneous transluminal removal of atheroma. *AJR* **1988**;150:799–801
2. Newman GE, Miner DG, Sussman SK, et al. Peripheral artery atherectomy: description of technique and report of initial results. *Radiology* **1988**;169:677–680
3. Hall-Craggs MA, Lees WR. Fine-needle aspiration biopsy: pancreatic and biliary tumors. *AJR* **1986**;147;399–403
4. Mendez G Jr, Russell E, Levi JU, et al. Percutaneous brush biopsy and internal drainage of biliary tree through endoprosthesis. *AJR* **1980**;134:653-659
5. Foutch PG, Harian JR, Kerr D, Sanowski RA. Wire-guided brush cytology: a new endoscopic method for diagnosis of bile duct cancer. *Gastrointest Endosc* **1989**;35:243-247
6. Cropper LD Jr, Gold RE. Simplified brush biopsy of the bile ducts. *Radiology* **1983**;148:307–308

Come to the
American Roentgen Ray Society
91st
ANNUAL MEETING

Boston, MA

Sheraton Boston Hotel
May 5-10, 1991

Scientific Program (200 papers)
Instructional Courses (60 hours)
Categorical Course on Body MR Imaging
The Caldwell Lecture
Award Papers
Scientific Exhibits
Social, Golf, and Tennis Programs
Guest Programs

Case Report

Obstructing Villous Adenoma and Papillary Adenomatosis of the Bile Ducts

David L. Harshfield,[1] Steven K. Teplick,[1] Mike Stanton,[2] Kishore Tunuguntla,[3] Wilma C. Diner,[1] and Raymond C. Read[2]

Benign mucosal tumors of the bile ducts are extremely uncommon [1], and the cholangiographic appearance of bile duct villous adenomas and papillary adenomas has not been described in the radiologic literature. We describe a patient who had obstructive jaundice caused by a large villous adenoma in the common bile duct. In addition, the patient had diffuse ductal papillary adenomatosis. The patient was followed up for 14 years before a definitive diagnosis was established.

Case Report

A 78-year-old man originally presented in 1975 with chest pain. Findings on a chest radiograph and an upper gastrointestinal series were normal. The patient had several normal gastrointestinal studies for nonspecific abdominal complaints in 1978 and 1980. In January 1982, he returned with persistent pain in the right upper quadrant. An oral cholecystogram revealed poor visualization of the gallbladder, and results of a sonogram were normal.

In April 1982, the patient presented with acute abdominal pain and subsequently underwent exploratory laparotomy. A cholecystectomy was performed, presumably because the acute abdominal symptoms were due to nonalcoholic pancreatitis. An intraoperative T-tube cholangiogram showed either a filling defect of the distal common bile duct or spasm of the papilla of Vater. This abnormality persisted on follow-up cholangiograms, and 1 month after the cholecystectomy, the patient underwent a common bile duct exploration, which revealed a polypoid lesion in the distal common bile duct (Fig. 1A). Multiple biopsy samples were obtained, and the histologic diagnosis was papillary adenoma. A T-tube was reinserted and choledochojejunostomy was performed. The decision to perform a definitive operation such as the Whipple procedure was deferred, because of the presumed benign nature of papillary adenomas in the common bile duct. In 1989, the patient presented with pain in the right lower quadrant and midepigastric area. An upper gastrointestinal series showed enlargement of the papilla of Vater (Fig. 1B). An ERCP was performed, which showed a mass in the common bile duct causing partial obstruction (Fig. 1C). A CT scan showed enlargement of the head of the pancreas, but was otherwise normal.

At surgery, the common bile duct was opened and biopsy samples were obtained, which revealed a benign villous adenoma. An attempt was made to take biopsy samples proximal to the tumor, but repeated biopsies showed tumor in the resected margins. Finally, a hepaticojejunostomy was performed. In addition to the villous adenoma, the patient had diffuse papillary adenomatosis extending into the right and left intrahepatic ducts. Biopsies of the head of the pancreas revealed chronic pancreatitis. The patient recovered uneventfully, and his postoperative course has remained uneventful.

Discussion

This case is unusual not only because of the rarity of bile duct obstruction from a benign tumor, but also because it is the first reported case documenting the progression of a single benign bile duct tumor to multiple benign tumors of different histologic types. The initial diagnosis was a papillary adenoma of the distal common bile duct, which, during 7 years, progressed to diffuse papillary adenomatosis plus the

---

Received November 20, 1989; accepted after revision January 3, 1990.

[1] Department of Radiology, University of Arkansas for Medical Sciences, 4301 W. Markham St., Little Rock, AR 72205. Address reprint requests to S. K. Teplick at Slot 556.

[2] Department of Surgery, University of Arkansas for Medical Sciences, 4301 W. Markham St., Little Rock, AR 72205.

[3] Department of Gastroenterology, University of Arkansas for Medical Sciences, 4301 W. Markham St., Little Rock, AR 72205.

AJR 154:1217–1218, June 1990 0361–803X/90/1546–1217 © American Roentgen Ray Society

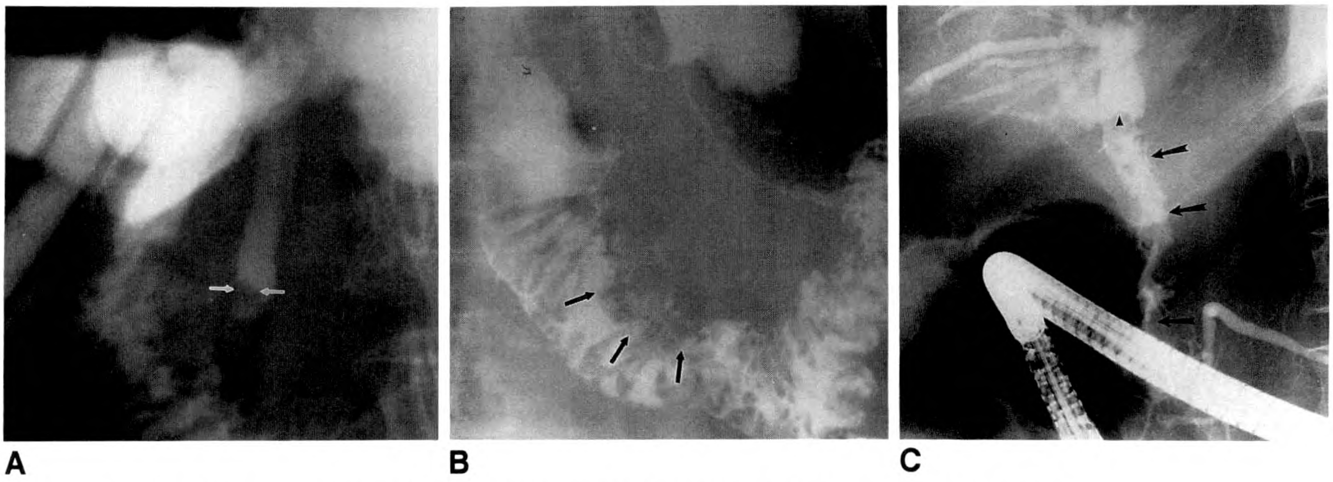

Fig. 1.—*A*, Cholangiogram reveals a polypoid filling defect in common bile duct just proximal to papilla of Vater (*arrows*).
B, Upper gastrointestinal series shows a mass in region of papilla of Vater (*arrows*).
C, ERCP reveals common bile duct to be diffusely abnormal from papilla to just proximal to level of bifurcation of right and left intrahepatic ducts (*arrows*), where there is an abrupt transition (*arrowhead*). In involved area, multiple polypoid filling defects with diffuse mucosal abnormality represent villous adenoma. More proximally located area of diffuse papillary adenomatosis is not shown.

formation of a large villous adenoma, causing obstruction of the common bile duct.

In 1967, Edmondson presented a classification of benign tumors of the bile ducts in which all benign epithelial tumors are classified as adenomas [2]. Distinctions were made according to the gross configuration of the tumors. The tumors were divided into papillary adenomas, pedunculated adenomas, and sessile adenomas; this classification replaced an earlier classification of papillomas, polyps, and adenomas, respectively [3]. Villous adenomas are thus classified as frondlike sessile adenomas, and papillomas are classified as papillary adenomas. Histologically, the most common benign tumors are adenomas [2]. These almost always arise in the common bile duct, with only a single case arising in the intrahepatic ducts [4]. Other histologic types reported are fibroma, lipoma, neuroma, granuloma, melanoma, and carcinoid [5].

The frequency of benign epithelial tumors in the bile ducts is not known, but is much lower than that in the gallbladder (these tumors occur in the gallbladder in about 1% of the population), even though the gallbladder and bile ducts are lined with the same mucosal epithelium.

In a few reported cases, benign bile duct tumors caused symptoms, but most were incidentally discovered during treatment for other biliary problems such as gallstones or cholecystitis. In our patient, the tumors themselves caused intermittent symptoms, which eventually led to definitive surgery. These benign lesions are thought to remain dormant for long periods and, in their early stages of the disease, cause vague and variable symptoms [5]. In other reported cases, the duration of symptoms referable to the gastrointestinal tract or biliary system varied from several weeks to 12 years. Usually, untreated patients eventually present with progressive biliary obstruction. Rarely these tumors cause acute severe biliary colic.

Several investigators think that any adenoma in the gastrointestinal tract is premalignant [3, 5]. Although only a few cases of villous adenomas in the common bile duct have been reported, most either were malignant or resulted in the patient's death because of their aggressive behavior [6, 7]. The serious prognosis of this tumor warrants aggressive treatment. Unfortunately, partial lobectomy, curettage, or debulking procedures have not had much success [6–8]. Some success was reported in one patient who was given systemic chemotherapy with BCNU (1,3-bis[2-choroethyl]-1-nitrosourea) late in the course of the disease [7]. This resulted in regression of tumor mass, although the patient eventually died. A technique described by Smith [8] indicates that direct instillation of chemotherapeutic agent into the biliary drainage catheter can be even more effective.

In our patient, the entire tumor was not excised. There might be residual malignant foci or eventual proliferation of the tumors causing ductal obstruction. However, for a 78-year-old patient without a diagnosis of malignancy, the operation performed was considered preferable to a Whipple procedure.

REFERENCES

1. Saxe J, Lucas C, Ledgerwood AM, Sugawa C. Villous adenoma of the common bile duct. *Arch Surg* **1988**;123:96–97
2. Edmondson HA. *Tumours of the gallbladder and extrahepatic bile ducts*. Washington, DC: Armed Forces Institute of Pathology, **1967**
3. Hulten J, Johannson H, Olding L. Adenomas of the gallbladder and extrahepatic bile ducts. *Acta Chir Scand* **1970**;136:203–207
4. McIntosh AM, Gilles AD. Two tumours of the extrahepatic bile ducts. *Med J Aust* **1940**;1:268–269
5. Chu PR. Benign neoplasms of the extrahepatic biliary ducts. *Arch Pathol Lab Med* **1950**;50:84–97
6. Neumann RD, LiVolsi VA, Rosenthal NS, Burrell M, Ball TJ. Adenocarcinoma in biliary papillomatosis. *Gastroenterology* **1976**;70:779–782
7. Madden JJ, Smith GW. Multiple biliary papillomatosis. *Cancer* **1974**;34:1316–1320
8. Smith R. Hepaticojejunostomy with transhepatic intubation. *Br J Surg* **1964**;51:186–194

Case Report

Combined Systemic and Portal Venous Gas: Sonographic and CT Detection in Two Cases

J. Scott Kriegshauser,[1] Carl C. Reading, Bernard F. King, and Timothy J. Welch

Portal venous gas is seen on plain abdominal films of patients with ischemic necrotic bowel and also occurs as a benign or incidental finding [1]. We report two cases with the unusual finding of systemic venous gas, seen by CT and sonography, in conjunction with portal venous gas. In one case, gas appeared to pass through the liver from the portal veins into the hepatic veins during observation with real-time sonography.

Case 1

A 68-year-old man with Gardner syndrome and multiple previous abdominal operations presented elsewhere with fever, leukocytosis, and one of three blood cultures positive for *Bacteroides*. He had a large palpable abdominal mass known to be a recurrent desmoid tumor. Fevers persisted intermittently, even after IV administration of antibiotics. He was referred to our institution after air in the portal venous system or biliary tree was seen on CT. A mass was palpated in the mid abdomen, and mild tenderness was noted in the right upper quadrant. Sonography revealed increased echogenicity throughout the liver. It was uncertain whether this was portal venous gas or air in the biliary tree because of the marked attenuation of the beam, which obscured most of the liver. CT showed air in the peripheral portions of the liver, consistent with portal venous gas (Fig. 1A). A large, partially necrotic mass in the right lower abdomen involved the small-bowel mesentery and surrounded or invaded several loops of small bowel (Fig. 1B). CT scans through the pelvis showed systemic venous gas within the prostatic venous plexus and the common femoral veins (Fig. 1C). At surgery, the mesenteric desmoid tumor was debulked, and several loops of jejunum and ileum were resected. Some of these loops had bluish discoloration suggesting ischemia. The patient did well postoperatively.

Case 2

A 54-year-old man had been treated with radiation and chemotherapy between 1964 and 1973 for Hodgkin lymphoma of the mediastinum. No evidence of recurrent lymphoma was found at surgery in October 1988, but mediastinal fibrosis had developed, obstructing the right ventricular outflow and causing progressive right heart failure. His postoperative course was complicated by recurrent pneumothoraces. Septicemia developed 2 weeks later; blood cultures were positive for *Candida* and coagulase-negative *Staphylococcus*. Subsequent blood cultures also grew *Corynebacterium*. Renal and liver failure developed, and blood cultures remained positive for *Candida*, even with amphotericin B treatment. The patient remained intubated with positive-pressure ventilation at 6 cm H_2O for 2 weeks; his systolic blood pressure was 40–50 mm Hg despite administration of dopamine and epinephrine. Sonography showed multiple discrete air bubbles flowing through the portal vein into the liver (Fig. 2A). These bubbles appeared as discrete echogenic foci that produced multiple spikes on the Doppler spectral display (Fig. 2B). Air bubbles also were seen in great numbers within the hepatic veins, flowing from the liver into the inferior vena cava (Fig. 2C). Physical examination of the abdomen was unremarkable, but the patient was unresponsive. Plain films showed evidence of pneumatosis coli but no air could be identified in the liver. Later that day, repeated sonography showed occasional bubbles in the portal vein, but many fewer than had been seen previously. No air was seen in the hepatic veins or inferior vena cava at that time. The patient died shortly after the

---

Received December 26, 1989; accepted after revision January 30, 1990.

[1] All authors: Department of Diagnostic Radiology, Mayo Clinic and Mayo Foundation, 200 First St. S.W., Rochester, MN 55905. Address reprint requests to C. C. Reading.

AJR 154:1219–1221, June 1990 0361–803X/90/1546–1219 © American Roentgen Ray Society

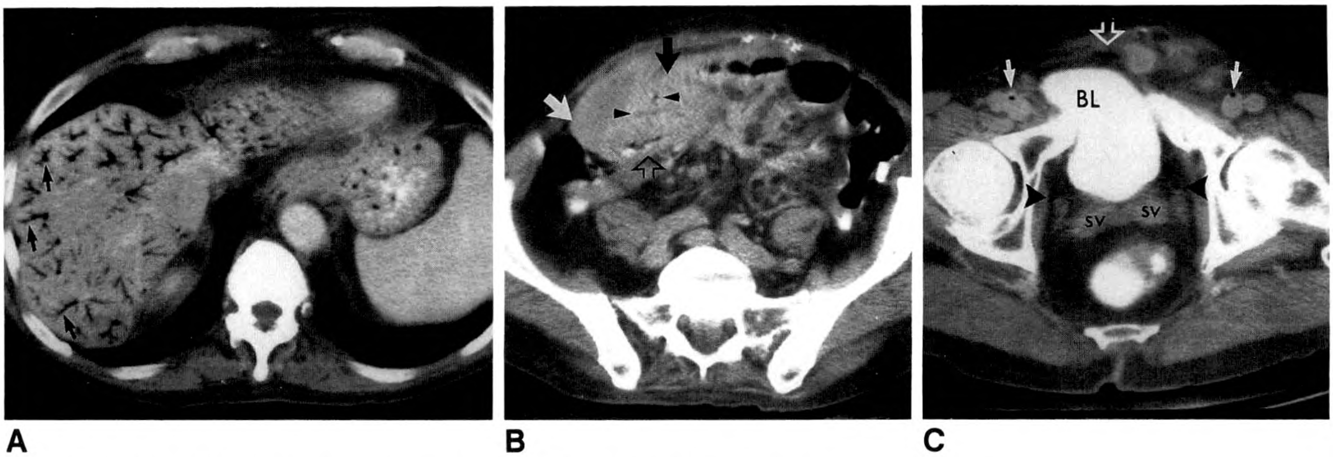

Fig. 1.—*A*, CT scan of upper abdomen shows gas in peripheral portal veins of liver (*arrows*).
B, CT scan of lower abdomen shows soft-tissue mass (*solid arrows*) containing small amount of gas (*arrowheads*). At surgery, mesenteric desmoid tumor was found involving several loops of small bowel (*open arrow*).
C, CT scan of lower pelvis shows gas in both common femoral veins (*white arrows*). Gas also was noted in periprostatic venous plexus (*arrowheads*) adjacent to seminal vesicles (SV). A small amount of gas also was present in several small veins (*open arrow*) just anterior to bladder (BL).

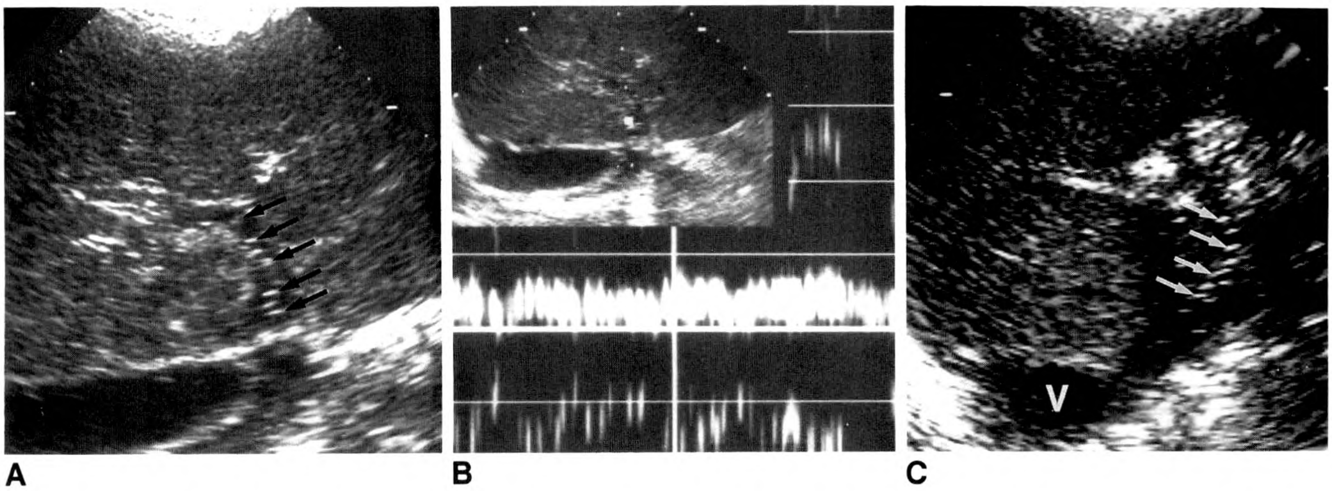

Fig. 2.—*A*, Sonogram of liver shows multiple discrete air bubbles (*arrows*) flowing through portal vein into liver.
B, Spectral Doppler display of air bubbles in portal vein.
C, Sonogram of liver shows multiple discrete air bubbles (*arrows*) flowing through middle hepatic vein into inferior vena cava (V).

second sonographic examination. Permission for autopsy was refused.

Discussion

Systemic venous gas most commonly occurs iatrogenically or after trauma [2]. It has never been shown to be a cause of portal venous gas because air emboli are trapped in the pulmonary or systemic capillaries. We have found only two reports of systemic venous gas associated with portal venous gas. One described an infant with necrotizing enterocolitis and a patent ductus venosus that allowed the portal venous gas to enter the inferior vena cava and the heart, which was detected by sonography [3]. In the other case, fulminant sepsis was due to a gas-forming organism; plain films showed portal venous gas and systemic venous gas [4].

In our first case, the portal venous gas almost certainly was related to ischemic bowel or an enterovenous fistula caused by the tumor. The systemic venous gas most likely was related to the multiple previous operations and the development of systemic venous drainage from the bowel or portosystemic fistulas so that the source of the air would be the same as for the portal venous gas. Septicemia as a cause of intravascular air is usually an agonal event and is unlikely to be the cause of systemic venous gas in this patient, who had only mild symptoms.

In our second case, the source of the portal venous gas was not documented pathologically but, given the plain film findings of pneumatosis coli and the clinical situation of hypotension, ischemic bowel was the most likely cause. Real-time visualization of portal venous gas, presumably extending from the portal veins through the liver sinusoids into the hepatic veins, as in this case, has never been reported, to our knowledge. One previous report specifically stated that air should not be seen within the hepatic veins or inferior vena cava [5]. It is known that the central vein and sinusoids in the liver become dilated and engorged when chronic right ventricular failure occurs. The perisinusoidal spaces open as an agonal event [6]. We suspect that the vascular spaces in this patient were large enough to allow tiny bubbles to pass through into the hepatic veins. A portal vein–to–hepatic vein fistula (e.g., with a hamartoma) is a less likely possibility. Septicemia with a gas-forming organism cannot be excluded, but this does not account for the apparent passage of air through the liver in this patient.

A potential source of confusion during sonography is the presence of multiple low-level echoes that can be seen within blood vessels that contain slowly flowing blood. These echoes are thought to be due to the erythrocytes or aggregates [7]. The echoes from intravascular air can be distinguished from those from erythrocytes by their highly reflective appearance and large spikes on the Doppler spectral display. Tiny microbubbles can be seen on sonography after IV injections and are used with echocardiography for detecting cardiac shunts. These microbubbles are presumably formed in the injection tubing or are caused by turbulence distal to the relatively narrow needle [8]. The location and circumstances of the intravascular gas found in the two cases presented here make this phenomenon an unlikely cause.

Thus, the two cases presented here represent two widely different presumed mechanisms of development of systemic venous gas. The first is communication of the systemic venous system with a gastrointestinal tract that has been involved by desmoid tumor in a patient who had had multiple abdominal operations; the second is the direct passage of gas from the portal vein into the hepatic veins through the liver as an agonal event.

REFERENCES

1. Griffiths DM, Gough MH. Gas in the hepatic portal veins. *Br J Surg* **1986**;73:172–176
2. Kizer KW, Goodman PC. Radiographic manifestations of venous air embolism. *Radiology* **1982**;144:35–39
3. Malin SW, Bhutani VK, Ritchie WW, Hall ML, Paul D. Echogenic intravascular and hepatic microbubbles associated with necrotizing enterocolitis. *J Pediatr* **1983**;103:637–640
4. Jones B. Massive gas embolism in *E. coli* septicemia. *Gastrointest Radiol* **1981**;6:161–163
5. Laing FC, Rego JD Jr, Jeffrey RB. Ultrasonographic identification of portal vein gas. *JCU* **1984**;12:512–514
6. Sherlock S. The liver in circulatory failure. In: Schiff L, ed. *Diseases of the liver*, 4th ed. Philadelphia: Lippincott, **1975**:1037–1042
7. Machi J, Sigel B, Beitler JC, Coelho JCU, Justin JR. Relation of in vivo blood flow to ultrasound echogenicity. *JCU* **1983**;11:3–10
8. Kort A, Kronzon I. Microbubble formation: in vitro and in vivo observation. *JCU* **1982**;10:117–120

Book Review

Clinical Urography. An Atlas and Textbook of Urological Imaging, vols. 1–3. Edited by Howard M. Pollack. Philadelphia: Saunders, vol. 1, 1152 pp.; vol. 2, 2169 pp.; vol. 3, 1072 pp.; 1990. $395/set

This work is divided into eight parts: an introduction to urologic imaging; urologic imaging techniques; specific diseases of the urinary tract; the adrenal glands; other retroperitoneal diseases; miscellaneous disorders of the urinary tract; renal failure, dialysis, and transplantation; and interventional uroradiology. It has 16 associate editors, all well-known uroradiologists; six consulting urologists; and 197 listed contributors, many of whom are recognized authorities. The illustrations include plain films, sonograms, CT scans, MR images, conventional urologic contrast examinations, nuclear scans, and angiograms. The quality of the radiologic images is, with few exceptions, excellent. Unavoidably in a work of this magnitude, some of the CT scans, sonograms, and MR images were produced with dated equipment; nevertheless, they make the intended points. The line drawings and tables are also excellent. The quality of the cover, binding, and paper is first-rate. The price is quite reasonable. The references at the end of each chapter are extensive and current through 1986; some 1987 and 1988 citations are given. The book was designed primarily for radiologists and urologists. The editor's aim is to "comprehensively cover the field of uroradiology in its broadest context." Befitting his training both as a urologist and as a radiologist, he has tried to "make [the book] above reproach as a source of urological information as well [as radiologic information]."

Part I (three chapters) is an introduction to urologic imaging, medicolegal issues, and radiation protection. This part will be of interest mostly to trainees and for reference. Part II comprises 15 chapters that discuss contrast material and all urologic imaging techniques. The chapter on contrast material is a relatively brief overview that concentrates on toxicity and on adverse reactions and their treatment. Unfortunately, probably because of time constraints, the controversies surrounding the newer, lower osmolar media are not addressed. The chapter on plain films covers a remarkable amount of material in 63 pages; by not limiting himself to genitourinary disease, the author has created a chapter in which the discussion is generally too superficial for radiologists but excellent for urologists. Excretory urography, retrograde pyelography, and cystourethrography of both adults and children are covered from a technical aspect. A short chapter discusses the radiologic evaluation of urinary diversions, seminal vesiculography and vasography, and cavernosonography. Many out-of-date illustrations weaken the otherwise excellent chapter on urosonography. Color Doppler imaging is not included. The chapters on CT and MR concentrate on technique and normal anatomy, whereas all the preceding chapters discuss diseases; this creates some overlap with Part III. Chapters on angiography, digital angiography, and lymphangiography are primarily technical, with some general principles of interpretation included. The chapter on urologic nuclear medicine is a good discussion of technique but is overly enthusiastic about the role of radionuclides in modern uroradiology.

Part III, which covers specific disorders of the urinary tract, is the meat of the book for my money. Separate sections on congenital anomalies, inflammatory disease, cystic disease, neoplastic disease, trauma, obstruction, calculous disease, neuromuscular disease, vascular disease, and renal parenchymal disease give masterful, encyclopedic discussions of genitourinary diseases. Part IV, on adrenal disease, and Part V, on retroperitoneal masses, pelvic lipomatosis, and retroperitoneal fibrosis, are equally excellent. Part VI includes conditions that do not fall neatly into earlier categories—genitourinary manifestations of endometriosis and amyloidosis, foreign bodies, hernias, fistulas, and postoperative appearances—and is excellent. Part VII on renal failure, dialysis, and transplantation is well done and is extraordinarily up to date, especially the chapter on imaging renal transplants. The field of interventional uroradiology has burgeoned in the past 10 years, and Part VIII is an excellent compendium of the latest techniques and their indications and complications. It competes favorably with similar material in other textbooks on interventional radiology.

This is the standard uroradiologic reference textbook for today, and it will remain so for at least the near future. I enthusiastically recommend it to all radiologists interested in uroradiology and to all urologists. It is essential for every radiology and urology departmental library. The text is easy to read and is illustrated profusely. It would not be unreasonable to expect all radiology residents to read it cover to cover at some time during their residency if enough copies are provided in each training program.

Arnold C. Friedman
Temple University Hospital
Philadelphia, PA 19140

Intrarenal Arterial Doppler Sonography in Patients with Nonobstructive Renal Disease:

Correlation of Resistive Index with Biopsy Findings

Joel F. Platt[1]
James H. Ellis[1]
Jonathan M. Rubin[1]
Michael A. DiPietro[1]
Aileen B. Sedman[2]

The resistive index (RI), calculated from the duplex Doppler waveform, was compared with clinical and laboratory findings and the results of renal biopsy in 41 patients with nonobstructive (medical) renal disease. Kidneys with active disease in the tubulointerstitial compartment had a mean RI of 0.75 ± 0.07. This was statistically significantly different ($p < .01$) from the RI in kidneys with disease limited to the glomeruli (mean RI of 0.58 ± 0.05). Acute tubular necrosis resulted in an elevated RI (mean RI = 0.78 ± 0.03) as did vasculitis/vasculopathy (mean RI = 0.82 ± 0.05). Patients with hypertension, proteinuria, or hematuria did not have kidneys with a significantly higher RI than did patients without these clinical factors. Kidneys found to be abnormally echogenic did not have an RI significantly different from kidneys of normal echogenicity. There was a weak correlation between creatinine level and RI value, reflected by a linear correlation coefficient of 0.34. In patients with normal renal RIs, the mean creatinine level was 1.7 ± 1.7, whereas in those with abnormal RI values (≥0.70), the mean creatinine level was 3.7 ± 3.6.

We conclude that some forms of nonobstructive renal disease can produce changes in the Doppler waveform detectable by RI measurement. The production of Doppler waveform changes is strongly influenced by the site of the main disease within the kidneys. Active disease within the tubulointerstitial compartment (acute tubular necrosis, interstitial nephritis) or vasculitis/vasculopathy generally resulted in an elevated RI, whereas disease limited to the glomeruli, no matter how severe, did not significantly elevate the RI. Degree of renal dysfunction as indicated by serum creatinine level probably affects the Doppler waveform to some degree, but the relationship is weak.

***AJR* 154:1223–1227, June 1990**

Sonography is often used as the initial imaging procedure in the examination of patients with renal failure. Aside from excluding hydronephrosis, sonography is generally not helpful in characterizing the type of renal disease, especially if the renal failure is acute [1–3]. Investigators have attempted to apply traditional sonographic parameters such as kidney size and relative echogenicity to the identification and characterization of renal disease [4–6]. In the vast majority of cases of renal failure (especially acute or subacute), the real-time sonographic examination is normal [1–3, 7, 8].

We recently reported the use of duplex Doppler sonography to assist in differentiating obstructive from nonobstructive pyelocaliectasis [9, 10]. As part of that study, we examined 50 patients with nonobstructive renal disease (renal medical disease) and found abnormal intrarenal arterial Doppler signals (resistive index [RI] ≥ 0.70) in just over half [10]. The other half had normal Doppler tracings despite often significant renal disease. It appeared clear that certain renal diseases produced states of increased renal vascular resistance (resulting in RI elevation), whereas other renal diseases produced no significant Doppler changes.

Recently two studies have demonstrated Doppler changes in small groups of children with renal failure [11, 12]. However, detailed pathologic correlation was

Received November 1, 1989; accepted after revision January 22, 1990.

[1] Department of Radiology, University of Michigan Medical Center, 1500 E. Medical Center Dr., Ann Arbor, MI 48109-0030. Address reprint requests to J. F. Platt at UH B1D520/0030.

[2] Department of Pediatrics, Section of Pediatric Nephrology, A. Alfred Taubmen Center, Rm. 1924, Box 0318, University of Michigan Medical Center, Ann Arbor, MI 48109-0318.

0361–803X/90/1546–1223
© American Roentgen Ray Society

not possible in these series because renal biopsies were not uniformly obtained. The purpose of this study is to determine if specific nonobstructive renal diseases alter the Doppler signal. We did this by correlating Doppler data with renal biopsy findings. The results may provide a basis for the use of duplex Doppler sonography in patients with renal failure.

Subjects and Methods

Between January 1989 and September 1989, bilateral duplex Doppler and standard gray-scale real-time sonography was performed prospectively on 86 kidneys in 43 patients (age range, 6–80 years) before renal biopsy. In two of the patients, the renal biopsy specimens were deemed inadequate for characterization of the renal disease and were therefore excluded from our study. Patients with hydronephrosis also would have been excluded, if any had been encountered. The study is therefore based on findings in 41 patients (82 kidneys) in whom unilateral kidney biopsy was adequate for diagnosis.

Real-time sonographic examination with a 3.5-MHz transducer (Acuson 128, Mountain View, CA) or a 3-MHz transducer (Advanced Technology Laboratories, Bothell, WA) and a pulsed Doppler examination of intrarenal arteries were performed on both kidneys before biopsy. For the Doppler study, the wall filter was set to the minimum (50 Hz for ATL and 125 Hz for Acuson) and the sample volume was set at 2–5 mm. Doppler signals were in general obtained from arcuate arteries at the corticomedullary junction and/or interlobar arteries along the border of medullary pyramids. At least two, and in most cases three, different renal vessels were studied with duplex Doppler imaging for each kidney.

Multiple Doppler tracings and a standard gray-scale examination of the kidney were recorded on film. From the hard copy, the RI (defined as [peak systolic frequency shift − minimum diastolic frequency shift]/peak systolic frequency shift) was determined from hand measurements made with a caliper. The RI for each vessel was calculated as an average value obtained from three to five waveforms. Mean RI measurements and standard deviations also were calculated for each kidney and each patient (averaging both kidneys). For purposes of RI correlation with other data, we considered an RI of 0.70 or higher as elevated. This value for a discriminatory RI level is based on our and others' experience with obstructed, medically diseased, and normal native kidneys [9–11, 13].

In addition to a detailed Doppler study, a real-time examination of each kidney was performed. This included longitudinal images of the right kidney and liver to allow assessment of relative renal cortical echogenicity. Kidneys were considered abnormally echogenic if the echo intensity of the cortex of the right kidney was greater than that of adjacent liver. Kidneys with echogenicity equal to that of the adjacent liver were not included as abnormal because our earlier work has shown that this criteria of abnormality includes too many normal kidneys [7].

Renal biopsies were performed with a Tru-Cut biopsy needle (Baxter Health Care Corp., Deerfield, IL) by using sonographic localization of the lower pole of the kidney. The paraffin-embedded sections of the biopsy specimens were reviewed by light microscopy, immunofluorescence, and electron microscopy to determine the diagnosis and the primary site of pathologic changes for each biopsy specimen. An attempt was made to determine if the dominant process was within the nephron (glomeruli), was in the tubulointerstitial compartment, or was vascular. In some biopsy specimens, more than one significant process was evident. The degree of activity and/or chronicity also was assessed if possible for each biopsy specimen. The most common renal diseases in our study were lupus nephritis (12 patients), IgA/IgM nephropathy (four patients), membranoproliferative glomerulonephritis (four patients), and acute tubular necrosis (five patients).

The sonographic and pathologic data were analyzed separately and blindly and correlated with the clinical history and laboratory studies. In all cases, creatinine values from within 24 hr of the biopsy were available for correlation. Creatinine values exceeding 1.3 mg/dl in adults and exceeding age-corrected levels in pediatric patients were considered abnormal. In addition, the presence or absence of proteinuria, hematuria, and hypertension was determined for each patient. The two-tailed Student's t test was used to determine significance of any difference between groups. Statistically, p values less than .05 were considered significant. Linear correlation analysis was performed for the data on RI and creatinine.

Results

The mean RI for the 41 patients (82 kidneys) in our study was 0.68 ± 0.10. Using a discriminatory RI value of 0.70, we found 35 abnormal kidneys and 47 normal kidneys.

As more than one vessel was studied within a particular kidney, we were able to determine any significant variation in mean RI measurements between different sites in the kidney. In general, the amount of variation in RI for different sites within a particular kidney was not great, averaging 4.0%. In addition, we compared the mean RI values between both kidneys in a given patient. The mean difference between the RIs was 0.02, with a range of 0.00 to 0.06. In only one case was the RI of one kidney below the discriminatory level of 0.70 and that of the other kidney above this level (RI values of 0.68 and 0.71).

Renal biopsy findings were analyzed and an attempt was made to classify the location of the primary abnormality as within the nephron (glomeruli), the tubulointerstitial compartment, or within the vascular compartment. However, in some cases more than one significant form of renal disease was present. In all, there were 16 patients (including one of the five patients with evidence for acute tubular necrosis) who had acute/active interstitial nephritis, often accompanied by chronic interstitial changes. In this group, the mean RI was 0.73 ± 0.07, and 24 of the 32 kidneys had an elevated RI ($\geq$0.70). In addition, there were four patients with acute tubular abnormality without significant interstitial nephritis. Therefore, a total of 20 patients had acute/active pathologic findings in the tubulointerstitial compartment of the kidney. In this patient group, the mean RI value was 0.75 ± 0.07, and 31 of these 40 kidneys had an abnormal RI (Fig. 1).

Two patients had a significant vasculitis/vasculopathy without associated glomerular or tubulointerstitial disease. The mean RI in these patients was 0.87 ± 0.04, with both patients' kidneys having abnormal RIs (Fig. 2).

The remaining 19 patients had renal disease essentially limited to the glomeruli with no active abnormalities in the tubulointerstitial region and no vasculitis. In these patients, the mean RI was 0.58 ± 0.05 (Fig. 3). This RI was statistically significantly different ($p < .01$) from the RI of patients with active tubulointerstitial disease. In fact, despite many kidneys having severe or acute glomerular disease, no kidney with disease essentially limited to the glomeruli had an abnormal Doppler waveform.

When all kidneys are considered, the renal biopsy revealed evidence for acute tubular necrosis in five patients with a mean RI of 0.78 ± 0.03 in this group. Nine of these 10 kidneys had an elevated RI. Five patients in this series had evidence for a significant vasculitis/vasculopathy with or without other pathologic findings. In these patients, the mean RI was 0.82 ± 0.05, with all kidneys having an elevated RI.

When the real-time sonographic data are analysed, 15 patients had echogenic kidneys and 26 patients had normal renal echogenicity. The abnormally echogenic kidneys had a mean RI of 0.71 ± 0.11, whereas normally echogenic kidneys had an RI of 0.66 ± 0.09; this difference was not statistically significant ($p > .05$).

Fourteen patients had hypertension with a mean RI of 0.70 ± 0.10, and 27 patients had no history of hypertension with a mean RI of 0.67 ± 0.09; this difference was not statistically significant. No statistically significant difference was found between mean RI values on the basis of the presence or absence of hematuria and proteinuria.

For purposes of correlating the Doppler data with creatinine level, a mean RI value was obtained for each patient by averaging the two kidneys' mean RI values. Table 1 details our data comparing RI values with creatinine levels. The linear correlation coefficient between creatinine and RI values in each patient was 0.34. In patients with a normal creatinine level, the mean RI was 0.61 ± 0.05. When all patients with an elevated creatinine level are considered, the mean RI was 0.71 ± 0.09; this was significantly different from the value for patients with a normal creatinine level ($p < .05$). For the 35 kidneys with an elevated RI (≥0.70), the mean creatinine value was 3.7 ± 3.6 (range, 1.2–16.1), whereas in the 47 kidneys with a normal RI, the patients' mean creatinine level was 1.7 ± 1.7 (range, 0.4–8.7). This difference was not statistically significant. In our series of 41 patients, two patients had an abnormal Doppler examination and a normal creatinine level, and 10 patients had a normal RI value despite an elevated creatinine level.

Discussion

Some investigators have found traditional renal sonography to be of limited value in most cases of renal failure after hydronephrosis has been excluded [1–3]. It has been our and others' experience that the sonogram is unremarkable in the majority of cases of nonobstructive renal disease [1–3]. A few investigators have attempted to use real-time sonographic parameters such as relative echogenicity and renal size to identify and characterize renal medical disease [4–6]. In our prospective study, we have found renal Doppler analysis with RI measurements to be promising in differentiating major types of renal medical disease.

Our results show the RI in kidneys with active/acute tubulointerstitial disease is significantly increased compared with the RI in kidneys that have disease essentially limited to the glomeruli ($p < .01$). This was true no matter how severe or acute the glomerular disease; without accompanying tubulointerstitial disease or vasculitis, all the RIs were normal (Fig. 3). Conversely, 31 of 40 kidneys with active tubulointerstitial disease had elevated RI measurements. The main diseases within this group were acute tubular necrosis (ATN) and interstitial nephritis (either primary or associated with other renal diseases such as lupus nephritis, cryoglobulinemia, or Wegener granulomatosis). In addition, five patients had significant vasculopathy/vasculitis in our series, and these kidneys all had abnormal Doppler waveform (mean RI, 0.82 ± 0.05) (Fig. 2). Similar changes in the Doppler waveform were recently observed with the renal microangiopathy associated with the hemolytic-uremic syndrome in children [11].

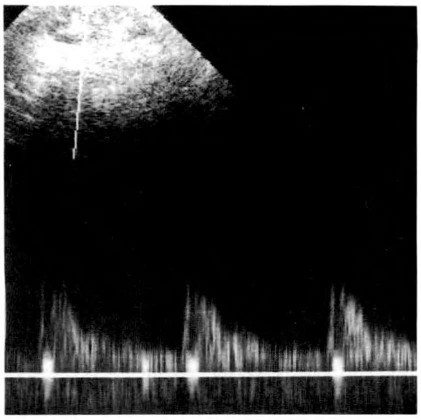

Fig. 1.—Renal Doppler sonogram of patient with acute tubular necrosis. Patient had a rapid rise in creatinine level from 1.4 to 3.1 mg/dl in 2 weeks. Standard real-time sonography of kidneys was normal. Doppler signal from intrarenal artery shows reduced end diastolic flow resulting in an elevated resistive index of 0.78. Renal biopsy was consistent with acute tubular necrosis.

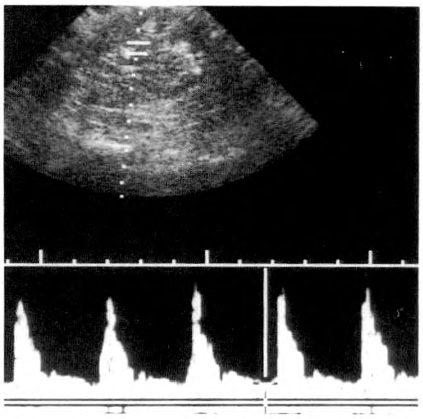

Fig. 2.—Renal Doppler sonogram of patient with vasculopathy. Creatinine level became elevated after a cardiac transplant. Standard real-time sonography was normal. Doppler signal obtained from intrarenal artery shows a significant reduction in end diastolic flow compared with peak systolic flow, resulting in an elevated resistive index of 0.83. Biopsy revealed changes consistent with cyclosporine vasculopathy.

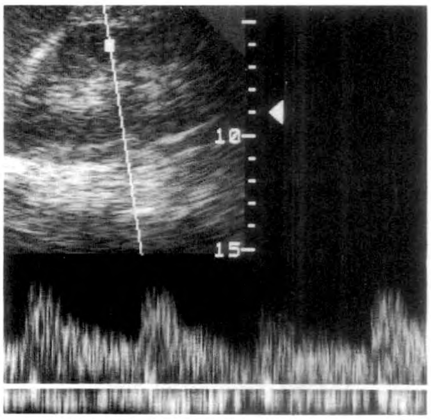

Fig. 3.—Renal Doppler sonogram of patient with glomerular disease. Patient had lupus nephritis and renal biopsy results were consistent with an active proliferative-type glomerulonephritis. Doppler signal from intrarenal artery in this patient with pure glomerular disease shows good diastolic flow, resulting in a normal resistive index of 0.55.

TABLE 1: Relationship of Creatinine Level to Resistive Index in 41 Patients

Resistive Index	No. of Patients per Creatinine Level (mg/dl)			
	Normal	1.4–1.9	2.0–3.9	≥4.0
≤0.54	2	1	0	0
0.55–0.59	4	3	1	1
0.60–0.64	6	0	0	0
0.65–0.69	2	1	1	2
0.70–0.74	1	1	1	0
0.75–0.79	0	2	1	2
≥0.80	1	2	4	2
Total no. of patients	16	10	8	7
Mean resistive index (± one standard deviation)	0.61 ± 0.05	0.69 ± 0.10	0.74 ± 0.08	0.73 ± 0.08

Acute tubular necrosis, the most common cause of acute renal failure, is an instructive example. Prior studies have shown that early in the course of the disease renal vascular resistance is elevated and renal blood flow is reduced [14, 15]. As in other instances of increased resistance, this should result in changes in the Doppler waveform with a more marked reduction in diastolic flow than in systolic flow and a resultant elevation in RI. In our study, the five patients with ATN had a mean RI of 0.78, most likely reflecting the high vascular resistance state (Fig. 1).

Previously, the major sonographic parameter used to characterize renal medical disease was relative renal cortical echogenicity. In one study, echogenic kidneys were positively correlated with pathologic changes such as global sclerosis, focal tubular atrophy, and focal leukocytic infiltration [5]. In our study, no significant difference was seen between the RI of abnormally echogenic kidneys (0.71) and the RI of normally echogenic kidneys (0.66). This suggests that factors affecting relative renal echogenicity are not identical to the processes that alter the Doppler signal. In our study, 37% (15/41) of patients with renal medical disease had echogenic kidneys, again reflecting the well-known finding that renal medical disease may result in increased renal echogenicity. However, echogenicity did not discriminate between major forms of renal disease as renal Doppler imaging did.

In addition to sonographic-pathologic correlation, we compared the RI values with clinical findings of the presence or absence of hypertension, hematuria, and proteinuria. For each clinical parameter, no statistically significant difference was found in the mean RI values when the parameter was present or absent.

For purposes of this study, serum creatinine level was used as an approximation of the degree of renal dysfunction. There did seem to be a trend toward more abnormal waveforms with higher creatinine levels, reflected by a mean creatinine level of 3.7 ± 3.6 in patients with an elevated RI and 1.7 ± 1.7 in patients with normal Doppler waveforms. However, this difference was not statistically significant, probably because of large standard deviations and possibly because of the relatively small population of patients. Dubbins [16] also has suggested that a coarse correlation exists between progressive uremia and increasing index values in his preliminary experience. We agree that the relationship is best categorized as weak, as reflected by the linear correlation coefficient of 0.34 between creatinine level and RI. Although a significant difference in mean RI was seen when comparing patients who had normal creatinine levels (0.61 ± 0.05) with patients who had elevated creatinine levels (0.71 ± 0.09), it would be a mistake to consider RI values as merely reflecting the creatinine level. Over a quarter of the patients in our series had discrepant Doppler-laboratory findings; two patients had abnormal RI values despite a normal creatinine level, and 10 patients had normal Doppler studies despite an elevated creatinine level. Our data therefore suggest that the site of disease within the kidney and its activity affect the Doppler signal more than the degree of renal dysfunction, although severe uremia most likely will have at least some effect on the RI.

Despite studying patients with a wide range of renal disease and pathologic findings that varied from very diffuse to more focal, we did not note a great difference between Doppler studies of the right and left kidneys within a given patient (mean RI difference, 0.02; range, 0.00–0.06). This agrees with the findings of Wong et al. [12], who found no significant difference between right and left kidney Doppler measurements in children. However, as it is still possible some specific forms of renal disease may produce discrepant or unilateral Doppler changes, we still recommend Doppler examination of both kidneys. Although use of a discriminatory RI level of 0.70 reflects our and others' current experience, it is certainly possible that in some instances or diseases a different value may be more appropriate; such determinations are beyond the scope of this study. The availability of a baseline Doppler study for comparison may in fact be even more useful than a single RI determination.

Another limitation that needs to be noted is that our findings may not apply to the infant's or younger child's kidney. This concern is well stressed in a recent editorial by Keller [17], which points out the existence of a high-resistance state (elevated RI) in the normal infant kidney. Although children were included in our series, none were younger than 6 years old. Prior renal functional maturation studies and a prior sonographic report suggest that normally high RI values should be observed in children less than 1 or 2 years old [12]. Hence, we believe inclusion of children 6 years old or older with the adults in our study is appropriate. However, we do not believe that our renal Doppler data based on observations in the essentially mature kidney should be blindly applied to the infant's kidney.

We conclude that duplex Doppler sonography detects a state of increased arterial vascular resistance (elevated RI) in some forms of renal medical disease but not in others. The main factor determining whether the RI is elevated appears to be the primary site of renal disease. Active or acute disease within the tubulointerstitial compartment and vasculitis generally elevated the RI, whereas disease limited primarily to the glomerulus did not. There appears to be a weak relationship between degree of renal dysfunction and RI; however, this seems less important than the type of renal medical disease present. Our data suggest that certain forms of renal medical disease such as interstitial nephritis and acute tubular necrosis, in which the traditional sonogram is generally unremarkable, should generally be expected to have abnormalities detected on Doppler study. The precise role that duplex Doppler sonography could play in the diagnosis, treatment, and follow-up of such patients requires further study.

REFERENCES

1. Green D, Carroll BA. Ultrasound of renal failure. In: Hricak H, ed. *Genitourinary ultrasound*. New York: Churchill Livingstone, **1986**:55–58
2. Hricak H. Renal medical disorders: the role of sonography. In: Sanders RC, ed. *Ultrasound annual*. New York: Raven Press, **1982**:43–80
3. Stuck KJ, White GM, Granke DS, Ellis JH, Weissfeld JL. Urinary obstruction in azotemic patients: detection by sonography. *AJR* **1987**;149:1191–1193
4. Stanley JH, Cornella R, Loevinger E, Schabel SI, Curry NS. Sonography of systemic lupus nephritis. *AJR* **1984**;142:1165–1168
5. Hricak H, Cruz C, Romanski R, et al. Renal parenchymal disease: sonographic–histologic correlation. *Radiology* **1982**;144:141–147
6. Paivansalo M, Huttunen K, Suramo I. Ultrasonographic findings in renal parenchymal diseases. *Scand J Nephrol* **1985**;10:119–123
7. Platt JF, Rubin JM, Bowerman RA, Marn CS. The inability to detect kidney disease on the basis of echogenicity. *AJR* **1988**;151:317–319
8. Mittelstaedt CA. *Abdominal ultrasound*. New York: Churchill Livingstone, **1987**:286–288
9. Platt JF, Rubin JM, Ellis JH, DiPietro M. Duplex Doppler US of the kidney: differentiation of obstructive from non-obstructive dilatation. *Radiology* **1989**;171:515–517
10. Platt JF, Rubin JM, Ellis JH. Distinction between obstructive and nonobstructive pyelocaliectasis with duplex Doppler sonography. *AJR* **1989**;153:997–1000
11. Patriquin HB, O'Regan S, Robitaille P, Paltiel H. Hemolytic-uremic syndrome: intrarenal arterial Doppler patterns as a useful guide to therapy. *Radiology* **1989**;172:625–628
12. Wong SN, Lo RNS, Yu ECL. Renal blood flow pattern by noninvasive Doppler ultrasound in normal children and acute renal failure patients. *J Ultrasound Med* **1989**;8:135–141
13. Schwaighofer B, Kainberger F, Fruehwald F, et al. Duplex sonography of normal renal allografts. *Acta Radiologica* **1989**;30:53–56
14. Brenner BM, Rector FC Jr. *The kidney*, 3rd ed. Philadelphia: Saunders, **1981**:745–751
15. Zollinger HU, Mihatsch MJ. *Renal pathology in biopsy*. New York: Springer-Verlag, **1978**:529–530
16. Dubbins PA. Doppler ultrasound in renal disease. *Curr Imaging* **1989**;1:32–38
17. Keller MS. Renal Doppler sonography in infants and children. *Radiology* **1989**;172:603–604

Book Review

Magnetic Resonance Workbook. By N. A. Matwiyoff. New York: Raven, 134 pp., 1990. $29.50, softcover

This softcover book reviews the underlying physics and some engineering aspects of MR imaging with a style and depth suitable for the intelligent and motivated nonphysicist. As such, the book is well suited to the radiologist who wishes to learn a bit more about the scientific basis of MR imaging than is contained in the many review chapters and articles that have appeared in the radiologic literature.

As noted, the book is written at a level that might be described as early college physics. Some simple mathematical relations are used, but nothing more complex than a little addition or multiplication. The derivations of most of the equations are considered beyond the scope of the text and are omitted. Physicists analyze MR phenomena from the perspectives of both classical and quantum mechanics; the descriptions in this text are limited to the former, which suffices for its intended audience.

The book contains eight chapters; the presentation is as a standard didactic text. The material is interspersed with straightforward questions, with an answer key provided at the end. The book is well illustrated with many line drawings and some MR images. The graphics are certainly clear and adequate, though they are not outstanding.

The bulk of the material addresses the basic physical principles of MR and of formation of MR images. The book begins with an overview of nuclear magnetic resonance and describes induction of an MR signal in a receiver coil. This is followed by a chapter on phase and frequency encoding. Another chapter describes the major components of an MR scanner, including RF coils, gradients, and the main magnet. This chapter has no significant discussion of the associated electronics, including amplifiers and computers, which is a bit unfortunate. A chapter expanding on the phenomenon of precession comes next. This is followed by a discussion of the basics of pulse sequences. The next chapter is an important description of image contrast and the effects of T1 and T2 on pixel intensity. The concluding chapters expand on previous discussions of image reconstruction and Fourier transformation and on the interaction of pulse sequences with tissue contrast. The order in which the subjects are presented is at times unorthodox; for example, most authors tend to present the material on precession at the beginning. However, the approach is a reasonable one.

The physics of MR is not a simple subject, and learning it cannot be made easy. This text provides a reasonable introduction that many radiologists may find helpful. The style and depth are likely to suit some but not others. The material on image correlation is a bit limited, but most of the coverage is appropriate to the apparent goals and intended audience. I recommend the book to the radiologist who wishes to learn something about physical phenomena that underlie MR imaging.

Alex M. Aisen
University of Michigan Hospitals
Ann Arbor, MI 48109-0030

Heating of the Scrotum by High-Field-Strength MR Imaging

Frank G. Shellock[1]
Barry Rothman
Dennis Sarti

Sterility can occur in mammals if spermatogenic tissue is acutely or chronically heated to levels equal to or greater than body temperature. High-field-strength MR imaging has been shown to elevate tissue temperatures, particularly if high levels of RF radiation are used. To determine if MR imaging above the recommended level for RF radiation is associated with heating of the scrotum, scrotal skin temperatures were measured in eight subjects immediately before and after MR imaging of the scrotum with a 1.5-T, 64-MHz MR scanner at mean whole-body average specific absorption rates ranging from 0.56 to 0.84 W/kg (mean, 0.72 W/kg). The average imaging time was 23 min. A statistically significant ($p < .01$) increase in average scrotal skin temperature was associated with MR imaging (before MR imaging, 30.8°C; after MR imaging, 32.3°C). The largest change in temperature was 3.0°C, and the highest temperature measured was 34.1°C.

MR imaging at relatively high specific absorption rates produced a statistically significant increase in average scrotal skin temperature. However, the recorded temperatures were below the threshold known to affect spermatogenesis in mammals.

***AJR* 154:1229–1232, June 1990**

MR imaging causes elevations in tissue temperatures as a result of RF radiation-induced heating [1–6]. It is known that the spermatogenic tissue of mammals is extremely sensitive to elevated temperatures. External application of heat to increase tissue temperatures to a level equivalent to or only slightly higher than body temperature is sufficient to affect spermatogenesis adversely [7–12].

Because high-field-strength MR imaging systems may deliver high levels of RF radiation to tissues [13] and MR imaging of the scrotum frequently is performed on patients for a variety of indications [14, 15], it is important to determine if any potentially hazardous tissue heating occurs at this site, especially at RF levels that exceed current U.S. Food and Drug Administration (FDA) guidelines [16]. Therefore, the purpose of this study was to evaluate temperature changes that can occur in association with high-field-strength MR imaging of the scrotum at specific absorption rates (SAR, the mass-normalized rate at which RF energy is coupled to biologic tissue) above the recommended level.

Subjects and Methods

Eight men, 20–61 years old (mean age, 42 years), who had been referred for MR imaging of the scrotum for suspected neoplastic disease, were studied under a protocol approved by the Human Subjects Committee that permitted MR imaging above the U.S. FDA recommended guideline for exposure to RF radiation (i.e., above a whole-body average specific absorption rate of 0.4 W/kg) [16].

A high-field-strength (1.5-T) MR imaging system operating at 64 MHz (Signa MR System, General Electric Company, Milwaukee, WI) was used. MR imaging was performed with a quadrature body coil and a 12.5-cm receive-only surface coil.

Received December 18, 1989; accepted after revision January 22, 1990.

This work was supported by PHS grant 1 RO1 CA44014-02 awarded by the National Cancer Institute, National Institutes of Health.

[1] All authors: Section of Magnetic Resonance Imaging, Department of Diagnostic Radiology, Cedars-Sinai Medical Center and UCLA School of Medicine, 8700 Beverly Blvd., Los Angeles, CA 90048. Address reprint requests to F. G. Shellock.

0361–803X/90/1546–1229
© American Roentgen Ray Society

Images were obtained as follows: (1) coronal plane, 600/20 (TR/TE), 10-mm slice thickness, 2.5-mm intersection gap, 20-cm field of view, two excitations, 256 × 128 matrix; (2) sagittal plane, 600/20, 5-mm slice thickness, 2.5-mm intersection gap, 20-cm field of view, two excitations, 256 × 128 matrix; (3) axial plane, 2000/25, 80, 5-mm slice thickness, 2-mm intersection gap, 20-cm field of view, two excitations, 256 × 256 matrix; (4) coronal plane, 2000/25, 80, 5-mm slice thickness, 2-mm intersection gap, 20-cm field of view, two excitations, 256 × 256 matrix.

These pulse sequences were selected in order to examine the scrotum thoroughly within a clinically acceptable time. We did not attempt to alter factors that would maintain exposure to RF radiation below the recommended level [16].

The Signa MR System is equipped to monitor and display the whole-body average SAR for each patient on the basis of an algorithm that takes into account the subject's weight and the scanning parameters [1–5]. The estimated whole-body average SARs and image acquisition times for each of the subjects are listed in Table 1. These SAR values are an average of the four series of pulse sequences used to image the scrotum, and therefore the temperature alterations recorded in this study reflect the response to the combined effect of the four series. Furthermore, because MR imaging was performed on the scrotum, this anatomic site was the primary site of RF power deposition [1, 3, 6, 17].

The U.S. FDA recommends that exposure to RF energy during MR imaging not exceed a whole-body average SAR of 0.4 W/kg [16]. The mean whole-body average SARs for the patients in this study ranged from 0.56 to 0.84 W/kg (mean, 0.72 W/kg).

Scrotal skin temperature was determined with a noncontact infrared thermometer (Medi-Therm; Everest Interscience, Tustin, CA). This fast-response (<1 sec) device has an accuracy and resolution of 0.1°C [18]. The calibration of the infrared thermometer was checked before each experiment by using a "black body" phantom (Everest Interscience, Tustin, CA).

Each patient wore a lightweight, cotton hospital gown without briefs so that a similar amount of skin surface was uncovered during the procedure. The penis was taped to the patient's abdomen to facilitate exposure of the scrotal skin area for temperature measurement and to position the scrotum optimally for MR imaging.

The patient was exposed to a constant ambient temperature of 21.0°C ± 1.0, a relative humidity of 40% ± 5%, and an air movement of less than 0.1 m/sec for at least 15 min. These conditions were maintained both within the preparation room and within the MR scanner. After this allotted time for temperature equilibration, the baseline scrotal skin temperature was measured with the infrared thermometer by using a circular area setting of approximately 15 mm in diameter. The scrotal skin temperature measurement site was selected at a position within the open portion of the circular surface coil so that no radiative heating effects would be produced by contact of the surface coil with the scrotal skin. The patients were not covered during the imaging procedure and their legs were positioned slightly apart to reduce the likelihood of tissue heating from conductive mechanisms. Immediately after MR imaging (<60 sec), measurement of scrotal skin temperature was repeated. Previous data indicates that because of the thermal inertia of biological tissues, only insignificant changes in temperature occur within 60 sec [4]. Therefore, the scrotal skin temperatures obtained immediately after MR imaging adequately represent maximal levels associated with this procedure [4, 6].

Scrotal skin temperatures obtained before MR imaging were compared with those obtained afterward by means of a standard paired Student t test. Data are reported as mean plus or minus one standard deviation. The changes in scrotal skin temperature were compared with the SARs by means of a linear regression statistical analysis.

Results

A statistically significant ($p < .01$) increase was seen in the average scrotal skin temperature associated with MR imaging of the scrotum (Table 1). The change in scrotal skin temperature ranged from 0.2 to 3.0°C, and the average change was 1.5°C. The highest scrotal skin temperature measured after MR imaging was 34.1°C. The correlation coefficient (R) was 0.047 ($p = .456$, $y = 1.01 + 0.6\ x$), indicating that no significant relationship existed between the scrotal skin temperature changes and the SARs.

None of the patients experienced any apparent temperature-related adverse effects after MR imaging of the scrotum. Six of the eight patients had signs of cutaneous flushing of the scrotal area, and all of them reported subjective sensations of warmth after the imaging procedure.

Discussion

Both the human testis and eye have a limited capacity for heat dissipation and are considered to be particularly susceptible to injuries caused by elevations in tissue temperature [19–22]. Consequently, these organs are designated as pri-

TABLE 1: Scrotal Skin Temperatures Before and After MR Imaging

Patient	Age (yr.)	SAR[a] (W/kg)	Imaging Time (min)	Temperature (°C)	
				Before	After
1	56	0.76	32.5	32.1	34.1
2	52	0.80	22.0	28.6	31.8
3	37	0.80	25.0	28.9	29.3
4	29	0.84	21.0	33.4	33.8
5	20	0.56	19.0	30.0	32.2
6	61	0.75	29.0	28.8	31.8
7	34	0.68	19.0	31.5	31.7
8	46	0.60	18.0	32.8	33.3
Mean ± S.D.	42 ± 14	0.72 ± 0.10	23.0 ± 5.0	30.8 ± 1.9	32.3 ± 1.5[b]

[a] SAR = specific absorption rate. Values for each patient are an average of the four series.
[b] $p < .01$.

mary sites that could be injured by excessive exposure to RF radiation during MR imaging [20]. Although a recent study reported that RF radiation-induced heating associated with MR imaging does not appear to cause any deleterious effects on human ocular tissues [5], there has yet to be a similar investigation on the male reproductive system. The only MR imaging-related study that has examined spermatogenic tissue of mammals was performed by Withers et al. [23], who concluded that 66 hr of continuous exposure to a 0.3-T static magnetic field did not produce any significant cytotoxicity in mouse sperm cells.

Research has indicated that there is a direct relationship between temperature and sperm motility and viability [7–12]. The adverse effect of heat on spermatogenic tissue is believed to be predominantly mediated by tissue anoxia related to vascular stagnation [8]. Extrinsic heating of scrotal/testicular tissues from a variety of sources, including hot water, infrared, ultrasound, fabric insulation, and electromagnetic fields are all capable of depressing spermatogenesis [7–9, 12]. Numerous investigators have examined the effects of exposure to RF radiation on mammalian spermatogenesis, primarily because the scrotum and testes are anatomically positioned so that they can be irradiated without subjecting the remainder of the body to RF energy [19, 21, 22]. These data have indicated that minimum threshold temperatures specific to the species studied were required for a single, short-term, acute exposure to disrupt spermatogenesis [19, 21, 22]. Obviously, MR imaging also entails a single, short-term acute exposure to RF radiation.

Experiments have suggested an apparent graded sensitivity of spermatogenic tissues to the damaging effects of heat related to the mode of heating, so that different tissue temperatures were required for the different methods of heating to produce a comparable degree of damage [8, 19, 21, 22]. Ultrasound required the lowest temperature changes, followed by electromagnetic fields, infrared, and simple externally applied heat [8]. Of further interest is that there appears to be a nonthermal component (an effect that occurs independently of the temperature level) to the disruption of spermatogenesis that is produced by exposure to electromagnetic radiation [8, 19, 21, 22]. Therefore, there may be a synergetic effect, because of the physical properties of electromagnetic fields, that results in temporary or permanent sterility at slightly lower temperatures than what would be observed by heating from another source [8, 19, 21, 22].

The temperature of the testis has been shown to correlate directly with the temperature of the scrotal skin [24]. This temperature relationship exists primarily because the scrotum has little or no associated subcutaneous fat or connective tissue, and consequently, no tissue-related temperature gradients are present [10, 24]. Accordingly, in this study, testicular temperature was evaluated indirectly by measuring scrotal skin temperature. A study that examined the skin temperature responses to RF radiation-induced heating during MR imaging indicated that the highest temperatures were observed at the end of scanning [6]. Therefore, the scrotal skin temperature recorded immediately after MR imaging is the most important and readily accessible data to obtain in human subjects to assess the potential heating hazards associated with this imaging procedure.

In this study, statistically significant increases in scrotal skin temperatures were associated with a protocol that provided a thorough examination of the scrotum at SARs up to 0.84 W/kg. The highest temperature recorded was 34.1°C. Therefore, the threshold for tissue temperatures where spermatogenesis may be affected (i.e., approximately body temperature for human subjects) was not reached during this study. Although scrotal skin temperature has been shown to be closely correlated with intratesticular temperature [24], RF radiation-induced heating during MR imaging has been observed to occur predominantly in superficial tissues as opposed to deeper body sites [1–6], and consequently, the increases in intratesticular temperature associated with MR imaging may not be as high as those observed for the scrotal skin. The lack of correlation between the changes in scrotal skin temperature and the SARs observed in this study is not surprising, considering the numerous problems with estimating SARs in human subjects [22, 25] combined with the myriad of factors that are known to affect scrotal skin temperature [7–12].

Control experiments (i.e., subjects placed inside the scanner and not exposed to MR imaging) were not performed in this study because it is highly unlikely that the elevated skin temperatures we observed were caused by mechanisms other than exposure to RF radiation [26]. Earlier studies performed under similar ambient and experimental conditions have shown that no statistically significant temperature changes are caused by the MR scanner itself (i.e., the static magnetic field or the environment within the bore) [26].

Studies examining RF radiation-induced heating during MR imaging have indicated that, although statistically significant increases in body and/or skin temperatures may occur, none of these are believed to be physiologically deleterious to human subjects [1–6]. A recent investigation reported an increase in abdominal skin temperature to 36.0°C in a subject undergoing MR imaging at a whole-body average SAR of 2.8 W/kg [6], suggesting that very high SAR studies may produce elevated tissue temperatures in the vicinity of the scrotum that could reach the threshold for affecting spermatogenesis. Furthermore, excessively heating the scrotum during MR imaging could exacerbate certain preexisting disorders associated with increased scrotal/testicular temperatures (e.g., acute febrile illnesses, varicocele) in patients who are already oligospermic and lead to temporary or permanent sterility [11]. Therefore, additional studies designed to investigate these issues are needed.

The FDA recommends limiting exposure to RF radiation during MR imaging to a whole-body average SAR of 0.4 W/kg [16]. Alternatively, the FDA has indicated that temperature criteria may be used, so that RF exposures that do not cause an increase in core temperature of greater than 1°C, local exposure of less than 38°C in the head, 39°C in the trunk, and 40°C in the extremities are acceptable [16]. Several manufacturers have received approval to perform MR imaging at whole-body average SARs ranging from 1.5 to 4.0 W/kg (R. Shuping, personal communication, FDA, Nov. 1989) on the basis of supporting safety data and their interpretation of the temperature criteria.

In view of the known thresholds for the effect of heat on spermatogenesis and assuming that the scrotum/testes are part of the trunk (as no specific criteria for the scrotum/testes are indicated by the FDA), following the temperature criteria for exposure to RF radiation during MR imaging could cause temporary sterility in human subjects at the highest approved SARs. Therefore, future FDA guidelines for safe levels of exposure to RF radiation during MR imaging may need to require specific criteria for scrotal/testicular tissues and/or require informed consent concerning this issue.

REFERENCES

1. Shellock FG, Schaefer DJ, Grundfest W, Crues JV. Thermal effects of high-field (1.5 T) magnetic resonance imaging of the spine: clinical experience above a specific absorption rate of 0.4 W/kg. *Acta Radiol Suppl* (Stockh) **1986**;369:514–516
2. Shellock FG, Gordon CJ, Schaefer DJ. Thermoregulatory responses to clinical magnetic resonance imaging of the head at 1.5 Tesla: lack of evidence for direct effects on the hypothalamus. *Acta Radiol Suppl* (Stockh) **1986**;369:512–513
3. Shellock FG, Crues JV. Temperature, heart rate, and blood pressure changes associated with clinical MR imaging at 1.5 T. *Radiology* **1987**;163:259–262
4. Shellock FG, Crues JV. Temperature changes caused by clinical MR imaging of the brain at 1.5 T using a head coil. *AJNR* **1987**;8:263–266
5. Shellock FG, Crues JV. Corneal temperature changes induced by high-field-strength MR imaging with a head coil. *Radiology* **1988**;167:809–811
6. Shellock FG, Schaefer DJ, Crues JV. Alterations in body and skin temperatures caused by MR imaging: is the recommended exposure for radiofrequency radiation too conservative? *Br J Radiol* **1989**;62:904–909
7. Robinson D, Rock J. Intrascrotal hyperthermia induced by scrotal insulation: effect on spermatogenesis. *Obstet Gynecol* **1967**;29:217–223
8. Kandeel FR, Swerdloff FR. Role of temperature in regulation of spermatogenesis and the use of heating as a method for contraception. *Fertil Steril* **1988**;49:1–23
9. Zorgniotti AW, MacLeod J. Studies in temperature, human semen quality, and varicocele. *Fertil Steril* **1973**;24:854–863
10. Zorgniotti AW, Sealfon AI. Measurement of intrascrotal temperature in normal and subnormal man. *J Reprod Fertil* **1988**;82:563–566
11. Procope B-J. Effect of repeated increase of body temperature on human sperm cells. *Int J Fertil* **1965**;10:333–339
12. Fahim MS, Fahim Z, Der R, Hall DG, Harman J. Heat in male contraception (hot water 60°C, infrared, microwave, ultrasound). *Contraception* **1975**;11:549–562
13. Crues JV, Shellock FG, Levy TL. Prevalence of high-field MRI procedures requiring specific absorption rates above 0.4 W/kg: experience in 639 patients (abstr). In: *Book of abstracts: Society of Magnetic Resonance in Medicine*. Berkeley, CA, **1986**:1032–1033
14. Baker LL, Hajek PC, Burkhard TK, et al. MR imaging of the scrotum: normal anatomy. *Radiology* **1987**;163:89–92
15. Baker LL, Hajek PC, Burkhard TK, et al. MR imaging of the scrotum: pathologic conditions. *Radiology* **1987**;163:93–98
16. Food and Drug Administration. Magnetic resonance diagnostic device; panel recommendation and report on petitions for MR reclassification. *Federal Register* **1988**;53:7575–7579
17. Bottomley PA, Redington RW, Edelstein WA, Schenck JF. Estimating radiofrequency power deposition in body NMR imaging. *Magn Reson Med* **1985**;2:336–349
18. Shellock FG, Rubin SA, Everest CE. Surface temperature measurement by IR. *Med Electron* **1984**;86:81–83
19. Berman E. Reproductive effects. In: *Biological effects of radiofrequency radiation.* Washington, DC: EPA, **1984**:5-29–5-52. Environmental Protection Agency-600/8-83-026A.
20. Saunders RD. Biological effects on NMR clinical imaging. *Appl Radiol* **1982**;Sept/Oct:43–46
21. Gordon CJ. Thermal physiology. In: *Biological effects of radiofrequency radiation.* Washington, DC: EPA, 1984:4-1–4-28. Environmental Protection Agency-600/8-83-026A.
22. Michaelson SM, Lin JC. Biological effects and health implications of radiofrequency radiation. New York: Plenum Press, **1987**:266–267, 289–294
23. Withers HR, Mason KA, Davis CA. MR effect on murine spermatogenesis. *Radiology* **1985**;156:741–742
24. Kurz KR, Goldstein M. Scrotal temperature reflects intratesticular temperature and is lowered by shaving. *J Urol* **1986**;135:290–292
25. National Council on Radiation Protection and Measurements. Radiofrequency electromagnetic fields: properties, quantities and units, biophysical interaction, and measurements. Washington, DC: NCRP, **1981**. NCRP Report No. 67.
26. Shellock FG, Schaefer DJ, Crues JV. Exposure to a 1.5 T static magnetic field does not alter body and skin temperatures in man. *Magn Reson Med* **1989**;11:371–375

Jogging Causes Acute Changes in the Knee Joint: An MR Study in Normal Volunteers

Sevil Kursunoglu-Brahme[1]
Bernhard Schwaighofer[1]
Cooper Gundry[1]
Charles Ho[1]
Donald Resnick[2]

As MR imaging allows evaluation of soft-tissue structures not previously possible with imaging techniques, we undertook a preliminary study to evaluate the effects of a popular form of exercise (jogging) on the knee. The specific question prompting our investigation was, does repetitive impulse loading produced by jogging cause acute structural changes within the knee that are visible by MR imaging? The knees of 10 healthy subjects were examined on a 1.5-T MR system before and immediately after 30 min of continuous jogging. The same extremity was examined each time, and the imaging sequences and photographic technique (meniscal windows) were identical for both examinations. Effusions developed in five of 10 subjects after exercise. In addition, five of 10 subjects had subtle increased signal intensity within their menisci.

These results suggest that jogging frequently leads to acute changes in the knee that are visible on MR imaging. The significance of these changes is unknown.

AJR 154:1233–1235, June 1990

In the past 15 years, jogging has become one of the most used and abused physical fitness activities [1]. In many patients, this has resulted in acute overuse syndrome and various injuries involving both soft-tissue and osseous structures [2]. Until recently, plain radiography, bone scanning, and arthrography were the only available methods for evaluating these injuries. With the advent of MR imaging, exquisite anatomic detail is provided, allowing critical scrutiny of intraarticular structures. The specific question prompting our investigation was, does repetitive impulse loading, as occurs with jogging, cause acute structural changes within the knee that are visible on MR imaging?

Materials and Methods

The knees of 10 healthy subjects (five men and five women, ages 20–35 years) were examined with a 1.5-T superconducting magnet (GE Signa System, Milwaukee, WI) and a dedicated extremity coil. The same extremity was examined before exercise and immediately (within 10 min) after continuous jogging for 30 min. The distance covered during the exercise was between 2 and 5 miles. Eight of 10 subjects were recreational joggers, running an average of 15–20 miles per week. All subjects were asymptomatic and had no complaints relating to their knees, nor had any undergone knee surgery.

Coronal T1-weighted images (800/20 [TR/TE]) and sagittal proton-density and T2-weighted images (2000/20–60) were obtained. Imaging was performed with a 5-mm slice thickness, 0.5-mm slice gap, 128 × 128 matrix, and a 16-cm field of view. Meniscal images (designed to promote visualization of intrameniscal signal) also were obtained at the same window width and level for similar slice locations.

All cases were reviewed independently by four radiologists. Both sets of images in each subject were reviewed simultaneously. The reviewers did not know which images were obtained before or after jogging. Each reviewer was given a score sheet and asked to evaluate three parameters qualitatively. These were (1) the ligaments (cruciate and collateral), whether they were normal or abnormal; (2) the menisci, the signal grade present within the

Received November 17, 1989; accepted after revision January 22, 1990.

Presented at the annual meeting of the American Roentgen Ray Society, New Orleans, LA, May 1989.

[1] Department of Radiology (H-756), University of California, San Diego, Medical Center, 225 Dickinson St., San Diego, CA 92103. Address reprint requests to S. Kursunoglu-Brahme.

[2] Department of Radiology, Veterans Administration Medical Center, San Diego, CA 92161.

0361-803X/90/1546-1233
© American Roentgen Ray Society

meniscus according to the Crues classification (I = punctate signal, noncontiguous with articular surface, II = linear signal, noncontiguous with articular surface, III = intrameniscal signal extending to articular surface); and (3) fluid, whether joint effusion was present [3]. The examinations were graded independently, and results were compared later. If disagreement existed among the reviewers, the studies were reviewed again and consensus opinion was established.

Before jogging, eight of 10 subjects had meniscal grades I and II. The two remaining subjects had no evidence of intrameniscal signal (one of these was a recreational jogger). No grade III changes were seen in the meniscus of any subject.

Results

In all subjects, MR images showed normal ligaments both before and after exercise. After jogging, five of 10 subjects had subtle increases in intrameniscal signal intensity, without change in grade (Figs. 1 and 2). Four of these five also showed small joint effusions (Fig. 3). One jogger developed an effusion without any change in meniscal signal.

The radiologists were in close agreement regarding both signal intensity differences within menisci and development of joint effusion. In one case, one of the four radiologists detected no fluid change, and in one case, one of the four detected no change in meniscal signal.

Discussion

Opinions vary regarding the effects of jogging on meniscal damage, although it appears that normal integrity and function of the menisci during strenuous exercise are important in preventing injuries from overuse. The early development of osteoarthritis in some studies of long-distance runners has not been confirmed [2, 4, 5]. A possible hypothesis to explain our findings of increased signal intensity within the meniscus after exercise may be the accumulation of fluid within the meniscus. Histologic studies show fissures in menisci, which may allow fluid to enter [6, 7]. Images of five of the 10 subjects showed accumulation of joint effusions after running. The development of effusions after exercise may represent a

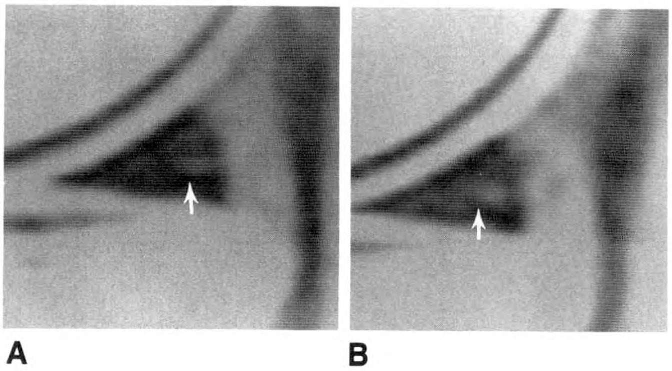

Fig. 1.—Changes in MR signal intensity seen in meniscal substance after exercise.

A, Before exercise, meniscal window (high contrast) MR image shows intrameniscal signal (*arrow*). Meniscal windows are designed to enhance visualization of intrameniscal signal.

B, After exercise, MR image obtained at same window width and level shows subtle increased signal intensity within meniscus (*arrow*).

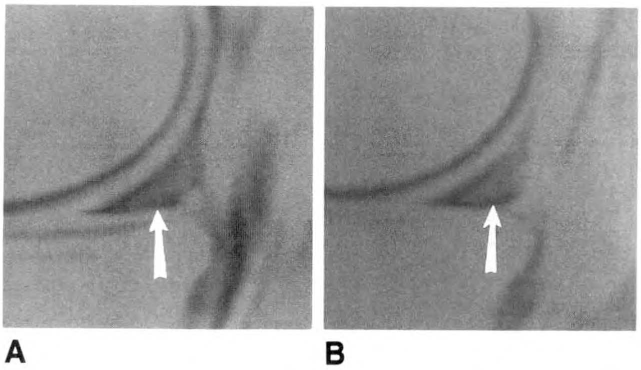

Fig. 2.—Increased MR signal intensity in meniscus after exercise.

A, MR image obtained before exercise shows linear signal in meniscus adjacent to capsular margin (*arrow*).

B, MR image obtained after exercise shows subtle increase in signal intensity in a similar location.

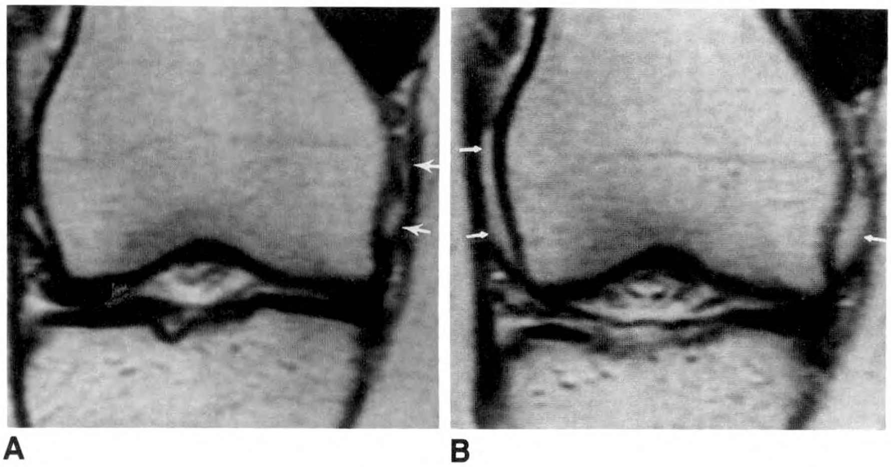

Fig. 3.—Development of knee effusion after exercise.

A, Before exercise, coronal T2-weighted MR image shows minimal effusion present around knee joint (*arrows*).

B, After exercise, a similar image shows increased size of effusion (*arrows*).

physiologic, protective response. Fluid may be expressed from articular hyaline cartilage as a normal sequela of loading forces, producing a film that minimizes cartilage-to-cartilage contact and thereby, wear and tear.

The presence of proteoglycans within the menisci also may be an explanation for the increase in intrameniscal signal intensity after exercise. The proteoglycan moieties are of high molecular weight and, therefore, relatively immobile [8, 9]. As they have a large number of hydroxyl groups, they are hydrophilic and function as a pump for water molecules. The increased intrameniscal signal observed after jogging may be due to imbibition of water by meniscal proteoglycans, owing to the presence of a joint effusion.

The results of our study indicate that mild effusions develop acutely within the knee joint after jogging and, further, that associated signal intensity changes appear on MR images of the menisci. The clinical significance of these findings is uncertain. Indeed, the volunteers were without complaints referable to their knees both before and after jogging, and they were subjected to minimal stress loading only. More pronounced changes may be detected after higher levels of stress such as may occur in marathon runners. If chronic biomechanical stress leads to degenerative changes within the menisci and subsequent injury, these findings may represent the earliest demonstrable evidence of such changes.

REFERENCES

1. Sohn RS, Micheli LJ. The effect of running on the pathogenesis of osteoarthritis of the hips and knees. *Clin Orthop* **1985**;198:106–109
2. Radin EL, Paul IL, Rose RM. Role of mechanical factors in pathogenesis of primary osteoarthritis. *Lancet* **1972**;1:519–521
3. Crues JV, Mink J, Levy TL, Lotysch M, Stoller DW. Meniscal tears of the knee: accuracy of MR imaging. *Radiology* **1987**;164:445–448
4. Kurosawa H, Fukubayashi T, Hiroyuki W. Load-bearing mode of the knee joint: physical behavior of the knee joint with or without menisci. *Clin Orthop* **1980**;149:283–290
5. Videman T. The effect of running on the osteoarthritic joint: an experimental matched-pair study with rabbits. *Rheumatol Rehabil* **1982**;21:1–7
6. Merkel KH. The surface of human menisci and its aging alterations during age. *Arch Orthop Trauma Surg* **1980**;97:185–191
7. Roca-Ferrer O, Vilalta C. Lesions of the meniscus. Part I: Macroscopic and histologic findings. *Clin Orthop* **1980**;146:289–300
8. Pedrini-Mille A, Pedrini VA, Maynard JA, et al. Response of immature chicken meniscus to strenuous exercise: biochemical studies of proteoglycan and collagen. *J Orthop Res* **1988**;6:196–204
9. Jones IL, Klamfeldt A, Sandstrom T. The effect of continuous mechanical pressure upon the turnover of articular cartilage proteoglycans in vitro. *Clin Orthop* **1982**;165:283–289

Book Review

Bone and Joint Imaging. By Donald Resnick. Philadelphia: Saunders, 1360 pp., 1989. $175

Once again, Donald Resnick has produced a masterpiece. Only 1 year after publication of the second edition of *Diagnosis of Bone and Joint Disorders,* he has produced a one-volume book entitled *Bone and Joint Imaging.* Although his previous six-volume book has become impractical for the individual, this book is a must for anyone involved in imaging and interpretation of skeletal disease. It was written in response to a request by residents and fellows in training that the multivolume book be "shortened a bit." Though this would appear to be an impossible task, Dr. Resnick accomplished it, in the fashion suggested by William Strunk, Jr., in the introduction: No sentence contains an unnecessary word and no paragraph an unnecessary sentence.

All clinical and pathologic data presented in the six-volume book have been culled to the minimal essentials. Chapters that are interesting but superfluous to the basic needs of interpreting the radiograph have been eliminated (e.g., the chapters on physiology, developmental anatomy, histomorphology, paleontology, and biomechanics). Superfluous description of radiographs has been removed. Only illustrations that graphically show important abnormalities have been used.

Three big changes have been made: First, an opening chapter of test cases has been included. The cases are used to introduce each of the 15 sections of the book and help illustrate the importance of each section. Second, citations within the text have been eliminated; pertinent references are listed at the end of each chapter. As a result, the text is more readable, and the references, on the whole, are more usable. However, in some chapters, this change has drawbacks. For example, both the chapter on physical trauma and the one on tumor and tumorlike lesions of bone have more than 125 references; it becomes difficult to read through the list to find the one reference needed to learn more about one specific disorder. Third, the summaries in the multivolume book have become large-print introductions to each chapter in this book. This is a helpful switch.

Readers should not feel that they are being shortchanged in purchasing a one-volume book condensed from a six-volume book. *Bone and Joint Imaging* actually has more information than any one book of the multivolume version. In fact, it is still too big and difficult to lift off the shelf. The paper is thinner, and the type is smaller. Actually, I find the size of the type a disadvantage; it is not easy to read—especially the legends to the figures. The book has more than 1700 multilettered figures; some have been cropped or reduced from the original figures used in the six-volume book. In some instances, especially the newly added test-case radiographs, the quality of the reproductions is not as good as that of past years. Occasionally, columns of print have been cut inappropriately, leaving words incomplete.

Dr. Resnick produced this book specifically for residents and fellows in training, hoping that they can read it in its entirety while still carrying out their many responsibilities. To this end, he has made it readable and pertinent to their training. Though it still may be too voluminous, I see no way to cut back and still present the complete picture of bone and joint disease. As a teacher of skeletal radiology, I am always asked by residents and fellows, "What one book should I buy that will cover all I need to know about bone and joint disease?" This particular book has become that one book I will recommend.

Anne C. Brower
Uniformed Services University of the Health Sciences
Bethesda, MD 20814-4799

MR Imaging of the Knee: Pseudotear of the Lateral Meniscus Caused by the Meniscofemoral Ligament

Thomas N. Vahey[1]
Harold T. Bennett[1, 2]
L. Eugene Arrington[1, 3]
K. Donald Shelbourne[4]
Judi Ng[5]

Sagittal MR images of the knee often show a linear band of increased signal in the medial aspect of the posterior horn of the lateral meniscus that can be confused with a meniscal tear. This pseudotear is due to the meniscal insertion of the meniscofemoral ligament. To study the normal appearance of the medial aspect of the posterior horn of the lateral meniscus, we analyzed 109 MR examinations and correlated the findings with the results of arthroscopy. The meniscofemoral ligament was visualized in 54 cases (50%), and in 42 cases (39%) it caused the appearance of a pseudotear on sagittal images. The pseudotear had one of two orientations. The most common (35/42) was an oblique orientation coursing from the superior surface posteriorly and inferiorly. The other (7/42) was a more vertical orientation parallel to the base of the meniscus.

Knowledge of the characteristic location and orientation of the meniscofemoral ligament should help to distinguish it from a true meniscal tear on MR images.

***AJR* 154:1237–1239, June 1990**

Sagittal MR imaging of the knee often shows a linear band of signal between the superior surface of the posterior horn of the lateral meniscus and the meniscofemoral ligament. This results in an appearance that can be confused with a meniscal tear. This study was performed to determine the normal appearance of the meniscofemoral ligament and to develop criteria to distinguish it from a true meniscal tear.

Materials and Methods

Between August 1987 and January 1989, all 109 patients at our institution who had both MR examinations of the knee and subsequent arthroscopy were reviewed. The patients ranged in age from 9 to 77 years, with a mean age of 33 years. All MR scans were obtained on a 1.5-T magnet (Signa; General Electric, Milwaukee, WI) with a dedicated solenoid surface coil (General Electric). As a portion of our routine examination, sagittal images were obtained with a 12- to 14-cm field of view, a 256 × 256 matrix, one excitation, a TR of 1600–2000 msec, and a dual-echo TE of 20 and 60–80 msec. Slice thickness was initially 5 mm with no interslice gap, but was subsequently decreased to 3 mm with a 1-mm gap. The frequency-encoding direction was always in the cephalocaudal axis to avoid wraparound artifact.

All cases were reviewed in a blinded retrospective fashion with special attention to the appearance of the posterior horn of the lateral meniscus for the presence of pseudotears caused by the insertion of the meniscofemoral ligament. The following were evaluated: (1) the frequency with which the meniscofemoral ligament was confidently visualized; (2) the frequency with which the meniscofemoral ligament's insertion into the lateral meniscus resulted in the appearance of a pseudotear; (3) the location and orientation of the pseudotear; (4) the number of consecutive images on which the meniscofemoral ligament was visualized before its meniscal insertion; (5) the number of consecutive images on which a pseudotear was present in each case; and (6) whether the meniscofemoral ligament coursed anterior or posterior to the posterior cruciate ligament.

MR examinations were correlated with arthroscopy reports to determine the exact location and extent of any lateral meniscal tears. Arthroscopies were performed with full knowledge

Received November 20, 1989; accepted after revision February 2, 1990.

[1] Department of Radiology, Methodist Hospital of Indiana, 1701 N. Senate Blvd., Indianapolis, IN 46202. Address reprint requests to T. N. Vahey.

[2] Present address: Radiology Department, University of California Hospitals and Clinics, 505 Parnassus Ave., San Francisco, CA 94143-2722.

[3] Present address: Radiology Department, Christ Hospital, 2139 Auburn Ave., Cincinnati, OH 45219-2989.

[4] Methodist Sports Center, 1815 N. Capitol Ave., Indianapolis, IN 46202.

[5] Department of Medical Research, Methodist Hospital of Indiana, 1701 N. Senate Blvd., Indianapolis, IN 46202.

0361–803X/90/1546–1237
© American Roentgen Ray Society

of MR findings. Discrepancies were correlated with videotape recordings of the arthroscopy.

Results

Of the 109 cases in this study, a meniscofemoral ligament was confidently identified on the MR scans in 54 cases (50%), and in 42 cases (39%) it caused the appearance of a pseudotear on sagittal images. The distal portion of the meniscofemoral ligament causing the pseudotear could be traced on at least one additional consecutive sagittal image in 40 of 42 cases, as it coursed superiorly and medially to its femoral insertion. In 23 cases, the meniscofemoral ligament was adequately visualized to determine if it ran anterior (10) or posterior (13) to the posterior cruciate ligament. In one additional case, two branches of the meniscofemoral ligament were seen; one passing anterior and the other posterior to the posterior cruciate ligament.

The pseudotear of the meniscofemoral ligament was constant in location, at its attachment site on the medial aspect of the posterior horn of the lateral meniscus (Fig. 1). When the meniscofemoral ligament caused the appearance of a pseudotear, the pseudotear had one of two orientations. The most common (35/42) was an oblique orientation coursing from the superior surface posteriorly and inferiorly (Fig. 2A). The other (7/42) was a more vertical orientation parallel to the base of the meniscus (Fig. 2B). The pseudotears were predominantly linear but occasionally had a curvilinear or slightly undulating course. In no case did a tear of the posterior horn of lateral meniscus mimic either of these orientations at that location. In one case, the insertions of both the anterior and posterior branches of the meniscofemoral ligament caused the appearance of a double pseudotear (Fig. 3). The visualized segment of the distal meniscofemoral ligament approximated the lateral meniscus closely enough to produce a pseudotear on one sagittal image in 24 cases, on two consecutive sagittal images in 15 cases, and on three consecutive sagittal images in three cases.

Discussion

A linear band of increased signal associated with the medial aspect of the posterior horn of the lateral meniscus is frequently identified on MR images in patients who subsequently have normal findings on arthroscopic examination. Our study suggests that this common and potentially confusing finding is a pseudotear due to the insertion of the meniscofemoral ligament.

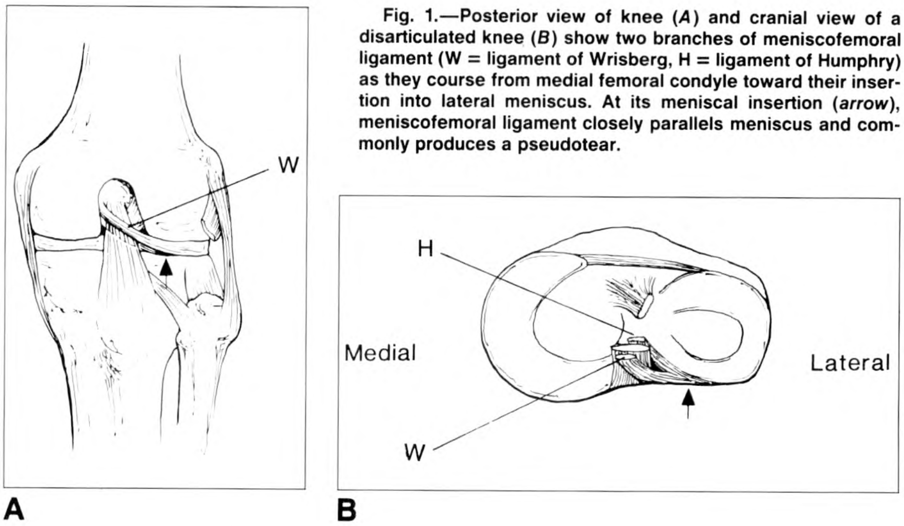

Fig. 1.—Posterior view of knee (*A*) and cranial view of a disarticulated knee (*B*) show two branches of meniscofemoral ligament (W = ligament of Wrisberg, H = ligament of Humphry) as they course from medial femoral condyle toward their insertion into lateral meniscus. At its meniscal insertion (*arrow*), meniscofemoral ligament closely parallels meniscus and commonly produces a pseudotear.

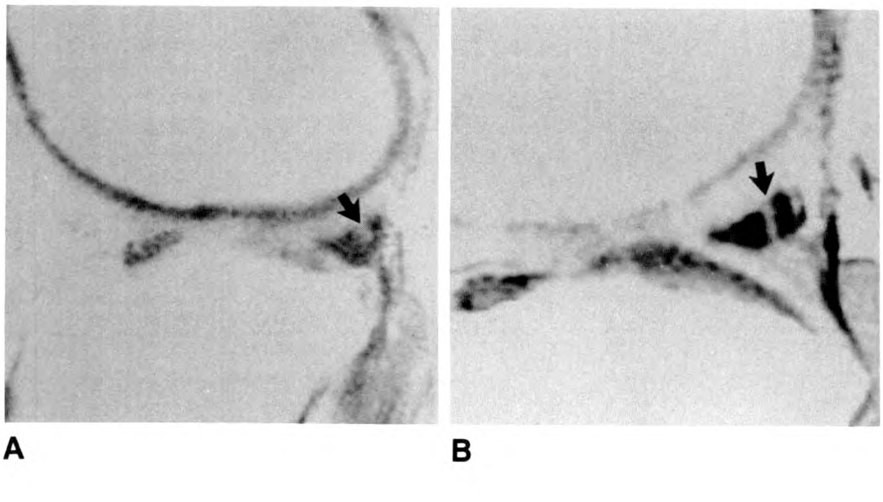

Fig. 2.—Sagittal MR images through medial aspect of lateral menisci show two characteristic orientations of meniscofemoral ligament pseudotear (*arrows*).

A, 43-year-old man with a normal lateral meniscus on arthroscopy. This pseudotear has an oblique orientation coursing from superior surface posteriorly and inferiorly.

B, 32-year-old man whose medial aspect of posterior horn of lateral meniscus was normal on arthroscopy. This pseudotear has a more vertical orientation parallel to base of meniscus.

Fig. 3.—31-year-old man with an arthroscopically normal lateral meniscus. MR image shows insertions of both anterior (*arrow*) and posterior (*arrowhead*) branches of meniscofemoral ligament, which causes a double pseudotear.

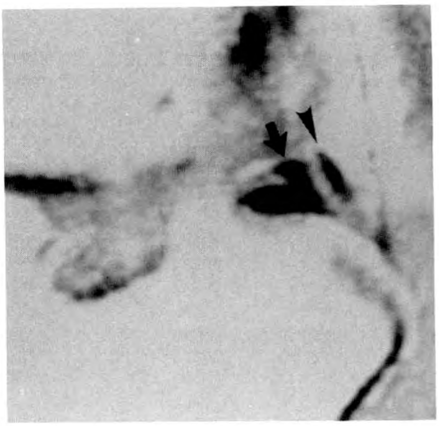

3

Fig. 4.—MR image of 42-year-old man with an arthroscopically proved tear (*arrow*) of posterior horn of lateral meniscus. Its oblique orientation (posterorsuperior to anterorinferior) is opposite of that expected in a pseudotear.

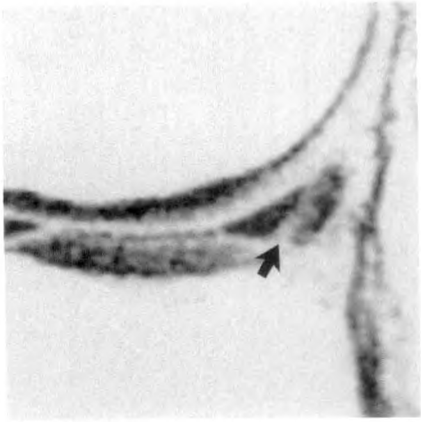

4

The meniscofemoral ligament is a strong fibrous band that connects the posterior horn of the lateral meniscus to the medial condyle of the femur (Fig. 1) and is composed of two branches. The anterior branch, or ligament of Humphry [1], is directed in an oblique craniomedial orientation anterior to the posterior cruciate ligament toward its medial condyle insertion site. The posterior branch, also known as the Wrisberg or Robert ligament [1], has the same orientation but runs posterior to the posterior cruciate ligament. Careful anatomic dissections reveal that at least one of these two branches is invariably present, and although both branches can coexist, generally one predominates [1, 2].

Several causes for meniscal pseudotears on MR images resulting from normal anatomic variants have been described [3–5]. Most pitfalls occur when a structure of low signal intensity (lateral inferior genicular artery, transverse ligament, popliteus tendon) closely parallels the outer margin of the meniscus. The linear signal between the low-intensity meniscus and the low-intensity parameniscal structure is misinterpreted as intrameniscal signal communicating with an articular surface. By an identical mechanism the meniscofemoral ligament, as it closely parallels the outer margin of the lateral meniscus, produced a linear band of signal that could be confused with a tear (Fig. 2) in 42 (39%) of 109 cases in our study.

When the meniscofemoral ligament insertion caused the appearance of a pseudotear, it did so in one of two orientations. The most common (35/42) was an oblique orientation extending from the superior articular surface posteriorly and inferiorly toward the base (Fig. 2A). The remainder (7/42) had a more vertical orientation and ran parallel to the base of the meniscus (Fig. 2B). None of the 16 true-positive lateral meniscal tears in our series had a similar appearance (Fig. 4). The typical location of the pseudotear near the meniscotibial attachment and its oblique or vertical orientation is characteristic.

Like many other low-intensity parameniscal structures, the meniscofemoral ligament often causes a pseudotear. The characteristic location and orientation of this pseudotear, and the ability to trace the ligament on consecutive sagittal images, allow its distinction from a true meniscal tear in the vast majority of cases.

ACKNOWLEDGMENTS

Thanks to Fran Shaul for secretarial assistance and to David Pennes and Terri Vahey for their help in manuscript preparation.

REFERENCES

1. Brantigan OC, Voshell AF. Ligaments of the knee joint: the relationship of the ligament of Humphry to the ligament of Wrisberg. *J Bone Joint Surg [Br]* **1945**;25-B:66–67
2. Kaplan EB. The lateral menisco-femoral ligament of the knee joint. *Bull Hosp J Dis Orthop Inst* **1956**;17:176–182
3. Herman LJ, Baltran J. Pitfalls in MR imaging of the knee. *Radiology* **1988**;167:775–778
4. Watanabe AT, Carter BC, Teitelbaun GP, Seeger LL, Bradley WG. Normal variations in MR imaging of the knee: appearance and frequency. *AJR* **1989**;153:341–344
5. Mink JH. Pitfalls in interpretation. In: Mink JH, Reicher MA, Crues JV, eds. *Magnetic resonance imaging of the knee.* New York: Raven, **1987**: 141–155

Book Review

Bone Tumors. Clinical, Radiologic, and Pathologic Correlations, vols. 1 and 2. By Joseph M. Mirra (in collaboration with Piero Picci and Richard H. Gold). Philadelphia: Lea & Febiger, 1829 pp., 1989. $250

This two-volume text is intended for all physicians—pathologists, orthopedic surgeons, radiologists, oncologists—involved in the workup and treatment of patients who have bone tumors. The main author, Dr. Mirra, is a pathologist. His coauthors include other distinguished pathologists, orthopedic surgeons, surgical oncologists, and a radiologist; all possess a wealth of experience in diagnosing and treating bone tumors.

The introductory chapter demonstrates the practicality of this text by stressing the authors' major goals: the importance of the clinical-radiologic-pathologic approach to diagnosis of bone tumors, the fallibility of "slide reading" alone, introduction of basic clinical and pathologic terminology, and suggestions for use of the text by residents according to medical speciality (i.e., pathology, radiology, or orthopedic surgery). The suggestions direct the resident to those chapters deserving of most intense scrutiny according to his or her chosen medical specialty. This useful guidance makes this two-volume textbook seem less overwhelming.

Volume 1 also contains valuable chapters devoted to such topics as workup of specimens, basics of clinical-radiologic interpretation, bone tumor terminology, and differential diagnostic tables. This background information takes up approximately 140 pages. Thereafter, individual chapters are devoted to typical bone tumors and tumorlike processes: osseous tumors of intramedullary origin, intramedullary cartilage- and chondroid-producing tumors, fibrohistocytic tumors of intramedullary origin, neurogenous tumors, smooth muscle tumors, Paget disease, giant-cell tumors, histiocytoses, Ewing sarcoma, lymphoma and lymphomalike disorders, mastocytosis, admantinoma and osteofibrous dysplasia, cyst and cystlike lesions of bone, vascular tumors, tumors of fat, metastases, unique tumors of the ribs, osseous soft-tissue tumors, parosteal tumors, and pseudotumors of bone that simulate primary malignancies. The final chapter is entitled "Quiz and Correlation" and includes six informative cases followed by general and supplemental questions and ultimately by solutions and answers. This chapter is intended to summarize some of the major teaching points of the text.

In addition to a thorough discussion of each topic, the book contains many useful charts, algorithms, and diagrams. The drawings and radiologic images are of the highest quality. Volume 2 has a series of 10 color plates dealing with a variety of bone tumors. These beautiful color illustrations include both histologic and gross specimens.

The typical chapter in this text begins with general definitions or a capsule summary. The authors include synonyms, classifications, and different subtypes of the various bone tumors. The pathologic, clinical, and radiologic features of each entity are discussed comprehensively and referenced reasonably. The spectrum of radiologic presentation of each entity includes plain radiographs and pertinent plain tomograms, angiograms, CT scans, and MR images.

No textbook is perfect, of course. For instance, it would be helpful if the pages listing the contributors or the table of contents indicated at the outset which contributor wrote which chapter. In addition, minor inconsistencies occur in the figure legends. To the reader, it is perhaps best to include uniformly the diagnosis being illustrated in the *beginning* of the figure legend. This practice is not used consistently throughout the text. A few of the radiologic images are printed upside down or in a bizarre orientation. For example, a pelvic CT scan of a giant-cell tumor of the sacrum is printed as though the patient were placed in the scanner prone rather than supine; this confusion is compounded when the caption states that the large mass filled the pelvis "anteriorly." This could be quite perplexing to a nonradiologist. It also is ironic that Dr. Mirra, who wrote the chapter on giant-cell tumors, begins by calling them "giant cell tumor of the epiphysis." Two of his coauthors (Sweet and Gilkey) maintain that giant-cell tumors arise in the metaphysis, rather than the epiphysis. Nevertheless, these criticisms are miniscule when contrasted with the overall superb content of this textbook.

The considerable cost of this two-volume book will preclude its inclusion in the personal library of many residents or general radiologists, but it is clearly the definitive textbook (in the English language) on bone tumors. It truly contains a wealth of valuable information. Any medical center responsible for managing patients who have bone tumors should have access to this marvelous textbook, which is likely to remain the definitive reference source for many years to come. Dr. Mirra and his colleagues are to be highly praised for contributing this monumental work to the medical literature.

Richard P. Moser, Jr.
Armed Forces Institute of Pathology
Washington, DC 20306-6000

Pictorial Essay

Intracapsular Osteoid Osteoma of the Proximal Femur: Findings on Plain Film and CT

Alan E. Schlesinger[1] and Ramiro J. Hernandez

Osteoid osteoma is a benign skeletal tumor that typically presents clinically with pain and radiologically with dense sclerosis and periosteal new bone formation in the cortex of a long bone. A radiolucent nidus (with or without a central ossified focus) may be seen [1]. When located in a portion of the bone that is within the capsule of a joint, an osteoid osteoma may present with clinical findings that are more indicative of an inflammatory synovitis and with atypical radiologic findings such as lack of both sclerosis and periosteal reaction [2–4]. Chronic changes of bone remodeling, such as widening and foreshortening of the femoral neck and reduction in height of the capital femoral epiphysis, also can be seen if the diagnosis is delayed for more than 3 months [4].

Subjects and Methods

Five patients between the ages of 6 and 18 years (median, 12 years) with osteoid osteomas of the intracapsular portions of the proximal femurs were examined at the University of Michigan Hospitals. Routine radiographs and CT scans were obtained in all five patients. Four patients underwent bone scintigraphy, and plain tomograms of the proximal femur were obtained in one patient. The diagnosis was made histologically in three patients. Two patients had characteristic clinical symptoms that responded to therapy with salicylates or naproxen and had typical bone scan and CT findings. They declined surgery and have been followed up conservatively.

Results

Plain Radiographs and Tomograms of the Pelvis

The radiolucent nidus or surrounding reactive sclerosis considered typical for osteoid osteoma was not visible in three of the five patients on routine radiographs. In one patient a definite area of sclerosis was seen in the femoral neck (Fig. 1). In a second patient, a faint area of sclerosis was suggested (Fig. 2A).

Evidence suggesting acute synovial inflammation or joint effusion (widening of the distance from the lateral aspect of the teardrop to the medial proximal femoral metaphysis) was seen on plain radiographs of the pelvis in four of five patients (Fig. 2). Signs of chronic involvement were seen in all five patients (osteopenia in two patients and widening of the femoral neck due to bone remodeling in four patients) (Fig. 2).

Tomography, performed in one patient, confirmed the area of sclerosis seen in the femoral neck on the routine radiograph and further showed a central radiolucent nidus that contained a calcific center (see Fig. 1).

Bone Scintigraphy

Three of the four patients imaged with bone scintigraphy had focal areas of increased radionuclide uptake (Fig. 3). Increased radionuclide uptake at the proximal femoral growth plate and at the growth plate of the apophysis of the greater

---

Received December 18, 1989; accepted after revision February 5, 1990.

[1] Both authors: Department of Radiology, The University of Michigan Medical Center, Section of Pediatric Radiology, C. S. Mott Children's Hospital C3123/0252, 1500 E. Medical Center Dr., Ann Arbor, MI 48109-0252. Address reprint requests to A. E Schlesinger at C. S. Mott Children's Hospital.

AJR 154:1241–1244, June 1990 0361–803X/90/1546–1241 © American Roentgen Ray Society

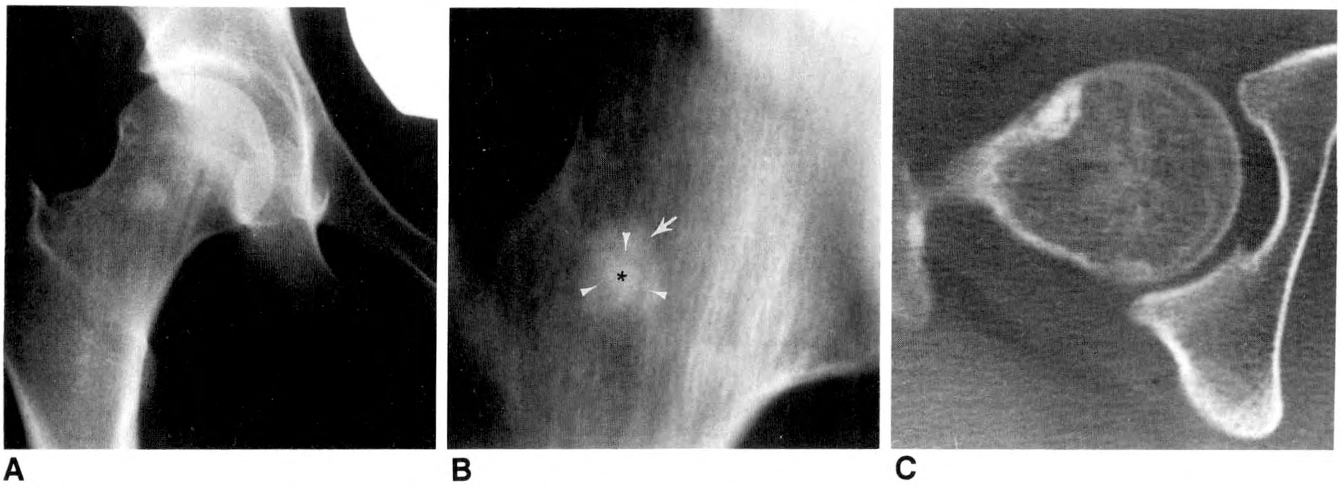

Fig. 1.—15-year-old girl with 5- to 6-month history of hip pain and dull aching in knee that awakened her at night and was relieved with aspirin.

A, Radiograph of hip shows a focal area of sclerosis in right femoral neck.

B, Tomogram further shows a radiolucent nidus (*arrowheads*) with a focal area of central sclerosis within nidus (*asterisk*). Sclerosis surrounding radiolucent nidus (*arrow*) also is noted.

C, Axial CT scan through osteoid osteoma confirms tomographic appearance. Symptoms improved dramatically with salicylate therapy. Patient refused surgery and is being treated conservatively.

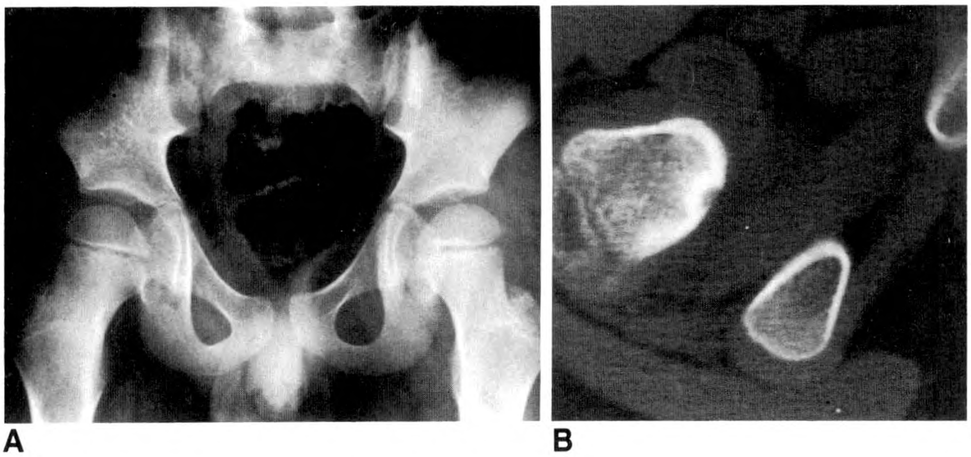

Fig. 2.—5-year-old boy with 4- to 6-month history of limp and right hip and knee pain.

A, Radiograph of pelvis suggests a right hip joint effusion (widening of distance from lateral aspect of teardrop to femoral metaphysis). In addition, note relative osteopenia of right proximal femur when compared with left as well as widening of right femoral neck. A suggestion of sclerosis is noted in medial, basal portion of femoral neck, but no radiolucent nidus is seen. Joint effusion suggests acute changes, whereas bony remodeling in femoral neck and osteopenia imply that process is long-standing. A CT scan (*not shown*) confirmed effusion.

B, Axial CT scan through proximal femur shows a radiolucent nidus without central calcification and with a small amount of sclerosis surrounding nidus. Patient improved with naproxen therapy and elected to have conservative therapy.

trochanter compared with the opposite unaffected side (without uptake at the site of the osteoid osteoma) was seen in one patient. The increased uptake at the growth plates was presumably due to increased blood flow.

CT

The location of the osteoid osteoma was identified on CT scans in all five patients. A radiolucent nidus within the cortex of the proximal femoral neck with a central calcific density was seen in three patients (Fig. 4). A radiolucent nidus within the cortex without a central calcific focus was seen in one patient (Fig. 2). A region of cortical irregularity along the anterior cortical surface of the proximal femoral neck corresponding to the location of the surgically proved osteoid osteoma was noted in the fifth patient (Fig. 3). There was no sclerosis surrounding the osteoid osteoma on CT in three of the five patients. Minimal sclerosis surrounding the radiolucent nidus was seen in one patient, and significant sclerosis was seen with CT in only the one patient whose plain films showed definite sclerosis in the proximal femoral neck (Fig. 1). In cases where 5-mm- or 1-cm-thick sections were obtained and no abnormality identified, thinner sections (2 mm) were required for successful identification of the osteoid osteoma.

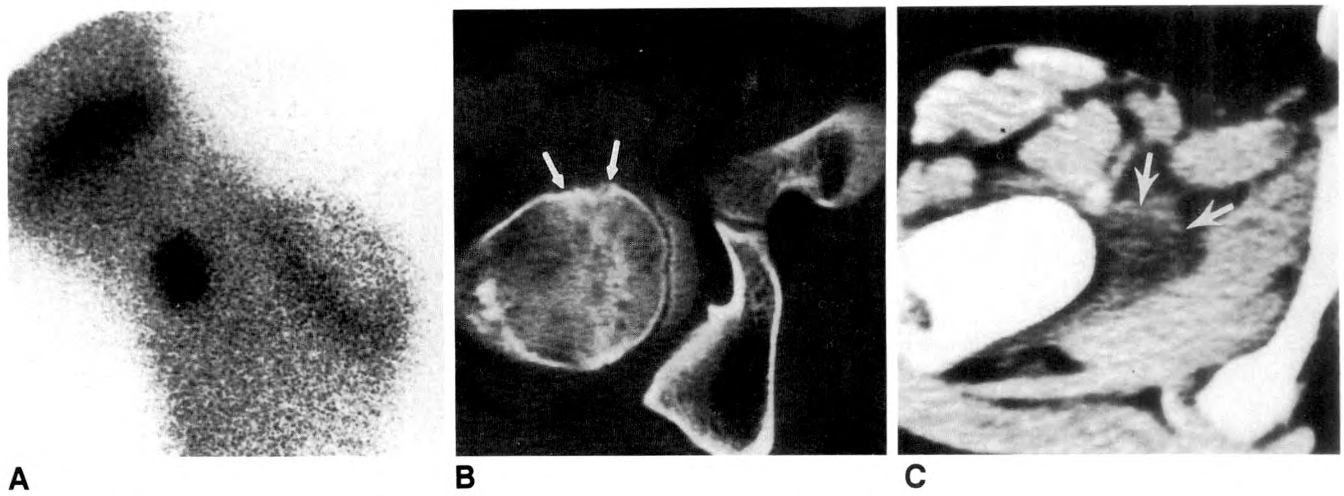

Fig. 3.—11-year-old boy with 3-year history of right groin and thigh pain relieved by aspirin.

A, Posterior view of right hip from a ^{99m}Tc-MDP scintigram shows a focal area of increased uptake of radionuclide in right femoral neck.

B, Axial CT scan through proximal femur shows an area of cortical irregularity in anterior aspect of right proximal femoral neck (*arrows*). This correlated with site of a surgically proved osteoid osteoma. This lesion was not detected on plain radiographs.

C, CT scan (1-cm-thick section), obtained approximately 21 months before *B*, shows a right hip effusion (*arrows*) with no bony abnormalities.

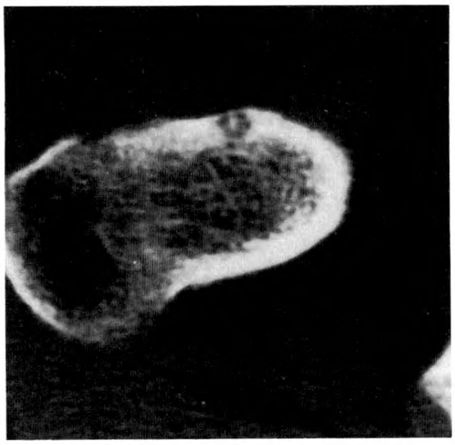

Fig. 4.—12-year-old girl with 6-month history of thigh pain radiating to knee that was relieved by salicylates. Axial CT scan through right femoral neck shows small radiolucent nidus with central calcification but without surrounding sclerosis. Neither nidus nor central calcification was detectable on plain radiographs. A small osteoid osteoma was removed at surgery.

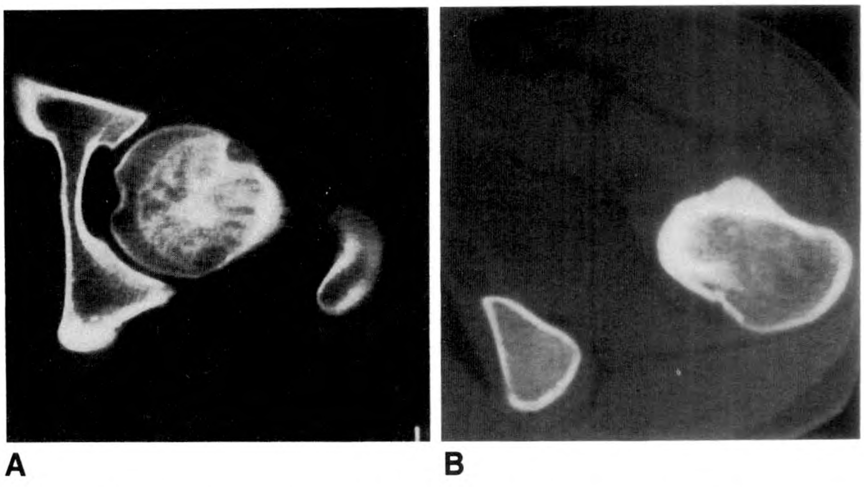

Fig. 5.—18-year-old boy with 1-year history of knee pain that was relieved by salicylates.

A, Axial CT scan through proximal femoral neck shows a radiolucent nidus with a focal area of central calcification but without surrounding sclerosis corresponding to surgically proved osteoid osteoma. Plain radiographs did not show lesion.

B, Axial CT scan through extracapsular femoral neck 3.25 cm more distal than *A* reveals periosteal reaction remote from site of osteoid osteoma.

Joint effusion was shown on CT scans in three of the five patients (Fig. 3). Periosteal reaction was seen in one case and was outside the limits of the joint capsule and remote from the intracapsular osteoid osteoma (Fig. 5).

Discussion

When an osteoid osteoma is located in the juxtaarticular portion of the proximal femur within the confines of the joint capsule, the clinical presentation can be atypical and mimic symptoms of synovial inflammation [1–4]. Therefore, osteoid osteoma should be considered early in the workup of the patient with symptoms of hip pain, limp, or pain referred to the knee [3].

The findings on plain radiographs in juxtaarticular osteoid osteoma also can be confusing because they differ from the typical findings seen in the extracapsular form of this benign bone tumor. Sclerosis may be lacking [4], and the intracapsular periosteum is less likely to produce new bone than the extracapsular periosteum [3]. Periosteal reaction associated with an intracapsular lesion also may occur at a remote (extracapsular) site [1]. A joint effusion may be present. If the diagnosis is delayed for several months, secondary changes in the femur such as widening in the femoral neck, osteopenia, and decreased height of the capital femoral epiphysis may develop [4].

Bone scintigraphy is highly sensitive in the detection of osteoid osteoma and is an excellent screening examination. The one patient we encountered in whom a bone scan showed no focal increased uptake of radionuclide at the site of the osteoid osteoma did have increased uptake in the adjacent growth plates. The scintigram was performed at another institution and was of good quality, but lacked pinhole views. Although the lack of radionuclide uptake by the osteoid osteoma may be due to the small size of the lesion and lack of sclerosis (see Fig. 4), a subtle abnormality might have been detected by pinhole views.

The appearance of a juxtaarticular osteoid osteoma on CT scans is that of a lucent nidus, with or without surrounding sclerosis. In one of our patients, there was irregularity of the cortex of the femoral neck rather than a well-defined radiolucent nidus. Central calcification may occur within the nidus in some patients. CT can confirm the presence of joint effusion and widening of the femoral metaphysis. Periosteal reaction remote from the site of the osteoid osteoma may be identified. If a patient presents with symptoms consistent with hip inflammation and an abnormal bone scan, CT may be helpful in confirming the diagnosis of osteoid osteoma and to monitor the lesion if conservative, nonsurgical therapy is elected.

REFERENCES

1. Fisher DR, Hinke ML. Musculoskeletal case of the day. *AJR* **1986**; 146:1087–1093
2. Kumar SJ, Harcke HT, MacEwen GD, Ger E. Osteoid osteoma of the proximal femur: new techniques in diagnosis and treatment. *J Pediatr Orthop* **1984**;4:669–672
3. Kattapuram SV, Kushner DC, Phillips WC, Rosenthal DI. Osteoid osteoma: an unusual cause of articular pain. *Radiology* **1983**;147:383–387
4. Alani WO, Bartal E. Osteoid osteoma of the femoral neck simulating an inflammatory synovitis. *Clin Orthop* **1987**;223:308–312

MR Imaging of the Temporomandibular Joint:

A Cadaver Study of the Value of Coronal Images

Bernhard W. Schwaighofer[1,2]
Terry T. Tanaka[3]
Michael V. Klein[1]
David J. Sartoris[1]
Donald Resnick[4]

Recent studies comparing cryosectional anatomy of the temporomandibular joint (TMJ) to its MR appearance have shown that the assessment of disk displacement is inaccurate when based on the sagittal plane alone. This article describes the MR appearance of the normal and abnormal (positional and osseous changes) TMJ in the coronal plane and compares these findings with their cryosectional anatomy. Twenty-two TMJs from unselected frozen cadavers were embedded in paraffin. Coronal and sagittal MR imaging was performed; specimens were then cut in the same plane as the coronal images. Disk position by cryosection was normal in 14 cases and abnormal in eight cases. Coronal MR images alone correctly depicted the TMJ disk position in 17 cases (77%) (13 normal, four abnormal). Complementary sagittal images were necessary for diagnosing anterior displacement in two cases (9%). MR was inaccurate in three cases (14%) of severe degenerative joint disease. Bone condition was correctly diagnosed on the basis of coronal images alone in all cases.

Our study shows that coronal MR imaging alone of the TMJ in cadavers accurately shows disk position in 77% of cases. Complementary sagittal images were of benefit in the diagnosis of an additional 9% with anterior displacement. Disk position was assessed inaccurately in either plane in patients with severe degenerative joint disease. For a full MR assessment of the TMJ for disk position and bone condition, we recommend imaging in both coronal and sagittal planes.

***AJR* 154:1245–1249, June 1990**

Pain and dysfunction of the temporomandibular joint (TMJ) are a common clinical syndrome seen in up to 39% of the population [1]. Patients' complaints include clicking, pain, crepitation, earache, and headache [2]. Potential causes are arthrosis, remodeling of the hard and soft structures, and internal derangements involving the articular disk and its attachments. Articular disk derangements frequently involve anterior [3, 4] and/or medial displacement [5, 6].

Different imaging techniques, including plain radiography, arthrography, and CT, were used to evaluate TMJ dysfunctions. Today, MR imaging has gained popularity among clinicians and radiologists with its ability to directly image disk margins and attachments. Sagittal MR imaging appears to be useful in the detection and delineation of disk configuration and displacement [2, 3, 7, 8]. The accuracy of MR imaging in assessing TMJ disk position has been found to be comparable with that of other imaging techniques, such as arthrography [9] and CT [8].

Recent studies comparing MR imaging with cryosectional anatomy have shown that the assessment of medial or lateral disk displacement based on the sagittal plane alone yields inaccurate results [4, 7, 9–12]. Additionally, rotational and sideways displacement of the disk frequently is misdiagnosed or missed entirely on sagittal MR imaging or arthrography [6]. Increased accuracy apparently can be achieved with MR by using a combination of sagittal and coronal views [6]. However, limitations of coronal plane MR imaging of both the normal and abnormal TMJ must be considered if it is routinely used to complement the sagittal images.

Received October 30, 1989; accepted after revision January 30, 1990.

This work was supported in part by fellowship J0283M (Erwin Schroedinger Stipendium), Austria, awarded to B. W. Schwaighofer.

[1] Department of Radiology and Magnetic Resonance Institute, University of California, San Diego, Medical Center, 225 Dickinson St., San Diego, CA 92103-1990. Address reprint requests to D. J. Sartoris.

[2] Present address: Department of Radiology, 2 Med. Univ. Klinik, Garnisongasse 13, A-1090 Vienna, Austria.

[3] Department of Radiology, University of California, San Diego, Medical Center, San Diego, CA 92103-1990.

[4] Department of Radiology, Veterans Administration Medical Center, 3350 La Jolla Village Dr., San Diego, CA 92161.

0361-803X/90/1546-1245
© American Roentgen Ray Society

In this study, we describe the MR appearance of both the normal and abnormal TMJ in the coronal plane and compare these findings with their cryosectional anatomy. Positional derangements and bone abnormalities as seen in the coronal plane are described, and the diagnostic accuracy and limitations of MR imaging in the coronal plane alone and in combination with the sagittal plane are discussed.

Materials and Methods

Twenty-two TMJs in the closed-jaw position were removed as blocks measuring approximately 5 × 5 × 5 cm from unselected fresh deep-frozen cadavers. No information about age, sex, or possible clinical premorbid TMJ symptoms of the cadavers was available. Standardized positioning during MR imaging and cryosectioning was achieved by embedding the specimens in square blocks of paraffin with one side oriented parallel to the condylar long axis. Plain radiographs were used to confirm position.

All scans were obtained on a commercially available Signa MR imager operating at 1.5 T (General Electric, Milwaukee, WI). Each specimen was thawed to room temperature and imaged with a 6.5-cm round planar surface coil operating in the receive mode. For best imaging quality, a special imaging protocol was used with an 8-cm field of view, 256 × 256 matrix, partial saturation pulse sequence with 600 msec repetition time and 20 msec echo time, and six excitations. Imaging was performed with 3-mm contiguous slices in the coronal plane (parallel to the long axis of the condyle) and a 3-mm slice thickness with a 1.5-mm interslice gap in the sagittal plane. The blocks were marked along these slices for sectioning.

After MR imaging, the specimens were refrozen. Fine-tooth metal-blade band saws and handsaws were used to cut each block in the same coronal plane as the coronal MR images. The cut surfaces of the specimens were photographed.

The MR images were independently evaluated for disk position and bone abnormalities by three radiologists who had no knowledge of the cryosectional results. Once the coronal images of all specimens were reviewed, the sagittal images were examined for additional information not present on the coronal images. The sagittal images were not evaluated separately as there were no cryosections in this plane for comparison. If a consensus opinion was not initially achieved, the image(s) in question were reviewed again by all evaluators, and a final consensus diagnosis was then made. MR findings subsequently were correlated with cryosection observations (as the morphologic standard).

The following criteria for disk position were used for both cryosections and MR images. The position of the TMJ disk was classified as normal or abnormal. If the disk was midway between the central portion of the condylar head and the apposing mandibular fossa, its position was considered normal [5, 11]. If the disk was displaced in either the coronal or sagittal plane, its position was considered to be abnormal. The position of an abnormal disk in the coronal plane was classified as either medial or lateral on the basis of its location relative to the superior surface of the condyle. Anterior displacement, if present, was diagnosed on the basis of the coronal MR image if the disk was seen on an image slice anterior to the condylar head and either no disk or only a small area of disk was noted above the condyle. Anterior disk displacement findings on coronal MR images then were correlated with the corresponding sagittal image. The cryosections and MR images of the TMJ joints were evaluated for evidence of osseous abnormalities, such as flattening and osteophytosis of the condyle, also.

Results

The results are summarized in Table 1. When compared with cryosectional anatomy, disk position was diagnosed correctly by coronal MR alone in 17 (77%) of the 22 joints and by the use of complementary coronal and sagittal MR images in 19 (86%) of the 22 joints.

In 14 (64%) of the 22 cadaver specimens, cryosectional analysis showed the disk in a normal position. In 13 (93%) of these 14 cases, the disk position was diagnosed as normal on both coronal and sagittal MR images. On coronal MR images, normal disks were located superior to the condyle and had a homogeneous relatively low signal intensity that was readily distinguishable from the surrounding tissues (Fig. 1). Only one of the 14 cryosectional specimens with normal disk position had a disk that was not visible on MR. This specimen had severe degenerative changes of the condyle with marked disk thinning. No perforations were found on either cryosection or MR imaging.

Abnormal disk position was noted on cryosection in eight (36%) of the 22 specimens. Seven cases had medially dislo-

TABLE 1: Disk Position and Bone Abnormalities Diagnosed on the Basis of Cryosection and MR Images in 22 Patients

Temporomandibular Joint Condition	Cryosection Diagnosis	Diagnosis by Coronal MR Images Only	Diagnosis by Complementary Coronal and Sagittal MR Images
Disk Position			
Normal	14	13	0
Abnormal displacement	8	4	2
Medial only	2	1	0
Lateral only	0	0	0
Anterior only	0	0	0
Anteromedial	5	3	2
Anterolateral	1	0	0
Bone Condition			
Normal	11	11	0
Abnormal	11	11	0
Osteoporosis	2	2	0
Degenerative changes	9	9	0

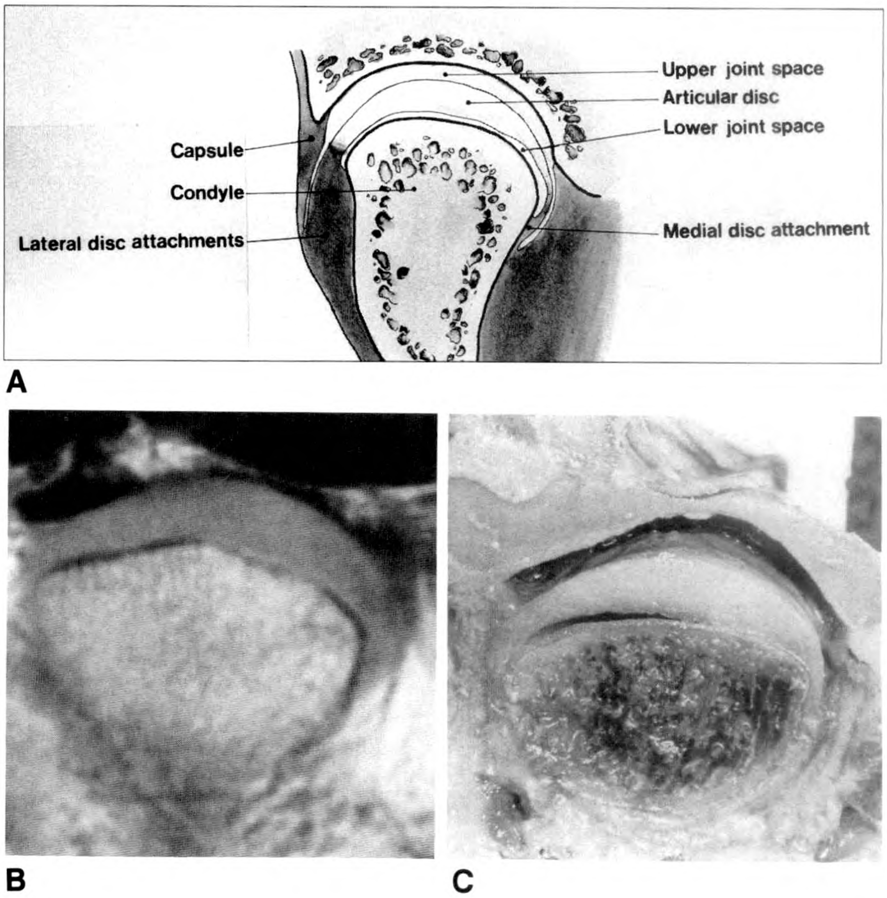

Fig. 1.—*A–C*, Coronal schematic illustration (*A*), spin-echo T1-weighted (600/20) MR image (*B*), and cryosection specimen (*C*) show normal right temporomandibular joint anatomy with disk positioned midway between central portion of condylar head and apposing mandibular fossa.

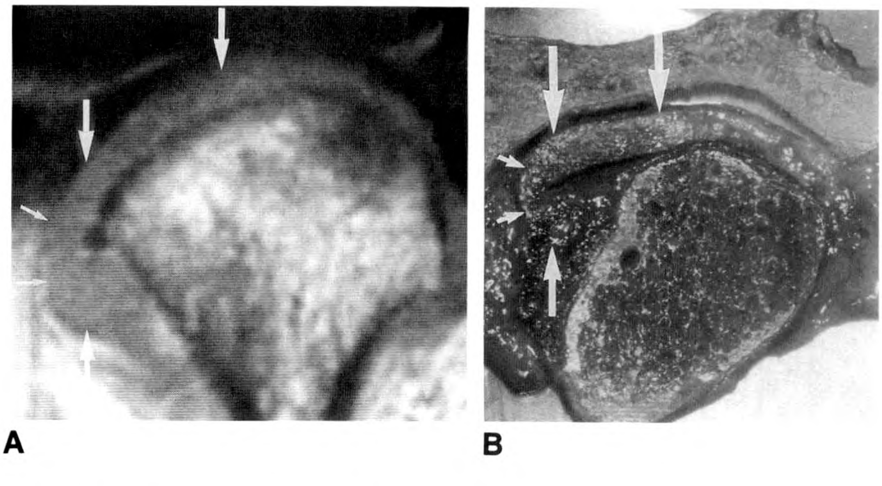

Fig. 2.—*A* and *B*, Coronal spin-echo T1-weighted (600/20) MR image (*A*) and cryosection specimen (*B*) show severe medial and mild anterior disk temporomandibular joint displacement. Marked medial displacement of disk (*arrows*) relative to medial pole of condyle is seen. Slight anterior displacement was evident on multiple coronal MR images and cryosection specimens.

cated disks; five also had anterior displacement. One specimen had anterolateral disk displacement. No specimens had isolated anterior or lateral disk displacement. MR images correctly depicted the position in all five specimens with anteromedial disk displacement (100%) (Fig. 2) and in one of two specimens with medial-only disk displacement (50%). MR images incorrectly depicted the TMJ disk position in the one specimen with anterolateral displacement (Fig. 3). The two specimens incorrectly diagnosed on the basis of MR findings had severe degenerative changes of the condyle with thinning of the disk (Fig. 3). Of the five specimens with anteromedial displacement diagnosed on the basis of MR findings, coronal views alone were sufficient for diagnosis of the anterior component of the displacement in three cases, and the use of complementary sagittal images was necessary in two cases.

MR images accurately correlated with the cryosections in the assessment of bone in all 22 cases (100%). The bone appeared normal in 11 of the 22 specimens.

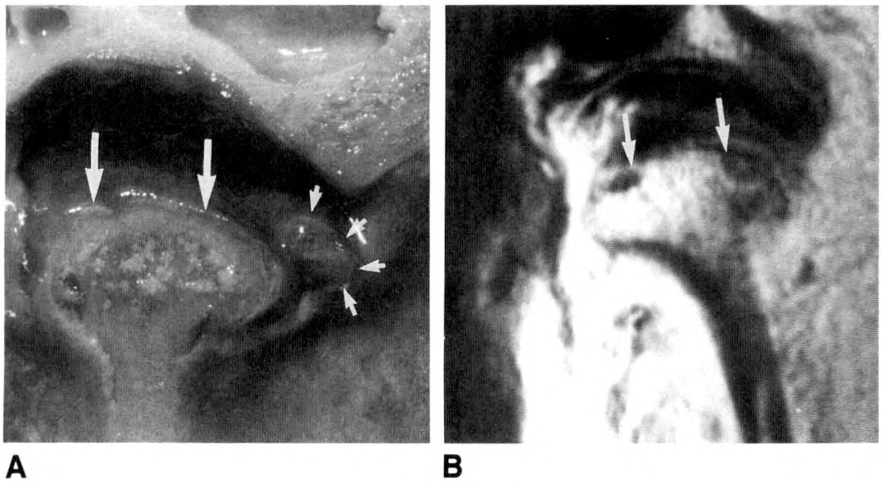

Fig. 3.—*A* and *B*, Coronal cryosection specimen (*A*) clearly shows anterolateral temporomandibular joint (TMJ) disk displacement (*small arrows*) on left side that was not diagnosed on the basis of coronal spin-echo T1-weighted (600/20) MR images (*B*). Incorrect MR diagnosis of TMJ disk position occurred in the presence of severe condylar degenerative changes and bony erosions, which are seen on both MR image and cryosection (*long arrows*).

Of the 11 specimens with bone abnormalities, two without degenerative changes had an accentuated trabecular bone pattern noted on both cryosectional examination and MR, which was interpreted as severe osteoporosis of the condyle. Nine specimens showed degenerative changes, including erosions, flattening, and osteophytosis of the condyle. The diagnosis of degenerative change was possible in all cases on the basis of coronal MR images alone. Erosions and flattening of the condyles, however, were better seen on coronal than on sagittal MR images (Fig. 4). Osteophytosis was better shown on sagittal than on coronal MR images.

Discussion

Our findings support previous studies showing that MR imaging clearly shows both normal [7, 11, 13] and abnormal TMJ position [7, 10, 13], except for cases involving severe degenerative joint disease. Coronal MR images alone allowed us to assess correctly the position of the TMJ disk in 77% of cases. The use of complementary sagittal MR images increased the accuracy to 86%. Our results correlate well with the only other published MR study that used both coronal and sagittal images [6], which revealed an accuracy of MR in the evaluation of disk position of 83% compared with cryosectional specimens. The inability of coronal views to provide additional information regarding disk position in a normal TMJ relative to the condylar head in our study is comparable to other reported results [8].

We found that inaccurate assessment of disk position by MR imaging occurred primarily in joints with severe degenerative changes involving a significantly thinned disk. For these cases, the joint spaces and surrounding tissues also had degenerative changes with an increase in MR signal intensity similar to that of the disk. Consequently, a distinct delineation of the thinned TMJ disk from surrounding tissue was not possible on MR. Several published reports discuss the occasional inability to differentiate the disk from the joint capsule, particularly in the presence of increased disk signal intensity resembling that of the capsule [9].

Mediolateral displacements of the TMJ disk are not uncommon [6]; sideways displacement occurred in 36% of our specimens. The large percentage of patients with rotational anteromedial and medial sideways disk displacements supports recent findings that indicate that these derangements are more common than rotational anterolateral or lateral displacements [6]. Importantly, standard protocols that use only sagittal MR images are not sufficiently accurate in the evaluation of sideways TMJ disk displacement [6]. Consequently, a full MR examination of the TMJ for positional disk abnormalities would include imaging in both coronal and sagittal planes.

Osseous abnormalities were diagnosed on all coronal images. The use of complementary sagittal MR images allowed better characterization of these changes. Coronal images more clearly depicted erosions and flattening of the condyles; sagittal images showed osteophytosis better. When sagittal MR imaging only is performed, accuracy in detecting the bone abnormalities may be as low as 60% [9]. Despite theoretical limitations of bone evaluation, MR has an accuracy rate in identifying osseous abnormalities (such as degenerative joint disease) comparable with that of CT [9], although these alterations may be less clearly visualized by MR [6]. Other reports suggest that CT remains superior in delineating osseous abnormalities [3, 8].

An important potential limitation of MR is its inability to reveal TMJ disk perforations, which are shown readily by arthrography [10, 14, 15]. Whereas an early study showed a TMJ disk perforation on sagittal T1-weighted images [3], more recent reports suggest that disk or posterior attachment perforations may be missed by either sagittal or coronal MR imaging [9, 10].

The use of a cadaveric model could limit the direct application of our results to the clinical setting. Although the unselected specimens used in this study may not match the age and sex distribution of a typical clinical population, the accuracy of MR in characterizing pathologic changes present in the specimens should be comparable with that of in vivo MR imaging. The ability of MR to show early pathologic changes underscores the importance of distinguishing symp-

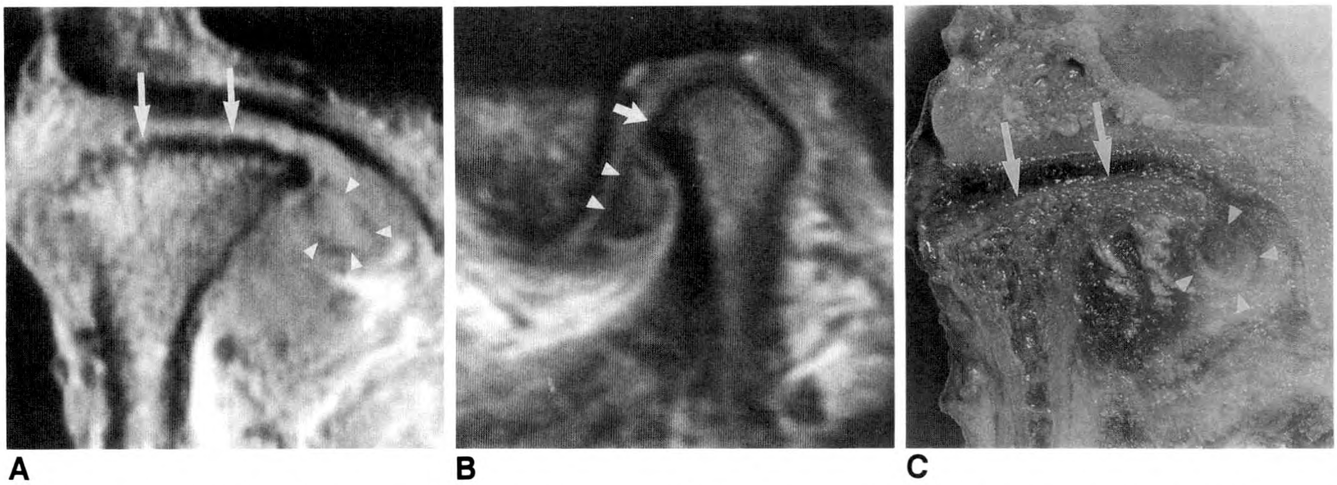

Fig. 4.—*A–C*, Right coronal (*A*) and sagittal (*B*) spin-echo T1-weighted (600/20) MR images and cryosection specimen (*C*) show condylar flattening and osteophytes. Cryosection specimen shows flattening and osteophytosis of condyle (*long arrows*) in addition to severe anteromedial disk displacement (*arrowheads*). Coronal image (*A*) shows condylar flattening (*long arrows*) better than sagittal image (*B*) does. Osteophytosis (*short arrow*) is shown more clearly on sagittal (*B*) than on coronal (*A*) image.

tomatic anatomic change from asymptomatic pathologic change or normal variation. In the present study, the absence of information about premorbid clinical symptoms as related to the cryosectional findings makes the significance of the more subtle findings difficult to assess. Also, cadaveric joint specimens may have components that move during the thawing process, thus increasing the prevalence of both false-positive and false-negative findings. The cadaveric model, however, provides an opportunity for accurate pathologic correlation that is unavailable in most clinical studies. Image quality of cadaver sections is maximized by the lack of movement and decreased noise from surrounding tissues. MR image quality in clinical studies may be degraded by patients' movements, noise from surrounding tissue, and older ferromagnetic orthodontic appliances or surgical implants [3, 4, 12]. Additionally, incomplete imaging frequently occurs as the result of claustrophobic episodes [3, 4, 12].

In summary, the use of the coronal plane alone allows a good assessment of the TMJ disk position and bone condition, with additional information on anterior disk displacement provided by the complementary sagittal image. Inaccuracies also occur in the presence of severe degenerative joint disease. For an optimal study of this joint, we recommend the combined use of coronal and sagittal MR images.

REFERENCES

1. Pullinger AG, Seligman DA, Solberg WK. Temporomandibular disorders. Part I: Functional status, dentomorphologic features, and sex differences in a nonpatient population. *J Prosth Dent* **1988**;59:228–235
2. Sokoloff R, Sartoris DJ, Resnick D. Uncovering the sources of temporomandibular joint malfunction. *J Musculoskel Med* **1988**;5:69–79
3. Harms SE, Wilk RM, Wolford LM, Chiles DG, Milan SB. The temporomandibular joint: magnetic resonance imaging using surface coils. *Radiology* **1985**;157:133–136
4. Harms SE, Wilk RM. Magnetic resonance imaging of the temporomandibular joint. *RadioGraphics* **1987**;7:521–542
5. Juniper RP. The pathogenesis and investigation of TMJ dysfunction. *Br J Oral Maxillofac Surg* **1987**;25:105–112
6. Katzberg RW, Westesson PL, Tallents RH, et al. Temporomandibular joint: MR assessment of rotational and sideways disk displacement. *Radiology* **1988**;169:741–748
7. Katzberg RW, Bessette RW, Tallents RH, et al. Normal and abnormal temporomandibular joint: MR imaging with surface coil. *Radiology* **1986**;158:183–189
8. Westesson P-L, Katzberg RW, Tallents RH, Sanchez-Woodworth RE, Svensson SA. CT and MR of the temporomandibular joint: comparison with autopsy specimens. *AJR* **1987**;148:1165–1171
9. Westesson P-L, Katzberg RW, Tallents RH, Sanchez-Woodworth RE, Svensson SA, Espeland MA. Temporomandibular joint: comparison of MR images with cryosectional anatomy. *Radiology* **1987**;164:59–64
10. Donlon WC, Moon KL. Comparison of magnetic resonance imaging, arthrotomograph and clinical and surgical findings in temporomandibular joint derangements. *Oral Surg Oral Med Oral Pathol* **1987**;64:2–5
11. Kaplan PA, Tu HK, Williams SM, Lydiatt DD. The normal temporomandibular joint: MR and arthrographic correlation. *Radiology* **1987**;165:177–178
12. Schellhas KP, Wilkes CH, Fritts HM, Omlie MR, Heithoff KB, Jahn JA. Temporomandibular joint: MR imaging of internal derangements and postoperative changes. *AJR* **1988**;150:381–389
13. Roberts D, Schenck J, Joseph P, et al. Temporomandibular joint: magnetic resonance imaging. *Radiology* **1985**;155:829–830
14. Westesson P-L, Bronstein SL, Liedberg J. Temporomandibular joint: correlation between single-contrast videoarthrography and postmortem morphology. *Radiology* **1986**;160:767–771
15. Westesson P-L, Rohlin M. Diagnostic accuracy of double-contrast arthrotomography of the temporomandibular joint: correlation with postmortem morphology. *AJR* **1984**;5:463–468

Book Review

Pediatric Bone Imaging. A Practical Approach. Edited by Soroosh Mahboubi. Boston: Little, Brown, 215 pp., 1989. $75, softcover

The purpose of this book is "to familiarize the reader with the different modalities used for musculoskeletal disorders in infants and children." The first chapter is an overview by John Kirkpatrick that briefly describes each modality. This is followed by 10 more chapters. Five give details on technique, indications, and findings in specific pathologic entities. The other five address radiologic and orthopedic approaches to specific musculoskeletal problems. Of special interest are the chapters on the radiologic approach to the evaluation of joint disease, primary soft-tissue lesions, and primary bone lesions in which a multitechnique assessment of different entities and lesions is given.

The text is well written, and the illustrations are of high quality. It is not a successor to or a competitor of a comprehensive text of pediatric orthopedic imaging, such as Ozonoff's *Pediatric Orthopedic Radiology* (Saunders, 1979). Rather it gives precept and example for integration of the newer techniques into the contemporary imaging practice, especially that of the pediatric radiologist. Its scope is broad, but the individual discussions are terse, although generously referenced. The essaylike discussion of an orthopedist's perspective of these modern procedures fills out the coverage.

Pediatric Bone Imaging is a contemporary, practical book indeed. It can give pediatric radiologists insight into what to do next, but it does not give the answers to all specific questions and problems.

M. Kathryn Garrett
Medical Center Radiology Group
Orlando, FL 32806
Alan E. Oestreich
Children's Hospital Medical Center
Cincinnati, OH 45229-2899

Staging of Hodgkin Disease in Children: Comparison of CT and Lymphography with Laparotomy

Lori L. Baker[1]
Bruce R. Parker[1]
Sarah S. Donaldson[2]
Ronald A. Castellino[1]

Proper therapy for Hodgkin disease requires accurate staging of the disease. We compared the value of CT and lymphography with that of laparotomy for staging newly diagnosed Hodgkin disease in 46 children. The laparotomy revealed disease in one or more subdiaphragmatic sites in 46%. Correlation of the imaging studies with the laparotomy findings showed that lymphography has a greater sensitivity (80%) than does CT (40%) in detecting retroperitoneal lymph nodes. The sensitivity of CT in detecting splenic involvement was only 19%, presumably because of the small size of tumor deposits in involved spleens. Staging laparotomy altered the clinical stage in 37% of children, which resulted in a significant change of therapy in those patients.

Although lymphography and, to a lesser degree, CT are useful for staging of Hodgkin disease, laparotomy continues to be the most important tool in choosing appropriate therapy for children with Hodgkin disease.

***AJR* 154:1251–1255, June 1990**

The appropriate methods for accurately staging subdiaphragmatic extent of disease in children with Hodgkin disease remains controversial. Although the relative usefulness of CT and lymphography in detection of retroperitoneal lymphadenopathy in Hodgkin disease in adults has been well addressed [1–4], only limited data are available regarding this issue in children [5–8]. In addition, debate continues over the justification for staging laparotomy with splenectomy in children with Hodgkin disease.

The present study was designed (1) to determine the sensitivity, specificity, and accuracy of CT and lymphography in detection of subdiaphragmatic involvement in a group of children with newly diagnosed Hodgkin disease that had been pathologically staged and (2) to assess the impact of staging laparotomy findings on clinical staging of the disease and treatment of patients.

Materials and Methods

This prospective study was performed from October 1979 to January 1989 and included 61 patients (38 boys, 23 girls), ranging in age from 5 to 16 years (mean, 12 years), who had newly diagnosed Hodgkin disease. All patients had posteroanterior and lateral chest radiographs; CT scans of chest, abdomen, and pelvis; and bipedal lymphography. The CT studies and lymphograms were interpreted without knowledge of the results of the other examination, and the interpretations of these studies at the formal staging conference were tabulated for this analysis. Patients were excluded if it was not possible to perform both imaging studies before staging laparotomy because of scheduling difficulties. In addition, many patients with clinical stage IV disease and some with medical contraindications were excluded because CT, lymphography, and staging laparotomies were not routinely performed. The final study group comprised 46 children with newly diagnosed Hodgkin disease. A few of our patients were included in an earlier study consisting primarily of adult patients [2].

CT studies were performed on GE 8800/9800 scanners (Milwaukee, WI) after administration of oral contrast material. Contiguous 10-mm slices were used. Patients routinely were scanned from the domes of the hemidiaphragms to the inferior tips of the liver and spleen

Received November 2, 1989; accepted after revision January 22, 1990.

Presented at the annual meeting of the American Roentgen Ray Society, New Orleans, LA, May 1989.

This work was supported in part by grant C-34233 from the National Cancer Institute, National Institutes of Health.

[1] Department of Diagnostic Radiology and Nuclear Medicine, Stanford University School of Medicine, Stanford, CA 94305. Address reprint requests to B. R. Parker.

[2] Department of Radiation Oncology, Stanford University School of Medicine, Stanford, CA 94305.

0361–803X/90/1546–1251
© American Roentgen Ray Society

before bolus IV administration of contrast material. The sequence was then repeated after the injection, and scanning was continued through the abdomen and pelvis to the level of the symphysis pubis. Dynamic imaging techniques were used early in the study because of data indicating superior results [9]. Technically comparable studies performed at other institutions on patients before their referral to Stanford University Medical Center also were accepted into this study. The CT diagnosis of lymphadenopathy was made when lymph nodes were larger than 1.0 cm or if there were clusters of smaller nodes. CT scans were considered positive for splenic or hepatic involvement when there was organ enlargement and/or parenchymal defects of low attenuation. CT studies were usually performed before lymphography.

Bipedal lymphography was performed in the standard fashion [10] after administration of local anesthesia. Sedation and/or general anesthesia was used in those children younger than 8 years old. The lymphograms were interpreted as positive for Hodgkin disease involvement when the opacified lymph nodes showed disruption of the normal internal architectural pattern, producing a foamy, lacelike appearance or focal filling defects.

Staging laparotomy included splenectomy, needle and wedge liver biopsies, bone marrow biopsy, and multiple lymph node biopsies (splenic hilar, paraaortic, porta hepatic, mesenteric, and celiac). A final pathologic stage was then determined in accordance with the Ann Arbor staging classification [11]. The postsurgical course was documented in each patient, follow-up ranged from 0.5 to 9.0 years (mean, 3.6 years). Histologic classification followed the Lukes-Butler classification [12].

The accuracy of CT and lymphography in detection of subdiaphragmatic involvement by Hodgkin disease at various anatomic sites was determined as a function of sensitivity, specificity, and overall accuracy [13]. Sensitivity indicates the percentage of patients with histologically proved disease whose imaging studies were correctly interpreted as positive. Specificity defines the percentage of patients histologically free of disease whose imaging studies were correctly interpreted as negative. Overall accuracy is the percentage of patients with true-positive and true-negative studies.

Pathologic stage was compared with initial clinical stage. Clinical stage is based on history, physical examination, and laboratory and radiologic findings. Pathologic stage is based on the histologic findings from splenectomy, retroperitoneal lymph node samplings, and liver and bone marrow biopsy. The Ann Arbor classification system [11] for staging of Hodgkin disease is based on anatomic extent of disease and presence or absence of constitutional symptoms. The impact of staging laparotomy findings on treatment of patients, particularly with respect to radiotherapy fields, was then evaluated.

Results

The histologic subtype and clinical stage for the disease in the 46 children who underwent staging laparotomy are shown in Table 1. Four patients had clinical stage I disease, on the basis of biopsy from a single lymph node site and otherwise normal physical examination and radiologic studies. The diagnosis of clinical stage II disease in 34 patients was based on presence of two or more supradiaphragmatic ($n = 33$) or infradiaphragmatic ($n = 1$) regions of disease. Six patients had clinical stage III disease on the basis of supradiaphragmatic disease and positive findings on lymphograms and/or abdominal CT scans. In the two patients with clinical stage IV disease, one had bone involvement on plain film and radionuclide scintigraphy studies, and the second had lung involvement on CT scan. The majority of patients (30/46, or 65%) had the nodular sclerosing histologic subtype.

Table 2 summarizes the extent of pathologically proved subdiaphragmatic disease by histologic subtype after staging

TABLE 1: Clinical Stage and Histologic Subtype in 46 Children with Newly Diagnosed Hodgkin Disease

Clinical Stage	No. of Patients	Histology				
		LP	NS	MC	LD	IF
I	4 (9)	2	0	1	0	1
II	34 (74)	2	25	6	0	1
III	6 (13)	0	3	3	0	0
IV	2 (4)	0	2	0	0	0
Total	46	4 (9)	30 (65)	10 (22)	0	2 (4)

Note.—LP = lymphocyte predominance; NS = nodular sclerosing; MC = mixed cellularity; LD = lymphocyte depletion; IF = interfollicular. Numbers in parentheses are percentages.

TABLE 2: Subdiaphragmatic Involvement at Staging Laparotomy by Histologic Subtype in 46 Children with Newly Diagnosed Hodgkin Disease

Histology	No. of Patients	No. with Subdiaphragmatic Involvement (%)	Spleen Only	Spleen + LN	LN Only
LP	4	1	0	1	0
NS	30	11 (37)	4	4	3
MC	10	8 (80)	2	4	2
IF	2	1	1	0	0
Total	46	21 (46)	7	9	5

Note.—LN = lymph nodes, including splenic hilar, retroperitoneal, and porta hepatic; LP = lymphocyte predominance; NS = nodular sclerosing; MC = mixed cellularity; IF = interfollicular. Of the 21 patients with subdiaphragmatic involvement, 19 had stage III and two had stage IV disease.

laparotomy. Almost half of the patients (46%) had positive findings at staging laparotomy. Subdiaphragmatic involvement by disease was most common in patients with the mixed cellularity subtype (8/10, or 80%).

Table 3 shows the sensitivity, specificity, and accuracy of lymphography and CT in the detection of subdiaphragmatic disease, with laparotomy findings used as the gold standard. In the five children with positive retroperitoneal lymph node involvement found at laparotomy, four had a positive lymphogram (sensitivity, 80%). In the one patient in whom the lymphogram was false-negative, the more cephalad paraaortic lymph nodes, which were positive at laparotomy, were not opacified; this patient's CT scan also was negative for retroperitoneal involvement. All 41 patients who were free of retroperitoneal lymph node involvement had negative lymphography studies (specificity, 100%). The overall accuracy of lymphography in evaluating the retroperitoneal lymph nodes in our patient series was 98% (45/46).

CT showed retroperitoneal lymph node enlargement in two of the five patients with positive retroperitoneal node biopsies (sensitivity = 40%). In the three patients in whom CT was false-negative, the lymph nodes sampled by biopsy were of normal size but were found histologically to be infiltrated by tumor. Thirty-nine of 41 patients with negative retroperitoneal lymph node biopsies also had negative CT studies (specificity, 95%). In the two patients with false-positive CT studies for retroperitoneal adenopathy, the excised lymph nodes were enlarged; however, they showed only reactive hyperplasia on histologic examination (and on the corresponding lymphography studies). The overall accuracy of CT in evaluating retroperitoneal lymph nodes in our patient population was 89% (41/46).

Other nodal groups sampled at laparotomy included splenic hilar, mesenteric, celiac, and porta hepatic lymph nodes. Splenic hilar nodes were sampled by biopsy in 36 patients. Of these, 10 had tumor involvement; none of those 10 patients had abnormalities on CT (sensitivity, 0%). All excised lymph nodes were normal in size. CT was true-negative in the remaining 26 patients who had histologically normal hilar nodes (specificity, 100%). Mesenteric and celiac nodes were sampled in 35 and 11 patients, respectively, all of whom showed absence of tumor involvement. All CT studies were normal with regard to mesenteric and celiac node abnormalities. Of the 12 patients in whom biopsies of the porta hepatic lymph nodes were done, only one child had tumor involvement. No patient showed porta hepatic abnormalities on CT.

In the 16 patients with splenic involvement at laparotomy, CT showed an abnormal spleen (splenomegaly with no focal regions of low attenuation) in only three children (sensitivity, 19%). The remaining 13 children had normal spleens on CT studies. The majority of children with splenic involvement (14/16, or 88%) had tumor deposits less than 5 mm in size; the largest deposit was 8 mm. CT showed normal spleens in 25/30 patients in whom splenectomy results were negative (specificity, 83%). The five children in whom CT was false-positive all showed splenomegaly with no parenchymal abnormalities; however, none of these spleens showed involvement by Hodgkin disease on histologic examination. Overall accuracy of CT in evaluation of splenic involvement was 61% (28/46).

No child in this series had histologic involvement of the liver by Hodgkin disease. All CT scans showed the liver to be of normal size and homogeneity.

Figure 1 summarizes the impact of staging laparotomy on initial clinical stage. Laparotomy findings resulted in alteration of clinical stage in 37% (17/46) of children. Clinical stage I disease in one patient and clinical stage II disease in 14 patients were upstaged to pathologic stage III disease on the basis of previously unsuspected splenic and/or splenic hilar node involvement at staging laparotomy, resulting in extension of radiation ports to include subdiaphragmatic sites. In two patients, clinical stage III disease diagnosed on the basis of splenic involvement suggested on CT was downstaged to

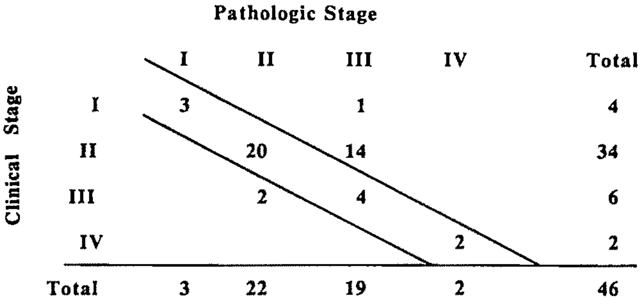

Clinical Stage \ Pathologic Stage	I	II	III	IV	Total
I	3		1		4
II		20	14		34
III		2	4		6
IV				2	2
Total	3	22	19	2	46

Fig. 1.—Comparison of clinical stage vs pathologic stage after staging laparotomy in children with newly diagnosed Hodgkin disease.

TABLE 3: Sensitivity, Specificity, and Accuracy of Lymphography and CT in Detection of Subdiaphragmatic Hodgkin Disease

Organ	Sensitivity (%)	Specificity (%)	Accuracy (%)
Lymph Nodes			
Retroperitoneal			
Lymphography	4/5 (80)	41/41 (100)	45/46 (98)
CT	2/5 (40)	39/41 (95)	41/46 (89)
Splenic hilar (CT)	0/10 (0)	26/26 (100)	26/36 (72)
Mesenteric (CT)	0/0	35/35 (100)	35/35 (100)
Celiac (CT)	0/0	11/11 (100)	11/11 (100)
Porta hepatic (CT)	0/1	11/11 (100)	11/12 (92)
Spleen (CT)	3/16 (19)	25/30 (83)	28/46 (61)
Liver (CT)	—	—	—

Note.—No patient had biopsy-proved hepatic involvement.

pathologic stage II after laparotomy, when histologic examination revealed no evidence of splenic disease. These children were thus spared subdiaphragmatic radiation. The remaining three patients with splenomegaly on CT, but negative splenectomy specimens, had positive retroperitoneal lymph nodes on CT and/or lymphography that were confirmed histologically, leaving them unchanged with stage III disease.

Discussion

Accurate staging followed by therapy tailored to the extent of disease has resulted in high 10-year survival rates in children with Hodgkin disease [14]. The therapeutic protocols used at Stanford for these patients rely heavily on accuracy of staging because the treatment regimen consists of multiagent chemotherapy and low-dose radiotherapy (15-25 Gy) to sites known to be involved. This individualized approach allows radiotherapy to be targeted maximally to involved sites, while minimizing short- and long-term treatment complications. Alternative therapeutic protocols that rely solely on clinical staging use extended field radiation with or without chemotherapy and consequently subject children to increased volumes and/or increased doses of radiation [15].

Our series of children showed lymphography to be slightly more accurate than CT in detecting retroperitoneal lymph node disease. Lymphography had a sensitivity of 80% and specificity of 100% compared with a sensitivity of 40% and specificity of 95% for CT. This difference may, in part, be explained by the ability of lymphography to show tumor deposits within normal-sized lymph nodes. In addition, lymphography often can differentiate nodal enlargement due to reactive hyperplasia from that due to lymphomatous infiltration. Our data, however, are limited by the small number of children with nodal disease at laparotomy, and therefore, the difference between lymphography and CT is not statistically significant ($p = .36$).

With the exception of splenic hilar nodes, which were positive in 10 of the 36 patients in whom they were sampled, involvement of other subdiaphragmatic nodal groups by Hodgkin disease was uncommon. All mesenteric and celiac lymph nodes sampled by biopsy were negative, as were corresponding CT findings. Previous studies have also documented a low frequency of mesenteric lymph node involvement, less than 5%, in Hodgkin disease [2, 16]. Involved mesenteric lymph nodes in these series were normal in size, and CT was unable to detect nodal involvement.

Splenic involvement was present in 35% of children. The sensitivity of CT for detecting splenic involvement was 19%. The poor sensitivity of CT reflects the fact that Hodgkin disease deposits in the spleen are small at presentation, generally less than 5 mm; in addition, tumor-involved spleens in these patients are often normal in size. Previous studies also have shown low sensitivities (33%) with regard to the capabilities of CT in detection of splenic involvement in adult patients [2]. Conventional sonography has yielded poor results in detection of lymphomatous spleens [17]. More recently, however, use of narrow-band filtration of backscattered ultrasound has shown promise in detection of splenic involvement [18]. Initial reports on the capability of MR imaging in this regard have shown no significant advantage of MR imaging over CT or conventional sonography [19, 20]. However, experimental studies have suggested that supraparamagnetic MR contrast agents may improve the sensitivity of MR imaging in tumor detection [21].

No child in our series had hepatic involvement. Therefore, the capabilities of CT in evaluating the liver for Hodgkin disease cannot be addressed.

Our series of patients was a consecutive group of newly diagnosed, previously untreated children who had both lymphography and CT performed before laparotomy. It does not represent a consecutive group of children who underwent staging laparotomy, as both imaging studies were not always done in all patients who underwent staging laparotomy because of scheduling difficulties. However, exclusion of specific patients was a random event. Furthermore, not all children with newly diagnosed Hodgkin disease ultimately underwent staging laparotomy. Those with clinical stage IV disease and/or medical contraindications for surgery did not routinely undergo laparotomy. Therefore, our population of children is skewed toward those with less advanced disease. Additionally, our data are not applicable to children with recurrent disease.

In conclusion, histologic evidence of splenic and retroperitoneal lymph node involvement at staging laparotomy had a significant impact on accurate determination of final stage of disease in 37% of patients. As a result, the therapy in these children was altered. Lymphography or CT performed before laparotomy serves as a means of discovering those children with clinical stage III disease in whom treatment would require subdiaphragmatic radiation, irrespective of laparotomy findings; surgical staging is not indicated in these patients. Lymphography also delineates suspicious nodes to be sampled by biopsy during surgery in equivocal cases. CT is less useful in detection of subdiaphragmatic involvement, given its low sensitivity in detection of lymphomatous deposits and inability to show disease within normal-sized lymph nodes.

REFERENCES

1. Castellino RA. Imaging techniques for staging abdominal Hodgkin's disease. *Cancer Treat Rev* **1982**;66:697-700
2. Castellino RA, Hoppe RT, Blank N, et al. Computed tomography, lymphography, and staging laparotomy: correlations in initial staging of Hodgkin disease. *AJR* **1984**;143:37-41
3. Marglin S, Castellino R. Lymphographic accuracy in 632 consecutive, previously untreated cases of Hodgkin disease and non-Hodgkin lymphoma. *Radiology* **1981**;140:351-353
4. Clouse ME, Harrison DA, Grassi CJ, Costello P, Edwards SA, Wheeler HG. Lymphangiography, ultrasonography, and computed tomography in Hodgkin's disease and non-Hodgkin's lymphoma. *J Comput Assist Tomogr* **1985**;9:1-8
5. Daneman A, Martin DJ, Fitz CR, Chan HS. Computed tomography and lymphogram correlation in children with Hodgkin's disease. *J Comput Assist Tomogr* **1983**;7:115-122
6. Parker BR, Castellino RA, Kaplan HS. Pediatric Hodgkin's disease. I. Radiographic evaluation. *Cancer* **1976**;37:2430-2435
7. Tschappeler H. Computed tomography (CT) and lymphoma in children. *Ann Radiol* **1980**;23:87-91
8. Sullivan M, Ramirez I, Jing B. Role of lymphogram in surgical staging of

children with Hodgkin disease. *Proc Annu Meet Am Assoc Cancer Res* **1986**;27:203

9. Young SW, Turner RJ, Castellino RA. A strategy for contrast enhancement of malignant tumors using dynamic computed tomography and intravascular pharmacokinetics. *Radiology* **1980**;137:137–147
10. Dunnick NR, Parker BR, Castellino RA. Pediatric lymphography: performance, interpretation, and accuracy in 193 consecutive children. *AJR* **1977**;129:639–645
11. Carbone PP, Kaplan HS, Mushoff K, Smithers DW, Tubiana M. Report of the Committeee of Hodgkin's Disease Staging Classification. *Cancer Res* **1971**;31:1860–1861
12. Lukes RJ, Butler JJ, Hicks EB. Natural history of Hodgkin's disease as related to its pathologic picture. *Cancer* **1966**;19:317–344
13. McNeil BJ, Keeler E, Adelstein SJ. Primer in certain elements of medical decision making. *N Engl J Med* **1975**;293:211–215
14. Donaldson SS, Link MP. Combined modality treatment with low-dose radiation and MOPP chemotherapy for children with Hodgkin's disease. *J Clin Oncol* **1987**;5:742–749
15. Jenkin D, Chan H, Freedman M, et al. Hodgkin's disease in children: treatment results with MOPP and low-dose extended-field irradiation. *Cancer Treat Rev* **1982**;66:949–959
16. Kaplan HS. *Hodgkin's disease*, 2d ed. Cambridge, MA: Harvard University Press, **1980**
17. Sekiva T, Meller ST, Cosgrove DO, McCread VR. Ultrasonography of Hodgkin's disease in the liver and spleen. *Clin Radiol* **1982**;33:635–639
18. Friedman PA, Sommer FG, Chen HS, Rachlin DJ, Hoppe R. Characterization of splenic structure in Hodgkin disease by using narrow-band filtration of backscattered ultrasound. *AJR* **1989**;152:1197–1203
19. Richards MA, Webb JA, Jewell SE, Stansfeld AG, Lister TA, Wrigley PF. Low field strength magnetic resonance imaging of the spleen: results from volunteers and patients with lymphoma. *Br J Cancer* **1988**;57:408–411
20. Nyman R, Rehn S, Glimelius B. Magnetic resonance imaging, chest radiography, computed tomography, and ultrasonography in malignant lymphoma. *Acta Radiol* **1987**;28:253–262
21. Fretz CJ, Stark DD, Metz CE, et al. Ferrite enhanced MRI of focal hepatic lesions: controlled comparison with contrast enhanced CT and noncontrast MR. Presented at the annual meeting of the American Roentgen Ray Society, New Orleans, LA, May **1989**

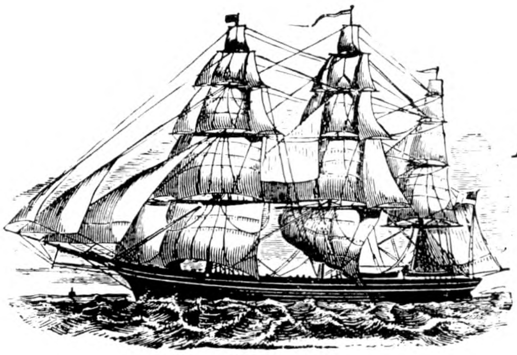

Come to the
American Roentgen
Ray Society
91st
ANNUAL MEETING
Boston, MA
Sheraton Boston Hotel
May 5-10, 1991

Scientific Program (200 papers)
Instructional Courses (60 hours)
Categorical Course on
Body MR Imaging
The Caldwell Lecture
Award Papers
Scientific Exhibits
Social, Golf, and Tennis Programs
Guest Programs

Book Review

Pros and Cons in PTA and Auxiliary Methods. Edited by Eberhard Zeitler and Walter Seyferth. New York: Springer-Verlag, 289 pp., 1989. $75, softcover

This is an excellent book. Under the able organization of Drs. Zeitler and Seyferth, it was written by an international cast of outstanding contributors and pioneers well known in the field of vascular dilatation and recanalization. The pioneering efforts of Charles Dotter and Andreas Grüntzig, to whom this book is dedicated, truly have revolutionized the nonsurgical treatment of atherosclerotic vascular disease and have spurred intense investigations for improving methods to prolong patency rates after angioplasty.

Three quarters of the text is devoted to feasibility studies and early clinical trials of evolving technologies with various types of laser-assisted angioplasty, mechanical recanalization devices, and endovascular stents. Concise introductory chapters on various types of laser energy are followed by a description of clinical trials with the hot metal-tip laser, the neodymium–yttrium-aluminum-garnet sapphire-tip contact laser, and the balloon-centered LASTAC system with a divergent argon laser beam, systems that today are used with only various degrees of success. Although unfocused laser treatment with bare fibers no longer is considered safe, the editors have included two chapters on the early clinical use of this method to provide a more complete historical perspective of the field. Various mechanical devices for recanalizing obstructed vessels are described by their inventors (i.e., Kensey, Vallbrecht, Wholey, and Zeitler). The Simpson atherectomy catheter is not mentioned.

The section on percutaneous endovascular stents covers the use of various auto- and balloon-expandable stents, which, in the United States, are still in clinical trials. This hot topic is extremely well presented. The reader should, however, be aware that this fascinating, evolving new technology not only is costly but also may not lead to improved patency rates over standard angioplasty and thrombolysis; the results of long-term comparative studies are not yet available. Short reviews of thrombolysis, percutaneous embolectomy, control of vasospasm, and platelet aggregation inhibitors are given for completeness.

Most of the information is available in the literature published from 1984 to early 1988, but not as conveniently as in this book, which provides, with its impressive sets of references, an excellent background of information for understanding present and future developments in this challenging field. The chapters are written in a clear and succinct style. Photographs and drawings are of excellent quality (the book contains 154 figures and 50 tables). Angiograms submitted by the authors to support the results of the interventional procedures range from adequate to good, except for those on pp. 86–87, which are barely interpretable. The quality of the paper, the printing, and the softcover binding is first-rate.

Because this easily readable and affordable book casts an eye on present and future percutaneous techniques for managing peripheral vascular disease, it should be useful as a reference for the vascular interventionist and fascinating for any physician who has an interest in the vascular system.

Constantin Cope
Hospital of the University of Pennsylvania
Philadelphia, PA 19104

Case Report

Arterial Embolization to Control Life-Threatening Hemorrhage from a Meckel's Diverticulum

Masatoshi Okazaki,[1] Hideyuki Higashihara,[1] Soichi Yamasaki,[1] Yuzo Akita,[1] Hiroshi Toriya,[2] and Zentaro Shirai[2]

A life-threatening hemorrhage from Meckel's diverticulum occurred in a 14-year-old boy. Superior mesenteric arteriography showed an abnormal vessel, a remnant of the omphalomesenteric artery with extravasation of contrast material. Because the patient was not a surgical candidate, a Tracker-18 catheter was used to embolize the artery with a Gelfoam fragment (Upjohn, Kalamazoo, MI). After hemostasis and stabilization, the Meckel's diverticulum was resected.

Case Report

A 14-year-old boy presented with a 7-day history of cramping periumbilical pain of moderate severity. Three days before admission to our hospital he first noted a bright red stool, after which he suffered a syncopal episode and was brought to another hospital. Initial hematocrit was 36.5% but fell to 26.7% after transfusion with two units (one unit = 200 ml) of packed RBCs. Gastroduodenoscopy was performed and was normal. Massive hemorrhage continued, and emergent visceral arteriography failed to reveal a bleeding site. After continued massive bleeding for 3 days, the patient became hypotensive despite repeated blood transfusions (30 units of packed RBCs) and volume replacement. A bleeding tendency and hypoproteinemia were noted at that time. The patient was transferred to the emergency department of Fukuoka University Hospital for further treatment.

On admission, the patient's blood pressure was 80/50 mm Hg, hemoglobin level was 6.3 g/dl, hematocrit 21%, and serum total protein 2.5 g/dl. Emergent angiography was performed while blood pressure was maintained by administration of packed RBCs, fresh frozen plasma, and dopamine infusion. Superior mesenteric arteriography with a 5-French Torcon blue catheter (Cook Inc., Bloomington, IN) disclosed an abnormally enlarged but unbranched vessel arising from the ileal artery (Fig. 1A). Selective arteriography with digital subtraction showed capillary staining and extravasation (Fig. 1B). A presumptive diagnosis of bleeding Meckel's diverticulum with heterotopic gastric mucosa was made. In order to embolize this abnormal vessel, a 2.2-French Tracker coaxial catheter and a Taper 0.016-in. (0.406 mm) platinum-tipped steerable guidewire (Target Therapeutics, Mountain View, CA) were introduced through the 5-French catheter (Fig. 1C). Embolization was performed by using a Gelfoam fragment (2–3 mm). Superior mesenteric arteriography after the embolization showed occlusion of this vessel without extravasation.

The ileum was partially resected on the first day after emergent embolization. The surgical specimen showed a deep peptic ulcer of the ileal bowel mucosa adjacent to the ectopic gastric mucosa in a Meckel's diverticulum. Histologically, arterial thrombosis was identified only in the Meckel's diverticulum, and no ischemic changes were observed in the remainder of the bowel.

After an initially stormy postoperative course, the patient made a good recovery and was discharged 5 days after surgery.

Discussion

Meckel's diverticulum, the most common congenital anomaly of the small intestine, is a true diverticulum that involves all layers of the gut wall. It results from incomplete obliteration of the vitelline or omphalomesenteric duct [1–3]. Meckel's

---

Received October 17, 1989; accepted after revision January 5, 1990.

This work was supported in part by a grant-in-aid for cancer research from the Ministry of Health and Welfare of Japan.

[1] Department of Diagnostic Radiology, Fukuoka University Hospital, 7-45-1 Nanakuma Jonan-ku Fukuoka, 814-01 Japan. Address reprint requests to M. Okazaki.

[2] First Department of Surgery, Fukuoka University Hospital, 7-45-1 Nanakuma Jonan-ku Fukuoka, 814-01 Japan.

AJR **154:1257–1258, June 1990** 0361–803X/90/1546–1257 © American Roentgen Ray Society

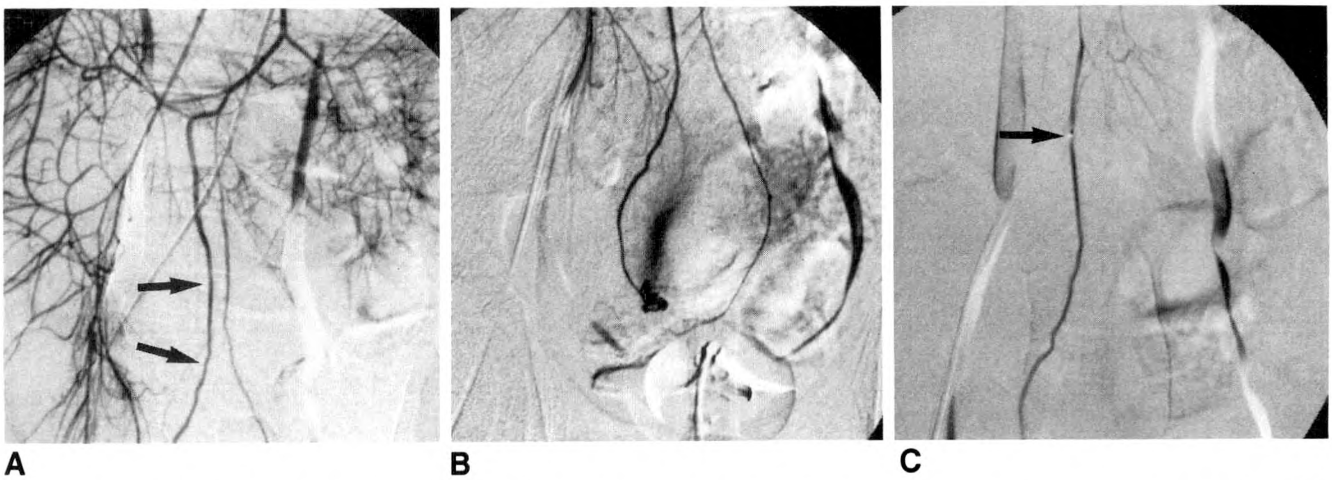

Fig. 1.—*A*, Superior mesenteric arteriogram shows an abnormally dilated artery (*arrows*) originating from ileal artery. This dilated vessel had no other branches until it reached pelvic cavity.

***B*, Ileal arteriogram shows extravasation and capillary staining of terminal portion of dilated vitelline artery.**

***C*, Superselective vitelline arteriography shows no branches of vitelline artery until it reaches site of extravasation. *Arrow* shows tip of a Tracker-18 catheter.**

diverticulum occurs in 1–3% of the population, and complications arise in approximately one third of those having this condition [4]. The most common complication in younger patients is hemorrhage, which is caused by peptic ulceration produced by secretion of acid and pepsin from ectopic gastric mucosa [2–4].

A 10.3% mortality rate and a 17.6% morbidity rate have been noted for symptomatic diverticuli [3]. In view of the potential for life-threatening hemorrhage, diagnosis and treatment of the bleeding is of considerable clinical importance. Angiography plays a dominant role, because it can show the bleeding site and, at the same time, provide effective treatment by embolization. However, although many reports have described treatment of bleeding Meckel's diverticulum, we are unaware of any reports of treatment of these lesions by means of embolization [1–6].

This patient was considered an extremely high-risk candidate for emergent surgical control of the bleeding because of hypoproteinemia and coagulopathy. Previous reports have identified an abnormal artery supplying the Meckel's diverticulum [6]. This artery is a remnant of the omphalomesenteric artery lying within the mesodiverticular band. By using a coaxial system, this artery can be selectively catheterized and embolization performed with limited risk to the adjacent bowel.

REFERENCES

1. Dennis WV, Karen WW, Jay LG. Vitelline duct anomalies: experience with 217 childhood cases. *Arch Surg* **1987**;122:542–547
2. Robert BR, David RA. Meckel's diverticulum: a review of 148 pediatric patients, with special reference to the pattern of bleeding and to mesodiverticular vascular bands. *Surgery* **1966**;59:618–626
3. William CM, Peter D. A fifty year experience with Meckel's diverticulum. *Surg Gynecol Obstet* **1983**;156:56–64
4. Leijonmarck CE, Kerstin BS, Frisell J, Raf L. Meckel's diverticulum in the adult. *Br J Surg* **1986**;73:146–149
5. Hogsbro OA, Fredens M. Arteriographic demonstration of bleeding from Meckel's diverticulum. *Scand J Gastroenterol* **1971**;6:109–110
6. Hall TJ. Meckel's bleeding diverticulum diagnosed by mesenteric arteriography. *Br J Surg* **1975**;62:882–884

Diagnosis of Tumors of the Parotid Gland with Anti-CEA Immunoscintigraphy

Kalevi J. A. Kairemo[1,2]
Erkki V. M. Hopsu[3]

Twenty-nine consecutive patients with a palpable unilateral tumor in the parotid gland region had scintigraphy 22–28 hr after they were injected with ^{111}In-labeled monoclonal anti–carcinoembryonic antigen (CEA) antibody (F023C5). Two patients were imaged at 48 hr also, and one patient was imaged additionally with single-photon emission CT. Twenty-seven of the patients had surgery within 2–3 weeks. The serum CEA concentrations were normal in 27 of 29 patients. Immunoglobulin G human anti-murine-antibody concentrations were elevated in three of 20 patients. Ten patients had scintigraphic findings suggesting a malignant tumor, six of them had histologically proved malignant tumors. The tumors associated with positive immunoscintigrams were stained immunohistochemically with anti-CEA, and four of the malignant tumors were positive in immunohistochemical staining.

The results suggest that nonspecific anti-CEA-antibody imaging is helpful in predicting the presence of a malignant tumor in the parotid area. The radioantibody method could provide useful clinical information that has a high negative predictive value.

AJR 154:1259–1262, June 1990

Radionuclides have been used in the diagnosis of salivary gland tumors: ^{99m}Tc-pertechnetate is accumulated in the normal salivary glands and is retained in patients with Warthin tumors [1]. Accumulation of ^{111}In-labeled WBCs in the lacrimal and salivary glands of a patient with Sjögren syndrome has been reported [2]. The efficacy of ^{67}Ga in the diagnosis of malignant neoplasms in the head and neck is limited by the normal uptake of this isotope by oral and pharyngeal minor salivary and secretory glands, thus hampering the differentiation of malignant neck and head neoplasms from normal tissues [3].

No reports have been published on the use of monoclonal radioantibodies to detect malignant salivary gland tumors, probably because of the problem caused by the great variety of malignant tumors in the salivary glands. A further difficulty is that the levels of common serum tumor markers, such as carcinoembryonic antigen (CEA), are rarely elevated [4]. The CEA is produced by many different malignant cell lines, especially different adenocarcinomas and carcinomas of epithelioid origin [5]. Radiolabeled polyclonal anti-CEA antibody has been used for detecting malignant tumors of the head and neck in five patients [6].

The aim of this study was to assess the value of anti-CEA scintigraphy for imaging malignant tumors in the parotid area and to compare the findings with the histology of the tumor.

Materials and Methods

A total of 29 consecutive patients (11 men, 18 women; 22–75 years old; average age, 52 years) with a palpable tumor in the parotid gland region were examined clinically and imaged radiologically. All patients gave their informed consent. All were outpatients with a suspicion of parotid tumor: three of 29 tumors later were found not to be of parotid origin. Twenty-five

Received July 10, 1989; accepted after revision November 21, 1989.

This work was supported by a grant from the Finnish Cancer Organizations (K.J.A. Kairemo) and the Finnish Academy Foundation (E.V.M. Hopsu).

[1] Department of Clinical Chemistry, Division of Nuclear Medicine, Helsinki University Central Hospital, Haartmaninkatu 4, SF-00290, Helsinki, Finland.

[2] Present address: Nuclear Medicine Service, Memorial Sloan-Kettering Cancer Center, 1275 York Ave., New York, NY 10021. Address reprint requests to K. J. A. Kairemo.

[3] Department of Otorhinolaryngology, Helsinki University Central Hospital, Helsinki, Finland.

AJR 0361–803X/90/1546–1259
© American Roentgen Ray Society

of these patients underwent surgery of the primary tumor. One patient with a local recurrence and one with a metastatic lesion also had surgery, but two patients were followed up clinically only, because the tumors decreased in size within 3 weeks. These tumors disappeared totally within 2 months and were regarded as lymphadenitis.

Surgery was performed 2–3 weeks after immunoscintigraphy. This study was done with the permission of the Ethical Committee of the Department of Otorhinolaryngology, Helsinki University Central Hospital.

The $F(ab')_2$ fragment, a DTPA conjugate of the anti-CEA antibody (clone F023C5) [7] (Indomab-K-2, Sorin Biomedica, Saluggia, Italy) was labeled with indium-111 ($InCl_3$ from Amersham International plc, Little Chalfont, U.K.) by using the standard method of conjugating the antibody with cyclic DTPA (c-DTPA) [8]. The maintenance of the immunoreactivity of the radiolabeled monoclonal antibody FO23C5 was checked by the manufacturer by in vitro assay in which the colorectal cancer cell line was used as the specific target and the lymphoblastoid cell line as the control [4]. The immunoreactivity was 90–95%.

The antibody dose was 0.3 mg, and the injected radioactive dose varied from 1.1 to 3.1 mCi (40–115 MBq). The labeling yield, measured in eight preparations, varied from 82% to 93%. Thin layer chromatography (ITLC SG, Gelman Sciences, Ann Arbor, MI) was used with 0.1 mol/l EDTA as solvent, and the elution time was approximately 5 min. The radioactivity was measured with a gamma counter (LKB Compugamma 1282, Wallac, Turku, Finland).

All patients were imaged 22–28 hr after the injection of radioantibody. No skin test was performed, but all the patients were asked for a history of allergies. Planar spot images were taken of the head (anteroposterior and lateral views) by using a General Electric Maxi 400 gamma camera (General Electric Co., Milwaukee, WI) with a medium-energy collimator. Into each scintigram, 300,000–450,000 counts were collected by using a 64 × 64 matrix. Both gamma energy peaks of ^{111}In (173 keV, 15% window; 245 keV, 15% window) were used. Two patients were imaged approximately 48 hr after injection also. One patient was imaged with single photon emission CT (SPECT) also, 72 hr after the injection. In the SPECT study, 64 angles were recorded at one frame per 35 sec. The camera, connected to a PDP-11 computer fitted with GAMMA-11/34 software, had a resolution of 350 dots and color display. The parotid regions were analyzed by using a region-of-interest (ROI) technique; the pulses were calculated in a square in both parotid regions and the tumor-to-background pulse ratio was calculated as the ratio of pulses of affected site and contralateral site after subtracting background pulses (square on corpus of mandible) on both sides.

TABLE 1: Tumor-to-Background Ratios in Different Salivary Gland Disorders

Diagnosis	No. of Cases	Average Ratio (range)
Benign lesions		
Pleomorphic adenoma	13	1.1 (0.9–1.5)
Mikulicz disease	3	1.1 (1.0–1.4)
Lymphoepithelial cyst	1	1.0
Adenolymphoma	1	1.4
Lymphadenitis[a]	3	1.0 (0.9–1.1)
Tuberculosis	1	1.0
Lipoma	1	1.0
Malignant lesions		
Adenocarcinoma metastases	1	1.2
Adenocystic carcinoma	1	1.2
Acinic cell carcinoma	2	1.3 (1.2–1.3)
Paraganglioma	1	1.6
Hemangiopericytoma	1	2.0

Note—Tumor-to-background ratios are expressed as ratios between suspected and contralateral sides (as explained in text).

[a] In two cases, diagnosis was based only on clinical investigations.

A superficial parotidectomy was performed on 24 patients, and three patients had a total parotidectomy. Histopathologic diagnoses of tumors are listed in Table 1. The scintigraphically malignant tumors (10/27) were stained for CEA. The immunohistochemically malignant tumors were acinic cell carcinomas, metastasis of an adenocarcinoma (possibly of renal origin), and an adenocystic carcinoma.

Serum samples in 27 patients were taken just before injecting the radioantibody. The concentration of CEA in serum was measured with a radioimmunoassay method.

Serum samples of the assay of human anti-murine antibodies (HAMAs) in 18 patients were taken within 2 weeks to 4 months after the radioantibody injection. Additional serum samples after 2–3 months were taken in three patients; in 14 patients the samples were taken within 2–4 weeks.

The IgG and IgM subclass HAMAs were determined with an enzyme-linked immunosorbent assay method (Enzygnost-HAMA-Micro, Behringwerke, Marburg, W. Germany).

Results

No adverse reactions to the radioantibody were observed. Ten of the 58 parotid gland regions appeared to contain a malignant neoplasm on scintigrams. Six of these malignant findings could be correlated with histologic findings of a malignant tumor: two acinic cell carcinomas (Fig. 1), one hemangiopericytoma (Fig. 2), one adenocystic carcinoma (Fig. 3), one metastasis of adenocarcinoma of unknown origin, and one paraganglioma. Four nonmalignant tumors appeared to be malignant on scintigrams. There were no normal scintigrams associated with malignant tumors.

Thus, the specificity (17/21) and sensitivity (6/6) as compared with the histologic findings (in order to detect malignant parotid tumors) were 81% and 100%, respectively. The specificity (19/23) and sensitivity (6/6) were 83% and 100%, respectively, if compared with the clinical and surgical findings. The carotid body tumor was considered malignant because of its potential fatality and ability to metastasize.

The serum CEA concentrations were below 4.0 $\mu g/l$ in 27 measured cases, and thus no one had an elevated concentration (abnormal values > 5.0 $\mu g/l$). The tumor-to-background ratios (TBR) were relatively low even if the scintigrams were regarded as suggesting a malignant tumor, except for one in which the TBR was greater than 2.0. The findings were regarded as suggestive of a malignant tumor if this ratio was 1.2 or more. The findings were considered suspicious when the TBR was 1.1–1.2. These lesions were analyzed carefully with the ROI technique and were considered malignant only if independent subjective evaluation by the two physicians suggested a malignant tumor. No disagreement in the interpretation between the two observers occurred. The average TBRs and ranges for the different parotid neoplasms are listed in Table 1.

Elevated HAMA trends of IgG subclass and the IgM subclass were observed in three and 16 of 20 cases, respectively.

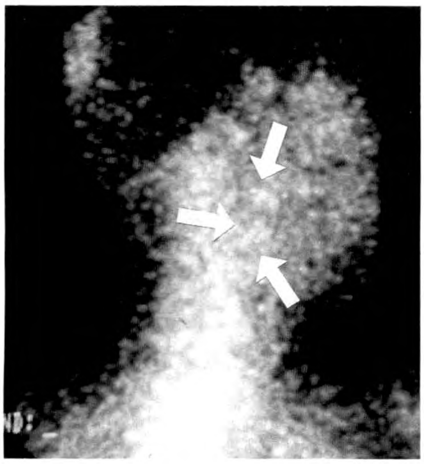

Fig. 1.—37-year-old man with an acinic cell carcinoma of parotid gland. Right lateral scintigram shows positive uptake in tumor site (*arrows*).

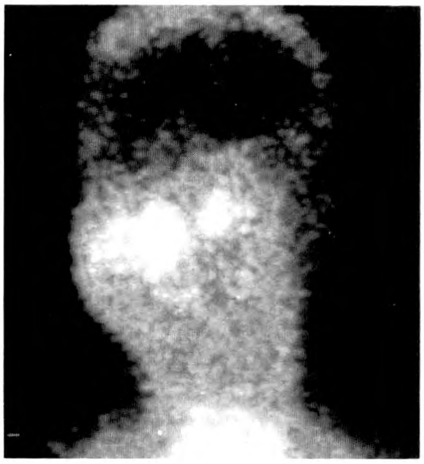

Fig. 2.—Planar spot scintigram (anterior view) of a 27-year-old man with hemangiopericytoma shows a large amount of uptake in right parotid region.

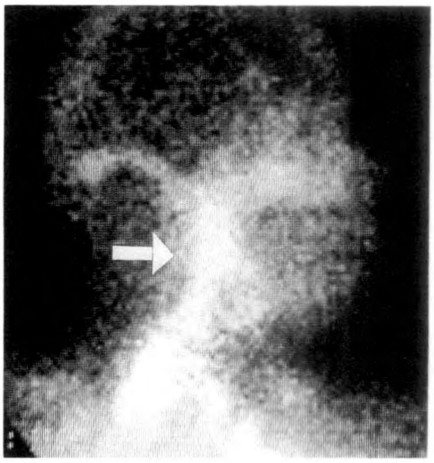

Fig. 3.—Right lateral scintigram of a 56-year-old woman with adenoid cystic carcinoma of parotid gland (*arrow*).

Discussion

With radiologic methods it is possible to obtain information concerning the character of salivary gland tumors [9]. Sialography, sonography, MR imaging, and CT can visualize the tumor. With these methods, however, it is difficult to draw conclusions about the possibility of a malignant tumor. In a recent low-field MR imaging study of 103 patients with suspected salivary gland disease, it was not possible to distinguish malignant invasion from chronic inflammatory disease [10]. CT and sonography have equal value in detection of parotid tumors, but CT is recommended in order to define whether the mass is benign or malignant [11]. The ultimate diagnosis rests on histology of the primary tumor.

Anti-CEA immunoscintigraphy had a high negative predictive value (100%). Our material, however, is limited, because we had only five different types of malignant tumors represented, all of which were visualized on scintigrams.

The mechanism of antibody uptake is not apparent because no clear correlation was seen between immunohistochemical and immunoscintigraphic findings. The highest uptakes were in the tumors with no stainability with anti-CEA.

One of the routes of the ^{67}Ga-citrate accumulation into malignant neoplasms is increased vascular permeability [12]. This same mode of uptake also could be valid for antibodies. The ^{67}Ga-citrate accumulates slightly in normal salivary glands, whereas ^{111}In-labeled anti-CEA antibodies do not show any affinity for normal salivary glands; this may be one of the major advantages when using antibodies in the diagnosis of salivary gland tumors.

Two cases with multiple lesions were considered false-positive; one of the reasons for abnormal scintigrams might be the superpositioning of tumors containing nonbinding circulating antibody.

One of the four false-positive findings was probably caused by infection because the parotid mass disappeared during the follow-up; anti-CEA antibodies can recognize structures on the granulocyte cell surface or granulocytes can entrap antibodies by pinocytosis. An anti-granulocyte antibody can be induced by CEA, and therefore anti-CEA antibodies occasionally can be observed to bind to granulocytes [13]. The tuberculoma in our material was not shown although it has been possible to image such a tumor in mice with another monoclonal antibody [14]. All but one of the pleomorphic adenomas (Fig. 4) appeared normal on immunoscintigrams. These can be diagnosed with MR imaging, and the differential diagnosis of Mikulicz disease, parotitis, and cysts also is possible with MR imaging [10]. The importance of paramagnetic contrast media in MR imaging of parotid tumors is still unknown; Gd-DPTA facilitated the interpretation of results in paragangliomas [15].

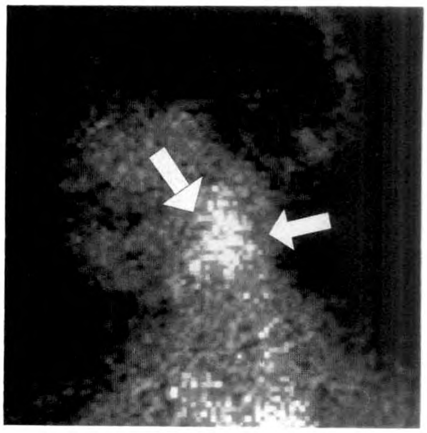

Fig. 4.—Left lateral scintigram of a 72-year-old woman with pleomorphic adenoma of parotid gland (*arrows*).

The serum CEA concentration did not correlate with our immunoscintigraphic findings. A similar discrepancy was reported by Mach et al. [16]. This indicates that it is probably difficult to find a suitable serum marker for malignant tumors of the parotid gland—at least CEA serum concentration determinations are not useful even though radiolabeled anti-

CEA is a promising diagnostic tool. However, we do not recommend immunoscintigraphy as a routine investigation because other monoclonal antibodies also have to be tested in larger series of various malignant tumors. CEA is expressed by many types of tumors (colorectal, breast, lung, pancreas, cervix carcinomas), and specificity causes problems that must be recognized when imaging parotid malignant tumors of various origins. The mechanism of the antibody uptake should be investigated further. Anti-CEA immunoscintigraphy is, however, a new and complementary radiologic tool in the diagnosis of tumors of the salivary glands.

ACKNOWLEDGMENTS

We thank Kristian Liewendahl and Lars-Göran Johnsson for their advisory comments.

REFERENCES

1. Greyson ND, Noyek AM. Radionuclide salivary scanning. *J Otolaryngol* **1982**;10[suppl]:1–47
2. Donnal JF, Beytas EM. In-111 WBC activity in salivary and lacrimal glands of a patient with Sjögren's syndrome. *Clin Nucl Med* **1988**;13:694–695
3. Kornblut AD, Silberstein EB, Saenger EL, Shumrick DA. Scintiscanning with gallium citrate 67: diagnosis of head and neck malignant neoplasms. *Arch Otolaryngol* **1974**;100:201–205
4. Silverman NA, Alexander JC, Chretien PB. CEA levels in head and neck cancer. *Cancer* **1976**;37:2204–2211
5. Toto PD. Fluorescent antibody detection of CEA in oral cancer. *J Oral Med* **1979**;34:45–46
6. Tranter RMD, Fairweather DS, Bradwell AR, Dykes PW, Watson-James S, Chandler S. The detection of squamous cell tumours of the head and neck using radio-labelled antibodies. *J Laryngol Otol* **1984**;98:71–74
7. Siccardi AG, Buraggi GL, Gallegaro L, et al. Immunoscintigraphy of adenocarcinomas by means of radiolabeled $F(ab')_2$ fragments of an anti-carcinoembryonic antigen monoclonal antibody: a multicenter study. *Cancer Res* **1989**;49:3095–3103
8. Paik CH, Ebbert MA, Murphy PR, et al. Factors influencing DTPA conjugations with antibodies by cyclic-DTPA anhydride. *J Nucl Med* **1983**;24:1158–1163
9. Mancuso AA, Harnsberger HR, Muraki AS, Stevens MH. Computed tomography of cervical and retropharyngeal lymph nodes: normal anatomy, variants of normal, and applications in staging head and neck cancer. *Radiology* **1983**;148:715–723
10. Smith FW, Deans HE, McLay KA, Rayner CW. Magnetic resonance imaging of the parotid glands using inversion-recovery sequences at 0.08 T. *Br J Radiol* **1988**;61:480–491
11. Isaza M, Ikezoe J, Morimoto S, et al. Computed tomography and ultrasonography in parotid tumors. *Acta Radiol [Diagn]* (Stockh)**1989**;30:11–15
12. Anghilieri LJ, Crone-Escanye M-C, Thouvenot P, Brunotte F, Ropert J. Mechanisms of gallium-67 accumulation by tumors: role of cell membrane permeability. *J Nucl Med* **1988**;29:663–668
13. Buchegger F, Schreyer M, Carrel S, Mach J-P. Monoclonal antibodies identify a CEA crossreacting antigen of 95 kD (NCA-95) distinct in antigenicity and tissue distribution from the previously described NCA of 55 kD. *Int J Cancer* **1984**;33:643–649
14. Hazra DK, Lahiri VL, Saran S, et al. In vivo tuberculoma creation and its radioimmunoimaging. *Nucl Med Commun* **1987**;8:139–142
15. Vogl T, Bauer M, Schedel H, Brüning R, Mees K, Lissner J. Kernspintomographische Untersuchungen von Paragangliomen des Glomus caroticum und Glomus jugulare mit Gd-DTPA. *Fortschr Geb Röntgenstr Nuklearmed Ergänzungsband* **1988**;148:38–46
16. Mach J-P, Bischof-Delaloye A, Curchod S, et al. L'immunoscintigraphie par les anticorps monoclonaux radiomarqués. *Schweiz Med Wochenschr* **1987**;117:1076–1086

Pictorial Essay

MR Imaging of the Cranial Nerves

Charles F. Lanzieri[1]

When imaging patients with cranial-nerve symptoms, it is useful to think of each cranial nerve as existing in a unique environment of vascular, bony, and dural structures (Figs. 1–5). Normal and pathologic anatomy are different for each cranial nerve, as are the clinical and imaging features [1–4]. This concept serves especially well when MR imaging is used because the cranial nerve itself as well as the adjacent structures can be seen with MR. Optimal radiologic evaluation of cranial-nerve abnormalities depends on a precise understanding of the cranial-nerve symptoms, precise focusing of the examination, and a complete understanding of the functional anatomy.

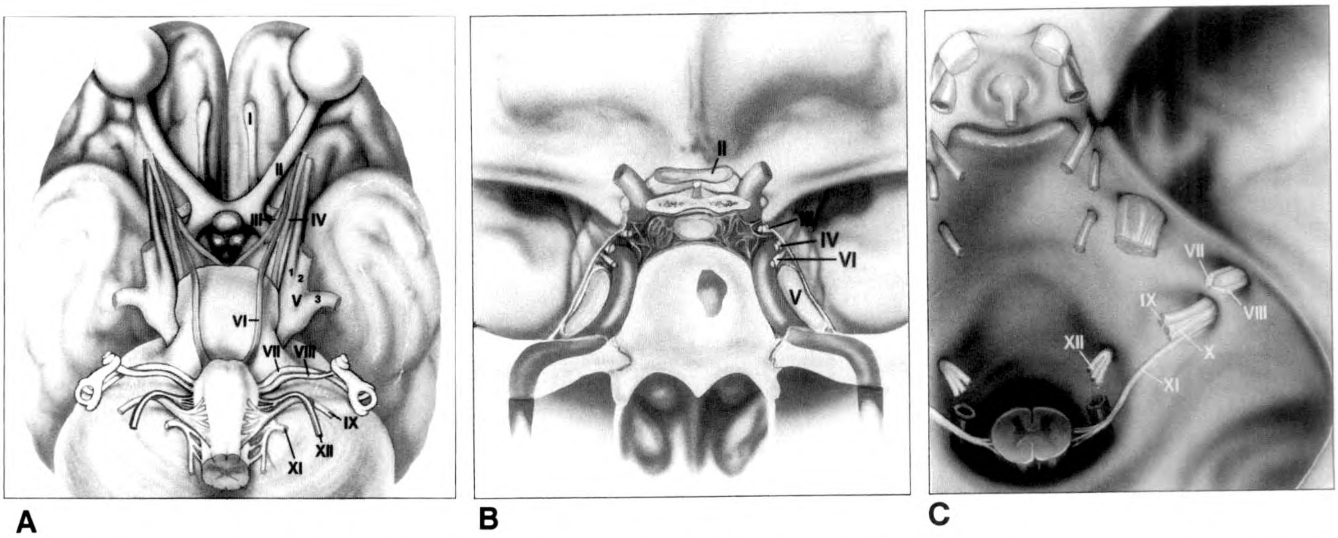

Fig. 1.—Normal anatomy. *A*, Sensory nerves enter and motor nerves exit brain from ventral surface. The only exception is the trochlear nerve (IV), which exits from the dorsal surface of the midbrain and travels in the perimesencephalic cistern to reach the cavernous sinus. Note long course of abducens (VI). Isolated sixth-nerve neuropathy may have any of a number of causes.

B, Cranial nerves III, IV, V, and VI are close together within cavernous sinus. Involvement of multiple cranial nerves in this group is commonly associated with inflammatory or neoplastic processes involving other adjacent structures such as the pituitary gland, carotid arteries, sphenoid sinus, and nasopharynx.

C, Glossopharyngeal (IX), vagus (X), and spinal accessory (XI) nerves all exit jugular foramen. Lower cranial nerve neuropathies tend to involve more than one of these at a time. Glossopharyngeal nerve, in particular, is hardly ever involved alone. Note that there is significant contribution from upper cervical segments to spinal accessory nerve, which ascends through foramen magnum to reach jugular foramen. Intraspinal masses, such as meningiomas, may produce isolated spinal accessory nerve palsy.

(Drawings courtesy of T. J. Masaryk, Cleveland, OH.)

Received October 11, 1989; accepted after revision January 5, 1990.
Presented at the American Society of Head and Neck Radiology, Toronto, Ontario, Canada, May 1989.

[1] Department of Radiology, University Hospitals of Cleveland, Case Western Reserve University, 2074 Abington Rd., Cleveland, OH 44106.

AJR **154:1263–1267, June 1990** 0361–803X/90/1546–1263 © American Roentgen Ray Society

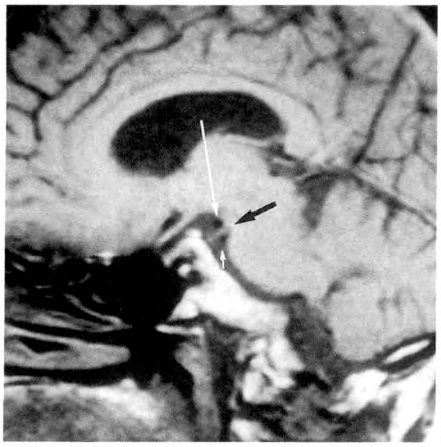

2

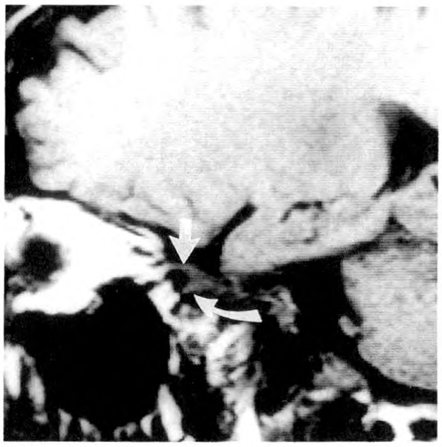

3

Fig. 2.—Normal anatomy of oculomotor nerve on parasagittal MR image, 500/30 (TR/TE). Oculomoter nerve (III) leaves midbrain and enters interpeduncular fossa (*black arrow*). In doing so it passes inferior to posterior cerebral artery (*long white arrow*) and superior to superior cerebellar artery (*short white arrow*). Ectasia, tortuosity, or aneurysms involving these vessels may produce third-nerve palsy.

Fig. 3.—Normal anatomy of trigeminal nerve on parasagittal spin-echo MR image, 506/32 (TR/TE). Gasserian nucleus (V) and first two divisions of trigeminal nerve lie within cavernous sinus. Ophthalmic division (V) (*straight arrow*) enters superior orbital fissure and provides sensory innervation to upper portion of face. Maxillary division (V_2) (*curved arrow*) enters foramen rotundum and provides sensory innervation to mid face.

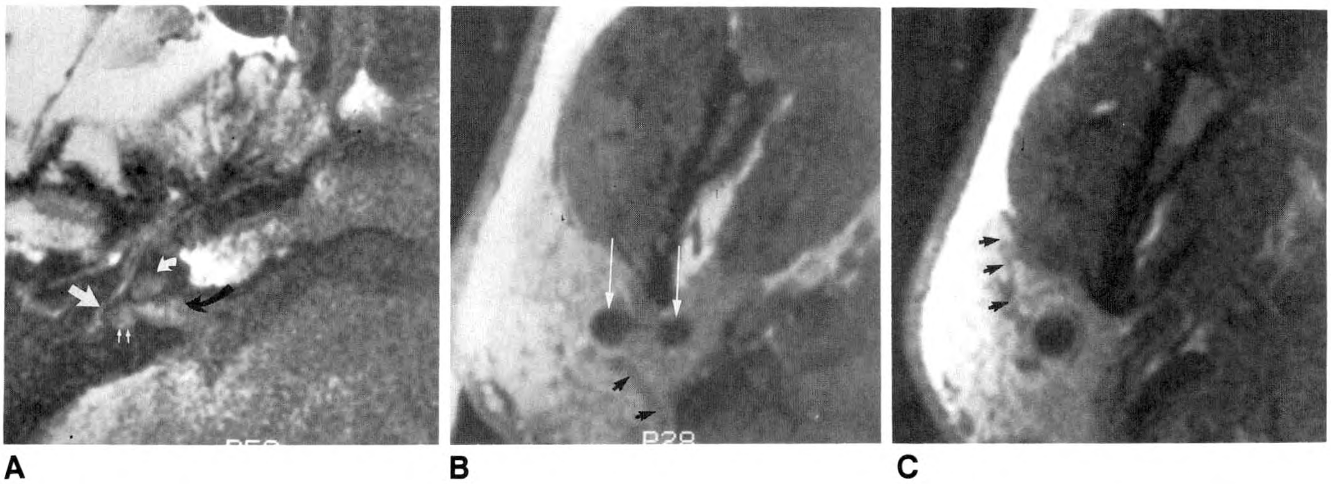

Fig. 4.—Normal anatomy of facial nerve.

A, MR image, 2000/60 (TR/TE). Facial nerve (VII) travels in anterior superior portion of internal auditory canal (*black arrow*). It leaves fundus of internal auditory canal and passes superior to cochlea (*curved white arrow*). Horizontal portion (*large straight white arrow*) travels lateral to vestibule (*small white arrows*) before turning inferiorly.

B and *C*, 500/32 MR images. After exiting stylomastoid foramen, facial nerve enters substance of parotid gland (*black arrows*, *B*) and serves as landmark between deep and superficial lobes of parotid. It passes lateral to retromandibular vein(s) (*white arrows*) and ramifies within superficial lobe (*black arrows*, *C*).

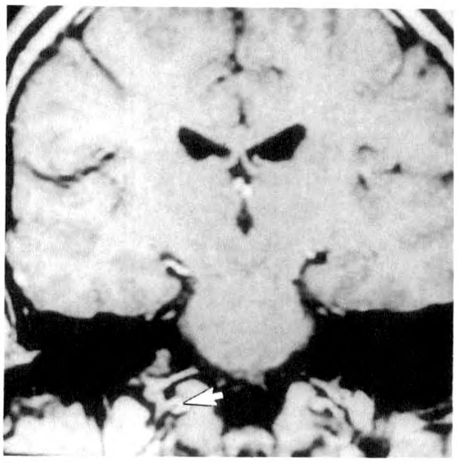

Fig. 5.—Normal anatomy of hypoglossal nerve. Coronal spin-echo MR image, 600/30 (TR/TE). Hypoglossal nerve (*arrow*) can be seen surrounded by fat in hypoglossal canal.

Olfactory Nerve

Nerve fibers subserving the sense of smell have their cell bodies within the olfactory mucosa. Obstruction of the flow of air and mucosal atrophy due to chronic inflammation, tumors, or trauma (Fig. 6) may affect the sense of smell.

Optic Nerve

The axons within the optic nerve are part of a white-matter tract that is surrounded by the subarachnoid space and covered with meninges. As such, the optic nerve is susceptible to gliomas and meningiomas. Primary neural tumors appear as fusiform enlargement of the optic nerve, as opposed to irregular enlargement of the optic nerve sheath due to meningiomas (Fig. 7).

Oculomotor Nerve

In addition to the posterior communicating artery, structures adjacent to the oculomotor nerve include the basilar

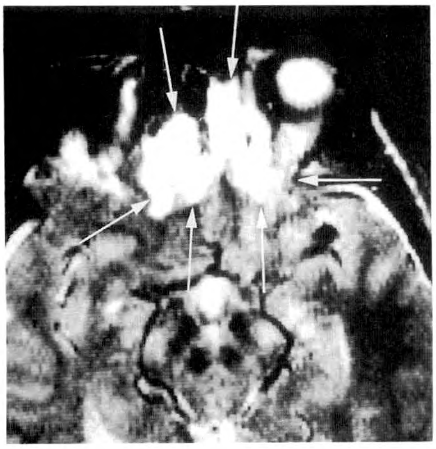

Fig. 6.—Olfactory dysfunction. The only lasting sequela of severe head trauma suffered by this patient is anosmia. T2-weighted image, 2000/60 (TR/TE), reveals edema involving subfrontal region and, presumably, olfactory bulbs (*arrows*). Posttraumatic anosmia may be permanent, in the case of fracture through the cribriform plate, or transient, from swelling and contusion of olfactory bulbs.

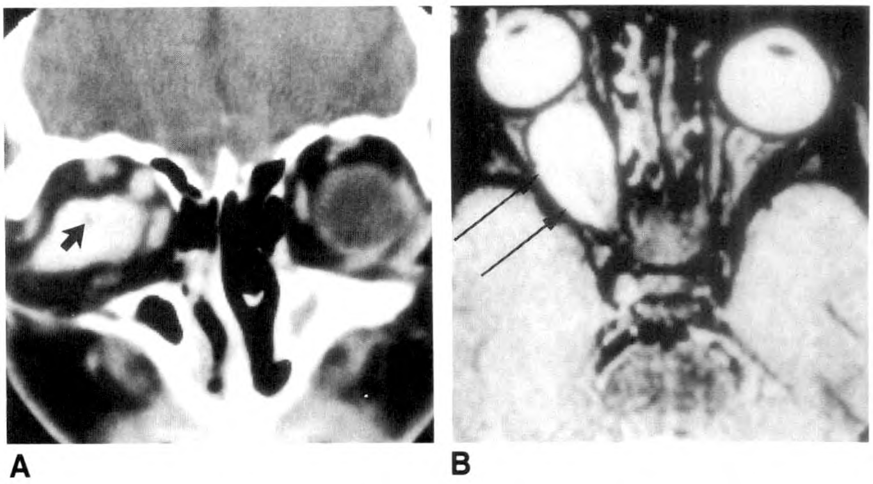

Fig. 7.—Optic nerve dysfunction. The common tumors of the optic nerve and sheath that affect visual acuity are optic-nerve meningiomas and optic gliomas. Meningiomas appear as irregular, enhancing masses with a filling defect representing optic nerve on both CT and MR.

A, Coronal contrast-enhanced CT scan of optic-nerve (*arrow*) meningioma.

B, Spin-echo MR image, 2010/120 (TR/TE). Optic glioma (*arrows*) presents a fusiform enlargement of optic nerve itself on MR and CT.

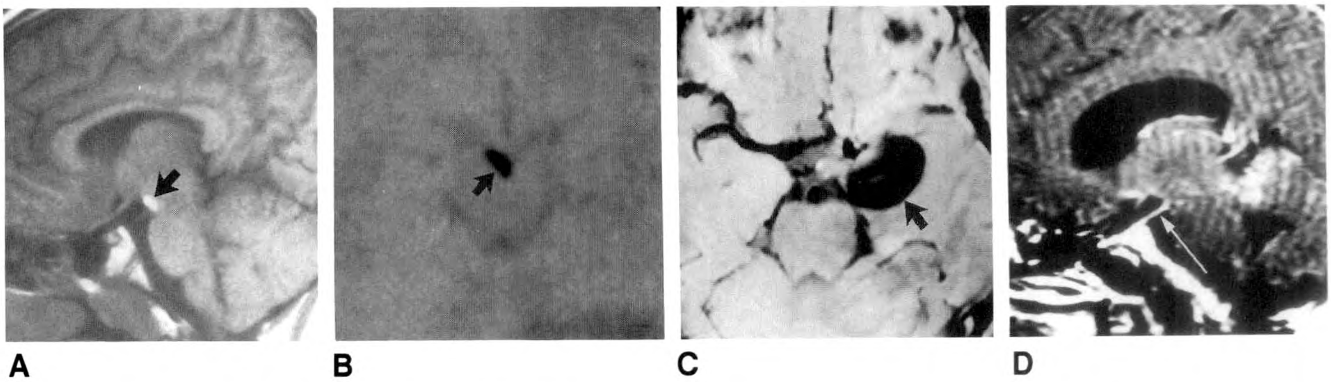

Fig. 8.—Oculomotor dysfunction.

A and *B*, 8-year-old girl with complete third-nerve palsy. Small lipoma (*black arrows*) seen at origin of third nerve on sagittal T1-weighted MR image, 600/30 (TR/TE) (*A*), is confirmed on axial CT scan (*B*).

C, Adult patient with complete third-nerve palsy. Axial MR image, 2010/30, shows large flow void (*arrow*) representing large aneurysm. There was concomitant dysfunction of cranial nerves IV, V, and VI.

D, In patients with diffuse meningeal involvement due to carcinomatous meningitis, lymphoma, tuberculosis, or sarcoidosis, enhancement of the meninges is seen. In this adult patient with sarcoidosis and multiple cranial-nerve palsies, enhancement is seen of the third cranial nerve (*arrow*).

artery, the posterior cerebral artery, and the superior cerebellar artery. In general, isolated third-nerve palsies are regarded as either complete (parasympathetic involvement) or incomplete (lack of parasympathetic involvement). If an isolated third-nerve palsy is accompanied by loss of pupillary function, MR imaging or angiography is indicated to rule out an aneurysm. MR imaging shows that fatty deposits at the origins of cranial nerves are common and may be symptomatic (Fig. 8).

Trochlear Nerve

Although primary tumors of the trochlear nerve have been reported, isolated fourth-nerve palsy is more commonly due to stretching of the superior medullary velum of the fourth ventricle, where the trochlear nerve decussates, by an intraventricular mass.

Trigeminal Nerve

The cranial nerves that are derived from the branchial apparatus (V, VII, IX, and X) are mixed nerves, that is, they contain both motor and sensory fibers. In each instance, there is sensory or motor dominance. For example, the trigeminal nerve is dominated by its sensory functions. Trigeminal neuralgia most often affects the mandibular and maxillary divisions. When compression by vascular structures is the cause, MR imaging can identify both the vessel and the compression of the trigeminal ganglia (Fig. 9).

Abducens Nerve

The sixth cranial nerve has a long sinuous course from low in the posterior fossa to the orbit. Because it passes through several anatomic areas, an isolated sixth-nerve palsy is nonspecific in terms of disease location. Lesions of the brainstem,

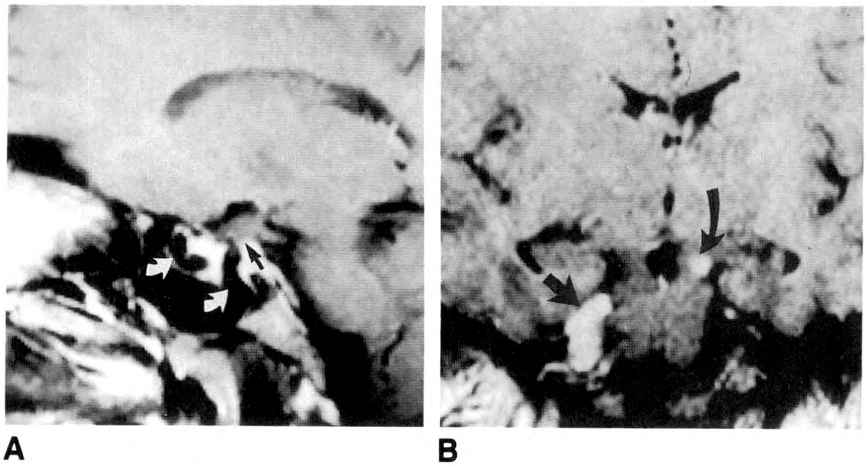

Fig. 9.—Trigeminal dysfunction.

A, Parasagittal T1-weighted MR image, 506/32 (TR/TE), in elderly patient with trigeminal neuralgia. Gasserian nucleus (*black arrow*) is being deformed and displaced by tortuous and ectatic internal carotid artery (*white arrows*).

B, Coronal gadolinium-enhanced T1-weighted MR image, 506/32, in patient with neurofibromatosis shows enhancement of mandibular division (V_3) as it leaves trigeminal ganglion (*straight arrow*) and descends through foramen ovale. Incidentally noted, on opposite side, is enhancing trochlear nerve (IV) neuroma (*curved arrow*).

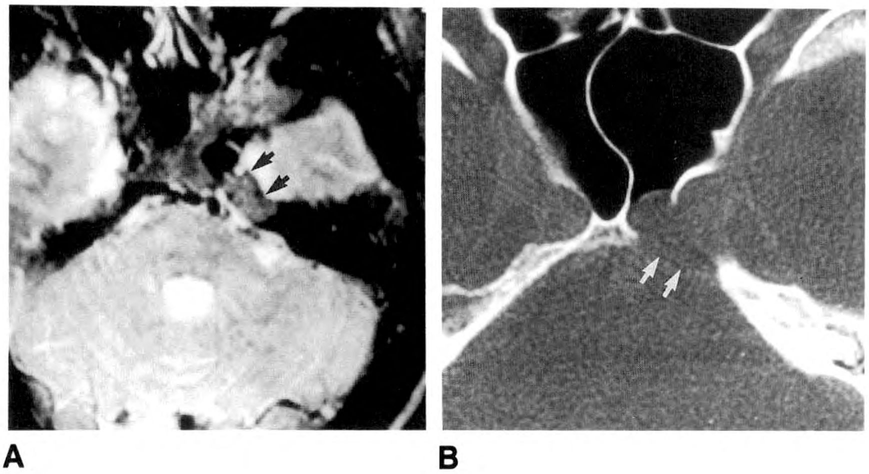

Fig. 10.—Abducens dysfunction. Because of its long course, the sixth cranial nerve is very sensitive to stretching.

A and *B*, Axial T2-weighted MR image, 2010/120 (TR/TE) (*A*), and CT scan (*B*) in patient with isolated sixth-nerve palsy. A very small metastasis to the petrous apex from carcinoma of the breast can be seen (*arrows*).

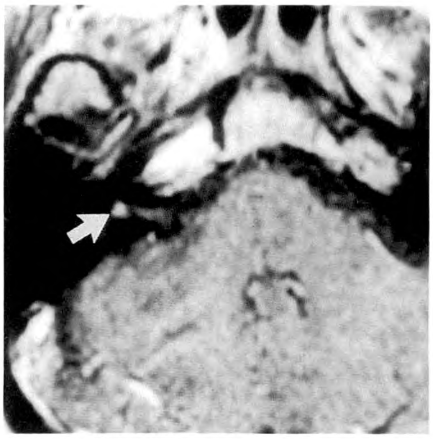

Fig. 11.—Vestibulocochlear dysfunction. Axial gadolinium-enhanced T1-weighted MR image, 500/30 (TR/TE), shows enhancing acoustic schwannoma in fundus of internal auditory canal (*arrow*). Further improvements in surface coils and pulse sequences will soon make visualization of intracochlear schwannomas possible.

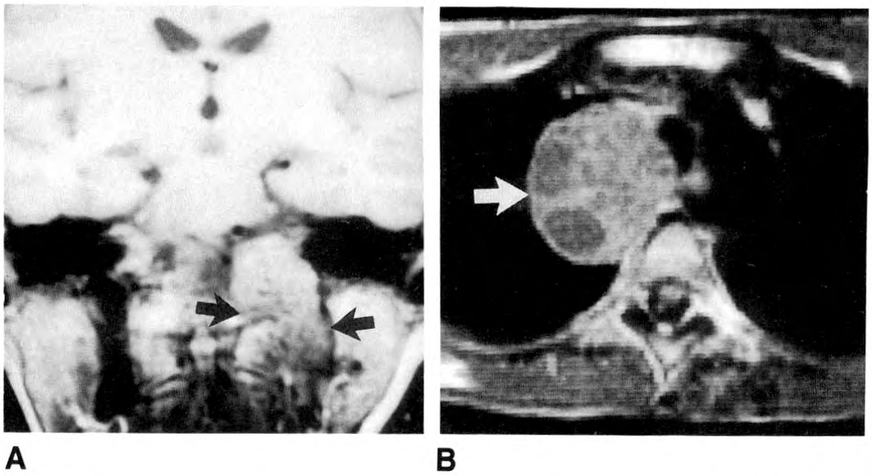

Fig. 12.—Vagal dysfunction. When tumors at or near the skull base affect the vagus nerve (X), both sensory and motor function of entire nerve are involved.

A, Large glomus jugular tumor (*arrows*) is seen on coronal MR image, 550/20 (TR/TE). Multiple other lower cranial nerves were affected, as is often the case.

B, Tumors located lower in the neck (infrahyoid) may only cause symptoms referable to the recurrent laryngeal nerve (motor) and present with hoarseness and vocal cord paralysis. A large schwannoma of the recurrent laryngeal nerve is shown in such a patient on axial MR image, 500/32 (*arrow*).

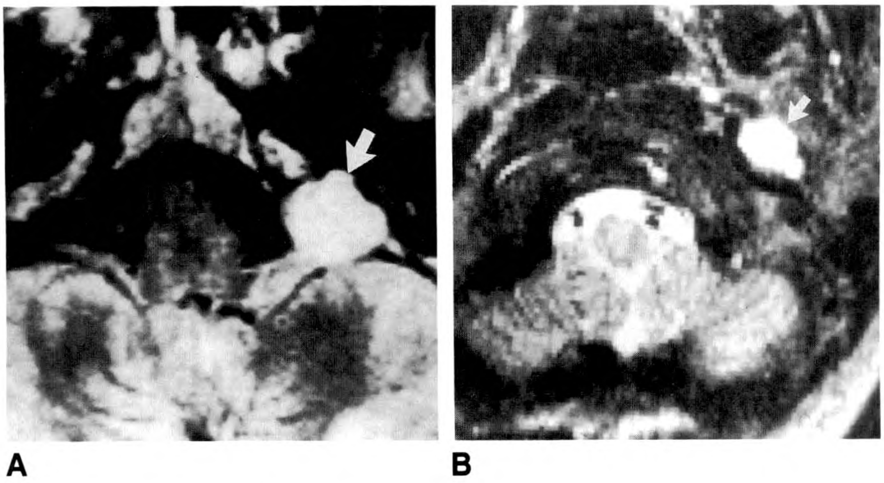

Fig. 13.—Spinal accessory dysfunction.
A and *B*, A schwannoma of the spinal accessory nerve is shown in these axial MR images. A T2-weighted, 2000/40 (TR/TE), image (*A*) shows the intracranial and intraosseous portion (*arrow*), and a slightly lower section (*B*) shows the extracranial component.

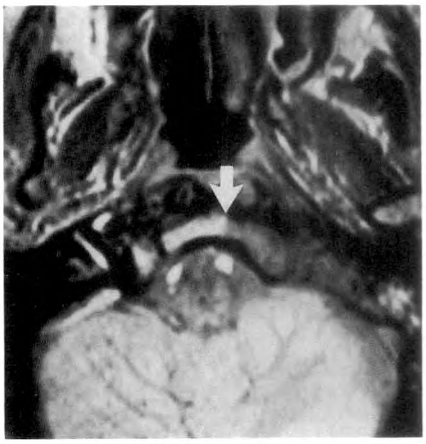

Fig. 14.—Hypoglossal dysfunction. This patient with metastatic breast carcinoma presented with left-sided twelfth nerve paresis. Findings on high-resolution CT of skull base were normal. Axial T1-weighted MR image, 500/30 (TR/TE), shows replacement of normal bright marrow-fat signal by lower-signal tumor infiltration on patient's left side. *Arrow* marks transition from normal (bright) to abnormal marrow signal.

extracranial posterior fossa, petrous apex, cavernous sinus, and orbital apex all may involve the sixth nerve (Fig. 10).

Facial Nerve

Every portion of the motor pathway for the nerves of facial expression, from the cerebral cortex through the parotid gland, can be demonstrated by one imaging technique or another. It is important to understand the normal anatomic and clinical findings that localize the abnormality and to be familiar with the pathologic lesions that occur at each level (Fig. 4). Recent improvements in MR surface-coil technology may soon make visualization of the intraparotid portion of the facial nerve routine.

Vestibulocochlear Nerve

The course of the eighth cranial nerve is short compared with that of most other cranial nerves. The most commonly encountered abnormalities are acoustic neuromas, meningiomas, and tortuous vascular structures. Currently, contrast-enhanced MR imaging is the first and usually the only imaging procedure required for evaluation of tumors in this region (Fig. 11).

Glossopharyngeal Nerve

The ninth cranial nerve is virtually always involved when there are associated symptoms of other lower cranial nerves (X, XI, or XII); isolated ninth-nerve symptoms are very rare.

Vagus Nerve

When a patient presents with hoarseness and a paralyzed vocal cord, it is vital to determine if there is complete vagal dysfunction or whether the recurrent laryngeal nerve alone is impaired. The most common causes of complete vagal dysfunction are masses affecting the proximal portion of the nerve such as glomus tumors; the most common causes of isolated recurrent laryngeal nerve paralysis are primary tumors of the head and neck (Fig. 12).

Spinal Accessory Nerve

The fibers that form cranial nerve XI arise from the medulla as well as from the upper cervical spinal cord. These coalesce and ascend through the foramen magnum. Thus, intraspinal, intracranial, or head and neck tumors such as lymphomas may cause dysfunction (Fig. 13).

Hypoglossal Nerve

The ability of MR imaging to identify abnormalities of the bone marrow at the base of the skull makes it useful for evaluating occult causes of cranial neuropathy such as infiltrating metastases (Fig. 14).

REFERENCES

1. Adams RD, Victor M. *Principles of neurology*, 2nd ed. New York: McGraw-Hill, **1981**
2. Kwan EF, Laucella M, Hedgeks TR III, Wolpert SM. A cliniconeuroradiologic approach to third cranial nerve palsies. *AJNR* **1987**;8:459–468
3. Chakeres DW, Kapila A. Normal and pathologic radiographic anatomy of the motor innervation of the face. *AJNR* **1984**;5:591–597
4. Jacobs JM, Harnsberger HR, Lufkin RB, et al. CT and MRI in the evaluation of vagal neuropathy. *Radiology* **1987**;164:97–102

Book Review

Pocket Atlas of Spinal MRI. By Leo F. Czervionke and Victor M. Haughton. New York: Raven, 95 pp., 1989. $13.95, softcover

This softcover book is a well-bound, pocket-sized (12.5 × 17.5 cm) monograph of normal MR spinal anatomy. Apart from the preface, which discusses technique, the book has no text. It has a basic table of contents, no index, and a limited bibliography.

The images were obtained with high- and mid-field-strength equipment. Each image occupies its own page and is annotated or provides the localizer for subsequent images. The cervical, thoracic, lumbar, and sacral segments are covered in 77 images. The images are all sharp and clearly labeled. The choice of structures labeled is often too obvious and repetitious. It would have been helpful to use the same numbers for tagging the same anatomic parts in each segment covered. Although most of the images are T1 weighted, T2-weighted and gradient-echo views are shown where appropriate.

I know of no book of similar size and cost that covers this material. However, in deciding where it fits into the spectrum of who needs what, I think this publication is best suited for medical students, X-ray technicians, and neuroclinicians because of its emphasis on fundamental anatomy and its lack of an index usable for reference. Radiology residents and practicing radiologists may be served better by the larger, more expensive, but more complete, *Magnetic Resonance Imaging: Atlas of the Head, Neck and Spine,* by Catherine M. Mill.

Edward V. Grayson
Memorial Hospital
Hollywood, FL 33021

MR Findings in Patients with Subacute Necrotizing Encephalomyelopathy (Leigh Syndrome):

Correlation with Biochemical Defect

L. Medina[1,2]
T. L. Chi[1,3]
D. C. DeVivo[4]
S. K. Hilal[1]

MR studies were correlated with biochemical results in nine children who presented with lactic acidosis and/or abnormal MR findings in the basal ganglia. Neurologic development was delayed in all nine children. Seven of these patients were diagnosed as having subacute necrotizing encephalomyelopathy (SNE, or Leigh syndrome) on the basis of history, clinical findings, and biochemical studies; of the remaining two, one had congenital lactic acidosis and the other had familial bilateral striatal necrosis with no known biochemical correlate. Although the clinical presentation of these patients was similar, we found distinctive MR abnormalities in characteristic locations in the seven patients with SNE, with or without detectable specific mitochondrial enzyme deficiency in cultured skin fibroblast assays. In our case studies of SNE patients with detectable enzyme deficiency states, defects in pyruvate dehydrogenase complex and cytochrome c oxidase have been found. The MR finding of note in SNE is the remarkably symmetrical involvement, most frequently of the putamen. In our study, lesions were also commonly found in the globus pallidus and the caudate nucleus, but never in the absence of putaminal abnormalities. Other areas of involvement included the paraventricular white matter, corpus callosum, substantia nigra, decussation of superior cerebellar peduncles, periaqueductal region, and brainstem.

In patients who present with lactic acidosis and whose MR findings show symmetrical abnormalities in the brain, but with sparing of the putamen, the diagnosis of SNE is in doubt.

***AJNR* 11:379–384, March/April 1990; *AJR* 154:1269–1274, June 1990**

Subacute necrotizing encephalomyelopathy (SNE, or Leigh syndrome) is a familial neurodegenerative disease conforming to an autosomal recessive mode of transmission, commonly manifested in infancy or childhood. The onset is usually insidious, and the course is intermittently progressive for several years. However, adult onset cases have been described, and the course can be acute [1, 2].

Clinical presentations may vary; however, most children are normal at birth. Common findings at the time of presentation include psychomotor regression and brainstem and cerebellar dysfunction resulting in ataxia, dystonia, and nystagmus. Limb weakness and optic nerve pallor are often noted [2, 3, 4]. Laboratory findings include metabolic acidosis with elevated lactate and pyruvate concentrations in the blood and CSF, suggesting that a disorder of pyruvate metabolism may be the primary biochemical defect. Specific mitochondrial enzyme deficiencies associated with SNE have been reported, including pyruvate carboxylase deficiency, pyruvate dehydrogenase complex defects, and cytochrome *c* oxidase deficiency [2, 5–7].

Pathologically, symmetrical focal necrotic lesions can be seen in the subcortical white matter, basal ganglia, thalamus, midbrain, medulla, and posterior column of the spinal cord. The mamillary bodies are rarely involved, which is a differential point in the diagnosis of Wernicke encephalopathy, in which the mamillary bodies are often involved [8, 9]. Microscopically, there is vascular proliferation, demyelination, and neuronal necrosis [10, 11].

Received March 16, 1989; revision requested May 5, 1989; revision received July 14, 1989; accepted July 23, 1989.

[1] Department of Radiology, Division of Neuroradiology, The Neurological Institute of New York, Columbia-Presbyterian Medical Center, New York, NY 10032.

[2] Present address: CT Radiology Complex, Box 2727, Bayamon, Puerto Rico 00619.

[3] Present address: Department of Radiology, Montefiore Medical Center, Albert Einstein School of Medicine, 11 E. 210th St., Bronx, NY 10467. Address reprint requests to T. L. Chi.

[4] Departments of Pediatrics and Neurology, Division of Pediatric Neurology, The Neurological Institute of New York, Columbia-Presbyterian Medical Center, New York, NY 10032.

0361-803X/90/1546-1269
© American Roentgen Ray Society

We describe here the characteristic MR findings in conjunction with the clinical and biochemical findings in the antemortem diagnosis of SNE.

Subjects and Methods

The MR images of nine patients who presented with progressive neurological involvement were reviewed. Patients' ages ranged from 6 months to 4 years old; eight had lactic acidosis and one had normal blood and CSF lactate values. Images were obtained on a 1.5-T superconductive magnet. Axial T2-weighted images were obtained with a multislice spin-echo pulse sequence, 3500–3700/80–120 (TR/TE), and 5-mm-thick sections. Image acquisition was done on a 512 × 512 matrix. All patients had axial images, and one patient also had coronal views. MR findings were correlated with the clinical history and laboratory findings. Skin biopsies were performed on all patients after obtaining informed consent from the parents. The cultured fibroblasts were assayed for a battery of oxidative enzymes: pyruvate dehydrogenase complex, pyruvate carboxylase, NADH cytochrome b_5 reductase, succinate cytochrome *c* reductase, NADH dehydrogenase, succinate dehydrogenase, and cytochrome *c* oxidase, as previously reported [2, 6, 7].

TABLE 1: Clinical, Laboratory, and MR Findings in Patients with Subacute Necrotizing Encephalomyelopathy

Patient No.	Age at Onset	Clinical Findings	Laboratory Findings	MR Findings (T2-Weighted Images)
1	6 months	Delayed neurologic development; feeding difficulties; hypotonia; hyporeflexia; dystonic posturing; bilateral Babinski signs; bilateral optic nerve pallor; nystagmus	Increased serum lactate and pyruvate; increased CSF lactate and pyruvate; cytochrome *c* oxidase deficiency (skin fibroblast assay)	Symmetrically increased SI in putamen, globus pallidus, subthalamic nuclei, substantia nigra, cerebral peduncles, decussation of superior cerebellar penducles, brachium of inferior colliculi, periaqueductal region, olivary nucleus, and inferior medulla
2	16 months	Delayed neurologic development; hypertonia; hyperreflexia; spasticity; dystonia; gait disturbance; bilateral Babinski signs; bilateral optic nerve pallor	Increased serum lactate and pyruvate; increased CSF lactate and pyruvate; pyruvate dehydrogenase deficiency (skin fibroblast assay)	Symmetrically increased SI in putamen, periaqueductal region, substantia nigra, olivary nucleus, and inferior medulla
3	15 months	Delayed neurologic development; ataxia; dystonia (L > R); spasticity; hyperreflexia; bilateral Babinski signs; bilateral optic nerve pallor (patient died with fulminant metabolic acidosis; no autopsy)	Increased serum lactate and pyruvate; increased CSF lactate and pyruvate; normal enzymes	Symmetrically increased SI in putamen, globus pallidus, caudate, and periaqueductal region
4	4 years	Delayed neurologic development; dysarthria; spasticity; hypertonia; dystonia (R > L); right hemiparesis; hyperreflexia; right Babinski signs; bilateral optic nerve pallor	Increased serum lactate and pyruvate; increased CSF lactate; normal enzymes	Symmetrically increased SI in putamen; cortical and subcortical involvement of frontal, parietal, and occipital regions
5	20 months	Delayed neurologic development; hypotonia; hyperreflexia; right hemiparesis	Increased serum lactate; increased CSF lactate; normal enzymes	Symmetrically increased SI in putamen and paraventricular white matter
6	3 years	Delayed neurologic development; mild hypotonia; hyporeflexia; optic atrophy and nystagmus; neurosensory hearing loss; Babinski equivocal	Increased serum lactate; increased CSF lactate; cytochrome *c* oxidase deficiency (skin fibroblasts)	Symmetrically increased SI in putamen and substantia nigra
7	1 year	Delayed neurologic development; hypotonia; ataxic; hyperreflexia; bilateral Babinski signs	Increased serum lactate; increased CSF lactate; cytochrome *c* oxidase deficiency (skin fibroblasts)	Symmetrically increased SI in putamen, medial geniculate body, restiform bodies, brachium of inferior colliculi, and inferior medulla

Note.—SI = signal intensity, L = left, R = right.

Results

Seven of our nine patients had a clinical picture compatible with the diagnosis of SNE (Table 1). CT scanning in four of these patients showed bilateral, hypodense, nonenhancing lesions in the basal ganglia. On the heavily T2-weighted MR images, all seven of the SNE patients had high-signal lesions, symmetrically involving the putamen. There also were lesions involving the globus pallidus (two patients), the caudate (one patient), the substantia nigra (three patients), the paraventricular white matter (two patients), the cortical gray matter (one patient), subthalamic nuclei (one patient), periaqueductal region (three patients), and the medulla (three patients) (Table 2).

Correlations made with enzyme activity assays revealed that of the seven patients with clinical diagnosis of SNE and characteristic MR findings, four had specific mitochondrial enzyme deficiencies. Patient 2 had pyruvate dehydrogenase deficiency; patients 1, 6, and 7 had cytochrome *c* oxidase deficiency; patients 3, 4, and 5 had normal enzyme activity in cultured fibroblasts. MR of patient 1 showed symmetrical foci of increased signal involving the medulla, substantia nigra, cerebral peduncles, decussation of superior cerebellar peduncles, brachium of inferior colliculi, subthalamic nuclei, periaqueductal region, putamen, and globus pallidus (Table 1 and Fig. 1). Patient 2 had symmetrical foci of increased signal in the substantia nigra, periaqueductal region, olives, and putamen (Table 1 and Fig. 2). Patient 3 showed symmetrical hyperintense foci in the periaqueductal region, putamen, globus pallidus, and caudate (Table 1). Patients 4 and 5 showed lesions on MR involving the paraventricular white matter and cerebral cortex, in addition to the lesions in the putamen; MR findings in patient 6 showed symmetrical lesions in the putamen and substantia nigra. Patient 7 showed lesions in the putamen, medial geniculate body, restiform bodies, brachium of inferior colliculi, and medulla. One of the nine patients presenting with lactic acidosis and developmental delay did not have clinical features of SNE. A review of this patient's MR studies showed areas of high signal involving the temporal lobes, paraventricular white matter, and centrum semiovale; there was no involvement of the putamen (patient 8 in Table 3). He has congenital lactic acidosis of undetermined origin.

TABLE 2: Distribution of Lesions in Seven Patients with Subacute Necrotizing Encephalomyelopathy

Location of Lesions	No. of Cases
Putamen	7
Globus pallidus	2
Caudate	1
Substantia nigra	3
Periaqueductal region	3
Inferior medulla	3
Paraventricular white matter	2
Cortical gray matter	1
Decussation of superior cerebellar penducles	1
Olivary nucleus	2
Medial geniculate body	1
Splenium	1
Brachium of inferior colliculi	2
Restiform bodies	1
Subthalamic nuclei	1

Discussion

The diagnosis of SNE can be confusing because of its variety of clinical manifestations and laboratory abnormalities. Most often, a definite diagnosis is made only at necropsy. Involvement of the basal ganglia has been described previously on CT [10, 12 13], which shows symmetrical, hypodense, nonenhancing lesions with predominant involvement of the putamen. In 1981, Chi et al. [4] reported autopsy and CT findings of a 28-month-old child with Leigh syndrome. The CT scan of this patient showed symmetrical lesions of low attentuation involving the basal ganglia and white matter. At autopsy, this patient showed typical histologic changes of Leigh syndrome with symmetrical involvement of the putamen. In addition, there was involvement of the periaqueductal region, which was not seen on CT.

With the increasing availability of MR for the examination of children with progressive degenerative diseases of the CNS, more cases of this disease are being recognized. Recently, there have been three reports of the MR findings in this disease [2, 14, 15]. These articles documented the higher sensitivity of MR in detecting lesions overall as compared with CT, and also noted a high frequency of involvement of the basal ganglia, in particular, the putamen. In patients who present with lactic acidosis without Leigh syndrome, MR findings often are abnormal. Focal hyperintense signal lesions can be seen predominantly in the deep white matter, paraventricular in distribution, perhaps related to watershed zones.

There have been several reports of the pathologic findings in SNE. The original case was described by Leigh in 1951 [9]. The case he presented showed symmetrical lesions involving the thalamus, midbrain, pons, medulla (inferior olives), and posterior column of the spinal cord. In 1971, Monpetit et al. [8] reviewed the pathologic findings of 50 cases of this disease. They found the basal ganglia to be involved in more than 65% of cases and the brainstem to be involved in 98%. Pathologically, the lesions consisted of areas of vascular proliferation and demyelination, which ultimately progressed to necrosis and cavitation [8–11].

Now with the discovery of the enzyme deficiencies in some of these patients and the advent of MR imaging, the diagnosis of SNE can be made more accurately, which permits early identification of these patients. SNE is a syndrome that embraces a wide spectrum of clinical severity associated with pyruvate carboxylase, pyruvate dehydrogenase, and cytochrome *c* oxidase deficiencies. It is expected that deficiencies of other enzymes involved in cerebral oxidative metabolism will be found soon. Some of these mitochondrial enzymes may be tissue specific. Normal enzyme activity in cultured skin fibroblasts, therefore, may not necessarily reflect brain mitochondrial enzyme activity [11].

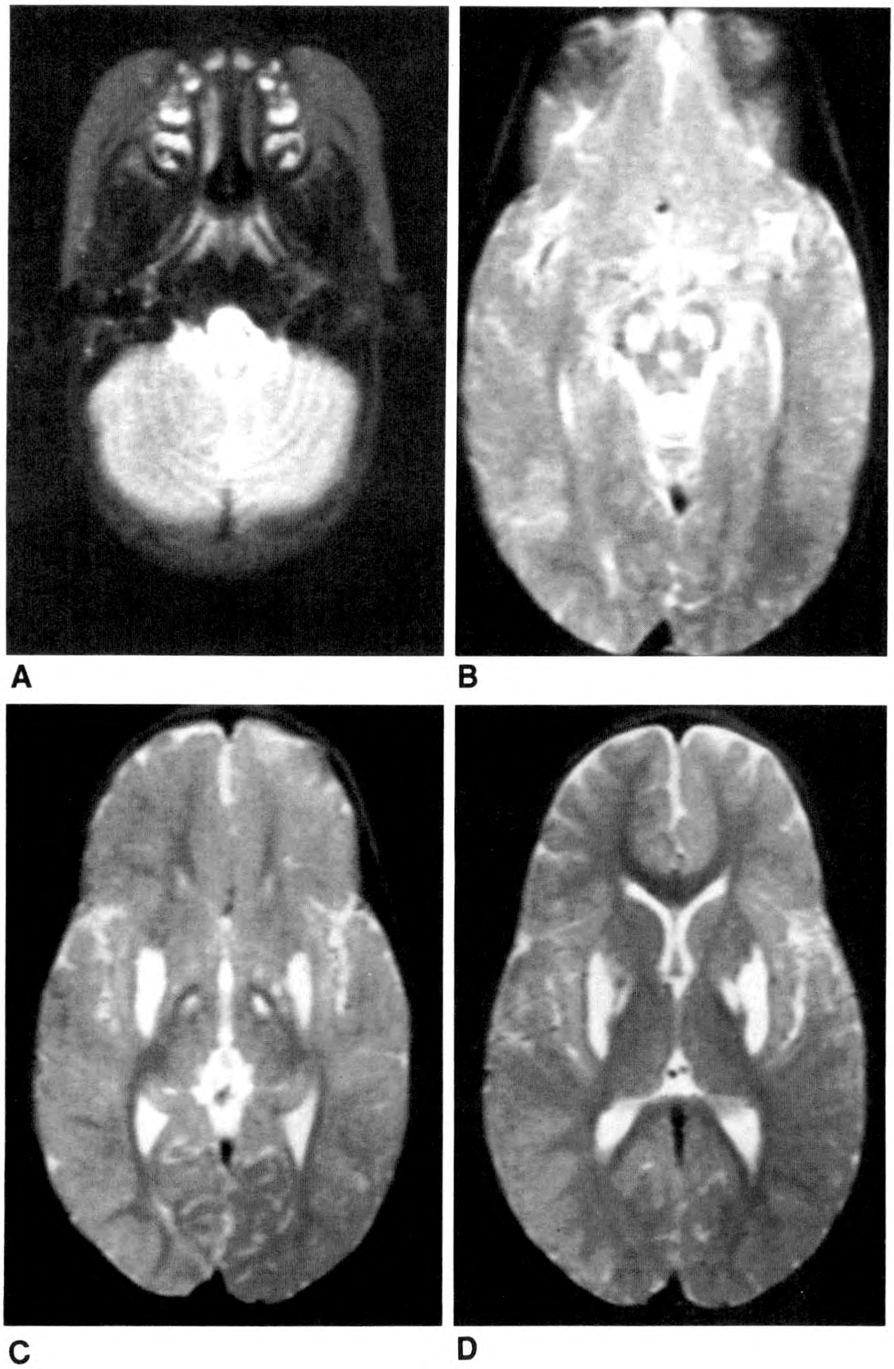

Fig. 1.—Case 1: T2-weighted axial MR images in 6-month-old patient with Leigh syndrome and cytochrome c oxidase deficiency.

A, Abnormal high signal involvement of medulla.

B, Abnormal high signal involvement of bilateral cerebral peduncles, substantia nigra, decussation of superior cerebellar peduncles, and periaqueductal region.

C, Symmetrically abnormal high signal involvement of putamina and, more medially, globus pallidi and subthalamic nuclei.

D, Higher section more clearly shows involvement of bilateral globus pallidus and putamen.

The differential diagnosis of disease entities with involvement of the basal ganglia manifesting in childhood include various toxic conditions such as carbon monoxide poisoning, cyanide poisoning, and a rare complication of viral encephalitis [11, 16, 17]. Such chronic conditions as familial striatal necrosis [18] (one case included in our study), Wilson disease, and Hallervorden-Spatz disease also have been noted to involve the basal ganglia. Wilson disease tends to occur in older children and has specific laboratory abnormalities [19–21].

In conclusion, a pattern of symmetrical, hyperintense lesions on T2-weighted images involving the basal ganglia and brainstem, with predominant involvement of the putamen, is highly specific for SNE. In these patients further attempts

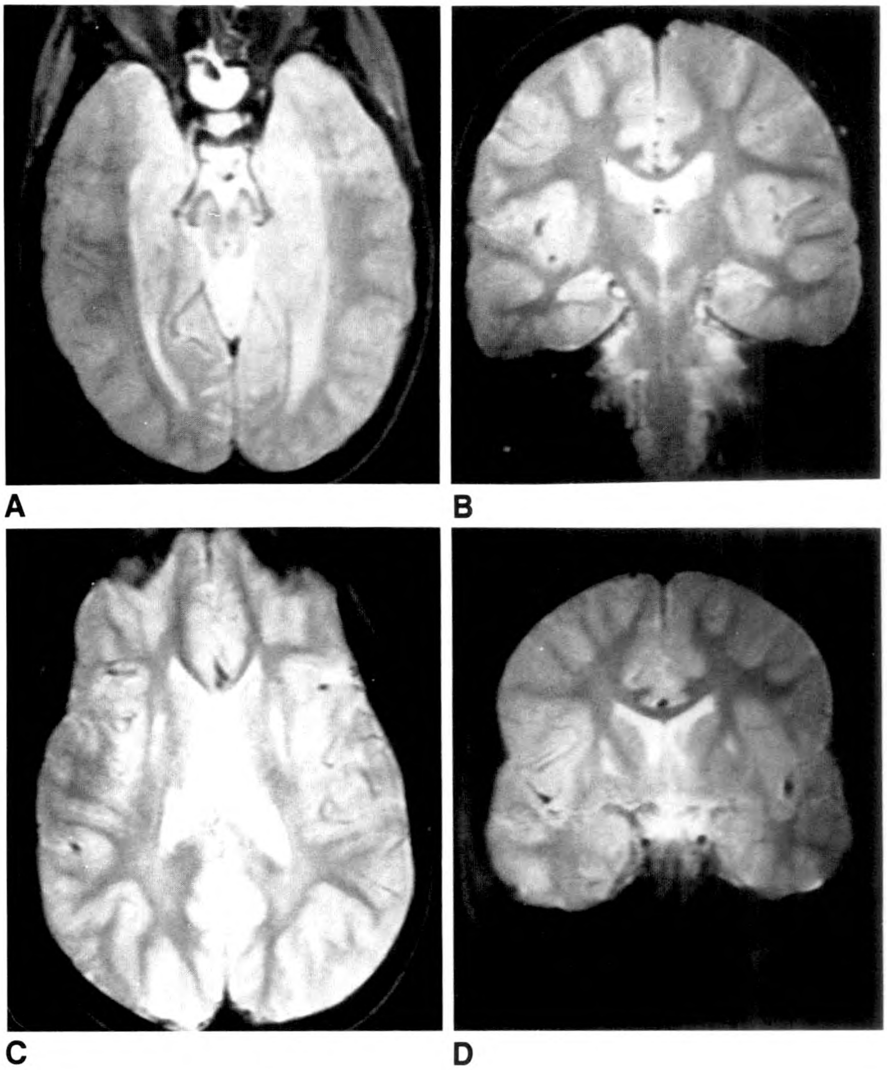

Fig. 2.—Case 2: T2-weighted axial and coronal MR images in 16-month-old patient with Leigh syndrome and pyruvate dehydrogenase deficiency.

***A* and *B*, Axial (*A*) and coronal (*B*) images show abnormal high signal involving substantia nigra and periaqueductal region.**

***C* and *D*, Axial (*C*) and coronal (*D*) images show high signal foci in putamen bilaterally.**

TABLE 3: Clinical, Laboratory, and MR Findings in Patients Without Subacute Necrotizing Encephalomyelopathy

Patient No.	Age at Onset	Clinical Findings	Laboratory Findings	MR Findings (T2-Weighted Images)
8	4 months	Delayed neurologic development; spasmus mutans; nystagmus	Increased serum lactate; normal enzymes	Increased SI in temporal lobes, paraventricular white matter of occipital region, and centrum semiovale
9	6½ years	Hypotonia; dystonia; family history for familial bilateral striatal necrosis	Normal serum lactate; normal enzymes	Increased SI in bilateral globus pallidus

Note.—SI = signal intensity.

should be made to identify a specific mitochondrial enzyme deficiency that has been associated with the diagnosis of subacute necrotizing encephalomyelopathy.

REFERENCES

1. DeVivo DC, DiMauro S, Rapin I. Mitochondrial disorders. In Rudolph AM ed. *Pediatrics*. E. Norwalk, CT: Appleton and Lange, **1987**;18:1736–1738
2. DiMauro S, Servidei S, Zeviani M, et al. Cytochrome *c* oxidase deficiency in Leigh syndrome. *Ann Neurol* **1987**;22:498–506
3. Koch TK, Yee MHC, Hutchinson HT, Berg BO. Magnetic resonance imaging in subacute necrotizing encephalomyelopathy (Leigh's disease). *Ann Neurol* **1986**;19:605–607
4. Chi JG, Yoo HW, Chang KH, Kim CW, Moon HR, Ko KW. Leigh's subacute necrotizing encephalomyelopathy: Possible diagnosis by CT scan. *Neuroradiology* **1981**;22:141–144

5. Van Erven PMM, Gabreels HJM, Ruitenbreek W, Renier WO, Fischer JC. *Arch Neurol* **1987**;44:775–778
6. DeVivo DC, Haymond M, Obert K, Nelson J, Pagliara A. Defective activation of the pyruvate dehydrogenase complex in subacute necrotizing encephalomyelopathy (Leigh disease). *Ann Neurol* **1979**;6:483–494
7. DeVivo DC, Russman BS, Dodson EW, DiMauro S. Leigh's syndrome and cytochrome *c* oxidase deficiency. *Ann Neurol* **1987**;22:445 (Abstr)
8. Montpetit VJA, Anderman F, Carpenter S, Fawcett JS, Zborowska-Sluis D, Giberson HR. Subacute necrotizing encephalomyelopathy. *Brain* **1971**;94:1–30
9. Leigh D. Subacute necrotizing encephalomyelopathy in an infant. *J Neurol Neurosurg Psychiatry* **1951**;14:216–221
10. Hall K, Gardner-Medwin D. Appearance in Leigh's disease (subacute necrotizing encephalomyelopathy). *Neuroradiology* **1978**;16:48–50
11. Berkovic SF, Karpati G, Carpenter S, Lang AE. Progressive dystonia with bilateral putaminal hypodensities. *Arch Neurol* **1987**;44:1184–1187
12. Schwartz W, Hutchinson HT, Berg BO. Computerized tomography in subacute necrotizing encephalomyelopathy (Leigh disease). *Ann Neurol* **1981**;10:268–271
13. Campistol J, Fernandez-Alvarez E, Cusi V. CT scan appearance in subacute necrotizing encephalomyelopathy. *Dev Med Child Neurol* **1984**;26:509–527
14. Davis PC, Hoffman JC, Braun IF, Ahman P, Krawiecki N. MR of Leigh's disease (subacute necrotizing encephalomyelopathy). *AJNR* **1987**;8:71–75
15. Geyer CA, Sartor KJ, Prensky AJ, Abramson CL, Hodges FJ, Gado MH. Leigh disease (subacute necrotizing encephalomyelopathy): CT and MR in five cases. *J Comput Assist Tomogr* **1988**;12:40–44
16. Hattori H, Kawamori J, Takao T, et al. Computed tomography in post influenza encephalitis. *Brain Dev* **1983**;5:564–567
17. Goutiers F, Aicardi J. Acute neurological dysfunction associated with destructive lesions of the basal ganglia in children. *Ann Neurol* **1982**;12:328–332
18. Mito T, Tanaka T, Becher LE, Takashima S, Tanaka J. Infantile bilateral striatal necrosis: clinicopathological classification. *Arch Neurol* **1986**;43:677–680
19. Aisen AM, Martel W, Gabrielson TO, et al. Wilson disease of the brain: MR imaging. *Radiology* **1985**;157:137–141
20. Starosta-Rubinstein S, Young AB, Kluin K, et al. Clinical assessment of 31 patients with Wilson's disease. Correlations with structural changes on magnetic resonance imaging. *Arch Neurol* **1987**;44:365–370
21. Lawler GA, Pennock JM, Steiner RE, Jenkins WJ, Sherlock S, Young IR. Nuclear magnetic resonance (NMR) imaging in Wilson disease. *J Comput Asst Tomogr* **1983**;7:1–8

Intracranial Chemical-Shift Artifacts on MR Images of the Brain: Observations and Relation to Sampling Bandwidth

Alison S. Smith[1,2]
Meredith A. Weinstein[3]
Gregory C. Hurst[1]
Dale R. DeRemer[3]
Richard A. Cole[4]
Paul M. Duchesneau[3]

The purpose of this study was to evaluate the presence of chemical-shift artifacts on cranial MR and to illustrate the interrelationship among chemical-shift artifacts, variable acquisition parameters, and field strength. Measurements of chemical-shift artifacts were performed on scans obtained from a volunteer imaged in a 1.5-T General Electric system at bandwidths of 8, 16, and 32 kHz, using a 24-cm field of view and an 8-kHz bandwidth with a 48-cm field of view. Chemical-shift displacements at 8 kHz were 6.6 and 14.2 mm at the respective fields of view. Retrospective review was also performed in 77 cases of cranial MR performed on a 1.4-T Technicare unit for the presence and source of chemical-shift artifact on spin-density and T2-weighted images. Most data reviewed showed no significant interference of chemical-shift artifacts on cranial images. An artifactual subdural fluid collection was a common artifact ($n = 30/77$). When present, this was due to shift of fat signal from subcutaneous tissues onto the brain in patients younger than 10 years old ($n = 4/10$) and correlated with the distance between brain and subcutaneous fat of less than the linear value of the chemical shift. When this artifact was present in adults ($n = 25/67$), it was due to shift of the medullary fat signal across the inner table of the skull. The latter also occurred in one child under 10. Apparent location shifts, consistent with the displacement expected from the chemical-shift artifact, were noted in five of five cases of intracranial lipoma. In one of these, the chemical-shift artifact disguised the presence of a large associated vessel. The method of calculating the linear displacement of chemical-shift artifact is reviewed, and the interrelationship of machine parameters and chemical-shift artifact is illustrated. Chemical-shift artifact increases proportionally with field strength and field of view. Increasing the bandwidth to decrease chemical-shift artifact has a resultant penalty in signal to noise but allows a lower time to echo. A lower time to echo can also be accomplished without increasing the bandwidth if asymmetric sampling is used.

Awareness of the relationships among chemical-shift artifacts, acquisition parameters, and field strengths can result in a more tailored examination when the chemical-shift artifact is going to be a significant factor. In addition, interpreter error can be avoided by awareness of these relationships when reviewing images from outside institutions.

***AJNR* 1990:303–311, March/April 1990; *AJR* 154:1275–1283, June 1990**

We observed that the chemical-shift artifacts causing apparent subdural hematomas were seen frequently on a Technicare 1.4-T Teslacon system and seen infrequently on General Electric 1.5-T Signa, Picker 1.5-T Vista, Technicare 0.6-T Teslacon II, and Picker 0.5-T Vista systems. We further observed that with the Technicare 1.4-T system, these apparent subdural hematomas were common in the first decade of life, less common between the ages of 10 and 39, and more common over the age of 40. The current study was performed to determine (1) what patient variables contribute to chemical-shift artifacts that mimic subdural hematomas; (2) which MR parameters contribute to these artifacts; and (3) what the relationships are among these parameters.

Received January 19, 1989; revision requested March 31, 1989; revision received September 7, 1989; accepted September 22, 1989.

[1] Department of Radiology, Cleveland Metropolitan General Hospital, Cleveland, OH 44109.

[2] Present address: Department of Radiology, University Hospitals of Cleveland, 2074 Abington Rd., Cleveland, OH 44106. Address reprint requests to A. S. Smith.

[3] Department of Radiology, Neuroradiology Section, Cleveland Clinic Foundation, Cleveland, OH 44106.

[4] Division of Research, Cleveland Clinic Foundation, Cleveland, OH 44106.

0361–803X/90/1546–1275
© American Roentgen Ray Society

Theory of Chemical Shift

The basis of chemical-shift artifact, chemical-shift imaging, and clinical-shift spectroscopy is the variation of the local magnetic field (nuclear environment) due to the magnetic moment of electrons near the nucleus of interest. If this electronic magnetic field opposes the main (applied) magnetic field, as in the vast majority of human tissues [1, 2], the effective local magnetic field is "shielded" so that nuclei in this environment experience a field less than that of the applied magnetic field. The net contribution of these distortions of the applied magnetic field is measured by diamagnetic susceptibility [3–5]. Paramagnetic effects are due to the "extra" magnetic field produced by electrons; this field augments rather than opposes the applied field, but due to molecular dynamics the principal observed effect of paramagnetism is shortened T1 and T2 relaxation times.

Hydrogen molecules bound to fat will precess at a slightly slower rate than hydrogen molecules of water because they are more shielded from the applied magnetic field and therefore experience a lower magnetic field. Because the MR system translates a received signal at a given frequency to a specific predictable location on the image, when the gradient field is applied during the "readout" mode of the imaging cycle, these fat protons will appear at a lower frequency. This "frequency misregistration," or "chemical-shift" artifact, results in a position shift (displacement) of fat signal relative to signal from water at the same physical location. This effect is most obvious on the MR image when a tissue containing predominantly fat is sharply interfaced with one that is predominantly of water content.

Chemical-shift artifact is directly proportional to the field strength because the frequency difference increases as the Larmor frequency increases. As can be seen in Figure 1, the steeper the gradient, the less the distance that the fat signal is displaced relative to the water signal. If the receiver bandwidth is doubled and the gradient is doubled to keep the same resolution and field of view (FOV), the chemical shift will be one-half as great. If the FOV in the frequency-encode direction is doubled, and resolution hence reduced by half, the gradient will be half as steep and the distance of the chemical-shift artifact will be twice as large. Because the fat signal is at a lower frequency, it appears on the image to be shifted in the lower field direction "downfield" of the gradient, relative to the water signal. The overlap of the fat signal with adjacent tissue can result in an artifact of extra, displaced signal, while the loss of signal from the fat at the original site results in a signal void at this location. The location of the chemical-shift artifact on the image can be changed by reorienting the frequency-encode axis or by reversing the gradient.

Bandwidth

For the purposes of this discussion, bandwidth will refer to either "signal" or "receiver" frequency ranges. The strength of the frequency-encoded gradient determines the range of frequencies contained in the image data signal. This range of frequencies is called the signal bandwidth. An increase in the signal bandwidth requires an equal increase in the system receiver sampling bandwidth to accommodate the greater range of signal frequencies. This is obtained by decreasing (narrowing) the time used for data collection (sampling). Steeper gradients result in a wider frequency bandwidth per pixel; therefore, the variance in fat and water signals are less significant, as shown in Figure 1.

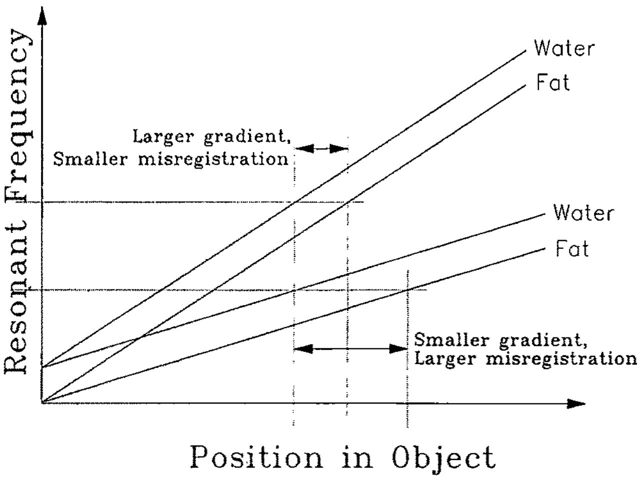

Fig. 1.—Because of different chemical shifts, water and fat in same external field will resonate at slightly different Larmor frequencies. In the presence of a spatially encoding field gradient, resonant frequency will depend on *both* position and chemical shift. Thus, water and fat at different positions will appear to be in the same place since they will have the same frequency. Position in the image is determined directly from resonant frequency, so that fat and water will be misregistered in the image. As gradient strength becomes smaller, this misregistration becomes larger; fat and water, which are farther apart in the subject, will have the same frequency, and hence be mapped to the same spot in the image.

Materials and Methods

With the use of the General Electric 1.5-T system, a 67-year-old volunteer was examined at bandwidths of 32, 16, and 8 kHz with a 24-cm FOV and at an 8-kHz bandwidth with a 48-cm FOV. Comparisons were made of measured vs calculated chemical-shift artifacts. The default and user-selectable sampling bandwidth and the minimum time to echo (TE) attainable with these bandwidths were determined for Technicare 0.6-T Teslacon II and 1.4-T Teslacon I, General Electric 1.5-T Signa, and Picker International 0.5-T and 1.5-T Vista systems.

Retrospective evaluation was made in 77 consecutive patient studies performed on a 1.4-T Teslacon I unit using a 25.6-cm FOV, 256 (x or frequency-encode) by 192 (y or phase-encode) matrix, 16.6-kHz sampling bandwidth, and frequency gradient strength of 0.1529 g/cm. Spin-echo images were obtained in axial and/or coronal planes using spin-density, 2010/32 (TR/TE), and T2-weighted, 2010/120, sequences. The frequency-encoding (x) axis was left-to-right in both planes with the gradient producing a higher field to the right. Qualitative assessment was made of the presence of chemical-shift artifacts at interfaces of fat and water. The presence of these artifacts was related to age, average skull thickness for age as determined by Orley [6], and measured biparietal diameter (BPD). BPD was measured at the level of the thalami. The presence of artifactual subdural fluid collections was correlated with these age groupings by decade. Quantitative linear measurements were made on the images after comparing magnification factors with cursor measurements on the imaging unit. Measurements were also made of shift artifacts seen in five cases of known intracranial lipomas, four studied with the 1.4-T Technicare system and one with the 1.5-T General Electric system (gradient strength = 0.31 g/cm). CT examinations in these cases were compared with the MR images for evaluation of the presence of calcifications, associated vessels, and apparent position change of the lipoma when compared with the MR images.

Results

Images in the volunteer obtained at a 24-cm FOV with progressive sampling bandwidths of 8, 16, and 32 kHz showed measured linear chemical-shift artifacts of 6.6, 3.8, and 1.9 mm compared with calculated values of 6.7, 3.4, and 1.7 mm, respectively (Fig. 1). Doubling the FOV from 24 to 48 cm at an 8-kHz bandwidth resulted in measured shifts of 6.6 and 14.2 mm compared with calculated values of 6.7 and 13.4 mm, respectively. Because it was difficult to define the edges of the artifact at a 48-cm FOV, the value is the mean of five measurements. Table 1 lists the default and selectable receiver bandwidths for the MR systems studied. Also listed are the minimal TEs attainable with these bandwidths.

On the 1.4-T Teslacon I system, the calculated shift of signal between juxtaposed fat and water was 3.2 mm (3.2 pixels). Of the 77 patient studies reviewed, 52 were in females and 25 were in males. The patients were 9 months to 85 years old. Chemical-shift artifacts caused a relative asymmetry of the brain within the surrounding ring of subcutaneous and/or diploic fat signal in all studies. Most studies reviewed showed no subdural artifact. When this asymmetry resulted in an artifactual subdural fluid collection, it was due to shift of fat signal from the subcutaneous tissue in those under 10 years of age (Fig. 2) and to shift of fat signal of the diploic cavity onto the brain in older individuals (Fig. 3). Shift of the subcutaneous tissue onto the brain was not observed beyond the age of 8.

TABLE 1: Relationships Among Machine Parameters, Chemical-Shift Artifacts, and Sampling Bandwidths

Variable	Increased Bandwidth	Increased Field of View	Increased Field Strength
Chemical-shift artifact	Decreased	Increased	Increased
Signal to noise	Decreased	Increased	Increased
TE	Decreased	–	–

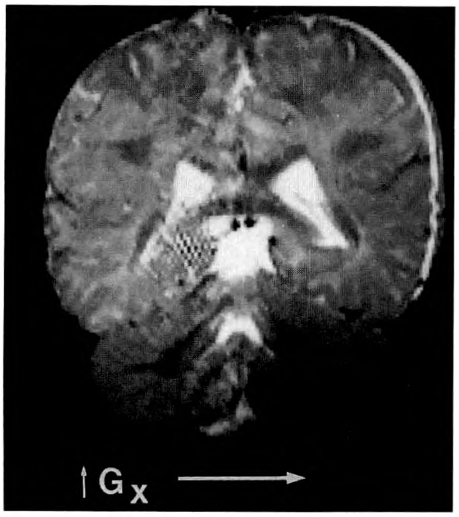

Fig. 2.—Overlap of brain with fat signal from subcutaneous tissue in this 1-year-old child results in artifactual subdural hematoma on 2000/120 image. Frequency encoding is left to right, with higher side of gradient to the right (G_x).

The presence of a subdural artifact from overlap of the diploic fat signal showed a generally increasing trend with increased age (see Fig. 4). The age differences between artifact groups that showed subdural effects due to subcutaneous tissue overlap vs no overlap and between subdural artifact due to shift of subcutaneous vs diploic fat signal were significant by the t test ($p = .0001$). The patients with a shift of the subcutaneous tissue onto the brain had an average BPD of 12.3 cm, patients with overlap of diploic fat signal had an average BPD of 14.2 cm, and patients who had no demonstrable overlap had an average BPD of 14.0 cm. The differences in BPD between the first two groups were significant by the t test ($p = .001$). Differences in BPDs between those having no artifact and overlap of the diploic fat signal were not significant.

Retrospective evaluation of the five cases of intracranial lipoma showed chemical-shift artifacts of 3–4 mm on the 1.4-T Technicare studies and approximately 2 mm on the 1.5-T General Electric examination. An area of decreased signal adjacent to these lipomas, representing the higher field direction of the gradient ("upfield") side of the artifact, had prospectively been called calcification or vessel in three of five cases. Calcification was not present in these sites on CT (Fig. 5). The downfield bright signal of the chemical-shift artifact obscured the presence of a large vessel adjacent to a sylvian fissure lipoma in one case (Fig. 6) and resulted in underestimation of calcification associated with a corpus callosum lipoma in another case.

Discussion

Relationship of Bandwidth to Chemical-Shift Artifacts and Other MR Parameters

Sampling bandwidth changes are related to the changes of strength of the read (x) gradient. The magnitude of the chemical-shift artifact depends on the effect of the inherent (chemical-shift) frequency difference between fat and water relative to the range of frequencies accountable to a given pixel. In other words, if the alteration of signal that occurs from the fat/water difference is small, relative to the range of signals expected in a given pixel, the chemical-shift artifact will not have a significant effect on the image (see Fig. 1). The amount of chemical shift can be determined by solving several simple equations. Needed values are FOV, bandwidth, and resonant frequency for the field strength of the MR unit.

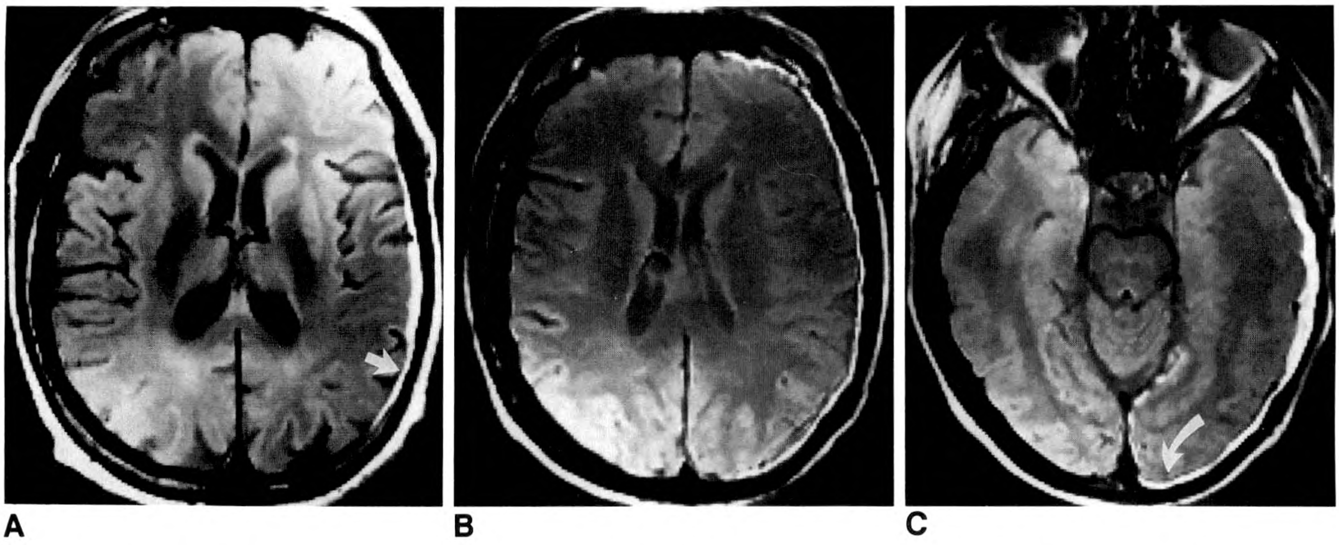

Fig. 3.—Rim of increased signal at left parietal cortex is evident in *A* and *B*.

***A*, Chemical-shift artifact from fat signal of diploic space has overlapped onto brain (*arrow*).**

***B* and *C*, Subdural hematoma is confirmed. Size of collection exceeds expected size of artifact, shows continuation of signal into posterior interhemispheric fissure, and does not taper at anterior and posterior poles where frequency-encoded artifact would be expected to diminish (*arrow*).**

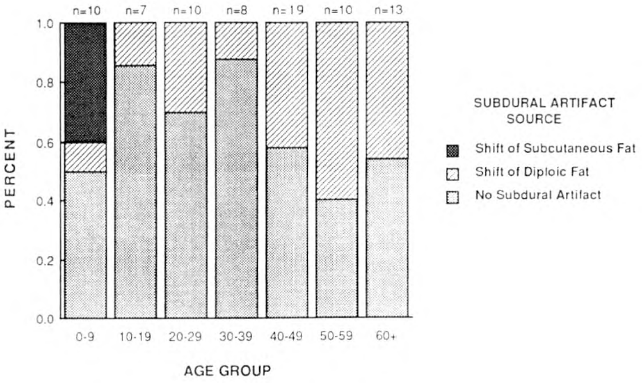

Fig. 4.—Artifact distribution within an age group.

Determine the frequency offset between fat and water in Hertz:

$$\text{Frequency offset (ppm)} = \text{shift (Hz)/resonant frequency (MHz)}. \qquad (1)$$

By using 3.5 ppm as the average chemical shift between fat and water, at 1.5 T, 3.5 ppm = frequency shift/64 MHz (frequency shift = 224 Hz).

After selecting the bandwidth (i.e., 32 kHz) at a given FOV (24 cm), determine the expected offset distance:

$$\begin{aligned}\text{Expected offset distance (mm)} &= [\text{frequency shift (Hz)} \times \text{FOV (mm)}]/\text{bandwidth (Hz)}\\ &= 224\ \text{Hz} \times 240\ \text{mm}/32{,}000\ \text{Hz}\\ &= 1.68\ \text{mm}. \qquad (2)\end{aligned}$$

The linear displacement of the chemical-shift artifact is estimated at 1.68 mm in the frequency-encoded axis in this example. However, allowance for pixel size and measurement error must be considered. The frequency shift between fat and water is between 3.0 and 3.5 ppm. We arbitrarily chose 3.5 ppm as the value of the protons providing the majority of human "fat" signal.

The following conclusions can be made about chemical shift if only one variable is altered at a time in the formulas 1 and 2.

1. The distance of the chemical-shift artifact is directly proportional to the strength of the magnetic field. Doubling the magnetic field will double the chemical-shift measurement in Hertz and in millimeters (see equation 1).

2. The distance of the chemical-shift artifact is inversely proportional to the sampling bandwidth. Doubling the sampling bandwidth will double the steepness of the gradient (to maintain the same resolution) and halve the distance of the chemical shift, as shown in Table 2. At 24-cm FOV, the artifact at 8, 16, and 32 kHz by cursor measurement was less than 1 mm from the calculated values of 6.7, 3.4, and 1.7 mm, respectively (Fig. 7).

3. The distance of chemical-shift artifact is directly proportional to the FOV. Doubling the FOV will halve the gradient and double the amount of chemical shift (Table 2). Measured artifact at 8 kHz with 24- and 48-cm FOVs differed by a factor of two, but the value at 48-cm FOV is an estimate since there was difficulty defining the margins of the fat signal on this image (Fig. 7).

It is important for the radiologist operating the MR system to understand the effects of and interrelationships involved in altering the sampling bandwidth, so the bandwidth can be optimized for each examination. At a given magnetic field

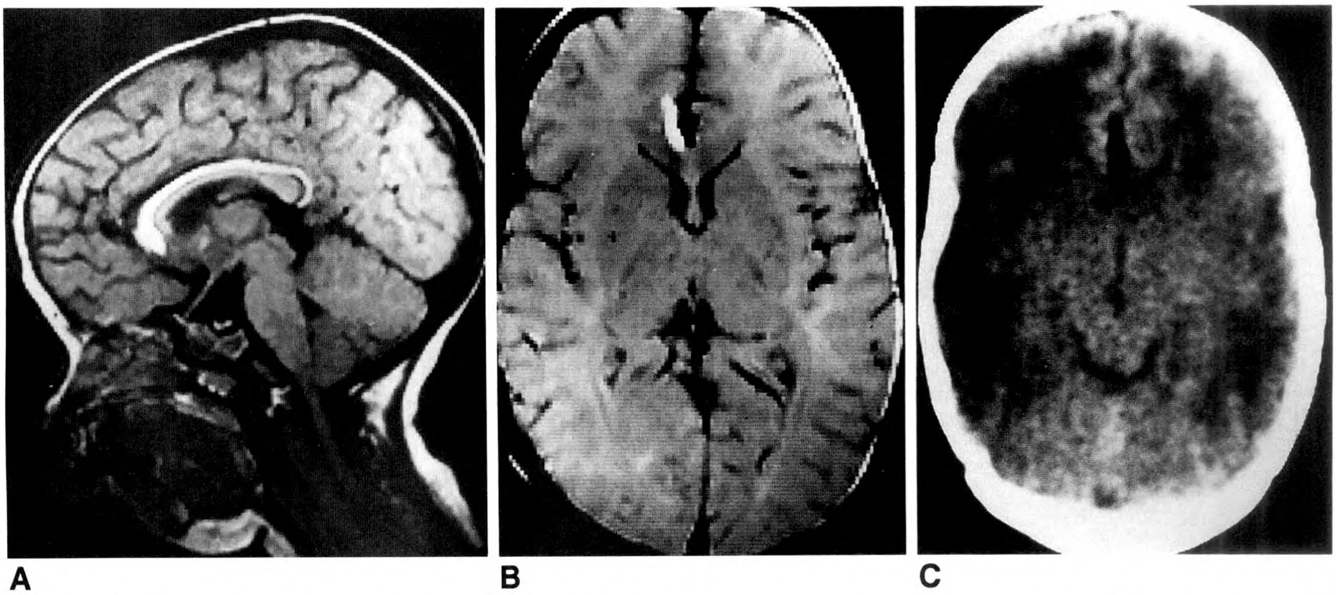

Fig. 5.—Fat signal in corpus callosum lipoma is superimposed on brain parenchyma by 3 mm, showing clinically insignificant but definite change from CT.

A, Sagittal image (500/30) shows downfield (right) shift of lipoma.

B, Axial MR image shows lipoma overlapping frontal cortex on downfield (left) side of image.

C, Axial CT scan indicates lipoma is closer to midline; there is no associated calcification.

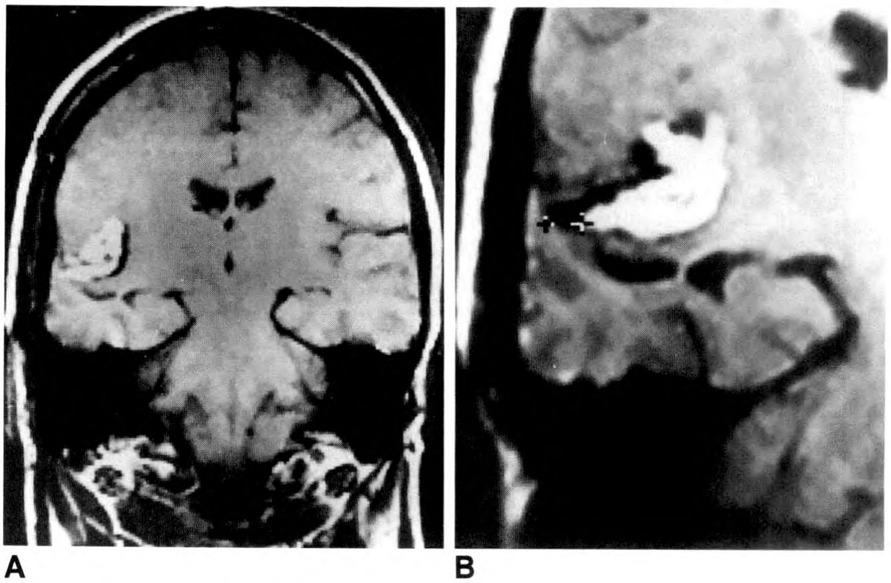

Fig. 6.—Reversal of gradient in frequency-encoded axis (left to right) changes appearance of sylvian fissure lipoma. Dark rim (upfield) part of chemical-shift artifact can mimic signal void of flowing blood or calcification, while bright (downfield) side of artifact structure may hide vessels or calcification.

A, Higher gradient to the right.

B, Higher gradient to the left. Signal void at indicated area measures 6 mm, larger than expected 3-mm artifact for system used; it correlated with a vessel at angiography and surgery.

strength, increasing the bandwidth lessens the distance of the chemical-shift artifact and decreases the signal to noise of the image. The signal to noise of the image is related to bandwidth by the formula, signal to noise $= 1/\sqrt{\text{bandwidth}}$. Therefore, an increase in bandwidth from 16 to 32 will decrease the signal to noise by a factor of 1.4 (Table 1).

Sampling bandwidths are inversely proportional to signal collection times. The signal collection time multiplied by the bandwidth (sampling frequency) equals the number of samples (read, × matrix). Therefore, with a constant number of samples, decreasing the sampling bandwidth to improve the signal to noise increases the time required to gather the returning signal and results in an increase in the minimal allowable TE. Asymmetric sampling is a method of data collection that allows a shorter TE without necessitating a change in bandwidth. Traditionally, sampling has been performed in a symmetric distribution around the returning signal. In the spin-echo sequence, after the 180° pulse, the read

TABLE 2: Technical Considerations of Operator-Selectable Bandwidth

Manufacturer/Field Strength	Limiting TE (msec)[a]	Bandwidth (kHz)	Comments
Technicare[b]			
0.6 T (Teslacon II)	43	8.3	–
	28	16.6	–
	20	33.0	Bandwidth is determined by TE and field of view
1.4 T (Teslacon I)	44	8.3	–
	29	16.6	–
	24	33.0	–
General Electric			
1.5 T (Signa)	142	2.0	2- to 32-kHz bandwidth selectable by modifying control variables
	78	4.0	–
	46	8.0	–
	29	16.0	–
	20	32.0	Default setting
Picker International[c]			
0.5 T (Vista)	40 (26)	12.5 (25)	Normal (shorter TE defaults to 25-kHz bandwidth)
	70	6.25	Extended sampling
1.5 T (Vista)	26	25.0	Normal
	60	12.5	Extended sampling

Note.—The selectability of the sampling bandwidth varies by manufacturer, may be run on a default setting, and affects the TE.

[a] Lower TEs are available with fast imaging techniques and asymmetric sampling.

[b] Bandwidth does not change on multiecho sequence.

[c] Bandwidth changes on multiecho sequence.

gradient is turned on while the slice gradient is turned off. Sampling cannot be performed during the interval in which the slice-select gradient is falling off and the read gradient is rising (Fig. 8) [7, 8]. The time between the gradient change and the beginning of signal collection limits how short the TE can be so that sampling does not overlap the gradient change interval. This can be compensated by a wider (higher) bandwidth (Fig. 9). By using asymmetric sampling, the TE can be shorter, allowing a closer spacing of signal collection and gradient change interval without requiring a narrower bandwidth (Fig. 9c).

Table 2 lists the specific parameters for the MR systems we have studied and indicates the degree of TE shortening with changes in sampling bandwidth. It should also be noted that the sampling bandwidth is an operative selectable parameter on the Picker International and General Electric units. If the sampling bandwidth is not selected by the user on these units, the sampling bandwidth will be set by the system (default setting). Default values will yield a high bandwidth, resulting in small chemical-shift artifacts and a shorter allowable TE. Since TE is inversely proportional to bandwidth, if a short TE image is needed to decrease the amount of T2-weighting and increase the amount of T1-weighting or to obtain gradient-recalled images, then a low sampling bandwidth cannot be used. Since chemical-shift artifacts increase with increasing FOV, in areas where a larger FOV is needed, such as the abdomen and pelvis, it is desirable to increase the sampling bandwidth in order to minimize the chemical-shift artifact. If the x matrix is increased, then either the bandwidth or the sampling time must be increased. If the sampling time is increased, the minimal allowable TE will also be increased.

Effect of Chemical-Shift Artifact on Cranial MR

With the Technicare 1.4-T system, the linear distance of chemical-shift artifacts as measured on spin-density-weighted images was 3.2 mm. Therefore, in children under the age of 8, the shift of the signal from fat in the subcutaneous tissues may exceed the average skull thickness and will overlap the brain causing artifactual subdural collection. In the first decade, skull thickness ranges from 2.9 to 3.3 mm, as measured 3 cm posterior to coronal suture [6, 9]. Less commonly between the ages of 8 and 40 and more commonly after age 40, the fat in the diploic space of the calvaria will be shifted over the brain when the distance between the brain and the medullary cavity is less than 3.2 mm. With increasing age, there is increased fat deposition within the marrow, which accounts for the increased prevalence of artifactual subdural hematomas with increasing age. Evaluation of the presence and source of fat signal resulting in subdural hematomas correlated with age-related changes of skull thickness and BPD. Skull thickness increases rapidly up to the teenage years, and then more gradually to age 40 or 50 [9]. The inner table of the skull has a relatively constant thickness of 0.5 mm. Although more variable, the outer table averages 1.5 mm in thickness [6, 10]. Differences in skull thickness are mainly due to the thickness of the diploic space. Between 4 and 20 years of age, the fat cell content of the marrow increases to approximately 21% [11, 12]. Analogous to hemopoietic marrow in other bones of the body, the fat content of the calvarial marrow begins to increase again in the eighth decade [13].

Usually, the appearance of the chemical-shift artifact is so characteristic that it is easily distinguishable from true subdural collections (Fig. 3). The chemical-shift artifact always occurs in the frequency-encoded direction and tapers as the source of fat signal becomes parallel to the frequency axis. Using the same machine and sequence, the frequency offset and apparent subdural location is always on the same side of the brain. Reversal of the direction of the gradient in the frequency-encoded axis results in the artifact being located on the opposite side. This artifact can be mistaken for a true subdural hematoma by those used to working at a different magnetic strength, in systems that alter bandwidth with TE, or when reviewing images from an unfamiliar unit. For questionable subdural hematomas, the phase- and frequency-encoded axes can be reversed or the direction of the gradient strength can be inverted. The dark side of the artifact will add

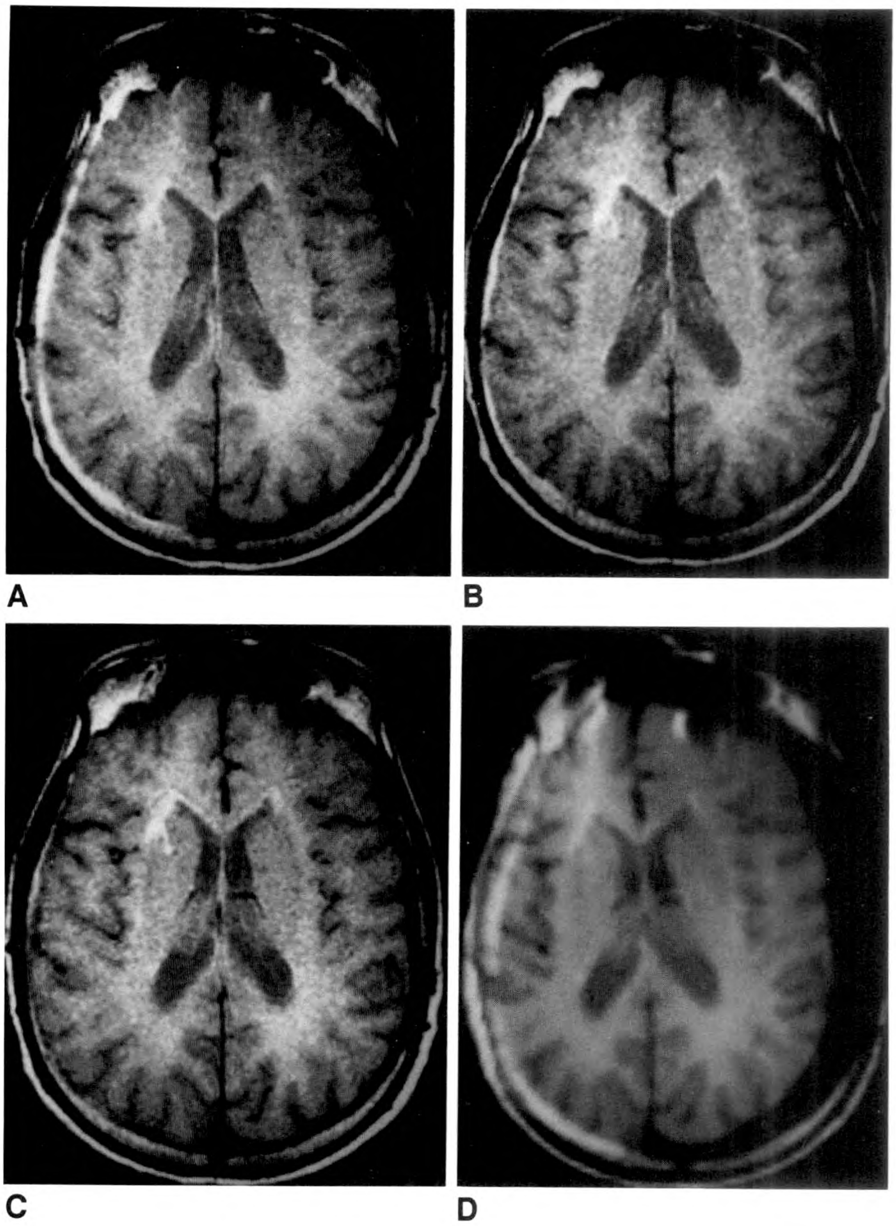

Fig. 7.—Chemical-shift artifact is inversely proportional to sampling bandwidth.

A–C, **8- (*A*), 16- (*B*), and 32- (*C*) kHz bandwidths, 500/60 images, 24-cm field of view, 256 × 256 matrix.**

D, **8-kHz bandwidth, 48-cm field of view.**

to the signal void of the inner table on the higher gradient side of the skull, and the shift of fat onto the inner table of the lower gradient side adds to the eccentricity of the brain within the halo of fat.

Comparison of CT and MR in the five patients with intracranial lipomas revealed discrete but insignificant apparent location shifts in the lipomas in the downfield direction (Fig. 5). Fat deposits in lipomas of the corpus callosum, interhemispheric fissure, and fat-containing tissues always shifted in the same direction as the subcutaneous fat. An area of decreased signal that may mimic calcification or blood vessels is always adjacent to the lesion in the direction opposite the shift of the fat. In the latter, the dark rim of the chemical-shift artifact is asymmetric and perpendicular to the axis of the frequency-encoded gradient, differentiating it from the concentric ring of decreased signal that surrounds intraparenchymal hemorrhage and represents hemosiderin deposit. Switching the direction of the frequency-encoded gradients or a gradient-echo pulse sequence [14] can be used to determine if calcification is present. The interpretation of the presence of calcifications associated with the intracranial lipomas in this study had no clinical significance. In the case of the sylvian fissure lipoma, deviation in size of the measured vs expected chemical-shift artifact correlated with angiographic and surgical verification of a large vessel. The flow void of the middle cerebral branch artery added to the artifact when the high gradient was to the left and was covered by the signal from the lipoma when the gradient was reversed (Fig. 6).

In conclusion, the relationship of machine-selectable variables on chemical-shift artifacts has been discussed. Chemical-shift artifact is directly proportional to field strength and FOV and inversely proportional to sampling bandwidth. Increasing the bandwidth to compensate for chemical-shift artifacts has consequences in terms of lower signal to noise while allowing a lower minimum TE. Furthermore, chemical-shift artifacts alter brain images in several ways: (1) apparent location shifts of lipomas and other fat-containing tumors, (2) rim artifacts mimicking associated vessels and calcifications while the bright side of the chemical shift can hide such associated structures, and (3) subdural hematomas appearing artifactual. Eccentricity of the brain occurs relative to the halo of subcutaneous fat and diploic fat. The apparent subdural hematomas can result from shift of either subcutaneous or diploic fat. The former occurs in children less than 8 years of age where the distance between brain and subcutaneous fat is less than the linear value of the chemical shift. Increase in the fat content of the enlarged diploic space in adults correlates with the presence of apparent subdural hematomas from the shift of the medullary fat signal across the inner table of the skull.

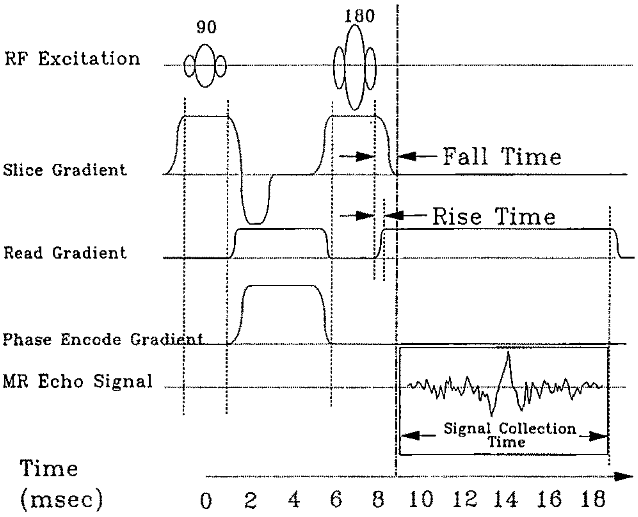

Fig. 8.—Beginning point of data sampling window is controlled by other events in the sequence. *Broken lines* indicate partitions for mutually exclusive events. For the spin-echo sequence, the earliest data sampling (*dot-dash line*) is controlled by falling edge of slice-select gradient, activated during 180° pulse. For other sequences (i.e., gradient echo), dominant factor is rise time of read gradient. These rise and fall times are 100–1500 msec for typical sequences in commercial whole-body MR systems.

ACKNOWLEDGMENTS

We thank Felix W. Wehrli, Hospital of the University of Pennsylvania, Philadelphia, and Linda M. Eastwood and Surya N. Mohapatra, Picker International, Highland Heights, OH, for technical information.

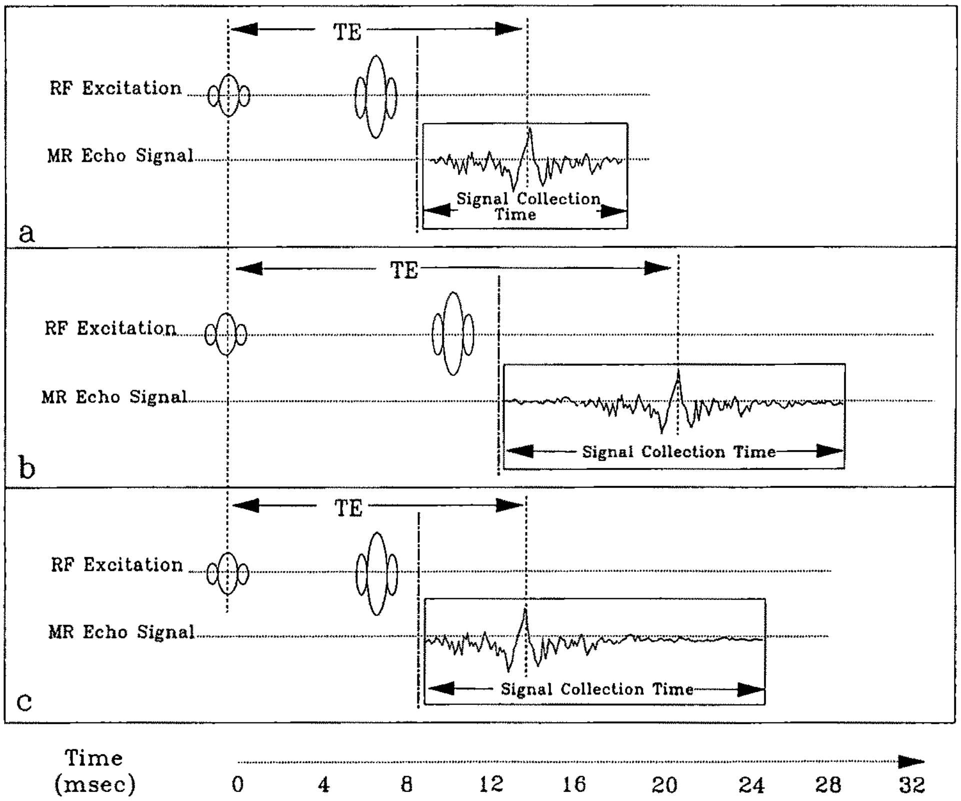

Fig. 9.—Returning echo is sampled at earliest possible interval (*a*). Increasing bandwidth to sample wider range of frequencies and decrease chemical-shift artifact requires a longer TE (*b*), or echo may be sampled asymmetrically (c).

REFERENCES

1. Pople JA, Schneider WG, Bernstein WG. General features of nuclear magnetic resonance spectra. In: Hume DN, King EL, Pope JA, Stork G, Williams HH, Herschbach DR, eds. *High-resolution nuclear magnetic resonance.* New York: McGraw-Hill, **1959**:12–21, 87–91
2. Wehrli FW. *Introduction to fast-scan magnetic resonance.* Milwaukee: General Electric Medical Systems, **1986** (G.E. publication no. 7299)
3. Abraham TJ, Loftus P. In: *Proton and carbon-13 NMR spectroscopy.* London: Heyden, **1979**:Chapter 2
4. Brady TJ, Wismer GL, Buxton R, Stark DD, Rosen BR. Magnetic resonance chemical shift imaging. In: Kressell HY, ed. *Magnetic resonance annual 1986.* New York: Raven, **1986**:55–80
5. Campbell IA, Dwek RA. *Biological spectroscopy.* Menlo Park, CA: Benjamin/Cummings, **1984**:361–367
6. Orley A. *Neuroradiology.* Springfield, IL: Thomas, **1949**:3
7. Provost TJ, Hurst GC. Asymmetric sampling of 2-D FT. Presented at the annual meeting of The Society of Magnetic Resonance in Medicine, Montreal, August **1986**
8. Hendrick RE. Sampling time effect on signal-to-noise, contrast-to-noise. *Magn Reson Imaging* **1987**:5;31–37
9. Adeloye A, Katten KR, Silverman FN. Thickness of normal skull in the American blacks and whites. *Am J Phys Anthopol* **1985**;43:23–30
10. Either R. Thickness and texture. In: Newton TH, Potts DG, eds. *Radiology of the skull and brain*, vol. 1, book 1. St. Louis: Mosby, **1971**:155–157
11. Russel WJ, Yoshinaga H, Antokir SH, Mizuno M. Active bone marrow distribution in the adult. *Br J Radiol* **1966**;39:735–739
12. Ellis RE. Distribution of active bone marrow in the adult. *Phys Med Biol* **1961**;5:255–258
13. Hartsock RJ, Smith EB, Petty CS. Normal variations with aging of the amount of hemapoietic tissue in bone marrow from the anterior iliac crest. *Am J Clin Pathol* **1965**;131:326–333
14. Atlas SW, Grossman RI, Hackney DB, et al. Calcified intracranial lesions: detection with gradient-echo-acquisition rapid MR imaging. *AJNR* **1988**;9:253–259, *AJR* **1988**;150:1383–1389

Memorial

Andrew Eccles Yeates, 1951–1989

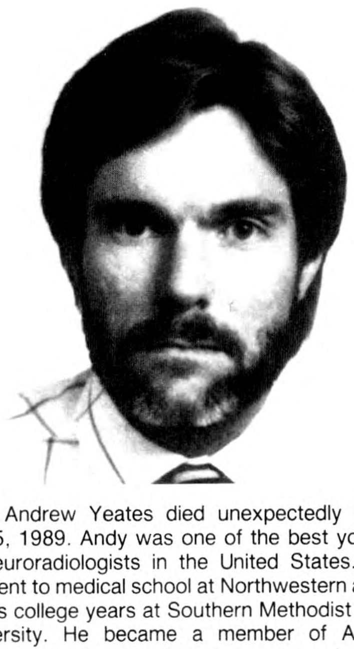

Andrew Yeates died unexpectedly May 15, 1989. Andy was one of the best young neuroradiologists in the United States. He went to medical school at Northwestern after his college years at Southern Methodist University. He became a member of Alpha Omega Alpha when he was a junior and came to Stanford on a 4-year internship-residency program in diagnostic radiology. From his first year there, he impressed us by his level of clinical knowledge, judgment, and radiologic acumen, as well as his outgoing personality, engaging wit, and zest for life. His professors commented on his ability to make teaching a stimulating and enjoyable experience. Evaluations made during his residency at Stanford note that he was exceptionally intelligent and that his knowledge, maturity, confidence, and poise were truly outstanding. He had a probing and imaginative mind. He was a joy to work with, making teaching a special delight.

After residency, Andy completed a neuroradiology fellowship and served 2 years at the University of California, San Francisco (UCSF), as a clinical instructor in the neuroradiology section where his academic skills were honed. While at UCSF, he wrote the first paper on the use of MR imaging in syringomyelia. He eventually was the author of 20 scientific papers and presented his research at many national meetings. He frequently was invited to speak at medical symposia. After his time at UCSF, Andy joined the faculty in the neuroradiology section at Duke, where his skills did not go unnoticed. He subsequently served as section chief and director of research on the neurologic applications of MR. He left Duke in 1985 for private practice in Northern California, the place he loved most dearly. He served as codirector of MR at Merritt Peralta Medical Center in Oakland. He missed academics and returned to Duke for 2 years, only to be tempted back to private practice in Northern California, again at Merritt Peralta Medical Center. During this time he served as assistant clinical professor of radiology at Stanford.

Andy was a natural athlete, and he combined this with a strong desire to win, making him a formidable opponent in most sports. Although he excelled at many sports, including tennis and skiing, his first love was golf. Andy was a scratch golfer, shooting routinely in the low 80s. It was not unusual for him to demonstrate his golf swing while conversing about unrelated topics in the hospital, at social gatherings, or in almost any situation. One of Andy's favorite activities was to spend a day off from private practice, teaching at Stanford and then playing a round of golf at the university's course.

His sharp wit, unique style of humor, and delightful charm made him a favorite companion for friends and fellow workers. Even hectic and otherwise tedious days at the hospital became pleasurable when Andy was on service entertaining his colleagues with practical jokes, enlightening them with his vast knowledge of neuroradiology, or inspiring them with his efficiency. He had an incisive mind and was always driven to excellence. Andy was such an outstanding radiologist and a charming individual that he continuously was besieged by attractive offers from both academic and private groups attempting to lure him to their institutions.

Andy leaves behind his parents, Robert and Cleone Yeates, two sisters, Shelley Blair and Elies McKowen, and a brother, Robert Yeates, Jr. All of us who taught him, learned from him, worked with him, and enjoyed his friendship for the brief time we had will also miss him dearly. Although those who knew Andy Yeates are shocked and saddened by his unexpected death, they are comforted by memories of the joy he brought into their lives that those less fortunate will never experience. In an effort to sustain Andy's memory and spirit, memorial funds have been established at Stanford and Duke universities to support teaching in neuroradiology.

Richard S. Breiman
Oakland, CA 94609
Michael Brant-Zawadzki
Newport Beach, CA 92658

MR Signal Abnormalities in Memory Disorder and Dementia

Brian C. Bowen[1]
William W. Barker[2]
David A. Loewenstein[3]
Jerome Sheldon[1]
Ranjan Duara[1,4]

MR imaging of the brain, performed in 86 normal subjects and 113 patients with objective memory disorder or dementia, demonstrated white- and gray-matter areas of high signal intensity on long TR images (short and long TE). Hyperintensities were analyzed with respect to size (on a scale of 0–3) and location: lesions were periventricular, subcortical, or cortical. The patients with memory disorder and dementia were categorized as having probable/possible Alzheimer disease, a combination of Alzheimer disease and multiinfarct cognitive disorder, or multiinfarct cognitive disorder alone on the basis of clinically determined Hachinski ischemic scores. Significant correlations were found between age and scores for periventricular lesions ($r = .40$, $p < .0005$) and subcortical lesions ($r = .39$, $p < .0005$) in normal subjects. Correlations were also found between the Hachinski ischemic score and scores for periventricular lesions ($r = .21$, $p < .01$), subcortical lesions ($r = .27$, $p < .0002$), and cortical lesions ($r = .32$, $p < .0005$) in subjects with memory disorder/dementia. Comparing multiinfarct cognitive disorder, Alzheimer disease, and normal groups, the mean scores for periventricular lesions were 12.0 ± 4.6, 7.6 ± 4.8, and 3.4 ± 2.6, while mean scores for subcortical lesions were 10.8 ± 12.2, 4.1 ± 6.4, and 0.8 ± 1.2, respectively. Periventricular lesions were present in 99–100% of patients with Alzheimer disease and multiinfarct cognitive disorder. On the other hand, subcortical lesions, which were identified in 100% of patients with multiinfarct cognitive disorder, were present in only about half of the patients with Alzheimer disease.

Thus, scores for both periventricular and subcortical lesions are positively correlated with age and risk factors for cerebrovascular disease and also are significantly increased in the presence of objective memory disorder or dementia. These results imply that in the subject groups considered here, elderly patients with vascular dementia are most likely to have severe white-matter abnormalities on MR scans. The score for subcortical lesions appears to be more helpful than the score for periventricular lesions in distinguishing vascular dementia from Alzheimer disease and normal aging, so that a patient with prominent subcortical white-matter abnormalities is more likely to have a diagnosis of vascular than degenerative dementia.

***AJNR* 11:283–290, March/April 1990; *AJR* 154:1285–1292, June 1990**

MR imaging is known to be sensitive in detecting periventricular and subcortical white-matter lesions, which appear as hyperintense areas of variable configuration and size on long TR spin-echo images. The number and size of these lesions correlate with chronologic age and with such risk factors for cerebrovascular disease as hypertension and prior ischemic event [1–3]. There are, however, conflicting reports as to how lesion severity correlates with the clinical diagnosis of dementia [1–5]. It has been suggested that the two main types of dementia, multiinfarct cognitive disorder (MICD) and Alzheimer disease (AD), may be differentiated by the severity of white-matter abnormalities [5]. An analysis based on CT characteristics has demonstrated significantly increased severity of periventricular white-matter abnormalities in MICD compared with AD [6]. Nevertheless, quantitation of white-matter lesions detected by MR in demented subjects, with consid-

Received March 24, 1989; revision requested June 7, 1989; revision received August 4, 1989; accepted August 16, 1989.

B. C. Bowen is the recipient of the Dauer Fellowship in Magnetic Resonance.

This work was supported in part under an agreement with the Aging and Adult Services Program Office, Department of Health and Rehabilitative Services, State of Florida.

[1] Department of Radiology, University of Miami School of Medicine, and Mount Sinai Medical Center, 4300 Alton Rd., Miami Beach, FL 33140. Address reprint requests to B. C. Bowen, Department of Radiology (R-130), University of Miami School of Medicine, P.O. Box 016960, Miami, FL 33101.

[2] Wien Center for Alzheimer's Disease and Memory Disorders, Mount Sinai Medical Center, Miami Beach, FL 33140.

[3] Department of Psychiatry, University of Miami School of Medicine, and Cognitive Neuropsychological Laboratory, Wien Center for Alzheimer's Disease and Memory Disorders, Mount Sinai Medical Center, Miami Beach, FL 33140.

[4] Department of Neurology, University of Miami School of Medicine, and Mount Sinai Medical Center, Miami Beach, FL 33140.

0361–803X/90/1546–1285
© American Roentgen Ray Society

eration given to the location of the lesions and clinical diagnosis of dementia, has not as yet been reported.

In this study, the location and size of white- and gray-matter lesions in clinically normal individuals and in those with memory disorder have been examined. The results have been analyzed with respect to the clinical diagnosis (MICD vs AD) in the memory disorder patients, and conclusions have been drawn regarding the contribution of MR to the proper diagnosis of dementia.

Subjects and Methods

Patients presenting with memory impairment underwent medical, neurologic, and psychiatric examinations; clinical laboratory tests; and MR examination of the brain. All patients included in this study were found to have objective memory disorders by neuropsychological testing. Patients who were considered to have a primary psychiatric diagnosis, such as depression, or a neurologic diagnosis other than AD or MICD (e.g., Parkinson disease) were excluded from this study. Eighty-six normal volunteers underwent the same evaluation as the patients, except that the psychiatric interview was not done. Patients with memory disorder who were also demented, according to the *Diagnostic and Statistical Manual of Mental Disorders* (DSM III) [7], were considered separately from those without dementia for certain analyses. Otherwise, the demented and nondemented patients with objective memory disorders were combined and then divided into three groups on the basis of their Hachinski ischemic score [8] (see Fig. 1). Those in the group with the lowest ischemic scores (0–4) were labeled probable or possible AD; patients in the group with the highest ischemic scores (7–14) were labeled MICD [9]. MICD was preferred to multiinfarct dementia [8, 10] because many patients with objectively determined memory disorders did not fulfill DSM III criteria for dementia. Patients in the group with intermediate Hachinski scores (5 and 6) were labeled mixed disorder (MIX). The degree of cognitive deficit was quantified by the Mini-mental State examination of Folstein et al. [11].

Spin-echo MR images were obtained using a Siemens Magnetom superconducting magnet operating at 0.5, 1.0, or 1.5 T and a 25-cm-diameter RF head coil. Seven- or 10-mm-thick contiguous axial images and contiguous sagittal images with long TRs and short TEs, 1500–3000/25–35 (TR/TE), and long TEs, 1500–3000/80–105, were obtained. Scans were interpreted by a radiologist who had no knowledge of the age, identity, or clinical diagnosis of the subjects.

MR signal abnormalities were identified as areas of increased signal intensity relative to surrounding brain parenchyma on both short and long TE images (Fig. 2) and were scored using the following scheme:

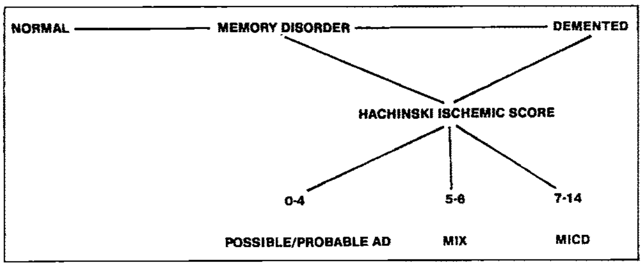

Fig. 1.—Classification of subjects. AD = Alzheimer disease; MIX = mixed disorder; MICD = multiinfarct cognitive disorder.

1. Lesions contiguous with the margins of each lateral ventricle were designated periventricular lesions (PVLs). They were arbitrarily assigned to anterior, central, and posterior periventricular regions to indicate lesions located respectively in the regions of frontal horn, body, or trigone/occipital horn of the lateral ventricle. The lesions in each region were given a score (similar to the scheme of Kinkel et al. [12]) of 0–3 based on severity (0 = none; 1 = punctate or thin band [less than 0.5 cm thick]; 2 = thick "cap" or broad band [approximately 0.5–1 cm thick]; 3 = lobular, irregular area [outer margin always greater than 1 cm from the ventricular margin]). Although central PVLs can be confused with the normal appearance of the caudate nucleus on short TE images, the caudate signal intensity decreases relative to the signal produced by PVLs on long TE images (Fig. 2). A total score was obtained by summing the scores for the right and left hemispheres (maximum score, 18).
2. White-matter lesions outside the periventricular domain (i.e., in the corona radiata of the frontal, parietal, temporal, and occipital lobes) and in the centrum semiovale, along with subcortical gray-matter lesions, were designated subcortical lesions (SCLs). MR axial images were assigned to one of four anatomic levels: supraventricular, high ventricular, low ventricular, and infraventricular. For each level, each cerebral hemisphere was divided into anterior, central, and posterior regions. SCLs in each region at each level were given a score of 0–3 (0 = none; 1 = punctate lesion [less than 0.5 cm in maximum diameter]; 2 = nodular lesion [approximately 0.5–1 cm in maximum diameter]; 3 = patchy, irregular lesion area always greater than 1 cm maximum diameter]). A total score was obtained by summing the scores of all regions in both right and left hemispheres for the four brain levels.
3. Cortical gray-matter lesions (CLs) were assigned to a location using the same scheme as for SCLs. Each lesion was given a score of 0–3 (none, small, moderate, and large, as for SCLs). A total score was obtained for both hemispheres and four brain levels.

Lesion was used to describe all periventricular and subcortical, as well as cortical, hyperintensities. For subjects in whom a perifrontal hyperintensity had an anterior PVL score of 1 or 2, the term lesion (meaning more or less circumscribed pathologic change) may not be correct since such hyperintensities can represent normal variation [13]. Because a spectrum of perifrontal hyperintensities, as well as hyperintensities located at other periventricular sites, were being evaluated, the term lesion was used throughout. Previous authors have used the term lesion similarly [1, 2, 4, 12].

Statistical Analysis

PVL, SCL, and CL scores were obtained for each subject. Because these data were not normally distributed, a nonparametric analytic strategy was used. Comparisons between various groups (young normal, elderly normal, AD, MICD, and MIX) were made using the Kruskal-Wallis one-way analysis of variance procedure. Post hoc tests were conducted using Mann-Whitney U tests. The relationship between MR scores and age, Hachinski ischemic score, and the Mini-mental status score of Folstein et al. [11] were examined using Spearman rank-order correlation coefficients.

Results

Table 1 gives the mean scores for right and left hemispheres for PVLs, SCLs, and CLs in each subject group. No significant differences were found in the laterality of these lesions in any subject group.

Table 2 gives the mean scores for anterior, central, and posterior regions of PVLs and SCLs in all subjects. It was found that for PVLs, the highest mean scores were in the anterior regions and the lowest mean scores were in the central region; intermediate scores were in the posterior region. For SCLs, no significant differences in mean scores were obtained for anterior, central, and posterior regions.

Table 3 gives the mean SCL scores in all subjects according to the horizontal level of the brain in which they were seen. The high ventricular level had the highest scores, followed by supraventricular and low ventricular levels, which had equal mean scores. The infraventricular level had the lowest mean scores.

In 86 clinically normal individuals between the ages of 23 and 84 (mean age, 53.6 ± 16.6 years), there was a significant increase with age in the average total score for PVLs ($r = .40, p < .0005$) and for SCLs ($r = .39, p < .0005$), but not for CLs ($r = .02, p < .42$) (Figs. 3 and 4). In 113 patients with memory disorders, significant positive correlations were found between Hachinski ischemic scores and PVL scores ($r = .21$, $p < .01$), SCL scores ($r = .27, p < .002$), and CL scores ($r = .32, p < .0005$). There was no significant correlation between PVL, SCL, or CL scores and Mini-mental State scores in memory disorder/dementia subjects.

The mean PVL and SCL scores for all memory disorder subjects without dementia were not significantly different from those for demented subjects. However, the scores for both demented and nondemented subjects with memory disorder were significantly higher than the corresponding scores for age-matched normal individuals (Table 4). Approximately 90% of elderly normals exhibited PVLs, with the majority of the subjects having scores between 1 and 4 (Fig. 3). In comparison, 99–100% of memory–disordered/demented individuals exhibited PVLs; the majority of these subjects had total scores between 5 and 18. For SCLs, a similar skewing of the score distribution toward higher scores (5–40) for memory–disordered/demented individuals was found (Fig. 4).

When memory–disordered/demented patients were divided into groups on the basis of their clinically determined ischemic score (Fig. 1), the data on white-matter lesions could be presented in another way. Mean PVL scores for probable/possible AD, MIX, and MICD patients, and for age-matched controls were compared (Table 4). The mean score for the MICD group was significantly greater than those for the AD and MIX groups, both of which in turn were significantly greater than that for normals. The mean SCL score for the MICD group was also significantly greater than that for the AD group but not the MIX group. MICD, MIX, and AD groups each had a mean SCL score significantly greater than that of the normal group.

Discussion

The goals in this study were to determine the prevalence and severity of white-matter abnormalities detected by MR in normal individuals and in elderly patients with memory disorders and dementia, and to correlate the MR results with clinical data such as Hachinski ischemic scores, which are routinely used in practice to determine whether a patient's cognitive deficits are due to primarily vascular or degenerative disease. The ischemic score has been used previously to classify patients with dementia in CT [6] and MR studies [5]. The Hachinski ischemic score, though not a simple linear, parametric scale, nevertheless assigns a semiquantitative value to risk factors for cerebrovascular disease [8].

Neuropathologic studies have demonstrated that patients who are diagnosed as having Alzheimer-type dementia on the basis of Hachinski ischemic scores of 4 or less, do have this pathologic diagnosis alone in 80–90% of cases [14, 15]. However, when multiinfarct dementia is diagnosed on the basis of a Hachinski ischemic score of 7 or greater, this pathologic diagnosis alone is found in approximately 25% of cases; most often, a mixed vascular and degenerative disorder is found [14]. We recognized this weakness in clinical categorization of patients by use of the Hachinski ischemic score, but were forced, because of the lack of an alternative clinical method, to employ this procedure. It is likely that some of the overlap in MR scores between clinical groups in this study may have resulted from this lack of specificity of the Hachinski ischemic scores.

In their study, Fazekas et al. [16] described large, confluent periventricular hyperintensities extending into the deep white matter in multiinfarct dementia, in contrast to the smooth, halolike periventricular hyperintensities and small focal deep white-matter hyperintensities seen in AD patients. By grading such lesions, we were able to examine their significance statistically.

Punctate and triangular perifrontal hyperintensities have been reported to be a common finding in normal individuals, secondary to locally decreased myelin content, focal ependymal breakdown ("ependymitis granularis"), and preferential centripetal drainage of interstitial fluid [13]. Perioccipital hyperintensities are also seen occasionally in normal individuals, secondary to focal ependymal breakdown [13, 17]. Pathologic hyperintensities can then represent extension from these "normal" foci, possibly related to primary or secondary vascular abnormalities occurring in the periventricular watershed or "border zones" [18, 19] in elderly normals and patients with memory disorder/dementia (see later discussion of MICD and AD).

In normal subjects, PVLs were a common finding in our study. They occurred in 74% of young normals (41.5 ± 9.9 years) and 89% of elderly normals (70.3 ± 6.1 years), while SCLs were seen in only 6% of young normals and in 39% of elderly normals (Figs. 3 and 4). The increase in the prevalence and severity of lesions with age was similar for PVLs and SCLs.

SCLs occurred most often in the high ventricular level and least frequently in the infraventricular level (Table 3). The predilection for the high ventricular level, which encompasses the bodies of the lateral ventricles and surrounding white matter, may be explained primarily by the vascular anatomy. At this level, the medullary branches of the anterior, middle, and posterior cerebral arteries reach their smallest size and

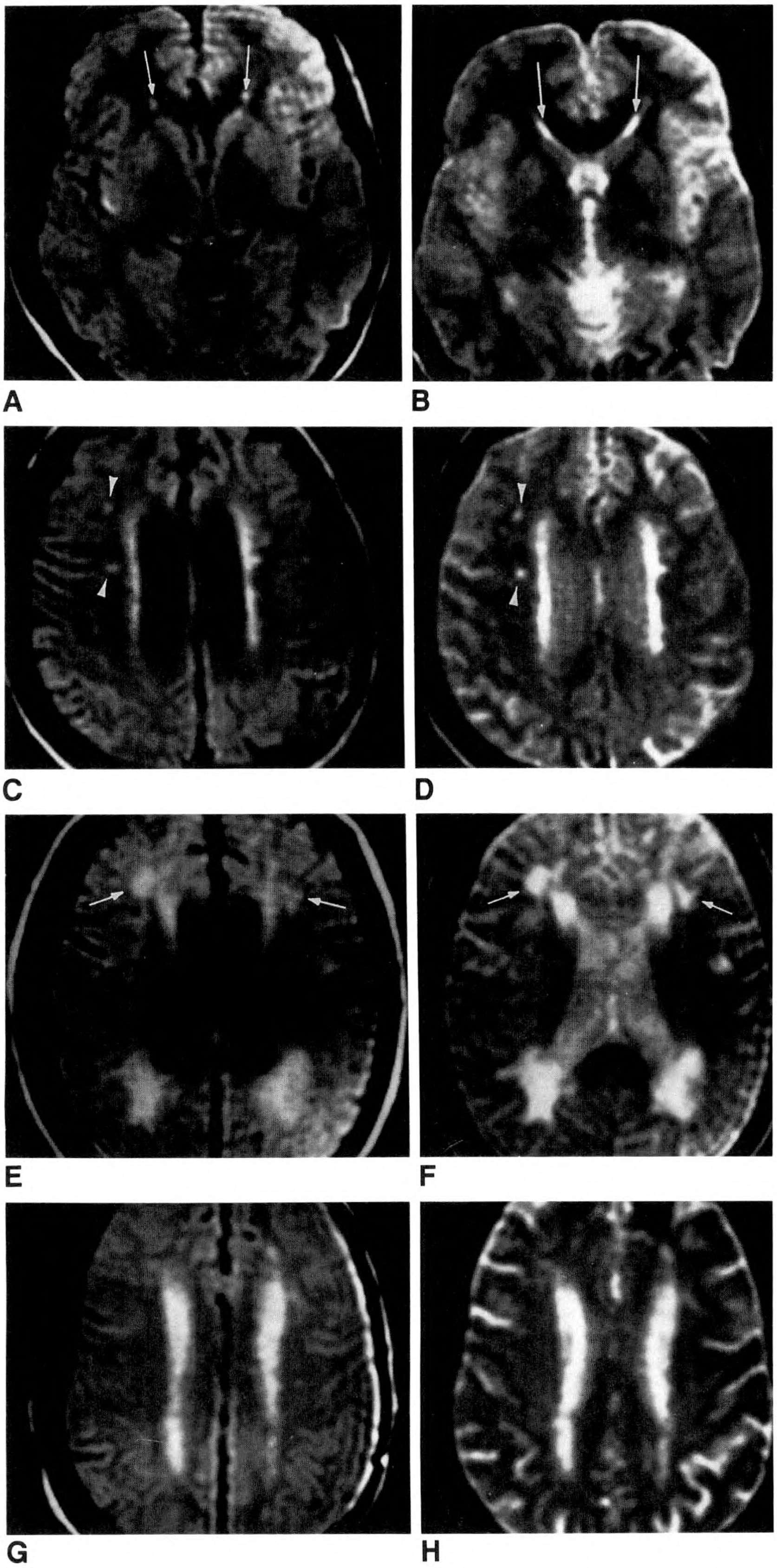

Fig. 2.—Scoring of white-matter lesions is illustrated on this and the next page.

A **and** ***B*****, 0.5-T MR images, 2000/35/1 (*****A*****) and 2000/105/1 (*****B*****). Score of anterior periventricular lesion is 1 for each hemisphere (*****arrows*****).**

C **and** ***D*****, 0.5-T MR images, 2000/35/1 (*****C*****) and 2000/80/1 (*****D*****). Score of central periventricular lesion is 2 for each hemisphere. Scores of anterior and central subcortical lesions (*****arrowheads*****) are 2.**

E **and** ***F*****, 0.5-T MR images, 2000/35/1 (*****E*****) and 2000/105/1 (*****F*****). Scores of anterior periventricular lesions, posterior periventricular lesions, and anterior subcortical lesions (*****arrows*****) are 3 for each hemisphere.**

G **and** ***H*****, 1.5-T MR images, 2500/28/1 (*****G*****) and 2500/84/1 (*****H*****). Score of central periventricular lesion is 3.**

(Fig. 2 is continued on the opposite page.)

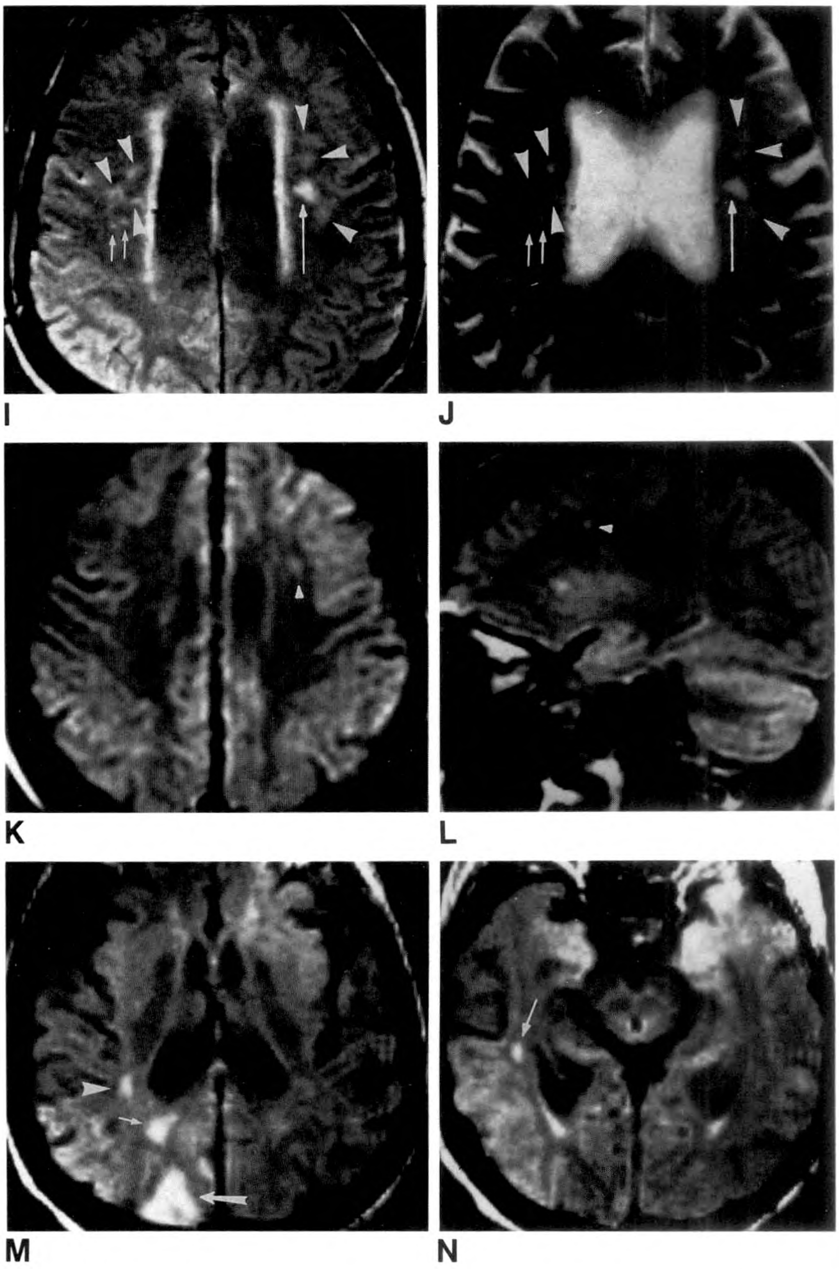

Fig. 2—(continued).

I and *J*, 1.5-T MR images, 2500/25/1 (*I*) and 2500/90/1 (*J*). Left hemisphere scores of high ventricular, central subcortical lesions are 3 (*long arrows*) and 2 (*arrowheads*); right hemisphere scores are 2 (*arrowheads*) and 1 (*short arrows*).

K and *L*, 0.5-T axial (*K*) and sagittal (*L*) MR images, 2000/35/1. Score of high ventricular/supraventricular, central subcortical lesion is 2 (*arrowheads*).

M, 1.0-T MR image, 2000/28/1. Scores of low ventricular posterior and central subcortical lesions are 3 (*small arrow*) and 2 (*arrowhead*), respectively. Score of right occipital cortical lesion is 3 (*large arrow*).

N, 1.0-T MR image, 2000/28/1. Score of low ventricular central subcortical lesion is 2 (*arrow*).

TABLE 1: Mean Scores of Periventricular, Subcortical, and Cortical Lesions by Hemisphere

Group	No.	Age	Periventricular Lesions		Subcortical Lesions		Cortical Lesions	
			Right	Left	Right	Left	Right	Left
All subjects	199	–	2.8 ± 2.5	2.7 ± 2.5	1.6 ± 3.4	1.4 ± 3.2	0.1 ± 0.4	0.1 ± 0.4
Young normals	50	41.5 ± 9.9	0.9 ± 0.8	0.9 ± 0.6	0.1 ± 0.5	0.03 ± 0.2	0.04 ± 0.2	0.03 ± 0.2
Elderly normals	36	70.3 ± 6.1	1.9 ± 1.6	1.5 ± 1.2	0.6 ± 1.1	0.2 ± 0.5	0.03 ± 0.2	0.0 ± 0.0
Probable and possible Alzheimer disease	87	73.1 ± 8.4	3.8 ± 2.5	3.8 ± 2.4	2.3 ± 3.5	1.9 ± 3.3	0.1 ± 0.4	0.1 ± 0.5
Mixed disorder	14	72.5 ± 11.2	3.5 ± 2.3	3.6 ± 2.5	2.6 ± 4.7	3.4 ± 5.0	0.4 ± 0.7	0.2 ± 0.6
Multiinfarct cognitive disorder	12	73.4 ± 9.3	6.0 ± 2.2	5.9 ± 2.6	5.7 ± 6.3	5.1 ± 6.0	0.3 ± 0.5	0.4 ± 0.7

Note.—No hemispheric difference was found in any subject group. Lesions were assessed on a scale of 0–3, with 0 reflecting no lesions and 3 being the most severe. Lesions were given separate grades for the anterior, central, and posterior regions of each hemisphere.

TABLE 2: Mean Scores of Periventricular and Subcortical Lesions by Region in All Subjects

Region	Lesion Score	
	Periventricular	Subcortical
Anterior	$2.8^a \pm 1.6$	0.7 ± 2.3
Central	$1.1^c \pm 1.7$	1.5 ± 3.2
Posterior	$1.7^b \pm 2.2$	0.8 ± 2.5

Note.—Lesions were assessed on a scale of 0–3, with 0 reflecting no lesions and 3 being the most severe.

[a–c] Mean scores with different superscripts a–c are significantly different ($p < .05$ by Mann-Whitney U test).

TABLE 3: Mean Scores of Subcortical Lesions by Horizontal Brain Level

Horizontal Brain Level	Lesion Score
Infraventricular	$0.1^c \pm 0.7$
Low ventricular	$0.7^b \pm 2.0$
High ventricular	$1.5^a \pm 2.9$
Supraventricular	$0.7^b \pm 2.0$

Note.—Lesions were assessed on a scale of 0–3, with 0 reflecting no lesions and 3 being the most severe.

[a–c] Mean scores with different superscripts a–c are significantly different ($p < .05$ by Mann-Whitney U test).

greatest depth of penetration into the white matter, and the opportunity for ischemic injury is greatest.

PVL and SCL scores for demented or memory-disordered patients were significantly higher than for age-matched normals (Table 4). As seen in Figures 3 and 4, the distributions of patient scores are skewed toward higher values in the memory disorder groups. These results agree with those of Brant-Zawadzki et al. [4], who found a higher prevalence of white-matter lesions in elderly subjects with dementia (non-AD) than in elderly subjects with normal neurologic examinations. At the same time, our results are not necessarily inconsistent with those of Awad et al. [1], who reported no correlation between the severity of white-matter "incidental lesions" and the presence of dementia. Awad et al. did not present a direct comparison between demented patients and age-matched normals, nor did they distinguish between memory disorder and dementia. If patients who had memory disorder but were not demented were included in the normal group in our study, we would also not have discovered a difference in mean PVL and SCL scores between demented and normal subjects. It has been reported that the severity of MR-detected [5] and CT-detected [20] white-matter lesions does not increase with the severity of dementia; our results imply this as well, since we found no correlation between Mini-mental State scores and PVL or SCL scores. We note, however, that our study included only ambulatory outpatients, and thus excluded severely demented, usually bedridden patients.

While the degree of the association between PVLs, SCLs, and CLs and the Hachinski score was small, our results emphasize the association of cerebrovascular risk factors with white-matter and cortical abnormalities. Awad et al. [1] previously indicated a positive correlation between the prevalence/severity of white-matter lesions and the presence of hypertension, as well as a history of previous brain ischemia. Our results show a trend toward a stronger correlation between SCLs and the Hachinski ischemic score than between PVLs and the ischemic score, suggesting that SCLs may be a more reliable indicator of cerebrovascular disease.

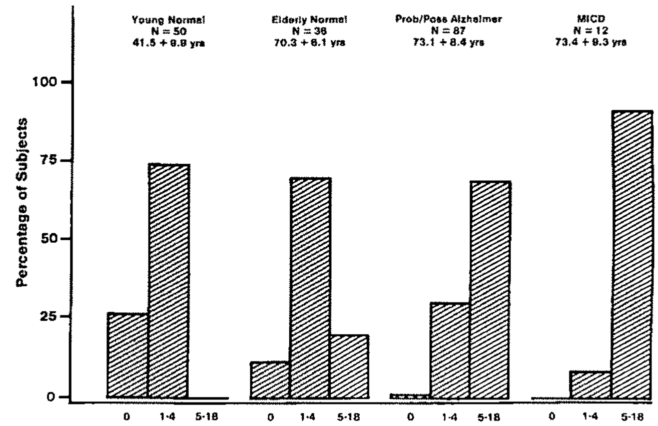

Fig. 3.—Scores of periventricular white-matter lesions for different subject groups. Ranges of scores illustrate major differences between groups.

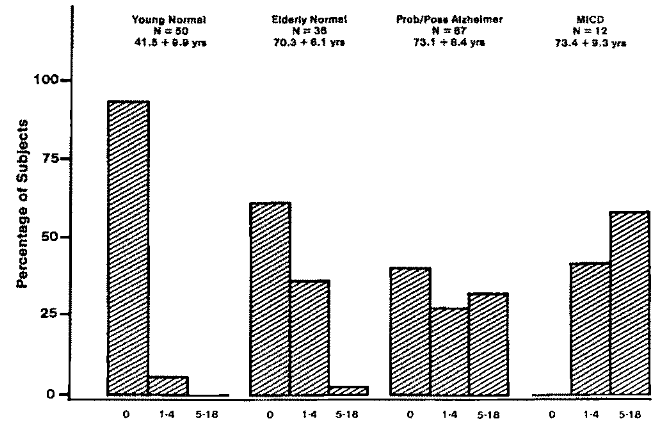

Fig. 4.—Scores of subcortical white-matter lesions for different subject groups. Ranges of scores illustrate major differences between groups.

We next compared MR results in those patients with a clinical diagnosis of possible/probable AD to those with a diagnosis of MICD (Table 4). The mean PVL score for the MICD group was 1.6 times greater than that for the AD group, and 3.5 times greater than that for elderly controls. The mean SCL score for the MICD group was 2.6 times greater than that for the AD group and 13.5 times greater than that for the elderly controls. While both PVL and SCL scores were higher in MICD than in AD, the SCL score better differentiated between MICD (primary vascular dementia) and AD (primary degenerative dementia). Thus, an MR scan showing bilateral subcortical nodular or confluent areas of prolonged T2 relaxation time in the centrum semiovale and corona radiata tends to favor a clinical diagnosis of vascular dementia over AD.

In pathologic studies of nondemented individuals, Awad et al. [21] found MR-detected, incidental white-matter lesions to

TABLE 4: Mean Scores of MR Lesions in Normal and Memory Disorder Subjects

Subject Classification	No. of Patients	Age (years)	Hachinski Score	Lesion Score	
				Periventricular	Subcortical
Clinical severity group					
Elderly normal	36	70.3[a] ± 6.1	–	3.4[a] ± 2.6	0.8[a] ± 1.2
Nondemented memory disorder	22	70.3[a,b] ± 10.7	3.5 ± 3.3	8.2[b] ± 5.0	6.5[b] ± 9.7
Demented memory disorder	91	73.8[b] ± 8.2	2.9 ± 2.9	7.9[b] ± 5.0	4.7[b] ± 7.2
ANOVA *p* value		.04	.45	.0001	.0009
Clinical diagnostic group					
Elderly normal	36	70.3 ± 6.1	–	3.4[x] ± 2.6	0.8[x] ± 1.2
Probable/possible Alzheimer dementia	87	73.1 ± 8.4	1.7 ± 1.3	7.6[y] ± 4.8	4.1[y] ± 6.4
Mixed disorder	14	72.5 ± 11.2	5.4 ± 0.5	6.8[y] ± 4.6	6.0[y,z] ± 9.4
Multiinfarct cognitive disorder	12	73.4 ± 9.3	9.9 ± 2.2	12.0[z] ± 4.6	10.8[z] ± 12.2
ANOVA *p* value		.38	.0001	.0001	.0001

Note.—Lesions were assessed on a scale of 0–3, with 0 reflecting no lesions and 3 being the most severe. Lesions were given separate grades for the anterior, central, and posterior regions of each hemisphere.

[a–c] For the clinical severity groups, mean scores with different superscripts a–c in each column are significantly different (Kruskal-Wallis analysis of variance [ANOVA] procedure [$p < .05$] and post hoc Mann-Whitney U test [$p < .05$]).

[x–z] For the clinical diagnostic groups, mean scores with different superscripts x–z in each column are significantly different (Kruskal-Wallis ANOVA procedures [$p < .05$] and post hoc Mann-Whitney U test [$p < .05$]).

be associated with arteriosclerosis, vascular ectasia, and dilated perivascular spaces (état criblé). According to Braffman et al. [22, 23] and others [24], however, dilated perivascular spaces such as those identified by Awad et al. are isointense relative to CSF, and thus not hyperintense compared with surrounding brain parenchyma on short TE images. The results of Braffman et al. indicate that in elderly patients the majority of lesions that are hyperintense on both short and long TE images represent subtle changes of gliosis and demyelination, possibly due to chronic vascular insufficiency [25] and/or frank infarction [26] in regions supplied by the medullary arteries of the hemispheres. In a pathoanatomic study without MR correlation, Brun and Englund [27] found that most of the 23 patients with multiinfarct dementia showed cerebral hypertensive angiopathy, and the white matter had multiple asymmetrically distributed, complete infarctions surrounded by a transitional zone of reactive gliosis and loss of tissue components. Thus, patients with diffuse cerebrovascular disease, at risk for multiinfarct dementia, would be expected to have prominent MR abnormalities in the periventricular watershed zone [18, 19, 28] and in the subcortical white matter. This would be consistent with the MR findings of our study.

The severity of MR-detected white-matter lesions seen in patients with a clinical diagnosis of possible/probable AD was intermediate between the findings in elderly normals and those of MICD patients (Figs. 3 and 4). Therefore, the MR abnormalities associated with primary degenerative disease and with vascular dementia may be different only on quantitative grounds.

Pathologically, changes in the deep white matter in elderly patients with AD have been characterized by symmetrically distributed, partial loss of myelin, axons, and oligodendroglial cells, with mild reactive gliosis and hyaline fibrosis of arterioles and capillaries, yet without complete infarctions and without hypertensive angiopathy [27, 29]. George et al. [20] described white-matter changes as typical pathologically of subcortical vascular disease. Rezek et al. [29] found the periventricular changes in AD patients indistinguishable from those occurring in normal elderly individuals, yet increased in prevalence and extent. Brun and Englund [27] and George et al. [20] also found white-matter changes to be quantitatively increased in AD.

A pathogenetic basis for the increase in deep white-matter changes in AD is uncertain, and some investigators argue that white-matter changes are incidental [1, 20, 21]. Brun and Englund [27] considered the possiblity of wallerian degeneration, secondary to the cortical gray-matter disease occurring in AD, to be unlikely because the severity of white-matter changes did not correlate with the regional or global severity of the cortical disease. Instead, regional cerebral hypoperfusion, secondary to cardiovascular dysfunction and systemic hypotension, in a brain with small-vessel disease was favored as the cause of the deep white-matter changes in AD. In other pathologic studies, vasculopathies associated with AD have been reported, including amyloid angiopathy [30] and, more recently, a denervation microangiopathy [31]. Regardless of origin, if the pathologic white-matter changes in AD cause only an exacerbation of the normal aging process, then MR would show signal abnormalities most prominent in the periventricular (watershed) zone and relatively less prominent in the subcortical white matter. The severity of white-matter abnormalities in a 60-year-old patient with AD would thus be expected to be similar to those of a normal 90-year-old individual.

In this study we were unable to show a high degree of specificity of MR findings for any subject group with memory disorder or dementia. In part, this may have been due to inaccuracies in clinical diagnoses. Nevertheless, the significant differences observed in the mean scores of white-matter lesions in different clinical groups can provide supportive data for a suspected clinical diagnosis. Alternatively, when the expected severity of MR signal abnormalities for a particular clinical diagnosis is not found, other diagnoses should be entertained.

ACKNOWLEDGMENTS

We thank Mary Ellen Bentham for MR technical assistance, Alice Kashuba for typing and preparing the manuscript, and M. J. D. Post for advice and criticism.

REFERENCES

1. Awad IA, Spetzler RF, Hodak JA, Awad CA, Carey R. Incidental subcortical lesions identified on magnetic resonance imaging in the elderly. I. Correlation with age and cerebrovascular risk factors. *Stroke* **1986**;17:1084–1089
2. Gerard G, Weisberg LA. MR periventricular lesions in adults. *Neurology* **1986**;36:998–1001
3. Bradley WG, Waluch V, Brant-Zawadzki M, Yadley RA, Wycoff RR. Patchy periventricular white matter lesions in the elderly: common observation during NMR imaging. *Noninvas Med Imaging* **1984**;1:35–41
4. Brant-Zawadzki M, Fein G, Van Dyke C, Kiernan R, Davenport L, de Groot J. MR imaging of the aging brain: patchy white-matter lesions and dementia. *AJNR* **1985**;6:675–682
5. Erkinjuntii T, Ketonen L, Sulkava R, Sipponen I, Vuorialho M, Ivanainen M. Do white matter changes on MR and CT differentiate vascular dementia from Alzheimer's disease? *J Neurol Neurosurg Psychiatry* **1987**;50:37–42
6. Aharon-Peretz J, Cummings JL, Hill MA. Vascular dementia and dementia of the Alzheimer type. *Arch Neurol* **1988**;45:719–721
7. American Psychiatric Association. *Diagnostic and statistical manual of mental disorders*, 3d ed. Washington, DC: American Psychiatric Assoc., **1980**
8. Hachinski VC, Zilhka E, DuBoulay GH, McAllister VL, Marshall J, Russell RWR, Symon L. Cerebral blood flow in dementia. *Arch Neurol* **1975**;32:632–637
9. Loewenstein DA, Barker WW, Chang JY, et al. Predominant left hemisphere metabolic dysfunction in dementia. *Arch Neurol* **1989**;46:146–152
10. Hachinski VC, Lassen NA, Marshall J. Multi-infarct dementia: a cause of mental deterioration in the elderly. *Lancet* **1974**;2:207–209
11. Folstein MF, Folstein SE, McHugh PR. Mini-mental State. *J Psychiatr Res* **1975**;12:189–198
12. Kinkel WR, Jacobs L, Polachini I, Bates V, Heffner RR Jr. Subcortical arteriosclerotic encephalopathy (Binswanger's disease). *Arch Neurol* **1985**;42:951–959
13. Sze G, De Armond SJ, Brant-Zawadzki M, Davis RL, Norman D, Newton TH. Foci of MRI signal (pseudo lesions) anterior to the frontal horns: histologic correlations of a normal finding. *AJNR* **1986**;7:381–387, *AJR* **1986**;147:331–337
14. Wade JPH, Mirsen TR, Hachinski VC, Fisman M, Lau C, Merskey H. The clinical diagnosis of Alzheimer's disease. *Arch Neurol* **1987**;44:24–29
15. Molsa PK, Paljarvi L, Rinne JO, Rinne UK, Sako E. Validity of clinical diagnosis in dementia: a prospective clinicopathological study. *J Neurol Neurosurg Psychiatry* **1985**;48:1085–1090
16. Fazekas F, Chawluk JB, Alvai A, Hurtig HI, Zimmerman RA. MR signal abnormalities at 1.5 T in Alzheimer's dementia and normal aging. *AJNR* **1987**;8:421–426
17. Dooling EC, Chi JG, Gilles FH. Developmental changes in ventricular epithelia. In: Gilles FH, Leviton A, Dooling EC, eds. *The developing human brain: growth and epidemiologic neuropathology*. Boston: John Wright, **1983**:113–116
18. Vander Bergh R. Centrifugal elements in the vascular pattern of the deep intracerebral blood supply. *Angiology* **1969**;20:88–94
19. DeReuck JL. The human periventricular arterial blood supply and the anatomy of cerebral infarction. *Eur Neurol* **1971**;5:321–334
20. George AE, deLeon MJ, Gentes CI, et al. Leukoencephalopathy in normal and pathologic aging: 1. CT of brain lucencies. *AJNR* **1986**;7:561–568
21. Awad IA, Johnson PC, Spetzler RF, Hodak JA. Incidental subcortical lesions identified on magnetic resonance imaging in the elderly. II. Postmortem pathological correlations. *Stroke* **1986**;17:1090–1097
22. Braffman BH, Zimmerman RA, Trojanowski JQ, Gonatas NK, Hickey WF, Schlaepfer WW. Brain MR: pathologic correlation with gross and histopathology. 1. Lacunar infarction and Virchow-Robin spaces. *AJNR* **1988**;9:621–628, *AJR* **1988**;151:551–558
23. Braffman BH, Zimmerman RA, Trojanowski JQ, Gonatas NK, Hickey WF, Schlaepfer WW. Brain MR: pathologic correlation with gross and histopathology. 2. Hyperintense white-matter foci in the elderly. *AJNR* **1988**;9:629–636, *AJR* **1988**;151:559–566
24. Jungreis CA, Kanal E, Hirsch WL, Marinez AJ, Moossy J. Normal periventricular spaces mimicking lacunar infarction: MR imaging. *Radiology* **1988**;169:101–104
25. Kirkpatrick JB, Hayman LA. White matter lesions in MR imaging of clinically healthy brains of elderly subjects: possible pathological basis. *Radiology* **1987**;162:509–511
26. Marshall VG, Bradley WG Jr, Marshall CE, Bhoopat T, Rhodes RH. Deep white matter infarction: correlation of MR and histopathological findings. *Radiology* **1988**;167:517–522
27. Brun A, Englund E. A white matter disorder in dementia of the Alzheimer type: a pathoanatomical study. *Ann Neurol* **1986**;19:253–262
28. Roman GC. Senile dementia of the Binswanger type: a vascular form of dementia in the elderly. *JAMA* **1987**;258:1782–1788
29. Rezek DL, Morris JC, Fulling KH, Gado MH. Periventricular white lucencies in senile dementia of the Alzheimer type and in normal aging. *Neurology* **1987**;37:1365–1368
30. Mandybur TI. The incidence of cerebral amyloid angiopathy in Alzheimer's disease. *Neurology* **1975**;25:120–126
31. Scheibel AS, Duong T, Tomiyasu U. Denervation angiopathy in senile dementia, Alzheimer type. *Alzheimer's Dis Associated Disorders* **1987**;1:19–37

Posttraumatic Cerebral Infarction Diagnosed by CT: Prevalence, Origin, and Outcome

[redacted]

Stuart E. Mirvis[1]
Aizik L. Wolf[2]
Yuji Numaguchi[1]
Gregory Corradino[2]
John N. Joslyn[1]

Posttraumatic cerebral infarction is a recognized complication of craniocerebral trauma, but its frequency, cause, and influence on mortality are not well defined. To ascertain this information, all cranial CT studies demonstrating posttraumatic cerebral infarction and performed during a 40-month period at our trauma center were reviewed. Posttraumatic cerebral infarction was diagnosed by CT within 24 hr of admission (10 patients) and up to 14 days after admission (mean, 3 days) in 25 (1.9%) of 1332 patients who required cranial CT for trauma during the period. Infarcts, in well-defined arterial distributions, were diagnosed either uni- or bilaterally in the posterior cerebral (17), proximal and/or distal anterior cerebral (11), middle cerebral (11), lenticulostriate/thalamoperforating (nine), anterior choroidal (three), and/or vertebrobasilar (two) territories in 23 patients. Two other patients displayed atypical infarction patterns with sharply marginated cortical and subcortical low densities crossing typical vascular territories. CT findings suggested direct vascular compression due to mass effects from edema, contusion, and intra- or extraaxial hematoma as the cause of infarction in 24 patients; there was postmortem verification in five. In one patient, a skull-base fracture crossing the precavernous carotid canal led to occlusion of the internal carotid artery and ipsilateral cerebral infarction.

Mortality in craniocerebral trauma with complicating posttraumatic cerebral infarction, 68% in this series, did not differ significantly from that in craniocerebral trauma patients without posttraumatic cerebral infarction when matched for admission Glasgow Coma Score results. Thus, aggressive management should be considered even in the presence of posttraumatic cerebral infarction.

***AJNR* 11:355–360, March/April 1990; *AJR* 154:1293–1298, June 1990**

Posttraumatic cerebral infarction (PTCI) is a known complication of craniocerebral trauma. A variety of mechanisms may account for this complication, including cerebral vasospasm, vascular compression, or attenuation due to adjacent mass effects producing cerebral displacement/herniation, direct vascular injury, embolization, and systemic hypoperfusion [1–13]. Infarction of the occipital pole following compression of the posterior cerebral artery (PCA) by the herniating medial temporal lobe is perhaps the most well-recognized mechanism leading to PTCI [1, 3]. The precise frequency with which cerebral infarction complicates craniocerebral trauma and its influence on mortality are not well established.

In order to ascertain this information, we retrospectively reviewed imaging studies and clinical histories of all patients with CT evidence of PTCI admitted to the University of Maryland Shock-Trauma Center during a 40-month period. The site(s) of infarction and probable etiology (based on CT, angiographic, and postmortem observations) and influence on patient mortality were evaluated.

Materials and Methods

From August 1985 through December 1988, 1332 patients were admitted to the Shock-Trauma Center of the University of Maryland Hospital with significant craniocerebral trauma.

Received June 10, 1989; revision requested August 2, 1989; revision received September 22, 1989; accepted September 25, 1989.

Presented at the annual meetings of the American Society of Neuroradiology, Orlando, FL, March 1989, and the American Roentgen Ray Society, New Orleans, May 1989.

[1] Department of Diagnostic Radiology, University of Maryland Hospital and Maryland Institute for Emergency Medical Services Systems, 22 S. Greene St., Baltimore, MD 21201. Address reprint requests to S. E. Mirvis.

[2] Department of Surgery, Division of Neurosurgery, University of Maryland Hospital and Maryland Institute for Emergency Medical Services Systems, Baltimore, MD 21201.

0361-803X/90/1546-1293
© American Roentgen Ray Society

Indications for cranial CT included a Glasgow Coma Score (GCS) less than 15, clinical evidence of a calvarial fracture, a history of loss of consciousness following trauma, foreign body localization, and postsurgical assessment. All study patients underwent at least one cranial CT study during admission or had cranial CT performed at an outside institution before transfer to our center. A computer data base of CT records was searched for all trauma patients diagnosed with cerebral infarction during this period. All CT scans, cerebral angiograms, medical records, and autopsy reports of these patients were reviewed. A CT diagnosis of PTCI was made when distinctly marginated area(s) of low attenuation in a known arterial territory was identified on unenhanced CT scans (23 patients) and persisted on all follow-up CT scans or when sharply marginated cortical and subcortical low densities crossed arterial territories (two patients). Patients with CT evidence of diffuse cerebral infarction due to hypoperfusion (with nontraumatic causes of infarction such as a spontaneous cerebrovascular accident) or with a history of CT findings indicating infarction as possible surgical or angiographic complications were not included in the study.

The 25 patients comprised 18 males and seven females 8–91 years old (mean, 38.1) who met the criteria for PTCI. Mechanisms of injury included motor vehicle collision (11), fall (six), pedestrian–motor vehicle impact (four), blunt assault (three), and gunshot wounds (one). All initial cranial CT scans were obtained without IV contrast material using a GE 9800 scanner (Milwaukee) or a Siemens DRH scanner (Iselin, NJ) unless performed at a referring institution. A selective cerebral angiogram was obtained in one patient to document evidence of vascular injury suggested by CT findings.

All cranial CT scans and the cerebral angiographic study were reviewed by two staff neuroradiologists and the staff trauma radiologist; interpretation was recorded by consensus. Information recorded included admission CT findings, site(s) of cerebral infarction on initial or follow-up CT scans, time to recognition of cerebral infarction by CT from the date of admission, and probable mechanism of infarction based on CT and cerebral angiographic findings. Medical chart review was conducted by two neurosurgeons to ascertain admission neurologic status as reflected by the GCS, history of surgical intervention following initial CT, and patient outcome. In addition, the mortality for *all* cranial trauma patients admitted during the period of review was obtained for two groups of patients based on an admission GCS of ≤5 or a GCS of >5 and ≤10. The results of postmortem examinations of the fixed and sectioned brain, performed in five patients, were reviewed.

Results

Sites of Infarction

Sites of cerebral infarction (Table 1) included the uni- or bilateral PCA distribution in 17 patients (Figs. 1–3), uni- or bilateral proximal and/or distal anterior cerebral artery (ACA) distributions in 11 (Figs. 1 and 2), and unilateral or bilateral middle cerebral artery (MCA) distributions in 11 patients. Among patients with ACA territory infarction, we observed five patients with unilateral and four patients with bilateral proximal ACA infarction. Eight of these patients had concurrent unilateral (six) or bilateral (two) distal ACA infarctions. In five of the 11 patients with MCA territory infarcts, concurrent infarction involving anterior cerebral and lenticulostriate distributions suggested proximal occlusion of the ipsilateral internal carotid artery. Lenticulostriate/thalamoperforating territory infarcts were diagnosed in nine patients (eight unilateral) (Fig. 1).

TABLE 1: Distribution of Posttraumatic Cerebral Infarction in 25 Patients

Vascular Territory	No.
Posterior cerebral artery	
Unilateral	12
Bilateral	5[a]
Middle cerebral artery	
Unilateral	9[b]
Bilateral	2[c]
Proximal anterior cerebral artery	
Unilateral	5
Bilateral	4
Distal anterior cerebral artery	
Unilateral	6
Bilateral	2
Lenticulostriate/thalamoperforating vascular territory	
Unilateral	8
Bilateral	1
Anterior choroidal artery vascular territory (unilateral)	3
Cortical compression	2
Basilar	2

[a] One with partial sparing of vascular territory.
[b] Two with partial sparing of vascular territory.
[c] Both with partial sparing of vascular territory.

Other areas of infarction included uni- or bilateral anterior choroidal (three) (Figs. 1 and 4) and vertebrobasilar (two) (Fig. 1) territories. In two patients, persistent cortical and subcortical uniform bands of low attenuation crossing vascular territories were compatible with infarction (Fig. 5).

Proposed Mechanism of Infarction

CT findings in 24 patients suggested that cerebral infarction was a result of focal mass effects and/or gross mechanical displacement of the brain producing transfalcine and/or transtentorial herniation (Figs. 1, 2, 4, 5). Large extraaxial hematomas with ipsilateral cerebral edema producing moderate to marked midline cerebral shift were the predominant injuries diagnosed by initial cranial CT in 17 patients. Fifteen of these 17 patients had cerebral infarctions in typical vascular distributions. Postmortem studies in three of these 15 patients confirmed the distribution of cerebral infarction(s) and demonstrated unilateral (one) or bilateral (one) medial temporal herniation. The other patient (Fig. 1) displayed left-to-right midline shift due to an epidural hematoma with left medial temporal and cingulate gyrus herniation. Infarction in this patient included the bilateral proximal and left distal ACA distribution among others.

Two of these 17 patients had cortical and subcortical bands of low density crossing arterial distributions following surgical decompression of large overlying subdural hematomas. Postmortem examination of the brain in one of these patients (Fig. 5) revealed cortical infarction in the frontoparietooccipital region adjacent to an ipsilateral overlying subdural hematoma. There was no evidence of cortical venous or dural sinus thrombosis.

Seven patients displayed multifocal cerebral contusions without significant midline shift, but with compression of basal cisterns compatible with downward transtentorial herniation.

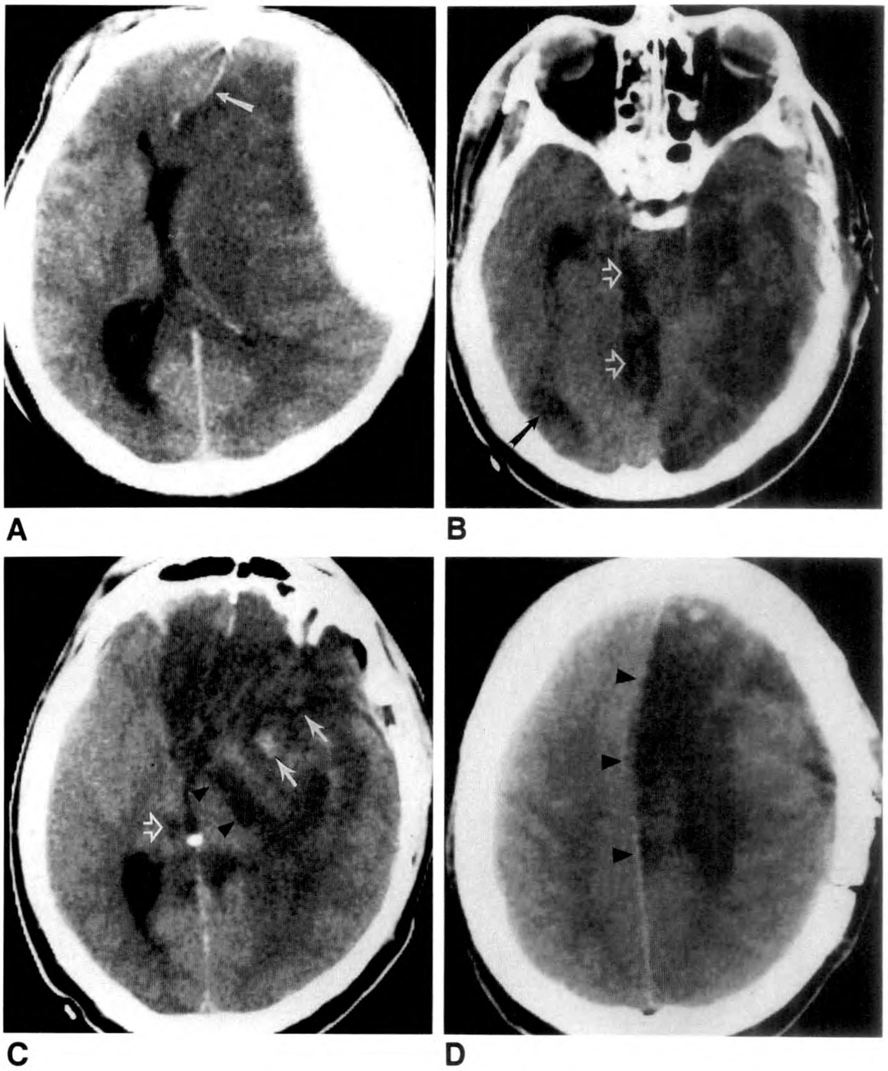

Fig. 1.—Multifocal cerebral infarction related to epidural hematoma.

***A,* Axial CT image on admission in 36-year-old man after assault. Large, hyperdense epidural hematoma produces marked shift of lateral ventricles. Note bowing of anterior falx (*arrow*).**

***B,* Postsurgical CT scan after evacuation of epidural hematoma reveals well-marginated low density in distribution of left posterior artery and focal low density in distribution of right posterior cerebral artery (*solid arrow*) suggestive of infarction. Low-attenuation area in superior vermis and right lateral rostral brainstem (*open arrows*) suggests infarction also. Low density in left anterior temporal lobe could result from contusion or medial temporal infarction.**

***C,* More rostral CT section reveals well-defined low density in distribution of left anterior choroidal artery (*arrowheads*) and bilateral decreased density involving proximal anterior cerebral distributions, suggesting infarction. Most of distribution of left middle cerebral artery appears spared, but hemorrhagic contusion or infarction involves anterior left temporal lobe (*solid arrows*). Focal low density in right thalamus (*open arrow*) may represent infarct.**

***D,* More rostral CT section reveals mixed anterior focal hemorrhage and low density along distribution of distal left anterior cerebral artery (*arrowheads*). Hemorrhagic component suggests either venous outflow obstruction or delayed reperfusion of infarcted tissue.**

Postmortem examination of fixed, sectioned brain confirmed subfalcine and bilateral medial temporal herniation and verified distribution of infarcts.

Postmortem examination of the brain in one of these patients confirmed the distribution of infarction diagnosed by CT and revealed bilateral medial temporal and cerebellar tonsillar herniation.

CT in one patient with posterior MCA and PCA infarction revealed a skull-base fracture traversing the ipsilateral precavernous carotid canal. Subsequent angiography revealed total occlusion of the ipsilateral internal carotid artery and a cavernous-carotid fistula (Fig. 3).

Mortality of Patients with PTCI vs General Trauma Admissions

Mortality in neurotrauma patients with complicating PTCI was compared with that in the general trauma population admitted during the same period without PTCI (Table 2). For 17 patients with PTCI admitted with a GCS of 5 or less, mortality was 76.5% compared with 64.3% for cranial trauma patients without PTCI admitted with a GCS of 5 or less ($p = .44$). Mortality was 33.3% for six patients with PTCI admitted with a GCS >5 and ≤10 compared with 17.2% for cranial trauma victims without PTCI admitted with the same GCS range ($p = .28$). The likelihood of mortality among the cranial trauma population with complicating PTCI was 1.96 times that of cranial trauma patients without PTCI when matched for admission GCS; the 95% confidence limit interval was 0.78–5.13 [14]. Thus, a statistically significant increase in mortality for patients with PTCI complicating craniocerebral trauma could not be demonstrated over that of craniocerebral trauma victims without this complication when matched for admission GCS.

Discussion

A variety of mechanisms are postulated to account for the development of posttrauamtic cerebral infarction [1–13]. In our series of 25 patients, CT findings either preceding or concurrent with evidence of cerebral infarction suggest that gross mechanical shift of the brain and herniation across the falx and/or tentorium accounted for infarction in 22 patients.

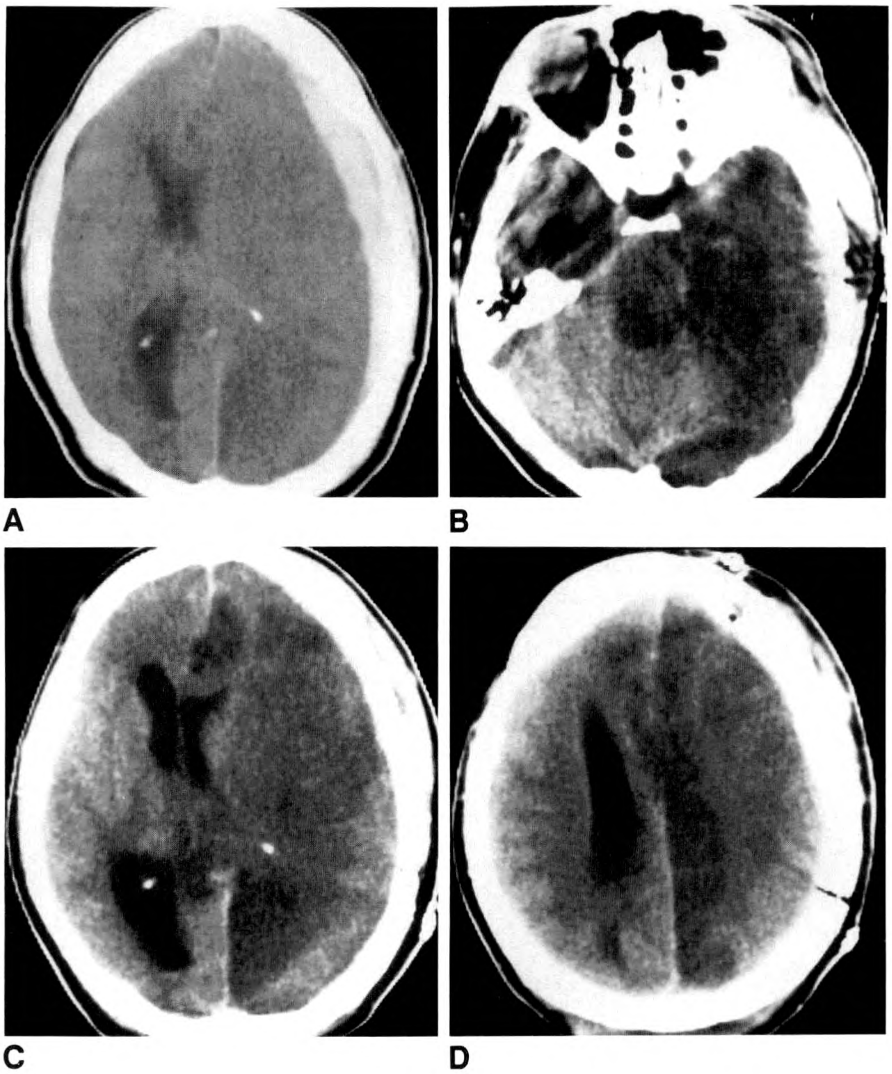

Fig. 2.—Cerebral infarction secondary to mass effect of subdural hematoma.

A, Axial CT scan in 45-year-old woman after a fall reveals large left convexity subdural hematoma producing marked left-to-right midline shift. Note complete effacement of left occipital horn. Low density is already observed in left posterior cerebral artery and focally in territory of right posterior cerebral artery.

B, CT scan 4 days after surgical evacuation reveals well-defined low density in brainstem and medial left anterior temporal lobe.

C, More rostral CT section. Low density in left anterior cerebral, left posterior cerebral, and anterior middle cerebral distributions was believed to represent infarction.

D, More rostral CT section reveals decreased attentuation involving left anterior and portion of left middle cerebral artery territory. Band of low density also involves distal right anterior cerebral distribution.

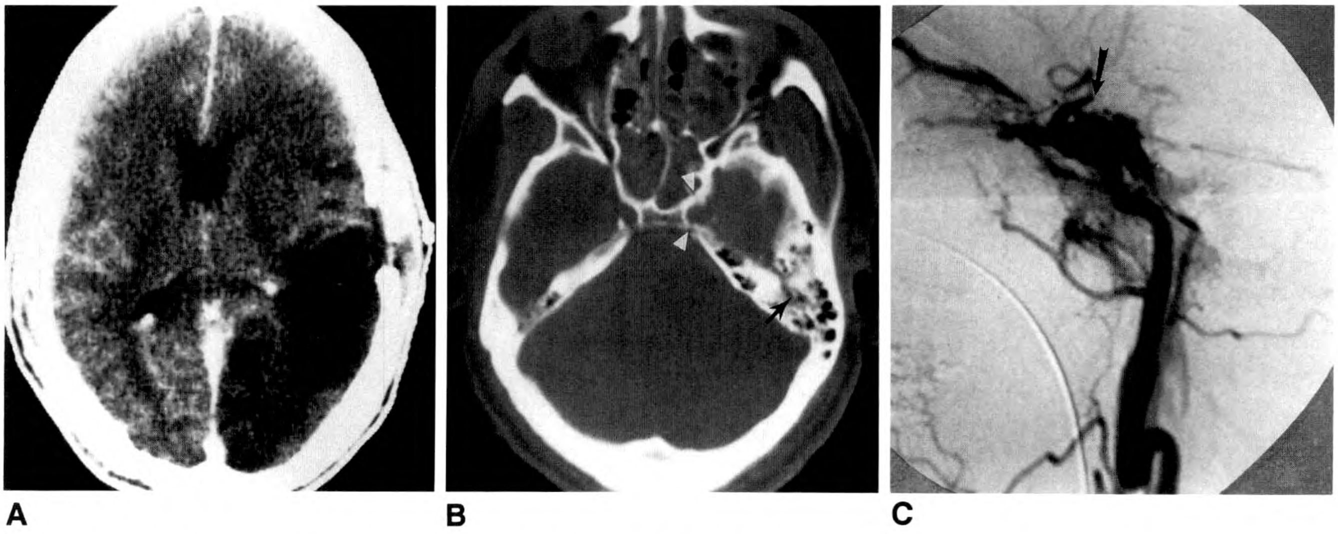

Fig. 3.—Traumatic occlusion of left internal carotid artery secondary to skull-base fracture.

A, Axial CT image in 25-year-old man after motor vehicle accident reveals wedge-shaped low density in region of left posterior cerebral and posterior left middle cerebral artery distributions. Surgical intervention in left parietal region was used for elevation of depressed fracture.

B, Axial CT scan through skull base at bone windows reveals longitudinal left mastoid fracture (*arrow*) and fracture crossing precavernous carotid canal (*arrowheads*).

C, Left internal carotid angiogram reveals complete occlusion of supraclinoid carotid artery (*arrow*) with carotid-cavernous fistula. Traumatic left internal carotid occlusion led to ipsilateral infarction.

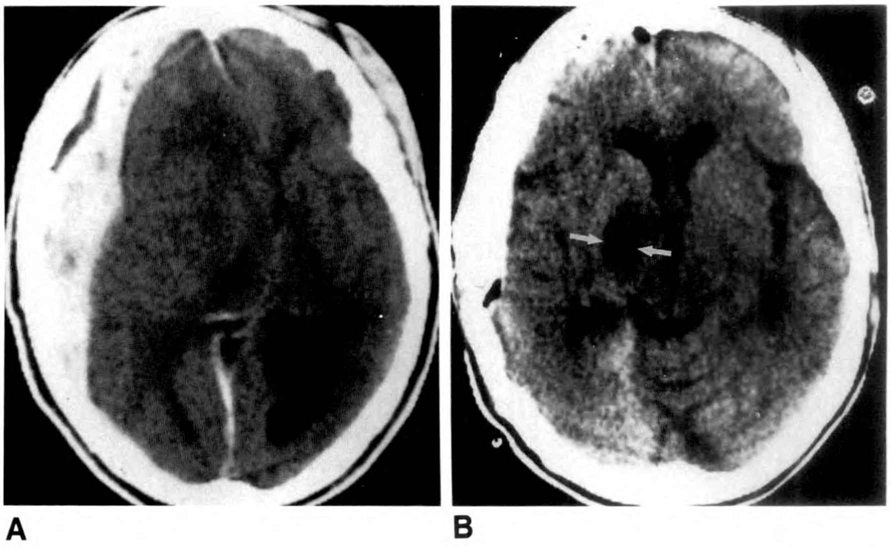

Fig. 4.—Anterior choroidal infarction due to mass effect of subdural hematoma.

A, Admission axial CT scan in 91-year-old woman after a fall reveals large right convexity subdural hematoma with marked midline shift. Left occipital horn appears trapped by mass effect.

B, CT scan after surgical evacuation of hematoma. Well-defined low density involving posterior limb of internal capsule (*arrows*) in right anterior choroidal artery distribution was believed to represent infarction.

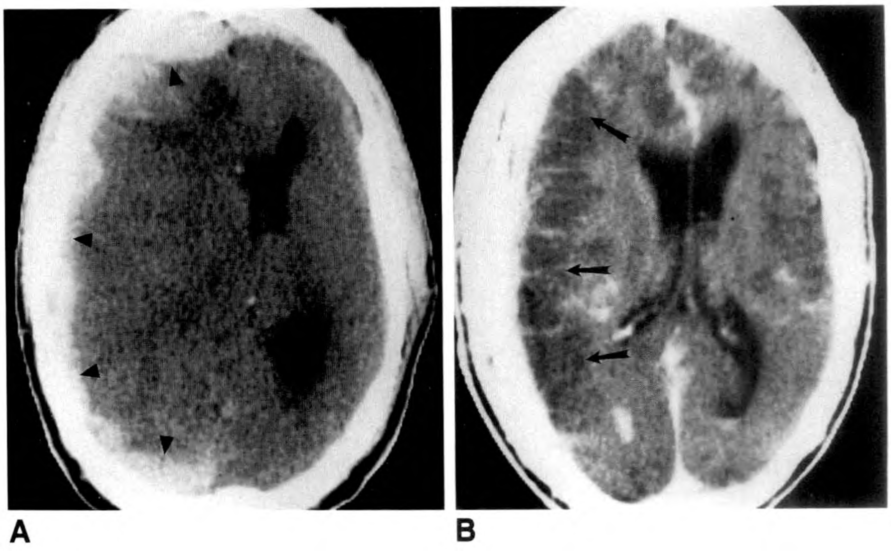

Fig. 5.—Cortical/subcortical posttraumatic infarction.

A, Axial nonenhanced CT image at midventricular level indicates diffuse right convexity subdural hematoma (*arrowheads*) and cortical hemorrhagic contusion with marked midline shift.

B, Axial CT image on postoperative day 6. Diffuse cortical and subcortical low density (*arrows*) over right frontoparietal region was believed to represent infarction related to direct pressure effects from overlying hematoma diminishing peripheral artery perfusion.

Postmortem examination of fixed and sectioned brain confirmed acute infarction of right frontotemporoparietal cortex at both gross and microscopic levels. No evidence was noted of cortical or dural sinus thrombosis.

TABLE 2: Mortality in Patients with Posttraumatic Cerebral Infarction (PTCI) vs Cranial Trauma Admissions Without Complicating Infarction by Admission Glasgow Coma Scale in 25 Patients

Glasgow Coma Scale	% Mortality (No. of Patients)		Exact Test (p)[a]
	With PTCI	All Trauma Patients	
≤5	76.5 (17)	64.3 (639)	.44
>5 and ≤10	33.3 (6)	17.2 (721)	.28
>10	50.0 (2)	2.7 (7946)	Not performed

[a] $p = .24$ for combined data for all groups using statistical guidelines of Mantel and Haenszel [14].

Infarctions due to mechanical shift were seen predominantly in the posterior and anterior cerebral vascular distributions. It is postulated [1, 3] that the PCA is compressed against the rigid edge of the tentorium by the herniating mass of the medial temporal lobe producing posterior cerebral infarction. Sato et al. [1] described the development of posterior cerebral infarction in nine (9%) of 100 patients with CT evidence of transtentorial herniation. The infarct size and location may vary depending on the precise point of compression of the PCA and the size of the tentorial aperture [1].

A recent report [2] describes the less well recognized development of infarction in the distal ACA distribution in three patients. The authors postulate that branches of the ipsilateral callosomarginal artery may be kinked against the free edge of the falx as the medial aspect of the hemisphere herniates across the midline. The precise extent of infarction would again vary depending on how anteriorly transfalcine herniation developed [2]. Infarction in the proximal distribution of the ACA was observed in nine of our patients, including four with bilateral proximal ACA infarction. Mechanical displacement of the anterior frontal lobe may produce stretching or attenuation of proximal ACA branches leading to infarction, or conversely, downward compression of the proximal ACA or its proximal branches against the posterior ridge of the body and lesser wing of the sphenoid may lead to infarction in both the proximal and distal anterior cerebral territories. In one of our patients with bilateral ACA infarction, cingulate gyrus herniation was found at postmortem examination. Distortion of cerebral vessels consequent to brain shift and internal herniation has been well documented neuropathologically [15].

Infarction was diagnosed in the MCA territory in 11 patients with either gross mass displacement and herniation or severe cerebral edema. Potential contributing factors include stretching and attenuation of the MCA, increased intracerebral pressure, direct pressure effects from overlying extraaxial hematomas [10], and vasospasm. Similarly, the mechanism of infarction confined to the distributions of the lenticulostriate and thalamoperforating vessels seen in nine of our patients is unclear. Presumably, these small perforating vessels could be stretched and attenuated by marked cerebral displacement leading to hypoperfusion of their vascular distributions.

Three patients in our series developed infarction confined to the posterior limb of the internal capsule, which is supplied by the anterior choroidal artery. The anterior choroidal artery may be compressed between the herniating medial temporal lobe and the cerebral peduncle medially [1]. All of the patients with infarction of the anterior choroidal distribution had massive shifts toward the side contralateral to the infarction.

The role of vascular spasm in producing cerebral infarction in our patients is unknown. Angiographically documented intracranial arterial vasospasm occurs in 5–57% of patients with craniocerebral trauma [8, 9]. Spasm is most prominent in the intradural portion of the distal internal carotid artery [6, 9]. Spasm may be due to direct vascular trauma or adjacent contusion and hemorrhage, or may be mediated by release of a vasoactive humoral factor [8]. MacPherson et al. [11] found that arterial spasm is most likely to produce ischemic damage to the cortex, but does not lead to ischemic damage of the deep gray nuclei or white matter. Since we did not perform arteriography in our patients with infarction arising from intracranial mass effects, we cannot determine what influence vasospasm had on producing infarction in these patients.

Two patients in our series developed bands of well-marginated low attenuation involving cortical and subcortical regions. These zones crossed known arterial vascular distributions. In both patients, overlying subdural hematomas produced significant mass effect on the adjacent cortex. Infarctions, particularly when hemorrhagic, may be due to direct compression of cortical veins. Postmortem examination in one of these two patients verified cortical infarction without evidence of cerebral venous thrombosis. Weisberg [10] has described infarction of brain underlying an epidural hematoma due to direct pressure effects, and underlying cerebral infarction has been reported in 8% of subdural hematomas. Presumably, direct pressure effects over the cerebral cortex result in diminished arterial perfusion leading to infarction peripherally.

Vascular injury, documented angiographically, was responsible for cerebral infarction in one of our patients with a skull-base fracture. Skull-base fractures that extend across the carotid canal can produce direct carotid vascular injury leading to occlusion, dissection with hypoperfusion and/or distal embolization, or pseudoaneurysm formation [12]. Such arterial injuries may present with either complete or fluctuating neurologic deficits, which are unaccounted for by findings on initial unenhanced cranial CT studies [5, 13] and suggest the need for immediate cerebral arteriography, particularly when skull-base fractures traverse the region of the carotid canal.

In summary, PTCI occurred in 1.9% of a large population of neurotrauma patients. Infarction was primarily due to gross mass effects producing transfalcine and/or transtentorial herniation and occurred in a wide variety of vascular territories. However, mortality for patients sustaining PTCI was not statistically significantly higher than that of craniocerebral trauma victims without PTCI admitted within a similar range of GCSs. This result suggests that the development of PTCI reflects severe cerebral injury already associated with a high mortality, but also suggests that aggressive management of the cerebral injury should not be abandoned despite the appearance of this complication.

REFERENCES

1. Sato M, Tanaka S, Kohama A, Fujii C. Occipital lobe infarction caused by tentorial herniation. *Neurosurgery* **1986**;18:300–305
2. Rothfus WE, Goldberg AL, Tabas JH, Deeb ZL. Callosomarginal infarction secondary to transfalcial herniation. *AJNR* **1987**;8:1073–1076
3. Keane JR. Blindness following tentorial herniation. *Ann Neurol* **1986**;8:186–190
4. Mauskop A, Wolintz AH, Valderrama R. Cerebral infarction and subdural hematoma. *J Clin Neuro Ophthalmol* **1984**;4:251–253
5. Mooney RP, Bessen HA. Delayed hemiparesis following nonpenetrating carotid artery trauma. *Am J Emerg Med* **1988**;6:341–345
6. Suwanwela C, Suwanwela N. Intracranial arterial narrowing and spasm in acute head injury. *J Neurosurg* **1972**;36:314–323
7. Marshall LF, Bruce DA, Bruno L, Langfitt TW. Vertebrobasilar spasm: a significant cause of neurologic deficit in head injury. *J Neurosurg* **1978**;48:560–564
8. Pasqualin A, Vivenza C, Licata C, Cavazzani P, De Pian R. Cerebral vasospasm after head injury. *Neurosurgery* **1984**;15:855–857
9. Wilkens RH, Odom GL. Intracranial arterial spasm associated with craniocerebral trauma. *J Neurosurg* **1970**;32:626–633
10. Weisberg LA. CT and acute head trauma. *Comput Radiol* **1979**;3:15–28
11. MacPherson P, Graham DI. Arterial spasm and slowing of the cerebral circulation in the ischaemia of head injury. *J Neurol Neurosurg Psychiatry* **1973**;36:1069–1072
12. Tsai FY, Teal JS, Heishima GB. *Neuroradiology of head trauma.* Baltimore: University Park, **1984**:221–241
13. Mears GD, Leonard RB. Blunt carotid artery trauma: a case report. *Am J Emerg Med* **1988**;6(4):281–284
14. Mantel N, Haenszel W. Statistical aspects of the analysis of data from retrospective studies of disease. *JNCI* **1959**;22:719–748
15. Graham DI, Adams JH, Doyle D. Ischemic damage in fatal non-missle head injuries. *J Neurosurg* **1978**;39:213–234

Neuroimaging of Disseminated Germ Cell Neoplasms

Vincent P. Mathews[1]
Dale R. Broome[1]
Richard R. Smith[1]
James R. Bognanno[1]
Lawrence H. Einhorn[2]
Mary K. Edwards[1]

The purpose of this study was to determine the role of neuroimaging in the management of patients with metastatic germ cell tumors. Retrospective evaluation of 299 patients treated in 1986 and 1987 for initial presentation or recurrence of testicular, retroperitoneal, and mediastinal germ cell tumors was performed to determine indications for neuroimaging, frequency and site of CNS metastases, and occurrence of other CNS abnormalities. Sixty-six patients required CNS imaging with myelography, CT, or MR. Studies were normal in 24 patients. Twenty patients had CNS metastases including 11 with intracranial metastases, eight with spine lesions, and one with both brain and spine involvement. Sixteen had cerebral or cerebellar atrophy of unclear origin and functional significance. Two patients had ventriculomegaly without symptoms of hydrocephalus. Four patients had questionable lesions that were never confirmed. None of the 25 asymptomatic patients with elevated serum tumor markers had brain metastases. Fifteen of 17 patients with focal neurologic deficits and three of six patients with seizures had CNS metastases.

CNS imaging to detect germ cell tumor metastases is most useful in the presence of neurologic deficits or seizures but is not useful in patients with unexplained elevation of serum tumor markers in the absence of neurologic deficits.

***AJNR* 11:319–324, March/April 1990; *AJR* 154:1299–1304, June 1990**

CNS involvement by disseminated germ cell neoplasms causes significant morbidity and mortality [1]. The most common of these tumors, testicular neoplasm, most frequently metastasizes to retroperitoneal and mediastinal lymph nodes, lung, and liver. CNS involvement is not uncommon; the reported prevalence was 30% in one autopsy series [2] and 15% in two large clinical reviews [3, 4]. The identification of CNS metastases is important in these patients since the therapeutic regimen will be altered by their presence. The purpose of this study was to evaluate the role of neuroimaging in the management of patients with disseminated germ cell neoplasms. The indications for neuroimaging, the frequency and site of CNS metastases, and the occurrence of other CNS abnormalities were examined.

Materials and Methods

We retrospectively evaluated 299 patients treated at our medical center for newly diagnosed or recurrent testicular, mediastinal, and retroperitoneal germ cell neoplasms from January 1, 1986, through December 31, 1987. The radiology records of these patients were reviewed to identify patients who had had neuroimaging. A complete medical chart review was then performed of 66 patients who had undergone neuroimaging with CT, MR, or myelography. The clinical indication for neuroimaging, clinical stage of disease, histologic cell type, and therapy before and after neuroradiologic evaluation were obtained from the medical records.

The patient population undergoing neuroimaging consisted of 66 males 15–51 years old (mean age, 28 years). Sites of origin included 51 testicular, nine primary mediastinal, and six primary retroperitoneal germ cell tumors. A total of 123 neuroradiologic studies were per-

Received June 20, 1989; revision requested August 8, 1989; revision received August 21, 1989; accepted August 29, 1989.

Presented at the annual meeting of the American Society of Neuroradiology, Orlando, FL, March 1989.

[1] Department of Radiology, Indiana University Medical Center, 926 W. Michigan St., Room X-64, Indianapolis, IN 46223. Address reprint requests to R. R. Smith.

[2] Department of Medicine, Indiana University Medical Center, Indianapolis, IN 46223.

0361-803X/90/1546-1299
© American Roentgen Ray Society

formed in the patient population; one to seven studies were performed for each patient. These included 95 head CT studies, two orbital CT studies, 11 spinal CT studies, four cranial MR studies, four spinal MR studies, and seven myelographic studies. Each study was reviewed independently by three radiologists with knowledge of the patient's age and clinical history. The radiologic findings were categorized on the basis of agreement between two or more of the reviewers. The data from the study were analyzed in terms of neuroimaging findings, clinical presentations, indications for neuroradiologic studies, and resultant therapy.

Results

The radiologic findings are summarized in Table 1. Twenty patients were noted to have CNS metastases including 11 with intracranial metastases, eight with spinal lesions, and one with both brain and spinal metastases. The overall rate of CNS metastases in all 299 patients was 6.7%. Seven (2.3%) of the 299 patients initially presented with CNS metastases. This group included three patients with brain metastases and four patients with spinal metastases. All had extensive metastatic involvement elsewhere, most frequently to the lungs and/or retroperitoneum. Of the 13 patients who presented later in their disease course with CNS metastases, all were in advanced stages with the exception of two patients with localized primary mediastinal disease. The sites of origin of the eight spine metastases were the testis in six patients, the mediastinum in one patient, and the retroperitoneum in one patient. Of the 11 patients with brain metastases, eight had testicular and three had mediastinal primary tumors. The patient with both brain and spine metastases had a testicular primary. At the time of diagnosis of brain metastases, all nine testicular cancer patients and two of three primary mediastinal tumor patients had prior or concomitant pulmonary metastases.

The location of the intracranial metastases was predominantly supratentorial ($n = 7$). However, a significant number were also located infratentorially ($n = 2$) or in both locations ($n = 3$). One patient who had multiple intracranial metastases also had a concomitant retinal metastasis. Multiple brain metastases were seen in five patients and hemorrhagic brain metastases were noted also in five patients. Three patients developed obstructive hydrocephalus resulting from cerebellar metastases (Fig. 1).

The nine spinal metastases were equally divided between epidural, bone, and combined involvement (Figs. 2 and 3). Epidural involvement was associated with mediastinal ($n = 2$) or retroperitoneal ($n = 3$) masses in five of six patients. One of the mediastinal masses was the primary tumor; the other four masses were due to distal nodal metastases. Four of the patients with bone invasion developed vertebral compression fractures. Involvement of a solitary vertebral level was not

TABLE 1: Neuroimaging Findings in Patients with Germ Cell Neoplasms

Finding	No. of Patients
CNS metastases	
Intracranial	
Supratentorial	7
Infratentorial	2
Both	3
Spinal	
Epidural	3
Bone	3
Epidural and bone	3
Subtotal	20[a]
Atrophy	
Focal	3[b]
Diffuse	13
Subtotal	16
Ventriculomegaly only	2
Questionable abnormality	4
Normal	24
Total	66

[a] One patient had both spinal and intracranial metastases.

[b] Includes one patient with cerebellar atrophy.

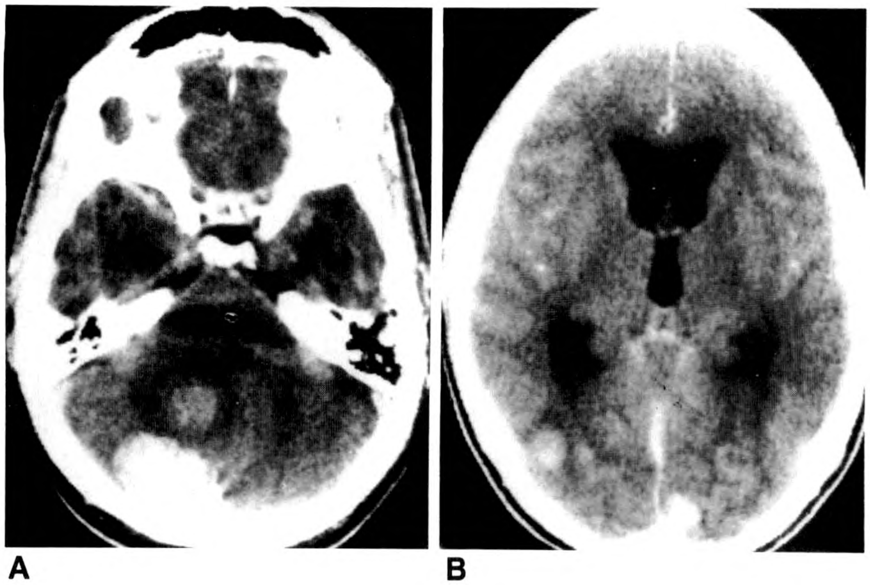

Fig. 1.—Brain metastases from testicular carcinoma in 19-year-old man.

***A*, Contrast-enhanced CT scan shows cerebellar metastases with mass effect compressing fourth ventricle.**

***B*, Image at more superior level shows multiple enhancing supratentorial metastases and obstructive hydrocephalus.**

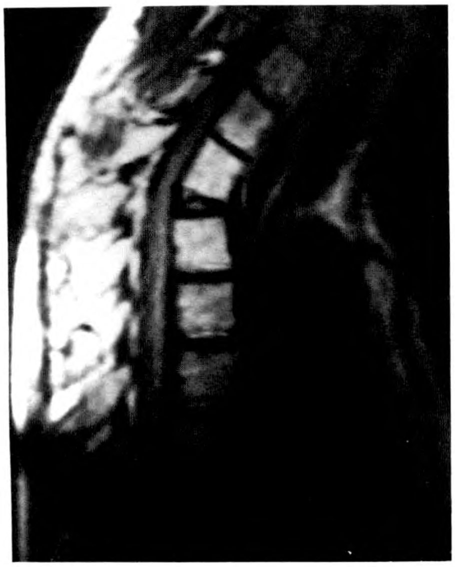

Fig. 2.—Vertebral body metastasis. Sagittal spin-echo MR image, 1500/20 (TR/TE), of thoracic spine shows compression fracture of third thoracic vertebral body due to metastasis in patient who initially presented with back pain and testicular mass.

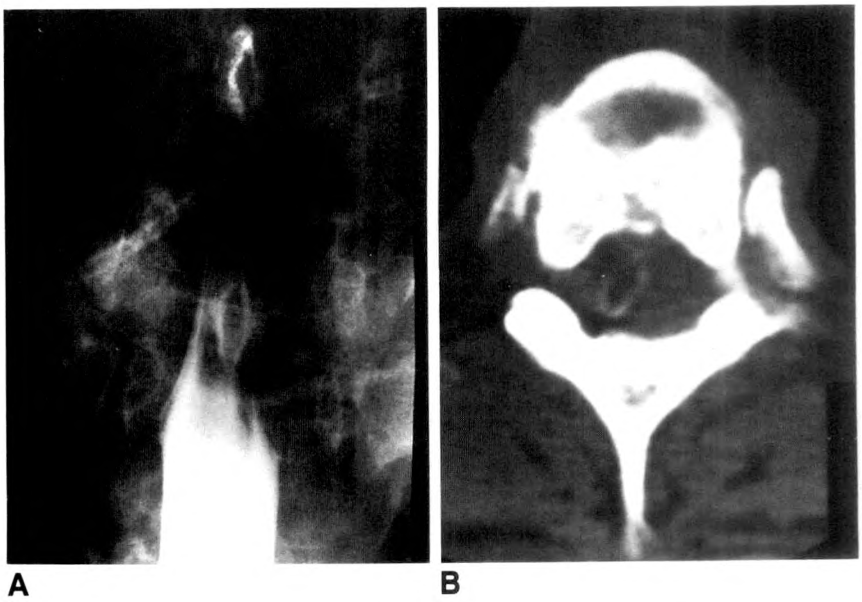

Fig. 3.—Thoracic spine metastasis in 30-year-old testicular cancer patient with lower extremity paralysis.

***A*, Thoracic myelogram shows extradural mass effect with nearly complete myelographic block.**

***B*, Postmyelogram CT scan shows metastasis to T4 vertebral body with epidural extension and spinal cord compression.**

uncommon and was noted in six of the nine patients. Five patients had evidence of cord compression on CT, MR, or myelography.

The frequencies of CNS metastases due to various types of germ cell tumors are listed in Table 2. There was a similar distribution of histologic types in patients with CNS metastases and in the total population undergoing CNS imaging. A majority of patients imaged and of patients with CNS metastases had mixed germ cell tumors.

Sixteen patients had either diffuse or focal cerebral atrophy and/or cerebellar atrophy. Mild to moderate diffuse cerebral atrophy was noted in 13 patients, as manifested by ventriculomegaly and sulcal and cisternal prominence (Fig. 4). None of these patients had prior cranial irradiation or symptoms of communicating hydrocephalus. All but two patients with diffuse atrophy had received varying amounts of systemic combination chemotherapeutic regimens composed of *cis*-platinum, bleomycin, and either etoposide or vinblastine. Focal atrophy was described as localized prominence of the sylvian fissures in two cases and as cerebellar atrophy in a third. The latter patient had no clinical signs of cerebellar dysfunction or history of alcohol abuse, phenylhydantoin therapy, or other predisposing factors. In addition, moderate ventricular enlargement was seen in two patients with normal cortical sulci and no clinical symptoms or signs of hydrocephalus (Fig. 5). Ventriculomegaly in these patients may have been due to central parenchymal loss, but hydrocephalus could not be excluded entirely.

In addition to patients with metastases and atrophy, four patients had questionable abnormalities that were never confirmed; the remaining 24 patients had normal studies.

TABLE 2: Germ Cell Tumor Histologies in Patients Requiring Neuroimaging and Patients with CNS Metastasis

Histology	No. (%)	
	Undergoing Neuroimaging	With Metastasis
Mixed germ cell tumor	39 (59.1)	12 (60)
Embryonal carcinoma	8 (12.1)	1 (5)
Choriocarcinoma	3 (4.5)	2 (10)
Yolk sac tumor	4 (6.1)	2 (10)
Seminoma	3 (4.5)	0 (0)
Malignant teratoma	1 (1.5)	0 (0)
Teratocarcinoma	1 (1.5)	0 (0)
Unknown	7 (10.6)	3 (15)
Total	66	20

The indications for neuroimaging are listed in Table 3 for patients with CNS metastases and in Table 4 for patients without CNS metastases. Focal neurologic deficits were noted in 17 patients and led to imaging, which detected metastases in 15, an unconfirmed questionable abnormality in one, and atrophy in another patient. The deficits in these latter two patients were transient and resolved within 24 hr. All patients with brain metastases had neurologic deficits. Eight patients with spinal metastases had presented with spinal pain; four of these had an associated neurologic deficit. Not listed in Table 3 is the fact that three patients with metastases had seizures in addition to their focal neurologic deficits. Overall, three of six patients with seizures had brain metastases. In 25 neurologically asymptomatic patients, head

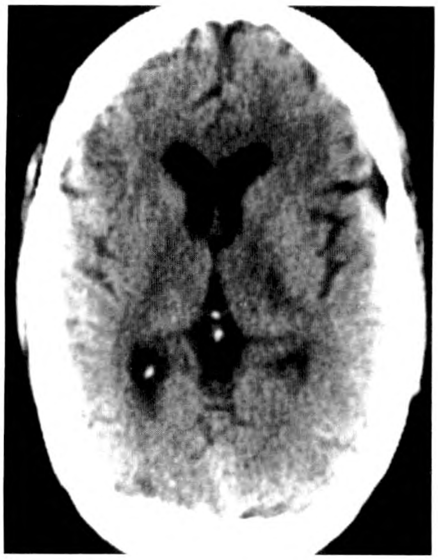

4

Fig. 4.—Cerebral atrophy. Noncontrast head CT scan in 35-year-old testicular cancer patient shows diffuse cerebral atrophy representative of that seen in our study.

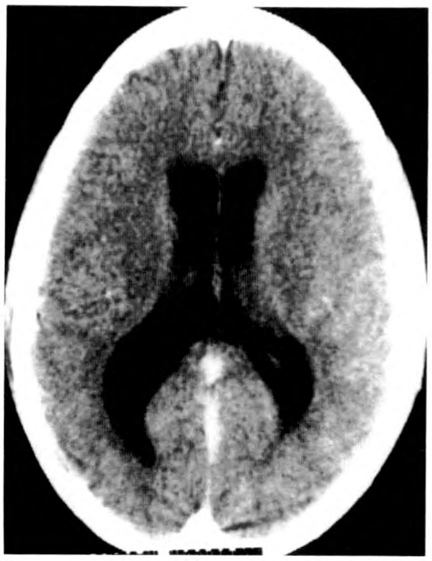

5

Fig. 5.—Ventriculomegaly. Noncontrast CT scan in 17-year-old testicular cancer patient shows ventriculomegaly without sulcal prominence. There were no signs or symptoms of hydrocephalus, possibly because of central atrophy.

TABLE 3: Clinical Presentation of Patients with CNS Metastases

Location of Metastasis	No. of Patients
Intracranial	
Focal neurologic deficit	11
Focal neurologic deficit with coma	1
Subtotal	12
Spinal	
Back/neck pain with neurologic deficit	4
Back/neck pain without neurologic deficit	4
Asymptomatic radiographic metastasis[a]	1
Subtotal	9
Total	20[b]

[a] One patient was asymptomatic for 4 months before developing pain.

[b] One patient had both intracranial and spinal metastases.

TABLE 4: Indications for CNS Imaging in 46 Patients Without CNS Metastasis and Imaging Findings

Indication	No. of Studies with These Radiographic Findings		
	Normal	Atrophy	Questionable Abnormality
Headaches without neurologic deficit	8	3	1
Mental status changes	0	3	1
Eye pain	3	0	0
Seizures	1	2	0
Syncope	0	1	0
Focal neurologic deficit			
Transient unilateral ptosis and facial nerve palsy	0	0	1
Transient unilateral reduced vision	0	1	0
Fever—rule out abscess	1	0	0
Rule out sanctuary site	15	9	1
Low back pain without neurologic deficit	1	0	0
Drug-induced dystonic reaction	1	0	0
No clear indication	2	1	0

CT scans were obtained to detect occult brain metastases or "sanctuary sites" in the setting of elevated serum tumor markers (human chorionic gonadotropin–beta subunit and alpha-fetoprotein) following chemotherapy. Brain metastases were seen in none of these.

The clinical therapy after the diagnosis of brain or spinal metastases included a variety of therapeutic protocols. Nineteen of 20 patients received subsequent systemic chemotherapy. One patient with brain metastases was lost to follow-up. Ten of 12 patients with intracranial metastases received subsequent whole-brain radiation therapy; five underwent craniotomy for resection of a solitary metastasis in addition to radiation therapy. Three patients required emergency ventricular shunting for obstructive hydrocephalus. Of the nine patients with spinal metastases, six received local spinal radiation therapy and two underwent decompressive laminectomy. In another spinal metastasis patient, spinal stabilization rods were placed surgically.

Discussion

The most common site of origin of germ cell neoplasm in our patients was the testis. This is an uncommon malignancy overall, accounting for only 1% of malignancies in males. However, testicular cancer is important since it is the most common malignancy in young adult males and may result in significant loss of productive years in this age group [5]. Approximately 75% of patients achieve a complete response to *cis*-platinum–containing chemotherapy regimens and postchemotherapy surgery. The estimated probability that these patients will be free of disease at 12 years is nearly 85% [6]. Extragonadal germ cell neoplasms are even less common than testicular cancer, but generally carry a poorer prognosis [5].

Although therapy for germ cell neoplasm is quite successful, in two large clinical series [3, 6] approximately 15% of the patients developed brain metastases some time during the course of their disease. Of the patients in our study, 2.3% initially presented with CNS metastases, but only 1.0% presented with brain metastases. Overall, 4% developed brain metastases during the course of their disease. This prevalence is much lower than the previously reported figure for at least three reasons. First, our follow-up has been for a much shorter interval than that in the other investigations. Second, because our institution is a referral center for these patients, many return to the care of their local physicians, sometimes resulting in incomplete follow-up. Third, our method of identifying patients who require neuroimaging by reviewing their radiology records at our medical center will fail to identify some patients who are studied at other institutions. Many of these studies are sent to us for review, but an unknown number are not.

An important characteristic of our population is that nearly all of our patients had nonseminomatous germ cell neoplasms (Table 2). This can be attributed to the fact that the majority of these patients are referred to our institution for treatment of advanced or refractory disease, which typically is nonseminomatous at histology. In addition, although seminomas account for 40% of testicular tumors [5], these tumors have a lower rate of CNS metastases than do other kinds of germ cell neoplasms [3]; therefore, neuroradiologic evaluation usually is not required.

The importance of identifying CNS metastases is that therapy is altered when these lesions are present. Radiation therapy was used in 80% of our patients, and orthopedic surgery or neurosurgery was used in 55% after brain or spinal lesions were discovered. The treatment philosophy at our medical center is to use radiation therapy in addition to standard chemotherapy when a patient has CNS metastases at the time of initial diagnosis. If a solitary CNS metastasis is the only manifestation of disease during a relapse, then surgical resection of the lesion is followed by chemotherapy and CNS irradiation. Surgery is not used when there are multiple metastases to the brain. Palliative cranial radiation therapy is often used in addition to chemotherapy in cases of CNS involvement associated with progressive neoplastic disease elsewhere [5].

Few MR studies were performed in our patients. MR was not performed with paramagnetic contrast material because Gd-DTPA was not clinically available when the studies were performed. A recent evaluation of 50 patients with suspected brain metastases found that Gd-DTPA–enhanced MR images were more sensitive for detecting intracranial metastases than contrast-enhanced CT scans were [7]. Nonenhanced MR was the least useful examination in this study because of a lack of specificity for discriminating metastatic lesions from ischemic or radiation changes. Since the identification of CNS metastases is very important in making treatment decisions for patients with germ cell tumors, future evaluation of these patients should be performed with Gd-DTPA–enhanced MR whenever clinically possible.

Brain metastases from germ cell neoplasms are thought to be spread hematogenously. Once malignant cells penetrate the lung they may enter the systemic circulation and involve the brain and other organs. Therefore, it is not surprising that in a study of 38 patients with brain metastases from testicular cancer, all had existing or preexisting pulmonary involvement [4]. In our nine patients with testicular cancer metastatic to the brain, pulmonary lesions were demonstrated also. However, one of the three patients with primary mediastinal germ cell tumors did not have lung metastases. Perhaps the tumor in this patient directly seeded the systemic arterial blood supply.

Although the leptomeninges are a site of metastases in some malignancies [8], carcinomatous meningitis was not found in germ cell tumor patients with brain metastases in one large series that specifically mentioned this entity [4], and it was not observed in our patients with intracranial metastases. Involvement of the leptomeninges also was not reported in an autopsy series of 78 patients with metastatic testicular carcinoma [2]. However, there was a case report of an acute subdural hematoma in a patient with testicular cancer metastatic to the dura [9]. Nevertheless, meningeal metastases from germ cell tumors originating outside the CNS appear to be uncommon.

The frequency of mild to moderate cerebral atrophy was unexpectedly high in our patients. Cerebral atrophy has been associated with intrathecal methotrexate [10, 11] but is not known to be associated with the systemic chemotherapeutic agents used to treat germ cell neoplasms. The patients at our institution are evaluated with histories, physical examinations, and a questionnaire [6], but no formal neuropsychological evaluation is performed routinely to determine if there are subtle deficits associated with the atrophy. There have been no controlled studies to determine whether or not the chemotherapeutic regimens in question have a causal relationship to cerebral atrophy. However, *cis*-platinum, the principal agent in combination chemotherapy for germ cell tumors, has well-documented neurotoxic effects including ototoxicity [10] and peripheral neuropathies [10, 12]. Although it is reported to cross an intact blood-brain barrier (BBB) poorly during IV therapy, a disrupted BBB, perhaps from subclinical metastases that are later ablated by the chemotherapy, will allow significant drug concentrations in the CNS [10, 13]. IV *cis*-platinum after BBB disruption has produced necrosis and hemorrhagic infarction of cerebral tissue in dog models [14]. In addition, combination chemotherapy with bleomycin, *cis*-platinum, and vinblastine has been associated with vascular toxicities that include acute cerebrovascular accidents [15]. Although no direct causal relationship has been shown, the potential for subclinical CNS toxicity as manifested by cerebral atrophy may exist. Two of the 16 patients with atrophy had not received chemotherapy before head CT studies, which suggests factors other than chemotherapy can be involved in the development of cerebral atrophy. There has been a report of cortical cerebellar degeneration occurring in conjunction with testicular neoplasm, presumably as a result of a paraneoplastic process [16]. However, to our knowledge there has been no description of diffuse atrophy resulting from a systemic effect of neoplasms. In one patient in our study, cerebellar atrophy was demonstrated on CT, but the neurologic deficits typically associated with cortical cerebellar atrophy were not present.

The indications for neuroimaging in our patients were evaluated to determine if guidelines could be developed for the efficacious use of radiologic studies. The presence of neurologic deficits and spine pain with or without neurologic deficits were the indications with the highest yield of positive examinations and are valid indications for imaging. However, many cancer patients with metastatic retroperitoneal lymphadenopathy have back pain and are not referred for spine imaging. The high percentage of positive spinal examinations in our study was likely due to the referral of patients with predominantly neurologic and/or positive plain film findings. Evaluation of seizures detected brain metastases in half the patients with this presentation; therefore, seizures are a useful indication for imaging. Examination of headaches without focal deficits detected no finding that altered therapy in these patients. Of 25 patients who were studied to rule out occult lesions, none had brain metastases. Therefore, screening the CNS in neurologically asymptomatic patients with unexplained elevations of serum tumor markers does not appear to be clinically useful.

In conclusion, the presence of CNS metastases significantly alters therapy in patients with germ cell tumors. Neuroradiologic studies are most useful in the presence of neurologic deficits, significant back pain, and recently developed seizures. However, screening neurologically asymptomatic patients with unexplained elevations of serum tumor markers for occult CNS lesions detected no metastases and is not recommended. Since Gd-DTPA–enhanced MR has greater sensitivity than other commonly used techniques [7], it should be the imaging technique of choice in screening germ cell tumor patients for CNS metastases. In addition, neuroimaging revealed an unexpectedly frequent occurrence of cerebral atrophy in our patients. The functional significance and etiology of this is unclear and should be studied further.

REFERENCES

1. Lester SG, Morphis JG, Hornback NB, Williams SD, Einhorn LH. Brain metastases and testicular tumors: need for aggressive therapy. *J Clin Oncol* **1984**;2:1397–1403
2. Johnson DE, Appelt G, Samuel ML, Luna M. Metastases from testicular carcinoma: study of 78 autopsied cases. *Urology* **1976**;8:234–239
3. Williams SD, Einhorn LH. Brain metastases in disseminated germinal neoplasms: incidence and clinical course. *Cancer* **1979**;44:1514–1516
4. Vugrin D, Cvitkovic E, Posner J, Hadju S, Golbey R. Neurological complications of malignant germ cell tumors of testis. *Cancer* **1979**;44:2349–2353
5. Einhorn LH, Williams SD, Donohue JP, Loehrer PJ, Peckham MJ. Cancer of the testes. In: DeVita VT, Hellman S, Rosenberg SA, eds. *Cancer: principles and practice of oncology.* Philadelphia: Lippincott, **1985**: 979–1011
6. Roth JR, Greist A, Kubilis PS, Williams SD, Einhorn LH. Cisplatin-based combination chemotherapy for disseminated germ cell tumors: long-term follow-up. *J Clin Oncol* **1988**;6:1239–1247
7. Sze G, Heier LA, Johnson CE, Krol G. Intracranial metastases: MR imaging versus contrast-enhanced CT. Presented at the annual meeting of the Radiologic Society of North America, Chicago, November **1988**
8. Olson ME, Chernik NL, Posner JB. Infiltration of the leptomeninges by systemic cancer: a clinical and pathologic study. *Arch Neurol* **1974**;30: 122–137
9. Rouah E, Goodman JC, Harper RL. Acute subdural hematoma and metastatic seminoma. *Neurology* **1986**;36:418–420
10. Kaplan RS, Wiernik PH. Neurotoxicity of antineoplastic drugs. *Semin Oncol* **1982**;9:103–130
11. Crosley CJ, Rorke LB, Evans A, Nigro M. Central nervous system lesions in childhood leukemia. *Neurology* **1978**;28:678–685
12. Thompson SW, Davis LE, Kornfield M, Hilgers RD, Standefer JC. Cisplatin neuropathy: clinical, electrophysiologic, morphologic, and toxicologic studies. *Cancer* **1984**;54:1269–1275
13. Ginsberg S, Kirshner J, Reich S, et al. Systemic chemotherapy for a primary germ cell tumor of the brain: a pharmacokinetic study. *Cancer Treat Rep* **1981**;65:477–483
14. Neuwelt EA, Glasberg M, Frenkel E, Barnett P. Neurotoxicity of chemotherapeutic agents after blood-brain barrier modification: neuropathologic studies. *Ann Neurol* **1983**;14:316–324
15. Samuels BL, Vogelzang NJ, Kennedy BJ. Vascular toxicity following vinblastine, bleomycin and cisplatin therapy for germ cell tumors. *Int J Androl* **1987**;10:363–369
16. Yamada M, Okeda R, Chen W, Nito H, Hatakeyama S, Tsukagoshi H. Cortical cerebellar degeneration with testicular neoplasm. *Acta Neuropathol* (Berl) **1985**;66:170–172

Case Report

Excretion of Gadopentetate Dimeglumine in Human Breast Milk

Udo Schmiedl,[1] Kenneth R. Maravilla,[1] Rebecca Gerlach,[1] and Catherine A. Dowling[2]

The excretion of iodinated contrast media in human breast milk has been documented [1–6]. Magnevist (gadopentetate dimeglumine, Berlex Inc., Wayne, NJ), a relatively new paramagnetic contrast agent for MR imaging with an extracellular distribution pattern similar to that of iodinated contrast agents, has been approved for clinical use in Europe and the United States. Although studies in rats have shown evidence that gadopentetate dimeglumine is excreted in breast milk [7], excretion of gadopentetate dimeglumine in human breast milk has, to our knowledge, not been reported or quantified. With the increasing use of contrast-enhanced MR procedures, knowledge of whether gadopentetate dimeglumine is excreted in breast milk and the time course of such excretion is important for treating lactating patients. We studied a lactating patient in whom a gadopentetate dimeglumine–enhanced MR study was performed. Serial measurements of gadolinium excretion in the patient's breast milk and urine form the basis of this report.

Subject and Methods

The patient, a 29-year-old lactating woman with a 13-year history of left ear deafness and mild left ear tinnitis, was referred for MR imaging to rule out an acoustic neuroma. After consulting with the patient and discussing the risks and options, it was decided to proceed with the contrast-enhanced MR study at the time because of personal and logistical considerations. After informed consent was obtained, Magnevist was injected IV at a dose of 0.1 mmol/kg. The total amount of administered gadopentetate dimeglumine was 5.8 mmol. Breast feeding was discontinued for 48 hr after the examination to minimize any potential risk to the infant. Serial samples of all expressed breast milk were collected at 135 min, 290 min, 12 hr 40 min, 17 hr 30 min, 22 hr 40 min, and 32 hr 40 min after injection of Magnevist. The patient attempted to empty both breasts completely at the time of each collection. Serial urine samples were obtained at the same time as the breast milk, together with a total urine collection for the 33-hr period of observation. Five-milliliter aliquots of all samples were lyophilized and analyzed for gadolinium concentration by using inductively coupled plasma atomic emission spectrometry (ICP-AES, wavelength 342.247 nm; Schering AG, Berlin). The lowest detectable gadolinium concentration with this method is 1×10^{-7} mol/l. The concentrations of gadolinium in the urine and milk samples were essentially equivalent to the concentration of gadopentetate dimeglumine as there is no endogenous source of gadolinium and no significant dissociation of the chelate within the body has been reported.

Results

A cumulative amount of gadolinium that accounted for only 0.011% of the total IV administered dose was excreted in the breast milk during the observation period of almost 33 hr. The cumulative excreted amounts of gadolinium in milk and urine vs time are shown in Figure 1. The highest concentration of gadolinium in breast milk was noted 4 hr 50 min after administration, and measured 5.1 μmol/l. At 22 hr after gadopentetate dimeglumine administration, the concentration in breast milk measured less than 1.0 μmol/l. The time course of gadopentetate dimeglumine concentration in excreted breast milk compared with that in urine is shown in Figure 2.

Received November 27, 1990; accepted after revision February 1, 1990
This work was supported in part by Schering AG, Berlin, W. Germany.

[1] Department of Radiology, University of Washington School of Medicine (SB-05), Seattle, WA 98195. Address reprint requests to U. P. Schmiedl.
[2] Department of Anesthesiology, University of Washington School of Medicine, Seattle, WA 98195.

AJR 154:1305–1306, June 1990 0361–803X/90/1546–1305 © American Roentgen Ray Society

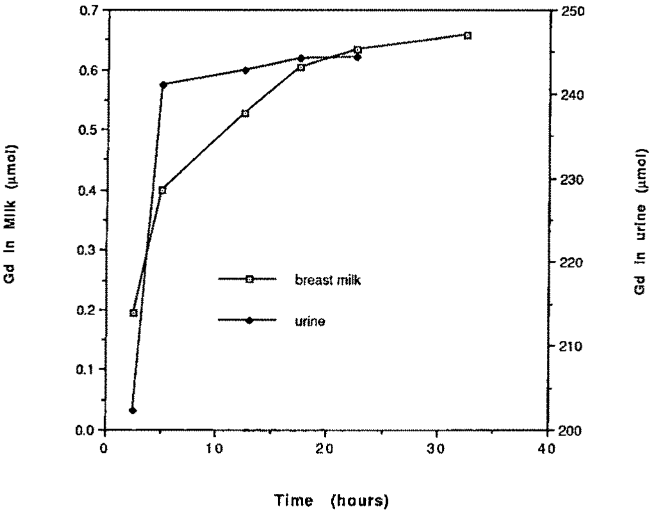

Fig. 1.—Total (cumulative) excretion of gadolinium in breast milk and urine over time after IV administration.

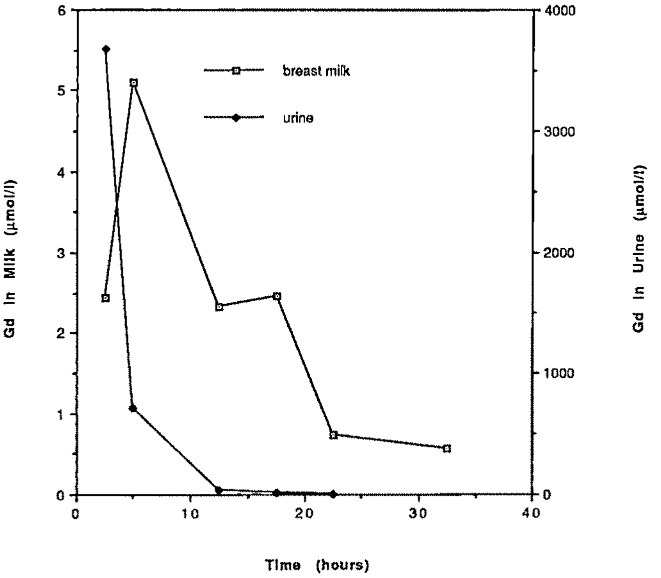

Fig. 2.—Concentration of gadolinium in breast milk and urine over time after IV administration.

Discussion

We have found that gadopentetate dimeglumine, which is an ionic contrast medium, is transferred to the breast milk in a very limited amount. Compared with the nonionic contrast agent iohexol, which is reported to be excreted in the breast milk in amounts of 0.5% of total injected dose [5], the excretion rate of gadopentetate dimeglumine appears even lower. Compared with the reported excretion of diatrizoate (<0.05%), an ionic contrast agent, the excretion of gadopentetate dimeglumine as measured in our study seems to be on the same order of magnitude [6]. Experimental studies of gadopentetate dimeglumine in lactating rats at a dose of 0.5 mmol/kg indicated an estimated cumulative mammary excretion of 0.2% [7]. One reason for the lower measured excretion found in our patient might be that she was weaning the infant at the time of the study, which resulted in a reduced amount of breast-milk production during this study. This effect was shown in an earlier study of iodinated contrast agents [5]. Other factors that have been shown to influence the degree of secretion of a substance from plasma to milk include: (1) the route, frequency, and dose of administered drug; (2) degree of protein binding; (3) molecular weight and degree of ionization at plasma and milk pH; (4) lipid solubility; and (5) time after parturition and frequency of breast feeding [1–3].

The extent of protein binding and blood cell partitioning of gadopentetate dimeglumine is not known [7]. Magnevist is a water-soluble gadopentetate dimeglumine salt that, upon injection, is completely dissociated, and the gadopentetate moiety is eliminated in the urine with 91± 13% of the total dose excreted by 24 hr after injection [7]. The small difference in molecular weight between the anion (the gadopentetate moiety) of Magnevist (550 daltons) and diatrizoate (614 daltons) may contribute to their similar excretion in breast milk.

The peak gadolinium concentration in breast milk (5.1 µmol/l), measured 5 hr after administration of Magnevist, equals approximately one tenth of estimated plasma concentration at this time (G. Schuhmann-Giampieri, personal communication). Assuming a body weight of 3 kg, the amount of gadolinium transferred to a nursing infant during the first 24 hr after injection would amount to only 0.21 µmol/kg. Theoretically, contrast media, if excreted in the breast milk, can cause either direct toxic effects on the nursing infants or allergic sensitization. Neither of these effects have been reported, to our knowledge, for gadopentetate dimeglumine or for iodinated contrast media. Although the present observation is limited because it is based on only one patient, our data indicate a low excretion rate of gadopentetate dimeglumine in the breast milk. The time course of excretion indicates that breast feeding can probably be safely resumed 24 hr after IV administration of gadopentetate dimeglumine. This conclusion is based on setting an arbitrary cutoff for gadopentetate dimeglumine concentration in breast milk at less than 1 µmol/l. Because of the uncertainties arising from the fact that our measurements are based on a single case, an additional waiting period of 12 or 24 hr could be used as an added safety factor, and breast feeding could be suspended for a total of 36–48 hr after gadopentetate dimeglumine administration.

REFERENCES

1. Anderson PO. Drugs and breast feeding: a review. *Drug Intell Clin Pharm* **1977**;11:208–223
2. Catz CS, Giacola GP. Drugs and breast milk. *Pediatr Clin North Am* **1972**;19:151–166
3. Wilson JT, Brown RD, Cherek DR, et al. Drug excretion in human breast milk: principles, pharmacokinetics and projected consequences. *Clin Pharmacokinet* **1980**;5:1–22
4. Vorherr H. Drug excretion in breast milk. *Postgrad Med* **1974**;56:97–104
5. Nielsen ST, Matheson I, Rasmussen JN, Skinnemoen K, Andrew E, Hafsahl G. Excretion of iohexol and metrizoate in human breast milk. *Acta Radiol* **1987**;28:523–526
6. Fitz-John TP, Williams GD, Laker MF, Owen JP. Intravenous urography during lactation. *Br J Radiol* **1982**;55:603–605
7. Magnevist product information. Wayne, NJ: Berlex Laboratories Inc., **1989**

Computerized On-line Reporting of Coronary Angiograms with the CLIP System

Ducksoo Kim[1] and Brian W. A. Leeming

Computerized language information processing (CLIP) is a computerized on-line radiology reporting system developed at Beth Israel Hospital, Boston, that permits the generation of a wide range of reports covering all radiologic studies including coronary angiographic studies. Each reporting area has a keyboard and monitor connected to computers situated in a central computer laboratory. By means of the keyboard and monitor, the radiologist accesses a data bank of information that is appropriate for each type of study and from which he or she selects data to compile the report. CLIP has been in use at Beth Israel Hospital in its current version since 1980. It is one of two reporting methods; the other is a manual system with dictaphones and transcriptionist entry of the dictated reports into the computer. The computerized system will be described in detail.

The system was evaluated by an experienced cardiac angiographer in the reporting of 107 consecutive coronary angiograms. We measured a number of parameters, and the results show the efficacy of the method in its ability to quickly deliver adequate angiographic reports in good English to the clinical staff.

Description of the CLIP Reporting System

A keyboard and television screen enable the radiologist at the film-viewing area to generate reports that, when electronically approved and signed, immediately become available for reading throughout the hospital [1, 2]. Each study has a unique access number (assigned when the patient arrives in the department). When this number is entered by the radiologist, the patient's name and other relevant data are displayed in the upper part of the screen. In the lower part of the screen is displayed a frame of statements that relate specifically to the type of examination being interpreted (Fig. 1).

All types of radiology reports can be generated by CLIP by using about 13,000 frames of data, which are grouped into large sets covering the different types of examination. Each statement is identified by a letter or number together with a brief precis of the statement. The radiologist selects one or more of these itemized statements to make the report. Selection of an item may cause the display of a new frame of more detailed information. Items from this frame may open to other frames in a hierarchic fashion until a precise but complete interpretation is developed. In addition, the statements may be modified further by selecting items from frames of anatomic or descriptive data automatically presented at appropriate points in the developing report. As each statement is selected and modified, it is added to the report narrative, which is developing in the center of the screen. Editing can take place at any time during the reporting or can be left until report completion. Unusual findings can be typed directly into the report. Once the report is completed (and, if necessary, edited), the radiologist can approve it and the report immediately becomes available for review by authorized personnel at any of the 1000 terminals located in all the patient areas and departments in the hospital.

Received November 9, 1989; accepted after revision December 26, 1989.

[1] Both authors: Charles A. Dana Research Institute, Department of Diagnostic Radiology, Beth Israel Hospital and Harvard Medical School, Boston, MA 02215. Address reprint requests to D. Kim, Beth Israel Hospital, 330 Brookline Ave., Boston, MA 02215.

AJR 154:1307–1310, June 1990 0361-803X/90/1546-1307 © American Roentgen Ray Society

In the case of the hierarchy of frames for coronary angiography, the master frame (Fig. 1) displays two columns of options. The left-hand column has a "Normal Report" option, a list of presenting features, and a description of the technical aspects of the study as well as other items relating to procedural complications. From the other column, one can select either diagnostic coronary angiography or percutaneous transluminal coronary angioplasty (PTCA). If desired, a summary and recommendation also can be entered. If coronary angiography is selected, a new frame appears (Fig. 2). This frame permits entry of any anatomic variations that are present, and also detailed left ventriculographic findings as well as the actual coronary angiography details, either preoperative or postoperative. For a diagnostic coronary angiogram, item B would be selected.

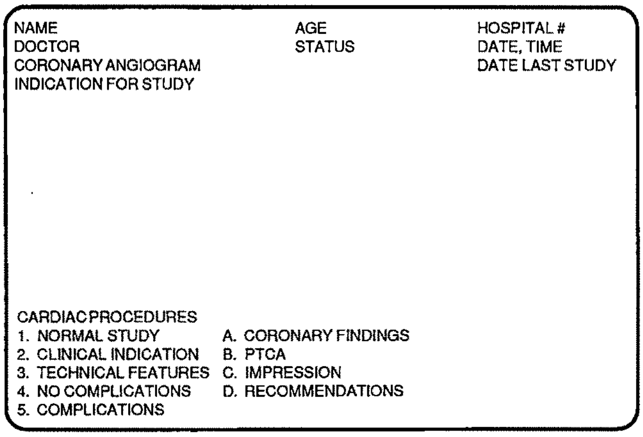

```
NAME                          AGE              HOSPITAL #
DOCTOR                        STATUS           DATE, TIME
CORONARY ANGIOGRAM                             DATE LAST STUDY
INDICATION FOR STUDY

CARDIAC PROCEDURES
1. NORMAL STUDY          A. CORONARY FINDINGS
2. CLINICAL INDICATION   B. PTCA
3. TECHNICAL FEATURES    C. IMPRESSION
4. NO COMPLICATIONS      D. RECOMMENDATIONS
5. COMPLICATIONS
```

Fig. 1.—Master frame that displays options available. Top part includes patient and examination information. Developing report is displayed in central area. Bottom part shows frame of reporting options. Each option opens to a new frame of options.

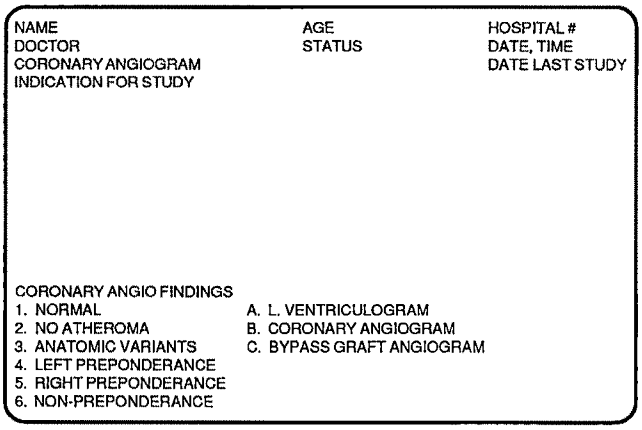

```
NAME                          AGE              HOSPITAL #
DOCTOR                        STATUS           DATE, TIME
CORONARY ANGIOGRAM                             DATE LAST STUDY
INDICATION FOR STUDY

CORONARY ANGIO FINDINGS
1. NORMAL                  A. L. VENTRICULOGRAM
2. NO ATHEROMA             B. CORONARY ANGIOGRAM
3. ANATOMIC VARIANTS       C. BYPASS GRAFT ANGIOGRAM
4. LEFT PREPONDERANCE
5. RIGHT PREPONDERANCE
6. NON-PREPONDERANCE
```

Fig. 2.—When coronary angiography is entered by pressing A (see Fig. 1), this frame replaces master frame. It contains all entries needed for a full report. Each entry causes display of a new frame. Pressing B will cause frame shown in Fig. 3 to appear (see Fig. 3).

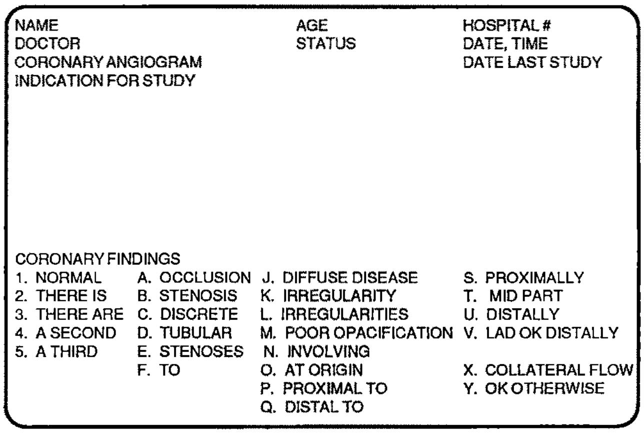

```
NAME                          AGE                  HOSPITAL #
DOCTOR                        STATUS               DATE, TIME
CORONARY ANGIOGRAM                                 DATE LAST STUDY
INDICATION FOR STUDY

CORONARY FINDINGS
1. NORMAL      A. OCCLUSION  J. DIFFUSE DISEASE      S. PROXIMALLY
2. THERE IS    B. STENOSIS   K. IRREGULARITY         T. MID PART
3. THERE ARE   C. DISCRETE   L. IRREGULARITIES       U. DISTALLY
4. A SECOND    D. TUBULAR    M. POOR OPACIFICATION   V. LAD OK DISTALLY
5. A THIRD     E. STENOSES   N. INVOLVING
               F. TO         O. AT ORIGIN            X. COLLATERAL FLOW
                             P. PROXIMAL TO          Y. OK OTHERWISE
                             Q. DISTAL TO
```

Fig. 3.—Narrative description is compiled by matching introductory and pathologic items from appropriate columns to specific vessels, which are accessed through item N.

The report is constructed by free selection from the displayed items to produce descriptions of the state of each coronary artery in succession (Fig. 3). As an example, with Figure 3 for guidance, the successive selection of items 2 (under which a list of grades of severity is automatically displayed), D, N, S, and X produces the following account in the narrative part of the screen:

> There is a severe tubular stenosis involving the left anterior descending artery proximally with distal retrograde filling by right to left collaterals from the posterior descending branch of the right coronary artery.

Similar descriptions of other coronary vessels are then compiled by returning to the frame shown in Figure 3. When the compilation of individual artery changes is completed, similar use of the "Impression" and "Recommendation" options (Fig. 1) rounds out the report.

A sample report generated by the CLIP system is shown in Figure 4.

Materials and Methods

One hundred seven successive coronary angiographic reports compiled by the CLIP system were prospectively included in the study. In each case, the angiogram was reviewed as soon as possible after it was completed. A coronary diagram was used to record by hand the position and grade of severity of any abnormalities. Then the report was entered immediately at a terminal as described earlier and was put on hold. At this point, the angiogram was briefly reevaluated and if no new information was added, the report was approved.

The following data were recorded for each study in the series. (1) Time between completion of the angiogram and the commencement of the reporting process. This time includes time for discussion of the case with the cardiology team and for the subsequent evaluation of the angiogram by using the coronary diagram. (2) Time required to enter the report. This time commences with the entry of the report access number into the computer and ends when the report is electronically approved. (3) The number of lines of printed text per report. (4) The number of lines of text derived as selections from the CLIP lexicon of statements. (5) The number of lines of the printed report that were entered as free text. The number of lines of free text is a measure of CLIP's inability to provide a complete lexicon of statements for coronary angiography. It is a design feature that the

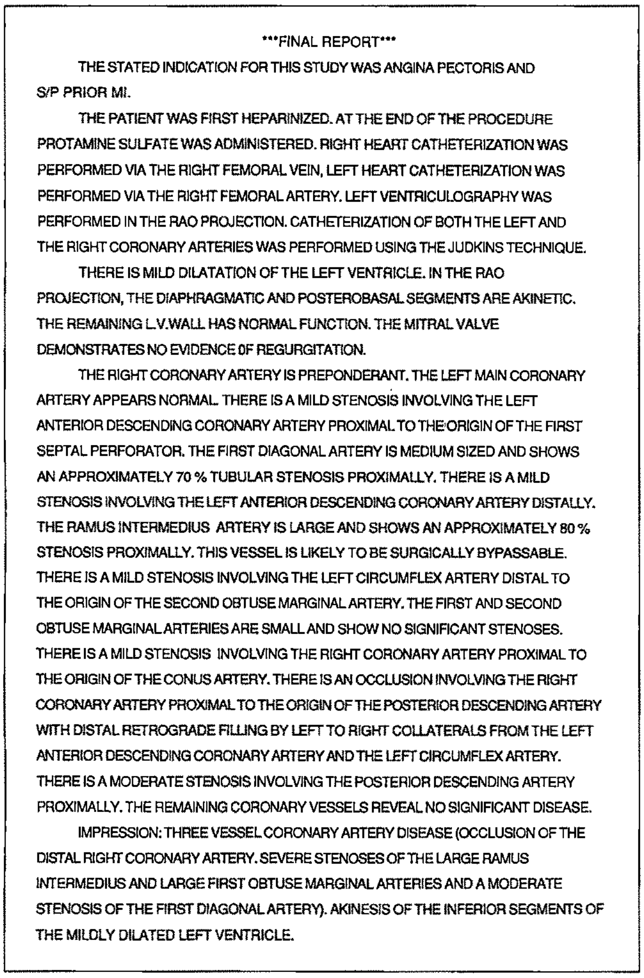

FINAL REPORT

THE STATED INDICATION FOR THIS STUDY WAS ANGINA PECTORIS AND S/P PRIOR MI.

THE PATIENT WAS FIRST HEPARINIZED. AT THE END OF THE PROCEDURE PROTAMINE SULFATE WAS ADMINISTERED. RIGHT HEART CATHETERIZATION WAS PERFORMED VIA THE RIGHT FEMORAL VEIN, LEFT HEART CATHETERIZATION WAS PERFORMED VIA THE RIGHT FEMORAL ARTERY. LEFT VENTRICULOGRAPHY WAS PERFORMED IN THE RAO PROJECTION. CATHETERIZATION OF BOTH THE LEFT AND THE RIGHT CORONARY ARTERIES WAS PERFORMED USING THE JUDKINS TECHNIQUE.

THERE IS MILD DILATATION OF THE LEFT VENTRICLE. IN THE RAO PROJECTION, THE DIAPHRAGMATIC AND POSTEROBASAL SEGMENTS ARE AKINETIC. THE REMAINING L.V.WALL HAS NORMAL FUNCTION. THE MITRAL VALVE DEMONSTRATES NO EVIDENCE OF REGURGITATION.

THE RIGHT CORONARY ARTERY IS PREPONDERANT. THE LEFT MAIN CORONARY ARTERY APPEARS NORMAL. THERE IS A MILD STENOSIS INVOLVING THE LEFT ANTERIOR DESCENDING CORONARY ARTERY PROXIMAL TO THE ORIGIN OF THE FIRST SEPTAL PERFORATOR. THE FIRST DIAGONAL ARTERY IS MEDIUM SIZED AND SHOWS AN APPROXIMATELY 70 % TUBULAR STENOSIS PROXIMALLY. THERE IS A MILD STENOSIS INVOLVING THE LEFT ANTERIOR DESCENDING CORONARY ARTERY DISTALLY. THE RAMUS INTERMEDIUS ARTERY IS LARGE AND SHOWS AN APPROXIMATELY 80 % STENOSIS PROXIMALLY. THIS VESSEL IS LIKELY TO BE SURGICALLY BYPASSABLE. THERE IS A MILD STENOSIS INVOLVING THE LEFT CIRCUMFLEX ARTERY DISTAL TO THE ORIGIN OF THE SECOND OBTUSE MARGINAL ARTERY. THE FIRST AND SECOND OBTUSE MARGINAL ARTERIES ARE SMALL AND SHOW NO SIGNIFICANT STENOSES. THERE IS A MILD STENOSIS INVOLVING THE RIGHT CORONARY ARTERY PROXIMAL TO THE ORIGIN OF THE CONUS ARTERY. THERE IS AN OCCLUSION INVOLVING THE RIGHT CORONARY ARTERY PROXIMAL TO THE ORIGIN OF THE POSTERIOR DESCENDING ARTERY WITH DISTAL RETROGRADE FILLING BY LEFT TO RIGHT COLLATERALS FROM THE LEFT ANTERIOR DESCENDING CORONARY ARTERY AND THE LEFT CIRCUMFLEX ARTERY. THERE IS A MODERATE STENOSIS INVOLVING THE POSTERIOR DESCENDING ARTERY PROXIMALLY. THE REMAINING CORONARY VESSELS REVEAL NO SIGNIFICANT DISEASE.

IMPRESSION: THREE VESSEL CORONARY ARTERY DISEASE (OCCLUSION OF THE DISTAL RIGHT CORONARY ARTERY. SEVERE STENOSES OF THE LARGE RAMUS INTERMEDIUS AND LARGE FIRST OBTUSE MARGINAL ARTERIES AND A MODERATE STENOSIS OF THE FIRST DIAGONAL ARTERY). AKINESIS OF THE INFERIOR SEGMENTS OF THE MILDLY DILATED LEFT VENTRICLE.

Fig. 4.—This report, selected from reports in study group, is entirely generated by computerized language information processing system except for second to fourth lines in impression section.

lexicon is not totally comprehensive. A very large lexicon would be self-defeating because the time required to probe it for wanted statements would be too long.

Results

Time between coronary angiogram completion and report entry (CAC-RE time). In 57 cases, the review of the study was promptly completed in 1 hr or less. In 32 cases, the CAC-RE time was between 2 and 5 hr and in 18 cases, the review was not completed until between 6 and 10 hr had passed. No review took more than 11 hr. These times are not directly related to use of CLIP. The times recorded reflect a variety of minor uncontrolled variables, such as the speed with which the cine film was processed. The times recorded might have been different were it not for the impact of the study.

Time required to complete each report on the computer. Lengths of time for the first 18 reports were not recorded, leaving 89 reports with available time lengths. Sixty-five reports (73%) were reported in 10 min or less. The remaining 24 reports (27%) required between 11 and 20 min to complete.

Number of lines of printed text per report. There were five reports (4.7%) that had 15 lines or fewer of printed text. Three of these were normal angiograms. There were 101 reports (95%) in which the number of lines of printed text was more than 15 and less than 45. Fifty-five of these cases had between 26 and 35 lines. Only one report exceeded 45 lines.

Number of CLIP-derived lines of printed text per report. No reports had less than 10 CLIP-generated lines of text. The number of lines of CLIP-generated text for any report was between 11 and 45 lines. Seventy of these reports (66%) had between 21 and 35 lines. Only two reports had more than 40 lines.

Number of lines of free text per report. In seven reports (6.5%), no free text was required. Five lines or fewer of free text were entered in 84 reports (78.5%). Thirteen reports (12%) required between six and 10 lines, and only three reports (3%) were complex or unusual enough to require more than 10 lines.

Discussion

CLIP is able to generate on-line coronary angiography reports for hospitalwide distribution without the delays inherent in the dictation and subsequent entry of the report into the computer, final editing, and approval by the radiologist. Our data show that with CLIP the time required to enter the contents of the report into the computer directly is acceptably fast, there is no requirement for massive entry of free text, and the reports are not merely brief telegraphic style summaries but are adequate descriptions of all the pertinent findings. Although concise, the reports are written in good English (Fig. 4).

In our radiology department, over 70% of all types of reports are generated with CLIP. Beth Israel Hospital is a 600-bed hospital and although there are about 110,000 radiology studies performed annually (not counting radionuclide studies), only three transcriptionists (including evening and weekend transcribing) are required to transcribe the dictated radiology reports.

CLIP is used less than 100% of the time because of several factors. First, the decision to report on line is voluntary, and not every radiologist is convinced that a computer can do a better job of reporting than he or she can. Second, there are definite drawbacks to direct report generation with a keyboard. The radiologist is compelled to divert his gaze from the radiologic images to the keyboard and the terminal. It is common for additional findings to be made by repeated visual scanning while dictating reports. The inability to do this is considered a drawback of keyboard use. Another objection is that it takes longer to generate a report directly than to dictate it, although radiologists experienced with the keyboard are able to compete successfully with dictation in the volume of reporting per hour.

We are planning to modify CLIP reporting by replacing the keyboards with voice transducers [3, 4]. The frames of data in CLIP can then be accessed by vocally summoning the wanted frames. Thus, saying "CHF" will result in the immediate appearance of this frame dealing with heart failure without having to step through several frames to find it. It is expected that keyboard usage will decline and perhaps even disappear as voice actuation becomes established. A commercial version that uses an accurate voice transducer is being developed and should be available in late 1990.

For clinical staff, the immediate availability of CLIP reports is considered a great benefit. There is no need to visit the radiology department except to discuss the case when this seems indicated. At our hospital, radiologic reports are just one of many reports directly accessible on multiple terminals. Clinical chemistry, microbiology, cytology, and other types of reports are easily reviewed from any of the many hospital terminals. Thus, the radiologic reports can be read with the other information, without having to go to a telephone or to a patient's records to obtain them. The radiologist should also feel a sense of satisfaction that his/her approved report is an integral component of the treatment strategy for the patient. This cannot be true when the report becomes available several hours or days later than the study itself.

The approval of reports by radiologists is often done perfunctorily, and occasionally necessary editing is overlooked or even avoided. Spelling errors by the transcriptionist are often ignored. Directly generated reports do not have these problems.

The amount of film handling by file clerks is less when reports are generated on line because the studies can be filed immediately and are thus more easily located because they are not circulating through the reporting rooms. The number of inquiries directed to the file room by clinical staff searching for either radiologic reports or for unreported films drops considerably.

All radiologic reports are held in computer memory for 2 years. They can be recalled instantaneously for review and comparison, including the most recent reports, which are frequently only hours old. The laborious task of maintaining a constantly updated file of reports in each patient's master folder is completely eliminated.

In summary, we claim that cardiac and coronary angiographic studies can be reported conveniently and rapidly by using the CLIP system without any sacrifice of style and with adequate detail for all purposes. The immediate availability of these reports, along with the 70% of all other radiologic reports on remote terminals located throughout the hospital, markedly improves efficiency. Finally, improved patient care resulting from the great reduction in the level of frustration and time-wasting associated with dealing with paper reports is a worthwhile achievement.

With on-line reporting that uses voice-activated transducers instead of keyboards to access the CLIP statements, most of the hostility toward keyboard use that is still expressed by some should disappear.

REFERENCES

1. Leeming BWA, O'Reilly GJ, Kleefield J, Simon M. Computerized reporting of cranial and spinal CT with the CLIP system. In: *Proceedings of the eighth conference on computer applications in radiology.* St. Louis: American College of Radiology, **1984**
2. Leeming BWA, Simon M. CLIP: A 1982 update. In: *Proceedings of the seventh conference on computer applications in radiology.* Boston: American College of Radiology, **1982**
3. Leeming BWA, Porter D, Jackson JD, Bleich HL, Simon M. Computerized radiologic reporting with voice data entry. *Radiology* **1981**;138:585–588
4. Leeming BWA, Simon M. On line reports to accompany digital x-ray images transmitted to satellite monitors. Presented at the 3rd PACS/PHD Symposium, Tokyo, Japan, July 9–12, **1986**

Meeting News

The Society of Gastrointestinal Radiologists: 19th Annual Meeting, January 1990

Elizabeth Whalen[1]

The nineteenth annual meeting of The Society of Gastrointestinal Radiologists (SGR) was held January 14–19, 1990, at the Hyatt Regency Waikoloa, Big Island of Hawaii. Participants had the opportunity to listen to scientific papers, panel discussions, categorical courses, and the annual Walter B. Cannon lecture. Also offered were poster sessions and workshops.

We regret that page limitations do not allow a comprehensive review of the entire program. However, this report does include some of the information presented in each of the major categories discussed at the meeting: pharyngoesophageal examinations, studies involving the gallbladder and bile ducts, hepatic and pancreatic radiology, imaging of the gastrointestinal tract, and new technology in gastrointestinal radiology.

Pharyngoesophageal Examinations

Presentations on pharyngoesophageal disorders covered the topics of pharyngeal tumors, mucosal abnormalities in Barrett esophagus, oral vs pharyngeal dysfunction as a cause of aspiration, evaluation of the oropharynx and esophagus in patients with cerebrovascular or immunosuppressive disease, esophageal motor disease as a cause of chest pain, and preservation of normal esophageal peristalsis in experimental esophageal dilatation and hypertrophy.

Stephen E. Rubesin (Hospital of the University of Pennsylvania, Philadelphia) discussed the importance of double-contrast studies of pharyngeal tumors in detecting primary carcinoma, defining the size and anatomic extent of the lesion, clarifying the degree of functional impairment, and ruling out coexistent esophageal carcinoma. Dr. Rubesin emphasized that good visualization requires lateral views and examinations performed in phonation. Radiologic appearance of pharyngeal carcinoma includes an intraluminal mass, decreased distensibility, and mucosal irregularities.

Certain abnormalities in the mucosal surface also can help diagnose Barrett esophagus, which is often premalignant. In each of nine patients discussed by Seth N. Glick (Hahnemann University Hospital, Philadelphia), the sole radiologic finding was an abnormal mucosal pattern. A previously described reticular pattern was found in five patients, and a villous pattern, not previously described, was found in six (both patterns were found in two).

To determine whether aspiration is caused by oral or pharyngeal dysfunction, Philadelphia researchers used a videofluorographic examination of swallowing to study 50 consecutive patients known to aspirate. Michael J. Feinberg (Albert Einstein Medical Center, Philadelphia, PA) discussed the results, which showed that the cause of aspiration was oral dysfunction in 46% of cases, pharyngeal dysfunction in 20%, and combined dysfunction in 34%. The most common causes of oropharyngeal impairment were dementia (21 patients) and stroke (15 patients).

Videofluoroscopic evaluations also were used in a study described by Michael Y. M. Chen (Bowman Gray School of

---

[1] Contributing editor, *American Journal of Roentgenology*, Ste. 200, 2223 Avenida de la Playa, La Jolla, CA 92037.

Editor's note.—"Meeting News" articles report the highlights of important national radiology meetings. The intent is to provide Journal readers with succinct, substantive, and accurate reviews of topics of current interest, written in a readable fashion and published promptly after the meeting.

The articles will not undergo the peer review usually required of *AJR* publications, nor will they offer a critique of the information provided. The sole purpose of the series is to apprise *AJR* readers of topics of current concern in an interesting and timely fashion.

***AJR* 154:1311–1316, June 1990** 0361–803X/90/1546–1311 © American Roentgen Ray Society

Medicine, Winston-Salem, NC). Chen and colleagues examined the oropharynx in 46 patients with cerebrovascular disease in order to assess oropharyngeal dysfunction, the prevalence and location of abnormalities, and the type and severity of aspiration. Although all patients were shown to have mild (18) or moderate (28) oropharyngeal abnormalities, the videofluoroscopic findings were not specific in predicting the type of cerebrovascular disease.

In immunosuppressed patients, such as those with AIDS, different types of esophagitis may be seen, including *Candida* esophagitis, herpes esophagitis, reflux esophagitis, and esophageal disease due to cytomegalovirus or drug reactions. Marc Levine (Hospital of the University of Pennsylvania, Philadelphia) stressed that diagnosis by double-contrast studies can obviate endoscopy in these severely ill patients and that esophagitis may be the first indication that a patient has AIDS.

David Ott (Bowman Gray School of Medicine, Winston-Salem, NC) discussed esophageal motor disease as a cause of chest pain. Radiologic evaluation of patients with chest pain is most effective in excluding esophageal disease; radiologic assessment of esophageal motility yields a high specificity by a low sensitivity and a low return on defining functional disorders.

In a study in opposums, C. Lu and colleagues (University of Iowa College of Medicine and Veterans Administration Medical Center, Iowa City) examined the preservation of normal esophageal contraction in induced esophageal dilatation and hypertrophy. Using barium esophagograms, videotaped dynamic studies, esophageal manometry, and anatomic studies, these researchers found that chronic esophageal obstruction and muscular hypertrophy do not interfere with normal contractility of the esophageal smooth muscle; the observed abnormalities in esophageal contraction seem to be caused by altered load (volume) conditions.

The Walter B. Cannon lecture, presented by H. Worth Boyce (University of South Florida, College of Medicine, Tampa), was entitled "Thirty Years of Looking and Learning: Endoscopic Observations from the Cricopharyngeus to the Cardia." Boyce reviewed the gross anatomy of the esophagus, as well as the important radiologic features and endoscopic appearances of the esophagus. After describing ways to locate and evaluate the esophagogastric junction, Boyce discussed in detail the sliding hiatal hernia, A-ring narrowing, static B-ring, Barrett esophagus, and reflux and drug-induced esophagitis. In his concluding remarks, Boyce stressed the importance of better training for radiologists in standard esophageal barium contrast diagnostic techniques, which at the present time may be either ignored or given less attention than the "more glamorous" techniques of CT and MR imaging.

Studies of the Gallbladder and Bile Ducts

The presentations concerning the biliary tree included reports on bile duct obstruction, biliary tract interventional procedures, cholecystitis, and gallstone imaging and treatment.

Bile Duct Obstruction

A categorical course on bile duct obstruction was moderated by Morton Burrell (Yale University, New Haven, CT). First, Dr. Burrell reviewed the basic principles of this type of obstruction and suggested an integrated diagnostic approach. His summary indicated that (1) sonography and CT are most effective when used in series skewed toward malignancy, (2) cholescintigraphy is most helpful in diagnosing low-grade (typically benign) obstructions, and (3) cholangiography is most useful in cases when the diagnosis is in doubt because of equivocal imaging or clinical results.

Abraham H. Dachman (Uniformed Services University, Bethesda, MD) discussed the radiologic-pathologic correlation of biliary obstruction. Included in the description of the various causes of biliary obstruction were the following:

1. Primary sclerosing cholangitis—distal common bile duct sparing in 20%; diffuse, short, multifocal involvement; diverticula; beading; mural irregularities (nodular, shaggy); and long, confluent strictures
2. AIDS cholangitis—fever, pain, increased alkaline phosphatase; appearance like that of primary sclerosing cholangitis with papillary stenosis on cholangiography
3. Oriental cholangitis—recurrent pain, fever, and/or jaundice; residual stones, strictures, anastomosis, and/or early duct change shown on percutaneous transhepatic cholangiography or ERCP
4. Cholangiocarcinoma—jaundice, weight loss, pruritus, and/or anorexia; mostly adenocarcinomas; infiltrating, nodular, and papillary patterns; prominent desmoplasia; stenotic, obstructive, or polypoid patterns (no diverticula) on cholangiography; no mass; obstruction and wall thickening on sonography.

Biliary Tract Interventional Procedures

Interventional radiology of the biliary tract was discussed in another categorical course. John P. McGahan (University of California, Davis, Medical Center, Sacramento) focused on two percutaneous techniques: diagnostic aspiration of the gallbladder and cholecystostomy. After diagnostic aspiration is performed for suspected acute cholecystitis, both a Gram stain (sensitivity, 48%) and a culture (sensitivity, 38%) of the bile should be obtained. A negative aspirate does not exclude acute cholecystitis, and Dr. McGahan concluded that aspiration is not likely to be used in the 1990s. Percutaneous cholecystostomy for suspected acute cholecystitis is a relatively simple procedure; however, (1) results of the patient's clotting studies should be appropriate, (2) the puncture should be transhepatic if possible, and (3) the procedure should not be delayed (even for a couple of days). Dr. McGahan predicted that percutaneous cholecystostomy would be widely used for a number of applications in the 1990s.

David S. Zimmon (St. Vincent's Hospital and Medical Center, New York) discussed the diverse techniques that make use of endoscopy for imaging. Diagnostic cholangiopancreatography is combined with a variety of therapeutic techniques that mimic percutaneous methods. Endoscopic sphincterotomy yields a permanent biliodigestive anastomosis and separates bile from the pancreatic duct to prevent recurrence of gallstone pancreatitis with a mortality rate of 0.5%, which is similar to that of elective cholecystectomy in patients who are not at high risk. Most unresectable periampullary tumors can be dealt with by using percutaneous assistance when the lesion cannot be passed endoscopically (20%). Large-bore (10–14 French) stents and brachytherapy are effective palliation. Percutaneous or endoscopic pancreatic cystenterostomy is replacing surgery unless drainage of the pancreatic duct is required. Pancreatic sphincter or duct stenoses are treated with stents, similar to the treatment of biliary stenosis.

In a study of 85 patients undergoing 159 major biliary percutaneous procedures, Stephen K. Teplick and colleagues investigated the most effective method for pain control during these often painful procedures. A high-thoracic epidural anesthesia was used for 64% of their patients, and narcotic sedation was used for the other 36%. A significant difference was found between the subjective pain measurements in the two groups of patients. In the epidural group, 93% of the patients experienced no pain or mild pain; however, in the patients who were under narcotic sedation, moderate or severe pain was reported by 60%, and only 40% reported no pain or mild pain. Moreover, more complications occurred in the narcotic sedation group (including the need for reversal of narcotic action, low blood pressure, and low respiratory rate). Dr. Teplick concluded that the increased cost and procedure time required by epidural anesthesia are outweighed by its benefits (including its ease of use, improved pain control, and continuous monitoring of the patient by an anesthesiologist).

Gallbladder Disease

In a study reported by Joe Ariyama (Juntendo University, Tokyo, Japan), endoscopic sonography was used to establish or exclude carcinoma of the gallbladder in 159 patients. Diagnoses included chronic cholecystitis (57), cholelithiasis (35), cholesterol polyp (34), adenomyomatosis (13), carcinoma (10), adenoma (one), and miscellaneous (nine). Endoscopic sonography always provided a complete view of the gallbladder, indicated the correct diagnosis in 90% of patients, and showed the depth of invasion in 55% of the resectable tumors.

R. L. MacCarty (Mayo Clinic, Rochester, MN) discussed the recurrence of sclerosing cholangitis after liver transplantation. Of 27 patients in whom liver transplantation was performed for primary sclerosing cholangitis, five showed changes suggestive of sclerosing cholangitis on posttransplantation cholangiography. In 35 other liver transplant patients, only one had changes suggestive of primary sclerosing cholangitis on posttransplantation cholangiography.

In a categorical course, Joseph F. Simeone (Harvard University, Cambridge, MA) talked about the diagnosis of chronic cholecystitis. He pointed out that the thickening of the gallbladder wall has several possible causes: failure of the patient to fast before the imaging procedure, acute cholecystitis, chronic cholecystitis, portal vein hypertension, hypoalbumenia, neoplasm, adenomyosis, or hepatitis. Imaging findings may clarify the cause; for example, the radiologist sometimes can redirect the diagnosis from acute cholecystitis to hepatitis (especially in young patients).

Gangrenous cholecystitis can be a difficult disease to diagnose. Sharlene A. Teefey (University of Washington and Veterans Administration Medical Center, Seattle) reported a study in which 27 patients with gangrenous cholecystitis were examined by sonography (24) and/or CT (seven). Of these 27 patients, 11 failed to show two or more of the disease's accepted clinical manifestations (abdominal pain, abdominal tenderness, fever, and leukocytosis). Acute cholecystitis was suggested first with sonography or CT in five of these 11 patients; striation of the gallbladder wall (seen in seven of 20 patients with wall thickening) may be a new sign indicative of gangrenous cholecystitis.

A study of the mechanism of cholecystokinin-octapeptide (CCK-OP) contraction of the opposum gallbladder was described by W. J. Dodds (the 1990 Walter B. Cannon medalist). Research at his institution (Medical College of Wisconsin, Milwaukee) indicated that the gallbladder contraction after infusion of CCK-OP was due to the action of CCK on cholinergic nerves (rather than to its action on the smooth muscle of the gallbladder, as was previously believed).

With the relatively recent advent of lithotripsy and bile acid therapy, much research has been performed and reported on gallstone treatment. In his presentation during a categorical course, Joseph F. Simeone emphasized that the "innocent" (or "silent") gallstone is not a myth; in a study of 103 subjects with gallstones, follow-up studies of up to 24 years showed that only 18% ever experienced any biliary pain.

In another categorical course, Eric vanSonnenberg (University of California, San Diego, Medical Center) reviewed recommendations for use of gallstone dissolution agents: (1) for few or multiple small stones, percutaneous dissolution may be an effective treatment; (2) methyl *tert*-butyl ether (MTBE) is good for dissolving "floating" (cholesterol) stones; (3) for stones with heavy calcium, dilatation of the tract followed by breakup and removal of the stone works better than does MTBE dissolution; (4) MTBE dissolution may be tried first with a stone that has a calcium nidus (MTBE dissolution can be followed by flushing or basketing of remaining fragments); (5) MTBE is an effective agent for dissolving intrahepatic stones and single or multiple large cholesterol stones; and (6) for stones in common duct obstruction, monooctanoin is preferred to MTBE as the dissolution agent. Dr. vanSonnenberg also gave guidelines for percutaneous gallstone dissolution (obtain a CT scan of the area before attempting dissolution; use a transhepatic approach and a small [5–7 French] catheter; and immediately stop the MTBE procedure if the patient becomes confused or sleepy, if MTBE can be smelled on the patient's breath, or if a net loss of MTBE is observed).

In the report of a recent project, Dr. vanSonnenberg stated that data showed no definite histopathologic effect on MTBE on the gallbladder wall. The study included 30 patients who underwent percutaneous cholecystostomy before MTBE therapy and 92 others who had percutaneous cholecystostomy for other reasons. In six of 30 MTBE patients, reversible thickening of the gallbladder occurred either during or within 5 days of therapy. In the three MTBE patients for whom histopathologic results were available (i.e., the patients underwent cholecystectomy), the mucosa was shown to be intact and without ulceration.

Two other studies on gallstone treatment were presented. Sanjay Saini and colleagues (Massachusetts General Hospi-

CENTRAL

tal, Boston) compared MTBE, monooctanoin, and sequential combination dissolution of stones shown to be calcified on radiographs. Twelve densely opaque gallstones were suspended in solvent for a total of 24 hr (the suspension technique kept the stones away from any mechanical destructive forces). MTBE used alone was found to be the most effective dissolution technique for calcified stones (decrease in stone weight: 82% for MTBE, 22% for monooctanoin, and 32% for MTBE/monooctanoin sequence).

Piezoelectric lithotripsy for gallstones was discussed by R. L. Baron (University of Washington, Seattle). In the past year, Baron and colleagues treated 37 patients with lithotripsy plus adjuvant ursodeoxycholic acid therapy; complete disappearance of stones was achieved in 37% of all patients (50% of those with one stone and 20% of those with two or three stones). Complications of the piezoelectric lithotripsy included colic, nausea, diarrhea, pancreatitis, petechiae, and hematuria. However, Baron sees this method as an effective, relatively painless treatment for patients who have a functioning gallbladder and a few gallstones that are small, symptomatic, and noncalcified.

Four presentations focused on gallstone imaging. In a prospective study of 30 consecutive patients, P. M. Bret and colleagues (Montreal General Hospital, Montreal, Quebec, Canada) used preoperative sonography to count and measure gallstones before elective cholecystectomy. Surgical results showed that sonography counted gallstones correctly in 27 of 30 patients (if more than five gallstones were imaged, the count was recorded as "more than five"). Stones were sized correctly (within 2 mm) in 89% of cases. Smaller stones tended to be overestimated and larger stones were underestimated. Another sonographic study, however, showed less accurate results: James A. Brink (Massachusetts General Hospital, Boston) presented in vitro data that indicate that accuracy of sonography in measuring stone fragments after lithotripsy can be as low as 60% because the fragments are admixed with debris and sludge. Discussion after Dr. Brink's presentation suggested that "physical agitation" of patients may separate fragments from debris and result in higher sonographic accuracy.

Frederick J. Schwab and colleagues (George Washington University, Washington, DC) imaged 111 human gallstones with plain film, CT, and sonography to find possible correlations between image characteristics and lithotripsy fragmentation time. No correlation was found between fragmentation and any radiologic characteristic or chemical composition, but significant correlations were found between fragmentation time and both size and weight of gallstones. Schwab suggested that calcification may not be an appropriate criterion for excluding lithotripsy in gallstone treatment.

In 1989, the group led by Richard L. Baron was given the SGR Research Award to aid their studies of CT of gallstones. In his summary report, Dr. Baron described the development of a body/gallbladder phantom to improve CT of gallstones in vitro. Results of the phantom's use for CT of 51 gallstones in vitro indicate no statistically significant correlation between CT appearance and fragmentation. However, tunable-dye laser lithotripsy of 27 gallstones in vitro (nine rimmed, nine dense, and nine faint) resulted in the surprising finding that CT can predict the number of pulses and energy needed for fragmentation.

Hepatic and Pancreatic Radiology

Three studies were presented comparing different imaging methods in hepatic disease. Bernard A. Birnbaum (NYU Medical Center, New York) discussed a blinded retrospective study comparing the diagnosis of hepatic hemangiomas with MR imaging and ^{99m}Tc-labeled RBC single-photon emission CT (^{99m}Tc-SPECT). Thirty-seven patients with 69 suspected lesions underwent MR imaging and ^{99m}Tc-SPECT. In the diagnosis of hepatic hemangiomas, MR imaging had a 91% sensitivity, 90% accuracy, and 80% specificity, compared with SPECT's 78% sensitivity, 80% accuracy, and 100% specificity. Dr. Birnbaum concluded that ^{99m}Tc-SPECT is the method of choice for diagnosis of hepatic hemangiomas, although MR imaging is best for imaging lesions that are small (<1.9 cm), near the dome of the liver, or adjacent to intrahepatic vessels.

Another hepatic imaging study was presented by William J. Miller (University of Pittsburgh, Pittsburgh, PA). Miller and colleagues compared results of CT and sonographic studies obtained before liver transplantation in 30 patients with hepatocellular carcinoma. Both types of studies missed some small tumors; altogether, CT showed 13 of 15 tumors, and sonography showed only eight. Also, CT indicated vascular invasion in 10 of 18 cases, whereas sonographic findings were suggestive of invasion in only four cases.

Dr. Miller also reported a study of CT, MR, and sonographic findings in Budd-Chiari syndrome. All 15 patients in the study underwent CT and Doppler sonography; 13 had MR studies. Based on pathologic findings, obstruction of the hepatic veins was correctly identified by MR imaging in 11, by sonography in nine, and by CT in five (eight CT examinations were indeterminate). However, CT was most effective in detecting the 15 liver parenchymal abnormalities (CT detected 14; MR, six; and sonography, 11).

CT of the pancreas was the subject of two presentations. E. J. Balthazar (NYU Medical Center, New York) discussed use of a CT severity index to stage acute pancreatitis on the basis of pancreatic necrosis and peripancreatic inflammation and collections. He and his colleagues found that patients with a high value on the CT severity index (>7 on a 1–10 scale) had a morbidity rate of 92% and a mortality rate of 17%, compared with a morbidity rate of 2% and mortality rate of 0% in patients with low values (0–2) on the same CT severity index.

Ruedi R. Thoeni (University of California, San Francisco, School of Medicine) presented a study of CT findings in 15 patients with pancreatic ampullary tumors and 14 with invasive pancreatic carcinomas (13 pancreatic carcinomas and one islet cell carcinoma). The results indicate that the CT features that distinguish the ampullary tumors from invasive carcinoma are density differences between the ampulla and the pancreas, extension of the dilated common bile duct into the ampulla as well as separation of the ampullary mass from the pancreas (both of which occur more often in ampullary tumors). However, dilatation of the biliary tree was seen in all patients and thus is not an accurate criterion to distinguish these two types of tumors.

Imaging of Colon and Bowel Disease

Many presentations concerned diseases of the gastrointestinal tract. Some dealt with the controversial issue of the most effective screening and diagnostic techniques for detecting colon cancer. In others, investigators discussed imaging of pneumatosis of intestinalis, gastrointestinal graft-vs-host disease, sigmoid diverticulitis, intestinal obstruction, and sigmoid polyps.

Colon Cancer

Because 50% of colon cancers recur, and resection of hepatic metastases improve 5-year survival rate (and resection of extrahepatic metastases may improve 5-year survival rate), detection of recurrent tumor is an important focus of research. W. F. Bennett (Ohio State University Hospitals) found that, in 13 of 22 patients studied, positive CT findings of recurrent malignant tumors were confirmed surgically. Moreover, preoperative CT findings benefited patients undergoing surgery by shortening surgery (there were seven cases in which negative CT findings increased confidence in negative surgical findings), by defining grossly positive areas as areas of surgical interest (three cases), and by guiding the surgeon to a deep liver lesion (one case). Moreover, positive CT findings led the surgeon to areas of recurrence in three patients in whom other test results and direct inspection were negative, and grossly positive CT findings obviated laparotomy in five patients. Another study, presented by G. Torres (University of Florida, Gainesville) showed that high-frequency sonography correlated perfectly with pathology in identifying tumor extension in seven patients with colorectal or gastric adenocarcinoma.

A two-session panel discussion on colon cancer highlighted the importance of this disease and the controversial imaging issues concerning its diagnosis. Richard Hunt (McMaster University Medical Centre, Hamilton, Ontario, Canada) cited U.S. incidence and prevalence rates of colon cancer at 70/100,000 and 75/100,000, respectively; he also listed the predisposing factors, including inherited, behavioral, and environmental factors. The screening methods available include fecal occult blood tests, single- and double-contrast barium enema, flexible sigmoidoscopy, and colonoscopy. The effectiveness of these various methods was the topic of spirited discussion. Giles Stevenson (McMaster University Medical Centre, Hamilton, Ontario, Canada) suggested that using flexible sigmoidoscopy first can direct cases without adenoma to studies by double-contrast barium enema and cases with adenomas to colonoscopy (during which detected polyps can be removed). David Gelfand (Bowman Gray School of Medicine, Winston-Salem, NC) disagreed with the panel's emphasis on endoscopic techniques and stated that use of sigmoidoscopy had failed to make any progress in the detection of colon cancer. All participants agreed that any of these methods can be valuable for detecting colon cancer if it is performed expertly.

In regard to preoperative screening of colorectal cancer patients, Dennis M. Balfe (Mallinckrodt Institute of Radiology, St. Louis, MO) believes that CT and MR of the liver may identify metastatic tumors at an operable stage and also may indicate when partial hepactectomy (which in itself has significant morbidity and mortality) is not indicated. The problem with CT and MR (as well as other models such as positron-emission tomography and monoclonal antibody imaging) is that they are not nearly as effective in diagnosing extrahepatic lesions. Finding a method that can precisely identify which patients will most benefit from hepatic surgery is an important challenge.

Dr. Hunt discussed the various methods of colorectal cancer screening, including barium enema, colonoscopy, CT, and MR imaging. He posed six questions that should be asked about each method and screening protocol: (1) What benefits accrue from this type of screening? (2) Who is in the high-risk category? (3) How sensitive and specific is the screening method or protocol? (4) Are accurate diagnoses and effective therapies available if this cancer is found? (5) Will the screening test be well accepted by patients? and (6) Is this screening method or protocol cost-effective?

Other Gastrointestinal Diseases

In a prospective evaluation of 27 patients with pneumatosis intestinalis, Mark Baker and colleagues (Duke University, Durham, NC) determined if any clinical, radiologic, or laboratory findings can be used to differentiate patients with pneumatosis caused by ischemia from those in whom the pneumatosis is due to more benign diseases. Radiologic studies were assessed for location and duration of the pneumatosis, a detectability index (on a scale of 1–3), appearance on plain film, and portal venous gas. No radiologic feature distinguished the 10 patients with ischemia from the others. The conclusion was that decisions about the need for surgery should be based on the severity of the patient's symptoms.

R. A. Halvorsen, Jr. (University of Minnesota Medical Center, Minneapolis), presented a study on gastrointestinal graft-vs-host disease (GVHD), in which the CT scans of 42 patients with biopsy-proved GVHD and 31 control subjects were evaluated. A significant relationship was found between colon wall thickening and GVHD: colon wall thickening was seen in 19% of the GVHD patients and in only 3% of the control subjects. Two conclusions were drawn about criteria for the diagnosis: (1) thickening of the colon wall that involved more than 10% of the colon had high sensitivity (100%) but low specificity (29%) and (2) colon wall thickening seen on two or more CT slices had low sensitivity (32%) and high specificity (94%).

In a prospective study of 56 hospitalized patients with suspected sigmoid diverticulitis, Kyunghee C. Cho and colleagues (Albert Einstein College of Medicine, Bronx, NY) compared the diagnostic values of CT and barium enema. The interpreters were not blinded to the final diagnosis. Both CT and barium enema proved to be effective methods (correct diagnoses of diverticulitis: CT, 93%; barium enema, 80%); however, CT was superior to barium enema in its ability to recognize other conditions that mimicked diverticulitis clinically.

Three studies concerned intestinal obstruction. P. Shrake (Indiana University School of Medicine, Indianapolis) described a blinded study of 117 consecutive patients with suspected small-bowel obstruction. In patients with varying degrees of small-bowel obstruction, plain films may be misleading (only 38% of the radiographs correctly indicated the level of obstruction); however, enteroclysis accurately predicted the level and cause of the obstruction (89% of predictions of level and 79% of predictions of cause were proved correct). In a study presented by Dean Maglinte and colleagues (Methodist Hospital of Indiana, Indianapolis), 27 patients with closed-loop bowel obstruction were evaluated. Their study indicated that closed-loop obstruction does not always indicate strangulation; these workers recommend routine use of small-bowel enteroclysis in patients with suspected obstruction who are being managed medically. Two of 27 patients in their study improved with medical management and avoided surgery. Finally, Robert Fulbright (St. Luke's-Roosevelt Hospital Center, New York) presented a study in which barium enema and colonoscopy were compared in the evaluation of constricting lesions of the colon in 80 patients. These investigators found that (1) the entire colon could be evaluated by barium enema in 65% of the cases and by colonoscopy in 17% (but in only 4% of those with constricting lesions on the left side); (2) if the lesion obstructs the flow of barium, it also obstructs the colonoscope; (3) if the constricting lesion is in the left side of the colon, colonoscopy did not result in any change in therapy; and (4) colonoscopic results may help make decisions about therapy if the lesion is on the right side.

S. Somers (McMaster University Medical Centre, Hamilton, Ontario, Canada) presented a study of 269 patients with sigmoid polyps who underwent flexible sigmoidoscopy before barium enema. He and his colleagues recommend the use of flexible sigmoidoscopy or a combination of sigmoidoscopy and barium enema, because use of barium enema alone had missed 71% of the significant sigmoid polyps (5–10 mm). Other reasons cited for using flexible sigmoidoscopy or the combination approach were reduction of radiation to the patient, reduction in cost (fewer colonoscopies would be needed), convenience for the patient (one preparation and one visit for both studies), and ease of learning how to perform an effective sigmoidoscopy.

A retrospective study of 33 cases of inflammatory fibroid polyps of the gastrointestinal tract was discussed by R. K. Harned (Armed Forces Institute of Pathology, Washington, DC). All the inflammatory fibroid polyps studied originated in the submucosa and were composed of fibroblasts, inflammatory cells, and a network of blood vessels; all were benign. Although these polyps appear to have no distinct radiologic appearance, the characteristic demographics (20 women, 13 men; average age, 45 years); clinical symptoms (abdominal pain and evidence of blood loss); and polyp composition may help prevent misdiagnosing such polyps as a malignant condition.

New Technology in Gastrointestinal Radiology

C. John Rosenquist (University of California, Davis, School of Medicine, Sacramento) moderated two panel discussions focused on new technology: "Abdominal MRI—Present and Future" and "Digital Imaging for the GI Radiologist." In his introductory remarks, Dr. Rosenquist noted that MR has been "the radiology development of the 1980s" and that digital imaging may well be "the radiology development of the 1990s."

Henry I. Goldberg (University of California, San Francisco, School of Medicine) presented the clinician's view of abdominal MR imaging by posing questions to an industry representative, S. Morry Blumenfield of General Electric Medical Systems (Milwaukee, WI). In answering Dr. Goldberg's questions, Dr. Blumenfield noted that, although MR images of the abdomen are still not equal in quality to CT images, we now can talk realistically about "MR of the abdomen." Dr. Blumenfield described the techniques that are being used to overcome motion problems: cardiac gating, phase encoding, spatial presaturation, and gradient-moment nulling. Adaptive moment correction and echoplanar imaging are two techniques that may be used in the future. Other new developments that may improve the quality of abdominal MR imaging include "spoiled" GRASS, chemical saturation, new contrast media, new surface-coil imaging techniques, and fluoroscopic MR imaging.

Three speakers discussed the future of digital imaging. Ronald P. Schwenker (Du Pont Medical Products, Wilmington, DE) talked about picture archiving and communications systems (PACS). The driving forces behind the development of these systems include the needs for better diagnostic information, better communication, increased convenience, better archive integrity, and increased revenue generation. The relatively slow development of efficient systems is due to the problems of high start-up cost; slow technologic improvements; and less than optimal image quality, system reliability, and overall productivity.

Kal Vizy (Eastman Kodak Company, Rochester, NY) stated that the processing, archiving, and hard-copy technologies are already established for an effective digital system. However, implementation of such systems is hampered by the problems of noncompatibility of systems and by the disappointing delays in the development of television monitors of sufficiently high resolution. Dr. Vizy predicts that radiologists may prefer use of hard copies for some time to come and that those films may be improved by the advent of laser scanner-based imagers.

Finally, Jean-Pierre Georges (General Electric Medical Systems) emphasized that the purpose of a digital image is *not* at this time to replace films. Rather, the digital image can provide immediate review and analysis, help guide the radiologist as the filming proceeds, simplify procedures and thus increase throughput, and increase the quality of image reproducibility, image archiving, and interdepartmental communication. Dr. Georges described two presently available digital imaging approaches: storage phosphor-based computer radiology (particularly applicable in intensive care and critical care units) and digital photospot imaging (most applicable when low-dose radiation is appropriate). The ideal digital imaging system was described as one that would provide a large image (14 × 17 in., like films themselves); fast, low-dose fluoroscopy; very high resolution (2000 × 2000 or even 4000 × 4000 pixels); user-friendly software; reliability; affordable peripheral systems; and cost-effectiveness.

ARRS Case of the Day

The answers to the Case of the Day exhibit at the 1990 American Roentgen Ray Society meeting in Washington, DC, are presented on the following pages. The original images, shown at the meeting and published in the April issue of the *AJR*, are reproduced along with supplementary illustrations and explanatory comments.

The cases were taken from the teaching files of the Departments of Radiology at Georgetown University Medical Center and at the National Naval Medical Center, Bethesda, MD. The authors are members of the faculty at Georgetown University School of Medicine, the Uniformed Services University of the Health Sciences, and the Armed Forces Institute of Pathology.

As the coordinator of this year's Case of the Day series, I thank the contributing authors for their cooperation and preparation of the cases and their respective secretaries for complying with my requests. I also thank the editorial staff of the *AJR* for their guidance and patience during the manuscript preparation.

I hope you found these cases challenging and educational. Congratulations to those who diagnosed the abnormalities correctly.

Margaret A. Stull
Department of Radiology
Georgetown University School of Medicine
Washington, DC 20007

Chest Case of the Day

Margaret A. Stull,[1] Letitia R. Clark,[1] Kathleen Reagan,[1] Curtis E. Green,[1] Cynthia M. Tracy,[2] Pamela W. Goose,[1] Paul V. Suhocki,[1] and Homer L. Twigg[1]

Case 1: Bronchoalveolar Carcinoma of the Lung

This 37-year-old man with a history of IV drug abuse had a 2-month history of dyspnea on exertion, fevers, sweating, coughing, and more recent onset of pleuritic chest pain. Physical examination was remarkable for a few fine rales on lung auscultation and a low-grade fever. Chest radiographs (Figs. 1A and 1B) showed bilateral mixed interstitial and acinar infiltrates with a focus of coalescence in the superior segment of the left lower lobe. The patient was admitted to the hospital with a tentative diagnosis of *Pneumocystis carinii* pneumonia complicating AIDS. He was treated with IV Bactrim (Roche, Nutley, NJ). The next morning, fiber-optic bronchoscopy revealed diffuse carbonaceous material in all lung fields. Transbronchial biopsy and bronchoalveolar lavage were performed. Results of lavage and human immunodeficiency virus antibody testing were negative, which made *Pneumocystis carinii* pneumonia less likely, leading to a second tentative diagnosis of aspiration pneumonia. Four days after admission, histologic examination of the transbronchial biopsy specimen revealed bronchoalveolar carcinoma. Subsequent CT scans (Figs. 1C and 1D) showed a heterogeneous mass with pleural tags in the left lower lobe superimposed on a background of bilateral mixed interstitial and acinar infiltrates.

Bronchoalveolar carcinoma of the lung is the least common (5–10%) [1–3] but perhaps the most controversial of all the lung cancers. Unlike other forms of lung cancer, a clear association with smoking has not been established [4]. Most series suggest a small percentage of cases are associated with a local parenchymal scar [2, 4, 5]. No correlation has been found between the patient's age, sex, smoking history, or occupational exposure and the occurrence or outcome of disease [4].

Symptoms depend on the stage of the lesion. Patients with peripheral solitary lesions are frequently asymptomatic (45–58%). Consequently, the tumor is found on routine chest radiographs. Less commonly, patients with solitary masses display coughing, dyspnea, or weight loss [2, 4]. Patients with diffuse disease generally complain of coughing, weight loss, chest pain, and dyspnea. Bronchorrhea is thought to be classic, but usually indicates extensive lung disease [5].

The neoplasm consists of columnar or cuboidal cells that invade the alveolar spaces [1]. Solitary lesions of bronchoalveolar carcinoma are confined to one lobe with no central adenopathy. These lesions are generally located peripherally, and range in size from 0.8 to 4.0 cm. Solitary lesions have a prolonged latent period and may be confused with benign disease because of their tendency to remain unchanged for years before spreading [4–6]. Hilar and mediastinal metastases are infrequent (18%) [6]. A solitary lesion that is less than 3 cm in diameter is expected to be cured by surgical resection in over 70% of patients [6]. Confluent disease is most likely the source of disseminated spread [3–6]. A dominant mass within diffuse disease is present in 89% of cases and is most likely the original tumor [6]. The mechanism of diffuse bilateral involvement is direct aerial spread through the bronchoalveolar tree. This spread is aided by tumor cells that produce mucus. Distant metastases are produced by lymphatic and hematogenous spread [6, 7]. The prognosis for patients with diffuse disease is poor, generally with less than 3 years survival. Unfortunately, this tumor is resistant to radiotherapy and chemotherapy [7].

The spectrum of radiologic findings is broad, ranging from solitary to diffuse disease. Air bronchogram is a common feature within the affected area. The margins of solitary lesions are irregular and are frequently associated with linear fibrous strands extending to the pleura (Fig. 1D) [2–6]. These pleural tags are ascribed to a desmoplastic host reaction to neoplasm [2, 3, 5, 6]. Although pleural tags can be seen in granulomatous disease, their association with air bronchograms is highly suggestive of bronchoalveolar carcinoma. On CT, heterogeneous attenuation within the mass can be present (Fig. 1C) [3]. The radiologic appearance of diffuse bronchoalveolar carcinoma is nonspecific and is frequently confused with inflammatory, granulomatous, or vascular conditions [1]. The basic radiologic manifestation is acinar shadows that are discrete or coalesce into an area of consolidation.

---

[1] Department of Radiology, Georgetown University Medical Center, 3800 Reservoir Rd., N.W., Washington, DC 20007. Address reprint requests to M. A. Stull.
[2] Division of Cardiology, Department of Medicine, Georgetown University Medical Center, 3800 Reservoir Rd., N. W., Washington, DC 20007.

***AJR* 154:1318–1324, June 1990** 0361–803X/90/1546–1318 © American Roentgen Ray Society

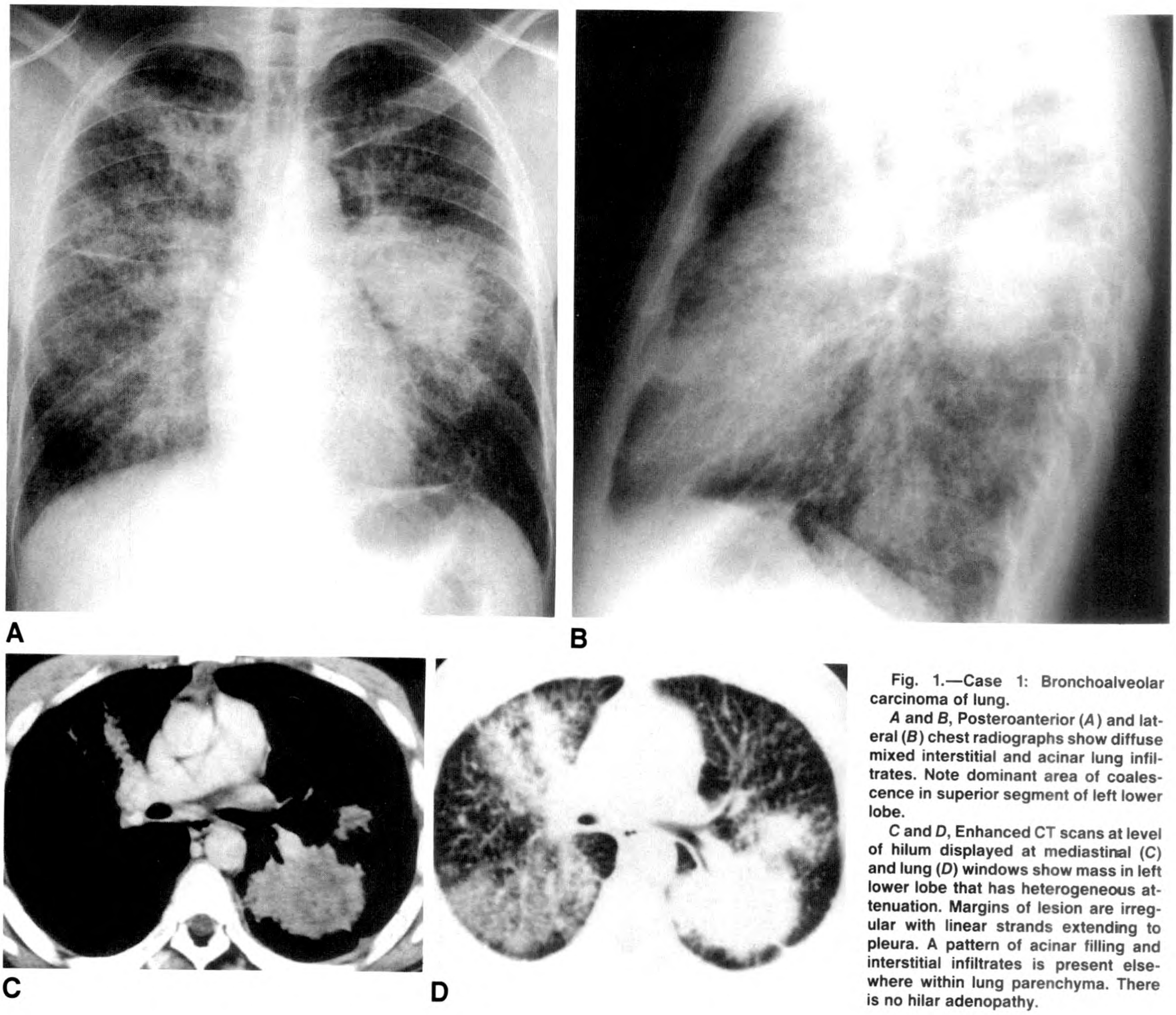

Fig. 1.—Case 1: Bronchoalveolar carcinoma of lung.

A and *B*, Posteroanterior (*A*) and lateral (*B*) chest radiographs show diffuse mixed interstitial and acinar lung infiltrates. Note dominant area of coalescence in superior segment of left lower lobe.

C and *D*, Enhanced CT scans at level of hilum displayed at mediastinal (*C*) and lung (*D*) windows show mass in left lower lobe that has heterogeneous attenuation. Margins of lesion are irregular with linear strands extending to pleura. A pattern of acinar filling and interstitial infiltrates is present elsewhere within lung parenchyma. There is no hilar adenopathy.

The spectrum of radiologic manifestations of bronchoalveolar carcinoma of the lung simulates that of many other diseases. Awareness of these patterns and of the slow-growth characteristics of this tumor will help suggest the diagnosis.

Letitia R. Clark
Margaret A. Stull
Homer L. Twigg

REFERENCES

1. Berkmen YM. The many facets of alveolar-cell carcinoma of the lung. *Radiology* **1969**;92:793–798
2. Edwards CW. Alveolar carcinoma: a review. *Thorax* **1984**;39:166–174
3. Kuhlaman JE, Fishman EK, Kuhajda FP, et al. Solitary bronchioalveolar carcinoma: CT criteria. *Radiology* **1988**;167:379–382
4. Greco RJ, Steiner RM, Goldman S, Cotler H, Patchefsky A, Cohn HE. Bronchoalveolar cell carcinoma of the lung. *Ann Thorac Surg* **1986**;41:652–656
5. Fraser RG, Paré JAP. Malignant neoplasms: bronchiolar (alveolar cell) carcinoma. In: *Diagnosis of diseases of the chest*, 2nd ed. Philadelphia: Saunders, **1977**:1055–1072
6. Hill CA. Bronchoalveolar carcinoma: a review. *Radiology* **1984**;150:15–20
7. Metzger RA, Mulhern CB, Arger PH, Coleman BG, Epstein DM, Gefter WB. CT differentiation of solitary from diffuse bronchoalveolar carcinoma. *J Comput Assist Tomogr* **1981**;5:830–833

Case 2: Tetralogy of Fallot with Pulmonary Atresia (Pseudotruncus Arteriosus)

This 44-year-old woman had a long history of progressive shortness of breath and recent development of cardiac arrhythmias. She had no history of surgery. Chest radiographs (Figs. 2A and 2B) showed a mildly enlarged heart and marked prominence of the thoracic aorta, primarily in its ascending portion. The aortic arch was on the left. The pulmonary trunk

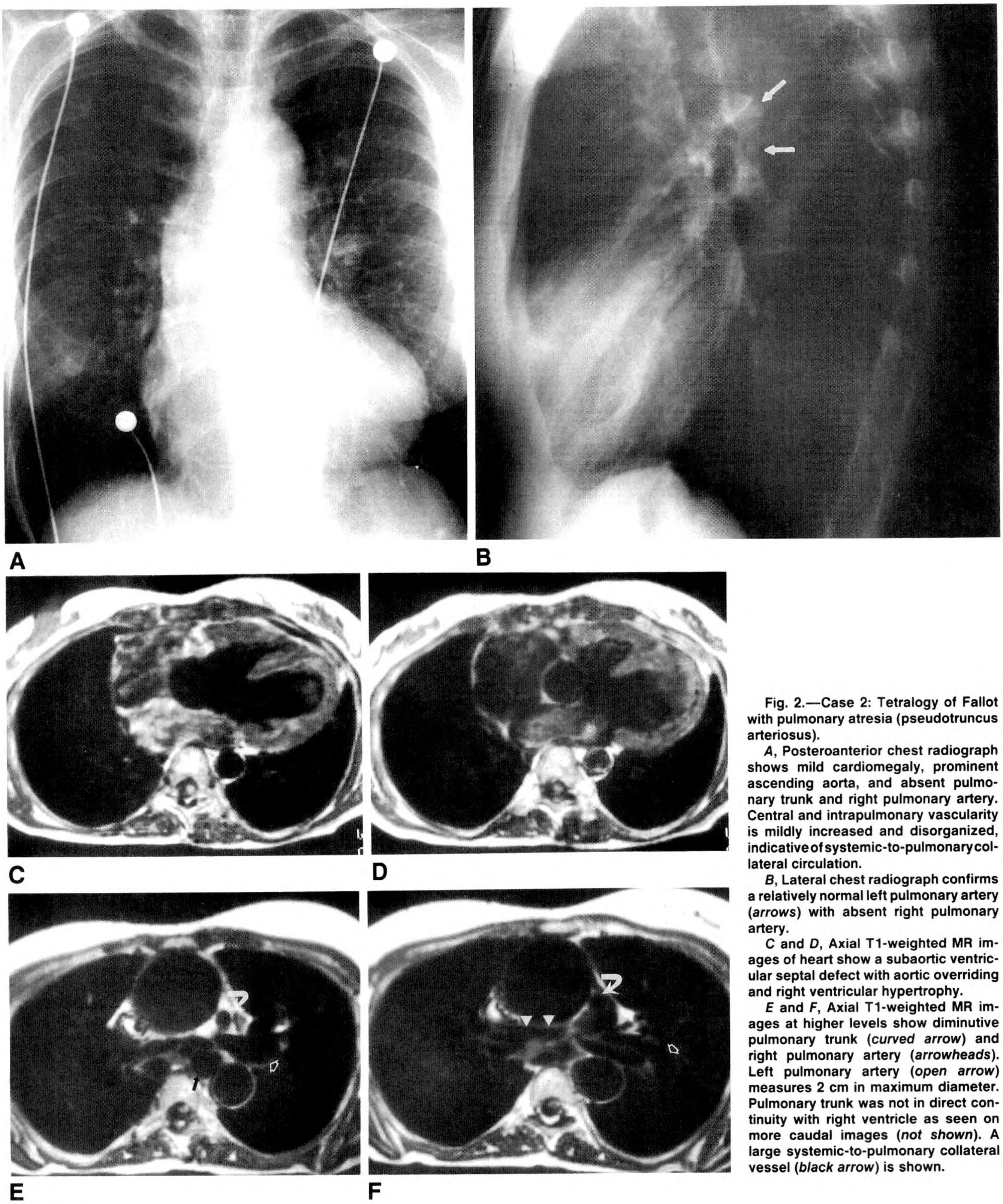

Fig. 2.—Case 2: Tetralogy of Fallot with pulmonary atresia (pseudotruncus arteriosus).

A, Posteroanterior chest radiograph shows mild cardiomegaly, prominent ascending aorta, and absent pulmonary trunk and right pulmonary artery. Central and intrapulmonary vascularity is mildly increased and disorganized, indicative of systemic-to-pulmonary collateral circulation.

B, Lateral chest radiograph confirms a relatively normal left pulmonary artery (*arrows*) with absent right pulmonary artery.

C and *D*, Axial T1-weighted MR images of heart show a subaortic ventricular septal defect with aortic overriding and right ventricular hypertrophy.

E and *F*, Axial T1-weighted MR images at higher levels show diminutive pulmonary trunk (*curved arrow*) and right pulmonary artery (*arrowheads*). Left pulmonary artery (*open arrow*) measures 2 cm in maximum diameter. Pulmonary trunk was not in direct continuity with right ventricle as seen on more caudal images (*not shown*). A large systemic-to-pulmonary collateral vessel (*black arrow*) is shown.

and right pulmonary artery were conspicuously absent; the left pulmonary artery shadow was relatively normal. Pulmonary vascularity was mildly increased and "disorganized" both centrally and peripherally, consistent with systemic-to-pulmonary collaterals. Axial MR images at the ventricular level (Figs. 2C and 2D) showed a large subaortic ventricular septal defect (VSD), with the aorta overriding the VSD. The thickness of the right ventricular wall approached that of the left ventricular wall, consistent with right ventricular hypertrophy. MR images obtained at more cephalic levels (Figs. 2E and 2F) showed dilatation of the ascending aorta (5 cm in maximal diameter) and a diminutive pulmonary trunk, which on more caudal images (not shown) was not continuous with the right ventricular infundibulum. The right and left pulmonary arteries appeared confluent. A well-developed systemic-to-pulmonary collateral vessel was seen. The left and right main pulmonary artery segments measured 2 cm and 1 cm, respectively. These MR images confirmed the findings on chest radiographs of the inapparent pulmonary trunk and right pulmonary artery.

A subaortic VSD, biventricular origin of the aorta, pulmonary atresia, and systemic-to-pulmonary collateral circulation characterize the severe form of tetralogy of Fallot (TOF) [1]. This entity is also commonly referred to as pseudotruncus arteriosus because only a single arterial trunk is present. The anatomic left and right pulmonary arteries (even though they may be small) also are present [2]. The basic physiology of VSD with pulmonary atresia mandates an alternative pulmonary blood supply, which may arise from a variety of sources: well-developed systemic-to-pulmonary collateral arteries; the ductus arteriosus; well-developed bronchial collateral arteries; innumerable, small systemic collateral vessels in an epibronchial or pleural distribution; or a combination of these [3]. The systemic-to-pulmonary collaterals vary in number and usually arise from the proximal aspect of the descending thoracic aorta; it is less common to see their origin from the abdominal aorta, brachiocephalic vessels, or coronary-to-pulmonary fistulas. Surgically created systemic-pulmonary arterial shunts are additional important routes of alternative pulmonary blood supply.

As TOF is one of the more common forms of cyanotic congenital heart disease, and advancements in surgical palliation and correction have resulted in improved survival of patients [4], thorough and accurate evaluation of intracardiac and extracardiac lesions is required. MR imaging has been shown to complement cardiac catheterization and cineangiography in the diagnosis of TOF [4, 5]. It is an important tool in the evaluation of the integrity and condition of the main and central pulmonary arteries as well as the lobar branches. Pulmonary blood flow is the main determinant for pulmonary arterial growth. Early surgical construction of a systemic-to-pulmonary connection in hypoplastic, confluent pulmonary arteries may provide adequate blood supply for their progressive enlargement, making possible sufficient pulmonary artery size for potential surgical correction. The noninvasive nature of MR imaging lends itself to the examination of the pediatric TOF patient in whom serial cardiac examinations after correction are needed. In adults, MR may be the imaging technique of choice to determine the presence or absence of confluent central pulmonary artery segments. Pulmonary artery and systemic-to-pulmonary collateral delineation by MR would avoid the inherent risks of selective catheterization and/or injection of contrast material into the pulmonary circulation of patients who may be nearly hypoxemic and prone to spells. Mirowitz et al. [4] note that MR is unlikely to replace cardiac catheterization in the initial examination of TOF patients, because of its inability to define coronary artery anomalies, which occur with a frequency of 4% to 11%. Furthermore, visualization of the pulmonary arteries in some cases of TOF with pulmonary atresia can be achieved only by selective injection of the systemic-to-pulmonary collaterals by using axial cineangiographic techniques, or by pulmonary vein wedge injections [6].

Other cyanotic congenital heart defects that mimic TOF clinically and radiologically include complete transposition with VSD and pulmonary atresia, double-outlet right (or left) ventricle with VSD and pulmonary atresia, single ventricle with VSD and pulmonary atresia, and corrected transposition with VSD and pulmonary atresia [7].

Kathleen Reagan
Curtis E. Green
Cynthia M. Tracy

REFERENCES

1. Soto B, Pacifico AD, Luna RF, Bargeron LM. A radiographic study of congenital pulmonary atresia with ventricular septal defect. *AJR* **1977**; 129:1027–1037
2. Pacifico AD, Kirklin JW, Bargeron LM, Soto B. Surgical treatment of common arterial trunk with pseudotruncus arteriosus. *Circulation* **1974**;49/50[suppl. II]:II-20–II-26
3. Liao PK, Edwards WD, Julsrud PR, Puga FJ, Danielson GK, Feldt RH. Pulmonary blood supply in patients with pulmonary atresia and ventricular septal defect. *J Am Coll Cardiol* **1985**;6:1343–1350
4. Mirowitz SA, Gutierrez FR, Canter CE, Vannier MW. Tetralogy of Fallot: MR findings. *Radiology* **1989**;171:207–212
5. Formanek AG, Witcofski RL, D'Souza VJ, Link KM, Karstaedt N. MR imaging of the central pulmonary arterial tree in conotruncal malformation. *AJR* **1986**;147:1127–1131
6. Diethelm E, Soto B, Nath PH, Bargeron LM, Kirklin JK. The pulmonary vascularity in patients with pulmonary atresia and ventricular septal defect. *RadioGraphics* **1985**;5:243–254
7. Elliott LP. Pathophysiology and roentgenologic findings in tetralogy of Fallot with pulmonary atresia. In: Taveras JM, Ferruci JT, eds. *Radiology: diagnosis, imaging, intervention,* rev. ed. Philadelphia: Lippincott, **1988**;2:1–4

Case 3: Metastatic Osteosarcoma to Lung

This 25-year-old man with osteosarcoma of the proximal right humerus (Fig. 3D) diagnosed 2½ years earlier was treated with disarticulation of the entire right upper extremity, scapula, and clavicle and adjuvant chemotherapy. Metastases subsequently developed in the left lung, and the patient underwent thoracotomy with resection of the tumor. His course was complicated by recurrent pleural effusions necessitating sclerotherapy. Recently, he complained of progressive dyspnea on exertion as well as back and left chest pain. He also experienced dysphagia for solids and liquids. On physical examination, the patient had mild tachycardia, tachypnea, and orthostatic hypotension. There was dullness to percussion over the left hemithorax and decreased breath sounds on the left side, sparing the apex. The left posterior chest wall was tender to palpation.

Chest radiographs (Figs. 3A and 3B) showed near complete

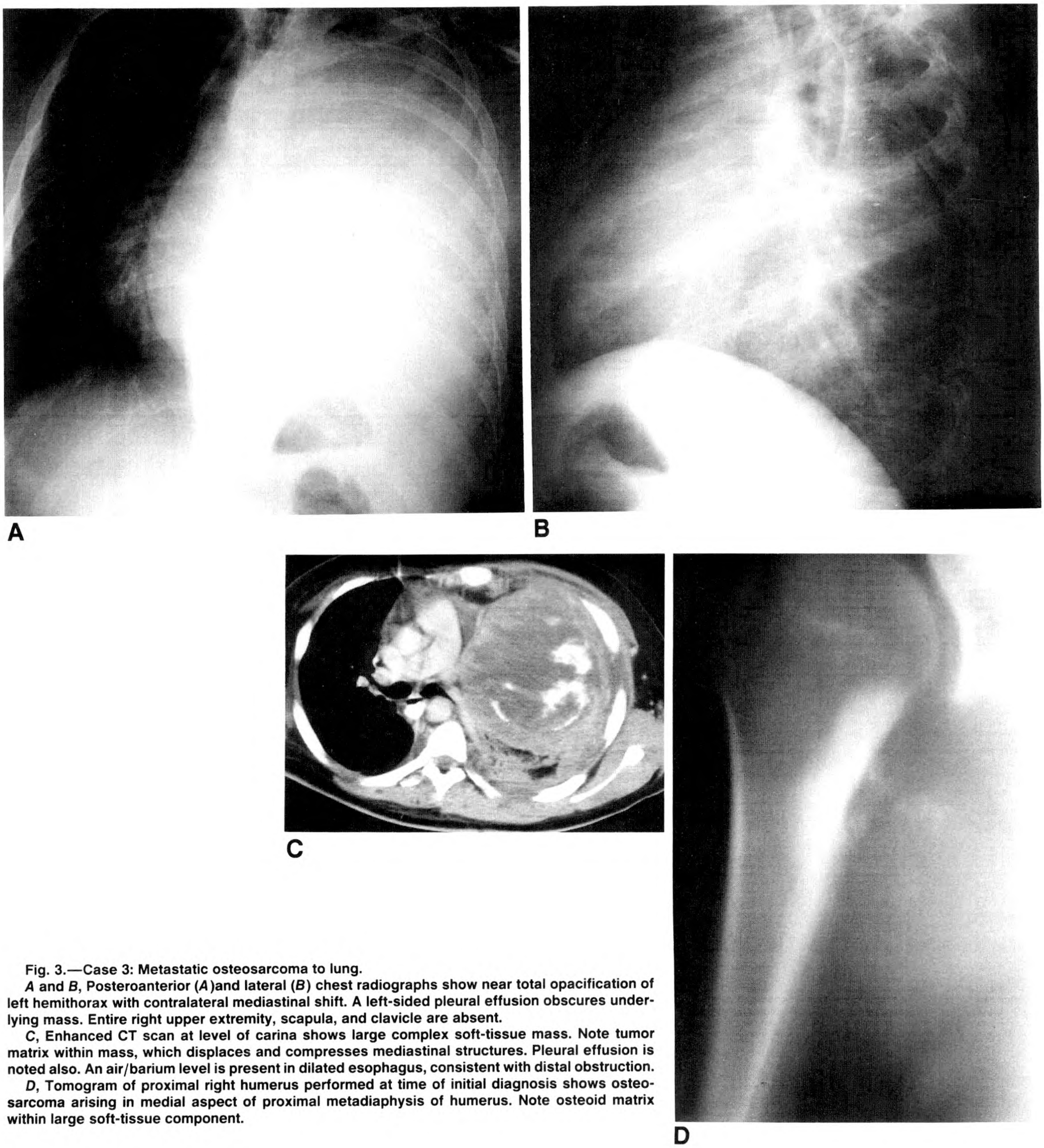

Fig. 3.—Case 3: Metastatic osteosarcoma to lung.

***A* and *B*, Posteroanterior (*A*)and lateral (*B*) chest radiographs show near total opacification of left hemithorax with contralateral mediastinal shift. A left-sided pleural effusion obscures underlying mass. Entire right upper extremity, scapula, and clavicle are absent.**

***C*, Enhanced CT scan at level of carina shows large complex soft-tissue mass. Note tumor matrix within mass, which displaces and compresses mediastinal structures. Pleural effusion is noted also. An air/barium level is present in dilated esophagus, consistent with distal obstruction.**

***D*, Tomogram of proximal right humerus performed at time of initial diagnosis shows osteosarcoma arising in medial aspect of proximal metadiaphysis of humerus. Note osteoid matrix within large soft-tissue component.**

opacification of the left hemithorax with marked shift of the mediastinum to the right. Right forequarter amputation was evident. Subsequent CT scanning of the thorax (Fig. 3C) revealed a large complex soft-tissue mass with intratumoral calcification and ossification filling the left hemithorax. Lower CT scans (not shown) showed compression and possible invasion of the esophagus and other mediastinal structures. Left pleural effusion also was identified.

Osteosarcoma is the most common primary malignant bone tumor in persons less than 30 years of age. The tumor usually arises in the metaphysis of long bones. The most common locations are the distal end of the femur (40%), the proximal tibia (16%), and humerus (15%) [1-3]. In patients over 35 years old, osteosarcoma arising in preexisting bone conditions, such as pagetoid or irradiated bone, is more common [1-3]. The flat bones, especially the ilium, are frequently involved in patients over 50 years old [2].

Osteosarcoma spreads by hematogenous dissemination. Pulmonary metastases are the most frequent. Patients may present with either a solitary pulmonary nodule, multiple nodules, a parenchymal mass, or large pleural effusion that obscures the underlying tumor. Spontaneous pneumothorax can be associated with lung metastases [1, 4, 5]. Death usually results from multiple pulmonary metastases. Histologically, metastases have a similar pathologic appearance to the primary tumor [5]. Ossification or calcification in lung metastases is believed to result from bone formation within the metastatic tumor [2].

Adjuvant chemotherapy, including preoperative and intraarterial chemotherapy, has resulted in prolonged survival [1, 4, 6]. Surgical excision of isolated pulmonary metastases also has improved survival [1-6].

Malignant effusion is the most common cause of unilateral opacified hemithorax with contralateral mediastinal shift. Large hemothorax, chylothorax, or empyema may produce similar thoracic alterations. Chest wall hematoma or collapsed lung can cause opacification of a hemithorax. The latter is associated with ipsilateral mediastinal shift. Intrathoracic tumors can attain large size when obscured by overlying pleural fluid, as in this case. Such masses arise from lung parenchyma, the mediastinum, or chest wall [7]. Benign tumors are less common than malignant tumors and are unlikely to have a large effusion. In adolescents and young adults, the differential considerations include Ewing sarcoma, lymphoma, and metastatic sarcoma [7]. The identification of the right forequarter amputation in a young adult with a large complex pulmonary mass with intratumoral ossification is consistent with the diagnosis of metastatic osteosarcoma.

Pamela W. Goose
Margaret A. Stull
Homer L. Twigg

REFERENCES

1. Resnick D, Kyriakos M, Greenway GB. Tumors and tumor-like lesions of bone: imaging and pathology of specific lesions. In: Resnick D, Niwayama G, eds. *Diagnosis of bone and joint disorders,* 2nd ed. Philadelphia: Saunders, **1988**:3648-3659
2. Edeiken-Monroe B, Edeiken J, Jacobson HB. Osteosarcoma. *Semin Roentgenol* **1989**;24:153-173
3. Unni KK, Dahlin DC. Osteosarcoma: pathology and classification. *Semin Roentgenol* **1989**;24:143-152
4. Hankins FD, DeSanto DA. Treatment of osteogenic sarcoma that had metastasized to the lungs. *West J Med* **1980**;132:245-248
5. Dunn D, Dehner LP. Metastatic osteosarcoma to lung: a clinicopathologic study of surgical biopsies and resections. *Cancer* **1977**;40:3054-3064
6. Carrasco CH, Charnsangavej C, Richli WR, Raymond AK, Wallace S, Benjamin RS. Osteosarcoma: interventional radiology in diagnosis and management. *Semin Roentgenol* **1989**;24:193-200
7. Cumming NA, Sabbah R. Large unilateral chest wall tumors in children. *J Can Assoc Radiol* **1985**;36:234-237

Case 4: Traumatic Pneumatocele

This previously healthy 17-year-old man sustained multiple injuries in a high-speed motor vehicle accident. His vital signs on admission to the emergency room were blood pressure 60 mm Hg/palpable, heart rate 120/min, and respiratory rate 24/min. Breath sounds were absent in the left hemithorax. A portable chest radiograph (not shown) revealed pneumothorax, a large pleural effusion, and rib fractures on the left side and bilateral atelectasis. After left-sided chest tube placement, abdominal CT (not shown) showed a fractured spleen, for which the patient underwent total splenectomy. A chest radiograph (Fig. 4C) obtained immediately after surgery showed extensive contusion in the left lung, persistent anterior pneumothorax, residual left-sided hemothorax, left-sided subcutaneous emphysema, and pneumomediastinum. In addition, an elongated, thin-walled, air-filled cavity, consistent with traumatic pneumatocele, was identified in the periphery of the left lung. Subsequent radiographs showed progressive resolution of the pulmonary contusion and persistence of the left lung cavity. Chest films (Figs. 4A and 4B) obtained before the patient was discharged from the hospital (9 days after surgery) showed the large left-sided traumatic pneumatocele.

Traumatic pneumatoceles represent air trapped within a pulmonary laceration [1-5]. Lung lacerations may result from perforation and penetrating injury or substantial blunt chest trauma, as in motor vehicle accidents [1-5]. The appearance on chest radiographs depends on the presence of blood and/or air trapped within the torn lung. Approximately half of lung lacerations appear as thin-walled, air-filled cavities (i.e., pneumatoceles) with or without air/fluid levels [1-3]. When blood is trapped within the torn lung (pulmonary hematoma), the laceration has a masslike appearance on chest radiographs [1, 3]. Traumatic pneumatoceles may appear immediately or within a few hours after injury. Lesions may be single or multiple, unilocular or multiloculated [1-3]. They are usually elliptical or spherical cavities, ranging from 2 to 14 cm in diameter. A subpleural, peripheral location is most common [1, 3]. Early radiologic evidence of traumatic pneumatocele is often obscured by an associated pulmonary contusion [1-3]. Contusions resolve within several days, whereas traumatic pneumatoceles tend to persist for longer periods, sometimes up to 4 months [1-3, 5].

Traumatic pneumatoceles most commonly develop in children and young adults [1, 3, 5]. This age distribution is felt to be related to the greater flexibility of the thoracic wall in this age group [1, 5]. The symptoms, physical findings, and clinical course of traumatic pneumatocele are generally innocuous. Hemoptysis is a common sign and may evacuate blood from the pneumatocele. Chest pain, coughing, and dyspnea may occur in the first few days. Associated low-grade fever and leukocytosis may result from resorption of injured lung tissue or blood clot and do not necessarily indicate superimposed infection [5]. Although fatal or nonfatal rupture of the pneumatocele into the pleural space with hemopneumothorax and superimposed lung abscess has been reported, complications are rare [1, 5].

In general, traumatic pneumatoceles require no treatment.

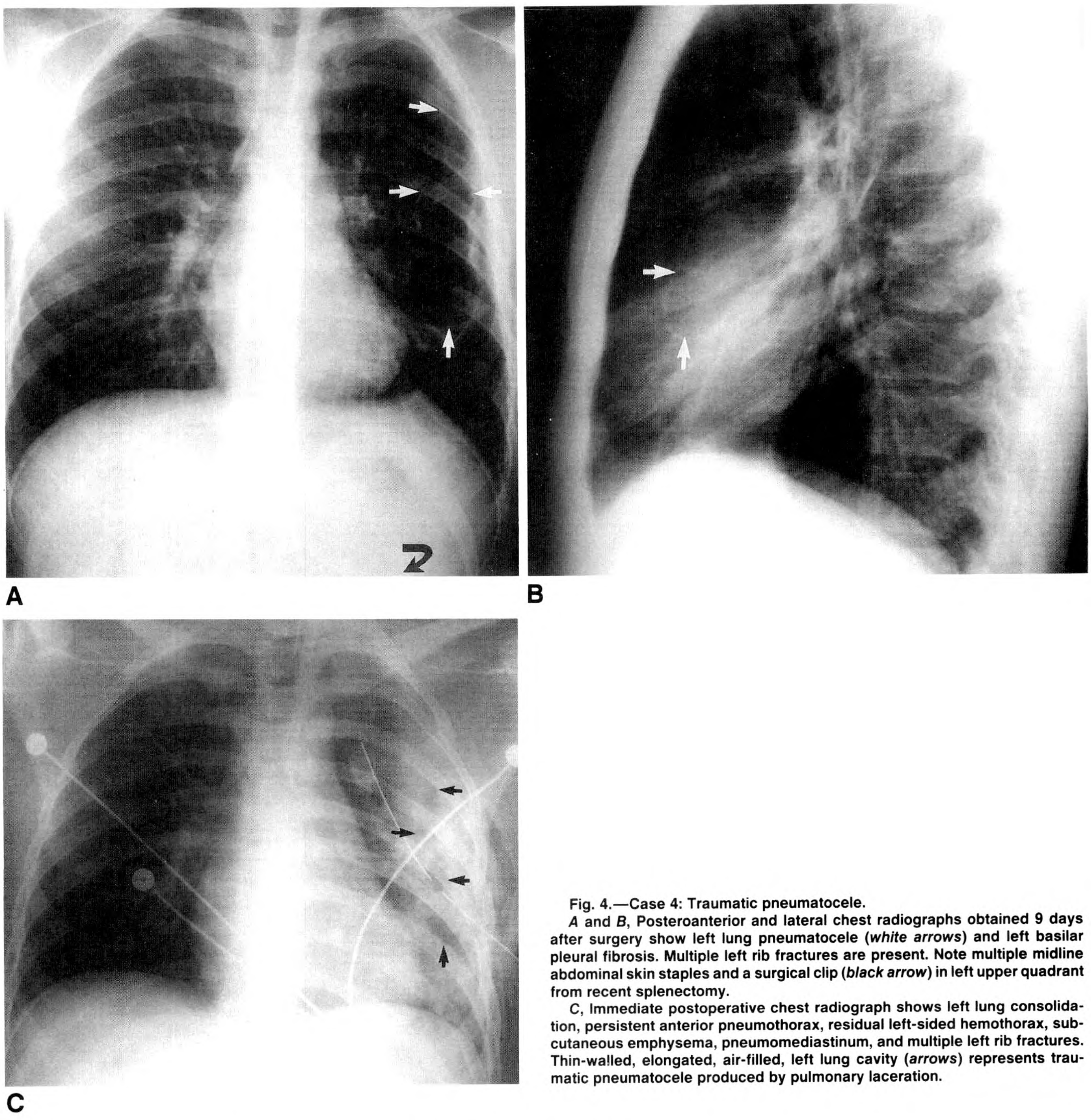

Fig. 4.—Case 4: Traumatic pneumatocele.

***A* and *B*, Posteroanterior and lateral chest radiographs obtained 9 days after surgery show left lung pneumatocele (*white arrows*) and left basilar pleural fibrosis. Multiple left rib fractures are present. Note multiple midline abdominal skin staples and a surgical clip (*black arrow*) in left upper quadrant from recent splenectomy.**

***C*, Immediate postoperative chest radiograph shows left lung consolidation, persistent anterior pneumothorax, residual left-sided hemothorax, subcutaneous emphysema, pneumomediastinum, and multiple left rib fractures. Thin-walled, elongated, air-filled, left lung cavity (*arrows*) represents traumatic pneumatocele produced by pulmonary laceration.**

Complete resolution without sequelae is typical. Residual pleural or parenchymal scars may occur [2, 5]. In-hospital observation is usually provided to monitor other injuries [5]. The differential diagnosis includes loculated hemopneumothorax, congenital lung cyst, postpneumonic pneumatocele, pneumatocele formation after hydrocarbon poisoning, thin-walled cavity produced by coccidioidomycosis, tuberculosis cavitation, lung abscess, and cavitating carcinoma [3, 5].

Paul V. Suhocki
Margaret A. Stull
Homer L. Twigg

REFERENCES

1. Wiot JF. The radiologic manifestations of blunt chest trauma. *JAMA* **1975**;231:500–503
2. Tocino I, Armstrong JD. Trauma to the lung. In: Taveras JM, Ferruci JT, eds. *Radiology: diagnosis, imaging, intervention,* rev. ed. Philadelphia: Lippincott, **1988**;1:1–16
3. Paré JA, Fraser RG. *Synopsis of diseases of the chest.* Philadelphia: Saunders, **1983**:601, 602, 616, 617
4. Wagner RB, Crawford WO, Schimpf PP. Classification of parenchymal injuries of the lung. *Radiology* **1988**;167:77–82
5. Ganske JG, Dennis DL, Vanderveer JB Jr. Traumatic lung cyst: case report and literature review. *J Trauma* **1981**;21:493–496

Abdominal Case of the Day

Paul M. Silverman,[1] Wendelin S. Hayes,[1] Cirrelda J. Cooper,[1] Daryl Fanney,[1] Michelle S. West,[1] Leslie Forer,[1] David S. Hartman,[2] Alan J. Davidson,[3] and Margaret A. Stull[1]

Case 1: Ileocolic Intussusception in AIDS

A 41-year-old man with AIDS presented to the emergency department with pain in the right lower quadrant, vomiting, and intermittent blood stools.

Plain film of the abdomen showed a large, ovoid soft-tissue mass in the right side of the abdomen (Fig. 1A). A CT scan at the level of the tip of the liver (Fig. 1B) showed a swirled, targetlike appearance of the bowel. A CT scan at the level of the umbilicus (Fig. 1C) showed features pathognomonic of intussusception. A dilated loop of bowel (intussuscipiens) with a thickened wall surrounds the intussusceptum with its accompanying low-attenuation pericolic fat. The patient underwent exploratory laparotomy, and an ileocolic intussusception was confirmed. Inspection of the bowel showed wall thickening and evidence of necrosis. A right hemicolectomy was performed. Pathologic examination of the specimen showed cytomegalovirus (CMV) colitis and hyperplastic lymphoid tissue thought to be the cause of the intussusception.

Intussusception is defined as telescoping of a segment of bowel into an adjacent segment. Unlike childhood intussusception, which is idiopathic in 90% of cases, adult intussusception has a demonstrable cause in over 90% of cases [1]. An intraluminal tumor, submucosal edema, or any process that causes dysrhythmic contractions may initiate an intussusception. Colonic intussusception is most commonly caused by a primary carcinoma, whereas small-bowel intussusception is usually related to benign tumors including submucosal masses. Meckel's diverticulum also may cause intussusception [2]. Gastrointestinal manifestations of AIDS that may potentially initiate an intussusception include lymphoma, lymphoid hyperplasia, CMV colitis, or Kaposi sarcoma [3].

The radiologic appearance of intussusception is often pathognomonic on CT [4]. The distended loop of bowel (intussuscipiens) has an apparent thickened wall because it represents two layers of bowel resulting from infolding of the intussusceptum. The intussusceptum usually occupies an eccentric location because the attached mesentery displaces it to the antimesenteric side. Within the intussuscipiens, the mesenteric fat appears as a crescentic low-attenuation fatty mass. Enhancing mesenteric vessels embedded in the mesentery support the diagnosis. A leading mass may sometimes be identified either as a soft-tissue tumor or a discrete low-attenuation lesion in the case of a lipoma. The entrapped mesenteric fat should not be misinterpreted as a lipoma. With compromise of the mesenteric blood supply, edema, ischemia, and thickening of the bowel wall result. The mesentery may become edematous and compressed, which may cause loss of a distinct central fatty density. Intussusception may then resemble other causes of bowel wall thickening such as ischemia, neoplasm, or inflammatory bowel disease.

Gastrointestinal disorders are second in frequency to pulmonary disease in patients with AIDS. Esophageal and gastric abnormalities include infection from CMV, *Candida*, and herpes, as well as neoplasms such as Kaposi sarcoma and lymphoma. Diarrhea, which can cause significant morbidity or mortality, may be due to numerous infections or drug therapy. Infectious cholangitis from CMV or *Cryptosporidium* produces morphologic changes similar to sclerosing cholangitis. Retroperitoneal and mesenteric adenopathy can result from numerous causes: progressive generalized lymphadenopathy, lymphoma, Kaposi sarcoma, and atypical mycobacterial infection [5]. Intussusception should be considered in patients with AIDS in the setting of acute abdominal pain. Familiarity with the CT appearance of intussusception will allow prompt diagnosis of this surgical emergency.

Daryl L. Fanney
Paul M. Silverman
Margaret A. Stull

The opinions and assertions contained herein are the private views of the authors and do not reflect the views of the Department of the Navy or of the Department of Defense.

[1] Department of Radiology, Georgetown University Medical Center, 3800 Reservoir Rd., N. W., Washington, DC 20007. Address reprint requests to M. A. Stull.

[2] Department of Radiology, F. Edward Hébert School of Medicine, Uniformed Services University of the Health Sciences, Bethesda, MD 20814-4799.

[3] Department of Radiologic Pathology, Armed Forces Institute of Pathology, Washington, DC 20306-6000.

P. M. Silverman is coordinator for the Abdominal Case of the Day. M. A. Stull is coordinator of the Case of the Day series.

AJR **154:1325–1330, June 1990** 0361–803X/90/1546–1325

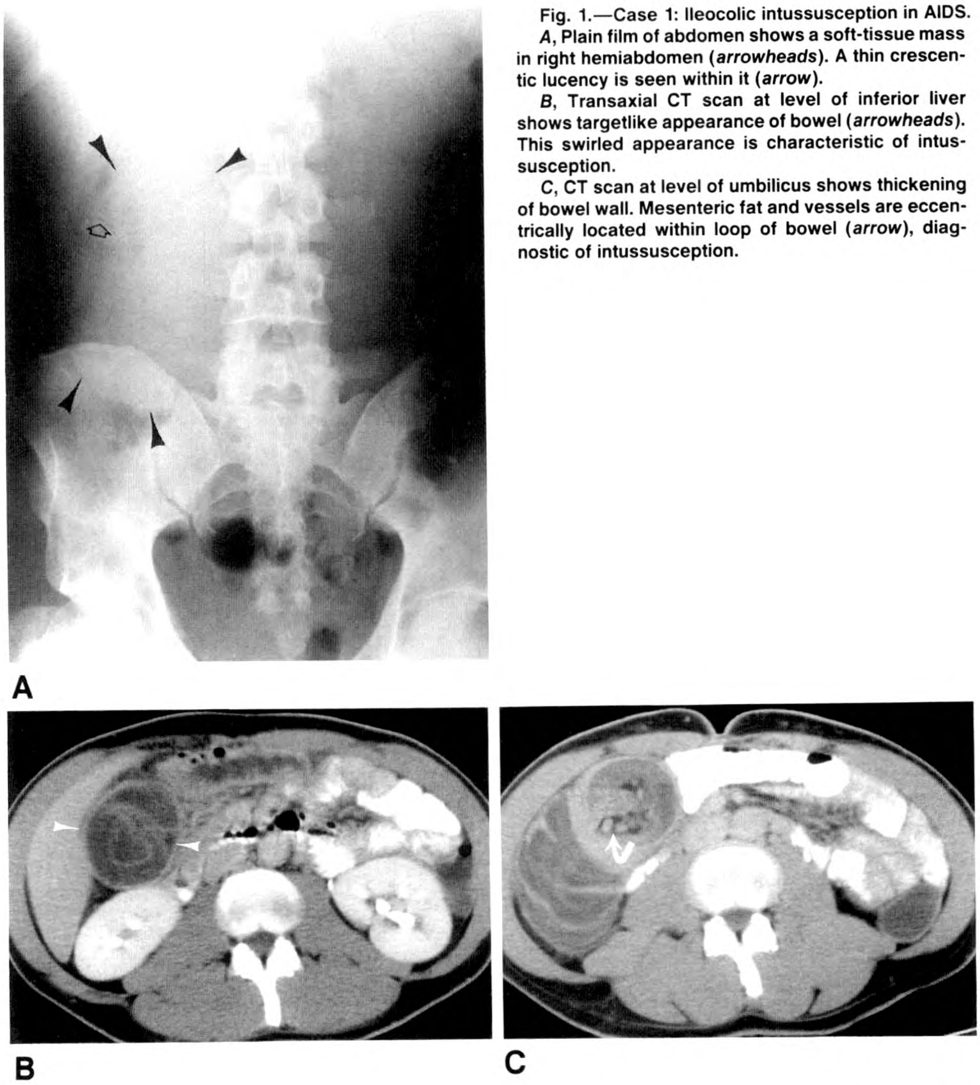

Fig. 1.—Case 1: Ileocolic intussusception in AIDS.

A, Plain film of abdomen shows a soft-tissue mass in right hemiabdomen (*arrowheads*). A thin crescentic lucency is seen within it (*arrow*).

B, Transaxial CT scan at level of inferior liver shows targetlike appearance of bowel (*arrowheads*). This swirled appearance is characteristic of intussusception.

C, CT scan at level of umbilicus shows thickening of bowel wall. Mesenteric fat and vessels are eccentrically located within loop of bowel (*arrow*), diagnostic of intussusception.

REFERENCES

1. Agha FP. Intussusception in adults. *AJR* **1986**;146:527–531
2. Curcio CM, Feinstein RS, Humphrey RL, Jones B, Siegelman SS. Computed tomography of entero-enteric intussusception. *J Comput Assist Tomogr* **1982**;6:969–974
3. Hofstetter SR, Stollman N. Adult intussusception in association with acquired immune deficiency syndrome and intestinal Karposi's sarcoma. *Am J Gastroenterol* **1986**;81:1073–1075
4. Iko BO, Teal JS, Siram SM, Chinwuba CE, Roux VJ, Scott VF. Computed tomography of adult colonic intussusception: clinical and experimental studies. *AJR* **1984**;143:769–772
5. Federle MP. A radiologist looks at AIDS: imaging evaluation based on symptom complexes. *Radiology* **1988**;166:553–562

Case 2: von Hippel-Lindau Disease

This previously healthy 24-year-old black man had a 1-year history of headaches, which had recently increased in severity and were now associated with nausea and difficulty walking. The patient had a twin brother with similar but less severe complaints. Physical examination was remarkable for bilateral papilledema, left retinal angioma, mild weakness in the upper extremity, and ataxic gait. Abdominal CT showed numerous pancreatic cysts and a few renal cysts (Figs. 2A and 2B). T2-weighted MR images of the brain and cervical cord showed three cerebellar lesions of high signal intensity and a syrinx of the cervical and upper thoracic cord (Fig. 2C). A cerebral angiogram showed mass effect on the left cerebellar hemisphere with displacement of the superior cerebellar and posterior inferior cerebellar arteries. Densely enhancing nodules were present in the left hemisphere, right cerebellar tonsil, and right lateral hemisphere (Fig. 2D). The patient underwent a low occipital craniotomy and excision of multiple hemangioblastomas.

Cerebelloretinal hemangioblastomatosis (von Hippel-Lindau disease) is a syndrome of multiple retinal and cerebellar vascular malformations, which include retinal capillary angiomas and hemangioblastomas. It is transmitted in an autosomal dominant fashion, with manifestations becoming more frequent with increasing age [1, 2]. Retinal and neurologic abnormalities are the most common source of symptoms. The retinal lesions result in progressive loss of vision. CNS hemangioblastomas are slow growing and frequently multiple, often arising in cerebellar and spinal locations. The most important differential diagnosis of CNS hemangioblastoma is

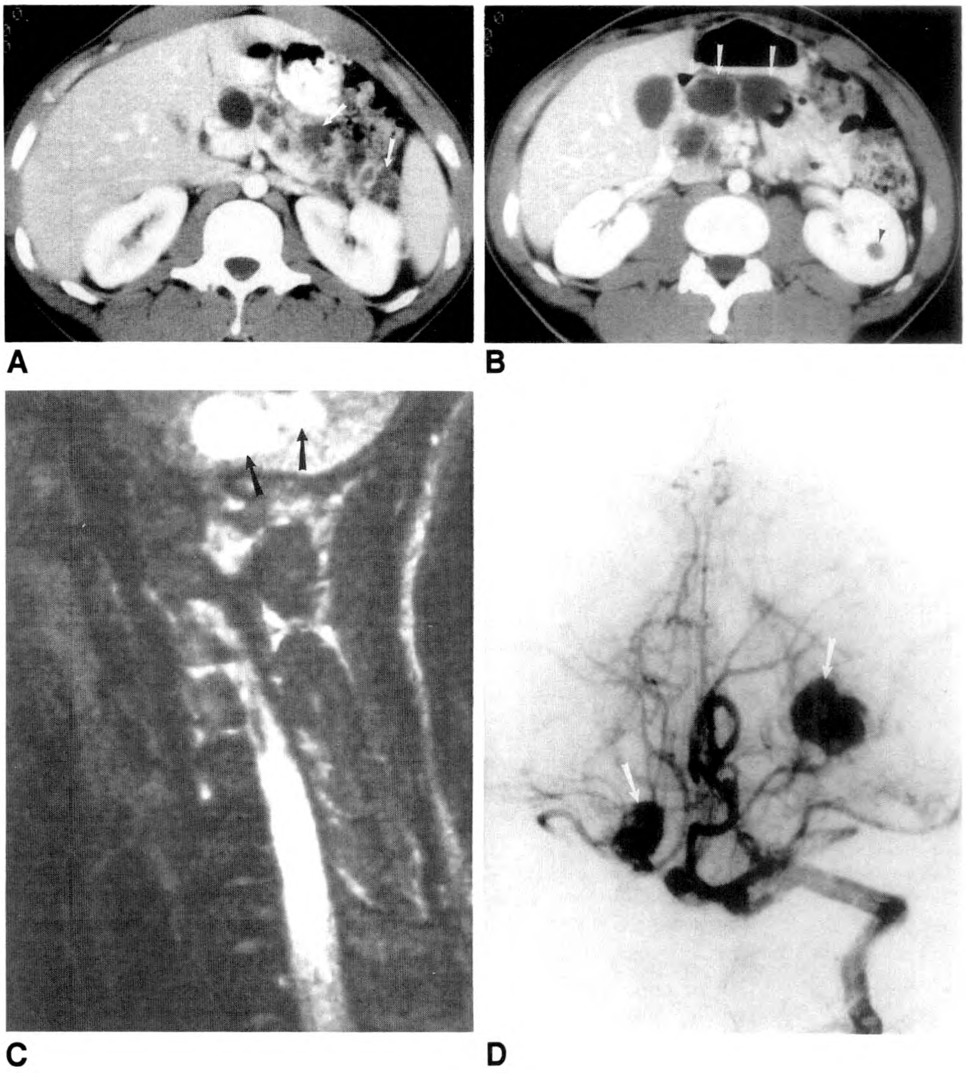

Fig. 2.—Case 2: von Hippel-Lindau disease.

A, **Transaxial contrast-enhanced CT scan of upper abdomen shows numerous cysts in body and tail of pancreas (*arrows*).**

B, **CT scan obtained 1 cm caudad to *A* shows multiple pancreatic cysts (*arrows*) and left renal cyst (*arrowhead*). Additional renal cysts were noted on other images.**

C, **Left parasagittal T2-weighted MR image shows two high-signal-intensity masses in cerebellar hemisphere (*arrows*).**

D, **Anteroposterior view from a left vertebral arteriogram shows densely enhancing nodules in left cerebellar hemisphere and superior right tonsil (*arrows*) consistent with hemangioblastomas.**

astrocytoma. Astrocytomas tend to be larger than hemangioblastomas and more frequently contain calcification [3].

Abdominal abnormalities associated with von Hippel-Lindau disease generally produce few or no symptoms. Abdominal manifestations include pancreatic and renal cysts, as well as a variety of benign and malignant tumors. There are higher incidences of renal cell carcinoma, pancreatic carcinoma, pheochromocytoma, visceral angioma, nonfunctional islet cell tumor, microcystic adenoma, hemangioblastoma, carcinoma of the ampulla of Vater, and retroperitoneal paragangliomas. Renal cysts, usually bilateral and multiple, are identified in up to three quarters of patients. Complex hemorrhagic cysts may be difficult to differentiate from neoplasm. In these cases, close interval follow-up with CT and sonography is helpful. Cystic areas in the pancreas have been identified on CT in 30% of patients but at autopsy are detected in nearly three quarters of cadavers [4]. Cysts also may arise in the liver, spleen, omentum, mesentery, adrenal glands, and epididymis. Differential diagnostic considerations of multiple pancreatic and renal cysts include adult polycystic renal disease, cystic pancreatic neoplasms such as cystadenoma/cystadenocarcinoma, and pancreatic pseudocysts with incidental simple renal cysts. Multiple pancreatic cysts also are seen in cystic fibrosis.

Renal neoplasms are a significant complication of this syndrome. Renal cell carcinoma arises in 25–38% of patients. In one series, these tumors were metastatic in 50% of cases and led to death in almost one third [2]. Tumors are usually multifocal (87%) and bilateral (75%) [5]. In view of the multiplicity of renal tumors, treatment can be managed in some patients by local excision in order to preserve renal function.

Pheochromocytomas are detected in approximately 10% of patients with von Hippel-Lindau disease [4]. These patients are less frequently symptomatic from excess catecholamine release than patients with sporadic tumors. Evaluation of serum or urine catecholamine levels in conjunction with CT screening is highly effective in detecting associated pheochromocytomas.

The constellation of clinical and radiologic findings in this case is characteristic of von Hippel-Lindau disease. Patients with the disease require periodic neurologic and abdominal examinations. Screening of patients should begin as early as the second decade. It is crucial that family members also be examined because early detection is probably the most important factor in the treatment of potentially lethal lesions in von Hippel-Lindau disease.

Michelle S. West
Paul M. Silverman
Margaret A. Stull

REFERENCES

1. Braunwald E, Isselbacher K, Petersdorf R, Wilson J, Martin J, Fauci A. *Harrison's principles of internal medicine*, 11th ed. New York: McGraw-Hill, **1987**:2031
2. Horton WA, Wong V, Eldridge R. von Hippel-Lindau disease: clinical and pathologic manifestations in nine families with 50 affected members. *Arch Intern Med* **1976**;136:769–777
3. Williams A, Haughton V. *Cranial computed tomography*. St. Louis: Mosby, **1985**:382
4. Levine E, Collins D, Horton W, Schimke R. CT screening of the abdomen in von Hippel-Lindau disease. *AJR* **1982**;139:505–510
5. Fill W, Lamiell J, Polk N. The radiographic manifestations of von Hippel-Lindau disease. *Radiology* **1979**;133:289–295

Case 3: Mesenteric Panniculitis

A 65-year-old diabetic man with a history of atherosclerotic vascular disease and intermittent diarrhea underwent an aortobifemoral graft procedure for increasing claudication. At surgery a 10 × 3 cm mass was palpated in the root of the small-bowel mesentery. Biopsy showed mesenteric panniculitis. The patient had no clinical or laboratory evidence of pancreatitis, inflammatory bowel disease, or fat necrosis at other sites. In view of his significant peripheral vascular disease and lack of abdominal symptoms, the patient was treated conservatively.

Abdominal CT was performed postoperatively to evaluate the extent of the mass. A discrete region of finely infiltrated fat was identified at the root of the small-bowel mesentery (Figs. 3A and 3B). The mass surrounded mesenteric vessels, some of which had an adjacent halo of preserved fat. There was no evidence of bowel wall thickening, tethering, or retraction.

Mesenteric panniculitis is an unusual inflammatory disorder of fat, often characterized by recurrent episodes of abdominal pain [1, 2]. The criteria for diagnosis include: (1) single, multiple, or diffuse masslike fatty lesions, (2) histologic confirmation of fat necrosis with inflammatory infiltrate and/or infiltration with lipid-laden macrophages, and (3) no evidence of pancreatitis, inflammatory bowel disease, or extraabdominal fat necrosis (i.e., Weber-Christian disease) [2]. The cause in most cases is idiopathic. However, infection, surgery, and trauma have been implicated as causes.

Patients can be affected throughout life, with the peak occurrence in the sixth and seventh decades. There is a slight male predominance. Patients may have abdominal pain, fever, anorexia, nausea, vomiting, and weight loss. Accurate preoperative diagnosis is infrequent because of the nonspecific symptoms. A poorly defined abdominal mass may be palpated in about 50% of patients [2].

Gross pathologic features include firm or hard masses that are loosely encapsulated with nodules of fat interspersed with irregular areas of discoloration representing necrotic or liquified fat. Variable amounts of hemorrhage and fibrosis are present also. The peritoneum may be adherent to the inflamed area. The jejunal mesentery is most often affected [1].

The most frequent radiologic finding on small-bowel series is displacement of loops by an extrinsic mass. Complete small-bowel obstruction is rare. Fixation or spiculation of bowel loops may simulate malignant disease. Sonography shows inhomogeneous masses with hyperechoic components related to fat. A spectrum of CT findings, ranging from well-defined inhomogeneous masses with interspersed areas of fat to ill-defined areas of soft-tissue infiltration in mesenteric fat, is encountered [2–4]. When the lesion has the latter appearance, the abnormality generally infiltrates along mesenteric vessels without vascular invasion. Calcifications are rare.

When the dominant feature of the lesions is linear or fibrotic strands, the entity is often termed retractile mesenteritis [5]. The presence of an associated soft-tissue mass raises concern for carcinoid tumor and consideration of clinical evaluation for elevated levels of 5-hydroxyindoleacetic acid. The differential considerations of a focal mass on CT include metastatic disease, lymphoma, liposarcoma, and teratoma [6, 7]. Torsion of the greater omentum, although rare, also can present as a mass, predominately of fatty density. The concentrically organized distribution of fibrous densities may help distinguish torsed omentum from other fatty masses [8]. Mesenteric lesions that have an infiltrative appearance should be distinguished from the sequelae of pancreatitis, inflammatory bowel disease, or trauma.

The clinical course of mesenteric panniculitis is usually

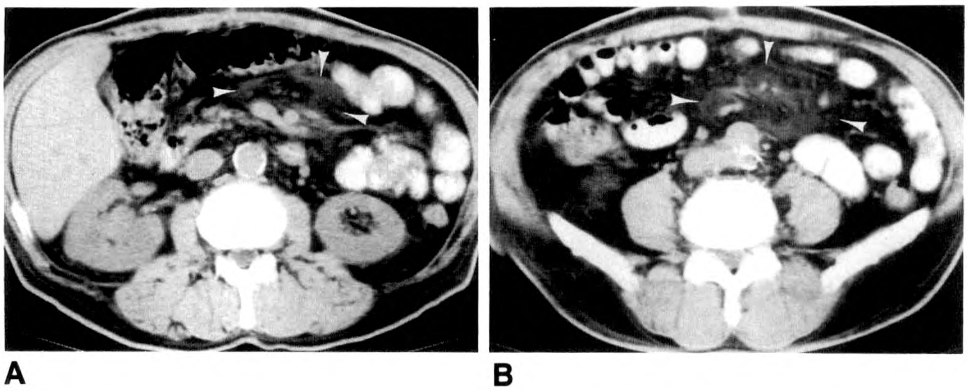

Fig. 3.—Case 3: Mesenteric panniculitis.

***A*, Transaxial CT scan of mid abdomen shows a poorly defined density (*arrowheads*), which produces mild mass effect in mesentery.**

***B*, Transaxial CT scan at top of iliac crests shows a poorly defined mass (*arrowheads*) that consists of soft-tissue density infiltrating mesenteric fat. Inflammatory process surrounds mesenteric vasculature.**

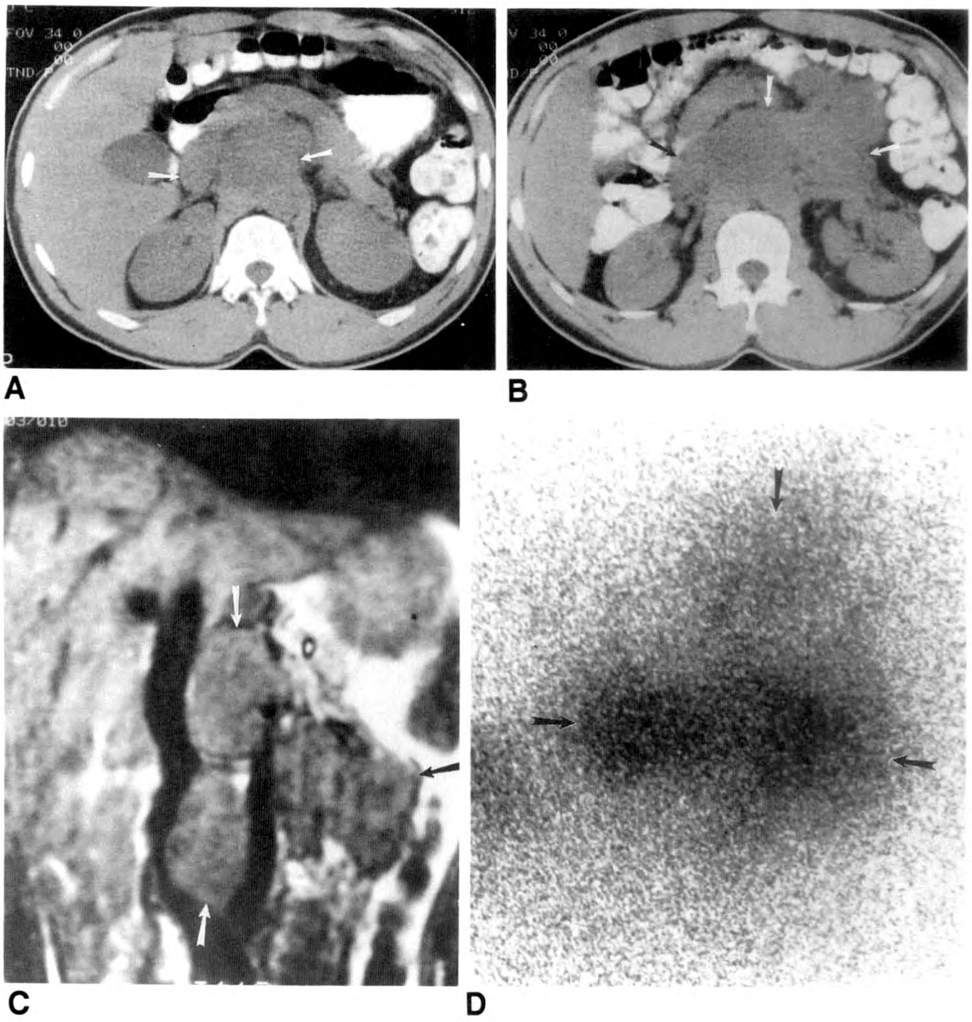

Fig. 4.—Case 4: Malignant extra-adrenal retroperitoneal paraganglioma.

***A* and *B*, Transaxial CT scans of upper (*A*) and mid (*B*) abdomen show a large, relatively homogeneous retroperitoneal mass (*arrows*) with irregular margins.**

***C*, Coronal T1-weighted MR image of abdomen shows multiple rounded masses (*arrows*) extending down sympathetic chain.**

***D*, Anterior metaiodobenzylguanidine scintigram shows abnormal tracer uptake in upper, mid, and lower abdomen (*arrows*).**

uneventful. Spontaneous remissions are common, and therefore the effect of various therapies including corticosteroids is difficult to assess. This patient continues to be treated conservatively.

Cirrelda J. Cooper
Paul M. Silverman
Leslie Forer
Margaret A. Stull

REFERENCES

1. Durst AL, Freund H, Rosenmann E, Birnbaum D. Mesenteric panniculitis: review of the literature and presentation of cases. *Surgery* **1977**;81:203–211
2. Katz ME, Heiken JP, Glazer HS, Lee JTK. Intraabdominal panniculitis: clinical, radiographic, and CT features. *AJR* **1985**;145:293–295
3. Mata JM, Inaraja L, Martin J, Olazabal A, Castilla MT. CT features of mesenteric panniculitis. *J Comput Assist Tomogr* **1987**;11:1021–1023
4. Waligore MP, Stephens DH, Soule EH, McLeod RA. Lipomatous tumors of the abdominal cavity: CT appearance and pathologic correlation. *AJR* **1981**;137:539–545
5. Seigel RS, Kuhns LR, Borlaza GS, McCormick TL, Simmons JL. Computed tomography and angiography in ileal carcinoid tumor and retractile mesenteritis. *Radiology* **1980**;134:437–440
6. Silverman PM, Baker ME, Cooper C, Kelvin FM. Computed tomography of mesenteric disease. *RadioGraphics* **1987**;7:309–320
7. Silverman PM, Kelvin FM, Korobkin M, Dunnick NR. Computed tomography of the normal mesentery. *AJR* **1984**;143:953–957
8. Ceuterick L, Baert AL, Marchal G, Kerremansi, Geboes K. CT diagnosis of primary torsion of greater omentum. *J Comput Assist Tomogr* **1987**;11:1083–1084

Case 4: Malignant Extraadrenal Retroperitoneal Paraganglioma

A healthy 30-year-old man with a 10-year history of hypertension and biochemical evidence of excess catecholamine secretion was evaluated by CT for a suspected pheochromocytoma. CT showed a large, homogeneous retroperitoneal mass with irregular margins following the distribution of the sympathetic chain (Figs. 4A and 4B). On T1-weighted MR images, the tumor comprised numerous soft-tissue masses consistent with multiple paragangliomas or paragangliomatosis (Fig. 4C). Scintigraphic evaluation with ^{131}I-metaiodobenzylguanidine (MIBG) showed abnormal tracer uptake corresponding to the location of the soft-tissue masses seen on CT (Fig. 4D). At surgery, the adrenal glands were found to be normal. Complete resection of the retroperitoneal mass was unsuccessful because of invasion of adjacent organs.

Retroperitoneal paragangliomas arise from the paraganglia (i.e., collections of specialized neural crest cells) that are distributed along the aorta in close association with the sympathetic chain. This tissue either aggregates in the adrenal medulla, where it gives rise to intraadrenal paragangliomas (pheochromocytoma) or remains in its paraaortic location where it may develop into extraadrenal retroperitoneal paragangliomas. Approximately 10–20% of retroperitoneal paragangliomas are extraadrenal [1–3].

Extraadrenal retroperitoneal paragangliomas are functional in 25–60% of patients [1–3], with males affected more frequently than females. Patients usually present between 30 and 45 years of age. Patients develop chronic or intermittent hypertension, palpitations, diaphoresis, or headache. If signs and symptoms of excess catecholamine secretion are recognized clinically, these tumors may be detected early. Nonfunctional tumors are rarely diagnosed preoperatively. These patients are frequently asymptomatic until the tumor reaches sufficient size to cause symptoms from compression of adjacent organs.

The predominant location of extraadrenal retroperitoneal paragangliomas is infrarenal, corresponding to the area of the fetal organ of Zuckerkandl [4]. These retroperitoneal paragangliomas (excluding those arising in the urinary bladder) have the highest incidence of malignant behavior (20–42% of patients [3]) when compared with paraganglioma arising in other locations [1–4]. Malignant paragangliomas are difficult to diagnose histologically. The diagnosis of malignancy is based on the presence of metastatic disease and invasion of adjacent organs, as in the illustrated case.

Extraadrenal retroperitoneal paragangliomas can be imaged accurately by CT, MR, or ^{131}I-MIBG scintigraphy. On CT, extraadrenal retroperitoneal paragangliomas are identified as soft-tissue masses along the course of the sympathetic chain. Differential diagnosis on CT includes primary retroperitoneal neoplasms (mesenchymal, neurogenic, or germ cell tumor), lymphoma, and metastatic disease. Malignant extraadrenal retroperitoneal paragangliomas tend to have irregular margins with heterogeneous density on CT [5]. On MR, these tumors are generally hypointense when compared with liver on T1-weighted images and extremely hyperintense on T2-weighted images [6]. MIBG is taken up by adrenergic tissue and is directly incorporated into the catecholamine neurotransmitter vesicles, allowing visualization of these tumors as areas of increased tracer uptake [7].

Owing to increased tissue characterization potential of ^{131}I-MIBG and MR imaging for these tumors, these imaging techniques may be superior to CT for evaluation of primary extraadrenal paragangliomas. For evaluation of metastatic or recurrent extraadrenal retroperitoneal tumors, ^{131}I-MIBG imaging may be superior to CT and MR, because whole-body images are obtained [6].

The treatment of choice for extraadrenal paragangliomas is surgical resection. Depending on the anatomic location and size of these tumors, complete resection may be difficult because of local extension and vascular involvement. As paragangliomas grow relatively slowly, prolonged follow-up is required [2–4, 7].

Wendelin S. Hayes
Alan J. Davidson
David S. Hartman
Paul M. Silverman
Margaret A. Stull

REFERENCES

1. Lack EE, Cubilla AL, Woodruff JM, Lieberman PH. Extra-adrenal paragangliomas of the retroperitoneum: a clinicopathologic study of 12 tumors. *Am J Surg Pathol* **1980**;4:109–120
2. Melicow MM. One hundred cases of pheochromocytoma (107) tumors at the Columbia-Presbyterian Medical Center, 1926–1976: a clinicopathological analysis. *Cancer* **1977**;40:1987–2004
3. Enzinger FM, Weiss SW. Paraganglioma. In: Enzinger FM, Weiss SW, eds. *Soft tissue tumors*, 1st ed. St. Louis: Mosby, **1983**:657–697
4. Glenn F, Gray GF. Functional tumors of the organ of Zuckerkandl. *Ann Surg* **1976**;183:578–586
5. Patel YD, Morehouse HT. Malignant paragangliomas of the retroperitoneum: value of computed tomography and angiography. *Clin Radiol* **1984**;35:185–188
6. Quint LE, Glazer GM, Francis IR, Shapiro B, Chenevert TL. Pheochromocytoma and paraganglioma: comparison of MR imaging with CT and I-131 MIBG scintigraphy. *Radiology* **1987**;165:89–93
7. Sisson JC, Fragel MS, Valk TW, et al. Scintigraphic localization of pheochromocytoma. *N Engl J Med* **1981**;305:12–17

Musculoskeletal Case of the Day

Margaret A. Stull[1] and Mark Glass-Royal

Case 1: Parosteal Osteosarcoma of the Humerus

About 6 months before presentation, this 62-year-old man noticed diffuse swelling and progressive loss of motion of the left shoulder and upper arm. About 4 months before presentation, he identified a nontender lump in the left shoulder. Physical examination revealed a large firm mass that extended into the root of the neck, medially to the chest wall, and inferiorly to the supracondylar region of the left elbow. Circulation, sensation, and function in the left hand were normal.

Twenty years earlier, he had undergone biopsy for a left shoulder mass, which was diagnosed as an osteochondroma. The patient's history did not reveal whether the mass had been completely surgically excised.

Radiologic examination of the left humerus and shoulder (Fig. 1A) revealed a massive, amorphous, irregularly calcified, and ossified mass replacing and infiltrating the shoulder and arm as well as encircling the humerus. An anterior ^{99m}Tc-methylene diphosphonate (MDP) scintigram (Fig. 1B) showed markedly increased tracer accumulation in the mass in the left upper extremity. Intramedullary invasion, cortical destruction, and infiltration of adjacent structures by the juxtacortical humeral mass were shown by CT (Fig. 1C). The extent of the tumor was delineated by MR examination. The T1-weighted coronal MR images (Fig. 1D) showed intermediate-signal tumor replacing the marrow of the left proximal humerus, enveloping the humerus, and infiltrating adjacent structures. The superior, medial, and inferior extent of the tumor was readily identified as bright signal infiltrating adjacent tissues on the T2-weighted MR coronal images (Fig. 1E). Histologic examination revealed a parosteal osteosarcoma.

Parosteal osteosarcoma is a rare, slow-growing, malignant, bone-forming neoplasm that arises from the surface of long bones. It has a better prognosis than conventional central osteosarcomas and other surface (juxtacortical) osteosarcomas [1–3]. Patients are generally affected in the second to fifth decades of life. They usually have gradual onset of pain, swelling, and a palpable mass [1, 4]. The indolent behavior of the tumor delays diagnosis. As illustrated in this case, the tumor may attain enormous size before the patient seeks clinical evaluation [1, 4]. In addition, radiologic and histologic misdiagnosis as benign osteochondroma [2] may result in inadequate surgical excision of the tumor—a distinct possibility in this patient.

The lesion most often arises from the metaphysis of a tubular bone, occasionally from the epiphysis, and rarely from the diaphysis [1, 4]. The most common location is the posterior aspect of the distal femur, followed by the proximal humerus, the tibia, fibula, and ulna [1, 4]. This malignant neoplasm grows circumferentially along the cortex of the involved bone, eventually enveloping the bone shaft. Cortical destruction and neoplastic invasion of the medullary cavity are uncommon except in cases of prior treatment or a long history of growth, as illustrated in this case [3–5].

On radiographs, early parosteal osteosarcomas are radiodense, lobulated, or oval masses with a broad base of attachment to the external cortex. A thin, radiolucent cleavage plane between the tumor and underlying bone is characteristic but not a constant finding [1, 3–5]. Progressive growth of the tumor may obliterate this plane. This tumor ossifies from the base of the lesion to its periphery in contradistinction to myositis ossificans, which initially ossifies from the periphery [1, 2, 4]. The differential diagnosis of a less advanced case of parosteal osteosarcoma includes osteochondroma, myositis ossificans, central osteosarcoma, extraosseous osteosarcoma, ossifying or calcifying hematoma, and exuberant callus [4, 5]. CT and MR studies assist in delineating the extent of the process and in preoperative planning [4, 5].

Margaret A. Stull
Mark Glass-Royal

REFERENCES

1. Resnick D, Kyriakos M, Greenway GD. Tumors and tumor-like lesions of bone: imaging and pathology of specific lesions. In: Resnick D, Niwayama G, eds. *Diagnosis of bone and joint disorders*, 2nd ed. Philadelphia: Saunders, **1988**:3648–3677
2. Hudson TM, Springfield DS, Benjamin M, Bertoni F, Present DA. Computed tomography of parosteal osteosarcoma. *AJR* **1985**;144:961–965
3. Schajowicz F, McGuire MH, Araujo ES, Muscolo DL, Gitelis S. Osteosarcomas arising on the surfaces of long bones. *J Bone Joint Surg [Am]* **1988**;70:555–564

---

[1] Both authors: Department of Radiology, Georgetown University Medical Center, 3800 Reservoir Rd., N. W., Washington, DC 20007. Address reprint requests to M. A. Stull, coordinator of the Case of the Day series.

***AJR* 154:1331–1336, June 1990** 0361-803X/90/1546-1331 © American Roentgen Ray Society

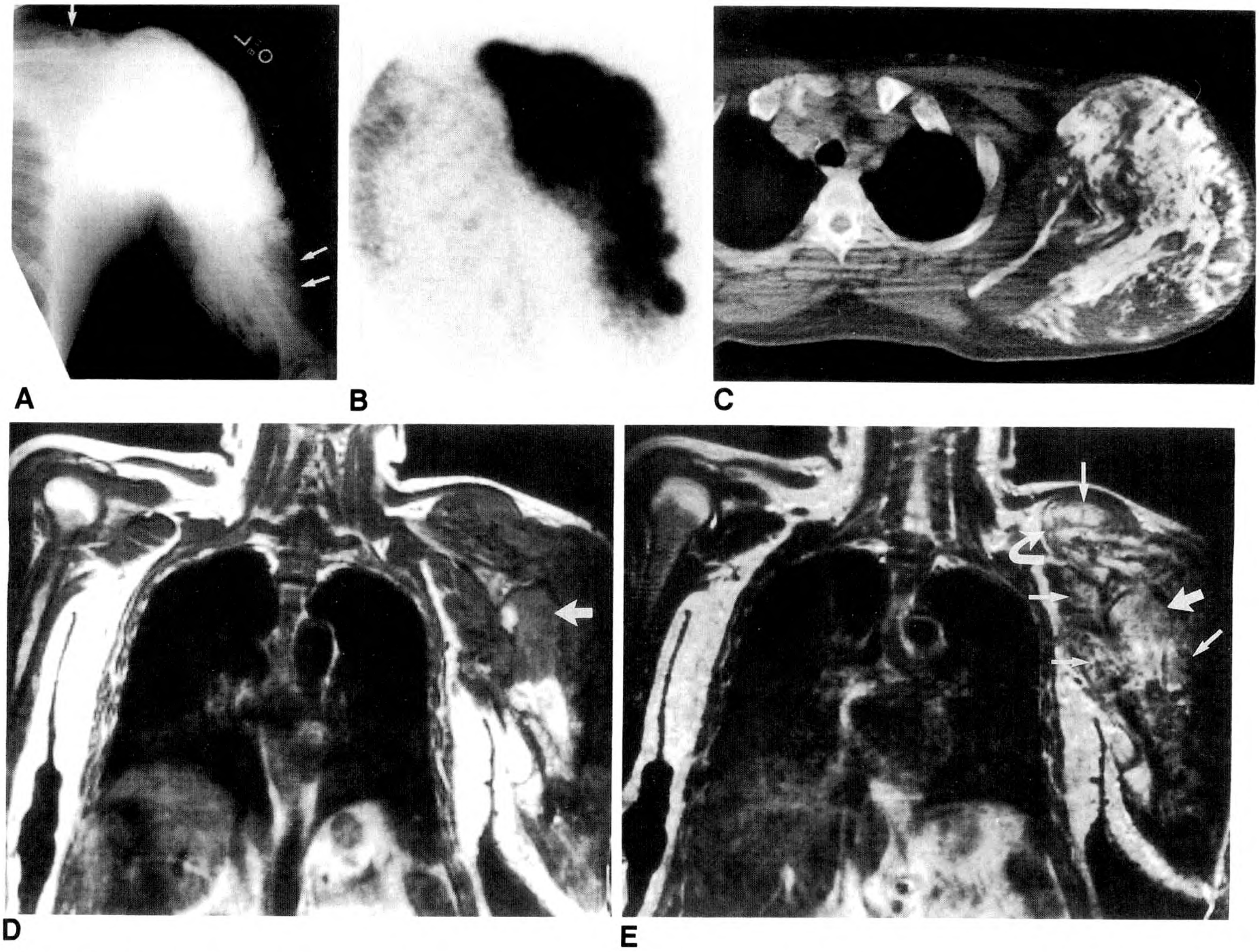

Fig. 1.—Case 1: Parosteal osteosarcoma of humerus.

***A*, Radiograph of left humerus shows massive amorphous and irregular calcification surrounding and replacing shoulder structures and majority of humerus. Lobulated soft-tissue mass (*white arrows*) is best seen along periphery of lesion.**

***B*, Anterior ^{99m}Tc-methylene diphosphonate scintigram shows inhomogeneous tracer uptake in a large, irregular, lobulated mass involving left shoulder structures and humerus.**

***C*, CT scan at level of left glenohumeral joint reveals extensive medullary invasion and cortical destruction by calcified juxtacortical humeral mass that infiltrates adjacent structures also.**

***D* and *E*, T1-weighted, 600/25, (*D*) and T2-weighted, 2000/80, (*E*) coronal MR images of thorax and upper extremities show intramedullary invasion of proximal left humerus (*large straight arrow*) and tumor extending medially, superiorly, and laterally into adjacent structures (*small straight arrows*). Tumor also extends into vicinity of left brachial plexus (*curved arrow*).**

4. Smith J, Ahuja SC, Huvos AG, Bullough PG. Parosteal (juxtacortical) osteogenic sarcoma: a roentgenological study of 30 patients. *J Can Assoc Radiol* **1978**;29:167–175
5. Lindell MM, Shirkhoda A, Raymond AK, Murray JA, Harle TS. Parosteal osteosarcoma: radiologic-pathologic correlation with emphasis on CT. *AJR* **1987**;148:323–328

Case 2: Osseous Sarcoidosis and Chronic Polyarthritis

This 26-year-old black man, with a 5-year history of quiescent intrathoracic sarcoidosis, presented with intermittent swelling and tenderness of his fingers for the past 2 years. The patient's symptoms partially improved by adjusting his steroid therapy. Physical examination revealed bilateral deformed, tender, and swollen fingers, hypertrophied nails, and skin lesions. In addition, multiple proximal and distal interphalangeal joints of both hands were tender and swollen. Other clinical findings related to active pulmonary sarcoidosis and left facial nerve involvement (i.e., Bell palsy) also had developed within the last 2 years and partially responded to steroid therapy. Radiographs of the hands (Figs. 2A and 2B) showed bilateral soft-tissue swelling, periarticular osteoporosis, deformity, and destructive osseous lesions of the digits. Localized "punched-out" lytic lesions, trabecular alterations resulting in a latticework pattern, pathologic fractures, and fragmentation were identified in the phalanges. Periostitis was absent. The metacarpals and wrists were spared, except for

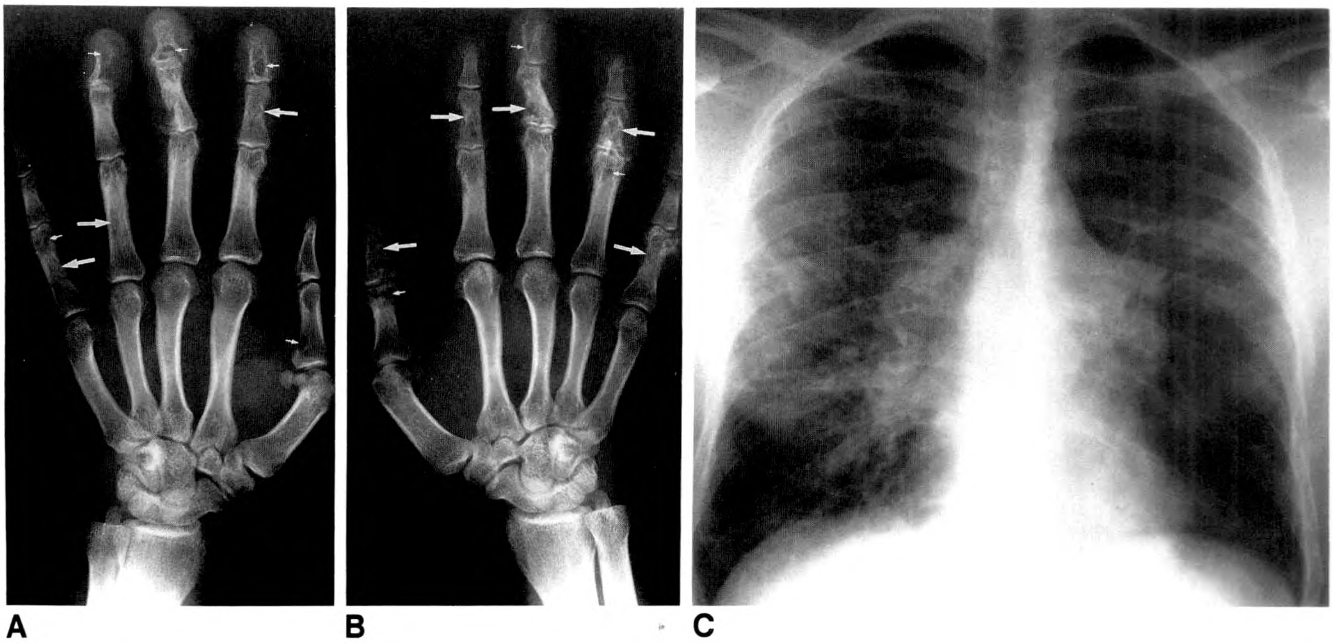

Fig. 2.—Case 2: Osseous sarcoidosis and chronic polyarthritis.

A and *B*, Radiographs of left (*A*) and right (*B*) hands show soft-tissue swelling, periarticular osteoporosis, deformity, and destructive lesions of digits. "Punched-out" lesions (*small arrows*) are seen in multiple phalanges. Cortical tunneling and trabecular alterations produce a latticework appearance in affected phalanges (*large arrows*). Middle and distal phalanges of left middle finger, the distal phalanx of left ring and right middle fingers, and the base of distal phalanx of right thumb have pathologic fractures. Absence of periosteal reaction is striking. An old healed intraarticular fracture of head of right fifth proximal phalanx is noted. There is limited involvement of several distal metacarpals, bilaterally. Wrists are spared. Joint spaces are relatively spared.

C, Chest radiograph shows bilateral hilar and mediastinal adenopathy. Bilateral reticulonodular infiltrates are more prominent on right side.

minor alterations in several distal metacarpals. The joint spaces were relatively spared. All of these radiologic findings are characteristic of skeletal alterations in sarcoidosis.

A concurrent chest radiograph (Fig. 2C) revealed mediastinal and hilar adenopathy and bilateral interstitial infiltrates consistent with stage 2 intrathoracic sarcoidosis. The combination of pulmonary and osseous abnormalities are characteristic of sarcoidosis.

Sarcoidosis is a generalized granulomatous disorder of unknown cause characterized by noncaseating granulomas. The frequency of radiologically apparent osseous involvement in sarcoidosis ranges from 1% to 13%, with an average of 5% [1–4]. Any bone can be affected; however, the small bones of the hands and feet are most often involved, with the hands as the predominant site. Osseous alterations are usually asymmetric and involve the distal and middle phalanges more often than the proximal phalanges and metacarpals. The bone lesions are usually asymptomatic, but can cause severe symptoms, as in this patient [1, 2]. Soft-tissue swelling, tenderness, stiffness, and deformities can accompany osseous disease. Skeletal involvement is generally associated with cutaneous lesions, which were present in this patient. Radiologic evidence of pulmonary involvement is found in 80% to 90% of patients with osseous sarcoidosis [1, 2].

Skeletal lesions in sarcoidosis have several radiologic manifestations. Cortical and trabecular alterations resulting in a reticular pattern or latticework appearance are the most characteristic radiologic findings of osseous sarcoid [2, 5]. Punched-out lytic lesions of bone destruction also are commonly described. Calcification, nodular opacities, and residual trabeculae may be present in these lytic lesions. Occasionally, rapid bone destruction results in a permeative pattern of osteolysis with cortical disruption and sequestration. Pathologic fracture, fragmentation, and telescoping of the digit are associated with more aggressive osseous lesions. Periostitis is distinctly unusual. The joint spaces are relatively spared despite extensive osseous destruction. Acroosteosclerosis characterized by opaque nodules in the terminal phalanges and endosteal thickening is a radiologic finding in osseous sarcoidosis, but also is present in rheumatoid arthritis, systemic lupus erythematosus, Hodgkin disease, and scleroderma [1, 2]. Generalized osteosclerosis, usually involving the spine, pelvis, skull, and ribs, is a less typical osseous manifestation of sarcoidosis [1].

Acute and chronic polyarthritis have been reported in 10% to 35% of sarcoidosis patients [1, 2]. An acute symmetrical peripheral polyarthritis affects small and medium-sized joints early in the course of sarcoidosis. The condition usually resolves in 4 to 6 weeks. Recurrent episodes of acute exacerbation are typical of chronic polyarthritis, which affects the ankles, knees, wrists, shoulders, and small joints of the hands. Alterations related to joint disease found on radiographs consist of soft-tissue swelling, periarticular osteoporosis, mild joint-space narrowing, and eccentric erosions. Coexistent osseous lesions can extend to the subchondral bone and result in articular destruction and collapse [1, 2]. This patient had a striking lack of interosseous alterations despite subjacent bone involvement and destruction.

Other entities to be considered in the differential diagnosis of bone lesions in this patient include tuberculosis and other granulomatous infections, hemangiomatosis, xanthomatosis, skeletal metastases, and enchondromatosis. The combination of intrathoracic and osseous abnormalities helps narrow the differential diagnosis to sarcoidosis with associated chronic polyarthritis.

Margaret A. Stull
Mark Glass-Royal

REFERENCES

1. Sartoris DJ, Resnick D, Resnik C, Yaghmai I. Musculoskeletal manifestations of sarcoidosis. *Semin Roentgenol* **1985**;20:376–386
2. Resnick D, Niwayama G. Sarcoidosis. In: Resnick D, Niwayama G, eds. *Diagnosis of bone and joint disorders*, 2nd ed. Philadelphia: Saunders, **1988**:4012–4032
3. Yaghmai I. Radiographic, angiographic and radionuclide manifestations of osseous sarcoidosis. *RadioGraphics* **1983**;3:375–396
4. Subbarao K. Sarcoidosis of bone. In: Taveras JM, Ferrucci JT, eds. *Radiology—diagnosis, imaging, intervention.* Philadelphia: Lippincott, **1989**;5:1–5
5. Holt JF, Owens WI. Osseous lesions of sarcoidosis. *Radiology* **1949**;53:11–30

Case 3: Primary Oxalosis with Renal Osteodystrophy

This 29-year-old woman with primary hyperoxaluria and consequent renal failure had required dialysis for the past 7 years. Her physical condition deteriorated progressively after a fall and injury to the extensor mechanism of both knees 5 years ago. The patient developed flexion contractures of both hips and knees related to these injuries. She complained of inability to walk and subsequently underwent bilateral soft-tissue contracture release procedures. Bone biopsy of the left iliac crest was performed at the request of the nephrology service. Histologic examination revealed numerous birefringent crystalline deposits consistent with calcium oxalate crystals within the bone tissue.

Radiographs of the left shoulder and pelvis from a metabolic survey revealed evidence of osteitis fibrosa cystica and diffuse "Paget-like" osteosclerosis (Figs. 3A and 3B). Bilateral renal calcification and nephrolithiasis also were identified. A lateral radiograph of the right foot (Fig. 3C) showed extensive vascular calcifications, which were denser than those commonly seen in diabetes or secondary hyperparathyroidism.

Primary hyperoxaluria is a rare autosomal recessive metabolic disorder of glyoxylate metabolism, characterized by excessive production and urinary excretion of oxalic acid,

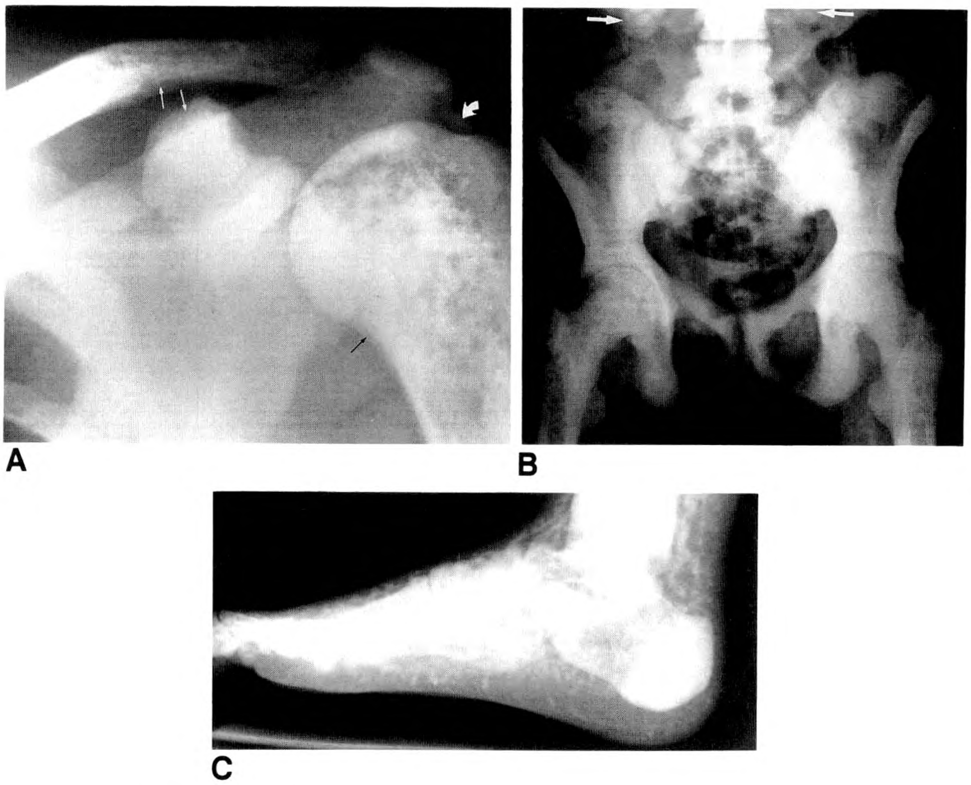

Fig. 3.—Case 3: Primary oxalosis with renal osteodystrophy.

A, **Radiograph of left shoulder shows subchondral resorption of distal clavicle and acromion, subligamentous resorption at sites of attachment of coracoclavicular ligament (*white straight arrows*), and subperiosteal resorption along medial aspect of humeral neck (*black arrow*). There is loss of normal trabecular pattern and diffuse patchy bone sclerosis. A focal soft-tissue calcification (*curved arrow*) is noted in region of tendinous portion of supraspinatus.**

B, **Radiograph of pelvis reveals diffuse "Paget-like" osteosclerosis, especially about hips, symphysis pubis, lumbar vertebrae, and sacroiliac joints. Nephrolithiasis and diffuse nephrocalcinosis are present in visualized portion of kidneys (*arrows*), which are disproportionately small.**

C, **Radiograph of right foot shows extensive vascular calcifications and diffuse osteosclerosis.**

calcium oxalate nephrolithiasis, and nephrocalcinosis with progressive renal failure that develops at an early age [1–4]. The metabolic derangement results from one of two enzymatic defects: the absence of α-ketoglutarate-glyoxylate carboligase activity resulting in glycolic aciduria (type 1 hyperoxaluria); or a deficiency of D-glycerate dehydrogenase causing 1-glyceric aciduria (type 2 hyperoxaluria). The second type is exceedingly rare [1–4].

Extrarenal deposition of calcium oxalate crystals, termed oxalosis, accompanies primary hyperoxaluria and is accelerated on renal failure. Major extrarenal sites of accumulation include bone, small blood vessels, eyes, and soft tissues [1–4]. There is also a predilection for sites of tissue injury. Crystal deposition is felt to be related to organ vascularity and not to active incorporation of oxalate crystals into growing tissue. Therefore, areas of high vascularity, such as the ends of bones, are preferentially affected [1].

The radiologic appearance of skeletal alterations in primary hyperoxaluria and oxalosis is produced by a combination of oxalate deposition and renal osteodystrophy, with the former predominating [1, 2]. Metaphyseal abnormalities in tubular bones include irregular transverse sclerotic bands and narrow translucent zones at the physis. Sclerosis in the subchondral areas of the humeri and femora can resemble osteonecrosis. Alternating lucent and sclerotic bands in the sternum and ilium have been described. Sclerotic zones along vertebral body end plates simulate the "rugger-jersey" spine of renal osteodystrophy. Delayed bone maturation and growth dysfunction resulting in drumstick-shaped metacarpals and epiphyseal invagination also have been noted. Eventually the trabecular pattern becomes blurred. Areas of cystic rarefaction followed by diffuse osteosclerosis are seen. End-stage renal failure leads to skeletal manifestations of renal osteodystrophy, including bone resorption, sclerosis, and osteomalacia [1, 2, 4]. In advanced disease, the skeletal alterations are produced not only by a direct response to oxalate deposition from hyperoxaluria, but also are affected by acquired or secondary oxalosis associated with chronic renal failure [4].

Secondary or acquired oxalosis is more common than the primary hereditary form. It is a known complication of renal failure, but also may result from excessive ingestion of substances that contain oxalate or are oxalate precursors, such as rhubarb, spinach, or ethylene glycol. In addition, pyridoxine deficiency and exposure to methoxyflurane anesthesia may result in secondary oxalosis. Patients with chronic gastrointestinal disorders, such as chronic inflammatory bowel disease, pancreatic and biliary tract diseases, bacterial overgrowth syndrome, and jejunoileal bypass surgery, which cause significant fat malabsorption, also may develop secondary oxalosis [3, 4]. The secondary causes of oxalosis usually do not produce skeletal and renal alterations as florid as those in the primary form.

Margaret A. Stull
Mark Glass-Royal

REFERENCES

1. Day DL, Scheinman JI, Mahan J. Radiological aspects of primary hyperoxaluria. *AJR* **1986**;146:395–401
2. Brancaccio D, Poggi A, Ciccarelli C, et al. Bone changes in end-stage oxalosis. *AJR* **1981**;136:935–939
3. Williams HE, Smith LH Jr. Primary hyperoxaluria. In: Stansbury JB, Wyngaarden JB, Fredrickson DS, Goldstein JL, Brown MS, eds. *The metabolic basis of inherited disease*, 5th ed. New York: McGraw-Hill, **1983**:204–228
4. Resnick D. Other crystal-induced diseases. In: Resnick D, Niwayama G, eds. *Diagnosis of bone and joint disorders*, 2nd ed. Philadelphia: Saunders, **1988**:1804–1814

Case 4: Gorham Syndrome of the Right Clavicle and Scapula

This 16-year-old boy suffered a fracture of the right clavicle on September 10, 1987, while playing football. Radiograph of the right shoulder on the day of injury (Fig. 4A) showed a pathologic fracture of the clavicle with a moth-eaten pattern of osteolysis destroying the distal half of the bone. Because of this appearance, biopsy was performed. Its results were interpreted as compatible with angioma or healing fracture, without evidence of malignancy. Subsequent radiographs taken on June 20, 1989, revealed complete disappearance of the right clavicle, adjacent superior scapula, and coracoid process (Fig. 4B). A right axillary arteriogram (Fig. 4C) showed an abnormal hypervascular blush in the neck of the scapula, without pooling of contrast material or arteriovenous shunting. In light of the progression of radiologic findings, the original biopsy specimen was reevaluated and Gorham syndrome was diagnosed.

Gorham syndrome (also known as Gorham disease, disappearing bone disease, phantom bone, massive osteolysis, hemangiomatosis with massive osteolysis, massive osteolysis, and angiomatosis) is a rare condition of unknown cause characterized by extensive localized osteolysis associated with proliferation of abnormal vascular channels [1, 2]. It is not hereditary, and no significant age or sex predilection is evident [3]. Approximately 100 cases have been reported, the first in 1838 [4].

Clinical presentation is variable. Some patients complain of pain; others experience limitation of motion or obvious deformity, without significant pain [3]. Antecedent trauma is present in slightly more than half the patients [2]. Laboratory values are usually normal.

Radiologically, the process is usually monocentric, but can spread to adjacent soft tissues and bones, despite an intervening joint space [3], as in our case. The process starts as small, focal areas of resorption that enlarge until complete dissolution of a portion of bone results, with tapering of the remaining osseous structure, resembling a licked stick of candy [2]. Pathologic fracture is frequent. Any bone may be involved. Arteriography usually does not reveal profound vascular abnormality, although a faint blush in the affected area may be seen [3, 5].

On histologic examination, multiple thin-walled vascular channels associated with bony destruction are noted [1]. These channels may be of vascular or lymphatic origin [2]. Osteoclasts are scarce, and no evidence is present for malignancy.

Therapeutic options that have been attempted include medical treatment, prosthetic devices, bone grafting, surgical extirpation, and radiotherapy; no clearly optimal approach has

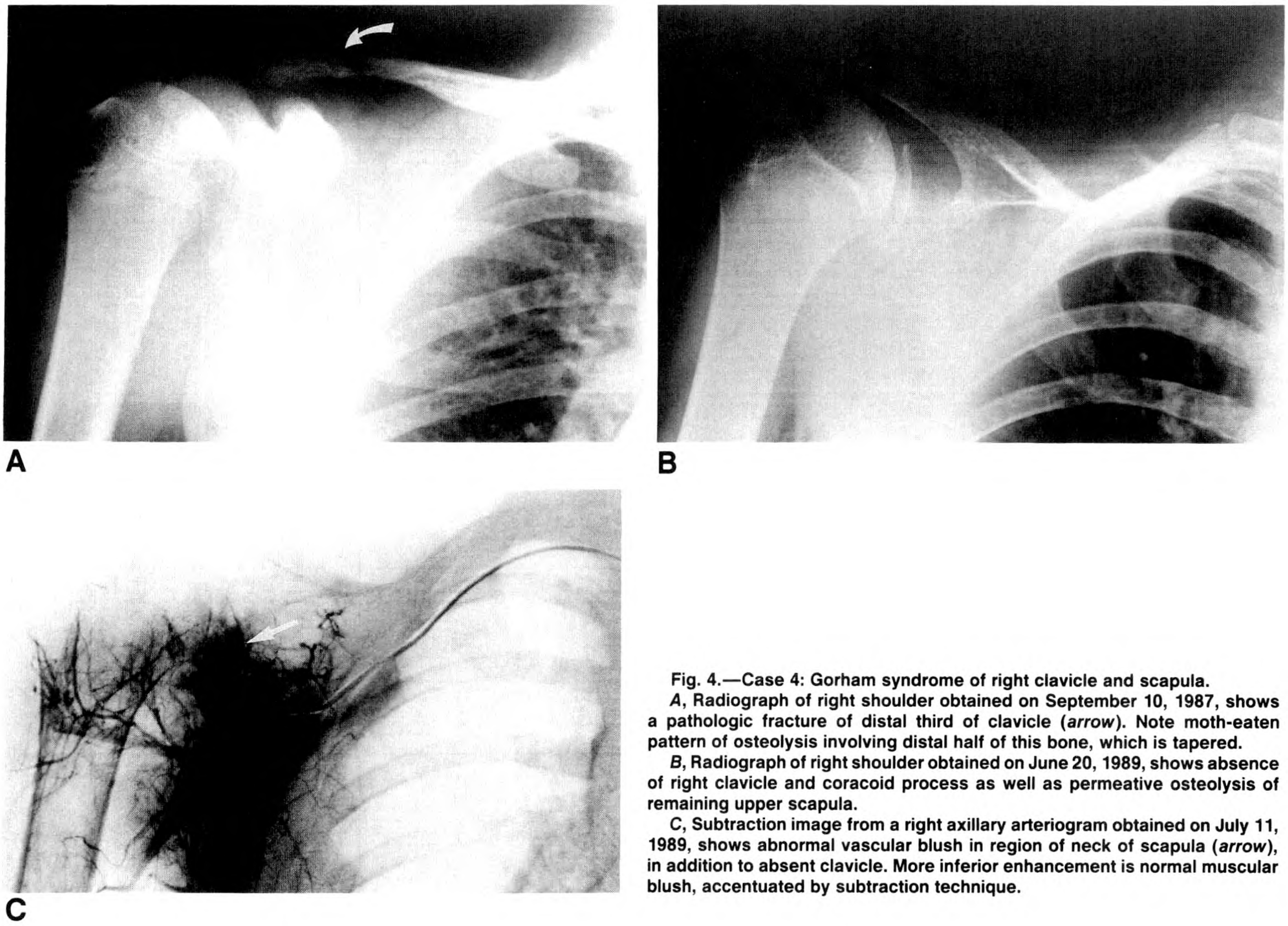

Fig. 4.—Case 4: Gorham syndrome of right clavicle and scapula.

A, Radiograph of right shoulder obtained on September 10, 1987, shows a pathologic fracture of distal third of clavicle (*arrow*). Note moth-eaten pattern of osteolysis involving distal half of this bone, which is tapered.

B, Radiograph of right shoulder obtained on June 20, 1989, shows absence of right clavicle and coracoid process as well as permeative osteolysis of remaining upper scapula.

C, Subtraction image from a right axillary arteriogram obtained on July 11, 1989, shows abnormal vascular blush in region of neck of scapula (*arrow*), in addition to absent clavicle. More inferior enhancement is normal muscular blush, accentuated by subtraction technique.

been defined. The condition often arrests spontaneously, but may be fatal if vital osseous structures are involved.

Mark Glass-Royal
Margaret A. Stull

REFERENCES

1. Gorham LW, Wright AW, Shultz HH, Maxon FC. Disappearing bones: a rare form of massive osteolysis. *Am J Med* **1954**;17:674–682
2. Choma ND, Biscotti CV, Bauer TW, Mehta AC, Licata AA. Gorham's syndrome: a case report and review of the literature. *Am J Med* **1987**; 83:1151–1156
3. Resnick D, Niwayama G. Osteolysis and chondrolysis. In: Resnick D, Niwayama G, eds. *Diagnosis of bone and joint disorders*, 2nd ed. Philadelphia: Saunders, **1988**:4141–4168
4. Jackson JBS. A boneless arm. *Boston Med Surg J* **1838**;18:368–369
5. Cannon SR. Massive osteolysis: a review of seven cases. *J Bone Joint Surg [Br]* **1986**;68-B:24–28

Neuroradiology Case of the Day

John P. Deveikis,[1] Curtis A. Cammarata, William M. Reid, Terri L. Ingram, Roland J. Mestayer, Dieter Schellinger, Nicholas J. Patronas, and Margaret A. Stull

Case 1: Neurofibromatosis 2

A 17-year-old white woman with a 6-year history of hearing loss had neurofibromatosis 2 (NF-2) diagnosed several years ago. More recently, she experienced increasing disequilibrium, severe headaches, progressive hearing loss, and difficulty concentrating in school.

An axial T1-weighted MR image (Fig. 1A) showed well-defined, bilateral, extraaxial masses causing enlargement and "trumpeting" of the internal auditory canals and severe compression of the brainstem. A gadolinium-enhanced T1-weighted MR study (Figs. 1B–E) also was performed. A coronal MR image (Fig. 1B) revealed intense, uniform enhancement typical of acoustic neuromas. Imaging at the level of the orbital apices (Fig. 1C) showed a homogeneously enhancing durally based mass in the right parietal convexity characteristic of meningioma. An axial MR image (Fig. 1D) showed a partly cystic medullary mass in an intraaxial location. A coronal MR image (Fig. 1E) showed a partly cystic, inhomogeneously enhancing intraaxial mass. Both intraaxial masses were compatible with primary brain gliomas.

Neurofibromatosis is the most common of the disorders classified as phakomatoses (neurocutaneous syndromes), with an incidence of one in 3000 live births [1]. At least two distinct forms exist (NF-1 and NF-2), having different genetic and clinical characteristics [2]. Both forms are transmitted in an autosomal dominant fashion with high penetrance (almost 100%) and variable phenotypic expression.

NF-1 is related to a gene locus on chromosome 17 [3], although half of all cases occur by spontaneous mutation [1]. Multiple cafe-au-lait spots, peripheral neurofibromas, axillary freckling, and Lisch nodules (pigmented iris hamartomas) characterize this disease [4]. The combined frequency of CNS tumors in these patients is 5–10%. Typical tumors include optic gliomas, acoustic and trigeminal nerve schwannomas, astrocytomas, ependymomas, hamartomas, and glioblastomas [4].

NF-2 is much less common and is related to a gene locus on chromosome 22 [5]. Bilateral acoustic neuromas are the hallmark of this disease. Symptoms in NF-2 patients typically begin in the teens or early twenties, with hearing loss as the presenting complaint (as in this case). Other symptoms include facial weakness, sensory changes, headache, or visual changes [2]. CNS tumors affect as many as 45% of these patients [6]. Schwann cell tumors are most common and may develop on any of the cranial nerves. Acoustic neuromas usually arise from the vestibular portion of the nerve. Hearing may be preserved in some cases if these tumors are partially or completely removed. Alternatively, bilateral tumors may progress relentlessly, leading to visual disturbance, paresis, and eventual death from brainstem compression. Meningiomas and gliomas also are common. Recent reports have emphasized the high incidence of spinal intramedullary tumors in an extended kindred with NF-2 [7] and that these tumors can remain asymptomatic or initially be confused with syringomyelia [7, 8].

The high incidence of CNS tumors in patients with NF-2 and the near 100% penetrance in this disease illustrate the need for periodic screening examinations of these patients and their family members at risk (i.e., first-degree relatives). Early detection of treatable lesions affords the best opportunity for successful intervention. MR is regarded as the screening technique of choice because of its greater sensitivity in lesion detection, high resolution, freedom from bone artifacts, multiplanar capability, and lack of ionizing radiation. Gadolinium-enhanced T1-weighted images should be included in the screening examination to afford additional increased sensitivity in lesion detection (especially in the case of small intracanalicular tumors and meningiomas).

Curtis A. Cammarata
John P. Deveikis
Dieter Schellinger
Nicholas J. Patronas
Margaret A. Stull

---

[1] All authors: Department of Radiology, Georgetown University Medical Center/NIH Clinical Center, 3800 Reservoir Dr., N. W., Washington, DC 20007. Address reprint requests to M. A. Stull, coordinator of the Case of the Day series.

AJR **154:1337–1342, June 1990** 0361–803X/90/1546–1337 © American Roentgen Ray Society

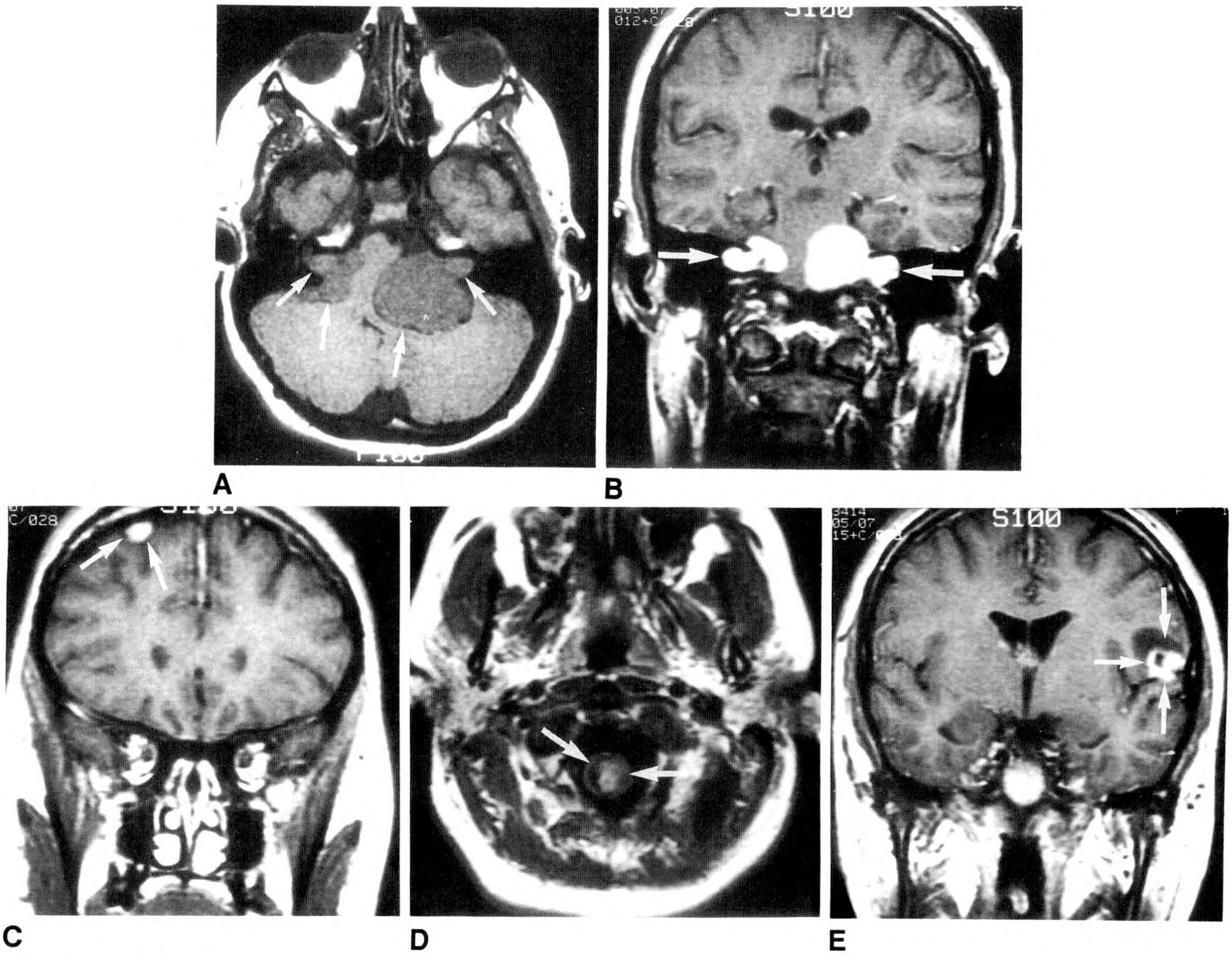

Fig. 1.—Case 1: Neurofibromatosis 2.

***A*, Axial T1-weighted MR image (600/20) shows bilateral intracanalicular and extracanalicular acoustic neuromas (*arrows*).**

***B*, Coronal gadolinium-enhanced T1-weighted MR image (600/20) shows intense homogeneous enhancement (*arrows*) of tumors.**

***C*, Coronal gadolinium-enhanced T1-weighted MR image (600/20) shows a homogeneously enhancing, durally based mass located in right parietal convexity (*arrows*).**

***D*, Axial gadolinium-enhanced T1-weighted MR image (600/20) shows a partially cystic mass in medulla (*arrows*).**

***E*, Coronal gadolinium-enhanced T1-weighted MR image (600/20) reveals intense enhancement of soft-tissue component of left parietal mass (*arrows*).**

REFERENCES

1. Crowe FW, Schull WJ, Neil JW. *A clinical, pathological and genetic study of multiple neurofibromatosis.* Springfield: Thomas, **1956**
2. Martuza R, Eldridge R. Neurofibromatosis 2 (bilateral acoustic neurofibromatosis). *N Engl J Med* **1988**;318:684–688
3. Barker D, Wright T, Nguyen K, et al. Gene for von Recklinghausen neurofibromatosis is in the pericentromeric region of chromosome 17. *Science* **1987**;236:1100–1102
4. Riccardi VM. Von Recklinghausen neurofibromatosis. *N Engl J Med* **1981**; 305:1617–1627
5. Seizinger BR, Martuza RL, Gusella JF. Loss of genes on chromosome 22 in tumorigenesis of human acoustic neuroma. *Nature* **1986**;322:644–647
6. Rodriquez HA, Berthrong M. Multiple primary intracranial tumors in von Recklinghausen's neurofibromatosis. *Arch Neurol* **1966**;14:467–474
7. Curran JG, Weissman JR, WIlliams JP, Wertelecki W. Superneau DW. High incidence of spinal intramedullary tumor in a kindred affected by neurofibromatosis 2: MR findings. *AJNR* **1989**;10:906
8. Kim T, Foust RJ, Mojtahedi S. MR imaging of asymptomatic brainstem and spinal cord lesions in sisters with neurofibromatosis. *AJNR* **1989**; 10[suppl.]:71–72

Case 2: Hypothalamic Histiocytosis X

This 37-year-old man presented with diabetes insipidus and panhypopituitarism. Coronal MR images (Figs. 2A and 2B) revealed a lesion in the right hypothalamus and a thickened pituitary stalk. Gadolinium-enhanced MR images (Figs. 2C and 2D) showed enhancement of the enlarged right hypothalamus and pituitary stalk. The workup included a chest radiograph (Fig. 2E), which showed diffuse interstitial disease. Histologic examination of a lung biopsy specimen revealed histiocytic infiltrates, consistent with histiocytosis X.

Histiocytosis X is an inflammatory process characterized by abnormal proliferating histocytes and other inflammatory

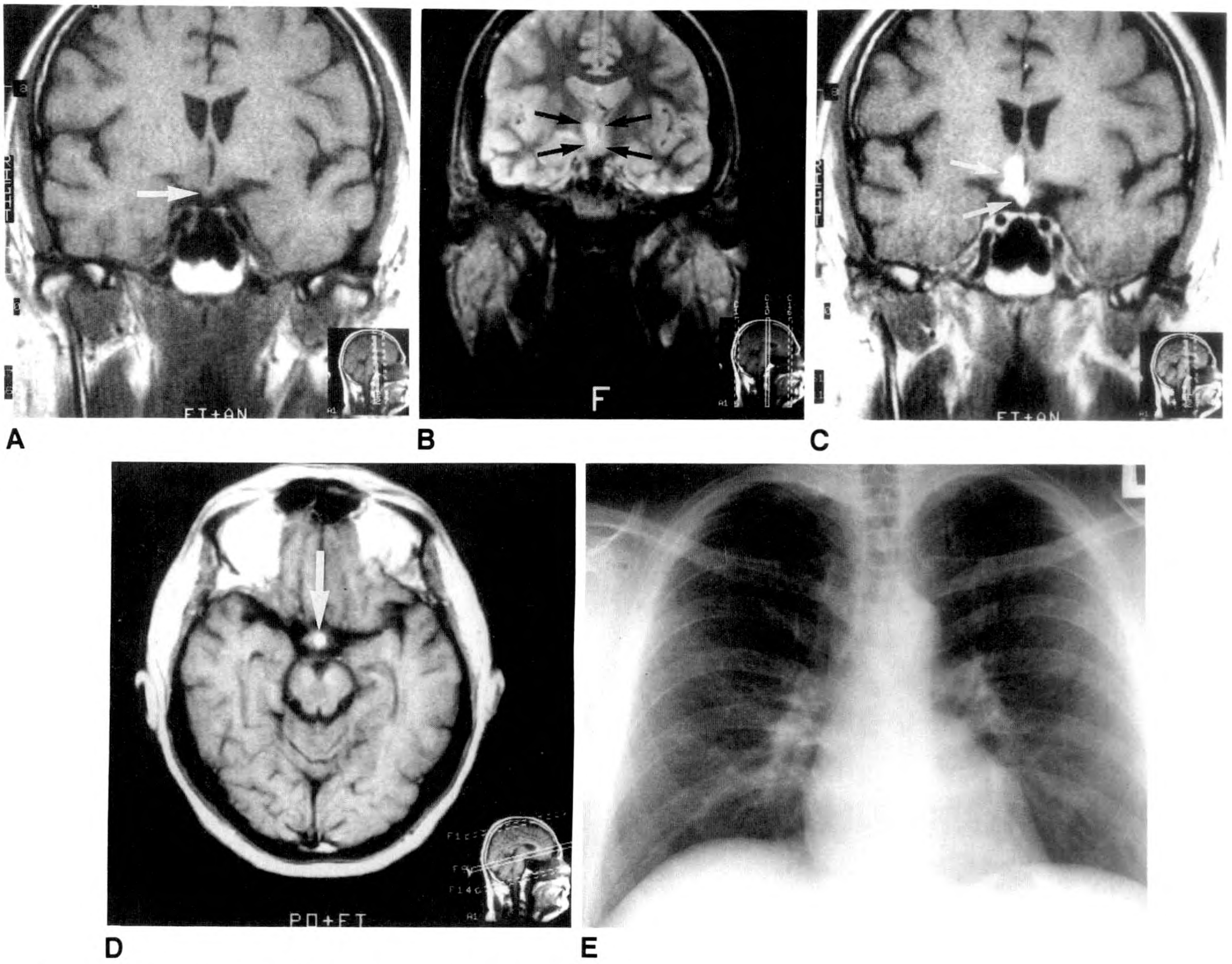

Fig. 2.—Case 2: Hypothalamic histiocytosis X.
A, Coronal T1-weighted MR image (400/26) shows subtle low signal intensity in right hypothalamus and a thickened pituitary stalk (*arrow*).
B, Coronal T2-weighted MR image (2000/80) shows increased signal intensity in right hypothalamus (*arrows*).
C, Coronal gadolinium-enhanced T1-weighted MR image (400/26) shows enhancement of enlarged right hypothalamus and pituitary stalk (arrows).
D, Axial gadolinium-enhanced T1-weighted MR image (533/20) shows an enhancing thickened pituitary stalk (*arrow*).
E, Posteroanterior chest radiograph shows diffuse interstitial lung disease, most prominent in upper and mid lung zones.

cells. Any part of the reticuloendothelial system may be involved. Clinical severity ranges from solitary or multifocal bone lesions in eosinophilic granuloma of bone, to chronic multiorgan involvement in Hand-Schüller-Christian disease, to the rapidly progressive and disseminated condition characteristic of Letterer-Siwe disease [1]. Less than 10% of patients have the classic Christian triad of diabetes insipidus, unilateral or bilateral exophthalmos, and skull lesions, reflecting hypothalamic, orbital, and calvarial involvement.

Eosinophilic granuloma occasionally affects the brain parenchyma, most commonly the hypothalamus and pituitary gland. However, almost any area of the brain may be involved [2–4]. On CT, parenchymal histiocytosis appears isodense to hyperdense and may enhance extensively [2–4]. On T1-weighted MR images, the lesions are usually isodense to hypointense compared with brain (Fig. 2C). Surrounding edema is variable [5]. Gadolinium enhancement on MR is analogous to the contrast enhancement on CT (Figs. 2D and 2E).

The differential diagnosis for the hypothalamic lesion in this patient includes primary glioma, metastases, lymphoma, and sarcoidosis [2].

William M. Reid
John P. Deveikis
Dieter Schellinger
Nicholas J. Patronas
Margaret A. Stull

REFERENCES

1. Fefer A. Diseases of the spleen and reticuloendothelial system. In: Isselbacher KJ, Adams RD, Brunwald E, Petersdord RG, Wilson JD, eds. *Harrison's principles of internal medicine,* 9th ed. New York: McGraw-Hill, **1980**:1581–1583
2. Williams AL. Infectious diseases. In: Williams AL, Haughton VM. *Cranial computed tomography.* St. Louis: Mosby, **1985**:269–315
3. Khant A, Fulco JD, Shende A, et al. Focal histiocytosis X of the parietal lobe. *J Neurosurg* **1980**;52:431–433
4. Sivalingann JS, Corkill G, Ellis WG, et al. Focal eosinophilic granuloma of the temporal lobe. *J Neurosurg* **1977**;47:941–945
5. Graif M, Pennock JM. MR imaging of histiocytosis X in the central nervous system. *AJNR* **1986**;7:21–23

Case 3: Parasellar Epidermoid

This 22-year-old woman had an 8-month history of intermittent dizziness, nausea, and headache. Workup included unenhanced and enhanced CT and MR scans and angiography. CT and MR studies (Figs. 3A–3E) showed a nonenhancing, calcified mass in a parasellar location, appearing to arise in Meckel's cave and protrude posteriorly into the cerebellopontine angle region. After surgery, histologic examination revealed an epidermoid.

Epidermoids (also called primary cholesteatomas) are congenital tumors that arise from inclusion of ectodermal elements into the neural tube during embryogenesis. Pathologically, they consists of keratin, epithelial debris, and cholesterin, unlike dermoids, which contain dermal appendages and teratomas, which contain all three germ cell layers [1]. Epidermoids are slow-growing, benign lesions. Patients may have headaches or seizures.

Common locations for intracranial epidermoids include the cerebellopontine angle, the suprasellar region, and the middle cranial fossa [1]. Lesions that extend from the middle cranial

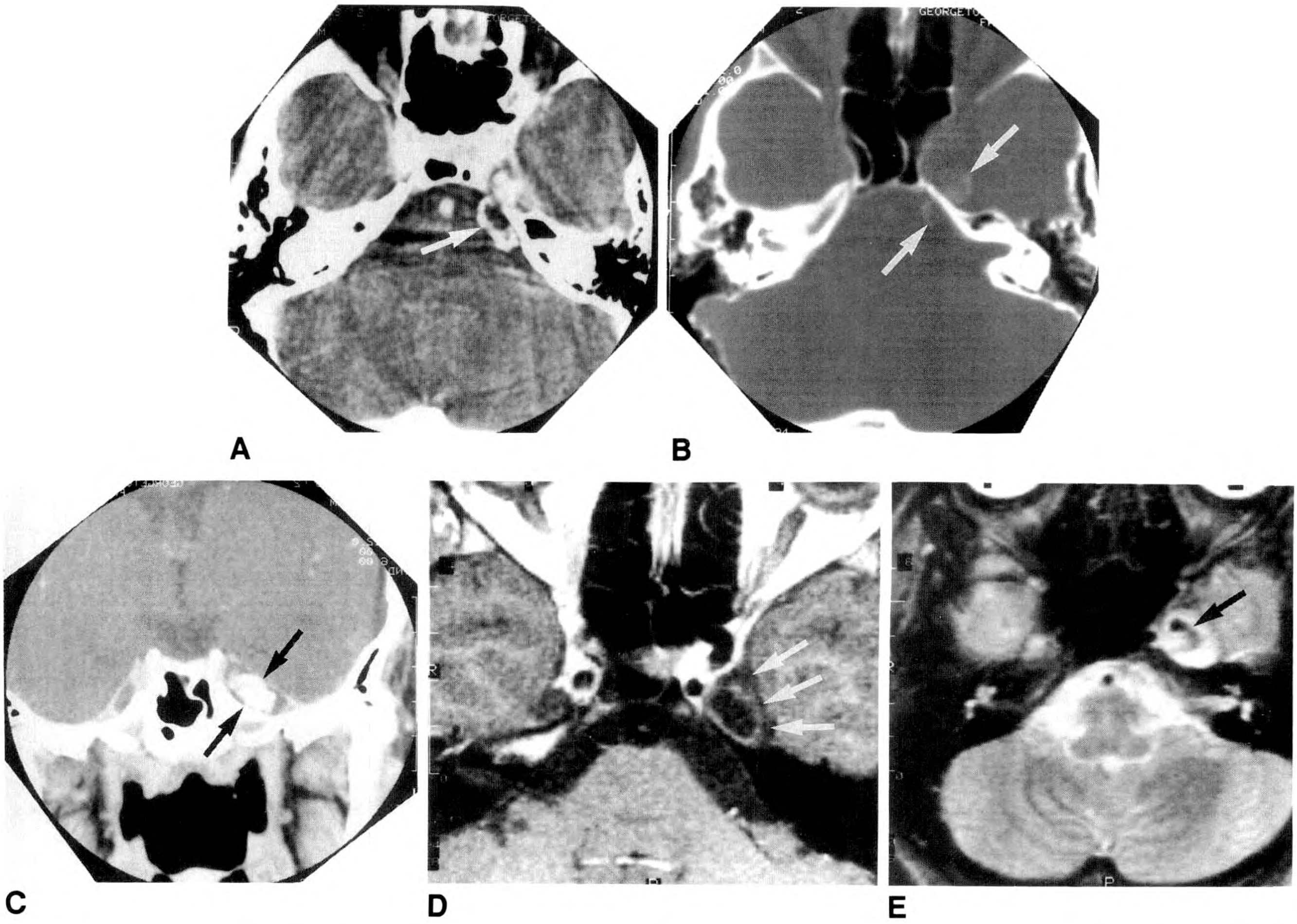

Fig. 3.—Case 3: Parasellar epidermoid.

***A*, Axial contrast-enhanced CT scan of head shows a nonenhancing calcified mass in parasellar region extending into cerebellopontine angle (*arrow*).**

***B*, Axial CT scan of head with bone windows reveals calcified mass on both sides of petrous tip (*arrows*).**

***C*, Coronal contrast-enhanced CT scan of head shows calcified lesion within Meckel's cave (*arrows*).**

***D*, Axial gadolinium-enhanced T1-weighted MR image (600/20) at level of cavernous sinus shows an extraaxial nonenhancing low-intensity lesion displacing medial temporal lobe (*arrows*).**

***E*, Axial T2-weighted MR image (2500/80) slightly inferior to *D* shows lesion is hyperintense and contains a curvilinear band of low signal intensity (*arrow*).**

fossa into the posterior fossa are called dumbbell or hourglass lesions, similar to those in this patient [2]. On CT, epidermoids characteristically appear as nonenhancing, well-demarcated, hypodense lesions with attenuation similar to CSF [3]. If contrast enhancement occurs, it is around the margin of the lesions. Hyperdense epidermoids have been reported rarely. This appearance is thought to be related to microcalcification [4]. The presence of gross calcifications within epidermoids, as in this case, has rarely been observed on CT [4].

MR has proved helpful in clearly defining the extraaxial location of these tumors. They may attain large size, yet characteristically do not produce edema in surrounding tissue [3]. The typical MR appearance of epidermoids is a somewhat inhomogeneous, low-signal-intensity mass on T1-weighted images that is hyperintense on T2-weighted images [5]. However, the imaging characteristics of epidermoids may vary depending on the relative contents of keratin and cholesterol.

Terri L. Ingram
John P. Deveikis
Dieter Schellinger
Nicholas J. Patronas
Margaret A. Stull

REFERENCES

1. Elster AD. *Cranial magnetic resonance imaging*. New York: Churchill Livingstone, **1988**:137
2. Albanese V, Tomasello F, Picozzi P, Sampaolo S, Spadaro A. Paramedian hourglass epidermoid extending above and below the tentorium. *Surg Neurol* **1982**;18:356–363
3. Vion-Dury J, Vincentelli F, Jiddane M, et al. MR imaging of the epidermoid cysts. *Neuroradiology* **1987**;29:333–338
4. Braun IF, Naidich TP, Leeds NE, Koslow M, Zimmerman HM, Chase NE. Dense intracranial epidermoid tumors. *Radiology* **1977**;122:717–719

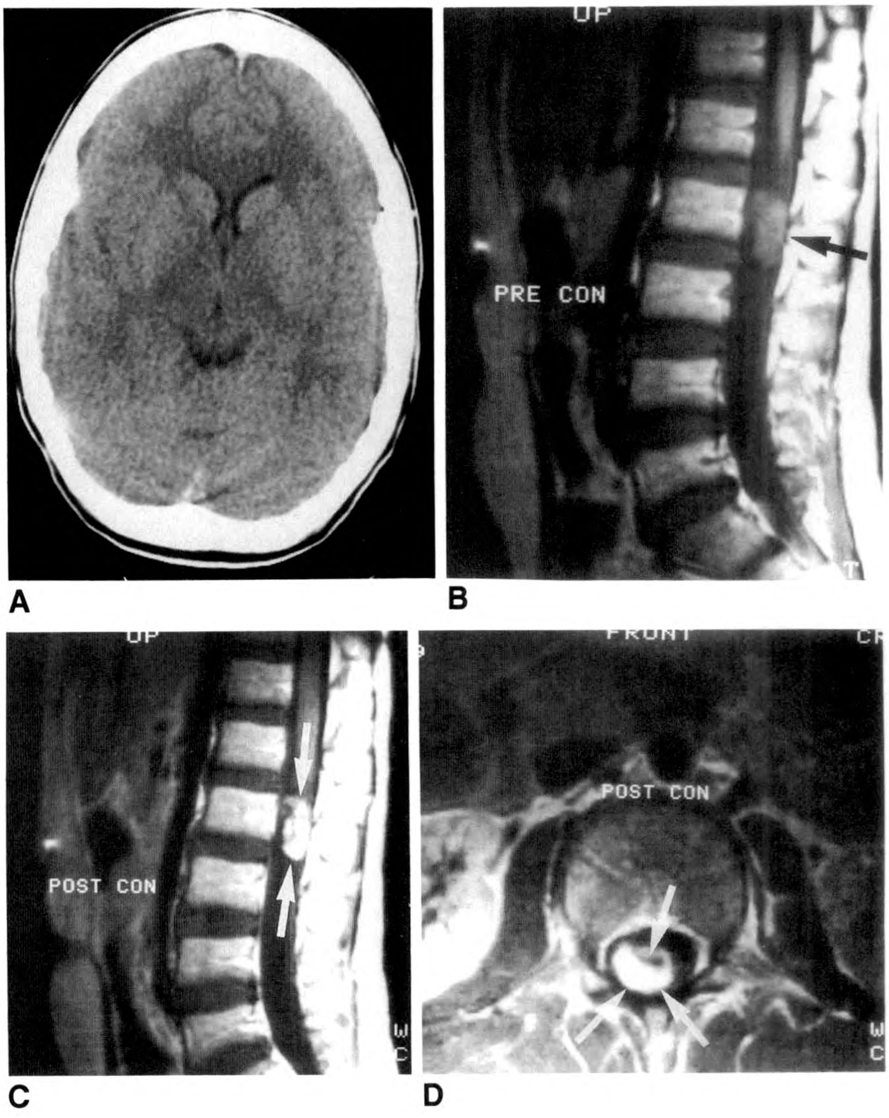

Fig. 4.—Case 4: Subarachnoid hemorrhage complicating an ependymoma of cauda equina.

***A*, Transaxial unenhanced CT scan of head is normal.**

***B*, Sagittal T1-weighted MR image (600/20) shows an extramedullary, intradural mass of cauda equina (*arrow*).**

***C* and *D*, Sagittal (*C*) and transaxial (*D*) gadolinium-enhanced T1-weighted MR images (600/20) show intense enhancement of mass (*arrows*).**

5. Olsen JJ, Beck DW, Crawford SC, Menezes AH. Comparative evaluation of intracranial epidermoid tumors with computed tomography and magnetic resonance imaging. *Neurosurgery* **1987**;21:357-360

Case 4: Subarachnoid Hemorrhage Complicating an Ependymoma of Cauda Equina

This 14-year-old boy had acute onset of severe headache, nausea, and vomiting. The patient also described a mild degree of back pain of several months duration. Neurologic examination was normal. Emergent CT scan of the head (Fig. 4A) showed no evidence of subarachnoid or intraparenchymal hemorrhage. Subsequently, lumbar puncture showed bloody CSF. Clinical suspicion of a ruptured berry aneurysm prompted a request for a cerebral arteriogram (not shown), which was normal.

The patient's back pain persisted and MR evaluation of the spine (Figs. 4B-4D) was performed. An intradural extramedullary mass of the cauda equina was evident. No other abnormalities of the spinal axis were identified. At surgery, a myxopapillary ependymoma of the cauda equina was confirmed.

Ependymomas are one of the most common tumors of the spinal cord in both children and adults [1]. Patients with intraspinal tumors generally present with back pain of many months duration. Radicular pain or weakness also can occur. Back pain is exacerbated by hemorrhage from the tumor.

Subarachnoid hemorrhage has been documented in patients with ependymomas and a variety of other intradural tumors [2, 3]. Hemorrhage may occur spontaneously or after minor trauma.

On MR images, ependymomas may present as intramedullary masses at any location along the spinal cord or as an extramedullary lesion of the cauda equina [4], as in this patient. On T1-weighted MR images they are characterized by mass effect and are typically isointense with the spinal cord. Homogeneous or slightly heterogeneous hyperintensity is noted on T2-weighted images. Intratumoral cysts also may be identified. Ependymomas usually enhance after the administration of paramagnetic contrast agents.

The treatment for intraspinal ependymomas is surgical excision. Extramedullary ependymomas are often easily resected. Prognosis for these extramedullary tumors after surgery and radiation therapy is generally excellent [1]. The myxopapillary histology, reflected in this case, also improves prognosis [5].

Roland J. Mestayer
John P. Deveikis
Dieter Schellinger
Nicholas J. Patronas
Margaret A. Stull

REFERENCES

1. Barone BM, Eluidoe AL. Ependymomas: a clinical survey. *J Neurosurg* **1970**;33:428-438
2. Fincher EF. Spontaneous subarachnoid hemorrhage in intradural tumors of the lumbar sac: a clinical syndrome. *J Neurosurg* **1951**;8:576-584
3. Ayres WW. Ependymoma of the cauda equina: a report of the clinicopathologic aspects and follow up studies of 18 cases. *Milit Med* **1958**;122:10-15
4. Wagle WA, Jaufman B, Mincey JE. Intradural extamedullary ependymoma: MR-pathologic correlation. *J Comput Assist Tomogr* **1988**;12:705-707
5. Sonneland PR, Scheithauer BW, Onofrio BM. Myxopapillary ependymoma, a clinicopathologic and immunocytochemical study of 77 cases. *Cancer* **1985**;56:883-893

Letters

Universal Premedication Before Use of Ionic Contrast Medium

I recently organized a genitourinary lecture series for the radiology residents in our department. One topic was the use of ionic vs nonionic contrast material. In reviewing the literature [1–4], several general principles are clear. No statistically significant difference has been found in mortality rates associated with the use of ionic vs nonionic contrast media. The prevalence of severe adverse reactions appears to be lower with nonionic agents. However, evidence exists that the prevalence of severe adverse reactions in patients receiving ionic contrast medium who have been pretreated with corticosteroids is comparable to that in patients receiving nonionic contrast medium without such pretreatment. An argument could be made that the patients most at risk are those first-time patients who have the potential for development of serious adverse reactions to ionic contrast agents but have not been identified and premedicated. My thought is, Why not premedicate all patients before they receive IV ionic contrast material? The risk associated with premedication is negligible and achieves the benefit of a lower prevalence of adverse reactions to contrast medium without accruing the additional cost of a nonionic contrast agent.

This argument has been presented in the literature but has not been implemented in daily clinical practice. I wonder if other physicians find this a logical approach and would consider universal premedication before the use of IV ionic contrast agents.

Alda F. Cossi
Brooke Army Medical Center
San Antonio, TX 78232

REFERENCES

1. McClennan BL. Low-osmolality contrast media: premises and promises. *Radiology* **1987**;182:1-8
2. Lasser EC, Berry CC, Talner LB, et al. Pretreatment with corticosteroids to alleviate reactions to intravenous contrast material. *N Engl J Med* **1987**;317:845-849
3. Wolf GL, Arenson RL, Cross AP. A prospective trial of ionic vs nonionic contrast agents in routine clinical practice: comparison of adverse effects. *AJR* **1989**;152:939-944
4. Lasser EC, Berry CC. Nonionic vs ionic contrast media: what do the data tell us? *AJR* **1989**;152:945-946

Note.—The opinions or assertions contained in the preceding letter are the private views of the author and are not to be construed as official or as reflecting the views of the Army Medical Department, the Department of the Army, or the Department of Defense.

Reply

Dr. Cossi asks whether additional thought should be given to the concept of routine pretreatment with corticosteroids before the use of IV ionic contrast agents. I also raised this question in a previous report [1] in the *AJR*. In that report, I also mentioned some of the potential logistic complications and suggested some possible modifications of an earlier corticosteroid protocol. Dr. Cossi suggests that the patients most at risk are those first-time patients who have the potential for development of serious adverse reactions to ionic contrast agents but who have not been identified and premedicated. In a study [2] of the potential protective effects of corticosteroids in patients receiving IV contrast material, my colleagues and I found that 93% of our patients either were not exposed to contrast media or were known nonreactors. In this group, the occurrence of grade 3 reactions (excluding dermatologic changes) was 1/2340 (0.04%) with the two-dose Medrol (methyl prednisolone) regimen and 19/3941 (0.5%) for the combined placebo and one-dose regimen ($p = .006$). This is a 12-fold difference. In the same series, 64% of our patients were either nonallergic or nonreacting. This category generally is considered the low-risk population in other studies. For this group, we found that the prevalence of grade 3 reactions in patients receiving the two-dose Medrol regmen was 1/1597 (0.06%) vs 12/2736 (0.44%) in patients receiving placebo or the one-dose regimen ($p = .04$). This is a sevenfold difference. The one-dose regimen in our study was completely indistinguishable statistically from the one-placebo or two-placebo groups.

The logistics of obtaining complete compliance with a two-dose corticosteroid regimen may seem daunting on first consideration. With some work, however, a two-dose pretreatment schedule may be feasible. I am aware of only one set of data (C. E. Seibert, personal communication) that addresses this point. That study covered the experience in two private hospitals and a private office over a 22-month period and included somewhat more than 10,000 patients. A review covering approximately the last 11 months of the study indicated that compliance was 95% or better in both hospitals and in the office. Approximately 47% of the total patients were receiving ionic media, according to the investigator's protocol, and hence the compliance figures come from this group.

I emphasize, as in previous reports, that the logistics, the economics, and the patient mix varies from institution to institution and therefore individual decisions on these matters should be made. Whatever the decision, it would seem prudent to use a written protocol that outlines the general course of action but makes allowances for appropriate individual exceptions.

Elliott C. Lasser
University of California, San Diego
La Jolla, CA 92093

REFERENCES

1. Lasser EC. Pretreatment with corticosteroids to prevent reactions to IV contrast material: overview and implications. *AJR* **1988**;150:257–259
2. Lasser EC, Berry CC, Talner LB, et al. Pretreatment with corticosteroids to alleviate reactions to intravenous contrast material. *N Engl J Med* **1987**;317:845–849

Reaction to Nonionic Contrast Medium During Arthrography of the Temporomandibular Joint

We are all aware that contrast material may cause reactions, but with the use of modern contrast agents, these reactions are rare, especially during arthrography [1]. In a series of 126,000 arthrograms performed by 84 radiologists, Newberg et al. [1] reported 61 cases of hives and nine cases of other complications that might be related to the use of contrast media, a prevalence of less than 0.06%. To the best of our knowledge, no description of a reaction to the contrast medium used during arthrography of the temporomandibular joint (TMJ) has been published.

A 27-year-old woman was referred for arthrography of her left TMJ because of pain and dysfunction. She had not previously had radiologic contrast medium. She reported that she had been allergic to room dust for the past 2 years.

After preparation of the skin (povidone-iodine) and local anesthesia (0.5 ml 2% lidocaine), about 0.5 ml of nonionic contrast medium (Omnipaque [Winthrop Pharmaceuticals, New York, NY], 300 mg iodine/ml) was injected into the left TMJ. Immediately after the injection, the patient experienced itching in her eyes, specifically on the left. Fluoroscopic evaluation of joint function was performed, and spot films were obtained. After about 2 min, mild periorbital edema (Fig. 1) developed, which was most pronounced around the left eye. The patient also felt mild congestion on breathing. She was given one tablet (25 mg) of Benadryl (diphenhydramine). The congestion lasted for another 10–15 min and then gradually resolved. Mild rhinitis was noted also. The periorbital edema increased gradually during the following 30 min. The itching in the eyes gradually decreased and was gone after about 30 min. The patient was observed for 1 hour and then left the department. At 24 hr, the periorbital swelling remained to some degree, but the other signs and symptoms were gone.

Reactions to contrast media after arthrography are rare [1], and to our knowledge, this is the first reported case involving the TMJ. This case shows that reactions to contrast media can occur even when a small amount of nonionic contrast medium is injected into a joint. It emphasizes the need to be prepared for these reactions, which nearly always occur unexpectedly [2].

Per-Lennart Westesson
James V. Manzione
University of Rochester Medical Center
Rochester, NY 14642

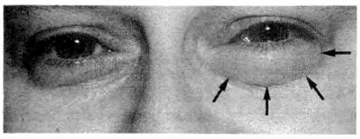

Fig. 1.—Mild periorbital edema caused by nonionic contrast medium.

REFERENCES

1. Newberg AH, Munn CS, Robbins AH. Complications of arthrography. *Radiology* **1985**;155:605–606
2. Ansell G, Tweedie MCK, West CR, Price-Evans DA, Couch L. The current status of reactions to intravenous contrast medium. *Invest Radiol* **1980**;15:32–39

Heart-Lung Transplantation: Postoperative Pleural Effusion

Pleural effusion is a frequent postoperative complication of heart and heart-lung transplantations [1–3]. In the current technique of heart-lung transplantation, the recipient's anterior paramediastinal parietal pleura on the right and left sides is incised widely, preserving the phrenic nerves within "ribbons" of pleura. The pulmonary ligaments are divided bilaterally, and the pericardium is incised widely [4]. On placement of the donor heart and lungs, no attempt is made to reestablish the integrity of pleural or pericardial barriers. The recipient heart is held in the usual mediastinal position, first by the inflated left lung and ultimately by the evolution of postoperative cicatricial changes (T. B. Icenogle, University of Arizona, Section of Cardiothoracic Surgery, personal communication).

We have encountered a case that graphically shows the absence of integrity of the normal pleural barriers between the right and left lungs postoperatively, allowing communication of a pleural effusion between both sides of the chest.

A 49-year-old man had heart-lung transplantation. Postoperatively, plain radiographs showed bilateral pleural effusions. Because thoracic CT suggested loculation of the pleural fluid collections (Fig. 1A), additional CT scans were obtained with the patient in the left lateral decubitus position in an attempt to confirm this finding. The scans showed immediate resolution of a pleural fluid component on the right side and a proportionate increase in the size of a pleural fluid component on the left side (Fig. 1B). This finding was thought to reflect absence of pleural integrity between the two sides of the chest.

This case shows the unusual form that a pleural fluid collection can take after heart-lung transplantation. It also points up the need for aggressive diagnosis and management of pleural effusion, empyema, and postoperative hemothorax to prevent problems that may

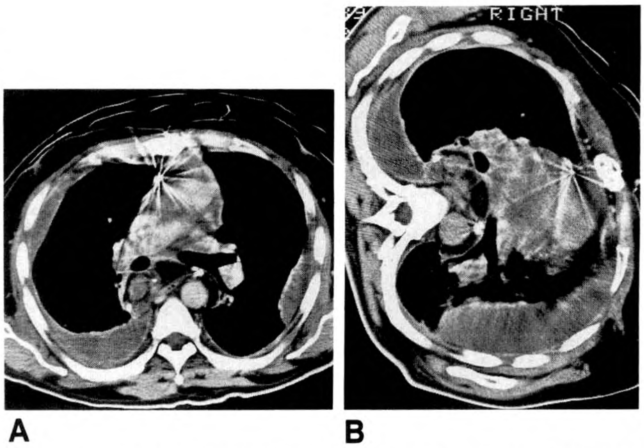

Fig. 1.—*A* and *B*, Postoperative pleural effusion after heart-lung transplantation. Thoracic CT scan (*A*) shows bilateral pleural effusions, and scan obtained with patient in left lateral decubitus position (*B*) shows resolution of anterolateral component of effusion on right side and proportionate increase in size of effusion on left side.

arise from these complications propagating from one hemithorax to the other.

Elliot M. Sacks
Evan C. Unger
University of Arizona
Tucson, AZ 85724

REFERENCES

1. Shirazi KK, Amendola MA, Tisnado J, Cho S, Beachley M, Lower R. Radiographic findings in the chest of patients following cardiac transplantation. *Cardiovasc Intervent Radiol* **1983**;6:1-6
2. Florence SH, Hutton LC, McKenzie FN, Kostuk WJ. Cardiac transplantation: postoperative chest radiographs. *J Can Assoc Radiol* **1988**;39: 115-117
3. Guthaner DF, Schnittger I, Wright A, Wexler L. Diagnostic challenges following cardiac transplantation. *Radiol Clin North Am* **1987**;25:367-376
4. Wallwork J. *Heart and heart-lung transplantation.* Philadelphia: Saunders, **1989**:277-280, 483-489

Collapse of a Breast Implant After Mammography

We recently saw a complication of mammography that was unique in our experience and is important to all who obtain mammograms on patients who have augmented breasts. A 53-year-old asymptomatic woman had her first screening mammogram. She had had bilateral breast augmentation approximately 10 years earlier with Heyer-Schulte saline-filled silicone implants (Mentor Corp., Goleta, CA). The cosmetic result had been satisfactory. A routine two-view study was done on dedicated mammography equipment with no apparent difficulty (Fig. 1). The technologist noted a firmness of the breasts and an inability to displace the implants away from the breast tissue for the "pinch technique" type of study [1]. The patient had no difficulty until 2 days later, when she noted a softening of one implant. By 7 days after mammography, the implant had deflated completely. The patient had suffered no breast trauma other than the mammogram.

Review of the literature found no reported case of collapse of an implant after mammography, although collapse related to other trauma and leakage from silicone-filled implants have been reported [2]. Neither the surgeon who did the original surgery nor the manufacturer of the implant was aware of a similar occurrence associated with mammography. The manufacturer indicated that the failure rate from all causes with this particular implant has been low.

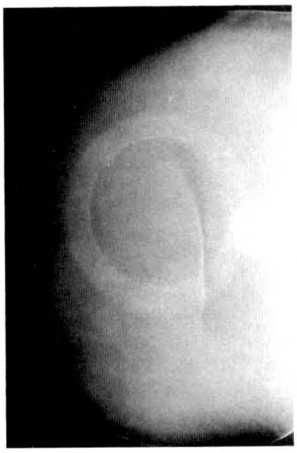

Fig. 1.—Oblique film-screen mammogram of right breast shows that implant fills breast with little mammary tissue evident. Implant valve is seen also.

We would be interested in hearing from any radiologist who knows of a similar experience.

Donald R. Hawes
University of Iowa Hospitals and Clinics
Iowa City, IA 52242

REFERENCES

1. Eklund GW, Busby RC, Miller SH, Job JS. Improved imaging of the augmented breast. *AJR* **1988**;151:469-473
2. Scott IR, Muller NL, Fitzpatrick DG, Burhenne LJ. Ruptured breast implant: computed tomographic and mammographic findings. *J Can Assoc Radiol* **1988**;39:152-154

Reply

Dr. Hawes has drawn attention to an interesting phenomenon: collapse of a breast implant after mammography. Although evidence implicating the mammographic procedure as the cause is circumstantial, it is certainly incriminating. I, too, have been unable to find a report in the literature of rupture of an implant after mammography. In more than 5 years of imaging augmented breasts by using the standard and modified compression views [1], I have observed no sign of damage to an implant.

We have had only one case of "capsulotomy" occurring during mammography. The patient had firm fibrous encapsulation of both breasts. During the final film of the examination of the second breast, an audible pop was heard when the compression paddle was applied in the oblique position. The involved breast was suddenly soft; it had a normal contour, but also a normal droop, unlike the firm, erect opposite breast. A repeat film of the now soft breast showed no difference compared with the first film. The patient was seen immediately by a plastic surgeon, who performed a closed, bimanual capsulotomy of the contralateral breast. The patient left the office with two symmetrical breasts, which were soft for the first time in 10 years.

The possibility of damage to an implant by compression during mammography certainly exists, although the event must be extremely rare. If an implant can deflate spontaneously, it seems quite reasonable to assume that applied pressure could result in such collapse. It would be interesting to know whether the collapsed implant was removed, and whether any unusual weakness or defect in the envelope could be detected. Figure 1 in Dr. Hawes's letter shows a crease in the implant wall, which may be a phenomenon of positioning and compression but also could have been present for a long time, resulting in a focal area of weakness. Such creases are seen commonly. I am unaware of any literature indicating a predisposition to weakening of the envelope by such a phenomenon, but the concept prompts interesting speculation.

I get the impression from Dr. Hawes's description that the implant was firmly encapsulated. If so, could the damage to the implant have been the result of a capsulotomy caused by the compression process? Collapse of an implant after vigorous bimanual closed capsulotomy has been described. Although I applaud the reporting of this event, it should not deter continued appropriate mammographic imaging of the augmented breast. These women are at no less risk for the development of breast cancer than women without breast implants. Lest inferences be drawn that the modified compression techniques [1] described for imaging the augmented breast are particularly damaging, it is important to appreciate that the implant is usually under less pressure when modified views are taken with the implant displaced or flattened against the chest wall than when compression is applied with the implant directly under the compression paddle.

G. W. Eklund
Susan G. Komen Breast Center
Saint Francis Medical Center
University of Illinois, College of Medicine at Peoria
Peoria, IL 61637

REFERENCE

1. Eklund GW, Busby RC, Miller SH, Job JS. Improved imaging of the augmented breast. *AJR* **1988**;151:469–473

Percutaneous Intracavitary Treatment of a Giant Aspergilloma

Surgery has been the primary choice of treatment of pulmonary aspergillomas, but it has high morbidity and mortality rates. Since the first description of the use of percutaneous intracavitary injection of antifungal agent in 1968, a success rate of 90% in 10 cases has been reported [1, 2]. This technique has a number of advantages, such as easy and rapid insertion of the catheter, prompt response to treatment, and relatively short hospitalization.

A 49-year-old man was admitted because of recurrent hemoptysis of 10 days duration. He had had pulmonary tuberculosis 23 years before that had been treated with antituberculous drugs. Chest radiograph on admission showed a huge aspergilloma in a large cavity in the right upper lobe (Fig. 1A). CT confirmed the presence of the aspergilloma (Fig. 1B). Percutaneous intracavitary introduction of an 8-French, Teflon-coated catheter (Cook Inc., Melbourne, Australia) was performed by using a posterior approach and fluoroscopic guidance. PAS staining of the cultured aspirates showed the fungus was *Aspergillus flavus*. Amphotericin B (50 mg) in 20 ml of 5% dextrose in water and then 8 mg of bromhexine (a mucolytic agent) mixed with 10 ml of normal saline were instilled into the cavity through the catheter daily for 15 days. The cavity was irrigated with 150 ml of normal saline 8 hr after each instillation. Hemoptysis subsided 2 days after the first instillation. A chest radiograph made on the 14th hospital day showed almost complete disappearance of the aspergilloma (Fig. 1C). Two months after discharge, follow-up chest radiograph showed no fungus ball and slight shrinkage of the previous cavity.

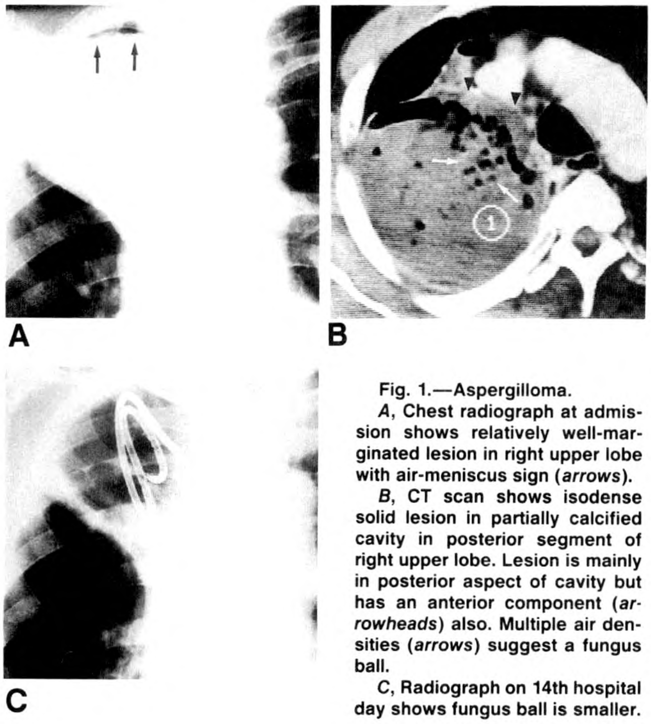

Fig. 1.—Aspergilloma.
***A*, Chest radiograph at admission shows relatively well-marginated lesion in right upper lobe with air-meniscus sign (*arrows*).**
***B*, CT scan shows isodense solid lesion in partially calcified cavity in posterior segment of right upper lobe. Lesion is mainly in posterior aspect of cavity but has an anterior component (*arrowheads*) also. Multiple air densities (*arrows*) suggest a fungus ball.**
***C*, Radiograph on 14th hospital day shows fungus ball is smaller.**

The mechanism of action of amphotericin B is not certain. Sclerosis of the cavity appears more likely than antifungal action because of the prompt cessation of the hemoptysis.

Complications of percutaneous intracavitary treatment of aspergillomas include pneumothorax, bronchospasm, and massive hemoptysis [1]. We had no complications in our patient except mild fever and general weakness. Percutaneous intracavitary treatment of aspergilloma may be a safe and reliable method and can be done even in patients who have giant aspergillomas.

Kyung Soo Lee
Yong Hoon Kim
Won Kyung Bae
Soonchunhyang University Hospital
Chunan, Korea

REFERENCES

1. Shapiro MJ, Albelda SM, Mayock RL, McLean GK. Severe hemoptysis associated with pulmonary aspergilloma: percutaneous intracavitary treatment. *Chest* **1988**;94:1225–1231
2. Hargis JL, Boine RC, Stewart J, Rector N, Hiller FC. Intracavitary amphotericin B in the treatment of symptomatic pulmonary aspergillomas. *Am J Med* **1980**;68:389–394

Cocaine-Induced Small-Bowel Perforation

Since the use of crack cocaine has become common, numerous complications associated with it have been described. Clinicians are aware of the more commonly occurring cardiac, cerebrovascular, pulmonary, and infectious complications. We describe a case of small-bowel ischemia with perforation and abscess induced by an overdose of crack cocaine.

A previously healthy 28-year-old man came to the emergency department because of abdominal pain in the right lower quadrant. The pain had developed 1 week earlier, after he had gotten high smoking crack cocaine. He remembered that he had passed out for approximately 30 min and that when he woke up, he had severe abdominal pain. He continued to smoke cocaine daily, but the abdominal pain persisted. He had been smoking cocaine daily or every other day for 4 years.

On admission, the patient had a body temperature of 103°F (39°C) and tenderness in the right lower quadrant of the abdomen. Plain abdominal radiographs showed ileus. He was admitted with the diagnosis of acute appendicitis. After admission, bloody diarrhea developed. Single-contrast barium enema showed a mass in the right lower quadrant with deformity and displacement of the ileum and sigmoid colon (Fig. 1A). The appendix was not visualized. The mass was thought to be an abscess most likely due to Crohn disease of the ileum. CT showed a large pelvic abscess (Fig. 1B). Surgery was performed with drainage of a pelvic abscess, small-bowel resection, and appendectomy.

The resected ileum was ischemic with focal areas of hemorrhage and ulceration. The ileum had an area of perforation with part of the wall incorporated into the wall of the abscess. The periappendiceal serosa was inflamed, but the appendiceal mucosa was normal. The patient had no complications after surgery and was discharged a week later. Four months later, he had recovered completely.

Cocaine is a common drug used in many forms through all social

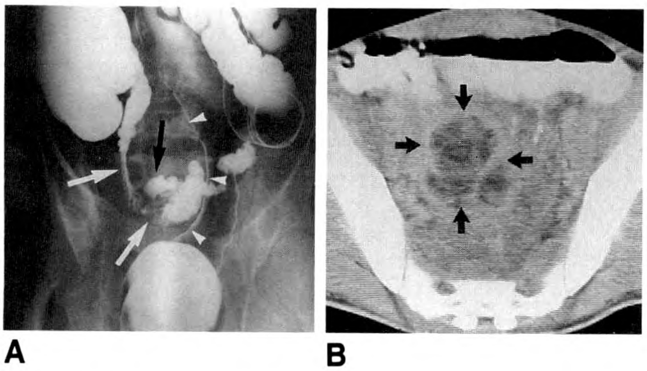

Fig. 1.—Cocaine-induced small-bowel perforation.
A, Barium enema shows a pelvic mass (*white arrows*) displacing sigmoid colon and ileum (*arrowheads*). Note barium entering mass (*black arrow*).
B, Contrast-enhanced CT scan shows large pelvic abscess (*arrows*).

strata. Bowel ischemia with perforation must be considered in any patient with abdominal pain who used cocaine shortly before the pain developed. The diagnosis may be missed or delayed because the symptoms may mimic other more common causes of acute abdomen such as acute appendicitis or Crohn disease. Cocaine is a potent vasoconstrictor. Its vasoconstrictive action probably results in ischemia of the bowel, which may be followed by hemorrhage and perforation.

Carmen Endress
George A. Kling
Wayne State University
Detroit, MI 48201

The Role of Imaging in the Diagnostic Evaluation of Impotence

We read with interest the article by Krysiewicz and Mellinger [1] on the role of imaging in the diagnostic evaluation of impotence. The authors mentioned penile arteriography, cavernosography, cavernosometry, duplex sonography, and pulsed-wave Doppler analysis. We are disappointed by their failure to include nuclear medicine procedures among the imaging techniques useful to clinicians who evaluate and treat impotence. We respectfully suggest that *AJR* readers would be interested in recent articles [2–4] on the role of radionuclide imaging in the measurement of penile blood flow.

T. K. Chaudhuri
S. Fink
Veterans Affairs Medical Center
Hampton, VA 23667

REFERENCES

1. Krysiewicz S, Mellinger BC. The role of imaging in the diagnostic evaluation of impotence. *AJR* **1989**;153:1133–1139.
2. Chaudhuri TK, Fink S, Burger RH, Netto ICV, Palmer JDK. Physiological considerations in radionuclide imaging of the penis during impotence therapy. *Am J Physiol Imaging* **1989**;4:75–80
3. Fanous HN, Jevtich MJ, Chen DCP, Edson M. Radioisotope penogram in diagnosis of vasculogenic impotence. *Urology* **1982**;20:499–502
4. Nseyo UO, Wilbur HJ, Kang SA, Flesh J, Bennett AH. Penile xenon (^{133}Xe) washout: a rapid method of screening for vasculogenic impotence. *Urology* **1984**;23:31–34

Reply

In response to Drs. Chaudhuri and Fink, few good studies have been done on large numbers of patients to assess the usefulness of radionuclide imaging in the evaluation of erectile dysfunction. Fanous et al. [1] evaluated 19 impotent patients and nine control volunteers. These investigators studied the penis in the flaccid state and made no attempt to induce erection with pharmacologic methods. As has been shown with Doppler studies that measure the penile-brachial index or flow index, normal results fail to provide information about the hemodynamic capabilities of the penis. Additionally, in the article by Fanous et al., the results of the radionuclide study appeared to correlate with the penile-brachial index, which then questions the need for the radionuclide study (with the attendant exposure to radiation) when the penile-brachial index would give the same information.

Regarding the article by Nseyo et al. [2], essentially the same criticisms apply. The authors evaluated three healthy men as controls and 16 impotent men. In these patients, the penis was studied in the flaccid state, and subcutaneous injections were given into the penile skin just proximal to the dorsal glans. The penile skin is drained primarily by the superficial dorsal vein, and so it is difficult to imagine that this method would provide an accurate evaluation of the cavernous arteries and deep venous structures. Additionally, correlation with penile-brachial indexes was good, again raising the question of the need for the radionuclide study.

One problem with such nuclear medicine studies is that they essentially measure the radioactivity at the level of the penis, providing a summation of arterial inflow and venous outflow. This makes it difficult to separate and define easily whether the problem is one of inflow, outflow, or a combination of the two. Additionally, as opposed to dynamic cavernosonography, the anatomy is not delineated clearly with the radionuclide imaging studies, which is necessary for planning a surgical approach.

Two pertinent articles were published recently in the *Journal of Nuclear Medicine*. Schwartz et al. [3] used intracorporal papaverine to assess blood flow during early tumescence. Haden et al. [4], however, obtained measurements of the penis only when it was flaccid. Again, the criticisms of using radionuclide studies are the same as those mentioned for the previous papers.

Brett C. Mellinger
Long Island Jewish Medical Center
New Hyde Park, NY 10042
Susan Krysiewicz
The New York Hospital–Cornell Medical Center
New York, NY 10021

REFERENCES

1. Fanous HN, Jevtich MJ, Chen DCP, Edson M. Radioisotope penogram in diagnosis of vasculogenic impotence. *Urology* **1982**;20:499–502
2. Nseyo UO, Wilbur HJ, Kang SA, Flesh J, Bennett AH. Penile xenon (^{133}Xe) washout: a rapid method of screening for vasculogenic impotence. *Urology* **1984**;23:31–34
3. Schwartz AN, Graham MM, Ferency GF, Miura RS. Radioisotope penile plethysmography: a technique for evaluating corpora cavernosal blood flow during early tumescence. *J Nucl Med* **1989**;30:466–473
4. Haden HT, Katz PG, Mulligan T, Zasler ND. Penile blood flow by xenon-133 washout. *J Nucl Med* **1989**;30:1032–1035

Bilateral Dorsal Defect of the Patella

Dorsal defect of the patella is a radiologic variant present in about 1% of contemporary clinical populations [1]. In archaeologic samples, however, the frequency is much lower in many historic and prehistoric groups. Because radiologists and orthopedists rarely have the opportunity to examine these lesions in dry-bone specimens, the following example is presented for comparison of gross and radiologic features.

The example is a 16- to 19-year-old Confederate soldier killed in 1862 in the Battle of Glorieta Pass, NM. The right patellar defect is 6

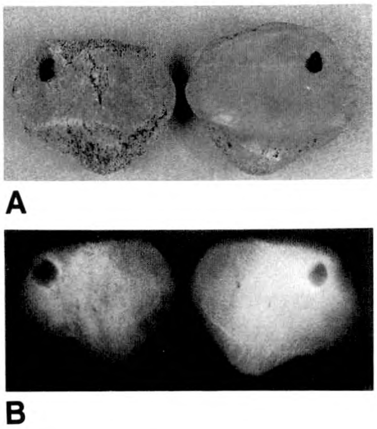

Fig. 1.—*A* and *B*, Photograph (*A*) and radiograph (*B*) of dry-bone archeologic specimen show dorsal defects of patellae.

× 6 × 7 mm (maximal length, breadth, and depth), and the left defect is 7 × 6 × 8 mm. The ovoid lesions are in the superolateral portions of the patellae and have well-defined, sloping margins (Fig. 1A). Radiographs show sclerotic margins with no evidence of inflammation or degenerative arthritis (Fig. 1B).

The cause of dorsal defect of the patella is unknown. In the few cases in which biopsies were performed, nonspecific fibrous tissue was found [2, 3]. The consistent gross and radiologic appearance and location of these defects suggest a developmental anomaly possibly resulting from delayed or faulty ossification [4].

Douglas W. Owsley
Robert W. Mann
Smithsonian Institution
Washington, DC 20560

REFERENCES

1. Johnson JF, Brogdon BG. Dorsal defect of the patella: incidence and distribution. *AJR* **1982**;139:339–340
2. Haswell DM, Berne AS, Graham CB. The dorsal defect of the patella. *Pediatr Radiol* **1976**;4:238–242
3. Hunter LY, Hensinger RN. Dorsal defect of the patella with cartilagenous involvement: a case report. *Clin Orthop* **1979**;143:131–132
4. Resnick D, Niwayama G. *Diagnosis of bone and joint disorders*, 2nd ed. Philadelphia: Saunders, **1988**:55–83

Agenesis and Lipoma of the Corpus Callosum: MR Findings

A 5-year-old girl with a 3-year history of epilepsy was admitted to the hospital because the number of seizures had increased and headaches had occurred. Results of the neurologic examination were normal. MR studies were performed on a resistive BMT 1100 imager (Bruker Co.) with an operating field of 0.282 T. A head coil was used to obtain rapid-acquisition relaxation-enhanced (RARE) [1] and spin-echo (SE) sequences. The RARE sequences provided fast heavily T2-weighted images. SE sequences with short TR and TE (400–600/33) were used for T1-weighted images. The slice thickness was 8 mm. Coronal, sagittal, and axial imaging was performed. Sagittal and coronal T1-weighted images showed a mass with a bright signal. The mass had well-defined margins and displaced the third ventricle downward (Fig. 1). On the midline sagittal image, no corpus callosum could be seen. At surgery, agenesis of the corpus callosum and lipoma of the corpus callosum were found. The lipoma was removed partially.

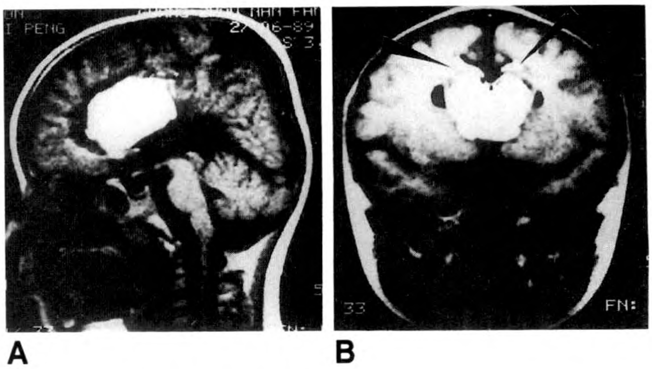

Fig. 1.—*A*, Midline sagittal spin-echo T1-weighted, 400/33, MR image shows bright-signal mass caused by lipoma of corpus callosum associated with complete agenesis of corpus callosum.

***B*, Coronal spin-echo T1-weighted, 600/33, MR image shows lipoma extends upward to both cerebral hemispheres (*arrowheads*), and third ventricle is displaced downward.**

Lipoma of the corpus callosum is an unusual tumor of the CNS. The diagnosis usually is made on the basis of CT findings [2, 3]. Recently, however, the advantages of MR imaging have been emphasized [4]. In the patient described here, the high signal intensity on T1-weighted images was characteristic of a lipoma. MR also showed agenesis of the corpus callosum.

Chen Long Hua
Nanfang Hospital
Guang Zhou, Peoples Republic of China, 510515

REFERENCES

1. Friedburg H, Hennig J. RARE-imaging: a rapid imaging technique in NMR tomography. *Med Rep* (Bruker) **1985**;1:13–14
2. Wallace D. Lipoma of the corpus callosum. *J Neurol Neurosurg Psychiatry* **1976**;39:1179–1185
3. Kazner E, Stochdorph O, Wende S, Grumme T. Intracranial lipoma: diagnosis and therapeutic considerations. *J Neurosurg* **1980**;52:234–235
4. Wolpert SM, Anderson M, Scott RM, Kwan ESK, Runge VM. Chiari II malformation: MR imaging evaluation. *AJR* **1987**;149:1033–1042

Standards for Color Doppler Imaging

As the use of color Doppler imaging has spread, and the number of lectures on it has burgeoned, the lack of standards has become increasingly disturbing. It appears that those who do cardiovascular Doppler imaging always attempt to show the arterial flow as red and venous flow as blue, regardless of the direction of flow in relation to the transducer. These same people also tend to have the arterial waveform always above the baseline and the venous waveform below. However, the folks doing abdominal and extremity Doppler imaging seem to have no standards at all.

I have asked several lecturers and "experts" about these rather haphazard methods, and the usual reply is something like, "If one really knows what one is doing, then it really doesn't matter." To this, I usually want to reply, "If it really doesn't matter, then it doesn't matter, so let's arrive at some standard so we can pay attention to the lecture and quit trying to figure out if the spectrum has been inverted or if the blood flow really is reversed!"

Basically, if a reflector is moving toward a transducer, then the returning echoes will have a higher frequency than the original sound frequency, and echoes from a reflector that is moving away will return lower frequencies. From analysis of these frequency shifts, it is possible to determine not only the direction of flow but also the velocity of the flow. How this directional information is displayed is the subject of this letter. In the beginning, only spectral (waveform) display and audio were available. In those days, it was simpler. However, today, with color display, we suddenly have the problem of torsions and arcuate vessels that change color in midstream, thus making it impossible to show all arteries as red and veins as blue, as Gray and Netter would have us display vessels.

In his widely used text [1], Kremkau says of the spectral analysis, "The plus sign is used when the reflector is moving toward the source, and a minus sign is used when the reflector is moving away from the source." Kremkau says of color displays, "Color choices for these applications are not standardized, and there is some debate regarding which are best." Other textbooks display the "negative" arterial carotid flow, which is clearly away from the transducer, above the baseline. Yet these same textbooks at other places show arterial spectra both above and below the baseline, depending on the direction of flow.

This lack of a standard and the frequent reversing of the spectral and color flow display create a situation that has a potential of erroneous diagnosis and complicates the educational process. Although it may not "really make a difference if one knows what one is doing," who among us has not had some difficulty remembering to label images left and right at the end of a long, busy day or has not experienced some degree of disorientation when learning a new technique such as transvaginal sonography? The frequent changes of Doppler display carry the same kind of potential confusion.

I wish to make two proposals: (1) that sonographic Doppler information should be displayed as a physical function of direction of flow to the transducer and not as an anatomic relationship and (2) that flow toward the transducer should be considered positive (+) flow and be displayed above the baseline and in blue and that flow away from the transducer should be considered negative (–) flow and be displayed below the baseline and in red. I realize that the momentum is considerable for always showing normal carotid arterial flow above the baseline regardless of the transducer angle. Momentum also was considerable before the 1980s for displaying gray-scale sonography as black on white, and now most of the world displays gray scale as white on black—even though it "really doesn't matter, if you know what you are doing."

Adopting my proposed standards also will be more congruent with the way the other physical sciences have been viewing Doppler information since the 1800s [2–4]. Although Doppler sonography does not deal with actual color spectral shifts, as cosmology does, it seems logical to have the color wavelength conform to the actual Doppler shift (longer or shorter wavelengths). It also will remove some of the subjectivity from the decision of how to display the flow in extremely turbulent vessels or in cases of severe distal stenosis in which flow may appear bidirectional. Or perhaps we should forget about expensive color processes and encourage manufacturers to provide an isobar-type velocity flow map with user-selected intervals for standard, high-contrast, black-and-white images. As Doppler imaging becomes as universal as real-time sonography is today, conventions will at least make it easier to explain the technique to new students of the discipline.

Terry J. DuBose
Austin Radiological Association
Austin Community College
Austin, TX 78765

REFERENCES

1. Kremkau FW. *Diagnostic ultrasound: principles, instruments, and exercises*, 3rd ed. Philadelphia: Saunders, **1989**:179, 194
2. Hawking SW. *A brief history of time.* New York: Bantam, **1988**:38–40
3. Weinberg S. *The first three minutes.* New York: Basic Books, **1988**:12–17
4. Ellis GFR, Williams RM. *Flat and curved space-times.* Oxford, England: Oxford University Press, **1988**:53–62

Reply

I would like to applaud Mr. DuBose's suggestion that some form of standardization be implemented in Doppler imaging. Certainly, the haphazard assignment of positive and negative Doppler spectra and the inconsistent use of the colors red and blue can lead to confusion. Although most institutions establish their own method of spectral and color display out of necessity, inconsistencies can be problematic when a scan is reviewed by a person other than the one who has performed it or when someone reviews a scan performed at an earlier time or at another institution. In practice, the likelihood of a true misdiagnosis on this basis is probably minimal as some form of identifying information usually appears somewhere in the image (positive or negative spectral values of a color bar). Nonetheless, a uniform code of display as is found in most other imaging techniques would be of benefit to all involved.

In complete agreement with Mr. DuBose, I am strongly opposed to any attempt to emulate Netter drawings by displaying arteries in red and veins in blue (or the spectral equivalent of always showing carotid flow as positive) without regard to their Doppler angle. Although this convention may produce pleasing color images in the relatively linear world of the normal carotid artery, it becomes completely untenable when dealing with the complex angular relationships encountered when a sector format is used to scan the abdomen or, for that matter, a tortuous carotid artery. These complexities undoubtedly lead Mr. DuBose to draw the conclusion (with which I take issue and assume refers only to our interest in color imaging) that those of us doing abdominal and extremity Doppler imaging "have no standards at all."

It is my opinion that Doppler information should be displayed as a function of the Doppler angle. Simply stated, flow toward the Doppler *beam* should be considered positive and flow away negative. This is seemingly self-explanatory when referring to spectral display but is obviously completely arbitrary when dealing with color. I am surprised, however, that Mr. DuBose advocates displaying flow toward the Doppler beam in blue. This goes against almost every display scheme I ever have encountered. Although color assignment is completely arbitrary and has no real physical basis (you could just as easily choose purple and green), I believe that almost all institutions display flow toward the Doppler beam as red and away as blue. The obvious exceptions are those who invariably feel compelled to display the carotid arteries in red.

Because Doppler imaging currently crosses a relatively large number of medical specialities (radiology, cardiology, and vascular surgery, to name a few), it seems unlikely that any one specialty, and probably least of all, radiology, would take it on itself to attack this problem directly. I would hope, therefore, that the members of the one relatively unbiased ultrasound organization, the American Institute of Ultrasound in Medicine, will shortly take it on themselves to solve this seemingly simple problem and establish guidelines.

Edward G. Grant
University of California, Los Angeles
Center for the Health Sciences
Los Angeles, CA 90024-1721

Intracaval Breakage of a Kimray-Greenfield Filter

An 87-year-old woman was admitted to the hospital because of malaise and vertigo without syncope associated with a sudden onset of right-sided chest pain suggestive of recurrent pulmonary embolism. Four years earlier, a Kimray-Greenfield filter had been implanted because of a pulmonary embolism associated with deep-vein thrombophlebitis of the left lower extremity. A plain radiograph of the abdomen obtained 48 hr after the implantation showed that the filter

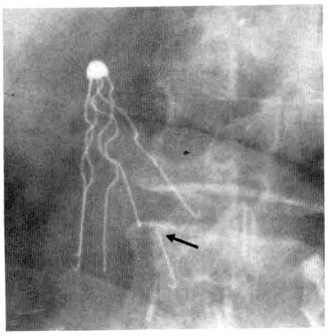

Fig. 1.—Plain radiograph of abdomen made 4 years after placement of a Kimray-Greenfield filter shows a broken strut (*arrow*).

was in good position with a 13° angulation from the vertical course of the vena cava and that all six struts were present and intact.

The results of physical examination on the present admission were unremarkable. A chest radiograph was normal except for a filter strut visible in the right hilum. Plain abdominal radiographs showed the same angulation of the filter as noted after the implantation, but one of the struts was broken (Fig. 1). The extremity of the broken strut and the five remaining struts were hooked into and penetrated the wall of the vena cava. The span of the filter was 30% larger than it had been 4 years before. Venacavograms showed narrowing of the inferior vena cava. Digital pulmonary angiography showed that the pulmonary arterial tree was free of thrombus. The fragment of the broken strut was trapped in the anterior basal artery of the right lower lobe. It was decided not to remove the fragment because no thrombus was associated with it. The patient's signs and symptoms disappeared spontaneously.

Fragmentation of a Mobin-Uddin or Kimray-Greenfield filter with local migration of the stent, most often as a consequence of trauma, has been described [1-3]. To our knowledge, fracture and embolization of a strut of a Kimray-Greenfield filter in the absence of trauma has not been reported. The cause of the fracture in our case is uncertain. Hypotheses include a manufacturing defect, damage during implantation, and repeated motion of the strut caused by changes in the diameter of the inferior vena cava during respiration. The principal reason may be the increase in the span of the filter, which was greater than increases described previously [4]. This case raises two issues: the necessity of long-term radiologic follow-up of inferior vena cava filters [4] and the diminished filtering capacity that occurs when Kimray-Greenfield or other filters are broken leading to possible recurrent pulmonary embolism.

X. Dufretay
J. Y. Pagny
J. Relland
J. C. Gaux
Broussais Hospital
75014 Paris, France
J. M. Coulaud
J. Lissac
Boucicaut Hospital
75105 Paris, France

REFERENCES

1. Cabrera JJ, Macht SH. Intracaval breakage of umbrella filter. *Surgery* **1987**;82:555–557
2. Plaus WJ, Hermann G. Structural failure of a Greenfield filter. *Surgery* **1988**;103:662–664
3. Kim D, Porter DH, Siegel JB, Simon M. Perforation of the inferior vena cava with aortic and vertebral penetration by a suprarenal Greenfield filter. *Radiology* **1989**;172:721–723
4. Mesmer JM, Greenfield LJ. Greenfield caval filters: long-term radiographic follow-up study. *Radiology* **1985**;156:613–618

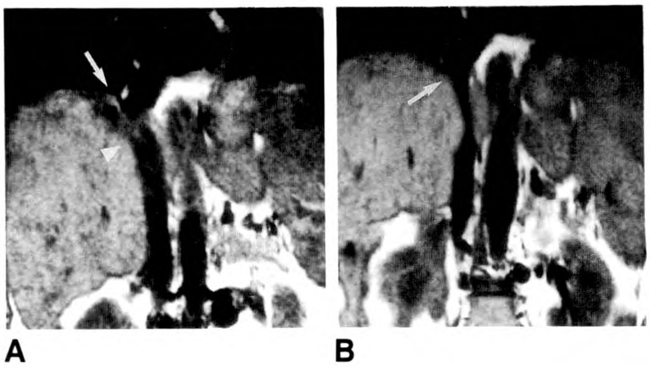

Fig. 1.—Budd-Chiari syndrome.

***A*, T1-weighted coronal MR image (600/15, presaturation) shows septumlike structure (*arrow*) and higher intensity (*arrowhead*) in inferior vena cava, suggesting membranous obstruction and stagnation of blood flow.**

***B*, T1-weighted coronal MR image (same level as *A*) obtained 5 days after percutaneous transluminal angioplasty shows "flow void" phenomenon (*arrow*) and disappearance of membranous septum, suggesting patency of inferior vena cava.**

MR Evaluation of Budd-Chiari Syndrome Treated by Percutaneous Transluminal Angioplasty

The Budd-Chiari syndrome has many manifestations, which makes the diagnosis difficult. We report a case treated by percutaneous transluminal angioplasty in which MR imaging was useful in evaluating patency of the inferior vena cava before and after treatment.

A 53-year-old woman had had upper abdominal pain for 3 months. Dynamic enhanced CT showed hepatocellular carcinoma in the left lobe and dilatation of the azygos and the hemiazygos veins, consistent with obstruction of the inferior vena cava. MR imaging showed a thin septumlike structure and increased intraluminal signal intensity in this vessel (Fig. 1). Venacavography showed membranous obstruction of the inferior vena cava; the superior vena cava was patent. Because the patient was a poor candidate for surgery, she had percutaneous transluminal angioplasty of the inferior vena cava with four 7-French Grüntzig balloon catheters. Immediately after the procedure, improvement in blood flow was confirmed by venacavography. MR imaging performed 5 days after the angioplasty showed patency of the inferior vena cava. The patient subsequently received radiation therapy and had transcatheter arterial embolization for hepatocellular carcinoma. She was well during a follow-up of 6 months.

MR has been useful in the diagnosis of Budd-Chiari syndrome. The advantages include the ability to obtain direct coronal and sagittal images, which can facilitate detection of the inferior vena caval web and evaluation of the blood vessels without the need for contrast material [1, 2]. The normal vessels are visible because of the "flow void" phenomenon, in which rapidly flowing blood causes no MR signal [3, 4]. The phenomenon is absent in the presence of slow flow or obstruction of the blood vessel. The presence of this phenomenon has been used to confirm patency of the inferior vena cava after angioplasty [2]. MR imaging also can be used to distinguish slowly flowing blood from intraluminal thrombus by examining first- and second-echo images. Slow flow usually will cause an increase in relative signal intensity on a second-echo image, whereas thrombus shows either less increase or a decrease in relative signal intensity (paradoxical enhancement) [3, 4].

Fumihiko Wakao
Kenichi Takayasu
Yukio Muramatsu
Shigeru Nawano

Noriyuki Moriyama
National Cancer Center Hospital
Tokyo 104, Japan

REFERENCES

1. Murphy FB, Steinberg HV, Shires GT III, Martin LG, Bernardino ME. The Budd-Chiari syndrome: a review. *AJR* **1986**;147:9–15
2. Stark DD, Hahn PF, Trey C, Clouse ME, Ferrucci JT Jr. MRI of the Budd-Chiari syndrome. *AJR* **1986**;146:1141–1148
3. Higgins CB, Goldberg H, Hricak H, Crooks LE, Kaufman L, Brasch R. Nuclear magnetic resonance imaging of vasculature of abdominal viscera: normal and pathologic features. *AJR* **1983**;140:1217–1225
4. Bernardino ME, Steinberg HV, Pearson TC, Gedgaudas-McClees RK, Torres WE, Henderson JM. Shunts for portal hypertension: MR and angiography for determination of patency. *Radiology* **1986**;158:57–61

Letters are published at the discretion of the Editor and are subject to editing.

Letters to the Editor must not be more than two *double-spaced*, typewritten pages. One or two figures may be included. Abbreviations should not be used. See Author Guidelines, page A5.

Material being submitted or published elsewhere should not be duplicated in letters, and authors of letters must disclose financial associations or other possible conflicts of interest.

Letters concerning a paper published in the *AJR* will be sent to the authors of the paper for a reply to be published in the same issue. Opinions expressed in the Letters to the Editor do not necessarily reflect the opinions of the Editor.

FORTHCOMING ARTICLES

SPECIAL ARTICLES

Review. MR spectroscopy of the heart. *Brown JJ, Mirowitz SA, Sandstrom JC, Perman WH*

Progress in Radiology. Pancreas transplant imaging: an overview. *Low RA, Kuni CC, Letourneau JG*

PULMONARY RADIOLOGY

Acute lung rejection after heart-lung transplantation: correlation of radiologic findings with lung biopsy results. *Bergin CJ, Castellino RA, Blank N, Berry GJ, Sibley RK, Starnes VA*

Case report. Pneumoperitoneum with catamenial pneumothorax. *Downey DB, Towers MJ, Poon PY, Thomas P*

Technical note. A one-piece unit for treatment of pneumothorax complicating needle biopsy: evaluation in 10 patients. *Molina PL, Solomon SL, Glazer HS, Sagel SS, Anderson DJ*

BREAST RADIOLOGY

Differentiation of benign and malignant local tumor recurrence after lumpectomy. *Dershaw DD, McCormick B, Cox L, Osborne MP*

The association of breast carcinoma and previous treatment for Hodgkin disease in women under age forty. *Cook KL, Adler DD, Lichter AS, Ikeda DM, Helvie MA*

Optical spectroscopy (INVOS) is unreliable in detecting breast cancer. *Bosanko CM, Baum JK, Clark K, Jones D, Levine AJ*

GASTROINTESTINAL RADIOLOGY

The diagnosis of small hepatocellular carcinomas: efficacy of various imaging procedures in 100 patients. *Takayasu K, Moriyama N, Muramatsu Y, et al.*

Hepatic hemangiomas versus metastases: MR differentiation at 1.5 T. *Lombardo DM, Baker ME, Spritzer CE, Blinder R, Meyers W, Herfkens RJ*

Differentiation between small hepatic hemangiomas and metastases on MR images: importance of size-specific quantitative criteria. *Itoh K, Saini S, Hahn PF, Imam N, Ferrucci JT*

Gallstone dissolution in methyl *tert*-butyl ether after mechanical fragmentation: an in vitro study. *Lu DS, Ho C-S, Allen LC*

CT density of mesenteric, retroperitoneal, and subcutaneous fat in cirrhotic patients: comparison with normal individuals. *Tyrrel RT, Montemayor KA, Bernardino ME*

Staging of esophageal carcinoma: comparison of results using endoscopic sonography and CT. *Vilgrain V, Mompoint D, Palazzo L, et al.*

Case report. Extrapulmonary *Pneumocystis carinii* in a patient with AIDS: sonographic findings. *Spouge AR, Wilson SR, Gopinath N, Sherman M, Blendis LM*

Technical note. Percutaneous gastrojejunostomy with a modified Cope-loop catheter. *Gehman KE, Elliott JA, Inculet RI*

GENITOURINARY RADIOLOGY

Percutaneous drainage of renal and perirenal abscesses: results in 30 patients. *Deyoe LA, Cronan JJ, Lambiase RE, Dorfman GS*

Diagnostic evaluation of cancer patients with pelvic pain: a comparison of scintigraphy, CT, and MR imaging. *Beatrous TE, Choyke PL, Frank JA*

Oblique plain radiographs are useful for detecting opaque presacral ureteral calculi. *Gatewood OMB, Berkowitz JE*

Case report. Epididymitis associated with Müllerian duct cyst and calculus: sonographic diagnosis. *Ardill RH, Manivel JC, Beier-Hanratty S, Ercole C, Letourneau JG*

MUSCULOSKELETAL RADIOLOGY

Cortical fracture of the femoral head associated with posterior hip dislocation: CT detection. *Richardson P, Young JWR, Porter D*

Does dysbaric osteonecrosis progress in the absence of further hyperbaric exposure? A 10-year radiologic follow-up of 15 patients. *VanBlarcom ST, Czarnecki DJ, Fueredi GA, Wenzel MS*

Pictorial essay. Musculoskeletal manifestations of the Marfan syndrome: radiologic features. *Magid D, Pyeritz RE, Fishman EK*

Coronal radiographs and videofluoroscopy improve the diagnostic quality of temporomandibular joint arthrography. *Duvoisin B, Klaus E, Schnyder P*

Metastases from malignant melanoma to the axial skeleton: a CT study of frequency and appearance. *Patten RM, Shuman WP, Teefey S*

Parosteal osteogenic sarcoma arising in cranial bones: clinical and radiologic features in eight patients. *Kumar R, Moser RP Jr, Madewell JE, Edeiken J*

Pictorial essay. Hallux valgus deformity: preoperative radiologic assessment. *Karasick D, Wapner KL*

PEDIATRIC RADIOLOGY

Importance of prenatal detection of hydronephrosis of the upper pole. *Winters WD, Lebowitz RL*

Technical note. Doppler flow monitoring of the dorsalis pedis artery facilitates puncture of the femoral artery in children. *Becker CJ, Towbin RB*

Case report. Pneumatosis intestinalis in children with AIDS. *Sivit CJ, Josephs SH, Taylor GA, Kushner DC*

NEURORADIOLOGY

Colloid cysts of the third ventricle: correlation of MR and CT findings with histology and chemical analysis. *Maeder PP, Holtås SL, Basibüyük LN, Salford LG, Tapper UAS, Brun A*

MR Imaging of pineal tumors. *Tien RD, Barkovich AJ, Edwards MSB*

Recurrent medulloblastoma: frequency of tumor enhancement on Gd-DTPA MR imaging. *Rollins N, Mendelsohn D, Mulne A, et al.*

Intracranial aneurysms: evaluation by MR angiography. *Ross JS, Masaryk TJ, Modic MT, Ruggieri PM, Haacke EM, Selman WR*

Three-dimensional phase-contrast MR angiography in the head and neck: preliminary report. *Pernicone JR, Siebert JE, Potchen EJ, Pera A, Dumoulin CL, Souza SP*

VASCULAR RADIOLOGY

MR angiography with gadopentatate dimeglumine polylysine: evaluation in rabbits. *Marchal G, Bosmans H, Van Hecke P, et al.*

Amplatz vena caval filter: clinical experience in 30 patients. *McCowan TC, Ferris EJ, Carver DK, Baker ML*

COMPUTER PAGE

Radiologic image communication methods. *Huang HK, Lou SL, Cho PS, Valentino DJ, Wong AWK, Chan KK*

PERSPECTIVES

How many radiologic technologists are necessary to efficiently image patients in a pediatric radiology department? *Carver CD, Slovis TL*

Fellowship training for all? *Green CE*

Review of Current Literature

Initials and addresses of corresponding authors are provided in parentheses for each article so that the reader can obtain reprints directly. Abstracts are printed verbatim from each journal.

The New England Journal of Medicine

Pancreatic function in infants identified as having cystic fibrosis in a neonatal screening program. Waters DL, Dorney SFA, Gaskin KJ, Gruca MA, O'Halloran M, Wilcken B (KJG, James Fairfax Institute of Paediatric Nutrition, Royal Alexandra Hospital for Children, Pyrmont Bridge Rd., Camperdown, NSW 2050, Australia). *N Engl J Med* 322(5):303–308, 1990

The use of the dried-blood immunoreactive-trypsin assay for the detection of cystic fibrosis in newborns has been questioned on the grounds that it may fail to identify patients with enough pancreatic function to have normal fat absorption. To investigate this possibility, we assessed pancreatic function in 78 patients identified in a neonatal screening program as having cystic fibrosis. The diagnosis of cystic fibrosis was confirmed by abnormal results on a sweat chloride test.

The results of measurements of fecal fat excretion, pancreatic-stimulation tests, and estimations of the serum level of pancreatic isoamylase indicated that 29 of the 78 children (37 percent) had substantial preservation of pancreatic function. These children (median age, four years) had growth that was close to normal and comparable to growth in children with severe pancreatic insufficiency who received oral enzyme therapy. Pancreatic insufficiency subsequently developed in 6 of the 29 patients, at 3 to 36 months of age.

We conclude that the serum immunoreactive-trypsin assay used in neonatal screening programs identifies patients with cystic fibrosis who have sufficient pancreatic function to have normal fat absorption and that a substantial proportion of infants identified as having cystic fibrosis are in this category.

Cathepsin D and prognosis in breast cancer. Tandon AK, Clark GM, Chamness GC, Chirgwin JM, McGuire WL (WLM, Dept. of Medicine, Division of Oncology, University of Texas Health Science Center, 7703 Floyd Curl Dr., San Antonio, TX 78284-7884). *N Engl J Med* 322(5):297–302, 1990

We investigated the possibility that cathepsin D, an estrogen-induced lysosomal protease, might have value as a prognostic factor in breast cancer by studying frozen tissue specimens from 397 patients. We measured the 34-kd mature form of the enzyme by Western blot assay and densitometry. Among 199 patients with node-negative disease, but not among 198 with node-positive disease, high levels of cathepsin D proved to be a significant predictor of reduced disease-free survival (median follow-up, 64 months), either as a continuous variable (log cathepsin D; $P = 0.018$) or as a dichotomous variable with an optimized cutoff point ($P = 0.0001$). Results were similar for overall survival ($P = 0.009$ and 0.0001, respectively).

Relating the level of cathepsin D to other prognostic factors in the patients with node-negative disease, we found an association with aneuploidy but none with estrogen or progesterone receptors, tumor size, or the age of the patient. In multivariate analyses, a high level of cathepsin D was the most important independent factor in predicting shorter disease-free and overall survival in patients with node-negative disease. As compared with the risk in women with low levels of cathepsin D, the relative risk of tumor recurrence was 2.6 (95 percent confidence interval, 1.6 to 4.4) and the relative risk of death was 3.9 (95 percent confidence interval, 2.1 to 7.3) among those with high levels of cathepsin D. For disease-free survival, cathepsin D status was predictive of outcome primarily among those with aneuploid tumors; the actuarial five-year recurrence rates of aneuploid tumors were 60 percent among women with high levels of cathepsin D and 29 percent among those with low levels, as compared with 22 percent for all diploid tumors. We conclude that cathepsin D may be an independent predictor of early recurrence and death in node-negative breast cancer.

Thiazide diuretic agents and the incidence of hip fracture. LaCroix AZ, Wienpahl J, White LR, et al. (AZL, Center for Health Studies, Group Health Cooperative of Puget Sound, 521 Wall St., Seattle, WA 98121). *N Engl J Med* 322:286–290, Feb 1990

Thiazide diuretic agents lower the urinary excretion of calcium. Their use has been associated with increased bone density, but their role in preventing hip fracture has not been established. We prospectively studied the effect of thiazide diuretic agents on the incidence of hip fracture among 9518 men and women 65 years of age or older residing in three communities.

At base line, 24 to 30 percent of the subjects were thiazide users. In the subsequent four years, 242 subjects had hip fractures. The incidence rates of hip fracture were lower among thiazide users than nonusers in each community; the Mantel-Haenszel relative risk of hip fracture, adjusted for community and age, was 0.63 (95 percent confidence interval, 0.46 to 0.86). The protective effect of the use of thiazides was independent of sex, age, impaired mobility, body-mass index, and current and former smoking status; the multivariate adjusted relative risk of hip fracture was 0.68 (95 percent confidence interval, 0.49 to 0.94). Furthermore, the protective effect was specific to thiazide diuretic agents, since there was no association between the use of antihypertensive medications other than thiazides and the risk of hip fracture.

These prospective data suggest that in older men and women the use of thiazide diuretic agents is associated with a reduction of approximately one third in the risk of hip fracture.

The risk of *Pneumocystis carinii* pneumonia among men infected with human immunodeficiency virus type 1. Phair J, Muñoz A, Detels R, et al. (JP, Comprehensive AIDS Center, Northwestern University Medical School, 680 N. Lake Shore Dr., Ste. 1106, Chicago, IL 60611). *N Engl J Med* 322(3):161–165, 1990

We assessed the risk of pneumonia due to *Pneumocystis carinii* in 1665 participants in the Multicenter AIDS Cohort Study who were seropositive for human immunodeficiency virus type 1 (HIV-1) but did not have the acquired immunodeficiency syndrome (AIDS) and were not receiving prophylaxis against *P. carinii*. During 48 months of follow-up, 168 participants (10.1 percent) had a first episode of *P. carinii* pneumonia.

The risk was greatly increased in participants with CD4+ cell counts at base line of 200 per cubic millimeter or less (relative risk, 4.9; 95 percent confidence interval, 3.1 to 8.0). Although most participants (60.7 percent) described no HIV-1-related symptoms at the clinic visit at which a CD4+ cell count of 200 per cubic millimeter or less was first noted, this finding during follow-up was also associated with an increased risk of *P. carinii* pneumonia. The development of thrush or fever significantly and independently increased the risk of *P carinii* pneumonia in these patients (adjusted relative risks, 1.86 and 2.15 for thrush and fever, respectively). Most participants with CD4+ cell counts above 200 per cubic millimeter who had *P. carinii* pneumonia within six months were symptomatic.

We conclude that *P. carinii* pneumonia is unlikely to develop in HIV-1-infected patients unless their CD4+ cells are depleted to 200 per cubic millimeter or below or the patients are symptomatic, and therefore that prophylaxis should be reserved for such patients.

Racial differences in susceptibility to infection by *Mycobacterium tuberculosis*. Stead WW, Senner JW, Reddick WT, Lofgren JP (WWS, Tuberculosis Program, Arkansas Dept. of Health, 4815 W. Markham St., Little Rock, AR 72205-3867). *N Engl J Med* 322:422–427, Feb. 1990

The prevalence of tuberculosis among blacks is known to be about twice that among whites. When we looked at infection rates among the initially tuberculin-negative residents of 165 racially integrated nursing homes in Arkansas, we were stimulated to investigate whether this difference could be due in part to racial differences in susceptibility to *Mycobacterium tuberculosis* infection. A new infection was defined by an increase of ≥12 mm of induration after a tuberculin skin test (5 tuberculin units) administered at least 60 days after a negative two-step test.

On repeat skin testing of the 25,398 initially tuberculin-negative nursing home residents, we found that 13.8 percent of the blacks and only 7.2 percent of the whites had evidence of a new infection (relative risk, 1.9; 95 percent confidence interval, 1.7 to 2.1). Blacks were infected more frequently, regardless of the race of the source patient. In homes with a single source patient who was white, 17.4 percent of the black and 11.7 percent of the white residents became infected (relative risk, 1.5; 95 percent confidence interval, 1.2 to 1.9); in homes with a single source patient who was black, 12.4 percent of the black and 7.7 percent of the white residents became infected (relative risk, 1.6; 95 percent confidence interval, 1.2 to 2.1). However, there was no racial difference in the percentage of residents who had recently converted to positive status who, in the absence of preventive therapy, were later found to have clinical tuberculosis (blacks, 11.5 percent; whites, 10.6 percent). Data from three outbreaks of tuberculosis in two prisons also showed that blacks have about twice the relative risk of whites of becoming infected with *M. tuberculosis*.

We conclude that blacks are more readily infected by *M. tuberculosis* than are whites. The data also suggest that susceptibility to *M. tuberculosis* infection varies independently of the factors governing the progression to clinical disease.

Association of hypokalemia, aldosteronism, and renal cysts. Torres VE, Young WF Jr, Offord KP, Hattery RR (VET, Mayo Clinic, 200 1st St. S.W., Rochester, MN 55905). *N Engl J Med* 322(6):345–351, Feb. 1990

The recognition of renal cysts in two patients with chronic hypokalemia and the renal effects of hypokalemia in certain species of animals prompted this study of the possible association of hypokalemia and renal cysts in patients with primary aldosteronism or primary renal potassium wasting.

Using CT scans, we studied 55 patients with primary aldosteronism, of whom 24 had cysts (44 percent). The cysts were more frequent in patients with adrenal tumors than in those with idiopathic adrenal hyperplasia. Sixteen of the 26 patients with tumors (62 percent) had renal cysts, which were often multiple and located in the medulla. Lower plasma potassium levels and higher serum aldosterone levels, urinary aldosterone excretion, and plasma renin activity were correlated with the extent of the cystic disease. Sequential observations indicated that prolonged hypokalemia can be accompanied by the development of renal scarring and that the size and number of cysts can decrease markedly in some patients after the removal of an adrenal adenoma. The association of hypokalemia, aldosteronism, and renal cysts was also supported by the finding of multiple medullary cysts in two patients with primary renal potassium wasting.

We conclude that chronic hypokalemia is accompanied by enhanced renal cystogenesis and may lead to interstitial scarring and renal insufficiency. Renal cysts are thus dynamic structures whose growth can be influenced by hormonal or pharmacologic interventions.

Intrafamilial clustering of *Helicobacter pylori* infection. Drumm B, Perez-Perez GI, Blaser MJ, Sherman PM (PMS, Division of Gastroenterology (Rm. 1448), Hospital for Sick Children, 555 University Ave., Toronto, Ontario M5G 1X8, Canada). *N Engl J Med* 322(6):359–363, 1990

Colonization of the gastric antrum by *Helicobacter pylori* (formerly *Campylobacter pylori*) has been associated with primary gastritis. We determined the frequency of colonization by *H. pylori* in gastric-antrum biopsy specimens from 93 children undergoing gastroscopy for the evaluation of upper gastrointestinal symptoms. We also determined *H. pylori* IgG antibody levels by enzyme-linked immunosorbent assay in coded serum samples from these children, family members, and control subjects of comparable ages.

Among 27 children with primary, or unexplained, gastritis, *H. pylori* was identified by silver staining in 24 biopsy specimens and by culture in 22; specific antibodies were present in 23 children (96 percent). Three children with unexplained gastritis had no evidence of *H. pylori* in the antrum, nor did any of 13 children with secondary gastritis or any of 53 children with normal antral histologic features; specific antibodies were present in only 1 of these 69 children. *H. pylori* antibody was detected in 25 of 34 parents of colonized children, but in only 8 of 33 parents of noncolonized children ($P < 0.001$). Of 22 siblings of children colonized by *H. pylori*, 18 had specific antibodies, as compared with only 5 of 37 controls ($P < 0.001$).

We conclude that *H. pylori*-specific IgG antibodies are associated with bacterial colonization of the gastric antrum by this organism. The intrafamilial clustering of *H. pylori* infection suggests that there may be person-to-person spread of these bacteria.

Cancer

Primary pulmonary Hodgkin's disease. Radin AI (AIR, Yale University School of Medicine, Hematology Section, L. C. I. 810, 333 Cedar St., P. O. Box 3333, New Haven, CT 06510). *Cancer* 65:550–563, 1990

Primary pulmonary Hodgkin's disease is a rare but distinct entity, to be distinguished from nodal Hodgkin's disease and from lymphomas involving the lung secondarily. Sixty-one cases have now been reported in the world's literature. This lymphoma affects women more frequently than men, and typically involves the superior portions of the lungs. Radiologically, it appears as a solitary mass or multinodular disease; inhomogeneity or cavitation of these lesions are common.

Since the presentation of this disease is nonspecific, and as noninvasive tests are rarely revealing, diagnosis requires an open thoracotomy and lung biopsy. Factors which correlate with a poorer prognosis include "B" symptoms, bilateral disease, multilobe involvement, penetration of the pleura, and cavitation. The staging and treatment of these lymphomas according to the extent of pulmonary involvement are recommended, as radiotherapy or combination chemotherapy may be effective in appropriately selected patients.

Reprinted by permission from the American Cancer Society.

Fatal pulmonary failure complicating high-dose cytosine arabinoside therapy in acute leukemia. Andersson BS, Luna MA, Yee C, Hui KK, Keating MJ, McCredie KB (BSA, Dept. of Hematology, Box 61, University of Texas, M. D. Anderson Cancer Center, 1515 Holcombe Blvd., Houston, TX 77030). *Cancer* 65:1079–1084, 1990

One hundred three relapsed leukemia patients were treated with high-dose cytosine arabinoside (Ara-C); 3 g/m^2 intravenously over 2 hours every 6 to 12 hours for a total of nine to 12 doses or 3 g/m^2 intravenously over 2 hours for two doses 12 hours apart followed by a continuous infusion of 1.5 g/m^2 over 24 hours daily for 3 to 4 days. Thirteen of them developed adult respiratory distress syndrome (ARDS) without having any recognized reason for the development of pulmonary edema. This problem showed no correlation with age or prior chemotherapy. Four of the patients recovered, but in nine this complication was fatal. The authors have reviewed the clinical course of these 13 patients and the postmortem findings of the seven patients who had an autopsy performed. The pulmonary tissue from six patients showed massive edema and one had diffuse alveolar damage. Histologic examination revealed a highly proteinaceous intraalveolar infiltrate without any inflammatory reaction in all cases. Intestinal tissue from all patients revealed changes compatible with cytotoxic damage, and pleura and/or pericardium from six of the seven patients showed an extensive fibrinous exudate suggestive of capillary leakage. The time sequence of the clinical events and the histologic findings indicate that high-dose Ara-C treatment in leukemia may cause a capillary leakage syndrome with ARDS that may progress to fatal respiratory failure.

Reprinted by permission from the American Cancer Society.

Chest

Anterior segment upper lobe tuberculosis in the adult: occurrence in primary and reactivation disease. Spencer D, Yagan R, Blinkhorn R, Spagnuolo PJ (PJS, Dept. of Medicine, Cleveland Metropolitan General Hospital, Cleveland, OH 44109). *Chest* 97:384–388, 1990

Nine patients with pulmonary tuberculosis involving predominantly or exclusively the anterior segment of one or both upper lobes were seen over a five-year period. The incidence of anterior segment upper lobe tuberculosis was 6.3 percent of 142 patients presenting with pulmonary tuberculosis during the same time period. Five of the nine patients with anterior segment upper lobe involvement had reactivation disease. An increased incidence of advanced age, diabetes, associated malignant neoplasms, alcoholism, and steroid use were noted in those patients with anterior segment involvement, although only the occurrence of diabetes was statistically significant. We suggest vigilance with regard to the diagnosis of tuberculosis in patients who are elderly, diabetic, or alcohol abusers, particularly where the roentgenographic appearance of anterior segment upper lobe involvement would tend to favor an alternative diagnosis.

Circulation

Silent ischemia during daily life is an independent predictor of mortality in stable angina. Deedwania PC, Carbajal EV (PCD, Division of Cardiology, Dept. of Medicine, UCSF Program/VAMC, 2615 E. Clinton Ave., Fresno, CA 93703). *Circulation* 81:748–756, 1990

We prospectively examined the prognostic significance of silent myocardial ischemia detected by ambulatory electrocardiogram (ECG) monitoring during daily life in 107 patients with long-term stable angina who were symptomatically controlled on conventional antianginal agents. Forty-six patients (group 1) demonstrated one or more episodes (87% silent) of myocardial ischemia; the remaining 61 patients (group 2) had no ischemic ST segment changes. During the mean follow-up period of 23 ± 8 months, 11 cardiac deaths (five sudden and six nonsudden) occurred in group 1, and five cardiac deaths (all nonsudden) occurred in group 2. Kaplan-Meier survival analysis between the groups confirmed that patients with silent ischemia (group 1) had worse prognoses during the follow-up period ($p = 0.023$). Although the higher incidence of hypertension, smoking, hypercholesterolemia, and diabetes in our patients might reflect a more sickly population of stable angina patients, the multivariate Cox's hazard function analysis of these and other variables including Q waves on ECG, exercise parameters, and ambulatory ECG findings revealed presence of silent ischemia during daily life as the most powerful and independent predictor of cardiac mortality ($p = 0.01$). These data indicate that, in such patients with stable angina, silent myocardial ischemia occurs frequently during treatment with conventional antianginal drugs and identifies a subset of patients who are at high risk of cardiac death.

Detection of dissection of the aortic intima and media after angioplasty of coarctation of the aorta: an angiographic, computer tomographic, and echocardiographic comparative study. Erbel R, Bednarczyk I, Pop T, et al. (RE, Medical Clinic, Johannes Gutenberg University, Langenbeckstr. 1, D-6500 Mainz, F. R. G.). *Circulation* 81:805–814, 1990

Balloon coarctation angioplasty (BCA) was performed in eight patients (five male and three female) who were 14–49 years old (mean, 27.3 years) with isolated discrete unoperated coarctation of the aorta ($n = 7$) and postoperative recoarctation ($n = 1$). BCA was successful in seven of eight patients, resulting in a decrease in the gradient (64 ± 19 to 16 ± 13 mm Hg, $p < 0.01$), an increase in the diameter at the coarctation site (0.9 ± 0.4 to 1.6 ± 0.4 mm, $p < 0.01$). Follow-up (6 months) has demonstrated continued gradient relief (6 ± 9 mm Hg) and diameter increase (1.6 ± 0.2 cm). Monitoring was performed by transesophageal echocardiography (TEE) during BCA, and before and after BCA angiography and after BCA computed tomography. In three of seven patients, immediately distal to the BCA site, intimal flaps (1–2 cm) could be detected by TEE but not by angiography or computed tomography. Follow-up TEE showed spontaneous healing in two and persistence in one patient. By TEE and computed tomography in one of eight patients during follow-up, intima and media dissection was found with pleural effusion and spontaneous healing. In one female patient, aortic dissection occurred after successful uneventful BCA, detected by TEE at the 6-month follow-up study and subsequently confirmed by biplane angiography, not detected by computed tomography and previous monoplane angiography. Because of the significant morbidity of BCA in this group of patients, its role in the management of adults with coarctation has yet to be determined. Further long-term follow-up studies will demonstrate whether the observed intima and media dissection by TEE after BCA are related to aneurysm formation.

Gastroenterology

Postprandial colonic transit and motor activity in chronic constipation. Bazzocchi G, Ellis J, Villanueva-Meyer J, et al. (GB, Dept. of Medicine, Harbor-University of California, Los Angeles Medical Center, Los Angeles, CA). *Gastroenterology* 98:686–693, 1990

The aim of this study was to correlate colonic motility and transit in patients with constipation and symptoms of the irritable bowel syndrome. Studies were performed in 16 patients with constipation and compared with the results in 12 healthy subjects. Intraluminal pressure was measured with perfused catheter ports in the transverse colon, splenic flexure, and descending and sigmoid colon. Movement of the luminal contents was measured by following the movement of Technetium-99m-DTPA that was instilled as a bolus in the splenic flexure. In both healthy subjects and patients with constipation there was no movement of the intraluminal tracer and no increase in intraluminal pressure during fasting. After eating a meal, healthy subjects and one group of the constipated patients had an increase in the radioactive marker in the transverse colon ($p < 0.03$) and in the sigmoid colon ($p < 0.03$). The movement of the intraluminal contents was associated with a positive pressure gradient between the descending colon and the transverse and sigmoid colon. There was no retrograde movement of the intraluminal contents and no postprandial increase in intraluminal pressure in the second group of patients with constipation. In healthy subjects, propagating contractions, which were associated with the rapid movement of intraluminal contents, began 60 min after eating. There were no propagating contractions in patients with constipation. These studies suggest that (a) the movement of intraluminal contents in healthy and constipated patients is determined by the postprandial pressure gradients within the colon, and (b) the propagating contraction is necessary for a normal bowel habit.

Reprinted with permission by the American Gastroenterological Association.

Extracorporeal lithotripsy of bile duct stones using ultrasonography for stone localization. Ponchon T, Martin X, Barkun A, Mestas J-L, Chavaillon A, Boustière C (TP, Dept. of Hepatogastroenterology, Hôpital Edouard Herriot, Lyons, France). *Gastroenterology* 98:726–732, 1990

In 19 patients, extraction of bile duct stones through the papilla using a Dormia basket or a mechanical lithotripter was not possible following endoscopic sphincterotomy. After the insertion of a nasobiliary drain, extracorporeal lithotripsy was performed with intravenous sedation using an ultrasonographic stone localization system. The number and location of stones were first determined by retrograde cholangiography. At the time of lithotripsy, saline was injected in the bile ducts to modify the acoustic impedance of tissues surrounding the stones, and subsequent ultrasonography was effective in localizing all stones present in 4 of 5 (80%) patients with intrahepatic stones, and 13 of 14 (93%) with common bile duct stones. In 10 patients (53%), fragmentation was satisfactory and the bile ducts were cleared completely. The mean single stone diameter was significantly smaller in successful cases of fragmentation compared with failures (22.8 ± 6.6 mm vs. 40 ± 10 mm). The results in patients with multiple stones were significantly worse than those in patients with single stones of similar size (25% vs. 100% successful fragmentation). Reasons for this difference in results included the small size of the focal area and the reduced ability of ultrasonography (1) to adequately visualize multiple calculi individually and (2) to assess the degree of stone destruction. Care was taken to first await the resolution of infection or the correction of coagulation abnormalities when present; no morbidity following extracorporeal lithotripsy was observed. Despite its 3-step approach (endoscopic sphincterotomy, lithotripsy, and endoscopic extraction), the need for only intravenous sedation and the absence of patient immersion in water render this technique attractive for elderly and frail patients.

Reprinted with permission by the American Gastroenterological Association.

Manometry and radiology: complementary studies in the assessment of esophageal motility disorders. Hewson EG, Ott DJ, Dalton CB, Chen YM, Wu WC, Richter JE (EGH, Dept. of Gastroenterology, Bowman Gray School of Medicine, Wake Forest University, Winston-Salem, NC). *Gastroenterology* 98:626-632, 1990

The relationship between radiological and manometric findings in esophageal motility disorders is poorly understood. Therefore, 20 subjects (4 normal; 13 diffuse spasm; 3 other motility disorders) were studied using synchronous manometry and videofluoroscopy with alternate 5-ml and 10-ml barium swallows. A total of 181 swallows were analyzed. Concordance between manometry and fluoroscopy was excellent for individual swallows (98%), groups of 5 swallows (97%), and final diagnoses (90%). Contraction onset intervals <0.8 s apart over 5 cm (velocity >6.25 cm/s) were critical in determining abnormal bolus transit (98% sensitivity and positive predictive value). Radiologically, segmental tertiary activity (complete luminal obliteration) was always associated with disrupted primary peristalsis, but nonsegmental tertiary activity was often seen with normal bolus transit and did not have a specific manometric correlate. Four patterns of interrupted peristalsis radiologically were found—segmental tertiary contractions, a generalized esophageal contraction, absence of motor activity, or discoordinated "to-and-fro" movement. Surprisingly, nearly complete barium clearance occurred by the first two mechanisms in two thirds of swallows. Thus, the authors believe radiology and manometry are both excellent studies for identifying abnormal esophageal peristalsis. In difficult cases, these tests give complementary information because radiology assesses bolus movement while manometry provides quantitative pressure data.

Reprinted with permission by the American Gastroenterological Association.

Digestive Diseases and Sciences

Esosphageal function in humans: effects of bolus consistency and temperature. Dooley CP, Lorenzo C, Valenzuela JE (CPD, Gastroenterology Section, Dept. of Medicine, U. S. C. School of Medicine, 2025 Zonal Ave., Los Angeles, CA 90033). *Dig Dis Sci* 35(2):167–172, Feb. 1990

We determined the effect of increased bolus consistency on esophageal motor function in 11 healthy volunteer subjects. Further, we sought to define the esophageal response to boluses with a wide range of temperatures in nine healthy volunteers. Intraluminal pressure events were measured with an infused catheter system, and lower esophageal sphincter pressure was monitored continuously with a Dent sleeve. Boluses (10 swallows each) consisted of 5 ml of a solid suspension (yogurt), 5 cm^3 of a soft solid (gelatin), and 5 ml of water were given in a randomized order. In a separate study, boluses with temperatures of 1°C, 5°C, 10°C, 15°C, room temperature, 30°C, 40°C, 50°C, and 60°C were given in a randomized fashion. Compared to the water bolus, the solid boluses elicited a significant ($P < 0.05$) reduction in peristaltic wave velocity, which was accompanied by significant ($P < 0.05$) increments in the durations of wave contraction and lower esophageal sphincter relaxation. The magnitude of the response elicited by the solid boluses was comparable to that noted with boluses of high viscosity suggesting that the esophagus responds to increments in bolus viscosity and consistency in a similar fashion. Alterations in bolus temperature did not elicit any significant changes in the parameters of esophageal peristalsis. it is concluded that bolus temperature does not have a significant role in the modulation of human esophageal peristalsis except under conditions that cause a change in esophageal wall temperature.

Manometric characteristics of glossopalatal sphincter. Dantas RO, Dodds WJ, Massey BT, Shaker R, Cook IJ (WJD, Medical College of Wisconsin, Dept. of Radiology, Froedtert Memorial Lutheran Hospital, 9200 W. Wisconsin Ave., Milwaukee, WI 53226). *Dig Dis Sci* 35(2):161-166, Feb. 1990

When a liquid bolus is held in the mouth, the posterior tongue and soft palate pinch together to prevent premature spillage of the bolus into the oropharynx. We propose that this glossopalatal closure acts as a glossopalatal sphincter (GPS). In this investigation, we studied glossopalatal closure by obtaining concurrent manometric and radiographic recordings of barium swallows in healthy volunteers. Manometry was done by both a continuous pullthrough method and also by a stationary catheter technique using a ribbon catheter with multiple sideholes spaced at 1-cm intervals. The results showed that when the mouth was loaded with a fluid bolus, the closed glossopalatal segment generated an asymmetric high-pressure zone with greater pressures toward the tongue and palate than laterally. With swallowing, the glossopalatal sphincter high-pressure zone relaxed and the glossopalatal sphincter opened to allow barium to flow from the mouth into the oropharynx. We conclude that the glossopalatal sphincter functions as a physiological sphincter in that it (1) generates a sustained high-pressure zone and closure when a liquid bolus is held in the mouth and (2) relaxes and opens with swallowing.

Gastrointestinal Endoscopy

Study of the gastric mucosal background in patients with gastric polyps. Nakano H, Persson B, Slezak P (HN, Dept. of Internal Medicine, Fujita-Gakuen Health University, Toyoake, 470-11, Japan). *Gastrointest Endosc* 36(1):39–42, 1990

The characteristics of gastric mucosal patterns in the polyp-bearing stomach were investigated by the endoscopic Congo red test and systemic four-points biopsy in 46 patients with hyperplastic polyps and 21 patients with gastric adenomas. In addition, function of the stomach in these patients was assessed by determination of gastric acidity and fasting serum gastrin level and by gastrin response test to a beef extract. In the investigation of the gastric mucosal pattern in hyperplastic polyp patients, Type A gastritis (involving the corpus but sparing the antrum) was most frequently found. On the other hand, extensive intestinal metaplasia from the pyloric antrum to the corpus was most often noted in the adenoma-bearing stomach. Hypergastrinemia was more marked in hyperplastic polyp patients, and may be involved in the pathogenesis of hyperplastic polyps. Attention should be paid to the detection of cancer in areas without polyps during endoscopic observation and reexamination of patients. On these occasions, the characteristics of the background mucosa for each type of polyp should be kept in mind.

Endoscopic versus operative gastrostomy: final results of a prospective randomized trial. Stiegmann GV, Goff JS, Silas D, Pearlman N, Sun J, Norton L (GVS, University of Colorado Health Sciences Center, C-313 4200 E. 9th Ave., Denver, CO 80262). *Gastrointest Endosc* 36(1):1–5, 1990

This study compared operative gastrostomy (OG) (by surgeons) with endoscopic gastrostomy (PEG) (by physicians) in a prospective randomized fashion to determine whether one technique was superior. PEG (Sachs-Vine) and OG (Stamm) were done using local anesthesia. Patients were assessed for complications, mortality, tube function, and cost. Groups were equally matched for indications and underlying disease. Fifty-seven had OG and 64 had attempted PEG. Complications occurred in 26% of OG patients and 9% died. Complications occurred in 25% of PEG patients and 12% died. Tube feeding was initiated in both groups within a mean of 29 (24 to 72) hours of the gastrostomy placement. OG cost $1675 and PEG $979 to perform. Twenty-one PEG patients required endoscopic tube change which raised their total cost to $1574. We conclude there is no difference between OG (using local anesthesia) and PEG with regard to morbidity, mortality, or tube function. The endoscopic technique does appear to have economic advantage.

The Journal of Bone and Joint Surgery

Magnetic resonance imaging of the femoral head after acute intracapsular fracture of the femoral neck. Speer KP, Spritzer CE, Harrelson JM, Nunley JA (JAN, Duke University Medical Center, P. O. Box 2919, Durham, NC 27710). *J Bone Joint Surg [Am]* 72-A:98–103, Jan. 1990

In fifteen patients who had a subcapital fracture of the femoral neck (twelve displaced fractures and three non-displaced fractures), magnetic resonance imaging of the femoral head was done with two-dimensional Fourier transform spin-echo technique within forty-eight hours of injury. The magnetic resonance image did not show avascular necrosis of the femoral head in any of the patients. In eleven patients, there was a decreased signal at the base of the femoral head, immediately adjacent to the fracture. This decreased signal corresponded to a recognized band of necrosis and hemorrhage next to the site of the fracture and was not related to the viability of the femoral head. No other changes were seen on the images. We concluded that this type of magnetic resonance imaging is inadequate to determine the viability of the femoral head within forty-eight hours after a patient sustains an acute intracapsular fracture of the femoral neck.

The Journal of Urology

The significance of the prostatic hypoechoic area: results in 226 ultrasonically guided prostatic biopsies. Devonec M, Fendler JP, Monsallier M, et al. (MD, Service d'Urologie, Hopital Antiquaille, 69321 Lyon, France). *J Urol* 143:316–319, Feb. 1990

A total of 666 patients with symptoms of urinary outflow obstruction underwent assessment of the prostate by digital rectal examination and transrectal ultrasonography. Of the patients 64 had a palpable abnormality suggestive of cancer (stages T1 to T4, or B to C). In the remainder the prostate was either palpably normal, firm or enlarged by benign prostatic hypertrophy. All 64 patients with a palpable abnormality and 162 of 602 with normal rectal examination findings had a hypoechoic area on transrectal ultrasound. Biopsy of the ultrasonic abnormality was done in 148 men by the transperineal route with linear array ultrasound guidance and in 78 by the transrectal route with a mechanical sector scanner in the sagittal plane.

Of the 64 patients with a nodular prostate 34 (53%) had cancer (31% of those with stages T1 and 2, 83% with stage T3 and 100% with stage T4 disease). In 14% of the patients with stages T1 and T2 cancer the biopsy showed prostatic intraepithelial neoplasia grade 3. Of the 162 patients with a palpably normal prostate who underwent ultrasound-guided biopsy 11 (6.7%) had cancer and 6 (3.7%) had grade 3 prostatic intraepithelial neoplasia detected in the biopsy material. Patients with stages T1 to T2 cancer and those with ultrasound-diagnosed impalpable cancer were not significantly different with respect to patient age (67 versus 70 years), cancer size (3.0 ± 1.6 versus 3.9 ± 2.5 cm.^2) or Gleason score (5.4 ± 1.2 versus 6.5 ± 0.9). The results demonstrate that ultrasound guidance improves the yield of prostate needle biopsy. Furthermore, it is suggested that prostate cancer found by ultrasound alone is not different from early palpable disease and should be treated in the same manner.

Pediatrics

Lack of transmission of human immunodeficiency virus from infected children to their household contacts. Rogers MF, White CR, Sanders R, et al. (MFR, AIDS Program, Mailstop G29, Centers for Disease Control, Atlanta, GA 30333). *Pediatrics* 85(2):210–214, Feb. 1990

The possibility of transmission of the human immunodeficiency virus (HIV) from infected children to their contacts has been confronted in households, schools, day-care centers, and other child care settings. Cases reported to the Centers for Disease Control and several studies of close contacts of HIV-infected patients suggested that the risk of transmission in these settings is extremely low. However, most of these studies involved infected adults or older children. Younger children, who drool, bite, mouth toys, and are incontinent, may be more likely to transmit HIV in these settings. To assess this possibility, the authors tested 89 members of households in which 25 children with HIV infection, most of whom were preschool-aged, resided. Household members had close personal contact with the infected children. They shared many items likely to be soiled with blood and body fluids, such as toys, toothbrushes, eating utensils, toilets, and bathtubs. Hugging, kissing, sharing a bed, and bathing together were common. Household members were tested no sooner than 4 months after initial contact with the infected child, to allow adequate time for seroconversion. All 89 participating household members were anti-HIV seronegative, and 78 who were tested were serum p24 antigen negative. It was concluded from this study and other evidence that the risk of transmission from children to their contacts is extremely low and has not been clearly documented in the household setting.

Reprinted by permission of PEDIATRICS © 1990.

The Journal of Pediatrics

Use of extracorporeal membrane oxygenation in the treatment of respiratory syncytial virus bronchiolitis: the national experience, 1983 to 1988. Steinhorn RH, Green TP (RHS, Minnesota Regional ECMO Program, Box 104 UMHC, Harvard St. at East River Rd., Minneapolis, MN 55455). *J Pediatr* 116:338–342, 1990

In an effort to obtain data to provide the basis for the design of controlled clinical trials, we contacted all U.S. participants in the National ECMO Registry to assemble the national experience on the use of extracorporeal membrane oxygenation in respiratory syncytial virus bronchiolitis during the past 5 years. Twelve infants were treated at nine centers between 1983 and 1988. Eight had been born prematurely, and five had bronchopulmonary dysplasia. The mean age at onset of infection with respiratory syncytial virus was 108 ± 102 days. The mean length of ventilator management before extracorporeal membrane oxygenation was 7.8 ± 7.1 days. All infants had persistent hypoxemia with a mean arterial oxygen pressure of 39.2 ± 11.7 torr (5.3 ± 1.6 kPa) despite high ventilator pressures (mean airway pressure 19.7 ± 6.4 cm H_2O) and 100% inspired oxygen; six had air leak syndrome. Seven infants survived (58%). The mean duration of extracorporeal membrane oxygenation for survivors was 233 ± 139 hours. Preexisting chronic lung disease did not predict a poor outcome: four of the five infants with bronchopulmonary dysplasia survived. Six of the survivors have subsequently achieved expected developmental milestones and one has slight motor delay. We conclude that, for infants with severe respiratory syncytial virus bronchiolitis whose condition deteriorates despite maximal ventilator management, extracorporeal membrane oxygenation may provide lifesaving support. The duration of successful treatment with this therapy may be longer than that for conventional neonatal indications, but excellent neurologic outcome may be expected in survivors.

Gastrointestinal Radiology

Percutaneous interventional gallbladder procedures: personal experience and literature review. Teplick SK, Brandon JC, Wolferth CC, Amron G, Gambescia R, Zitomer N (SKT, Dept. of Radiology, University of Arkansas Medical Center, Mail Slot 556, 4301 W. Markham, Little Rock, AR 72205). *Gastrointest Radiol* 15:133–136, 1990

Our experience with 58 percutaneous gallbladder procedures in 48 patients are discussed. Diagnostic procedures consisted of needle aspiration of bile ($n = 5$) to evaluate the gallbladder as a source of infections and transcholecystic cholangiography (TCC) ($n = 32$) for bile duct visualization. Percutaneous cholecystostomy (PC) ($n = 21$) was performed for gallbladder or bile duct decompression or stone dissolution. Ultrasound and/or fluoroscopic guidance were used, and the procedures were successful in all but one patient. The overall complication rate was 13.8% (8/58 procedures) but only 5.2% were considered serious (three instances of bile peritonitis). No vasovagal reactions or hemorrhage occurred. We also reviewed the complications in 231 cases of PC that have been reported in the English literature. The overall complication rate was 7.8%, and the most significant problems were death ($n = 1$), peritonitis ($n = 3$), and severe vasovagal reactions ($n = 4$).

Nonvisualized gallbladder on oral cholecystography: implications for lithotripsy. Wong K, Ekberg O, Laufer I, Malet PF, Arger P (OE, Dept. of Radiology, Hospital of the University of Pennsylvania, 3400 Spruce St., Philadelphia, PA 19104). *Gastrointest Radiol* 15:126–128, 1990

Currently, most protocols evaluating the efficacy of gallstone lithotripsy require a visualized gallbladder on oral cholecystography (OCG). The primary purpose of the OCG is to establish that the cystic duct is patent. When the gallbladder is visualized on OCG, it can also be used to number and size gallstones accurately. Patients with nonvisualization of the gallbladder on OCG are excluded from consideration for lithotripsy. The purpose of this study was to evaluate retrospectively the ultrasonographic findings (i.e., number and size of stones in 32 patients with nonvisualization on the OCG). In 11 patients (34%) ultrasound (US) did not detect any stone, and it is presumed that the gallbladder failed to visualize for other reasons. Six patients (19%) had one or two stones and 15 (47%) patients had more than three stones. This suggests that 20% of patients with nonvisualization of the gallbladder on OCG would otherwise be eligible for lithotripsy provided that patency of the cystic duct can be demonstrated by other means, such as computed tomographic (CT) examination with oral biliary contrast or cholescintigraphy.

Comparison of computed tomography and magnetic resonance imaging in the evaluation of focal hepatic lesions. Barakos JA, Goldberg HI, Brown JJ, Gilbert TJ (JAB, Dept. of Radiology, P. O. Box 0628, University of California, San Francisco, CA 94131). *Gastrointest Radiol* 15:93–101, 1990

Two combined magnetic resonance (MR) spin-echo pulse sequences at 0.35 T were compared with dynamic bolus contrast-enhanced computed tomography (CT) in the evaluation of focal hepatic lesions. Each combined MR sequence was performed in a separate group of patients. The first group consisted of 76 patients in whom a moderately T1-weighted sequence (spin echo [SE] 500/30 [repetition time/echo time]) was combined with a T2-weighted sequence (SE 2000/60). In the second group, consisting of 68 patients, a more heavily T1-weighted sequence (SE 250/15) was combined with the T2-weighted sequence. All studies were evaluated in a retrospective blinded fashion, with construction of receiver operating characteristic curves.

We conclude that, in detection of patients with one or more focal hepatic lesions, either combined MR sequence was comparable to CT. In the detection of individual hepatic lesions, the sensitivity of the combined MR sequence with a moderately T1-weighted sequence (SE 500/30 and 2000/60) was essentially equivalent to CT (79 vs 77%, respectively). Additionally, a combined MR sequence with a heavily T1-weighted pulse sequence (SE 250/15 and 2000/60) was not statistically different than CT (86 vs 80%, respectively). These findings were supported by the receiver operating characteristic analysis.

Journal of Ultrasound in Medicine

Sonographic fetal growth standards: are current data applicable to a racially mixed population? Hadlock FP, Harrist RB, Shah YP, Sharman RS, Park SK (FPH, Dept. of Radiology, Baylor College of Medicine, Houston, TX 77030). *J Ultrasound Med* 9:157–160, March 1990

Currently available sonographic growth standards for fetal head size, abdominal size, and limb length are based primarily on studies from white populations. To determine whether these published standards are appropriate for a racially mixed, indigent population, we compared our published data from a middle-class white population with data generated from a black/Hispanic population seen at a county hospital in Houston, Texas. No statistically significant differences were found for any of the following fetal sonographic parameters (20 to 41 weeks): biparietal diameter, head circumference, abdominal circumference, femur length.

Reprinted with permission by the American Institute of Ultrasound in Medicine.

Journal of Computer Assisted Tomography

MR characterization of hepatic lesions by t-null inversion recovery sequence. Patrizio G, Pavone P, Testa A, Marsili L, Tettamanti E, Passariello R (GP, Departimento di Radiologia, Ospedale Santa Maria di Collemaggio, 67100 L'Aquila, Italy). *J Comput Assist Tomogr* 14(1):96–101, Jan./Feb. 1990

Tissue characterization of focal hepatic lesions was performed employing an inversion recovery sequence with short repetition time and short inversion time (TI) values. Different and specific TI values, correlated to the in vivo measured T1 relaxation times, were used to null the signal intensity of each type of lesion. In 40 patients studied, we observed the nulling effect of normal liver in 10 of 10 cases with a TI of 136 ms, of metastases in 7 of 8 cases with a TI of 175 ms, of hemangiomas in 15 of 16 cases with a TI of 200 ms, and of cysts in 6 of 7 cases with a TI of 235 ms. A quantitative analysis of the nulled signal was performed by measuring the signal/noise values. A further qualitative and quantitative characterization was carried out by evaluating the signal intensity of hepatic lesions at the null point of normal liver. The method provided the possibility of discriminating different focal lesions with specificity values of 83–94%, according to the type of lesion.

News

Courses in MR Imaging at Emory University

The Magnetic Resonance Education Center, Emory University, Atlanta, GA, is offering courses in MR imaging for physicians, scientists, and technologists. Course topics include principles and methods of MR imaging; neurologic, abdominal, cardiovascular, and musculoskeletal applications; MR spectroscopy; and operation and management of MR facilities. The format includes lectures, case reviews, clinical observation, teaching file study, and computer simulation activities. Course director: Perry Sprawls. Category 1 credit: 30 hr; credit for technologists: 3 CEUs. Introduction to Magnetic Resonance Imaging for physicians will be held Sept. 10–14, Sept. 24–28, Oct. 1–5, Oct. 29–Nov. 2, Nov. 12–16, and Dec. 3–7. The course for technologists will be held June 4–8, July 9–13, Aug. 6–10, Oct. 15–19, and Nov. 4–10. Fee: physicians, $1100; technologists, $550. Information: Continuing Medical Education, 1440 Clifton Rd., N.E., 111-A WHSCAB, Atlanta, GA 30322; (404) 727-5695.

Workshops on New Cardiac and Peripheral Vascular Devices

The Pittsburgh Vascular Institute and the Pittsburgh Heart Institute of Shadyside Hospital are sponsoring New Devices for the Cardiac and Peripheral Vascular Laboratories, July 2–6, at the Walt Disney World Swan Hotel, Orlando, FL. Attendees will acquire hands-on experience in using the new devices; workshops will be taught by leading cardiologists, radiologists, cardiovascular surgeons, and biomedical engineers. Topics will include angioscopy, complex multilesional angioplasty, intravascular stents, intravascular ultrasound, lasers, and percutaneous atherectomy. Course directors: James D. O'Toole and Mark H. Wholey. Category 1 credit: 15 hr. Fee: physicians, $500; nursing and technical personnel, $300; 2-day session only, $250. Information: Shadyside Hospital, New Devices Technology Workshop, 5230 Centre Ave., Pittsburgh, PA 15232; (412) 622-1051.

Diagnostic Imaging Seminar

The Dept. of Radiology, Hospital of the University of Pennsylvania, is sponsoring its 12th annual Diagnostic Imaging Seminar, July 9–13, at the Harbor House Hotel, Nantucket Island, MA. The seminar will provide updates on procedures for imaging the chest, musculoskeletal system, brain, spine, and children. Some aspects of pelvic and obstetric imaging will be included. Course director: Peter H. Arger. Guest faculty: D. P. Naidich and R. L. Teele. Category 1 credit: 23 hr (pending). Fee: physicians, $495; residents, $325; technologists (letter required), $200. Information: Janice Ford or Gwen Mallard-Winter, Dept. of Radiology, Continuing Education, 3440 Market St., Ste. 420, Philadelphia, PA 19104; (215) 662-6904 or 622-6877.

Tomography for Technologists

The Division of Nuclear Medicine, Dept. of Radiology, Emory University School of Medicine, Atlanta, GA, is sponsoring Tomography for Technologists, July 16–17, Sept. 17–18, and Nov. 12–13. The program is intended for experienced nuclear medicine technologists who are beginning to perform SPECT studies. Participants should be familiar with nuclear medicine computer systems and data processing techniques. Basic principles will be presented in lectures, and practical aspects will be emphasized in hands-on sessions. Course director: James Galt. Credit: 0.7 CEUs and 0.6 VOICE credits. Fee: $200. Information: Continuing Medical Education, 1440 Clifton Rd., N.E., 111-A WHSCAB, Atlanta, GA 30322; (404) 727-5695.

Annual Symposium on Breast Disease

The Dept. of Radiology, University of Michigan Medical School, is sponsoring the 4th Annual Symposium on Breast Disease, July 22–25, at the Grand Traverse Resort, Grand Traverse Village, MI. Highlights of the course will include presentation of the newest developments in breast imaging and diagnostic techniques, including mammography, breast sonography, and fine-needle aspiration biopsy; update of the role and implications of breast cancer screening; summary of the latest cytologic, surgical, and oncologic approaches to breast cancer; and workshops to allow small group discussions of various diagnostic, management, and technical issues. Course director: Dorit D. Adler. Category 1 credit: 13 hr. Fee: physicians, $395; residents and fellows, $295. Information: Ted Ciganik, Program Assistant, Office of Continuing Medical Education, G-1100 Towsley Center, Box 0201, University of Michigan Medical School, Ann Arbor, MI 48109-0201; (313) 763-1400.

Imaging on Lake Coeur d'Alene

The Depts. of Radiology, University of Washington, Seattle, and Sacred Heart Medical Center, Spokane, are cosponsoring their 4th annual Imaging on Coeur d'Alene—A Summer Radiology Meeting, Aug. 2–4, at the Coeur d'Alene Resort, Coeur d'Alene, ID. The course is designed primarily to meet the needs of practicing general diagnostic radiologists. Sessions will cover thoracic, cardiovascular, abdominal, pelvic, and musculoskeletal imaging and diagnostic sonography. Category 1 credit: 20 hr. Fee: $350 ($400 after July 15). Information: Kathy Fischer, Course Secretary, Dept. of Radiology, Sacred Heart Medical Center, TAF-C9, Spokane, WA 99220; (509) 455-3352 or 455-3330.

Mackinac Island Imaging Conference

The Dept. of Diagnostic Radiology, William Beaumont Hospital, Royal Oak, MI, is offering Mackinac Island Imaging Conference, Aug. 6–9, at the Grand Hotel, Mackinac Island, MI. The conference is intended to be a refresher course and an updating in the practical aspects of modern radiologic imaging and interventional techniques. Guest faculty: L. W. Bassett, R. R. Edelman, W. D. Foley, and Elias Kazam. Category 1 credit: 22 hr. Fee: physicians, $400; residents and Beaumont alumni, $200. Information: Miss Mary Anne Smith, William Beaumont Hospital, Royal Oak, MI 48073; (313) 551-6199.

Summer Imaging and Interventional Techniques VIII

The Dept. of Radiology, Emory University School of Medicine, is sponsoring Summer Imaging and Interventional Techniques VIII, Aug. 13–17, at the Westin Resort on Port Royal Plantation, Hilton Head Island, SC. State-of-the-art imaging techniques, including MR, CT, sonography with Doppler imaging, scintigraphy, and interventional procedures, will be demonstrated. The material will be presented in an organ-oriented format. Course director: Michael E. Bernardino. Category 1 credit: 20.5 hr. Fee: physicians, $550; residents (letter required), $250. Information: Continuing Medical Education, 1440 Clifton Rd., N.E., 111-A WHSCAB, Atlanta, GA 30322; (404) 727-5695.

Neurotransmitters: Brain, Heart, and Tumor Response

The American College of Nuclear Physicians (ACNP) and the United States Dept. of Energy are cosponsoring Neurotransmitters: Brain, Heart, and Tumor Response, Aug. 24–27, at the Hotel Des Couverneurs Le Grand, Montreal, Quebec. Chairman: David E. Kuhl. Category 1 credit: 11.5 hr. Fee: ACNP members: physicians and scientists, $250; technologists and residents, $150; nonmembers: physicians and scientists, $350; technologists and residents, $200. Information: Margie Kilty, American College of Nuclear Physicians, 1101 Connecticut Ave. N.W., #700, Washington, DC 20036; (202) 857-1191.

Registry Preparation Courses for Sonographers

The Center for Medical Ultrasound, Bowman Gray School of Medicine, is offering several registry preparation courses for sonographers. Ultrasound Physics will be held Sept. 7–8 at the Dallas–Fort Worth Hilton Executive Conference, Dallas; Sept. 24–25 at the Marina Del Rey Marriott, Los Angeles; Sept. 29–30 at the Hyatt Regency Crystal City, Washington, DC; and Oct. 5–6 at the Stouffer Hotel, Chicago. Doppler Physics will be held Sept. 9 at the Dallas–Fort Worth Hilton Executive Conference Center; Sept. 26 at the Marina Del Rey Marriott; Oct. 1 at the Hyatt Regency Crystal City; and Oct. 7 at the Stouffer Hotel. Course director for both physics courses: Frederick W. Kremkau. Fee: Ultrasound Physics, $250; Doppler Physics, $150; both courses, $350. Abdominal Ultrasound Review and OB/GYN Ultrasound Review will be offered at the Hyatt Regency Crystal City, Washington, DC, Sept. 26–27 and Sept. 28, respectively. Course director: Kenneth J. W. Taylor. Fee: Abdominal, $200; OB/GYN, $120. Information for all courses: Louise Nixon, Center for Medical Ultrasound, Bowman Gray School of Medicine, Winston-Salem, NC 27103; (919) 748-4505.

International Symposium on Biliary Lithotripsy

The 3rd International Symposium on Biliary Lithotripsy will be held Sept. 13–15 at the Sheraton Hotel, Munich, Germany. Information: Ms. J. Steinberg, Secr. to Prof. Paumgartner, Dept. of Medicine II, Klinikum Grosshadern, Marchioninistrasse 15, D-8000 Munich 70, F. R. G.; telephone: 49-89-70952380; fax: 49-89-70958887.

Advances in Mid and Low Field Magnetic Resonance Imaging

Sacred Heart General Hospital and Pacific Northwest MR Forums, Eugene, OR, are cosponsoring the 2nd annual Advances in Mid and Low Field Magnetic Resonance Imaging, Sept. 14–16, at the Portland Marriott Hotel, Portland, OR. The meeting will address the practical, clinical, and economic needs of physicians and technologists who use or wish to purchase a mid or low field strength MR system. The program also will include an update of the clinical relevance and usefulness of low-field imaging. Meeting cochairmen: D. D. Stark and R. M. Quencer. Guest faculty: L. F. Czervionke, R. B. Dietrich, E. Fram, R. J. Herzog, C. B. Higgins, R. B. Lufkin, D. W. Nelson, W. W. Orrison, B. A. Porter, M. A. Solomon, E. C. Unger, and J. V. Welch. Category 1 credit: 18 hr. Fee: physicians, $395; residents and fellows (letter required), $295. Information: Sacred Heart MRI Dept., 1255 Hilyard St., Eugene, OR 97401; (503) 686-6741; or Pacific Northwest MR Forums, 28132 Spencer Ck. Rd., Eugene, OR 97405; (503) 683-4930.

Interdisciplinary Management of Dysphagia

The Audie L. Murphy Memorial Veterans Hospital and the University of Texas Health Science Center at San Antonio are sponsoring Interdisciplinary Management of Dysphagia, Sept. 15, at the Geriatric Education Center, University of Texas Health Science Center. The symposium will highlight physiology and pathophysiology of the oropharyngeal and esophageal swallow, recent advances in diagnosis and treatment of dysphagia, and the team approach to evaluation and patient management. Course director: Jean K. Patterson. Guest faculty: M. V. Donner, J. A. Logemann, and E. W. Massey. Category 1 credit: pending. Fee: non-VA Hospital participants, $35; VA Hospital staff members, $15. Information: Geriatric Education Center, University of Texas Health Science Center, 7703 Floyd Curl Dr., San Antonio, TX 78284-7919; telephone: (512) 567-3370; fax: (512) 567-2490.

Interventional Neuroradiology: Current Practices and Techniques

The Dept. of Radiology and Radiological Science, The Johns Hopkins University, School of Medicine, is sponsoring Interventional Neuroradiology: Current Practices and Techniques, Sept. 16–18, at The Johns Hopkins Medical Institutions, Baltimore, MD. The course will have a didactic component and an in-depth practicum given by leading authorities in interventional neuroradiology, anesthesiology, neurosurgery, neurology, and plastic surgery. Course director: Gerard M. Debrun. Category 1 credit: 27 hr. Fee: physicians, $550; residents and fellows (letter required), $350; technicians, $350. Information:

Program Coordinator, The Johns Hopkins Medical Institutions, Office of Continuing Education, Turner Bldg., 720 Rutland Ave., Baltimore, MD 21205; (301) 955-2959.

Quantitative Thallium Myocardial Tomography

The Division of Nuclear Medicine, Dept. of Radiology, Emory University School of Medicine, Atlanta, GA, is sponsoring Quantitative Thallium Myocardial Tomography, Sept. 24–25 and Oct. 22–23. The program is designed for nuclear medicine physicians, radiologists, and cardiologists. It is intended to familiarize participants with basic principles and the clinical usefulness of quantitative thallium tomography. Objectives include knowledge of image reconstruction and its application to quantitative thallium analysis, appreciation of factors that influence image quality and accuracy of the technique, knowledge of quality control techniques used to monitor tomographic camera imaging systems, development of skills in interpreting quantitative thallium images, and appreciation of clinical applications of this technique. Category 1 credit: 13.5 hr. Fee: $500. Information: Continuing Medical Education, 1440 Clifton Rd., N.E., 111-A-WHSCAB, Atlanta, GA 30322; (404) 727-5695.

Neuroradiology Courses at Harvard

Harvard Medical School is offering two postgraduate courses in neuroradiology. Current Concepts in Neuroradiology will be given Oct. 1–3; and Head and Neck Radiology and Neuro-MRI, Oct. 4–5. Both courses will be held at the Lafayette Hotel, Boston. Category 1 credit (both courses): 40 hr. Fee: combined course: physicians, $620; residents and fellows, $530; Current Concepts course only, $505; Head and Neck course only, $480. Information: Dept. of Continuing Education, Harvard Medical School, Boston, MA 02114; (617) 432-1525.

Cardiovascular Imaging and Interventional Radiology

The Dept. of Radiology, Brigham and Women's Hospital, and the Dept. of Continuing Education, Harvard Medical School, in cooperation with the Society of Cardiovascular and Interventional Radiology, are offering Cardiovascular Imaging and Interventional Radiology, Oct. 9–12, at the Hyatt Regency Hotel, Cambridge, MA. Program director: Donald P. Harrington. Category 1 credit: approximately 25 hr. Fee: physicians, $525; residents, fellows, nurses, and technologists, $350. Information: Harvard Med-CME, P. O. Box 825, Boston, MA 02117; (617) 432-1525.

Digital Imaging and Other New Trends in Clinical Practice

Massachusetts General Hospital, Boston, is sponsoring Digital Imaging and Other New Trends in Clinical Practice, Oct. 15–18. Course director: Reginald E. Greene. Category 1 credit: 31 hr. Fee: $495. Information: Dept. of Continuing Education, Harvard Medical School, Boston, MA 02115; (617) 432-1525.

Update on MR Imaging and CT

The Dept. of Radiology, Brigham and Women's Hospital, and the Dept. of Continuing Education, Harvard Medical School, are sponsoring Magnetic Resonance Imaging and Computed Tomography Update, Oct. 22–26, at the Hyatt Regency Hotel, Cambridge, MA. Program directors: Steven E. Seltzer, Ferenc Jolesz, and Daniel O'Leary. Category 1 credit: approximately 31 hr. Fee: physicians, $550; residents, fellows, and technologists, $325. Information: Harvard Med-CME, P. O. Box 825, Boston, MA 02117; (617) 432-1525.

Advanced Neuroradiology Seminar

The Depts. of Radiology, The Tampa General Hospital and the University of South Florida College of Medicine, are sponsoring the 8th annual Advanced Neuroradiology Seminar, Oct. 25–27, at the Hyatt Regency Grand Cypress, Orlando, FL. The course will emphasize recent advances in MR imaging; CT; and neurosurgical techniques, including radiosurgery. Topics will include optimizing parameters for MR imaging; MR imaging of brain tumors, infarcts, hemorrhage, and trauma; MR imaging of the lumbar spine, cervical spine, and spinal cord; CT and MR of the orbits; and therapy of intracranial aneurysms and arteriovenous malformations. Course directors: Carlos R. Martinez and Charles H. Fisher. Guest faculty: Eben Alexander III, S. W. Atlas, R. M. Quencer, J. S. Ross, and Gordon Sze. Category 1 credit: 15 hr. Fee: physicians, $395; residents and fellows, $300. Information: Agnes Bridges, Radiological Services, The Tampa General Hospital, P. O. Box 1289, Tampa, FL 33601; (813) 251-7778.

The American Board of Radiology Examinations

Written examinations for the American Board of Radiology (ABR) are scheduled for Sept. 27–28, 1990, and Oct. 3–4, 1991. Oral examinations will be held at the Executive West Hotel in Louisville, KY, June 4–8, 1990, and June 3–7, 1991. The ABR will accept applications for admission to the examinations after July 1, but not later than Sept. 30, in the year *preceding* the year in which the examination is to be taken. For application forms and further information: Office of the Secretary, The American Board of Radiology, 300 Park, Ste. 440, Birmingham, MI 48009.

Meeting and Course Review

For the reader's convenience, a summary of upcoming meetings and courses is provided. Detailed listings are given in the *AJR* issue given in parentheses.

Visiting Fellowship in Interventional Radiology, times arranged, Baltimore (Sept 1989)
Visiting Fellowships at UCSF, times arranged, San Francisco (Sept 1989)
Preceptorships in Transrectal Ultrasound of the Prostate, Ann Arbor, MI (Sept 1989)
Musculoskeletal MRI for Orthopedists and Radiologists, May 28–June 1, Sonesta Beach Hotel (Dec 1989)
Emergency Radiology 1990, May 29–June 1, Boston (March)
Italian Society of Radiology and Nuclear Medicine, May 30–June 3, Turin, Italy (Nov 1989)
Contemporary Medical Imaging VII, May 30–June 3, Hilton Head Island, SC (April)
Diagnostic Imaging of the Eye and Orbit, June 1–2, New York City (May)
American Society of Emergency Radiology Annual Meeting, June 2, Boston (Feb)
Fellowships in Biliary Lithotripsy, June 7–9, Baltimore, MD (Dec 1989)

American College of Medical Physics Annual Meeting, June 7–10, Austin, TX (Dec 1989)
Abdominal Ultrasound, June 11–14, Philadelphia, (Jan)
Prostate Ultrasound, June 15, Philadelphia (Jan)
Advanced Techniques in MRI, June 16–22, Kiawah Island, SC (March)
Radiology in Scandinavia and the Soviet Union, June 16–30, Copenhagen, Malmo, Stockholm, Helsinki, and Leningrad (Feb)
Diagnostic Radiology, June 17–22, Myrtle Beach, NC (March)
Pediatric Nuclear Medicine Categorical Seminar, June 18, Washington, DC (March)
Liver Imaging, June 25–27, Boston (March)
International Course in Cardiovascular Interventional Radiology, July 11–13, Leeds, United Kingdom (Dec 1989)
Mammography and the Search for Breast Cancer, July 13–14, Rochester, NY (April)
Annual Pittsburgh Breast Imaging Seminar, July 13–15, Pittsburgh (May)
Advances in Radiation Oncology Physics, July 16–20, Lawrence, KS (March)
American Association of Physicists in Medicine Annual Meeting, July 22–26, St. Louis (Feb)
Napa Valley Imaging Update—MRI 1990, July 22–26, Napa, CA (April)
Musculoskeletal Imaging, July 23–25, Laguna Niguel, CA (March)
Symposium on Magnetic Resonance Imaging, July 26–29, Laguna Niguel, CA (March)
Annual Northern Imaging Meeting, Aug. 4–8, Winnipeg, Manitoba (March)
Copenhagen Symposium on Uroradiology, Aug. 27–30, Herlev, Denmark (Feb)
Uroradiology Postgraduate Course, Sept. 10–14, Vancouver, B.C. (April)
Mammography for the General Radiologist, Sept. 10–13 and Oct. 22–25, Boston (March)
European Society of Head and Neck Radiology Annual Meeting, Sept. 12–15, Bresica (Lake of Garda), Italy (Feb)
Applied Ultrasound: Accent on Doppler, Sept. 12–15, Naples, FL (April)
Musculoskeletal Disorders, Sept. 12–15, Salzburg, Austria (April)
Interventional Radiology/2nd Marmara Medical Days, Sept. 19–21, Haydarpasa-Istanbul, Turkey (March)
International Meeting on Topics of Interventional Radiology, Sept. 20–22, Hotel Oranje Noordwyk, the Netherlands (May)
Nuclear Medicine Technology Certification Examination, Sept. 22; application deadline, July 21 (Nov 1989)
Radiology in Britain and Brussels, Sept. 23–30, Eastbourne, Sussex, England, and Brussels, Belgium (May)
International Conference on Ultrasound Angiography, Sept. 25–28, London, United Kingdom (Feb)
Royal Australasian College of Radiologists Annual Meeting, Oct. 5–11, Perth, Western Australia (April)
Practical Radiology, Oct. 8–11, Charlottesville, VA (May)
Magnetic Resonance Imaging 1990: Back to the Future, Oct. 10–13, Cincinnati (May)
American Lithotripsy Society Annual Meeting, Oct. 11–14, San Diego (March)
MR Imaging Course in Riyadh, Saudi Arabia, Oct. 14–17 Riyadh, Saudi Arabia, (April)
Advances in Color Doppler Sonography, Nov. 1–3, White Sulphur Springs, WV (May)
Symposium on Bone and Soft-Tissue Tumors, Nov. 9–10, Sacramento, CA (May)
International Congress of Radiation Research, July 7–12, 1991, Toronto. Deadline for Junior Investigators Awards, Oct. 15, 1990; for abstracts, Jan. 15, 1991 (May)

AJR carries announcements of courses, symposia, and meetings of interest to its readers if received a minimum of 5 months before the event. There is no charge; receipt of items by the *AJR* Editorial Office is not acknowledged. Submit items for publication typed double-spaced. Provide title, date, location, brief description, sponsor, course directors, fees, category I credit, and address and telephone number for additional information. Faculty from the host institution will not be listed. Guest faculty names will appear **only** if initials are provided. Mail news items to *AJR* Editorial Office, 2223 Avenida de la Playa, Suite 200, La Jolla, CA 92037-3218.

American Roentgen Ray Society 91st Annual Meeting
May 5–10, 1991, Boston, MA
Sheraton Boston Hotel

Registration and Hotel Reservations

Forms for advance registration and hotel reservations will be in the February and March 1991 issues of the *AJR*.

Scientific Program

Abstracts of papers to be considered for the program must be submitted by November 1, 1990. Forms on which to submit abstracts are in this issue of the *AJR*. The ARRS Program Committee will select papers and notify authors in early January. The *AJR* has first rights to all papers accepted for presentation at the ARRS meeting. Send abstract, application, and four copies of the abstract to

ARRS President-Elect
c/o Paul R. Fullagar
American Roentgen Ray Society
1891 Preston White Dr.
Reston, VA 22091

Refresher Course Program

A summary of the refresher courses will appear in the *AJR* in February along with advance registration forms. Early registration is an advantage in assuring preferred courses in this popular program.

Scientific Exhibits

Proposals for scientific exhibits must reach the Chairman of Exhibits by November 1, 1990. Forms, which may be photocopied, are in this issue of the *AJR*. Send completed form to

Chairman, Scientific Exhibits Committee
c/o Paul Fullagar
American Roentgen Ray Society
1891 Preston White Drive
Reston, VA 22091
Telephone (703) 648-8992

Local Program

A program of sightseeing, shopping, and entertainment will be developed by the Local Arrangements Chairman. Information and advance registration forms will be in the February issue of the *AJR*.

Residents' Award Papers

The society offers several cash awards for the best scientific papers prepared by residents in radiology. The President's Award has a $2000 prize. There are two Executive Council awards of $1000 each. All are presented at the annual meeting. Papers should be submitted by February 15, 1991, for consideration in this competition. Send entries to

Nancy O. Whitley, M.D.
Dept. of Radiology
University of Maryland Medical Systems Hospital
22 S. Greene St.
Baltimore, MD 21201

Deadlines

Abstracts of papers: November 1, 1990
Scientific exhibit proposals: November 1, 1990
Residents' Award papers: February 15, 1991

Call for Papers

American Roentgen Ray Society 1991 Annual Meeting: May 5–10, 1991, Boston, MA

ADDRESS OF PRESENTING AUTHOR

Department

Institution

Street

City, State Zip

Phone: ____________

Type title, authors, and abstract in the space provided below. (Instructions are on reverse side of this page. Abstract should not exceed 300 words.)

Select one category: ______Angio/Interventional ______Breast ______Chest ______CT ______Gastrointestinal Tract ______Genitourinary Tract ______MR ______Neuroradiology ______Skeletal ______Sonography

Projection Requirements: ______35 mm, single or double (circle one) ______16 mm silent film ______½"VHS ______¾"

Has this been presented elsewhere? ______yes ______no. If yes, please describe on reverse side of this page.

Instructions for Scientific Abstracts

1. Type the information single-spaced within the lines. Underline the name of the presenting author. Append as a last line of the abstract any research grant support, if applicable (e.g., Supported by USPHS Grant HE-80144). If the abstract is accepted, it will not be proofread; it will appear exactly as typed. Use the following format:

   MR IMAGING OF THE SPINE AND NECK
   F. S. Lau, M.D., A. N. Kirk, M.D., and R. A. Beck, Ph.D.
   University of California, Bakersfield, Bakersfield, CA 92338

2. Abstracts should include four paragraphs devoted sequentially to the following topics: (1) object or purpose of the study, (2) materials, methods, and procedures, (3) results, (4) significance of the results and conclusions. The text should not exceed 300 words. Specific data are essential. The abstract should be a succinct summary of work done rather than a promissory note.
3. The Program Committee will grade each abstract and determine acceptance. Further information will be forwarded to those whose abstracts are accepted for presentation.

Deadline for submission of abstract is November 1, 1990. Mail abstract and two copies to

ARRS President-Elect
c/o Paul R. Fullagar
American Roentgen Ray Society
1891 Preston White Dr.
Reston, VA 22091

Call for Scientific Exhibits

American Roentgen Ray Society
1991 Annual Meeting:
May 5–10, 1991, Boston, MA

FOR COMMITTEE USE ONLY

Date Received ______ Application No. ______
Subject ______ Score ______
Rejected ______ Accepted ______
Assigned ______ Space No. ______

Principal Exhibitor's Mailing Address

Name ______ Institution ______

Department ______ Street Address ______ City ______

State ______ Zip Code ______ Telephone: office (   ) ______ home (   ) ______

Names of Exhibitors (List principal exhibitor first and telephone number of each person.)

Last	First	Middle	Telephone	Degree (one only)	Member ARRS?

Title of Exhibit ______

Type abstract single-spaced in the space provided below. (See instructions on the reverse side of this page.)

Instructions for Abstract

The abstract should be a brief paragraph that states the purpose, principal information, and conclusions of the exhibit. Promissory statements are not acceptable. Type single-spaced in the space provided on the reverse side. Brevity is desirable but not at the expense of specific information. **The abstract will appear in the program book as submitted.** Please use typewriter and complete the application form on both sides. List space requirements.

What Sort of Exhibit Is Proposed? (Check one and fill in all appropriate blanks.)

_____ **Free-standing.** This is a self-contained display created in total by the exhibitor. It may be a fold-open unit, a unit shipped in cases and assembled on site, or a tabletop unit. Linear feet required _____.

_____ **Poster Board (backboard panels).** Backboard panels are 4 × 6 or 4 × 8 ft. (1.2 × 1.8 or 1.2 × 2.5 m). Number of panels required _____ 4 × 6 or _____ 4 × 8. If two panels are needed, there will be a ¼-in. frame separating the panels, thus requiring a separation in the presentation.

_____ **Viewbox.** Mounted materials (radiographs and other transparencies) for display on the society's illuminators. Each illuminator is 39.5 × 59.5 in. (100 × 151 cm). Number of illuminators required _____. Slides should not be glass mounted.

_____ **Audiovisual.**

Please Indicate Most Appropriate Category.

Diagnostic Radiology

_____ Bone _____ Cardiovascular System _____ Chest _____ Pediatric Radiology _____ Gastrointestinal Tract

_____ Genitourinary Tract _____ Neuroradiology _____ Mammography

Other

_____ Medical Physics _____ Nuclear Medicine _____ Radiation Oncology _____ Radiobiology _____ Sonography

Has the exhibit been shown in whole or in part at any previous meeting? _____ (Previous display does not preclude acceptance.)

If so, where? _____________________ When? _____________

Nature of meeting or name of society _____________________

Signature of Principal Exhibitor _____________________

Exhibitors will receive instructions for exhibit preparation.

Applications must be received no later than November 1, 1990. Mail original and five copies to

Chairman, Scientific Exhibits Committee
c/o Paul R. Fullagar
American Roentgen Ray Society
1891 Preston White Dr.
Reston, VA 22091

Telephone: (703) 648-8900

Classified Advertisements

Positions Available

FACULTY ULTRASOUND RADIOLOGIST, THOMAS JEFFERSON UNIVERSITY HOSPITAL Jefferson's Dept. of Radiology wishes to recruit a faculty radiologist to work in our division of diagnostic ultrasound. Candidates at all levels will be considered. This division is housed in 1 of the largest and best equipped facilities in the world and is extensively involved in the full range of ultrasound studies including obstetrical, vascular, echocardiography, invasive, endoluminal, and both biliary and kidney stone lithotripsy. A new outpatient ultrasound facility is under construction adjacent to the main campus. The position provides excellent salary and benefits, protected research time each wk, and an opportunity to become associated with 1 of the most academically productive ultrasound groups anywhere. Interested individuals should contact either Barry Goldberg, M.D. (Director of Ultrasound), or David C. Levin, M.D. (Dept. Chairman), at the Dept. of Radiology, Thomas Jefferson University Hospital, Philadelphia, PA 19107. Jefferson is an equal opportunity/affirmative action employer. 6xa

IMMEDIATE OPENING - BOSTON SUBURBAN RADIOLOGY GROUP—300-bed, university-affiliated, community hospital seeks partner with skills or experience in all modalities. Send CV to Box B2, *AJR* (see address this section). 6–8ap

CHIEF, PULMONARY RADIOLOGY—The University of California, Davis, School of Medicine has a faculty position available in the Diagnostic Division of the Dept. of Radiology. Appointment will be at the assistant, associate, or full professor level. Candidates must be board-certified in diagnostic radiology, eligible for licensure in California, and have an academic and clinical background in pulmonary radiology, with an interest in CT, interventional radiology, and MRI. Please forward a CV, a letter outlining background and interests in teaching/research, and the names and addresses of 5 references to C. John Rosenquist, M.D., Chair, Dept. of Radiology, University of California, Davis, 2516 Stockton Blvd., Sacramento, CA 95817. This position will be "open until filled," but not later than Oct. 31, 1990. The University of California is an equal opportunity/affirmative action employer and encourages applications from members of minority groups and women. 6–7a

GENERAL RADIOLOGIST (ER/TRAUMA INTEREST)—The University of California, Davis, School of Medicine has a faculty position available in the Diagnostic Division of the Dept. of Radiology. Appointment will be at the assistant, associate, or full professor level. Candidates must be board-certified in diagnostic radiology, eligible for licensure in California, and have an academic and clinical background in general radiology, including ER/trauma. Please forward a CV, a letter outlining background and interests in teaching/research, and the names and addresses of 5 references to C. John Rosenquist, M.D., Chair, Dept. of Radiology, University of California, Davis, 2516 Stockton Blvd., Sacramento, CA 95817. This position will be "open until filled," but not later than Oct. 31, 1990. The University of California is an equal opportunity/affirmative action employer and encourages applications from members of minority groups and women. 6–7a

FLORIDA DIAGNOSTIC CENTER (east central coast) seeks a board-eligible/certified radiologist with recent training in nuclear medicine, ultrasound, CT scanning, and skeletal imaging. Must be personable. Send CV and salary requirements to Administrator. P. O. Box 693, Melbourne, FL 32902. 6ap

VERMONT—Diagnostic radiologist to join busy practice affiliated with modern, 90-bed, acute-care hospital. In-house CT, new ultrasound, nuclear, mammography, and angiography capabilities. Beautiful 4-season recreational area. Lakeside community 10 mi. from skiing. Competitive first-yr. compensation leading to early partnership. Send CV to New England Health Search, 63 Forest Ave., Orono, ME 04473; (207) 866-5680 or (207) 866-5685. 6–7ap

DIAGNOSTIC RADIOLOGIST, IMMEDIATE OPENING—Board-certified/eligible radiologist to join 11-member diagnostic/therapeutic radiology group in an incorporated practice to metropolitan St. Louis County at second largest area hospital. All state-of-the-art modalities with current expansion underway. Compensation commensurate with experience. Excellent fringe benefits and exceptional time-off scheduling. In excess of 160,000 exams/yr. Additional opening available July 1, 1990. Send CV to South County Radiologists, Inc., 9914 Kennerly Rd., St. Louis, MO 63128. 6ap

RADIOLOGIST/INTERVENTIONAL ANGIOGRAPHER—The Dept. of Diagnostic Imaging, Temple University School of Medicine and Hospital is recruiting an interventional angiographer to be head of the Section of Vascular/Interventional Radiology. We have an active practice in angiography, angioplasty, and interventional radiology. A research vascular suite is available to support research interests. Candidate should be board-certified, fellowship-trained in angiography/interventional radiology, and should be experienced in teaching, administration, and patient care service. Contact Francis J. Shea, M.D., Professor and Acting Chairman, Dept. of Diagnostic Imaging, Temple University School of Medicine, Broad and Ontario Sts., Philadelphia, PA 19140. Temple University is an affirmative action, equal opportunity educator and employer. 6a

HOSPITAL/PRIVATE OFFICE DIAGNOSTIC RADIOLOGISTS—Excellent opportunity in well-established Rhode Island practice for general radiologist. Prefer experience or interest in neuroradiology or interventional procedures. Reply to Box B4, *AJR* (see address this section). 6–9ap

THE DEPT. OF RADIOLOGY, VIRGINIA COMMONWEALTH UNIVERSITY/MEDICAL COLLEGE OF VIRGINIA (VCU/MCV) AND THE MCGUIRE VA MEDICAL CENTER, RICHMOND, VA seek faculty for positions in diagnostic radiology (chest, GI, mammography, CT/ultrasound/MR, neuroradiology, pediatrics, ER, angio/interventional, and general), and nuclear medicine. MCV is a 1058-bed facility (205 for pediatric patients) and is a Level 1 trauma center. The McGuire VAMC is an 800-bed facility (pediatrics excluded). ABR certification or eligibility required. Academic rank and salary commensurate with experience. For position description or to submit CV, write A. V. Proto, M.D., Dept. of Radiology, MCV, Box 470, Richmond, VA 23298-0470; (804) 786-7212. VCU/MCV is an equal opportunity/affirmative action employer. Women and minorities are encouraged to apply. 6–8a

DARTMOUTH-HITCHCOCK MEDICAL CENTER is seeking a BC/BE radiologist to be part of a community-based hospital practice undergoing rapid growth. All modalities except angio; approx. 10,000 exams/yr. Will be part of multispecialty group at a teaching hospital 40 mi. away. Coverage provided for meetings, vacation, and rotation through parent dept. Unlimited recreational opportunities in college town with nearby lakes and mountains. Competitive benefits and salary. Write to Harte C. Crow, M.D., Dept. of Radiology, Dartmouth-Hitchcock Medical Center, 2 Maynard St., Hanover, NH 03756. AA/EEO. 6–8a

MARY HITCHCOCK MEMORIAL HOSPITAL is seeking a permanent, BC/BE, interventional radiologist to be a member of a 200-physician, academic multispecialty group that forms the clinical faculty of Dartmouth Medical School. Hospital has 400 beds and 80 radiology dept. personnel. 50,000 inpatient and 45,000 outpatient exams are performed per yr. Dept. consists of 13 staff and 9 resident radiologists with full range of modern radiologic practice. Position entails the responsibility for a full spectrum of invasive and interventional procedures with 3 other radiologists. Vigorous interest in teaching essential, research interest highly desirable. Write to P. K. Spiegel, M.D., Dept. of Radiology, Dartmouth-Hitchcock Medical Center, 2 Maynard St., Hanover, NH 03756. AA/EEO. 6–8a

MARY HITCHCOCK MEMORIAL HOSPITAL is seeking a permanent nuclear radiologist to be a member of a 200-physician, academic multispecialty group that forms the clinical faculty of Dartmouth Medical School. 420-bed hospital. 58,000 inpatient and 48,000 outpatient exams are performed per yr. Dept. consists of 13 staff and 9 resident radiologists with a full range of modern radiologic practice. ABR/ABNM preferred, experience in nuclear cardiology and SPECT essential. Interest in teaching is essential. Strong clinical orientation with research program developing with monoclonal antibody imaging. Will direct nuclear medicine equipment acquisitions for new medical center to be occupied in late 1991. Write to: Donald L. Herzberg, M.D., Dept. of Radiology, Dartmouth-Hitchcock Medical Center, 2 Maynard St., Hanover, NH 03756. AA/EEO. 6–8a

THIRD BC DIAGNOSTIC RADIOLOGIST needed to join rapidly expanding group in a progressive community hospital. Practice includes all diagnostic modalities as well as basic interventional angiography, CT, and MRI. Extremely competitive salary/partnership terms. Please reply to Paul Zipp, M.D., 16917 33rd Ave., S.W., Seattle, WA 98166. 6ap

RADIOLOGIST/NEURORADIOLOGIST—The Dept. of Diagnostic Imaging, Temple University School of Medicine and Hospital, is recruiting a board-certified radiologist with fellowship training and experience in neuroradiology for a faculty position. Candidate should be skilled in teaching, interested in research, and experienced in patient care delivery. Contact Francis J. Shea, M.D., Professor and Acting Chairman, Dept. of Diagnostic Imaging, Temple University School of Medicine, Broad and Ontario Sts., Philadelphia, PA 19140. Temple University is an affirmative action, equal opportunity educator and employer. 6a

TWO STAFF INTERVENTIONAL RADIOLOGISTS SOUGHT at New York Hospital-Cornell University Medical Center for July 1990. The positions include clinical and teaching responsibilities as well as the opportunity for research. Equipment includes 3 state-of-the-art Philips digital labs and a 4-bed recovery room. Applicants should be trained in all aspects of peripheral, vascular, and nonvascular interventions. For further information, please contact Thomas A. Sos, M.D.; (212) 746-2600. 6a

FLORIDA SUNCOAST RADIOLOGY GROUP seeks board-certified radiologist for unique employment opportunity. Have every other week and weekend (26 wk/yr) entirely off while providing night and weekend night coverage during alternate weeks. Daytime and evenings are also free time during coverage weeks. Multiple modality skills including basic angiography are necessary. The opportunity for extra daytime employment during off weeks is an option. Competitive salary, excellent benefits. Interested candidates should forward a CV to Radiology Practice, P. O. Box 17319, Tampa, FL 33682. 6–7a

NEURORADIOLOGIST, BRIGHAM AND WOMEN'S HOSPITAL—The Dept. of Radiology at Brigham and Women's Hospital/Harvard Medical School is seeking a neuroradiologist for a full-time academic position. Research and teaching opportunities are available. Candidate must be BC/BE, with fellowship training in neuroradiology. Please send CV to B. Leonard Holman, M.D., Chairman, Dept. of Radiology, Brigham and Women's Hospital, 75 Francis St., Boston, MA 02115. Brigham and Women's Hospital/Harvard Medical School is an affirmative action/equal opportunity educator and employer. 6–11a

THERAPEUTIC RADIOLOGIST/RADIATION ONCOLOGIST—The VA Medical Center, Dayton, OH, is actively recruiting a radiation oncologist to staff our new radiation therapy unit. Our equipment will include a dual energy linear accelerator with multiple electron beam capability. Patient care services will include brachytherapy. Our medical center is a full-service, 1454-bed facility affiliated with Wright State University School of Medicine with a new acute-care facility under construction. We offer an excellent salary program, flexible benefit package, and relocation expenses. Dayton is an expanding community located in southwestern Ohio, 1½ hr from Columbus and 1 hr from Cincinnati. Contact Judy Williams (05), VA Medical Center, 4100 W. Third St., Dayton, OH 45428; (513) 268-6511, ext. 2509. An equal opportunity employer. 6a

CHIEF RADIOLOGIST needed to fill retirement vacancy at county hospital in Oakland, CA, 20 min. from downtown San Francisco. Highland General Hospital is a Level 2 trauma center and has residency programs in medicine, surgery, oral surgery, and emergency medicine. Additionally, residents rotate from other teaching hospitals in orthopedic surgery and ophthalmology. Currently radiology residents affiliated with the University of California at Davis rotate through East Bay hospitals including Highland General Hospital. Faculty appointment available for appropriate candidate. The dept. has 6.2 FTE radiologists and 50 technical and support staff. Nuclear medicine is a separate service. 66,000 exams performed per annum. Ten radiographic rooms, 1 mammography room, 3 ultrasound machines (including Acuson 128 with Doppler), 1 CT (Picker 1200SX), 1 angiography suite (Picker Digicon). Position available June 1991 and will be as an independent contractor to Alameda County. Attendant must be board-certified or have equivalent certification, and possess or be able to obtain California licensure. Highland General Hospital is an EOE. Applications, including CV and references, to Medical Staff Office, Attn. Radiology Chairman Search Committee, 1411 E. 31st St., Oakland, CA 94602. 6–8a

FULL/PART-TIME BC/BE RADIOLOGIST wanted for 187-bed GM&S VA Medical Center. Excellent GE equipment, duplex Doppler ultrasound, diagnostic, and fluroscopic. CT interpretation desirable. 18,000 procedures/yr. State university city amid hills and lakes in northwest Arkansas with cultural and recreational attractions. Competitive salary and excellent benefits/retirement. Call chief of staff; (501) 444-5050. 6–8a

BREAST IMAGING RADIOLOGIST—BC/BE, part/full-time to join 2-member group for outpatient Women's Diagnostic Center. Mammography, OB/GYN sonography expertise required. Flexible hr/no call. Ideal for radiologist with family responsibilities or semi-retired. Immediate availability. Contact Frankie Weier, Director, Women's Center for Radiology, 615 E. Princeton Street, Ste. 101, Orlando, FL 32803; (407) 894-2466. 6ap

IMMEDIATE OPENING, PART-TIME, SUBURBAN BOSTON—300-bed, university-affiliated, community teaching hospital seeks BE/BC radiologist. Flexible hr. Send CV to Box B6, *AJR* (see address this section). 6–8ap

IMMEDIATE OPENING—BC/BE neuroradiologist to join medium-sized group in Austin, TX. Practice covers major trauma center and outpatient radiology facility. In addition to general diagnostic services, outpatient facility also provides CT and MRI service on 2 GE 9800 scanners, GE 1.5-T, and 0.5-T MR units. Applicants are requested to contact Drs. Boyd, Gray, or Lava, 711 W. 38th St., Ste. B-8, Austin, TX 78705; (512) 454-8718. 6–11ap

SALEM, MA—Immediate opportunity for BC, fellowship-trained angio/interventionalist to practice in 10-person group at large community teaching hospital on Boston's beautiful North Shore. Available July 1990. Contact Courtney Neff, M.D.; (508) 741-1200, ext. 4420. 6ap

PEDIATRIC RADIOLOGIST—Full-time faculty position, Dept. of Radiology, Children's Hospital Medical Center, Cincinnati, OH, at academic rank of assistant professor to professor, Dept. of Radiology and Pediatrics, University of Cincinnati College of Medicine, available July 1, 1990. Salary and fringe benefits are highly competitive; salary is based on academic rank and experience. Candidates must be certified in diagnostic radiology by the American Board of Radiology or its equivalent, must have completed a fellowship in pediatric radiology, and must be eligible for active membership in The Society for Pediatric Radiology. Duties include clinical service, teaching, and research. Children's Hospital Medical Center is a 355-bed institution where over 100,000 radiologic exams are performed annually by 12 full-time faculty radiologists. Professional coverage includes conventional radiography, ultrasonography, CT, MRI, nuclear medicine, vascular/interventional procedures, and digital radiography. The candidate also must have a demonstrated interest and qualifications in basic and/or clinical pediatric imaging research. Children's Hospital Medical Center and the University of Cincinnati College of Medicine are affirmative action/equal opportunity employers. Address inquiry and CV to Donald R. Kirks, M.D., Director, Dept. of Radiology, Children's Hospital Medical Center, Cincinnati, OH 45229-2899; (513) 559-8058. 6ap

PACIFIC NORTHWEST, SEATTLE AREA — Board-certified radiologist needed to join dynamic growing practice at 4 breast and ultrasound diagnostic centers. Mammography and/or ultrasound experience desirable. Average 4½ days/wk. 8-9 mo/yr. NO NIGHT CALL. Attractive salary. All inquiries strictly confidential. Send letter or CV to Irwin Schiller, D.O., or Marita Achenson, M.D., Breast Diagnostic Center, 411 Strander Blvd. #303, Seattle, WA 98188; (206) 575-9123. 6–7ap

ALASKA, ANCHORAGE/SITKA—Need public service-oriented diagnostic radiologists. Medical school loan repayment available. Excellent benefits. CT/some interventional. Contact: Ken Bartline, Alaska Area Native Health Service, 250 Gambell Street, Anchorage, AK 99501; (907) 257-1457 collect. EOE. 6–10a

NEW ENGLAND—BC/BE diagnostic radiologist with expertise in ultrasound, CT, and mammography sought by 6-member office practice dept. in an established, rapidly expanding, multispecialty, prepaid, and FFS group practice. New imaging center. Physician owned and directed. Send CV to Medical Director, Fallon Clinic, Inc., 630 Plantation St., Worcester, MA 01605. 6–7ap

IMMEDIATE, UNEXPECTED OPENING for B/C, recently trained diagnostic radiologist, preferably with fellowship experience. Busy, 4-member, hospital-based practice in beautiful university town in central PA, home of Penn State University, seeks fifth radiologist. All modalities including mobile MRI, fixed MRI planned. Excellent salary and benefits leading to early partnership. Send CV with references to R. A. Rockower, M.D., Centre Community Hospital, 1800 E. Park Ave., State College, PA 16803; (814) 234-6137. 6–8ap

UCSD SCHOOL OF MEDICINE—The Dept. of Radiology is seeking an ultrasonologist to direct clinical service, medical student and resident teaching, and research projects. Participation in other diagnostic subspecialties is available. Qualifications required: board-eligibility/certification, California medical license, and 1-yr. fellowship in ultrasound. Title Series: associate/full professor (in-residence or clinical series — not currently a tenure-track position); level based on yr. experience; salary commensurate with rank and step of appointment based on the established salary schedule of the UCSD School of Medicine Faculty Compensation Plan. The University of California, San Diego, is an equal opportunity/affirmative action employer. All CVs received before Aug. 1, 1990, will be given full consideration. Send to George R. Leopold, M.D., Professor and Chairman, Dept. of Radiology, UCSD Medical Center, 225 Dickinson St., San Diego, CA 92103. 6a

OPENING FOR BC/BE GENERAL RADIOLOGIST with experience in interventional and vascular radiology to join a group of 4 radiologists for a 160-bed hospital located in Allentown, PA, about 60 mi. N.W. of Philadelphia. The daily practice includes all aspects of general radiology, CT, ultrasound, and nuclear medicine. Please call or send CV to: Asad Shohadai, M.D., Allentown Osteopathic Medical Center, 1736 Hamilton Street, Allentown, PA 18104; (215) 770-8700. 6xap

RADIOLOGY SERVICES OPPORTUNITY, BOULDER, CO—Progressive, 265-bed, full-service hospital located within 1 hr. of Denver, CO, is seeking proposals for the provision of complete radiology services. Comprehensive services include diagnostic, CT, nuclear medicine, mammography, and interventional cardiology. Total of over 40,000 radiologic procedures per yr. Regional trauma center. Located near abundant cultural, educational, recreational, and scenic resources at the base of the Rockies. Request for proposal may be obtained from Mr. Joe McDonald, Vice President, Finance, Boulder Community Hospital, P. O. Box 9019, Boulder, CO 80301-9019; (303) 440-2214. 6a

RADIOLOGISTS—New York City combined private radiology practice and fee-for-service hospital practice has an immediate opening for a board-certified radiologist with experience in CT, ultrasound, and interventional radiology. In addition, MRI and mammography experience is preferred. This well-established practice has 3 private offices on the upper east side of Manhattan as well as operations in 2 hospitals in Manhattan. Other studies performed in the practice include diagnostic radiology, nuclear imaging, and vascular duplex imaging. The practice continues to expand in all imaging modalities with its recent opening of a second, state-of-the-art MRI unit. Excellent benefit package includes health, life, disability, and malpractice insurance, profit sharing plan, continuing medical education, and a travel and entertainment account for professional use. Send CV to Box B8, *AJR* (see address this section). 6ap

CONNECTICUT—Immediate opening for BC/BE radiologist to join a group of 7 radiologists. Proficiency in MRI preferred. Practice includes a 435-bed, fully equipped, university-affiliated, community hospital and a 47-physician, multispecialty clinic. Excellent salary and benefits leading to full partnership after second yr. For information, call or send CV to Paul C. Lakin, M.D., Dept. of Radiology, New Britain General Hospital, 100 Grand St., New Britain, CT 06050. 6–9ap

DIAGNOSTIC RADIOLOGIST/MUSCULOSKELETAL IMAGING—Yale University School of Medicine, Yale-New Haven Medical Center, is seeking a board-eligible/certified radiologist for a full-time faculty appointment in musculoskeletal imaging. Academic rank is at a nontenured or tenured assistant/associate professor level, depending on qualifications. Clinical and research opportunities are in the areas of general orthopedic radiology, CT, MRI, arthrography, 3-D reconstruction, bone density analysis, and interventional orthopedics. Additional areas of collaboration include the Yale Sports Medical Center, Yale Metabolic Bone Center, and the Yale Biomechanics Laboratory. Please send inquiries along with CV to Jack P. Lawson, M.D., Dept. of Diagnostic Radiology, Yale University School of Medicine, 333 Cedar St., New Haven, CT 06510. Yale University is an equal opportunity/affirmative action employer; applications from women and minority group members are encouraged. Application deadline is Aug. 15, 1990. 6–7a

DIAGNOSTIC RADIOLOGIST/MAMMOGRAPHY Yale University School of Medicine, Yale-New Haven Medical Center, is seeking a board-eligible/certified radiologist with additional experience or training in mammography for a full-time faculty appointment. The Mammography Section performs approximately 900 screening mammograms, 200 diagnostic mammograms, and 20 needle localization procedures per mo. The second also participates in ultrasound exams of the breast, including Doppler. The position also includes duties in other areas of diagnostic imaging. A strong interest in patient care, research, and teaching is required. Rank (nontenured or tenured) and salary are commensurate with experience. Please send inquiries along with current CV to Carol H. Lee, M.D., Dept. of Diagnostic Radiology, Yale University School of Medicine, 333 Cedar St., New Haven, CT 06510. Yale University is an equal opportunity/affirmative action employer; applications from women and minority group members are encouraged. Application deadline is Aug. 15, 1990. 6–7a

TEN-PERSON RADIOLOGY GROUP located in Corpus Christi is seeking a new associate to start July 1990, or as late as July 1991. Must be board-certified or eligible. Will perform all diagnostic studies, including interventional, CT, MRI, nuclear medicine, and ultrasound. Please send CV to Search Committee, P. O. Box 5608, Corpus Christi, TX 78465-5608. 5–6ap

IMMEDIATE OPENING—Four board-certified radiologists seek a 5th for a dynamic diagnostic and interventional practice in a multispecialty clinic attached to a 200-bed hospital. All imaging modalities are represented. Excellent benefit package includes health, life, disability and malpractice insurance, profit-sharing plan, and continuing medical education. Fargo is on the Minnesota-North Dakota state line, 30 mi. from the Minnesota lake country, 250 mi. from both Minneapolis-St. Paul, MN, and Winnipeg, Canada. Contact Douglas Landers, M.D., Dakota Clinic, Ltd., Box 6001, Fargo, ND 58108; (701) 280-3321. 5–10a

KEARNEY, NE, A BUSTLING COLLEGE TOWN Excellent opportunity for a BE/BC diagnostic radiologist to join a progressive, expanding, 3-person radiology group. 197-bed, community hospital-based practice with all imaging modalities. Presently have busy interventional practice; assistance needed with angiography. Prefer someone with neuroradiology interest. Other areas considered would be CT, MRI, and ultrasound. Above-average salary and fringe benefits. Rapid pathway to full partnership. Inquire at (308) 234-7555, or write to Great Plains Radiology, P. O. Box 2051, Kearney, NE 68848. 5–6ap

SUMMIT, NJ—Excellent opportunity for diagnostic radiologist with special interest in mammography to join private-practice group of 13 radiologists. University-affiliated, 600-bed community hospital with a radiology residency, located in a pleasant suburban setting 25 mi. from New York City. State-of-the-art equipment including Acuson with color Doppler, Siemens Somatom Plus CT, and a 1.5-T Magnetom. Competitive salary leading to partnership. Please send CV to A. Salomon, M.D., 151 Summit Ave., Summit, NJ 07901. 5–8ap

NORTHERN NEW JERSEY DIAGNOSTIC RADIOLOGIST—Half- or full-time position available for BC/BE radiologist to join established group in hospital and expanding outpatient practice. Applicant should be interested and experienced in all modalities of diagnostic radiology, except nuclear medicine, including MRI. Send letter and CV to Box A17, *AJR* (see address this section). 5–6ap

WANTED—Full- and/or part-time BE/BC diagnostic radiologist, with MRI experience and interventional training desirable, to join 4-person group in 200-bed community hospital and private office setting doing 50,000 exams per yr. All imaging modalities offered. Located in Reading, PA, with population in metropolitan area of 300,000. Family-oriented suburban life with excellent schools, recreation, and cultural activities. One hr to Philadelphia, 2½ hr to New York City or Washington, and 2 hr to the Poconos or seashore. Competitive salary and benefits leading to partnership for full-time position. Write with CV to Jonathan L. Stolz, M.D., Director, Dept. of Radiology, Community General Hospital, 145 N. Sixth St., Reading, PA 19601. 5–6ap

NUCLEAR MEDICINE—Excellent opportunity for diagnostic radiologist with special interest in nuclear medicine, special competency preferred, to join private-practice group of 13 radiologists. University-affiliated, 600-bed community hospital with a radiology residency, located in a pleasant suburban setting 25 mi. from New York City. State-of-the-art equipment including Acuson with color Doppler, Siemens Somatom Plus CT, and 1.5-T Magnetom. Competitive salary leading to partnership. Please send CV to A. Salomon, M.D., 151 Summit Ave., Summit, NJ 07901. 5–8ap

RADIOLOGIST—BC/BE to join a group of 4 radiologists at the university/county hospital complex in El Paso, TX. Should be skilled in all forms of imaging and general diagnostic radiology including pediatrics. The hospital is a major trauma center with a busy emergency room and obstetrical practice. The work is interesting and challenging. The candidate will have time for clinical research and will have the support of the Texas Tech School of Medicine, including a large library and complete audiovisual facilities. Compensation is negotiable depending on the candidate's qualifications and experience. El Paso is a city of 500,000 people with yr-round sunny and warm weather. Contact Lloyd K. Mark, M.D., Professor and Associate Chairman, Dept. of Radiology, Texas Tech University HSC, 4800 Alberta St., El Paso, TX 79905; (915) 545-6845. 5–7a

PEDIATRIC RADIOLOGISTS—Vacancies are available in various parts of the pediatric radiology dept. at The Hospital for Sick Children, Toronto. The hospital is a 560-bed, tertiary-care pediatric center situated in downtown Toronto and affiliated with the University of Toronto. Staff includes 17 full-time pediatric radiologists and 7 fellows; 100,000 exams are performed each yr. Positions are available in general pediatric radiology areas and in more specialized areas such as neuroradiology. The dept. is equipped with state-of-the-art equipment. Applicants must have had previous pediatric radiology experience including 1- and preferable 2-yr fellowship. Staff radiologists with greater experience are certainly most welcome. For further information, please contact A. Daneman, M.D., Radiologist-in-Chief, Dept. of Radiology, The Hospital for Sick Children, 555 University Ave., Toronto, Ontario, M5G 1X8, Canada; (416) 598-6026. 5–6a

MAINE—Excellent opportunity for BC/BE, MRI or neuroradiology fellowship-trained radiologist for general diagnostic position with progressive, well-established, small group. Live and work in college community in southern region close to coast, mountains, and lakes. Competitive compensation package leading to partnership. Affiliate with 200-bed, modern community hospital. Send CV to New England Health Search, 63 Forest Ave., Orono, ME 04473; (207) 866-5680 or (207) 866-5685. 5–6ap

BC/BE IN RADIOLOGY—Excellent opportunity to join 5-member group based at MacNeal Hospital, a 427-bed, progressive teaching facility with university affiliation, in western suburb of Chicago. All state-of-the-art modalities including 2 GE 9800 CT scanners, ultrasound, nuclear medicine with SPECT, mammography, and interventional radiology suite, all located in the newly rebuilt, modern replacement facility of the hospital. MRI located in free-standing adjacent facility. Ideal candidate should be BC/BE in radiology, energetic, and progressive, with an interest in general diagnostic radiology. Competitive salary and benefits leading to equal parity. Send CV to Jeanette Simons, Division of Physician Affairs, MacNeal Hospital, 3249 S. Oak Park Ave., Berwyn, IL 60402. 5–6a

NEURORADIOLOGIST—Immediate faculty opening for a fellowship-trained neuroradiologist to join an evolving neuroimaging center at the University of Oklahoma Health Sciences Center, Oklahoma City, OK. Academic rank determined by previous experience. Salary and benefits are highly competitive. Strong commitment to teaching and research desired. Must be board-certified and eligible for senior membership in the ASNR. Send cover letter and CV to Don A. Wilson, M.D., MR Center of Oklahoma (BMR-10), P. O. Box 26307, Oklahoma City, OK 73126. Affirmative action/equal opportunity employer. 5–10a

CHALLENGING LOCUM TENENS POSITIONS AVAILABLE NOW—Work at your convenience, full- or part-time. Competitive compensation. No hassles, politics, or paperwork. Paid malpractice insurance, housing, and transportation. Put an experienced leader to work for you! Contact LOCUM Medical Group, 30100 Chagrin Blvd., Cleveland, OH 44124; (800) 752-5515. 5–8xap

NORTHWEST WASHINGTON—Progressive, 7-person group seeks a BC radiologist preferably with a fellowship in body imaging or nuclear medicine. Complete imaging including CT, MR, angio/interventional, ultrasound, nuclear medicine, and mammography provided at 2 hospitals and 3 offices. Excellent salary and benefits with potential for early partnership. Reply Box A13, *AJR* (see address this section). 5–7a

WANTED, JULY 1991—Young, outgoing, BC/BE general radiologist to work in 120-bed community medical center (1 of 2 Missoula, MT, hospitals) covered by 6-person group. We seek someone with special interest in ultrasound and mammography, but also experienced in angiography, CT, and MRI. Position leads to directorship of dept. in 3 yr. One yr to full partner income, 2 yr to full partnership. Missoula, in mountainous western Montana, is the home of the University of Montana and offers a progressive medical environment with over 150 physicians, as well as abundant recreational opportunities including skiing, fishing, hunting, and backpacking. Send CV to Missoula Radiology, Inc., P. O. Box 2039, Missoula, MT 59806. 5–9ap

BC DIAGNOSTIC RADIOLOGIST—Private office imaging center. Five-day work wk, no call. MRI (GE 1.5), CT (GE 9800), ultrasound, nuclear medicine, SPECT, mammography, routine radiography, and fluoroscopy. First yr salary and benefits, $175,000. Send CV to Desmond Fischer, M.D., 1301 McCallie Ave., Chattanooga, TN 37404; (615) 622-7212. 5–8ap

NUCLEAR MEDICINE/IMAGING—Twelve-person radiology practice has an opening for a diagnostic radiologist with experience/expertise in nuclear medicine. Practice is hospital-based with full range of equipment. Will share duties with 1 other fellowship-trained nuclear medicine radiologist. Cardiac nuclear imaging experience required. Please send letter of inquiry and CV to Richard D. Herman, M.D., Chairman, Dept. of Radiology, St. Luke's Hospital, Bethlehem, PA 18015. 4–6ap

TWO BOARD-CERTIFIED/ELIGIBLE GENERAL DIAGNOSTIC RADIOLOGISTS to join expanding, 11-person group covering 2 hospitals and 2 MR sites. Ideal private practice in a stable midwest community using all imaging modalities and interventional techniques. Can start immediately or wait until July 1990. Excellent opportunity with excellent salary and benefits. Send CV to Joseph F. Norfray, M.D., MR Center of Springfield, 319 E. Madison, Springfield, IL 62701. 4–7ap

NUCLEAR MEDICINE—Immediate opening in large, progressive radiology group in the Central New Jersey/Bucks County, PA, region for recently trained person with a nuclear medicine fellowship with emphasis on cardiac imaging. Must be willing to do all other facets of noninvasive radiology. Four-hospital group has 8 cameras and 3 SPECT units. Send letter and CV to L. Ratner, M.D., 838 W. State St., Trenton, NJ 08618. 4–6a

OREGON—Group of 12 radiologists in Salem, OR, seeks BC/BE radiologist with general radiology skills. Special competence in nuclear medicine desirable, but not mandatory. Practice includes 450-bed community hospital, large office, and a multispecialty clinic. Send CV to John Eyre, M.D., c/o Salem Radiology, 919 Oak St. S.E., Salem, OR 97301. 4–6ap

UNIQUE OPPORTUNITY—Permanent part-time position for diagnostic radiologist to work weekends, or more if desired, in exciting Las Vegas at a university-affiliated hospital with a large private group. Ample time to enjoy the many regional recreational activities. Candidates should be well-trained general radiologists with basic skills in ultrasound and CT. Angiography not required. Generous salary and fringe benefits. Contact Brent Birkin, M.D., 3848 Pima Ln., Las Vegas, NV 89109; (702) 384-5210 (7 a.m. to 5 p.m.) or (702) 732-0559 (after 6 p.m.). 4–6ap

OPPORTUNITY FOR YOUNG, WELL-TRAINED, AGGRESSIVE RADIOLOGIST to join 5-person group in a small, midwestern city near St. Louis. Excellent equipment including mobile MRI. Competitive salary leading to early partnership. Reply to Box U40, *AJR* (see address this section). 6xa

SOUTHERN OREGON—Opportunity for BC/BE, general diagnostic radiologist to join group of 5 board-certified radiologists. Experience in all modalities desired. Practice includes 2 hospitals and own private office. Competitive starting salary with early full partnership. Excellent lifestyle with many outdoor activities from Pacific Coast to Oregon Cascades. Send CV to Larry Strickland, Administrator, Roseburg Radiologists, P.C., P. O. Box 1547, Roseburg, OR 97478. 5–10ap

DIAGNOSTIC RADIOLOGIST/GASTROINTESTINAL IMAGING, Yale New Haven Medical Center, Yale University School of Medicine. Superb opportunity for a person interested in the highest quality practice combining the best of academic and clinical resources. Applicant should be an enthusiastic person interested in all aspects of gastrointestinal imaging including conventional barium radiography and CT. An effort will be made to accommodate additional interests. Salary and rank are most competitive and commensurate with experience, in addition to an excellent fringe package. Please send inquiries along with CV to Morton Burrell, M.D., Professor of Radiology, Director of Gastrointestinal Radiology, Yale University School of Medicine, 333 Cedar St., New Haven, CT 06510. Yale University is an equal opportunity/affirmative action employer; applications from women and minority groups are encouraged. Application deadline is June 30, 1990. 5–6a

NEURORADIOLOGIST/MRI—Two positions available; Fellowship training a necessity. Group of 7 radiologists seek BC colleague in multihospital practice. Must be capable as general diagnostic radiologist as well. Position available July 1990. Send letter and CV to Neel E. Bennett, M.D., Medical Director and Chairman, Dept. of Radiology, Holy Cross Hospital, 1050 E. South Temple, Salt Lake City, UT 84102; (801) 350-4636. 6xa

DARTMOUTH-HITCHCOCK MEDICAL CENTER, DEPT. OF RADIOLOGY is offering 2 permanent positions for BC/BE, GI/GU radiologists at the Mary Hitchcock Memorial Hospital. This is a 400-bed hospital with 80 radiology personnel who perform 55,000 inpatient and 45,000 outpatient exams/yr. The dept. consists of 13 staff and 9 residents covering the full range of modern radiologic practice. Become a member of the 200-physician, academic, multispecialty group that forms the clinical faculty of Dartmouth Medical School. Position has responsibility for a full scope of general diagnostic procedures. Interest in teaching essential, research desirable. Interested candidates should write to P. K. Spiegel, M.D., Dartmouth-Hitchcock Medical Center, Dept. of Radiology, 2 Maynard St., Hanover, NH 03756. AA/EOE. 6xa

ASSISTANT OR ASSOCIATE PROFESSOR OF NEURORADIOLOGY—The University of Texas Medical School at Houston has openings for neuroradiologists at the Lyndon Baines Johnson General Hospital and the Hermann Hospital to perform clinical neuroradiology and participate in resident and medical student teaching. Candidates must have completed an approved residency in diagnostic radiology and a 2-yr neuroradiology fellowship. Candidates must be board-certified by the ABR, or equivalent, and must have a Texas medical license. Compensation will be based on the most recent AAMC survey and the candidate's qualifications. Applicants should send a CV, along with the names and addresses of 3 references, to John H. Harris, Jr., M.D., D.Sc., Professor and Chairman, Dept. of Radiology, The University of Texas Medical School at Houston, 6431 Fannin St., Ste. 2.132, Houston, TX 77030. The University of Texas Health Science Center at Houston is an equal opportunity employer and encourages women and minority candidates to apply. 1–6a

ISRAEL, DIAGNOSTIC RADIOLOGY. Opportunities for 3–4 week or longer working vacations in a number of Israeli medical centers, on a volunteer basis. Positions varied, arrangements flexible. For information contact: Jonathan H. Fish, M.D., 1844 San Miguel Dr., #302, Walnut Creek, CA 94596; (415) 947-0560. 5–7xa

FULL-TIME BC RADIOLOGIST needed to staff outpatient women's diagnostic center in suburban Dallas. Experience in mammography and OB/GYN sonography preferred. No call responsibilities. Attractive compensation package. Send CV to Box Y56, *AJR* (see address this section). 6xa

ASHEVILLE, NC—BC/BE general diagnostic radiologist needed to join 6-person group. Practice consists of 320-bed private hospital and office practice with 80,000 procedures/yr. Excellent benefits and compensation in a beautiful mountain setting. Contact D. T. Milton, M.D., 445 Biltmore Center, Ste. 301, Asheville, NC 28801; (704) 255-3761. 6ap

PEDIATRIC RADIOLOGIST, PORTLAND, OR Immediate opening for a pediatric radiologist at Emanuel Hospital in Portland, OR. Either a pediatric fellowship or significant work experience is required. Opportunity to do general radiology as well. The hospital is a Level I trauma center, as well as a major pediatric referral center. The position leads to full partnership after second yr. Please send CV to Blaine E. Kozak, M.D., Chairman, Dept. of Radiology, Emanuel Hospital, 2801 N. Gantenbein, Portland, OR 97227; (503) 280-4032. 6ap

DIRECTOR OF CLINICAL MAGNETIC RESONANCE—The Dept. of Radiology at the University of Texas Medical School at Houston has an opening for a radiologist at the assistant, associate, or full professor level, who will direct clinical activities, medical student and resident teaching, and clinical research in the university MRI center at Hermann Hospital. Candidate will be expected to conduct or direct clinical or basic research in MR leading to grant support. Candidates must have demonstrated experience in direction of a clinical MRI unit, teaching, research, writing, and obtaining grant support, and have a strong publication background. Candidate must be board-certified by the ABR and must have a Texas medical license. Compensation will be based on the most recent AAMC survey and candidate's qualifications. Please forward a CV, and the names and addresses of 3 references, to John H. Harris, Jr., M.D., D. Sc., Professor and Chairman, Dept. of Radiology, The University of Texas Medical School at Houston, 6431 Fannin, Ste. 2.132, Houston, TX 77030. The University of Texas Health Science Center at Houston is an equal opportunity employer and encourages women and minority candidates to apply. 1–6a

ORTHOPEDIC RADIOLOGIST—A position is available at the University of Rochester Medical Center, Strong Memorial Hospital, Dept. of Radiology, a 750-bed, tertiary-care facility. An appointment as assistant professor or higher is available at a level appropriate to experience. Research and teaching opportunities are available in a strong academic dept. with state-of-the-art radiologic equipment. Send CV to Robert E. O'Mara, M.D., Professor and Chair, Diagnostic Radiology, Box 648, University of Rochester Medical Center, Rochester, NY 14642. EO/AA/M-F employer. 3–6ap

NEURORADIOLOGIST—The University of Texas Health Science Center at San Antonio is seeking a qualified academic neuroradiologist to fill an immediate opening. Send cover letter and CV to John R. Jinkins, M.D., Director of Neuroradiology, The University of Texas Health Science Center, 7703 Floyd Curl Dr., San Antonio, TX 78284-7800. 3–8ap

PRACTICE IN THE COASTAL PLAIN OF NORTH CAROLINA at a well-established 100-bed hospital seeks third radiologist. 23,000/24,000 procedures/yr. General radiology including mammography, CT, ultrasound, and nuclear medicine. No angio, interventional, or MRI. Compensation and benefits competitive. Available immediately. Contact Roanoke-Chowan Radiology Associates, Inc., P. O. Box 459, Ahoskie, NC 27910; (919) 332-6011. 3–6ap

DIAGNOSTIC RADIOLOGIST—BC/BE to join 2 radiologists in 50-physician, multispecialty clinic. Fellowship in body imaging preferred. Practice includes general radiography, CT, ultrasound, MRI, and film-screen mammography. Excellent first yr salary leading to partnership. Send CV to Michael D. Lavine, M.D., 333 Dixie Hwy., Chicago Heights, IL 60411. 5–7ap

DIAGNOSTIC RADIOLOGY, PACIFIC NORTHWEST, MRI, CT AND ULTRASOUND—Progressive group of 4 radiologists seeks board-certified radiologist with subspecialty interest and expertise in MRI, CT, and ultrasound. Busy, dynamic practice in regional medical center hospital, privately owned MRI center (presently mobile unit—planning for fixed site in spring 1990), plus private outpatient office. Located in beautiful recreation area in the inland Northwest. World-class lakes for boating and sailing. Excellent skiing, hunting, and fishing. Family-oriented environment 30 min from Spokane. Competitive starting salary with full partnership in 1 yr. Send CV to Richard Hehn, M.D., Radiology Associates of North Idaho, 1104 Ironwood Dr., Coeur d'Alene, ID 83814; (208) 667-0686- 5–7ap

FACULTY POSITIONS AVAILABLE IN DIAGNOSTIC RADIOLOGY—On July 1, 1990, the faculty of the University of Texas Medical School at Houston (UTMSH) will assume clinical practice, teaching, and research at the Lyndon Baines Johnson (LBJ) General Hospital, newly constructed by the Harris County Hospital District, in Houston, TX. LBJ General will be a principal medical student teaching affiliation of the UTMSH, is certified for 300 beds (with expansion capabilities to approximately 500 beds) and is projected to perform approximately 130,000 imaging procedures the first yr. The Dept. of Radiology at LBJ is fully equipped with new, state-of-the-art GE equipment, including a 9800 Quick CT scanner with 3-D software and an LU angiographic unit, and comparable routine, R&F, ultrasound, and nuclear equipment. Full-time UTMSH faculty positions exist for 5 associate professors and 10 assistant professors with clinical, teaching, and research interests in all aspects of diagnostic imaging. Residents who have just completed training and are board-certified will be offered the rank of assistant professor at an annual salary of $90,000. Fellows who have completed training and are board-certified will be offered the rank of assistant professor at an annual salary of $100,000. These salaries may be increased depending on the candidate's education and experience beyond either residency or fellowship, and in addition to base salary, total fringe benefits of approximately 20% of the base salary will be provided. Associate professor compensation will be based on the most recent AAMC survey and the candidate's qualifications. Candidates must be diplomates of the ABR, or its equivalent, and must have a Texas medical license. Applicants are requested to send their CV to John H. Harris, Jr., M.D., D.Sc., Professor and Chairman, Dept. of Radiology, The University of Texas Medical School at Houston, 6431 Fannin St., Ste. 2.132, Houston, TX 77030. The University of Texas Health Science Center at Houston is an equal opportunity employer. Women and minorities are encouraged to apply. 1–6a

ULTRASOUND/CT/MRI—Opportunity for board-certified radiologist specializing in ultrasound, body CT, and body MRI to pursue academic career at The New York Hospital-Cornell Medical Center. Dept. provides state-of-the-art equipment, including Acuson ultrasound, GE 9800 CT, and GE Signa 1.5-T MR. Wide variety of ultrasound exams include abdominal, OB-GYN, color Doppler, small parts, neonatal head, transvaginal, and transrectal. Prefer candidate with prior fellowship in sectional imaging or ultrasound. Responsibilities include clinical practice, teaching, and research. Position available 7/1/90 or earlier. Please send CV to Elias Kazam, M.D., Dept. of Radiology, The New York Hospital-Cornell Medical Center, 525 E. 68th St., New York, NY 10021. 4–6ap

ASSISTANT, ASSOCIATE, OR FULL PROFESSOR OF DIAGNOSTIC RADIOLOGY—The University of Texas Medical School at Houston has an opening for a general diagnostic radiologist to perform clinical radiologic exams and procedures and to participate in resident and medical student teaching. Candidates should have completed an approved residency in diagnostic radiology. Postresidency experience or training would be preferable, but not mandatory, at the assistant professor level. Candidates must be board-certified by the ABR, or equivalent, and must have a Texas medical license. Compensation will be based on the most recent AAMC survey and the candidate's qualifications. Applicants should send a CV, along with the names and addresses of 3 references, to John H. Harris, Jr., M.D., D.Sc., Professor and Chairman, Dept. of Radiology, The University of Texas Medical School at Houston, 6431 Fannin St., Ste. 2.132, Houston, TX 77030. The University of Texas Health Science Center at Houston is an equal opportunity employer and encourages women and minority candidates to apply. 1–6a

NORTHERN CALIFORNIA/SAN FRANCISCO BAY AREA—The Permanente Medical Group is seeking a BC radiologist with multimodality interests and fellowship training in MR or interventional radiology to join a 10-person group serving a 337-bed acute-care hospital and 2 outpatient clinics. Teaching opportunities are available with residents of subspecialty services on rotation from Stanford University Hospital and our own medical residents. We are currently siting a GE 1.5-T MRI system and installing a new LU arm. Competitive salary and excellent benefits. Please send inquiries and CV to Bruce Baker, M.D., Chief, Dept. of Radiology, Kaiser-Permanente Medical Center, 900 Kiely Blvd., Santa Clara, CA 95051; (408) 236-4444. EOE. 5–7a

ASSISTANT, ASSOCIATE, OR FULL PROFESSOR OF THORACIC RADIOLOGY—The University of Texas Medical School at Houston has an opening for a thoracic radiologist to perform clinical thoracic radiology exams and procedures and participate in resident and medical student teaching. Candidates should have completed an approved residency in diagnostic radiology and must have postresidency experience or training in thoracic radiology. Candidates must be board-certified by the ABR, or equivalent, and must have a Texas medical license. Compensation will be based on the most recent AAMC survey and the candidate's qualifications. Applicants should send a CV, along with the names and addresses of 3 references, to John H. Harris, Jr., M.D., D.Sc., Professor and Chairman, Dept. of Radiology, The University of Texas Medical School at Houston, 6431 Fannin St., Ste. 2.132, Houston, TX 77030. The University of Texas Health Science Center at Houston is an equal opportunity employer and encourages women and minority candidates to apply. 1–6a

DIAGNOSTIC RADIOLOGIST WITH SPECIAL INTEREST IN ANGIOGRAPHY AND INTERVENTIONAL RADIOLOGY—The Dept. of Radiology at the University of Texas Medical School at Houston has an immediate opening at the Hermann Hospital, and an opening for July 1, 1990, at the Lyndon Baines Johnson General Hospital, for an experienced interventionist/angiographer with strong interest in patient care and teaching. Research interest and experience are important, but not essential. Although the principal responsibilities will be in intervention/angiography, there will be an opportunity to be involved in other clinical areas of the candidate's interest. The position will include teaching at the medical student and resident levels. Candidate must be a diplomate of the ABR and have completed at least a 1-yr. interventional/angiography fellowship, have a Texas state medical license, and have had at least 1 yr. postfellowship experience. Candidates with the qualifications for a senior assistant professor or associate professor appointment are preferred. Academic rank will be commensurate with qualifications. Compensation will be based on the most recent AAMC survey and the candidate's qualifications and experience. Please submit CV, along with the names and addresses of 3 references, to John H. Harris, Jr., M.D., D.Sc., Professor and Chairman, Dept. of Radiology, The University of Texas Medical School at Houston, 6431 Fannin, Ste. 2.132, Houston, TX 77030. The University of Texas Health Science Center at Houston is an equal opportunity employer. Women and minorities are encouraged to apply. 1–6a

Positions Desired

JULY 1990 PGY-3 RADIOLOGY RESIDENCY SOUGHT—Current PGY-2 radiology resident seeking PGY-3 position. Have training in plain film, CT, ultrasound, nuclear medicine, and angiography. Reply to Box A9, *AJR* (see address this section). 5–7bp

GENERAL DIAGNOSTIC RADIOLOGIST — Board-certified, MRI fellowship. Four yr. angio/interventional experience in busy practice. Prefer general diagnostic with some subspecialization. Competent in nuclear medicine and ultrasound. Desire partnership opportunity. Impeccable references. Available July 1990. Reply Box Y52, *AJR* (see address this section). 3–6bp

Fellowships and Residencies

FELLOWSHIP IN MUSCULOSKELETAL RADIOLOGY—The Emory University, Dept. of Radiology, offers a 1-yr. fellowship in musculoskeletal radiology starting July 1, 1991. Clinical activities include MRI, CT, needle biopsies, arthrography, and QCT. The musculoskeletal section is staffed by 3 full-time radiologists. Experience includes a wide range of musculoskeletal disease and trauma through a 600-bed university hospital, a 900-bed county hospital, a 160-bed pediatric hospital, and 2 outpatient clinics. Candidates should be eligible for Georgia medical licensure. Contact Terry M. Hudson, M.D., Section of Radiology, The Emory Clinic, 1365 Clifton Rd., N.E., Atlanta, GA 30322; (404) 248-4354 or (404) 248-5834. Emory University is an equal opportunity/affirmative action employer. 6–9cp

PG II OR PG III—Unexpected opening available for a PG II or PG III in our diagnostic radiology residency program as of July 1, 1990. Inquire in writing to Dorothy Klegerman, Director of Human Resources, St. Francis Hospital of Evanston, 355 Ridge Ave., Evanston, IL 60202. An equal opportunity employer. 6c

CARDIOVASCULAR/INTERVENTIONAL RADIOLOGY—The Dept. of Radiology at the University of Minnesota has four 1- to 2-yr. postresidency fellowship training positions in cardiovascular/interventional radiology available at the rank of instructor (temporary, annual renewable) beginning July 1, 1991. Minimum requirements include successful completion of an accredited radiology residency and board ceritification in radiology by beginning date of fellowship appointment. In addition to clinical practice and training, responsibilities will include graduate and undergraduate medical instruction in cardiovascular/interventional radiology as well as assisting with related departmental research projects. Salary is negotiable and competitive and dependent on past scholarly productivity and post-M.D. experience. Applicants must be licensed or able to obtain license to practice medicine in the state of Minnesota before appointment date. Applications for these positions will be accepted through Feb. 28, 1991. Send letters to Kurt Amplatz, M.D., Dept. of Radiology, Box 292 UMHC, University of Minnesota, 420 Delaware St., S.E., Minneapolis, MN 55455. The University of Minnesota is an equal opportunity, affirmative action educator and employer and specifically encourages applications from women and minorities. 6c

BODY IMAGING FELLOWSHIPS—One yr. beginning July 1, 1990, and July 1, 1991. Emphasis on ultrasound (including high-risk obstetrics). Vascular lab (full range of procedures), and body CT; limited volume of MRI. Excellent location. If interested, please contact by phone or mail CV to William J. Zwiebel, M.D., Director of Ultrasound and CT, Dept. of Radiology, University of Utah Medical Center, 50 N. Medical Dr., Salt Lake City, UT 84132; (801) 581-8188. 6–7cp

BODY IMAGING FELLOWSHIP, JULY 1990 CT/ultrasound/MRI. Clinical and research activities in all areas tailored to the fellow's and dept.'s goals. Should have interest in teaching and research. GE 9800 CT, GE 1.5-T Signa MRI, and Acuson and Diasonics ultrasound. Full resident complement. Four body imaging faculty. Send CV to Fred Flickinger, M.D., Body Imaging Section, Dept. of Radiology, Medical College of Georgia, 1120 15th St., Augusta, GA 30912-3900. EEO/AA. Women/minorities encouraged to apply. 6c

MAGNETIC RESONANCE IMAGING—The Dept. of Radiology at the University of Minnesota has four 1- to 2-yr. postresidency fellowship training positions in MRI available at the rank of instructor (temporary, annual renewable) beginning July 1, 1991. Minimum requirements include successful completion of an accredited radiology residency and board certification in radiology by beginning date of fellowship appointment. In addition to clinical practice and training, responsibilities will include graduate and undergraduate medical instruction in MRI as well as assisting with related departmental research projects. We have 2 MR scanners (a 1.0-T unit and a 1.5-T unit) and apart from experience with MR scanning of the brain and spine, a large amount of experience with musculoskeletal and body MR will be possible. Salary is negotiable and competitive and dependent on past scholarly productivity and post-M.D. experience. Applicants must be licensed or able to obtain license to practice medicine in the state of Minnesota before appointment date. Applications for these positions will be accepted through Feb. 28, 1991. Send letters to Arthur E. Stillman, M.D., Ph.D., Dept. of Radiology, Box 292 UMHC, University of Minnesota, 420 Delaware St., S.E., Minneapolis, MN 55455. The University of Minnesota is an equal opportunity, affirmative action educator and employer and specifically encourages applications from women and minorities. 6c

NUCLEAR MEDICINE FELLOWSHIP—The Dept. of Radiology at the University of Minnesota has 1- to 2-yr. postresidency fellowship training positions in nuclear medicine available at the rank of instructor (temporary, annual renewable) beginning July 1, 1991. Minimum requirements include successful completion of an accredited radiology residency and board certification in radiology by beginning date of fellowship appointment. In addition to clinical practice and training, responsibilities will include graduate and undergraduate medical instruction in nuclear medicine as well as assisting with related departmental research projects. Salary is negotiable and competitive and dependent on past scholarly productivity and post-M.D. experience. Applicants must be licensed or able to obtain license to practice medicine in the state of Minnesota before appointment date. Applications for these positions will be accepted through Feb. 28, 1991. Send letters to Robert Boudreau, M.D., Dept. of Radiology, Box 292 UMHC, University of Minnesota, 420 Delaware St., S.E., Minneapolis, MN 55455. The University of Minnesota is an equal opportunity, affirmative action educator and employer and specifically encourages applications from women and minorities. 6c

MUSCULOSKELETAL RADIOLOGY—The Dept. of Radiology at the University of Minnesota has 1- to 2-yr. postresidency fellowship training positions in musculoskeletal radiology available at the rank of instructor (temporary, annual renewable) beginning July 1, 1991. Minimum requirements include successful completion of an accredited radiology residency and board certification in radiology by beginning date of fellowship appointment. In addition to clinical practice and training, responsibilities will include graduate and undergraduate medical instruction in musculoskeletal radiology as well as assisting with related departmental research projects. This fellowship will encompass all aspects of musculoskeletal radiology including CT, arthrography, and MR. Salary is negotiable and competitive and dependent on past scholarly productivity and post-M.D. experience. Applicants must be licensed or able to obtain license to practice medicine in the state of Minnesota before appointment date. Applications for these positions will be accepted through Feb. 28, 1991. Send letters to Harry Griffiths, M.D., Dept. of Radiology, Box 292 UMHC, University of Minnesota, 420 Delaware St., S.E., Minneapolis, MN 55455. The University of Minnesota is an equal opportunity, affirmative action educator and employer and specifically encourages applications from women and minorities. 6c

NEURORADIOLOGY—The Dept. of Radiology at the University of Minnesota has four 1- to 2-yr. postresidency fellowship training positions in neuroradiology available at the rank of instructor (temporary, annual renewable) beginning July 1, 1991. Minimum requirements include successful completion of an accredited radiology residency and board certification in radiology by beginning date of fellowship appointment. In addition to clinical practice and training, responsibilities will include graduate and undergraduate medical instruction in neuroradiology as well as assisting with related departmental research projects. Salary is negotiable and competitive and dependent on past scholarly productivity and post-M.D. experience. Applicants must be licensed or able to obtain license to practice medicine in the state of Minnesota before appointment date. Applications for these positions will be accepted through Feb. 28, 1991. Send letters to Benjamin C. P. Lee, M.D., Dept. of Radiology, Box 292 UMHC, University of Minnesota, 420 Delaware St., S.E., Minneapolis, MN 55455. The University of Minnesota is an equal opportunity, affirmative action educator and employer and specifically encourages applications from women and minorities. 6c

ABDOMINAL IMAGING—The Dept. of Radiology at the University of Minnesota has five 1- to 2-yr. postresidency fellowship training positions in abdominal imaging available at the rank of instructor (temporary, annual renewable) beginning July 1, 1991. Minimum requirements include successful completion of an accredited radiology residency and board certification in radiology by beginning date of fellowship appointment. The fellowship will consist of body MRI, CT, and ultrasound rotations. Fellows will perform biopsy and drainage procedures using CT and ultrasound guidance. State-of-the-art equipment is available in all these imaging areas. In addition to clinical practice and training, responsibilities will include graduate and undergraduate medical instruction in abdominal, thoracic, and musculoskeletal CT imaging as well as assisting with related departmental research projects. Salary is negotiable and competitive and dependent on past scholarly productivity and post-M.D. experience. Applicants must be licensed or able to obtain license to practice medicine in the state of Minnesota before appointment date. Applications for these positions will be accepted through Feb. 28, 1991. Send letters to Stephen Trenkner, M.D., Dept. of Radiology, Box 292 UMHC, University of Minnesota, 420 Delaware St., S.E., Minneapolis, MN 55455. The University of Minnesota is an equal opportunity, affirmative action educator and employer and specifically encourages applications from women and minorities. 6c

ULTRASOUND—The Dept. of Radiology at the University of Minnesota has two 1- to 2-yr. postresidency fellowship training positions in ultrasound available at the rank of instructor (temporary, annual renewable) beginning July 1, 1991. Minimum requirements include successful completion of an accredited radiology residency and board certification in radiology by beginning date of fellowship appointment. In addition to clinical practice and training, responsibilities will include graduate and undergraduate medical instruction in ultrasound as well as assisting with related departmental research projects. The clinical practice will provide experience in general abdominal, obstetric, gynecologic, and vascular ultrasound using conventional, color Doppler, intracavitary, and intravascular technology. It will also provide experience with interventional procedures under sonographic guidance. Salary is negotiable and competitive and dependent on past scholarly productivity and post-M.D. experience. Applicants must be licensed or able to obtain license to practice medicine in the state of Minnesota before appointment date. Applications for these positions will be accepted through Feb. 28, 1991. Send letters to Janice Letourneau, M.D., Dept. of Radiology, Box 292 UMHC, University of Minnesota, 420 Delaware St., S.E., Minneapolis, MN 55455. The University of Minnesota is an equal opportunity, affirmative action educator and employer and specifically encourages applications from women and minorities. 6c

FELLOWSHIP IN EMERGENCY IMAGING—One-yr. fellowship available July 1, 1990, offers training in imaging of traumatic and nontraumatic emergencies from Massachusetts General Hospital Emergency Ward. Total of 170–200 cases performed daily. The division is equipped with a GE 9800 Quick CT scanner, ultrasound, fluoroscopy, and tomography. Experience with three-dimensional and MR imaging is available. In addition to clinical responsibilities, there are opportunities for research and teaching. For further information, please contact Robert A. Novelline, M.D., Dept. of Radiology, Massachusetts General Hospital, Boston, MA 02114; tel. (617) 726-8796; fax (617) 726-6808. 6cp

PEDIATRIC RADIOLOGY—The Dept. of Radiology at the University of Minnesota and Minneapolis Children's Medical Center has 1- to 2-yr. postresidency fellowship training positions in pediatric radiology available at the rank of instructor (temporary, annual renewable) beginning July 1, 1991. Minimum requirements include successful completion of an accredited radiology residency and board certification in radiology by beginning date of fellowship appointment. In addition to clinical practice and training, responsibilities will include graduate and undergraduate medical instruction in pediatric radiology as well as assisting with related departmental research projects. Seven experienced pediatric radiologists will be actively involved in the training process. The clinical experience will be equally distributed between the Minneapolis Children's Medical Center and the University Hospital. Salary is negotiable and competitive and dependent on past scholarly productivity and post-M.D. experience. Applicants must be licensed or able to obtain license to practice medicine in the state of Minnesota before appointment date. Applications for these positions will be accepted through Feb. 28, 1991. Send letters to Deborah Day, M.D., Dept. of Radiology, Box 292 UMHC, University of Minnesota, 420 Delaware St., S.E., Minneapolis, MN 55455. The University of Minnesota is an equal opportunity, affirmative action educator and employer and specifically encourages applications from women and minorities. 6c

BODY CT—The Dept. of Radiology at the University of Minnesota has 1- to 2-yr. postresidency fellowship training positions in body CT available at the rank of instructor (temporary, annual renewable) beginning July 1, 1991. Minimum requirements include successful completion of an accredited radiology residency and board certification in radiology by beginning date of fellowship appointment. In addition to clinical practice and training, responsibilities will include graduate and undergraduate medical instruction in abdominal, thoracic, and musculoskeletal CT imaging as well as assisting with related departmental research projects. Percutaneous biopsy and drainage techniques using CT guidance will be emphasized. Salary is negotiable and competitive and dependent on past scholarly productivity and post-M.D. experience. Applicants must be licensed or able to obtain license to practice medicine in the state of Minnesota before appointment date. Applications for these positions will be accepted through Feb. 28, 1991. Send letters to Robert Halvorsen, M.D., Dept. of Radiology, Box 292 UMHC, University of Minnesota, 420 Delaware St., S.E., Minneapolis, MN 55455. The University of Minnesota is an equal opportunity, affirmative action educator and employer and specifically encourages applications from women and minorities. 6c

IMAGING FELLOWSHIP (CT, ULTRASOUND, MRI)—William Beaumont Hospital, a 970-bed, modern, tertiary-care, teaching and academic institution in southeast Michigan, offers a 1-yr fellowship in sectional body imaging. The fellowship will provide extensive clinical experience in body CT, ultrasound, and MRI, including CT- and ultrasound-guided procedures, conventional and color flow Doppler exams, prostatic and endovaginal sonography. Ample elective time is also provided for other rotations of interest to fellow. Candidates must be board-certified or board-eligible in diagnostic radiology and have a valid Michigan medical license. Four positions are available for July 1991. Salary and fringe benefits are highly competitive. For further information, write to Ali Shirkhoda, M.D., Chief of Imaging Division, William Beaumont Hospital, 3601 W. 13 Mile Rd., Royal Oak, MI 48073; (313) 551-1001. 4–6c

FELLOWSHIPS AT THOMAS JEFFERSON UNIVERSITY HOSPITAL—The Dept. of Radiology at Thomas Jefferson University Hospital in Philadelphia offers the following fellowship programs each yr. Ultrasound/CT/MRI—Jefferson has 1 of the largest and most modern ultrasound facilities in the world, performing 40,000 exams of all types per yr. This includes obstetrical, vascular, lithotripsy, invasive, endoluminal, etc. We also operate 3 CT scanners and 4 GE 1.5-T MRI units. Contact Barry Goldberg, M.D., regarding this program. Cardiovascular/interventional—This division is housed in a new suite with state-of-the-art Philips units with digital subtraction angiography, and performs the full range of both vascular and nonvascular interventional procedures. Contact Geoffrey Gardiner, Jr., M.D. Neuro/ENT radiology—Very active clinical services supply a wealth of material to this division, which is housed in a Neurosciences Imaging Center containing all imaging modalities in a single comprehensive facility. Contact Carlos Gonzalez, M.D. Chest/breast imaging—Jefferson's new Breast Imaging Center performs approximately 85 studies/day. Contact Stephen Feig, M.D., or Robert Steiner, M.D. MRI—This is a dedicated body MRI program and includes excellent research opportunities, in addition to a large clinical caseload. Contact Matthew Rifkin, M.D. Musculoskeletal—This program includes MRI of the musculoskeletal system. Contact David Karasick, M.D. All program directors listed above can be contacted at the Dept. of Radiology, Thomas Jefferson University Hospital, Philadelphia, PA 19107. Jefferson is an equal opportunity/affirmative action employer. 6xc

FELLOWSHIP IN MR IMAGING at Central Massachusetts Magnetic Imaging Center, July 1991 through June 1992. CMMIC is a consortium of 3 area teaching hospitals, including a university hospital with a mixture of clinical and research responsibilities, dedicated to furthering the applications and addressing the educational requirements of MRI. CMMIC currently uses 2 clinical 1.5-T GE Signa systems capable of multifaceted imaging as well as a 2.0-T GE Fremont CSI research system. The fellowship will include thorough training in MRI physics, imaging principles, clinical applications, and image interpretation. Duties will include image interpretation of neurologic, musculoskeletal, pediatric, and cardiac studies; daily supervision of scanning; teaching file maintenance; and participation in CMMIC's numerous teaching and research responsibilities. Requirements include satisfactory completion of a 4-yr accredited radiology training program and board-eligibility or certification. Please send inquiries to Ronald Ragland, M.D., Medical Director, CMMIC, Inc., 367 Plantation St., Worcester, MA 01605. 5–6cp

BODY IMAGING FELLOWSHIP, JULY 1990—CT/ultrasound/MRI. Clinical and research activities in all areas tailored to the fellow's and dept. goals. Should have interest in teaching and research. GE 9800 CT, GE 1.5-T Signa MRI, Acuson and Diasonics ultrasound. Full resident complement. Four body-imaging faculty. Send CV to Fred W. Flickinger, M.D., Body Imaging Section, Dept. of Radiology, Medical College of Georgia, 1120 15th St., Augusta, GA 30912-3900. 5–7c

A FELLOWSHIP IN VASCULAR/INTERVENTIONAL RADIOLOGY is offered at the University of Maryland beginning July 1, 1990. The fellow will participate in all aspects of diagnostic vascular radiology, as well as nonvascular interventional procedures, including percutaneous and laser angioplasty, embolization, biliary and GU intervention, and insertion of IVC filters. Contact Gerald S. Johnston, M.D., Dept. of Diagnostic Radiology, 22 S. Greene St., Baltimore, MD 21201. 6c

FELLOWSHIPS IN NEURORADIOLOGY—The Dept. of Radiology at the University of Texas Medical School at Houston has openings for 1- and 2-yr neuroradiology fellowships to begin July 1990 and July 1991. Under faculty supervision, candidates will be responsible for neuroradiologic exams and procedures (i.e., angiograms, myelograms, CT, MR imaging, and in vivo spectroscopy). The candidate will participate in teaching at the medical student and resident levels and will conduct basic or clinical research. Candidate must be a graduate of an approved U.S. medical school or its equivalent, must have completed an approved residency in diagnostic radiology, must be a diplomate of the ABR, and must have a Texas medical license. Please submit CV, along with the names and addresses of 3 references, to John H. Harris, Jr., M.D., D.Sc., Professor and Chairman, Dept. of Radiology, The University of Texas Medical School at Houston, 6431 Fannin St., Ste. 2.132, Houston, TX 77030. The University of Texas Health Science Center at Houston is an equal opportunity employer. Women and minorities are encouraged to apply. 1–6c

FELLOWSHIPS IN PEDIATRIC RADIOLOGY, JULY 1991—The Dept. of Radiology, Children's Hospital Medical Center, Cincinnati, OH, offers 1- or 2-yr fellowships in pediatric radiology beginning July 1991. Children's Hospital Medical Center is a 355-bed institution where approximately 100,000 radiological exams are performed annually by 13 full-time faculty radiologists. Four fellowship positions are available annually. Training includes all aspects of pediatric imaging: neonatal radiology, neuroimaging, musculoskeletal radiology, cardiovascular and thoracic imaging, abdominal imaging, oncologic imaging, ultrasonography, nuclear medicine, CT, MRI, and vascular/interventional techniques. Facilities include digital fluoroscopy, Acuson and ATL ultrasound units with Doppler and color-flow Doppler capabilities, Gamma and SPECT tomographic nuclear cameras, GE 9800 Quick CT scanner, 1.5-T GE MRI, and cardiac catheterization/angiographic suite with digital vascular imaging. Numerous opportunities to participate in both clinical and basic research. Salary and fringe benefits are highly competitive. Candidates must be board-certified or board-qualified in diagnostic radiology and must be able to obtain an Ohio medical license. Children's Hospital Medical Center and the University of Cincinnati College of Medicine are affirmative action/equal opportunity employers. Address inquiry and CV to Donald R. Kirks, M.D., Director, Dept. of Radiology, Children's Hospital Medical Center, Elland and Bethesda Aves., Cincinnati, OH 45229-2899; (513) 559-8058. 1–12cp

FELLOWSHIP IN ULTRASOUND AND BODY CT/MRI—July 1, 1991 to June 30, 1992, at the New York Hospital/Cornell Medical Center. Dept. provides state-of-the-art equipment, including Acuson ultrasound, GE 9800 CT, and GE Signa 1.5-T MR. Wide variety of ultrasound exams include abdominal, OB-GYN, color Doppler, small parts, neonatal head, transvaginal, and transrectal. Applicants should be ABR eligible or certified. Send CV to Elias Kazam, M.D., Dept. of Radiology, The New York Hospital/Cornell Medical Center, 525 E. 68th St., New York, NY 10021. 4–6cp

CARDIOVASCULAR-INTERVENTIONAL RADIOLOGY FELLOWSHIP—Available July 19, 1989. One-year fellowship program at a 750-bed teaching hospital. Extensive clinical experience involving all aspects of cardiovascular imaging, interventional vascular and nonvascular procedures, and availability for clinical or animal research. Send CV and Inquiries to Oscar H. Gutierrez, M.D., Dept. of Radiology, Box 648, University of Rochester Medical Center, Rochester, NY 14642. An equal opportunity employer (M/F). 1–6c

MRI FELLOWSHIP AT THOMAS JEFFERSON UNIVERSITY HOSPITAL—A new MRI fellowship position has been created in the Dept. of Radiology of Thomas Jefferson University Hospital, Philadelphia. This 1-yr position encompasses a full range of clinical and research activities. The MRI division includes 6 staff physicians, 2 MRI physicists, and 3 Signa systems (1.5T). The position is available as of Jan. 1990, but applications will also be taken for the academic year beginning in July 1990. Send inquiries to Matthew Rifkin, M.D., Dept. of Radiology, Thomas Jefferson University Hospital, Philadelphia, PA 19107. Jefferson is an equal opportunity/affirmative action employer. 9–6c

NEURORADIOLOGY FELLOWSHIP, THOMAS JEFFERSON UNIVERSITY HOSPITAL—An unexpected opening for a neuroradiology fellow is available in the Dept. of Radiology at Thomas Jefferson University Hospital, beginning July 1990. The Division of Neuroradiology has close clinical and research relationships with Jefferson's very active neurology, neurosurgery, orthopedic surgery, and otolaryngology depts. Complete training in ENT radiology is part of this program. Five full-time faculty members currently staff this division. Clinical facilities include 2 dedicated CT scanners, a myelography room, a biplane angiography room with DSA, and a GE 1.5-T MRI unit. Two more MRI units will be operational by the summer of 1990. Contact Carlos Gonzalez, M.D., Director of Neuroradiology, 1009 Main Bldg., Thomas Jefferson University Hospital, Philadelphia, PA 19107; (215) 928-5447. Jefferson is an affirmative action/equal opportunity employer. 6xc

THE UNIVERSITY OF PITTSBURGH offers fellowships in angiography/interventional radiology, abdominal imaging (CT/ultrasound/MRI), neuroradiology, pediatric radiology, and MRI. Positions in all of these areas are available to begin July 1991. A fellowship position in pediatric radiology and 1 in abdominal imaging are also available to begin July 1990. Interested applicants should send letters of inquiry and CV to Lawrence A. Cooperstein, M.D., Dept. of Radiology, Presbyterian-University Hospital, DeSoto at O'Hara Sts., Pittsburgh, PA 15213. 3–7cp

FELLOWSHIP POSITIONS—Applications are invited now for July 1991. Positions are available in neuroradiology, vascular/interventional radiology, and body imaging (CT/ultrasound/MRI). For information, contact James R. Schmidgall, M.D. or Richard W. Katzberg, M.D., Chairman, Dept. of Radiology, L-340, Oregon Health Sciences University, 3181 S. W. Sam Jackson Park Rd., Portland, OR 97201. 7–6c

FELLOWSHIPS IN ABDOMINAL IMAGING—The Dept. of Radiology at the University of Texas Medical School at Houston has openings for 2 abdominal imaging fellowships to begin July 1991. Under faculty direction and supervision, candidates will further their training in the specialty of abdominal imaging including CT, ultrasound, and MRI through 4-mo rotations in each service. Candidate will participate in teaching in each section at the medical student and resident levels, will have the opportunity to conduct basic or clinical research, and will be expected to prepare and submit at least 1 scientific article to an appropriate refereed journal. Candidate must be a graduate of an approved U.S. medical school or its equivalent, must have completed an approved residency in diagnostic radiology, must be a diplomate of the ABR, and must have a Texas medical license. Please submit CV, along with the names and addresses of 3 references, to John H. Harris, Jr., M.D., D.Sc., Professor and Chairman, Dept. of Radiology, The University of Texas Medical School at Houston, 6431 Fannin St., Ste. 2.132, Houston, TX 77030. The University of Texas Health Science Center at Houston is an equal opportunity employer. Women and minorities are encouraged to apply. 1–6c

Tutorials/Courses

WORKSHOP—NATO Advanced Study Institute (ASI), Picture Archiving and Communication System (PACS) in Medicine, Evian, France, Oct. 14–26, 1990. The aim of this ASI workshop is to bring 80 participants for intensive presentation and probing discussions on PACS. The theme of this meeting is to emphasize "how to." Cost per person including room and board for the full duration is $645 single, $585 double. No registration fee is required. There is limited funding to support participation. For more information, please contact Professor H. K. Huang, M.D., Division of Medical Imaging, Dept. of Radiological Sciences, UCLA School of Medicine, Los Angeles, CA 90024-1721, U.S.A.; (213) 206-1045. FAX: (213) 206-2967. 5–8d

SIXTH ANNUAL LONDON-PARIS ULTRASOUND CONGRESS, SEPTEMBER 15–22, 1990—Category I accreditation followed by OPTIONAL LOIRE VALLEY BICYCLE TOUR. For information contact Medical Seminars International, Inc., 9800 D Topanga Canyon Blvd., Ste. 232, Chatsworth, CA 91311; (818) 700-9821. 3–8d

ALASKA 90—CRUISE THE INLAND PASSAGE, July 6–13, 1990. Patrick Colletti, M.D., University of Southern California, MRI tutorial and course. Category I CME credits. For information, contact Medical Seminars International, Inc., 9800 D Topanga Canyon Blvd., Ste. 232, Chatsworth, CA 91311; (818) 700-9821. 1–6d

Other

X-RAY FILM FOR SALE FROM NATIONWIDE DISTRIBUTOR—Very attractive prices and excellent service. Freight prepaid and no sales tax. Orders phoned in before noon are shipped out by UPS the same day. We ship anywhere in the world. No minimum order necessary. For information, prices, and free samples, please contact Dacco Enterprises, 7350 S.W. 48th St., Miami, FL 33155; USA (800) 222-8242. 5–8ep

VISITING PROFESSORSHIP, THOMAS JEFFERSON UNIVERSITY HOSPITAL—The Dept. of Radiology at Thomas Jefferson University Hospital in Philadelphia offers a visiting professorship in our Division of General Diagnostic Radiology. The position commences July 1990 and will be available for 2 yr, while several of our faculty members are on sabbatical leave. Funding for the position is appropriate for a senior faculty member from another institution on sabbatical with partial funding or for a junior faculty member. In addition to working in the General Diagnostic Division, the visiting radiologist will have access, for research or educational purposes, to state-of-the-art MRI, CT, and ultrasound units, and to well-equipped physics and physiology research laboratories. Liberal research time will be available. Interested individuals should contact David C. Levin, M.D., Chairman, Dept. of Radiology, Thomas Jefferson University Hospital, Philadelphia, PA 19107. Jefferson is an equal opportunity/affirmative action employer. 11–10e

AJR Classified Advertisements Information

Box Responses and Address for Ad Placement

Write Box ______, AJR, 2223 Avenida de la Playa, Suite 200, La Jolla, CA 92037-3218; (619) 459-2229; FAX: (619) 459-8814.

Author Index
Volume 154

Authors of *AJR* articles are also included in the 5-year cumulative index published in *Radiology*.

A

Aabed MY, **154:**989
Abbitt PL, **154:**849
Ablin DS, **154:**1035
Abu-Yousef M, **154:**721
Adachi N, **154:**423
Agee MW, **154:**135
Aideyan OA, **154:**989
Aisen AM, **154:**1228
Akins EW, **154:**1091
Akita Y, **154:**1257
Alberhasky MT, **154:**261
Alexander PW, **154:**493
Alford BA, **154:**785
Allgood M, **154:**181
Alrowaih A, **154:**331
Ambrosino MM, **154:**797
Amis ES Jr, **154:**1028
Anderson CM, **154**623
Andersson I, **154:**1191
André MP, **154:**32
Ansari A, **154:**114
Arisawa J, **154:**1181
Arrington LE, **154:**1237
Arthur RH, **154:**603
Aruny JE, **154:**1105
Atkinson DJ, **154:**937
Atlas SW, **154:**167, **154:**1069
Avolio RE, **154:**1127, **154:**1128

B

Babcock DS, **154:**202
Bae WK, **154:**1346
Bair JH, **154:**405
Bakal CW, **154:**171
Baker EL, **154:**27
Baker KS, **154:**129
Baker LL, **154:**1251
Baker ME, **154:**67
Ball WS Jr, **154:**361
Balthazar EJ, **154:**27, **154:**72, **154:**281, **154:**499
Banner H, **154:**797
Barker WW, **154:**1285
Barkoff ND, **154:**295
Barloon TJ, **154:**271, **154:**301
Baron NW, **154:**327
Baron RL, **154:**79
Bassett LW, **154:**713, **154:**1196
Baumann MH, **154:**481
Baumgartner BR, **154:**105, **154:**291
Baum PA, **154:**633
Bean WJ, **154:**659
Bell SA, **154:**121
Benedikt RA, **154:**16
Bennett HT, **154:**1237
Benson LN, **154:**789
Berbaum KS, **154:**301
Bergin CJ, **154:**251, **154:**495
Berman E, **154:**770
Bernardino ME, **154:**45
Berquist TH, **154:**323
Berrey BH, **154:**563
Berry CC, **154:**477
Bescos JM, **154:**525
Bhalla M, **154:**51
Bilaniuk LT, B154:585
Bindman DJ, **154:**533
Binkovitz LA, **154:**323
Birnbaum BA, **154:**761
Bisset GS III, **154:**202
Bjorkengren AG, **154:**331, **154:**1025
Black WC, **154:**17
Blandino A, **154:**654
Blask AN, **154:**657
Bloem JL, **154:**763
Boechat MI, **154:**573
Bognanno JR, **154:**1299
Bohlman H, **154:**151
Boiskin I, **154:**529
Borushok KF, **154:**275
Bosley TM, **154:**167
Bowen BC, **154:**1285
Bowie JD, **154:**903
Boxt LM, **154:**788
Bradley MJ, **154:**900
Brady TJ, **154:**1053
Brahme F, 154:158
Brant-Zawadzki M, **154:**1284
Braunstein EM, **154:**134
Bree RL, **154:**656
Breiman RS, **154:**1284
Brendler CB, **154:**741
Brenner B, **154:**175
Brenner JS, **154:**199
Brenner RJ, **154:**420
Briggs SE, **154:**1003
Brogdon BG, **154:**867, **154:**1111
Brooks BS, **154:**577
Broome DR, **154:**1299
Brower AC, **154:**309, **154:**1236
Brown AT, **154:**1003
Brown BP, **154:**721
Brown MD, **154:**821
Brown RC, **154:**301
Bruner JM, **154:**351
Bryant RG, **154:**175
Budzik RF Jr, **154:**459
Buetow PC, **254:**563
Bunchman TE, **154:**785
Burhenne HJ, **154:**1015
Burk DL Jr, **154:**549
Burke DR, **154:**183
Burnstein MI, **154:**555
Burrows PE, **154:**789
Burton D, **154:**521
Busuttil RW, **154:**393, **154:**573

C

Callen PW, **154:**459
Cammarata CA, **154:**893, **154:**1337
Campbell JA, **154:**1177
Carella I, **154:**654
Carlsen SE, **154:**495
Caroline DF, **154:**1124
Carroll BA, **154:**398
Carter J, **154:**151
Casarella WJ, **154:**1007
Cascade PN, **154:**1117
Castellino RA, **154:**251, **154:**1251
Castillo M, **154:**607, **154:**1051
Chalif M, **154:**45
Chaloupka JC, **154:**1051
Chamberlain DW, **154:**999
Chan KK, **154:**415, **154:**635
Chandnani V, **154:**1025
Chang C-h, **154:**900
Chang KH, **154:**809
Chang P, **154:**521
Charboneau JW, **154:**1
Charles HC, **154:**67
Chaudhuri TK, **154:**1347
Chen C, **154:**1025
Chi TL, **154:**1269
Cho PS, **154:**415, **154:**635
Choplin RH, **154:**23
Clark DC, **154:**989
Clark LR, **154:**884, **154:**1318
Clark RA, **154:**54, **154:**744
Clore FC, **154:**655
Cohen EP, **154:**1126
Cohen J, **154:**903
Colby JM, **154:**532
Coldwell DM, **154:**1101
Cole RA, **154:**1275
Coombs RJ, **154:**1011
Cooper CJ, **154:**119, **154:**888, **154:**1325
Cooperstein LA, **154:**709
Cope C, **154:**183, **154:**203, **154:**1256
Corcoran HL, **154:**255
Cormier JM, **154:**425
Corradino G, **154:**1293
Cossi AF, **154:**1343
Coulaud JM, **154:**1349
Courchesne E, **154:**593
Cox JF, **154:**1124
Cronan JJ, **154:**851
Curry NS, **154:**307
Cynamon J, **154:**171
Czarnecki DJ, **154:**902

D

Daffner RH, **154:**554
Daniel TB, **154:**1091
Dännert W, **154:**691
Das KM, **154:**421
David G, **154:**863
Davidson AJ, **154:**888, **154:**1325
Davis LP, **154:**327
Davis PC, **154:**607, **154:**831
Day DL, **154:**729, **154:**785
De Courten-Meyers G, **154:**361
Defalque D, **154:**515
Degryse HRM, **154:**343
DeMarino GB, **154:**709
Demeure R, **154:**515
Demirci A, **154:**1126
Demopoulos R, **154:**295
De Pena CA, **154:**351
DeRemer DR, **154:**1275
De Schepper AMA, **154:**343
De Smet AA, **154:**555
Deveikis JP, **154:**893, **154:**1337
DeVivo DC, **154:**1269
Diamond JJ, **154:**867
Diaz MJ, **154:**315
Dickson BA, **154:**255
Dillon W, **154:**375
Diner WC, **154:**1217
DiPietro MA, **154:**1223
Distell BM, **154:**903
Dobkin GR, **154:**857
Dodd GD III, **154:**459
Dodds WJ, **154:**87, **154:**953, **154:**965
Dodero P, **154:**1049
Doi K, **154:**1107
Donaldson MC, **154:**857
Donaldson SS, **154:**1251
Doppman JL, **154:**1075
Dorfman GS, **154:**851
Dowling CA, **154:**1305
Drake DG, **154:**785
Drayer BP, **154:**163
Dresel S, **154:**585
D'Souza VJ, **154:**621
Duara R, **154:**1285
DuBose TJ, **154:**1348
Duchesneau PM, **154:**1275
Duerinckx AJ, **154:**393
Dufretay X, **154:**1349
Dunaway HE Jr, **154:**735
Dunbar JS, **154:**149
Dunnick NR, **154:**927
Dyer RB, **154:**621

E

Eber O, **154:**423
Edell SL, **154:**572
Edelman RR, **154:**901, **154:**937
Edwards MK, **154:**1299
Ehara S, **154:**777
Ehrlich SM, **154:**779
Einhorn LH, **154:**1299
Eisenberg RL, **154:**1125
Eismont F, **154:**821
Eklund GW, **154:**1345
El Gammal T, **154:**577
Elizondo G, **154:**287
Elkadi TAF, **154:**1060
Ellis JH, **154:**1223
Endoh W, **154:**1124
Endress C, **154:**1346
Engelstad B, **154:**73
English JT, **154:**199
Epstein JI, **154:**741
Erickson SJ, **154:**87, **154:**399, **154:**1126
Esparza J, **154:**525
Eulderink F, **154:**763

F

Fagerholm M, **154:**545
Fakhry J, **154:**124
Fanney D, **154:**888, **154:**1325
Farner R, **154:**721
Faro SH, **154:**757
Feczko PJ, 154:199
Felker RE, **154:**241
Fell SC, **154:**73
Felmlee JP, **154:**185
Fermand M, **154:**425
Fernback SK, **154:**142
Ferrucci JT Jr, **154:**287, **154:**1003
Fiessinger JN, **154:**425
Filly RA, **154:**459
Finck EJ, **154:**181
Finestone H, **154:**201, **154:**657
Fink S, **154:**1347
Fisher DR, **154:**555
Fish G, **154:**307
Fishman EK, **154:**741, **154:**1017
Flack MR, **154:**1075
Flaherty LE, **154:**327
Flanigin HF, **154:**577
Fleischer AC, **154:**529
Fletcher G, **154:**817
Foley WD, **154:**399, **154:**1126
Forcade C, **154:**51
Forer L, **154:**888, **154:**1325
Forman BH, **154:**1003
Formanek AG, **154:**898
Forsberg DA, **154:**751
Foster MA, **154:**79
Foster TH, **154:**175
Francis CW, **154:**175
Frank SJ, **154:**1075
Franken EA Jr, **154:**271, **154:**345, **154:**1123
Franquet T, **154:**525
Freedom RM, **154:**789
Freeny PC, **154:**79
Frey GD, **154:**870
Fried AM, **154:**544
Friedland GW, 154:1100
Friedman AC, **154:**1124, **154:**1222
Friedman D, **154:**797
Friedman PJ, **154:**33
Friefeld GD, **154:**405
Froehlich JA, **154:**851
Fujita M, **154:**509
Fulcher AS, **154:**259

G

Gaa J, **154:**1003
Gado M, **154:**369
Gaeta M, **154:**654
Gagliardi RA, **154:**94, **154:**899, **154:**952
Gallego F, **154:**997
Gamstaetter G, **154:**654
Gareen IF, **154:**265
Garneau RA, **154:**271
Garrett MK, **154:**1250
Garvin AJ, **154:**307
Gaux JC, **154:**1349
Gay JN, **154:**577
Gay SB, **154:**55, **154:**871
Gebarski SS, **154:**360, **154:**1074
Gebauer A, **154:**656
Gelfand DW, **154:**279
Gelfand MJ, **154:**202
Genez BM, **154:**315
Genieser NB, **154:**797
Gennari RC, **154:**709
Gerlach R, **154:**1305
Geubel A, **154:**515
Gibney RG, **154:**203, **154:**1015
Giger ML, **154:**1107
Gigot J-F, **154:**515
Gilula LA, **154:**129, **154:**559
Gingrich R, **154:**721
Giovanniello J, **154:**424
Glassberg RM, **154:**47
Glasser SA, **154:**1069
Glass-Royal M, **154:**890, **154:**1331
Glazer HS, **154:**200
Glenthøj A, **154:**1087
Godwin JD, **154:**41
Goell WS, **154:**902
Goldberg ME, **154:**286
Goldfarb CR, **154:**201, **154:**657
Goldman ML, **154:**1101
Gold RE, **154:**69
Gold RH, **154:**568, **154:**713
Goldstein RB, **154:**459
Goldwag S, **154:**849
Gomes AS, **154:**393, **154:**975
Good BC, **154:**709
Goodman P, **154:**1207
Goose PW, **154:**884, **154:**1318
Gorden P, **154:**1075
Gordon RB, **154:**281, **154:**499, **154:**761
Gornbein JA, **154:**713
Gotoh M, **154:**1124
Govoni AF, **154:**265
Graf BK, **154:**555
Grafe M, **154:**593
Grafton WD, **154:**1125
Gramm HF, **154:**476, **154:**1198
Grant EG, **154:**393, **154:**573, **154:**1349
Grantham JR, **154:**655
Grasl MCh, **154:**411
Gray JE, **154:**185
Grayson EV, **154:**576, **154:**1268
Green BA, **154:**821
Green CE, **154:**884, **154:**1318
Greenspan A, **154:**1035
Grevers G, **154:**585
Gritzmann N, **154:**411
Grix A, **154:**1025
Gross GM, **154:**1097
Gross GW, **154:**779
Grossman RI, **154:**167, **154:**1069
Gudi K, **154:**424
Guenin M, **154:**897
Guenther RW, **154:**617
Gundry CR, **154:**337, **154:**1233
Gur D, **154:**709

H

Hackney DB, **154:**1069
Haddad MC, **154:**989
Hahn PF, **154:**287, **154:**1003
Hall FM, **154:**897, **154:**903
Hall TR, **154:**573
Hamilton P, **154:**1187
Hanafee W, **154:**374, **154:**584
Han BK, **154:**202, **154:**361
Han MC, **154:**809
Han MH, **154:**809
Harris K, **154:**424
Harris RD, **154:**1122
Harshfield DL, **154:**1217
Hartman DS, **154:**888, **154:**1325
Hartman GW, **154:**645
Hasegawa H, **154:**1203
Hathorn JW, **154:**67
Haughton VM, **154:**817
Hawes DR, **154:**1345
Hawkins IF Jr, **154:**1091
Hawkins RA, **154:**975
Hayes WS, **154:**888, **154:**1325
Hegedüs L, **154:**1087
Heitbrink MA, **154:**202
Helmer E, **154:**603
Helmer M, **154:**411
Helms CA, **154:**319
Hendee WR, **154:**647
Henderson JM, **154:**1007
Hennerici M, **154:**1061
Hermans J, **154:**763
Herman SJ, **154:**999
Herman TE, **154:**806
Hernandez RJ, **154:**1241
Hernanz-Schulman M, **154:**797
Herndon JH, **154:**851
Hertzberg BS, **154:**903
Hesselink JR, **154:**593, **154:**837
Heveron ED, **154:**867
Hicks ME, **154:**725
Higashihara H, **154:**1257
Higgs JB, **154:**315
Hilal SK, **154:**1269
Hindman BW, **154:**1127, **154:**1128
Ho BKT, **154:**415, **154:**635
Ho C, **154:**1233
Ho K-C, **154:**817
Hoffman JC Jr, **154:**607, **154:**831
Holm HH, **154:**1087
Holmes CL, **154:**393
Holscher HC, **154:**763
Honda H, **154:**271
Hoogewoud HM, **154:**901, **154:**937
Hopper KD, **154:**115
Hopsu EVM, **154:**1259
Houlle D, **154:**425
Howard JM, **154:**1011
Hua CL, **154:**1348
Huang HK, **154:**415, **154:**635
Hubner KF, **154:**1024
Hudgins P, **154:**1051
Hulnick D, **154:**499
Hunter DW, **154:**729
Hurst GC, **154:**1275
Huskison WT, **154:**118

I

Iio M, **154:**505
Ikeya S, **154:**1203
Ikezoe J, **154:**1079, **154:**1181
Imazato M, **154:**201
Ingram TL, **154:**893, **154:**1337
Isik V, **154:**1126
Isobe Y, **154:**201
Itai Y, **154:**505

J

Jackson FI, **154:**899, **154:**1121
Jackson VP, **154:**1196
Jain CU, **154:**424
Jamart J, **154:**515
Janick PA, **154:**1069
Jeffrey RB Jr, **154:**27, **154:**275
Jelinek JS, **154:**563
Joffe N, **154:**897
Joffre F, **154:**613
Johnson CD, **154:**99
Johnson JO, **154:**539
Johnson KK, **154:**405
Jolles H, **154:**259
Josephs SH, **154:**803
Joslyn JN, **154:**1293

K

Kahn CE Jr, **154:**635
Kairemo KJA, **154:**1259
Kanai T, **154:**1124
Kanal E, **154:**384
Kandarpa K, **154:**1105
Kang HS, **154:**337, **154:**1025
Kang K, **154:**585
Kangarloo H, **154:**635
Kao SCS, **154:**345
Kaplan ID, **154:**745
Kaplan P, **154:**319, **154:**1025
Karasick D, **154:**549
Karstrup S, **154:**1087
Kasi LP, **154:**796
Kaszar-Seibert DJ, **154:**533
Kaude JV, **154:**199
Kaufman RA, **154:**569
Kaufman SL, **154:**1007
Keller FS, **164:**1097
Kerns SR, **154:**55
Kilcoyne RF, **154:**1029
Kim C-W, **154:**809
Kim D, **154:**421, **154:**1213, **154:**1307
Kim EE, **154:**796
Kim IO, **154:**809
Kim YH, **154:**1346
Kimizu K, **154:**385
Kimme-Smith C, **154:**713
Kimmey M, **154:**1101
Kimura K, **154:**345
King BF, **154:**1219
King DW, **154:**577
King GA, **154:**1346
Kirks DR, **154:**202
Kitagawa M, **154:**419
Kitamura T, **154:**509
Klatt EC, **154:**27
Klein MV, **154:**1245
Kleinman PK, **154:**1047
Kling GA, **154:**327
Kloetzsch C, **154:**1061
Knudson GJ, **154:**399
Ko YT, **154:**107
Kobayashi T, **154:**1079
Kochhar R, **154:**421
Koike K, **154:**789
Kok FP, **154:**202
Költringer P, **154:**423
Korn WT, **154:**533
Korobkin M, **154:**1096
Kostrubiak IS, **154:**125
Kowall NW, **154:**1053
Koyama H, **154:**1079
Kozuka T, **154:**1079, **154:**1181
Kransdorf MJ, **154:**309, **154:**563
Kriegshauser JS, **154:**1219
Kronthal AJ, **154:**741
Krysiewicz S, **154:**1347
Kuboya Y, **154:**777
Kuhlman JE, **154:**741
Kulik WJ, **154:**1127, **154:**1128
Kuroda C, **154:**1124
Kursunoglu-Brahme S, **154:**337, **154:**1233
Kurtz AB, **154:**691

L

LaBrecque D, **154:**721
La Fontaine RL, **154:**975
Lai A, **154:**1053
Laing FC, **154:**275
Lally JF, **154:**757
Lang EK, **154:**735
Lang EV, **154:**33, **154:**725
Lange RH, **154:**555
Langsteger W, **154:**423
Lanzieri CF, **154:**1263
Lask D, **154:**111
Lasser EC, **154:**1343
Lauerman WC, **154:**315
Lawson TL, **154:**399, B154:87
Lecumberri FJ, **154:**525
Lee DH, **154:**107
Lee EL, **154:**65
Lee G, **154:**1127, **154:**1128
Lee KS, **154:**1346
Lee MJ, **154:**1003
Lee RE, **154:**623
Lee SH, **154:**1015
Lee Y-Y, **154:**351
Leeming BWA, **154:**1307
Leetzow ML, **154:**185
Leitman BS, **154:**51
Leonidas JC, **154:**1123
Letourneau JG, **154:**729, **154:**785
Leung AN, **154:**487
Levine E, **154:**771
Levine MS, **154:**1157
Lev-Toaff AS, **154:**982, **154:**1124
Levy A, **154:**903
Lim JH, **154:**107
Lindfors KK, **154:**261
Lindholm K, **154:**1191
Lind P, **154:**423
Lindstrand A, **154:**331
Lipchik EO, **154:**399
Lissac J, **154:**1349
Lissner J, **154:**585
Lituania M, **154:**1049
Liu SS, **154:**163
Lo H-H, **154:**1078
Loewenstein DA, **154:**1285
Löfgren M, **154:**1191
Logemann JA, **154:**953, **154:**965
Longmaid HE III, **154:**1034
Lott SA, **154:**261
Lowrey CE, **154:**315
Lu CT, **154:**1107
Lubat E, **154:**761
Lucigrai G, **154:**1049

M

Mack LA, **154:**143
MacMahon H, **154:**1107
Magid D, **154:**1017
Mahoney MC, **154:**255
Maldonado V, **154:**899
Mali WPTM, **154:**902
Mann RW, 58, **154:6**, **154:**420,
154:658, **154:**1347
Mannick JA, **154:**857
Mansoory A, **154:**757
Mantineo G, **154:**654
Mantoni M, **154:**535
Manzione JV, **154:**1344
Maravilla KR, **154:**1305
Marcus RE, **154:**151
Marder VJ, **154:**175
Markivee CR, **154:**659
Martinez S, **154:**751
Martin LG, **154:**1007
Marukawa T, **154:**1124
Marx MV, **154:**725
Masaryk TJ, **154:**151, **154:**159
Matalon TAS, **154:**847
Mathews VP, **154:**1299
Matsen FA III, **154:**1029
Mattle HP, **154:**901, **154:**937
Mattrey RF, **154:**539
Mattsson TA, **154:**989
Mauer SM, **154:**785
McCabe DJ, **154:**656
McCauley DI, **154:**51
McClennan BL, B154:645
Mc Diarmid SV, **154:**573
McGahan JP, **154:**143
McGrath FP, **154:**1015
McKee A, **154:**1053
McKinstry RC, **154:**1053
McKusick MA, **154:**422
McLaurin RL, **154:**361
McLeod RA, **154:**323
Meador K, **154:**577
Medina L, **154:**1269
Megibow AJ, **154:**27, **154:**281,
154:295, **154:**761
Meizner I, **154:**903
Mellinger BC, **154:**1347
Meranze SG, **154:**183
Merchant S, **154:**426
Merriam GR, **154:**1075
Merrick HW, **154:**1011
Mestayer RJ, **154:**893, **154:**1337
Metreweli C, **154:**900
Metz CE, **154:**419, **154:**1121
Metzger TS, **154:**847
Mewissen MW, **154:**399
Meyers PC, **154:**86, **154:**1125
Meza MP, **154:**899
Micheli L, **154:**657
Michelson JD, **154:**1017
Miketic LM, **154:**709
Miller DL, **154:**1075
Miller RR, **154:**487, **154:**983
Millikan WJ Jr, **154:**1007
Mills DG, **154:**375
Milner LB, **154:**486
Mirowitz SA, **154:**369
Mirvis SE, **154:**1293
Mitchell DG, **154:**549
Miyata S, **154:**419
Modic MT, **154:**151, **154:**159
Moes CAF, **154:**789
Mojtahedi S, **154:**1107
Monden M, **154**1124
Montalvo BM, **154:**821
Montemayor KA, **154:**105
Montes M, **154:**525
Moore J, **154:**1053
Moore SG, **154:**745
Mori T, **154:**1124
Morimoto S, **154:**1079, **154:**1181
Moriyama N, **154:**1350
Morparia H, **154:**426
Morris DM, **154:**1125
Morris M, **154:**1029
Morris TW, **154:**300
Morrison MC, **154:**1003
Morse S, **154:**1103
Moser RP Jr, **154:**309, **154:**563,
154:1176, **154:**1240
Moss GD, **154:**1086
Mostbeck G, **154:**656
Movson JS, **154:**903
Mowschenson PM, **154:**1213
Mueller PR, **154:**233, **154:**1003
Mukai K, **154:**1203
Müller NL, **154:**487, **154:**983
Mullhollan TJ, **154:**65
Mullin DM, **154:**659
Munk PL, **154:**391
Muñoz A, B154:997
Murakami JW, **154:**593
Muramatsu Y, **154:**1203, **154:**1350
Murphy FB, **154:**45
Muz J, **154:**327

N

Naidich DP, **154:**51
Nakahara K, **154:**1181
Nakanishi K, **154:**509
Nakasato T, **154:**777
Nath H, **154:**493
Nawano S, **154:**1350
Nelson RC, **154:**291
Newbold R, 154:119
Newmark H III, **154:**1164
Newton TH, **154:**375
Ney DR, **154:**1017
Ng J, **154:**1237
Nino-Murcia M, **154:**521
Nishiyama K, **154:**1079
Nooy MA, **154:**763
Norman D, **154:**375
Numaguchi Y, **154:**1293
Nyberg DA, **154:**143
Nylander WA, **154:**529

O

O'Brien MJ, **154:**50
Oestreich AE, **154:**1250
Ohtomo K, **154:**505
Ohtomo Y, **154:**505
Okamura J, **154:**1124
Okazaki M, **154:**1257
Okimura T, **154:**385
Okuda S, **154:**509
Oldfield EH, **154:**1075
O'Leary DH, **154:**857
Olmedilla G, **154:**997
Olson DL, **154:**1126
O'Neil J, **154:**199
Ongseng F, **154:**201, **154:**657
Osborn AG, **154:**630
Ott DJ, **154:**279
Owsley DW, **154:**1347
Ozcan U, **154:**1126

P

Pagny JY, **154:**1349
Paley D, **154:**125
Park JH, **154:**898
Parker BR, **154:**1251
Parvey HR, **154:**1125
Patel YD, **154:**179
Patronas NJ, **154:**893, **154:**1075,
154:1337
Patt RH, **154:**633
Patterson K, **154:**803
Paulin S, **154:**898
Payne WD, **154:**729
Pedersen JF, **154:**535
Pedersen MI, **154:**203
Peñarrocha L, **154:**997
Pentecost MJ, **154:**181
Perkash I, **154:**521
Perrella RR, **154:**393
Pettersson H, **154:**331
Pfister RC, **154:**233
Phillipson J, **154:**539
Phillips WC Jr, **154:**1149
Picus D, **154:**725
Pierce ME, **154:**1127
Platt JF, **154:**1223
Poch-Broto J, **154:**997
Polak JF, **154:**857
Popovich MJ, **154:**603
Porter DH, **154:**421, **154:**1213
Porter RM, **154:**659
Post MJD, **154:**821
Pozniak MA, **154:**545
Press GA, **154:**593, **154:**837
Price JC, **154:**185
Price SC, **154:**863
Pringot J, **154:**515
Proto AV, **154:**259

Q

Quencer RM, **154:**821
Quinn SF, **154:**1103

R

Rabin AM, **154:**305
Rabinson S, **154:**111
Racette CD, **154:**757
Radecki PD, **154:**1124
Radin DR, **154:**27
Raillat C, **154:**613
Ralls PW, **154:**27
Ramakantan R, **154:**61, **154:**200
Rapaport SI, **154:**239
Raptopoulos V, **154:**532
Raval B, **154:**1207
Read RC, **154:**1217
Reading CC, **154:**1, **154:**1219
Reagan K, **154:**884, **154:**1318
Recht MP, **154:**183
Reed JC, **154:**23
Reid WM, **154:**893, **154:**1337
Reifsnyder AC, **154:**65
Reinhart M, **154:**1025
Relland J, **154:**1349
Remmele W, **154:**654
Renner JB, **154:**135
Resnick D, 37, **154:**3, **154:**337,
154:1025, **154:**1233, **154:**1245
Resnik CS, **154:**125
Rice S, **154:**149
Rifkin MD, **154:**549, **154:**691
Rockette HE, **154:**709
Rockwood CA, **154:**1029
Roe D, **154:**975
Roh JK, **154:**809
Rohrmann CA Jr, **154:**79, **154:**1002
Roniger WE, **154:**735
Rose BS, **154:**425
Rosen BR, **154:**1053
Rosenberg MA, **154:**342, **154:**988
Rosenquist CJ, **154:**644, **154:**652
Rosenthal RE, **154:**658
Ross JS, **154:**151, **154:**159
Rothman B, **154:**1229
Rousseau H, **154:**613
Routh WD, **154:**1097
Roux D, **154:**613
Rowland GA, **154:**291
Rubesin SE, **154:**1157
Rubin JM, **154:**1223
Rumancik W, **154:**797
Rummeney E, **154:**287
Russ PD, **154:**405

S

Sacks BA, **154:**421
Sacks EM, **154:**1344
Safirstein BH, **154:**897
Safrit H, **154:**119
Sagel SS, **154:**200
Sahn DJ, **154:**1060
Sahn SA, **154:**481
Saini S, **154:**287, **154:**1003
Sakon M, **154:**1124
Sakurai M, **154:**1124
Salerno MD, **154:**425
Saloner D, **154:**623
Samuels T, **154:**1187
Sanders C, **154:**493
Sanders RC, **154:**741
Sandler MP, **154:**529
Sargent EN, **154:**64
Sarti D, **154:**1229
Sartor K, **154:**369

Sartoris DJ, **154:**337, **154:**882, **154:**1245
Sasaki K, **154:**385
Sasaki M, **154:**777
Sato T, **154:**777
Sato Y, **154:**345
Savino PJ, **154:**167
Saxey R, **154:**657
Scanlan KA, **154:**545
Schabel SI, **154:**307
Schaighofer B, **154:**1233
Scheinbaum K, **154:**171
Schellinger D, **154:**893, **154:**1337
Schenck J, **154:**205
Schils JP, **154:**1025
Schinella RA, **154:**281
Schlesinger AE, **154:**1241
Schlueter FJ, **154:**202
Schmidt RA, **154:**419, **154:**1107, **154:**1121
Schmiedl U, **154:**1305
Schoeneman MJ, **154:**201
Schrock TB, **154:**73
Schulte SJ, **154:**79, **154:**1002
Schwaighofer BW, **154:**337, **154:**1245
Scott JA, **154:**1149
Scott MD, **154:**621
Scudamore CH, **154:**203
Sedman AB, **154:**1223
Sekiya M, **154:**1107
Selby HG, **154:**871
Selby JB Jr, **154:**871
Sener RN, **154:**1126
Serchuk L, **154:**904
Sergott RC, **154:**167
Shah P, **154:**61, **154:**200
Shapeero LG, **154:**623
Shapiro S, **154:**545
Sharif HS, **154:**989
Shaw DWW, **154:**1101
Shaw P, **154:**1187
Sheflin JR, **154:**1177
Shelbourne KD, **154:**1237
Sheldon J, **154:**1285
Shellock FG, **154:**631, **154:**1229
Shiga J, **154:**505
Shiina S, **154:**947
Shipley RT, **154:**255
Shirai Z, **154:**1257
Shortsleeve MJ, **154:**533
Shuman WP, **154:**79, **154:**1029
Sibley RK, **154:**785
Siegel HA, **154:**504, **154:**964
Siegel JB, **154:**1213
Siegel ME, **154:**114
Siegel MJ, **154:**139, **154:**200, **154:**806
Silver B, **154:**847
Silverman FN, **154:**784
Silverman PM, **154:**633, **154:**888, **154:**1325
Silverman SG, **154:**233, **154:**1003
Sisler CL, **154:**139
Sisler WJ, **154:**1127
Sivit CJ, **154:**803
Sklar E, **154:**821
Skolnick L, **154:**1125
Slimp G, **154:**631
Small WC, **154:**45
Smerud MJ, **154:**99
Smit FW, **154:**202
Smith AS, **154:**1275
Smith DK, **154:**559
Smith GM, **154:**23
Smith HJ, **154:**65
Smith JL, **154:**271
Smith JR, **154:**577
Smith RR, **154:**1299
Smith WL, **154:**345
Solomon M, **154:**837
Sonntag VKH, **154:**163
Soper RT, **154:**345
Sorensen AG, **154:**1053
Sostman D, **154:**67
Spencer RP, **154:**40
Spetzler RF, **154:**163
Spoto GP, **154:**837
Spouge AR, **154:**999
Sprayregen S, **154:**171
Sprecher S, **154:**904
Stalker HP, **154:**569
Stanton M, **154:**1217
Staples CA, **154:**983
Stark DD, **154:**287
Stedje K, **154:**569
Steele RD, **154:**899
Steer ML, **154:**1213
Steinberg FL, **154:**901
Steinberg R, **154:**904
Steiner E, **154:**411
Steinke W, **154:**1061
Stephens DH, **154:**99, **154:**422
Stern E, **154:**51
Stevens SK, **154:**745
Stewart ET, **154:**87, **154:**953, **154:**965
Stone J, **154:**521
Strange C, **154:**481
Strazzella WD, **154:**897
Strife JL, **154:**202
Stull MA, **154**, **154:**884, **154:**888, **154:**890, **154:**893, **154:**1317, **154:**1318, **154:**1325, **154:**1331, **154:**1337, 1337
Sugisawa M, **154:**777
Suhocki PV, **154:**884, **154:**1318
Sundaram M, **154:**776
Suri S, **154:**421
Surratt RS, **154:**725
Sussman SK, **154:**47

T

Tagawa K, **154:**947
Taira RK, **154:**415, **154:**635
Takai S, **154:**1079
Takarada A, **154:**385
Takashima S, **154:**1079, **154:**1181
Takashima T, **154:**419
Takasugi JE, **154:**41
Takayasu K, **154:**1203, **154:**1350
Takei Y, **154:**607, **154:**831
Tamakawa Y, **154:**777
Tamamura H, **154:**385
Taminiau AHM, **154:**763
Tanaka S, **154:**509
Tanaka TT, **154:**1245
Taylor AJ, **154:**87, **154:**1126
Taylor GA, **154:**803
Teefey SA, **154:**79
Teele RL, **154:**797
Tein AB, **154:**305
Teitelbaum GP, **154:**633
Teixidor HS, **154:**265
Teplick SK, **154:**1217
Terano A, **154:**947
Terasaki KK, **154:**181
Terriff BA, **154:**203
Tessler FN, **154:**393
Thaler H, **154:**423
Thoeni RF, **154:**73
Thomford NR, **154:**1011
Thompson GP, **154:**1177
Thompson R, **154:**803
Thorngren K-G, **154:**331
Thulborn KR, **154:**1053
Tien RD, **154:**351
Tjon A Tham RTO, **154:**95
Tocino IM, **154:**1122
Toi A, **154:**1199
Tomà P, **154:**1049
Tonami H, **154:**385
Tonkin ILD, **154:**241
Toriya H, **154:**1257
Torres WE, **154:**291
Totterman S, **154:**175
Totty WG, **154:**559
Towbin RB, **154:**149, **154:**361
Townsend RR, **154:**275
Tracy CM, **154:**884, **154:**1318
Trambert JJ, **154:**305
Treves ST, **154:**657
Tsuruda JS, **154:**375, **154:**623
Tung GA, **154:**1003
Tunuguntla K, **154:**1217
Twedt G, **154:**203
Twigg HL, **154:**884, **154:**1318
Tyrrel RT, **154:**105

U

Ueno E, **154:**201
Umeshita K, **154:**1124
Unger EC, **154:**1344
Unger JM, **154:**1123
Unuma T, **154:**947
Urbanek PJ, **154:**851
Urbanski S, **154:**849
Usselman JA, **154:**404

V

Vahey TN, **154:**1237
Valdivieso M, **154:**327
Van Beers B, **154:**515
van Heesewijk HPM, **154:**202
Van Tassel P, **154:**351
Veith FJ, **154:**171
Vick CW, **154:**121
Vlasveld LT, **154:**95
Vogl T, **154:**585
Vogler JB III, **154:**751
Volta S, **154:**654
Vorwerk D, **154:**617

W

Wakao F, **154:**1350
Wakasa K, **154:**1124
Wakhloo AK, **154:**654
Walter RM, **154:**656
Waltman AC, **154:**901
Wang Y, **154:**779
Webb WR, **154:**701
Webber, MM, **154:**975
Wehrli FW, **154:**1069
Weidenfeld M, **154:**654
Weinreb JC, **154:**295
Weinstein MA, **154:**1275
Weintraub BD, **154:**1075
Weisbrod GL, **154:**999
Weiss KL, **154:**305
Weiss MA, **154:**656
Weissleder R, **154:**287
Welch TJ, **154:**1, **154:**1219
West MS, **154:**888, **154:**1325
Westesson PL, **154:**1344
Wetzel LH, **154:**771
Whalen E, **154:**11, **154:**875, **154:**1311
Whittemore AR, **154:**204
Wichman RD, **154:**45, **154:**831
Wiedmeyer DA, **154:**399
Wiener MD, **154:**751
Willemze R, **154:**95
Williams KD, **154:**163
Williams WG, **154:**789
Willis JJ, **154:**315
Wills JS, **154:**757
Wilson G, **154:**789
Wilson SR, **154:**1199
Winer-Muram HT, **154:**69
Wingstrand H, **154:**331
Witko J, **154:**897
Wittenberg J, **154:**287
Wojtasek DA, **154:**265
Wolf AL, **154:**1293
Woodring JH, **154:**1165
Woodruff W, **154:**315
Wootton P, **154:**862

X

Xu X-W, **154:**1107

Y

Yachia D, **154:**111
Yaghmai F, **154:**577
Yakes WF, **154:**115
Yamada A, **154:**201
Yamamoto I, **154:**385
Yamasaki S, **154:**1257
Yamashita T, **154:**423
Yoon Y, **154:**107
Yoshikawa J, **154:**419
Young JWR, **154:**125
Young LW, **154:**1156
Yousem DM, **154:**167, **154:**1069
Yu S, **154:**817
Yucel EK, **154:**901

Z

Zagoria R J, **154:**521
Zeiss J, **154:**1011
Zheutlin J, **154:**713

Subject Index
Volume 154

AJR articles are also included in the 5-year cumulative index published in *Radiology*.

Index Key: a = abstract, b = book review, e = editorial, l = letter, m = memorial, p = pictorial essay, v = videotape review

Subjects in this index are cataloged by body part where possible. Disease entities unique to a body part are listed by that part; other more general diseases have separate listings by name. Technical procedures are also listed by part, as appropriate. Because of general interest, subjects dealing with computed tomography, magnetic resonance imaging, sonography, radionuclide imaging, and pediatric radiology are listed under those headings as well as under appropriate body part and/or disease.

A

Abdominal aorta
  aneurysm, prognosis (a), **154:**661
  ruptured stump, transcatheter embolization, **154:**181
Abdominal wall, abnormalities, CT (p), **154:**1207
Abortion, threatened, subchorionic hemorrhage in, sonography, **154:**535
Acetabula, allografts, after bipolar revision arthroplasty, hip (a), **154:**1131
Acquired immune deficiency syndrome
  bowel obstruction in, infant, **154:**803
  ileocecal tuberculosis, CT, **154:**499
  ileocolic intussusception in, **154:**1325
  infection related to, visceral and nodal calcification, **154:**27
Acromegaly, diagnosis, inferior petrosal sinus sampling, **154:**1075
Adrenal gland
  bilateral hemorrhage, adrenocorticotropic hormone-induced (l), **154:**424
  imaging, **154:**927
Adrenocorticotropic hormone, bilateral adrenal hemorrhage induced by (l), **154:**424
Airway, collapse, infant, ultrafast CT, **154:**345
Aldosteronism, hypokalemia, renal cysts and (a), **154:**1354
American College of Radiology, summit meeting, August 1989, **154:**645
American Roentgen Ray Society
  information and application for membership, **154:**220, **154:**448, **154:**1138
  1989 meeting, summary, **154:**219
  1990 meeting
    instructional courses and symposium, **154:**438, **154:**676, **154:**914
    local activities and tennis and golf tournaments, **154:**441
    summary, **154:**437, **154:**675, **154:**913
    Washington, DC, **154:**216, **154:**435, **154:**673
  1991 meeting, Boston, MA, **154:**1364
  Melvin M. Figley Fellowship in Radiology Journalism, **154:**470
  officers, committees, and membership information, **154:**223, **154:**444, **154:**682, **154:**917, **154:**1141
Anatomy
  Pernkopf anatomy (b), **154:**374
  sectional, basic atlas (b), **154:**882, **154:**1034
  sectional (b), **154:**504
Angina, stable, silent ischemia during (a), **154:**1355
Angiography
  coronary
    CLIP system, on-line reporting, **154:**1307
    pulmonary atresia, hypoplastic right ventricle, and ventriculocoronary communications, **154:**789
  digital, cardiac applications (b), **154:**788
  miniature catheters, high-flow jets from, **154:**1091
  MR, **154:**937
    maximum-intensity-projection display (p), **154:**623
    portal vein (l), **154:**901
Angioplasty
  coarctation of the aorta, intima and media dissection after (a), **154:**1355
  long-term, treatment of Budd-Chiari syndrome, **154:**1007
  percutaneous transluminal
    Budd-Chiari syndrome, MR (l), **154:**1350
    infrapopliteal arteries, **154:**171
Ano-rectal strictures, balloon dilatation, infant (a), **154:**211
Anti-carcinoembryonic antigen, immunoscintigraphy, parotid gland tumors, **154:**1259
Aorta
  coarctation
    after surgical correction (a), **154:**208
    angioplasty of, intima and media dissection after (a), **154:**1355
Appendicitis, perforation with, sonographic diagnosis, **154:**275
Arthrectomy, balloon dilatation and, intimal hyperplasia in vascular endoprostheses, **154:**617
Arthritis
  degenerative, atlantoodontoid joint, CT (p), **154:**315
  rheumatoid, nodular pulmonary opacities in (a), **154:**663
  suppurative, percutaneous catheter drainage, **154:**135
Arthrography
  temporomandibular joint, reaction to nonionic contrast medium (l), **154:**1344
  wrist ligaments, MR comparison, **154:**337
Arthroplasty, bipolar revision, acetabular allografts after (a), **154:**1131
Arthrotomography, conventional and computed, shoulder evaluation (a), **154:**666
Artifacts, intracranial chemical-shift, brain, MR, **154:**1275
Asbestos, diseases associated with, cigarette filter workers (a), **154:**661
Ascites, extraperitoneal mass effect (a), **154:**908
Aspergilloma, giant, percutaneous intracavitary treatment of (l), **154:**1346
Atlantoodontoid joint, degenerative arthritis, CT (p), **154:**315
Autoradiology, patient-performed procedures, **154:**871
Azygos system, retroaortic anastomoses, CT, **154:**41

B

Bacteriuria, untreated, renal scarring and, pediatric girls (a), **154:**907
Balloon dilatation, atherectomy and, intimal hyperplasia in vascular endoprostheses, **154:**617
Barium studies
  double-contrast, sigmoidoscopy and (a), **154:**906
  hypersensitivity reaction during (l), **154:**199
Biello criteria, diagnosis of pulmonary emboli, lung scans, **154:**975
Bile duct
  biopsy, Simpson atherectomy catheter, **154:**1213
  extrahepatic, CT, **154:**79
  hilar cholangiocarcinoma, enhanced CT, **154:**1203
  benign strictures, endoscopic therapy for (a), **154:**428
  necrosis, after partial hepatectomy (l), **154:**1124
  papillary adenomatosis, obstructing villous adenoma and, **154:**1217
  stones, sonography for localization, ESWL and (a), **154:**1356
Biliary endoprostheses, clogging, aspirin and doxycycline in (a), **154:**906
Biliary tract
  fistulas, endoscopic treatment (a), **154:**906
  Hawkins-Hunter rocket wire in, **154:**1101
Biopsy
  CT and sonographically guided, **154:**1

fine-needle aspiration
  hepatic hemangioma, fatality from (l), **154:**203
  hepatocellular carcinoma (a), **154:**664
  metastatic lung tumor (a), **154:**905
needle
  sonographically guided, simple phantom for, **154:**847
  sonographically guided, hepatic cavernous hemangioma (a), **154:**908
  sonographically guided, prostatic hypoechoic area (a), **154:**1357
occult breast lesions, new device for evaluation, **154:**261
percutaneous needle, thoracic lesions, **154:**1181
Simpson atherectomy catheter, bile duct, **154:**1213
stereotactic fine-needle, nonpalpable breast lesions, **154:**1191, **154:**1196 (commentary)

Bladder, transitional cell carcinoma, cavitary pulmonary metastases in, **154:**493
Blastomycosis, pulmonary, chest radiographs, **154:**1177
Blood flow, cerebral, newborn, mechanical ventilation effects (a), **154:**211
Blood pressure, high, adult, childhood risk factors for (a), **154:**209
Blue rubber bleb nevus syndrome, CT, **154:**105
Bone
dome of talus, osteochondral fractures (a), **154:**208
Ilizarov limb-lengthening procedures, sonography, **154:**125
imaging (b), **154:**1236
  pediatric (b), **154:**1250
metastasis, hepatocellular carcinoma presenting as (a), **154:**662
pathologic formation (a), **154:**208
sarcoma, chemotherapy effects, MR monitoring of, **154:**763
scan, ballet dancers (l), **154:**657
tibia vara (a), **154:**208
tumors (b), **154:**1240
Bone marrow, changes after irradiation, MR, **154:**745
Book reviews
assurance of quality in the diagnostic x-ray department, **154:**32
avulsion and stress injuries of the musculoskeletal system, **154:**134
basic atlas of sectional anatomy with correlated imaging, **154:**882, **154:**1034
basic medical techniques and patient care for radiologic technologists, **154:**476
basic principles of radiographic exposure, **154:**862
bone and joint imaging, **154:**1236
bone tumors, **154:**1240
breast imaging, **154:**572
cardiac applications of digital angiography, **154:**788
cerebral and spinal computerized tomography, **154:**1074
cerebral computed tomography, **154:**360
chest radiographic analysis, **154:**486
clinical pelvic imaging, **154:**988
clinical radiology of the small intestine, **154:**72
clinical renal imaging, **154:**1096
clinical urography, **154:**1222
CT and sonography of the acute abdomen, **154:**982
dento maxillo facial radiology, **154:**584
Doppler ultrasound, **154:**398
dynamic functional studies in nuclear medicine in developing countries (b), **154:**40
dysphagia, **154:**532
emergency interventional radiology, **154:**1028
ERCP atlas, **154:**1002
evaluation of renal function and disease with radionuclides, **154:**114
exposure of the U.S. population from diagnostic medical radiation, **154:**50
gastrointestinal radiology, **154:**1198
guidance on radiation received in space activities, **154:**870
handbook of breast imaging, **154:**568
house officer, becoming a medical specialist, **154:**16
imaging of sports injuries, **154:**342
imaging of the pediatric urinary tract, **154:**142
magnetic resonance imaging of bone and soft tissue tumors and their mimics, **154:**554
magnetic resonance imaging, **154:**770
magnetic resonance imaging workbook, **154:**1228
manual of diagnostic radiology, **154:**286
nuclear medicine annual 1989, **154:**404
pediatric bone imaging, **154:**1250
Pernkopf anatomy, **154:**374
pocket atlas of head and neck MR anatomy, **154:**630
pocket atlas of spinal MR, **154:**1268
positron emission tomography in clinical research and clinical diagnosis, **154:**1024
procedures in diagnostic radiology, **154:**1164
pros and cons in PTA and auxiliary methods, **154:**1256
radiographic measurements, **154:**744
radiologic clinics of North America, MR of the head and neck, **154:**158
radiology administration (b), **154:**644
radiology of occupational chest diseases, **154:**64
scintigraphy of inflammation with nanometer-sized colloid tracers, **154:**796
sectional human anatomy, **154:**504
textbook of color Doppler echocardiography, **154:**1060
the radiologic clinics of North America, CT of the gastrointestinal tract, **154:**86
tomographic methods in nuclear medicine, **154:**1078
ultrasonography of muscles and tendons, **154:**124
ultrasound and infertility, **154:**544
urologic pathology with clinical and radiologic correlations, **154:**1100
videofluoroscopic studies of speech in patients with cleft palate, **154:**1156
Borgerson, Robert James (m), 154:1086
Bowel
infarction, CT, **154:**99
inflammatory disease, geographic origins of Jewish patients (a), **154:**208
Bowel, small, perforation, cocaine-induced (l), **154:**1346
Brain
intracranial chemical-shift artifacts, MR, **154:**1275
MR signal abnormalities, memory disorder and dementia, **154:**1285
posttraumatic infarction, CT, **154:**1293
Breast
cancer
  after irradiation of thymus in infancy (a), **154:**905
  irradiation for tuberculosis (a), **154:**905
  prognosis, cathepsin D and (a), **154:**1353
carcinoma, secondary acute myelocytic leukemia after (a), **154:**662
imaging (b), **154:**568, **154:**572
implant, collapse after mammography (l), **154:**1345
lesions, nonpalpable, stereotactic fine-needle biopsy, **154:**1191, **154:**1196 (commentary)
occult lesions, biopsy specimens, **154:**261
simulation of mass on mammogram (l), **154:**900
Breast milk, gadopentetate dimeglumine excretion, **154:**1305
Bronchoalveolar lavage, chest radiographs with, interstitial lung disease (a), **154:**905
Bronchopulmonary dysplasia, long-term diuretic therapy for (a), **154:**210
Bronchoscopy, flexible, pulmonary filtrates in pediatric cancer patients (a), **154:**209
Bronchus, left lower lobe, anterior wall stripe, CT, **154:**33
Budd-Chiari syndrome
angioplasty for long-term treatment, **154:**1007
percutaneous transluminal angioplasty treatment, MR (l), **154:**1350
Bursography, current role of, **154:**129

C

Calculi, *see* specific type
Campylobacter pylori, gastrointestinal disease related to, children (a), **154:**427
Cancer
see also specific type or site
lung, radiologic diagnosis, pitfalls, **154:**1165
metastatic, samarium-153 EDTMP (a), **154:**665
Carcinoma, *see* specific organ, region
Carotid artery, disease, color Doppler flow imaging, **154:**1061
Case of the day
abdominal, **154:**888, **154:**1325
chest, **154:**884, **154:**1318
musculoskeletal, **154:**890, **154:**1331
neuroradiology, **154:**893, **154:**1337
Castleman disease
greater omentum (l), **154:**654
mother and daughter (l), **154:**899
neck, CT, **154:**1051
Cathepsin D, breast cancer prognosis and (a), **154:**1353
Catheter
conversion of retrograde to antegrade, femoral artery, **154:**179
double-J, transgastric cystogastrostomy (l), **154:**421
magnetic, removal of foreign bodies, **154:**149
miniature angiographic, high-flow jets from, **154:**1091
percutaneous drainage, suppurative arthritis, **154:**135
Simpson atherectomy, biopsy, **154:**1213
small drainage, malignant pleural effusions (a), **154:**662
transvaginal, selective osteal salpingography and, fallopian tube obstruction, **154:**735
venous, malpositioned, redirection of, **154:**183
Catheterization, gastrojejunal, directable cannula for (l), **154:**203
Cauda equina, ependymoma of, subarachnoid hemorrhage and, **154:**1342
Caudate lobe, liver (p), **154:**87
Cerebellum, anatomic MR correlation, **154:**593
Cerebral hemorrhage, CT appearance, ferritin and hemosiderin role in, **154:**1053
Chemotherapy
bone sarcoma, MR monitoring of, **154:**763
cytosine-arabinoside, GI complications of, **154:**95
intraarterial infusion, metastatic liver tumors, lipid contrast medium and (a), **154:**662
Child abuse, differentiation from osteogenesis imperfecta, **154:**1035, **154:**1047 (commentary)
Cholangiography, papillary adenomatosis, obstructing villous adenoma and, bile ducts, **154:**1217
Cholangiopancreatography, endoscopic retrograde, biliary complications in hydatid disease of liver (a), **154:**210
Cholecystectomy, bile duct diameter after (a), **154:**664
Cholecystography, oral, nonvisualization of gallbladder, lithotripsy and (a), **154:**1358
Cholelithiasis
early recurrence rate, after shock-wave therapy (a), **154:**1131
ESWL, **154:**291

- partially calcified, ESPL and methyl *tert*-butyl ether (a), **154:**427

Chondroblastoma, periostitis in, frequency and diagnostic significance, **154:**309
Chondrosarcoma, laryngeal, CT, **154:**997
Cigarette smoking
- cigarette filter workers, asbestos-associated diseases (a), **154:**661
- neutrophil kinetics and, lung (a), **154:**661

Cirrhosis
- alcoholic, peritoneovenous shunting compared with medical treatment (a), **154:**1129
- gastroesophageal endoscopic features in (a), **154:**906
- regenerating nodules of, MR, **154:**505

Cisplatin, suspended in lymphographic agent, chemotherapy for hepatocellular carcinoma (a), **154:**662
Cocaine
- coronary artery vasoconstriction and (a), **154:**1130
- small bowel perforation and (l), **154:**1346

Coloboma, real-time sonography, **154:**391
Colon
- acute diverticulitis, sonography, **154:**1199
- cancer, diagnosis, cost containment and, **154:**875
- filling, double-contrast enema, **154:**279
- postprandial transit and motor activity, after chronic constipation (a), **154:**1355

Colonoscopy, pediatric patient (a), **154:**429
Computed tomography, biopsy guided by, **154:**1
Computed tomography, abdomen
- abnormalities of abdominal wall (p), **154:**1207
- acute (b), **154:**982
- acute diverticulitis, **154:**281
- after Whipple procedure for malignancy, **154:**1011
- blue rubber bleb nevus syndrome, **154:**105
- blunt trauma, hematuria in, children, **154:**569
- bowel infarction, **154:**99
- combined systemic and portal venous gas, **154:**1219
- gallium scan comparison, synthetic vascular graft infection, **154:**405
- hilar cholangiocarcinoma, **154:**1203
- ileocecal tuberculosis, **154:**499
- staging of Hodgkin disease, children, **154:**1251
- traumatic mesenteric venous thrombosis (l), **154:**425

Computed tomography, adrenal gland, current status, **154:**927
Computed tomography, ankle, plain film comparison, adult fractures, **154:**1017
Computed tomography, biliary system, extrahepatic bile ducts, **154:**79
Computed tomography, bone
- degenerative arthritis, atlantoodontoid joint (p), **154:**315
- occult fractures, carpals and metacarpals (l), **154:**1127
- subtalar arthrorisis, **154:**559

Computed tomography, cranium
- anoxic/ischemic cerebral injury, reversal sign, children, **154:**361
- cerebral (b), **154:**360
- intracranial cryptococcosis, **154:**603
- intracranial ganglioglioma, **154:**607
- intracranial leptomeningeal metastases, **154:**351
- meningitis, comparison with Gd-DTPA-enhanced MR, **154:**809
- posttraumatic cerebral infarction, **154:**1293
- primary cerebral neuroblastoma, **154:**831

Computed tomography, fetus, estimated radiation dose, multislice studies, **154:**185
Computed tomography, gallbladder, high-density bile (a), **154:**908
Computed tomography, humerus, displaced proximal fractures, Neer classification of (p), **154:**1029
Computed tomography, kidney
- long-term dialysis patients (l), **154:**1125
- oncocytoma, intratumoral fat on, **154:**307
- percutaneous procedures, risk of puncturing lung, spleen, and liver, **154:**115

Computed tomography, larynx, chondrosarcoma, **154:**997
Computed tomography, leg, intracapsular osteoid osteoma, proximal femur (p), **154:**1241
Computed tomography, liver
- after transplantation, biliary complications (p), **154:**729
- focal lesions, MR comparison (a), **154:**1358
- focal nodular hyperplasia, contrast material retention in (l), **154:**422
- hemangiomatosis (l), **154:**423

Computed tomography, lung
- adenoid cystic carcinoma, calcification in (l), **154:**419
- bronchiolitis obliterans, organizing pneumonia, **154:**983
- pulmonary infarction (a), **154:**665

Computed tomography, neck
- Castleman disease, **154:**1051
- ultrafast, laryngeal and tracheobronchial obstruction in infants, **154:**345

Computed tomography, pelvis
- clinical imaging (b), **154:**988
- ovarian cyst, herniation through inguinal canal (l), **154:**202
- posterior perineal hernia, **154:**761
- postsurgical complications, ileoanal pouches, **154:**73
- surgical lateral ovarian transposition, **154:**119

Computed tomography, spine
- cerebral and spinal (b), **154:**1074
- cervical facet joints, age-related changes, **154:**817
- cervical spondylolysis, **154:**751
- traumatic lumbar hernia, **154:**757

Computed tomography, thorax
- blunt chest trauma (p), **154:**55
- diffuse pleural disease, **154:**487
- Kaposi's sarcoma (a), **154:**427
- left lower lobe bronchus, anterior wall stripe of, **154:**33
- lung carcinoma, calcification in, **154:**255
- mediastinal lymph node enlargement, usual interstitial pneumonitis, **154:**251
- mediastinal masses, low-attenuation (l), **154:**199
- pulmonary interventional procedures guided by, detection of pneumothorax after, **154:**45
- retroaortic anastomoses, azygos system, **154:**41
- solitary pulmonary nodules, **154:**701
- superior pericardial recess, simulating mediastinal mass, **154:**69
- Whipple disease, mediastinum, **154:**1187
- wooden foreign body in lung parenchyma, **154:**999

Computed tomography, thyroid, anaplastic carcinoma, **154:**1079
Computed tomography, uterus, perforating, simulating urachal carcinoma, **154:**741
Computed tomography, wrist, what is abnormal (l), **154:**1127
Computer page
- coronary angiogram, CLIP system, **154:**1307
- JCAHO dose calculations, microcomputer spreadsheet program, **154:**863
- residents' on-call and vacation schedules, management of, **154:**641

Constipation, chronic, postprandial colonic transit and motor activity in (a), **154:**1355
Contrast medium
- Gd-DTPA
  - extradural degenerative disease, spine, **154:**151
  - tears of anulus fibrosus, **154:**159
- ionic, universal premedication before (l), **154:**1343
- lipid, anti-cancer agents suspended in, chemotherapy (a), **154:**662
- nonionic, reaction during arthrography (l), **154:**1344
- retention, focal nodular hyperplasia of liver (l), **154:**422

Coronary artery
- left ventricle fistula (l), **154:**898
- vasoconstriction, cocaine-induced (a), **154:**1130

Corpus callosum, agenesis and lipoma of, MR (l), **154:**1348
Corticosteroids, withdrawal, sarcoidosis during, chest radiography, **154:**481
Cranial nerves, MR (p), **154:**1263
Craniosynostosis, enlarged parietal foramina and, American Indian child (l), **154:**658
Crohn's disease, cyclosporine therapy (a), **154:**207
Cronkhite-Canada syndrome, radiologic features (a), **154:**211
Cryomicrotomy, cervical facet joints, age-related changes, **154:**817
***Cryptococcus neoformans*,** intracranial infection, CT, **154:**603
Cyclosporine
- organ transplant recipients, malignant neoplasms in, **154:**271
- therapy, Crohn's disease (a), **154:**207

Cyst, *see* specific organ or site
Cystic fibrosis, neonatal screening program, pancreatic function in (a), **154:**1353
Cystic teratoma, mediastinum, **154:**259
Cystogastrostomy, transgastric, double-J catheter for (l), **154:**421
Cytosine arabinoside, high-dose therapy, acute leukemia, fatal pulmonary failure and (a), **154:**1355

D

Dementia, MR signal abnormalities in, **154:**1285
Diastematomyelia, cervical and basicranial, neonate, **154:**806
Diffuse pleural disease, CT, **154:**487
Diverticulitis
- acute, colon, sonography, **154:**1199
- CT diagnosis, **154:**281

Ductus arteriosus, transcatheter closure, pediatric (a), **154:**209
Dysphagia
- diagnosis and treatment (b), **154:**532
- radiologic investigation, **154:**1157

E

Echocardiography, color Doppler (b), **154:**1060
Embolization
- arterial, life-threatening hemorrhage from Meckel's diverticulum, **154:**1257
- transcatheter, ruptured abdominal aortic stump, **154:**181

Endoprosthesis, Wallstent, iliac artery stenoses, **154:**613
Endoscopic therapy
- benign bile duct strictures (a), **154:**428
- biliary tract fistulas (a), **154:**906
- upper gastrointestinal tract, pediatric patient (a), **154:**429

Endosonography, anal (a), **154:**210
Endotracheal tube, malpositioning, radiologic detection, **154:**23
Enema
- contrast
  - acute diverticulitis, **154:**281
  - postsurgical complications, ileoanal pouches, **154:**73
- double-contrast, filling the colon, **154:**279

Ependymoma, subependymoma and, intracranial, MR, **154:**831
Epilepsy, intractable complex partial seizures, MR, **154:**577
ERCP, *see* Cholangiopancreatography, endoscopic retrograde

Esophagitis, reflux, patients with Zollinger-Ellison syndrome (a), **154:**1131
Esophagus
  acute food impaction, glucagon, effervescent agent, and water combination, **154:**533
  function, bolus consistency and temperature (a), **154:**1356
  malpositioning of endotracheal tubes, radiologic detection, **154:**23
  motility disorders, manometry and radiology in (a), **154:**1356
  tuberculosis, peptic strictures and (l), **154:**200
ESWL, *see* Extracorporeal shock-wave lithotripsy
Ethanol
  percutaneous injection therapy, hepatocellular carcinoma, **154:**947
  sonographically guided percutaneous injection, hyperparathyroidism, **154:**1087
Extracorporeal membrane oxygenation, respiratory syncytial virus bronchiolitis, children (a), **154:**1358
Extracorporeal shock-wave lithotripsy
  abdominal radiography, renal ultrasound and excretory urography comparison (a), **154:**1132
  bile duct stones, sonography for localization of stones (a), **154:**1356
  gallstone recurrence after (a), **154:**1131
  gallstones, **154:**291
  methyl *tert*-butyl ether and, partially calcified gallstones (a), **154:**427

F

Fallopian tube, obstruction, selective osteal salpingography and transvaginal catheter in, **154:**735
Femoral artery, catheterization, conversion of retrograde to antegrade, **154:**179
Femur
  acute intracapsular fracture, MR (a), **154:**1357
  fractures, scintimetry after, prognostic accuracy (a), **154:**1131
  proximal
    intracapsular osteoid osteoma, CT (p), **154:**1241
    metastatic carcinoma, MR (l), **154:**902
Ferritin, cerebral hemorrhage appearance on CT and, **154:**1053
Fetus, nuchal cystic hygroma, spontaneous resolution in second trimester of pregnancy (l), **154:**903
Fluoroscope, gastrostomy guided by, **154:**725

G

Gadopentetate dimeglumine, excretion, breast milk, **154:**1305
Gallbladder
  contractility, spinal cord injuries, sonography, **154:**521
  nonvisualized, oral cholecystography, lithotripsy and (a), **154:**1358
  percutaneous interventional procedures (a), **154:**1358
Gallstones, *see* Cholelithiasis
Ganglioglioma, intracranial, MR, CT and clinical findings, **154:**607
Gastric polyps, gastric mucosal background study in (a), **154:**1357
Gastroenterostomy, percutaneous, fluoroscopically guided, **154:**725
Gastrointestinal tract
  complications, cytosine-arabinoside chemotherapy, **154:**95
  CT (b), **154:**86
Gastropexy, with percutaneous gastrostomy, **154:**1003
Gastrostomy
  endoscopic vs operative (a), **154:**1357
  percutaneous
    fluoroscopically guided, **154:**725
    gastropexy with, **154:**1003
Germ cell tumors, neuroimaging, **154:**1299
Gibbs phenomenon (l), 154:204
Glazer, Norman (m), 154:784
Glossopalatal sphincter, manometric characteristics (a), **154:**1356
Gorham syndrome, right clavicle and scapula, **154:**1335
Guidewires, floppy platinum-tip, complications from, **154:**1103

H

Halo vest, cervical spine fixation during MR, **154:**631
Hartman, Glen W. (m), 154:952
Hawkins-Hunter rocket wire, biliary system, **154:**1101
Heart disease, congenital, angiography in, **154:**789
Heart-lung transplantation, postoperative pleural effusion (l), **154:**1344
Helicobacter pylori
  histologic gastritis (a), **154:**1129
  intrafamilial clustering of infection (a), **154:**1354
Hemangioma
  hepatic, fatality from fine-needle aspiration biopsy (l), **154:**203
  intramuscular, MR (p), **154:**563
Hematuria, blunt abdominal trauma, children, CT, **154:**569
Hemosiderin, cerebral hemorrhage appearance on CT and, **154:**1053
Hemostasis, before abdominal interventions, **154:**233, **154:**239 (commentary)
Hepatectomy, partial, bile duct necrosis after (l), **154:**1124
Hepatic artery, transcatheter embolization, bile duct necrosis after (l), **154:**1124
Hepatocellular carcinoma
  comparison with other lesions, Doppler studies (a), **154:**664
  fine-needle aspiration biopsy (a), **154:**664
  hepatic arterial injection chemotherapy, cisplatin suspended in lymphographic agent for (a), **154:**662
  percutaneous ethanol injection therapy, **154:**947
  presenting as bone metastasis (a), **154:**662
Hepaturia, dipsticks, urinary tract cancer detected with (a), **154:**663
Hilar cholangiocarcinoma, enhanced CT, **154:**1203
Histiocytoma, malignant fibrous, lung, asbestos exposure and, **154:**65
Hodgkin disease
  children, CT and lymphography comparison with laparotomy, **154:**1251
  leukemia after (a), **154:**1130
  primary pulmonary (a), **154:**1354
Holoprosencephaly, alobar and semilobar, sonography of fetal facial features, **154:**143
Human immunodeficiency virus
  transmission, children (a), **154:**1357
  type 1, *Pneumocystis carinii* pneumonia risk in (a), **154:**1354
Humerus, displaced proximal fractures, Neer classification of (p), **154:**1029
Hyaline membrane disease, mechanical breathing, surfactant therapy effects, infant (a), **154:**1132
Hydatid cysts, multiple (l), **154:**1126
Hydatid disease, spleen, imaging findings, **154:**525
Hydronephrosis, carcinoma of the vermiform appendix and (l), **154:**654
Hyperparathyroidism, ethanol injection, sonographically guided percutaneous, **154:**1087
Hypertension
  portal, ultrasonic measurements (a), **154:**908
  radiation and (l), **154:**659
Hypokalemia, aldosteronism, renal cysts and (a), **154:**1354
Hypothalamic histiocytosis, CT, **154:**1338

I

Ileitis, pouch (a), **154:**428
Ileoanal pouches, CT, scintigraphy, and contrast enema comparison, **154:**73
Iliac artery, stenoses, Wallstent endoprosthesis treatment, **154:**613
Ilizarov limb-lengthening procedures, distraction site, sonography, **154:**125
Immunoscintigraphy, anti-CEA, parotid gland tumors, **154:**1259
Impotence
  diagnostic evaluation, role of imaging in (l), **154:**1347
  vasculogenic erectile, penile duplex sonography (a), **154:**907
Infertility, sonography (b), **154:**544
Infrapopliteal arteries, percutaneous transluminal angioplasty, **154:**171
Interleukin-2, shoulder pain caused by, scintigraphy, **154:**327
Intestine, small, clinical radiology (b), **154:**72
Intraocular lesions, patients with systemic disease, MR, **154:**385
Intraurethral stent, self-retaining, alternative for prostatism, **154:**111
Intraventricular hemorrhage
  indomethacin and (a), **154:**210
  preterm infants (a), **154:**665
Intussusception, hydrostatic reduction of (l), **154:**1123
Irradiation, bone marrow changes after, MR, **154:**745
Ischemia, recurrent (a), **154:**663

K

Kaposi's sarcoma, CT (a), **154:**427
Kidney
  abnormalities, bacterial attachment and, boys with urinary tract infection (a), **154:**907
  blood flow, transcatheter thrombosis of leaking saccular aneurysm, **154:**1097
  carcinoma, venacavography and MR comparison (a), **154:**428
  clinical imaging (b), **154:**1096
  crossed renal ectopia without fusion, sonography (l), **154:**657
  function, evaluation with radionuclides (b), **154:**114
  imaging, long-term dialysis patients, CT and sonography comparison (l), **154:**1125
  intrarenal arteriovenous fistula, pseudoaneurysm and, duplex Doppler sonography (l), **154:**424
  nonobstructive renal disease, intrarenal arterial Doppler sonography, **154:**1223
  percutaneous procedures, posterior intercostal approach, **154:**115
  polycystic disease, pediatric (a), **154:**907
  transplantation, children, Doppler evaluation of, **154:**785
Kimray-Greenfield filter
  intracaval breakage (l), **154:**1349
  percutaneous insertion, **154:**621
Knee
  acute changes in joint, jogging and, MR, **154:**1233
  lateral meniscus, pseudotear, MR, **154:**1237
  spontaneous osteonecrosis, MR, **154:**331

L

Laparatomy, comparison with CT and lymphography, staging of Hodgkin disease in children, **154:**1251
Larynx, chondrosarcoma, CT, **154:**997
Leigh syndrome, MR, correlation with biochemical defect, **154:**1269
Leiomyoma, distinguished from pelvic masses, MR, **154:**295
Leptomeningeal metastases, intracranial, CT and MR, **154:**351

- **Leukemia**
  - acute, high-dose Ara-C therapy, fatal pulmonary failure and (a), **154:1355**
  - after chemotherapy for ovarian cancer (a), **154:1129**
  - after Hodgkin's disease (a), **154:1130**
  - myelocytic, secondary, after breast carcinoma therapy (a), **154:662**
- **Ligaments,** wrist, arthrography and MR comparison, **154:337**
- **Linguinal cortical defect,** unknown cause (l), **154:420**
- **Lithotripsy**
  - *see also* Extracorporeal shock-wave lithotripsy
  - biliary, hepatic subcapsular hematoma and, **154:1015**
- **Liver**
  - caudate lobe (p), **154:87**
  - cavernous hemangioma, fine-needle aspiration biopsy (a), **154:908**
  - extramedullary hematopoiesis, sonography (l), **154:900**
  - focal lesions
    - CT and MR comparison (a), **154:1358**
    - t-null inversion recovery sequence MR (a), **154:1359**
  - focal nodular hyperplasia, contrast material retention in (l), **154:422**
  - hydatid disease, biliary complications, ERCP value in (a), **154:210**
  - imaging, ghost artifact on gradient-echo, **154:633**
  - inflammatory pseudotumor (l), **154:201**
  - iron overload, noninvasive imaging (a), **154:908**
  - ringed lesions, MR (p), **154:287**
  - subcapsular hematoma, complication of biliary lithotripsy, **154:1015**
  - transplantation, biliary complications after (p), **154:729**
  - tumors
    - color Doppler imaging, **154:509**
    - Gd-DTPA-enhanced spin-echo imaging, **154:515**
  - venocclusive disease, Doppler sonography, **154:721**
- **Lung**
  - adenoid cystic carcinoma, calcification in, CT (l), **154:419**
  - blastomycosis, chest radiographs, **154:1177**
  - bronchoalveolar carcinoma, CT, **154:1318**
  - calcification in carcinoma, CT, **154:255**
  - cancer, radiologic diagnosis, pitfalls, **154:1165**
  - endobronchial sarcoidosis, upper lobe collapse (l), **154:897**
  - hernia, radiologic features, **154:51**
  - infarction, CT (a), **154:665**
  - interstitial disease, chest radiographs with bronchoalveolar lavage (a), **154:905**
  - left lower lobe bronchus, anterior wall stripe, CT, **154:33**
  - malignant fibrous histiocytoma, asbestos exposure and, **154:65**
  - malignant pleural effusions, small bore catheter drainage and sclerotherapy (a), **154:662**
  - metastatic osteosarcoma to, **154:1321**
  - metastatic tumors, fine needle aspiration biopsy (a), **154:905**
  - neutrophil kinetics, smoking effects (a), **154:661**
  - parenchyma, wooden foreign body in, **154:999**
  - radiation fibrosis, Gd-DTPA enhancement (a), **154:666**
  - scans, criteria for diagnosis of pulmonary emboli, **154:975**
  - sequestration, imaging of, **154:241**
  - solitary nodule, radiologic evaluation, **154:701**
  - transplantation, reactivation of tuberculosis after, **154:495**
- **Lymphangioma,** peripancreatic retroperitoneal, similarities to other lesions (l), **154:1125**
- **Lymphedema,** periportal, trauma patients (l), **154:1124**
- **Lymph node,** metastases, carotid artery and jugular vein, sonography, **154:411**
- **Lymphography,** staging of Hodgkin disease, children, **154:1251**
- **Lymphoma,** intraabdominal and retroperitoneal, fine needle aspiration diagnosis (a), **154:1130**

M

- **Magnetic resonance imaging**
  - angiography, **154:937**
  - physical principles and instrumentation (b), **154:770**
  - workbook (b), **154:1228**
- **Magnetic resonance imaging, abdomen**
  - Budd-Chiari syndrome, percutaneous transluminal angioplasty treatment (l), **154:1350**
  - femoropopliteal venous thrombosis, **154:175**
  - prenatal detection of abdominal mass, pancuronium bromide and, **154:1049**
  - thorax and, comparison with other procedures, **154:989**
  - transposition of great vessels, congenitally corrected (l), **154:898**
- **Magnetic resonance imaging, adrenal gland,** current status, **154:927**
- **Magnetic resonance imaging, ankle,** osteochondritis dissecans, **154:555**
- **Magnetic resonance imaging, bone**
  - sarcoma, chemotherapy effects, **154:763**
  - soft tissue tumors and their mimics (b), **154:554**
- **Magnetic resonance imaging, bone marrow,** changes after irradiation, **154:745**
- **Magnetic resonance imaging, cranium**
  - basal ganglion lesions, neurofibromatosis, **154:369**
  - cerebellum, **154:593**
  - cerebral hemorrhage, ferritin and hemosiderin role in, **154:1053**
  - corpus callosum, agenesis and lipoma (l), **154:1348**
  - cranial nerves (p), **154:1263**
  - Gd-DTPA-enhanced, meningitis, CT comparison, **154:809**
  - head and neck anatomy (b), **154:630**
  - intracranial chemical-shift artifacts on, **154:1275**
  - intracranial ependymoma, subependymoma and, **154:837**
  - intracranial ganglioglioma, **154:607**
  - intracranial leptomeningeal metastases, **154:351**
  - intractable complex partial epileptic seizures, **154:577**
  - Leigh syndrome, children, **154:1269**
  - primary cerebral neuroblastoma, **154:831**
  - sella and para-sella region (b), **154:384**
  - signal abnormalities, memory disorder and dementia, **154:1285**
  - temporomandibular joint, **154:1245**
  - Tolosa-Hunt syndrome, **154:167**
  - trichilemmal cyst, scalp (l), **154:423**
- **Magnetic resonance imaging, eyes,** intraocular lesions, patients with systemic disease, **154:385**
- **Magnetic resonance imaging, foot,** ankle and (v), **154:776**
- **Magnetic resonance imaging, hand and wrist,** detection of masses, **154:323**
- **Magnetic resonance imaging, heart,** mitral regurgitation (a), **154:1133**
- **Magnetic resonance imaging, hip,** metastatic carcinoma (l), **154:902**
- **Magnetic resonance imaging, kidney,** renal carcinoma, extending to renal vein and inferior vena cava (a), **154:428**
- **Magnetic resonance imaging, knee**
  - acute changes in joint, jogging and, **154:1233**
  - osteonecrosis, **154:331**
  - popliteal artery, entrapment, **154:425**
  - pseudotear of lateral meniscus, **154:1237**
- **Magnetic resonance imaging, leg,** femoral head, acute intracapsular fracture (a), **154:1357**
- **Magnetic resonance imaging, liver**
  - cirrhosis, regenerating nodules of, **154:505**
  - focal lesions
    - CT comparison (a), **154:1358**
    - t-null inversion recovery sequence (a), **154:1359**
  - Gd-DTPA-enhanced, spin-echo, differentiation of tumors, **154:515**
  - gradient-echo, ghost artifact on, **154:633**
  - ringed lesions (p), **154:287**
  - t-null inversion recovery sequence, characterization of lesions (a), **154:1133**
- **Magnetic resonance imaging, muscle,** intramuscular hemangiomas (p), **154:563**
- **Magnetic resonance imaging, neck,** Gd-DTPA-enhanced, tumors of nasopharynx and adjacent areas, **154:585**
- **Magnetic resonance imaging, pelvis**
  - clinical imaging (b), **154:988**
  - leiomyoma, distinguished from pelvic masses, **154:295**
- **Magnetic resonance imaging, sacrum,** lesions (p), **154:771**
- **Magnetic resonance imaging, scrotum,** high-field-strength, heating, **154:1229**
- **Magnetic resonance imaging, shoulder**
  - correlation with plain film radiographs (p), **154:549**
  - 0.2T permanent-magnet unit, **154:777**
- **Magnetic resonance imaging, spine**
  - cervical, halo vest for fixation, **154:631**
  - cervical facet joints, age-related changes, **154:817**
  - cervical portion, pseudoatrophy, **154:1069**
  - Gd-DTPA-enhanced
    - central nervous system, von Hippel-Lindau disease (a), **154:211**
    - extradural degenerative disease, **154:151**
    - tears of anulus fibrosus, **154:159**
  - lumbosacral, synovial cysts, **154:163**
  - pocket atlas (b), **154:1268**
  - three-dimensional gradient-recalled, cervical radiculopathy, **154:375**
- **Magnetic resonance imaging, spleen,** visceroatrial situs (p), **154:797**
- **Magnetic resonance imaging, testes,** seminomatous and nonseminomatous tumors, **154:539**
- **Magnetic resonance imaging, thorax**
  - abdominal wall and, comparison with other procedures, **154:989**
  - ascending aortic prosthetic conduits by (a), **154:1131**
- **Magnetic resonance imaging, wrist,** ligament evaluation, arthrography comparison, **154:337**
- **Mammary artery,** importance, percutaneous transthoracic intervention, **154:47**
- **Mammography**
  - breast mass simulation (l), **154:900**
  - collapse of breast implant after (l), **154:1345**
  - dual-screen and dual-emulsion film combination, quality of, **154:265**
  - screen/film combinations, radiation dose, **154:713**
  - sensitivity of (l), **154:419**
- **Mandible,** incipient lingual cortical defect, American Indian child (l), **154:658**
- **Manometry**
  - glossopalatal sphincter (a), **154:1356**
  - radiology and, esophageal motility disorders (a), **154:1356**
  - sphincter of Oddi in (a), **154:1131**
- **Mastication,** muscles of (l), **154:658**
- **McNeil criteria,** diagnosis of pulmonary emboli, lung scans, **154:975**
- **Meckel's diverticulum,** life-threatening hemorrhage from, arterial embolization, **154:1257**

Mediastinum
  cystic teratoma, **154:**259
  fibrosis, dysphagia due to, pulmonary tuberculosis and, **154:**61
  low-attenuation masses, CT (l), **154:**199
  mass, superior pericardial recess simulating, **154:**69
  Whipple disease, **154:**1187
Melanoma metastases, sonographic diagnosis, liver, gallbladder, and spleen (a), **154:**211
Memorials
  Andrew Eccles Yeates, 1951–1989, **154:**1284
  Glen W. Hartman, 1936–1990, **154:**952
  Norman Glazer, 1920–1989, **154:**784
  Paul L. Rogers, 1931–1989, **154:**118
  Robert James Borgerson, 1919–1989, **154:**1086
Memory disorder, MR signal abnormalities in, **154:**1285
Meningitis, Gd-DTPA-enhanced MRI, CT comparison, **154:**809
Metastatic disease, long bones (a), **154:**906
Mitral commissurotomy, percutaneous transvenous, indications, complications, and outcome (a), **154:**207
Monochorionic twinning, sonography, **154:**459
Motility disorders, gastrointestinal, stress and (a), **154:**664
Musculoskeletal system, avulsion and stress injuries (b), **154:**134
Mycobacterium tuberculosis**,** susceptibility to infection by, racial differences (a), **154:**1354
Myocardial infarction, noninfarcted myocardium, functional significance of hypertrophy (a), **154:**207
Myopathy, pentazocine-induced, imaging in, **154:**343

N

Nasopharynx, tumors, MR, **154:**585
Necrotizing enterocolitis, neonates, portable abdominal radiography in, **154:**779
Neuroblastoma, primary cerebral, CT and MR, **154:**831
Neurofibromatosis, basal ganglion lesions in, MR, **154:**369
Neurofibromatosis 2, etiology, **154:**1337
Neuroimaging, germ cell neoplasms, **154:**1299
Nuclear medicine
  1989 annual (b), **154:**404
  developing countries (b), **154:**40
  pulmonary, thromboembolic disease (a), **154:**907
  spine fracture probability, multi-site BMC measurements for (a), **154:**210
  tomographic methods (b), **154:**1078
Nutcracker phenomenon, pericaliceal varices due to, **154:**305

O

Omentum, Castleman disease (l), **154:**654
Oncocytoma, renal, mimicking angiomyolipoma, CT, **154:**307
Organ transplantation, cyclosporine treatment, malignant neoplasms in, **154:**271
Osteochondritis dissecans, staging, MRI, **154:**555
Osteodystrophy, renal, primary oxalosis with, **154:**1334
Osteogenesis imperfecta, differentiation of child abuse from, **154:**1035, **154:**1047 (commentary)
Osteogenic sarcoma, bleomycin-related pulmonary injury in (a), **154:**661
Osteoid osteoma, intracapsular, proximal femur, CT (p), **154:**1241
Osteonecrosis, spontaneous, knee, MRI, **154:**331
Osteopenia, insufficiency fracture of sternum and, **154:**1025
Osteosarcoma, parosteal, humerus, CT, **154:**1331
Ovary
  cancer, chemotherapy for, leukemia after (a), **154:**1129
  herniation of cyst through inguinal canal, CT (l), **154:**202
  surgical lateral transposition, CT, **154:**119
  teratomas, sonographic appearance, **154:**139

P

Pancreas
  function, neonatal screening for cystic fibrosis (a), **154:**1353
  sonographic changes, renal failure (a), **154:**210
  transplantation, acute venous thrombosis after, sonography and scintigraphy, **154:**529
Pancuronium bromide, immobilization of fetus during MR, detection of abdominal mass, **154:**1049
Panniculitis, mesenteric, CT, **154:**1328
Paraganglioma, malignant extraadrenal retroperitoneal, CT, **154:**1329
Parasellar epidermoid, CT, **154:**1340
Parotid gland, tumors, anti-CEA immunoscintigraphy, **154:**1259
Patella, bilateral dorsal defect (l), **154:**1347
Pediatric radiology
  ano-rectal strictures, balloon dilatation of, infant (a), **154:**211
  anoxic/ischemic cerebral injury, CT, reversal sign on, **154:**361
  biomedical research, informed consent (a), **154:**1132
  blunt abdominal trauma, hematuria in, **154:**569
  bone imaging (b), **154:**1250
  bowel obstruction, infant with AIDS, **154:**803
  Campylobacter pylori, gastrointestinal disease related to (a), **154:**427
  childhood risk factors, adult high blood pressure (a), **154:**209
  colonoscopy (a), **154:**429
  congenital rubella syndrome, calcific epiphyseal stippling and peroxisomal dysfunction (a), **154:**1132
  coronary angiography, pulmonary atresia, hypoplastic right ventricle, and ventriculocoronary communications, **154:**789
  craniosynostosis, enlarged parietal foramina and, American Indian child (l), **154:**658
  diastematomyelia, cervical and basicranial, **154:**806
  endoscopy, upper gastrointestinal tract (a), **154:**429
  hepatic artery thrombosis, after liver transplantation, duplex Doppler studies, **154:**573
  HIV transmission (a), **154:**1357
  Hodgkin disease, CT and lymphography comparison with laparotomy, **154:**1251
  holoprosencephaly, sonography of fetal facial features, **154:**143
  hyaline membrane disease, mechanical breathing, surfactant therapy effects, infant (a), **154:**1132
  incipient lingual cortical mandibular defect, American Indian child (l), **154:**658
  intraventricular hemorrhage, preterm infants (a), **154:**665
  intraventricular hemorrhage, indomethacin and (a), **154:**210
  laryngeal and tracheobronchial obstruction, ultrafast CT of, **154:**345
  Leigh syndrome, MR correlation with biochemical defect, **154:**1269
  long-term diuretic therapy, bronchopulmonary dysplasia (a), **154:**210
  magnetic catheter, removal of foreign bodies, **154:**149
  mechanical ventilation effects, cerebral blood flow, newborn (a), **154:**211
  moderate head trauma, intracranial injury after (a), **154:**428
  necrotizing enterocolitis, neonates, portable abdominal radiographs in, **154:**779
  ovarian teratomas, prepubertal and postpubertal, **154:**139
  polycystic kidney disease (a), **154:**907
  pulmonary infiltrates, cancer patients, flexible bronchoscopy in (a), **154:**209
  renal abnormalities, boys with urinary tract infection (a), **154:**907
  renal transplants, Doppler evaluation of, **154:**785
  respiratory syncytial virus, extracorporeal membrane oxygenation for (a), **154:**1358
  transcatheter closure, patient ductus arteriosus (a), **154:**209
  untreated bacteriuria, renal scarring and, girls (a), **154:**907
  urinary tract imaging (b), **154:**142
Pelvic mass, solid, distinguished from leiomyoma, MR, **154:**295
Pentazocine, myopathy induced by, imaging in, **154:**343
Percutaneous transthoracic intervention, hemorrhage due to, **154:**47
Pericaliceal varices, due to nutcracker phenomenon, **154:**305
Perineal hernia, posterior, CT, **154:**761
Periostitis, chondroblastoma, **154:**309
Phlegmasia cerulea dolens, after placement of bird's nest vena cava filter, **154:**1105
Picture archiving, communication systems and, Japan, **154:**415
PIOPED criteria, diagnosis of pulmonary emboli, lung scans, **154:**975
Pneumatocele, traumatic, **154:**1323
Pneumocystis carinii
  AIDS-related infection, visceral and nodal calcification, **154:**27
  risk, HIV type 1 men (a), **154:**1354
Pneumonia, bronchiolitis obliterans organizing, **154:**983
Pneumonitis, usual interstitial, lymph node enlargement on CT scans, **154:**251
Pneumoperitoneum, acute abdomen, sonography, **154:**107
Pneumothorax, after CT-guided pulmonary interventional procedures, CT and chest radiographs, **154:**45
Polyarthritis, chronic, **154:**1332
Popliteal artery, entrapment, MR, **154:**425
Portosystemic shunts, color Doppler sonography, **154:**393
Positron emission tomography, clinical research and diagnosis (b), **154:**1024
Posttraumatic cerebral infarction, CT, **154:**1293
Pregnancy
  second trimester, nuchal fetal cystic hygroma, spontaneous resolution of (l), **154:**903
  transvaginal sonography in (l), **154:**656
Prostate
  endorectal sonography, **154:**691
  hypoechoic area, sonographically guided biopsy (a), **154:**1357
Prostatism, self-retaining intraurethral stent, **154:**111
Prune belly syndrome, comprehensive approach (a), **154:**209
Pulmonary sequestration, imaging of, **154:**241

R

Radiation
  diagnostic medical, exposure (b), **154:**50
  dose, new mammography screen/film combinations, **154:**713
  estimated dose, multislice CT studies, fetus, **154:**185
  hypertension and (l), **154:**659
  space activities (b), **154:**870
Radiculopathy, cervical, MR, **154:**375
Radiography

- developed by new ultrarapid film processing system, **154:**1107
- exposure (b), **154:**862
- measurements (b), **154:**744
- retained firearm projectiles, **154:**471

Radiography, technique
- chest
  - analysis (b), **154:**486
  - interpretation, clinical history effects, **154:**709
  - newer methods (a), **154:**1133
  - pulmonary blastomycosis, **154:**1177
  - sarcoidosis during corticosteroid withdrawal, **154:**481
- GI complications, cytosine-arabinoside chemotherapy, **154:**95
- malpositioning of endotracheal tubes, esophagus, **154:**23
- portable abdominal, necrotizing enterocolitis in infants, **154:**779

Radiologic technologists, medical techniques and patient care (b), **154:**476

Radiologists
- attitude toward practice, **154:**867
- implications of technology assessment (commentary), **154:**652
- medical decision making, **154:**1149

Radiology
- administration (b), **154:**644
- diagnostic
  - manual for (b), **154:**286
  - proportions in , **154:**477
  - quality improvement (perspective), **154:**1117
- diagnostic (b), **154:**1164
- gastrointestinal (b), **154:**1198
- interventional, emergency (b), **154:**1028
- journalism, Melvin M. Figley Fellowship, **154:**470
- literature, evaluation of, **154:**17
- occupational chest diseases (b), **154:**64
- oral and pharyngeal phases of swallowing, **154:**953, **154:**965
- perception of images (l), **154:**1121
- statistical terminology, specifics of (l), **154:**1121

Radiology, technique
- dento maxillo facial (b), **154:**584
- diagnostic X-ray department, quality assurance (b), **154:**32
- dysphagia investigation, **154:**1157
- lung cancer diagnosis, pitfalls, **154:**1165

Radiology, training, manpower equation (perspective), **154:**1111

Radiology department, planning of (perspective), **154:**635

Radionuclides, evaluation of renal function (b), **154:**114

Renal artery, endovascular stented (l), **154:**902

Reversal sign, CT and MR, anoxic/ischemic cerebral injury, children, **154:**361

Roentgen diagnosis, index for (l), **154:**659

Rogers, Paul L. (m), **154:**118

Rotator cuff, tears, sonography, **154:**121

S

Sacrum, lesions, MR (p), **154:**771

Salpingography, selective osteal, fallopian tube obstruction, **154:**735

Samarium-153 EDTMP, pharmacokinetics of, metastatic cancer (a), **154:**665

Saphenous vein, arterial bypass graft stenosis, color Doppler sonography, **154:**857

Sarcoidosis
- during corticosteroid withdrawal, chest radiographic findings in, **154:**481
- endobronchial, upper lobe collapse (l), **154:**897
- osseous, **154:**1332

Scintigraphy
- acute venous thrombosis, after pancreas transplantation, **154:**529
- gallium, CT comparison, synthetic vascular graft infection, **154:**405
- inflammation (b), **154:**796
- postsurgical complications, ileoanal pouches, **154:**73
- shoulder pain, caused by interleukin-2, **154:**327

Sclerotherapy, small drainage catheter and, malignant pleural effusions (a), **154:**662

Scrotum
- blunt trauma, ultrasound and (a), **154:**665
- skin temperature after MR, **154:**1229

Sequential images, method of identification (l), **154:**426

Sigmoidoscopy, double-contrast barium enema and (a), **154:**906

Single photon emission computed tomography, ^{99m}Tc-RBC, hemangiomatosis (l), **154:**423

Sinus, inferior petrosal, sampling, diagnosis of acromegaly, **154:**1075

Society for Pediatric Radiology, 1990 annual meeting, **154:**671

Society of Gastrointestinal Radiologists, 19th annual meeting, **154:**1311

Society of Uroradiology
- abstracts from 1989 meeting, **154:**191
- 1989 scientific session, **154:**11
- survey of members, current status of adult uroradiology, **154:**301

Soft tissue, masses, hand and wrist, MRI, **154:**323

Sonography
- biopsy guided by, **154:**1
  - needle placement for, **154:**847
- color Doppler
  - carotid artery disease, **154:**1061
  - liver tumor, **154:**509
  - physics, instrumentation, and clinical application (b), **154:**398
  - portosystemic shunts, **154:**393
  - saphenous vein arterial bypass graft stenosis, **154:**857
  - standards for (l), **154:**1348
  - upper-extremity deep venous thrombosis, **154:**399
- Doppler
  - hepatic venocclusive disease, **154:**721
  - hepatocellular carcinoma and other lesions (a), **154:**664
  - renal transplantation in children, **154:**785
- duplex Doppler
  - hepatic artery thrombosis after liver transplantation, children, **154:**573
  - intrarenal arteriovenous fistula and pseudoaneurysm (l), **154:**424
  - normal native kidneys with urinary tract obstruction (a), **154:**429
- muscles and tendons (b), **154:**124

Sonography, abdomen
- acute appendicitis, perforation in, **154:**275
- acute (b), **154:**982
- combined systemic and portal venous gas, **154:**1219
- gallbladder contractility, spinal cord injuries, **154:**521
- melanoma metastases, liver, gallbladder, and spleen (a), **154:**211
- pneumoperitoneum, **154:**107

Sonography, adrenal gland, current status, **154:**927

Sonography, bone, limb lengthening, Ilizarov procedures, **154:**125

Sonography, colon, acute diverticulitis, **154:**1199

Sonography, eye, coloboma, **154:**391

Sonography, fetus
- alobar and semilobar holoprosencephaly, **154:**143
- femur length (a), **154:**665
- growth standards, racial differences (a), **154:**1358
- monochorionic twinning, **154:**459

Sonography, hip, lower-extremity venous thrombosis, acute fractures, **154:**851

Sonography, kidney
- crossed renal ectopia without fusion (l), **154:**657
- intrarenal arterial Doppler, nonobstructive renal disease, **154:**1223
- long-term dialysis patients (l), **154:**1125

Sonography, liver
- extramedullary hematopoiesis (l), **154:**900
- hemangiomatosis (l), **154:**423
- inflammatory pseudotumor (l), **154:**201
- portal vasculature, diagnosis of portal hypertension (a), **154:**908

Sonography, lymph node, metastases, carotid artery and jugular vein, **154:**411

Sonography, pancreas
- after transplantation, acute venous thrombosis, **154:**529
- changes in chronic renal failure (a), **154:**210

Sonography, pelvis
- clinical imaging (b), **154:**988
- endovaginal, draining pelvic fluid collections, **154:**849
- infertility (b), **154:**544
- ovarian teratomas, prepubertal and postpubertal, **154:**139
- threatened abortion, subchorionic hemorrhage in, **154:**535

Sonography, penis, vasculogenic erectile impotence (a), **154:**907

Sonography, prostate
- endorectal, **154:**691
- hypoechoic area, sonographically guided biopsy (a), **154:**1357

Sonography, shoulder, rotator cuff tears, **154:**121

Sonography, spine, intraoperative, lumbar disk herniation and canal stenosis, **154:**821

Sonography, thorax, percutaneous needle biopsy, lesions, **154:**1181

Sonography, thyroid, hyperparathyroidism, sonographically guided percutaneous injection of ethanol, **154:**1087

Sonography, transabdominal, gynecologic disease (a), **154:**1133

Sonography, transperineal, assessment of vaginal atresia, 154:545

Sonography, transvaginal
- early pregnancy (l), **154:**656
- gynecologic disease (a), **154:**1133

Spectroscopy, ^{31}P MR, radiation fibrosis and recurrent neoplasia, **154:67**

Sphincter of Oddi, manometry in (a), **154:**1131

Spine
- cervical
  - halo vest for fixation, **154:**631
  - pseudoatrophy, MR, **154:**1069
- cervical radiculopathy, MR, **154:**375
- cervical spondylolysis, CT, **154:**751
- cord compression, epidural, vertebral metastasis and (a), **154:**1130
- extradural degenerative disease, Gd-DTPA-enhanced MR, **154:**151
- injuries, gallbladder contractility and, sonography, **154:**521
- lumbar, traumatic hernia, CT, **154:**757
- lumbar disk herniation, canal stenosis and, intraoperative sonography, **154:**821
- lumbosacral, synovial cysts, MR, **154:**163
- tears of anulus fibrosus, Gd-DTPA-enhanced MR, **154:**159

Spleen, hydatid disease, **154:**525

Splenosis, subcutaneous (l), **154:**655

Sports injuries, imaging (b), **154:**342

Sterility, MRI heating of scrotum and, **154:**1229

Sternoclavicular joint, spontaneous atraumatic anterior subluxation of (a), **154:**428

Sternum, insufficiency fracture, osteopenia and, **154:**1025

Subacute necrotizing encephalomyelopathy, *see* Leigh syndrome

Subtalar arthrorisis, CT, **154:**559

Swallowing
- oral and pharyngeal phases, physiology and radiology, **154:**953, **154:**965

upper esophageal sphincter opening and modulation during (a), **154:663**

T

Talus, dome of, osteochondral fractures (a), **154:208**
Technology assessment
  implications for the radiologist (commentary), **154:652**
  professional organizations and, **154:647**
Temporomandibular joint
  diagnostic imaging, **154:319**
  MR, **154:1245**
Tenography, current role of, **154:129**
Testes, seminomatous and nonseminomatous tumors, MRI, **154:539**
Tetralogy of Fallot, pulmonary atresia with, **154:1319**
Thiazide, diuretic agent, hip fracture and (a), **154:1353**
Thorax, blunt chest trauma, CT (p), **154:55**
Thromboembolic disease, pulmonary nuclear medicine (a), **154:907**
Thrombosis
  deep venous, upper-extremity, color Doppler sonography, **154:399**
  hepatic artery, after liver transplantation, duplex Doppler studies in children, **154:573**
  mesenteric venous, CT (l), **154:425**
  transcatheter, leaking saccular aneurysm, **154:1097**
  venous
    after pancreas transplantation, sonography and scintigraphy, **154:529**
    lower-extremity, compression sonography, **154:851**
Thymus, irradiation, infancy, breast cancer after (a), **154:905**
Thyroid gland, anaplastic carcinoma, CT, **154:1079**
Tibia vara, critical review (a), **154:208**
Tolosa-Hunt syndrome, MR, **154:167**
Trachea, rupture (l), **154:1122**
Transitional cell carcinoma, bladder, cavitary pulmonary metastases in, **154:493**
Trichilemmal cyst, scalp, MR (l), **154:423**
Trisegmentectomy, right, percutaneous biliary drainage after (l), **154:656**
Tuberculosis
  ileocecal, CT and radiologic evaluation, **154:499**
  pulmonary, mediastinal fibrosis in, dysphagia and, **154:61**
  reactivation, after lung transplantation, **154:495**
  treatment for, breast cancer after (a), **154:905**
  upper lobe, adult (a), **154:1355**

U

Ultrarapid film processing system, radiographs developed by, **154:1107**
Urethra, obstruction, self-retaining intraurethral stent, **154:111**
Urinary tract
  cancer, home screening with hematuria dipsticks (a), **154:663**
  imaging, pediatric (b), **154:142**
  infection
    boys, renal abnormalities and (a), **154:907**
    imaging (l), **154:201**
  obstruction, normal native kidneys with, duplex sonography evaluation (a), **154:429**
Urography, clinical (b), **154:1222**
Urologic pathology, clinical and radiologic correlations (b), **154:1100**
Uroradiology, adult, current status, **154:301**
Uterus, perforation, simulating urachal carcinoma, CT, **154:741**

V

Vaginal atresia, assessment, transperineal sonography, **154:545**
Vena cava, bird's nest filter, phlegmasia cerulea dolens after, **154:1105**
Venacavography, renal carcinoma, extending to renal vein and inferior vena cava (a), **154:428**
Venous thrombosis, femoropopliteal, MRI, **154:175**
Videofluoroscopy, speech, cleft palate (b), **154:1156**
Videotape reviews
  MR of the foot and ankle, **154:776**
  MR of the sella and para-sella region, **154:384**
  RSNA today, vol. 3, no. 2, **154:54**
  RSNA today, vol. 3, no. 3, **154:94**
  RSNA today, vol. 3 special edition, **154:300**
  RSNA today, vol. 3, no. 4, **154:964**
Villonodular synovitis, pigmented, knee, radiologic findings (a), **154:664**
Visceroatrial situs, abnormal (p), **154:797**
von Hippel-Lindau disease
  CT, **154:1326**
  radiologic screening (a), **154:211**

W

Whipple disease, mediastinum, **154:1187**
Whipple procedure, recurrence of tumor, CT after, **154:1011**

Y

Yeates, Andrew Eccles (m), 154:1284

Z

Zollinger-Ellison syndrome, reflux esophagitis in (a), **154:1131**

Volume 154

Official Journal of the American Roentgen Ray Society

American Journal of Roentgenology

Diagnostic Imaging and Related Sciences

Editor-In-Chief Robert N. Berk, *La Jolla, California*
University of California, San Diego
School of Medicine and Medical Center

Editor Emeritus Melvin M. Figley, *Seattle, Washington*

Associate Editor Saskia von Waldenburg Hilton, *San Diego, California*

Consulting Editor Michael S. Huckman, *Chicago, Illinois*

Statistician Charles C. Berry, *San Diego, California*

Editorial Board

John R. Amberg
Itamar Aviad
Mark E. Baker
Lawrence W. Bassett
Michael A. Bettman
Felix S. Chew
N. Reed Dunnick
David K. Edwards
Ronald G. Evens
David S. Feigin
Sandra K. Fernbach
Richard H. Gold
William R. Hendee
John R. Hesselink
Charles B. Higgins
Melvyn T. Korobkin
Faye C. Laing
Thomas L. Lawson
Robert G. Levitt
Bruce L. McClennan
Richard P. Moser
Albert A. Moss
Jeffrey H. Newhouse
Donald L. Resnick
Stewart R. Reuter
Charles A. Rohrmann, Jr.
Peter M. Ronai
Sjef H. J. Ruijs
Stuart S. Sagel
David J. Sartoris
Stefan C. Schatzki
William P. Shuman
Edward A. Sickles
Barry A. Siegel
David D. Stark
Edward T. Stewart
Murali Sundaram
Eric vanSonnenberg
Robert K. Zeman

Editorial Staff: Margaret Levene, *managing editor*; Katie L. Spiller, Barbara Rose, Barbara L. Halliburton, and Janine Anderson, *manuscript editors*; Nancy Rydbeck, *office manager*; Sheri Smith, *administrative assistant*; Sandra L. Griffin, *administrative secretary*.

AJR, AMERICAN JOURNAL OF ROENTGENOLOGY (ISSN 0361 803X) is the official journal of the American Roentgen Ray Society, and is published monthly by Williams & Wilkins, 428 E. Preston St., Baltimore, MD 21202. Annual dues include $50 for journal subscription. Second-class postage paid at Baltimore, MD, and at additional mailing offices. Postmaster, send address changes (Form 3579) to AJR, 428 E. Preston St., Baltimore, MD 21202. Subscription rates $110 ($155 foreign, $244 Japan); institutions $120 ($165 foreign, $254 Japan); in training $25 ($70 foreign, $159 Japan); single copy $16 ($19 foreign). Japanese rates include airfreight. Japanese yen price is available from our sole agent USACO Corporation, 13-12, Shimbashi 1-Chome, Minato-Ku, Tokyo 105, Japan, telephone 03-502-6471. Airmail rates furnished on request. Indexed by *Current Contents* and *Index Medicus*. Copyright © 1990 by American Roentgen Ray Society. 0361-803X/89$2.00

January 1990

SPECIAL ARTICLES

1 **Expert Advice. CT and sonographically guided needle biopsy: current techniques and new innovations.** *Charboneau JW, Reading CC, Welch TJ*

11 **Meeting News. The Society of Uroradiology scientific session, September 1989.** *Whalen E*

17 **Perspective. How to evaluate the radiology literature.** *Black WC*

CHEST RADIOLOGY

23 **Radiographic detection of esophageal malpositioning of endotracheal tubes.** *Smith GM, Reed JC, Choplin RH*

27 **Visceral and nodal calcification in patients with AIDS-related *Pneumocystis carinii* infection.** *Radin DR, Baker EL, Klatt EC, et al.*

33 **The anterior wall stripe of the left lower lobe bronchus on the lateral chest radiograph: CT correlative study.** *Lang EV, Friedman PJ*

41 **CT appearance of the retroaortic anastomoses of the azygos system.** *Takasugi JE, Godwin JD*

45 **CT and chest radiography are equally sensitive in the detection of pneumothorax after CT-guided pulmonary interventional procedures.** *Murphy FB, Small WC, Wichman RD, Chalif M, Bernardino ME*

47 **Case report. Life-threatening hemorrhage due to percutaneous transthoracic intervention: importance of the internal mammary artery.** *Glassberg RM, Sussman SK*

51 **Lung hernia: radiographic features.** *Bhalla M, Leitman BS, Forcade C, Stern E, Naidich DP, McCauley DI*

55 **Pictorial essay. CT of blunt chest trauma.** *Kerns SR, Gay SB*

61 **Dysphagia due to mediastinal fibrosis in advanced pulmonary tuberculosis.** *Ramakantan R, Shah P*

65 **Case report. Malignant fibrous histiocytoma of the lung in a patient with a history of asbestos exposure.** *Reifsnyder AC, Smith HJ, Mullhollan TJ, Lee EL*

67 **Case report. The differentiation of radiation fibrosis from recurrent neoplasia: a role for ^{31}P MR spectroscopy?** *Charles HC, Baker ME, Hathorn JW, Sostman D*

69 **Case report. Effusion in the superior pericardial recess simulating a mediastinal mass.** *Winer-Muram HT, Gold RE*

GASTROINTESTINAL RADIOLOGY

73 **Ileoanal pouches: comparison of CT, scintigraphy, and contrast enemas for diagnosing postsurgical complications.** *Thoeni RF, Fell SC, Engelstad B, Schrock TR*

79 **CT of the extrahepatic bile ducts: wall thickness and contrast enhancement in normal and abnormal ducts.** *Schulte SJ, Baron RL, Teefey SA, et al.*

87 **Pictorial essay. Caudate lobe of the liver: anatomy, embryology, and pathology.** *Dodds WJ, Erickson SJ, Taylor AJ, Lawson TL, Stewart ET*

95 **Gastrointestinal complications of cytosine-arabinoside chemotherapy: findings on plain abdominal radiographs.** *Tjon A Tham RTO, Vlasveld LT, Willemze R*

99 **The diagnosis of bowel infarction: a comparison of plain films and CT scans in 23 cases.** *Smerud MJ, Johnson CD, Stephens DH*

105 **Case report. Blue rubber bleb nevus syndrome: CT diagnosis of intussusception.** *Tyrrel RT, Baumgartner BR, Montemayor KA*

107 **Sonographic detection of pneumoperitoneum in patients with acute abdomen.** *Lee DH, Lim JH, Ko YT, Yoon Y*

GENITOURINARY RADIOLOGY

111 **Self-retaining intraurethral stent: an alternative to long-term indwelling catheters or surgery in the treatment of prostatism.** *Yachia D, Lask D, Rabinson S*

115 **The posterior intercostal approach for percutaneous renal procedures: risk of puncturing the lung, spleen, and liver as determined by CT.** *Hopper KD, Yakes WF*

119 **Case report. Surgical lateral ovarian transposition: CT appearance.** *Newbold R, Safrit H, Cooper C*

MUSCULOSKELETAL RADIOLOGY

121 **Rotator cuff tears: diagnosis with sonography.** *Vick CW, Bell SA*

125 **Sonographic evaluation of bone production at the distraction site in Ilizarov limb-lengthening procedures.** *Young JWR, Kostrubiak IS, Resnik CS, Paley D*

129 **Review. The current role of tenography and bursography.** *Baker KS, Gilula LA*

135 **Treatment of suppurative arthritis by percutaneous catheter drainage.** *Renner JB, Agee MW*

PEDIATRIC RADIOLOGY

139 **Ovarian teratomas: a comparison of the sonographic appearance in prepubertal and postpubertal girls.** *Sisler CL, Siegel MJ*

143 **Sonography of facial features of alobar and semilobar holoprosencephaly.** *McGahan JP, Nyberg DA, Mack LA*

149 **Technical note. Magnet catheter for removal of magnetic foreign bodies.** *Towbin RB, Dunbar JS, Rice S*

NEURORADIOLOGY

151 **Assessment of extradural degenerative disease with Gd-DTPA–enhanced MR imaging: correlation with surgical and pathologic findings.** *Ross JS, Modic MT, Masaryk TJ, Carter J, Marcus RE, Bohlman H*

159 **Tears of the anulus fibrosus: assessment with Gd-DTPA–enhanced MR imaging.** *Ross JS, Modic MT, Masaryk TJ*

163 **Synovial cysts of the lumbosacral spine: diagnosis by MR imaging.** *Liu SS, Williams KD, Drayer BP, Spetzler RF, Sonntag VKH*

167 **MR imaging of Tolosa-Hunt syndrome.** *Yousem DM, Atlas SW, Grossman RI, Sergott RC, Savino PJ, Bosley TM*

VASCULAR RADIOLOGY

171 **Percutaneous transluminal angioplasty of the infrapopliteal arteries: results in 53 patients.** *Bakal CW, Sprayregen S, Scheinbaum K, Cynamon J, Veith FJ*

175 **Diagnosis of femoropopliteal venous thrombosis with MR imaging: a comparison of four MR pulse sequences.** *Totterman S, Francis CW, Foster TH, Brenner B, Marder VJ, Bryant RG*

179 **Technical note. Catheter for conversion of retrograde to antegrade femoral artery catheterization.** *Patel YD*

181 **Case report. Transcatheter embolization of a ruptured abdominal aortic stump.** *Terasaki KK, Allgood M, Finck EJ, Pentecost MJ*

183 **Technical note. Simple technique for redirecting malpositioned central venous catheters.** *Recht MP, Burke DR, Meranze SG, Cope C*

RADIATION BIOLOGY

185 **Estimated fetal radiation dose from multislice CT studies.** *Felmlee JP, Gray JE, Leetzow ML, Price JC*

OTHER CONTENT

Book reviews and videotape reviews 16, 32, 40, 50, 54, 64, 72, 86, 94, 114, 124, 134, 142, 158

71 **ARRS 1990 resident award papers information**

118 **Memorial, Paul L. Rogers**

191 **The Society of Uroradiology 1989 meeting abstracts from 1989**

199 **Letters**

206 **Books received**

207 **Review of current literature**

212 **Forthcoming articles**

213 **News**

216 **Invitation to the 1990 ARRS meeting**

219 **1990 ARRS meeting summary**

220 **ARRS membership information and application**

223 **American Roentgen Ray Society information**

224 **Classified advertisements**

A3 **Guidelines for authors**

A8 ***AJR* business and subscriber information**

February 1990

SPECIAL ARTICLES

233 **Perspective. Hemostatic evaluation before abdominal interventions: an overview and proposal.** *Silverman SG, Mueller PR, Pfister RC*

239 **Commentary. Assessing hemostatic function before abdominal interventions.** *Rapaport SI*

CHEST RADIOLOGY

241 **Review. Imaging of pulmonary sequestration.** *Felker RE, Tonkin ILD*

251 **Mediastinal lymph node enlargement on CT scans in patients with usual interstitial pneumonitis.** *Bergin C, Castellino RA*

255 **CT demonstration of calcification in carcinoma of the lung.** *Mahoney MC, Shipley RT, Corcoran HL, Dickson BA*

259 **Case report. Cystic teratoma of the mediastinum: demonstration of fat/fluid level.** *Fulcher AS, Proto AV, Jolles H*

BREAST RADIOLOGY

261 **Technical note. A new device for evaluation of biopsy specimens of occult breast lesions.** *Lindfors KK, Lott SA, Alberhasky MT*

265 **Diagnostic quality of mammograms obtained with a new low-radiation-dose dual-screen and dual-emulsion film combination.** *Wojtasek DA, Teixidor HS, Govoni AF, Gareen IF*

GASTROINTESTINAL RADIOLOGY

271 **Clinical and radiologic features of malignant neoplasms in organ transplant recipients: cyclosporine-treated vs untreated patients.** *Honda H, Barloon TJ, Franken EA Jr, Garneau RA, Smith JL*

275 **Sonographic diagnosis of perforation in patients with acute appendicitis.** *Borushok KF, Jeffrey RB Jr, Laing FC, Townsend RR*

279 **Technical note. Double-contrast enema: a simplified method for filling the colon.** *Gelfand DW, Ott DJ*

281 **Limitations in the CT diagnosis of acute diverticulitis: comparison of CT, contrast enema, and pathologic findings in 16 patients.** *Balthazar EJ, Megibow A, Schinella RA, Gordon R*

287 **Pictorial essay. The differential diagnosis of ringed hepatic lesions in MR imaging.** *Hahn PF, Stark DD, Saini S, et al.*

291 **Gallstone extracorporeal shock wave lithotripsy: time and treatment considerations.** *Nelson RC, Rowland GA, Torres WE, Baumgartner BR*

GENITOURINARY RADIOLOGY

295 **The value of MR imaging in distinguishing leiomyomas from other solid pelvic masses when sonography is indeterminate.** *Weinreb JC, Barkoff ND, Megibow A, Demopoulos R*

301 **Perspective. Current status of adult uroradiology: a survey of members of the Society of Uroradiology.** *Barloon TJ, Brown RC, Berbaum KS*

305 **Case report. Pericaliceal varices due to the nutcracker phenomenon.** *Trambert JJ, Rabin AM, Weiss KL, Tein AB*

307 **Case report. Intratumoral fat in a renal oncocytoma mimicking angiomyolipoma.** *Curry NS, Schabel SI, Garvin AJ, Fish G*

MUSCULOSKELETAL RADIOLOGY

309 **The frequency and diagnostic significance of periostitis in chondroblastoma.** *Brower AC, Moser RP, Kransdorf MJ*

315 **Pictorial essay. CT findings of degenerative arthritis of the atlantoodontoid joint.** *Genez BM, Willis JJ, Lowrey CE, et al.*

319 **Expert advice. Diagnostic imaging of the temporomandibular joint: recommendations for use of the various techniques.** *Helms CA, Kaplan P*

323 **Masses of the hand and wrist: detection and characterization with MR imaging.** *Binkovitz LA, Berquist TH, McLeod RA*

327 **Scintigraphic findings in patients with shoulder pain caused by interleukin-2.** *Baron NW, Davis LP, Flaherty LE, Muz J, Valdivieso M, Kling GA*

331 **Spontaneous osteonecrosis of the knee: value of MR imaging in determining prognosis.** *Björkengren AG, AlRowaih A, Lindstrand A, Wingstrand H, Thorngren K-G, Pettersson H*

337 **Is MR better than arthrography for evaluating the ligaments of the wrist? In vitro study.** *Gundry CR, Kursunoglu-Brahme S, Schwaighofer B, Kang HS, Sartoris DJ, Resnick D*

343 **Case report. Imaging findings in a patient with pentazocine-induced myopathy.** *De Schepper AMA, Degryse HRM*

PEDIATRIC RADIOLOGY

345 **Ultrafast CT of laryngeal and tracheobronchial obstruction in symptomatic postoperative infants with esophageal atresia and tracheoesophageal fistula.** *Kao SCS, Smith WL, Sato Y, Franken EA Jr, Kimura K, Soper RT*

NEURORADIOLOGY

351 **Loculated intracranial leptomeningeal metastases: CT and MR characteristics.** *Lee Y-Y, Tien RD, Bruner JM, De Pena CA, Van Tassel P*

361 **Reversal sign on CT: effect of anoxic/ischemic cerebral injury in children.** *Han BK, Towbin RB, De Courten-Myers G, McLaurin RL, Ball WS Jr*

369 **High-intensity basal ganglia lesions on T1-weighted MR images in neurofibromatosis.** *Mirowitz SA, Sartor K, Gado M*

375 **Three-dimensional gradient-recalled MR imaging as a screening tool for the diagnosis of cervical radiculopathy.** *Tsuruda JS, Norman D, Dillon W, Newton TH, Mills DG*

385 **Intraocular lesions in patients with systemic disease: findings on MR imaging.** *Tonami H, Tamamura H, Kimizu K, et al.*

391 **Case report. Coloboma: evaluation with real-time sonography.** *Munk PL*

VASCULAR RADIOLOGY

393 **Color Doppler imaging of portosystemic shunts.** *Grant EG, Tessler FN, Gomes AS, et al.*

399 **Color Doppler sonographic imaging in the assessment of upper-extremity deep venous thrombosis.** *Knudson GJ, Wiedmeyer DA, Erickson SJ, et al.*

405 **Diagnosis of synthetic vascular graft infection: comparison of CT and gallium scans.** *Johnson KK, Russ PD, Bair JH, Friefeld GD*

411 **Invasion of the carotid artery and jugular vein by lymph node metastases: detection with sonography.** *Gritzmann N, Grasl MCh, Helmer M, Steiner E*

COMMENTARY

415 **Picture archiving and communication systems in Japan: 3 years later.** *Huang HK, Cho PS, Taira R, Ho BK, Chan KK*

OTHER CONTENT

Book and videotape reviews 286, 300, 342, 360, 374, 384, 398, 404

254 **ARRS 1990 resident award papers information**

418 **Forthcoming articles**

419 **Letters**

427 **Review of current literature**

430 **News**

435 **Invitation to the 1990 ARRS meeting**

437 **1990 ARRS meeting summary**

438 **1990 ARRS meeting courses and symposium**

441 **1990 ARRS meeting local activities**

444 **American Roentgen Ray Society information**

445 **1990 ARRS meeting registration forms**

448 **ARRS membership information and application**

451 **Classified advertisements**

A3 **Guidelines for authors**

A8 ***AJR* business and subscriber information**

March 1990

PROGRESS IN RADIOLOGY

459 **Review article. Monochorionic twinning: sonographic assessment.** *Filly RA, Goldstein RB, Callen PW*

SPECIAL ARTICLES

471 **Pictorial essay. Identification of retained firearm projectiles on plain radiographs.** *Dodd GD III, Budzik RF Jr*

477 **Perspective. A tutorial on confidence intervals for proportions in diagnostic radiology.** *Berry CC*

PULMONARY RADIOLOGY

481 **Do chest radiographic findings reflect the clinical course of patients with sarcoidosis during corticosteroid withdrawal?** *Baumann MH, Strange C, Sahn SA*

487 **CT in differential diagnosis of diffuse pleural disease.** *Leung AN, Müller NL, Miller RR*

493 **Case report. Cavitary pulmonary metastases in transitional cell carcinoma of urinary bladder.** *Alexander PW, Sanders C, Nath H*

495 **Case report. Reactivation of tuberculosis in a donor lung after transplantation.** *Carlsen SE, Bergin CJ*

GASTROINTESTINAL RADIOLOGY

499 **Ileocecal tuberculosis: CT and radiologic evaluation.** *Balthazar EJ, Gordon R, Hulnick D*

505 **Regenerating nodules of liver cirrhosis: MR imaging with pathologic correlation.** *Ohtomo K, Itai Y, Ohtomo Y, Shiga J, Iio M*

509 **Color Doppler flow imaging of liver tumors.** *Tanaka S, Kitamura T, Fujita M, Nakanishi K, Okuda S*

515 **Dynamic spin-echo imaging with Gd-DTPA: value in the differentiation of hepatic tumors.** *Van Beers B, Demeure R, Pringot J, et al.*

521 **Gallbladder contractility in patients with spinal cord injuries: a sonographic investigation.** *Nino-Murcia M, Burton D, Chang P, Stone J, Perkash I*

525 **Hydatid disease of the spleen: imaging findings in nine patients.** *Franquet T, Montes M, Lecumberri FJ, Esparza J, Bescos JM*

529 **Case report. Acute venous thrombosis after pancreas transplantation: diagnosis with duplex Doppler sonography and scintigraphy.** *Boiskin I, Sandler MP, Fleischer AC, Nylander WA*

533 **Technical note. Treatment of acute esophageal food impaction with a combination of glucagon, effervescent agent, and water.** *Kaszar-Seibert DJ, Korn WT, Bindman DJ, Shortsleeve MJ*

GENITOURINARY RADIOLOGY

535 **Prevalence and significance of subchorionic hemorrhage in threatened abortion: a sonographic study.** *Pedersen JF, Mantoni M*

539 **Differentiation of seminomatous from nonseminomatous testicular tumors with MR imaging.** *Johnson JO, Mattrey RF, Phillipson J*

545 **Value of transperineal sonography in the assessment of vaginal atresia.** *Scanlan KA, Pozniak MA, Fagerholm M, Shapiro S*

MUSCULOSKELETAL RADIOLOGY

549 **Pictorial essay. MR imaging of the shoulder: correlation with plain radiography.** *Burk DL Jr, Karasick D, Mitchell DG, Rifkin MD*

555 **Value of MR imaging in staging osteochondral lesions of the talus (osteochondritis dissecans): results in 14 patients.** *De Smet AA, Fisher DR, Burnstein MI, Graf BK, Lange RH*

559 **Subtalar arthrorisis: evaluation with CT.** *Smith DK, Gilula LA, Totty WG*

563 **Pictorial essay. Radiologic appearance of intramuscular hemangioma with emphasis on MR imaging.** *Buetow PC, Kransdorf MJ, Moser RP Jr, Jelinek JS, Berrey BH*

PEDIATRIC RADIOLOGY

569 **The significance of hematuria in children after blunt abdominal trauma.** *Stalker HP, Kaufman RA, Stedje K*

573 **False-negative duplex Doppler studies in children with hepatic artery thrombosis after liver transplantation.** *Hall TR, Mc Diarmid SV, Grant EG, Boechat MI, Busuttil RW*

NEURORADIOLOGY

577 **MR imaging in patients with intractable complex partial epileptic seizures.** *Brooks BS, King DW, El Gammal T, et al.*

585 **Tumors of the nasopharynx and adjacent areas: MR imaging with Gd-DTPA.** *Vogl T, Dresel S, Bilaniuk LT, Grevers G, Kang K, Lissner J*

593 **The cerebellum: 3. Anatomic-MR correlation in the coronal plane.** *Press GA, Murakami JW, Courchesne E, Grafe M, Hesselink JR*

603 **CT of intracranial cryptococcosis.** *Popovich MJ, Arthur RH, Helmer E*

607 **Intracranial ganglioglioma: MR, CT, and clinical findings in 18 patients.** *Castillo M, Davis PC, Takei Y, Hoffman JC Jr*

VASCULAR RADIOLOGY

613 **Treatment of iliac artery stenoses with the Wallstent endoprosthesis.** *Raillat C, Rousseau H, Joffre F, Roux D*

617 **Technical note. Removal of intimal hyperplasia in vascular endoprostheses by atherectomy and balloon dilatation.** *Vorwerk D, Guenther RW*

621 **Technical note. A simple device to facilitate percutaneous insertion of the Kimray-Greenfield filter.** *Zagoria RJ, Scott MD, D'Souza VJ, Dyer RB*

MR IMAGING

623 **Pictorial essay. Artifacts in maximum-intensity-projection display of MR angiograms.** *Anderson CM, Saloner D, Tsuruda JS, Shapeero LG, Lee RE*

631 **Technical note. Halo vest for cervical spine fixation during MR imaging.** *Shellock FG, Slimp G*

633 **Technical note. Ghost artifact on gradient-echo imaging: a potential pitfall in hepatic imaging.** *Silverman PM, Patt RH, Baum PA, Teitelbaum GP*

COMPUTER PAGE

635 **Planning a totally digital radiology department.** *Huang HK, Kangarloo H, Cho PS, Taira RK, Ho BKT, Chan KK*

641 **Computer-aided management of residents' on-call and vacation schedules.** *Kahn CE Jr*

MEETING NEWS

645 **Summary of the 1989 American College of Radiology summit meeting.** *McClennan BL, Hartman GW*

COMMENTARIES

647 **Review article. Technology assessment: The contribution of professional organizations.** *Hendee WR*

652 **Implications of technology assessment for the radiologist.** *Rosenquist CJ*

OTHER CONTENT

470 **Melvin M. Figley Fellowship recipient**

Book reviews 476, 486, 504, 532, 544, 554, 568, 572, 576, 584, 630, 644

640 **Forthcoming articles**

654 **Letters**

661 **Review of current literature**

667 **News**

671 **SPR Scientific Program: 33rd annual meeting, April 19–22**

673 **Invitation to 1990 ARRS meeting**

675 **ARRS 1990 meeting summary**

676 **ARRS 1990 meeting courses and symposium**

679 **1990 ARRS meeting registration forms**

682 **American Roentgen Ray Society information**

683 **Classified advertisements**

A3 **Guidelines for authors**

A16 ***AJR* business and subscriber information**

April 1990

SPECIAL ARTICLES

691 **Progress in radiology. State of the art: endorectal sonography of the prostate gland.** *Rifkin MD, Dähnert W, Kurtz AB*
701 **Review article. Radiologic evaluation of the solitary pulmonary nodule.** *Webb WR*

PULMONARY RADIOLOGY

709 **Does knowledge of the clinical history affect the accuracy of chest radiograph interpretation?** *Good BC, Cooperstein LA, DeMarino GB, et al.*

BREAST RADIOLOGY

713 **New mammography screen/film combinations: imaging characteristics and radiation dose.** *Kimme-Smith C, Bassett LW, Gold RH, Zheutlin J, Gornbein JA*

GASTROINTESTINAL RADIOLOGY

721 **Doppler sonography: a noninvasive method for evaluation of hepatic venocclusive disease.** *Brown BP, Abu-Yousef M, Farner R, LaBrecque D, Gingrich R*
725 **Fluoroscopically guided percutaneous gastrostomy and gastroenterostomy: analysis of 158 consecutive cases.** *Hicks ME, Surratt RS, Picus D, Marx MV, Lang EV*
729 **Pictorial essay. Imaging of and intervention for biliary complications after hepatic transplantation.** *Letourneau JG, Hunter DW, Payne WD, Day DL*

GENITOURINARY RADIOLOGY

735 **Selective osteal salpingography and transvaginal catheter dilatation in the diagnosis and treatment of fallopian tube obstruction.** *Lang EK, Dunaway HE Jr, Roniger WE*
741 **Case report. Uterine perforation simulating urachal carcinoma: CT diagnosis.** *Kronthal AJ, Fishman EK, Sanders RC, Epstein JI, Kuhlman JE, Brendler CB*

MUSCULOSKELETAL RADIOLOGY

745 **Early and late bone-marrow changes after irradiation: MR evaluation.** *Stevens SK, Moore SG, Kaplan ID*
751 **Cervical spondylolysis: imaging findings in 12 patients.** *Forsberg DA, Martinez S, Vogler JB III, Wiener MD*
757 **Traumatic lumbar hernia: CT diagnosis.** *Faro SH, Racette CD, Lally JF, Wills JS, Mansoory A*
761 **Case report. CT diagnosis of posterior perineal hernia.** *Lubat E, Gordon RB, Birnbaum BA, Megibow AJ*
763 **The value of MR imaging in monitoring the effect of chemotherapy on bone sarcomas.** *Holscher HC, Bloem JL, Nooy MA, Taminiau AHM, Eulderink F, Hermans J*
771 **Pictorial essay. MR imaging of sacral and presacral lesions.** *Wetzel LH, Levine E*
777 **Technical note. MR of the shoulder with a 0.2-T permanent-magnet unit.** *Sasaki M, Ehara S, Nakasato T, et al.*

PEDIATRIC RADIOLOGY

779 **Diagnostic quality of portable abdominal radiographs in neonates with necrotizing enterocolitis: digitized vs nondigitized images.** *Gross GW, Ehrlich SM, Wang Y*
785 **Doppler evaluation of renal transplants in children: a prospective analysis with histopathologic correlation.** *Drake DG, Day DL, Letourneau JG, et al.*
789 **Coronary angiography of pulmonary atresia, hypoplastic right ventricle, and ventriculocoronary communications.** *Burrows PE, Freedom RM, Benson LN, et al.*
797 **Pictorial essay. Current evaluation of the patient with abnormal visceroatrial situs.** *Hernanz-Schulman M, Ambrosino MM, Genieser NB, et al.*
803 **Case report. Bowel obstruction in an infant with AIDS.** *Sivit CJ, Taylor GA, Patterson K, Thompson R, Josephs SH*
806 **Case report. Cervical and basicranial diastematomyelia.** *Herman TE, Siegel MJ*

NEURORADIOLOGY

809 **Gd-DTPA–enhanced MR imaging of the brain in patients with meningitis: comparison with CT.** *Chang KH, Han MH, Roh JK, Kim IO, Han MC, Kim C-W*
817 **Age-related changes in the cervical facet joints: studies with cryomicrotomy, MR, and CT.** *Fletcher G, Haughton VM, Ho K-C, Yu S*
821 **Lumbar disk herniation and canal stenosis: value of intraoperative sonography in diagnosis and surgical management.** *Montalvo BM, Quencer RM, Brown MD, et al.*
831 **Primary cerebral neuroblastoma: CT and MR findings in 12 cases.** *Davis PC, Wichman RD, Takei Y, Hoffman JC Jr*
837 **Intracranial ependymoma and subependymoma: MR manifestations.** *Spoto GP, Press GA, Hesselink JR, Solomon M*

INTERVENTIONAL RADIOLOGY

847 **Technical note. A simple phantom for learning needle placement for sonographically guided biopsy.** *Silver B, Metzger TS, Matalon TAS*
849 **Technical note. Endovaginal sonography for guidance in draining pelvic fluid collections.** *Abbitt PL, Goldwag S, Urbanski S*

VASCULAR RADIOLOGY

851 **Lower-extremity venous thrombosis in patients with acute hip fractures: determination of anatomic location and time of onset with compression sonography.** *Dorfman GS, Froehlich JA, Cronan JJ, Urbanek PJ, Herndon JH*
857 **Early detection of saphenous vein arterial bypass graft stenosis by color-assisted duplex sonography: a prospective study.** *Polak JF, Donaldson MC, Dobkin GR, Mannick JA, O'Leary DH*

RADIATION PHYSICS

863 **Computer page. Performing JCAHO dose calculations with the aid of a microcomputer spreadsheet program.** *David G, Price SC*

PERSPECTIVES

867 **Attitudes of American radiologists toward their practices: present and future.** *Brogdon BG, Heveron ED, Diamond JJ*
871 **Technical note. Autoradiology: patient heal thyself.** *Gay SB, Selby JB Jr, Selby HG*

MEETING NEWS

875 **Colon cancer: diagnosis in an era of cost containment. ACR Conference, November 8, 1989.** *Whalen E*

CASE OF THE DAY

883 **Introduction.** *Stull MA*
884 **Chest case of the day.** *Stull MA, Clark LR, Reagan K, et al.*
888 **Abdominal case of the day.** *Silverman PM, Hayes WS, Cooper CJ, et al.*
890 **Musculoskeletal case of the day.** *Stull MA, Glass-Royal MW*
893 **Neuroradiology case of the day.** *Deveikis JP, Cammarata CA, Reid WM, et al.*

OTHER CONTENT

Book and videotape reviews 744, 770, 776, 788, 796, 862, 870, 882
784 **Memorial, Norman Glazer**
856 **Forthcoming articles**
897 **Letters**
905 **Review of current literature**
909 **News**
913 **ARRS 1990 meeting summary**
914 **ARRS 1990 meeting courses and symposium**
916 **Books received**
917 **American Roentgen Ray Society information**
918 **Classified advertisements**
A3 **Guidelines for authors**
A18 ***AJR* business and subscriber information**

May 1990

HANSON LECTURE

927 **Adrenal imaging: current status.** *Dunnick NR*

PROGRESS IN RADIOLOGY

937 **MR angiography.** *Edelman RR, Mattle HP, Atkinson DJ, Hoogewoud HM*

947 **Percutaneous ethanol injection therapy for the treatment of hepatocellular carcinoma.** *Shiina S, Tagawa K, Unuma T, Terano A*

REVIEW ARTICLES

953 **Physiology and radiology of the normal oral and pharyngeal phases of swallowing.** *Dodds WJ, Stewart ET, Logemann JA*

965 **Radiologic assessment of abnormal oral and pharyngeal phases of swallowing.** *Dodds WJ, Logemann JA, Stewart ET*

CHEST RADIOLOGY

975 **Comparison of Biello, McNeil, and PIOPED criteria for the diagnosis of pulmonary emboli on lung scans.** *Webber MM, Gomes AS, Roe D, La Fontaine RL, Hawkins RA*

983 **Bronchiolitis obliterans organizing pneumonia: CT features in 14 patients.** *Müller NL, Staples CA, Miller RR*

989 **MR imaging of thoracic and abdominal wall infections: comparison with other imaging procedures.** *Sharif HS, Clark DC, Aabed MY, Aideyan OA, Haddad MC, Mattsson TA*

997 **Case report. Laryngeal chondrosarcoma: CT findings in three patients.** *Muñoz A, Peñarrocha L, Gallego F, Olmedilla G, Poch-Broto J*

999 **Case report. Wooden foreign body in the lung parenchyma.** *Spouge AR, Weisbrod GL, Herman SJ, Chamberlain DW*

GASTROINTESTINAL RADIOLOGY

1003 **Percutaneous gastrostomy with gastropexy: experience in 125 patients.** *Saini S, Mueller PR, Gaa J, et al.*

1007 **Angioplasty for long-term treatment of patients with Budd-Chiari syndrome.** *Martin LG, Henderson JM, Millikan WJ Jr, Casarella WJ, Kaufman SL*

1011 **CT of the abdomen after the Whipple procedure: value in depicting postoperative anatomy, surgical complications, and tumor recurrence.** *Coombs RJ, Zeiss J, Howard JM, Thomford NR, Merrick HW*

1015 **Case report. Hepatic subcapsular hematoma: an unusual complication of biliary lithotripsy.** *McGrath FP, Lee SH, Gibney RG, Burhenne HJ*

MUSCULOSKELETAL RADIOLOGY

1017 **Adult ankle fractures: comparison of plain films and interactive two- and three-dimensional CT scans.** *Magid D, Michelson JD, Ney DR, Fishman EK*

1025 **Insufficiency fracture of the sternum caused by osteopenia: plain film findings in seven patients.** *Chen C, Chandnani V, Kang HS, et al.*

1029 **Pictorial essay. The Neer classification of displaced proximal humeral fractures: spectrum of findings on plain radiographs and CT scans.** *Kilcoyne RF, Shuman WP, Matsen FA III, Morris M, Rockwood CA*

PEDIATRIC RADIOLOGY

1035 **Review article. Differentiation of child abuse from osteogenesis imperfecta.** *Ablin DS, Greenspan A, Reinhart M, Grix A*

1047 **Commentary. Differentiation of child abuse and osteogenesis imperfecta: medical and legal implications.** *Kleinman PK*

1049 **Case report. Prenatal detection of an abdominal mass by MR imaging performed while the fetus is immobilized with pancuronium bromide.** *Tomà P, Lucigrai G, Dodero P, Lituania M*

1051 **Case report. Castleman disease in the neck: atypical appearance on CT.** *Chaloupka JC, Castillo M, Hudgins P*

NEURORADIOLOGY

1053 **The role of ferritin and hemosiderin in the MR appearance of cerebral hemorrhage: a histopathologic biochemical study in rats.** *Thulborn KR, Sorensen AG, Kowall NW, et al.*

1061 **Carotid artery disease assessed by color Doppler flow imaging: correlation with standard Doppler sonography and angiography.** *Steinke W, Kloetzsch C, Hennerici M*

1069 **Pseudoatrophy of the cervical portion of the spinal cord on MR images: a manifestation of the truncation artifact?.** *Yousem DM, Janick PA, Atlas SW, et al.*

ENDOCRINE RADIOLOGY

1075 **The diagnosis of acromegaly: value of inferior petrosal sinus sampling.** *Doppman JL, Miller DL, Patronas NJ, et al.*

1079 **CT evaluation of anaplastic thyroid carcinoma.** *Takashima S, Morimoto S, Ikezoe J, et al.*

1087 **Nonsurgical treatment of primary hyperparathyroidism with sonographically guided percutaneous injection of ethanol: results in a selected series of patients.** *Karstrup S, Holm HH, Glenthøj A, Hegedüs L*

ANGIOGRAPHY AND INTERVENTIONAL RADIOLOGY

1091 **A solution to the problem of high-flow jets from miniature angiographic catheters.** *Daniel TB, Akins EW, Hawkins IF Jr*

1097 **Case report. Transcatheter thrombosis of a leaking saccular aneurysm of the main renal artery with preservation of renal blood flow.** *Routh WD, Keller FS, Gross GM*

1101 **Technical note. Use of the Hawkins-Hunter rocket wire in the biliary system.** *Shaw DWW, Coldwell DM, Kimmey M, Goldman ML*

1103 **Technical note. Complications from 0.018-in. floppy platinum tip guidewires.** *Quinn SF, Morse S*

1105 **Case report. Phlegmasia cerulea dolens, a complication after placement of a bird's nest vena cava filter.** *Aruny JE, Kandarpa K*

RADIOLOGIC TECHNOLOGY

1107 **Evaluation of radiographs developed by a new ultrarapid film processing system.** *Schmidt RA, Doi K, Sekiya M, et al.*

PERSPECTIVES

1111 **The radiology manpower equation: a new look.** *Brogdon BG*

1117 **Quality improvement in diagnostic radiology.** *Cascade PN*

OTHER CONTENT

952 **Memorial, Glen W. Hartman**

Book and videotape reviews 964, 982, 988, 1002, 1024, 1028, 1034, 1060, 1074, 1078, 1096, 1100

1086 **Memorial, Robert James Borgerson**

1121 **Letters**

1129 **Review of current literature**

1134 **Forthcoming articles**

1135 **News**

1138 **ARRS membership information and application**

1141 **American Roentgen Ray Society Information**

1142 **Classified advertisements**

A3 **Guidelines for authors**

A8 ***AJR* business and subscriber information**

June 1990

SPECIAL ARTICLES

1149 **Review. Medical decision making: practical points for practicing radiologists.** *Phillips WC Jr, Scott JA*
1157 **Expert advice. Radiologic investigation of dysphagia.** *Levine MS, Rubesin SE*
1165 **Review. Pitfalls in the radiologic diagnosis of lung cancer.** *Woodring JH*

CHEST RADIOLOGY

1177 **Pulmonary blastomycosis: findings on chest radiographs in 63 patients.** *Sheflin JR, Campbell JA, Thompson GP*
1181 **Percutaneous biopsy of thoracic lesions: value of sonography for needle guidance.** *Ikezoe J, Morimoto S, Arisawa J, Takashima S, Kozuka T, Nakahara K*
1187 **Case report. Whipple disease of the mediastinum.** *Samuels T, Hamilton P, Shaw P*
1189 **Case report. Bilateral internal mammary artery aneurysms: a previously unreported cause for an anterior mediastinal mass.** *Giles JA, Sechtin AG, Waybill MM, Moser RP Jr*

BREAST RADIOLOGY

1191 **Stereotactic fine-needle aspiration for cytologic diagnosis of nonpalpable breast lesions.** *Löfgren M, Andersson I, Lindholm K*
1196 **Commentary. Stereotactic fine-needle aspiration biopsy for nonpalpable breast lesions.** *Jackson VP, Bassett LW*

GASTROINTESTINAL RADIOLOGY

1199 **The value of sonography in the diagnosis of acute diverticulitis of the colon.** *Wilson SR, Toi A*
1203 **CT of hilar cholangiocarcinoma: late contrast enhancement in six patients.** *Takayasu K, Ikeya S, Mukai K, Muramatsu Y, Makuuchi M, Hasegawa H*
1207 **Pictorial essay. CT of the abdominal wall.** *Goodman P, Raval B*
1213 **Technical note. Common bile duct biopsy with the Simpson atherectomy catheter.** *Kim D, Porter DH, Siegel JB, Mowschenson PM, Steer ML*
1217 **Case report. Obstructing villous adenoma and papillary adenomatosis of the bile ducts.** *Harshfield DL, Teplick SK, Stanton M, Tunuguntla K, Diner WC, Read RC*
1219 **Case report. Combined systemic and portal venous gas: sonographic and CT detection in two cases.** *Kriegshauser JS, Reading CC, King BF, Welch TJ*

GENITOURINARY RADIOLOGY

1223 **Intrarenal arterial Doppler sonography in patients with nonobstructive renal disease: correlation of resistive index with biopsy findings.** *Platt JF, Ellis JH, Rubin JM, DiPietro MA, Sedman AB*
1229 **Heating of the scrotum by high-field-strength MR imaging.** *Shellock FG, Rothman B, Sarti D*

MUSCULOSKELETAL RADIOLOGY

1233 **Jogging causes acute changes in the knee joint: an MR study in normal volunteers.** *Kursunoglu-Brahme S, Schwaighofer B, Gundry C, Ho C, Resnick D*
1237 **MR imaging of the knee: pseudotear of the lateral meniscus caused by the meniscofemoral ligament.** *Vahey TN, Bennett HT, Arrington LE, Shelbourne KD, Ng J*
1241 **Pictorial essay. Intracapsular osteoid osteoma of the proximal femur: findings on plain film and CT.** *Schlesinger AE, Hernandez RJ*
1245 **MR imaging of the temporomandibular joint: a cadaver study of the value of coronal images.** *Schwaighofer BW, Tanaka TT, Klein MV, Sartoris DJ, Resnick D*

PEDIATRIC RADIOLOGY

1251 **Staging of Hodgkin disease in children: comparison of CT and lymphography with laparotomy.** *Baker LL, Parker BR, Donaldson SS, Castellino RA*
1257 **Case report. Arterial embolization to control life-threatening hemorrhage from a Meckel's diverticulum.** *Okazaki M, Higashihara H, Yamasaki S, Akita Y, Toriya H, Shirai Z*

NEURORADIOLOGY

1259 **Diagnosis of tumors of the parotid gland with anti-CEA immunoscintigraphy.** *Kairemo KJA, Hopsu EVM*
1263 **Pictorial essay. MR imaging of the cranial nerves.** *Lanzieri CF*
1269 **MR findings in patients with subacute necrotizing encephalomyelopathy (Leigh syndrome): correlation with biochemical defect.** *Medina L, Chi TL, DeVivo DC, Hilal SK*
1275 **Intracranial chemical-shift artifacts on MR images of the brain: observations and relation to sampling bandwidth.** *Smith AS, Weinstein MA, Hurst GC, DeRemer DR, Cole RA, Duchesneau PM*
1285 **MR signal abnormalities in memory disorder and dementia.** *Bowen BC, Barker WW, Loewenstein DA, Sheldon J, Duara R*
1293 **Posttraumatic cerebral infarction diagnosed by CT: prevalence, origin, and outcome.** *Mirvis SE, Wolf AL, Numaguchi Y, Corradino G, Joslyn JN*
1299 **Neuroimaging of disseminated germ cell neoplasms.** *Mathews VP, Broome DR, Smith RR, Bognanno JR, Einhorn LH, Edwards MK*

CONTRAST MATERIAL

1305 **Case report. Excretion of gadopentetate dimeglumine in human breast milk.** *Schmiedl U, Maravilla KR, Gerlach R, Dowling CA*

COMPUTER PAGE

1307 **Computerized on-line reporting of coronary angiograms with the CLIP system.** *Kim D, Leeming BWA*

MEETING NEWS

1311 **The Society of Gastrointestinal Radiologists: 19th annual meeting, January 1990.** *Whalen E*

ARRS CASE OF THE DAY

1317 **Introduction.** *Stull MA*
1318 **Chest case of the day.** *Stull MA, Clark LR, Reagan K, et al.*
1325 **Abdominal case of the day.** *Silverman PM, Hayes WS, Cooper CJ, et al.*
1331 **Musculoskeletal case of the day.** *Stull MA, Glass-Royal M*
1337 **Neuroradiology case of the day.** *Deveikis JP, Cammarata CA, Reid WM, et al.*

OTHER CONTENT

Book reviews 1156, 1164, 1198, 1222, 1228, 1236, 1240, 1250, 1256, 1268
1176 **Robert D. Pugatch, sixth distinguished scientist, AFIP.** *Moser RP, Jr*
1186 **ARRS 1991 resident award papers information**
1284 **Memorial, Andrew E. Yeates**
1343 **Letters**
1352 **Forthcoming articles**
1353 **Review of current literature**
1360 **News**
1364 **ARRS 1991 meeting announcement, calls for papers and exhibits**
1369 **Classified advertisements**
1387 **Index, Volume 154**
A3 **Guidelines for authors**
A8 ***AJR* business and subscriber information**

New look.
New shape.

GoLYTELY®
PEG-3350 and Electrolytes for Oral Solution

The name that started a revolution now comes in a narrow, stackable container.

Now GoLYTELY takes up less storage space and less space in your patient's refrigerator.

More convenient for
Patients
Pharmacists
Physicians
Nurses

NDC #52268-0100-01
GoLYTELY®
PEG–3350 and Electrolytes for Oral Solution
When reconstituted with water to a volume of 4 liters, this solution contains 125 mmol/L sodium, 10 mmol/L potassium, 40 mmol/L sulfate, 20 mmol/L bicarbonate, 35 mmol/L chloride, and 17.6 mmol/L polyethylene glycol 3350
CAUTION: Federal law prohibits dispensing without prescription
LOT NO. / EXPIRES: SEE BOTTOM
Each disposable jug contains, in powdered form: polyethylene glycol 236 g, sodium sulfate (anhydrous) 22.74 g, sodium bicarbonate 6.74 g, sodium chloride 5.86 g, potassium chloride 2.97 g
LABORATORIES INC. Braintree Braintree, MA 02184
© 1985

New look.
New shape.
GoLYTELY.

Made by Lyne Laboratories, Stoughton, MA 02072, for BRAINTREE LABORATORIES, INC., P.O. Box 361, Braintree, MA 02184.

LABORATORIES · INC
Braintree

© 1989 BRAINTREE LABORATORIES, INC.
TRE-1039

Circle 35 on the Reader Service Card

Volume 154 **American Journal of Roentgenology** June 1990

SPECIAL ARTICLES

1149 **Review. Medical decision making: practical points for practicing radiologists.** *Phillips WC Jr, Scott JA*
1157 **Expert advice. Radiologic investigation of dysphagia.** *Levine MS, Rubesin SE*
1165 **Review. Pitfalls in the radiologic diagnosis of lung cancer.** *Woodring JH*

CHEST RADIOLOGY

1177 **Pulmonary blastomycosis: findings on chest radiographs in 63 patients.** *Sheflin JR, Campbell JA, Thompson GP*
1181 **Percutaneous biopsy of thoracic lesions: value of sonography for needle guidance.** *Ikezoe J, Morimoto S, Arisawa J, Takashima S, Kozuka T, Nakahara K*
1187 **Case report. Whipple disease of the mediastinum.** *Samuels T, Hamilton P, Shaw P*
1189 **Case report. Bilateral internal mammary artery aneurysms: a previously unreported cause for an anterior mediastinal mass.** *Giles JA, Sechtin AG, Waybill MM, Moser RP Jr*

BREAST RADIOLOGY

1191 **Stereotactic fine-needle aspiration for cytologic diagnosis of nonpalpable breast lesions.** *Löfgren M, Andersson I, Lindholm K*
1196 **Commentary. Stereotactic fine-needle aspiration biopsy for nonpalpable breast lesions.** *Jackson VP, Bassett LW*

GASTROINTESTINAL RADIOLOGY

1199 **The value of sonography in the diagnosis of acute diverticulitis of the colon.** *Wilson SR, Toi A*
1203 **CT of hilar cholangiocarcinoma: late contrast enhancement in six patients.** *Takayasu K, Ikeya S, Mukai K, Muramatsu Y, Makuuchi M, Hasegawa H*
1207 **Pictorial essay. CT of the abdominal wall.** *Goodman P, Raval B*
1213 **Technical note. Common bile duct biopsy with the Simpson atherectomy catheter.** *Kim D, Porter DH, Siegel JB, Mowschenson PM, Steer ML*
1217 **Case report. Obstructing villous adenoma and papillary adenomatosis of the bile ducts.** *Harshfield DL, Teplick SK, Stanton M, Tunuguntla K, Diner WC, Read RC*
1219 **Case report. Combined systemic and portal venous gas: sonographic and CT detection in two cases.** *Kriegshauser JS, Reading CC, King BF, Welch TJ*

GENITOURINARY RADIOLOGY

1223 **Intrarenal arterial Doppler sonography in patients with nonobstructive renal disease: correlation of resistive index with biopsy findings.** *Platt JF, Ellis JH, Rubin JM, DiPietro MA, Sedman AB*
1229 **Heating of the scrotum by high-field-strength MR imaging.** *Shellock FG, Rothman B, Sarti D*

MUSCULOSKELETAL RADIOLOGY

1233 **Jogging causes acute changes in the knee joint: an MR study in normal volunteers.** *Kursunoglu-Brahme S, Schwaighofer B, Gundry C, Ho C, Resnick D*
1237 **MR imaging of the knee: pseudotear of the lateral meniscus caused by the meniscofemoral ligament.** *Vahey TN, Bennett HT, Arrington LE, Shelbourne KD, Ng J*
1241 **Pictorial essay. Intracapsular osteoid osteoma of the proximal femur: findings on plain film and CT.** *Schlesinger AE, Hernandez RJ*
1245 **MR imaging of the temporomandibular joint: a cadaver study of the value of coronal images.** *Schwaighofer BW, Tanaka TT, Klein MV, Sartoris DJ, Resnick D*

PEDIATRIC RADIOLOGY

1251 **Staging of Hodgkin disease in children: comparison of CT and lymphography with laparotomy.** *Baker LL, Parker BR, Donaldson SS, Castellino RA*
1257 **Case report. Arterial embolization to control life-threatening hemorrhage from a Meckel's diverticulum.** *Okazaki M, Higashihara H, Yamasaki S, Akita Y, Toriya H, Shirai Z*

NEURORADIOLOGY

1259 **Diagnosis of tumors of the parotid gland with anti-CEA immunoscintigraphy.** *Kairemo KJA, Hopsu EVM*
1263 **Pictorial essay. MR imaging of the cranial nerves.** *Lanzieri CF*
1269 **MR findings in patients with subacute necrotizing encephalomyelopathy (Leigh syndrome): correlation with biochemical defect.** *Medina L, Chi TL, DeVivo DC, Hilal SK*
1275 **Intracranial chemical-shift artifacts on MR images of the brain: observations and relation to sampling bandwidth.** *Smith AS, Weinstein MA, Hurst GC, DeRemer DR, Cole RA, Duchesneau PM*
1285 **MR signal abnormalities in memory disorder and dementia.** *Bowen BC, Barker WW, Loewenstein DA, Sheldon J, Duara R*
1293 **Posttraumatic cerebral infarction diagnosed by CT: prevalence, origin, and outcome.** *Mirvis SE, Wolf AL, Numaguchi Y, Corradino G, Joslyn JN*
1299 **Neuroimaging of disseminated germ cell neoplasms.** *Mathews VP, Broome DR, Smith RR, Bognanno JR, Einhorn LH, Edwards MK*

CONTRAST MATERIAL

1305 **Case report. Excretion of gadopentetate dimeglumine in human breast milk.** *Schmiedl U, Maravilla KR, Gerlach R, Dowling CA*

COMPUTER PAGE

1307 **Computerized on-line reporting of coronary angiograms with the CLIP system.** *Kim D, Leeming BWA*

MEETING NEWS

1311 **The Society of Gastrointestinal Radiologists: 19th annual meeting, January 1990.** *Whalen E*

ARRS CASE OF THE DAY

1317 **Introduction.** *Stull MA*
1318 **Chest case of the day.** *Stull MA, Clark LR, Reagan K, et al.*
1325 **Abdominal case of the day.** *Silverman PM, Hayes WS, Cooper CJ, et al.*
1331 **Musculoskeletal case of the day.** *Stull MA, Glass-Royal M*
1337 **Neuroradiology case of the day.** *Deveikis JP, Cammarata CA, Reid WM, et al.*

OTHER CONTENT

Book reviews 1156, 1164, 1198, 1222, 1228, 1236, 1240, 1250, 1256, 1268
1176 **Robert D. Pugatch, sixth distinguished scientist, AFIP.** *Moser RP, Jr*
1186 **ARRS 1991 resident award papers information**
1284 **Memorial, Andrew E. Yeates**
1343 **Letters**
1352 **Forthcoming articles**
1353 **Review of current literature**
1360 **News**
1364 **ARRS 1991 meeting announcement, calls for papers and exhibits**
1369 **Classified advertisements**
1387 **Index, Volume 154**
A3 **Guidelines for authors**
A8 ***AJR* business and subscriber information**

1991 ARRS Meeting: May 5–10, Boston, MA